

Emilio Bombardieri
John Buscombe
Giovanni Lucignani
Otmar Schober

Advances in **Nuclear Oncology**

Diagnosis and
Therapy

informa
healthcare

Advances in Nuclear Oncology

Advances in Nuclear Oncology Diagnosis and Therapy

Edited by

Emilio Bombardieri

*Director, Department of Diagnostic Imaging and Therapy, Nuclear Medicine Division,
IRCCS Foundation, National Cancer Institute, Milan, Italy*

John Buscombe

Consultant, Department of Nuclear Medicine, Royal Free Hospital, London, UK

Giovanni Lucignani

*Director, Unit of Nuclear Medicine, Hospital San Paolo,
Institute of Radiological Sciences, University of Milan, Milan, Italy*

Otmar Schober

Director, Department of Nuclear Medicine, University of Münster, Münster, Germany

informa
healthcare

© 2007 Informa UK Ltd

First published in the United Kingdom in 2007 by Informa Healthcare,
Telephone House, 69-77 Paul Street, London EC2A 4LQ.
Informa Healthcare is a trading division of Informa UK Ltd.
Registered Office: 37/41 Mortimer Street, London W1T 3JH.
Registered in England and Wales number 1072954.

Tel: +44 (0)20 7017 5000
Fax: +44 (0)20 7017 6699
Website: www.informahealthcare.com

All rights reserved. No part of this publication may be reproduced, stored in a retrieval system, or transmitted, in any form or by any means, electronic, mechanical, photocopying, recording, or otherwise, without the prior permission of the publisher or in accordance with the provisions of the Copyright, Designs and Patents Act 1988 or under the terms of any licence permitting limited copying issued by the Copyright Licensing Agency, 90 Tottenham Court Road, London W1P 0LP.

Although every effort has been made to ensure that all owners of copyright material have been acknowledged in this publication, we would be glad to acknowledge in subsequent reprints or editions any omissions brought to our attention.

Although every effort has been made to ensure that drug doses and other information are presented accurately in this publication, the ultimate responsibility rests with the prescribing physician. Neither the publishers nor the authors can be held responsible for errors or for any consequences arising from the use of information contained herein. For detailed prescribing information or instructions on the use of any product or procedure discussed herein, please consult the prescribing information or instructional material issued by the manufacturer.

A CIP record for this book is available from the British Library.
Library of Congress Cataloging-in-Publication Data

Data available on application

ISBN-10: 1 84184 614 7
ISBN-13: 978 1 84184 614 9

Distributed in North and South America by
Taylor & Francis
6000 Broken Sound Parkway, NW, (Suite 300)
Boca Raton, FL 33487, USA

Within Continental USA
Tel: 1 (800) 272 7737; Fax: 1 (800) 374 3401
Outside Continental USA
Tel: (561) 994 0555; Fax: (561) 361 6018
Email: orders@crcpress.com

Distributed in the rest of the world by
Thomson Publishing Services
Cheriton House
North Way
Andover, Hampshire SP10 5BE, UK
Tel: +44 (0)1264 332424
Email: tps.tandfsalesorder@thomson.com

Composition by Cepha Imaging Pvt. Ltd., Bangalore, India
Printed and bound in India by Replika Press Pvt. Ltd

Contents

List of contributors	vii	9. Ovarian cancer	133
Preface	xi	<i>Sandro Sironi, Maria Picchio, Luca Guerra, Cristina Messa, and Ferruccio Fazio</i>	
Acknowledgments	xii	10. Breast cancer	143
I: Biology of cancer		<i>Emilio Bombardieri, Marco Maccauro, Orazio Schillaci, and Flavio Crippa</i>	
1. What is cancer?	1	11. Thyroid cancer	161
<i>Uwe Haberkorn</i>		<i>Peter Lind and Susanne Kohlfürst</i>	
2. Targets	17	12. Adrenal tumors	177
<i>Christoph Bremer and Michael Schäfers</i>		<i>Christiane Franzius and Otmar Schober</i>	
II: Diagnostic applications		13. Neuroendocrine	189
3. Primary brain tumors	23	<i>gastroenteropancreatic tumors</i>	
<i>Eva Orunesu, Andreas Jacobs, Andrea Falini, Angelo Del Sole, and Giovanni Lucignani</i>		<i>Emilio Bombardieri, Angela Coliva, Marco Maccauro, Ettore Seregni, and Irene Virgolini</i>	
4. Head and neck cancer	51	14. Lymphoma	203
<i>Flavio Crippa, Alberto Gerali, and Alessandra Alessi</i>		<i>Simona Ben-Haim and Ora Israel</i>	
5. Lung cancer	61	15. Bone and soft tissue tumors	223
<i>Richard P Baum, Vikas Prasad, and Wolfgang A Weber</i>		<i>Gopinath Gnanasegaran, Gary Cook, Sanjay Vijayanathan, and Ignac Fogelman</i>	
6. Esophageal cancer	89	16. Malignant melanoma	253
<i>Cristina Nanni, Sara Taddayon, Guido Biasco, Stefano Fanti, and Arturo Chiti</i>		<i>Ehab M Kamel and Angelika Bischof Delaloye</i>	
7. Colorectal cancer	99	17. Cancer of unknown primary	265
<i>Ken Herrmann and Bernd Joachim Krause</i>		<i>Emilio Bombardieri, Stefano Fanti, Arturo Chiti, Cristina Nanni, Angela Coliva, Enrico Pelosi, and Gianni Bisi</i>	
8. Prostate cancer	109		
<i>Werner Langsteger, Mohsen Beheshti, Reza Vali, Avi Beri, Michael Nader, and Guenter Janetschek</i>			

III: Therapeutic applications

18. Therapy of differentiated thyroid cancer 275
Martin Biermann, and Otmar Schober
19. Therapy of medullary thyroid cancer 293
Aurore Oudoux, Catherine Ansquer, Jacques Barbet, David M Goldenberg, Jean-François Chatal, and Françoise Kraeber-Bodéré
20. Therapy of lymphoma 299
Tim Illidge and Yong Du
21. Therapy of neuroendocrine tumors 315
Irene Virgolini, Ulrich Andergassen, Tatjana Traub-Weidinger, Dirk Heute, Elisabeth von Guggenberg, Dorota Kendler, Margarida Rodrigues, Georg Dobrozemsky, Boris Warwitz, Daniel Putzer, Roy Moncayo, Clemens Decristoforo, and Michael Gabriel
22. Therapy of bone metastases 341
Holger Palmedo
23. Therapy of liver tumors 351
John Buscombe
24. Therapy of colorectal cancer 359
John Buscombe
25. Therapy of brain tumors 367
Chiara Maria Grana, Mirco Bartolomei, Mahila Ferrari, and Giovanni Paganelli
26. Therapy of ovarian cancer 383
Angela Coliva, Ettore Seregni, Mariangela Figini, Alberto Zacchetti, Rosanna Fontanelli, Francesco Raspagliesi, Silvana Canevari, and Emilio Bombardieri

IV: Methods and technology

27. New instrumentation 397
Jörg Eckardt, Klaus Schäfers, and Lars Stegger
28. New radiopharmaceuticals for cancer diagnosis 413
Jane K Sosabowski, Matthias Glaser, and Stephen J Mather
29. Radiopharmaceuticals for therapy 433
Margaret S Cooper and John Buscombe
30. New concepts in dosimetry and radiation protection 443
Michael Lassmann, Manuel Bardies, Carlo Chiesa, Wolfgang Eschner, Glenn Flux, Myriam Monsieurs, Sauli Savolainen, and Sven-Erik Strand
31. Advances in nuclear medicine imaging in oncology 467
Carlo Chiesa, Roberta Matheoud, Marco Brambilla, and Gian Luca Poli
32. Nuclear medicine-guided radiotherapy 499
Diana Salvo, Annibale Versari, Cinzia Iotti, and Marta Paiusco
- Index** 521

Contributors

Ulrich Andergassen

Medical University Innsbruck, Innsbruck, Austria

Catherine Ansquer

Service de Gynecologie-Obstetrique, Hopital de la Mere-et-de-l'Enfant, France.

Alessandra Alessi

PET Unit, Division of Nuclear Medicine, National Cancer Institute, Milan, Italy

Jacques Barbet

Institut National de la Sante et de la Recherche Medicale, Institut de Biologie, Nantes France

Manuel Bardies

INSERM UMR, Nantes, France

Mirco Bartolomei

European Institute of Oncology, Milan, Italy

Richard P Baum

Department of Nuclear Medicine /Centre for PET, Zentralklinik Bad Berka, Bad Berka, Germany

Mohsen Beheshti

PET/CT Center Linz, St Vincent's Hospital, Linz, Austria

Simona Ben-Haim

Institute of Nuclear Medicine, University College London, London, UK

Avi Beri

Endourology and Laparoscopic Surgery, Elisabethinen Hospital, Linz, Austria

Guido Biasco

Institute Haematology and Oncology, Universita di Bologna, Policlinico S. Orsola-Maplighi, Bologna, Italy

Martin Biermann

University of Bergen, Haukeland University Hospital, Bergen, Norway

Angelika Bischof Delaloye

Nuclear Medicine, Lausanne University Hospital, Lausanne, Switzerland

Gianni Bisi

Nuclear Medicine Division, University of Turin, Turin, Italy

Emilio Bombardieri

Nuclear Medicine Division, National Cancer Institute, Milan, Italy

Marco Brambilla

Ospedale Maggiore della Carità, Novara, Italy

Christoph Bremer

Department of Clinical Radiology, University of Münster, Münster, Münster, Germany

John Buscombe

Department of Nuclear Medicine, Royal Free Hospital, London, UK

Silvana Canevari

Experimental Oncology, National Cancer Institute, Milan, Italy

Jean-François Chatal

Centre de Reserche sur le Cancer, Universite de Nantes, Nantes, France

Carlo Chiesa

Division of Nuclear Medicine, National Cancer Institute, Milan, Italy

Arturo Chiti

Istituto Clinico Humanitas, Rozzano – Milano, Italy

Angela Coliva

Division of Nuclear Medicine, National Cancer Institute, Milan, Italy

Gary Cook

Royal Marsden Hospital, London, UK

Margaret S Cooper

St Bartholomew's Hospital, London, UK

Flavio Crippa

PET Unit, Division of Nuclear Medicine, National Cancer Institute, Milan, Italy

Clemens Decristoforo

Medical University Innsbruck, Innsbruck, Austria

Angelo Del Sole

Institute of Radiological Sciences, University of Milan, Italy

Georg Dobrozemsky

Medical University Innsbruck, Innsbruck, Austria

Yong Du

Institute of Nuclear Medicine, University College Hospital, London, UK

Jörg Eckardt

University Hospital, Westfälische Wilhelms-University Münster, Münster, Germany

Wolfgang Eschner

Klinik und Poliklinik für Nuklearmedizin der Universität zu Köln, Köln, Germany

Andrea Falini

Department of Neuroradiology, Scientific Institute and University Ospedale San Raffaele, Milan, Italy

Stefano Fanti

University of Bologna, Policlinico S Orsola-Malpighi, Bologna, Italy

Ferruccio Fazio

University of Milano-Bicocca, Milan, and Scientific Institute San Raffaele, Milan, and IBFM-CNR, Milan, Italy

Mahila Ferrari

European Institute of Oncology, Milan, Italy

Mariangela Figini

National Cancer Institute, Experimental Oncology, Milan, Italy

Glenn Flux

Royal Marsden Hospital, London, UK

Ignac Fogelman

Guys and St Thomas' Hospital NHS Trust, London, UK

Rosanna Fontanelli

Division of Gynecological Oncology, National Cancer Institute, Milan, Italy

Christiane Franzius

University Hospital, Westfälische Wilhelms-University Münster, Münster, Germany

Michael Gabriel

Medical University Innsbruck, Innsbruck, Austria

Alberto Gerali

PET Unit, Division of Nuclear Medicine, National Cancer Institute, Milan, Italy

Matthias Glaser

Hammersmith Imanet Ltd, Hammersmith Hospital, London, UK

Gopinath Gnanasegaran

Guys and St Thomas' Hospital NHS Trust, London, UK

David M Goldenberg

Center for Molecular Medicine and Immunology, Garden State Cancer Center Belleville, New Jersey, USA

Chiara Maria Grana

European Institute of Oncology, Milan, Italy

Luca Guerra

San Gerardo Hospital, Monza, Italy

Uwe Haberkorn

University of Heidelberg Clinical Cooperation Unit Nuclear Medicine German Cancer Research Center, Heidelberg, Germany

Ken Herrmann

Clinic and Polyclinic of Nuclear Medicine, Klinikum Rechts der Isar, Technical University of Munich, Munich, Germany

Dirk Heute

Medical University Innsbruck, Innsbruck, Austria

Tim Illidge

Cancer Studies Division, Christie Hospital, University of Manchester, UK

Cinzia Iotti

Hospital 'Santa Mario Nuova', Reggio Emilia, Italy

Ora Israel

Rambem Medical Center, Haifa, Israel, & The Bruce Rappaport Faculty of Medicine, Technion, Israel Institute of Technology, Haifa,

Andreas Jacobs

Laboratory for Gene Therapy and Molecular Imaging, Max Planck Institute for Neurological Research, University of Cologne, Cologne, Germany

Guenter Janetschek

Elisabethinen Hospital, Linz, Austria

Ehab M Kamel

Department of Nuclear Medicine, Lausanne University Hospital, Lausanne, Switzerland

Dorota Kandler

Medical University Innsbruck, Innsbruck, Austria

Susanne Kohlfürst

PET/CT Center Klagenfurt, Klagenfurt, Austria

Françoise Kraeber-Bodéré

Réné Gauducheau Cancer Center, Nantes, France

Bernd Joachim Krause

Clinic and Polyclinic of Nuclear Medicine, Klinikum Rechts der Isar, Technical University of Munich, Munich, Germany

Werner Langsteiger

PET/CT Center Linz, St Vincent's Hospital, Linz, Austria

Michael Lassmann

*Clinic for Nuclear Medicine, University Clinic,
University of Würzburg, Würzburg, Germany*

Peter Lind

PET/CT Center Klagenfurt, Klagenfurt, Austria

Giovanni Lucignani

*Unit of Nuclear Medicine, Hospital San Paolo,
Institute of Radiological Sciences, University of Milan,
Milan, Italy*

Marco Maccauro

*Division of Nuclear Medicine, National Cancer Institute,
Milan, Italy*

Roberta Matheoud

Ospedale Maggiore della Carita Novara, Italy

Stephen J Mather

*Centre for Cancer Imaging, Barts and the London, Queen
Mary's School of Medicine and Dentistry, University of
London, UK*

Cristina Messa

*University of Milano-Bicocca, Milan, Italy, San Gerardo
Hospital, Monza, Italy and IBFM-CNR, Milan, Italy*

Roy Moncayo

Medical University Innsbruck, Innsbruck, Austria

Myriam Monsieurs

Ghent University, Ghent, Belgium

Michael Nader

*ARGOS Zyklotron Ltd, Member of the IASON Group, Linz,
Austria*

Cristina Nanni

*University of Bologna Policlinico S Orsola-Malpighi,
Bologna, Italy*

Eva Orunesu

*Institute of Radiological Sciences, University of Milan,
Milan, Italy*

Aurore Oudoux

Réné Gauducheau Cancer Center, Nantes, France

Giovanni Paganelli

European Institute of Oncology, Milan, Italy

Marta Paiusco

Hospital 'Santa Maria Nuova', Reggio Emilia, Italy

Enrico Pelosi

Nuclear Medicine Division, University of Turin, Turin, Italy

Holger Palmedo

*Nuclear Medicine Department, University Hospital,
Bonn, Germany*

Maria Picchio

Scientific Institute San Raffaele, Milan, Italy

Gian Luca Poli

Ospedali Riuniti, Bergamo, Italy

Vikas Prasad

Zentralklinik Bad Berka, Bad Berka, Germany

Daniel Putzer

Medical University Innsbruck, Innsbruck, Austria

Francesco Raspagliesi

*Division of Gynecological Oncology, National Cancer
Institute, Milan, Italy*

Margarida Rodrigues

Medical University Innsbruck, Innsbruck, Austria

Diana Salvo

Hospital 'Santa Maria Nuova', Reggio Emilia, Italy

Sauli Savolainen

*HUS, Medical Imaging Centre and Department of Physical
Sciences, University of Helsinki, Helsinki, Finland*

Klaus Schäfers

*University Hospital, Westfälische Wilhelms-University
Münster, Münster, Germany*

Michael Schäfers

*University Hospital, Westfälische Wilhelms-University
Münster, Münster, Germany*

Orazio Schillaci

*Department of Biopathology and Diagnostic Imaging,
University 'Tor Vergata', Rome, Italy*

Otmar Schober

*Department of Nuclear Medicine, University of Münster,
Münster, Germany*

Ettore Seregni

*Division of Nuclear Medicine, National Cancer Institute,
Milan, Italy*

Sandro Sironi

*University of Milano-Bicocca, Milan, Italy and San Gerardo
Hospital, Monza, Italy*

Jane K Sosabowski

*Centre for Cancer Imaging, Barts and the London, Queen
Mary's School of Medicine and Dentistry, University of
London, UK*

Lars Stegger

*University Hospital, Westfälische Wilhelms-University
Munster, Munster, Germany*

Sven-Erik Strand

Medical Radiation Physics, Lund University, Lund, Sweden

Sara Taddayon

Istituto Clinico Humanitas, Rozzano, Milano, Italy

Tatjana Traub-Weidinger

Medical University Innsbruck, Innsbruck, Austria

Reza Vali

PET/CT Center Linz, St Vincent's Hospital, Linz, Austria

Annibale Versari

Hospital 'Santa Maria Nuova', Reggio Emilia, Italy

Sanjay Vijayanathan

Musculoskeletal Radiology, Guys and St Thomas' Hospital NHS Trust, London, UK

Irene Virgolini

Medical University Innsbruck, Innsbruck, Austria

Elisabeth von Guggenberg

Medical University Innsbruck, Innsbruck, Austria

Boris Warwitz

Medical University Innsbruck, Innsbruck, Austria

Wolfgang A Weber

Zentralklinik Bad Berka, Bad Berka, Germany

Alberto Zacchetti

Experimental Oncology, National Cancer Institute, Milan, Italy

Preface

There has been enormous progress in nuclear medicine in recent years, and the impact of this progress has been particularly noticeable in oncology. Research into molecular imaging has led to the development of radiopharmaceuticals that can explore the cellular metabolism, and visualize at molecular and subcellular levels the pathological processes specific to cancer. Equipment development has produced high-technology instruments such as those used in positron emission tomography (PET), able to produce high-quality images that have become indispensable in the diagnostic work-up of cancer patients, because they often reveal alterations and lesions not demonstrated by conventional morphologically oriented techniques such as X-ray imaging, ultrasound, computed tomography (CT), or magnetic resonance imaging (MRI). Research in the area of image fusion techniques has led to the design of software programs able to merge in a single image the molecular, functional, and metabolic information of nuclear medicine with the morphological information provided by radiology. Hybrid instruments (PET/CT, SPECT/CT) are now available which allow the fusion of images of a patient in just one diagnostic session. Intensive research is ongoing to obtain detectors, hardware, and software able to perform whole-body scans faster and with increasing spatial resolution, so that it may become possible to detect lesions on a submillimeter level. Nuclear medicine has made the step from bench to bedside, to a significant extent.

All of these achievements have had a great impact on not only the diagnosis but also the treatment of cancer. Improved, individually tailored therapy is now on the horizon.

Radiopharmaceuticals developed specifically to target and visualize malignant tumors can also be used, at high doses, for therapeutic purposes. Nuclear medicine therapeutics thus takes advantage of selective radiopharmaceuticals that have demonstrated marked anticancer efficacy in many types of tumors. For example, in recent years, these techniques have been used and shown greatest efficacy in the treatment of lymphomas and neuroendocrine tumors.

The diagnostic and therapeutic achievements in nuclear medicine are the result of the interdisciplinary research efforts of cell biologists, chemists, pharmacologists, physicists, computer scientists, engineers, nuclear medicine physicians, and oncologists. The clinical implications of these achievements have made nuclear medicine indispensable in the management of cancer.

This textbook on modern nuclear medicine applications in the diagnosis and treatment of cancer describes the state of the art and the current position of nuclear medicine in the light of these recent developments. It is intended as a valuable update also for non-nuclear medicine specialists working in oncology. Nuclear medicine as part of molecular imaging and therapy has changed radically in the past decade. The growing importance and clinical impact of these changes for the near future has impelled the authors to record them in this book.

Emilio Bombardieri
John Buscombe
Giovanni Lucignani
Otmar Schober

Acknowledgments

The Editors are grateful to Ms Anna Luisa De Simone Sorrentino for her secretarial help in organizing this book. We also appreciate the initial approach from our publisher at Informa Healthcare, Alan Burgess and members of his team: Lindsay Campbell and Kathryn Dunn.

1

What is cancer?

Uwe Haberkorn

At first sight cancer is a disease induced by the failure of control mechanisms. The cancer cell does not respond to control signals because of damage to its DNA, the presence of oncogene products, or because the homeostatic control mechanisms themselves are disturbed. Biologically this corresponds to uncontrolled proliferation occurring at the wrong place and time driven by oncogenic signals, impaired differentiation, and invasion of other tissues leading to metastases.

In a recent review, Hanahan and Weinberg mentioned six essential alterations in cell physiology which are seen as the hallmarks of cancer: self-sufficiency in growth signals, insensitivity to growth-inhibitory signals, evasion of programmed cell death (apoptosis), limitless replicative potential, sustained angiogenesis, and tissue invasion and metastasis. These alterations are interpreted as results of genetic changes in the cancer cell. However, mutations in the tumor genome may not be the only cause.¹

Genetic and epigenetic background

Cancer has been viewed as a multistep process of genetic alterations that result in the transformation of benign cells into malignant ones. These genetic abnormalities include mutations in tumor-suppressor genes and oncogenes, and chromosomal abnormalities such as chromosomal gain, loss, and/or rearrangement (Table 1.1).^{1,2} Such events are thought to be followed by a clonal selection of variant cells that show increasingly aggressive behavior.³

Although it is still commonly thought that aneuploidy occurs as a late-stage effect rather than as a cause of cancer development, this might not always be true, as carcinogens such as asbestos and arsenic initially do not cause gene mutations, but rather lead to aneuploid lesions. Furthermore, normal cells exposed to chemical carcinogens can become aneuploid long before they show signs of being cancerous. Therefore, it is possible that gains and losses of

whole chromosomes may disturb the balances that regulate normal growth control. On the other hand, many normal cells, both in vitro and in vivo, may become cancerous after the right combination of oncogenes is introduced.⁴ However, only a fraction of these cells will give rise to cancer, implying that other yet unknown factors might also be involved in tumor initiation. Therefore, both mutations and chromosomal derangements are important in the initial stages of tumor development, and both mechanisms might be involved in establishment of the cancer stem cell.

Many of the oncogenes act by mimicking normal growth signaling. This can be accomplished by alteration of extracellular growth signals, or alterations of transcellular transducers of those signals or of intracellular circuits that translate those signals into cellular response. Many cancer cells acquire the ability to synthesize growth factors to which they are responsive, creating a positive feedback signaling loop. Examples of this autocrine stimulation are platelet derived growth factor (PDGF) and transforming tumor growth factor β (TGF β). Furthermore, there is overexpression of growth factor receptors, which often carry tyrosine kinase activities in their cytoplasmic domains. This results in cells becoming hyperresponsive even to low growth factor levels that normally would not trigger proliferation. As an example, members of the epidermal growth factor receptor family such as EGFR/erbB are upregulated in non-small-cell lung cancer (NSCLC) and head and neck, renal cell, brain, and breast tumors, and HER2/neu receptors are overexpressed in stomach and mammary tumors. Ligand independent signaling can also be achieved through structural alteration of receptors: truncated versions of the EGFR lacking parts of the cytoplasmic domain act constitutively. Finally, there are alterations of the downstream cytoplasmic signaling pathways, which receive and process the signals emitted by ligand-activated growth factor receptors and integrins. In that respect, the Ras–Raf–MAPK (mitogen-activated protein kinase) cascade plays a central role. In about 25% of human tumors, Ras proteins are present in structurally altered forms. This has been exemplified in human colon carcinomas where about 50% of the tumors bear mutant

Table 1.1 Regulatory proteins for tumorigenesis, apoptosis, and drug resistance

<i>Protein</i>	<i>Role in tumorigenesis, apoptosis, and drug resistance</i>
<i>Suppressor proteins</i>	
p53	Mutated or altered expression in many cancers. Initiates the intrinsic apoptotic pathway. p53-negative cells are resistant to drug-induced apoptosis
ATM	Mutated in ataxia–telangiectasia syndrome. Senses DNA double strand breaks and stabilizes p53. Increased risk for hematological malignancies and breast cancer
CHK2	Mutated in Li–Fraumeni syndrome. Senses DNA double strand breaks and phosphorylates and stabilizes p53
Rb	Mutated in some cancers, functionally disrupted in many cancers. Inhibits E2F-mediated transcription. Loss of Rb function induces p53-dependent and -independent apoptosis
Bax	Mutated or decreased expression in some tumors. Mediates mitochondrial membrane damage
Bak	Mutated or decreased expression in some tumors. Mediates mitochondrial membrane damage
PTEN	Mutated or altered expression in cancers. Regulates Akt activation and subsequent phosphorylation of Bad. Loss of PTEN results in resistance to many apoptotic stimuli
APAF1	Mutated and transcriptionally silenced in melanoma and leukemia cell lines. Necessary for activation of caspase-9 following cytochrome c release. Chemoresistance
CD95/Fas	Mutated and downregulated in lymphoid and solid tumors. Initiates the extrinsic apoptotic pathway. Resistance to drug-induced cell death
TRAIL-R	Mutated in metastatic breast cancers. Initiates the extrinsic apoptotic pathway. Mutations lead to suppression of death receptor-mediated apoptosis
Caspase-8	Silenced in neuroblastomas. Activates both extrinsic and intrinsic apoptotic pathways. Resistance to drug-induced apoptosis
<i>Oncogenes</i>	
Bcl-2	Frequently overexpressed in many tumors. Antagonizes Bax and/or Bak and inhibits mitochondrial membrane disruption. Inhibits drug-induced apoptosis
MDM2	Overexpressed in some tumors. Negative regulator of p53. Inhibits drug-induced p53 activation
IAPs	Frequently overexpressed in cancer. Downregulation of XIAP induces apoptosis in chemoresistant tumors
NFκB	Deregulated activity in many cancers. Transcriptionally activates expression of antiapoptotic members of the Bcl-2 and IAP families. Can inhibit both the extrinsic and intrinsic death pathways and induce drug resistance
Myc	Deregulated expression in many cancers. Induces proliferation in the presence of survival factors, such as Bcl-2, and apoptosis in the absence of survival factors. Can sensitize cells to drug-induced apoptosis
Akt	Frequently amplified in solid tumors. Phosphorylates Bad. Hyperactivation induces resistance to a range of apoptotic stimuli
PI3K	Overexpressed or deregulated in some cancers. Responsible for activation of Akt and downstream phosphorylation of Bad. Inhibition of PI3K enhances chemotherapeutic drug-induced apoptosis
Ras	Mutated or deregulated in many cancers. Activates PI3K and downstream pathways. Induces proliferation and inhibits c-myc and drug-induced apoptosis

ATM, ataxia telangiectasia mutated; Chk2, checkpoint kinase 2; PTEN, phosphatase and tensin homolog; Apaf-1, apoptotic protease activating factor 1; TRAIL-R, TNF-related apoptosis-inducing ligand receptor; MDM2, transformed 3T3 cell double minute 2; IAPs, inhibitor of apoptosis proteins; NFκB, nuclear factor κB; Akt, protein kinase B; PI3K, phosphatidylinositol 3-kinase.

ras oncogenes. It is suggested that the remaining colonic tumors carry defects in other components of the growth signaling pathways, with similar functional results to those obtained after ras oncogene activation.¹

Besides response to growth signals, resistance to antigrowth signals is an equally important feature of cancer. These antiproliferative signals are coordinated mainly by the retinoblastoma protein (pRb) and its two relatives p107 and p130. Hypophosphorylated pRb blocks proliferation by sequestering and altering the function of E2F transcription factors that control the expression of several genes which are essential for the progression from G1 into S phase.⁵ Disruption of the pRb pathway liberates E2F and allows cell proliferation, rendering cells insensitive to antigrowth factors. In this respect, transforming growth factor β (TGF β) is an important regulator of pRb modification by preventing the inactivating phosphorylation of the protein. Response to TGF β can be lost after downregulation of TGF β receptors, or mutant, dysfunctional receptors.⁶ In addition, changes in the signaling pathway may occur: the function of proteins such as Smad4, which transduces signals from ligand-activated TGF β receptors to downstream targets, or p15INK4B may be changed by mutation of the corresponding genes.^{7,8}

Differentiation is also a condition which results in the inhibition of proliferation and is disturbed in a variety of tumor cells. One of the target genes in this respect is the c-myc oncogene, which encodes a transcription factor. During normal development, the growth-stimulating action of Myc, in association with another factor, Max, can be inhibited by the formation of complexes of Max with a group of Mad transcription factors. These Mad–Max complexes result in differentiation-inducing signals.⁹ Overexpression of the c-Myc oncoprotein occurs in many tumors and shifts the balance to Myc–Max complexes, which impairs differentiation and thereby promotes tumor growth. A further example is inactivation of the APC/ β -catenin pathway in colon carcinoma, which results in a block of the differentiation of enterocytes in the colonic crypts.²

The characteristics mentioned above are subsumed under the term ‘somatic mutation theory of carcinogenesis’, which has been the dominant force driving cancer research during the 20th century. In brief, it proposes that successive DNA mutations in a single cell cause cancer. This theory places carcinogenesis at the cellular and subcellular hierarchical levels of biological complexity. However, increasing evidence has been obtained that epigenetic changes and also changes in surrounding or tumor infiltrating non-tumor cells such as fibroblasts and endothelial cells are important. These may interact with tumor cells by secretion of a variety of signaling factors such as diffusible growth factors, extracellular matrix components, or cell-to-cell adhesion/interaction molecules. Evidence of a promotion of cancer cells by inflammatory cells infiltrating the tumor site has also been found.¹⁰

Epigenetic changes are realized by three different mechanisms: DNA methylation, RNA-associated silencing, and histone modification, which are known to initiate and sustain epigenetic silencing, and to interact with each other.^{11–13}

Methylation of the C5 position of cytosine residues in DNA is maintained by a number of DNA methyltransferases and has multiple roles for the silencing of transposable elements, for defense against viral sequences, and for the transcriptional repression of genes. The resulting metabolite, 5-methylcytosine, is highly mutagenic, causing C:G to T:A transitions, and leads to a suppression of the methylated site in the human genome. The predominant sites, CpG islands, are regions of more than 500 base pairs in size and with a GC content greater than 55%,¹⁴ and have been conserved during evolution because they are normally kept free of methylation. They are located within the promoter regions of about 40% of mammalian genes and can be transcriptionally silenced by methylation. Extensive de novo methylation of CpG islands is a common feature of many cancers.¹⁵

Histone modifications such as acetylation, phosphorylation, and methylation of conserved lysine residues on the amino-terminal tail domains have also been defined as epigenetic modifiers. Acetylation of histones causes transcriptionally active DNA regions, whereas hypoacetylated histones are associated with transcriptionally inactive DNA regions. Since there is a considerable variation of all possible histone modifications, and also interactions between histone deacetylases, histone methyltransferases, and methylcytosine-binding proteins occur, this is seen as a histone code which is used by a variety of cellular factors.^{16,17}

The role of epigenetic changes in cancer has been shown for the MLH1 gene, where methylation and silencing of the gene may lead to a variety of cancers.^{18,19} Chromatin-modifying enzymes have also been associated with human leukemias, with histone acetyltransferases and histone methyltransferases engaged in the modification of fusion protein activity, such as the oncogenic PML–RAR α (promyelocytic leukemia–retinoic acid receptor α) in acute promyelocytic leukemia, which recruits a histone deacetylase to repress genes essential for the differentiation of hematopoietic cells, or AML1–ETO (AML refers to acute myeloid leukaemia) fusions, which recruit a histone deacetylase 1 complex to inhibit myeloid development.^{20,21} Furthermore, loss or mutations of adenosine triphosphate (ATP)-dependent chromatin remodeling complexes such as SWI–SNF, BRM, and BRG1 have been found to be associated with pediatric cancer as well as a variety of cancer cell lines and tumor tissues.²²

A simple way to induce a carcinogenic phenotype is the transcriptional repression of tumor suppressor genes, which may represent an alternative mechanism to genetic mutation. In addition, cancer-cell genomes simultaneously show global hypomethylation and gene promoter-specific

hypermethylation. This might contribute to genomic instability, structural changes in chromosomes, and increases in gene expression.^{15,23–25} These alterations may occur at early stages of carcinogenesis and may determine the subsequent genetic changes and progression of these mutated clones.

Many genes are epigenetically silenced in cancer cells, and many epigenetically silenced genes have not been found to contain any genetic mutations at all, even though they are transcriptionally repressed in many different cancer-cell types. These facts underscore the potential value of screening for all epigenetic modifications, as well as genetic changes, that are associated with human tumor types. Examples of a combination for genetic and epigenetic changes were found in the colon cancer cell line HCT116, which contains several mutations, including the DNA mismatch-repair protein, MLH1, and p16, which contribute to the mismatch-repair phenotype and to disruption of the cyclin D-RB1 (retinoblastoma 1) cell-cycle-control pathway, the transforming growth factor- β 2 receptor, which causes a loss of control of a cell differentiation pathway, and an activating mutation in the gene that encodes β -catenin, resulting in constitutive Wnt (wingless type) signaling and cell proliferation.^{26–30} In addition to these mutations, there are at least 14 epigenetically silenced genes in these cells, all of which can be reactivated by either treating the cells with DNA-demethylating agents or disrupting the genes that encode DNA methyltransferases, which catalyze DNA methylation.^{31–35} Reactivating expression of these growth-control genes results in phenotypic changes that range from reducing proliferation to inducing senescence or apoptosis.^{26,27,33} Epigenetic alterations of these genes seem to complement mutations in determining the phenotype of these cells. Examples of a collaboration between epigenetic and genetic abnormalities are MLH1 and CDKN2A (the gene that encodes p16) in HCT116 cells: while one allele of each of these genes is mutated in these cells, the wild-type allele becomes silenced by hypermethylation. Therefore, genetic and epigenetic changes can collaborate to prevent expression of a functional gene product in cancer cells.

Another epigenetic–genetic collaboration in HCT116 cells is found in the Wnt pathway. Four members of the secreted frizzled-related gene family (SFRP1, SFRP2, SFRP4, and SFRP5) that encode Wnt antagonists are epigenetically silenced in these cells. This contributes to the abnormal activation of Wnt signaling, even in cells that already carry activating mutations in β -catenin.³³ In addition, silencing of the genes that encode the transcription factors GATA4 and GATA5, as well as their downstream activation targets trefoil factor 1 (TFF1), TFF2, TFF3, and inhibin- α ,³² could impair maturation of endoderm-derived epithelial cells.^{36–39} Finally, TIMP3 (tissue inhibitor of metalloproteinase 3) is silenced in HCT116 cells, and loss of function of its product might increase the invasive ability of these cells.³⁵

Epigenetic silencing may occur during the early stages of tumor progression, possibly during the abnormal expansion of stem and progenitor cells. This silencing predisposes the stem cells to abnormal clonal exposition. Changes that are known to contribute to tumor formation such as chronic inflammation, which leads to the production of reactive oxygen species, induce cell renewal dedicated to repair of tissue damage. This is associated with epigenetic events which lead to heritable transcriptional repression and activation of stem-cell and progenitor-cell expansion at the expense of normal cell differentiation and maturation. The subsequent progression to malignancy would then depend not only on gene mutations but also on the collection of epigenetic alterations. These epigenetic changes might occur continuously not only in epithelial cells but also in surrounding stromal cells.⁴⁰

The reductionist approach, which sees cancer solely as a disease reducible to mutations, has been challenged not only by the finding of epigenetic changes but also by the number of mutations occurring in cancers. These range from three to anywhere from 11 000 to 100 000 mutations.^{41–43} In principle these data, obtained from high-throughput technologies such as gene arrays, may be used to introduce new classifications.⁴⁴ However, these new technologies face problems associated with bias, reproducibility, overfitting, and data interpretation.⁴⁵

This has led to the proposal of an alternative theory, the tissue organization field theory of carcinogenesis and neoplasia. Its assumptions are that proliferation is the default state of all cells and that carcinogenesis and neoplasia are defects of tissue architecture. Carcinogens would act initially by disrupting the normal interactions between parenchymal cells and the stroma of the organ. In this model the stroma appears as the primary target of carcinogens, stating that carcinogenesis and neoplasia occur exclusively through supracellular phenomena. This implies that neoplastic cells may be reprogrammed to behave as non-tumor cells when placed in the context of normal tissues.⁴⁶ Evidence is derived from early studies with teratocarcinomas, where the stem cells generated not only more stem cells but also more differentiated cells that gave rise to non-tumorigenic tissue. The teratocarcinoma cells were generated from tumors resulting from the implantation of normal embryos into ectopic locations. Teratocarcinoma cells injected into normal blastocysts were shown to generate normal tissues in viable mosaic individuals resulting from this manipulation.^{47,48} In subsequent generations, normal offspring resulted from the genome of a cell that was once a cancer cell. If cancer indeed results from the accumulation of DNA mutations in a previously normal cell, it becomes problematic to explain these data. More recently, ectopic expression of stromelysin-1 by mammary gland epithelial cells in transgenic animals resulted in mammary gland carcinoma. In this case, expression of this enzyme induces stromal changes that in turn would lead to carcinoma.

Treatment with specific protease inhibitors blocked carcinogenesis in this model.⁴⁹ Also, irradiation of the stroma of epithelium-free mammary glands results in carcinogenesis in non-irradiated mammary epithelial cells inoculated into the irradiated stroma.⁵⁰ In all these experiments, the parenchyma–stroma interaction seems to be an important factor for cancer progression.^{51,52} From the evidence mentioned above it follows that cancer is more than a disease of specific genes. Rather, instability of the genome as a whole must be seen as a hallmark of malignant tumors.^{53–56} Furthermore, the concept that epigenetic abnormalities could be as important as genetic ones in determining the course of tumor development, and also be involved in tumor-specific signaling pathway abnormalities, is relevant to the future design of both preventive and therapeutic approaches to cancer.¹³

Cell death: Apoptosis and more

To control abnormal proliferation a cell can either enter a quiescence-like growth arrest phase, or undergo apoptosis or senescence. These antiproliferative programs are induced by tumor suppressors such as p53 and pRb in response to potential oncogenic signals.

The most common and well-defined form of programmed cell death is apoptosis, which is a physiological cell-suicide program that is essential for embryonic development, function of the immune system, and the maintenance of tissue homeostasis in multicellular organisms. Apoptosis in mammalian cells is mediated by a family of cysteine proteases known as the caspases. To keep the apoptotic program under control, caspases are initially expressed in cells as inactive procaspase precursors. When initiator caspases such as caspase-8 and caspase-9 are activated by oligomerization, they cleave the precursor forms of effector caspases, such as caspase-3, caspase-6, and caspase-7.^{57,58} Activated effector caspases cleave a specific set of cellular substrates, resulting in specific biochemical and morphological changes (Table 1.2) that are associated with the apoptotic phenotype. Dysregulation of apoptosis has been implicated in numerous pathological conditions, including neurodegenerative diseases, autoimmunity, and cancer.⁵⁹

There are two pathways by which caspase activation is triggered, the extrinsic and intrinsic apoptotic pathways. The extrinsic pathway is induced by activation of death receptors on the cell surface. Binding of ligands such as FasL and tumor necrosis factor (TNF) to Fas and the TNF receptor (TNFR), respectively, leads to formation of the death induced signaling complex (DISC). DISC recruits caspase-8 and promotes the cascade of procaspase activation (Figure 1.1).⁶⁰ The intrinsic pathway is triggered by various extracellular and intracellular stresses, such as growth-factor withdrawal, hypoxia, DNA damage, and

Table 1.2 Morphological and biochemical differences between apoptosis and necrosis

Features	Apoptosis	Necrosis
Tissue distribution	Single cells	Multiple cells
Tissue reaction	Phagocytosis	Cellular exudate
Cell morphology	Shrinkage	Swelling
Organelles	Intact	Damaged
Chromatin	Marginated, condensed	Fragmented
Membrane	Intact	Damaged
Biochemistry	Activated endonucleases DNA cleavage Activated caspases	Defective ion pump Activated lysosomal enzymes

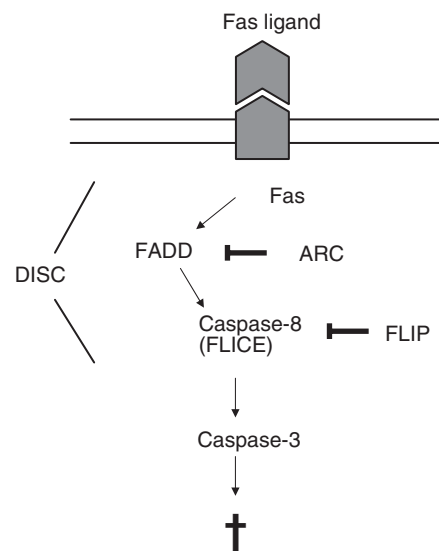


Figure 1.1

Simplified scheme of the death receptor-mediated or extrinsic apoptosis pathway. Binding of the Fas ligand is followed by formation of the death inducing signaling complex (DISC): the adaptor molecule FADD binds to the death domain of Fas and recruits procaspase-8 via its death effector domain. Autocatalytic activation of procaspase-8 leads to activation of the downstream effector caspase-3. The cascade may be inhibited by FLICE inhibitory protein (FLIP) or by the apoptosis repressor with a CARD domain (ARC).

oncogene induction. Signals that are transduced in response to these stresses converge mainly on the mitochondria. A series of biochemical events is induced that results in the permeabilization of the outer mitochondrial membrane, the release of cytochrome c and other proapoptotic molecules, the formation of the apoptosome, a large protein complex that contains cytochrome c, apoptotic protease activating factor 1 (APAF1), and caspase-9, and caspase activation. Once cytochrome c is released, the downstream cascade of caspase activation is irreversible. Cell death is also modified by other proteins such as endonuclease G21 and apoptosis-inducing factor (AIF), which may induce cell death independently of caspase activation.

In order to survive, tumor cells need to avoid apoptosis that can be induced by unregulated oncogene expression, and a limited supply of growth factors, oxygen, or nutrients. Protection from apoptosis may be achieved by modification of the activities of antiapoptotic genes such as Bcl-2 or suppressor genes such as p53. In human B-cell follicular lymphomas, a chromosomal translocation linking the Bcl-2 gene to an immunoglobulin locus was identified in the transformed cells, resulting in constitutively active Bcl-2 and survival of the lymphoma cells.⁶¹

The tumor suppressor p53 is an important regulator of apoptosis and is the most commonly mutated gene in cancer.⁶² Normal function of p53 induces apoptosis in the presence of genotoxic stress, causing DNA damage that cannot be repaired during cell-cycle arrest, growth-factor withdrawal, hypoxia, and dysregulated expression of mitogenic oncogenes. In addition to the fact that most human cancers have either mutations in p53 or defects in the pathway, p53-null mice are highly prone to developing cancers.

As the Fas pathway regulates the immune system through its proapoptotic function, disruption of this pathway may lead to lymphoproliferative disorders and hematopoietic cancers. Somatic mutations of the Fas gene or its downstream effectors have been found in patients with multiple myeloma, non-Hodgkin's lymphoma, and other cancers.^{63,64} Alterations to cell-survival pathways may also be involved in the suppression of apoptosis. The PI3K–Akt (phosphatidylinositol 3-kinase–protein kinase B) survival signaling pathway is activated by various intracellular and extracellular stimuli and modulates apoptotic pathways, resulting in the resistance of tumor cells to death signals. Akt signaling induces expression of the antiapoptotic molecule Bcl-XL, inhibits the proapoptotic activity of FKHRL1 (FOXO3A), and leads to negative regulation of p53 mediated apoptosis.⁶⁵ Akt activation also provides cells with a survival advantage through its promotion of glucose metabolism.^{66,67} Another survival factor that is relevant to human tumorigenesis is nuclear factor κ B (NF κ B), a transcription factor that is activated by numerous cytokines and oncogenes. De novo gene transcription that is induced by NF κ B prevents apoptosis that is induced by the engagement of death receptors.⁶⁸ Therefore, many

different modes of inactivating proapoptotic signaling pathways underlie tumorigenesis.

Several non-apoptotic cell death mechanisms have been identified, including necrosis, autophagy, mitotic catastrophe, and senescence. In contrast to apoptotic cell death, necrosis is an unregulated process with membrane distortion, organelle degradation, and cellular swelling, resulting in cell destruction and the release of intracellular components. Necrosis is usually a consequence of a pathophysiological condition, such as infection, inflammation, or ischemia, which leads to the failure of normal physiological pathways that are essential for maintaining cellular homeostasis, such as regulation of ion transport, energy production, and pH balance.

Primary cells in culture initially proliferate rapidly, with a significant shortening of the telomeres of their chromosomes. This may lead to a form of permanent cell-cycle arrest that has been described as replicative senescence. A senescent cell is characterized by flattened cytoplasm, increased granularity, changes in metabolism, and the induction of senescence-associated β -galactosidase activity. Furthermore, alterations in chromatin structure and gene-expression patterns are seen. The phenomenon is inducible by various cellular stresses, DNA damage, and oncogene activity.⁶⁹ The senescence program then induces the activation of various cell-cycle inhibitors and requires the functions of p53, the CDKN1A gene product WAF1/p21, the CDKN2A gene product INK4A/p16, and the retinoblastoma protein (pRb). The involvement of these tumor suppressors implies that one of the main functions of the senescence program is to suppress tumorigenesis, a hypothesis that has been confirmed in mutant mice.^{70,71}

In normal cells, unwanted proteins or proteins that are no longer required are degraded by two independent mechanisms: ubiquitin mediated proteolysis in proteasomes, and autophagy, a mechanism by which long-lived proteins and organelle components are directed to and degraded within lysosomes.⁷² Autophagy is conserved in various species, and is activated in response to growth-factor withdrawal, differentiation, starvation, and stress. After the induction of autophagy, autophagic vesicles (autophagosomes) are formed by the assembly and expansion of membrane-bound structures, probably originating in the endoplasmic reticulum around organelles and isolated proteins. The autophagosome encapsulates the cytosolic materials and fuses with lysosomes or other vacuoles, causing degradation of its content. The signaling pathway that leads to autophagy involves at least the activities of phosphatidylinositol 3-kinase (PI3K) and the kinase target of rapamycin (TOR).⁷³ The TOR pathway coordinates signaling pathways that are initiated by nutritional and mitogenic factors, and also controls both protein synthesis and degradation. Although the components of the autophagic machinery are highly conserved in a wide range of organisms, the physiological role of the process varies. There is evidence that lysosomal

degradation of organelles is required for cellular remodeling due to differentiation, stress, or damage following exposure to cytotoxins, and that dysregulation of autophagy can result in pathological states such as neurodegenerative diseases, cardiomyopathy, and cancer.⁷⁴

Uncontrolled protein degradation by the proteasomal pathway can contribute to tumorigenesis. Examples are the Wnt and hedgehog (HH) signaling pathways, which are regulated by the turnover of β -catenin and cubitus interruptus (CI). Mutations in the corresponding genes that lead to constitutive activation of Wnt and HH pathways are common in human colon cancer and basal-cell skin carcinomas.⁷⁵ Defects in the autophagic pathway of protein degradation might also be connected to cancer via some oncogenes and tumor-suppressor genes. Autophagy is partly controlled by the PI3K pathway, and constitutive activation of PI3K signaling is common in human cancer cells.⁷⁶ PI3K and its downstream effectors, Akt and TOR, might normally contribute to the suppression of autophagy, whereas PTEN (phosphatase and tensin homolog), a tumor suppressor that negatively regulates PI3K signaling, might normally promote autophagy. Furthermore, beclin 1 (BECN1) that interacts with PI3K and participates in the induction of autophagy in response to starvation is monoallelically deleted in a high percentage of human ovarian, breast, and prostate cancers.^{77,78} Transfection of BECN1 into a transformed cell line can decrease its tumorigenic potential, and studies of mice that are deficient for this protein have shown that BECN1-mediated regulation of autophagy is required for normal mammalian development, and that animals with heterozygous deletions in *Becn1* show a marked increase in the incidence of lymphomas and carcinomas of the lung and liver. Without autophagy, the natural turnover of a protein that acts as a positive regulator of cell growth might be blocked, promoting proliferation. Autophagy is also involved in removing damaged organelles and, therefore, in maintaining cellular homeostasis. Damage to mitochondria or sections of the endoplasmic reticulum might result in the production of endogenous cellular oxidants that increase the basal mutation rate. Removal of these damaged internal cellular structures by autophagy might therefore limit the genotoxic damage that is caused by oxidants. Conversely, reduced autophagy might increase oxidant stress and promote the accumulation of tumorigenic mutations.

Mitotic catastrophe is caused by aberrant mitosis and is associated with the formation of multinucleate, giant cells that contain uncondensed chromosomes. In normal somatic cells, the M phase of the cell cycle encompasses two processes: mitosis, in which sister chromatids are aligned and segregated into two daughter cells; and cytokinesis, in which the cytoplasm and its contents are partitioned into those cells. Mitosis is further subdivided into prophase, prometaphase, metaphase, anaphase, and telophase. The G2 checkpoint of the cell cycle is responsible for blocking

mitosis when a cell has been hit by DNA damage. This activates a number of molecules that promote cellular activities such as cell-cycle arrest, DNA repair, or apoptosis, if the damage cannot be repaired. However, if the G2 checkpoint is defective, a cell can enter mitosis prematurely, before DNA replication is complete or DNA damage has been repaired. This aberrant mitosis causes the cell to undergo death by mitotic catastrophe. Activation of the G2 checkpoint begins with the detection of DNA damage by the sensory molecules ataxia telangiectasia mutated (ATM) and ATM- and Rad3-related (ATR). The further process involves activation of checkpoint kinase 2 (CHK2) and checkpoint kinase 1 (CHK1), and phosphorylation of CDC25C and several G2 checkpoint genes. The inhibition or inactivation of any of these G2-checkpoint genes results in the death of cells that have sustained DNA damage by mitotic catastrophe. Recent evidence suggests an important role of the cytoprotective protein survivin in checkpoint regulation.⁷⁹

Defects in genes such as the polo-like kinase (PLK) family, the NIMA (for never in mitosis, gene A) family, the aurora kinase family, and a regulator of the spindle checkpoint called BUB that are required for mitotic catastrophe can also contribute to tumorigenesis.⁸⁰ Overexpression of aurora-A, which occurs in a wide range of human cancers, increases genetic instability, aneuploidy, and centrosomal aberrations. Furthermore, the overexpression of other mitotic kinases results in multinucleation and an increase in centrosome number.^{81,82}

Cancer cells often have a defect in a particular cell-death pathway, but the cells can still die because of the redundancy of cell-death mechanisms. However, the nature of the cell-death defect ultimately affects the clinical outcome of treatment, depending on which mechanism is missing. At present it is not clear whether apoptosis, senescence, necrosis, autophagy, and mitotic catastrophe are entirely independent programs, whether these mechanisms overlap to some degree, or whether one mechanism may compensate for another that is inactivated by a tumorigenic mutation.

Factors influencing tumor growth

Since Virchow postulated that inflammation stimulates the progression of cancer, evidence has been found that immune-cell infiltration is a characteristic of malignant tumors. Tumor cells produce various cytokines and chemokines that attract macrophages, dendritic cells, mast cells, T cells, and hematopoietic progenitors. These stromal cells sometimes even outnumber cancer cells. Besides releasing mitogenic and survival factors, stimulating DNA damage, facilitating invasion by remodeling the extracellular

matrix, and evading the host defense, inflammatory cells also stimulate angiogenesis in tumors.⁸³ For instance, tumor-associated macrophages accumulate in hypoxic tumor regions and produce angiogenic factors such as vascular endothelial growth factor (VEGF), VEGF-C, and VEGF-D. Tie2-expressing monocytes, mast cells, and platelets also release proangiogenic factors.⁸⁴ Bone marrow-derived hematopoietic cells become recruited to tumors in response to VEGF and placenta growth factor (PGF) and extravasate around nascent vessels, where they stimulate growth of resident vessels by releasing angiogenic factors such as VEGF, PlGF and angiopoietin-2. In addition, these cells function as hemangioblasts, producing both hematopoietic and endothelial progenitors that result in new blood vessels.⁸⁵ Furthermore, leukocyte-attracting chemokines such as interleukin-8 (IL-8) directly stimulate endothelial cell growth. Moreover, in response to PlGF released by tumor cells, VEGFR-1 positive hematopoietic bone-marrow progenitors home to tumor-specific premetastatic sites, where they recruit tumor cells and endothelial progenitor cells.⁸⁶

As mentioned above, growth factor peptides and their receptors are often overexpressed in human cancer and are involved in cell proliferation, differentiation, and survival. One of the best known systems is the HER/erbB family which consists of four structurally similar, transmembrane tyrosine kinase (TK) receptors: endothelial growth factor receptor (EGFR or HER1/erbB-1), HER2/erbB-2, HER3/erbB-3, and HER4/erbB-4.⁸⁷ Multiple ligands bind to the EGFR: endothelial growth factor (EGF), transforming growth factor β (TGF β), heparin-binding EGF, amphiregulin, betacellulin, epiregulin, and neuregulin G2b. After binding, the receptors dimerize and trigger intracellular signaling pathways.⁸⁸ HER2 heterodimerizes with either EGFR or HER3, and binds to their ligands for receptor activation. The downstream pathways of activated EGFR/HER2 involve at least two major pathways: the Ras/mitogen activated protein kinase (MAPK)-dependent pathway and the phosphatidylinositol 3-kinase (PI3K)-dependent pathway.

The HER receptors and their ligands are frequently overexpressed in many tumor types and are often associated with advanced disease and poor prognosis (Table 1.3).⁸⁹ Therefore, EGFR and HER2 have been defined as promising targets of anticancer therapy, which has been realized mostly using monoclonal antibodies such as trastuzumab, to prevent ligand binding, and tyrosine kinase inhibitors, to interact with receptor autophosphorylation and signaling.

In addition to overexpression mutations may occur. Mutations in exons 18–21 lead to increased EGFR activity through overactivation of PI3K/Akt signaling and confer sensitivity towards TK inhibitors, such as gefitinib or erlotinib.⁹⁰ On the other hand, there are mutations in exon 20 that confer resistance to TK inhibitors.⁹¹

Another important system is the ras signal transduction pathway. It is activated by growth factor receptors,

Table 1.3 Human cancers with overexpression of the epidermal growth factor receptor

<i>Tumor type</i>	<i>Expression (%)</i>	<i>Prognostic significance</i>
NSCLC	40–80	Shorter overall survival, metastases
Head and neck	80–100	Shorter disease-free and overall survival
Renal cell	50–90	Poor prognosis, shorter survival
Bladder	31–48	More prevalent in recurrent invasive tumors
Gastric	40	Shorter survival in tumors positive for TGF β and EGFR
Pancreatic	30–50	Reduced survival
Colon	25–77	Poor patient outcome
Breast	14–91	Worse overall survival, steroid receptor-negative tumors
Ovary	35–70	Reduced disease-free survival, overall survival, drug resistance

NSCLC, non-small-cell lung cancer; TGF, transforming growth factor; EGFR, epidermal growth factor.

cytokines (IL-2, IL-3, GM-CSF (granulocyte macrophage-colony stimulating factor)), and hormones (insulin, insulin-like growth factor (IGF)).⁹² Ras activity is regulated by cycling between the inactive guanosine diphosphate (GDP)-bound and the active guanosine triphosphate (GTP)-bound forms. Active ras triggers several downstream effector pathways that mediate cell proliferation and suppression of apoptosis. The hydrolysis of GTP by Ras is facilitated by GTPase-activating proteins (GAPs) such as p120GAP and NF1.⁹² Point mutations in the ras gene render Ras insensitive to GAP stimulation and result in a permanent activation of the downstream pathways. Furthermore, continuous activation of Ras also occurs in the absence of any mutation in the ras gene, as a result of continuous upstream signals, for example by activation of HER family receptors. Overexpression of Ras isoforms is reported in many solid and hematologic malignancies and is associated with a worse outcome.⁹³ Ras protein function depends on its physical association with the inner surface of the membrane and transmission of the signal to Raf-1, which involves complex post-translational modifications

of the protein such as farnesylation, which is catalyzed by the enzyme farnesyl-transferase.⁹⁴ Mutations may also occur downstream of the ras pathway. The Raf kinase proteins include three isoforms, ARAF, BRAF, and RAF-1, which differ in their expression profile, regulation, and ability to function in the context of the Ras–Raf–MAPK pathway. Activating mutations in the BRAF gene have been demonstrated in 70% of human malignant melanomas and 15% of human colon cancers.⁹⁵

Akt/protein kinase B (PKB) is a serine/threonine protein kinase that interacts with the membrane lipid phosphatidylinositol-trisphosphate (PIP3), which is produced by PI3K after activation by growth factor receptors. Activation of Akt is prevented by PTEN, a phosphatase that removes from PIP3 the phosphate attached by PI3K.⁹⁶ Akt is a positive regulator of the mammalian target of rapamycin (mTOR), a central control element for cell growth and proliferation, by phosphorylation and inactivation of mTOR inhibitors, such as tuberlin (TSC2).⁹⁷ Furthermore, Akt activation leads to phosphorylation and thereby inactivation of proapoptotic proteins, such as BAD and caspase-9, and several transcriptional factors. There are multiple lines of evidence relating Akt to carcinogenesis: Akt is overexpressed in a variety of human cancer types; PTEN, a major antagonist of Akt activity, is frequently lost or inactivated by mutation in human cancer; and the Akt positive regulator, PI3K, or one of its downstream effectors, mTOR, is commonly upregulated in cancer.^{96,98}

Angiogenesis

The dependence of tumor growth on the development of a neovasculature is now a well-established aspect of cancer biology.^{99,100} In general, increased tumor vascularization and tumor expression of proangiogenic factors has been associated with advanced tumor stage and poor prognosis in a variety of human cancers.^{101–104}

Tumor angiogenesis is regulated by a balance of pro- and antiangiogenic factors (Table 1.4). A shift in this balance in favor of proangiogenesis molecules activates the normally quiescent vasculature to develop new blood vessels, often together with enlargement of the pre-existing vasculature. This process involves the recruitment of sprouting vessels from existing blood vessels and the incorporation of endothelial progenitors into the growing vascular bed. This relies on the proliferation, migration, and invasion of endothelial cells, organization of endothelial cells into functional tubular structures, maturation of vessels, and vessel regression.¹⁰⁵

The normal vasculature is usually quiescent in the adult, and endothelial cells are among the longest-lived cells outside the nervous system. There are only a few adult tissues that require ongoing angiogenesis, including female

Table 1.4 Most important pro- and antiangiogenic factors

<i>Molecule</i>	<i>Function</i>
<i>Proangiogenic</i>	
VEGF	Angiogenesis, permeability, leukocyte adhesion
VEGFR	Integration of angiogenic signals
Ang-1/Tie-2	Stabilization of vessels
PDGF	Recruitment of smooth muscle cells
TGF β , TGF β R	Extracellular matrix stimulation
FGF, HGF, MCP-1	Angiogenesis
Integrins	Receptors for matrix proteinases
VE-cadherin	Endothelial junction
Plasminogen activators	Matrix remodeling, release of growth factors
Chemokines	Pleiotropic role
<i>Antiangiogenic</i>	
Soluble VEGFR-1	Secreted molecule, binds VEGF
Ang-2	Antagonist of Ang-1, function depends on other factors
Angiostatin	Suppresses angiogenesis
Endostatin	Inhibition of endothelial survival and migration
Vasostatin	Inhibition of endothelial growth
Platelet factor 4	Inhibition of bFGF and VEGF binding
MMP inhibitors	Suppression of pathological angiogenesis

VEGF, vascular endothelial growth factor; VEGFR, VEGF receptor; PDGF, platelet derived growth factor; FGF, fibroblast growth factor; HGF, hepatocyte growth factor; MCP-1, monocyte chemotactic protein 1; VE-cadherin, vascular endothelial cadherin; MMP, matrix metalloproteinase.

reproductive organs, organs that are undergoing physiological growth, or injured tissue. Under normal physiological angiogenesis, new vessels rapidly mature and become stable. One characteristic feature of tumor blood vessels is that they fail to become quiescent, resulting in a constant angiogenesis. The tumor vasculature presents unique characteristics being different in architecture compared to their normal counterparts. Tumor vessels are usually irregularly shaped, dilated, tortuous, and sometimes with dead ends, and they lack organization into definitive venules, arterioles,

and capillaries. In consequence, the vascular network that forms in tumors is often chaotic, leaky, and hemorrhagic. Blood flows irregularly in tumor vessels, moving slowly, and sometimes even shows oscillations. Tumors can be heterogeneous in their vascular patterns, and are able to overproduce their capillary networks. In normal tissues, by contrast, vessel density is dynamically controlled by the metabolic need for nutrients and oxygen.^{106–108}

The molecular basis of angiogenesis has been studied extensively and has identified a number of growth factor receptor pathways that promote tumor angiogenesis. One of the major pathways involved in this process is the vascular endothelial growth factor (VEGF) family of proteins and receptors.^{109,110} Activation of the VEGF/VEGF-receptor (VEGFR) axis triggers multiple signaling networks that result in endothelial cell survival, mitogenesis, migration, and differentiation, and vascular permeability and mobilization of endothelial progenitor cells from the bone marrow into the peripheral circulation. In addition, VEGF mediates vessel permeability, and leads to deposition of proteins in the interstitium that facilitate angiogenesis. Especially VEGF-A has been found to be expressed in many human tumors and to be associated with a broad spectrum of oncogenes such as mutant ras, erbB-2/Her2, activated EGFR, and bcr-abl21.^{111,112} VEGF-A binds to two receptor tyrosine kinases (RTK), VEGFR-1 (Flt-1) and VEGFR-2 (KDR, Flk-1).¹¹¹ VEGFR-2 is the major mediator of the mitogenic, angiogenic, and permeability-enhancing effects of VEGF-A. In contrast, VEGFR-1 may function as a decoy receptor that sequesters VEGF and prevents its interaction with VEGFR-2.¹¹¹ Furthermore, VEGFR-1 has significant roles in hematopoiesis, the recruitment of monocytes and other bone marrow-derived cells that may home to tumor vasculature and promote angiogenesis.^{113,114} In addition, VEGFR-1 is involved in the induction of matrix metalloproteinases (MMPs) and in the paracrine release of growth factors from endothelial cells.¹¹⁵

Other signaling molecules involved in angiogenesis are platelet derived growth factor β and its receptor (PDGF-B/PDGFR- β) and the angiopoietins (Ang), the ligands of the Tie-2 receptor.^{110,116} PDGF-B is required for the recruitment of pericytes and maturation of the microvasculature. Inhibition of PDGFR- β signaling has been reported to result in a tumor microvascular tree that is dependent on VEGF-mediated survival signals. Furthermore, tumor-derived PDGF-A and PDGFR- β signaling has been shown to be involved in the recruitment of an angiogenic stroma that produces VEGF-A and other angiogenic factors.¹¹⁷ Ang-1 is required for the remodeling and maturation of the immature vasculature. Ang-1 is the major agonist for Tie-2, whereas Ang-2 may act as an antagonist or a partial agonist.¹¹⁸ However, recent studies present evidence that Ang-2 may also play a positive role in tumor angiogenesis.¹¹⁹

Several endogenous inhibitors of angiogenesis have been identified such as thrombospondin, a multifunctional

glycoprotein secreted by most epithelial cells in the extracellular matrix, and fragments of larger proteins including endostatin, tumstatin, vasostatin, and vasohibin.¹²⁰ The precise mechanism of action of these proteins is not fully defined, although several hypotheses have been proposed, including that they bind to specific integrins.¹²⁰

Hypoxia

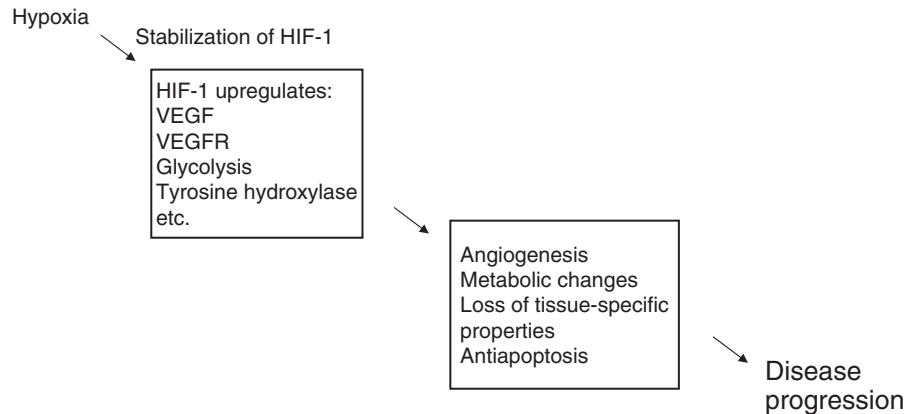
Due to uncontrolled growth and a misbalance between tumor mass and vascularization, oxygen limitation is a common feature of malignant tumors. Oxygen concentration inside solid tumors is reduced, which contributes to the tumor aggressiveness and poor prognosis of patients.¹²¹ Genomes of tumor cells become unstable under hypoxic conditions, and hypoxia can be the selective pressure for the expansion of clones with antiapoptotic, treatment resistant, or highly metastatic potential.^{122,123} Resistance to chemotherapy and radiation therapy can be attributed, at least in part, to the hypoxic condition of tumor cells.¹²⁴ Hypoxia confers these aggressive properties on the tumors through either the remodeling of tumor vasculature or the direct phenotypic changes of tumor cells themselves. Tumor cells under hypoxia can acquire antiapoptotic and chemoresistant properties through changes in the expression of apoptosis-related molecules. Furthermore, the involvement of HIF-1 α in tumor progression to an antiapoptotic phenotype was reported.¹²⁵

Oxygen deprivation is encountered by the induction of various genes. Hypoxia inducible factor 1 (HIF-1) plays a central role in this regulatory system (Figure 1.2). HIF-1 can induce the production of a variety of gene products relevant for metabolism, vascularization, survival, pH, and cell migration. Active HIF-1 is a heterodimer composed of two subunits, HIF-1 α and HIF-1 β . HIF-1 β is constitutively expressed independent of environmental oxygen concentration, while the expression of HIF-1 α is negligible under normoxia and induced under hypoxia. Up to now, HIF-1 α , HIF-2 α , and HIF-3 α have been identified and cloned as the members of the HIF α family that can dimerize with HIF-1 α and bind to hypoxia responsible elements (HRE) in the genes of hypoxia responsive molecules.

Among HIF α family members, HIF-1 α is thought to be the key molecule regulating the cellular response to physiological and pathological hypoxia. Mechanisms of hypoxia-induced expression of HIF-1 α have been intensively studied, and the intracellular level of HIF-1 α protein under reduced oxygen concentration was found to be increased mainly through stabilization of the protein. Turnover of the HIF-1 α protein is regulated by the ubiquitin–proteasome system, in which target proteins are degraded by proteasome depending on their ubiquitylation.¹²⁶ Under normoxia, the level of the HIF-1 α protein is kept low

Figure 1.2

HIF-mediated reactions to hypoxia leading to disease progression. Since hypoxia inducible factor (HIF) induces the expression of a variety of genes, multiple reactions at the physiological and biochemical level result. VEGF, vascular endothelial growth factor; VEGFR, VEGF receptor.



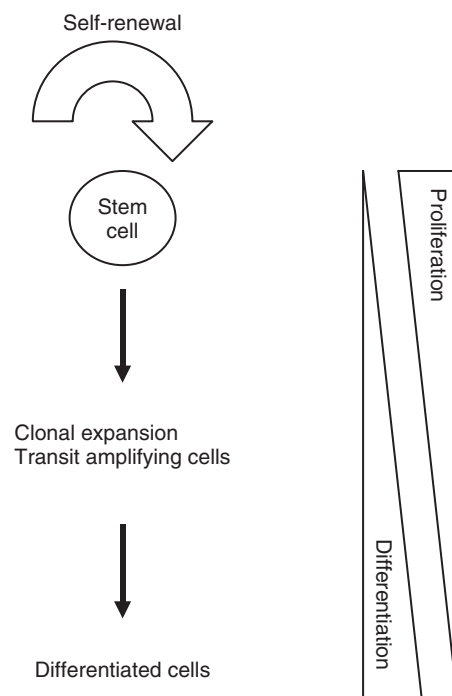
through rapid ubiquitylation and subsequent proteasomal degradation. HIF-1 α becomes susceptible to rapid ubiquitylation through hydroxylation of proline residues at Pro-402 and Pro-564 by prolyl hydroxylase 2 (PHD2), which requires oxygen for its enzyme activity.¹²⁷ In cells under hypoxia, the ubiquitylation and subsequent degradation of HIF-1 α are suppressed due to the decrease in PHD2 activity, and therefore the level of HIF-1 α protein increases. In addition, the activity of HIF-1 as a transcription factor is also controlled by hydroxylation of HIF-1 α protein. Hydroxylation of the asparagine residue at Asn-803 inhibits the interaction between HIF-1 α and p300, which is essential for the transcriptional activity of HIF-1.¹²⁸ Because the factor inhibiting HIF (FIH) that hydroxylates Asn-803 is also an oxygen-dependent enzyme, the transcriptional activity of HIF-1 increases under hypoxia due to the suppressed hydroxylation at Asn-803.^{129,130} Cells can control the transcription of HIF-1-regulated genes by sensing the oxygen concentration through the activities of oxygen dependent enzymes PHD2 and FIH, and consequently regulating the intracellular level as well as the transcriptional activity of HIF-1.¹³¹

Although HIF-1 can be activated by non-hypoxic pathways, hypoxia inside the growing tumor mass is the most probable candidate for the activation of HIF-1 α cascade in tumor cells. This is supported by the fact that both HIF-1 α and VEGF expression are upregulated predominantly in tumor cells around the necrotic areas of highly vascularized tumor mass in glioblastoma.¹³² Therefore, angiogenesis triggered by the hypoxia–HIF-1 α –VEGF cascade seems to play an important role in tumor progression to the more aggressive phenotypes.

Cancer stem cells

Stem cells are defined as cells that have the ability to perpetuate themselves through self-renewal and to generate

mature cells of a particular tissue through differentiation (Figure 1.3). The term ‘cancer stem cell’ is an operational term defined as a cancer cell that has the ability to self-renew, dividing to give rise to another malignant stem cell and a cell that gives rise to the phenotypically diverse tumor cell population. Stem cells in different tissues vary with respect to their intrinsic abilities to self-renew and to

**Figure 1.3**

Stem cell paradigm. It is postulated that within every tissue a small fraction of cells exist which have the following properties: self-renewal, pluripotency giving rise to other cells of the lineage, and longevity. The transit amplifying cells show rapid division and end up in terminally differentiated cells which lose their ability to proliferate.

differentiate into particular cell types. Most cancers consist of a heterogeneous population of cells with differences in their proliferative potential as well as their ability to reconstitute the tumor on transplantation. Evidence for cancer stem cells was first documented in hematological malignancies where only a small subset of cancer cells were capable of forming new tumors.^{133–137} Because the differences in clonogenicity among the leukemia cells mirrored the differences in clonogenicity among normal hematopoietic cells, the clonogenic leukemic cells were described as leukemic stem cells. It has also been shown for solid cancers that the cells are phenotypically heterogeneous and that only a small proportion of cells are clonogenic in culture and in vivo.^{138–142} As in the context of leukemic stem cells, these observations led to the hypothesis that only a few cancer cells are actually tumorigenic and that these tumorigenic cells could be considered as cancer stem cells. However, two possible explanations remain: either all solid cancer cells have a low probability of proliferating extensively and behaving in clonogenic assays as cancer stem cells, or most cancer cells have only a limited proliferative potential and cannot behave as cancer stem cells, but a small, definable subset of cells is enriched for the ability to proliferate extensively and form tumors. In both cases, some of the cancer cell heterogeneity would arise as a result of environmental differences within the tumor and continuing mutagenesis.

On transplantation, cancer stem cells give rise to tumors consisting of both new cancer stem cells and heterogeneous populations of non-tumorigenic cells, reminiscent of the developmental hierarchy in the tissues from which the tumors arose. To date, cancer stem cell-like cells have been identified in breast and central nervous system tumors.^{143–148} It is still not clear whether the cancer stem cells are derived from true tissue-derived stem cells, bone marrow stem cells or mature cells that have undergone dedifferentiation or a transdifferentiation process. It is also not entirely clear whether the cancer stem cell represents one or multiple phenotypes.^{149,150}

Further evidence for cancer stem cells comes from the study of signaling pathways. Since normal stem cells and cancer cells share the ability to self-renew, it seems reasonable to propose that newly arising cancer cells apply the machinery for self-renewal that is normally expressed in stem cells. Evidence shows that many pathways that are classically associated with cancer may also regulate normal stem cell development. For example, the prevention of apoptosis by enforced expression of the oncogene *bcl-2* results in increased numbers of hematopoietic stem cells (HSCs) in vivo, suggesting that cell death has a role in regulating the homeostasis of HSCs.¹⁵¹ Other signaling pathways associated with oncogenesis, such as the Notch, Sonic hedgehog (Shh) and Wnt signaling pathways, may also regulate stem cell self-renewal (Table 1.5).⁷⁵ In vivo data from transgenic mice suggest that activation of the Wnt signaling pathway in epidermal stem cells leads to epithelial cancers.¹⁵²

Table 1.5 Signaling pathways in stem cells and cancer

Pathway	Stem cell	Cancer
Wnt	Hematopoietic stem cells	Lymphoblastic leukemia
	Intestinal epithelial stem cells	Colorectal cancer
	Keratinocyte stem cells	Pilomatricoma
	Cerebellar granule-cell progenitors	Medulloblastoma
	CNS stem cells	Gliomas
Shh	Hair-follicle progenitors	Basal-cell carcinoma
	Cerebellar granule-cell progenitors	Medulloblastoma
	CNS stem cells	Gliomas
BMI1	Hematopoietic stem cells	B-cell lymphomas, AML
Notch	Hematopoietic stem cells	Lymphoblastic leukemia
	Mammary epithelial stem cells	Breast cancer
PTEN	Neural stem cells	Gliomas

Wnt, wingless type; Shh, Sonic hedgehog; BMI1, B lymphoma MO-MLV insertion region; AML, acute myeloid leukemia.

If the signaling pathways that normally regulate stem cell self-renewal lead to tumorigenesis when dysregulated, then the stem cells themselves may represent the target of transformation in certain types of cancer.^{153,154} There are two lines of evidence in support of this hypothesis. First, because stem cells have the machinery for self-renewal already activated, maintaining this activation may be simpler than turning it on de novo in a more differentiated cell: fewer mutations may be required to maintain self-renewal than to activate it ectopically. Second, by self-renewing, stem cells often persist for long periods of time, instead of dying after short periods of time like many mature cells in highly proliferative tissues. Therefore, there is a much greater opportunity for mutations to accumulate in individual stem cells than in most mature cell types.

If cancer stem cells are responsible for tumor growth, this would have profound implications for cancer therapy. One possible reason for the failure of current cancer therapy is the acquisition of drug resistance by cancer cells; another possibility is that existing therapies fail to kill cancer stem cells effectively. Normal stem cells from various tissues tend to be more resistant to chemotherapeutics than mature cell types from the same tissues. This may be due to high levels of expression of antiapoptotic proteins or ABC (ATP-binding cassette) transporters such as the multidrug resistance gene.^{151,155,156} If the same were true of cancer

stem cells, then it could be expected that these cells would be more resistant to chemotherapeutics than would be tumor cells with limited proliferative potential. Even therapies that cause the complete regression of tumors might spare enough cancer stem cells to allow regrowth of the tumors. Therefore, it is hoped that therapies that are more specifically directed against cancer stem cells might result in much more durable responses and even cures of metastatic tumors.

References

- Hanahan D, Weinberg RA. The hallmarks of cancer. *Cell* 2000; 100: 57–70.
- Kinzler KW, Vogelstein B. Lessons from hereditary colorectal cancer. *Cell* 1996; 87: 159–70.
- Novell PC. The clonal evolution of tumor cell populations. *Science* 1976; 194: 23–8.
- Hahn WC, Weinberg RA. Rules for making human tumor cells. *N Engl J Med* 2002; 347: 1593–603.
- Weinberg RA. The retinoblastoma protein and cell cycle control. *Cell* 1995; 81: 323–30.
- Fyran TM, Reiss M. Resistance to inhibition of cell growth by transforming growth factor-beta and its role in oncogenesis. *Crit Rev Oncog* 1993; 4: 493–540.
- Schutte M, Hruban R, Hedrick L et al. DPC4 gene in various tumor types. *Cancer Res* 1996; 56: 2527–30.
- Chin L, Pomerantz J, DePinho RA. The INK4a/ARF tumor suppressor: one gene—two products—two pathways. *Trends Biochem Sci* 1998; 23: 291–6.
- Foley KP, Eisenman RN. Two MAD tails: what the recent knockouts of Mad1 and Mx1 tell us about the MYC/MAX/MAD network. *Biochim Biophys Acta* 1999; 1423: M37–47.
- Cordon-Cardo C, Prives C. At the crossroads of inflammation and tumorigenesis. *J Exp Med* 1999; 190: 1367–70.
- Holliday R, Pugh JE. DNA modification mechanisms and gene activity during development. *Science* 1975; 187: 226–32.
- Baylin SB, Ohm JE. Epigenetic gene silencing in cancer—a mechanism for early oncogenic pathway addiction? *Nat Rev Cancer* 2006; 6: 107–16.
- Egger G, Liang G, Aparicio A, Jones PA. Epigenetics in human disease and prospects for epigenetic therapy. *Nature* 2004; 429: 457–63.
- Takai D, Jones PA. Comprehensive analysis of CpG islands in human chromosomes 21 and 22. *Proc Natl Acad Sci USA* 2002; 99: 3740–5.
- Jones PA, Baylin SB. The fundamental role of epigenetic events in cancer. *Nat Rev Genet* 2002; 3: 415–28.
- Fischle W, Wang Y, Allis CD. Binary switches and modification cassettes in histone biology and beyond. *Nature* 2003; 425: 475–9.
- Strahl BD, Allis CD. The language of covalent histone modifications. *Nature* 2000; 403: 41–5.
- Gazzoli I, Loda M, Garber J, Syngal S, Kolodner RD. A hereditary nonpolyposis colorectal carcinoma case associated with hypermethylation of the MLH1 gene in normal tissue and loss of heterozygosity of the unmethylated allele in the resulting microsatellite instability-high tumor. *Cancer Res* 2002; 62: 3925–8.
- Suter CM, Martin DI, Ward RL. Germline epimutation of MLH1 in individuals with multiple cancers. *Nat Genet* 2004; 36: 497–501.
- Grignani F, DeMatteis S, Nervi C, et al. Fusion proteins of the retinoic acid receptor-alpha recruit histone deacetylase in promyelocytic leukaemia. *Nature* 1998; 391: 815–18.
- Jones LK, Saha V. Chromatin modification, leukaemia and implications for therapy. *Br J Haematol* 2002; 118: 714–27.
- Roberts CW, Orkin SH. The SWI/SNF complex—chromatin and cancer. *Nature Rev Cancer* 2004; 4: 133–42.
- Jones PA, Laird PW. Cancer epigenetics comes of age. *Nat Genet* 1999; 21: 163–7.
- Feinberg AP, Tycko B. The history of cancer epigenetics. *Nat Rev Cancer* 2004; 4: 143–53.
- Herman JG, Baylin SB. Gene silencing in cancer in association with promoter hypermethylation. *N Engl J Med* 2003; 349: 2042–54.
- Herman JG, Kumar A, Polyak K, et al. Incidence and functional consequences of hMLH1 promoter hypermethylation in colorectal carcinoma. *Proc Natl Acad Sci USA* 1998; 95: 6870–5.
- Bachman KE, Park BH, Rhee I, et al. Histone modifications and silencing prior to DNA methylation of a tumor suppressor gene. *Cancer Cell* 2003; 3: 89–95.
- Myohanen SK, Baylin SB, Herman JG. Hypermethylation can selectively silence individual p16ink4A alleles in neoplasia. *Cancer Res* 1998; 58: 591–3.
- Parsons R, Myeroff LL, Liu B, et al. Microsatellite instability and mutations of the transforming growth factor β type II receptor gene in colorectal cancer. *Cancer Res* 1995; 55: 5548–50.
- Morin PJ, Sparks AB, Krinh V, et al. Activation of β -catenin—Tcf signaling in colon cancer by mutations in β -catenin or APC. *Science* 1997; 275: 1787–90.
- Suzuki H, Gabrielson E, Chen W, et al. A genomic screen for genes upregulated by demethylation and histone deacetylase inhibition in human colorectal cancer. *Nature Genet* 2002; 31: 141–9.
- Akiyama Y, Watkins N, Suzuki H, et al. GATA-4 and GATA-5 transcription factor genes and potential downstream antitumor target genes are epigenetically silenced in colorectal and gastric cancer. *Mol Cell Biol* 2003; 23: 8429–39.
- Suzuki H, Watkins DN, Jair KW, et al. Epigenetic inactivation of SFRP genes allows constitutive WNT signaling in colorectal cancer. *Nat Genet* 2004; 36: 417–22.
- Rhee I, Bachman KE, Park BH, et al. DNMT1 and DNMT3b cooperate to silence genes in human cancer cells. *Nature* 2002; 416: 552–6.
- Bachman KE, Herman JG, Corn PG, et al. Methylation-associated silencing of the tissue inhibitor of metalloproteinase-3 gene suggest a suppressor role in kidney, brain, and other human cancers. *Cancer Res* 1999; 59: 798–802.
- Gao X, Sedgwick T, Shi YB, Evans T. Distinct functions are implicated for the GATA-4, -5, and -6 transcription factors in the regulation of intestine epithelial cell differentiation. *Mol Cell Biol* 1998; 18: 2901–11.
- Al-azhah E, Dittrich O, Vervoorts J, et al. Gastroprotective peptide trefoil factor family 2 gene is activated by upstream

- stimulating factor but not by c-Myc in gastrointestinal cancer cells. *Gut* 2002; 51: 685–90.
38. Bossenmeyer-Pourie C, Kannan R, Ribieras S, et al. The trefoil factor 1 participates in gastrointestinal cell differentiation by delaying G1–S phase transition and reducing apoptosis. *J Cell Biol* 2002; 157: 761–70.
 39. Wright NA, Hoffmann W, Otto WR, Rio MC, Thim L. Rolling in the clover: trefoil factor family (TFF)-domain peptides, cell migration and cancer. *FEBS Lett* 1997; 408: 121–3.
 40. Hu M, Yao J, Cai L, et al. Distinct epigenetic changes in the stromal cells of breast cancers. *Nat Genet* 2005; 37: 899–905.
 41. Hahn WC, Counter CM, Lundberg AS, et al. Creation of human tumor cells with defined genetic elements. *Nature* 2000; 400: 464–8.
 42. Stoler DL, Chen N, Basik M, et al. The onset and extent of genomic instability in sporadic colorectal tumor progression. *Proc Natl Acad Sci USA* 1999; 96: 15121–6.
 43. Ionov Y, Peinado MA, Alkhosyan S, et al. Ubiquitous somatic mutations in simple repeated sequences reveal a new mechanism for colonic carcinogenesis. *Nature* 1993; 363: 558–61.
 44. Quackenbush J. Microarray analysis and tumor classification. *N Engl J Med* 2006; 354: 2463–72.
 45. Tinker AV, Boussioutas A, Bowtell DDL. The challenges of gene expression microarrays for the study of human cancer. *Cancer Cell* 2006; 9: 333–9.
 46. Sonnenschein C, Soto AM. Somatic mutation theory of carcinogenesis: why it should be dropped and replaced. *Mol Carcinog* 2000; 29: 205–11.
 47. Mintz B, Illmensee K. Normal genetically mosaic mice produced from malignant teratocarcinoma cells. *Proc Natl Acad Sci USA* 1975; 72: 3585–9.
 48. Illmensee K, Mintz B. Totipotency and normal differentiation of single teratocarcinoma cell cloned by injection into blastocysts. *Proc Natl Acad Sci USA* 1976; 73: 549–53.
 49. Sternlicht MD, Lochter A, Sympton CJ, et al. The stromal proteinase MMP3/stromelysin-1 promotes mammary carcinogenesis. *Cell* 1999; 98: 137–46.
 50. Barcellos-Hoff MH, Ravani SA. Irradiated mammary gland stroma promotes the expression of tumorigenic potential by unirradiated epithelial cells. *Cancer Res* 2000; 60: 1254–60.
 51. Bissell MJ, Weaver VM, Lelievre SA, et al. Tissue structure, nuclear organization, and gene expression in normal and malignant breast. *Cancer Res* 1999; 59: S1757–63.
 52. Huang S, Ingber DE. The structural and mechanical complexity of cell-growth control. *Nat Cell Biol* 1999; 1: E131–8.
 53. Loeb LA. Many mutations in cancers. *Cancer Surv* 1996; 28: 329–42.
 54. Cahill DP, Kinzler KW, Vogelstein B, Lengauer C. Genetic instability and Darwinian selection in tumors. *Trends Cell Biol* 1999; 9: M57–60.
 55. Strohmman RC. The coming Kuhnian revolution in biology. *Nature Biotechnol* 1997; 15: 194–200.
 56. Folkman J, Hahnfeldt P, Hlatky L. Cancer: looking outside the genome. *Nat Rev Mol Cell Biol* 2000; 1: 76–9.
 57. Salvesen GS, Dixit VM. Caspases: intracellular signaling by proteolysis. *Cell* 1997; 91: 443–6.
 58. Cryns V, Yuan J. Proteases to die for. *Genes Dev* 1998; 12: 1551–70.
 59. Thornberry NA, Lazebnik Y. Caspases: enemies within. *Science* 1998; 281: 1312–16.
 60. Budihardjo I, Oliver H, Lutter M, Luo X, Wang X. Biochemical pathways of caspase activation during apoptosis. *Annu Rev Cell Dev Biol* 1999; 15: 269–90.
 61. Tsujimoto Y, Finger LR, Yunis J, Nowell PC, Croce CM. Cloning of the chromosome breakpoint of neoplastic B cells with the t(14;18) chromosome translocation. *Science* 1984; 226: 1097–9.
 62. Vogelstein B, Lane D, Levine AJ. Surfing the p53 network. *Nature* 2000; 408: 307–10.
 63. Gronbaek K, Straten PT, Ralfkiaer E, et al. Somatic Fas mutations in non-Hodgkin's lymphoma: association with extranodal disease and autoimmunity. *Blood* 1998; 92: 3018–24.
 64. Park WS, Oh RR, Kim YS, et al. Somatic mutations in the death domain of the Fas (Apo-1/CD95) gene in gastric cancer. *J Pathol* 2001; 193: 162–8.
 65. Brunet A, Bonni A, Zigmond MJ, et al. Akt promotes cell survival by phosphorylating and inhibiting a Forkhead transcription factor. *Cell* 1999; 96: 857–68.
 66. Gottlob K, Majewski N, Kennedy S, et al. Inhibition of early apoptotic events by Akt/PKB is dependent on the first committed step of glycolysis and mitochondrial hexokinase. *Genes Dev* 2001; 15: 1406–18.
 67. Barthel A, Okino ST, Liao J, et al. Regulation of GLUT1 gene transcription by the serine/threonine kinase Akt1. *J Biol Chem* 1999; 274: 20281–6.
 68. Wang CY, Mayo MW, Baldwin AS Jr. TNF- and cancer therapy-induced apoptosis: potentiation by inhibition of NFκB. *Science* 1996; 274: 784–7.
 69. Campisi J. Cellular senescence as a tumor-suppressor mechanism. *Trends Cell Biol* 2001; 11: S27–31.
 70. Kamijo T, Bodner S, van de Kamp E, Randle DH, Sherr CJ. Tumor spectrum in ARF-deficient mice. *Cancer Res* 1999; 59: 2217–22.
 71. Serrano M, Lee H, Chin L, et al. Role of the INK4a locus in tumor suppression and cell mortality. *Cell* 1996; 85: 27–37.
 72. Kim J, Klionsky DJ. Autophagy, cytoplasm-to-vacuole targeting pathway, and pexophagy in yeast and mammalian cells. *Annu Rev Biochem* 2000; 69: 303–42.
 73. Noda T, Ohsumi Y. Tor, a phosphatidylinositol kinase homologue, controls autophagy in yeast. *J Biol Chem* 1998; 273: 3963–6.
 74. Liang XH, Jackson S, Seaman M, et al. Induction of autophagy and inhibition of tumorigenesis by beclin 1. *Nature* 1999; 402: 672–6.
 75. Taipale J, Beachy PA. The Hedgehog and Wnt signalling pathways in cancer. *Nature* 2001; 411: 349–54.
 76. Mochizuki T, Asai A, Saito N, et al. Akt protein kinase inhibits non-apoptotic programmed cell death induced by ceramide. *J Biol Chem* 2002; 277: 2790–7.
 77. Tassa A, Roux MP, Attaix D, Bechet DM. Class III phosphoinositide 3-kinase–Beclin1 complex mediates the amino acid-dependent regulation of autophagy in C2C12 myotubes. *Biochem J* 2003; 376: 577–86.
 78. Qu X, Yu J, Bhagat G, et al. Promotion of tumorigenesis by heterozygous disruption of the beclin 1 autophagy gene. *J Clin Invest* 2003; 112: 1809–20.
 79. Carvalho A, Carmena M, Sambade C, Earnshaw WC, Wheatley SP. Survivin is required for stable checkpoint activation in taxol-treated HeLa cells. *J Cell Sci* 2003; 116: 2987–98.

80. Nigg EA. Mitotic kinases as regulators of cell division and its checkpoints. *Nat Rev Mol Cell Biol* 2001; 2: 21–32.
81. Sen S, Zhou H, White RA. A putative serine/threonine kinase encoding gene BTAK on chromosome 20q13 is amplified and overexpressed in human breast cancer cell lines. *Oncogene* 1997; 14: 2195–200.
82. Meraldi P, Honda R, Nigg EA. Aurora-A overexpression reveals tetraploidization as a major route to centrosome amplification in p53^{-/-} cells. *EMBO J* 2002; 21: 483–92.
83. Coussens LM, Werb Z. Inflammation and cancer. *Nature* 2002; 420: 860–7.
84. De Palma M, Venneri MA, Galli R, et al. Tie2 identifies a hematopoietic lineage of proangiogenic monocytes required for tumor vessel formation and a mesenchymal population of pericyte progenitors. *Cancer Cell* 2005; 8: 211–26.
85. Orimo A, Gupta PB, Sgroi DC, et al. Stromal fibroblasts present in invasive human breast carcinomas promote tumor growth and angiogenesis through elevated SDF-1/CXCL12 secretion. *Cell* 2005; 121: 335–48.
86. Kaplan RN, Riba RD, Zachoroulis S, et al. VEGFR1-positive hematopoietic bone marrow progenitors initiate the premetastatic niche. *Nature* 2005; 438: 820–7.
87. Yarden Y, Sliwkowski MX. Untangling the ErbB signalling network. *Nat Rev Mol Cell Biol* 2001; 2: 127–37.
88. Bianco R, Melisi D, Ciardiello F, Tortora G. Key cancer cell signal transduction pathways as therapeutic targets. *Eur J Cancer* 2006; 42: 290–4.
89. Salomon DS, Brandt R, Ciardiello F, et al. Epidermal growth factor-related peptides and their receptors in human malignancies. *Crit Rev Oncol Hematol* 1995; 19: 183–232.
90. Pao W, Miller VA. Epidermal growth factor receptor mutations, small-molecule kinase inhibitors, and non-small-cell lung cancer: current knowledge and future directions. *J Clin Oncol* 2005; 23: 2556–68.
91. Kobayashi S, Boggon TJ, Dayaram T, et al. EGFR mutation and resistance of non-small-cell lung cancer to gefitinib. *N Engl J Med* 2005; 352: 786–92.
92. Shields JM, Pruitt K, McFall A, et al. Understanding Ras: it ain't over 'til it's over. *Trends Cell Biol* 2000; 10: 147–54.
93. Eberhard DA, Johnson BE, Amler LC, et al. Mutations in the epidermal growth factor receptor and in KRAS are predictive and prognostic indicators in patients with non-small-cell lung cancer treated with chemotherapy alone and in combination with erlotinib. *J Clin Oncol* 2005; 23: 5900–9.
94. Kato K, Cox AD, Hisaka MM, et al. Isoprenoid addition to ras protein is the critical modification for its membrane association and transforming activity. *Proc Natl Acad Sci USA* 1992; 89: 6403–7.
95. Davies H, Bignell GR, Cox C, et al. Mutations of the BRAF gene in human cancer. *Nature* 2002; 417: 949–54.
96. Sansal I, Sellers WR. The biology and clinical relevance of the PTEN tumor suppressor pathway. *J Clin Oncol* 2004; 22: 2954–63.
97. Bjornsti MA, Houghton PJ. The TOR pathway: a target for cancer therapy. *Nat Rev Cancer* 2004; 4: 335–48.
98. Barnett SF, Bilodeau MT, Lindsley CW. The Akt/PKB family of protein kinases: a review of small molecule inhibitors and progress towards target validation. *Curr Top Med Chem* 2005; 5: 109–25.
99. Folkman J. Tumor angiogenesis: therapeutic implications. *N Engl J Med* 1971; 285: 1182–6.
100. Folkman J. What is the evidence that tumors are angiogenesis dependent? *J Natl Cancer Inst* 1990; 82: 4–6.
101. Fidler IJ, Ellis LM. The implications of angiogenesis for the biology and therapy of cancer metastasis. *Cell* 1994; 79: 185–8.
102. Ikeda N, Adachi M, Taki T, et al. Prognostic significance of angiogenesis in human pancreatic cancer. *Br J Cancer* 1999; 79: 1553–63.
103. Fontanini G, Lucchi M, Vignati S, et al. Angiogenesis as a prognostic indicator of survival in non-small-cell lung carcinoma: a prospective study. *J Natl Cancer Inst* 1997; 89: 881–6.
104. Hicklin DJ, Ellis LM. Role of the vascular endothelial growth factor pathway in tumor growth and angiogenesis. *J Clin Oncol* 2005; 23: 1011–27.
105. Rafii S, Lyden D, Benezra R, et al. Vascular and haematopoietic stem cells: novel targets for anti-angiogenesis therapy. *Nat Rev Cancer* 2002; 2: 826–35.
106. Hanahan D, Folkman J. Patterns and emerging mechanisms of the angiogenic switch during tumorigenesis. *Cell* 1996; 86: 353–64.
107. Carmeliet P. Mechanisms of angiogenesis and arteriogenesis. *Nat Med* 2000; 6: 389–95.
108. Dvorak HF. Tumors: wounds that do not heal. Similarities between tumor stroma generation and wound healing. *N Engl J Med* 1986; 315: 1650–9.
109. Ferrara N, Gerber HP, LeCouter J. The biology of VEGF and its receptors. *Nat Med* 2003; 9: 669–76.
110. Yancopoulos GD, Davis S, Gale NW, et al. Vascular-specific growth factors and blood vessel formation. *Nature* 2000; 407: 242–8.
111. Ferrara N. Vascular endothelial growth factor: basic science and clinical progress. *Endocr Rev* 2004; 25: 581–611.
112. Rak J, Mitsuhashi Y, Bayko L, et al. Mutant ras oncogenes upregulate VEGF/VPF expression: implications for induction and inhibition of tumor angiogenesis. *Cancer Res* 1995; 55: 4575–80.
113. Hattori K, Heissig B, Wu Y, et al. Placental growth factor reconstitutes hematopoiesis by recruiting VEGFR1+ stem cells from bone-marrow microenvironment. *Nat Med* 2002; 8: 841–9.
114. Gerber HP, Malik AK, Solar GP, et al. Vascular endothelial growth factor regulates haematopoietic stem cell survival by an internal autocrine loop mechanism. *Nature* 2002; 417: 954–8.
115. LeCouter J, Moritz DR, Li B, et al. Angiogenesis-independent endothelial protection of liver: role of VEGFR-1. *Science* 2003; 299: 890–3.
116. Lindhal P, Johansson BE, Leveen P, Betsholtz C. Pericyte loss and microaneurysm formation in PDGF-B-deficient mice. *Science* 1997; 277: 242–5.
117. Dong J, Grunstein J, Tejada M, et al. VEGF-null cells require PDGFR alpha signaling-mediated stromal fibroblast recruitment for tumorigenesis. *EMBO J* 2004; 23: 2800–10.
118. Maisonpierre PC, Suri C, Jones PF, et al. Angiopoietin-2, a natural antagonist for Tie-2 that disrupts in vivo angiogenesis. *Science* 1997; 277: 55–60.

119. Oliner J, Min H, Leal J, et al. Suppression of angiogenesis and tumor growth by selective inhibition of angiopoietin-2. *Cancer Cell* 2004; 6: 507–16.
120. Ferrara N, Kerbel RS. Angiogenesis as a therapeutic target. *Nature* 2005; 383: 967–74.
121. Stadler P, Becker A, Feldmann HJ, et al. Influence of the hypoxic subvolume on the survival of patients with head and neck cancer. *Int J Radiat Oncol Biol Phys* 1999; 44: 749–54.
122. Young SD, Marshall RS, Hill RP. Hypoxia induces DNA overreplication and enhances metastatic potential of murine tumor cells. *Proc Natl Acad Sci USA* 1988; 85: 9533–7.
123. Graeber TG, Osmanian C, Jacks T, et al. Hypoxia-mediated selection of cells with diminished apoptotic potential in solid tumors. *Nature* 1996; 379: 88–91.
124. Teicher BA. Hypoxia and drug resistance. *Cancer Metastasis Rev* 1994; 13: 139–68.
125. Erler JT, Cawthorne CJ, Williams KJ, et al. Hypoxia-mediated down-regulation of Bid and Bax in tumors occurs via hypoxia-inducible factor 1-dependent and -independent mechanisms and contributes to drug resistance. *Mol Cell Biol* 2004; 24: 2875–89.
126. Semenza GL. HIF-1 and tumor progression: pathophysiology and therapeutics. *Trends Mol Med* 2002; 8: S62–7.
127. Berra E, Benizri E, Ginouves A, et al. HIF prolyl-hydroxylase 2 is the key oxygen sensor setting low steady-state levels of HIF-1 α in normoxia. *EMBO J* 2003; 22: 4082–90.
128. Lando D, Peet DJ, Whelan DA, Gorman JJ, Whitelaw ML. Asparagine hydroxylation of the HIF transactivation domain a hypoxic switch. *Science* 2002; 295: 858–61.
129. Lando D, Peet DJ, Gorman JJ, et al. FIH-1 is an asparaginyl hydroxylase enzyme that regulates the transcriptional activity of hypoxia-inducible factor. *Genes Dev* 2002; 16: 1466–71.
130. Hewitson KS, McNeill LA, Riordan MV, et al. Hypoxia-inducible factor (HIF) asparagine hydroxylase is identical to factor inhibiting HIF (FIH) and is related to the cupin structural family. *J Biol Chem* 2002; 277: 26351–5.
131. Haddad JJ. Oxygen-sensing mechanisms and the regulation of redox-responsive transcription factors in development and pathophysiology. *Respir Res* 2002; 3: 26.
132. Plate KH, Breier G, Weich HA, Risau W. Vascular endothelial growth factor is a potential tumor angiogenesis factor in human gliomas in vivo. *Nature* 1992; 359: 845–8.
133. Park CH, Bergsagel DE, McCulloch EA. Mouse myeloma tumor stem cells: a primary cell culture assay. *J Natl Cancer Inst* 1971; 46: 411–22.
134. Bruce WR, Gaag H. A quantitative assay for the number of murine lymphoma cells capable of proliferation in vivo. *Nature* 1963; 199: 79–80.
135. Wodinsky I, Swinarski J, Kensler CJ. Spleen colony studies of leukemia L1210. I. Growth kinetics of lymphocytic L1210 cells in vivo as determined by spleen colony assay. *Cancer Chemother Rep* 1967; 51: 415–21.
136. Bergsagel DE, Valeriote FA. Growth characteristics of a mouse plasma cell tumor. *Cancer Res* 1968; 28: 2187–96.
137. Bonnet D, Dick JE. Human acute myeloid leukemia is organized as a hierarchy that originates from a primitive hematopoietic cell. *Nat Med* 1997; 3: 730–7.
138. Fidler IJ, Kripke ML. Metastasis results from preexisting variant cells within a malignant tumor. *Science* 1977; 197: 893–5.
139. Fidler IJ, Hart IR. Biological diversity in metastatic neoplasms: origins and implications. *Science* 1982; 217: 998–1003.
140. Heppner GH. Tumor heterogeneity. *Cancer Res* 1984; 44: 2259–65.
141. Nowell PC. Mechanisms of tumor progression. *Cancer Res* 1986; 46: 2203–7.
142. Southam CM, Brunschwig A. Quantitative studies of autotransplantation of human cancer. *Cancer* 1961; 14: 971–8.
143. Al-Hajj M, Clarke MF. Self-renewal and solid tumor stem cells. *Oncogene* 2004; 23: 7274–82.
144. Al-Hajj M, Wicha MS, Benito-Hernandez A, Morrison SJ, Clarke MF. Prospective identification of tumorigenic breast cancer cells. *Proc Natl Acad Sci USA* 2003; 100: 3983–8.
145. Singh SK, Clarke JD, Terasaki M, et al. Identification of a cancer stem cell in human brain tumors. *Cancer Res* 2003; 63: 5821–8.
146. Singh SK, Hawkins C, Clarke JD, et al. Identification of human brain tumor initiating cells. *Nature* 2004; 432: 396–401.
147. Singh SK, Clarke ID, Hide T, Dirks PB. Cancer stem cells in nervous system tumors. *Oncogene* 2004; 23: 7267–73.
148. Galli R, Binda E, Orfanelli U, et al. Isolation and characterization of tumorigenic, stem-like neural precursors from human glioblastoma. *Cancer Res* 2004; 64: 7011–21.
149. Reya T, Morrison SJ, Clarke MF, Weissman IL. Stem cells, cancer, and cancer stem cells. *Nature* 2001; 414: 105–11.
150. Passegue E, Jamieson CH, Ailles LE, Weissman IL. Normal and leukemic hematopoiesis: are leukemias a stem cell disorder or a reacquisition of stem cell characteristics? *Proc Natl Acad Sci USA* 2003; 100 (Suppl): 11842–9.
151. Domen J, Gandy KL, Weissman IL. Systemic overexpression of BCL-2 in the hematopoietic system protects transgenic mice from the consequences of lethal irradiation. *Blood* 1998; 91: 2272–82.
152. Gat U, DasGupta R, Degenstein L, Fuchs E. De novo hair follicle morphogenesis and hair tumors in mice expressing a truncated b-catenin in skin. *Cell* 1998; 95: 605–14.
153. Sell S, Pierce GB. Maturation arrest of stem cell differentiation is a common pathway for the cellular origin of teratocarcinomas and epithelial cancers. *Lab Invest* 1994; 70: 6–22.
154. Sawyers C, Denny C, Witte O. Leukemia and the disruption of normal hematopoiesis. *Cell* 1991; 64: 337–50.
155. Peters R, Leyvraz S, Perey L. Apoptotic regulation in primitive hematopoietic precursors. *Blood* 1998; 92: 2041–52.
156. Zhou S, Schuetz JD, Bunting KD, et al. The ABC transporter Bcrp1/ABCG2 is expressed in a wide variety of stem cells and is a molecular determinant of the side-population phenotype. *Nat Med* 2001; 7: 1028–34.

Targets

Christoph Bremer and Michael Schäfers

Genomics–proteomics

The human genome consists of approximately 34 000 genes encoding numerous protein structures in the body. Disease-specific aberrations of gene expression profiles are being discovered with ever-increasing speed, and are therefore unraveling the underlying ‘molecular pathology’ of cancer. Thus, innumerable molecular structures can potentially serve as novel tissue specific markers for oncological imaging *in vivo*. High-throughput analysis tools in genomics and proteomics help to identify new target molecules which are specifically regulated (up- and/or downregulation) in cancer. The term functional genomics refers to the systematic generation and analysis of information on what specific genes do. Moreover, the genome-wide analysis of gene expression (analysis of the transcriptome), the analysis of protein expression levels (proteomics), and their phenotypic effects are fundamental research advances which will help to discover ever new relevant targets for oncology in general, and imaging in oncological disorders specifically.

The investigation of how genes and proteins interact to finally carry out cellular functions, which is also referred to as ‘systems biology’, will moreover improve our understanding of the ‘molecular anatomy’ as well as ‘molecular pathology’.

Whereas many activities in basic research on molecular pathology in cancer are pursued by analytical methods applied to blood or tissue samples, molecular and functional imaging is uniquely able to discover molecular target expression and function on a protein level non-invasively *in vivo*. Thus, profiling-mediated discovery of novel disease-specific targets will also spur the development of new and more specific imaging agents for molecular imaging.¹ Based on this knowledge, new ligands with high affinity towards newly discovered molecular targets in cancer will form the basis for new imaging as well as therapeutic agents (see below).

Targets for oncological molecular imaging *in vivo* should generally be (1) clinically relevant (i.e. linked to a certain type of disease or be predictive of disease outcome),

(2) abundantly overexpressed (or significantly downregulated) as compared to healthy tissue (warranting appropriate imaging contrast), and (3) easily accessible by intravenously applied molecular tracers (e.g. extracellular). Typically, specific proteins (e.g. cell receptors) are chosen as molecular targets, since the ‘natural amplification’ mechanism from gene to protein (i.e. 1 gene = several copies of proteins) can be exploited and – depending on the site of expression – proteins may be more easily accessible in general.

While targeting extracellular proteins seems relatively easily achievable using a huge variety of compounds (peptidyl vs. non-peptidyl structures) coupled to an isotope or fluorescent dye (tracer), intracellular targets can only be reached with a more complex chemical approach, since pharmacological barriers are substantial (see below). In a ‘classical’ approach, tracers are constructed to bind in a 1:1 fashion to the molecular target. A typical example is given by the binding of a receptor antagonist to a cellular surface receptor² or an inhibitor of an enzyme binding selectively to the activated enzyme.³ As a distinct group of molecular targets, enzymes can be exceptionally interesting when combined, for example, with radiolabeled substrates which are trapped intracellularly after enzymatic conversion, since one target structure (e.g. hexokinase) can process several hundreds of reporter probes and thus vastly amplify the signal *in vivo*. Optical imaging approaches have taken the advantages of fluorescence resonance energy transfer (FRET) techniques to design enzymatically activatable fluorophores (so-called ‘smart’ probes), which can be exploited to visualize a broad spectrum of oncologically relevant enzyme systems (e.g. matrix metalloproteinases, cathepsins, etc.).^{4,5}

However, theoretically even intracellular structures (e.g. caspases, RNA, DNA) can be targeted by different molecular imaging approaches. For this purpose, membrane translocation signals can facilitate entry of the probe into the intracellular space. Different approaches have been described to achieve improved transmembrane migration of reporter probes, including the human immunodeficiency virus (HIV) derived tat-peptide, dendrimers, and polyamine residues.¹

Targets

To date, numerous molecular targets have been explored to serve as targets for new molecular imaging tools. Therefore, we here refer to only a few classes of currently applied molecular imaging targets in cancer. Generally speaking, among the huge spectrum of targets being evaluated for preclinical purposes using different imaging modalities such as scintigraphy and fluorescence imaging, there are only a few molecular imaging targets which have been validated and established for clinical applications, in the vast majority using scintigraphic approaches such as positron emission tomography (PET) and single photon emission computed tomography (SPECT). Recent advances, especially in the field of molecular imaging, have prompted the development of new tracers being specific for molecular imaging of molecular targets in oncology.⁶ A review of new molecular imaging tracers for diagnostic purposes is additionally given in Chapter 31.

Clinically established targets for oncological imaging

Glucose transporters and hexokinase

Positron emission tomography with [¹⁸F]fluoro-2-deoxy-D-glucose (FDG) is one of the first molecular imaging techniques which has been extensively validated experimentally and has now provided a substantial clinical benefit for oncological imaging. In a first step, FDG (as the original molecule glucose) is taken up intracellularly via glucose transporters (e.g. GLUT1 and GLUT4) and subsequently phosphorylated by hexokinase. In contrast to glucose-6-phosphate, FDG-6-phosphate cannot enter the citrate cycle, and thus is trapped and increasingly accumulated intracellularly. While the target enzyme, hexokinase, is not specific for malignancy (being activated in inflammation, remodeling, etc.) the specificity of the FDG imaging approach is limited per se. However, a vast number of malignant tumors indeed show an increased rate of glycolysis, so that FDG-PET is becoming an increasingly important mainstay of molecular imaging in clinical oncology (see Chapter 28).

Neuroendocrine tumors

Some of the earliest reported peptide based receptor imaging agents developed and investigated in cancer patients were radiolabeled analogs of the hormone somatostatin. Somatostatin receptors (SSTRs) are found on the cell surface in a number of organs, including the central nervous

system, the gastrointestinal tract, and the endocrine and exocrine pancreas. A large number of human tumors express the somatostatin receptor subtype SSTR2. SSTR has a very short biological half-life; however, somatostatin analogs such as octreotide have much longer residence times. Octreotide labeled with ¹¹¹In using DTPA (diethylene-triaminepentaacetic acid) is approved for human use in the USA and Europe as a diagnostic imaging agent for neuroendocrine tumors. There are numerous other octreotide based imaging agents which have been extensively validated for oncological molecular imaging. Recently, new SSTR ligands for PET imaging of SSTR expression in cancer patients have been described.^{7,8}

Metaiodobenzylguanidine (MIBG) was developed in the early 1980s to visualize tumors arising from the adrenal medulla. Today, MIBG scintigraphy using MIBG labeled with ¹²³I in combination with SPECT represents the imaging modality of choice for pheochromocytomas, paragangliomas, and neuroblastomas. It has a complementary function in other neuroendocrine tumors such as carcinoids, medullary thyroid carcinomas, and non-functioning paragangliomas.⁹ Future developments might translate the SPECT technology to PET, e.g. labeling MIBG with the positron emitter ¹²⁴I.

Sodium iodide symporter

Sodium iodide symporter (NIS) is a membrane glycoprotein that couples the transport of iodine and sodium into cells using a sodium gradient maintained by the sodium–potassium adenosine triphosphatase (ATPase). Secondary active transport of iodine occurs in the thyroid gland, lactating breast, salivary glands, and gastric mucosa. Radioactive isotopes of iodine (e.g. ¹²³I and ¹³¹I) and [^{99m}Tc] pertechnetate are well established tracers in nuclear medicine for the diagnosis and targeted therapy of thyroid gland pathology. NIS transport is maintained in thyroid malignancies at lower levels compared to normal thyroid tissue, which can help to detect recurrent thyroid cancer and its metastasis as hot spots.

Preclinical imaging targets

Over recent years substantial progress has been made in the development of target specific anticancer drugs. Successful molecular targeting in cancer by treatment with target-avid drugs include, for example: the anti-HER2/neu antibody (trastuzumab) for erbB2-expressing breast cancers,¹⁰ and the kinase inhibitor imatinib for chronic myelogenous leukemia and gastrointestinal stroma tumors. Moreover, molecularly targeted drugs have shown efficacy in lung cancer (e.g. the epidermal growth factor receptor (EGFR) inhibitor erlotinib¹¹), multiple myeloma (e.g. the proteasome

inhibitor bortezomib¹²), advanced colorectal cancer (e.g. the EGFR antibody cetuximab¹³), and other breast cancer entities (e.g. the aromatase inhibitor letrozole¹⁴).

However, the response to target specific treatment regimens can be difficult to predict, which spurs the development of new target specific imaging probes that may help to enhance the clinical risk stratification due to improved diagnostic capabilities, optimize therapy based on molecular target characterization, and improve efficacy assessments.

Generally speaking, fundamental biological properties of oncological processes that are desirable to measure by means of molecular imaging include *angiogenesis*, *proliferation*, *apoptosis*, and *hypoxia*; these will be briefly reviewed hereafter.

Imaging of angiogenesis

Angiogenesis is a key oncological feature that is essential for tumor growth and for the formation of tumor metastases.¹⁵ Different key features are important hallmarks of angiogenesis in solid tumors.

Cell surface *tyrosine kinase receptors* are closely linked to cancer progression. Angiogenic endothelial cells depend on activation of the vascular endothelial growth factor (VEGF) receptor VEGFR2, and undergo apoptosis upon withdrawal of VEGF.¹⁶

A large array of *adhesion molecules* is important for the interaction of endothelial with other endothelial cells¹⁷ and with perivascular smooth muscle cells and pericytes respectively.¹⁸ The $\alpha_v\beta_3$ integrin is one prominent example of an adhesion molecule that can be targeted for both therapeutic and diagnostic purposes. Finally, enzymes degrading the extracellular matrix are an integral part of tumor angiogenesis, including matrix metalloproteinases, cathepsins, or hyaluronidase.

Different non-specific, parametric imaging modalities have been developed to quantify tumor perfusion, vascular permeability, and intravascular and interstitial volume fractions.^{19–23} For direct imaging of angiogenesis related molecules, various endothelial targets can be successfully visualized, including VEGF and the $\alpha_v\beta_3$ integrin (see above). The $\alpha_v\beta_3$ integrin receptor, for example, is upregulated in angiogenic endothelium, and has been imaged using Arg-Gly-Asp containing peptidic linkers which exhibit a high affinity for integrins.^{24,25} E-selectin is another potential angiogenesis-related target that can be imaged by appropriate affinity ligands. Other factors that are related to or trigger angiogenesis include the hypoxia inducible factor 1 (HIF-1; see below) that induces the expression of VEGF. VEGF in turn causes an increase in vessel leakiness, extravasation of plasma proteins, and activation of the coagulation cascade, which leads to an alteration of the extracellular matrix, making it supportive of endothelial

and tumor cell invasion. Migration and invasion of cells requires the degradation of components of the extracellular matrix, which is triggered by a cascade of enzymes (e.g. matrix metalloproteinases and cathepsins), and finally the establishment of new cell adhesion contacts mediated by integrins.

Imaging of proliferation

The nucleoside thymidine (e.g. labeled with ¹¹C) as well as [¹²⁴I] iododeoxyuridine has been successfully applied to monitor tumor cell proliferation and response to tumor treatment.^{26–28} ¹⁸F-labeled thymidines include 3'-deoxy-3'-fluorothymidine (FLT). FLT is trapped intracellularly in a manner analogous to FDG, since following initial phosphorylation by thymidine kinase the resulting monophosphate cannot be incorporated into DNA due to lack of a hydroxyl group. In general, FLT provides complementary information to FDG imaging, showing a good correlation with histological markers for tumor proliferation.²⁹ FLT may substantially improve the sensitivity of assessing treatment response in cancers, since responding tumor cells may continue to metabolize FDG but stop synthesizing DNA (and thus stop accumulating FLT).

Moreover, molecules that are involved in cell cycle regulation and thus trigger tumor growth can be imaged. The estrogen receptor is one prominent example that can be monitored, e.g. by ¹⁸F-labeled estrogens (FES).³⁰ FES estrogen receptor (ER) imaging has been validated and tested in preliminary patient studies as a tool for measuring ER expression and a predictive assay for hormonal therapy.¹⁰ Likewise, the androgen receptor can be successfully targeted by [¹⁸F] fluoro-5-dihydrotestosterone (FDHT). FDHT-PET is feasible in patients with advanced prostate cancer with testosterone levels that are in the castrate range. Recent data suggest that FDHT may be a valuable tracer to study prostate cancer biology and to determine the treatment efficacy of receptor blockage in these patients.³¹

Tyrosine kinases (TKs) represent another highly relevant class of oncological targets that regulate most of the signal transduction in eukaryotic cells and control many processes in cancer cells, including metabolism, transcription, cell-cycle progression, cytoskeletal rearrangement and cell movement, apoptosis, and differentiation.^{32,33} There are more than 90 known protein kinase genes in the human genome: 58 encode transmembrane receptor TKs distributed into 20 subfamilies, and 32 encode cytoplasmatic, non-receptor TKs in ten subfamilies. The epidermal growth factor receptor (EGFR) is a transmembrane receptor of TK of the erbB (also known as HER) family that is abnormally activated in many epithelial tumors³³ and has been targeted both therapeutically and diagnostically with good success.^{33,34}

Imaging of apoptosis

Cancer is as much a failure of apoptosis as it is a result of unchecked proliferation.³⁵ Apoptosis also plays a significant role in cancer response to therapy. Programmed cell death pathways, many of which are p53 dependent, are triggered when tumor cells detect damaged DNA. These pathways lead to the activation of effector caspases that trigger a proteolytic cascade resulting in a fragmentation of intracellular components.³⁶ One of the earliest effects of caspase activation is disruption of the translocase system that normally maintains phosphatidylserine on the interior of the cell membrane. Together with an upregulation of the scramblase activity, a redistribution of phosphatidylserine to the outer membrane leaflet occurs, serving as a signal of digestion by phagocytic cells.³⁷ Annexin 5 is a 36-kDa protein that binds with high affinity to externalized phosphatidylserine and has been successfully applied for scintigraphic, optical, and magnetic resonance (MR)-based imaging of apoptotic events. Apoptosis imaging probes could potentially be applied in the evaluation of cancer therapies, particularly in lymphoma and leukemia.^{38,39}

Imaging of hypoxia

Hypoxia may result from unregulated cell growth, but is also a common attribute of the tumor phenotype and may even be a factor in tumorigenesis. Hypoxia enhances the expression of endothelial cytokines such as VEGF, interleukin-1, tumor necrosis factor α , and transforming growth receptor β , and a cellular O₂ sensing mechanism triggers the production of hypoxia inducible factor 1 (HIF-1). HIF-1 initiates a cascade of events resulting in angiogenesis (see above). Hypoxia promotes radioresistance of tumors as well as chemoresistance through various mechanisms. Hypoxia impedes drug delivery to tumors, slows cellular proliferation, and induces gene expression changes that enable cellular rescue from severe damage.¹⁰

Derivatives of misonidazole, hypoxic cell sensitizer which binds covalently to intracellular molecules at a rate inversely proportional to the intracellular O₂ concentration, have successfully been developed for PET imaging of tumor hypoxia.⁴⁰ Because hypoxia is associated with poor response to both radiation and chemotherapy, identifying hypoxia should have prognostic value.¹⁰

References

1. Feindegen LE, Shreeve WW, Eckelman WC, Wagner HNJ. *Molecular Nuclear Medicine—The Challenge of Genomics and Proteomics to Clinical Practice*. Berlin: Springer-Verlag, 2003.
2. Wagner S, Kopka K, Law M et al. Synthesis and first in vivo evaluation of new selective high affinity β 1-adrenoceptor radioligands for SPECT based in ICI 89,406. *Bioorg Med Chem* 2004; 12: 4117–32.
3. Schäfers M, Riemann B, Kopka K et al. Scintigraphic imaging of matrix metalloproteinase activity in the arterial wall in vivo. *Circulation* 2004; 109: 2554–9.
4. Bremer C, Tung CH, Weissleder R. In vivo molecular target assessment of matrix metalloproteinase inhibition. *Nat Med* 2001; 7: 743–8.
5. Weissleder R, Tung CH, Mahmood U, Bogdanov A Jr. In vivo imaging of tumors with protease-activated near-infrared fluorescent probes. *Nat Biotechnol* 1999; 17: 375–8.
6. Weissleder R, Mahmood U. Molecular imaging. *Radiology* 2001; 219: 316–33.
7. Koukouraki S, Strauss LG, Georgoulas V et al. Comparison of the pharmacokinetics of (68)Ga-DOTATOC and [(18)F]FDG in patients with metastatic neuroendocrine tumours scheduled for (90)Y-DOTATOC therapy. *Eur J Nucl Med Mol Imaging* 2006; 33: 1115–22.
8. Meisetschlager G, Poethko T, Stahl A et al. Gluc-Lys([18F]FP)-TOCA PET in patients with SSTR-positive tumors: biodistribution and diagnostic evaluation compared with [111In]DTPA-octreotide. *J Nucl Med* 2006; 47: 566–73.
9. Bombardieri E, Seregini E, Villano C, Chiti A, Bajetta E. Position of nuclear medicine techniques in the diagnostic work-up of neuroendocrine tumors. *Q J Nucl Med Mol Imaging* 2004; 48: 150–63.
10. Kelloff GJ, Krohn KA, Larson SM et al. The progress and promise of molecular imaging probes in oncologic drug development. *Clin Cancer Res* 2005; 11: 7967–85.
11. Dowell J, Minna JD, Kirkpatrick P. Erlotinib hydrochloride. *Nat Rev Drug Discov* 2005; 4: 13–14.
12. Kane RC, Bross PF, Farrell AT, Pazdur R. Velcade: US FDA approval for the treatment of multiple myeloma progressing on prior therapy. *Oncologist* 2003; 8: 508–13.
13. Cunningham D, Humblet Y, Siena S et al. Cetuximab monotherapy and cetuximab plus irinotecan in irinotecan-refractory metastatic colorectal cancer. *N Engl J Med* 2004; 351: 337–45.
14. Cohen MH, Johnson JR, Li N, Chen G, Pazdur R. Approval summary: letrozole in the treatment of postmenopausal women with advanced breast cancer. *Clin Cancer Res* 2002; 8: 665–9.
15. Folkman J. Role of angiogenesis in tumor growth and metastasis. *Semin Oncol* 2002; 29 (6 Suppl 16): 15–18.
16. Abramovitch R, Dafni H, Smouha E, Benjamin LE, Neeman M. In vivo prediction of vascular susceptibility to vascular susceptibility endothelial growth factor withdrawal: magnetic resonance imaging of C6 rat glioma in nude mice. *Cancer Res* 1999; 59: 5012–16.
17. Cavallaro U, Liebner S, Dejana E. Endothelial cadherins and tumor angiogenesis. *Exp Cell Res* 2006; 312: 659–67.
18. Baluk P, Hashizume H, McDonald DM. Cellular abnormalities of blood vessels as targets in cancer. *Curr Opin Genet Dev* 2005; 15: 102–11.
19. Brasch RC, Li KC, Husband JE et al. In vivo monitoring of tumor angiogenesis with MR imaging. *Acad Radiol* 2000; 7: 812–23.

20. Bremer C, Mustafa M, Bogdanov A Jr et al. Steady-state blood volume measurements in experimental tumors with different angiogenic burdens – a study in mice. *Radiology* 2003; 226: 214–20.
21. Turetschek K, Roberts TP, Floyd E et al. Tumor microvascular characterization using ultrasmall superparamagnetic iron oxide particles (USPIO) in an experimental breast cancer model. *J Magn Reson Imaging* 2001; 13: 882–8.
22. Boellaard R, Knaapen P, Rijbroek A, Luurtsema GJ, Lammertsma AA. Evaluation of basis function and linear least squares methods for generating parametric blood flow images using 15O-water and Positron Emission Tomography. *Mol Imaging Biol* 2005; 7: 273–85.
23. Bruehlmeier M, Roelcke U, Schubiger PA, Ametamey SM. Assessment of hypoxia and perfusion in human brain tumors using PET with 18F-fluoromisonidazole and 15O-H₂O. *J Nucl Med* 2004; 45: 1851–9.
24. Chen X, Park R, Shahinian AH et al. 18F-labeled RGD peptide: initial evaluation for imaging brain tumor angiogenesis. *Nucl Med Biol* 2004; 31: 179–89.
25. Pasqualini R, Koivunen E, Ruoslahti E. Alpha v integrins as receptors for tumor targeting by circulating ligands. *Nat Biotechnol* 1997; 15: 542–6.
26. Blasberg RG, Roelcke U, Weinreich R et al. Imaging brain tumor proliferative activity with [124I]iododeoxyuridine. *Cancer Res* 2000; 60: 624–35.
27. Carnochan P, Brooks R. Radiolabelled 5'-iodo-2'-deoxyuridine: a promising alternative to [18F]-2-fluoro-2-deoxy-D-glucose for PET studies of early response to anticancer treatment. *Nucl Med Biol* 1999; 26: 667–72.
28. Wells P, Aboagye E, Gunn RN et al. 2-[11C]thymidine positron emission tomography as an indicator of thymidylate synthase inhibition in patients treated with AG337. *J Natl Cancer Inst* 2003; 95: 675–82.
29. Pinder SE, Wencyk P, Sibbering DM et al. Assessment of the new proliferation marker MIB1 in breast carcinoma using image analysis: associations with other prognostic factors and survival. *Br J Cancer* 1995; 71: 146–9.
30. Katzenellenbogen JA, Welch MJ, Dehdashti F. The development of estrogen and progestin radiopharmaceuticals for imaging breast cancer. *Anticancer Res* 1997; 17: 1573–6.
31. Dehdashti F, Picus J, Michalski JM et al. Positron tomographic assessment of androgen receptors in prostatic carcinoma. *Eur J Nucl Med Mol Imaging* 2005; 32: 344–50.
32. Manning G, Whyte DB, Martinez R, Hunter T, Sudarsanam S. The protein kinase complement of the human genome. *Science* 2002; 298: 1912–34.
33. Baselga J, Arteaga CL. Critical update and emerging trends in epidermal growth factor receptor targeting in cancer. *J Clin Oncol* 2005; 23: 2445–59.
34. Ke S, Wen X, Gurfinkel M et al. Near-infrared optical imaging of epidermal growth factor receptor in breast cancer xenografts. *Cancer Res* 2003; 63: 7870–5.
35. Hajra KM, Liu JR. Apoptosome dysfunction in human cancer. *Apoptosis* 2004; 9: 691–704.
36. Kelloff GJ, Hoffman JM, Johnson B et al. Progress and promise of FDG-PET imaging for cancer patient management and oncologic drug development. *Clin Cancer Res* 2005; 11: 2785–808.
37. Schlegel RA, Williamson P. Phosphatidylserine, a death knell. *Cell Death Differ* 2001; 8: 551–63.
38. Lahorte CM, Vanderheyden JL, Steinmetz N et al. Apoptosis-detecting radioligands: current state of the art and future perspectives. *Eur J Nucl Med Mol Imaging* 2004; 31: 887–919.
39. Reed JC, Pellicchia M. Apoptosis-based therapies for hematologic malignancies. *Blood* 2005; 106: 408–18.
40. Rasey JS, Hofstrand PD, Chin LK, Tewson TJ. Characterization of [18F]fluoroetanidazole, a new radiopharmaceutical for detecting tumor hypoxia. *J Nucl Med* 1999; 40: 1072–9.

Primary brain tumors

Eva Orunesu, Andreas Jacobs, Andrea Falini, Angelo Del Sole, and Giovanni Lucignani

Background

Cancerous transformation entails major biochemical changes including modifications of the energy metabolism of the cell, e.g. utilization of glucose and other substrates, protein synthesis, and expression of receptors and antigens. Tumor growth also leads to heterogeneity in blood flow owing to focal necrosis, angiogenesis, and metabolic demands, as well as disruption of transport mechanisms of substrates across cell membranes and other physiological boundaries such as the blood–brain barrier. These biochemical and histological changes, along with their macroscopic anatomical effects, can be assessed with different non-invasive imaging tools, such as X-ray computed tomography (CT), magnetic resonance imaging (MRI), magnetic resonance spectroscopy (MRS), positron emission tomography (PET), and single photon emission computed tomography (SPECT). Whereas anatomical imaging (i.e. CT and MRI) is aimed at defining the size and exact localization of brain tumors, along with the assessment of invasion of surrounding structures, functional imaging (MRS, PET, SPECT) is better suited for characterization of the biological properties. The identification of a tumoral mass and the assessment of its size and vascularization are best achieved with CT and MRI, while functional imaging can provide additional information that is crucial for tumor classification, differential diagnosis, and follow-up.¹

Classification and epidemiology

Intracranial brain neoplasms can be classified into primary brain neoplasms and metastatic tumors. Primary brain tumors may arise from various cell types of the brain, including glial cells, neurons, neuroglial precursor cells, pinealocytes, the meninges, choroid plexus, pericytes of the vessels, cells of the hypophysis, and lymphocytes. Brain metastases are more common than primary brain tumors, since lung neoplasms, as well as breast, gastrointestinal and

genitourinary tumors, and melanomas frequently give rise to a metastatic tumor in the central nervous system (CNS).

The incidence of primary brain tumors varies between subtypes. Incidence rates of all primary non-malignant and malignant brain and central nervous system tumors published by the Central Brain Tumor Registry of the United States (CBTRUS) for the year 2000 are 14.8 cases per 100 000 person-years (7.4 per 100 000 person-years for benign and borderline tumors and 7.4 per 100 000 person-years for malignant tumors).² These incidence rates are substantially similar to those from other institutions, including the International Agency for Research on Cancer (IARC) (<http://www-dep.iarc.fr>). Considering all tumors (benign and malignant), the rate is higher in females, but malignant tumors show slight predominance in males. In other words males have a 0.65% and females a 0.50% lifetime risk of being diagnosed with a primary malignant brain/central nervous system tumor. Pediatric incidence (ages 0–19) is 4.3 cases per 100 000 person-years.

Despite aggressive multimodal treatment strategies (surgery, radiation, chemotherapy), median survival of patients with gliomas is limited, depending on the grade and age at diagnosis, varying from 1 year for glioblastoma, to 2–3 years for grade 3 and to 5–10 years for a grade 2 glioma. Overall, the 5-year relative survival rate following diagnosis of a primary malignant brain and central nervous system tumor decreases with age, from 64.8% (ages 0–19) to 23.1% (ages 45–54) and 4.8% (over 75).

In adults, about two-thirds of brain tumors arise from supratentorial structures, while in children about two-thirds of brain tumors are infratentorial. Over one-half of brain neoplasms are metastases from tumors outside the CNS, and involve the skull or any intracranial structure.

The most frequent primary brain tumors in adults are gliomas, accounting for over 90% of primary brain tumors in patients older than 20 years and for more than 60% of all intracranial brain tumors in all patients.¹ Their incidence is 5–10 per 100 000 in the general population. Gliomas are divided histologically into astrocytomas, oligodendrogliomas, mixed gliomas, ependymal tumors, and tumors of the choroid plexus. Grading is performed according to World

Health Organization (WHO) criteria, taking into account the presence of nuclear changes, mitotic activity, endothelial proliferation, and necrosis. The most frequent (65%) and most malignant histological subtype of glioma in adults is the glioblastoma, with a peak incidence in the seventh decade and survival of less than 2 years for most patients. Even in low-grade astrocytomas, 5-year survival is only 30% due to malignant progression. If we consider glioma subtypes as distinct entities, the single most frequent brain tumor in adults is not glioma but meningioma. Decreasing frequencies are reported for pituitary adenomas, schwannomas, congenital tumors, and others.

In children, the most common brain tumors are low-grade gliomas, mostly the pilocytic astrocytoma and the benign cerebellar astrocytoma. Other frequent brain tumors are the medulloblastoma (the most common pediatric malignant brain tumor), the ependymoma (which grows into the brain ventricles), and brainstem glioma. They occur more often between the 4th and 11th years of life, rarely below the first year.

Metastatic brain tumors are more frequent than primary ones. Up to 15% of cancer patients may have metastatic spread into the brain, and the incidence of brain metastasis increases as cancer patients live longer. The most common primary cancers metastasizing to the brain are lung cancer (50%), breast cancer (15–20%), unknown primary cancer (10–15%), melanoma (10%), and colon cancer (5%).⁴ Eighty percent of brain metastases are localized in the cerebral hemispheres, 15% occur in the cerebellum, and 5% in the brainstem.³ For diagnostic purposes it is important to consider that in over 70% of cases there are multiple brain metastases at the time of diagnosis, but solitary metastases may also occur.⁴ It is important to avoid the mistake of considering an intracranial tumor a metastasis just because the patient has had previous cancer; in this case a correct diagnosis and appropriate treatment could be missed. Brain involvement can occur with cancers of the nasopharyngeal region by direct extension along the cranial nerves or through the foramina at the base of the skull.

Brain tumors are named after the brain cell type they histologically appear most similar to. This does not mean that the tumor originates from the type of cell it is named after. Certain tumors are composed of cells that are so undifferentiated that no similarity to a histological category can be determined, such as glioblastoma cells.⁵ In general, the malignancy grade of the tumor is based on nuclear atypia, number of mitoses, vascular proliferation, and foci of necrosis, but specific differences between the different tumor types must be considered. The commonly applied terminology follows the rules of the WHO classification published in 2002,⁶ consisting of classification of the malignancy grade of brain tumors into four different grades, from the least aggressive (grade 1) to the most malignant (grade 4).

The three main categories of gliomas are astrocytomas, oligodendrogliomas, and mixed oligoastrocytomas.

Astrocytomas can then be graded according to their histological malignancy grade into the four WHO grades, while oligodendrogliomas and mixed oligoastrocytomas are graded only into two grades, although a reassessment of this classification is in progress, concerning the grading criteria with the possible addition of a grade 4 oligodendroglioma, a subclass of glioblastoma with an oligodendroglial component.^{7,8} Even low-grade tumors are infiltrative, with a marked potential to increase the malignancy grade over time.

The only WHO grade 1 tumor is the pilocytic astrocytoma, which occurs mainly in children and can be located in the posterior fossa (cerebellum and brainstem), hypothalamus, basal ganglia, or optic tracts (often associated with neurofibromatosis type 1). It is characterized by a slow growth rate with good prognosis and a long-term survival.

Grade 2 gliomas include the diffuse astrocytoma, the oligodendroglioma and the oligoastrocytoma. Most low-grade gliomas affect young adults, the incidence slowly increasing from birth up to 40 years of age, with a subsequent decrease.

Most oligodendrogliomas are low-grade; the malignant form represents only 20% of cases. Approximately one-third of patients survive for 5 years after diagnosis. Like most slowly growing brain tumors, low-grade gliomas usually present with partial or generalized seizures. Usually they develop over a year-long silent period with slow subclinical progression, followed either by diffuse spread of the tumor throughout one or both hemispheres or by malignant transformation into grade 3 or 4 gliomas.⁷

The most frequent grade 3 and 4 gliomas are the anaplastic astrocytoma (WHO grade 3) and the glioblastoma (WHO grade 4), which account for more than half of all astrocytomas after the age of 60, with survival less than 2 years for most patients. The peak age of incidence is the fifth decade for the anaplastic astrocytoma and the sixth decade for the glioblastoma. Typically these tumors, although highly malignant, do not spread beyond the CNS. Despite most modern therapy approaches, these tumors virtually always recur, usually arising within 2 cm of surgical resection margins. Treatment of these tumors is palliative, and must be individually tailored through a multidisciplinary approach to preserve or restore the highest possible quality of life for as long as possible. There are no strict guidelines for the timing of treatment options. External radiation therapy seems to slightly improve survival in these patients. A recent large randomized phase-3 study, including 573 glioblastoma patients, has shown that the addition of the alkylating drug temozolomide to radiotherapy as initial treatment prolongs the 2-year survival rate from 10.4% to 26.5% in patients with glioblastoma.⁹ Large efforts are aimed at identifying molecular markers predictive of treatment response. This may, in the future, permit the selection of a particular treatment based on specific molecular features of the tumor. Molecular tumor profiles may also allow identification of novel and promising treatment targets for malignant gliomas.¹⁰

The anaplastic oligodendroglioma which arises either from a lower grade oligodendroglioma or de novo is well known to be chemosensitive, in contrast to malignant astrocytomas.¹¹ Several subgroups of patients with different response rates for chemotherapy can be differentiated through genetic analysis.^{7,12,13}

Meningiomas are not strictly brain tumors, as they occur outside the brain, in the meninges. Nevertheless they grow inside the cranial cavity and present some of the features of brain tumors. Meningiomas arise especially in areas of arachnoid villi, mostly along the sagittal sinus, over the cerebral convexity, at the base of the skull, and in the parasellar regions. They are mostly asymptomatic and discovered accidentally, but constitute approximately 30% of all brain neoplasms. The median age at diagnosis is 64 years, and the female to male ratio is almost 2:1. Slow, progressive enlargement of the tumor leads to focal or generalized seizure disorders or neurological deficits caused by compression of adjacent neural tissue.¹⁴ Most of these tumors present with histological well-differentiated tissue, low proliferative capacity, limited invasiveness, and good long-term prognosis after surgical treatment. Ninety percent of meningiomas are classified as benign, 6% atypical, and 2–4% malignant. There is increased incidence of meningiomas in patients with breast cancer, for which a hormonal relationship has been proposed.¹⁵ All meningiomas show loss of chromosome 22q, a feature common to neurofibromatosis type 2. In fact, neurofibromatosis type 2 is often associated with multiple meningiomas.¹⁶

Adenomas of the pituitary gland are often composed of well differentiated cells that produce anterior pituitary hormones, which can cause syndromes of hormone excess as in acromegaly and gigantism for growth hormone-, galactorrhea for prolactin-, and Cushing's syndrome for adrenocorticotrophic hormone-producing tumors. They can also be non-secreting, and all can cause hormonal imbalances or other symptoms due to the compression of surrounding structures, such as hormonal deficiencies and visual problems due to compression of the optic chiasm. Aids to diagnosis are plasma hormone measurements in addition to MRI of the sella turcica. Pituitary adenomas are typically divided on the basis of their size into 'microadenomas' when their size is below 10 mm in diameter and 'macroadenomas' when they are bigger. Nearly all of these tumors are benign. Life expectancy is normal if complete surgical removal is achieved and the subsequent hormone deficiency is corrected by drugs.

Primary central nervous system lymphoma is a rare form of extranodal non-Hodgkin's lymphoma that is confined to the CNS and the eye.¹⁷ In immunocompromised patients, the incidence is several thousand-fold higher than the baseline rate in the general population, namely about 5 per 1000 person-years among patients with acquired immunodeficiency syndrome (AIDS) and 0.3 per 100 000 person-years in the immunocompetent population.^{7,18}

The incidence rate is low in children and rises steadily with age, reaching its maximum in the seventh and eighth decades. In the immunocompetent subject the tumor is often localized in the subcortical region and is multifocal in 40% of cases.¹⁹ The tumor is characterized by the tendency to spread diffusely throughout the CNS and to the eye; therefore, surgical excision is not considered useful as in other brain tumors. Nevertheless, diagnostic surgery or stereotactic biopsy are necessary to establish a histological diagnosis, showing in almost all cases a malignant large-cell diffuse B-cell lymphoma that expresses pan-B cell markers such as CD20. These tumors are sometimes called 'ghost tumors' because of spontaneous or steroid-induced regression of the mass.⁷ As a consequence, administration of steroids prior to diagnostic procedures such as imaging procedures or biopsy with histological evaluation should be avoided.

Primary brain tumors are the most frequent neoplastic disease in children after leukemia. In children, up to 50% of brain tumors are located in the infratentorial region; this region is rarely affected by brain neoplasms in adults. In general, tumors in infants and children tend to show high variability and low specificity of clinical symptoms. General symptoms of rising intracranial pressure such as irritability, reduced alertness, vomiting, failure to grow, and progressive macrocephaly can be observed in infants; older children can sometimes show focal symptoms, but it is not the rule.²⁰ The three most common brain tumors in children are the pilocytic astrocytoma (21%), the medulloblastoma (17%), and the diffuse low-grade cerebellar astrocytoma (9%).

The medulloblastoma is an infratentorial primitive neuroectodermal tumor that shows local invasiveness, subarachnoid dissemination, and extraneural metastases. Its frequency decreases from the first decade by approximately halving every decade. The 5-year disease-free survival for medulloblastoma is variable, with an average of approximately 50%. Increased risk of recurrence is mainly determined by the presence of metastases, age below 4 years, and extensive residual disease after surgery. In addition to surgical resection, treatment is based on craniospinal radiotherapy to prevent leptomeningeal dissemination through cerebrospinal fluid. Chemotherapy is added to radiotherapy in selected cases.²⁰

Ependymomas are commonly diagnosed in children under 4 years of age, but they occur also in adults at any age. They usually arise in the ependymal lining of the ventricles and may occur anywhere within the CNS. Most frequently they lie within the posterior fossa arising from the lining of the fourth ventricle or cerebellopontine angle, but they may also arise in the filum terminale and the central spinal canal. Advances in neuroimaging, neurosurgery, and radiation therapy have improved disease control and functional outcomes for children with ependymoma, including children under the age of 3 years.²¹ Supratentorial ependymomas are often larger and have a cystic component. The 5-year survival rate depends on the histopathological

grading, being 87% for low-grade tumors and 27% for high-grade tumors, and localization: 97% for tumors of the spine, 68% for infratentorial tumors, and 62% for supratentorial tumors.²²

Other primary brain tumors in children include choroid plexus papilloma and carcinoma. They are rare tumors which arise from the cerebral spinal fluid (CSF) producing neuroepithelial tissue. Almost half of these tumors occur under 12 years of age, and represent 2–4% of all pediatric brain tumors. The choroid plexus papilloma is the most common brain tumor in children less than 1 year of age. Most of these tumors are located in the lateral ventricles, less often in the fourth and rarely the third ventricle. Because papillomas tend to grow slowly within ventricles, they expand to fill the ventricle and block CSF flow. When a complete surgical resection can be achieved, the prognosis of choroid plexus papilloma is good, in contrast to the choroid plexus carcinoma which has an extremely poor prognosis.²³

Molecular basis of brain tumorigenesis

Understanding glial tumorigenesis is crucial for the development of molecular therapeutic targets to overcome current therapeutic limitations. Molecular changes are the basis of dysregulation of the cell cycle, alterations of apoptosis and cell differentiation, neovascularization, and tumor cell migration and invasion into the brain parenchyma. Genetic alterations which play an important role in glioma development include a loss, mutation, or hypermethylation of the tumor suppressor gene TP53 or other genes involved in the regulation of the cell cycle, such as cyclin-dependent kinase N2A/p16, p14ARF, and primitive neuroectodermal tumor (PTEN), as well as activation or amplification of oncogenes and growth factors and/or their receptors, such as MDM2, cyclin-dependent kinase 4, cyclin D1 and D3, epidermal growth factor receptor (EGFR), vascular endothelial growth factor (VEGF), PDGFR (platelet-derived growth factor (PDGF) receptor), and transforming growth factor β .^{24–26} During progression from low-grade astrocytoma (WHO grade 2) to anaplastic astrocytoma (WHO grade 3) and to glioblastoma multiforme (WHO grade 4), a step-wise accumulation of genetic alterations occurs. Whereas TP53 mutation and PDGF and PDGFR- α overexpression represent early changes during low-grade glioma development, progression to anaplastic astrocytoma is associated with pRb (retinoblastoma protein) alteration and loss of heterozygosity (LOH) of 19q, further malignant progression to glioblastoma including LOH 10q, and mutations of the PTEN gene.²⁷ These secondary glioblastomas, which develop from better differentiated

astrocytomas, can be distinguished from primary de novo glioblastomas on the basis of molecular genetic findings,²⁸ with amplification and/or overexpression of the EGFR, p16 deletion, PTEN mutation, pRb alteration, and LOH 10p and 10q associated with primary glioblastoma. Most important, molecular alterations have been identified which indicate the therapeutic response of patients and, thus, are prognostically relevant: anaplastic oligodendrogliomas with LOH 1p and/or LOH 19q are characteristically sensitive to PCV (procarbazine, lomustine, vincristine) chemotherapy, and patients' survival is significantly prolonged.^{12,29–31}

Diagnostic modalities

The goals of diagnostic procedures in brain oncology include: primary diagnosis, ideally obviating the need for stereotactic biopsy; planning of stereotactic biopsy and surgical resection; radiation therapy planning for target volume definition; evaluation for chemotherapy in selected cases as well as experimental therapies; and re-evaluation after treatment.

When clinical signs and symptoms lead to the suspicion of a brain tumor, the differential diagnosis includes a number of non-oncologic causes of expanding intracranial lesions such as granulomas, paracystic cysts, abscesses, hemorrhages (intracerebral, extradural, or subdural), or aneurysms.

The first diagnostic evaluation is based on neuroradiologic imaging, and when the diagnosis of brain tumor is highly suspicious, it is necessary to characterize the type of tumor and its grade of malignancy, as the morphologic imaging alone is not specific enough to give full comprehension of brain lesions. The gold standard for diagnosis is histopathological evaluation, which requires the use of tissue sampling, either surgically or by stereotactic biopsy, both of which are invasive procedures. However, because of tumor heterogeneity, even biopsy does not always hit the site of highest malignancy, which should best define the grade of the tumor. Hence the histological evaluation yields a 'minimum grading' which is not always the real grade of the tumor.⁵ Non-invasive functional imaging techniques can then be applied with the aim of characterizing more subtle tissue differences and enable successful targeting of the biopsy to the site of highest malignancy.

Most clinical manifestations of tumors located in the brain parenchyma are due to the 'mass effect' of the growing tumor and the consequence of non-specific events such as increased intracranial pressure, edema, and shift and destruction of surrounding brain tissue. There is a tendency for slowly growing tumors to cause partial or generalized seizures, especially if they are located in the cortex (as often observed in low-grade gliomas). Rapidly growing tumors tend to cause symptoms of progressively rising intracranial pressure, which results from the growing

tumor mass itself, from cerebral edema, or from obstructed cerebrospinal fluid flow. These symptoms are headache, nausea, vomiting, drowsiness, and visual abnormalities. Other symptoms are focal neurological deficits, which can show the localization of the tumor. Mental status changes, such as memory loss and decreased alertness, can be associated with tumors of the frontal lobe, diffuse meningeal spread, or diffuse brain infiltration.⁷

Unfortunately, as mentioned above, tumor misclassification can occur with morphologic imaging techniques. The first crucial step to achieving correct diagnosis through histological evaluation is to target the biopsy to the most malignant region within the tumor. Especially gliomas can be regionally extremely heterogeneous, so biopsy-targeting is of crucial importance for a correct grading of the tumor and for subsequent management planning, otherwise sampling errors may lead to malignancy-grade underestimation. Furthermore, low-grade gliomas have the tendency to infiltrate throughout the brain parenchyma and to increase malignancy grade over time, so again exact sampling of the site of highest malignancy is crucial.⁷ For correct biopsy-targeting, the ideal imaging procedure would design a precise map of regional malignancy within the tumor. Thus, if such a technique was sufficiently sensitive and specific, it could allow a non-invasive diagnosis obviating the need for biopsic sampling prior to surgical intervention. Nevertheless, mostly for gliomas, in addition to the problem of correct sampling there is another frequent source of error, namely the poor within- and between-observer reproducibility in the morphological classification of glioma subclasses, especially for differentiating astrocytic from oligodendroglial tumors or identification of anaplastic astrocytomas.^{31,32}

Detection of a brain lesion is the first diagnostic step in patients with symptoms and signs suggesting the presence of a brain tumor. Imaging is primarily done to prove or rule out the presence of such a lesion. To this end, both direct and indirect signs are sought. A direct sign of a brain tumor is an area with a density (CT) or signal (MRI) different from that of normal cerebral tissue, including changes secondary to contrast media infusion. Such changes in density or signal occur secondary to the structural features of neoplasms.

X-ray computed tomography, magnetic resonance imaging and magnetic resonance spectroscopy

For many years, X-ray CT with contrast enhancement has been the gold standard for the diagnosis of brain tumors due to its ability to ascertain the presence of a brain lesion, to define its dimension and relation with surrounding

brain structures, to assess perilesional edema, and to define the presence of multiple brain lesions. Most tumors are characterized by contrast enhancement; the increased accumulation of contrast results primarily from the leakage of contrast into the tumor's interstitium because of the absence of a blood-brain barrier in the blood vessels derived from tumor neoangiogenesis. The region of contrast-enhancement corresponds to the main tumor mass; however, malignant tumor cells are commonly found beyond the contrast-enhanced region, particularly in gliomas. X-ray CT is superior to MRI for detecting calcification, skull lesions, and hyperacute hemorrhage (bleeding less than 24 hours old), and helps in direct differential diagnosis as well as immediate management. On the other hand, it is less sensitive than MRI in some brain regions, namely those near bony areas of irregular shape, such as the posterior fossa and the floor of the middle fossa, due to the presence of beam-hardening artifacts. Nevertheless, the X-ray CT depiction of bone structures is valuable for defining bone destruction or sclerosis associated with metastatic tumors, pituitary adenomas, meningiomas or carcinomas from the sinuses or pharynx, and for studying lesions with calcific components or localized close to bone structures. The use of multislice high speed X-ray CT is desirable for evaluating clinically unstable patients in whom motion would result in degraded MR images due to artifacts. Contrast-enhanced X-ray CT allows us to detect any blood-brain barrier disruption which occurs in most brain tumors, but also in many neurological disorders including acute stroke, inflammatory, infectious cerebral diseases, and multiple sclerosis. X-ray CT can also miss non-enhancing tumors such as low-grade gliomas.³³

Continuous developments in MRI provide new insights into the diagnosis, classification, and understanding of the biology of brain tumors. MRI offers several advantages as compared to X-ray CT. MRI studies are characterized by higher contrast resolution associated with multiplanarity. MRI is characterized by high sensitivity for structural alterations caused by tumoral growth, also in brain regions that are poorly assessed by X-ray CT, such as the infratentorial, sellar, temporal, and meningeal regions. The already high sensitivity for structural alterations can be further enhanced by the use of paramagnetic contrast agents. For these reasons, MRI is the procedure of choice for the primary diagnosis of all types of brain tumor.³³ Standard T₁- and T₂-weighted MRI acquisitions display high sensitivity for brain tumors and give information on the size and localization of the tumor.³⁴ MRI is characterized by high soft-tissue resolution, and it allows the detection with high definition of lesions that are isodense on X-ray CT, tumor enhancement, and secondary concurrent alterations such as edema, mass effects, signs of intracranial pressure, all phases of hemorrhagic states (except hyperacute), and necrosis. MRI is also the procedure of choice in the evaluation of intramedullary and extramedullary spinal cord lesions.

A normal contrast-enhanced MRI scan essentially rules out the possibility of a brain tumor.

There are several available MRI acquisition parameters: T_1 -, T_2 -, proton density-, diffusion-, and perfusion-weighted images, as well as fluid attenuated inversion recovery (FLAIR). They display characteristic patterns depending on tumor type and grade. Usually most brain tumors are hypointense on T_1 -weighted images and hyperintense on FLAIR and T_2 -weighted images (unless fat or hemorrhage is present (Figure 3.1)). In highly proliferative brain tumors, such as the glioblastoma, the blood–brain barrier is often disrupted, resulting in leakage of contrast media, visible in gadolinium-enhanced T_1 images and contrast-enhanced X-ray CT. On plain images, without contrast agent, the margins of gliomas are ill defined. Gliomas tend to spread to the opposite hemisphere along the white matter through the corpus callosum. Due to their fast proliferation, high-grade gliomas such as the glioblastoma often display central necrotic areas, fluid, and hemorrhage;

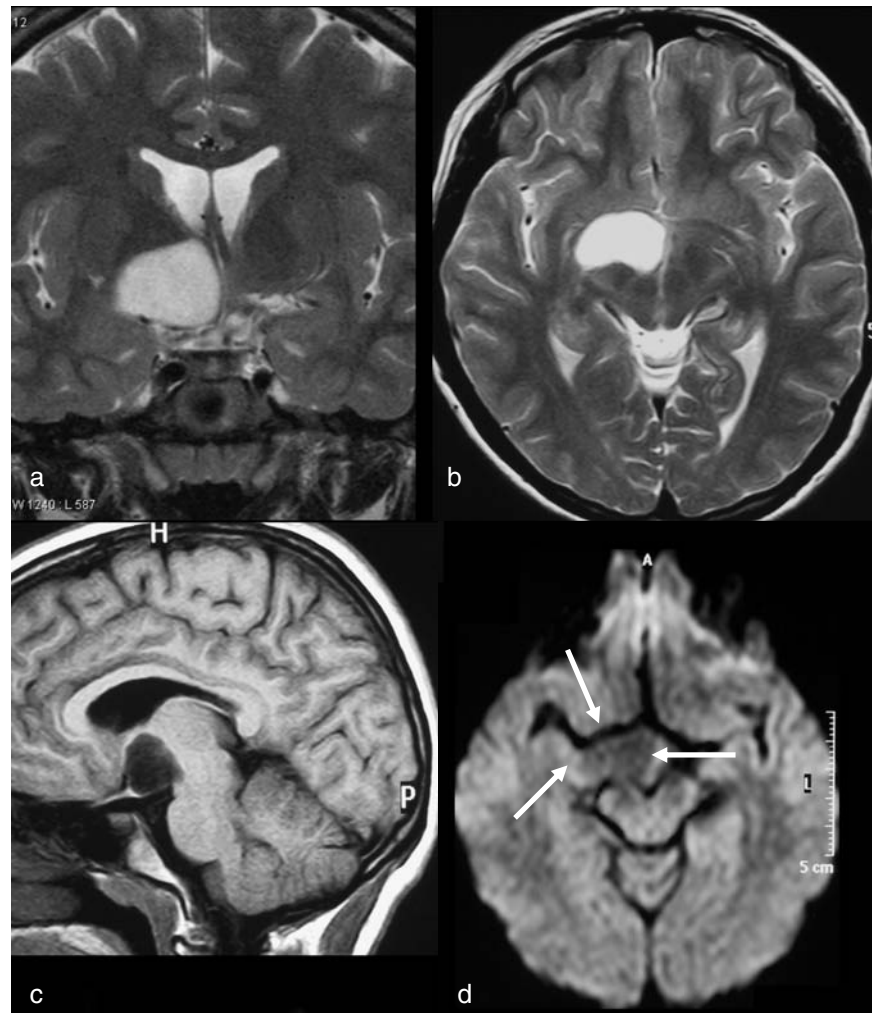
the fast expansion leads to mass effect and peritumoral edema. Lower grade gliomas can have large cystic components; they are usually more homogeneous without central necrosis.

Three main variables differentiate tumors from normal tissue: water content, regressive events, and vascular architecture.

Most types of brain tumor typically exhibit an increased water content due to the high cellularity. Changes are more pronounced in those lesions having a low nucleus/cytoplasm ratio (e.g. astrocytoma) than in lesions with a high nucleus/cytoplasm ratio (e.g. medulloblastoma). Another factor responsible for the increased water content in neoplasms is the high quantity of interstitial fluids, that is, the cytotoxic intratumoral edema. Increase of water content is the explanation of CT hypodensity and the increase in T_1 and T_2 relaxation times on MRI (T_1 hypointensity and T_2 hyperintensity). Regressive events include the presence of cysts, necrotic and hemorrhagic areas, calcifications, and fatty degenerative areas.

Figure 3.1

Left hypothalamic astrocytoma typically showing a bright hyperintensity on T_2 images (a, b), hypointensity on T_1 images (c), and a hypointense signal on diffusion-weighted images (d), suggesting increased water molecule movement.



The cystic appearance of some neoplasms has long been utilized as an aid for differential diagnosis (Figure 3.2). Preoperative delineation of cysts is also helpful to the neurosurgeon when planning the surgical approach. Intratumoral cysts are secondary to focal mucoid degeneration, and further enlargement of the cavity occurs due to fluid transudation from cyst walls. Large cysts are commonly found in low-grade lesions (pilocytic astrocytoma, hemangioblastoma, ganglioglioma, pleomorphic xantho-astrocytoma, ependymomas, craniopharyngiomas, pituitary adenoma, acoustic neurinoma, meningioma). Cysts can be filled with pure water, or contain considerable amounts of protein or other debris deriving from prior hemorrhage. A homogeneous content is a common finding in large cysts; in some cases, cysts and solid tumors display similar imaging characteristics and cannot be differentiated. The characteristics of the fluid contained in the cysts influence the MR signal characteristics. If the water is pure and does not contain proteins, the fluid in the cyst will have the same signal as cerebrospinal fluid (CSF). When the protein content increases, protons become bound in a hydration layer adjacent to the protein, significantly decreasing the T_1 relaxation time of the water solution, with a final increase in the signal intensity on both T_1 and T_2 images. The most benign tumors commonly show cystic fluid with an intensity near to that of CSF. On CT scans, cysts are characterized by a low density, similar to that of CSF. Higher protein density is reflected in greater CT density and may lead to simulation

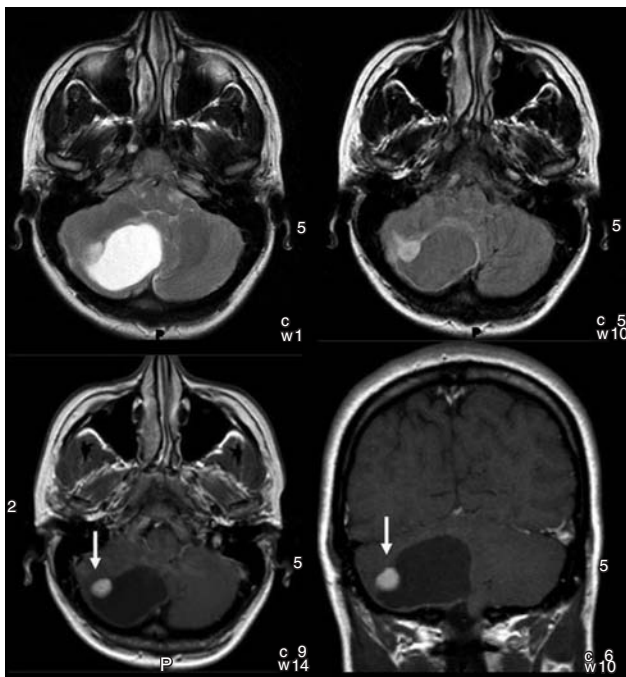


Figure 3.2
Cerebellar pilocytic astrocytoma, characterized by a cystic mass with enhancing mural nodule (arrows).

of a solid tumor. Necrotic areas are due to ischemic cell damage or intralesional hemorrhagic events that result in the formation of pseudocystic areas. Both the discrepancy between tumoral growth and blood supply and microvessel thrombosis due to wall infiltration or hyalinosis can cause intralesional ischemia. On CT and MRI, the density and signal characteristics can be similar to those of true cysts. Morphological criteria, including an irregular shape of cavities, with indented borders and heterogeneous content, may suggest the necrotic origin of the cyst. Generally, lesions containing areas of necrosis are more likely to be malignant. A large hemorrhage originating from a tumor is a relatively uncommon event (1% in neuroepithelial lesions), and when it occurs it is usually very difficult to immediately identify a tumor as the cause. However, small hemorrhages are frequently seen within tumors. Certain primary intracranial neoplasms (e.g. glioblastoma, ependymoma, and oligodendroglioma) and metastases from various tumors (e.g. melanoma, lung carcinoma, renal cell carcinoma, choriocarcinoma) demonstrate a characteristic tendency to bleed, and this behavior can be useful for the diagnosis. This implies that it is necessary to use methods that are sensitive and specific for the detection of hemorrhage. Both CT and MRI are useful for depicting the presence of hemorrhage, but the ability of CT to define its etiology is very poor. On MR images it is possible to distinguish between the signal intensity pattern of intratumoral hemorrhage and that of benign intracranial hematomas.³⁵ The signal intensity is heterogeneous in the former, with concurrent areas of edema and hemorrhage.³⁵ Furthermore, the evolution of blood within tumor tissue may be slow, as compared to the evolution of benign hematomas. These delayed changes are probably related to the hypoxic state typical of human neoplasms,³⁶ or to repeated episodes of bleeding.³⁷ Another finding that helps to differentiate intratumoral bleeding from benign hematomas is the reduction or irregularity of the hemosiderin halo that can usually be found in the periphery of chronic benign intracranial haematomas.³⁵ The presence of non-hemorrhagic tumor tissue inside the lesion represents a clear sign of neoplasm. Lastly, the presence on long TR (repetition time) images of high-intensity signal in the parenchyma surrounding tumoral hemorrhage³⁵ requires follow-up by MRI or a biopsy.³⁸ In the presence of any of these signs the hemorrhagic event can be due to a benign cause, such as an occult cerebrovascular malformation; however, a work-up must be performed to exclude a tumor.³⁸ The presence of calcifications in brain tumors is common and it has a diagnostic relevance. Tumors that commonly undergo some calcification include meningioma, craniopharyngioma, oligodendroglioma, astrocytoma, ependymoma, choroid plexus papilloma, ganglioglioma, dysgerminoma, chordoma, and all tumors after irradiation. Calcification patterns vary from punctate to diffuse, and calcifications are best seen on CT as high-density areas. Calcium produces a void signal on MRI,

and calcifications are thus difficult to identify by this technique. Areas of fatty degeneration occur secondary to macrophagic phagocytosis in necrotic areas (most common in glioblastomas). They are seen as hypodense lipidic areas on CT and with a marked reduction in relaxation time, especially T_1 , on MRI. An abnormal vascular architecture is a feature of most tumors. Tumors stimulate neoangiogenesis within the tumoral tissue and sometimes in the adjacent areas, so the detection of vascularity is not specific enough to characterize morphologic images. Thus, several efforts have focused on the development of further MR-based techniques including diffusion and perfusion imaging, and spectroscopy studies. The implementation of echo planar imaging sequences on clinical MR scanners has allowed the rapid acquisition of images with new types of contrast mechanisms.³⁹ One possibility that is beginning to be investigated in association with brain tumors is the use of diffusion-weighted MRI (Figure 3.3). With this technique, magnetic field gradients are applied before and after the 180i pulse in spin echo imaging sequences. The reversal of spins by the 180i pulse means that these gradients do not contribute any net phase shift for static spins, whereas protons that are diffusing in the medium undergo a loss of phase coherence that is detected as a loss of MR signal

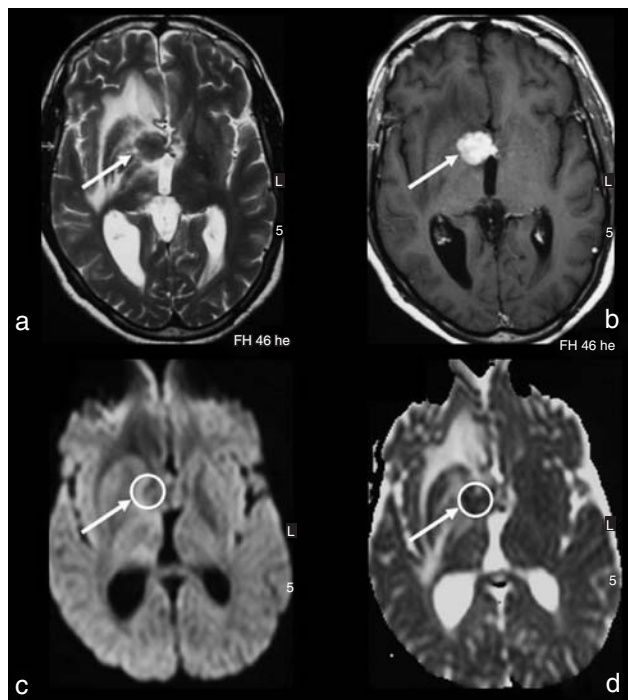


Figure 3.3

Deep right basal ganglia primary central nervous system lymphoma characterized by a very low signal on T_2 images (a), a sharp enhancement after gadolinium (b), and a clear restriction of apparent diffusion coefficient on diffusion-weighted images (c) and maps (d).

amplitude.³⁹ Spins with higher diffusion rates generally produce a greater loss of phase coherence and a lower MR signal than those with slower diffusion rates.³⁹ The apparent diffusion coefficient (ADC) reflects physical factors, such as temperature and viscosity, in addition to the restricted motion of the molecules resulting from the presence of semi-permeable tissues and membranes. Differences in ADC are expected to reflect changes in cellularity, cell membrane permeability, intracellular and extracellular diffusion, and tissue structure.³⁹ Preliminary studies in brain tumors have typically shown low anisotropy in abnormal regions, which reflects the loss of normal tissue structure, with an increased ADC in necrosis, edema, and cysts relative to normal-appearing white matter. There have been reports that the ADC of regions of tumor is correlated with cellularity, with a tendency towards lower ADC values in high-grade as compared with low-grade gliomas.⁴⁰ The minimum ADC value in patients with tumors tends to be higher in regions of low anisotropy than in regions of normal tissue anisotropy. This parameter may be important in the effort to distinguish regions of edema from non-enhancing tumor.³⁹ Moreover, diffusion-weighted MRI can be successfully used to differentiate between extra-axial cysts and epidermoid tumors.⁴¹ Another application of echo planar imaging is in the estimation of parameters that reflect tissue vascularization.³⁹ This is achieved by acquiring multiple repeated images during the first pass of a bolus of MR contrast agent. Changes in signal intensity of such dynamic data may be used to calculate an image of regional cerebral blood volume (rCBV).³⁹ Although the detailed mechanisms underlying perfusion and vascular contrast MRI are under investigation, the potential of the technique to provide useful information in patients with brain tumors is clear.³⁹ Neovascularization has been shown to be an important factor in the regulation and malignant potential of many tumors,⁴² and as an increasing number of new therapies that specifically target angiogenesis are available, it is desirable to have an imaging technique able to depict angiogenesis.³⁹ With such a methodology, necrosis may be differentiated from tumor by virtue of its low rCBV relative to normal-appearing white matter in the contralateral hemisphere. The differentiation between viable tumor and adjacent gray matter is more difficult because these tissues may appear isointense on rCBV images.³⁹ A study of glioma patients suggested a positive correlation between rCBV and tumor grade.⁴³ The potential for use of rCBV imaging to define the radiation target and monitor therapeutic success was demonstrated in a study of eight glioma patients investigated three to four times serially.⁴⁴ This study showed similar results for rCBV data and positron emission tomography (PET) scans obtained at the same time points. In a more recent study the authors state that dynamic susceptibility contrast MRI is more useful for grading glioma than conventional MRI, and that it can also provide complementary information that facilitates differentiation

between malignant lymphoma and glioma. The absence of tumor neovascularization in malignant lymphoma leads to a low rCBV, which is in contrast to findings in malignant gliomas. Moreover, this technique can be used to differentiate between extra-axial tumors, e.g. between meningioma and neurinoma.⁴⁵

Two new MRI modalities attempt to highlight functional or metabolic properties of the tumor: perfusion-weighted and diffusion-weighted MRI.

Perfusion-weighted MRI is able to assess the tumor blood volume, which can be useful in defining the tumor extent. With an intact blood–brain barrier, this measure is reliable, but in most brain tumors, where the blood–brain barrier is disrupted or absent, there is a variable underestimation of the tumor extent.⁴⁶ New techniques have been developed to overcome this problem, but there is yet no application in clinical practice.

The apparent diffusion coefficient in diffusion-weighted MRI sequences does not seem to be helpful for distinguishing tumor tissue from peritumoral brain tissue in gliomas.⁴⁷ In vivo white matter tractography by diffusion tensor imaging (DTI) has become a popular tool for investigation of white matter architecture in the normal brain (Figure 3.4). DTI studies for delineating white matter organization in the vicinity of brain tumors have demonstrated that edema, tissue compression, and degeneration may cause significant interpretation problems, but also that the combination of functional MRI (fMRI) and DTI may represent a useful tool to define the seed region of interest for DTI-based tractography and to provide more comprehensive, functionally related, white matter mapping in presurgical assessment.⁴⁸

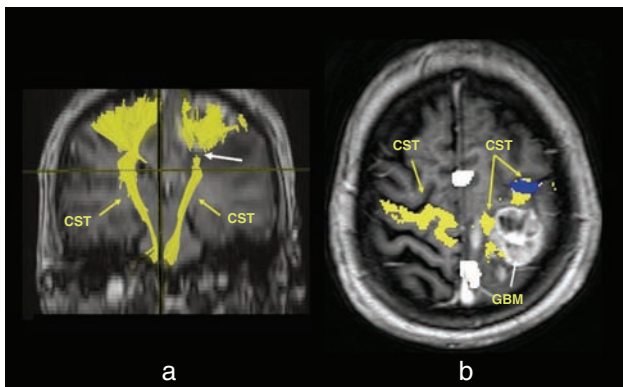


Figure 3.4

Diffusion tensor imaging (DTI) tractography combined with functional magnetic resonance imaging (fMRI) in a patient with left Rolandic glioblastoma multiforme (GBM). In (a), three-dimensional reconstruction of the corticospinal tract (CST) depicts the destructive effect of the lesion on the white matter tract (white arrow). In (b), the anterior displacement of part of the left CST and of the hand motor area, demonstrated with fMRI (blue spot), is shown.

The MRI finding of most intracranial tumors without contrast enhancement consists of iso- or hypointensity on T₁-weighted, and hyperintensity on T₂-weighted images, to a variable extent of mass effect on other structures inside the cranial cavity. These features alone are not reliable enough to differentiate between the different tumors. To discriminate between the different tumors before histological evaluation, other features can be helpful, such as morphology, contrast enhancement, and the presence of a cystic component, of calcifications, of necrosis, hemorrhage, and edema.

MR spectroscopy (MRS) shares with MRI the principle that makes the production of images feasible, namely that of nuclear magnetic resonance. In MRS the signal obtained from a single element is further separated into its different chemical forms. This is possible because the effect of a magnetic field on nuclei is not direct: it is shielded by the distribution of the bonding electrons around the nuclei being detected. Therefore, nuclei in different chemical environments give rise to signals at different frequencies. This separation of nuclear resonance frequencies is termed chemical shift, depends on the magnetic field strength, and is expressed in dimensionless units termed parts per million (ppm). It is thus possible to define a spectrum of nuclear magnetic resonance signal, in which the several chemical forms of an element (where ‘element’ indicates hydrogen, carbon, etc.) give peaks in specific positions.

With ¹H-MRS, a non-invasive in vivo approach for the determination of some cerebral metabolites of clinical relevance is possible. Unfortunately, the in vivo resolution of this method is poor; only molecules small and mobile enough to tumble freely in solution can be detected. There is no way to detect signals from proteins, from most membrane components, or from small molecules bound to larger ones. Moreover, only compounds present in concentrations of about 1 mmol can be measured directly. The rationale for considering that signals originating from certain metabolites are of use in defining the viability of, or the damage to, any cellular structure is based on in vitro histochemical and cellular studies. These studies demonstrated that individual metabolites are localized in specific cells or cerebral structures; on the basis of this evidence, signal modifications of a particular metabolite could reflect death or injury to a certain cell population. In a brain proton MRS study the main marker resonances include: the generally defined choline peak at 3.2 ppm, which encompasses choline-containing compounds, such as membrane phospholipids (phosphocholine and glycerophosphocholine), and their respective degradation products; creatine and phosphocreatine, which are elements of cellular energetic metabolism; mobile lipids and triglycerides; N-acetyl-aspartate (NAA) and N-acetyl groups, considered to be the markers of the neuronal population; and the lactic acid peak, which can be measured when the glycolysis terminal metabolite concentration exceeds the normal value, as in hypoxic conditions.

In addition to these metabolites, it is possible to detect other compounds utilizing short echo time (TE) sequences (10–50 ms). Short TEs allow the recognition of substances with a short T_2 , or that are strongly spin-coupled, such as glutamate, glutamine, taurine, glycine, myoinositol, and γ -aminobutyric acid (GABA), which is very informative from the clinical point of view, but very difficult to quantify with the 1.5-T magnetic field that is normally used for clinical studies.

The major clinical application of MRS considered for brain tumor patients has been its potential for non-invasive tumor grading.^{49–51} These studies have predominantly used MRS techniques that detect a signal spectrum from a small region of interest (single-voxel MRS). Trends such as higher mean choline and lower mean NAA levels in higher-grade tumors have been reported (Figures 3.5 and 3.6). However, most of the studies have found large standard deviations in metabolite ratios and substantial overlap in individual values, which may restrict the accuracy of the technique. Studies using sophisticated data analysis techniques have shown a higher degree of accuracy for in vitro and in vivo spectroscopy studies.⁵² A significant improvement in accuracy was obtained using a two-dimensional MRS imaging technique.⁵¹ Multivoxel techniques (chemical shift imaging or spectroscopic imaging) provide spatially encoded chemical information from large tissue slices composed of several voxels. The combination of improved spatial resolution and increased number of voxels provides many more data about tumor heterogeneity and assists in exploration of the tumor margin (Figure 3.7). As a result it is possible to measure the metabolite content of different areas of neoplasms and surrounding normal tissue. This is very useful for better characterization of glial tumors, in which areas with different grading very often coexist, and for more accurate monitoring of possible malignant degeneration of benign tumors. In a serial proton MRS imaging study it was clearly demonstrated that an increased choline signal is associated with malignant

progression of cerebral gliomas and that serial MRS imaging effectively and accurately differentiates between stable and progressive disease.⁵³

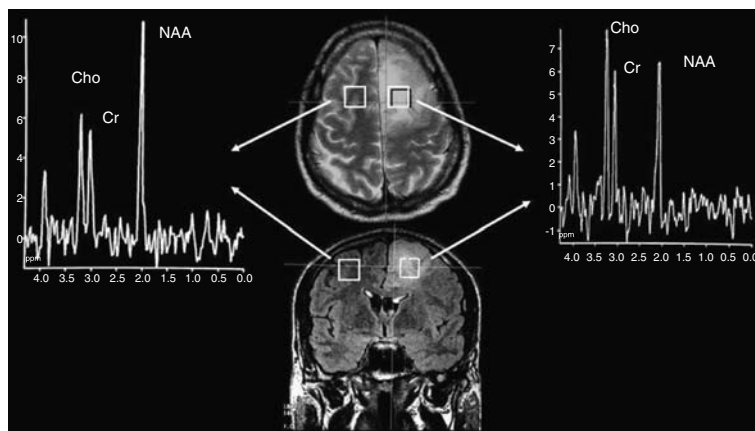
Spectroscopy studies are also very useful in the assessment of response to therapy. The sensitivity of this technique in fact exceeds that of conventional MRI, with useful information being provided in lesions treated with chemotherapy or radiation therapy. There is general agreement that within high-dose regions that correspond to the radiation target, treatment response is reflected in reduction in the levels of choline, creatine, and NAA 2–3 months after treatment. In regions that are not responsive to the radiation treatment, levels of choline may increase, corresponding to residual or recurrent tumor. This different behavior is of paramount importance in helping to differentiate between radionecrosis and recurrence, one of the most difficult topics in oncological neuroradiology. The possibility of monitoring the efficacy of new antitumoral compounds explains why MRS is included as the main tool in most new experimental protocols.

The high sensitivity of MRS is not paralleled by its specificity. Although several studies have reported that MRS permits the differentiation of diverse histological tumor types or of abscesses or cystic lesions from neoplasms, the experience of routine daily practice has drawn attention to the risks related to the technique, and warrants caution when considering differential diagnosis. This is true not only for differentiation of neoplastic lesions, but even more so when distinction between tumoral and non-neoplastic lesions is addressed.

The absolute quantitation of metabolites and short TE spectra may provide additional data to improve specificity. However, absolute quantitation is complex and time consuming, and short TE spectra have a poor signal to noise ratio. Although the problems of absolute quantitation and reduction of TE without impairment of quality may soon be resolved, it is still debatable whether different metabolic patterns correspond to different types of tumors.

Figure 3.5

Single-voxel spectroscopy (echo time (TE) 135 ms) of a subcortical low-grade glioma. Compared to the normal spectral profile (top left), the tumoral spectrum (top right) shows a slight increase of choline (Cho) and N-acetyl-aspartate (NAA) reduction.



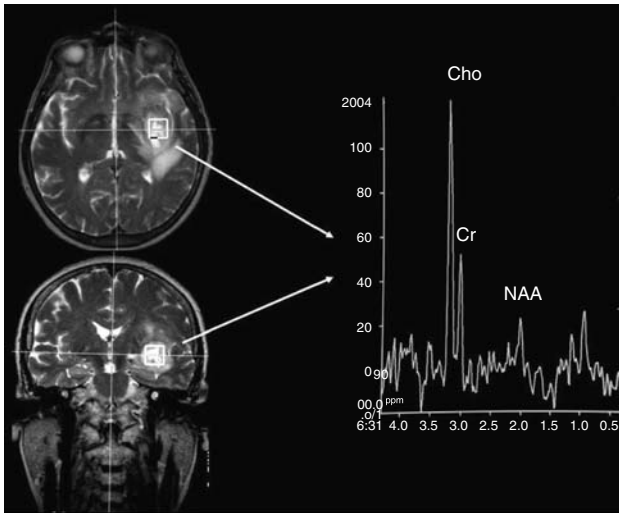


Figure 3.6

Single-voxel spectroscopy (TE 135 ms) of a glioblastoma multiforme (GBM). The single volume of interest comprises different tumoral areas (solid and cystic). There is a clear increase of choline (Cho) content; N-acetyl-aspartate (NAA) is severely reduced.

Radionuclide imaging of brain tumors

In the early 1970s, before X-ray CT had an established role in medicine, the aim of nuclear medicine studies was to image a tumor which was suspected on a clinical basis. Nowadays, such a demand is easily answered by X-ray CT and/or MRI, but great effort has been spent on the characterization of brain lesions beyond what is possible using

simple imaging. Intracellular biochemical processes can be measured and visualized with nuclear medicine techniques.

For radionuclide imaging, there are two available three-dimensional techniques: single photon emission computed tomography (SPECT) and positron emission tomography (PET). They rely on the detection of different types of radioactive emission of radionuclides, namely β^+ emission for the more sophisticated and expensive PET and photon emission for the SPECT. PET has a better spatial resolution (up to 4 mm) than SPECT (8–10 mm).

There are several applications for radionuclide brain imaging, including: delineating tumors from non-neoplastic tissue, grading and prognosis, localizing the optimum site for biopsy, distinguishing radionecrosis from tumor recurrence, assessing response to therapy, predicting malignant progression, distinguishing high- from low-grade glioma, and therapy follow-up.

Single photon emission computed tomography

Even today the most important SPECT tracer in neuro-oncology is thallium-201 chloride ($[^{201}\text{Tl}]$ chloride), a potassium analog.^{54–59} The uptake of $[^{201}\text{Tl}]$ chloride in neoplastic tissue was observed in patients referred for myocardial perfusion studies with this tracer. In those patients who had tumors, $[^{201}\text{Tl}]$ chloride uptake was also evident in those extramyocardial areas where the tumors were localized. The mechanism of $[^{201}\text{Tl}]$ chloride uptake is not completely understood; however, it is thought to be largely dependent upon delivery, i.e. blood flow and blood–brain barrier permeability, cellular metabolism, and efficiency of the sodium–potassium adenosine phosphatase (ATPase) activity.

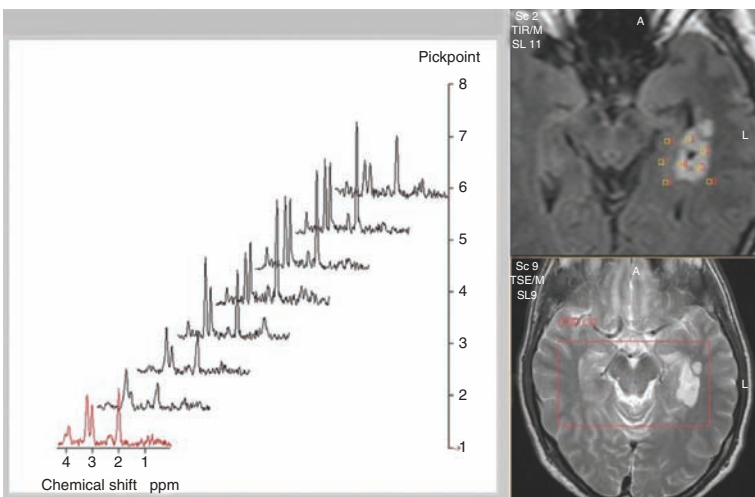


Figure 3.7

Multivoxel technique on a 3-T scanner in a subject with temporal lobe low-grade glioma. Multiple spectra on the left side show the differences existing between tumoral tissue (spectra 1–4) and peritumoral tissue normal (5–8).

Factors affecting the uptake of [^{201}Tl]chloride in brain tumors include tissue viability, tumor type, co-transport system, calcium ion channel system, vascular immaturity with leakage, and increased cellular permeability. [^{201}Tl]chloride has been shown to accumulate in viable tumor tissue more than in connective tissue, especially in inflammatory cells, and it is barely detectable in necrotic tissue. [^{201}Tl]chloride has a much higher affinity for brain tumor than for white and gray matter, as the latter show little or no [^{201}Tl]chloride uptake. Disruption of the blood–brain barrier allows for greater [^{201}Tl]chloride uptake in tumors; however, in radiation necrosis and resolving hematoma, blood–brain barrier disruption can occur without [^{201}Tl]chloride accumulation. The time course of [^{201}Tl]chloride uptake in brain tumors depends upon several variables. Early uptake, i.e. within 5 min of tracer injection, depends on regional blood flow, blood volume, and permeability of the blood–brain barrier. By contrast, delayed uptake depends on active transport by the membrane pump of the tumor. Sodium–potassium ATPase activity has been shown to account for ten times more [^{201}Tl]chloride uptake than tumor blood flow.

Depending on the patient selection process, the sensitivity and specificity of [^{201}Tl]chloride in localizing brain tumors have been estimated to be about 70% and 80%, respectively.^{58,59} Sensitivity is lower in low-grade gliomas, while specificity is lower in cases with hemorrhagic infarction.⁶⁰ Small tumor size and a location in the posterior fossa may further reduce the sensitivity of [^{201}Tl]chloride imaging.⁵⁸ The highest sensitivity has been observed in glioblastoma multiforme and metastatic lesions. By comparing the uptake of [^{201}Tl]chloride in tumors of different histological type,⁶¹ it has been demonstrated that the mean retention index (tumor/non-tumor activity) is higher than 0.7 for each type of malignant tumor, whereas it is lower than 0.6 in all benign tumors, except pituitary adenomas. Moreover, it has been shown that the early uptake of [^{201}Tl]chloride correlates with contrast enhancement on MRI, except in the case of schwannomas and cavernous hemangiomas. Ricci et al. have reported⁵⁹ that the extent of necrosis may affect the uptake of [^{201}Tl]chloride when the volume included within the region examined encompasses both necrotic areas and highly malignant tumor tissue. Since necrosis is related to tumor proliferative activity and represents a negative prognostic factor in astrocytoma, a possible underestimation of [^{201}Tl]chloride uptake due to intratumoral necrosis must be carefully evaluated. It must be noted that the administration of steroids diminishes the uptake of [^{201}Tl]chloride by more than 20%.⁵⁸ Thallium-201 has also been found to be useful for evaluating the histological grade of astrocytomas. In a study comparing this tracer with [^{18}F]FDG (fluro-2-deoxy-D-glucose) in 23 patients, [^{201}Tl]chloride uptake was statistically different both between grades 2 and 3 and between grades 3 and 4, while FDG was negative in all grade 2 patients, positive in six out

of seven grade 4 patients, but highly variable in grade 3 patients.⁶²

Thallium-201 SPECT has been utilized to characterize treatment response and to detect recurrence after initial treatment. Patients who showed recurrence presented with a high uptake of [^{201}Tl]chloride, but this technique failed to diagnose the viability of tumors that were less than 1.5 cm in diameter, owing to the partial volume effect and/or the limited resolution of [^{201}Tl]chloride SPECT. In order to improve the quality of SPECT images, [$^{99\text{m}}\text{Tc}$]sestamibi has been applied in the detection of recurrent gliomas after radiotherapy; this method is able to identify recurrent gliomas with a higher accuracy than [^{201}Tl]chloride.^{63–65}

[$^{99\text{m}}\text{Tc}$]methoxyisobutylisonitrile (MIBI),^{63,64} was originally developed for the evaluation of myocardial perfusion. This tracer is a cationic complex that is concentrated in cytoplasm and mitochondria as a result of passive diffusion across highly negative transmembrane potentials in relation to metabolic demand. The entry of [$^{99\text{m}}\text{Tc}$]MIBI into cells depends on a combination of charge and lipophilicity. The negative potential on the inner mitochondrial membrane traps the tracer within the organelle matrix.⁶⁶ Its retention in the mitochondria is not organ specific, and appears to be a mechanism common to most tissues. Studies with this tracer have shown that its sensitivity to detect malignant tumors and recurrences is similar to that of [^{201}Tl]chloride. The uptake of [$^{99\text{m}}\text{Tc}$]MIBI in brain tumors was first compared with that of [^{201}Tl]chloride in 1993 by O'Tuama et al.,⁶⁷ and it was concluded that the spectrum of avidity is similar for both tracers. Later, the uptake of MIBI was studied in a greater number of patients and it was demonstrated that this tracer is of value in distinguishing low- from high-grade gliomas, and at the same time enables differentiation from other non-malignant lesions such as radiation necrosis, cerebral abscess, or ischemic stroke.^{68,69}

For brain tumors and cerebral metastases, [$^{99\text{m}}\text{Tc}$]MIBI has a sensitivity and a specificity of 85%, with a positive predictive value (PPV) of 97% and a negative predictive value (NPV) of 53%. The best results are obtained in gliomas (sensitivity 88%, specificity 92%, PPV 98%, and NPV 63%), without differences between low- and high-grade tumors.⁶⁴ The use of [$^{99\text{m}}\text{Tc}$]MIBI for the assessment of tumor response to chemotherapy has also been advocated. This proposal is based on the observation that the efflux of [$^{99\text{m}}\text{Tc}$]MIBI is related to the expression of the multidrug-resistance MDR₁ gene and amplification or increased expression of its product, P-glycoprotein (Pgp), and to the expression of the multidrug resistance-associated protein.⁷⁰ Tests in gliomas⁶⁴ and pediatric neuroblastomas and ganglioneuromas⁷¹ have suggested that the results of [$^{99\text{m}}\text{Tc}$]MIBI imaging may correlate with the presence of functional Pgp in gliomas and neural crest tumors, as has been shown for other tumors. It has also been suggested that

[^{99m}Tc]MIBI imaging might be used to assess recurrent gliomas after radiation therapy.^{63,64}

[^{99m}Tc]tetrafosmin is a lipophilic cationic tracer which shares many of the properties of [^{99m}Tc]MIBI and is extensively used in nuclear cardiology. It has been shown that this tracer has a trapping mechanism which is similar to that of [^{99m}Tc]MIBI, depending on both cell membrane and mitochondrial potentials.⁷¹ Recently it has been suggested that it may be a suitable radiotracer for brain tumor imaging.⁷² Preliminary results with [^{99m}Tc]tetrafosmin indicate that this tracer does not accumulate in low-grade gliomas (grade 2), but is taken up avidly by high-grade gliomas and other malignant brain tumors. Uptake in the tumor region correlates well with that of [^{99m}Tc]MIBI, so it has been concluded that [^{99m}Tc]tetrafosmin may also be useful for the non-invasive grading of brain tumors.⁷³

Imaging modalities based on the use of SPECT and monoclonal antibodies have attracted increasing interest, and this is particularly true in those aimed at signal amplification and dose reduction by tumor pre-targeting techniques. This is best achieved by the administration of biotinylated monoclonal antibody followed by administration of the radioactive tracer (two-step technique), or by the administration of avidin after the monoclonal antibody, and then tracer administration (three-step technique). The additional steps are aimed at enhancement of the signal to noise ratio by allowing a longer time for antibody localization on the tumor (two-step technique), and the removal of free antibody by conjugation with avidin (three-step technique), prior to the administration of low doses of radioactive tracer.

These approaches overcome the limitations deriving from the low tumor/non-tumor ratio and high dosimetry when using monoclonal antibodies directly labeled with iodine-131. In practice, one of the procedures used entails the following three steps: administration of biotinylated BC2 anti-tenascin immunoglobulins; administration of cold avidin at 24 h; and administration of ^{99m}Tc-labeled PnAO-biotin (where PnAO is propylene amine oxime) after a further 24 h. In glioma patients, Paganelli et al.⁷⁴ have shown a correlation between in vitro immunohistochemistry for tenascin and in vivo immunodetection with this pre-targeting technique (sensitivity 93%, specificity 75%, accuracy 90%).

Somatostatin receptor imaging in intracranial tumors is usually performed with [¹¹¹In]DTPA-D-Phe₁-octreotide (where DTPA is diethylenetriamine pentaacetic acid) or [¹²³I]Tyr₃-octreotide. Uptake depends upon receptor expression and absence or disruption of the blood-brain barrier. Non-specific uptake is commonly observed in lesions other than tumors.

Somatostatin receptor imaging in intracranial tumors has already been the object of a review summarizing 15 studies in a total of 535 patients carried out between 1989 and 1996. The analysis demonstrated the usefulness of

somatostatin analogs in meningiomas but not in gliomas; its role in pituitary adenomas is also considered doubtful.⁷⁵

The use of tracers which specifically bind to receptors has been applied mostly to pituitary adenomas, in particular in the assessment of non-secreting tumors in the parasellar region, where radiological differential diagnosis may occasionally be difficult. The in vivo characterization of the biochemical and functional properties of the tissue may provide useful information about the nature of the pituitary mass. PET and SPECT have been used for the assessment of adenomas and other parasellar tumors with [¹¹C]deprenyl, ¹¹C- and ¹⁸F-labeled spiperone analogs, [¹²³I]IBZM (iodobenzamide), and [¹²³I]epidepride.⁷⁶⁻⁸¹ Some brain tumors show a high density of benzodiazepine receptors compared with normal tissue. [¹¹C]PK11195 is a ligand which binds with high affinity to peripheral benzodiazepine receptors and has been used to image human gliomas.^{82,83}

The limited spatial resolution of the SPECT technique may restrict its value in assessment of the extent of the disease. Nevertheless, attempts have been made to delineate tumor tissue with [²⁰¹Tl]chloride and with [¹²³I]α-methyl-tyrosine (IMT), and it has been concluded that [¹²³I]IMT shows greater tumor extent especially in grade 3 gliomas, while the size of glioblastomas is shown in a comparable manner.⁸⁴

Positron emission tomography

The tumor variable most commonly assessed with PET is glucose uptake. Tumor glycolysis can be assessed with 2-[¹⁸F]fluoro-2-deoxy-D-glucose ([¹⁸F]FDG), which differs from glucose only in the replacement of the hydroxyl group on the second carbon atom by radioactive fluorine. Glucose and [¹⁸F]FDG share the same saturable carriers between blood and tissue, and [¹⁸F]FDG competes with glucose for hexokinase. [¹⁸F]FDG-6-phosphate is trapped in cells in proportion to the glucose metabolic rate, and its accumulation can be detected by PET. By fitting the data of [¹⁸F]FDG accumulation under a region of interest in a dynamic study, three constants may be derived which represent the glucose transport from blood to brain, the reverse transport from brain to blood, and the phosphorylation of glucose. [¹⁸F]FDG is the most important tracer for PET oncological studies: its relatively simple synthesis and long half-life along with extensive knowledge of the mechanisms determining its uptake and retention have made it quite popular in neuro-oncology. It is well established that brain neoplasms present changes in glucose utilization in comparison with normal tissue. In vitro tumor cells have a high rate of glucose degradation into lactic acid even in the presence of oxygen.⁸⁵ With this tracer, changes in the oxidative metabolism were first demonstrated in vivo in brain neoplasms.^{86,87}

Alterations of glucose transport in experimental cancer cells have been demonstrated and related both to an increased metabolism and to an increased number of existing glucose transporters.⁸⁸ Activation of the gene encoding the synthesis of glucose transporter GLUT1 is a major early marker of malignant transformation. An overexpression of GLUT1 and GLUT3 has been observed in several tumor types, including brain tumors,⁸⁹ and this may explain the raised level of glucose extraction demonstrated with PET.⁹⁰

In both experimental and human gliomas it was demonstrated that even in the presence of a normal unidirectional glucose influx into tumor cells, the glucose metabolism was doubled in comparison with normal gray matter, and that there was an uncoupling between glucose transport and phosphorylation.^{91,92}

The [¹⁸F]FDG uptake into malignant cells is therefore the consequence of both increased expression of glucose transporter molecules and glycolysis. Quantitative assessment of glucose metabolism with PET in human brain neoplasms is considered to be highly reproducible⁹³ but cumbersome. The use of semiquantitative methods such as the standardized uptake value (SUV) has become popular for the analysis of tumor activity in sites other than the brain. However, some doubts have been raised as to the usefulness of quantitation or even semiquantitation in a clinical setting, where simple visual assessment of tracer accumulation by an experienced reader or measurement of the radioactivity distribution ratio between tumor and contralateral normal brain has been found to be sufficient in most cases. The latter methods remain the most common means of [¹⁸F]FDG-PET analysis in brain tumors.^{94,95}

Most [¹⁸F]FDG-PET studies have been performed on gliomas and on correlation between brain tumor-^{[18F]FDG} uptake and survival,^{96–99} histology,^{99–106} tumor grading,^{99,103,107} different histological subtypes of glioma,^{102,108} histology, other imaging methods,^{103,109,110} and PET with other tracers.^{98,99,103,105,111–114} Most studies have been performed in a limited number of patients. A sum of studied patients among all available studies would yield a high number of patients, but this cannot be done, due to extreme heterogeneity in patient characteristics, histology, evaluation parameters of diagnostic procedures, and reference parameters. In sum, the level of evidence would be too low, and thus insufficient to draw definitive guidelines. Nevertheless, it can be concluded that only in high-grade gliomas can the accuracy of conventional radiological methods with high sensitivity, such as MRI, be improved by the concomitant use of [¹⁸F]FDG-PET, which contributes to the accuracy through improved specificity. Initial studies with [¹⁸F]FDG were able to identify elevated uptake of tracer in brain tumors,¹¹⁵ and it was rapidly concluded that the uptake of [¹⁸F]FDG is correlated with the grade of malignancy. Thus, low-grade gliomas are not easily identified, or appear as cold spots surrounded by normal uptake in the cerebral cortex, which may hinder

clear definition of tumor extension. Overall, insufficient correlation between [¹⁸F]FDG uptake and histological grade, and low diagnostic accuracy for low-grade gliomas, led to recommend the use of [¹⁸F]FDG only in selected cases, mostly for restaging after treatment to differentiate tumor persistence/recurrence from radiation necrosis in high-grade gliomas or to visualize malignant transformation of low-grade gliomas.^{62,102,103,105,108}

There are various applications of FDG in the assessment of brain tumors. Prior to any treatment, PET scan with [¹⁸F]FDG is considered useful in the diagnostic work-up of suspected brain tumors and metastases as it may identify focal hypermetabolic abnormalities. Different studies have related the grade of malignancy of gliomas to the rate of [¹⁸F]FDG uptake, and shown that while low-grade astrocytomas display low [¹⁸F]FDG uptake, anaplastic astrocytomas and glioblastomas have markedly elevated uptake.^{62,97,116,117} [¹⁸F]FDG-PET has also been proposed as a useful tool to assess the tumor grade in oligodendrogliomas¹¹⁸ and gangliogliomas.¹⁰⁹ In some other rare intracranial tumors such as hemangiopericytomas, low uptake of [¹⁸F]FDG was not correlated with high malignancy.¹¹⁹ On the other hand, the high uptake of [¹⁸F]FDG that has been observed in juvenile pilocytic astrocytomas is not an expression of malignancy, as these tumors are associated with a relatively good prognosis.¹²⁰ Anaplasia is considered the factor that determines the elevated uptake of glucose, and PET has therefore been proposed as a tool to guide biopsy in the high metabolic area, where it is most likely to provide diagnostic results.^{121,122} [¹⁸F]FDG-PET has been used to predict the survival of untreated patients. In low-grade gliomas, the natural history of the disease is variable, and malignant transformation is difficult to predict. [¹⁸F]FDG-PET is useful in this context in that detection of areas of increased [¹⁸F]FDG uptake in histologically proven low-grade gliomas is predictive of malignant transformation.^{123,124} In the early postoperative period, [¹⁸F]FDG-PET can be used to differentiate residual tumor from the effect of surgery.¹²⁵ It seems clear that a decline in tumoral uptake of [¹⁸F]FDG weeks or months after therapy is suggestive of a good response to treatment, indicating either a reduced number of viable cells or reduced metabolism of damaged cells.¹²⁶ After treatment, [¹⁸F]FDG may differentiate recurrence from other therapy-related changes. Furthermore, when recurrence is confirmed, no visible uptake of [¹⁸F]FDG or uptake lower than adjacent cortical activity is associated with a longer survival than is observed in patients in whom tumor [¹⁸F]FDG uptake is higher than in the adjacent cortex.^{127,133}

Malignant gliomas and gray matter structures take up FDG avidly, whereas lower grade gliomas do so to a lesser degree. Thus, when tumors are in or near gray matter, it may be difficult to distinguish between the two. Improvement in the delineation of gliomas with FDG-PET imaging, by extending the interval between FDG administration and PET data acquisition, has been preliminarily

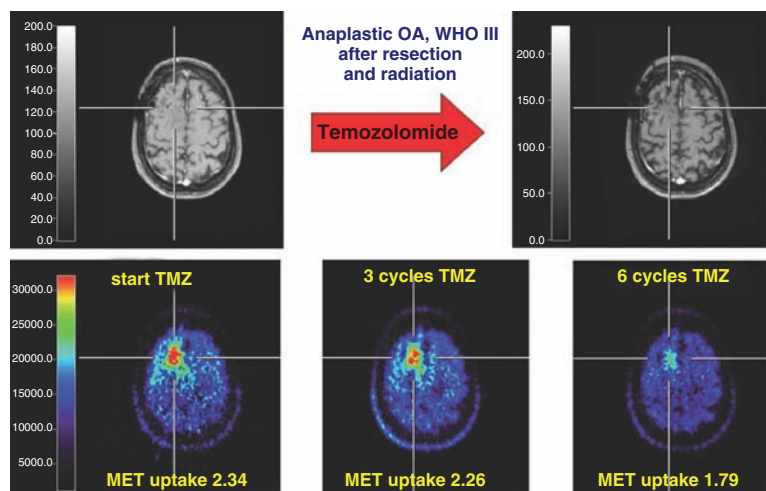
reported.¹³⁴ Delayed images by visual analysis showed better delineation of the FDG uptake of tumors relative to gray matter. This result likely stems from a greater effect of glucose-6-phosphatase degradation of FDG-6-phosphate in normal brain relative to the gliomas. Delayed FDG-PET imaging is simple, is technically feasible, and may improve glioma diagnosis in tumors in or near the cortex or deep nuclei.

Imaging with radiolabeled amino acids visualizes protein synthesis and amino acid transport phenomena, which are accelerated in tumors.¹³⁵ Because the uptake of amino acids in macrophages and other inflammatory cells is low, these tracers might be more tumor specific than [¹⁸F]FDG for the assessment of abnormal tissue. Methionine and other large neutral amino acids, e.g. phenylalanine, leucine, tyrosine, isoleucine, valine, tryptophan, and histidine, are normally supplied to the brain from systemic protein breakdown and diet. A transport system in the blood–brain barrier mediates the transcapillary movement of structurally related amino acids that compete with each other for entry into the brain, which occurs at a rate of approximately 3–10 nmol/g per minute. Use of carbon-11 methionine avoids many of the problems related to the tumor/non-tumor uptake ratio that are encountered with [¹⁸F]FDG, and overcomes the difficulty in differentiating tumors from other cerebral pathologies that may cause abnormal [¹⁸F]FDG uptake, i.e. infections, radiation necrosis, and edema.¹³⁶ In tumors without obvious breakdown of the blood–brain barrier, a stereospecific process with similar properties to those in the normal brain tissue is responsible for the accumulation of labeled methionine.¹³⁷ Amino acid uptake, evaluated by administration of ¹¹C-labeled L-methionine, has been found to be different in tumors compared with normal brain tissue.¹³⁸ In contrast to [¹⁸F]FDG, tumor tissue, like glioma, shows avid uptake of radiolabeled amino acids, while uptake in macrophages, other inflammatory cells, and normal cerebral tissue is low. Therefore these tracers might be more tumor specific than

the radiolabeled glucose analog.³³ Accumulation of ¹¹C-labeled L-methionine in brain tumors does not seem to be dependent on disruption of the blood–brain barrier, like contrast enhancement in CT and MRI. In fact, most low-grade gliomas do not show any blood–brain barrier leakage, but they display increased ¹¹C-labeled L-methionine uptake.^{139–143} Many authors have found a positive correlation between ¹¹C-labeled L-methionine uptake and the histological grade of gliomas.^{99,142,144} Less clear results can be found on the possible correlation between ¹¹C-labeled L-methionine uptake and prognosis: other factors must be taken into account in the evaluation of patient prognosis, such as histology, presenting symptoms, and clinical performance status.^{141,145} ¹¹C-labeled L-methionine has proved to be useful to target stereotactic biopsy.^{143,146} Another interesting application of this method is functional brain mapping: Kaplan et al. used PET scans and co-registered MR images prior to neurosurgical tumor excision of brain tumors in children to maximize resection and minimize the risk of neurological sequelae. Good results have also been found for restaging of brain tumors after treatment, especially for differentiation between recurrent glioma from radiation necrosis^{147–149} and to evaluate chemotherapy effectiveness^{142,144} (Figure 3.8). There are several applications of ¹¹C-labeled L-methionine that complement those of FDG and of anatomical imaging. [¹¹C]methionine allows earlier and more accurate delineation of tumor extension than does anatomical imaging,^{150–152} and has been proved to be better than [¹⁸F]FDG in delineating low-grade gliomas^{99,108} (Figure 3.9). [¹¹C]methionine enters several biochemical pathways; therefore, modeling of its kinetics in brain tumor tissue presents even more difficulties than those deriving from the heterogeneous features of tumor masses. Non-specific uptake has been reported in non-neoplastic lesions, including hematomas and abscesses, while the administration of branched chain amino acids inhibits the accumulation of methionine in brain tumors without severe disruption

Figure 3.8

Value of methionine-positron emission tomography (MET-PET) in the follow-up of chemotherapy. A patient presented with the clinical signs of tumor progression (increase in seizure frequency). Magnetic resonance imaging (MRI) was non-remarkable, MET-PET showed substantial tumor activity (uptake ratio: 2.34). After three and six cycles of chemotherapy with temozolomide (TMZ), MRI did not exhibit any changes; however, MET-PET clearly shows the antitumor activity with a decreased uptake ratio of 1.79. OA,; WHO, World Health Organization.



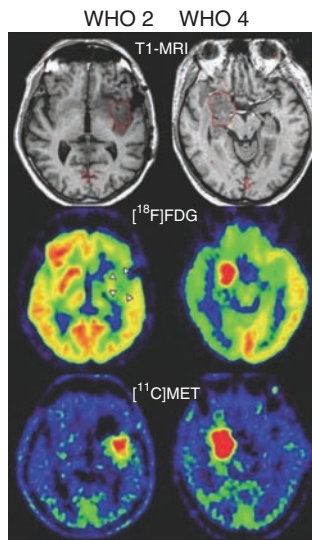


Figure 3.9

Non-invasive differentiation between low- and high-grade gliomas. In low-grade gliomas (WHO 2) glucose metabolism is similar to that of white matter (arrowheads) and amino acid uptake is only moderately increased. In high-grade gliomas (GBM; WHO 4), both glucose metabolism and amino acid uptake are increased. (Reproduced with permission from reference 153.)

of the blood–brain barrier, as in normal brain tissue.¹³⁸ The use of [¹¹C]methionine is justified by its relatively simple synthesis and its rapid uptake in tumors and clearance from blood and other tissues. In conclusion, in brain oncology, PET with ¹¹C-labeled L-methionine can add substantial information to MRI or CT, for primary diagnosis, planning of stereotactic biopsy, target volume definition prior to radiation therapy and surgical resection, and for restaging after treatment. Nevertheless MRI and CT can detect the tumor with high sensitivity, and to date they cannot be replaced by any functional imaging procedure.

Experience with other tracers is limited, but in a quantitative evaluation of [¹¹C]methionine uptake in patients with low-grade gliomas, those patients with a low tumor uptake in the baseline study had a significantly better prognosis than those with a high uptake.¹⁵⁴

More recently, [¹¹C]methionine PET has been applied to guide, in a stereotactic environment, the biopsy of a brain tumor. In comparison with [¹⁸F]FDG, this tracer has the advantage of offering better detection of non-anaplastic tumor zones and brain regions with infiltrating neoplastic cells.¹⁰²

Many studies have demonstrated that [¹¹C]methionine imaging is highly accurate in the detection of brain tumor boundaries both in primary lesions and in recurrences, regardless of their pathological grading.^{108,155,156} In a large series of gliomas, 35 out of 37 lesions were clearly depicted as hot spots on the [¹¹C]methionine images; by contrast, [¹⁸F]FDG (45 patients) visualized 23 lesions as hot spots (these were mostly high-grade gliomas) and 18 as hypometabolic

lesions, while four were difficult to distinguish from surrounding brain tissue.¹⁰⁸ The reported advantage of [¹¹C]methionine over [¹⁸F]FDG in delineating gliomas is probably not relevant in CNS lymphoma, where [¹⁸F]FDG uptake in tumor is much higher than in normal cortex.¹⁵⁷

Highly significant differences in amino acid uptake were demonstrated between low-grade and high-grade oligodendrogliomas, and in one recent study it was found that [¹¹C]methionine was even better than [¹⁸F]FDG in grading this type of tumor.¹⁰³

The use of [¹¹C]methionine-PET has been evaluated in low-grade gliomas after radiotherapy. It was demonstrated that stable or decreasing uptake of methionine in tumors during follow-up is apparently a favorable sign.¹⁵⁴

Other amino acids used for brain tumor imaging are tyrosine, thymidine, glutamate, and phenylalanine and their labeled derivatives. Tyrosine uptake in brain tumors can be assessed with its labeled derivatives: O-(2-[¹⁸F]fluoroethyl)-L-tyrosine (FET), L-[3-¹⁸F]methyltyrosine (FMT), and [¹²³I]iodomethyltyrosine (IMT).^{158,159} Also, the uptake of tyrosine-labeled derivatives is higher in brain tumors than in normal brain tissue. They are not incorporated into proteins, and their distribution patterns parallel that of methionine. Other labeled amino acids for the evaluation of brain tumors include [¹⁸F]fluorophenylalanine, which has a marked uptake in oligodendrogliomas,¹⁶⁰ and [¹¹C]choline, a tracer that has a higher uptake in glioblastoma cells than in normal brain tissue.¹⁶¹

Oxygen-15 is a short-lived positron-emitting isotope that can be used to measure hemodynamic parameters. Using mathematical modeling techniques, functional images of cerebral blood flow (CBF), oxygen extraction (OER), oxygen metabolic rate (rCMRO₂), and regional blood volume (CBV) can be derived from the combination of sequential studies with ¹⁵O₂, C¹⁵O₂, and C¹⁵O. Blood flow in tumors is variable, while oxygen metabolism has been found to be depressed in patients with gliomas, in keeping with the relatively anaerobic energy metabolism. The low OER implies that the tumor is not ischemic and that perfusion is sufficient to meet the metabolic need for oxygen in brain tumors before the initiation of any therapy.^{162,163}

The use of oxygen relative to that of glucose, i.e. metabolic ratio, is reduced in malignant gliomas. In normal brain, the metabolic ratio is 5.2 moles of oxygen per mole of glucose, whereas in gliomas it is 1.9. A low metabolic ratio concurrent with adequate blood flow and reduced oxygen extraction indicates aerobic glycolysis in tumors, i.e. the non-oxidative metabolism of glucose described by Warburg. Although oxygen metabolism in gliomas differs from that in normal brain, hypoxia appears to be an important factor in determining glioma aggressiveness and response to therapy. Low oxygen tension levels are associated with poor response to radiation therapy and recurrences. Spontaneous necrosis suggests the presence of hypoxic regions that are radioresistant. [¹⁸F]fluoromisonidazole (FMISO) is a

hypoxia agent for in vivo imaging with PET. FMISO is not retained in non-hypoxic tissues, and high-grade lesion uptake of FMISO is frequently heterogeneous and incompletely overlapping with FDG uptake.

The most direct measure of tumor growth and proliferation is the rate of DNA synthesis. Because thymidine is present in DNA and not in RNA, many tracer approaches for measuring tumor growth based on the rate of DNA synthesis have been based on the use of a labeled form of thymidine. The most popular compound for this purpose is [^{18}F]fluoro-L-thymidine (FLT).^{164,165} This compound has little degradation after injection and slow incorporation into DNA, but the lack of labeled metabolites generates high-contrast images in high-grade brain tumors, possibly related to increased expression of nucleoside transporters and cellular thymidine kinase activity²⁹ (Figure 3.10).

Tracers of cell membrane synthesis, including 1- $^{[11\text{C}]}$ acetate, $^{[11\text{C}]}$ choline, or [^{18}F]fluorocholine, show retention in tumor tissue but not by gray matter. For 1- $^{[11\text{C}]}$ acetate, in particular, in non-tumor regions of brain, $^{11\text{C}}$ will egress quickly as CO_2 by way of the tricarboxylic acid cycle. 1- $^{[11\text{C}]}$ acetate may be selectively taken up by glioma cells, because exogenous acetate is preferentially metabolized by astrocytes in the central nervous system and the uptake in astrocytes is by a carrier similar to the monocarboxylic acid transporter.¹⁶⁶

$^{[11\text{C}]}$ choline or [^{18}F]fluorocholine are alternative tracers that are being evaluated for lipid/membrane biosynthesis. Choline uptake could reflect choline transporter or choline kinase activity rather than lipid/membrane biosynthesis.¹⁶⁷ Choline uptake in low-grade tumors could be difficult to distinguish from that in gray matter structures.¹⁶⁸

Nuclear medicine images usually lack the anatomical information needed to define treatment margins with the accuracy requisite for surgery and radiotherapy planning. Nevertheless, functional brain mapping with H_2^{15}O -PET

associated with $^{11\text{C}}$ -methionine or [^{18}F]FDG has been proposed as an effective tool to define higher cortical functions near a brain tumor (Figure 3.11), with the aim of achieving aggressive resections with a reduced risk of neurological impairment.¹⁶⁹ Similar results have recently been obtained with SPECT and [$^{99\text{m}}\text{Tc}$]ethyl-cysteinate dimer (ECD), a tracer approved for the assessment of CBF. When this tracer is injected during a motor activation test, it clearly depicts sensorimotor and supplementary motor areas in patients with brain lesions near the central sulcus,¹⁷⁰ and this information is relevant in planning as extensive a resection as possible.

The same objective can be achieved with MRI of brain functions in relationship to intracranial tumors, to determine the risk for performing surgical excision and selecting the optimal surgical approach to a lesion. A variety of paradigms are used to produce a blood oxygen level-dependent response in various brain regions, which can be identified with fMRI. The paradigms used include active motor, language, or cognitive tasks, and passive tactile, auditory, or visual stimuli. Activation usually indicates the location of eloquent cortex. Lack of function in a region cannot be assumed when fMRI shows an absence of activation within the region.¹⁷¹

Conclusions and future outlook

Anatomical imaging procedures are essential tools for brain tumor assessment. No patient presenting with symptoms suggesting the presence of a brain tumor can be assessed properly unless an X-ray CT and/or an MRI scan is performed, with and without the administration of contrast agents and, in the case of MRI, with various acquisition sequences.¹⁷² Additional information can be obtained from functional imaging with emission tomography and MRS.

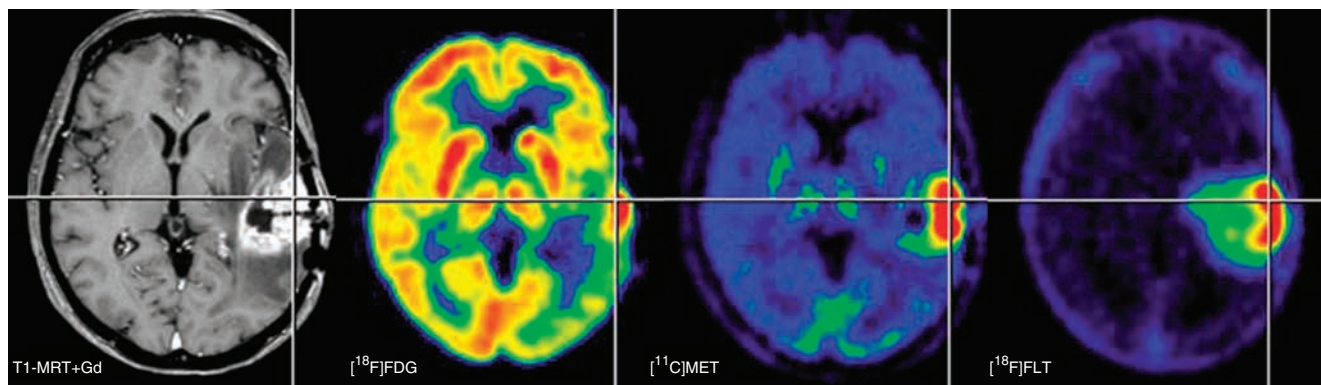


Figure 3.10

Parameters of interest in the non-invasive diagnosis of brain tumors. Alteration of the blood–brain barrier and the extent of peritumoral edema are detected by MRI. Signs of increased cell proliferation can be observed by means of multitracer PET imaging using [^{18}F]FDG (fluro-2-deoxy-D-glucose), $^{[11\text{C}]}$ MET, and [^{18}F]FLT (fluro-L-thymidine) as specific tracers for glucose consumption, amino acid transport, and DNA synthesis, respectively. Secondary phenomena, such as inactivation of ipsilateral cortical cerebral glucose metabolism, may be observed ([^{18}F]FDG) and are of prognostic relevance. (Reproduced with permission from reference 153.)

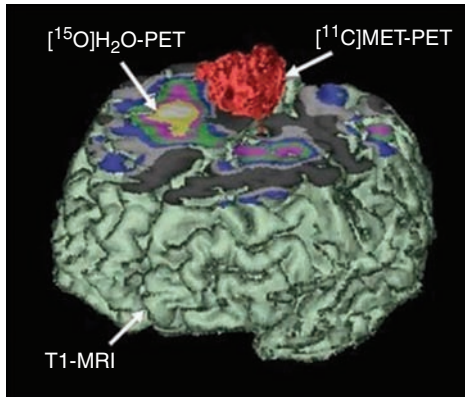


Figure 3.11

Preoperative differentiation of tumor tissue from functionally important neuronal tissue through multimodal and multitracer imaging. These combined imaging procedures guide the neurosurgeon to operate as much tumor as possible but at the same time to leave the functionally important tissue intact. (Reproduced with permission from reference 153.)

SPECT and PET with different tracers are indicated during the diagnostic work-up to determine the degree of malignancy and as a substitute or guide for biopsy, as well as to assess prognosis. After surgery and radiotherapy, anatomical and functional imaging is indicated to assess persistence of the tumor, to monitor progression and changes in the degree of malignancy, and to differentiate recurrence from radiation necrosis. Although somewhat similar information can be obtained with either MRI or X-ray CT, and with either SPECT or PET, each technique has unique features and provides information complementary to that acquired with the other techniques. The choice of which method to use, or of synergistic use of different methods, depends upon the availability, the question addressed, and the stage of the disease. In most cases SPECT methods may be perfectly adequate and provide results that parallel those obtained with PET. To claim that any single method (X-ray CT, PET, SPECT, MRI, etc.) is the ultimate magical one for brain tumor assessment is simply to limit one's opportunity to achieve a proper diagnosis. Best results are achieved when anatomical imaging (X-ray CT, MRI) and functional imaging (PET/SPECT) are used sequentially and to complement each other. Studies are being conducted to investigate the ability of some of the methods based on the use of radionuclides to assess processes that are relevant for disease management, such as the presence and expression of multidrug resistance in cancer. Imaging studies in experimental brain tumor models over the past 10 years aimed towards (1) the development of new radiotracers for cellular proliferation and protein synthesis, (2) characterization of these tracers with respect to their ability to detect responses to radio- and chemotherapy at a relatively early stage, (3) strategies for imaging transcriptional regulation and migration of tumor cells, and (4) imaging the expression of exogenous

genes carrying a marker or therapeutic function and introduced into experimental gliomas for the purpose of developing improved gene therapeutic vectors (Figure 3.12). These experimental strategies have been reviewed in detail

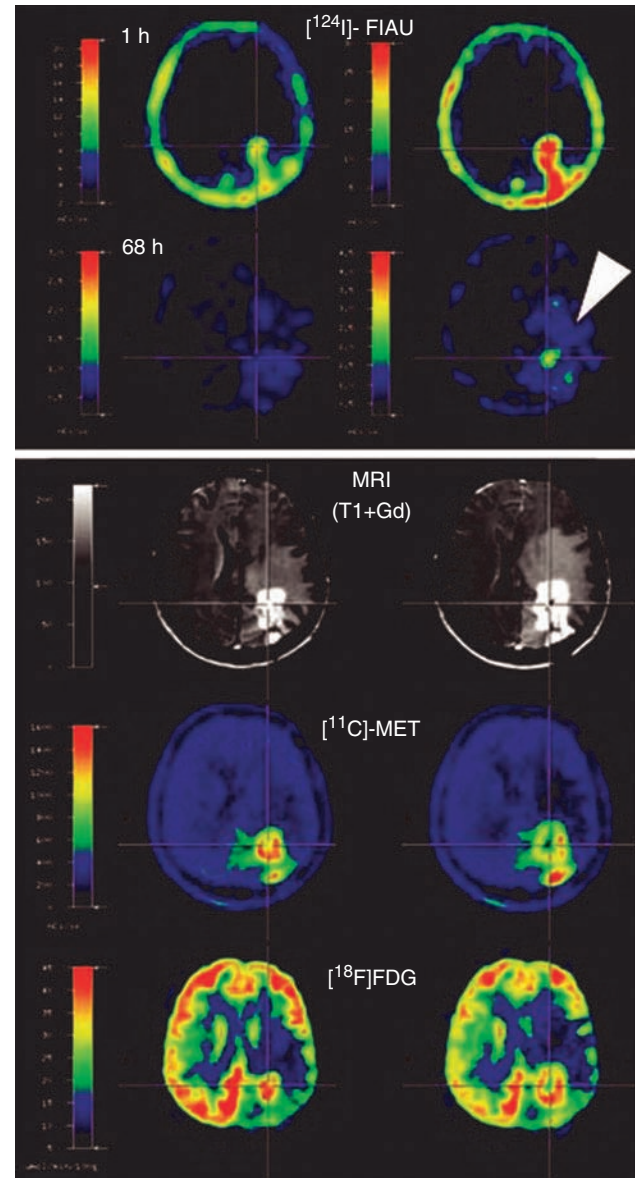


Figure 3.12

Multimodal imaging for the establishment of imaging-guided experimental treatment strategies. Co-registration of $[^{124}\text{I}]\text{FIAU}$, $[^{11}\text{C}]\text{MET}$, $[^{18}\text{F}]\text{FDG}$ -PET, and MRI before (left column) and after (right column) targeted application (stereotactic infusion) of a gene therapy vector. The region of specific $[^{124}\text{I}]\text{FIAU}$ retention (white arrowhead) resembles the proposed 'tissue dose' of vector-mediated gene expression and shows signs of necrosis (cross right column; reduced methionine uptake (MET) and glucose metabolism (FDG)) after ganciclovir treatment. (Reproduced with permission from reference 173.)

previously.¹⁷⁴ New developments aim towards (1) the detection of tumor cell migration in vivo,¹⁷⁵ the establishment of in vivo assays for direct imaging of tumor-specific signal transduction pathways (e.g. p53, E2F-1, and HIF-1- α regulated pathways),¹⁷⁵⁻¹⁷⁸ (3) the design of labeled peptides binding specifically to the cell adhesion receptor integrin $\alpha_v\beta_3$ or other tumor-specific antigens and of labeled bone marrow-derived endothelial precursor cells to allow highly specific tumor visualization and the study of glioma angiogenesis and neovascularization,¹⁷⁹⁻¹⁸³ (4) the generation and in vivo characterization of transgenic mice with gliomas induced by signaling through Ras and Akt pathways,¹⁸⁴ and (5) the construction of bifunctional imaging marker and therapeutic genes to allow direct assessment of therapeutic gene expression in culture and in vivo models

by directly corresponding assays.^{185,186} Especially the design of small tumor-specific antibody fragments is an attractive way for specific detection of tumor cells by imaging in vivo, as well as for targeted therapy by radioimmunotherapy. Many of the current experimental protocols investigating new drug and treatment strategies for experimental gliomas include MRI, optical or PET imaging of either the distribution of therapeutic agents,¹⁸⁷⁻¹⁸⁹ or therapy-induced tumor changes,^{185,190-198} with the overall attempt of designing image-guided treatments.^{173,199} Most intriguing for potential clinical application is the design of multifunctional nanoparticles that can be detected by both MRI and fluorescence imaging, allowing the non-invasive pre-operative assessment of the tumor and the intraoperative visualization of tumor margins by optical imaging.²⁰⁰

Table 3.1 Revised classification of primary intracranial tumours according to the World Health Organization (WHO)

<i>Histological class</i>	<i>Histology</i>	
	<i>Predominantly in adults</i>	<i>Predominantly in children</i>
Tumors of neuroepithelial tissue	Diffuse astrocytoma Anaplastic astrocytoma Astrocytoma Glioblastoma Oligodendroglioma Anaplastic oligodendroglioma Ependymoma/anaplastic ependymoma Mixed glioma	Pilocytic astrocytoma Ependymoma/anaplastic ependymoma Choroid plexus tumors Embryonal/primitive/medulloblastoma
Tumors of cranial and spinal nerves	Nerve sheath, benign and malignant	
Tumors of meninges	Meningioma Other mesenchymal, benign and malignant	
Lymphomas and hemopoietic neoplasms	Lymphoma	
Germ cell tumors and cysts		Germ cell tumors, cysts and heterotopias
Tumors of sellar region	Pituitary	
	Craniopharyngioma	

Table 3.2 Simplified classification of gliomas according to the World Health Organization (WHO)

<i>WHO grade</i> <i>(from least to most aggressive)</i>	<i>Classes of gliomas</i>		
	<i>Astrocytomas</i>	<i>Oligodendrogliomas</i>	<i>Mixed oligoastrocytomas</i>
1	Pilocytic astrocytoma (frequent in children, localized in the cerebellum)	—	—
2	Diffuse astrocytoma	Oligodendroglioma	Oligoastrocytoma
3	Anaplastic astrocytoma	Anaplastic oligodendroglioma	Anaplastic oligoastrocytoma
4	Glioblastoma	—	—

Table 3.3 Typical traditional neuroimaging findings of the main intracranial tumors

Type of tumor	Percentage of all primary intracranial tumors	Median age at diagnosis (years)	MR/CT findings	PET tracer
Gliomas	40% of all brain tumors (78% of malignant brain tumors)			
<i>High grade gliomas</i>				
Glioblastoma (grade 4)	20.3%	64	CT: irregular lesion MR: T ₁ hypointense inhomogeneous lesion with ring-like CE (contrast enhancement) around irregular foci of necrosis and edema, mass effect	[¹⁸ F]FDG: high uptake [¹¹ C]MET: very high uptake
Anaplastic astrocytoma (grade 3)	3.2%	51	CT: inhomogeneous lesion MR: T ₁ hypointense, CE and perifocal edema; T ₂ hyperintense	[¹⁸ F]FDG: usually high uptake [¹¹ C]MET: very high uptake
Anaplastic oligodendroglioma (grade 3)	1.2%	48	CT: inhomogeneous lesion with focal CE and calcifications	[¹⁸ F]FDG: variable uptake [¹¹ C]MET: very high uptake
<i>Low grade gliomas</i>				
Diffuse astrocytoma (grade 2)	0.7%	46	MR: diffuse, non-enhancing mass; distinct borders; no edema; T ₁ hypointense; T ₂ hyperintense	[¹⁸ F]FDG: low uptake [¹¹ C]MET: high uptake
Oligodendroglioma (grade 2)	2.5%	41		[¹⁸ F]FDG: variable uptake [¹¹ C]MET: high uptake
Mixed glioma (grade 2)	1.1%	42	FLAIR hyperintense (oligodendroglioma can have calcifications and hemorrhage)	[¹⁸ F]FDG: variable uptake [¹¹ C]MET: high uptake
Pilocytic astrocytoma (grade 1)	2.3% (20.9% of tumors occurring within ages 0–14)	12	CT and MR: well-circumscribed, contrast-enhancing cystic tumor	[¹⁸ F]FDG: variable uptake [¹¹ C]MET: high uptake
Ependymoma	2%	39	CT: hypodense MR: solid structure with heterogeneous signal intensity, CE, typical localization in fourth ventricle (if supratentorial: periventricular localization) or intramedullary; often cystic, hemorrhages	[¹⁸ F]FDG: low uptake [¹¹ C]MET: very high uptake
Choroid plexus papilloma	0.3%	21	CT: iso/hyperdensity MR/CT: characteristic localization in ventricles; sharp tumor border; gross contrast enhancement	[¹¹ C]MET: high uptake

Table 3.3 Typical traditional neuroimaging findings of the main intracranial tumors—cont'd

<i>Type of tumor</i>	<i>Percentage of all primary intracranial tumors</i>	<i>Median age at diagnosis (years)</i>	<i>MR/CT findings</i>	<i>PET tracer</i>
Meningioma	30.1%	64	<p>Localization: adjacent to bone with typical growth along the dura ('dural tail') in the typical localizations (see text)</p> <p>CT: hyperdensity, possible calcifications</p> <p>MR: T₁ isointense; T₂ hypointense; infiltration of bone; dural artery; dural tail sign</p> <p>Diffuse contrast enhancement</p>	<p>[¹⁸F]FDG: variable uptake</p> <p>[¹¹C]MET: high uptake</p> <p>[¹⁸F]FES: high uptake</p>
Pituitary adenoma	6.3%	49	<p><i>Microadenomas:</i></p> <p>MR: high variability (for details see reference 201)</p> <p>Most commonly: T₁ hypo- or isointense; no contrast enhancement in contrast with the healthy pituitary gland</p> <p><i>Macroadenomas:</i> T₁ and T₂ inhomogeneous</p> <p>Utility of contrast enhancement relies on the contrast between slight contrast enhancement of the tumor, and strong enhancement of healthy pituitary tissue</p>	[¹⁸ F]FESP: high uptake
Medulloblastoma	1.7% (16.8% of tumors occurring within ages 0–14)	9	<p>(Brain and spinal MR for risk of dissemination through cerebrospinal fluid)</p> <p>Localized in fourth ventricle (75%) or cerebellum (25%)</p> <p>MR: homogeneously enhancing masses; T₁ hypointense; T₂ hyperintense</p>	<p>[¹⁸F]FDG: very high uptake</p> <p>[¹¹C]MET: high uptake</p>
Lymphoma	3.1%	60	<p>CT, MR: diffuse and homogeneous pattern of enhancement</p> <p>Localization: periventricular, in 50% of cases multiple sites (at diagnosis in 25% of cases spinal dissemination, in 20% of cases infiltration of the eye)</p>	<p>[¹⁸F]FDG: very high uptake</p> <p>[¹¹C]MET: high uptake</p>

MR, magnetic resonance; CT, computed tomography; PET, positron emission tomography; FDG, fluro-2-deoxy-D-glucose; MET, methionine; FES, fluroethylspiperone; FESP, fluroestradiol.

Table 3.4 Summary of indications for use of radionuclide imaging of brain tumors**[¹⁸F]FDG-PET**

- 1 Grading: 90% accurate for tumor grading (low grade versus high grade) and prognosis
- 2 Progression: monitoring of progression from low-grade to high-grade glioma
- 3 Together with amino acid tracer: differentiating radionecrosis and recurrence. However, recurrence may be undetectable due to high glucose consumption in surrounding normal brain tissue
- 4 Differentiation between primary CNS lymphoma and toxoplasmosis

L-amino acids PET/SPECT

- 1 Grading: together with [¹⁸F]FDG-PET
- 2 Delineation: good separation of tumor from surrounding normal brain tissue (in comparison to [¹⁸F]FDG-PET)
- 3 Residuuum/progression: good delineation of residual tumor and determination of tumor progression
- 4 Differentiation between radiation necrosis and recurrent tumor

²⁰¹Tl-SPECT

- 1 Accurate for glioma grading (low uptake in glioma WHO 1–2 vs. high uptake in glioma 3–4, non-Hodgkin's lymphoma, metastases)
- 2 Poor separation of gliomas 1–2 from non-tumoral lesions and of gliomas 3–4 from meningiomas
- 3 Good prediction of malignancy, accurate estimation of therapeutic efficacy, early detection of recurrence and of malignant transformation

[^{99m}Tc]sestamibi SPECT

- 1 Accurate for glioma grading (low uptake in glioma WHO 1–2 vs. high uptake in glioma 3–4, non-Hodgkin's lymphoma, metastases)
- 2 High positive predictive value but low negative predictive value in tumor relapse after radiotherapy

CNS, central nervous system; SPECT, single photon emission computed tomography.

References

1. Del Sole A, Falini A, Ravasi L et al. Anatomical and biochemical investigation of primary brain tumours. *Eur J Nucl Med* 2001; 28: 1851–72.
2. 2005–2006 Statistics Reports of the Central Brain Tumor Registry of the United States. <http://www.cbtrus.org/>, 2006.
3. Wen PY BPLJ. Treatment of metastatic cancer. In: DeVita VT Jr HSRS, eds. *Cancer: Principles and Practice of Oncology*. Philadelphia: Lippincott Williams & Wilkins, 2001: 2655–70.
4. Patchell RA. The management of brain metastases. *Cancer Treat Rev* 2003; 29: 533–40.
5. Collins VP. Brain tumours: classification and genes. *J Neurol Neurosurg Psychiatry* 2004; 75 (Suppl 2): ii2–11.
6. Kleihues P, Louis DN, Scheithauer BW et al. The WHO classification of tumors of the nervous system. *J Neuropathol Exp Neurol* 2002; 61: 215–25.
7. Behin A, Hoang-Xuan K, Carpentier AF, Delattre JY. Primary brain tumours in adults. *Lancet* 2003; 361: 323–31.
8. He J, Mokhtari K, Sanson M et al. Glioblastomas with an oligodendroglial component: a pathological and molecular study. *J Neuropathol Exp Neurol* 2001; 60: 863–71.
9. Stupp R, Mason WP, van den Bent MJ et al. Radiotherapy plus concomitant and adjuvant temozolomide for glioblastoma. *N Engl J Med* 2005; 352: 987–96.
10. Stupp R, Hegi ME, van den Bent MJ et al. Changing paradigms—an update on the multidisciplinary management of malignant glioma. *Oncologist* 2006; 11: 165–80.
11. Cairncross JG, Macdonald DR. Successful chemotherapy for recurrent malignant oligodendroglioma. *Ann Neurol* 1988; 23: 360–4.
12. Cairncross JG, Ueki K, Zlatescu MC et al. Specific genetic predictors of chemotherapeutic response and survival in patients with anaplastic oligodendrogliomas. *J Natl Cancer Inst* 1998; 90: 1473–9.
13. Ino Y, Betensky RA, Zlatescu MC et al. Molecular subtypes of anaplastic oligodendroglioma: implications for patient management at diagnosis. *Clin Cancer Res* 2001; 7: 839–45.
14. Whittle IR, Smith C, Navoo P, Collie D. Meningiomas. *Lancet* 2004; 363: 1535–43.
15. Markopoulos C, Sampalis F, Givalos N, Gogas H. Association of breast cancer with meningioma. *Eur J Surg Oncol* 1998; 24: 332–4.
16. Antinheimo J, Sankila R, Carpen O, Pukkala E, Sainio M, Jaaskelainen J. Population-based analysis of sporadic and

- type 2 neurofibromatosis-associated meningiomas and schwannomas. *Neurology* 2000; 54: 71–6.
17. Plotkin SR. Update on primary central nervous system lymphoma. *Curr Opin Neurol* 2005; 18: 645–53.
 18. Cote TR, Manns A, Hardy CR, Yellin FJ, Hartge P. Epidemiology of brain lymphoma among people with or without acquired immunodeficiency syndrome. AIDS/Cancer Study Group. *J Natl Cancer Inst* 1996; 88: 675–9.
 19. Deangelis LM. Brain tumors. *N Engl J Med* 2001; 344: 114–23.
 20. Pollack IF. Brain tumors in children. *N Engl J Med* 1994; 331: 1500–7.
 21. Merchant TE, Fouladi M. Ependymoma: new therapeutic approaches including radiation and chemotherapy. *J Neurooncol* 2005; 75: 287–99.
 22. Schild SE, Nisi K, Scheithauer BW et al. The results of radiotherapy for ependymomas: the Mayo Clinic experience. *Int J Radiat Oncol Biol Phys* 1998; 42: 953–8.
 23. McEvoy AW, Harding BN, Phipps KP et al. Management of choroid plexus tumours in children: 20 years experience at a single neurosurgical centre. *Pediatr Neurosurg* 2000; 32: 192–9.
 24. Barker FG IM. Molecular genetics. In: Berger MS WC, eds. *The Gliomas*. Philadelphia: WB Saunders Co, 1999: 39–51.
 25. Ichimura K, Bolin MB, Goike HM et al. Deregulation of the p14ARF/MDM2/p53 pathway is a prerequisite for human astrocytic gliomas with G1–S transition control gene abnormalities. *Cancer Res* 2000; 60: 417–24.
 26. Morrison RS. Growth factor mediated signaling pathways. In: Berger MS WC, eds. *The Gliomas*. Philadelphia: WB Saunders Co, 1999: 52–64.
 27. Kleihues P BPCVNEOHCW. Glioblastoma. In: Kleihues P CW, eds. *Pathology and Genetics of Tumours of the Nervous System*. World Health Organisation Classification of Tumours. Lyon: IARC Press, 2000: 29–39.
 28. Lang FF, Miller DC, Koslow M, Newcomb EW. Pathways leading to glioblastoma multiforme: a molecular analysis of genetic alterations in 65 astrocytic tumors. *J Neurosurg* 1994; 81: 427–36.
 29. Deangelis LM, Burger PC, Green SB, Cairncross JG. Malignant glioma: who benefits from adjuvant chemotherapy? *Ann Neurol* 1998; 44: 691–5.
 30. Reifenberger G, Louis DN. Oligodendroglioma: toward molecular definitions in diagnostic neuro-oncology. *J Neuropathol Exp Neurol* 2003; 62: 111–26.
 31. Sasaki H, Zlatescu MC, Betensky RA et al. Histopathological-molecular genetic correlations in referral pathologist-diagnosed low-grade 'oligodendroglioma'. *J Neuropathol Exp Neurol* 2002; 61: 58–63.
 32. Coons SW, Johnson PC, Scheithauer BW, Yates AJ, Pearl DK. Improving diagnostic accuracy and interobserver concordance in the classification and grading of primary gliomas. *Cancer* 1997; 79: 1381–93.
 33. Del Sole A, Moncayo R, Tafuni G, Lucignani G. Position of nuclear medicine techniques in the diagnostic work-up of brain tumors. *Q J Nucl Med Mol Imaging* 2004; 48: 76–81.
 34. Jacobs AH, Kracht LW, Gossman A et al. Imaging in neurooncology. *NeuroRx* 2005; 2: 333–47.
 35. Hackney DB, Atlas SW, Grossman RI et al. Subacute intracranial hemorrhage: contribution of spin density to appearance on spin-echo MR images. *Radiology* 1987; 165: 199–202.
 36. Gatenby RA, Coia LR, Richter MP et al. Oxygen tension in human tumors: in vivo mapping using CT-guided probes. *Radiology* 1985; 156: 211–14.
 37. Sze G, Krol G, Olsen WL et al. Hemorrhagic neoplasms: MR mimics of occult vascular malformations. *AJR Am J Roentgenol* 1987; 149: 1223–30.
 38. Atlas SW, ed. *Magnetic Resonance Imaging of the Brain and Spine*. Philadelphia: Raven Press, 1996.
 39. Nelson SJ. Imaging of brain tumors after therapy. *Neuroimaging Clin North Am* 1999; 9: 801–19.
 40. Sugahara T, Korogi Y, Kochi M et al. Usefulness of diffusion-weighted MRI with echo-planar technique in the evaluation of cellularity in gliomas. *J Magn Reson Imaging* 1999; 9: 53–60.
 41. Tsuruda JS, Chew WM, Moseley ME, Norman D. Diffusion-weighted MR imaging of the brain: value of differentiating between extraaxial cysts and epidermoid tumors. *AJNR Am J Neuroradiol* 1990; 11: 925–31.
 42. Black PM. Brain tumors. Part 1. *N Engl J Med* 1991; 324: 1471–6.
 43. Aronen HJ, Gazit IE, Louis DN et al. Cerebral blood volume maps of gliomas: comparison with tumor grade and histologic findings. *Radiology* 1994; 191: 41–51.
 44. Pardo FS, Aronen HJ, Kennedy D et al. Functional cerebral imaging in the evaluation and radiotherapeutic treatment planning of patients with malignant glioma. *Int J Radiat Oncol Biol Phys* 1994; 30: 663–9.
 45. Sugahara T, Korogi Y, Shigematsu Y et al. Value of dynamic susceptibility contrast magnetic resonance imaging in the evaluation of intracranial tumors. *Top Magn Reson Imaging* 1999; 10: 114–24.
 46. Uematsu H, Maeda M. Double-echo perfusion-weighted MR imaging: basic concepts and application in brain tumors for the assessment of tumor blood volume and vascular permeability. *Eur Radiol* 2006; 16: 180–6.
 47. Pauleit D, Langen KJ, Floeth F et al. Can the apparent diffusion coefficient be used as a noninvasive parameter to distinguish tumor tissue from peritumoral tissue in cerebral gliomas? *J Magn Reson Imaging* 2004; 20: 758–64.
 48. Arfanakis K, Gui M, Lazar M. Optimization of white matter tractography for pre-surgical planning and image-guided surgery. *Oncol Rep* 2006; 15 Spec no: 1061–4.
 49. Demaerel P, Johannik K, Van Hecke P et al. Localized 1H NMR spectroscopy in fifty cases of newly diagnosed intracranial tumors. *J Comput Assist Tomogr* 1991; 15: 67–76.
 50. Negendank WG, Sauter R, Brown TR et al. Proton magnetic resonance spectroscopy in patients with glial tumors: a multicenter study. *J Neurosurg* 1996; 84: 449–58.
 51. Preul MC, Caramanos Z, Collins DL et al. Accurate, noninvasive diagnosis of human brain tumors by using proton magnetic resonance spectroscopy. *Nat Med* 1996; 2: 323–5.
 52. Somorjai RL, Dolenko B, Nikulin AK et al. Classification of 1H MR spectra of human brain neoplasms: the influence of preprocessing and computerized consensus diagnosis on classification accuracy. *J Magn Reson Imaging* 1996; 6: 437–44.
 53. Tedeschi G, Lundbom N, Raman R et al. Increased choline signal coinciding with malignant degeneration of cerebral gliomas: a serial proton magnetic resonance spectroscopy imaging study. *J Neurosurg* 1997; 87: 516–24.

54. Kaplan WD, Takvorian T, Morris JH et al. Thallium-201 brain tumor imaging: a comparative study with pathologic correlation. *J Nucl Med* 1987; 28: 47–52.
55. Elgazzar AH, Fernandez-Ulloa M, Silberstein EB. 201Tl as a tumour-localizing agent: current status and future considerations. *Nucl Med Commun* 1993; 14: 96–103.
56. Kim KT, Black KL, Marciano D et al. Thallium-201 SPECT imaging of brain tumors: methods and results. *J Nucl Med* 1990; 31: 965–9.
57. Yoshii Y, Komatsu Y, Yamada T et al. Malignancy and viability of intraparenchymal brain tumours: correlation between Gd-DTPA contrast MR images and proliferative potentials. *Acta Neurochir (Wien)* 1992; 117: 187–94.
58. Dierckx RA, Martin JJ, Dobbeleir A et al. Sensitivity and specificity of thallium-201 single-photon emission tomography in the functional detection and differential diagnosis of brain tumours. *Eur J Nucl Med* 1994; 21: 621–33.
59. Ricci M, Pantano P, Pierallini A et al. Relationship between thallium-201 uptake by supratentorial glioblastomas and their morphological characteristics on magnetic resonance imaging. *Eur J Nucl Med* 1996; 23:524–9.
60. Staffen W, Hondl N, Trinka E et al. Clinical relevance of 201Tl-chloride SPET in the differential diagnosis of brain tumours. *Nucl Med Commun* 1998; 19: 335–40.
61. Taki S, Kakuda K, Kakuma K et al. 201Tl SPET in the differential diagnosis of brain tumours. *Nucl Med Commun* 1999; 20: 637–45.
62. Sasaki M, Kuwabara Y, Yoshida T et al. A comparative study of thallium-201 SPET, carbon-11 methionine PET and fluorine-18 fluorodeoxyglucose PET for the differentiation of astrocytic tumours. *Eur J Nucl Med* 1998; 25: 1261–9.
63. Soler C, Beauchesne P, Maatougui K et al. Technetium-99m sestamibi brain single-photon emission tomography for detection of recurrent gliomas after radiation therapy. *Eur J Nucl Med* 1998; 25: 1649–57.
64. Maffioli L, Gasparini M, Chiti A et al. Clinical role of technetium-99m sestamibi single-photon emission tomography in evaluating pretreated patients with brain tumours. *Eur J Nucl Med* 1996; 23: 308–11.
65. Park CH, Kim SM, Zhang JJ, Intenzo CM, McEwan JR. Tc-99m MIBI brain SPECT in the diagnosis of recurrent glioma. *Clin Nucl Med* 1994; 19: 57–8.
66. Piwnica-Worms D, Kronauge JF, Chiu ML. Uptake and retention of hexakis (2-methoxyisobutyl isonitrile) technetium(I) in cultured chick myocardial cells. Mitochondrial and plasma membrane potential dependence. *Circulation* 1990; 82: 1826–38.
67. O'Tuama LA, Treves ST, Larar JN et al. Thallium-201 versus technetium-99m-MIBI SPECT in evaluation of childhood brain tumors: a within-subject comparison. *J Nucl Med* 1993; 34: 1045–51.
68. Baillet G, Albuquerque L, Chen Q, Poisson M, Delattre JY. Evaluation of single-photon emission tomography imaging of supratentorial brain gliomas with technetium-99m sestamibi. *Eur J Nucl Med* 1994; 21: 1061–6.
69. Bagni B, Pinna L, Tamarozzi R et al. SPET imaging of intracranial tumours with 99Tcm-sestamibi. *Nucl Med Commun* 1995; 16: 258–64.
70. Piwnica-Worms D, Chiu ML, Budding M et al. Functional imaging of multidrug-resistant P-glycoprotein with an organotechnetium complex. *Cancer Res* 1993; 53: 977–84.
71. De Moerloose B, Van de Wiele C, Dhooge C et al. Technetium-99m sestamibi imaging in paediatric neuroblastoma and ganglioneuroma and its relation to P-glycoprotein. *Eur J Nucl Med* 1999; 26: 396–403.
72. Soricelli A, Cuocolo A, Varrone A et al. Technetium-99m-tetrofosmin uptake in brain tumors by SPECT: comparison with thallium-201 imaging. *J Nucl Med* 1998; 39: 802–6.
73. Choi JY, Kim SE, Shin HJ, Kim BT, Kim JH. Brain tumor imaging with 99mTc-tetrofosmin: comparison with 201Tl, 99mTc-MIBI, and 18F-fluorodeoxyglucose. *J Neurooncol* 2000; 46: 63–70.
74. Paganelli G, Magnani P, Zito F et al. Pre-targeted immunodetection in glioma patients: tumour localization and single-photon emission tomography imaging of [99mTc]PnAO-biotin. *Eur J Nucl Med* 1994; 21: 314–321.
75. Schmidt M, Scheidhauer K, Luyken C et al. Somatostatin receptor imaging in intracranial tumours. *Eur J Nucl Med* 1998; 25: 675–86.
76. Muhr C, Bergstrom M, Lundberg PO et al. Dopamine receptors in pituitary adenomas: PET visualization with 11C-N-methylspiperone. *J Comput Assist Tomogr* 1986; 10:175–80.
77. Daemen BJ, Zwertbroek R, Elsinga PH et al. PET studies with L-[1-11C]tyrosine, L-[methyl-11C]methionine and 18F-fluorodeoxyglucose in prolactinomas in relation to bromocryptine treatment. *Eur J Nucl Med* 1991; 18: 453–60.
78. Bergstrom M, Muhr C, Jossan S et al. Differentiation of pituitary adenoma and meningioma: visualization with positron emission tomography and [11C]-L-deprenyl. *Neurosurgery* 1992; 30: 855–61.
79. Pirker W, Riedl M, Luger A et al. Dopamine D2 receptor imaging in pituitary adenomas using iodine-123-epidepride and SPECT. *J Nucl Med* 1996; 37: 1931–7.
80. Lucignani G, Losa M, Moresco RM et al. Differentiation of clinically non-functioning pituitary adenomas from meningiomas and craniopharyngiomas by positron emission tomography with [18F]fluoro-ethyl-spiperone. *Eur J Nucl Med* 1997; 24: 1149–55.
81. de Herder WW, Reijs AE, de Swart J et al. Comparison of iodine-123 epidepride and iodine-123 IBZM for dopamine D2 receptor imaging in clinically non-functioning pituitary macroadenomas and macroprolactinomas. *Eur J Nucl Med* 1999; 26: 46–50.
82. Junck L, Olson JM, Ciliax BJ et al. PET imaging of human gliomas with ligands for the peripheral benzodiazepine binding site. *Ann Neurol* 1989; 26: 752–8.
83. Pappata S, Cornu P, Samson Y et al. PET study of carbon-11-PK 11195 binding to peripheral type benzodiazepine sites in glioblastoma: a case report. *J Nucl Med* 1991; 32: 1608–10.
84. Weckesser M, Matheja P, Rickert C et al. Evaluation of the extension of cerebral gliomas by scintigraphy. *Strahlenther Onkol* 2000; 176: 180–5.
85. Warburg O. PKNE. Ueber den Stoffwechsel der Carcinomzelle. *Biochem Z* 1924; 309–4.
86. Rhodes CG, Wise RJ, Gibbs JM et al. In vivo disturbance of the oxidative metabolism of glucose in human cerebral gliomas. *Ann Neurol* 1983; 14: 614–26.
87. Mineura K, Yasuda T, Kowada M et al. Positron emission tomographic evaluation of histological malignancy in gliomas using oxygen-15 and fluorine-18-fluorodeoxyglucose. *Neurol Res* 1986; 8: 164–8.

88. Hatanaka M. Transport of sugars in tumor cell membranes. *Biochim Biophys Acta* 1974; 355: 77–104.
89. Nishioka T, Oda Y, Seino Y et al. Distribution of the glucose transporters in human brain tumors. *Cancer Res* 1992; 52: 3972–9.
90. Brooks DJ, Beaney RP, Lammertsma AA et al. Glucose transport across the blood–brain barrier in normal human subjects and patients with cerebral tumours studied using [¹¹C]3-O-methyl-D-glucose and positron emission tomography. *J Cereb Blood Flow Metab* 1986; 6: 23–9.
91. Mies G. Measurement of in vivo glucose transport from blood to tissue of experimentally-induced glioma in rat brain. *J Neurooncol* 1992; 12: 13–23.
92. Herholz K, Rudolf J, Heiss WD. FDG transport and phosphorylation in human gliomas measured with dynamic PET. *J Neurooncol* 1992; 12: 159–65.
93. Weber WA, Ziegler SI, Thodtmann R, Hanauske AR, Schwaiger M. Reproducibility of metabolic measurements in malignant tumors using FDG PET. *J Nucl Med* 1999; 40: 1771–7.
94. Di Chiro G, Brooks RA. PET quantitation: blessing and curse. *J Nucl Med* 1988; 29: 1603–4.
95. Hustinx R, Smith RJ, Benard F, Bhatnagar A, Alavi A. Can the standardized uptake value characterize primary brain tumors on FDG-PET? *Eur J Nucl Med* 1999; 26: 1501–9.
96. Barker FG, Chang SM, Valk PE, Pounds TR, Prados MD. 18-Fluorodeoxyglucose uptake and survival of patients with suspected recurrent malignant glioma. *Cancer* 1997; 79: 115–26.
97. Kim CK, Alavi JB, Alavi A, Reivich M. New grading system of cerebral gliomas using positron emission tomography with F-18 fluorodeoxyglucose. *J Neurooncol* 1991; 10: 85–91.
98. Kim S, Chung JK, Im SH et al. 11C-methionine PET as a prognostic marker in patients with glioma: comparison with 18F-FDG PET. *Eur J Nucl Med Mol Imaging* 2005; 32: 52–9.
99. Kaschten B, Stevenaert A, Sadzot B et al. Preoperative evaluation of 54 gliomas by PET with fluorine-18-fluorodeoxyglucose and/or carbon-11-methionine. *J Nucl Med* 1998; 39: 778–85.
100. Goldman S, Levivier M, Pirotte B et al. Regional glucose metabolism and histopathology of gliomas. A study based on positron emission tomography-guided stereotactic biopsy. *Cancer* 1996; 78: 1098–106.
101. Kracht LW, Friese M, Herholz K et al. Methyl-[¹¹C]-l-methionine uptake as measured by positron emission tomography correlates to microvessel density in patients with glioma. *Eur J Nucl Med Mol Imaging* 2003; 30: 868–73.
102. Goldman S, Levivier M, Pirotte B et al. Regional methionine and glucose uptake in high-grade gliomas: a comparative study on PET-guided stereotactic biopsy. *J Nucl Med* 1997; 38: 1459–62.
103. Derlon JM, Chapon F, Noel MH et al. Non-invasive grading of oligodendrogliomas: correlation between in vivo metabolic pattern and histopathology. *Eur J Nucl Med* 2000; 27: 778–87.
104. Kaplan AM, Lawson MA, Spataro J et al. Positron emission tomography using [¹⁸F] fluorodeoxyglucose and [¹¹C] l-methionine to metabolically characterize dysembryoplastic neuroepithelial tumors. *J Child Neurol* 1999; 14: 673–7.
105. Pirotte B, Goldman S, Massager N et al. Comparison of 18F-FDG and 11C-methionine for PET-guided stereotactic brain biopsy of gliomas. *J Nucl Med* 2004; 45: 1293–8.
106. Herholz K, Pietrzyk U, Voges J et al. Correlation of glucose consumption and tumor cell density in astrocytomas. A stereotactic PET study. *J Neurosurg* 1993; 79: 853–8.
107. Delbeke D, Meyerowitz C, Lapidus RL et al. Optimal cutoff levels of F-18 fluorodeoxyglucose uptake in the differentiation of low-grade from high-grade brain tumors with PET. *Radiology* 1995; 195: 47–52.
108. Derlon JM, Petit-Taboue MC, Chapon F et al. The in vivo metabolic pattern of low-grade brain gliomas: a positron emission tomographic study using 18F-fluorodeoxyglucose and 11C-L-methylmethionine. *Neurosurgery* 1997; 40: 276–87.
109. Kincaid PK, El Saden SM, Park SH, Goy BW. Cerebral gangliogliomas: preoperative grading using FDG-PET and 201Tl-SPECT. *AJNR Am J Neuroradiol* 1998; 19: 801–6.
110. Pirotte B, Levivier M, Morelli D et al. Positron emission tomography for the early postsurgical evaluation of pediatric brain tumors. *Childs Nerv Syst* 2005; 21: 294–300.
111. Pirotte B, Goldman S, Massager N et al. Combined use of 18F-fluorodeoxyglucose and 11C-methionine in 45 positron emission tomography-guided stereotactic brain biopsies. *J Neurosurg* 2004; 101: 476–83.
112. Narayanan TK, Said S, Mukherjee J et al. A comparative study on the uptake and incorporation of radiolabeled methionine, choline and fluorodeoxyglucose in human astrocytoma. *Mol Imaging Biol* 2002; 4: 147–56.
113. Chung JK, Kim YK, Kim SK et al. Usefulness of 11C-methionine PET in the evaluation of brain lesions that are hypo- or isometabolic on 18F-FDG PET. *Eur J Nucl Med Mol Imaging* 2002; 29: 176–82.
114. Voges J, Herholz K, Holzer T et al. 11C-methionine and 18F-2-fluorodeoxyglucose positron emission tomography: a tool for diagnosis of cerebral glioma and monitoring after brachytherapy with 125I seeds. *Stereotact Funct Neurosurg* 1997; 69: 129–35.
115. Di Chiro G, DeLaPaz RL, Brooks RA et al. Glucose utilization of cerebral gliomas measured by [¹⁸F] fluorodeoxyglucose and positron emission tomography. *Neurology* 1982; 32: 1323–9.
116. Di Chiro G, Bairamian D. Brain imaging of glucose utilization in cerebral tumors. *Am J Physiol Imaging* 1988; 3: 56.
117. Gupta NC, Nicholson P, Bloomfield SM. FDG-PET in the staging work-up of patients with suspected intracranial metastatic tumors. *Ann Surg* 1999; 230: 202–6.
118. Mineura K, Shioya H, Kowada M et al. Blood flow and metabolism of oligodendrogliomas: a positron emission tomography study with kinetic analysis of 18F-fluorodeoxyglucose. *J Neurooncol* 1999; 43: 49–57.
119. Kracht LW, Bauer A, Herholz K et al. Positron emission tomography in a case of intracranial hemangiopericytoma. *J Comput Assist Tomogr* 1999; 23: 365–8.
120. Fulham MJ, Melisi JW, Nishimiya J, Dwyer AJ, Di Chiro G. Neuroimaging of juvenile pilocytic astrocytomas: an enigma. *Radiology* 1993; 189: 221–5.
121. Wong TZ, van der Westhuizen GJ, Coleman RE. Positron emission tomography imaging of brain tumors. *Neuroimaging Clin North Am* 2002; 12: 615–26.

122. Levivier M, Goldman S, Pirotte B et al. Diagnostic yield of stereotactic brain biopsy guided by positron emission tomography with [18F]fluorodeoxyglucose. *J Neurosurg* 1995; 82: 445–52.
123. Francavilla TL, Miletich RS, Di Chiro G et al. Positron emission tomography in the detection of malignant degeneration of low-grade gliomas. *Neurosurgery* 1989; 24: 1–5.
124. De Witte O, Levivier M, Violon P et al. Prognostic value positron emission tomography with [18F]fluoro-2-deoxy-D-glucose in the low-grade glioma. *Neurosurgery* 1996; 39: 470–6.
125. Kim EE, Chung SK, Haynie TP et al. Differentiation of residual or recurrent tumors from post-treatment changes with F-18 FDG PET. *Radiographics* 1992; 12: 269–79.
126. Haberkorn U, Strauss LG, Dimitrakopoulou A et al. Fluorodeoxyglucose imaging of advanced head and neck cancer after chemotherapy. *J Nucl Med* 1993; 34: 12–17.
127. Di Chiro G, Oldfield E, Wright DC et al. Cerebral necrosis after radiotherapy and/or intraarterial chemotherapy for brain tumors: PET and neuropathologic studies. *AJR Am J Roentgenol* 1988; 150: 189–97.
128. Ishikawa M, Kikuchi H, Miyatake S et al. Glucose consumption in recurrent gliomas. *Neurosurgery* 1993; 33: 28–33.
129. Patronas NJ, Di Chiro G, Kufta C et al. Prediction of survival in glioma patients by means of positron emission tomography. *J Neurosurg* 1985; 62: 816–22.
130. Alavi JB, Alavi A, Chawluk J et al. Positron emission tomography in patients with glioma. A predictor of prognosis. *Cancer* 1988; 62: 1074–8.
131. Glantz MJ, Hoffman JM, Coleman RE et al. Identification of early recurrence of primary central nervous system tumors by [18F]fluorodeoxyglucose positron emission tomography. *Ann Neurol* 1991; 29: 347–55.
132. Schifter T, Hoffman JM, Hanson MW et al. Serial FDG-PET studies in the prediction of survival in patients with primary brain tumors. *J Comput Assist Tomogr* 1993; 17: 509–61.
133. Barker FG, Chang SM, Valk PE, Pounds TR, Prados MD. 18-Fluorodeoxyglucose uptake and survival of patients with suspected recurrent malignant glioma. *Cancer* 1997; 79: 115–26.
134. Spence AM, Muzi M, Mankoff DA et al. 18F-FDG PET of gliomas at delayed intervals: improved distinction between tumor and normal gray matter. *J Nucl Med* 2004; 45: 1653–9.
135. Isselbacher KJ. Sugar and amino acid transport by cells in culture—differences between normal and malignant cells. *N Engl J Med* 1972; 286: 929–33.
136. Kubota R, Kubota K, Yamada S et al. Methionine uptake by tumor tissue: a microautoradiographic comparison with FDG. *J Nucl Med* 1995; 36: 484–92.
137. Bergstrom M, Ericson K, Hagenfeldt L et al. PET study of methionine accumulation in glioma and normal brain tissue: competition with branched chain amino acids. *J Comput Assist Tomogr* 1987; 11: 208–13.
138. Bergstrom M, Ericson K, Hagenfeldt L et al. PET study of methionine accumulation in glioma and normal brain tissue: competition with branched chain amino acids. *J Comput Assist Tomogr* 1987; 11: 208–13.
139. Mosskin M, Ericson K, Hindmarsh T et al. Positron emission tomography compared with magnetic resonance imaging and computed tomography in supratentorial gliomas using multiple stereotactic biopsies as reference. *Acta Radiol* 1989; 30: 225–32.
140. Ogawa T, Shishido F, Kanno I et al. Cerebral glioma: evaluation with methionine PET. *Radiology* 1993; 186: 45–53.
141. Ribom D, Eriksson A, Hartman M et al. Positron emission tomography (11C)-methionine and survival in patients with low-grade gliomas. *Cancer* 2001; 92: 1541–9.
142. Nariai T, Tanaka Y, Wakimoto H et al. Usefulness of L-[methyl-11C] methionine-positron emission tomography as a biological monitoring tool in the treatment of glioma. *J Neurosurg* 2005; 103: 498–507.
143. Hara T, Kondo T, Hara T, Kosaka N. Use of 18F-choline and 11C-choline as contrast agents in positron emission tomography imaging-guided stereotactic biopsy sampling of gliomas. *J Neurosurg* 2003; 99: 474–9.
144. Tang BN, Sadeghi N, Branle F et al. Semi-quantification of methionine uptake and flair signal for the evaluation of chemotherapy in low-grade oligodendroglioma. *J Neurooncol* 2005; 71: 161–8.
145. Ribom D, Smits A. Baseline 11C-methionine PET reflects the natural course of grade 2 oligodendrogliomas. *Neurol Res* 2005; 27: 516–21.
146. Kracht LW, Miletic H, Busch S et al. Delineation of brain tumor extent with [11C]L-methionine positron emission tomography: local comparison with stereotactic histopathology. *Clin Cancer Res* 2004; 10: 7163–70.
147. Tsuyuguchi N, Takami T, Sunada I et al. Methionine positron emission tomography for differentiation of recurrent brain tumor and radiation necrosis after stereotactic radiosurgery—in malignant glioma. *Ann Nucl Med* 2004; 18: 291–6.
148. Van Laere K, Ceyskens S, Van Calenbergh F et al. Direct comparison of 18F-FDG and 11C-methionine PET in suspected recurrence of glioma: sensitivity, inter-observer variability and prognostic value. *Eur J Nucl Med Mol Imaging* 2005; 32: 39–51.
149. Sonoda Y, Kumabe T, Takahashi T, Shirane R, Yoshimoto T. Clinical usefulness of 11C-MET PET and 201Tl SPECT for differentiation of recurrent glioma from radiation necrosis. *Neurol Med Chir (Tokyo)* 1998; 38: 342–7.
150. Mosskin M, von Holst H, Bergstrom M et al. Positron emission tomography with 11C-methionine and computed tomography of intracranial tumours compared with histopathologic examination of multiple biopsies. *Acta Radiol* 1987; 28: 673–81.
151. Mineura K, Sasajima T, Kowada M et al. Early delineation of cerebral glioma using amino acid positron tracers. *Comput Med Imaging Graph* 1997; 21: 63–6.
152. Tovi M, Thuomas KA, Bergstrom K et al. Tumour delineation with magnetic resonance imaging in gliomas. A comparison with positron emission tomography and computed tomography. *Acta Radiol Suppl* 1986; 369: 161–3.
153. Jacobs AH. PET in gliomas. In: Schlegel, Weller, Westphal, eds. *Neuroonkologie*. Berlin: Thieme-Verlag, 2003: 72–6.
154. Nuutinen J, Sonninen P, Lehtikoinen P et al. Radiotherapy treatment planning and long-term follow-up with [(11)C]

- methionine PET in patients with low-grade astrocytoma. *Int J Radiat Oncol Biol Phys* 2000; 48: 43–52.
155. Ogawa T, Kanno I, Shishido F et al. Clinical value of PET with 18F-fluorodeoxyglucose and L-methyl-11C-methionine for diagnosis of recurrent brain tumor and radiation injury. *Acta Radiol* 1991; 32: 197–202.
 156. Ogawa T, Inugami A, Hatazawa J et al. Clinical positron emission tomography for brain tumors: comparison of fludeoxyglucose F 18 and L-methyl-11C-methionine. *AJNR Am J Neuroradiol* 1996; 17: 345–53.
 157. Roelcke U, Leenders KL. Positron emission tomography in patients with primary CNS lymphomas. *J Neurooncol* 1999; 43: 231–6.
 158. Biersack HJ, Coenen HH, Stocklin G et al. Imaging of brain tumors with L-3-[123I]iodo-alpha-methyl tyrosine and SPECT. *J Nucl Med* 1989; 30: 110–12.
 159. Langen KJ, Ziemons K, Kiwit JC et al. 3-[123I]iodo-alpha-methyltyrosine and [methyl-11C]-L-methionine uptake in cerebral gliomas: a comparative study using SPECT and PET. *J Nucl Med* 1997; 38: 517–22.
 160. Mineura K, Shioya H, Kowada M, Uemura K. Tumor extent of slowly progressive oligodendroglioma determined by 18F-fluorophenylalanine positron emission tomography. *Eur J Radiol* 1997; 25: 30–5.
 161. Shinoura N, Nishijima M, Hara T et al. Brain tumors: detection with C-11 choline PET. *Radiology* 1997; 202: 497–503.
 162. Lammertsma AA, Wise RJ, Cox TC, Thomas DG, Jones T. Measurement of blood flow, oxygen utilisation, oxygen extraction ratio, and fractional blood volume in human brain tumours and surrounding oedematous tissue. *Br J Radiol* 1985; 58: 725–34.
 163. Tyler JL, Diksic M, Villemure JG et al. Metabolic and hemodynamic evaluation of gliomas using positron emission tomography. *J Nucl Med* 1987; 28: 1123–33.
 164. Grierson JR, Shields AF. Radiosynthesis of 3'-deoxy-3'-[(18)F]fluorothymidine: [(18)F]FLT for imaging of cellular proliferation in vivo. *Nucl Med Biol* 2000; 27: 143–56.
 165. Shields AF, Grierson JR, Dohmen BM et al. Imaging proliferation in vivo with [F-18]FLT and positron emission tomography. *Nat Med* 1998; 4: 1334–6.
 166. Waniewski RA, Martin DL. Preferential utilization of acetate by astrocytes is attributable to transport. *J Neurosci* 1998; 18: 5225–33.
 167. Yoshimoto M, WAYYFY. Acetate and choline as cell growth markers provide different perspectives of lipid synthesis. *J Nucl Med* 2001; 42: 275.
 168. Ohtani T, Kurihara H, Ishiuchi S et al. Brain tumour imaging with carbon-11 choline: comparison with FDG PET and gadolinium-enhanced MR imaging. *Eur J Nucl Med* 2001; 28: 1664–70.
 169. Kaplan AM, Bandy DJ, Manwaring KH et al. Functional brain mapping using positron emission tomography scanning in preoperative neurosurgical planning for pediatric brain tumors. *J Neurosurg* 1999; 91: 797–803.
 170. Nishiyama Y, Yamamoto Y, Fukunaga K et al. Visualization of the motor activation area using SPECT in neurosurgical patients with lesions near the central sulcus. *J Nucl Med* 2000; 41: 411–15.
 171. Moritz C, Haughton V. Functional MR imaging: paradigms for clinical preoperative mapping. *Magn Reson Imaging Clin N Am* 2003; 11: 529–42, v.
 172. Gilman S. Imaging the brain. Second of two parts. *N Engl J Med* 1998; 338: 889–96.
 173. Jacobs A, Voges J, Reszka R et al. Positron-emission tomography of vector-mediated gene expression in gene therapy for gliomas. *Lancet* 2001; 358: 727–9.
 174. Jacobs AH, Dittmar C, Winkeler A, Garlip G, Heiss WD. Molecular imaging of gliomas. *Mol Imaging* 2002; 1: 309–35.
 175. Su H, Forbes A, Gambhir SS, Braun J. Quantitation of cell number by a positron emission tomography reporter gene strategy. *Mol Imaging Biol* 2004; 6: 139–48.
 176. Serganova I, Doubrovin M, Vider J et al. Molecular imaging of temporal dynamics and spatial heterogeneity of hypoxia-inducible factor-1 signal transduction activity in tumors in living mice. *Cancer Res* 2004; 64: 6101–8.
 177. Uhrbom L, Nerio E, Holland EC. Dissecting tumor maintenance requirements using bioluminescence imaging of cell proliferation in a mouse glioma model. *Nat Med* 2004; 10: 1257–60.
 178. Wen B, Burgman P, Zanzonico P et al. A preclinical model for noninvasive imaging of hypoxia-induced gene expression; comparison with an exogenous marker of tumor hypoxia. *Eur J Nucl Med Mol Imaging* 2004; 31: 1530–8.
 179. Anderson SA, Glod J, Arbab AS et al. Noninvasive MR imaging of magnetically labeled stem cells to directly identify neovasculature in a glioma model. *Blood* 2005; 105: 420–5.
 180. Chen X, Park R, Shahinian AH et al. 18F-labeled RGD peptide: initial evaluation for imaging brain tumor angiogenesis. *Nucl Med Biol* 2004; 31: 179–89.
 181. Haubner R, Wester HJ, Weber WA et al. Noninvasive imaging of alpha(v)beta3 integrin expression using 18F-labeled RGD-containing glycopeptide and positron emission tomography. *Cancer Res* 2001; 61: 1781–5.
 182. Sundaresan G, Yazaki PJ, Shively JE et al. 124I-labeled engineered anti-CEA minibodies and diabodies allow high-contrast, antigen-specific small-animal PET imaging of xenografts in athymic mice. *J Nucl Med* 2003; 44: 1962–9.
 183. van Waarde A, Buursma AR, Hospers GA et al. Tumor imaging with 2 sigma-receptor ligands, 18F-FE-SA5845 and 11C-SA4503: a feasibility study. *J Nucl Med* 2004; 45: 1939–45.
 184. Koutcher JA, Hu X, Xu S et al. MRI of mouse models for gliomas shows similarities to humans and can be used to identify mice for preclinical trials. *Neoplasia* 2002; 4: 480–5.
 185. Jacobs AH, Winkeler A, Hartung M et al. Improved herpes simplex virus type 1 amplicon vectors for proportional coexpression of positron emission tomography marker and therapeutic genes. *Hum Gene Ther* 2003; 14: 277–97.
 186. Ponomarev V, Doubrovin M, Serganova I et al. A novel triple-modality reporter gene for whole-body fluorescent, bioluminescent, and nuclear noninvasive imaging. *Eur J Nucl Med Mol Imaging* 2004; 31: 740–51.
 187. Hamstra DA, Lee KC, Tychevicz JM et al. The use of 19F spectroscopy and diffusion-weighted MRI to evaluate differences in gene-dependent enzyme prodrug therapies. *Mol Ther* 2004; 10: 916–28.
 188. Mamot C, Nguyen JB, Pourdehnad M et al. Extensive distribution of liposomes in rodent brains and brain tumors

- following convection-enhanced delivery. *J Neurooncol* 2004; 68: 1–9.
189. Saito R, Bringas JR, McKnight TR et al. Distribution of liposomes into brain and rat brain tumor models by convection-enhanced delivery monitored with magnetic resonance imaging. *Cancer Res* 2004; 64: 2572–9.
 190. Grohn OH, Valonen PK, Lehtimäki KK et al. Novel magnetic resonance imaging contrasts for monitoring response to gene therapy in rat glioma. *Cancer Res* 2003; 63: 7571–4.
 191. Rehemtulla A, Stegman LD, Cardozo SJ et al. Rapid and quantitative assessment of cancer treatment response using in vivo bioluminescence imaging. *Neoplasia* 2000; 2: 491–5.
 192. Ross BD, Chenevert TL, Garwood M et al. Evaluation of (E)-2'-deoxy-2'-(fluoromethylene)cytidine on the 9L rat brain tumor model using MRI. *NMR Biomed* 2003; 16: 67–76.
 193. Rubin JB, Kung AL, Klein RS et al. A small-molecule antagonist of CXCR4 inhibits intracranial growth of primary brain tumors. *Proc Natl Acad Sci USA* 2003; 100: 13513–18.
 194. Schmidt NO, Ziu M, Carrabba G et al. Antiangiogenic therapy by local intracerebral microinfusion improves treatment efficiency and survival in an orthotopic human glioblastoma model. *Clin Cancer Res* 2004; 10: 1255–62.
 195. Schmidt KF, Ziu M, Schmidt NO et al. Volume reconstruction techniques improve the correlation between histological and in vivo tumor volume measurements in mouse models of human gliomas. *J Neurooncol* 2004; 68: 207–15.
 196. Sun Y, Schmidt NO, Schmidt K et al. Perfusion MRI of U87 brain tumors in a mouse model. *Magn Reson Med* 2004; 51: 893–9.
 197. Valonen PK, Lehtimäki KK, Vaisanen TH et al. Water diffusion in a rat glioma during ganciclovir-thymidine kinase gene therapy-induced programmed cell death in vivo: correlation with cell density. *J Magn Reson Imaging* 2004; 19: 389–96.
 198. Vooijs M, Jonkers J, Lyons S, Berns A. Noninvasive imaging of spontaneous retinoblastoma pathway-dependent tumors in mice. *Cancer Res* 2002; 62: 1862–7.
 199. Voges J, Reszka R, Gossmann A et al. Imaging-guided convection-enhanced delivery and gene therapy of glioblastoma. *Ann Neurol* 2003; 54: 479–87.
 200. Kircher MF, Mahmood U, King RS, Weissleder R, Josephson L. A multimodal nanoparticle for preoperative magnetic resonance imaging and intraoperative optical brain tumor delineation. *Cancer Res* 2003; 63: 8122–5.
 201. Bonneville JF, Bonneville F, Cattin F. Magnetic resonance imaging of pituitary adenomas. *Eur Radiol* 2005; 15: 543–8.

4

Head and neck cancer

*Flavio Crippa, Alberto Gerali,
and Alessandra Alessi*

Background

Head and neck cancers constitute approximately 5% of all malignancies. Most head and neck cancers are squamous cell carcinomas (HNSCCs) of paranasal sinuses, the aerodigestive tract (nasopharynx, oral cavity and oropharynx, hypopharynx), and larynx.¹ Currently, the management of these cancers demands a multidisciplinary approach for therapy, including surgery, radiotherapy, and chemotherapy. The role of imaging in HNSCC is somewhat different from that applied in other malignancies. Many tumors (in particular of the naso-, oro-, and hypopharynx) present late, with bulky disease, invasion of the contiguous structures, and enlarged lymph nodes. The clinical diagnosis is often obvious, with direct access for biopsy. Therefore, imaging usually has a minor role in the initial diagnosis of the primary tumor, but it is essential for the success of treatment, which is based on accurate staging. Staging aims to evaluate the local extent of the tumor and to detect regional lymph node involvement, distant metastases, and synchronous/metachronous primary lesions. After primary therapy, imaging plays a major role in assessment of the response to treatment and early detection of cancer relapse.²⁻⁴

The normal anatomy of the head and neck is complex, and structures traverse many different planes and angles; therefore, cross-sectional imaging is required to study HNSCC. Currently, the most widely accepted cross-sectional imaging modality is computed tomography (CT), and in some institutions magnetic resonance imaging (MRI). During recent years, positron emission tomography (PET) has been proposed as an additional cross-sectional technique to evaluate patients with HNSCC.⁵⁻⁹ CT and MRI detect and characterize tumors by studying their changes in morphology, electronic density (CT), or proton environment and density (MRI). PET studies the metabolic differences between tumors and normal tissues. Metabolism in tumors is different from that in normal tissues in several ways. Some of these differences can be visualized with PET, taking advantage of the peculiar physical and chemical properties of particular radiolabeled compounds

called PET radiopharmaceuticals. After intravenous injection into the patient, these radiopharmaceuticals are incorporated into metabolic pathways, and the signals emitted by the cells, which have actively accumulated them, can be registered by dedicated instruments (the PET scanners), which produce multiplanar tomographic images of the radiopharmaceutical distribution. Cancer cells usually have a higher metabolic activity than do normal cells, and thus, in PET imaging, cancer is depicted as a focal area of increased accumulation of the radiopharmaceutical (Figure 4.1).

Functional alterations can precede morphological alterations in the development of many diseases, and this is particularly true for cancer. Therefore, it is intuitive that imaging based on metabolic changes may give a different perspective of cancer than imaging based on morphological changes, with potential advantages in staging of the disease, in evaluation of the response to therapy, and in diagnosis of cancer relapse.

This chapter addresses the current role of PET in the management of HNSCC, considering also some limitations

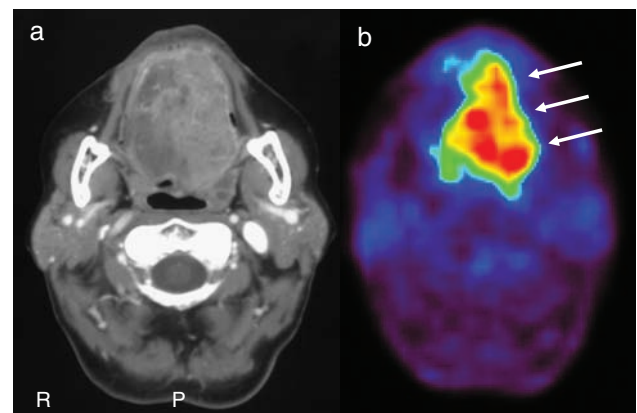


Figure 4.1 Locally advanced tongue squamous cell carcinomas. Axial fluoro-2-deoxy-D-glucose (FDG) image (b) shows intense glucose hypermetabolism of the tumor (arrows).

of this technique that, according to our experience and literature data, may lead to the misinterpretation of PET images.

Principle of positron emission tomography imaging

The advantages and limitations of PET imaging are basically determined by the biological properties of the radiopharmaceutical. The type of instrumentation used to generate PET images decides the quality of imaging and, consequently, the level of confidence in interpreting PET findings, but it cannot compensate for radiopharmaceutical limitations.

As in the vast majority of oncological applications of PET, also in HNSCC the most extensively studied and clinically used radiopharmaceutical is [^{18}F]fluoro-2-deoxy-D-glucose (FDG).^{10–12} With FDG-PET, cancer detection and characterization is based on changes in glucose metabolism in tumor cells, which usually show a high FDG uptake as a consequence of their well-known high rate of glycolysis (the Warburg effect).¹¹ FDG-PET imaging is performed in the fasting state (at least 5–6 hours) in order to reduce blood insulin and glucose levels. FDG competes with glucose for intracellular carrier-mediated transport, and serves as an alternative substrate for hexokinase; therefore, an increase of blood glucose leads to competitive tumor displacement of FDG (Figure 4.2). The blood glucose level should be checked before FDG injection, and diabetic patients with a value > 200 mg/dl should be rescheduled for PET when their glycemia is under control. Tumor uptake of FDG may increase even up to 2.5 hours after injection, and therefore it is important to use a standardized uptake time (at least 50 minutes) before imaging. Imaging should include at least the regions extending from the frontal sinuses to the liver.

PET imaging is characterized by poorer spatial resolution than CT or MRI, and the normal distribution of FDG in the head and neck region is complex, with a paucity of identifiable anatomic structures to accurately localize FDG uptake (Figure 4.3).^{13,14} In the head and neck, numerous structures show physiological uptake of FDG, such as muscles (tongue, muscles of the floor of the mouth and particularly the genioglossus muscle, masticator, laryngeal, scalene, sternocleidomastoid, and paraspinal muscles), lymphoid tissue (adenoidal, palatine and lingual tonsillar tissue), salivary glands, and brown tissue. Adopting a procedure to minimize muscular uptake can be crucial for correct image reading. In this regard, ensuring that during the uptake time the patient is not chewing gum, talking or reading is important. In young and tense patients, the use of benzodiazepine to reduce muscle uptake may be an

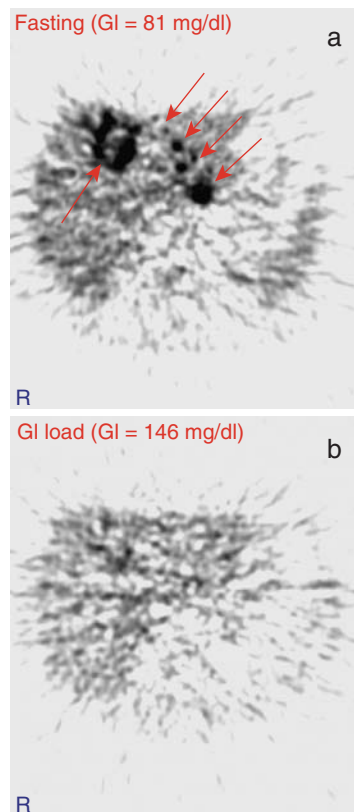


Figure 4.2

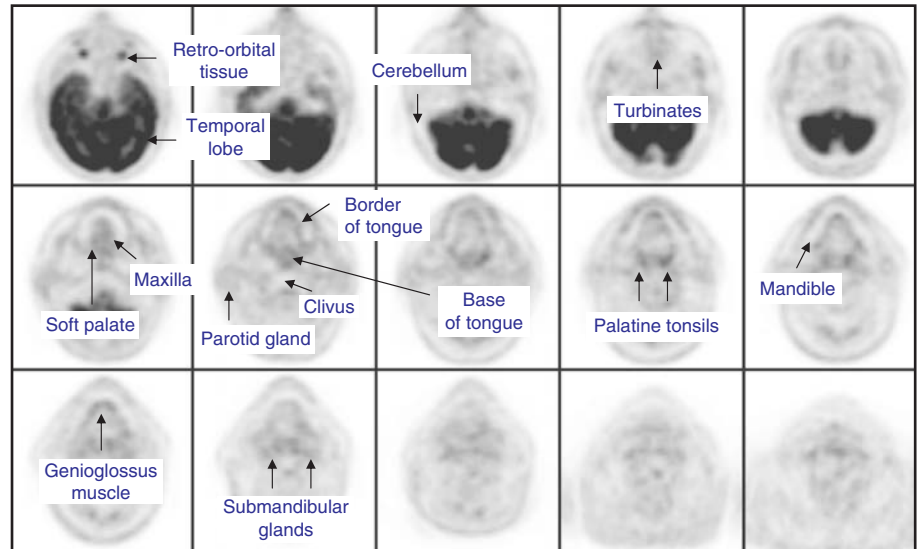
Liver metastases from colorectal cancer studied with FDG-PET in fasting state and after oral glucose load. The metastases (arrows) are clearly detected in the axial FDG image performed in fasting state and normal blood glucose level (a) and they are not still visible in the corresponding image performed after glucose load and with high blood glucose level (b).

advantage (Figure 4.4). The pattern of normal distribution of FDG is variable among different patients, and even in the same patient in repeated PET studies for follow-up. Sometimes, high and/or asymmetric uptakes can be found (Figures 4.5 and 4.6), and the differentiation between normal and abnormal findings may be very difficult. According to some investigators, semiquantitative analysis of FDG imaging with a standardized uptake value (SUV) may help to distinguish benign from pathological uptakes, and a SUV > 3.0 has been proposed as a threshold value suggestive of malignancy. However, in our experience the utility of SUV in this clinical setting is rather questionable.

A substantial improvement in FDG imaging of HNSCC has been represented by combined in-line PET–CT, a dual imaging modality in which CT and PET are performed sequentially during a single diagnostic session with a hybrid PET–CT scanner. The PET and CT images can be independently analyzed, or accurately co-registered using fusion software which produces superimposed PET–CT multiplanar tomographic images. This permits

Figure 4.3

Sequential axial FDG images showing a pattern of normal FDG distribution in head and neck.



the accurate anatomic designation of FDG-PET findings, increasing the level of confidence in the reading of PET images.¹⁵⁻²¹

PET-CT has introduced some sources of potential artifacts which may lead to the wrong interpretation of fused PET-CT images.²²⁻²⁶ PET-CT imaging can be affected by lateral head movement of the patient between the CT scan and the subsequent PET scan. This produces artifacts which can lead to wrong localization of asymmetric FDG

uptakes in the fused PET-CT images, simulating malignant findings. In these cases, it is important to evaluate the non-attenuation corrected emission PET images to obtain an accurate interpretation (Figure 4.7). Metals used for dental work can produce artifacts in PET-CT imaging, characterized by stripe artifacts in CT and fused PET-CT images, totally photopenic areas in PET images because of overadsorption of photons by the metal, and fictional FDG uptake in the space close to the metal dental work in the

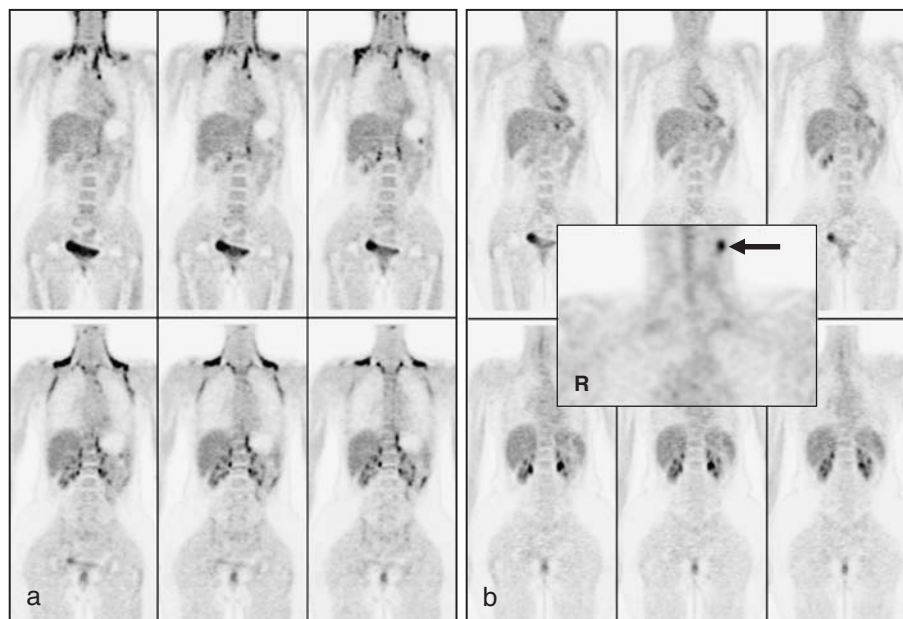


Figure 4.4

Coronal whole body FDG images showing high uptakes in the muscles of neck and shoulders (a). These uptakes may be reduced with muscle relaxation with benzodiazepine (b). After this preparation, an abnormal focal area of FDG uptake very consistent with a metastatic node is visible in the left neck (arrow).

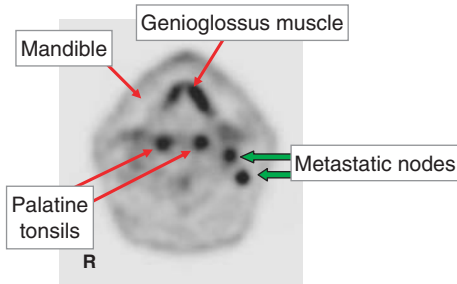


Figure 4.5
Axial FDG image showing intense uptake in two metastatic retro-mandibular nodes (green arrows) as well in normal structures. Normal bone is usually hypometabolic.

attenuation corrected PET images. Also in these cases it is advisable to analyze FDG uptake using the non-attenuation-corrected emission PET images (Figure 4.8).

The main limitations of FDG imaging are related to the spatial resolution of the current PET technology (about 5–10 mm), not adequate to detect very small foci of cancer, and the suboptimal specificity of FDG in some situations for accumulation in inflammatory alterations, particularly those with dense granulation tissue and infiltration of macrophages.

Initial staging with FDG-PET

The contribution of FDG-PET to the staging of a primary tumor (T-staging) has been addressed in several

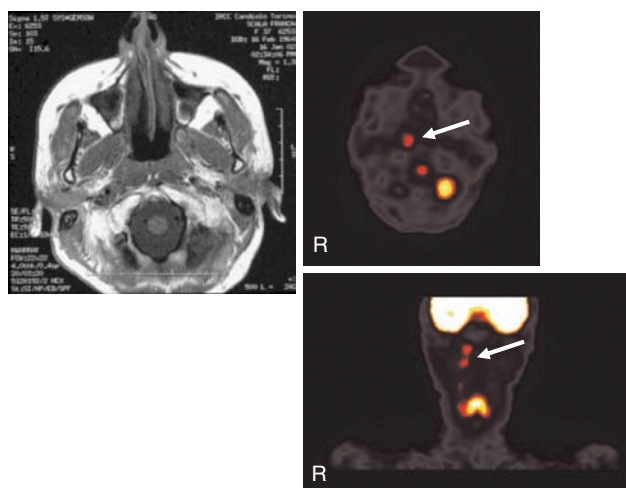


Figure 4.6
Axial and coronal FDG images showing asymmetric uptake (arrows) in the right posterolateral wall of nasopharynx due to physiological uptake in tissue with benign hyperplasia of lymphoid tissue.

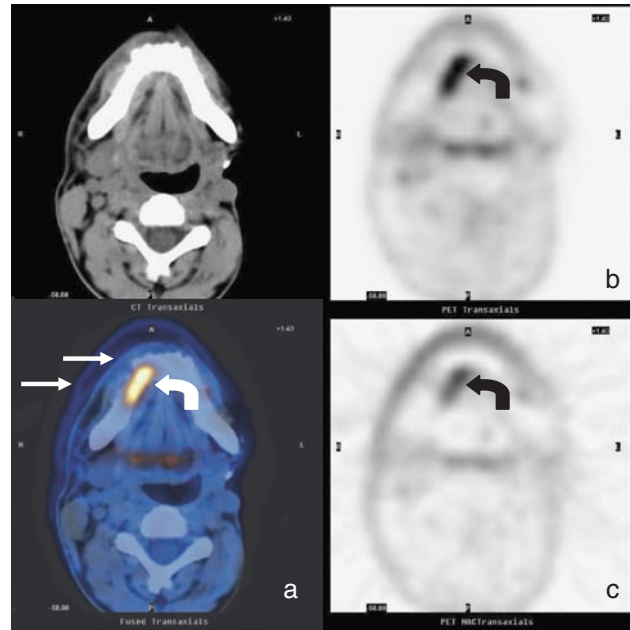


Figure 4.7
In combined PET-CT imaging, patient movement between CT scan and PET scan (arrows) may induce wrong anatomic localization of FDG uptake in the fused PET-CT images (a) mimicking cancer. In this example, the FDG uptake (curved arrow), apparently localized in the right mandible (a), can be repositioned in the floor of the mouth analyzing the corresponding PET alone image (b) and, particularly, the not-corrected PET image (c). Therefore, the FDG finding can be interpreted as normal uptake in the right genioglossus muscle.

published studies.²⁷ They have demonstrated that FDG-PET can accurately detect primary HNSCC without, however, advantages over CT/MRI. However, many of these studies have been performed with outdated imaging systems (i.e. coincidence γ cameras or old-generation PET scanners producing only non-attenuation corrected images), and their conclusions might have been different had PET-CT been used. All the same, recent and preliminary studies with PET-CT in the evaluation of mandible involvement of HNSCC of the oral cavity have given contradictory results.^{28,29} It makes sense that T-staging of HNSCC should remain a critical indication for FDG imaging also using PET-CT. In fact, in order to have a clear definition of the tumor margins, we need enough spatial resolution to separate close and complicated anatomical structures, a fast imaging technique to minimize movement artifacts (particularly when the site of interest is in the oral cavity or the neck), and to be able to distinguish the tumor from surrounding inflammatory secretions. The resolution of current PET scanners is about 5–10 mm, they take at least 6–8 minutes to provide good quality FDG images of the head and neck, and differentiation between

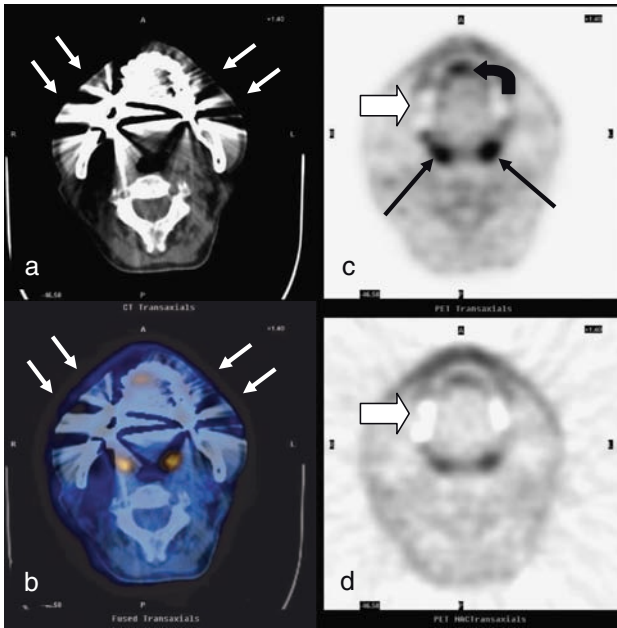


Figure 4.8

In combined PET–CT imaging, metal dental works may induce errors in the interpretation of photon attenuation-corrected PET images. In CT (a) and fused PET–CT (b) images dental works typically produces stripe artifact (short arrows). In attenuation-corrected (c) and not-corrected PET images (d) metal dental works are seen as totally photopenic areas (large arrows) with unreal FDG uptakes in contiguous tissues (curved arrow). The evaluation of not-corrected PET images (d) is useful to recognize the presence of these artifacts. In this example, inflammatory FDG uptake is visible in the soft palate, and the finding is emphasized in corrected-PET imaged for the same reasons (c, long arrows).

normal and abnormal FDG uptake may be difficult because of the complicated pattern of normal distribution of FDG and possible accumulation in inflammatory cells. On the basis of this performance, PET imaging may be inadequate to study precisely the local extension of HNSCC, unless there are further improvements in technology and/or radiopharmaceuticals other than FDG are used.

Many studies have described the high sensitivity and specificity of FDG-PET in the evaluation of lymph node involvement (N-staging) of HNSCC^{30–37} (Figure 4.9). Even if PET cannot detect micrometastases, it performs better than radiologic modalities for detecting metastases in normal lymph nodes according to morphological criteria. The sensitivity and specificity of PET is about 90% and 94%, respectively, as compared to 82% and 85% (CT), 80% and 79% (MRI), and 72% and 70% (ultrasound).¹⁷ However, being a functional imaging procedure and having less spatial resolution than CT/MRI, PET alone cannot provide some important parameters for nodal staging: the level and

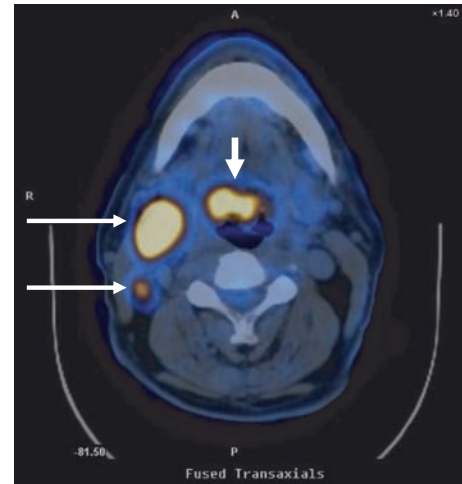


Figure 4.9

57-year-old man with primary squamous cell carcinoma of hypopharynx. Fused axial PET–CT image shows intense FDG uptake in the primary lesion (short arrow) and in two metastatic lymph nodes (long arrows) in the right neck, one of them with size < 10 mm.

size of the metastatic nodes, their number and distribution (ipsilateral, contralateral, bilateral), and the presence of extracapsular spread. In particular, extracapsular spread decreases the expected survival by 50%.³⁸ Therefore, a combination of PET and CT is likely to provide more accurate nodal staging.

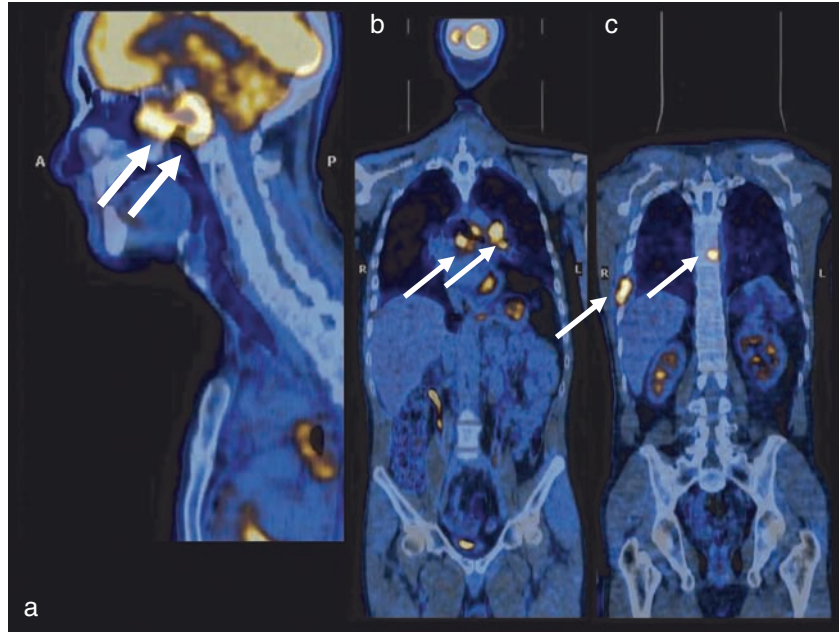
A particular indication of FDG-PET is the evaluation of patients with cervical lymph node metastases from an unknown primary tumor. The aim of PET imaging in this clinical setting is to localize a focal and asymmetric area of abnormal uptake, to guide direct examination and biopsy. PET can detect the site of the primary lesion in about 30–50% of patients, as compared to 10–20% with CT/MRI.^{39,40}

Distant metastases are less common in HNSCC than in other cancers. Because of the low prevalence (< 5%) of distant metastases at presentation, PET is unlikely to change the staging in a clinically significant fraction of patients. Whole-body PET, however, could be recommended as part of the initial staging in patients with advanced disease or recurrent cancer who have a higher risk of distant lung, liver, and bone metastases.^{27,30,34} In these patients, PET could reduce the need for other, additional investigations and affect the therapeutic strategy (palliative vs. curative) (Figure 4.10).

Whole-body PET may also help in the detection of a second primary tumor in patients with HNSCC, who have an increased risk of synchronous or metachronous carcinomas which are localized in the aerodigestive tract, esophagus, and lung.⁴¹

Figure 4.10

Axial (a) and coronal (b and c) PET-TC images showing abnormal FDG uptakes in a locally advanced nasopharyngeal squamous carcinoma with skull base invasion (arrows a) and distant metastases in mediastinal lymph nodes (arrows b) and bone (arrows c).



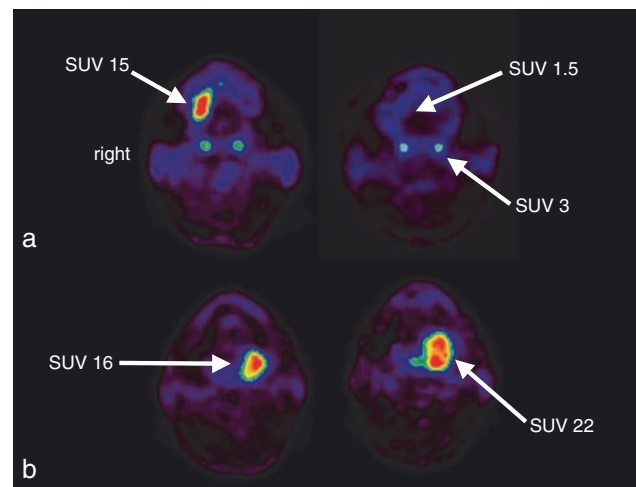
Post-therapy evaluation with FDG-PET

In the past 20 years, therapeutic management of HNSCC has changed from a primarily surgical approach to a multidisciplinary approach which contemplates different combinations of therapy, including surgery, preoperative or postoperative radiation therapy, and neoadjuvant or induction chemotherapy, depending on the stage of disease. As a consequence of these growing treatment options, imaging plays a major role in guiding the therapeutic strategy, by means of essential contributions to the initial staging and the detection of residual or recurrent cancer.

Many investigators have shown that FDG-PET has greater accuracy than CT or MRI in assessing the response to chemotherapy and radiotherapy.^{42–55} The superiority of PET in detecting residual/recurrent disease is for several reasons. First, the biological properties of FDG are unique among nuclear medicine tracers and radiological contrast agents. It provides a non-invasive evaluation of the cancer vitality as a consequence of the close relationship between the amount of uptake and the number of viable tumor cells. Second, volume changes measured with conventional imaging during therapy are rather late events, and a reduction in the viable tumor-cell fraction does not always result in a volume reduction if tumor tissue is replaced by necrotic or fibrotic tissue. Additionally, new anticancer therapy based on antivascular and cytostatic agents aim at tumor growth stabilization rather than tumor shrinkage, and during these therapies no major volume changes are to be expected. Finally, the interpretation of PET imaging is not affected by post-surgery and/or post-radiotherapy anatomical distortions and the FDG uptake can be

calculated, providing semiquantitative (SUV) or quantitative parameters useful for evaluating the metabolic changes during therapy (Figure 4.11).

The procedures for using PET in the assessment of therapy response are not yet completely standardized.

**Figure 4.11**

Two patients with locally advanced tongue cancer treated with chemotherapy and monitored with FDG-PET. Pre-treatment axial FDG images (right column) show hypermetabolic cancer in both patients (SUV_{max} 15 and 16, respectively). After the completion of therapy, axial FDG images (left column) shows complete metabolic response in patient a: SUV_{max} 1.5 equal to background activity and less than FDG uptake in normal tissue as palatin tonsils. In patient b, axial FDG images shows a larger metabolic diameter of the tumor and increased SUV_{max} (22), indicating a not-responding cancer.

Pretreatment imaging is generally recommended to evaluate the FDG avidity of the tumor and obtain a baseline measure of its metabolic activity. The time-point of PET reevaluation after therapy depends on the treatment modality used, but different choices can be found among investigators. Chemotherapy does not usually induce intense inflammatory alteration, which may interfere with PET imaging, and the PET scan can be repeated as early as after 1–2 cycles of therapy to evaluate the chemosensitivity, or after the completion of therapy to evaluate the chemoresistance. Radiotherapy may induce an early acute inflammatory reaction with dense infiltration of macrophages and fibroblasts, which causes a high rate of false-positive results in PET imaging within 4–6 weeks after the completion of therapy. When FDG uptake occurs in irradiated regions, it may remain visible for several months. A conventional time-point for PET imaging is 3–4 months after the completion of radiotherapy.

A particular field of application of FDG-PET is the use of combined PET–CT for the definition of the radiotherapy target volume (BTV, biological target volume) and dose in HNSCC patients.^{56,57} In the literature, there are an expanding number of studies which demonstrate that FDG-PET imaging may be useful for radiotherapy planning in different ways: first, excluding from radiotherapy patients with unknown distant metastases detected by PET (16% of cases), and, then, providing modified target volumes thanks to metabolic evaluation of the extent of viable tumor and/or detection of a malignant, normal-size lymph node. The obtained BTV might reduce the risk for geographic misses and minimize the dose of ionizing radiation applied to non-target organs. However, this is still an area of clinical research, and the impact on treatment outcome of these procedures remains to be demonstrated.

All HNSCC patients are at high risk of cancer recurrence and a second primary tumor. Most recurrences appear within the first 24 months of follow-up, but long-term

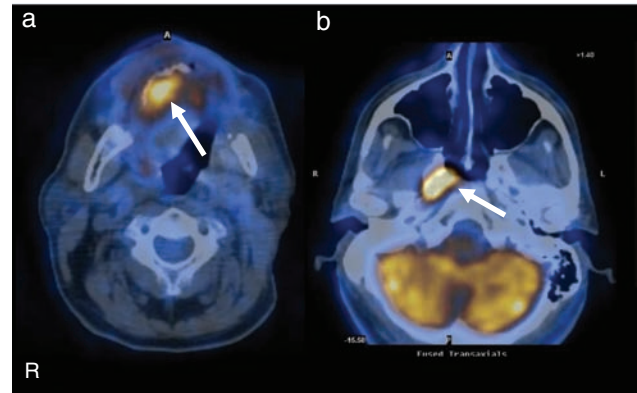


Figure 4-12

Axial fused PET–CT images showing abnormal areas of FDG uptake (arrows) very consistent with cancer relapse (biopsy confirmation) of squamous cell carcinomas of the oral cavity (a) and nasopharynx (b).

surveillance is required. The sensitivity and specificity of FDG-PET for detecting recurrent disease are approximately 88–100% and 75–100%, respectively, compared with 70–92% and 50–57% for CT and MRI. The superiority of FDG-PET compared with conventional imaging is based on the detection of abnormalities in metabolism rather than in anatomy, which can be greatly distorted after radiation or surgery (Figure 4.12). Such distortions are particularly complicated after reconstructive surgery of the maxillofacial region or neck. After surgery and/or radiotherapy, FDG findings are analyzed with greater confidence using combined PET–CT rather than PET alone. However, FDG uptake in the treated region due to inflammation tissue may mimic cancer relapse, and differential diagnosis between post-therapy alteration and recurrence may present particular challenges (Figure 4.13). Some authors use a

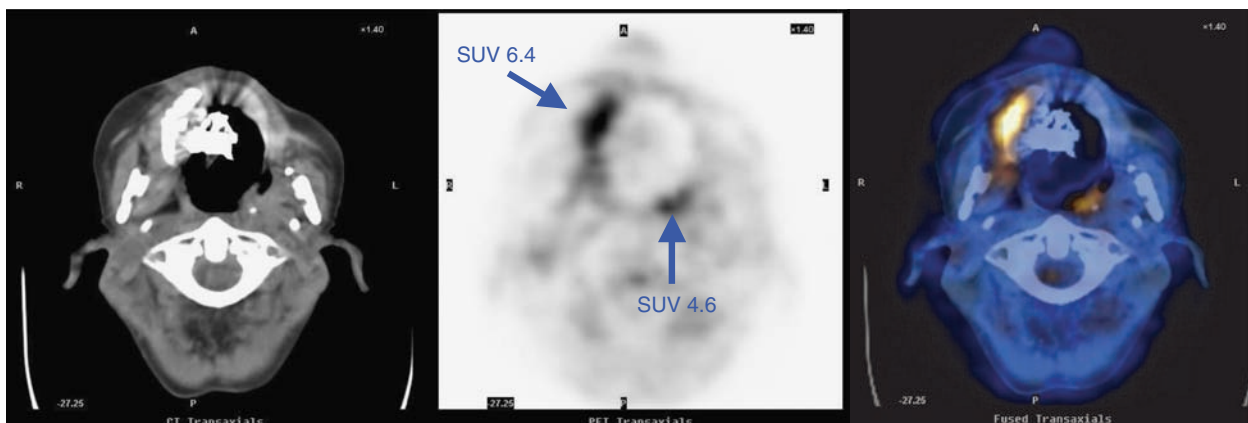
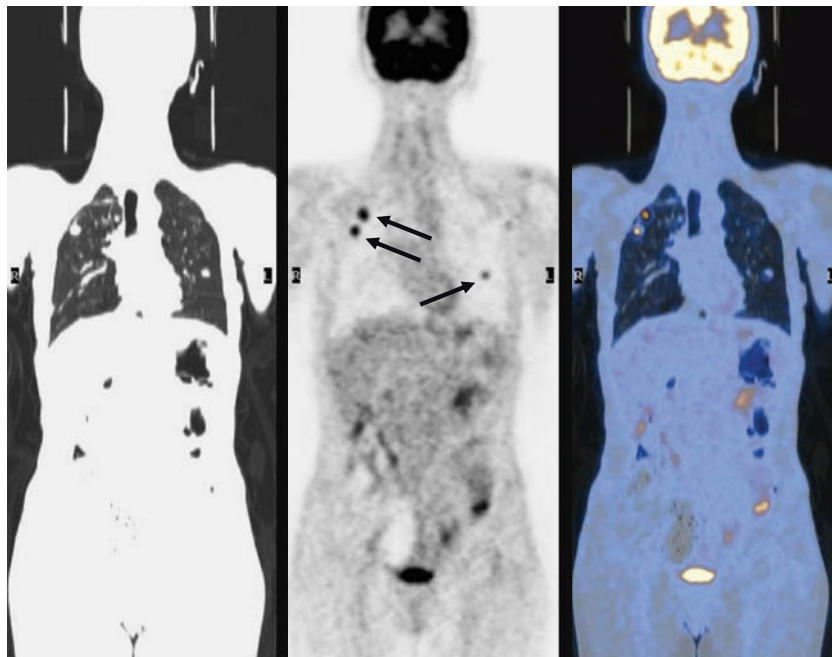


Figure 4.13

Axial PET–CT images showing FDG uptakes (arrows) in bone and soft tissues ($SUV_{max} > 3.0$) after major surgery for maxillary cancer. FDG findings are ambiguous between cancer relapse and inflammation both in visual and semi-quantitative analyses.

Figure 4.14

Coronal whole body PET-CT images showing unknown lung metastases (arrows). This example stresses the additional diagnostic value of PET in the restaging of HNSCC.



SUV value > 3.0 as a parameter consistent with malignant uptake, but in our experience SUV is often confusing because of the overlap between SUV values found in inflammation and those in recurrent tumor. In our opinion, better results are obtained by repeating PET imaging after 1–2 months and calculating the SUV, to monitor evolution of the FDG uptake. Regression or no significant variation of SUV is generally associated with post-therapy alteration. In some difficult cases, biopsy of ambiguous lesions visualized on FDG-PET may be needed to reach the correct diagnosis. The negative predictive value of PET imaging for recurrent disease is high; nevertheless false-negative results may occur if the tumor is not FDG-avid, the relapse is located in structures with a physiologically elevated FDG uptake, and the tumor size is below the resolution of current PET imaging.

Finally, in recurrent HNSCC, PET has the value of a whole-body procedure that may detect unknown distant metastases which completely change the therapeutic strategy and the patient's prognosis (Figure 4.14).

Conclusions

FDG-PET imaging can improve the management of patients with HNSCC, providing additional and valuable diagnostic information for the selection of therapeutic options. In fact, PET imaging can detect, with higher sensitivity than conventional imaging, metastases in a normal-size lymph node, distant metastases and/or a secondary

primary tumor, and residual/recurrent disease. The use of combined PET–CT improves significantly the accuracy of FDG imaging, but false-positive results are inevitable in some situations because of the biological properties of FDG, and false-negative results can be found if the tumor size is below the spatial resolution of current PET imaging (about 5–10 mm). A new and promising indication of PET–CT is the definition of a metabolic target volume to improve radiotherapy planning. The clinical validation of new radiopharmaceuticals (i.e. $[^{11}\text{C}]$ methionine, $[^{18}\text{F}]$ thymidine, and $[^{18}\text{F}]$ MISO (misonizadole)) might expand the role of PET imaging in HNSCC.

References

1. Barnes L, Eveson JW, Reichart P, Sidransky D, eds. World Health Organization Classification of Tumors. Pathology and Genetics of Head and Neck Tumours. Lyon: IARC Press, 2005.
2. Rankin S. Paranasal sinus tumour. In: Husband JES, Reznik RH, eds. Imaging in Oncology. Oxford: ISIS Medical Media, 1998: 415–28.
3. King M. Tumours of the pharynx, tongue and mouth. In: Husband JES, Reznik RH, eds. Imaging in Oncology. Oxford: ISIS Medical Media, 1998: 429–56.
4. Lev M, Silverman P, Curtin H. Laryngeal tumour. In: Husband JES, Reznik RH, eds. Imaging in Oncology. Oxford: ISIS Medical Media, 1998: 457–79.
5. Adams S, Baum RP, Stuckensen T et al. Prospective comparison of FDG PET with conventional imaging techniques

- (CT, MRI, US) in lymph node staging of head and neck cancer. *Eur J Nucl Med* 1998; 25: 1255–60.
6. Kau RJ, Alexiou C, Laubenbacher C et al. Lymph node detection of head and neck squamous cell carcinomas by positron emission tomography with fluorodeoxyglucose F 18 in a routine clinical setting. *Arch Otolaryngol Head Neck Surg* 1999; 125: 1322–8.
 7. Kostakoglu L, Goldsmith SJ. PET in the assessment of therapy response in patients with carcinoma of the head and neck and of the esophagus. *J Nucl Med* 2004; 45: 56–68.
 8. Goerres GW, Schmid DT, Bandhauer F et al. Positron emission tomography in the early follow-up of advanced head and neck cancer. *Arch Otolaryngol Head Neck Surg* 2004; 130: 105–9.
 9. Menad Y, Graham MM. Uptodate on 18F-fluorodeoxyglucose/positron emission tomography and positron emission tomography/computer tomography imaging of squamous head and neck cancers. *Semin Nucl Med* 2005; 35: 214–19.
 10. Wahl RL. Targeting glucose transporters for tumor imaging: 'sweet' idea, 'sour' result. *J Nucl Med* 1996; 37: 1038–41.
 11. Kostakoglu L, Agress H Jr, Goldsmith SJ. Clinical role of FDG PET in evaluation of cancer patients. *Radiographics* 2003; 23: 315–40.
 12. Warburg O, Posener K, Negelein E. On the metabolism of cancer cells. *Biochem Z* 1924; 152: 319–44.
 13. Blodgett T, Branstetter B, Fukui M, Meltzer C. Physiologic uptake in the head and neck on PET/CT. *Radiographics* 2007; in press.
 14. Shreve PD, Anzai Y, Wahl RL. Pitfalls in oncologic diagnosis with FDG PET imaging: physiologic and benign variants. *Radiographics* 1999; 19: 61–77.
 15. Kapoor V, McCook BM, Torok FS. An introduction to PET-CT imaging. *Radiographics* 2004; 24:523–43.
 16. Beyer T, Townsend DW, Brun T et al. A combined PET/CT scanner for clinical oncology. *J Nucl Med* 2000; 41: 1369–79.
 17. Schoder H, Yeung HW, Gonen M, Kraus D, Larson SM. Head and neck cancer: clinical usefulness and accuracy of PET/CT image fusion. *Radiology* 2004; 231: 65–72.
 18. Branstetter BF, Blodgett TM, Zimmer LA et al. Head and neck malignancies: is PET/CT more accurate than PET or CT alone? *Radiology* 2005; 235: 580–6.
 19. Syed R, Bomanji JB, Nagabhushan N et al. Impact of combined 18F-FDG PET/CT in head and neck tumours. *Br J Cancer* 2005; 92: 1046–50.
 20. Bar-Shalom R, Yefremov N, Guralnik L et al. Clinical performance of PET/CT in evaluation of cancer: additional value for diagnostic imaging and patient management. *J Nucl Med* 2003; 44: 1200–9.
 21. Kluetz P, Meltzer C, Villemagne V et al. Combined PET/CT imaging in oncology: impact on patient management. *Clin Positron Imaging* 2000; 3: 223–30.
 22. Goerres GW, Hany TF, Kamel E, von Schulthess GK, Buck A. Head and neck imaging with PET and PET/CT: artefacts from dental metallic implants. *Eur J Nucl Med Mol Imaging* 2002; 29: 367–70.
 23. Kamel EM, Burger C, Buck A, von Schulthess GK, Goerres GW. Impact of metallic dental implants on CT-based attenuation correction in a combined PET/CT scanner. *Eur Radiol* 2003; 13: 724–8.
 24. Goerres GW, Burger C, Kamel E et al. Respiration-induced attenuation artifact at PET/CT: technical considerations. *Radiology* 2003; 226: 906–10.
 25. Bujenovic S, Mannting F, Chakrabarti R, Ladnier D. Artifacts of 2-deoxy-2-[(18)F]fluoro-D-glucose localization surrounding metallic objects in a PET/CT scanner using CT-based attenuation correction. *Mol Imaging Biol* 2003; 5: 20–2.
 26. Nakamoto Y, Chin BB, Kraitchman DL et al. Effects of nonionic intravenous contrast agents at PET/CT imaging: phantom and canine studies. *Radiology* 2003; 227: 817–24.
 27. Lowe VJ, Stack BC Jr. PET imaging in head and neck cancer. In: Valk PE, Bailey DL, Townsend DW, Maisey MN, eds. *Positron Emission Tomography. Basic Science and Clinical Practice*. London: Springer-Verlag, 2003; 535–46.
 28. Goerres GW, Schmid DT, Schknecht B, Eyrych GK. Bone invasion in patients with oral cavity cancer: comparison of conventional CT with PET/CT and SPECT/CT. *Radiology* 2005; 237: 281–7.
 29. Babin E, Hamon M, Benateau H et al. Interest of PET/CT scan fusion to assess mandible involvement in oral cavity and oropharyngeal carcinomas. *Ann Otolaryngol Chir Cervicofac* 2004; 121: 235–40.
 30. Schwartz DL, Ford E, Rajendran J et al. FDG-PET/CT imaging for preradiotherapy staging of head and neck squamous cell carcinoma. *Int J Radiat Oncol Biol Phys* 2005; 61: 129–36.
 31. Adams S, Baum RP, Stuckensen T et al. Prospective comparison of 18F-FDG PET with conventional imaging modalities (CT, MRI, US) in lymph node staging of head and neck cancer. *Eur J Nucl Med* 1998; 25: 1255–60.
 32. Bailet JW, Abeymayor E, Jabour BA et al. Positron emission tomography. A new, precise imaging modality for detection of primary head and neck tumours and assessment of cervical adenopathy. *Laryngoscope* 1992; 102: 281–8.
 33. Braams JW, Pruim J, Freling et al. Detection of lymph node metastases of squamous-cell cancer of the head and neck with FDG-PET and MRI. *J Nucl Med* 1995; 36: 211–16.
 34. Hannah A, Scott AM, Tochon-Danguy H et al. Evaluation of 18F-fluorodeoxyglucose positron emission tomography and computed tomography with histopathologic correlation in the initial staging of head and neck cancer. *Ann Surg* 2002; 236: 208–17.
 35. Mendenhall WM, Mancuso AA, Parsons JT, Stringer SP, Cassisi NJ. Diagnostic evaluation of squamous cell carcinoma metastatic to cervical lymph nodes from unknown head and neck primary site. *Head Neck* 1998; 20: 739–44.
 36. Myers LL, Wax WK, Nabi H, Simpson GT, Lamonica D. Positron emission tomography in the evaluation of the N0 neck. *Laryngoscope* 1998; 108: 232–6.
 37. McGuirt WF, Williams DW 3rd, Keyes JW Jr et al. A comparative diagnostic study of head and neck nodal metastases using positron emission tomography. *Laryngoscope* 1995; 105: 373–5.
 38. Jones AS, Roland NJ, Field JK, Phillips DE. The level of cervical lymph node metastases: their prognostic relevance and relationship with head and neck squamous carcinoma primary sites. *Clin Otolaryngol* 1994; 19: 63–9.
 39. Assar OS, Fischbein NJ, Caputo GR et al. Metastatic head and neck cancer: role and usefulness of FDG PET in locating occult primary tumors. *Radiology* 1999; 210: 177–81.

40. Manolidis S, Donald PJ, Volk P, Pounds TR. The use of positron emission tomography scanning in occult and recurrent head and neck cancer. *Acta Otolaryngol Suppl* 1998; 534: 1–11.
41. Leon X, Quer M, Diez S et al. Second neoplasm in patients with head and neck cancer. *Head Neck* 1999; 21: 204–10.
42. Mukherji SK, Wolf GT. Evaluation of head and neck squamous cell cancer after treatment. *AJNR Am J Neuroradiol* 2003; 24: 1743–6.
43. Som PM, Lawson W, Urken ML. The posttreatment neck: clinical and imaging considerations. In: Som PM, Curtin HD, eds. *Head and Neck Imaging*, 4th edn. St Louis, MO: Mosby, 2003: 2239–72.
44. Farber LA, Benard F, Machtay M et al. Detection of recurrent head and neck squamous cell carcinomas after radiation therapy with 2-18F-fluoro-2-deoxy-d-glucose positron emission tomography. *Laryngoscope* 1999; 109: 970–5.
45. Sakamoto H, Nakai Y, Ohashi Y et al. Monitoring of response to radiotherapy with fluorine-18 deoxyglucose PET of head and neck squamous cell carcinomas. *Acta Otolaryngol* 1998; 538 (Suppl): 254–60.
46. Lowe VJ, Dunphy FR, Varvares M et al. Evaluation of chemotherapy response in patients with advanced head and neck cancer using [F-18] fluorodeoxyglucose positron emission tomography. *Head Neck* 1997; 19: 666–74.
47. Greven KM, Williams DW 3rd, Keyes JW Jr et al. Positron emission tomography of patients with head and neck carcinoma before and after high dose irradiation. *Cancer* 1994; 4: 1355–9.
48. Fischbein NJ, Assar OS, Caputo GR et al. Clinical utility of positron emission tomography with 18F-fluorodeoxyglucose in detecting residual/recurrent squamous cell carcinoma of the head and neck. *AJNR Am J Neuroradiol* 1998; 19: 1189–96.
49. Anzai Y, Carroll WR, Quint DJ et al. Recurrence of head and neck cancer after surgery or irradiation: prospective comparison of 2-deoxy-2-[F-18]fluoro-d-glucose PET and MR imaging diagnoses. *Radiology* 1996; 200: 135–41.
50. Wong WL, Chevretton EB, McGurk M et al. A prospective study of PET-FDG imaging for the assessment of head and neck squamous cell carcinoma. *Clin Otolaryngol* 1997; 22: 209–14.
51. Farber LA, Benard F, Machtay M et al. Detection of recurrent head and neck squamous cell carcinomas after radiation therapy with 2-18F-fluoro-2-deoxy-D-glucose positron emission tomography. *Laryngoscope* 1999; 109: 970–5.
52. Haberkorn U, Strauss LG, Dimitrakopoulou A et al. Fluorodeoxyglucose imaging of advanced head and neck cancer after chemotherapy. *J Nucl Med* 1993; 34: 12–17.
53. Greven KM, Williams DW 3rd, McGuirt WF Sr et al. Serial positron emission tomography scans following radiation therapy of patients with head and neck cancer. *Head Neck* 2001; 23: 942–6.
54. Keyes JW Jr, Watson NE Jr, Williams DW 3rd, Greven KM, McGuirt WF. FDG PET in head and neck cancer. *AJR Am J Roentgenol* 1997; 169: 1663–9.
55. Mukherji SK, Fischbein NJ, Castelijns JA. New imaging modalities. In: Som PM, Curtin HD, eds. *Head and Neck Imaging*, 4th edn. St Louis, MO: Mosby, 2003: 2294–322.
56. Koshy M, Paulino AC, Howell R et al. F-18 FDG PET-CT fusion in radiotherapy treatment planning for head and neck cancer. *Head Neck* 2005; 27: 494–502.
57. Scarfone C, Lavelly WC, Cmelak AJ et al. Prospective feasibility trial of radiotherapy target definition for head and neck cancer using 3-dimensional PET and CT imaging. *J Nucl Med* 2004; 45: 543–52.

Lung cancer

Richard P Baum, Vikas Prasad, and Wolfgang A Weber

Background

Lung cancer, the commonest cancer in the world and accounting for 12.3% of all new cancer cases, is responsible for millions of deaths per year, greater than the total number of deaths from breast, colon, and prostate cancer combined. More than 160 000 patients died of lung cancer in the USA in 2005 (estimated figure of American Cancer Society). In Europe, nearly 400 000 new cases of lung cancer are diagnosed every year, and it continues to be the leading cause of cancer deaths in man above the age of 45 years.¹ The 5-year survival rates are 16% in the United States and 5% in the UK. In Europe, there is substantial geographical difference in the incidence and mortality of lung cancer. Males have a four time higher chance of getting lung cancer as compared to females, and the average time of diagnosis is 61 years. The association of tobacco smoking was first reported in 1950, and it is now well established as the main cause of lung cancer, with around 90% of cases thought to be related to tobacco consumption.¹⁻³ The strong association is related to the amount and type of tobacco product used, the duration of use, and the age at initiation.⁴

Histologically, lung cancer is classified into two main categories: non-small-cell lung cancer (NSCLC) and small-cell lung cancer (SCLC). NSCLC accounts for roughly 80% of lung cancer cases, the rest being SCLC. Although there are many histological variants of NSCLC (such as squamous cell carcinoma, adenocarcinoma, large-cell carcinoma, adenosquamous carcinoma, etc.), the broader classification SCLC/NSCLC mainly determines clinical management and prognosis.

The average survival time for untreated NSCLC and SCLC is only 6 months and 2 months, respectively. If diagnosed at an early stage, NSCLC can be cured by surgical resection. Locally advanced disease is treated by preoperative chemoradiotherapy followed by surgical resection. In contrast, the primary therapy of SCLC is systemic chemotherapy, since this tumor type is highly sensitive to chemotherapy and has usually metastasized at the time of diagnosis.⁵

Diagnostic strategies and treatment options

Lung cancer often presents as a solitary pulmonary nodule (SPN) diagnosed on chest radiographs, after initial presentation of the patient with a broad spectrum of non-specific symptoms. Chest radiographs are frequently used as a screening method. Approximately one-third of SPNs in patients more than 35 years old are malignant. However, the non-invasive identification of malignant nodules is a diagnostic challenge, and approximately 50% of radiographically indeterminate nodules resected at thoracoscopy are benign.⁶

In patients with lung cancer, a battery of investigations is required for staging and restaging after therapy. Knowledge about the cardiopulmonary status prior to therapy is essential to ascertain whether a patient is fit for surgery and to predict residual lung function. Preoperative assessment of residual lung volume is important in the management of patients with lung cancer.⁷⁻⁹ Scintigraphic assessment of residual lung volume – predicted as a relative value from the percentage loss of radioactivity in the lung segments, or lobes, intended for resection or irradiation – is essential for the estimation of functional resectability. All patients suspected of harboring lung cancer should undergo the tests recommended by the American Thoracic Society (ATS) and by the German Pneumology Society (Table 5.1).^{5,7} Once the diagnosis has been confirmed, the next level of investigation should be adapted according to the available therapeutic options as described in Table 5.2.^{2,3,5,9,10}

Staging should be performed in accordance with the International Staging System (ISS).^{5,9,11} The TNM system depicts the size and proximity of the primary tumor (T) to important structures, the lymph node status (N), and the presence of metastases (M) (Table 5.3).¹¹ The involvement of ipsilateral peribronchial, hilar lymph nodes is designated as N1, ipsilateral mediastinal lymph node metastases are designated as N2, and contralateral mediastinal or supraclavicular lymph node metastases are

Table 5.1 Tests recommended by American Thoracic Society and German Pneumology Society for patients suspected of having lung cancer

Thorough medical history
Complete physical examination
Total blood count
Laboratory investigations for following: electrolytes, calcium, alkaline phosphatase, albumine, AST, ALT, GGT, LDH, bilirubin, creatinine
Chest X-ray
CECT of chest and upper abdomen covering the adrenals
Bronchoscopy for cytological and histological examination and staging biopsy for central tumors

described as N3. Further, thoracic lymph nodes are classified into four groups: superior mediastinal, inferior mediastinal, aortic and N1 nodes. These nodal groups can be subdivided into different levels (Table 5.4).¹² One of the uses of this classification of lymph nodes is for selection

of a proper method of lymph node sampling. There are numerous invasive methods for lymph node sampling such as mediastinoscopy,¹³ video-assisted thoracic surgery (VATS), thoracotomy, and ultrasound-guided and endoscopic transbronchial biopsy, as well as computed tomography (CT)-guided percutaneous needle biopsy (Table 5.5).¹⁴ Mediastinoscopy is commonly used for the evaluation of levels 2, 4, and 7, whereas VATS is mostly used for lymph nodes at levels 5, 6, and 7. However, VATS, depending upon the approach, can evaluate multiple stations. Sampling of lymph nodes at all levels is performed during thoracotomy. Pulmonary metastases outside the lung lobe of the primary tumor are designated as M1, including distant lymph nodes above the supraclavicular level and other organ sites. The brain, central nervous system, bone, liver, and adrenal glands are common sites for distant metastases. The combination of T, N, and M results in the ISS stages 1–4. In the new guidelines, ISS is also recommended for small-cell lung cancer.⁹

Prior to the initiation of any tumor-specific treatment, a histopathologic or at least a cytological diagnosis needs to be obtained. Management strategies are based on the stage of the disease. Current recommendations for stage-specific treatment of NSCLC and SCLC are summarized in Tables 5.6 and 5.7 respectively.^{2,3,5,7,10} Because of the

Table 5.2 Indications for further work-up of patients having confirmed lung cancer

<i>Investigation</i>	<i>Indication</i>
CECT of liver	Deranged liver function on LFT; abnormal NCECT of liver/ abnormal clinical evaluation
CECT or MRI of brain	Presence of CNS symptoms or abnormal clinical evaluation
MRI of thoracic wall/spine	In case of Pancoast tumor or if there is suspicion of infiltration of the spine
Whole body bone scintigraphy	Complaint of bone pain, or documented evidence of elevated alkaline phosphatase (bony fraction), elevated calcium or abnormal clinical evaluation
Biopsy/MRI/FDG-PET	Potentially resectable patients having an isolated adrenal enlargement/liver lesion
PFT	In case lung resection or thoracic radiotherapy is planned
Quantitative lung perfusion scintigraphy or exercise testing to evaluate maximum oxygen consumption	Patients with borderline resectability (having limited cardiopulmonary status)
Concentration of arterial blood gases	Patients with borderline resectability (having limited cardiopulmonary status)
Mediastinoscopy	Evidence of mediastinal lymph nodes of 10 mm short axis diameter or left-sided tumor on chest CT
Diagnostic thoracotomy	For pathological confirmation of malignancy (only if no other less invasive techniques are not successful)
Thoracoscopy	For pathological confirmation of malignancy in pleural effusion (only if aspiration of pleural biopsy is not successful)

Table 5.3 International Staging System (ISS)/TNM stage and 5-year survival rate

ISS stage	TNM stage	5-year survival rate (%)	
		Clinical staging	Pathological staging
1A	T1N0M0	61	67
1B	T2N0M0	38	57
2A	T1N1M0	34	55
2B	T2N1M0	24	39
	T3N0M0	22	38
3A	T3N1M0	9	25
	T1-3N2M0	13	23
3B	T4N0-2M0	7	—
	T1-4N3M0	3	—
4	T1-4N0-3M1	1	—

Table 5.4 Thoracic lymph node stations

Superior mediastinal nodes	Highest mediastinal Upper paratracheal Prevascular and retrotracheal Lower paratracheal (including azygos)
Inferior mediastinal nodes	Subcarinal Paraesophageal (below carina) Pulmonary ligament
Aortic nodes	Subaortic (AP window) Para-aortic (ascending aorta or phrenic)
N1 nodes	Hilar Interlobar Lobar Segmental Subsegmental

AP, aortopulmonary.

Table 5.5 Procedures used for sampling of lymph node (LN) according to level

Level of LN	Esophageal sonography	Thoracotomy	Mediastinoscopy	Chamberlain/VATS
Paratracheal (L&R)		+	+	
Lower paratracheal (L&R)	+	+	+	
Subaortic, para-aortic	+	+		+
Subcarinal	+	+	+	
Paraesophageal, pulmonary ligament	+	+		
Hilar (L&R)		+		+
Interlobar, lobar, segmental, subsegmental		+		

L&R, left and right; VATS, video-assisted thoracic surgery.

Table 5.6 Therapy for non-small-cell lung cancer adapted to stage

Stage	Therapy used in current practice	Recommended therapy	Future directions with a view upon improving the prognosis
1A	Surgery If inoperable: radiotherapy	Surgery If inoperable: radiotherapy	Neoadjuvant or adjuvant systemic therapy Optimization of radiotherapy
1B/2	Surgery If inoperable: radiotherapy	Treatment in controlled trials*	Neoadjuvant or adjuvant systemic therapy Optimization of radiotherapy
3A	Surgery and radiotherapy	Treatment in controlled trials*	Use of multimodality treatment approach
3B	Radiotherapy as most are inoperable	Platin-based chemotherapy followed by radiotherapy Simultaneous with radiotherapy or treatment in controlled trials*	Use of multimodality treatment approach Optimization of chemotherapy and radiotherapy
4	Chemotherapy Palliative treatment	Chemotherapy or treatment in controlled trials*	New chemotherapeutic combinations or tyrosine kinase/angiogenesis inhibitors

*For patients suitable for participation in phase 3 studies with the intent of optimization of therapy.

Table 5.7 Therapy for small-cell lung cancer adapted to stage

Stage	Therapy used in current practice	Recommended therapy	Future directions with a view upon improving the prognosis
1	Surgery followed by RT and PCI or CTx followed by TRT and PCI if there is complete remission	Surgery followed by RT and PCI or CTx/TRT with addition of PCI (if CR) treatment in studies*	Optimization of multimodality therapeutic options
2	Surgery followed by CTx, TRT, and PCI or CTx followed by TRT and PCI if there is complete remission	Surgery followed by CTx, TRT, and PCI or CTx/TRT with addition of PCI (if CR) treatment in studies*	Experimental studies mainly taking into account: the efficacy of resection in stage 1–3A; use of different concepts for TRT (fractionation, target volume, dose) in stage 1–3B for the purpose of improved local control
3A	CTx followed by TRT and PCI if there is complete remission	CTx/TRT and PCI if there is complete remission, treatment in controlled trials*	Experimental studies mainly taking into account: the efficacy of high-dose CTx in stage 1–3B;
3B	CTx followed by TRT and PCI if there is complete remission	CT/TRT and PCI (if CR) treatment in controlled trials*	The efficacy of biological therapy principles (metalloproteinase inhibitors, angiogenesis inhibitors) for the purpose of achieving improved systemic control
4	CTx or palliative treatment	CTx or treatment in controlled trials*	New chemotherapeutic combinations or tyrosine kinase/angiogenesis inhibitors

*For patients suitable for participation in phase 3 studies with the intent of optimization of therapy.
RT, radiotherapy; PCI, prophylactic cranial irradiation; CTx, chemotherapy; TRT, thoracic radiotherapy; CR, complete remission.

largely unchanged overall 5-year survival rate in the past decade (only 15%), there are frequent changes in the guidelines, especially for locally advanced lung cancer, in an effort to improve the prognosis.

In the absence of mediastinal (N2 or N3) or distant metastases (M), surgical treatment is potentially curative in patients with NSCLC. Nearly 45% of all lung cancers are confined to the chest, and surgical resection with curative intent is a possibility in such patients,¹⁵ provided the surgeon is well versed in bronchoplastic and angioplastic techniques, including expanded resection techniques if there is involvement of the neighboring organs, especially the mediastinum and/or the chest wall. If there is suspicion of involvement of N2 lymph nodes on CT, mediastinoscopy is currently the recommended procedure to confirm the lymph node status.¹⁰ If the results of histopathology suggest metastatic involvement of N2 nodes, then multimodality treatment should be used. Involvement of the contralateral mediastinal or supraclavicular lymph node

(N3) is considered as a contraindication for surgical resection.¹⁰

Palliative chemotherapy is the standard treatment for SCLC and stage 4 NSCLC. The main aim of such a treatment strategy is to increase survival and quality of life.^{2,3} In patients having locally advanced NSCLC with metastatic involvement of the mediastinal lymph nodes, or in non-resectable tumors, the use of chemotherapy and radiotherapy followed by surgery is currently under investigation.

Inoperable early-stage patients (due to concurrent diseases or non-compliance) can be treated with primary radiotherapy using tumor doses of at least 60 Gy. For pancoast tumors (T3N0M0), preoperative radiotherapy with a tumor dose of 50 Gy is recommended. Patients having mediastinal lymph node metastases or incomplete tumor resection should be treated with adjuvant radiotherapy (50 Gy), subsequently followed by a boost dose of 10–16 Gy for the residual tumor. Radiotherapy is also

useful for palliation of symptoms. Combined radiotherapy and chemotherapy has been extensively studied, especially in stage 3 NSCLC.⁵

In SCLC, the recommended treatment is irradiation of the tumor site after chemotherapy, followed by prophylactic cranial irradiation.

Diagnostic modalities

Various imaging modalities play an important role in the management of lung cancer. The selection of these imaging modalities depends on the tumor stage and the available therapeutic options. This chapter will outline the role of various imaging modalities in relation to patient management, focusing on nuclear medicine procedures.

Lung nodules

By definition, a solitary pulmonary nodule (SPN) is an opacity in the lung parenchyma measuring up to 3 cm that is not associated with mediastinal adenopathy or atelectasis. Lesions greater than 3 cm are categorized as masses.¹⁶ Approximately 75% of pulmonary nodules are found incidentally during chest radiographs. Signs and symptoms (coughing, hemoptysis, or thoracic pain) suggesting a lung problem are found in only 20–25% of patients with SPN. A German study has shown that there is an average delay of 7 months before a definitive diagnosis is reached.¹⁷ The same study has documented that the younger is the patient and smaller is the lesion, the longer is the delay in reaching the final diagnosis.

There are numerous etiologies (approximately 80) for lung nodules, ranging from infections to inflammation and malignancies.¹⁸ Approximately 130 000 SPNs are diagnosed per year in the USA, with an incidence of 52 per 100 000 population. Invasive techniques such as bronchoscopy have a sensitivity of only 65%, whereas transbronchoscopic biopsy reaches a sensitivity of 79%.¹⁹ Although transthoracic fine needle biopsy (TTFB) has a very high sensitivity (94–98%) and specificity (91–96%), the risk factors associated with its use (mainly pneumothorax) reach 19–26%, with approximately 10–15% of patients requiring pleural drainage after TTFB, resulting in hospital stay and increased expenditure.²⁰

Conventional imaging (chest radiographs and CT) and metabolic imaging (using positron emission tomography (PET)) play a complementary role in the diagnosis of lung cancer.

Conventional imaging

The evaluation (additional work-up) of a SPN starts after its incidental detection on a chest radiography to rule out malignancy. Uniformly dense calcified nodules on chest radiography are mostly benign in nature.⁴ Serial chest radiographs taken over a longer period of time (2 years or more) showing no signs of change in the appearance also make the diagnosis of a benign nodule very likely.

Prior to the advent of PET, a radiographically indeterminate SPN was best evaluated using CT.²¹ Although CT remains an integral part of the work-up of SPN, other options are available. CT is used for the evaluation of shapes, borders, and densities of nodules. With the use of CT densitometry, calcifications can be detected within the nodules. Calcified nodules are mostly benign; however, the list of differential diagnoses is long, including metastasis from primary tumors (e.g. bone tumor, mucin-producing adenocarcinomas, and soft-tissue sarcomas) or internal hemorrhage in metastases (e.g. choriocarcinoma and melanoma).⁴ A nodule is presumably benign only if the attenuation consistent with calcification is present in the majority of the region of the nodule. The calcification has to be present in the center of the nodule for it to be considered benign.⁴ Diffuse calcification measuring more than 300 HU (Hounsfield units) is indicative of a benign nodule.¹⁶ The pattern of contrast enhancement can also help to differentiate between benign and malignant nodules. Nodules showing less than 15 HU enhancement in the center are more likely to be benign, whereas those showing enhancement greater than 25 HU are more likely to be malignant.^{22,23}

A report from the Early Lung Cancer Action Program (ELCAP) study has documented that 20% of pulmonary nodules on baseline screening are like ground-glass, or sub-solid (they are less dense than the solid nodules and the surrounding pulmonary vasculature and, thus, do not obscure the lung parenchyma). Ground-glass opacities are associated with bronchoalveolar carcinoma, whereas other adenocarcinomas present more frequently as solid nodules.²⁴

Apart from the calcification and ground-glass appearance, certain morphological characteristics of pulmonary nodules such as a speculated outer margin, a hazy and indistinct margin, extension to pulmonary veins, focal retraction of adjacent pleura, and endobronchial extension are also suggestive of malignancies. Inhomogeneous internal composition and the evidence of central necrosis point towards a malignant nature of the lesion. Some malignant lesions create air bronchograms, commonly associated with pneumonia. Sometimes, CT scan features of lymphoma and bronchoalveolar cell carcinoma can be confused with benign lung lesions.⁴

In spite of all these morphologic criteria, 25–39% of malignant nodules are inappropriately classified as benign.²⁵ Although constancy of the nodule in terms of its morphologic characteristic over time is reliable for labeling a nodule benign, the predictive value of stability in size may be only 65%, probably because doubling in volume amounts to only 26% increase in nodular diameter, a change very difficult to perceive.^{26,27} Clinical information combined with the radiographic characteristics can be used to calculate the likelihood ratio of malignant disease. This strategy, having its origin in Bayesian analysis, is also a way of choosing the appropriate management protocol. If the probability of cancer is less than 5%, then the patient is monitored over time; if the probability is between 5 and 60%, the lesion is biopsied. For a likelihood ratio greater than 60%, resection of the nodule is recommended.^{28,29} However, 50% of patients undergoing surgical biopsy of an indeterminate SPN have benign disease. Because of the inadequacy of these radiographic characteristics, there was a need to find a better alternative, resulting in the rapid development of PET in lung cancer diagnosis.^{6,30–32}

Nuclear imaging

Somatostatin receptor imaging

[^{99m}Tc]depreotide, a somatostatin analog with a high affinity for the receptor subtypes 2, 3, and 5, has been used for the differentiation of indeterminate lung nodules.³³ A study by Blum et al. in 114 patients showed a sensitivity of 97% with a specificity of 73% and a negative predictive value of 86%.³⁴ [^{99m}Tc]depreotide has been approved in Europe and the United States for the differentiation of benign and malignant nodules. Although the results are encouraging, it is mainly recommended for institutions having no PET facility.³⁵

Positron emission tomography with fluoro-2-deoxy-D-glucose (FDG-PET)

The rapidly increasing role of FDG-PET in the work-up of lung cancer in the past decade can be related to the advancement in instrumentation and associated software, resulting in image resolution of 6 mm or less in clinical applications.³⁶ In lung cancer, there are numerous approved indications for performing FDG-PET (Table 5.8). Because of its immense potential in oncology, whole-body FDG-PET should be used with diligence in order to reproduce the results with a high degree of sensitivity and specificity. Optimal patient preparation is the stepping-stone and should be followed strictly (Table 5.9). Sufficient time interval between injection and scanning should be given

so that there is good blood clearance of FDG, especially from the mediastinum and lung.^{37,38} In order to detect small mediastinal lymph nodes, use of attenuation correction is necessary. Nowadays, iterative reconstruction is standard, and is especially useful to avoid reconstruction artifacts and to detect lymph node metastases near the primary tumor when there is intense uptake in the primary tumor or the myocardium. Respiratory movements during scanning produce their own artifacts, which can be minimized using four-dimensional (4D) PET (gated PET).^{39–41} In order to minimize the impact of respiratory artifacts on the fusion of PET and CT data, often the CT images are acquired in the mild expiratory phase. This might compromise the detection of lung metastases. Juergens et al.⁴² have shown that additional low-dose chest CT in inspiration improves the detection of solitary pulmonary nodules while using FDG-PET-CT.

There are specific guidelines for acquisition and image reconstruction, as summarized in Table 5.10.^{43–45} Calculation of the maximum standardized uptake value (SUV_{max}) is recommended in all or at least in the most relevant tumor lesions.^{46,47} Bryant and Cerfolio⁴⁶ have shown in a large prospective series in 585 patients that, if the pulmonary nodule is less than 2.5 cm (indeterminate pulmonary nodules), a SUV_{max} between 0 and 2.5 suggests 24% chance of malignancy. If the SUV_{max} is between 2.6 and 4 the chance of the nodule being malignant is 80%, which increases to 96% for SUV_{max} greater than 4.1. However, for solid pulmonary lesions with low FDG uptake (SUV_{max} < 2.5), semiquantitative approaches do not improve the accuracy of [¹⁸F]FDG-PET over that obtained with visual analysis. Pulmonary lesions with visually absent uptake suggest that the probability of malignancies is very low. On the other hand, the probability of malignancy in any visually evident lesion is about 60%.⁴⁸

The results of the PET study should always be analyzed in conjunction with a CT image, because of the poor anatomic localization on PET images alone. The advent of PET-CT and the possibility of image fusion has been heralded as a major breakthrough in oncologic PET imaging.⁴⁹

For characterization of SPN, FDG-PET alone better predicts malignancy than a combination of clinical and morphologic criteria. A meta-analysis,^{50,51} covering the results of numerous studies in approximately 1400 patients,^{52–76} proved that FDG-PET can differentiate between benign and malignant SPN with a sensitivity and specificity of approximately 96.8% and 77.8%,⁵⁰ respectively. The counter argument put forward is the relatively high cost of a PET study. A group from Italy compared the traditional SPN work-up using CT, fine-needle aspiration cytology, and thoracoscopic biopsy with a diagnostic work-up including FDG-PET.⁷⁷ This study demonstrated a reduction in cost of approximately 50 euros (~\$60) per patient if PET was included in the work-up. Lejeune et al.

Table 5.8 Nuclear medicine techniques in the work-up of lung cancer

<i>Nuclear medicine techniques and commonly used radiopharmaceuticals (sorted according to their clinical relevance)</i>	<i>Indications</i>
[¹⁸ F]FDG [^{99m} Tc]SMS (depreotide) [^{99m} Tc]MIBI [^{99m} Tc]tetrofosmin [²⁰¹ Tl]chloride [⁶⁷ Ga]citrate [^{99m} Tc](5)DMSA	Differentiating benign from malignant pulmonary lesions
FDG-PET Somatostatin receptor scintigraphy ([^{99m} Tc]depreotide) [^{99m} Tc]MIBI [⁶⁷ Ga]citrate	Staging of mediastinal lymph node in NSCLC
FDG-PET Immunoscintigraphy (mAb NR-LU-10)	Staging of NSCLC for extrathoracic metastases
Bone scanning (^{99m} Tc-labeled phosphonates) [¹⁸ F]fluoride PET FDG-PET [^{99m} Tc](5)DMSA	Ruling out or detection of bone metastases
FDG-PET Immunoscintigraphy (MAb NR-LU-10) Somatostatin receptor scintigraphy ([¹¹¹ In]pentetreotide)	Staging of SCLC
[^{99m} Tc]MIBI [^{99m} Tc]tetrofosmin	Evaluation of resistance to cytostatic chemotherapy
Lung perfusion scintigraphy	Assessment of lung function prior to therapy
FDG-PET [²⁰¹ Tc]chloride [⁶⁷ Ga] citrate	Diagnosis of recurrence
FDG-PET [²⁰¹ Tc]chloride	Evaluation of treatment response

FDG-PET, fluoro-2-deoxy-D-glucose-positron emission tomography; SMS, somatostatin; MIBI, methoxyisobutylisonitrile; DMSA, dimercaptosuccinic acid; mAb, monoclonal antibody; NSCLC, non-small-cell lung cancer; SCLC, small-cell lung cancer.

Table 5.9 Patient preparation prior to [¹⁸F]FDG-PET scan

Fasting: 12 hours (minimum 6 hours)

Hydration of the patient: intake of at least 0.75 liter of mineral water (or other non-caloric fluids) before injection

Blood glucose estimation prior to FDG administration (not to exceed 150 mg/dl or 7.5 mmol/l)

Intravenous injection of 230–500 MBq (5–6 MBq/kg) [¹⁸F]FDG

Emission scan to be acquired after a resting period of 60 (to 90) minutes

Enforced diuresis (furosemide 20 mg intravenously after FDG injection)

Table 5.10 Imaging techniques for [¹⁸F]FDG-PET

First the transmission scan is acquired

Emission scan should include neck, thorax, abdomen, and pelvis

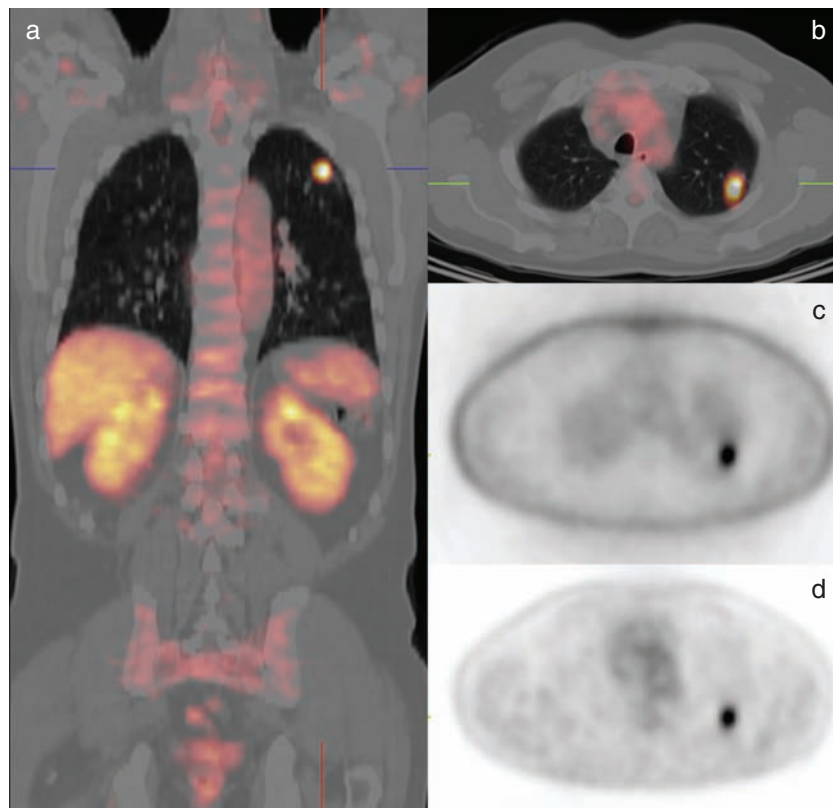
use lower ¹⁸F activity in case of three-dimensional scanning

Image reconstruction including

- iterative algorithms
- scatter compensation
- attenuation correction

Figure 5.1

Singular pulmonary nodule (SPN) left upper lung lobe. Clinical stage based on contrast enhanced (ce) CT scan: cT1 (16 x 13 mm) N2 M1 (enlarged mediastinal lymph nodes and enlarged right adrenal gland). Metabolic tumor stage (based on F-18 FDG PET/CT): mT1(SUV 6.1) N0 M0. a: coronal PET/CT slice, b: transversal PET/CT slice, c: transversal PET slice (non-attenuation corrected), d: attenuation corrected transversal PET slice. Histopathological stage: pT1 pN0 Mx (adenocarcinoma G3, stage IA, R0 L0 V0 C4 after lobectomy and radical lymphadenectomy). The enlargement of mediastinal lymph nodes on CT was due to anthracosilicosis. Follow-up showed no change in size of the right adrenal gland (incidentaloma). Influence on clinical management (ICM) by PET/CT: operation instead of chemotherapy, exclusion of distant metastasis.



compared the cost-effectiveness ratio of three management strategies for SPN: wait and watch with periodic CT, PET, and a combination of CT plus PET. It was concluded that CT plus PET is the most cost-effective strategy in those patients having a risk of malignancy in the range 5.7–87%, whereas patients having a risk of 0.3–5% should be followed under the wait and watch strategy.⁷⁸

In ground-glass nodules, preliminary PET studies have found a sensitivity of only 10% and a specificity of only 20%.⁷⁹ The ELCAP report has suggested a limited role of FDG-PET in the evaluation of these nodules, because of the small size of the nodules and the potential for false-negative findings in focal bronchoalveolar cell carcinoma.⁴ Chhajed et al.⁸⁰ have demonstrated in their study the significant role of FDG-PET when combined with bronchoscopy in the diagnosis of non-calcified chest radiologic lesions ≤ 3 cm in size.

An important issue that determines the diagnostic accuracy of an imaging modality in the evaluation of SPN is the size of the nodule. Pulmonary nodules having a diameter of less than 5 mm on CT scan were found to be non-malignant in 378 patients monitored with CT in the New York (NY)-ELCAP study. For FDG-PET, Bastarikka et al.⁸¹ found a sensitivity of 69% for the detection of malignancy in nodules having a size in the range 5–10 mm

and a sensitivity of 95% in nodules greater than 10 mm in size. The authors also observed a reduction in the apparent uptake of FDG in nodules if the size of the nodule was less than twice the system resolution (7–8 mm), underlining the need for generating different criteria for determination of malignancy in patients having SPN smaller than 15 mm. The inability of PET to reliably detect nodules smaller than 7 mm has also been documented in a phantom study by Coleman et al.⁸²

A meta-analysis of five prospective studies by Hellwig et al.,⁵¹ including at least 35 patients per study and fulfilling the quality criteria as specified by the German Consensus Conference, has shown that FDG-PET has a sensitivity and specificity of 93% and 87%, respectively (Table 5.11). The positive and negative predictive values are 94% and 89%, respectively; the probability to miss a malignant nodule is 11%. This risk has to be weighed against possible life-threatening complications of surgery. The method of interpretation of a PET study is also a matter of debate.⁷⁰ Hubner et al. have shown that there is an improvement of approximately 10% in the specificity of FDG-PET if Patlak analysis is applied for quantitation.⁸³ Cerfolio et al.,⁸⁴ in their retrospective analysis to evaluate the role of maximum SUV in prediction of stage, recurrence, and survival in NSCLC patients, clearly demonstrated that

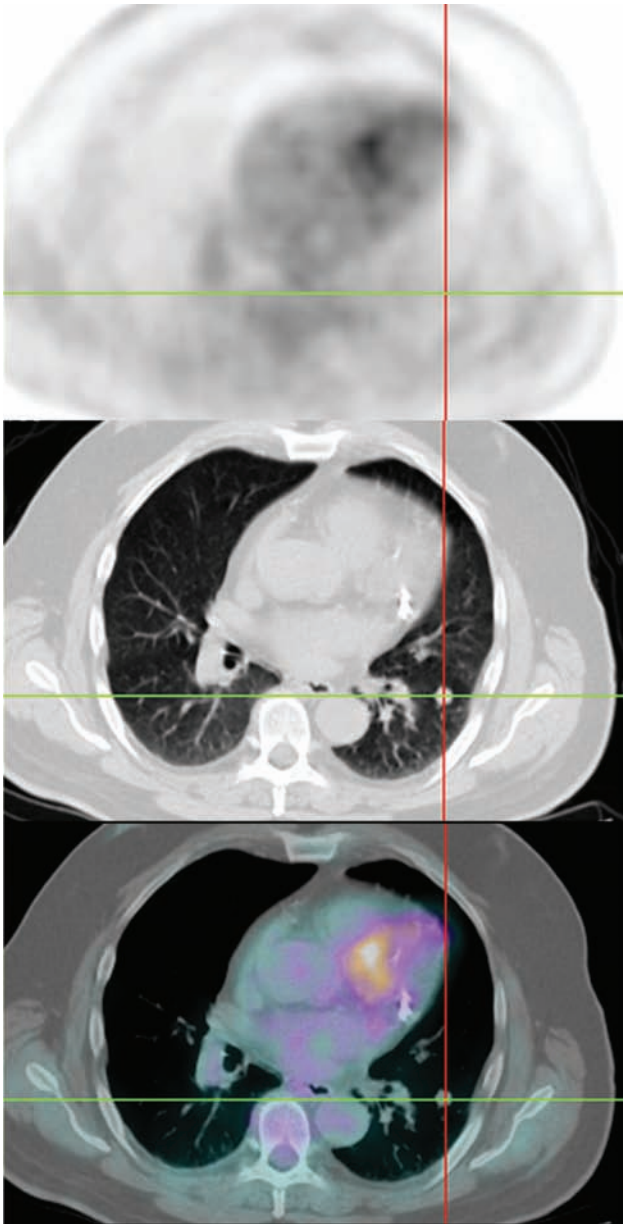


Figure 5.2

SPN left lower lung lobe in a 52-year-old patient at high risk for lung operation (NYHA IV due to aortic valve insufficiency, hypertension, diabetes mellitus). CT scan shows a well-rounded nodule, 1.1 cm in diameter in segment S 10. F-18 FDG PET/CT demonstrates no increased glucose metabolism of the SPN (benign nodule). Follow-up CT scans showed no increase in size. ICM by PET/CT: no operation, exclusion of malignancy.

the maximum SUV of a pulmonary nodule on [^{18}F]FDG-PET is an independent predictor of aggressiveness of NSCLC. The maximum SUV predicted more accurately the recurrence rate for stages 1B and 2 NSCLC and survival for patients with stage 1B, 2 or 3A than did TNM stage.

In a recent study by Yi et al.,⁸⁵ it has been shown that integrated PET-CT is more sensitive and accurate than helical dynamic CT for malignant nodule characterization; therefore, PET-CT may be performed as the first-line evaluation tool for SPN characterization. The authors have also concluded that since helical dynamic CT has high specificity and acceptable sensitivity and accuracy, it may be a reasonable alternative for nodule characterization when PET-CT is unavailable.

When interpreting FDG-PET studies in patients with SPN, several causes of false-positive and false-negative findings (Table 5.12) need to be considered.⁸⁶⁻⁸⁸ In order to increase the sensitivity and specificity of FDG-PET, dual-phase (over time) studies have been performed in which the images were acquired at 1 h and 2 h after the injection of FDG.^{89,90} Matthies et al.⁸⁹ compared single-phase and dual-phase imaging in patients with SPN using a cut-off SUV value of 2.5% and a 10% increase in SUV as a marker of malignancy. They found a sensitivity and specificity of 89% and 94%, respectively, in the single-phase study and of 100% and 89%, respectively, in the dual-phase study. Ponzo et al. have explained this phenomenon on the basis of the difference in levels of glucose-6-phosphatase and hexokinase within benign and malignant cells.⁹¹ However, other studies have indicated that active granulomas, a common reason for false-positive FDG-PET scans, demonstrate the same time course of FDG uptake as that of malignant tumors. Therefore, more data are needed before the dual-phase study becomes routine clinical practice.

Staging of lung cancer: distant metastases

Conventional imaging

At the time of first presentation, occult metastases are present in approximately 30% of patients with adenocarcinoma or large-cell carcinoma as compared to 15% in patients with squamous cell carcinoma.⁹² The adrenal glands and liver are the most common sites of extrathoracic occult metastases. Without clinical or laboratory evidence, routine use of radiology is not advised for the work-up of occult metastases. Approximately 10% of patients with bronchogenic cancer have an adrenal mass on CT. However, benign adenoma needs to be ruled out, as these are found to occur in 3–5% of the overall population.^{93,94} Non-contrast-enhanced CT followed by magnetic resonance

Table 5.11 Evaluation of solitary pulmonary nodules using FDG-PET⁵¹

Author	Year	Cases	Prevalence(%)	Sensitivity(%)	Specificity(%)
Pitman	2002	36	58	90	93
Lowe	1998	89	67	91	89
Gupta	1996	61	73	93	87
Bury	1996	50	66	100	88
Duhaylonsod	1995	47	65	100	81

imaging (MRI) has been reported as the most cost-effective morphologic evaluation for the assessment of suspected adrenal masses.⁹⁵ Adrenal masses less than 10 HU on non-contrast-enhanced CT are generally benign; those adrenal masses which fail to fulfill the CT criteria for a benign lesion are followed up with MRI.

Nuclear imaging

Conventional nuclear medicine procedures

Osteoblastic activity induced by bone metastases can be imaged by osteotropic tracers very early, whereas conventional radiographic imaging is able to detect bone metastases only

if the size of the lesion is more than 1 cm and if there is a focal loss of at least 50% or a focal increase of 30% of the bone mineral.⁹⁶ In lung cancer patients, [^{99m}Tc]MDP (methylene diphosphonate) bone scan is indicated for further evaluation of bone pain, elevated serum calcium, or elevated alkaline phosphatase levels.^{2,3} Although the sensitivity of the technique is reasonably high, it suffers from lack of specificity (40–90%) because of the increased uptake of MDP in various benign conditions that are associated with increased osteoblastic activity. In order to minimize false-positive findings, proper history taking is essential prior to acquiring a whole-body bone scan. In the absence of PET-CT, single photon emission computed tomography (SPECT)-CT has also been shown to have a significant role in diagnosis, staging, response evaluation, follow-up, and dosimetry evaluation of patients with lung cancer.⁹⁷

Figure 5.3

SPN right upper lung lobe. Clinical stage based on ceCT scan: cT1 (15 x 15 mm) N0 M1 (enlarged adrenal glands), differential diagnosis (DD) tuberculoma vs. lung cancer (Tbc known since 38 years). Metabolic tumor stage (based on F-18 FDG PET/CT): mT1(SUV 14.9) N0 M0. a: coronal PET/CT slice, b: transversal PET slice, c: transversal CT slice, d: fused PET/CT slice. There is high FDG uptake in the posterior lesion which has contact to the pleura. No uptake is seen in a morphologically similar lesion more anteriorly. Histopathological stage: pT1 pN0 Mx (squamous cell carcinoma, so-called scar-derived cancer, stage IA, R0 L0 V0 C4 (after lobectomy and radical lymphadenectomy). The enlarged adrenal glands were shown to be incidentalomas in the follow-up. ICM by PET/CT: operation, exclusion of distant metastases.

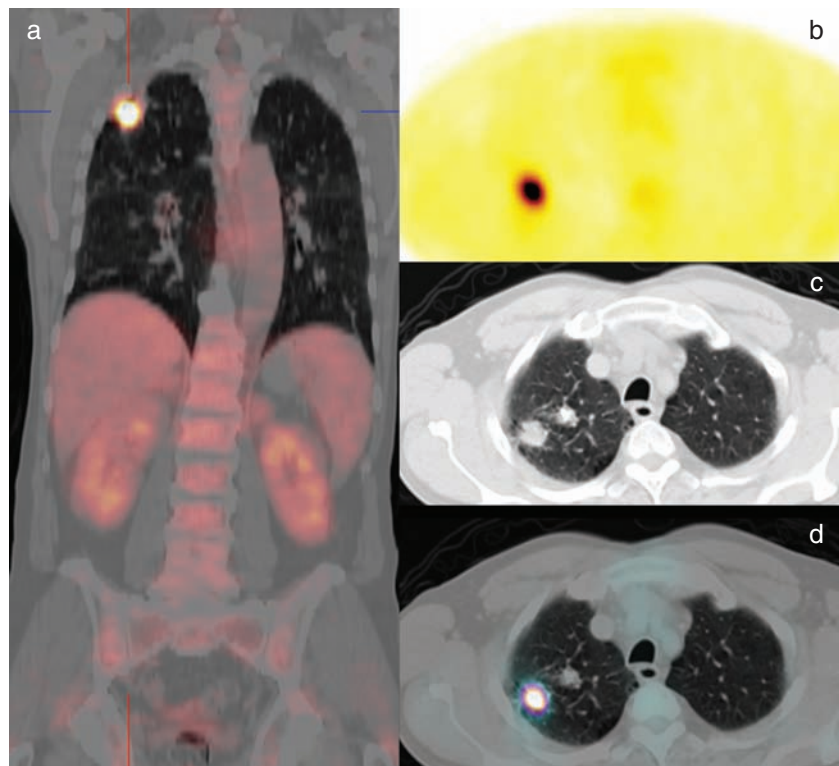


Table 5.12 Possible causes of false-positive findings in FDG-PET studies in the chest (modified from reference 88)

1. Physiologic uptake	
Muscle	Hypermetabolism after activation
Thymus	Normal until puberty
	Hyperplasia after chemotherapy
Bone marrow	Hyperplasia after chemotherapy
Brown fat	Non-shivering thermoregulation
2. Infection/inflammation	
Lung	
bacterial	Pneumonia, nocardiosis, abscess
mycobacterial	Active tuberculosis, atypical mycobacteriosis
fungal	Aspergillosis, coccidioides-mycosis, cryptococcosis, blastomycosis
granuloma	Granuloma, necrotizing granuloma, Wegener's granulomatosis, sarcoidosis, histoplasma granuloma, rheumatoid arthritis-associated lung disease, plasma cell granuloma
interstitial fibrosis	Fibrosing alveolitis, radiation pneumonitis
allergic	Airway inflammation with asthma
occupational	Inflammatory anthracosilicosis
non-specific	Acute inflammation with bronchiectasis and atelectasis, tumor necrosis, reactive mesothelial cell, histiocytic infiltrate, fibrous histiocytic infiltrate, aspiration pneumonia with barium, aspiration pneumonia with salivary and tracheal secretions, inflammatory pseudotumor, organizing pneumonia
Mediastinum	
esophagus	Esophagitis
lymph node	Chronic non-specific lymphadenitis; cryptococcal; tuberculosis; anthracosilicosis; active granuloma
Pleura	
	Empyema
	Pleural effusion
3. Non-malignant tumors	
Lung	
	Chondrohamartoma
Pleura	
	Fibrous mesothelioma
Bone	
	Enchondroma
Nerve root	
	Schwannoma
	Aggressive neurofibroma
4. Iatrogenic	
Trachea	
	Tracheostomy tube
Skin and soft tissue	
	Open lung biopsy
	Irradiation

FDG-PET

One of the major advantages of PET over other imaging modalities is the feasibility of performing a whole-body scan in a single examination, thereby allowing the detection of distant and lymph node metastases along with the primary tumor. Once a patient is diagnosed with distant metastases, palliative treatment is the only available therapy option, except for a single brain metastasis, which, in selected cases can be cured by complete surgical resection followed by cranial radiotherapy and thoracic surgery. At this stage it is essential to know the detection limit of PET in terms of the number of cells. Fischer et al.⁹⁸ have shown in their experimental model that the detection limit of PET is in the order of 10^5 – 10^6 malignant cells.

It has been documented in several studies^{38,59,99–108} that FDG-PET is superior to CT and other conventional imaging techniques in detecting distant metastases in patients with lung cancer. The average frequency of occult extrathoracic metastases in these studies was 13%; FDG-PET resulted in a change in treatment management in 18% of patients. A significant correlation was observed between the ISS stage and the frequency of metastases in clinical trial in patients with suspected stage 3 NSCLC prior to conformational radiotherapy. The frequency of metastases was found to increase with the increase in ISS stage of the disease: 7.5%, 18%, and 24% in stage 1, stage 2 and stage 3, respectively. van Tinteren et al.¹⁰⁹ enrolled 188 patients with NSCLC in a prospective, randomized, multicenter study to investigate the utility of preoperative FDG-PET in improving the outcome of surgery.

The patients were divided into two groups: one group (96 patients) was worked up with conventional imaging (mainly CT); in the other group (92 patients) FDG-PET was added to the conventional work-up. The authors observed that the addition of FDG-PET to conventional imaging resulted in a significant reduction in the frequency of futile surgery (defined as relapse or death within 1 year after surgery, or intraoperative proof of advanced disease), from 41% to 21%. This study proved that in NSCLC, the selection of patients for surgical resection can be improved significantly by the addition of FDG-PET. Some studies have shown the superiority of integrated PET-CT over CT or PET alone in the staging of lung cancer.^{110,111} In places where integrated PET-CT is not available, visually correlated PET-CT is a valuable alternative. In a recent study, FDG-PET and helical CT were found to be complementary to each other, with similar performances in the mediastinal staging of NSCLC.¹¹²

FDG-PET has been shown to have high sensitivity in the detection of adrenal metastases.¹¹³ An enlarged adrenal is

present in approximately 20% of patients at the time of the initial presentation.¹¹⁴ Pooled data from smaller and larger data series on whole-body FDG-PET yielded a sensitivity and specificity of 97% and 98%, respectively.^{59,105,114-116} The negative and positive predictive values were 98% and 94%, respectively. These data demonstrate that a negative PET scan rules out the malignant nature of a suspicious adrenal mass, thereby avoiding unnecessary surgical trauma.

In the detection of brain metastases, FDG-PET has no role,⁵¹ as the positive and negative predictive values are lower than with conventional imaging using MRI. For bone metastases, FDG-PET can be used, because it has higher specificity (98% vs. 61%) than skeletal scintigraphy.^{100,104}

Kramer et al. have shown that the tumor stage on FDG-PET is the most significant prognostic factor for survival in patients with NSCLC.¹¹⁷ A study of immense importance is the one conducted by Nguyen et al.,¹¹⁸ in which they have shown that FDG tumor uptake is more valuable than glucose transporter GLUT1 or Ki-67 protein

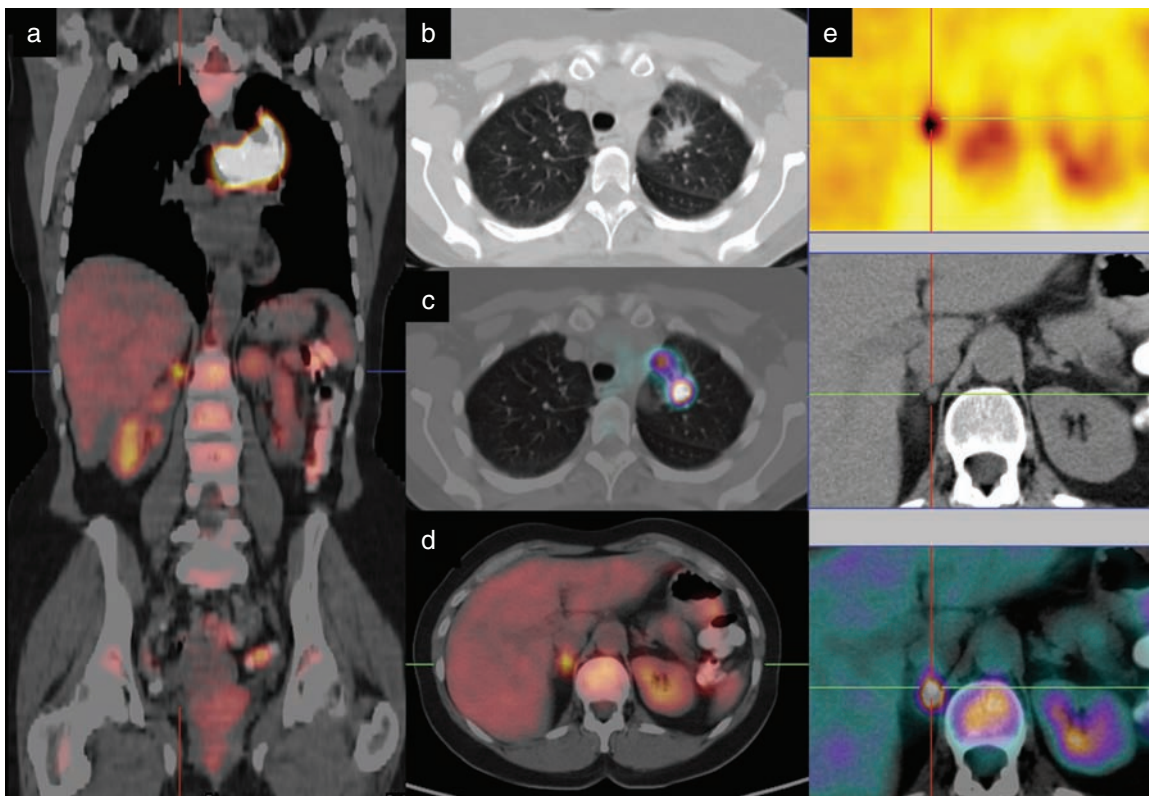


Figure 5.4

Staging of NSCLC. Clinical stage based on ceCT scan: cT4 N2 M0. Metabolic tumor stage (based on F-18 FDG PET/CT): mT4(SUV 35.9) N2 M1_{adrenal}. a: coronal PET/CT (large, left central primary tumor of the upper lobe with invasion of the mediastinum; CT (b) and transversal PET (c) slices, revealing an intrapulmonary metastasis in segment 1 (17 x17 mm in diameter). Transversal PET/CT slice at the level of the adrenals (d) showing focal FDG uptake on the right; e: small (5 x 5 mm) right adrenal metastasis as confirmed by follow up. PET scan (upper row), CT (middle) and fusion image (lower right). ICM by PET/CT: Upstaging of patient (M1 stage).

expression in terms of predicting prognosis in patients with resected NSCLC. The authors have shown that SUV_{max} is the only determinant of disease-free survival. In the analyses of 498 patients with lung cancer, including surgical and non-surgical cases, Davies et al. have also concluded that a higher tumor uptake of FDG is associated with worse survival.¹¹⁹ In stage 1 lung adenocarcinoma also, FDG uptake was found to be predictive of disease-free survival.¹²⁰

Lymph node staging

The prognosis of patients and therapeutic options available in NSCLC depend upon whether the mediastinal lymph nodes are involved or not. The presence of contralateral mediastinal lymph node metastases rules out surgical intervention; chemotherapy and/or radiotherapy then becomes the treatment option.⁵ Patients with ipsilateral lymph node metastasis are candidates for multimodality therapy, including preoperative chemoradiotherapy followed by surgical resection. Specifically, patients having so-called ‘minimal N2’ status have been found to have reasonable prognosis after complete resection and adjuvant radiotherapy. The 5-year survival rate is found to be 40% in this subgroup of patients as compared to 8% in ‘bulky N2’.¹⁵ These observations underline the importance of accurate mediastinal staging of NSCLC.

Conventional imaging

Lymph nodes greater than 1 cm in size are considered abnormal by CT criteria.^{121–123} However, 15% of patients with stage 1 disease have the probability of having micrometastases in lymph nodes which otherwise appear normal.¹²⁴ A prospective Radiological Diagnostic Oncologic Group Study has shown that CT and MRI have low sensitivity and specificity (approximately 50% and 65%, respectively) in the detection of mediastinal lymph node metastases.¹⁰¹ Some 30–40% of enlarged lymph nodes (2–4 cm in diameter) exhibit no tumor cells on histopathology.¹²⁵ CT has very high false-negative (7–39%) and false-positive (20–50%) values for the detection of mediastinal lymph nodes.¹⁶ The presence of fat in an enlarged lymph node suggests a benign lesion. The introduction of spiral CT has not been shown to significantly improve the accuracy of mediastinal lymph node staging, as is shown by meta-analyses on mediastinal staging using CT and FDG-PET.^{51,126}

Nuclear imaging

Several studies have investigated the role of FDG-PET in mediastinal lymph node staging.^{38,52,59,61,74,101,105,106,108,125–146} The results of three meta-analyses have also proved that FDG-PET is significantly more accurate than CT in the

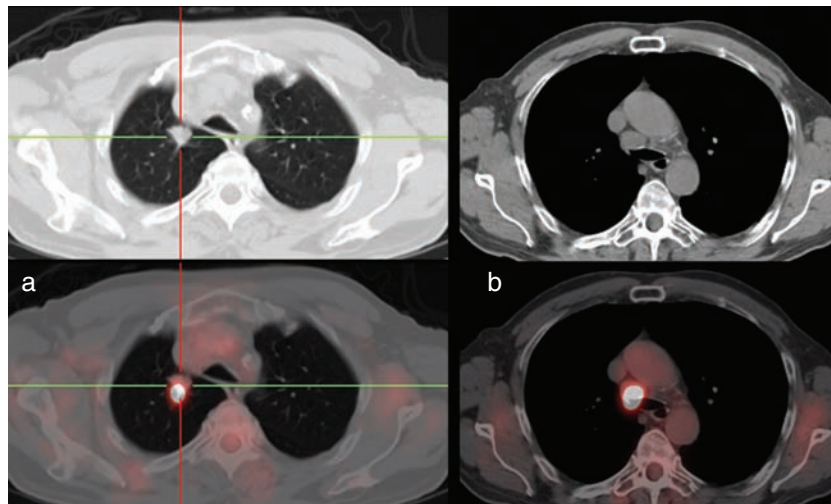


Figure 5.5

Staging of NSCLC. Bronchoscopy: centrally located squamous cell carcinoma with invasion of the bronchus. Clinical stage based on ceCT scan: cT2 (diameter 4,5 cm) N2 (enlarged paratracheal and para-aortic lymph nodes) M0. Metabolic tumor stage (based on F-18 FDG PET/CT): mT2(SUV 14.2) N0 M0. a: coronal PET/CT slice, b: transversal CT and PET/CT slice, c: zoomed CT and PET/CT slice. Intense FDG uptake in the primary tumor, which is invading the left main bronchus. No lymph node or distant metastases. Histopathological stage: pT1 pN0/30 Mx (squamous cell carcinoma G3, stage IB, R0 L0 V0 C4 after lobectomy and radical lymphadenectomy). ICM by PET/CT: operation (instead of neoadjuvant chemo-/radiation therapy), exclusion of mediastinal lymph node and distant metastases.

Table 5.13 Studies comparing computed tomography (CT) and [¹⁸F]FDG-PET for mediastinal lymph node staging (modified from reference 35)

Author	Year	No. of cases	CT		PET	
			Sensitivity (%)	Specificity (%)	Sensitivity	Specificity (%)
Valk	1995	76	63	54	83	94
Bury	1997	66	79	72	88	87
Vansteenkiste	1998	68	75	63	92	95
Marom	1999	79	64	78	97	87
Liewald	2000	80	NR	NR	92	76
Pieterman	2000	102	75	66	90	85
Roberts	2000	100	NR	NR	87	90
Poncelet	2001	61	56	68	66	84
Kernstine	2002	237	NR	NR	81	81
Vesselle	2002	118	NR	NR	80	96
von Haag	2002	52	50	65	66	91

NR, not reported.

staging of lymph nodes in non-small-cell lung cancer, irrespective of the instrumentation used for CT scan.^{51,147,148} Table 5.13 shows studies (including more than 35 patients) of mediastinal lymph node staging (N0/1 versus N2/3) in patients with NSCLC. Pooled data from these 11 studies in 1039 patients suggest that FDG-PET has an overall sensitivity of 87% and a specificity of 87%, as compared to a sensitivity and specificity of 69% and 65%, respectively, for CT scan (in seven studies with a total of 505 patients).

False-negative findings may occur in small-sized lymph nodes. Similarly, false-positive findings are also possible. In order to decrease the impact of false-positive findings on patient management, lymph nodes showing increased FDG uptake on PET (and hence inducing a change in management of the patient, e.g. altering planned surgery) should be histologically verified, for example by mediastinoscopy.³⁵

The ways and means to assess patients with stage 3A–N2 after induction therapy remains a matter of debate, specifically when it comes to deciding upon potential surgical treatment.¹⁰⁸ The performance of PET alone has not been as satisfactory in restaging as it was for the baseline lymph node staging. Studies have documented the superiority of PET–CT as compared to PET alone in lymph node staging.¹⁴⁹ By allowing accurate localization of focally increased FDG uptake, PET–CT facilitates the identification of FDG uptake by normal structures such as brown adipose tissue or skeletal muscles. Consequently, the number of false-positive findings is significantly reduced. PET–CT has also been found to be more

accurate than visual comparison of PET and CT images or software fusion of independently acquired PET and CT images.^{150–152} Some studies.^{153–155} have demonstrated the superiority of endobronchial ultrasound-guided trans-bronchial needle aspiration as being superior to CT or PET in mediastinum and hilar lymph node staging. In a recent meta-analysis, the dependency of FDG-PET on the size of the lymph node has been evaluated by de Langen et al.¹⁵⁶ In order to stratify patients for mediastinoscopy or thoracotomy, depending upon the test (PET and CT) results, it is essential to establish the relationship between size and likelihood of malignancy. In this meta-analysis, de Langen et al.¹⁵⁶ have shown that post-test probability for N2 disease is 5% for lymph nodes measuring 10–15 mm on CT in patients with a negative FDG-PET result, suggesting that these patients should be planned for thoracotomy, as the yield of mediastinoscopy will be extremely low. For patients with lymph nodes measuring ≥ 16 mm on CT and a negative FDG-PET result, a post-test probability for N2 disease is 21%, indicating that these patients should be planned for mediastinoscopy prior to possible thoracotomy, to prevent too many unnecessary thoracotomies in this subset.

Just as hand-held γ probes have helped in the lymph node staging of breast cancer patients, Nwogu et al.¹⁵⁷ have demonstrated that it is feasible to detect occult metastases in lymph nodes using an FDG sensitive intraoperative γ probe. More studies are needed to elucidate further the role of these γ probes in the lymph node staging of lung cancer patients.

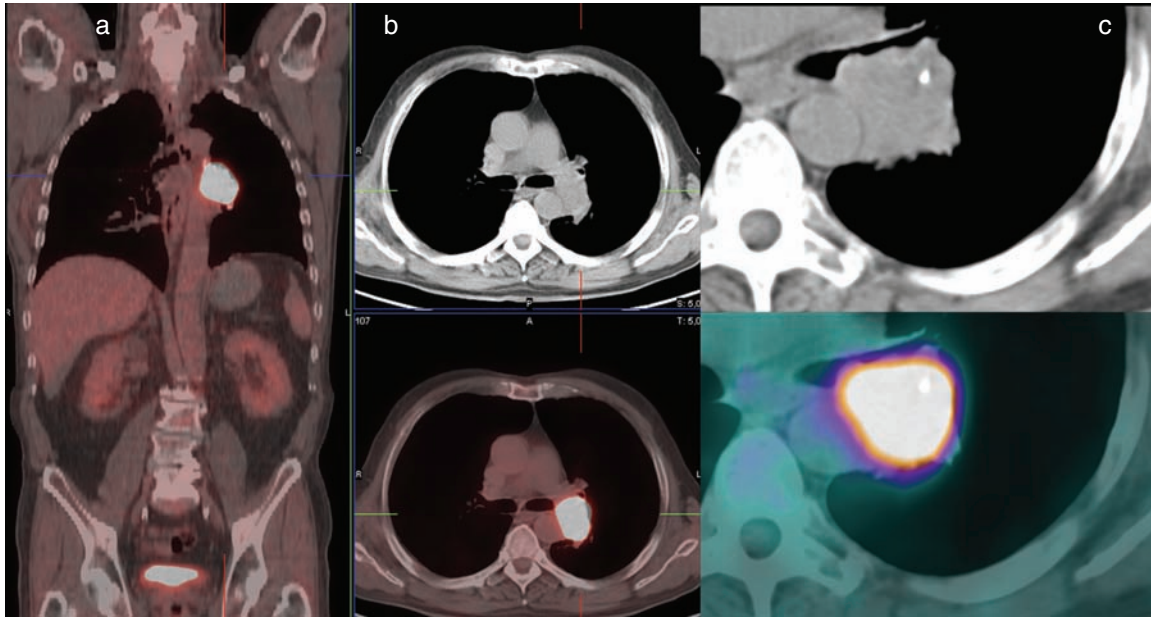


Figure 5.6

Staging of NSCLC. Clinical stage based on ceCT scan: cT1 N2 (enlarged mediastinal lymph nodes) M0. Metabolic tumor stage (based on F-18 FDG PET/CT): mT1(SUV 8.0) N2 M0. a: transversal CT and PET/CT slice (primary tumor in segment S 1, b: CT and PET/CT slice (mediastinal lymph node metastases, region 4R according to the ATS classification). Mediastinoscopy confirmed pN2 lymph node metastases. ICM by PET/CT: Neoadjuvant chemo-/radiation therapy, confirmation of mediastinal lymph node metastases.

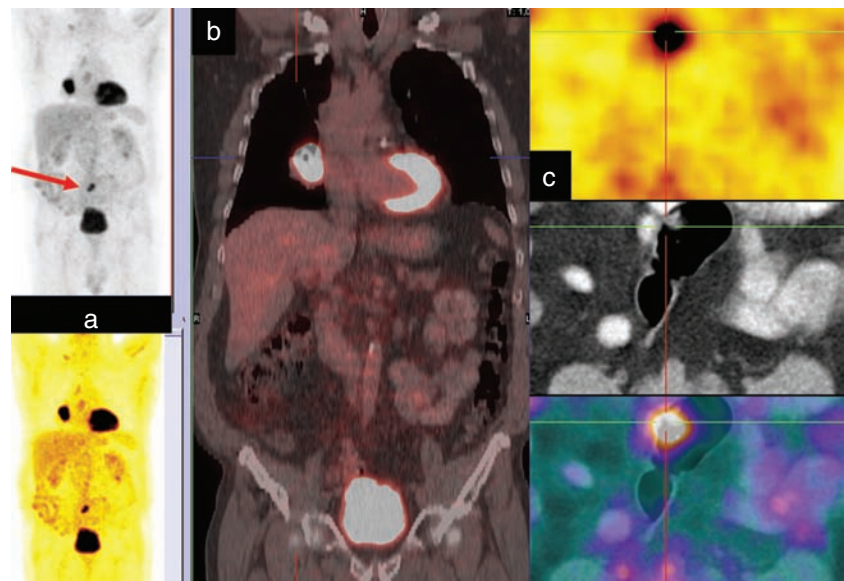
Detection of recurrence

Conventional imaging and FDG-PET play a complementary role in the detection of tumor recurrences, where PET is used to differentiate scar from viable tumor tissue based upon the increased glucose metabolism in tumor tissue as compared to non-viable fibrotic tissue.

FDG-PET detects local recurrences of lung cancer with an average sensitivity of 98% and a specificity of 87%.¹¹⁴ False-positive findings¹¹⁴ can occur, especially after external radiation therapy (so-called radiation pneumonitis). PET-CT has been shown to be of significant importance in detecting recurrent tumor/residual tissue.¹⁵⁸

Figure 5.7

Staging of NSCLC. Clinical stage based on ceCT scan: cT2 N2 (enlarged mediastinal lymph nodes) M0. Metabolic tumor stage (based on F-18 FDG PET/CT): mT2(SUV 15.9) N3 M0. a: Maximum intensity projection (MIP) images showing the primary lung tumor, lymph node metastases and a focus in the pelvis (red arrow); b: coronal PET/CT slice showing the primary tumor in right middle lobe centrally, extending to the right atrium; c: transversal PET, CT and PET/CT fusion slices at the level of focal FDG uptake in the pelvis. Colonoscopy confirmed a second primary tumor (adenocarcinoma pT1) in the recto-sigmoid colon.



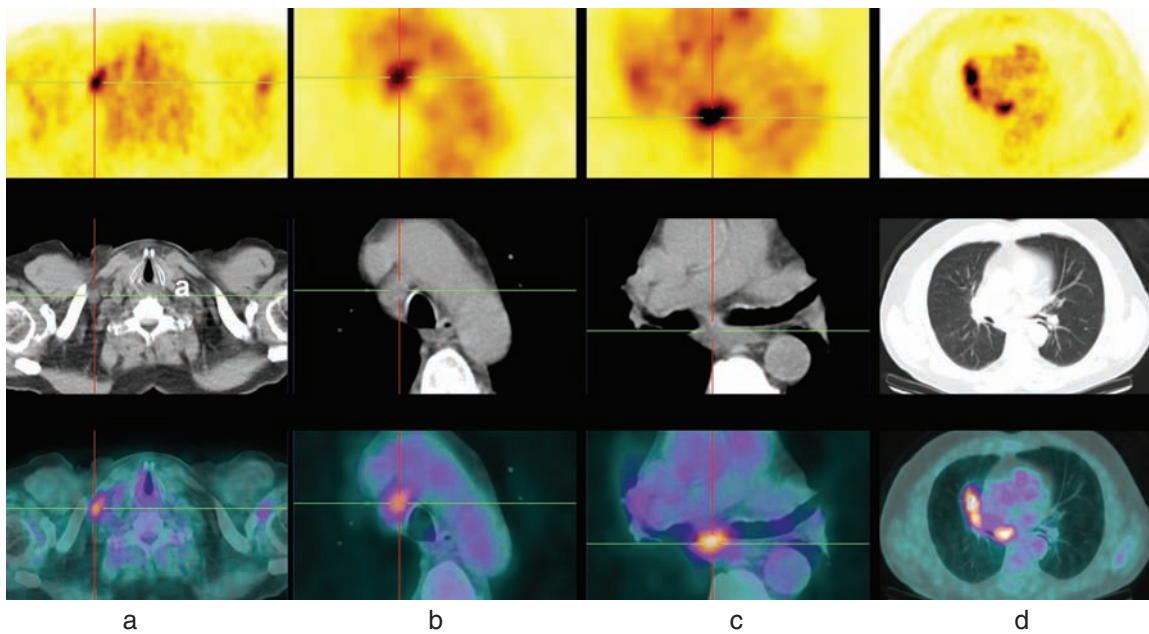
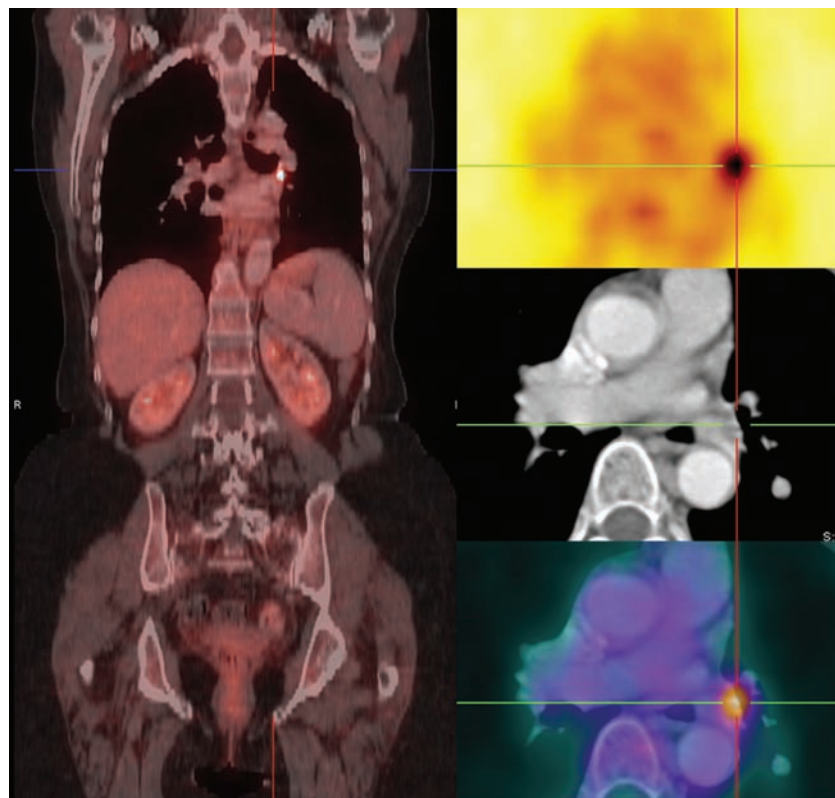


Figure 5.8

Staging of NSCLC. Same patient as shown in fig. Y. Hypermetabolic lymph node metastases in the retroclavicular region on the right (a), in the aorto-pulmonary window (b), at the level of tracheal bifurcation (c), and in the right central hilus (d). Mediastinoscopy confirmed pN3 lymph node metastases. ICM by PET/CT: Chemo-/radiation therapy, confirmation of mediastinal (N2) and detection of N3 lymph node metastases, therefore upstaging from stage 3A to stage 3B. Detection of an asymptomatic second primary tumor in the colon.

Figure 5.9

Restaging of NSCLC (adenosquamous cell carcinoma, primary stage pT2 (G3) N1 M0) after resection of the left upper lobe 3 years ago. F-18 FDG PET/CT (coronal and transversal PET/CT slices) show a 15 mm soft tissue dense nodular lesion in the left hilus region at the resection rim (local recurrence). No other hypermetabolic lesions are evident on the FDG-PET whereas CT shows additionally multiple, up to 20 mm large lesions in the parenchyma of the left lung. The patient was treated by left pneumonectomy. Histology confirmed local recurrence as well as multiple intrapulmonary metastases. Two years follow-up was unremarkable. ICM by PET/CT: confirmation of local recurrence. As a consequence, surgery was performed.



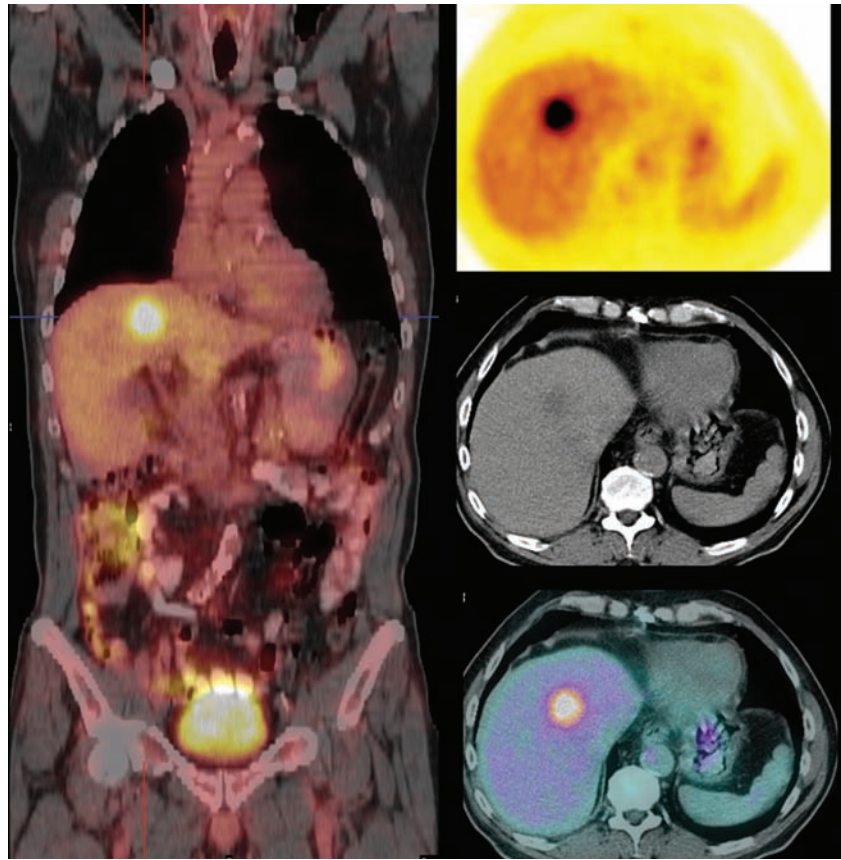


Figure 5.10

Restaging of NSCLC (squamous cell carcinoma, primary stage pT2 N1 M0) after chemotherapy. F-18 FDG PET/CT (coronal and transversal PET/CT slices) shows a solitary, hypodense liver metastasis in segment IVa (35 x 35 mm in diameter, SUV 7.2. Metabolic tumor volume 15.3 ml). No other metastases are present. ICM by PET/CT: Confirmation of a single liver metastasis. As a consequence, radiofrequency ablation (RFA) was performed.

Metabolic/molecular radiation therapy planning

In patients with lung cancer, radiotherapy is used with curative as well as with palliative intent. For effective radiation therapy, exact staging of the disease is essential in order to deliver the killing dose of radiation to all suspected metastatic sites with least toxicity to the surrounding normal tissues.¹⁵⁹ However, one has to keep in mind that the main cause of death after primary radiation therapy of lung cancer is local recurrence,¹¹⁴ thereby necessitating the need for having precise delineation of the extent of the tumor and its size. MRI and CT scans sometimes fail to differentiate malignant from normal tissues, particularly when atelectasis, pleural effusion, or normal tissue displacement occurs. During the calculation of gross tumor volume (GTV) and ultimately planning target volume (PTV), this may lead to wide intraobserver variation and radiation exposure to normal and benign tissues.^{160,161}

The concept of using radiopharmaceuticals such as [¹⁸F]FDG, directed towards detecting the metabolic activity of cancerous cells, for radiation therapy planning had its origin in 1993,^{35,159,162–167} and this was soon coined a special term by Baum as ‘metabolic or molecular

radiation treatment planning’ using HERMES software (now registered as a trademark by HERMES Medical as MRTPTM). Until the early 1990s, radiation dose based on two-dimensional (2D) radiotherapy plans was still much in vogue. It is now proven that 2D planning leads to a lower dose to the tumor and a higher dose to the surrounding normal tissue, e.g. spinal cord and lung.¹⁶⁸ In the early 1990s, three-dimensional (3D) radiotherapy plans were introduced. The calculation of unconventional field configurations was soon possible. Since in 3D conformational radiation therapy the isodoses can maximally follow the delineated target volume, it is possible to increase the dose without causing damage to normal tissue.^{106,169} The co-registration of planning CT and PET, with the patient in the same treatment position, is an exciting new tool for improving the planning target volume by treating the metabolically active tumor (‘biological target volume’ or BTV) and not – as is routine today – an anatomical or morphological target volume based only on the CT scan.¹⁷⁰ Several studies have shown the importance of incorporating PET in the radiotherapy planning of lung cancer,^{171–177} and different methods for the delineation of target volume on PET have already been described.¹⁷⁸

In the first prospective study of its kind, describing the use of PET in the 3D planning of radiation therapy in 27 patients with NSCLC, Schmucking et al.¹⁵⁹ concluded that: (1) PET is an important complementary tool to morphological imaging used for exact localization of nodal tumor involvement as well as for determining the extent of the primary tumor, (2) radiation therapy can be delivered with less toxicity in most patients, and (3) better tumor control may be possible by MRTP.

Recent research has focused on establishing the optimum thresholds for maximum standardized uptake value calculation. The result suggests that 15–20% may be the appropriate threshold value; however, Biehl et al.¹⁷⁹ have shown in their study that there is no single threshold delineating the PET(GTV) that is accurate for volume definition when compared with that provided by the CT(GTV) in the majority of NSCLC patients. There are several issues that have to be taken into consideration for defining the target volumes.^{180,181}

The role of PET in radiotherapy is also highlighted in a study by Cherk et al.¹⁸² The authors have shown (using FDG-PET and [¹⁸F]fluoromisonidazole-PET) that the hypoxic cell fraction of primary NSCLC is consistently low. Since the response to external beam radiotherapy is highly dependent on the oxygen concentration in the target tissue, this study has far-reaching consequences.

Prediction and monitoring response to therapy

[^{99m}Tc]methoxyisobutylisonitrile (MIBI) is one of the substrates for P-glycoprotein (Pgp), a product of the multidrug resistance gene MDR1, which is responsible for resistance to chemotherapy in patients with unresectable lung cancer.^{35,183} Studies have demonstrated the scintigraphic retention of [^{99m}Tc]MIBI as a model for the non-invasive assessment of Pgp expression.^{64,132,184–187} By measuring the [^{99m}Tc]MIBI uptake, Ceriani et al. reported a sensitivity and specificity of 83% and 84% for predicting the response to chemotherapy of lung cancer.¹⁸⁴ However, more studies will be needed supporting these observations before [^{99m}Tc] MIBI is incorporated into the management protocol of lung cancer patients.

Inductive chemotherapy or chemoradiation therapy followed by resection is one of the treatment options available for patients with locally advanced NSCLC, especially ISS stage 3A-2,⁵ where the success of downstaging is usually assessed by histological analysis of a surgical specimen of the primary tumor and/or mediastinal lymph nodes. Based upon the observation that metabolic changes precede morphologic alterations, metabolic imaging using PET radiopharmaceuticals has shown

encouraging results for monitoring response to therapy.^{159,188–191} Using morphological imaging, tumor response is usually assessed according to the World Health Organization (WHO) or the Response Evaluation Criteria in Solid Tumors (RECIST) criteria. In solid tumors, morphologic changes induced by therapy usually take several weeks to months, thereby subjecting non-responding patients to unnecessary side-effects of chemotherapy or radiotherapy. Apart from that, the relative inability of morphologic imaging to differentiate scar tissue from viable tumor with a high degree of specificity may lead to a masking of tumor regression.

In the therapy monitoring of patients with lung cancer, PET is used in three main areas: assessment of response to neoadjuvant chemotherapy,^{192,193} early assessment of response to therapy, and restaging after completion of therapy.¹⁹ The potential of FDG-PET in the evaluation of response to inductive chemotherapy in lung cancer patients has been assessed by Baum et al.¹⁹⁴ by showing a close correlation between histomorphometric studies and the results of PET imaging. In 26 patients treated with neoadjuvant chemotherapy, Ryu et al.¹⁹⁵ found a sensitivity and specificity of FDG-PET of 88% and 67%, respectively, for the diagnosis of tumor viability and a sensitivity and specificity of 58% and 97%, respectively, in nodal restaging. Akhurst et al.¹⁹⁶ reported a high negative predictive value of 98% for the detection of viable residual tumor tissue, but a low diagnostic accuracy (52%) for nodal tumor status. Pottgen et al.¹⁹⁷ in their study have come to the conclusion that corrected SUV_{max} from two serial PET–CT scans, before and after three chemotherapy cycles or later, allows the prediction of histopathologic response in the primary tumor and mediastinal lymph nodes and has prognostic value.

Su et al.¹⁹⁸ have shown that glucose metabolic activity as measured by FDG-PET reflects the response to gefitinib (endothelial growth factor receptor kinase inhibitor). Weber et al.¹⁹⁰ used FDG-PET for the early assessment of response to chemotherapy in 57 patients with NSCLC, 1 and 3 weeks after the first cycle of chemotherapy, and found a significant correlation between the metabolic activity and the final outcome after therapy. Whereas the early metabolic response predicted a better survival after the first three cycles of chemotherapy, a poor response was associated with disease progression, which opens the possibility of excluding non-responders from the treatment regimen and thereby reducing the morbidity and cost of treatment.

Since the inception of integrated PET–CT in clinical practice, studies have been conducted to determine the role of this new technology over that of stand-alone PET. PET–CT has been found to have the possibility to make a difference in monitoring the tumor response to therapy by integrating anatomic and functional measures of treatment effects. Perhaps even more important, PET–CT is

expected to increase the acceptance of PET as a tool for assessing the tumor response in medical research and clinical practice, since anatomic and functional measurements can be obtained in just one imaging session and jointly reported.^{151,199,200} Cerfolio et al.,²⁰¹ in their recent study, have shown that repeat integrated PET–CT is superior to repeat CT for the restaging of patients with stage 3a non-small-cell lung cancer after neoadjuvant chemoradiotherapy. The authors also conclude that the percentage decrease in SUV_{max} of the primary and of the involved lymph node is predictive of pathology; however, nodal biopsy is required, as a persistently high SUV_{max} does not equate to residual cancer.

Patz et al.²⁰² have shown that patients with a positive FDG-PET after completion of therapy have a worse prognosis than that of patients with a negative FDG-PET. Based upon FDG-PET for treatment monitoring, Hicks et al.²⁰³ demonstrated a change in patient management in 63% of patients, and that tumor response assessed by FDG-PET predicted better patient survival than did CT criteria, the pretreatment tumor stage, or patient performance status. The correlation between tumor FDG uptake after chemoradiotherapy and patient outcome was also confirmed in a recent study by Hellwig et al.²⁰⁴ in 47 patients after preoperative chemoradiotherapy. Patients were classified as responders if the SUV of the primary was less than 4. Median survival after resection was greater than 56 months for PET responders and 19 months for PET non-responders ($p < 0.001$). Schmucking et al.²⁰⁵ have demonstrated significant correlation between histologic results and the PET findings for tumor regression and survival in locally advanced non-small-cell lung cancer after neoadjuvant treatment.

Cost-effectiveness

One of the major concerns in the routine use of PET in clinical practice in oncology is the costs associated with FDG-PET studies. However, FDG-PET also has the potential to lead to cost savings by reducing the number of expensive invasive procedures. Several studies have demonstrated the cost-effectiveness of PET in the management of NSCLC patients. Cost of patient care and life expectancy were taken as criteria for the assessment of cost-effectiveness. In spite of differences in medicoeconomic data due to diversities in the healthcare structure, various studies from the United States, Europe, Japan, and Australia have come to the common conclusion that FDG-PET is cost-effective for the differentiation of lung nodules as well as for the preoperative staging of NSCLC.^{78,206–216} A study comparing confirmatory and selective mediastinoscopy in patients with positive FDG-PET has shown approximately double the cost savings per patient

(\$2267 vs. \$1154) at the expense of missing 1.7% of patients who might have been cured.²¹⁰

Pleural disease

FDG-PET has also been used for the assessment of pleural mass or pleural effusion for evidence of malignancy.²¹⁷ In a study conducted by Erasmus et al.²⁵ in 25 patients with suspected malignant pleural effusion, the sensitivity, specificity, and positive predictive value of FDG-PET were found to be 95%, 67%, and 95%, respectively. Such a high positive predictive value of FDG-PET for the detection of malignant pleural effusion will help in the appropriate staging of NSCLC. Schaffler et al.²¹⁸ have compared the utility of FDG-PET with that of CT in 92 patients for the ability to differentiate benign from malignant pleural effusion. FDG-PET was found to have a sensitivity, specificity, and positive predictive value of 100%, 71%, and 63%, respectively. The difference in the positive predictive value from the previous study by Erasmus et al. is attributed to the inclusion of a relatively large number of patients with benign pleural disease. This study also demonstrated that use of CT was indeterminate in 71% of the patients. Pleural dissemination of lung adenocarcinoma is best diagnosed using the CT component of FDG-PET–CT, since lesions causing pleural involvement without pleural effusion are beyond the resolution of PET.²¹⁹ Research is ongoing to determine the role of FDG-PET–CT in pleural mesothelioma, and initial results are promising.²²⁰

Staging of small-cell lung cancer

Small-cell lung cancer (SCLC) is a tumor of neuroendocrine origin with an aggressive growth pattern, often metastasizing early and proliferating rapidly.²²¹ There is a two-stage classification scheme²²² proposed by the Veterans Administration Lung Cancer Study Group: limited disease (limited to the thorax) or extensive disease (distant metastases, including those to the contralateral lung). The role of FDG-PET in the staging of SCLC is still controversial. According to Detterbeck et al.,²²³ the clinical presentation and radiographic appearance of the disease are sufficiently characteristic to negate the need for further evaluation. However, the few studies that have evaluated the role of FDG-PET as compared to conventional radiographic imaging have demonstrated that PET changed patient management in 8.3–29% of patients.^{34,224,225} Patients having extensive disease were treated with chemotherapy whereas those having limited disease received chemoradiotherapy. Kruger et al.²²⁶ have demonstrated low FDG uptake in patients with pulmonary carcinoids necessitating biopsy

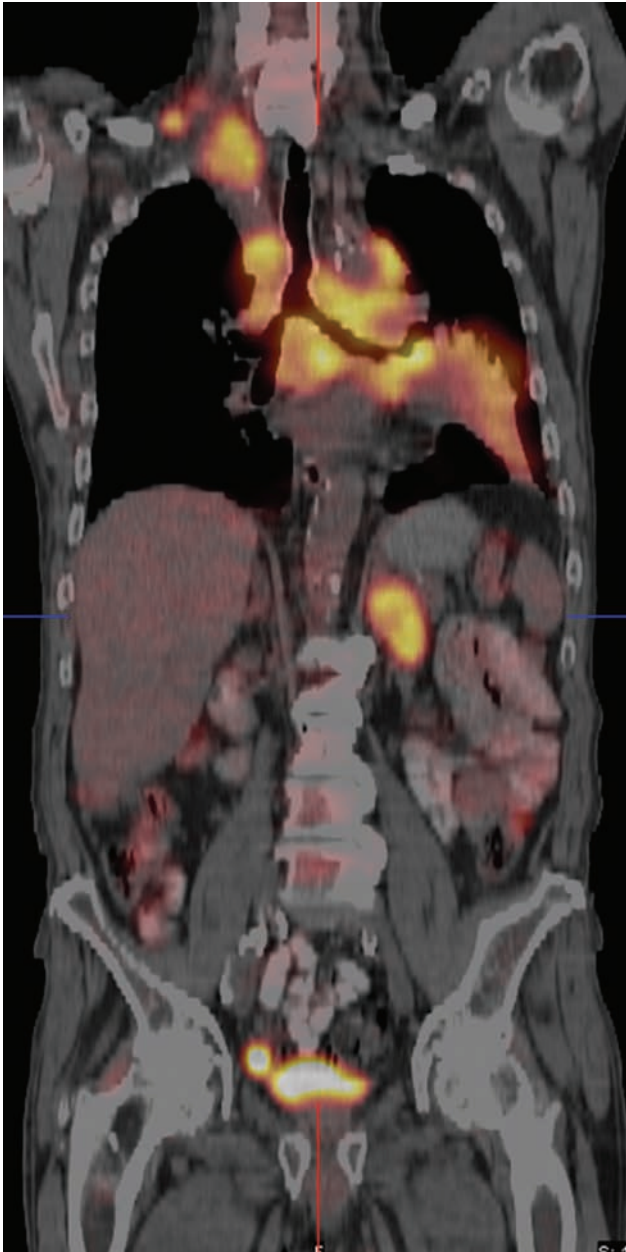


Figure 5.11

Staging of small-cell lung cancer (SCLC). Extensive disease. Hypermetabolic primary tumor (SUV_{max} 12.5) in the left central region (8 x 5 cm) with bilateral mediastinal (SUV_{max} 10.4) and right supra- and infraclavicular metastases measuring 5.5 x 5.8 cm (SUV_{max} 9.1). Atelectasis in the left lower lobe (poststenotic, inflammatory infiltrations, SUV_{max} 6.4). Additionally, CT scan revealed pericardial effusion. Large (4.8 x 2.7 cm), hypermetabolic (SUV_{max} 10.2) left adrenal metastasis with central necrosis.

and surgical resection, even if the FDG-PET study did not show hypermetabolic activity. Recent research into SCLC has shown some promising results for the use of integrated PET-CT in SCLC by simplifying and even improving the accuracy of the current staging protocol,²²⁷ as well as in response evaluation.^{228,229} Further prospective studies are needed to assess the exact role of FDG-PET in the restaging of patients with SCLC and in therapy monitoring.

References

1. Tyczynski JE, Bray F, Parkin DM. Lung cancer in Europe in 2000: epidemiology, prevention, and early detection. *Lancet Oncol* 2003; 4: 45–55.
2. ESMO Minimum Clinical Recommendations for diagnosis, treatment and follow-up of non-small-cell lung cancer (NSCLC). *Ann Oncol* 2001; 12: 1049–50.
3. ESMO Minimum Clinical Recommendations for diagnosis, treatment and follow-up of small-cell lung cancer (SCLC). *Ann Oncol* 2001; 12: 1051–2.
4. Bunyaviroch T, Coleman RE. PET evaluation of lung cancer. *J Nucl Med* 2006; 47: 451–69.
5. Spaepen K, Stroobants S, Dupont P et al. Early restaging positron emission tomography with (18)F-fluorodeoxyglucose predicts outcome in patients with aggressive non-Hodgkin's lymphoma. *Ann Oncol* 2002; 13: 1356–63.
6. Mack MJ, Hazelrigg SR, Landreneau RJ, Acuff TE. Thoracoscopy for the diagnosis of the indeterminate solitary pulmonary nodule. *Ann Thorac Surg* 1993; 56: 825–30; discussion 830–2.
7. The American Thoracic Society and The European Respiratory Society. Pretreatment evaluation of non-small-cell lung cancer. *Am J Respir Crit Care Med* 1997; 156: 320–32.
8. Clinical practice guidelines for the treatment of unresectable non-small-cell lung cancer. Adopted on May 16, 1997 by the American Society of Clinical Oncology. *J Clin Oncol* 1997; 15: 2996–3018.
9. Thomas M, Gatzemeier U, Goerg R et al. Empfehlungen zur Diagnostik des Bronchialkarzinoms. *Deutsche Gesellschaft für Pneumologie. Pneumologie* 2000; 54: 361–71.
10. BTS guidelines: guidelines on the selection of patients with lung cancer for surgery. *Thorax* 2001; 56: 89–108.
11. Mountain CF. Revisions in the International System for Staging Lung Cancer. *Chest* 1997; 111: 1710–17.
12. Mountain CF, Dresler CM. Regional lymph node classification for lung cancer staging. *Chest* 1997; 111: 1718–23.
13. Cerfolio RJ, Bryant AS, Eloubeidi MA. Routine mediastinoscopy and esophageal ultrasound fine-needle aspiration in patients with non-small cell lung cancer who are clinically N2 negative: a prospective study. *Chest* 2006; 130: 1791–5.
14. Cerfolio RJ, Ojha B, Bryant AS, et al. The role of FDG-PET scan in staging patients with nonsmall cell carcinoma. *Ann Thorac Surg* 2003; 76: 861–6.

15. Deslauriers J. Current surgical treatment of nonsmall cell lung cancer 2001. *Eur Respir J Suppl* 2002; 35: 61s–70s.
16. Lee JKT SS, Stanley RJ, Heiken JP. *Computed Body Tomography with MRI Correlation*, 3rd edn. Philadelphia: Lippincott Williams & Wilkins, 1998.
17. Hoffmann H, Dienemann H. *Der pulmonale Rundherd: Prinzipien der Diagnostik*. *Dtsch Arztebl* 2000; 97: A1065–71.
18. Jeong YJ, Yi CA, Lee KS. Solitary pulmonary nodules: detection, characterization, and guidance for further diagnostic workup and treatment. *AJR Am J Roentgenol* 2007; 188: 57–68.
19. Mavi A, Lakhani P, Zhuang H, Gupta NC, Alavi A. Fluorodeoxyglucose-PET in characterizing solitary pulmonary nodules, assessing pleural diseases, and the initial staging, restaging, therapy planning, and monitoring response of lung cancer. *Radiol Clin North Am* 2005; 43: 1–21, ix.
20. Gambhir SS, Shepherd JE, Shah BD et al. Analytical decision model for the cost-effective management of solitary pulmonary nodules. *J Clin Oncol* 1998; 16: 2113–25.
21. Proto AV, Thomas SR. Pulmonary nodules studied by computed tomography. *Radiology* 1985; 156: 149–53.
22. Swensen SJ, Brown LR, Colby TV, Weaver AL. Pulmonary nodules: CT evaluation of enhancement with iodinated contrast material. *Radiology* 1995; 194: 393–8.
23. Swensen SJ, Brown LR, Colby TV, Weaver AL, Midthun DE. Lung nodule enhancement at CT: prospective findings. *Radiology* 1996; 201: 447–55.
24. Henschke CI, Yankelevitz DF, Mirtcheva R et al. CT screening for lung cancer: frequency and significance of part-solid and nonsolid nodules. *AJR Am J Roentgenol* 2002; 178: 1053–7.
25. Erasmus JJ, McAdams HP, Rossi SE et al. FDG PET of pleural effusions in patients with non-small cell lung cancer. *AJR Am J Roentgenol* 2000; 175: 245–9.
26. Gould MK, Lillington GA. Strategy and cost in investigating solitary pulmonary nodules. *Thorax* 1998; 53 (Suppl 2): S32–7.
27. Yankelevitz DF, Henschke CI. Does 2-year stability imply that pulmonary nodules are benign? *AJR Am J Roentgenol* 1997; 168: 325–8.
28. Grills IS, Yan D, Black QC et al. Clinical implications of defining the gross tumor volume with combination of CT and (18)FDG-positron emission tomography in non-small-cell lung cancer. *Int J Radiat Oncol Biol Phys* 2006.
29. Gurney JW. Determining the likelihood of malignancy in solitary pulmonary nodules with Bayesian analysis. Part I. Theory. *Radiology* 1993; 186: 405–13.
30. Fischer BM, Mortensen J. The future in diagnosis and staging of lung cancer: positron emission tomography. *Respiration* 2006; 73: 267–76.
31. Christensen JA, Nathan MA, Mullan BP et al. Characterization of the solitary pulmonary nodule: 18F-FDG PET versus nodule-enhancement CT. *AJR Am J Roentgenol* 2006; 187: 1361–7.
32. Bernard A. Resection of pulmonary nodules using video-assisted thoracic surgery. The Thorax Group. *Ann Thorac Surg* 1996; 61: 202–4; discussion 204–5.
33. Halley A, Hugentobler A, Icard P et al. Efficiency of 18F-FDG and 99mTc-depreotide SPECT in the diagnosis of malignancy of solitary pulmonary nodules. *Eur J Nucl Med Mol Imaging* 2005; 32: 1026–32.
34. Blum J, Handmaker H, Lister-James J, Rinne N. A multicenter trial with a somatostatin analog (99m)Tc depreotide in the evaluation of solitary pulmonary nodules. *Chest* 2000; 117: 1232–8.
35. Baum RP, Hellwig D, Mezzetti M. Position of nuclear medicine modalities in the diagnostic workup of cancer patients: lung cancer. *Q J Nucl Med Mol Imaging* 2004; 48: 119–42.
36. Shon IH, O'Doherty M J, Maisey MN. Positron emission tomography in lung cancer. *Semin Nucl Med* 2002; 32: 240–71.
37. Lowe VJ, DeLong DM, Hoffman JM, Coleman RE. Optimum scanning protocol for FDG-PET evaluation of pulmonary malignancy. *J Nucl Med* 1995; 36: 883–7.
38. Pieterman RM, van Putten JW, Meuzelaar JJ, et al. Preoperative staging of non-small-cell lung cancer with positron-emission tomography. *N Engl J Med* 2000; 343: 254–61.
39. Nehmeh SA, Erdi YE, Ling CC, et al. Effect of respiratory gating on reducing lung motion artifacts in PET imaging of lung cancer. *Med Phys* 2002; 29: 366–71.
40. Nehmeh SA, Erdi YE, Pan T, et al. Four-dimensional (4D) PET/CT imaging of the thorax. *Med Phys* 2004; 31: 3179–86.
41. Allen-Auerbach M, Yeom K, Park J, Phelps M, Czernin J. Standard PET/CT of the chest during shallow breathing is inadequate for comprehensive staging of lung cancer. *J Nucl Med* 2006; 47: 298–301.
42. Juergens KU, Weckesser M, Stegger L, et al. Tumor staging using whole-body high-resolution 16-channel PET-CT: does additional low-dose chest CT in inspiration improve the detection of solitary pulmonary nodules? *Eur Radiol* 2006; 16: 1131–7.
43. Reinhardt MJ, Wiethoelter N, Matthies A, et al. PET recognition of pulmonary metastases on PET/CT imaging: impact of attenuation-corrected and non-attenuation-corrected PET images. *Eur J Nucl Med Mol Imaging* 2006; 33: 134–9.
44. Kuehl H, Veit P, Rosenbaum SJ, Bockisch A, Antoch G. Can PET/CT replace separate diagnostic CT for cancer imaging? Optimizing CT protocols for imaging cancers of the chest and abdomen. *J Nucl Med* 2007; 48 (Suppl 1): 45S–57S.
45. Mawlawi O, Erasmus JJ, Munden RF et al. Quantifying the effect of IV contrast media on integrated PET/CT: clinical evaluation. *AJR Am J Roentgenol* 2006; 186: 308–19.
46. Bryant AS, Cerfolio RJ. The maximum standardized uptake values on integrated FDG-PET/CT is useful in differentiating benign from malignant pulmonary nodules. *Ann Thorac Surg* 2006; 82: 1016–20.
47. Bryant AS, Cerfolio RJ, Klemm KM, Ojha B. Maximum standard uptake value of mediastinal lymph nodes on integrated FDG-PET-CT predicts pathology in patients with non-small cell lung cancer. *Ann Thorac Surg* 2006; 82: 417–22; discussion 422–3.
48. Hashimoto Y, Tsujikawa T, Kondo C et al. Accuracy of PET for diagnosis of solid pulmonary lesions with 18F-FDG uptake below the standardized uptake value of 2.5. *J Nucl Med* 2006; 47: 426–31.
49. Slomka PJ, Dey D, Przetak C, Aladl UE, Baum RP. Automated 3-dimensional registration of stand-alone (18)F-FDG whole-body PET with CT. *J Nucl Med* 2003; 44: 1156–67.

50. Gould MK, Maclean CC, Kuschner WG, Rydzak CE, Owens DK. Accuracy of positron emission tomography for diagnosis of pulmonary nodules and mass lesions: a meta-analysis. *JAMA* 2001; 285: 914–24.
51. Hellwig D, Ukena D, Paulsen F, Bamberg M, Kirsch CM. [Meta-analysis of the efficacy of positron emission tomography with F-18-fluorodeoxyglucose in lung tumors. Basis for discussion of the German Consensus Conference on PET in Oncology 2000]. *Pneumologie* 2001; 55: 367–77. [in German]
52. Albes JM, Lietzenmayer R, Schott U et al. Improvement of non-small-cell lung cancer staging by means of positron emission tomography. *Thorac Cardiovasc Surg* 1999; 47: 42–7.
53. Bury T, Dowlati A, Paulus P et al. Evaluation of the solitary pulmonary nodule by positron emission tomography imaging. *Eur Respir J* 1996; 9: 410–14.
54. Croft DR, Trapp J, Kernstine K et al. FDG-PET imaging and the diagnosis of non-small cell lung cancer in a region of high histoplasmosis prevalence. *Lung Cancer* 2002; 36: 297–301.
55. Dewan NA, Gupta NC, Redepenning LS, Phalen JJ, Frick MP. Diagnostic efficacy of PET-FDG imaging in solitary pulmonary nodules. Potential role in evaluation and management. *Chest* 1993; 104: 997–1002.
56. Dewan NA, Shehan CJ, Reeb SD et al. Likelihood of malignancy in a solitary pulmonary nodule: comparison of Bayesian analysis and results of FDG-PET scan. *Chest* 1997; 112: 416–22.
57. Duhaylongsod FG, Lowe VJ, Patz EF Jr et al. Detection of primary and recurrent lung cancer by means of F-18 fluorodeoxyglucose positron emission tomography (FDG PET). *J Thorac Cardiovasc Surg* 1995; 110: 130–9; discussion 139–40.
58. Duhaylongsod FG, Lowe VJ, Patz EF Jr et al. Lung tumor growth correlates with glucose metabolism measured by fluoride-18 fluorodeoxyglucose positron emission tomography. *Ann Thorac Surg* 1995; 60: 1348–52.
59. Gupta NC, Graeber GM, Rogers JS 2nd, Bishop HA. Comparative efficacy of positron emission tomography with FDG and computed tomographic scanning in preoperative staging of non-small cell lung cancer. *Ann Surg* 1999; 229: 286–91.
60. Gupta NC, Maloof J, Gunel E. Probability of malignancy in solitary pulmonary nodules using fluorine-18-FDG and PET. *J Nucl Med* 1996; 137: 943–8.
61. Hagberg RC, Segall GM, Stark P, Burdon TA, Pompili MF. Characterization of pulmonary nodules and mediastinal staging of bronchogenic carcinoma with F-18 fluorodeoxyglucose positron emission tomography. *Eur J Cardiothorac Surg* 1997; 12: 92–7.
62. Hain SF, Curran KM, Beggs AD et al. FDG-PET as a 'metabolic biopsy' tool in thoracic lesions with indeterminate biopsy. *Eur J Nucl Med* 2001; 28: 1336–40.
63. Halter G, Storck M, Guhlmann A et al. FDG positron emission tomography in the diagnosis of peripheral pulmonary focal lesions. *Thorac Cardiovasc Surg* 2000; 48: 97–101.
64. Hung GU, Shiau YC, Tsai SC et al. Value of 18F-fluoro-2-deoxyglucose positron emission tomography in the evaluation of recurrent colorectal cancer. *Anticancer Res* 2001; 21: 1375–8.
65. Imdahl A, Reinhardt MJ, Nitzsche EU et al. Impact of 18F-FDG-positron emission tomography for decision making in colorectal cancer recurrences. *Langenbecks Arch Surg* 2000; 385: 129–34.
66. Knight SB, Delbeke D, Stewart JR, Sandler MP. Evaluation of pulmonary lesions with FDG-PET. Comparison of findings in patients with and without a history of prior malignancy. *Chest* 1996; 109: 982–8.
67. Lee J, Aronchick JM, Alavi A. Accuracy of F-18 fluorodeoxyglucose positron emission tomography for the evaluation of malignancy in patients presenting with new lung abnormalities: a retrospective review. *Chest* 2001; 120: 1791–7.
68. Lowe VJ, Duhaylongsod FG, Patz EF et al. Pulmonary abnormalities and PET data analysis: a retrospective study. *Radiology* 1997; 202: 435–9.
69. Lowe VJ, Fletcher JW, Gobar L et al. Prospective investigation of positron emission tomography in lung nodules. *J Clin Oncol* 1998; 16: 1075–84.
70. Lowe VJ, Hoffman JM, DeLong DM, Patz EF, Coleman RE. Semiquantitative and visual analysis of FDG-PET images in pulmonary abnormalities. *J Nucl Med* 1994; 35: 1771–6.
71. Menda Y, Bushnell DL, Madsen MT et al. Evaluation of various corrections to the standardized uptake value for diagnosis of pulmonary malignancy. *Nucl Med Commun* 2001; 22: 1077–81.
72. Pitman AG, Hicks RJ, Binns DS et al. Performance of sodium iodide based (18)F-fluorodeoxyglucose positron emission tomography in the characterization of indeterminate pulmonary nodules or masses. *Br J Radiol* 2002; 75: 114–21.
73. Prauer HW, Weber WA, Romer W et al. Controlled prospective study of positron emission tomography using the glucose analogue [18f]fluorodeoxyglucose in the evaluation of pulmonary nodules. *Br J Surg* 1998; 85: 1506–11.
74. Sazon DA, Santiago SM, Soo Hoo GW et al. Fluorodeoxyglucose-positron emission tomography in the detection and staging of lung cancer. *Am J Respir Crit Care Med* 1996; 153: 417–21.
75. Scott WJ, Schwabe JL, Gupta NC et al. Positron emission tomography of lung tumors and mediastinal lymph nodes using [18F]fluorodeoxyglucose. The Members of the PET-Lung Tumor Study Group. *Ann Thorac Surg* 1994; 58: 698–703.
76. Coates G, Skehan SJ. Emerging role of PET in the diagnosis and staging of lung cancer. *Can Respir J* 1999; 6: 145–52.
77. Gugiatti A, Grimaldi A, Rossetti C et al. Economic analyses on the use of positron emission tomography for the work-up of solitary pulmonary nodules and for staging patients with non-small-cell-lung-cancer in Italy. *Q J Nucl Med Mol Imaging* 2004; 48: 49–61.
78. Lejeune C, Al Zahouri K, Woronoff-Lemsi MC et al. Use of a decision analysis model to assess the medicoeconomic implications of FDG PET imaging in diagnosing a solitary pulmonary nodule. *Eur J Health Econ* 2005; 6: 203–14.
79. Nomori H, Watanabe K, Ohtsuka T et al. Evaluation of F-18 fluorodeoxyglucose (FDG) PET scanning for pulmonary nodules less than 3 cm in diameter, with special reference to the CT images. *Lung Cancer* 2004; 45: 19–27.
80. Chhajed PN, Bernasconi M, Gambazzi F et al. Combining bronchoscopy and positron emission tomography for the

- diagnosis of the small pulmonary nodule ≤ 3 cm. *Chest* 2005; 128: 3558–64.
81. Bastarrika G, Garcia-Velloso MJ, Lozano MD et al. Early lung cancer detection using spiral computed tomography and positron emission tomography. *Am J Respir Crit Care Med* 2005; 171: 1378–83.
 82. Coleman RE, Laymon CM, Turkington TG. FDG imaging of lung nodules: a phantom study comparing SPECT, camera-based PET, and dedicated PET. *Radiology* 1999; 210: 823–8.
 83. Hubner KF, Buonocore E, Gould HR et al. Differentiating benign from malignant lung lesions using 'quantitative' parameters of FDG PET images. *Clin Nucl Med* 1996; 21: 941–9.
 84. Cerfolio R, Bryant A, Ohja B. The maximum standardised uptake values on positron emission tomography of non-small cell lung cancer predict stage, recurrence and survival. *J Thorac Cardiovasc Surg* 2005; 130: 151–9.
 85. Yi CA, Lee KS, Kim BT et al. Tissue characterization of solitary pulmonary nodule: comparative study between helical dynamic CT and integrated PET/CT. *J Nucl Med* 2006; 47: 443–50.
 86. Low SY, Eng P, Keng GH, Ng DC. Positron emission tomography with CT in the evaluation of non-small cell lung cancer in populations with a high prevalence of tuberculosis. *Respirology* 2006; 11: 84–9.
 87. Mackie GC, Pohlen JM. Mediastinal histoplasmosis: F-18 FDG PET and CT findings simulating malignant disease. *Clin Nucl Med* 2005; 30: 633–5.
 88. Bakheet SM, Saleem M, Powe J et al. F-18 fluorodeoxyglucose chest uptake in lung inflammation and infection. *Clin Nucl Med* 2000; 25: 273–8.
 89. Matthies A, Hickeson M, Cuchiara A, Alavi A. Dual time point 18F-FDG PET for the evaluation of pulmonary nodules. *J Nucl Med* 2002; 43: 871–5.
 90. Zhuang H, Pourdehnad M, Lambright ES et al. Dual time point 18F-FDG PET imaging for differentiating malignant from inflammatory processes. *J Nucl Med* 2001; 42: 1412–17.
 91. Gupta P, Ponzo F, Kramer EL. Fluorodeoxyglucose (FDG) uptake in pulmonary rheumatoid nodules. *Clin Rheumatol* 2005; 24: 402–5.
 92. Sider L, Horejs D. Frequency of extrathoracic metastases from bronchogenic carcinoma in patients with normal-sized hilar and mediastinal lymph nodes on CT. *AJR Am J Roentgenol* 1988; 151: 893–5.
 93. Oliva JP, Pimentel G, Borron M, et al. [Pilot study with the monoclonal antibody IOR-C5 as a potential agent of radioimmunoscintigraphy in colorectal cancer]. *Rev Esp Med Nucl* 2001; 20: 282–8. [in Spanish]
 94. Sandler MA, Pearlberg J, Madrazo B, Gitschlag K, Gross S. Computed tomography evaluation of the adrenal gland in the preoperative assessment of bronchogenic carcinoma. *Radiology* 1982; 145: 733–6.
 95. Remer EM, Obuchowski N, Ellis JD et al. Adrenal mass evaluation in patients with lung carcinoma: a cost-effectiveness analysis. *AJR Am J Roentgenol* 2000; 174: 1033–9.
 96. Van den Wall H. *The Evaluation of Malignancy: Metastatic Bone Disease*. Edinburgh: Churchill Livingstone; 1998.
 97. Schillaci O. Single-photon emission computed tomography/computed tomography in lung cancer and malignant lymphoma. *Semin Nucl Med* 2006; 36: 275–85.
 98. Fischer BM, Olsen MW, Ley CD et al. How few cancer cells can be detected by positron emission tomography? A frequent question addressed by an in vitro study. *Eur J Nucl Med Mol Imaging* 2006; 33: 697–702.
 99. Boland GW, Goldberg MA, Lee MJ et al. Indeterminate adrenal mass in patients with cancer: evaluation at PET with 2-[F-18]-fluoro-2-deoxy-D-glucose. *Radiology* 1995; 194: 131–4.
 100. Bury T, Barreto A, Daenen F et al. Fluorine-18 deoxyglucose positron emission tomography for the detection of bone metastases in patients with non-small cell lung cancer. *Eur J Nucl Med* 1998; 25: 1244–7.
 101. Bury T, Dowlati A, Paulus P et al. Whole-body 18FDG positron emission tomography in the staging of non-small cell lung cancer. *Eur Respir J* 1997; 10: 2529–34.
 102. Collins BT, Lowe VJ, Dunphy FR. Initial evaluation of pulmonary abnormalities: CT-guided fine-needle aspiration biopsy and fluoride-18 fluorodeoxyglucose positron emission tomography correlation. *Diagn Cytopathol* 2000; 22: 92–6.
 103. Erasmus JJ, Patz EF Jr, McAdams HP et al. Evaluation of adrenal masses in patients with bronchogenic carcinoma using 18F-fluorodeoxyglucose positron emission tomography. *AJR Am J Roentgenol* 1997; 168: 1357–60.
 104. Kao CH, Hsieh JF, Tsai SC, Ho YJ, Yen RF. Comparison and discrepancy of 18F-2-deoxyglucose positron emission tomography and Tc-99m MDP bone scan to detect bone metastases. *Anticancer Res* 2000; 20(3B): 2189–92.
 105. Poncelet AJ, Lonnew M, Coche E, Weynand B, Noirhomme P. PET-FDG scan enhances but does not replace preoperative surgical staging in non-small cell lung carcinoma. *Eur J Cardiothorac Surg* 2001; 20: 468–74; discussion 474–5.
 106. Vanuytsel LJ, Vansteenkiste JF, Stroobants SG et al. The impact of (18)F-fluoro-2-deoxy-D-glucose positron emission tomography (FDG-PET) lymph node staging on the radiation treatment volumes in patients with non-small cell lung cancer. *Radiother Oncol* 2000; 55: 317–24.
 107. Schmid RA, Hillinger S, Bruchhaus H et al. [Detection of unexpected extrathoracic metastases in preoperative staging of non-small-cell bronchial carcinoma (NSCLC) with positron emission tomography (PET)]. *Langenbecks Arch Chir Suppl Kongressbd* 1998; 115: 1264–7. [in German]
 108. Vansteenkiste J, Doooms C. Positron emission tomography in nonsmall cell lung cancer. *Curr Opin Oncol* 2007; 19: 78–83.
 109. van Tinteren H, Hoekstra OS, Smit EF et al. Effectiveness of positron emission tomography in the preoperative assessment of patients with suspected non-small-cell lung cancer: the PLUS multicentre randomised trial. *Lancet* 2002; 359: 1388–93.
 110. De Wever W, Ceyssens S, Mortelmans L et al. Additional value of PET-CT in the staging of lung cancer: comparison with CT alone, PET alone and visual correlation of PET and CT. *Eur Radiol* 2007; 17: 23–32.
 111. Shim SS, Lee KS, Kim BT et al. Non-small cell lung cancer: prospective comparison of integrated FDG PET/CT and CT alone for preoperative staging. *Radiology* 2005; 236: 1011–19.
 112. Pozo-Rodriguez F, Martin de Nicolas JL, Sanchez-Nistal MA et al. Accuracy of helical computed tomography and

- [18F] fluorodeoxyglucose positron emission tomography for identifying lymph node mediastinal metastases in potentially resectable non-small-cell lung cancer. *J Clin Oncol* 2005; 23: 8348–56.
113. Kumar R, Xiu Y, Yu JQ et al. 18F-FDG PET in evaluation of adrenal lesions in patients with lung cancer. *J Nucl Med* 2004; 45: 2058–62.
 114. Nestle U, Hellwig D, Schmidt S et al. 2-Deoxy-2-[18F]fluoro-D-glucose positron emission tomography in target volume definition for radiotherapy of patients with non-small-cell lung cancer. *Mol Imaging Biol* 2002; 4: 257–63.
 115. Eschmann SM, Friedel G, Paulsen F et al. FDG PET for staging of advanced non-small cell lung cancer prior to neoadjuvant radio-chemotherapy. *Eur J Nucl Med Mol Imaging* 2002; 29: 804–8.
 116. MacManus MP, Hicks RJ, Ball DL et al. F-18 fluorodeoxyglucose positron emission tomography staging in radical radiotherapy candidates with nonsmall cell lung carcinoma: powerful correlation with survival and high impact on treatment. *Cancer* 2001; 92: 886–95.
 117. Kramer H, Post WJ, Pruim J, Groen HJ. The prognostic value of positron emission tomography in non-small cell lung cancer: analysis of 266 cases. *Lung Cancer* 2006; 52: 213–17.
 118. Nguyen XC, Lee WW, Chung JH et al. FDG uptake, glucose transporter type 1, and Ki-67 expressions in non-small-cell lung cancer: correlations and prognostic values. *Eur J Radiol* 2007 Jan 17. [Epub ahead of print]
 119. Davies A, Tan C, Paschalides C et al. FDG-PET maximum standardised uptake value is associated with variation in survival: Analysis of 498 lung cancer patients. *Lung Cancer* 2007; 55: 75–8.
 120. Ohtsuka T, Nomori H, Watanabe K et al. Prognostic significance of [(18)F]fluorodeoxyglucose uptake on positron emission tomography in patients with pathologic stage I lung adenocarcinoma. *Cancer* 2006; 107: 2468–73.
 121. Libshitz HI, McKenna RJ Jr. Mediastinal lymph node size in lung cancer. *AJR Am J Roentgenol* 1984; 143: 715–18.
 122. Verschakelen JA, Bogaert J, De Wever W. Computed tomography in staging for lung cancer. *Eur Respir J Suppl* 2002; 35: 40s–8s.
 123. Glazer GM, Gross BH, Quint LE et al. Normal mediastinal lymph nodes: number and size according to American Thoracic Society mapping. *AJR Am J Roentgenol* 1985; 144: 261–5.
 124. Shields TW. The significance of ipsilateral mediastinal lymph node metastasis (N2 disease) in non-small cell carcinoma of the lung. A commentary. *J Thorac Cardiovasc Surg* 1990; 99: 48–53.
 125. Berlangieri SU, Scott AM, Knight SR et al. F-18 fluorodeoxyglucose positron emission tomography in the non-invasive staging of non-small cell lung cancer. *Eur J Cardiothorac Surg* 1999; 16 (Suppl 1): S25–30.
 126. Chin R Jr, Ward R, Keyes JW et al. Mediastinal staging of non-small-cell lung cancer with positron emission tomography. *Am J Respir Crit Care Med* 1995; 152: 2090–6.
 127. Diederich S, Das M. Solitary pulmonary nodule: detection and management. *Cancer Imaging* 2006;6: S42–6.
 128. Farrell MA, McAdams HP, Herndon JE, Patz EF Jr. Non-small cell lung cancer: FDG PET for nodal staging in patients with stage I disease. *Radiology* 2000; 215: 886–90.
 129. Guhlmann A, Storck M, Kotzerke J et al. Lymph node staging in non-small cell lung cancer: evaluation by [18F]FDG positron emission tomography (PET). *Thorax* 1997; 52: 438–41.
 130. Gupta NC, Graeber GM, Bishop HA. Comparative efficacy of positron emission tomography with fluorodeoxyglucose in evaluation of small (<1 cm), intermediate (1 to 3 cm), and large (>3 cm) lymph node lesions. *Chest* 2000; 117: 773–8.
 131. Gupta NC, Tamim WJ, Graeber GG, Bishop HA, Hobbs GR. Mediastinal lymph node sampling following positron emission tomography with fluorodeoxyglucose imaging in lung cancer staging. *Chest* 2001; 120: 521–7.
 132. Higashi K, Nishikawa T, Seki H et al. Comparison of fluorine-18-FDG PET and thallium-201 SPECT in evaluation of lung cancer. *J Nucl Med* 1998; 39: 9–15.
 133. Kernstine KH, McLaughlin KA, Menda Y et al. Can FDG-PET reduce the need for mediastinoscopy in potentially resectable nonsmall cell lung cancer? *Ann Thorac Surg* 2002; 73: 394–401; discussion 401–2.
 134. Kernstine KH, Stanford W, Mullan BF et al. PET, CT, and MRI with Combidex for mediastinal staging in non-small cell lung carcinoma. *Ann Thorac Surg* 1999; 68: 1022–8.
 135. Liewald F, Grosse S, Storck M et al. How useful is positron emission tomography for lymphnode staging in non-small-cell lung cancer? *Thorac Cardiovasc Surg* 2000; 48: 93–6.
 136. Magnani P, Carretta A, Rizzo G et al. FDG/PET and spiral CT image fusion for mediastinal lymph node assessment of non-small cell lung cancer patients. *J Cardiovasc Surg (Torino)* 1999; 40: 741–8.
 137. Marom EM, McAdams HP, Erasmus JJ et al. Staging non-small cell lung cancer with whole-body PET. *Radiology* 1999; 212: 803–9.
 138. Patz EF Jr, Lowe VJ, Goodman PC, Herndon J. Thoracic nodal staging with PET imaging with 18FDG in patients with bronchogenic carcinoma. *Chest* 1995; 108: 1617–21.
 139. Roberts PF, Follette DM, von Haag D et al. Factors associated with false-positive staging of lung cancer by positron emission tomography. *Ann Thorac Surg* 2000; 70: 1154–9; discussion 1159–60.
 140. Scott WJ, Gobar LS, Terry JD, Dewan NA, Sunderland JJ. Mediastinal lymph node staging of non-small-cell lung cancer: a prospective comparison of computed tomography and positron emission tomography. *J Thorac Cardiovasc Surg* 1996; 111: 642–8.
 141. Steinert HC, Hauser M, Allemann F et al. Non-small cell lung cancer: nodal staging with FDG PET versus CT with correlative lymph node mapping and sampling. *Radiology* 1997; 202: 441–6.
 142. Tatsumi M, Yutani K, Watanabe Y et al. Feasibility of fluorodeoxyglucose dual-head gamma camera coincidence imaging in the evaluation of lung cancer: comparison with FDG PET. *J Nucl Med* 1999; 40: 566–73.
 143. Valk PE, Pounds TR, Hopkins DM et al. Staging non-small cell lung cancer by whole-body positron emission

- tomographic imaging. *Ann Thorac Surg* 1995; 60: 1573–81; discussion 1581–2.
144. Vansteenkiste JF, Stroobants SG, De Leyn PR et al. Lymph node staging in non-small-cell lung cancer with FDG-PET scan: a prospective study on 690 lymph node stations from 68 patients. *J Clin Oncol* 1998; 16: 2142–9.
 145. Eubank WB, Mankoff DA, Vesselle HJ et al. Detection of locoregional and distant recurrences in breast cancer patients by using FDG PET. *Radiographics* 2002; 22: 5–17.
 146. von Haag DW, Follette DM, Roberts PF et al. Advantages of positron emission tomography over computed tomography in mediastinal staging of non-small cell lung cancer. *J Surg Res* 2002; 103: 160–4.
 147. Dwamena BA, Sonnad SS, Angobaldo JO, Wahl RL. Metastases from non-small cell lung cancer: mediastinal staging in the 1990s—meta-analytic comparison of PET and CT. *Radiology* 1999; 213: 530–6.
 148. Weber WA, Dietlein M, Hellwig D et al. [PET with (18)F-fluorodeoxyglucose for staging of non-small cell lung cancer]. *Nuklearmedizin* 2003; 42: 135–44. [in German]
 149. Bruzzi JF, Munden RF. PET/CT imaging of lung cancer. *J Thorac Imaging* 2006; 21: 123–36.
 150. Kayani I, Groves AM, Ell PJ, George PJ, Bomanji J. Imaging bronchial carcinoma in situ: possible roles for combined positron emission tomography (PET)-CT. *Lancet Oncol* 2005; 6: 190.
 151. Halpern BS, Schiepers C, Weber WA et al. Presurgical staging of non-small cell lung cancer: positron emission tomography, integrated positron emission tomography/CT, and software image fusion. *Chest* 2005; 128: 2289–97.
 152. Lardinois D, Weder W, Hany TF et al. Staging of non-small-cell lung cancer with integrated positron-emission tomography and computed tomography. *N Engl J Med* 2003; 348: 2500–7.
 153. Eloubeidi MA, Cerfolio RJ, Chen VK et al. Endoscopic ultrasound-guided fine needle aspiration of mediastinal lymph node in patients with suspected lung cancer after positron emission tomography and computed tomography scans. *Ann Thorac Surg* 2005; 79: 263–8.
 154. Yasufuku K, Nakajima T, Motoori K et al. Comparison of endobronchial ultrasound, positron emission tomography, and CT for lymph node staging of lung cancer. *Chest* 2006; 130: 710–18.
 155. Takamochi K, Yoshida J, Murakami K et al. Pitfalls in lymph node staging with positron emission tomography in non-small cell lung cancer patients. *Lung Cancer* 2005; 47: 235–42.
 156. de Langen AJ, Raijmakers P, Riphagen I, Paul MA, Hoekstra OS. The size of mediastinal lymph nodes and its relation with metastatic involvement: a meta-analysis. *Eur J Cardiothorac Surg* 2006; 29: 26–9.
 157. Nwogu C, Fischer G, Tan D et al. Radioguided detection of lymph node metastasis in non-small cell lung cancer. *Ann Thorac Surg* 2006; 82: 1815–20; discussion 1820.
 158. Gilman MD, Aquino SL. State-of-the-art FDG-PET imaging of lung cancer. *Semin Roentgenol* 2005; 40: 143–53.
 159. Schmucking M, Baum RP, Griesinger F et al. Molecular whole-body cancer staging using positron emission tomography: consequences for therapeutic management and metabolic radiation treatment planning. *Recent Results Cancer Res* 2003; 162: 195–202.
 160. Bosmans G, van Baardwijk A, Dekker A, et al. Intra-patient variability of tumor volume and tumor motion during conventionally fractionated radiotherapy for locally advanced non-small-cell lung cancer: a prospective clinical study. *Int J Radiat Oncol Biol Phys* 2006; 66: 748–53.
 161. Mah K, Caldwell CB, Ung YC, et al. The impact of (18)FDG-PET on target and critical organs in CT-based treatment planning of patients with poorly defined non-small-cell lung carcinoma: a prospective study. *Int J Radiat Oncol Biol Phys* 2002; 52: 339–50.
 162. Baum RP, Adams S, Kiefer J et al. A novel technetium-99m labeled monoclonal antibody (174H.64) for staging head and neck cancer by immuno-SPECT. *Acta Oncol* 1993; 32: 747–51.
 163. Baum RP. Nuclear immunology: at the crossroads of immunology and nuclear medicine. *Jpn J Nucl Med* 1993; 30: 836.
 164. Baum RP, Schmucking M, Przetak C et al. NET-based data transfer and automatic image fusion of metabolic (PET) and morphologic (CT/MRI) images for metabolic radiation treatment planning of brain tumors. *Eur J Nucl Med* 2003; 30: S182.
 165. Rahn AN, Baum RP, Adamietz IA et al. [Value of 18F fluorodeoxyglucose positron emission tomography in radiotherapy planning of head-neck tumors]. *Strahlenther Onkol* 1998; 174: 358–64. [in German]
 166. Adamietz IA, Schemmann F, Baum RP et al. [Value of SPECT-immunoscintigraphy in radiation treatment planning for patients with squamous cell carcinomas in the head and neck area]. *Strahlenther Onkol* 1995; 171: 278–83. [in German]
 167. Hamm KD, Surber G, Schmucking M et al. Stereotactic radiation treatment planning and follow-up studies involving fused multimodality imaging. *J Neurosurg* 2004; 101 (Suppl 3): 326–33.
 168. Wilson EM, Joy Williams F, Lyn BE, Aird EG. Comparison of two dimensional and three dimensional radiotherapy treatment planning in locally advanced non-small cell lung cancer treated with continuous hyperfractionated accelerated radiotherapy weekend less. *Radiother Oncol* 2005; 74: 307–14.
 169. Rosenman J, Chaney EL, Sailer S et al. Recent advances in radiotherapy treatment planning. *Cancer Invest* 1991; 9: 465–81.
 170. Touboul E, Deniaud-Alexandre E, Moureau-Zabotto L, Lerouge D. [The impact of integrating images of positron emission tomography with computed tomography simulation on radiation therapy planning]. *Cancer Radiother* 2004; 8 [Suppl 1]: S29–35. [in French]
 171. Lavrenkov K, Partridge M, Cook G, Brada M. Positron emission tomography for target volume definition in the treatment of non-small cell lung cancer. *Radiother Oncol* 2005; 77: 1–4.
 172. Messa C, Ceresoli GL, Rizzo G et al. Feasibility of [18F]FDG-PET and coregistered CT on clinical target volume definition of advanced non-small cell lung cancer. *Q J Nucl Med Mol Imaging* 2005; 49: 259–66.
 173. De Ruyscher D, Wanders S, Mincken A et al. Effects of radiotherapy planning with a dedicated combined PET-CT-simulator of patients with non-small cell lung cancer

- on dose limiting normal tissues and radiation dose-escalation: a planning study. *Radiother Oncol* 2005; 77: 5–10.
174. De Ruyscher D, Wanders S, van Haren E et al. Selective mediastinal node irradiation based on FDG-PET scan data in patients with non-small-cell lung cancer: a prospective clinical study. *Int J Radiat Oncol Biol Phys* 2005; 62: 988–94.
 175. Grosu AL, Piert M, Weber WA et al. Positron emission tomography for radiation treatment planning. *Strahlenther Onkol* 2005; 181: 483–99.
 176. Brianzoni E, Rossi G, Ancidei S et al. Radiotherapy planning: PET/CT scanner performances in the definition of gross tumour volume and clinical target volume. *Eur J Nucl Med Mol Imaging* 2005; 32: 1392–9.
 177. Senan S, De Ruyscher D. Critical review of PET-CT for radiotherapy planning in lung cancer. *Crit Rev Oncol Hematol* 2005; 56: 345–51.
 178. Nestle U, Kremp S, Schaefer-Schuler A et al. Comparison of different methods for delineation of 18F-FDG PET-positive tissue for target volume definition in radiotherapy of patients with non-small cell lung cancer. *J Nucl Med* 2005; 46: 1342–8.
 179. Biehl KJ, Kong F-M, Dehdashti F et al. 18F-FDG PET definition of gross tumor volume for radiotherapy of non-small cell lung cancer: is a single standardized uptake value threshold approach appropriate? *J Nucl Med* 2006; 47: 1808–12.
 180. Nestle U, Kremp S, Grosu AL. Practical integration of [(18F)-FDG-PET and PET-CT in the planning of radiotherapy for non-small cell lung cancer (NSCLC): the technical basis, ICRU-target volumes, problems, perspectives. *Radiother Oncol* 2006; 81: 209–25.
 181. Nestle U, Schaefer-Schuler A, Kremp S et al. Target volume definition for (18)F-FDG PET-positive lymph nodes in radiotherapy of patients with non-small cell lung cancer. *Eur J Nucl Med Mol Imaging* 2007; 34: 453–62.
 182. Cherk MH, Foo SS, Poon AM et al. Lack of correlation of hypoxic cell fraction and angiogenesis with glucose metabolic rate in non-small cell lung cancer assessed by 18F-fluoromisonidazole and 18F-FDG PET. *J Nucl Med* 2006; 47: 1921–6.
 183. Oka M, Fukuda M, Sakamoto A et al. The clinical role of MDR1 gene expression in human lung cancer. *Anticancer Res* 1997; 17(1B): 721–4.
 184. Ceriani L, Giovannella L, Bandera M et al. Semi-quantitative assessment of ⁹⁹Tcm-sestamibi uptake in lung cancer: relationship with clinical response to chemotherapy. *Nucl Med Commun* 1997; 18: 1087–97.
 185. Dirlik A, Burak Z, Goksel T et al. The role of Tc-99m sestamibi imaging in predicting clinical response to chemotherapy in lung cancer. *Ann Nucl Med* 2002; 16: 103–8.
 186. Hsu WH, Yen RF, Kao CH et al. Predicting chemotherapy response to paclitaxel-based therapy in advanced non-small-cell lung cancer (stage IIIb or IV) with a higher T stage (> T2). Technetium-99m methoxyisobutylisonitrile chest single photon emission computed tomography and P-glycoprotein expression. *Oncology* 2002; 63: 173–9.
 187. Yuksel M, Cermik TF, Karlikaya C et al. Monitoring the chemotherapeutic response in primary lung cancer using ^{99m}Tc-MIBI SPET. *Eur J Nucl Med* 2001; 28: 799–806.
 188. Baum RP, Przetak C. Evaluation of therapy response in breast and ovarian cancer patients by positron emission tomography (PET). *Q J Nucl Med* 2001; 45: 257–68.
 189. Vansteenkiste JF. Imaging in lung cancer: positron emission tomography scan. *Eur Respir J Suppl* 2002; 35: 49s–60s.
 190. Weber WA, Petersen V, Schmidt B et al. Positron emission tomography in non-small-cell lung cancer: prediction of response to chemotherapy by quantitative assessment of glucose use. *J Clin Oncol* 2003; 21: 2651–7.
 191. Weber W, Young C, Abdel-Dayem HM et al. Assessment of pulmonary lesions with 18F-fluorodeoxyglucose positron imaging using coincidence mode gamma cameras. *J Nucl Med* 1999; 40: 574–8.
 192. Cerfolio RJ, Bryant AS, Winokur TS, Ohja B, Bartolucci AA. Repeat FDG-PET after neoadjuvant therapy is a predictor of pathologic response in patients with non-small cell lung cancer. *Ann Thorac Surg* 2004; 78: 1903–9; discussion 1909.
 193. Eschmann SM, Friedel G, Paulsen F et al. Repeat (18)F-FDG PET for monitoring neoadjuvant chemotherapy in patients with stage III non-small cell lung cancer. *Lung Cancer* 2007; 55: 165–71.
 194. Baum RP, Griesinger F, Niesen A. Correlation of FDG-PET measurements with morphometric tumor response after induction chemotherapy and adjuvant radiotherapy in stage III non-small cell lung cancer (NSCLC). Presented at 25th International Symposium Radioactive Isotopes in Clinical Medicine and Research, Bad Gastein, Austria, 2002.
 195. Ryu JS, Choi NC, Fischman AJ, Lynch TJ, Mathisen DJ. FDG-PET in staging and restaging non-small cell lung cancer after neoadjuvant chemoradiotherapy: correlation with histopathology. *Lung Cancer* 2002; 35: 179–87.
 196. Akhurst T, Downey RJ, Ginsberg MS et al. An initial experience with FDG-PET in the imaging of residual disease after induction therapy for lung cancer. *Ann Thorac Surg* 2002; 73: 259–64; discussion 264–6.
 197. Pottgen C, Levegrun S, Theegarten D et al. Value of 18F-fluoro-2-deoxy-D-glucose-positron emission tomography/computed tomography in non-small-cell lung cancer for prediction of pathologic response and times to relapse after neoadjuvant chemoradiotherapy. *Clin Cancer Res* 2006; 12: 97–106.
 198. Su H, Bodenstein C, Dumont RA, et al. Monitoring tumor glucose utilization by positron emission tomography for the prediction of treatment response to epidermal growth factor receptor kinase inhibitors. *Clin Cancer Res* 2006; 12: 5659–67.
 199. Weber WA, Figlin R. Monitoring cancer treatment with PET/CT: does it make a difference? *J Nucl Med* 2007; 48 (Suppl 1): 36S–44S.
 200. Hoekstra CJ, Stroobants SG, Smit EF et al. Prognostic relevance of response evaluation using [18F]-2-fluoro-2-deoxy-D-glucose positron emission tomography in patients with locally advanced non-small-cell lung cancer. *J Clin Oncol* 2005; 23: 8362–70.
 201. Cerfolio RJ, Bryant AS, Ojha B. Restaging patients with N2 (stage IIIa) non-small cell lung cancer after neoadjuvant

- chemoradiotherapy: a prospective study. *J Thorac Cardiovasc Surg* 2006; 131: 1229–35.
202. Patz EF Jr, Connolly J, Herndon J. Prognostic value of thoracic FDG PET imaging after treatment for non-small cell lung cancer. *AJR Am J Roentgenol* 2000; 174: 769–74.
203. Hicks RJ, Kalff V, MacManus MP et al. The utility of (18)F-FDG PET for suspected recurrent non-small cell lung cancer after potentially curative therapy: impact on management and prognostic stratification. *J Nucl Med* 2001; 42: 1605–13.
204. Hellwig D, Graeter TP, Ukena D et al. Value of F-18-fluorodeoxyglucose positron emission tomography after induction therapy of locally advanced bronchogenic carcinoma. *J Thorac Cardiovasc Surg* 2004; 128: 892–9.
205. Schmucking M, Baum RP, Bonnet R, Junker K, Muller KM. [Correlation of histologic results with PET findings for tumor regression and survival in locally advanced non-small cell lung cancer after neoadjuvant treatment]. *Pathologie* 2005; 26: 178–89. [in German]
206. Alzahouri K, Lejeune C, Woronoff-Lemsi MC, Arveux P, Guillemain F. Cost-effectiveness analysis of strategies introducing FDG-PET into the mediastinal staging of non-small-cell lung cancer from the French healthcare system perspective. *Clin Radiol* 2005; 60: 479–92.
207. Nguyen VH, Peloquin S, Lacasse Y. Cost-effectiveness of positron emission tomography for the management of potentially operable non-small cell lung cancer in Quebec. *Can Respir J* 2005; 12: 19–25.
208. Dietlein M, Moka D, Weber K, Theissen P, Schicha H. [Cost-effectiveness of PET in the management algorithms of lung tumors: comparison of health economic data]. *Nuklearmedizin* 2001; 40: 122–8. [in German]
209. Dietlein M, Weber K, Gandjour A et al. Cost-effectiveness of FDG-PET for the management of potentially operable non-small cell lung cancer: priority for a PET-based strategy after nodal-negative CT results. *Eur J Nucl Med* 2000; 27: 1598–609.
210. Gambhir SS, Hoh CK, Phelps ME, Madar I, Maddahi J. Decision tree sensitivity analysis for cost-effectiveness of FDG-PET in the staging and management of non-small-cell lung carcinoma. *J Nucl Med* 1996; 37: 1428–36.
211. Valkema R, De Jong M, Bakker WH et al. Phase I study of peptide receptor radionuclide therapy with [In-DTPA] octreotide: the Rotterdam experience. *Semin Nucl Med* 2002; 32: 110–22.
212. Kosuda S, Ichihara K, Watanabe M, Kobayashi H, Kusano S. Decision-tree sensitivity analysis for cost-effectiveness of chest 2-fluoro-2-D-[(18)F]fluorodeoxyglucose positron emission tomography in patients with pulmonary nodules (non-small cell lung carcinoma) in Japan. *Chest* 2000; 117: 346–53.
213. Kosuda S, Ichihara K, Watanabe M, Kobayashi H, Kusano S. Decision-tree sensitivity analysis for cost-effectiveness of whole-body FDG PET in the management of patients with non-small-cell lung carcinoma in Japan. *Ann Nucl Med* 2002; 16: 263–71.
214. Miles KA, Griffiths MR, Fuentes MA. Standardized perfusion value: universal CT contrast enhancement scale that correlates with FDG PET in lung nodules. *Radiology* 2001; 220: 548–53.
215. Scott WJ, Shepherd J, Gambhir SS. Cost-effectiveness of FDG-PET for staging non-small cell lung cancer: a decision analysis. *Ann Thorac Surg* 1998; 66: 1876–83; discussion 1883–5.
216. Valk PE, Pounds TR, Tesar RD, Hopkins DM, Haseman MK. Cost-effectiveness of PET imaging in clinical oncology. *Nucl Med Biol* 1996; 23: 737–43.
217. Talbot JN, Kerrou K, Grahek D et al. [PET in primary pulmonary or pleural cancer]. *Presse Med* 2006; 35: 1387–400. [in French]
218. Schaffler GJ, Wolf G, Schoellnast H et al. Non-small cell lung cancer: evaluation of pleural abnormalities on CT scans with 18F FDG PET. *Radiology* 2004; 231: 858–65.
219. Shim SS, Lee KS, Kim BT et al. Integrated PET/CT and the dry pleural dissemination of peripheral adenocarcinoma of the lung: diagnostic implications. *J Comput Assist Tomogr* 2006; 30: 70–6.
220. Truong MT, Marom EM, Erasmus JJ. Preoperative evaluation of patients with malignant pleural mesothelioma: role of integrated CT-PET imaging. *J Thorac Imaging* 2006; 21: 146–53.
221. Elias A. Small cell lung cancer: state of the art therapy in 1996. *Chest* 1997; 112 (Suppl): 251S–8S.
222. Abrams J, Doyle LA, Aisner J. Staging, prognostic factors, and special considerations in small cell lung cancer. *Semin Oncol* 1988; 15: 261–77.
223. Detterbeck FC, Falen S, Rivera MP, Halle JS, Socinski MA. Seeking a home for a PET, part 2: Defining the appropriate place for positron emission tomography imaging in the staging of patients with suspected lung cancer. *Chest* 2004; 125: 2300–8.
224. Bradley JD, Dehdashti F, Mintun MA et al. Positron emission tomography in limited-stage small-cell lung cancer: a prospective study. *J Clin Oncol* 2004; 22: 3248–54.
225. Kamel EM, Zwahlen D, Wyss MT et al. Whole-body (18)F-FDG PET improves the management of patients with small cell lung cancer. *J Nucl Med* 2003; 44: 1911–17.
226. Kruger S, Buck AK, Blumstein NM et al. Use of integrated FDG PET/CT imaging in pulmonary carcinoid tumours. *J Intern Med* 2006; 260: 545–50.
227. Fischer BM, Mortensen J, Langer SW et al. A prospective study of PET/CT in initial staging of small-cell lung cancer: comparison with CT, bone scintigraphy and bone marrow analysis. *Ann Oncol* 2007; 18: 338–45.
228. Fischer BM, Mortensen J, Langer SW et al. PET/CT imaging in response evaluation of patients with small cell lung cancer. *Lung Cancer* 2006; 54: 41–9.
229. Brink I, Schumacher T, Mix M et al. Impact of [18F]FDG-PET on the primary staging of small-cell lung cancer. *Eur J Nucl Med Mol Imaging* 2004; 31: 1614–20.

Esophageal cancer

Cristina Nanni, Sara Taddayon, Guido Biasco, Stefano Fanti, and Arturo Chiti

Background

Esophageal cancer is a malignant disease characterized by a poor prognosis, which accounts for about 4% of all digestive tract cancers. In developed countries the incidence is 4–5 per 100 000 people, with a significant higher incidence in China, in the Caspian region of Iran, and in South Africa. Males are affected two to four times more often than females, and black men present the highest incidence in squamous cell carcinoma. The overall 5-year survival rate in patients amenable to definitive treatment ranges from 5% to 30%, although patients diagnosed with early disease may have a better chance of survival.

Several risk factors are associated with the development of esophageal cancer. These factors are responsible for inflammation of the mucosa first, which may evolve into metaplasia, dysplasia, and eventually cancer. The strongest association with esophageal cancer has been found with tobacco use, dietary habits (very hot food), alcohol consumption, obesity, Barrett's esophagus, chronic gastro-esophageal reflux disease, Plummer–Vinson syndrome, caustic injury, chronic achalasia, and tylosis.

Two major pathologic types account for more than 98% of all esophageal cancers: squamous cell carcinoma, frequently arising in the upper two-thirds of the organ, and adenocarcinoma, commonly located in the distal esophagus. The other 2% of esophageal malignant lesions include lymphomas, leiomyosarcoma, and neuroendocrine tumors. Worldwide, squamous cell carcinoma is more prevalent than adenocarcinoma.

In many patients, the tumor is metastatic before the initial diagnosis. The distal esophagus is most often involved, and the overall prognosis is generally poor. Surgery is the only curative option, although characterized by a high 5% mortality risk and a low 20% overall 5-year survival rate. Radiation therapy is commonly associated with surgery to improve overall survival. Neoadjuvant chemoradiotherapy, used as a multimodality approach with surgery, may reduce local recurrence and improve survival.

The TNM system is used to determine the patient's staging, commonly based on the American Joint Committee

on Cancer (AJCC) system. The T stage relates to local invasion of esophageal structures by the tumor, not to its size. The N stage is based on the presence of metastatic regional lymph nodes and is simply divided into N0 and N1. The presence of any metastases determines stage M1, which differs depending on the third of the organ which harbors the primary site. Tables 6.1 and 6.2 illustrate the TNM and AJCC systems.¹ Prognosis is strongly dependent on stage, and while early stages are treated by limited surgical or endoscopic procedures, multimodality strategies are required for advanced tumor stages. In patients with systemic metastases the therapy is palliative, with the aim of relieving dysphagia.

Diagnostic modalities

Accurate staging is essential for an effective therapeutic approach to both limited and advanced disease.² Diagnostic modalities must be chosen in order to assess the potential resectability of the primary tumor with its locoregional lymphatic drainage, and the presence of systemic tumor spread.

This assessment relies on endoscopic ultrasound (EUS), computed tomography (CT) scan, and positron emission tomography (PET) using [¹⁸F]fluoro-2-deoxy-D-glucose (FDG).

Endoscopic ultrasound

EUS is established as the diagnostic modality of choice for evaluating local tumor growth and depth of invasion. Since it is widely employed, the advantages and limitations of EUS are well defined. A recent paper suggested that the accuracy of EUS is dependent on the size and location of the tumor³ and that it is better in small tumors (< 5 cm) than in large tumors (> 5 cm). These data are most probably related to a bias in patient selection, namely the exclusion

Table 6.1 TNM definitions in esophageal cancer*Primary tumor (T)*

TX: Primary tumor cannot be assessed

T0: No evidence of primary tumor

Tis: Carcinoma in situ

T1: Tumor invades lamina propria or submucosa

T2: Tumor invades muscularis propria

T3: Tumor invades adventitia

T4: Tumor invades adjacent structures

Regional lymph nodes (N)

NX: Regional lymph nodes cannot be assessed

N0: No regional lymph node metastasis

N1: Regional lymph node metastasis

Distant metastasis (M)

MX: Distant metastasis cannot be assessed

M0: No distant metastasis

M1: Distant metastasis

Tumors of the lower thoracic esophagus

M1a: Metastasis in celiac lymph nodes

M1b: Other distant metastasis

Tumors of the mid-thoracic esophagus

M1a: Not applicable

M1b: Non-regional lymph nodes and/or other distant metastasis

Tumors of the upper thoracic esophagus

M1a: Metastasis in cervical nodes

M1b: Other distant metastasis

Table 6.2 American Joint Committee on Cancer (AJCC) stage groupings

Stage 0: TisN0M0

Stage 1: T1N0M0

Stage 2A: T2N0M0; T3N0M0

Stage 2B: T1N1M0; T2N1M0

Stage 3: T3N1M0; T4 any N M0

Stage 4: Any T any N M1

Stage 4A: Any T any N M1a

Stage 4B: Any T any N M1b

of non-resectable cancers. The same study concludes that EUS is more accurate in staging esophageal tumors than esophagogastric junction tumors, which is a common finding. EUS is particularly effective in visualizing lymph node metastases at the celiac axis, which is strongly correlated with survival.⁴ In fact, the medium-term survival of surgically treated patients harboring large celiac (> 20 mm) lymph nodes is reported to be in the same range of that of non-surgically treated patients without detectable celiac lymph node enlargement.

Computed tomography

CT scan is able to detect the primary tumor in up to 80% of cases; however, the sensitivity is low for local regional nodal metastases, ranging from 50% to 70%.⁵

Moreover, although CT scans may accurately predict resectability in as many as 75% of cases, it has not been demonstrated to be useful for assessing the response to induction therapy.

FDG-PET

Positron emission tomography (PET) is the leading method in nuclear molecular imaging.

Its principle is based on the possibility of labeling biological molecules with a positron emitting isotope. These radionuclides are able to emit a positron from their nucleus; the positron has a high probability of being annihilated by an electron after a short time of travel. This annihilation leads to the production of two 511-keV photons which travel at 180° apart. These coincidence photons can be detected using dedicated scanners, which have particular crystals for photon detection and electronic circuits to localize the emissions in time and space coordinates.

FDG is a glucose analog which enters cells through specific glucose receptors (GLUT). Once inside the cell, FDG is phosphorylated and trapped, without being further metabolized. This mechanism allows the *in vivo* labeling of cells in proportion to their glucose metabolism.

Since malignant lesions, including those from esophageal cancer, have a high mitotic index and an increased glucose metabolism, they can be easily detected using PET, often earlier than with CT. This approach allows identification of malignant lesions at a very early stage, since the spatial resolution of new scanners approaches 4.0 mm. A favourable characteristic of PET is that it allows measurement of the metabolic activity of the lesion in a very simple way. The maximum standardized uptake value (SUV_{max}) is widely used to quantify the uptake of a lesion

and can give an index of disease response to therapy or disease progression.

A clinical PET examination requires the intravenous injection of 5–6 MBq/kg of FDG. Since insulin alters the tracer distribution, the patient fasts for at least 6 h before injection and is not allowed to have insulin or oral antidiabetic drugs. Therefore, this poses a problem when dealing with diabetic patients, who must be strictly followed and instructed. After the injection the patient rests for an optimal uptake time of 60 minutes, during which he or she is hydrated. Eventually the patient undergoes the image acquisition procedure, which may last from 15 to 45 minutes, depending on the scanner type and patient's size.

To improve PET accuracy in the localization of positive findings, hybrid PET–CT scanners have recently been implemented. Hybrid scanners are able to co-register a PET with a CT scan acquired within a short time interval, without moving the patient from the scanner bed. Images are fused slice by slice, superimposing PET on the anatomical map created by CT. In these scanners CT data are also used to measure attenuation correction.

The value of PET is also related to its whole-body view, which gives a complete overview of disease extent, and allows early detection of lymph node involvement and distant metastasis for staging, assessment of therapy response, evaluation of disease relapse, and follow-up.

On the other hand, although PET is very sensitive for the detection of primary lesions, as both adenocarcinoma and squamous cell carcinoma are easily detected, the exact

infiltration of the esophageal wall cannot be evaluated by means of functional imaging because of the poor spatial resolution compared to EUS.

For N staging, PET is considered to be more sensitive than CT because of its ability to make a diagnosis based on a functional index, the tracer uptake, and not on a morphological alteration. In fact, normal-sized, CT-negative, lymph nodes may harbor metastatic cells and show increased tracer uptake. Nonetheless, metastatic lymph nodes close to the primary tumor cannot be seen on PET, due to the high activity of the primary tumor that masks the lower signal coming from small lymph nodes.

PET positivity criteria

PET is considered to be consistent with esophageal cancer when a focal area of increased tracer uptake is detected in correspondence to the esophageal wall as seen on CT. SUV_{max} is indicative of malignancy when greater than 2.0–2.5 according to international guidelines (Figures 6.1–6.3). Esophagitis is frequently associated with esophageal cancer and can be misinterpreted. Inflammation, in fact, is the main cause of false-positive results in PET, and must always be taken into account. The only characteristic that differentiates esophageal inflammation from cancer is that the former is usually diffuse and the latter is

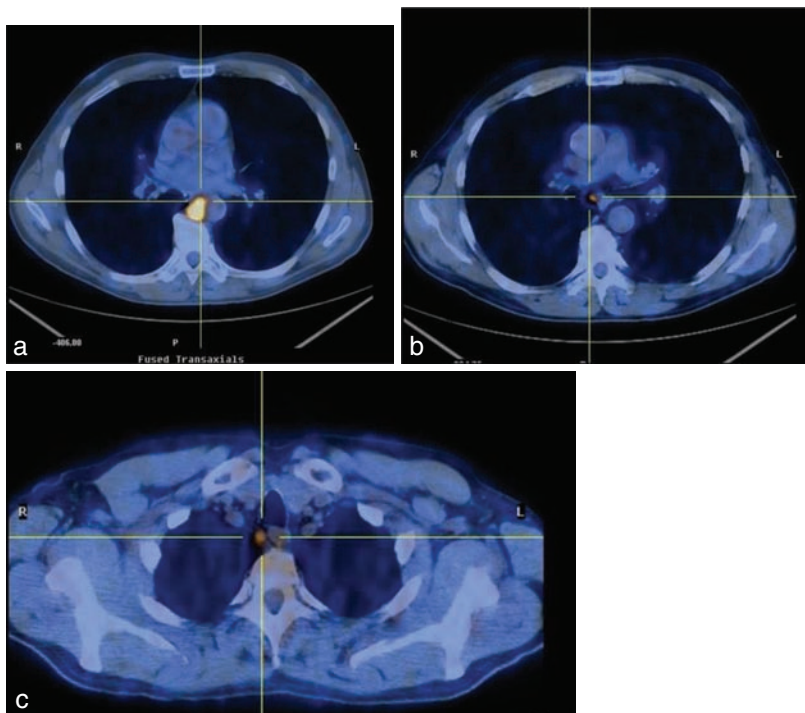


Figure 6.1

$[^{18}F]$ fluro-2-deoxy-D-glucose-positron emission tomography–computed tomography (FDG-PET–CT) fused axial images of a patient with an esophageal cancer upstaged by PET to N+M0. Panel (a) shows the primary tumor, while panels (b) and (c) show paraesophageal and superior paratracheal metastatic lymph nodes.

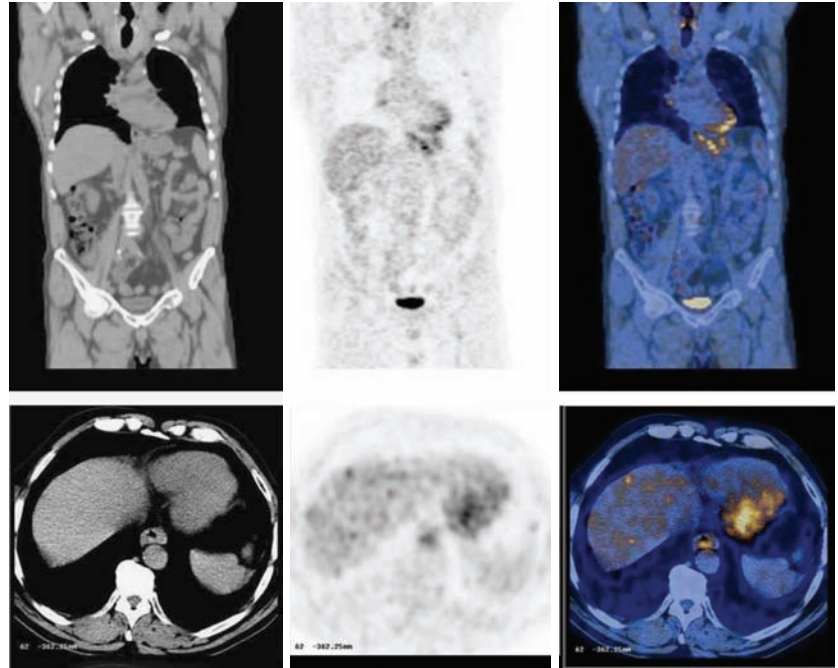


Figure 6.2

Coronal slices of CT (upper panel, left), PET (center), and fused PET-CT (right) images of a T2N0M0 tumor. Lower panel shows the corresponding axial images.

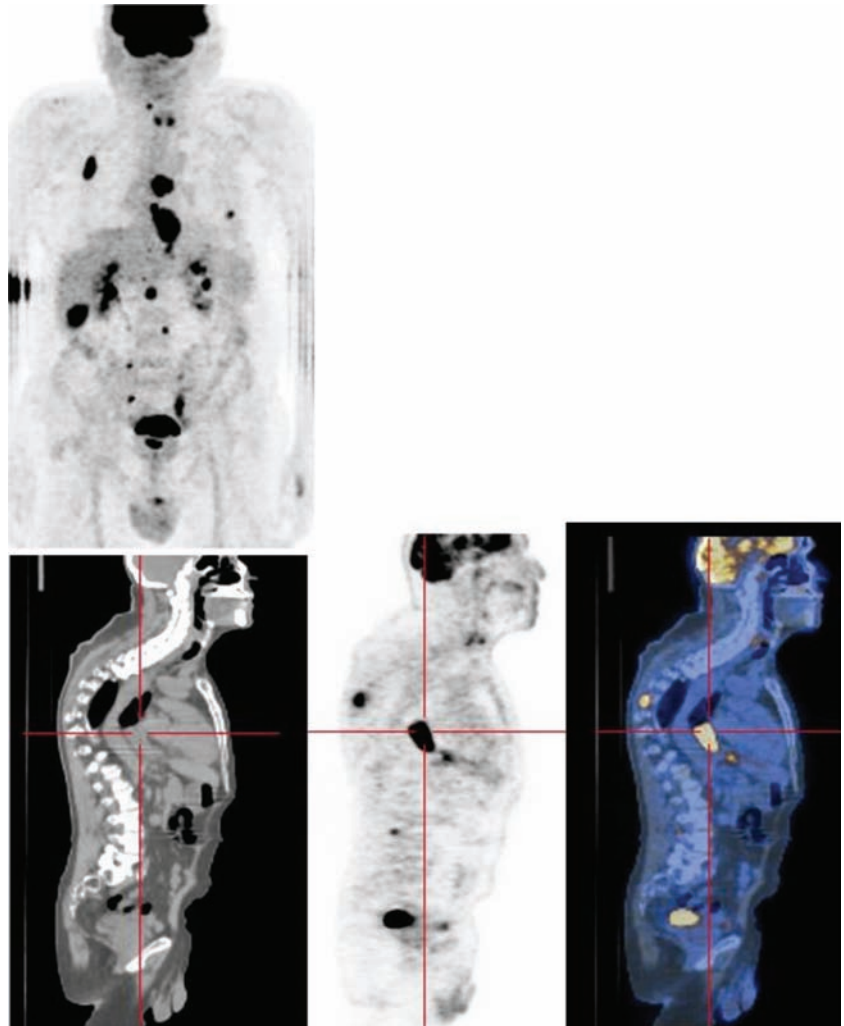


Figure 6.3

Coronal PET slice and sagittal images (CT, PET, and fused) of a metastatic tumor at staging.

usually focal. These criteria are not strict, and extension of the uptake cannot be considered a reliable method.

FDG-PET is falsely negative also for lesions smaller than the scanner spatial resolution (4–6 mm) or for flat lesions thinner than this size, growing parallel to the major axis of the esophagus. In situ carcinoma and severe dysplasia are, therefore, not usually detected.

The advantage of PET–CT over stand-alone PET has been assessed by Bar-Shalom et al.,⁶ who published a study prospectively comparing PET–CT and PET reviewed side by side with CT. The authors concluded that PET–CT has additional value over PET and plays an important role in defining tumor involvement in cervical and abdominal–pelvic sites, as well as in the pretherapy assessment of locoregional disease involvement. Precise characterization of abnormalities in areas of post-surgical distorted anatomy using PET–CT has a particular value in this tumor, as surgery may be the only curative chance.

Staging

A recent review and meta-analysis of 12 studies summarizes and evaluates FDG-PET as a staging method for esophageal cancer.⁷ Pooled specificity and sensitivity data for detection of either locoregional or distant metastases have been calculated as 84% and 51%, respectively. FDG-PET has been shown to have high sensitivity and specificity for the detection of distant (lymphatic and hematogenous) metastases. By contrast, the method has been confirmed to be poor in delineation of locoregional lymph node metastases.

The incremental value of the use of FDG-PET in addition to a CT scan has been demonstrated in a Japanese study⁸ in which relevant additional information was derived from FDG-PET imaging in 20 of 149 patients. Whether the additional information obtained by FDG-PET has a direct impact on the surgical management is still not clear.^{9,10} Some authors suggest that unnecessary surgical explorations could be avoided due to additional information on systemic tumor burden given by FDG-PET, whereas others conclude that the method does not lead to a change in surgery indication. Further advancements in this field are expected using PET–CT technology in larger studies,¹¹ although the fusion of PET and CT will not overcome the intrinsic limitations of the two imaging technologies. In particular, both PET and CT are poor in detecting locoregional lymph node metastases. In CT imaging, lymph nodes are considered metastatic based on size criteria, while a positive PET is dependent on glucose metabolism of the tumor cells, the number of tumor cells, and the distance of the lesion from the primary tumor. Thus, preoperative information about lymph node status may still be unclear. Consequently, it is some authors'

opinion that information on locoregional lymph node status should not influence the therapeutic decision.

A recent paper¹² reports that CT, EUS, and PET have similar performances in nodal staging, with sensitivity and specificity of 84% and 67% for CT, 86% and 67% for EUS, and 82% and 60% for FDG-PET. This paper also reports a trend towards improved locoregional assessment for EUS and better distant disease staging with CT or PET, but concludes that each test contributes by means of unique patient staging information on an individual basis, suggesting that a combination of the three diagnostic methods should always be used.

SUV_{max} measured during staging procedures has been proposed as a prognostic index.¹³ In this study, patients were clustered into two groups depending on the primary lesion SUV_{max} value. The two groups eventually presented a significant difference in the overall survival (613 ± 89 vs. 262 ± 47 days). Another recent paper on 50 patients¹⁴ concludes that SUV_{max} of the primary tumor in esophageal adenocarcinoma predicts clinical stage, pathologic stage, and overall survival. The authors also state that a high SUV_{max} identifies a subset of patients with early-stage clinical and pathologic stage disease but poor prognosis. Therefore, FDG SUV_{max} can potentially be used at diagnosis to select patients for induction therapy or to stratify patients for entry into clinical trials, testing novel multimodality treatment strategies.

Another study¹⁵ suggests that the number of PET abnormalities detected at baseline independently correlates with overall survival, and may become a useful factor for patient stratification in randomized trials. It can also become a tool for individualizing therapy. The study also determines that baseline EUS correlates with neither patient outcome nor any of the PET parameters.

The impact of FDG-PET in patients with locally advanced disease has been determined in a group of patients enrolled in a phase 2 trial of preoperative chemoradiation therapy.¹⁶ This study showed that the addition of PET imaging after conventional staging resulted in the upstaging of a significant percentage of patients. The authors report that patients with locally advanced esophageal cancer on conventional staging, but subsequently found to have PET findings consistent with distant disease, experience a worse outcome after receiving definitive or preoperative chemoradiation therapy. Therefore, it is suggested that the use of FDG-PET is considered a fundamental part of the routine staging.

Relapse

In patients operated on for esophageal cancer, the presence of post-surgical fibrotic tissue causes difficulties in interpretation of the CT scan. In fact, distinguishing vital tissue,

indicating cancer relapse, from non-vital tissue resulting from a surgical scar may be difficult. PET has proved to have a high accuracy for the detection of early relapse in different tumors, and has also been demonstrated to be useful in assessing recurrent and distant metastatic disease.^{17,18} For the detection of recurrent disease, PET is very sensitive (Figure 6.4), although the combination of

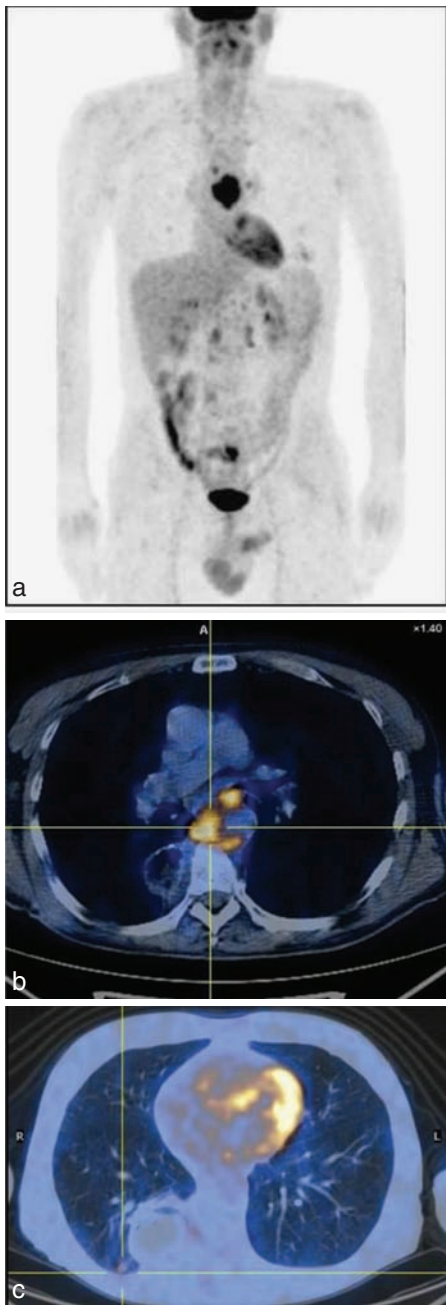


Figure 6.4
Demonstration of a relapse suspected on CT with PET-CT, which shows local relapse (a), mediastinal lymph nodes (b), and a lung metastasis (c).

conventional methods and PET is the most helpful in characterizing anastomotic recurrences.¹⁹ PET is more sensitive than CT and has at least an equal specificity for the detection of systemic metastatic disease, and may detect distant metastases in up to 10–20% of patients that were not identified with CT.^{20,21} Pooled sensitivity and specificity for the detection of locoregional metastases are reported to be 51% and 84%, respectively, while for distant metastases pooled sensitivity and specificity are 67% and 97%.²² PET may also provide additional diagnostic information over CT, which may lead to management changes in 4–30% of patients.^{23,24}

Response to neoadjuvant therapy

As previously described, many investigators have demonstrated that FDG-PET has a high sensitivity as a staging procedure in esophageal cancer. Fewer studies have examined the use of this imaging method for evaluation of the response to a combination of chemotherapy and radiotherapy,^{25–27} reporting very high sensitivity and specificity as well (Figures 6.5 and 6.6).

Since a significant number of patients are diagnosed with esophageal cancer in a late phase, when the disease is so extended that a surgical approach is useless or even dangerous, neoadjuvant chemoradiotherapy has been proposed to reduce the primary mass and allow successful post-treatment surgery. FDG-PET results have been correlated to the pathologic response and the percentage change of SUV_{max} before and after therapy, and this is considered to be an accurate index for the early evaluation of therapy response. Nevertheless, it is not clear whether an early recognition of neoadjuvant therapy response is significantly correlated to a better prognosis, although Swisher et al.²⁸ found that after neoadjuvant chemoradiotherapy, patients with $SUV_{max} \leq 4$ within the residual lesion had a significantly longer overall survival compared to patients with $SUV_{max} > 4$.

Although it is commonly accepted that FDG-PET is an effective modality for assessing pathologic tumor response to neoadjuvant chemoradiotherapy in esophageal cancer, it must be stressed that methodological differences may play an important role when assessing response in clinical practice and also when comparing data from different studies. For instance, Brucher et al.²⁹ report an extremely high sensitivity (100%) and a relatively low specificity (55%) in the prediction of pathologic response with FDG-PET, defining sensitivity as the proportion of responding tumors showing a reduction in FDG uptake equal to or greater than a cut-off value. Their methods and definitions seem to be very helpful in depicting the change in tumor

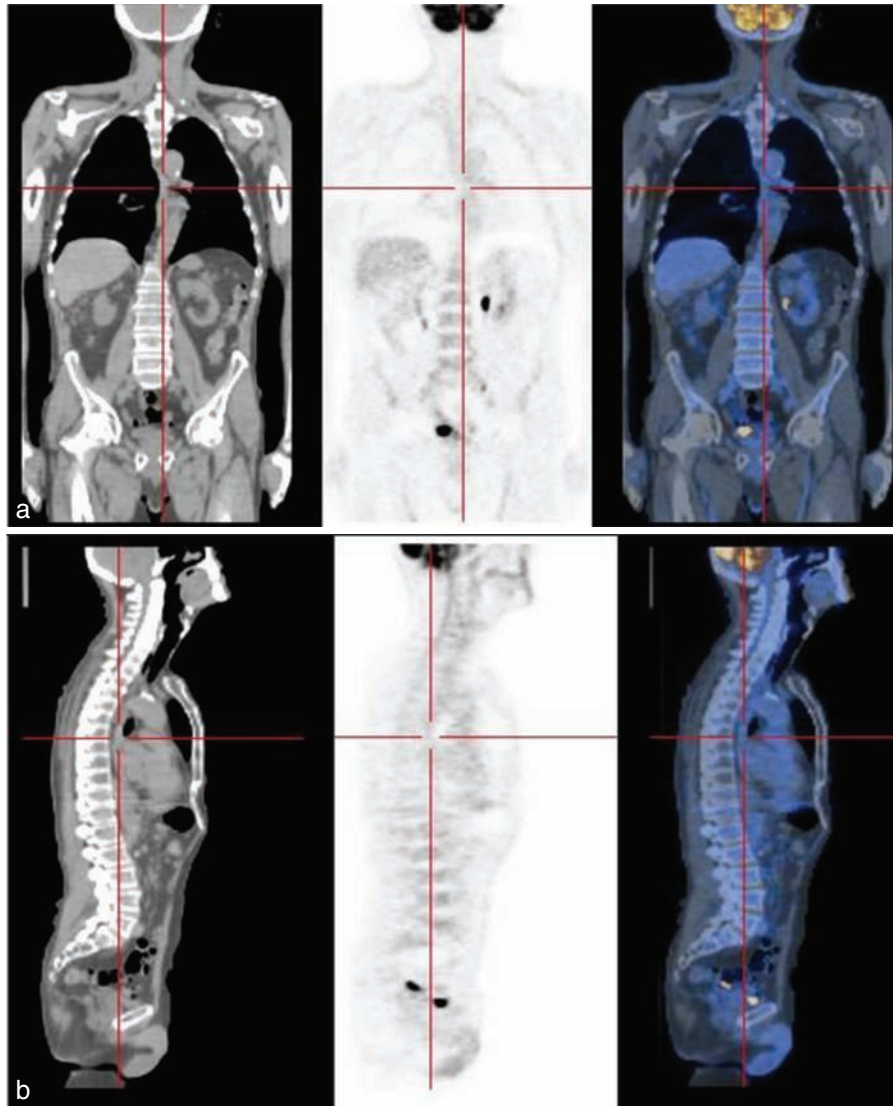


Figure 6.5

Coronal (a) and sagittal (b) slices of a patient with a complete response after neoadjuvant therapy.

size, but not in detecting a residual tumor before surgery, as the relatively small amount of residual tumor may lead to recurrence and a poor prognosis. Also, different definitions of pathologic response in published studies lead to a great variation in reported sensitivity and specificity.¹⁵ Using single-center defined cut-off values in the measurement of SUV variation, reported sensitivity is in the range from 71 to 100% and specificity from 54.5 to 95%.

Esophagitis is also often mentioned as a source of false-positive results, which may be a common finding in patients treated with aggressive chemotherapeutic regimens. Song et al.¹⁵ did not find any correlation between the absolute value of SUV post-therapy or its relative change from baseline level and the pathologic response, but

reported that when patients with highly metabolic tumors (SUV > 4.0) were selected, the result became comparable to that of other investigators. This study also showed a lower sensitivity in assessing pathologic response in lymph nodes than in primary tumors, after chemoradiotherapy. Refuting established data, they affirm that FDG-PET is not effective for detecting lymph node metastasis or evaluating response after chemoradiotherapy because of the low diagnostic sensitivity.

Duong et al.³⁰ qualitatively evaluated PET images on an SUV-calibrated scale, without calculating the tumor SUV. PET after chemoradiotherapy was interpreted only as being negative or positive for residual disease, thus using a dichotomous classification of images. In the authors'

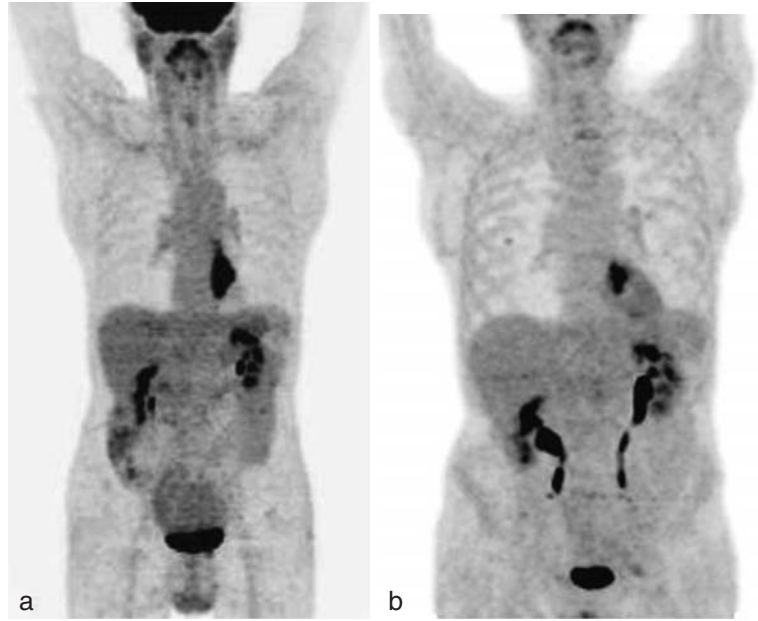


Figure 6.6

Coronal PET slices of a patient with advanced disease. Panel (a) shows the image at staging (maximum standardized uptake value, $SUV_{max} = 11$) and panel (b) after therapy, 5 months later ($SUV_{max} = 6$).

report, the advantage of this method is that a baseline study is not required, and it is not subject to methodological variation. They also promote this approach, since most pretreatment primary esophageal tumors are already demonstrated to be FDG-avid.^{31,32} On the other hand, the absence of a baseline study limits this approach only to assessing which patients could be considered for non-surgical treatment or in whom aggressive surgical treatment would be inappropriate based on the extent of residual disease. Nevertheless, a PET scan before treatment is always advisable, since this is likely to be beneficial in terms of both tumor staging and treatment planning, as well as providing further prognostic stratification.

Levine et al.³³ recently suggested incorporating FDG-PET to identify a patient subgroup with a high probability of response, based on a pretreatment scan. In this way, patients with a low SUV_{max} could be managed with surgery alone or chemoradiotherapy followed by esophagectomy, while potential responders may be managed by chemoradiotherapy alone. The authors concluded that FDG-PET is a useful tool for identifying esophageal cancer patients likely to experience a significant response to preoperative chemoradiotherapy.

Follow-up

FDG-PET is not routinely used for follow-up, and should only be employed when the patient has equivocal findings upon conventional imaging.

Other PET radiopharmaceuticals

[¹¹C]choline is commonly used for clinical studies, particularly for the evaluation of prostate cancer, giving an index of cell membrane metabolism.

According to the literature, [¹¹C]choline is feasible for the study of esophageal cancer, but, from preliminary studies, it has a significantly lower sensitivity, specificity, and accuracy for the detection of primary tumors and distant metastases, missing abdominal lesions due to high uptake in the liver and spleen. Concerning nodal involvement [¹¹C]choline-PET seems to be more sensitive than FDG-PET, and its use has been suggested to increase the accuracy of N evaluation,³⁴ although clinical studies with a significant number of patients are still lacking, probably due to the low availability of this radiopharmaceutical. [¹⁸F]fluorothymidine has been also used to evaluate esophageal cancer, being a direct marker of cell proliferation. This tracer also showed a lower sensitivity when compared to FDG, but limited the number of false-positive results as it is not taken up in inflammatory lesions.³⁵

References

1. Greene FL, Page DL, Fleming ID et al., eds. *AJCC Cancer Staging Manual*, 6th edn. New York: Springer-Verlag; 2002.
2. von Rahden BHA, Stein HJ. Staging and treatment of advanced esophageal cancer. *Curr Opin Gastroenterol* 2005; 21: 472–7.

3. Heeren PA, van Westreenen HL, Geersing GJ, van Dullemans HM, Plukker JT. Influence of tumor characteristics on the accuracy of endoscopic ultrasonography in staging cancer of the esophagus and esophagogastric junction. *Endoscopy* 2004; 36: 966–71.
4. Marsman WA, van Wissen M, Bergman JJ et al. Outcome of patients with esophageal carcinoma and suspicious celiac lymph nodes as determined by endoscopic ultrasonography. *Endoscopy* 2004; 36: 961–5.
5. Devita VT, Hellman S, Rosenberg SA, Eds. *Cancer: Principles and Practice of Oncology*, 6th edn. Philadelphia: Lippincott Williams & Wilkins, 2001.
6. Bar-Shalom R, Guralnik L, Tsalic M et al. The additional value of PET/CT over PET in FDG imaging of esophageal cancer. *Eur J Nucl Med Mol Imaging* 2005; 32: 918–24.
7. van Westreenen HL, Westerterp M, Bossuyt PM et al. Systematic review of the staging performance of 18F fluorodeoxyglucose positron emission tomography in esophageal cancer. *J Clin Oncol* 2004; 22: 3805–12.
8. Kato H, Miyazaki T, Nakajima M et al. The incremental effect of positron emission tomography on diagnostic accuracy in the initial staging of esophageal carcinoma. *Cancer* 2005; 103: 148–56.
9. Kneist W, Schreckenberger M, Bartenstein P. Prospective evaluation of positron emission tomography in the preoperative staging of esophageal carcinoma. *Arch Surg* 2004; 139: 1043–9.
10. van Westreenen HL, Heeren PA, van Dullemans HM et al. Positron emission tomography with F-18-fluorodeoxyglucose in a combined staging strategy of esophageal cancer prevents unnecessary surgical explorations. *J Gastrointest Surg* 2005; 9: 54–61.
11. Larson SM, Schoder H, Yeung H. Positron emission tomography/computerized tomography functional imaging of esophageal and colorectal cancer. *Cancer J* 2004; 10: 243–50.
12. Lowe VJ, Booya F, Fletcher JG et al. Comparison of positron emission tomography, computed tomography, and endoscopic ultrasound in the initial staging of patients with esophageal cancer. *Mol Imaging Biol* 2005; 7: 422–30.
13. van Westreenen HL, Plukker JT, Cobben DC et al. Prognostic value of the standardized uptake value in esophageal cancer. *AJR Am J Roentgenol* 2005; 185: 436–40.
14. Rizk N, Downey RJ, Akhurst T et al. Preoperative 18[F]-fluorodeoxyglucose positron emission tomography standardized uptake values predict survival after esophageal adenocarcinoma resection. *Ann Thorac Surg* 2006; 81: 1076–82.
15. Song SY, Kim JH, Ryu JS, et al. FDG-PET in the prediction of pathologic response after neoadjuvant chemoradiotherapy in locally advanced, resectable cancer. *Int J Radiat Oncol Biol Phys* 2005; 63: 1053–9.
16. Blackstock AW, Farmer MR, Lovato J et al. A prospective evaluation of the impact of 18-F-fluoro-deoxy-D-glucose positron emission tomography staging on survival for patients with locally advanced esophageal cancer. *Int J Radiat Oncol Biol Phys* 2006; 64: 455–60.
17. Jadvar H, Henderson RW, Conti PS. 2-deoxy-2-[F-18] fluoro-D-glucose-positron emission tomography/computed tomography imaging evaluation of esophageal cancer. *Mol Imaging Biol* 2006; 8: 193–200.
18. Flanagan FL, Dehdashti F, Siegel BA et al. Staging of esophageal cancer with 18F-fluorodeoxyglucose positron emission tomography. *AJR Am J Roentgenol* 1997; 168: 417–24.
19. Flamen P, Lerut A, van Cutsem E et al. The utility of positron emission tomography for the diagnosis and staging of recurrent esophageal cancer. *J Thorac Cardiovasc Surg* 2000; 120: 1085–92.
20. Kim K, Park SJ, Kim BT, Lee KS, Shim YM. Evaluation of lymph node metastases in squamous cell carcinoma of the esophagus with positron emission tomography. *Ann Thorac Surg* 2001; 71: 290–4.
21. Larson SM, Schoder H, Yeung H. Positron emission tomography/computerized tomography functional imaging of esophageal and colorectal cancer. *Cancer J* 2004; 10: 243–50.
22. Rasanen JV, Sihvo EI, Knuuti MJ. Prospective analysis of accuracy of positron emission tomography, computed tomography, and endoscopic ultrasonography in staging of adenocarcinoma of the esophagus and the esophagogastric junction. *Ann Surg Oncol* 2003; 10: 954–60.
23. Yeung HW, Macapinlac HA, Mazumdar M, et al. FDG-PET in esophageal cancer. Incremental value over computed tomography. *Clin Positron Imaging* 1999; 2: 255–60.
24. Imdahl A, Hentschel M, Kleimaier M, Hopt UT, Brink I. Impact of FDG-PET for staging of esophageal cancer, *Langenbecks Arch Surg* 2004; 389: 283–8.
25. Brink I, Hentschel M, Bley TA et al. Effects of neoadjuvant radio-chemotherapy on 18F-FDG-PET in esophageal carcinoma. *Eur J Surg Oncol* 2004; 30: 544–50.
26. Downey RJ, Akhurst T, Ilson D et al. Whole body 18FDG-PET and the response of esophageal cancer to induction therapy: Results of a prospective trial. *J Clin Oncol* 2003; 21: 428–32.
27. Kato H, Kuwano H, Nakajima M et al. Usefulness of positron emission tomography for assessing the response of neoadjuvant chemoradiotherapy in patients with esophageal cancer. *Am J Surg* 2002; 184: 279–83.
28. Swisher SG, Maish M, Erasmus JJ et al. Utility of PET, CT, and EUS to identify pathologic responders in esophageal cancer. *Ann Thorac Surg* 2004; 78: 1152–60.
29. Brucher BL, Weber W, Bauer M et al. Neoadjuvant therapy of esophageal squamous cell carcinoma: response evaluation by positron emission tomography. *Ann Surg* 2001; 233: 300–9.
30. Duong CP, Hicks RJ, Weih L et al. FDG-PET status following chemoradiotherapy provides high management impact and powerful prognostic stratification in oesophageal cancer. *Eur J Nucl Med Mol Imaging* 2006; 33: 770–8.
31. McAteer D, Wallis F, Couper G et al. Evaluation of 18F-FDG positron emission tomography in gastric and oesophageal carcinoma. *Br J Radiol* 1999; 72: 525–9.
32. Rankin SC, Taylor H, Cook GJ, Mason R. Computed tomography and positron emission tomography in the pre-operative staging of oesophageal carcinoma. *Clin Radiol* 1998; 53: 659–5.
33. Levine EA, Farmer MR, Clark P et al. Predictive value of 18-fluoro-deoxy-glucose-positron emission tomography (18F-FDG-PET) in the identification of responders to chemoradiation therapy for the treatment of locally advanced esophageal cancer. *Ann Surg* 2006; 243: 472–8.
34. Jager PL, Que TH, Vaalburg W et al. Carbon-11 choline or FDG-PET for staging of esophageal cancer? *Eur J Nucl Med* 2001; 28: 1845–9.
35. van Westreenen HL, Cobben DCP, Jager PL et al. Comparison of 18F-FLT PET and 18F-FDG PET in esophageal cancer. *J Nucl Med* 2005; 46: 400–4.

Colorectal cancer

Ken Herrmann and Bernd Joachim Krause

Background

Colorectal cancer is one of the most common neoplasms in Western countries. In 2002 it ranked second for men and women.¹ After a slight increase in frequency over recent years, the incidence is expected to remain stable over the coming years. Epidemiologic and experimental studies suggest that an unbalanced fatty nutrition with low dietary fibers may promote tumor growth. Two inherited syndromes, familial adenomatous polyposis (FAP) and hereditary non-polyposis colorectal cancer (HNPCC), associated with colorectal cancer have been identified so far. In Germany, the mortality rate for colorectal cancer in 2000 was 29.8/100 000 for men and 19.3/100 000 for women.¹

In most cases colorectal cancer is located in the rectum (40%), followed by the sigmoid and cecum. Of diagnosed tumors around 70% are resectable. However, around 40% of patients undergoing surgery will relapse in the first 2 years after initial resection. Up to 30% develop hepatic metastases and around 15% lung metastases. Reported 5-year survival rates range between 40% and 60%. Early stages (Dukes A) are well curable, resulting in 5-year survival rates of around 90%. However, only 39% of colorectal cancers are diagnosed at this early stage. For advanced stages (Dukes D) the reported 5-year survival rate is only around 10%.² The goal of treatment is cure in the early stages (Dukes A and B), prolongation of survival in stage C, and palliation in stage D. Resection of metastases isolated to the liver has been associated with improved survival.^{3,4}

The initial detection of primary colorectal cancer is a domain of endoscopy. Additional imaging for therapy planning is discussed controversially, especially due to the lack of a single comprehensive imaging method.⁵ Conventional imaging modalities, comprising endoluminal ultrasound, computed tomography (CT), and magnetic resonance imaging (MRI), are limited to give morphological information. Differentiation between malignant and benign

lesions is not always reliable. For assessment of lymph node involvement, size and morphology remain the only criteria. Regarding MRI and CT, lymph nodes larger than 1 cm are considered to be suspicious, but of course also smaller lymph nodes can contain malignancies. Therefore, there is a high demand for imaging methods providing functional information.

Imaging modalities play an even more important role in the setting of suspected recurrence of colorectal cancer. In around 40% of cases, recurrence occurs within 2 years of the initial diagnosis. Of these, around 30% appear to have limited recurrent disease, but only 25% of them are actually curable by surgery.⁶ At surgery, up to 75% of patients are revealed to have non-resectable disease due to distant metastases or widespread disease.^{7,8} In order to decrease the number of futile surgeries it is essential to improve the accuracy of preoperative detection of recurrent disease.

Positron emission tomography (PET) is based on imaging biochemical processes in vivo, which represent molecular processes underlying metabolic activity.⁹ The most common tracer is the glucose analog [¹⁸F]fluoro-2-deoxy-D-glucose (FDG). FDG accumulation is proportional to the amount of glucose utilization.^{10,11} Increased consumption of glucose is a characteristic of most cancers, and is in part related to overexpression of the GLUT1 glucose transporters in many cancers.¹² According to the 3rd German Interdisciplinary Consensus Conference, FDG-PET is rated as a 1a indication (established clinical use) for restaging in suspected relapse and as a 1b indication (clinical use probable) for therapy control, whereas staging of colorectal cancer is not indicated.¹³

In 1989, a first study of PET in patients with recurrent colorectal cancer was published comparing PET with CT. The aim of the study was to differentiate between scar tissue and recurrent disease in the follow-up of patients with colorectal cancer. In a group of 29 patients, Strauss et al. detected recurrent disease in 21 patients all showing an increased FDG uptake in PET cross-sections.¹⁴ Since then, a considerable number of PET studies of different

groups regarding staging,¹⁵ detection of recurrence,^{6,16–23} and changes of therapy management^{24–26} have been published (for reviews see Huebner et al.⁶ and Dietlein et al.¹⁸).

In 1998, the first PET–CT scanner, combining functional information with morphological information, was introduced by Townsend and co-workers.²⁷ Combined PET–CT devices offer an efficient tool for whole-body staging and functional assessment within one imaging modality. PET–CT scanners allow a merging of complementary information from CT and PET, leading to an exact anatomic localization. Furthermore, a more precise assessment of tumor volume is possible in comparison with PET. Since then, the number of institutions and imaging centers operating combined PET–CT scanners has been steadily increasing. After its introduction into clinical routine in 2001, first studies concerning the restaging of colorectal cancer were published (Figures 7.1 and 7.2).^{28–32}

This chapter will focus on the main indications of PET and PET–CT in patients with colorectal cancer and analyze

the published data separately regarding staging, detection of recurrent disease (Figure 7.1), therapy monitoring (Figure 7.2), early response evaluation, and tumor control.

Positron emission tomography Staging

In 1994, Falk et al.³³ reported on a comparison of PET and CT for preoperative staging of colorectal carcinoma in 16 patients. PET proved to be more accurate than CT (accuracy 83% for PET vs. 56% for CT). Abdel-Nabi et al.¹⁵ preoperatively investigated 48 consecutive patients with biopsy-proven or highly clinically suspected colorectal cancer. PET depicted all primaries, resulting in a sensitivity of 100%, and the related specificity was 43%. PET also proved to be very sensitive for the detection of liver metastases

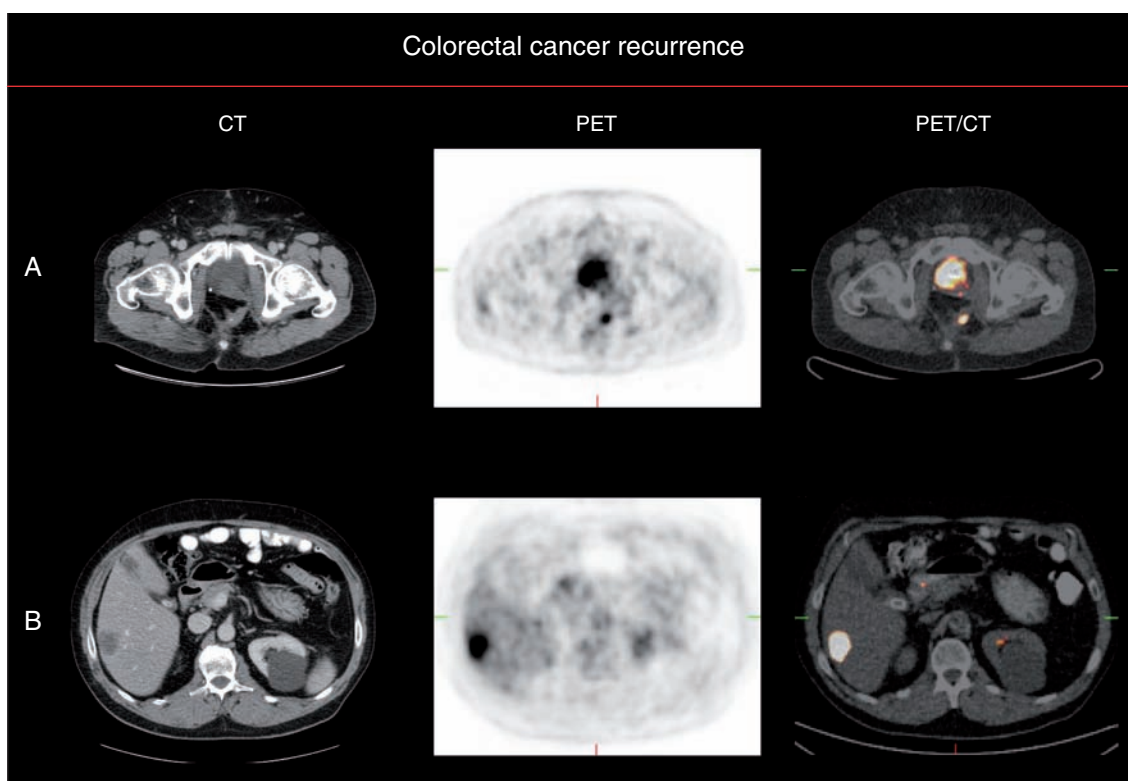


Figure 7.1

Positron emission tomography–computed tomography (PET–CT) with [¹⁸F]Fluoro-deoxy-glucose (FDG) in an 81-year-old patient with recurrent rectal carcinoma (local/pelvic recurrence and solitary hepatic metastasis) 15 months after initial diagnosis and surgical resection. (A) Transaxial sections of the liver in CT, PET, and fused PET–CT. (B) Transaxial sections of the pelvis.

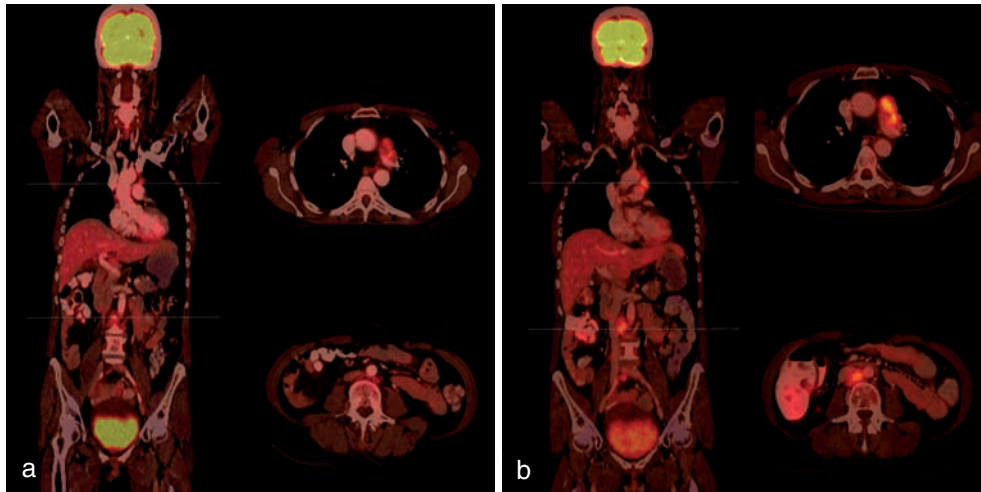


Figure 7.2

PET–CT with [^{18}F]Fluoro-deoxy-glucose (FDG) in a patient with mediastinal and retro peritoneal lymph node recurrence of colorectal cancer (a) before and (b) after 6 weeks of chemotherapy. (a,b) Left coronal sections of the whole body, right upper, and lower transaxial sections of thorax and pelvis.

(sensitivity 83%) whereas it was positive only in 29% of the lymph node metastases. Overall, Abdel-Nabi et al.¹⁵ concluded that PET is superior to CT for the staging of primary colorectal carcinoma. In a study of 24 patients, Mukai et al.²¹ confirmed earlier published results regarding PET examinations by detecting a sensitivity of 96% for staging of primary colorectal cancer. Only 22% of the histologically confirmed lymph node metastases were depicted by PET. In a more recent publication, Kantorova et al.¹⁹ compared FDG–PET with CT in the preoperative staging of colorectal cancer. In 38 consecutive patients with histologically proven colorectal cancer, PET was more sensitive than CT and ultrasound (95%, 49%, and 14% respectively) in staging primary disease. Despite a low sensitivity of 29%, PET had an accuracy of 75% in depicting lymph node metastases. Compared to ultrasound (accuracy 81%), PET and CT appeared to be more accurate (both 91%) in detecting hepatic metastases. Additional information provided by PET led to a change of treatment modality for 8% of patients and influenced the range of surgery for 13%.

Regarding the prognostic relevance of the initial maximum standardized uptake value (SUV_{max}), Calvo et al.¹⁷ showed that initial SUV_{max} in PET staging was predictive for long-term patient outcome in a cohort of 25 consecutive patients. The definition of a cut-off of $\text{SUV}_{\text{max}} \leq 6$ correlated with a significantly better 3-year survival (92% vs. 60%).

T-staging is the domain of morphological imaging methods (CT and MRI). Sensitivity for N-staging remains low for morphological as well as functional imaging

modalities (PET). PET can provide important additional information regarding M-staging.

Recurrent disease

In 1989, the first study evaluating PET for the differentiation between scar tissue and recurrent disease was published.¹⁴ In a group of 29 patients, PET detected recurrent disease in 21 patients, all showing an increased FDG uptake in the cross-sections. In a meta-analysis by Huebner et al.,⁶ 11 studies met the inclusion criteria defined, and the reported data were analyzed. The overall sensitivities and specificities of PET for the local/pelvic region on a patient basis, hepatic metastases on a patient and lesion-by-lesion basis, and the whole body on a patient basis were determined separately. Imaging results for the detection of local/pelvic recurrence were available in a total of 366 patients. Analysis of the pooled data resulted in a sensitivity of 94% (range 90–97%) and a specificity of 98% (range 89–100%). Analysis of the imaging results of FDG–PET of the liver in a total of 393 patients included in five studies showed a sensitivity ranging between 94% and 100% and a specificity reaching from 67% to 100%. Hepatic involvement reported in lesion data was published in two studies including a total of 182 patients. Sensitivity (90% vs. 91%) and specificity (96% vs. 100%) were similar in both publications. Five studies reported on sensitivity and specificity data for FDG–PET, depicting colorectal recurrences in the whole body.

In a total of 281 patients the sensitivity ranged from 95% to 100%, whereas the specificity showed a wider spread (69–83%). This led to an overall sensitivity of 97% and an overall specificity of 76%. All studies are summarized in Table 7.1.

Whiteford et al.²³ compared the clinical efficacy of FDG-PET with that of CT plus other conventional imaging methods in patients with recurrent or metastatic colorectal cancer. In the detection of clinically relevant tumor or metastases, PET showed a significantly higher sensitivity (87% vs. 66%) and specificity (68% vs. 59%) than CT plus other conventional imaging. Reported sensitivities for PET were higher than for conventional imaging, including CT

detecting hepatic metastases (89% vs. 71%), extrahepatic metastases (94% vs. 67%), and local recurrence (90% vs. 71%). The determined specificities showed no significant difference for both imaging methods (Table 7.1).

In another study with a total of 100 patients, the influence of FDG-PET on surgical decision-making was studied. PET showed an overall sensitivity of 98% and specificity of 90% (Table 7.1) for detecting malignant lesions compared to CT, 91% and 72% respectively, and to CEA (carcinoembryonic antigen) level measurements, 76% and 90% respectively.²² PET was more sensitive in the detection of hepatic metastases than ultrasound (98% vs. 87%), whereas ultrasound revealed a higher specificity

Table 7.1 Reported sensitivity and specificity for positron emission tomography (PET)^{6,16,20,22,23}

<i>Author</i>	<i>Year</i>	<i>Patients (n)</i>	<i>Type</i>	<i>Part</i>	<i>Modality</i>	<i>Sensitivity (%)</i>	<i>Specificity (%)</i>
Schiepers	1995	83	Studies	Local/pelvic	PET	96	97
		83	Studies	Hepatic	PET	94	100
Vitola	1996	24	Patients	Whole body	PET	95	80
		55	Lesions	Hepatic	PET	90	100
Lai	1996	34	Patients	Hepatic	PET	100	67
Delbeke	1997	61	Patients	Whole body	PET	98	83
		127	Lesions	Hepatic	PET	91	96
Keogan	1997	18	Patients	Local/pelvic	PET	92	80
Ogunbiyi	1997	58	Patients	Hepatic	PET	96	100
		47	Patients	Local/pelvic	PET	90	100
Ruhlmann	1997	59	Patients	Whole body	PET	100	69
Flanagan	1997	22	Patients	Whole body	PET	100	71
Valk	1999	115	Patients	Whole body	PET	95	79
		115	Patients	Hepatic	PET	95	100
		115	Patients	Local/pelvic	PET	97	96
Flamen	1999	103	Patients	Local/pelvic	PET	94	100
		103	Patients	Hepatic	PET	98	100
Whiteford	2000	109	Patients	Whole body	PET	87	68
		70	Patients	Local/pelvic	PET	90	92
		101	Patients	Hepatic	PET	89	98
		101	Patients	Extrahepatic	PET	94	98
Staib	2000	100	Patients	Whole body	PET	98	90
			Patients	Hepatic	PET	100	99
			Patients	Local/pelvic	PET	96	96
Arulampalam	2001	42	Patients	Whole body	PET	93	58
		15	Patients	Hepatic	PET	100	100
		15	Patients	Local/pelvic	PET	100	86
Lonneux	2002	79	Patients	Whole body	PET	97	72
		32	Patients	Hepatic	PET	97	100
		15	Patients	Local/pelvic	PET	100	98

than PET (96% vs. 90%) resulting in similar accuracies (PET: 95%, ultrasound: 93%). According to this study, additional PET information regarding correct diagnosis of hepatic and distant metastases influenced surgical decisions in 61% of the cases, separated into very high relevance (14%) and high relevance (47%).

Arulampalam et al.¹⁶ investigated the impact of FDG-PET on clinical management in a group of 42 patients with suspected recurrence. Due to the additional information provided by PET, 27% of the patients were upstaged, and in a total of 16 (38%) patients the clinical management was altered. Follow-up and histological confirmation of diagnosis proved that in 14 cases a change of treatment was to the benefit of the patient, whereas two patients ultimately did not benefit from the alteration of clinical management. Determination of sensitivity for the detection of recurrence showed that PET was more sensitive than CT (93% vs. 73%). The related specificity of PET was 58% compared to a specificity of 75% for CT (Table 7.1). In staging local recurrence, PET (sensitivity 100%, specificity 86%) proved to be more accurate than CT (sensitivity 75%, specificity 100%). Additionally, PET proved to be superior to CT for the detection of liver metastases (sensitivity: 100% vs. 45% and specificity both 100%).

In a study of 79 patients with known or suspected recurrence, Lonneux et al.²⁰ analyzed the impact of PET on selecting candidates for curative resection more accurately than with conventional imaging modalities. PET predicted resectability significantly more accurately (82% vs. 65%, $p = 0.02$) than conventional imaging modalities consisting of CT abdomen, CT pelvis, and chest X-ray, and led to a reduction of unnecessary surgeries of 53%. PET was also more accurate (overall sensitivity 97%, specificity 72%) than conventional imaging modalities (overall sensitivity 61%, specificity 36%) in detecting recurrence at all sites except for the liver (Table 7.1).

PET-CT

The combination of whole-body anatomical (CT) and functional (PET) imaging offers an efficient tool for whole-body staging and functional assessment in one device. PET-CT enables assessment of the exact tumor volume. Recently, studies evaluating the impact of PET-CT on diagnosing and treating colorectal cancer have been published (Tables 7.1 and 7.2).^{28,30–32}

In 45 patients with known colorectal cancer, Cohade et al.³² compared retrospectively the accuracies for staging and restaging of PET-CT vs. PET alone. All PET and PET-CT studies were evaluated separately in randomized order. ⁶⁸Ge attenuation-corrected images were assessed to reassure that only the added value of CT information was evaluated. Patient scans were evaluated on a lesion-by-lesion

and on a patient-by-patient basis. Lesion location was scored on a three-point scale (0 = uncertain, 1 = probable, 2 = certain) and certainty of lesion characterization on a five-point scale (0 = definitely benign, 1 = probably benign, 2 = equivocal, 3 = probably malignant, 4 = definitely malignant). PET-CT reduced the number of lesions rated as uncertain location by 55% and the number of lesions characterized as equivocal or probable by 50%. On a patient-by-patient basis the overall accuracy was raised by 11% (PET-CT: 89%, PET alone: 78%), resulting in a reduction of incorrectly staged patients by 50%. Additional information provided by PET-CT in comparison to PET alone seems to be of greater importance for the evaluation of extrahepatic disease than for liver evaluation. In extrahepatic regions a better localization of [¹⁸F]FDG uptake appeared to be crucial for staging. In this study, follow-up data for at least 6 months was available only in 56% of the analyzed patients.

Kamel et al.³¹ evaluated the contribution of dedicated CT interpretation to the accuracy of PET-CT in patients with suspected primary or metastatic colorectal carcinoma. In 100 PET-CT scans in 90 consecutive patients, this group analyzed the impact of the additional CT information to the overall accuracy of PET-CT. The CT component of the PET-CT scans was reviewed retrospectively by two experienced CT radiologists and findings classified as primary lesion, local recurrence, or distant metastases. Comparison of sensitivity, specificity, and accuracy of combined PET-CT with dedicated CT interpretation (99%, 100%, and 98% respectively) to the PET-CT reports (91%, 63%, and 83% respectively) showed a statistically significant higher accuracy ($p < 0.05$). The 15% increase of the overall accuracy was mainly due to an increase of specificity by a significant reduction of false-positive scans consisting of post-liver resection or radiofrequency ablation, inflammatory pulmonary or hilar uptake, and non-neoplastic increased activity. These results demonstrate the high impact of combined PET-CT devices in clinical routine by combining functional information with valuable anatomic and pathologic information.

Kim et al.³⁰ compared the accuracies of [¹⁸F]FDG-PET, in-line PET-CT, and software fusion for the restaging of recurrent colorectal cancer. A total of 51 patients underwent a PET-CT examination and 34 patients of this cohort received an additional CT scan within 4 weeks of PET-CT. For evaluation of the accuracy of the software fusion, defined landmarks, including normal anatomic structures such as the lower poles of both kidneys and the lower pole of the spleen, were identified on CT and PET scan and the distances measured. PET, PET-CT, and software fusion of PET and CT were interpreted separately by independent observers. Findings were validated by histological evaluation or clinical follow-up of at least 6 months. Staging accuracy on a patient basis was significantly higher for PET-CT (88%) than for PET alone (71%; $p = 0.01$) due to an

additional identification of metastases in five regions and correct exclusion of metastases in seven regions. Additionally detected metastases included peritoneal lesions, small pulmonary metastases, and a sclerotic bone metastasis. Better anatomic localization of increased FDG uptake led to a reduction of false-positive findings. Analysis of software fusion of independently acquired PET and CT scans revealed a comparable accuracy to that of in-line PET–CT (95% vs. 97% respectively), but software fusion was successful in only 76% of the patients. In accordance with the results published by Kamel et al.,³¹ Kim et al.³⁰ concluded that CT scans should also be evaluated for signs of metastatic disease and not only for anatomic localization of abnormalities identified in the PET study, leading to significantly higher accuracies than with PET alone. Additionally, in-line PET–CT reduces the time required for the diagnostic work-up, and is therefore likely to become the new standard for the staging of patients with recurrent colorectal cancer.

Strunk et al.²⁸ compared retrospectively, in a cohort of 29 patients referred for restaging due to suspected recurrent colorectal carcinoma, PET alone, CT alone, and PET and CT virtually fused with simultaneously co-registered PET–CT scans. Detection of lesions was most sensitive with co-registered PET–CT scans. Discrepancies were mainly found in the lung, where PET alone often detected lymph nodes and soft tissue masses, while CT alone was negative. Co-registered PET–CT scans provided additional information in seven of 29 patients, leading to a higher accuracy in diagnosis and anatomic localization of metastases in colorectal cancer patients.

Management

This section gives an overview of the consequences of additional information provided by PET on the clinical therapy management of patients with recurrent colorectal carcinoma. PET is expected to allow earlier treatment evaluation when CT-negative lesions can already be detected by PET. Detection of distant metastases and better preoperative assessment of tumor spread can avoid unnecessary surgeries, sparing patients significant morbidity and mortality associated with aggressive and futile therapeutic approaches.

Seven of the 11 studies reviewed by Huebner et al.⁶ evaluated the change of therapy management as a consequence of PET imaging (Table 7.2). In a total of 349 patients the pooled change of management rate was 29% (range 20–44%). In the study by Whiteford et al.²³ clinical management based on the results of FDG-PET was changed in 30 patients (30%). Histological analysis and clinical follow-up proved that in 26 cases (26%) FDG-PET had a beneficial effect by upstaging disease from resectable

Table 7.2 Change of management^{6,16,20,24–26}

Author	Year	Change (%)	Patients (n)
Fong	1999	23	40
Whiteford	2000	30	101
Arulampalam	2001	33	42
Huebner	2001	29	349
Strasberg	2001	14	43
Simo	2002	48	120
Kalff	2002	59	102
Lonneux	2002	41	79
Ruers	2002	20	51
Pooled management change		34.9	927

to unresectable ($n = 14$), disproving a positive CT finding ($n = 8$), or detecting a previously unrecognized resectable ($n = 4$) tumor. In four cases false-positive FDG-PET scans had a negative clinical effect, leading to non-therapeutic interventions. Arulampalam et al.¹⁶ reported a change of clinical management in a beneficial manner due to additional information provided by PET in 14 of 42 patients (33%). In nine patients with a negative CT scan, PET detected local recurrence, and in five patients PET allowed a more accurate staging of liver metastases, avoiding futile surgery in three cases. In two other cases (5%) PET led to invasive investigations which had no benefit for the patient.

In a study by Lonneux et al.²⁰ PET correctly modified the disease stage in 33 of 79 patients (41%). In 18 patients recurrence was detected by PET. PET ruled out recurrence in seven patients and upstaged the disease in eight cases, avoiding surgery in seven patients. Kalff et al.²⁴ aimed to confirm the earlier claimed beneficial influence of PET in treatment planning in a prospective study. In a total of 102 patients, an alteration of clinical management was found in 59% (60 patients) of the cases. Three patients were lost to follow-up. In 52 of the 57 evaluable patients, follow-up revealed a beneficial effect of management changes induced by PET. These 52 included seven patients with a true-negative PET scan and 45 patients with a true-positive PET result. In five patients, consisting of one case with a false-positive PET and four studies underestimating disease spread, changes of therapy management had no therapeutic benefit for the patients.

In another study with 120 patients, FDG-PET led to a major management change in 58 (48%) of the referred patients.²⁶ Clinical management changes due to additional information provided by PET had a beneficial effect in 54 (45%) cases. Three patients with a negative PET scan relapsed within 9 months of follow-up, and another one referred for preoperative planning showed no FDG uptake

in a histologically proven lesion. Ruers et al.²⁵ investigated prospectively the value of FDG-PET for treatment planning in candidates for resection of colorectal liver metastases. In ten of 51 patients (20%), additional information provided by PET resulted in a change of clinical management. In six cases, PET detected unresectable metastases (pulmonary: $n = 5$, hepatic: $n = 1$). In two patients, extrahepatic disease, and in another two, hepatic disease, could be ruled out by PET. Regarding the additional information provided by PET in a retrospective analysis, PET revealed a potential change of management in 15 patients (29%). PET and conventional imaging consisting of spiral CT of the lung, abdomen, and pelvis showed discordant results for extrahepatic disease in eleven patients (22%) and for hepatic disease in eight patients (16%). According to follow-up and histological confirmation of discrepant results in PET and conventional imaging, PET resulted in true upstaging ($n = 11$, 22%), true downstaging ($n = 5$, 10%), false upstaging ($n = 1$, 2%), and false downstaging ($n = 2$, 4%). Pooling the data of all reviewed studies with a total of 927 patients shows that additional information provided by PET led to a change of clinical management in around 35% of the cases. All studies are summarized in Table 7.2.

Cost-effectiveness

New techniques must be assessed with respect to efficiency and cost-effectiveness in comparison to already existing strategies. So far, only a few cost-effective analyses of the management of recurrent colorectal cancer based on decision analysis models have been published. Cost calculations of two studies were based on US Medicare reimbursement rates,^{34–38} whereas one other economic analysis was performed from the French national health insurance's perspective.³⁷

Gambhir and co-workers³⁴ compared carcinoembryonic antigen (CEA) + CT with CEA + CT + PET for detecting and restaging patients with suspected hepatic metastases. In comparison to the CEA + CT strategy, the calculations for CEA + CT + PET resulted in savings of \$220 per patient and were accompanied by a calculated gain in life expectancy of 2 days. The study by Park et al.³⁵ also focused on patients with a positive CEA and suspected hepatic recurrence who were potentially curable through surgical hepatic resection. Compared to the CEA + CT strategy, the CEA + CT + PET strategy was higher in mean cost by \$429 per patient, but was associated with a calculated increase of life expectancy of 9.5 days. The incremental cost-effectiveness ratio (ICER) of \$16 437 per life-year gained, calculated by $ICER = (Cost_a - Cost_b) / (life\ expectancy_a - life\ expectancy_b)$, was significantly lower than the maximum ICER (\$50 000 per life-year gained) accepted by many health-care economists as indicating a cost-effective strategy.

Recently, Lejeune et al.³⁷ published a study assessing the cost-effectiveness of FDG-PET in the management of liver metastases of colorectal cancer based on a decision analysis model and survival data provided by the Burgundy Digestive Cancer Registry (France). In contrast to the other two studies, patient selection was based on an abdominal ultrasound with suspicious findings. The CT + PET strategy presented an expected incremental cost saving of \$3213 per patient, mainly caused by a decreasing number of futile surgeries (88% less than CT alone). CT + PET did not generate an additional survival effectiveness compared to CT alone. In conclusion, the use of FDG-PET for diagnosis and staging of recurrent colorectal cancer might prove to be cost-effective, and its introduction into clinical routine economically justifiable.

Methods and limitations

Spatial resolution of PET scanners is lower, compared to morphological imaging techniques such as CT and MR. However, PET possesses specific molecular markers resulting in high lesion-to-background contrasts. One of the consequences of the low spatial resolution is a partial loss of signal in structures which are smaller than twice the resolution of the PET scanner, leading to measured activity concentrations which are lower than the real activity concentration. This effect, described as the partial volume effect, represents one of the main limitations of qualitative and quantitative analysis of PET studies of small anatomical structures. As a result, PET has difficulties in detecting lesions smaller than 1 cm such as small lymph nodes and lesions in the liver and lung.

A wide spectrum of methods and algorithms for the evaluation and interpretation of FDG metabolism signals from PET, ranging from visual analysis to kinetic modeling, are available. For quantitation of FDG metabolism, individual rate constants and uptake kinetics have to be determined, requiring arterial blood sampling or arterialized venous blood sampling simultaneous with dynamic image acquisition or look-up tables. Due to its complexity, kinetic modeling remains mainly limited to scientific investigations. Semiquantitative analysis of static PET images using the standardized uptake value has proved to be suitable for clinical routine. Calculation of the standardized uptake value (SUV) is defined as the ratio of measured activity in the lesion in mCi/ml and the injected dose in mCi/g of body weight. Normalization of the SUV to the body surface area,³⁸ lean body weight,³⁹ and blood glucose level⁴⁰ has been reported. Graham et al.⁴¹ compared, in a study population of 40 patients with colon cancer and liver metastases, complex kinetic modeling methods with simplified quantitative analysis methods of FDG uptake. The best predictor of outcome and best discriminator between

normal tissue and tumor was the Patlak graphical analysis, nevertheless SUV normalized to body surface area also revealed good results. Regarding therapy monitoring, Stahl et al.⁴² investigated the influence of different imaging protocols and SUV normalizations on the prediction of tumor response in a cohort of 43 patients with gastric carcinomas. The SUV decrease was not essentially influenced by any of the methodological variations investigated, demonstrating the robustness of FDG SUV for therapeutic monitoring.

Metabolic response plays a decisive role in therapy monitoring and evaluation of tumor response to therapy. So far, only a reduction of SUV has been taken into account, whereas a change of tumor volume is not included in semiquantitative analyses. The PET–CT technique, combining metabolic and anatomic information, allowing the precise location of FDG uptake, might potentially lead to a more detailed evaluation of changes in therapy response. Comparison of in-line PET–CT, with software fusion of PET and CT, with so-called mental fusion of PET and CT, with PET only, proved superiority of the new in-line devices in staging and restaging of colorectal carcinoma.^{28,30}

Image acquisition in PET scanners takes several minutes per acquisition field of view, during which the patient breathes freely. As a consequence, PET images represent an average of different organ positions during breathing cycles. In contrast, state of the art CT scans are performed in a few seconds, and can be acquired in any desirable state of respiratory arrest.⁴³ Motion artifacts can result in suboptimal co-registration of PET and CT images, leading to breathing-related non-rigid mismatches and possible misinterpretation of lesions, especially in the lung and liver. Respiratory gating, a possible approach to solve this problem, was introduced by Nehmeh et al.,⁴⁴ proving a reduction of respiratory motion artifacts in PET imaging. Another approach reported by Shekhar et al.⁴⁵ was the development of an automated three-dimensional elastic registration algorithm of whole-body PET and CT, correcting non-rigid misalignments as well as improving mechanical registration.

Another limitation of PET relates to false-positive findings. FDG is an excellent tumor-localizing tracer but is not tumor-specific. Benign processes associated with increased glucose uptake include physiologic processes such as brown fat, colonic and gynecologic activity, infectious and inflammatory processes, hyperplastic bone marrow, and rebounding thymic hyperplasia in children and young adults.⁴⁶

Therapy monitoring

Guillem et al.⁴⁷ investigated the prediction of response by FDG-PET to preoperative chemoradiation in patients with rectal cancer. In a cohort of 15 patients, a decrease of $SUV_{max} > 62.5\%$ in the second PET, 4 weeks after completion of chemoradiation, correlated significantly with a

better recurrence-free survival ($p = 0.02$). In a recently published study by Cascini et al.,⁴⁸ early assessment of response to radiochemotherapy by FDG-PET was investigated in 33 patients with locally advanced rectal cancer. Patients underwent FDG-PET scans before start of therapy and twelve days after starting treatment. Retrospective ROC-analysis revealed that a cut-off of 52% SUV_{mean} decrease separated histological responders from non-responders with a high sensitivity, specificity and accuracy as early as twelve days after the start of radiochemotherapy. Wieder et al.⁴⁹ used the amino-acid tracer methionine (MET) to investigate assessment of response to radiochemotherapy in 26 patients with locally advanced rectal cancer. The degree of SUV decrease showed no correlation with histopathological tumor response. In a study of 22 consecutive patients, Amthauer et al.⁵⁰ correlated SUV decrease between the initial FDG-PET and second PET, 2–4 weeks after completion of neoadjuvant radiochemotherapy, with histopathology. Applying a cut-off of 36% SUV decrease revealed a sensitivity of 100% and a specificity of 86% in histopathological response prediction.

Conclusions

FDG-PET and PET–CT imaging in the setting of recurrent colorectal cancer provide a unique opportunity for detecting recurrence, exclusion of distant metastases, and monitoring response to therapy. The combination of morphological information with functional information guarantees functional assessment and whole-body staging within one imaging modality. Particular advantages of PET–CT lie in its ability to assess exact tumor volume and its time saving for the patient in reducing the number of examinations to one scan. Furthermore, additional information provided by PET and PET–CT allows a specific patient and therapy selection, risk stratification, and individual therapy monitoring.

The introduction of new tracers such as [¹⁸F]MISO (misonizadole) and [¹⁸F]FAZA (fluoroazomycinaraabinofuranoside) for hypoxia imaging and [¹⁸F]galacto-RGD (arginine-glycine-aspartate) for angiogenesis imaging make PET a promising non-invasive tool to accurately characterize individual tumor biology and offer the potential to optimize and individualize therapy for cancer patients.^{51–53}

References

1. Krebs in Deutschland, Häufigkeiten und Trends. Berlin: Robert Koch Institut, 2006.
2. Adam IJ, Mohamdee MO, Martin IG et al. Role of circumferential margin involvement in the local recurrence of rectal cancer. *Lancet* 1994; 344: 707–11.

3. Willmanns W, Huhn D, Wilms K. *Internistische Onkologie*. Stuttgart: Georg Thieme, 1994.
4. Djulbegovic B, Sullivan DM. *Decision Making in Oncology: Evidence-Based Management*. New York: Churchill Livingstone, 1997.
5. Ott DJ, Wolfman NT, Scharling ES, Zagoria RJ. Overview of imaging in colorectal cancer. *Dig Dis* 1998; 16: 175–82.
6. Huebner RH, Park KC, Shepherd JE et al. A meta-analysis of the literature for whole-body FDG PET detection of recurrent colorectal cancer. *J Nucl Med* 2000; 41: 1177–89.
7. Saenz NC, Cady B, McDermott WV Jr, Steele GD Jr. Experience with colorectal carcinoma metastatic to the liver. *Surg Clin North Am* 1989; 69: 361–70.
8. Steele G Jr, Bleday R, Mayer RJ et al. A prospective evaluation of hepatic resection for colorectal carcinoma metastases to the liver: Gastrointestinal Tumor Study Group Protocol 6584. *J Clin Oncol* 1991; 9: 1105–12.
9. Phelps ME. Inaugural article: positron emission tomography provides molecular imaging of biological processes. *Proc Natl Acad Sci USA* 2000; 97(16): 9226–33.
10. Higashi K, Clavo AC, Wahl RL. Does FDG uptake measure proliferative activity of human cancer cells? In vitro comparison with DNA flow cytometry and tritiated thymidine uptake. *J Nucl Med* 1993; 34: 414–19.
11. Higashi K, Clavo AC, Wahl RL. In vitro assessment of 2-fluoro-2-deoxy-D-glucose, L-methionine and thymidine as agents to monitor the early response of a human adenocarcinoma cell line to radiotherapy. *J Nucl Med* 1993; 34: 773–9.
12. Flier JS, Mueckler MM, Usher P, Lodish HF. Elevated levels of glucose transport and transporter messenger RNA are induced by ras or src oncogenes. *Science* 1987; 235: 1492–5.
13. Reske SN, Kotzerke J. FDG-PET for clinical use. Results of the 3rd German Interdisciplinary Consensus Conference, 'Onko-PET III', 21 July and 19 September 2000. *Eur J Nucl Med* 2001; 28: 1707–23.
14. Strauss LG, Clorius JH, Schlag P et al. Recurrence of colorectal tumors: PET evaluation. *Radiology* 1989; 170: 329–32.
15. Abdel-Nabi H, Doerr RJ, Lamonica DM et al. Staging of primary colorectal carcinomas with fluorine-18 fluorodeoxyglucose whole-body PET: correlation with histopathologic and CT findings. *Radiology* 1998; 206: 755–60.
16. Arulampalam T, Costa D, Visvikis D et al. The impact of FDG-PET on the management algorithm for recurrent colorectal cancer. *Eur J Nucl Med* 2001; 28: 1758–65.
17. Calvo FA, Domper M, Matute R et al. 18F-FDG positron emission tomography staging and restaging in rectal cancer treated with preoperative chemoradiation. *Int J Radiat Oncol Biol Phys* 2004; 58: 528–35.
18. Dietlein M, Weber W, Schwaiger M, Schicha H. [18F-Fluorodeoxyglucose positron emission tomography in restaging of colorectal cancer]. *Nuklearmedizin* 2003; 42: 145–560. [in German]
19. Kantorova I, Lipska L, Belohlavek O. Routine (18)F-FDG PET preoperative staging of colorectal cancer: comparison with conventional staging and its impact on treatment decision making. *J Nucl Med* 2003; 44: 1784–8.
20. Lonneux M, Reffad AM, Detry R et al. FDG-PET improves the staging and selection of patients with recurrent colorectal cancer. *Eur J Nucl Med Mol Imaging* 2002; 29: 915–21.
21. Mukai M, Sadahiro S, Yasuda S et al. Preoperative evaluation by whole-body 18F-fluorodeoxyglucose positron emission tomography in patients with primary colorectal cancer. *Oncol Rep* 2000; 7: 85–7.
22. Staib L, Schirrmester H, Reske SN, Beger HG. Is (18)F-fluorodeoxyglucose positron emission tomography in recurrent colorectal cancer a contribution to surgical decision making? *Am J Surg* 2000; 180: 1–5.
23. Whiteford MH, Whiteford HM, Yee LF et al. Usefulness of FDG-PET scan in the assessment of suspected metastatic or recurrent adenocarcinoma of the colon and rectum. *Dis Colon Rectum* 2000; 43: 759–67.
24. Kalff V, Hicks RJ, Ware RE et al. The clinical impact of (18)F-FDG PET in patients with suspected or confirmed recurrence of colorectal cancer: a prospective study. *J Nucl Med* 2002; 43: 492–9.
25. Ruers TJ, Langenhoff BS, Neeleman N et al. Value of positron emission tomography with [F-18]fluorodeoxyglucose in patients with colorectal liver metastases: a prospective study. *J Clin Oncol* 2002; 20: 388–95.
26. Simo M, Lomena F, Setoain J et al. FDG-PET improves the management of patients with suspected recurrence of colorectal cancer. *Nucl Med Commun* 2002; 23: 975–82.
27. Beyer T, Townsend DW, Brun T et al. A combined PET/CT scanner for clinical oncology. *J Nucl Med* 2000; 41: 1369–79.
28. Strunk H, Bucerius J, Jaeger U et al. [Combined FDG PET/CT imaging for restaging of colorectal cancer patients: impact of image fusion on staging accuracy]. *Rofo* 2005; 177: 1235–41. [in German]
29. Stollfuss J, Wieder H, Rummeny E, Schwaiger M. [PET/CT for colorectal and hepatic tumors.] *Radiologe* 2004; 44: 1068–78. [in German]
30. Kim JH, Czernin J, Ien-Auerbach MS et al. Comparison between 18F-FDG PET, in-line PET/CT, and software fusion for restaging of recurrent colorectal cancer. *J Nucl Med* 2005; 46: 587–95.
31. Kamel IR, Cohade C, Neyman E, Fishman EK, Wahl RL. Incremental value of CT in PET/CT of patients with colorectal carcinoma. *Abdom Imaging* 2004; 29: 663–8.
32. Cohade C, Osman M, Leal J, Wahl RL. Direct comparison of (18)F-FDG PET and PET/CT in patients with colorectal carcinoma. *J Nucl Med* 2003; 44: 1797–803.
33. Falk PM, Gupta NC, Thorson AG et al. Positron emission tomography for preoperative staging of colorectal carcinoma. *Dis Colon Rectum* 1994; 37: 153–6.
34. Gambhir SS, Valk P, Shepherd JE et al. Cost-effective analysis modeling of the role of FDG PET in the management of patients with recurrent colorectal cancer. *J Nucl Med* 1997; 38: 90–1.
35. Park KC, Schwimmer J, Shephard JE et al. Decision analysis for the cost-effective management of recurrent colorectal cancer. *Ann Surg* 2001; 233: 310–19.
36. Valk PE, Pounds TR, Tesar RD, Hopkins DM, Haseman MK. Cost-effectiveness of PET imaging in clinical oncology. *Nucl Med Biol* 1996; 23: 737–43.
37. Lejeune C, Bismuth MJ, Conroy T et al. Use of a decision analysis model to assess the cost-effectiveness of 18F-FDG PET in the management of metachronous liver metastases of colorectal cancer. *J Nucl Med* 2005; 46: 2020–8.

38. Kim CK, Gupta NC, Chandramouli B, Alavi A. Standardized uptake values of FDG: body surface area correction is preferable to body weight correction. *J Nucl Med* 1994; 35: 164–7.
39. Zasadny KR, Wahl RL. Standardized uptake values of normal tissues at PET with 2-[fluorine-18]-fluoro-2-deoxy-D-glucose: variations with body weight and a method for correction. *Radiology* 1993; 189: 847–50.
40. Calvo R, Marti-Climent JM, Richter JA et al. Three-dimensional clinical PET in lung cancer: validation and practical strategies. *J Nucl Med* 2000; 41: 439–48.
41. Graham MM, Peterson LM, Hayward RM. Comparison of simplified quantitative analyses of FDG uptake. *Nucl Med Biol* 2000; 27: 647–55.
42. Stahl A, Ott K, Schwaiger M, Weber WA. Comparison of different SUV-based methods for monitoring cytotoxic therapy with FDG PET. *Eur J Nucl Med Mol Imaging* 2004; 31: 1471–8.
43. Goerres GW, Burger C, Schwitter MR et al. PET/CT of the abdomen: optimizing the patient breathing pattern. *Eur Radiol* 2003; 13: 734–9.
44. Nehmeh SA, Erdi YE, Pan T et al. Four-dimensional (4D) PET/CT imaging of the thorax. *Med Phys* 2004; 31: 3179–86.
45. Shekhar R, Walimbe V, Raja S et al. Automated 3-dimensional elastic registration of whole-body PET and CT from separate or combined scanners. *J Nucl Med* 2005; 46: 1488–96.
46. Juweid ME, Cheson BD. Positron-emission tomography and assessment of cancer therapy. *N Engl J Med* 2006; 354: 496–507.
47. Guillem JG, Moore HG, Akhurst T et al. Sequential preoperative fluorodeoxyglucose-positron emission tomography assessment of response to preoperative chemoradiation: a means for determining longterm outcomes of rectal cancer. *J Am Coll Surg* 2004; 199: 1–7.
48. Cascini GL, Avallone A, Delrio P, et al. 18F-FDG PET is an early predictor of pathologic tumor response to preoperative radiochemotherapy in locally advanced rectal cancer. *J Nucl Med* 2006; 47(8): 1241–8.
49. Wieder H, Ott K, Zimmermann F et al. PET imaging with [11C]methyl-L-methionine for therapy monitoring in patients with rectal cancer. *Eur J Nucl Med Mol Imaging* 2002; 29: 789–96.
50. Amthauer H, Denecke T, Rau B et al. Response prediction by FDG-PET after neoadjuvant radiochemotherapy and combined regional hyperthermia of rectal cancer: correlation with endorectal ultrasound and histopathology. *Eur J Nucl Med Mol Imaging* 2004; 31: 811–19.
51. Loi S, Ngan SY, Hicks RJ et al. Oxaliplatin combined with infusional 5-fluorouracil and concomitant radiotherapy in inoperable and metastatic rectal cancer: a phase I trial. *Br J Cancer* 2005; 92: 655–61.
52. Beer AJ, Haubner R, Goebel M et al. Biodistribution and pharmacokinetics of the alphavbeta3-selective tracer 18F-galacto-RGD in cancer patients. *J Nucl Med* 2005; 46: 1333–41.
53. Krause BJ, Beck R, Souvatzoglou M, Piert M. PET and PET/CT studies of tumor tissue oxygenation. *Q J Nucl Med Mol Imaging* 2006; 50: 28–43.

Internet links

- <http://www.cancer.gov/cancertopics/types/colon-and-rectal>
<http://www.ccalliance.org/>
<http://www.preventcancer.org/colorectal/>
<http://www.krebsinfo.de/ki/dkg/sleit/kolon/kolon.html>
<http://www.cancerworld.org/>
<http://www.startoncolology.net>

Prostate cancer

Werner Langsteger, Mohsen Beheshti, Reza Vali, Avi Beri, Michael Nader, and Guenter Janetschek

Background

Prostate cancer is the fourth most common cancer worldwide. In men it is the most common malignant tumor, accounting for approximately one-third of all cancer diagnosis; in the United States 230 000 new cases were diagnosed in 2004.¹

Prostate cancer has a variable biology, ranging from indolent low grade to spreading aggressiveness and a tendency to metastasize finally. Characteristically it originates in the peripheral zone. Since this part of the gland is attached to the anterior rectal wall, palpation of the prostate during digital rectal examination (DRE) is a cornerstone in the diagnosis and local staging of prostate cancer. DRE has a sensitivity of 52% and a specificity of 81% for the prediction of organ-confined disease.² In DRE, which is sometimes subjective and poorly reproducible, very often understaging and overstaging will be seen.

According to the pathologic features, impalpable prostate cancers detected by elevated serum prostate specific antigen (PSA) only and those diagnosed by DRE are equivalent in their potential to be indolent (9–10%).³ However, only about 20% of tumors diagnosed by PSA alone have advanced pathologic features, compared with 40% of palpable cancers.

The staging of prostate cancer using clinical examination alone will in 30–60% of patients usually be underestimated.⁴ Patients underestimated for cancer extent may suffer from morbidity of local treatment, with limited therapeutic benefit. For this reason, proper staging estimation is of pivotal importance; nevertheless, a precise staging (Table 8.1) in an individual patient cannot always be obtained.^{5–7}

Prognostic factors

The probability of recurrence after radical prostatectomy is related to the clinical stage, tumor grading in the biopsy specimen, and serum PSA level. In multivariate analysis,

all three of these were found to be independent risk factors for tumor progression after radical prostatectomy.⁸

To obtain an early diagnosis, individual nomograms including PSA, Gleason score (GSc) at biopsy, and clinical stage (at presentation) are used. More than 70% of prostate cancers are diagnosed when the tumor is still within the organ,^{5–7} and in most cases patients die from bone and/or bone marrow involvement.

Staging

Prostate cancer, predominantly a disease of the elderly, is becoming a disease of middle age. In comparison to more advanced metastatic disease, the incidence of localized disease has increased.

Nevertheless, the clinical stage is closely related to the risk of disease recurrence after local treatment. After surgical treatment, 5-year disease progression-free probabilities for non-palpable (T1c) and palpable disease (T2) are 85–90% and 63–85% respectively.^{8–11} In clinical stage T3 prostate cancer (with extraprostatic extension and/or seminal vesicle involvement), surgical treatment has not been widely accepted, due to the potential for incomplete excision of the primary tumor and a high incidence of lymph node metastases.¹² Due to the possibility of occult metastases before diagnosis, patients with clinical stage T3 prostate cancers very often have a poor prognosis. In carefully selected patients with minimal extraprostatic protrusion, seminal vesicle invasion will be seen in 67% and lymph node metastases in 20%.¹³ Seminal vesicle invasion in itself is a strong predicting factor of distant disease progression.

The Gleason grading system (GSc)

Numerous grading systems exist for the pathological evaluation of prostatic adenocarcinoma. In general, cytological features do not play an important role in tumor grading.

Table 8.1 Prostate cancer: TNM and grading system

Primary Tumor (T)				
Tx	cannot be assessed			
T0	no evidence			
T1	clinically unapparent – not palpable or visible by imaging			
	a – incidental discovery, found in < 5% of the gland			
	b – incidental discovery, found in > 5% of the gland			
	c – incidental discovery, elevated PSA and biopsy			
T2	confined within the prostate			
	a – involves one lobe			
	b – involves both lobes			
T3	extends outside the gland			
	a – extracapsular extensions (unilateral or bilateral)			
	b – involves seminal vesicles			
T4	fixed in the pelvis a/o locally invades regional tissue			
Regional Lymph Nodes (N)				
Nx	cannot be assessed			
N0	no nodal involvement			
N1	spread to regional nodes in the pelvis			
Distant Metastasis (M)				
Mx	cannot be assessed			
M0	no metastases			
M1	metastases			
	a – lymph nodes outside the pelvis			
	b – bone			
	c – other sites			
Stage				
Stage 1	T1a	N0	M0	grade 1
Stage 2	T1–T2	N0	M0	grade 2–4
Stage 3	T3	N0	M0	any grade
Stage 4	T4	N0–1	M0–1	any grade

The most widely accepted Gleason grading system is based on the glandular pattern of the tumor. Two architectural patterns, the predominant primary and the most prevalent secondary pattern, are identified and assigned a grade from 1 to 5: 1 is the most and 5 is the least differentiated. Because both patterns have an influence on the prognosis, the Gleason sum is obtained by adding the primary and secondary grades; the minimum score is 2, and the maximum could be 10. Patients with higher biopsy grades mostly have worse pathologic stages. The probability of having lymph node spread is 4% with Gleason 6, 12% with Gleason 7, and 28% with a higher Gleason score on prostate biopsy.¹⁴

PSA

The introduction of widespread prostate specific antigen (PSA) testing in the early 1990s has been associated with

dramatic shifts in the incidence, age, and stage at diagnosis. Currently it is the most commonly used screening method for diagnosis and follow-up management, followed by ultrasound-guided biopsies. PSA is a glycoprotein that acts as a serine protease, and is found almost exclusively in the epithelial cells of the prostate. It is secreted in large quantities into the seminal fluid, responsible for liquefaction of the coagulum. A small amount of PSA is reabsorbed via the ductal epithelial cells into the circulating bloodstream. A disruption of the normal prostatic structure allows a greater amount of PSA to enter the serum. This may occur in benign as well as malignant prostatic diseases. Preoperative serum PSA level and velocity are highly predictive of the risk of progression after radical prostatectomy. Almost 80% of patients with PSA values below 4 ng/ml have pathologically organ-confined disease. In those with PSA levels between 4 and 10 ng/ml approximately 66% have organ-confined cancer, and more than 50% of men with PSA levels above 10 ng/ml have extraprostatic involvement.^{15,16}

About 20% of patients with PSA levels more than 20 ng/ml and the majority of patients (approximately 75%) with PSA levels more than 50 ng/ml have pelvic LN involvement.²

Risk stratification

The results of staging and prognostic evaluation allow the risk posed by each individual's tumor to be assessed. Initially, the risk of progression without treatment is estimated. If treatment is judged to be preferable, a prediction of the outcome of a specific therapeutic intervention is made. Patients with very low-risk tumors might be considered for deferred treatment or watchful waiting, or brachytherapy. Those with intermediate-risk cancers are generally considered for definitive surgery or external-beam irradiation. Patients with high-risk cancers should be considered for combined-modality programs. For those cancers likely to be curable with single-modality therapy, the treatment approach should focus on reducing complications while optimizing cancer control. For aggressive, high-risk cancers, increased toxicity can be justified in an effort to increase the chances of cancer control.

Therapeutic approaches

Definitive treatment in prostate cancer, which is indicated in organ-confined disease, means local tumor ablation. This might be achieved by means of surgery, radiation (internal or external), and cryotherapy. However, the most recognized form of localized prostate cancer treatment is radical prostatectomy.

Treatment directed at eradication of the primary tumor is not likely to affect the prognosis when the disease is no longer organ-confined or metastatic. Reliable adjuvant therapy capable of eradicating extraprostatic disease is currently unavailable.

Surgery

Radical prostatectomy is defined as entire surgical ablation of the prostatic gland and seminal vesicles, followed by urinary bladder neck to urethra anastomosis. The goal of the operation is to excise all the cancer with the least morbidity to continence and potency.

Radical perineal prostatectomy was first performed by Billroth in 1867 and further popularized by Young in 1905.¹⁷ The retropubic approach was pioneered by Millin in 1947.¹⁸ Over the years this technique was adopted by others and modified, but never gained widespread popularity because of poor oncologic outcomes aside from significant

complications of bleeding, incontinence, and impotence. With a large series of anatomic discoveries and variations, Walsh et al. improved the surgeon's ability to remove the entire tumor, thus substantially reducing perioperative morbidity, including functional significance in erectile function.^{19–21} As a result, modern radical prostatectomy provides good cancer control with reasonable morbidity. In the past two decades, shifts in the stage and age on diagnosis of the disease have led to wide popularization of the operation. Today, radical prostatectomy is one of the most frequently performed operations in urology; nevertheless, it should be reserved for men who are likely to be cured and will live long enough to benefit from the cure.

Other therapeutic modalities

In symptomatic advanced prostate cancer, hormone therapy including antiandrogen, luteinizing hormone releasing hormone (LH-RH) agonists, and orchiectomy shows symptomatic relief in the majority of patients.

Realizing high rates of postoperative disease progression after radical prostatectomy, investigators turned to the issue of neoadjuvant therapy prior to surgery. In this context, androgen deprivation therapy was evaluated. Neoadjuvant hormonal regimens lead to a lowering of the PSA level and downstaging of the disease; however, this form of treatment has no influence in long-term follow-up.^{22,23}

Radiation therapy (RT) has been established in the management of prostate cancer in stages 1 and 2. With the introduction of advanced techniques it has become a useful modality in patients who are not primarily scheduled for surgery, especially in cases of distant metastases, high-risk conditions, or by patient request. However, its benefit should be regarded in the light of different complications, such as impotence, incontinence, dysuria, and radiation-induced inflammation (e.g. proctitis).^{24,25}

Recent advances in chemotherapy of metastatic prostate cancer treatment have influenced the investigation of new drugs in neoadjuvant and adjuvant protocols. Cisplatin, 5-FU (fluorouracil), estramustine, mitoxantrone, and docetaxel (Taxotere®) are agents which have been used in different regimens;^{26–28} nevertheless, outcomes of these studies do not yet exist.

Follow-up management

After radical prostatectomy, serum PSA levels should decline to undetectable values. Detectable and rising PSA levels almost always precede clinical recurrence, usually after 6–8 years.^{9,29,30}

After an initial curative therapeutic approach (radical prostatectomy or radiation), recurrences – revealed by a rise in the PSA level – are not uncommon.^{31,32}

To distinguish local recurrence from distant metastases, the velocity of PSA increase is used.^{33,34} The PSA doubling time (DT) provides additional information concerning the course of the disease. This is the time taken for the PSA value to double, based on at least three values separated by at least 3 months each. Semeniuk et al.³⁵ showed in one study that PSA DT serves as an independent prognostic marker for survival in patients with metastatic hormone refractory prostate cancer (HRPC). They concluded that the inclusion of PSA DT with other clinical data could help clinicians to select men at high risk of early mortality who may benefit most from aggressive treatment regimens, such as docetaxel-based regimens.

For patients with histologically organ-confined prostate cancer, 5-year disease-free recurrence determined by measurement of the serum PSA level is greater than 90%.^{8,10} Advanced pathologic grade and stage, involvement of surgical margins, and positive lymph nodes are all independent predictors of postoperative disease recurrence aside from preoperative clinical assessment tools. Extracapsular extension and seminal vesicle and lymph node involvement are associated with descending probability of disease-free survival: 76%, 37%, and 18% progression rate in 5 years, respectively. Positive surgical margins are associated with a 40–74% 5-year progression rate.^{8,36,37}

Nomograms based on pathological characteristics are available for the prediction of tumor progression in a period of 10 years after prostatectomy.³⁸

The sentinel lymph node concept

The concept of the sentinel lymph node (SLN) originally described by Cabanas for penile cancer is based on the assumption that the lymph flow is orderly, sequential, and predictable.³⁹ The SLN is the first lymph node encountered by tumor cells, and a negative SLN excludes distant lymph basin involvement. The concept of radioisotope-guided sentinel lymph node dissection, which has already proved its value for the management of melanoma and breast cancer, has been successfully introduced into prostate cancer management by Wawroschek et al.⁴⁰ They succeeded in using this innovative technique to decrease the morbidity of PLND (pelvic lymph node dissection) while maintaining sensitivity.⁴¹

General aspects

Lymph node status is of crucial significance for the estimation of prognosis and treatment planning in the prostate cancer patient. Unfortunately, at present there is no non-invasive imaging modality that can reliably identify those

individuals with nodal involvement. Surgical staging by way of PLND therefore remains the mainstay of diagnosis of lymph node metastases. At least 26% of patients with small, organ-confined T1c cancer who undergo radical prostatectomy and have negative lymph nodes during standard PLND later develop distant metastases.⁴²

Lymphangiography studies showed that the prostate has three sets of draining vessels. The most important set of lymphatics drains into the internal iliac nodes, which are not routinely dissected.⁴³ Frequently, solitary nodes are also found around the external iliac vessels.

Thus, the so-called ‘standard’ PLND is actually a limited dissection of the obturator fossa only. It is still commonly neglected that primary lymph node metastases may occur on a much larger template. Studer and his group were among the first to clearly demonstrate that the detection rate of small solitary lymph node metastases markedly increases when performing an extended PLND, and almost half of the metastases are missed by a PLND of the obturator fossa only.⁴⁴ Heidenreich et al. also observed a higher incidence of metastases in extended PLND as compared to standard PLND (26% vs. 12%).⁴⁵ Substratifying the risk categories, they noted that 95.8% of patients with lymph node metastases had a preoperative PSA of more than 10.5 ng/ml and a biopsy Gleason score of 7 or more. They concluded that these high-risk patients benefit from the extended template. Stone et al. noted that the incidence of positive lymph node was three times higher (23.1% vs. 7.3%) with extended PLND.⁴⁶

Technical aspects

Prior to surgery, the radioactive tracer technetium-99m (Tc), bound to large particle size colloids, is injected into the peripheral zone of the prostate. The tracer travels to the first lymph node echelon which will be marked by the radioactivity. By means of a γ probe it can be identified and removed during surgery. Provided that the sentinel nodes are negative, further metastases can be excluded. A total of 335 of 350 patients showed at least one sentinel node in lymphoscintigraphy, and 24.7% had lymph node metastases. Only in two of these patients, were metastases found in a node not marked by radioactivity without at least one sentinel node being affected.⁴⁷

PLND is routinely performed in conjunction with radical retropubic prostatectomy. Surgical staging of the lymph node may precede other local treatment modalities, or be performed by a different access in cases of perineal prostatectomy. However, PLND is not recommended as a separate operation except in selected patients with high-grade, high-stage cancer and a markedly elevated serum PSA level who still have a chance of localized disease and in whom retropubic prostatectomy is unsuitable.

Compared to limited dissection, extended PLND is a time-consuming procedure with increased morbidity. Clark et al.⁴⁸ evaluated extended versus limited PLND and stated a trend towards an increased risk of complications after extended PLND. To simplify dissection and reduce morbidity while maintaining the diagnostic accuracy of extended PLND is of substantial clinical interest.

Laparoscopic lymphadenectomy

The ability to gain access to the lymphatic drainage of the prostate gland in a minimally invasive fashion has a major impact on the diagnosis and treatment of prostate cancer.

Laparoscopy for pelvic lymphadenectomy was first described for cervical carcinoma in 1991.⁴⁹ In the same year, Schuessler et al. reported their initial experience in the use of laparoscopic PLND in prostate cancer.⁵⁰

A significant reduction of morbidity as compared to open PLND enables application of the procedure in conjunction with perineal prostatectomy and other forms of definitive prostate cancer treatment. The most important application of laparoscopic PLND is in combination with laparoscopic radical prostatectomy.

Numerous papers have addressed the question regarding the efficacy of the procedure, showing no difference when compared with the open alternative.^{51,52} The complication rate is strictly related to the learning curve and decreases with experience.⁵³ The conclusion of the abovementioned studies was that the laparoscopic approach provides the same staging accuracy as the open surgical technique, and is superior with respect to morbidity.

As shown in our studies (Table 8.2), both extended and sentinel PLND can be performed by a laparoscopic approach.^{47,54–57} The prerequisite, therefore, is the availability of a laparoscopic γ probe with a diameter of 11 mm and a lateral energy window at 90° (Figure 8.1). The detection rate of lymph node metastases (Figure 8.2) was 12.9% in 71 patients with a mean PSA of 8.9 ng/ml; 72.7% of the metastases were outside the obturator fossa. Lymph node metastases were exclusively found in the nodes marked with radioactive tracer (Figure 8.3). The smallest metastasis was 0.2 mm in diameter; additionally several micrometastases were detected. The transperitoneal approach proved superior to the extraperitoneal since exposure of the internal iliac nodes is more precise, and the risk of lymphocele formation lower.

Imaging

Many morphological imaging modalities have been introduced for staging and follow-up reasons. However, early stages of disease will only be detected if structural abnormalities are

seen already. In cases of disease progression and/or in significant structural abnormalities, anatomic imaging techniques will become more and more successful. Nevertheless, in some cases structural abnormalities may never be obvious throughout the course of certain diseases.⁵⁸

Conventional imaging modalities

Transrectal ultrasound

The use of transrectal ultrasound (TRUS) for the local staging of prostate cancer remains controversial. TRUS has a sensitivity of 66%, a specificity of 46%, a positive predictive value (PPV) of 63%, and a negative predictive value (NPV) of 49% in predicting extraprostatic extension of the disease.⁵⁹ However, ultrasound is frequently used to guide biopsy for optimal sampling.

Computed tomography and magnetic resonance imaging for TNM staging

T staging

Recently, molecular expression imaging techniques have been introduced for local staging purposes. Normal prostate tissue is rich in citrate, and prostate cancer contains high levels of choline and often diminished citrate. This is due to conversion from a citrate-producing to a citrate-oxidizing metabolism and a high cell membrane phospholipid turnover in prostate cancer cells. This is behind the application of magnetic resonance spectroscopy (MRS) in diagnosis and local staging of the disease. In combination with pelvic phased array and an endorectal coil, MRI (magnetic resonance imaging) with MRS has a sensitivity of 54% and a specificity of 96% in predicting the extracapsular extension.⁶⁰ Though promising, the major limitations of MRS are cost, availability, and lack of supporting clinical data.

N staging

Imaging is not indicated as a routine staging procedure to search for lymph node metastases in men with clinically localized prostate cancer unless in high-risk patients. Grossly positive nodes are encountered in less than a third of patients with positive nodes and in less than 1% of candidates for radical prostatectomy.⁶¹

Due to the limited sensitivity (< 20 %) of cross-sectional imaging, computed tomography (CT) and MRI are not routinely used for the evaluation of lymph node metastases.^{59,62,63} This is probably because early metastatic lesions from prostate cancer usually take the form of small nodules rather than large metastatic deposits. Nevertheless, it is currently useful in detecting advanced lymphatic spread only.

Table 8.2 Results of sentinel lymph node (SLN) staging in prostate cancer

	Year	Patients (n)	Colloid	Colloid size (nm)	Dose (MBq)	Volume injected (ml)	Injection before operation (h)	Injections to each lobe (n)	SLN detection rate (%)	Dissected nodes (n)	Patients POS (%)
Wawroschek ⁴⁶	2003	350	Nanocoll	80	90–400	2–3	24	1	97	5, 6 (1–17)	24, 7
Takahshima ⁵⁵	2004	24	Phytate		80	0, 2	6	1	87	4, 2 (1–10)	12, 5
Jeschke ⁵³	2005	71	Senti-Scint	100–600	200	2, 0	24	3	97	4, 7 (1–20)	12, 8
Brenot-Rossi ⁵⁶	2005	27	Nanocis	100	60	0, 6	24	1	100	3, 5 (1–9)	15, 0
Haecker ⁵⁴	2006	20	Senti-Scint	100–600	200	2, 0	24	3	90		50, 0

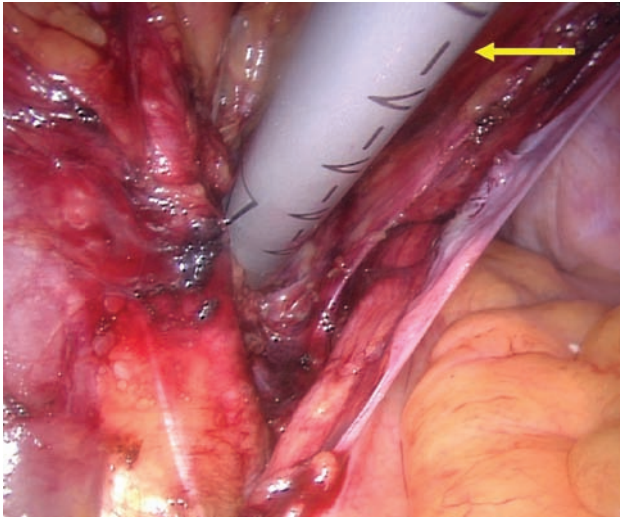


Figure 8.1

Laparoscopic view of pelvic side wall with γ probe scanning (arrow) for sentinel lymph node.

Limitations of these modalities in the imaging of small lesions are well recognized. The probability of detectable lymph node enlargement increases in high-risk patients as defined by clinical prognostic factors. However, one should remember that enlarged lymph nodes in prostate cancer are frequently secondary to regressive or hyperplastic alterations and not to metastatic disease.⁶⁴

Highly lymphotropic superparamagnetic nanoparticles, which gain access to lymph nodes by means of interstitial lymphatic fluid transport, could be used in conjunction with high-resolution MRI for prostate cancer LN staging.

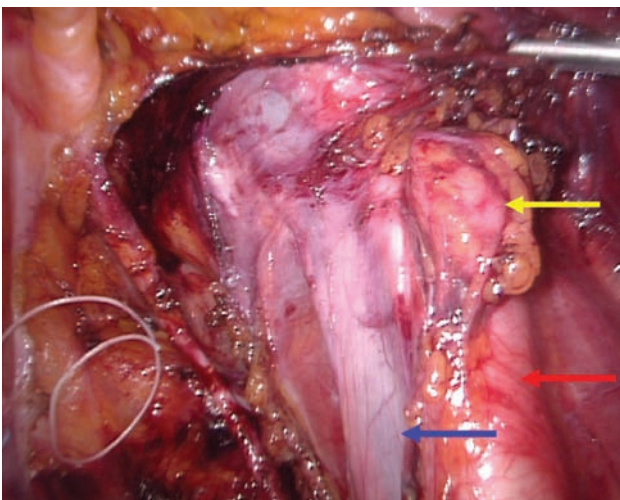


Figure 8.2

Metastatic lymph node (LN) (yellow arrow) attached to the external iliac artery (red arrow) and vein (blue arrow).

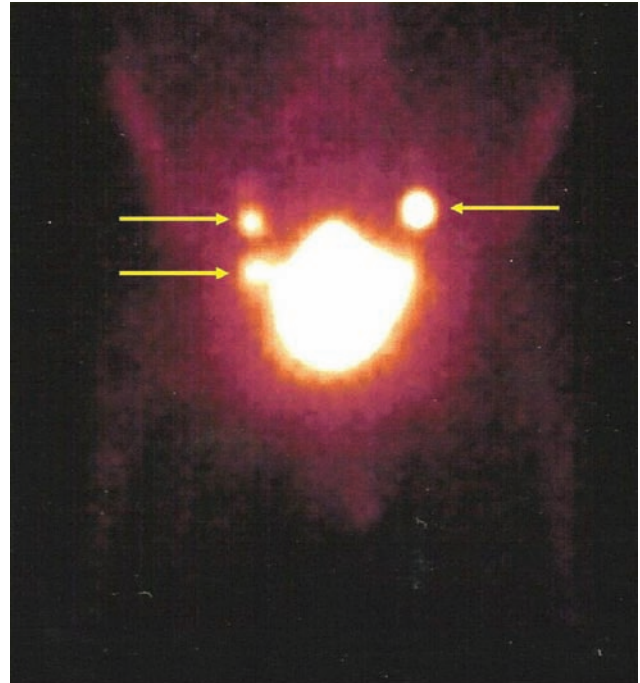


Figure 8.3

Three positive iliac LN metastases (yellow arrows) detected by lymphoscintigraphy.

Limited clinical data available at this time show extremely promising results, with an overall sensitivity of 90.5% in metastatic lymph node detection and of 41.1% in the nodes smaller than 5 mm.⁶⁵

M staging

For staging of distant metastases, CT is used due to its high sensitivity and specificity.^{66–68} In the detection of bone metastases it has only a limited role, and therefore its routine use is not strongly recommended.

A major dimension in the investigation of bone and soft tissue abnormalities, sometimes in combination with multiple organ disorders, was added with MRI.^{69–72} For the detection of vertebral metastases, it is accepted as the most accurate and sensitive (97–100%) imaging modality today,^{73,74} distinctly better for imaging the spinal cord, adjacent soft tissue structures, and bone marrow, than for evaluating bone itself.⁷⁵ MRI is more sensitive than planar bone scintigraphy (BS) in the spine and pelvis, whereas in the skull and ribs BS is more sensitive.^{73,76–78}

Bone scintigraphy in the detection of early metastatic disease has been reported to be superior to radiographs as well as to clinical evaluation, alkaline phosphatase, and acid phosphatase, due to the fact that 15% of patients have no pain and both enzymes at normal levels.⁷⁹ For further evaluation of scintigraphic bone lesions, correlation with CT

and/or MRI is the most common approach, visualizing normal and malignant tissues in great detail.^{80–82}

Nuclear medicine modalities

Radioimmunoscinigraphy

During recent decades, radioimmunotargeting has led to the development of specific agents for applications in both imaging and therapy. Capromab pendetide (ProstaScint®) – conjugated to ¹¹¹indium – is a murine monoclonal antibody which binds to an intracellular component of the prostate specific membrane antigen (PSMA). PSMA is a transmembrane glycoprotein on the surface of prostatic epithelial cells with three recognized extracellular, transmembrane, and intracellular components. The intracellular component⁸³ will only be available when the membrane is disrupted (e.g. dead or dying cells).⁸⁴ This is probably responsible for the limitation of the capromab pendetide scan to detect metastases accurately, especially in bone lesions. Recently, labeling of monoclonal antibodies to the extracellular component of PSMA has been tried as possible second-generation scans that could probably improve the accuracy of detecting extraprostatic disease.⁸⁵ In order to contribute to anatomic localization of revealed lesions, fusion with cross-sectional imaging is gaining increased popularity.

The reported sensitivity, specificity, PPV, and NPV for nodal disease as compared to the results of obturator fossa-limited lymph node dissection are 63%, 72%, 62%, and 72% respectively.⁸⁶ Of note, this study revealed that 14 of 25 patients (56%) showed PSA progression following radical prostatectomy. This suggests that the true positive predictive value may actually be higher than that reported based on limited lymph node dissection. However, in patients with a low probability of pelvic metastases, positive findings should be confirmed using other procedures before changing treatment regimens.

Availability and cost-effectiveness are major limitations for wider clinical application in preoperative staging. On the other hand, due to a normal faint uptake in the intact prostate gland and also in prostate hyperplasia, an evaluation of the local extent of prostate cancer is not yet established. Due to the presence of PSMA, the differentiation of inflammatory changes (after surgery or radiotherapy) from recurrent tumor is also not reliable.

Bone scintigraphy

General aspects of bone metastases

After pelvic lymph nodes, the second most prevalent target of metastatic prostate cancer is the skeleton, where bone

metastases occur in up to 70% of patients.⁸⁷ Therefore, BS is the most commonly used test in patients with suspected recurrent disease. A survey among urologists revealed that 70% order a bone scan in a case of rising PSA levels after radical prostatectomy or radiation therapy.⁸⁸

There are well-known pathophysiological mechanisms clearly showing that the mineralization process of bone formation as well as activated osteoclasts, osteoblasts, cancer, and inflammatory cells coexist in bone metastases. Additional factors such as increasing vascularity in areas of red marrow, as well as tumor cells producing adhesive molecules (binding them to bone matrix and marrow stromal cells), will account for the frequency of bone metastases.¹⁰ Patients can have osteolytic, osteoblastic, or mixed lesions containing both elements.

Currently, the most commonly used tracer for imaging the skeleton in conventional nuclear medicine is methylene diphosphonate (MDP) labeled with ^{99m}Tc. The exact mechanism of this tracer uptake is not fully understood, but it is believed that this compound is chemisorbed onto bone surfaces. The uptake depends on local blood flow and osteoblastic activity. Therefore, there is focal accumulation of this tracer, because nearly all bone metastases are accompanied by an osteoblastic reaction.

Clinical impact

In patients with an abnormal bone scan, the extent of skeletal metastatic disease from prostate cancer is an independent prognostic marker.^{89–91} Lund et al.⁹² were also able to show the prognostic role of skeletal scintigraphy in prostatic carcinoma; they found that patients with an abnormal scan initially have a mortality rate of approximately 45% at 2 years, compared with 20% for those with a normal scan.

In the preoperative management, BS is not required in asymptomatic patients and in those with serum PSA levels < 10 ng/ml, but in symptomatic patients with bone pain and low or raised PSA levels it will be recommended by urologists.⁹³ Nevertheless, in a large retrospective analysis, the yield for bone metastases was less than 1% in patients with PSA < 20 ng/ml: among 306 men only one (PSA 18.2 ng/ml) had a positive bone scan, yielding a negative predictive value of 99.7%.^{94–98}

The value of serum PSA as a marker for patient follow-up is more than established. BS is indicated in the case of any PSA elevation following total prostatectomy,⁹⁹ as well as in patients treated with antiandrogen therapy, since 35% have been reported to have bone metastases with normal PSA levels.¹⁰⁰

For treatment monitoring BS could be misleading, especially if performed too early,^{101,102} due to an intense osteoblastic response following successful therapy – the ‘flare’ response.

Bone metastases that are not detected in bone scintigraphy may be explained due to an absence of reactive changes

and/or slow-growing lesions, in which reactive bone is not detectable.^{105–106}

Planar and SPECT techniques

Especially in elderly patients, FP (false positive) scintigraphic findings are common in benign bone diseases (inflammatory processes, trauma, degenerative changes, Paget's disease, etc.). Mostly, experienced readers will provide a clear-cut diagnosis; nevertheless, in some cases additional diagnostic procedures are required.

In several studies it could be shown that the sensitivity of BS could be improved by additional single photon emission computed tomography (SPECT) imaging.^{74,106,107} Particularly in the detection of lesions in the posterior vertebral region, SPECT is superior; on the other hand it is less evident in the body of the vertebra.¹⁰⁸ Nevertheless, definitive clinically relevant data for this issue are not yet published.

Conventional planar γ camera imaging as well as SPECT is a routine, but still powerful, imaging technique. However, due to recent findings we expect both to be much less frequently used at the end of this decade. For the detection of bone abnormalities we assume that [¹⁸F]fluoride PET will replace completely conventional bone imaging with ^{99m}Tc-labeled diphosphonates within the next few years.^{58,109}

Radiopharmacy of prostate cancer: positron emission tomography-tracers

Positron emission tomography (PET) is considered a new modality for metabolic tumor imaging. The design of the corresponding PET-radiopharmaceuticals is based on different metabolic models showing a specific alteration in prostate cancer.

[¹⁸F]fluoro-2-deoxy-D-glucose

[¹⁸F]fluoro-2-deoxy-D-glucose (FDG) was first introduced in 1976. FDG is transported in cancer cells by GLUT1 (glucose transporter protein) and is then phosphorylated by hexokinases (HK2) to FDG-6-phosphate, which is retained within the malignant cells, due to the increased glucose metabolism of tumors.

[¹⁸F]FDG has been used as the 'workhorse' of PET imaging for more than 30 years, and can therefore be regarded as a well-established radiopharmaceutical. Its preparation is mostly based on sterile disposable kit systems which allow multiple high-scale productions. Furthermore, the quality control of [¹⁸F]FDG has been standardized in

monographs of the European Pharmacopoeia as well as the United States Pharmacopoeia (USP).

The first studies with labeled glucose and prostate tumors started at the end of the 1990s. There are many limitations in the results of these studies due to renal excretion, which produces an accumulation in the urinary tract and does not correctly show the prostate zone and locoregional lymph node.⁹⁴ In general, well-differentiated prostate cancer has, because of the low expression of GLUT1 transporters, a lower glucose utilization than many other tumor types.¹¹⁰ The urinary excretion of [¹⁸F]FDG combined with the close proximity of the prostate to the bladder, with its intense accumulation of [¹⁸F]FDG, results in difficulties in diagnosing primary prostate cancer.¹¹¹

However, since the imaging of prostate cancer based on glucose metabolism is connected with several disadvantages, leading to many misinterpretations, investigators have focused their interest on the development of PET-tracers related to alternative metabolic approaches.

¹¹C- and ¹⁸F-labeled choline derivatives

Since ³¹P magnetic resonance spectroscopy in vivo and in vitro has revealed an elevated level of phosphatidylcholine in tumors, which is the most abundant phospholipid in the cell membranes of eukaryotic cells, it is thought that this elevation is the result of increased uptake of choline, a precursor of the biosynthesis of phosphatidylcholine. Thus, Hara et al.¹¹² successfully used [¹¹C]choline (CH) in identifying locally extensive prostate cancer and associated metastases, compared with [¹⁸F]FDG. Choline is a quaternary ammonium base which, in the first step of its metabolic pathway, is phosphorylated to phosphorylcholine under the catalysis of choline kinase, utilizing adenosine triphosphate (ATP). Choline kinase is widely distributed in tissues such as the brain, liver, and lung. In a further step, phosphorylcholine is converted to cytidine diphosphate (CDP) – choline catalyzed by cytidine triphosphate (CTP) by means of phosphocholine cytidyltransferase. The two alternative pathways consist of enzyme-catalyzed oxidation or acetylation of free choline. Following the oxidation pathway, choline is oxidized to betaine aldehyde, which is mainly converted to betaine in the liver and kidneys by choline oxidase. Just a small amount of the choline is acetylated via acetyl coenzyme A to the neurotransmitter acetylcholine, catalyzed by choline acetyltransferase, which is highly concentrated in the cholinergic nerve terminals. Roivainen et al. studied the biodistribution and metabolism of CH in rats and humans.¹¹³ They could show that, after an initial rapid metabolism, the ratio of CH and [¹¹C]betaine, which was the major metabolite, remained constant after 20 min. The late clearance pattern was attributed by

Roivainen et al. to reflect the metabolism of CH to [^{11}C]betaine and the subsequent clearance of the latter by the urinary system, because most ^{11}C in arterial plasma is in the form of [^{11}C]betaine > 5 min after administration. Although most of the circulating CH in blood is transported to tissues, it did not disappear totally from the blood during the study time of 40 min PET imaging. The practical advantages of working with the longer lived radioisotope ^{18}F (half-life 110 min) led Hara et al. to synthesize and evaluate the choline analog [^{18}F]fluoroethylcholine (FECH).¹¹⁴ In vitro experiments showed an incorporation into tumor cells by active transport, intracellular phosphorylation, and a final integration into phospholipids.

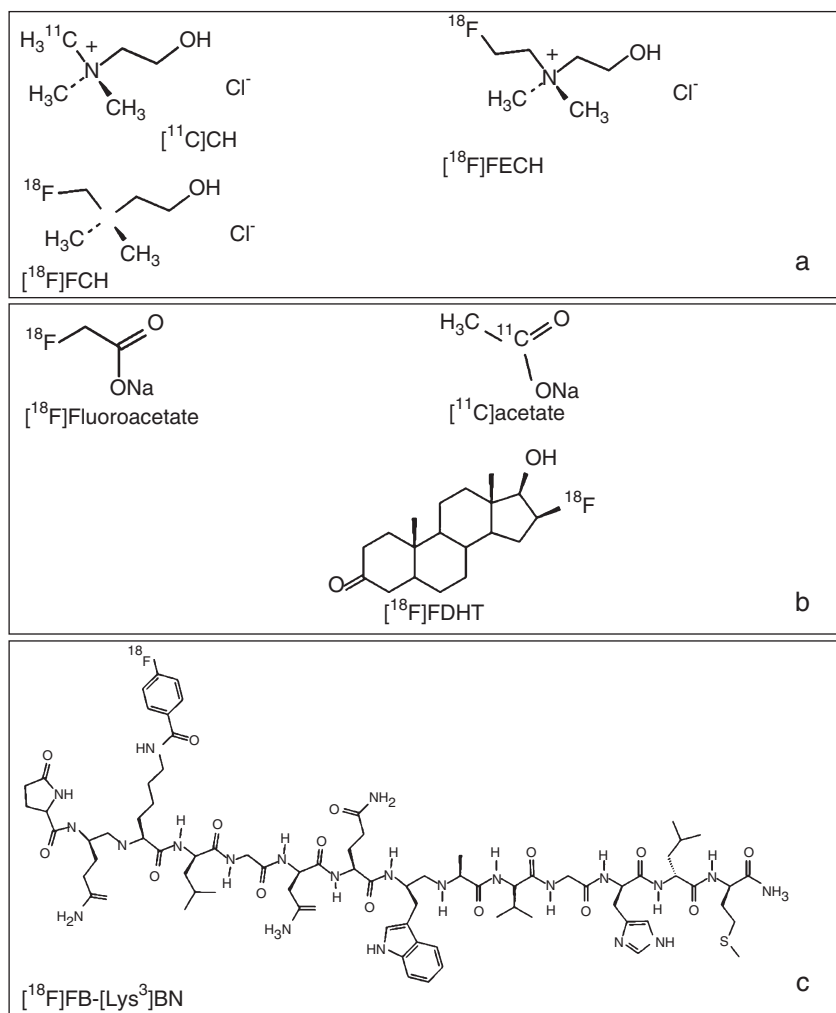
DeGrado et al.¹¹⁵ developed an ' ^{18}F -fluoromethylated' choline derivative (H atom of choline substituted by ^{18}F), anticipating that this tracer would mimic choline transport and metabolism more closely than FECH because of its structural similarity, with lower excretion of ^{18}F radioactivity. In fact, an increased uptake of [^{18}F]choline (FCH) has been shown in PC3 prostate cancer cells compared to FECH.

Furthermore, DeGrado et al. measured the in vitro phosphorylation rates of FCH and FECH using yeast choline kinase, and showed that the phosphorylation rate of FCH was comparable to that of choline, whereas the phosphorylation rate of FECH was 30% lower. Bender et al.¹¹⁶ compared both derivatives, and reported a 1.5–3 times higher uptake of FCH in known metastases, but also in normal organs (1.2–2.5) as compared to FECH. Both ^{18}F -labeled choline derivatives (Figure 8.4a) have a significant urinary excretion.

In general, the production of all choline derivatives is based on the alkylation of dimethylaminoethanol (DMAE), either in solid phase or in a reactor system. CH is synthesized by the ^{11}C methylation of DMAE on a ^{18}C solid phase, and the final product is purified by a cation exchange cartridge followed by formulation in saline.^{112,117} In a similar way, Hara et al.¹¹⁴ described the synthesis of FECH by the production of [^{18}F]fluoroethyltosylate and subsequent fluoroethylation of DMAE in a reaction vessel. The final product is purified by high performance liquid chromatography (HPLC) separation.

Figure 8.4

Structural formula of [^{18}F]choline (FCH) (a), 16 β -[^{18}F]-fluoro-5 α -dihydrotestosterone (FDHT) (b), and ^{18}F -labeled bombesin (c).



The synthesis of FCH starts with synthesis of the ^{18}F -fluoromethylation agent [^{18}F]fluoromethylbromide by the reaction of [^{18}F]fluoride with dibromomethane, followed by conversion of the intermediary to the more reactive [^{18}F]fluoromethyltriflate.¹¹⁸ Afterwards, DMAE is fluoromethylated in solid phase and the final product is purified as described for CH. Meanwhile, the synthesis process could be fully automated and integrated in a sterile disposable kit system.¹¹⁹ The quality control of all choline derivatives is performed analogously. The radiochemical purity of CH, FECH, and FCH is determined by HPLC. A central point in the quality control of both tracers is the quantitation of DMAE, which is proposed to be performed by either HPLC or gas chromatography.

[^{11}C]acetate

Another approach to the molecular imaging of prostate cancer is using the malignant transformation of the specific citrate metabolism of prostate epithelial cells.¹²⁰ The normal human prostate gland is producing, accumulating, and secreting extraordinarily high levels of citrate. This is a unique capability, which does not exist in any other soft tissue cells of the body. Furthermore, citrate-producing prostate epithelial cells exhibit an extremely low capability for oxidizing citrate due to a limiting mitochondrial m-aconitase activity that results in a truncated Krebs cycle. m-Aconitase is generally described as catalyzing an equilibrium between citrate via cis-aconitate and isocitrate, and this is not a rate-limiting reaction. Consequently, a rate-limiting m-aconitase activity is the most metabolic characteristic of these cells, and the equilibrium is significantly shifted in the direction of citrate. As a result, the supply of substrate for citrate oxidation is hampered, and just 40% of the usual energy in the form of ATP can be provided, which means that the main task of epithelial prostate cells is the secretion of citrate. Malignant prostate epithelial cells undergo a metabolic transformation from citrate-producing normal cells to citrate-oxidizing malignant cells. This alteration leads to an increased turnover of acetate again. Opposite to this mechanism, Yoshimoto et al.¹²¹ suggest that acetate is incorporated into the lipid pool in cancer tissue with low oxidative metabolism and high lipid synthesis. They showed that tumor cells incorporated [^{11}C]acetate into the lipid soluble fraction, mostly consisting of phosphatidylcholine and neutral lipids. These data suggest that the acetate accumulation was caused by enhanced lipid synthesis. The preparation of [^{11}C]acetate was already described in the early 1980s, where methylmagnesium bromide was carboxylated with [^{11}C]carbon dioxide, followed by hydrolysis with HCl and ether extraction.^{122,123} Several procedures for the radiosynthesis of [^{11}C]acetate have been presented in subsequent years, all based on the

^{11}C -carboxylation of magnesium halides. The published procedures mainly differ in the isolation method of the resulting [^{11}C]acetate. Isolation methods were described as liquid-liquid extraction^{122,124} or – avoiding this troublesome procedure – as column extraction through anion-exchange columns, Kieselguhr columns,¹²⁵ commercial cartridges,¹²⁶ or on specially designed AG11A8- ^{18}C columns. A further isolation method is the distillation of [^{11}C]acetate into aqueous buffer solutions.¹²⁷

[^{18}F]fluoroacetate

Similar to other ^{11}C tracers, sodium [^{18}F]fluoroacetate has been developed as a longer living analog of [^{11}C]acetate to facilitate diagnostic studies by PET. Sodium fluoroacetate is well known as a salt with very high mammalian toxicity, and is often used as a rodenticide or insecticide.¹²⁸ This salt is metabolized to fluorocitrate, which cannot be further metabolized to carbon dioxide, and blocks the tricarboxylic acid cycle of the Krebs cycle in the body and might therefore accumulate in proportion to oxidative metabolism.^{129–130} A toxic effect by using the ^{18}F -labeled analog cannot be expected since the tracer is prepared carrier-free. Recent studies using sodium [^{18}F]fluoroacetate as a tumor imaging agent have been reported, and the results suggested that defluorination of sodium [^{18}F]fluoroacetate was species dependent and occurred in rodents but not in primates.¹³² Sodium [^{18}F]fluoroacetate has also been reported to be a useful PET tracer for prostate cancer imaging.¹³³ In the past decade, several groups reported the synthesis of [^{18}F]fluoroacetate starting from either O-mesyl glycolate or O-tosyl glycolate, which react with potassium [^{18}F]fluoride/Kryptofix® 2.2.2, followed by hydrolysis with aqueous sodium hydroxide solution and HPLC purification. Sun et al.¹³⁴ were able to automate the synthesis and to integrate the production of [^{18}F]fluoroacetate into a sterile, disposable kit system.

16β -[^{18}F]fluoro- 5α -dihydrotestosterone

PET has also been used to analyze androgen receptors (ARs) and their impact on the clinical management of prostate cancer by using 16β -[^{18}F]fluoro- 5α -dihydrotestosterone (FDHT). A reliable and practical in vivo method is needed to better understand the mechanism of progression of prostate cancer and to determine the activity levels of ARs in order to monitor therapeutics that target ARs. FDHT has been shown to accumulate in the prostate gland of non-human primates. In addition, the biodistribution and radiation dosimetry of FDHT in non-human primates

suggest that this agent holds promise for studying ARs in human prostate carcinoma.¹³⁵

FDHT (Figure 8.4b) has been synthesized by nucleophilic substitution of the corresponding trifluoromethane sulfonate precursor, reduction by lithium aluminum hydride, and subsequent HPLC purification.

Labeled bombesin derivatives

The bombesin/gastrin-releasing peptide (GRP) receptor is overexpressed on prostate cancer cells, and has been the target for the imaging of prostate cancer. Rogers et al.¹³⁶ introduced [⁶⁴Cu]DOTA-Aoc-bombesin (DOTA is tetraazacyclododecanetetraacetic acid, and Aoc is 8-aminooctanoic acid) as the first radiolabeled bombesin (BN) analog suitable for PET. Micro-PET images showed good tumor localization in a PC3 xenograft mouse model, but high retention in normal tissues prevented clinical application of corresponding radiotracer. The incorporation of polyethylene glycol (PEG) linker resulted in significantly reduced receptor avidity and lower receptor-specific accumulation.¹³⁶ Chen et al.¹³⁷ reported the synthesis and pharmacologic evaluation of [⁶⁴Cu]DOTA-Lys³-BN in PC3 and 22RV1 tumor models, observing a fast washout of activity from PC-3 tumors. Schuhmacher et al.¹³⁸ synthesized [⁶⁸Ga]DOTA-PEG2-D¹³Tyr⁶-β-Ala¹¹-Thi¹³-Nle¹⁴-BN(6–14) amide (BZH3), which is conjugated with the macrocyclic chelator DOTA through a PEG2 linker and labeled with generator produced ⁶⁸Ga. They investigated the tracer imaging of AR4-2J rat pancreatic cancer-bearing nude mice and reported a clear delineation of tumors in the mediastinal area by means of [⁶⁸Ga]-BZH3. Recently, Zhang et al.¹³⁹ achieved the synthesis of ¹⁸F-labeled Lys³-BN and aminocaproic acid-bombesin(7–14) (Aca-BN(7–14)) by coupling the Lys³ amino group and Aca amino group with N-succinimidyl-4-[¹⁸F]fluorobenzoate ([¹⁸F]-SFB) as prosthetic group. It has been shown that [¹⁸F]FB-Lys³-BN is superior to [¹⁸F]FB-Aca-BN(7–14) in terms of GRP receptor avidity, receptor-mediated internalization rate, intracellular retention, tumor-targeting efficacy, and in vivo pharmacokinetics. Although [¹⁸F]FB-Lys³-BN (Figure 8.4c) is relatively metabolically unstable, dynamic PET scans demonstrated the ability of this tracer to visualize both subcutaneous and orthotopic PC3 tumor in murine xenograft models.

Future perspectives

Some new PET-radiopharmaceuticals and their corresponding derivatives have been developed in recent years for the diagnosis and staging of prostate cancer which are based on different metabolic models. However, efforts need to be

made to evaluate and compare these tracers with respect to their efficacy. Furthermore, approximately 80–90% of prostate cancers are androgen dependent at initial diagnosis, whereas some aggressive forms of prostate cancer have lost the expression of the androgen receptor. Although this receptor is the main target of prostate cancer therapy, its outcome remains uncertain. Thus, the design of new, more suitable PET-tracers for the prediction and monitoring of antiandrogen therapy should be a major goal for the future.

PET and PET–CT imaging

General aspects

Within the past 10 years PET has become one of the most important and innovative clinical applications in oncology. In comparison with CIM (conventional imaging modalities) such as CT, ultrasound (US), MRI, etc., PET has many important advantages. PET images have higher resolution and provide three-dimensional anatomical information,¹⁴¹ thus leading to superior sensitivity and specificity compared with conventional planar and SPECT techniques. Even with persisting high costs, PET is almost routinely used in the clinical management of certain cancer patients.^{141–143}

New, combined in-line PET–CT scanners are providing more detailed and precise CT anatomic localization of tumor lesions, especially in the skeletal system. In a recent study, PET–CT was able to clearly differentiate benign from malignant lesions in the majority of cases, even when only low-dose CT was performed.¹⁴⁴ With the newest CT scanner development (e.g. 64 slices) an increasing number of additional and/or unexpected tumor lesions will be detected and more easily visualized.¹⁴⁵

From the clinical point of view in PET imaging, more and more radiopharmaceuticals are now available for detecting different cancers. [¹⁸F]FDG has proved to be sensitive, specific, and also cost-effective.¹⁴⁶ Additionally, [¹⁸F]fluoride as a non-specific bone tracer is also widely accepted in daily clinical routine.⁸⁰

In the clinical setting of PET scanning, the semiquantitative parameter SUV (standardized uptake value) – which represents the tissue activity within a region of interest (ROI) corrected for the injected activity and for patient weight or lean body mass – is most widely used.^{147–150} For measuring the true tissue activity in attenuation corrected (AC) images a transmission scan is required.

[¹⁸F]FDG

Increased glycolysis in cancer cells is directly associated with the accumulation of FDG in PET imaging. FDG is most

effectively trapped by tumors with slow or absent dephosphorylation, due to the fact that malignant lesions have a higher glycolytic rate than normal tissue.¹⁵¹ Moreover, FDG accumulation is increased in tumor hypoxia through activation of the glycolytic pathway.¹⁴⁶

However, there is no clear relationship between defined biochemical alteration in glycolysis processes and FDG uptake in prostate cancer.^{152,153} Early studies with FDG-PET were disappointing due to the fact that in prostate cancer a low FDG accumulation was generally demonstrated. These unsatisfactory results might be due to the urinary excretion of FDG, increased uptake in benign prostatic hyperplasia (BPH), and/or inflammatory processes. Moreover, older reconstruction techniques or PET systems and/or the lack of appropriate patient selection were further limitations.^{154–156}

However, higher FDG uptake in tumors with higher Gleason score and close correlation between PSA level and FDG uptake were shown in some clinical¹⁵⁷ and in vitro studies.^{158,159} FDG might sometimes be suitable for prostate imaging in carefully selected patient groups when using adequate imaging techniques (iterative reconstruction, segmented attenuation correction, and application of PET–CT imaging).^{78,109,160,161} Although some involved regional lymph nodes show abnormal FDG uptake, it is not reliable enough for use in preoperative assessment.⁹⁴

In 17 patients with progressive metastatic prostate cancer, Morris et al.¹⁶² showed that FDG was able to discriminate active from quiescent osseous lesions. Finally, FDG-PET – which is generally known to be highly effective in the early detection of bone marrow metastases – could be useful for the evaluation of lymph node and distant metastases in advanced disease (Figures 8.5 and 8.6).

¹¹C]acetate

Due to the lack of urinary excretion and the good tumor/background ratio, [¹¹C]acetate has also been used for the imaging of prostate cancer during the past few years.^{159,163–166} Shreve et al.¹⁶⁴ suggested acetate as a potential and more suitable tracer for the imaging of the genitourinary system. Although many mechanisms were introduced for the accumulation of acetate in malignant cells (see section on ‘Radiopharmacy’ above), the final pathway is still unclear. However, acetate also accumulates in BPH.

The relationship between the intensity of acetate uptake in prostate cancer and PSA is unclear.^{159,166} When comparing SUVs, no significant differences could be shown between the normal prostate of older subjects and patients with proven prostate cancer, thus being unreliable for preoperative staging.



Figure 8.5

[¹⁸F]fluoro-2-deoxy-D-glucose (FDG)-positron emission tomography–computed tomography (PET–CT): multiple LN metastases (cervical, mediastinum, retroperitoneal, pelvis) in a patient with postoperatively increasing prostate specific antigen (PSA) values (after hormone and chemotherapy). Current PSA 8.0 ng/ml.

Some studies evaluated also the potential role of [¹¹C]acetate-PET in the detection of prostate cancer recurrence.^{165,166} In operated patients with PSA values below 3 ng/ml it also showed a low sensitivity and discouraging results.¹⁶⁵ These results could be due to methodological limitations such as the absence of SUV measurement and the low number of histological confirmations, as shown by Dimitrakopoulou-Strauss and Strauss.¹⁶⁷

Nevertheless, recent published data showed that it might have a significant potential for the detection of recurrences¹⁶⁸ when using more advanced PET-CT instrumentations.

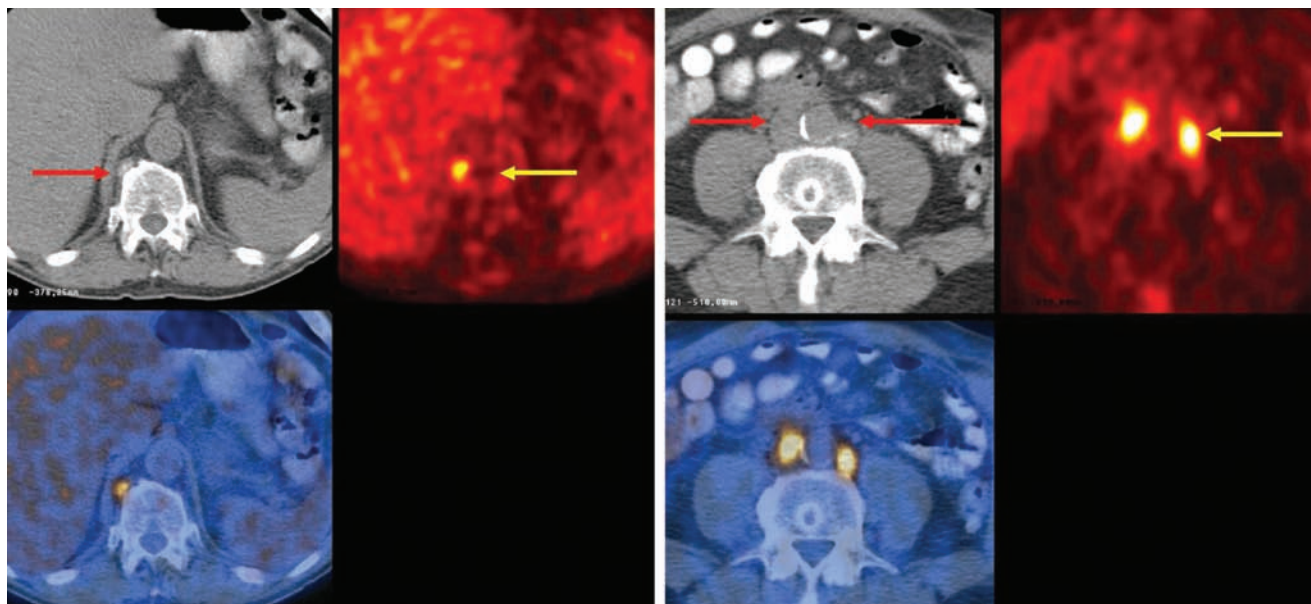


Figure 8.6

FDG-PET-CT (axial slices): in the same patient retrocrural (left) and para-aortal LN metastases (right).

$[^{11}\text{C}]$ choline

CH was first introduced by Hara and co-workers for the imaging of prostate malignancies;^{112,169–171} nevertheless, it also accumulates in BPH and inflammation. The rapid blood clearance of $[^{11}\text{C}]$ choline (approximately 7 minutes) allows imaging as early as 3–5 minutes after injection, and provides images of good diagnostic quality.^{112,169–171}

In prostate cancer, de Jong et al. used $[^{11}\text{C}]$ choline for the detection of recurrences after surgery or radiotherapy. The site of recurrence was detected correctly in 78% of the patients after external beam radiotherapy, compared to 38% postoperatively.⁸⁸ In a second series the accuracy of $[^{11}\text{C}]$ choline PET in the preoperative staging of pelvic lymph nodes was shown.⁸⁸

Although it was previously published that $[^{11}\text{C}]$ choline PET-CT cannot reliably distinguish between benign changes and malignant disease,¹⁷² Reske et al. were able to show, in a recent study, a clear differentiation between prostate cancer and benign processes (BPH or chronic prostatitis). In that study, the SUV_{max} correlated significantly with T stage but not with PSA or Gleason score.¹⁷³

$[^{18}\text{F}]$ choline

Recent successful labeling of choline compounds with ^{18}F overcomes the limitations of ^{11}C (e.g. short half-life of 20 minutes). $[^{18}\text{F}]$ fluoroethylcholine (FECH)

and -fluoromethyl-dimethyl-2-hydroxyethylammonium (fluorocholine, FCH) are two ^{18}F -labeled choline tracers which are currently used in PET imaging.^{114,115,174,175} Both compounds show rapid blood pool clearance, appearing in the urinary bladder 3–5 minutes after injection. The highest activity of FECH concentration occurs at 55 minutes post-injection,¹¹⁴ whereas FCH uptake shows a peak of activity at about 3 minutes post-injection followed by a plateau.¹¹⁵ It is unclear whether this difference would be clinically relevant, because beyond 5–8 minutes post-injection, the increasing accumulation of excreted tracer in the urinary bladder exceeds activity in the prostate and may interfere with visualization of abnormalities in the prostate (similar to FDG). This is in contrast to $[^{11}\text{C}]$ choline, which shows only small urinary excretion, and therefore lower activity in the bladder. It has been suggested that early urinary appearance of $[^{18}\text{F}]$ choline compounds is caused by incomplete tubular resorption of intact tracer, or by enhanced excretion of oxidized metabolites.¹¹⁵

Physiologically, FCH accumulation is seen in the salivary gland, lung, liver, kidneys, adrenal glands and also immediately post-injection in the bowel (Figure 8.7). In prostate cancer, in lymph node and/or bone metastases an intense tracer accumulation will be seen even 1 minute post-injection.

Some studies are now underway performing early dynamic acquisition 1 minute after injection of $[^{18}\text{F}]$ choline, which is supposed to overcome the abovementioned limitations. In particular, it could be useful to differentiate focal tracer activities in the ureters against tumor infiltrated lymph nodes (Figure 8.8).



Figure 8.7

Physiological distribution of $[^{18}\text{F}]$ choline to renal cortex, liver, spleen, bowel, pancreas, and salivary glands.

Our group evaluated the potential value of $[^{18}\text{F}]$ choline PET-CT for preoperative staging of patients with prostate cancer. FCH-PET-CT was performed consecutively in 103 patients with biopsy proven prostate cancer. However, in our series, the sensitivity for the detection of pelvic lymph node metastases > 5.0 mm in diameter was 63%, with a specificity of 99%.^{176,177} The PPV and NPV in that series were 83% and 96% respectively. Furthermore, due to lymph node and/or bone metastases, seven of 103 patients were upstaged with FCH-PET, with concomitant changes in the therapeutic management; instead of surgery, radiation or hormone therapy was performed.

In conclusion, the authors believe that for preoperative staging, choline-PET might be an effective method for evaluation of regional lymph node and distant metastases; nevertheless, further studies are essential to validate its accuracy.

Similar to FDG,¹⁰⁹ the choline uptake under hormone (e.g. antiandrogen) therapy or chemotherapy (Figure 8.9) is sometimes markedly reduced (this is also seen in bone metastases). In patients who have already received hormone therapy PSA level is likely to be suppressed, and may not correlate well with tumor size or metabolism. Although there are reports of choline uptake decreasing after initiating hormone therapy,¹⁷⁸ we do not know whether the influence on choline metabolism and on PSA level occurs in parallel. It cannot be ruled out that the FCH-PET signal is influenced less strongly than the PSA level.

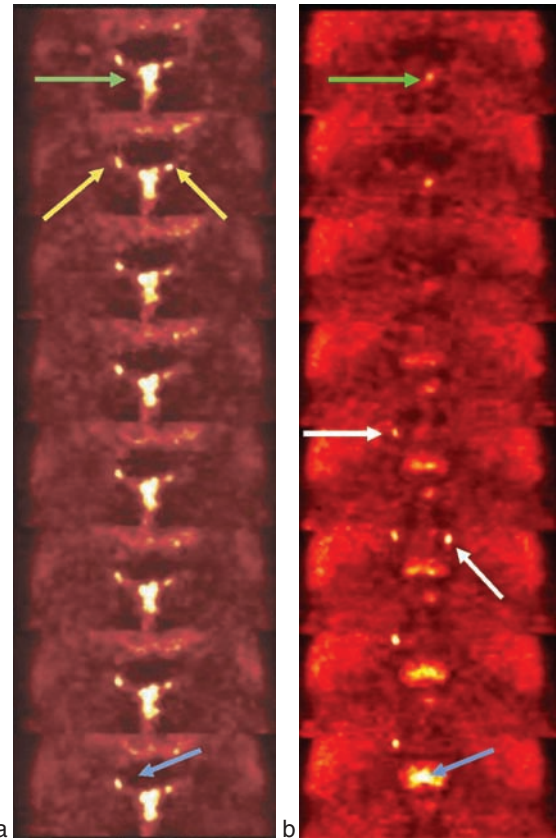


Figure 8.8

FCH-PET-CT (dynamic images). (a) Green arrow: intense FCH uptake in minute 1 in prostate cancer; blue arrow: still no FCH secretion in the urinary bladder (minute 8); yellow arrows: FCH uptake on both sides (minute 1) in the pelvic region due to iliac LN metastases. (b) Green arrow: small focal FCH uptake in minute 1 in prostate cancer; blue arrow: urinary bladder uptake (minute 5) of FCH; white arrows: FCH uptake on the right (minute 5) and on the left (minute 6) in the pelvic region due to ureter activity.

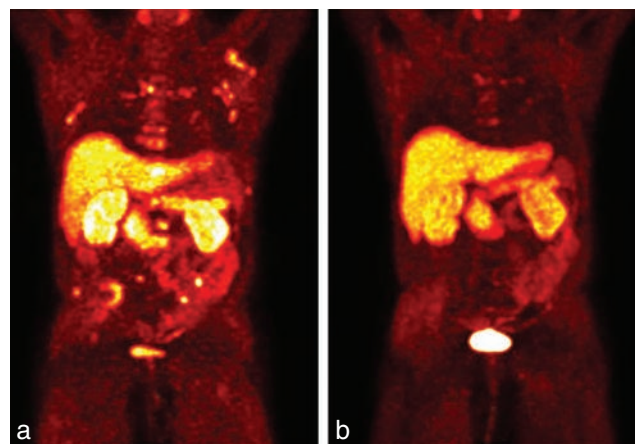


Figure 8.9

FCH-PET-CT: significant decrease of FCH uptake before (a) and 3 months after (b) chemotherapy (docetaxel) in a patient with prostate cancer. Current PSA 170 ng/ml.

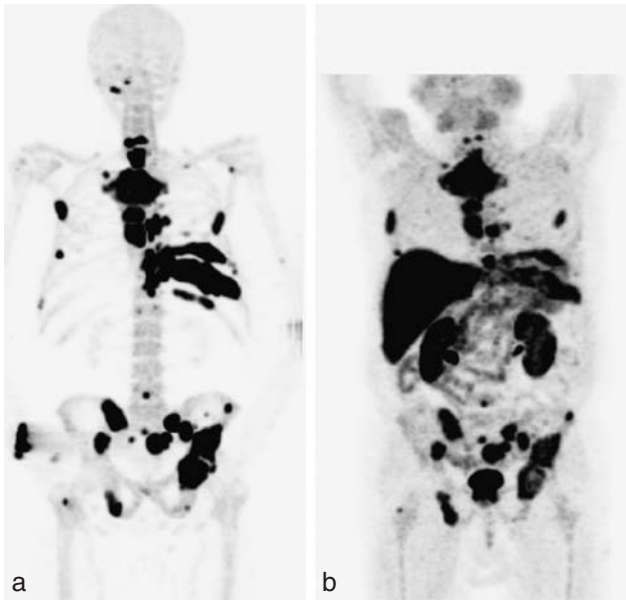


Figure 8.10

Comparison of FCH- (a) and $[^{18}\text{F}]$ fluoride-PET-CT (b): multiple bone metastases in a patient with postoperatively increasing PSA values (after hormone and chemotherapy). Current PSA 79.2 ng/ml.

In follow-up management, FCH-PET-CT seems also to be a suitable tool for detecting local recurrences and/or distal metastases. In 113 cases of elevated PSA levels, FCH-PET-CT was performed; in 20% lymph node, in 15% bone (Figure 8.10), and in 8% lymph node and bone metastases

were diagnosed.¹⁷⁷ In our experience, in almost all cases with bone metastases there was an increase in the SUV when comparing early and late (approximately 120 minutes post-injection) FCH images¹⁷⁹ (Figure 8.11).

Although de Jong et al.⁸⁸ raised the question whether the use of FCH-PET after initial therapy should be restricted to patients with PSA > 5 ng/ml, we were clearly able to show in a former study by our group¹⁸⁰ that FCH-PET-CT should not be limited to PSA values below 5.0 ng/ml; these findings were confirmed by other imaging modalities (CT, MRI, biopsy, and/or histology) or clinical follow-up. Moreover, we also believe that in patients under hormone therapy (with PSA levels < 5.0 ng/ml), FCH-PET-CT is of additional value for the detection of pathological lesions.

$[^{18}\text{F}]$ fluoride

For skeletal imaging $[^{18}\text{F}]$ fluoride as a non-specific bone scanning agent was first described in 1962.¹⁸¹ With the introduction of γ cameras it was replaced by $^{99\text{m}}\text{Tc}$ -labeled diphosphonates such as MDP, the most commonly used bone-seeking substance.

Due to the improvements of new PET scanner generations, high-resolution imaging of the bone became more and more interesting, thus reintroducing $[^{18}\text{F}]$ fluoride for clinical and research investigations. In comparison to only 64% of the larger phosphonate complexes, the smaller ^{18}F has almost 100% 'first-pass' extraction from blood through the capillary membrane into the bone.^{182,183}

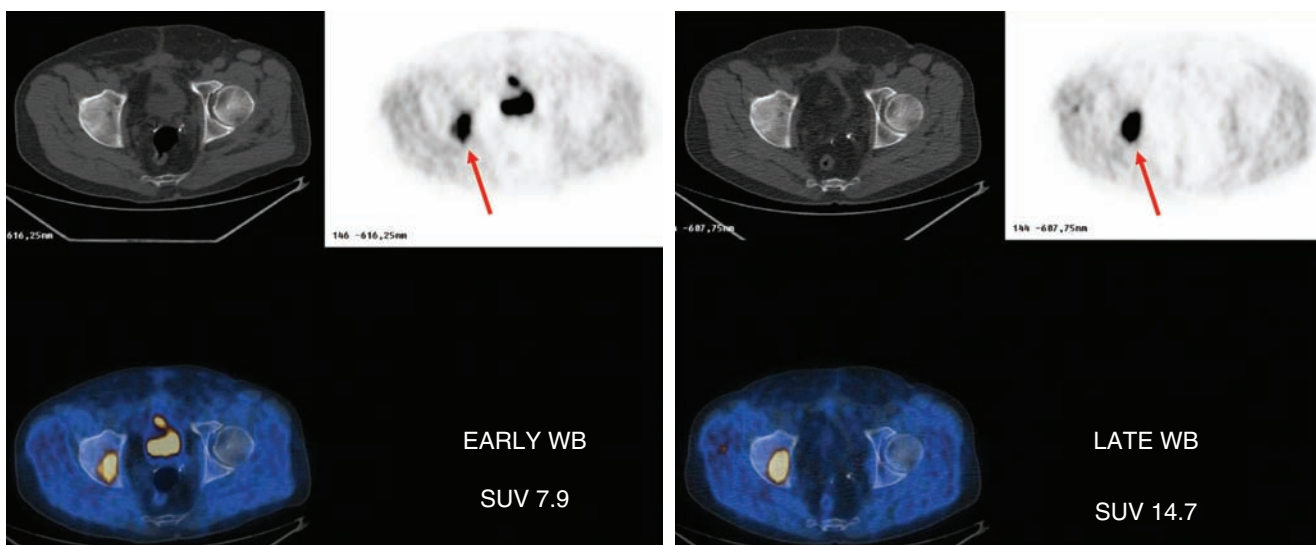


Figure 8.11

FCH-PET-CT: comparison of early and late axial images in bone metastasis (arrow) with 30-mm diameter – increasing standardized uptake values (SUVs) in the delayed images.

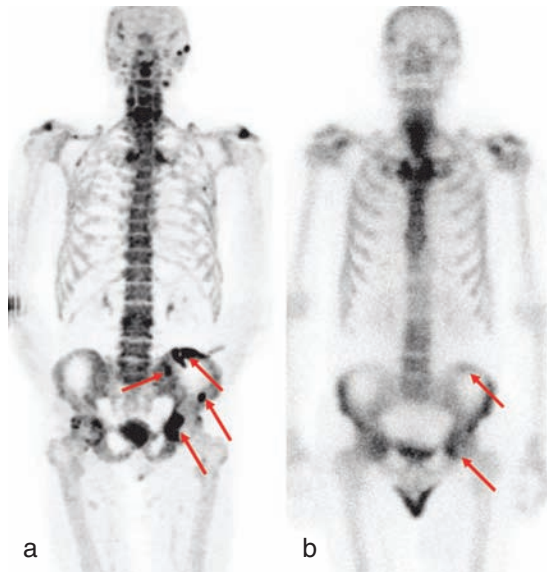


Figure 8.12
Comparison of [^{18}F]fluoride-PET-CT (a) and whole-body bone scintigraphy ($^{99\text{m}}\text{Tc}$]MDP (methylene diphosphonate)) (b) in a patient under chemotherapy.

Although there are only a few studies available which compare [^{18}F]fluoride with [$^{99\text{m}}\text{Tc}$]MDP, for the diagnosis of bone metastases [^{18}F]fluoride-PET seems to be more sensitive than conventional BS (Figure 8.12).⁸¹ Showing a higher contrast between normal and abnormal tissue, additional lesions, especially in the spine, were identified.^{80,81,109,145,184,185}

[^{18}F]fluoride-PET has a high sensitivity in the detection of non-malignant bone pathologies but limited specificity in the differentiation of malignant and/or benign lesions.¹⁸⁶ However, the use of integrated PET-CT technology, recently introduced to overcome this limitation, provides additional information (Figure 8.13).¹⁴⁴

Especially in high-risk prostate cancer patients (GSc > 7 and/or PSA DT < 3 months), [^{18}F]fluoride-PET-CT and not BS as an additional staging procedure should be performed. Therefore, as already mentioned, the authors believe that [^{18}F]fluoride may replace BS in the coming years.¹⁰⁹

Multitracer imaging

Multitracer imaging will provide in some cases an insight into the variations of intra- as well as interindividual tumor metabolism, thus improving our knowledge about special pathophysiological mechanisms and/or complex tumor metabolism.

Due to excessive and rapid changes in tumor metabolism, the early repetition of a diagnostic procedure may be useful. Not always knowing the ideal 'time curve' for when to perform diagnostic procedures,¹⁰⁹ FCH or FDG at 'the beginning' of a disease seems to have clear advantages over [^{18}F]fluoride.

In order to more fully evaluate the distribution of skeletal and soft tissue metastases, some authors¹⁸⁷ have proposed combining FDG and [^{18}F]fluoride imaging (two-in-one PET method). This is an approach which has not been accepted into daily clinical routine.

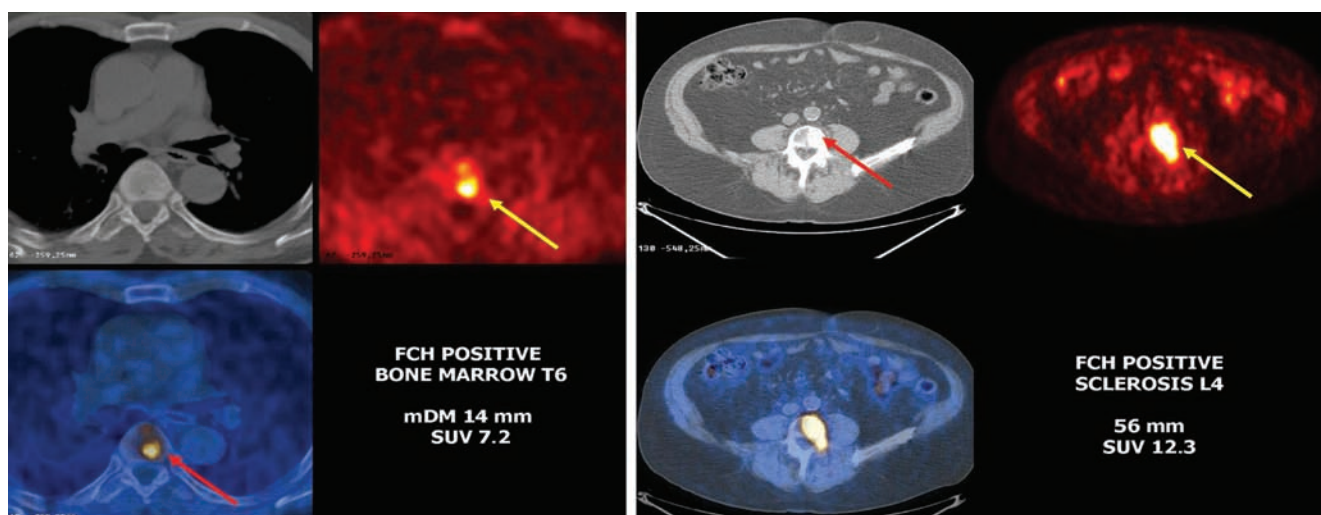


Figure 8.13
FCH-PET-CT (axial images): prostate cancer with bone marrow metastasis only seen in FCH-PET images (left) and sclerotic bone metastases detected by FCH-PET-CT (right).

References

- Jemal A, Tiwari RC, Murray T et al. Cancer statistics, 2004. *CA Cancer J Clin* 2004; 54: 8–29.
- Partin AW, Yoo J, Carter HB et al. The use of prostate specific antigen, clinical stage and Gleason score to predict pathological stage in men with localized prostate cancer. *J Urol* 1993; 150: 110–14.
- Ohori M, Wheeler TM, Dunn JK, Stamey TA, Scardino PT. The pathological features and prognosis of prostate cancer detectable with current diagnostic tests. *J Urol* 1994; 152: 1714–20.
- D'Amico AV, Whittington R, Schnall M et al. The impact of the inclusion of endorectal coil magnetic resonance imaging in a multivariate analysis to predict clinically unsuspected extraprostatic cancer. *Cancer* 1995; 75: 2368–72.
- Partin AW, Kattan MW, Subong EN et al. Combination of prostate-specific antigen, clinical stage, and Gleason score to predict pathological stage of localized prostate cancer. A multi-institutional update. *JAMA* 1997; 277: 1445–51.
- Kattan MW, Wheeler TM, Scardino PT. Postoperative nomogram for disease recurrence after radical prostatectomy for prostate cancer. *J Clin Oncol* 1999; 17: 1499–507.
- Kattan MW, Eastham JA, Stapleton AM, Wheeler TM, Scardino PT. A preoperative nomogram for disease recurrence following radical prostatectomy for prostate cancer. *J Natl Cancer Inst* 1998; 90: 766–71.
- Hull GW, Rabbani F, Abbas F et al. Cancer control with radical prostatectomy alone in 1,000 consecutive patients. *J Urol* 2002; 167: 528–34.
- Pound CR, Partin AW, Eisenberger MA et al. Natural history of progression after PSA elevation following radical prostatectomy. *JAMA* 1999; 281: 1591–7.
- Catalona WJ, Smith DS. 5-year tumor recurrence rates after anatomical radical retropubic prostatectomy for prostate cancer. *J Urol* 1994; 152: 1837–42.
- Zincke H, Oesterling JE, Blute ML et al. Long-term (15 years) results after radical prostatectomy for clinically localized (stage T2c or lower) prostate cancer. *J Urol* 1994; 152: 1850–7.
- Zincke H, Utz DC, Taylor WF. Bilateral pelvic lymphadenectomy and radical prostatectomy for clinical stage C prostatic cancer: role of adjuvant treatment for residual cancer and in disease progression. *J Urol* 1986; 135: 1199–205.
- Ohori M, Wheeler TM, Scardino PT. The New American Joint Committee on Cancer and International Union Against Cancer TNM classification of prostate cancer. Clinicopathologic correlations. *Cancer* 1994; 74: 104–14.
- Gleason D. The Veterans Administration Cooperative Urological Research Group: histological grading and clinical staging of prostatic carcinoma. In: Tannenbaum M, ed. *Urologic Pathology: The Prostate*. Philadelphia: Lea & Febiger, 1977: 171–97.
- Catalona WJ, Smith DS, Ornstein DK. Prostate cancer detection in men with serum PSA concentrations of 2.6 to 4.0 ng/mL and benign prostate examination. Enhancement of specificity with free PSA measurements. *JAMA* 1997; 277: 1452–5.
- Rietbergen JB, Hoedemaeker RE, Kruger AE, Kirkels WJ, Schroder FH. The changing pattern of prostate cancer at the time of diagnosis: characteristics of screen detected prostate cancer in a population based screening study. *J Urol* 1999; 161: 1192–8.
- Young H. The early diagnosis and radical cure of carcinoma of the prostate. Being a study of 40 cases and presentation of a radical operation which was carried out in four cases. *Johns Hopkins Hosp Bull* 1905; 16: 315–21.
- Millin T. *Retropubic Urinary Surgery*. London: Livingstone, 1947.
- Walsh PC. Anatomic radical prostatectomy: evolution of the surgical technique. *J Urol* 1998; 160: 2418–24.
- Walsh PC, Donker PJ. Impotence following radical prostatectomy: insight into etiology and prevention. *J Urol* 1982; 128: 492–7.
- Walsh PC, Lepor H, Eggleston JC. Radical prostatectomy with preservation of sexual function: anatomical and pathological considerations. *Prostate* 1983; 4: 473–85.
- Fair WR, Cookson MS, Stroumbakis N et al. The indications, rationale, and results of neoadjuvant androgen deprivation in the treatment of prostatic cancer: Memorial Sloan-Kettering Cancer Center results. *Urology* 1997; 49 (3A Suppl): 46–55.
- Klotz LH, Goldenberg SL, Jewett M et al. CUOG randomized trial of neoadjuvant androgen ablation before radical prostatectomy: 36-month post-treatment PSA results. Canadian Urologic Oncology Group. *Urology* 1999; 53: 757–63.
- Peeters ST, Hoogeman MS, Heemsbergen WD et al. Rectal bleeding, fecal incontinence, and high stool frequency after conformal radiotherapy for prostate cancer: normal tissue complication probability modeling. *Int J Radiat Oncol Biol Phys* 2006; 66: 11–19.
- Bhatnagar V, Stewart ST, Huynh V, Jorgensen G, Kaplan RM. Estimating the risk of long-term erectile, urinary and bowel symptoms resulting from prostate cancer treatment. *Prostate Cancer Prostatic Dis* 2006; 9: 136–46.
- Maki Y, Tsushima T, Nasu Y et al. [Combination chemotherapy with cis-platinum and ifosfamide for hormone unresponsive prostate cancer]. *Nippon Hinyokika Gakkai Zasshi* 1998; 89: 657–64. [in Japanese]
- Mike S, Harrison C, Coles B et al. Chemotherapy for hormone-refractory prostate cancer. *Cochrane Database Syst Rev* 2006; (4): CD005247.
- Kelly WK, Curley T, Slovin S et al. Paclitaxel, estramustine phosphate, and carboplatin in patients with advanced prostate cancer. *J Clin Oncol* 2001; 19: 44–53.
- Abi-Aad AS, Macturlane MT, Stein A, deKernion JB. Detection of local recurrence after radical prostatectomy by prostate specific antigen and transrectal ultrasound. *J Urol* 1992; 147: 952–5.
- Paulson DF. Impact of radical prostatectomy in the management of clinically localized disease. *J Urol* 1994; 152: 1826–30.
- Roehl KA, Han M, Ramos CG, Antenor JA, Catalona WJ. Cancer progression and survival rates following anatomical radical retropubic prostatectomy in 3,478 consecutive patients: long-term results. *J Urol* 2004; 172: 910–14.
- Kamat AM, Rosser CJ, Levy LB et al. Rise in serum PSA of 1.5 ng/mL above 24-month nadir after external beam radiotherapy is predictive of biochemical failure. *Urology* 2004; 63: 1132–7.
- Partin AW, Pearson JD, Landis PK et al. Evaluation of serum prostate-specific antigen velocity after radical prostatectomy

- to distinguish local recurrence from distant metastases. *Urology* 1994; 43: 649–59.
34. Okotie OT, Aronson WJ, Wieder JA et al. Predictors of metastatic disease in men with biochemical failure following radical prostatectomy. *J Urol* 2004; 171: 2260–4.
 35. Semeniuk RC, Venner PM, North S. Prostate-specific antigen doubling time is associated with survival in men with hormone-refractory prostate cancer. *Urology* 2006; 68: 565–9.
 36. Epstein JI, Pizov G, Walsh PC. Correlation of pathologic findings with progression after radical retropubic prostatectomy. *Cancer* 1993; 71: 3582–93.
 37. Ohori M, Wheeler TM, Kattan MW, Goto Y, Scardino PT. Prognostic significance of positive surgical margins in radical prostatectomy specimens. *J Urol* 1995; 154: 1818–24.
 38. Stephenson AJ, Scardino PT, Eastham JA et al. Postoperative nomogram predicting the 10-year probability of prostate cancer recurrence after radical prostatectomy. *J Clin Oncol* 2005; 23: 7005–12.
 39. Cabanas RM. An approach for the treatment of penile carcinoma. *Cancer* 1977; 39: 456–66.
 40. Wawroschek F, Vogt H, Weckermann D et al. Radioisotope guided pelvic lymph node dissection for prostate cancer. *J Urol* 2001; 166: 1715–19.
 41. Weckermann D, Hamm M, Dorn R et al. Sentinel lymph node dissection in prostate cancer: experience after more than 800 interventions. *Urologe A* 2006; 45: 723–7.
 42. Ghavamian R, Blute ML, Bergstralh EJ, Slezak J, Zincke H. Comparison of clinically nonpalpable prostate-specific antigen-detected (cT1c) versus palpable (cT2) prostate cancers in patients undergoing radical retropubic prostatectomy. *Urology* 1999; 54: 105–10.
 43. Raghavaiah NV, Jordan WP Jr. Prostatic lymphography. *J Urol* 1979; 121: 178–81.
 44. Bader P, Burkhard FC, Markwalder R, Studer UE. Disease progression and survival of patients with positive lymph nodes after radical prostatectomy. Is there a chance of cure? *J Urol* 2003; 169: 849–54.
 45. Heidenreich A, Varga Z, Von Knobloch R. Extended pelvic lymphadenectomy in patients undergoing radical prostatectomy: high incidence of lymph node metastasis. *J Urol* 2002; 167: 1681–6.
 46. Stone N, Stock R, Unger P. Laparoscopic pelvic lymph node dissection for prostate cancer: comparison of extended and modified techniques. *J Urol* 1997; 158: 1891–4.
 47. Wawroschek F, Vogt H, Wengenmair H et al. Prostate lymphoscintigraphy and radio-guided surgery for sentinel lymph node identification in prostate cancer. Technique and results of the first 350 cases. *Urol Int* 2003; 70: 303–10.
 48. Clark T, Parekh DJ, Cookson MS et al. Randomized prospective evaluation of extended versus limited lymph node dissection in patients with clinically localized prostate cancer. *J Urol* 2003; 169: 145–7; discussion 147–8.
 49. Querleu D, Leblanc E, Castelain B. Laparoscopic pelvic lymphadenectomy in the staging of early carcinoma of the cervix. *Am J Obstet Gynecol* 1991; 164: 579–81.
 50. Schuessler WW, Vancaillie TG, Reich H, Griffith DP. Transperitoneal endosurgical lymphadenectomy in patients with localized prostate cancer. *J Urol* 1991; 145: 988–91.
 51. Parra RO, Andrus CH, Boullier JA. Staging laparoscopic pelvic lymph node dissection. Experience and indications. *Arch Surg* 1992; 127: 1294–7.
 52. Kerbl K, Clayman RV, Petros JA, Chandhoke PS, Gill IS. Staging pelvic lymphadenectomy for prostate cancer: a comparison of laparoscopic and open techniques. *J Urol* 1993; 150: 396–8; discussion 399.
 53. Kavoussi LR, Sosa E, Chandhoke P et al. Complications of laparoscopic pelvic lymph node dissection. *J Urol* 1993; 149: 322–5.
 54. Jeschke S, Nambirajan T, Leeb K et al. Detection of early lymph node metastases in prostate cancer by laparoscopic radioisotope guided sentinel lymph node dissection. *J Urol* 2005; 173: 1943–6.
 55. Takashima H, Egawa M, Imao T et al. Validity of sentinel lymph node concept for patients with prostate cancer. *J Urol* 2004; 171: 2268–71.
 56. Brenot-Rossi I, Bastide C, Garcia S et al. Limited pelvic lymphadenectomy using the sentinel lymph node procedure in patients with localised prostate carcinoma: a pilot study. *Eur J Nucl Med Mol Imaging* 2005; 32: 635–40.
 57. Häcker A, Jeschke S, Leeb K et al. Detection of pelvic lymph node metastases in patients with clinically localized prostate cancer: comparison of FCH PET-CT and laparoscopic radioisotope-guided sentinel lymph node dissection. *J Urol* 2006; 176: 2014–19.
 58. Alavi A, Kung JW, Zhuang H. Implications of PET based molecular imaging on the current and future practice of medicine. *Semin Nucl Med* 2004; 34: 56–69.
 59. Rifkin MD, Zerhouni EA, Gatsonis CA et al. Comparison of magnetic resonance imaging and ultrasonography in staging early prostate cancer. Results of a multi-institutional cooperative trial. *N Engl J Med* 1990; 323: 621–6.
 60. Yu KK, Scheidler J, Hricak H et al. Prostate cancer: prediction of extracapsular extension with endorectal MR imaging and three-dimensional proton MR spectroscopic imaging. *Radiology* 1999; 213: 481–8.
 61. Gervasi LA, Mata J, Easley JD et al. Prognostic significance of lymph nodal metastases in prostate cancer. *J Urol* 1989; 142: 332–6.
 62. Tempany CM, Zhou X, Zerhouni EA et al. Staging of prostate cancer: results of Radiology Diagnostic Oncology Group project comparison of three MR imaging techniques. *Radiology* 1994; 192: 47–54.
 63. Wolf JS Jr, Cher M, Dall'era M et al. The use and accuracy of cross-sectional imaging and fine needle aspiration cytology for detection of pelvic lymph node metastases before radical prostatectomy. *J Urol* 1995; 153: 993–9.
 64. Weingartner K, Ramaswamy A, Bittinger A et al. Anatomical basis for pelvic lymphadenectomy in prostate cancer: results of an autopsy study and implications for the clinic. *J Urol* 1996; 156: 1969–71.
 65. Harisinghani MG, Barentsz J, Hahn PF et al. Noninvasive detection of clinically occult lymph-node metastases in prostate cancer. *N Engl J Med* 2003; 348: 2491–9.
 66. Schaner EG, Chang AE, Doppman JL et al. Comparison of computed and conventional whole lung tomography in detecting pulmonary nodules: a prospective radiologic-pathologic study. *AJR Am J Roentgenol* 1978; 131: 51–4.

67. Vanel D, Henry-Amar M, Lumbroso J et al. Pulmonary evaluation of patients with osteosarcoma: roles of standard radiography, tomography, CT, scintigraphy, and tomoscintigraphy. *AJR Am J Roentgenol* 1984; 143: 519–23.
68. Muhm JR, Brown LR, Crowe JK et al. Comparison of whole lung tomography and computed tomography for detecting pulmonary nodules. *AJR Am J Roentgenol* 1978; 131: 981–4.
69. Crim JR, Cracchiolo A, Bassett LW et al. Magnetic resonance imaging of the hindfoot. *Foot Ankle* 1989; 10: 1–7.
70. Hilpert PL, Friedman AC, Radecki PD et al. MRI of hemorrhagic renal cysts in polycystic kidney disease. *AJR Am J Roentgenol* 1986; 146: 1167–72.
71. Semelka RC, Shoenut JP, Ascher SM et al. Solitary hepatic metastasis: comparison of dynamic contrast-enhanced CT and MR imaging with fat-suppressed T2-weighted, breath-hold T1-weighted FLASH, and dynamic gadolinium-enhanced FLASH sequences. *J Magn Reson Imaging* 1994; 4: 319–23.
72. Stark DD, Wittenberg J, Butch RJ, Ferrucci JT Jr. Hepatic metastases: randomized, controlled comparison of detection with MR imaging and CT. *Radiology* 1987; 165: 399–406.
73. Haubold-Reuter BG, Duewelling S, Schilcher BR, Marincek B, von Schulthess GK. The value of bone scintigraphy, bone marrow scintigraphy and fast spin-echo magnetic resonance imaging in staging of patients with malignant solid tumours: a prospective study. *Eur J Nucl Med* 1993; 20: 1063–9.
74. Kosuda S, Kaji T, Yokoyama H et al. Does bone SPECT actually have lower sensitivity for detecting vertebral metastasis than MRI? *J Nucl Med* 1996; 37: 975–8.
75. Athanasoulis T, Koutsikos J, Zerva C. What is the source of the skeletal affinity of ^{99m}Tc-V-DMSA? *Eur J Nucl Med Mol Imaging* 2004; 31: 1673–4; author reply 1675–6.
76. Smoker WR, Godersky JC, Knutzon RK et al. The role of MR imaging in evaluating metastatic spinal disease. *AJR Am J Roentgenol* 1987; 149: 1241–8.
77. Frank JA, Ling A, Patronas NJ et al. Detection of malignant bone tumors: MR imaging vs scintigraphy. *AJR Am J Roentgenol* 1990; 155: 1043–8.
78. Steinborn MM, Heuck AE, Tiling R et al. Whole-body bone marrow MRI in patients with metastatic disease to the skeletal system. *J Comput Assist Tomogr* 1999; 23: 123–9.
79. Schaffer DL, Pendergrass HP. Comparison of enzyme, clinical, radiographic, and radionuclide methods of detecting bone metastases from carcinoma of the prostate. *Radiology* 1976; 121: 431–4.
80. Petren-Mallmin M, Andreasson I, Ljunggren O et al. Skeletal metastases from breast cancer: uptake of ¹⁸F-fluoride measured with positron emission tomography in correlation with CT. *Skeletal Radiol* 1998; 27: 72–6.
81. Schirrmeyer H, Guhlmann A, Elsner K et al. Sensitivity in detecting osseous lesions depends on anatomic localization: planar bone scintigraphy versus ¹⁸F PET. *J Nucl Med* 1999; 40: 1623–9.
82. Bury T, Barreto A, Daenen F et al. Fluorine-18 deoxyglucose positron emission tomography for the detection of bone metastases in patients with non-small cell lung cancer. *Eur J Nucl Med* 1998; 25: 1244–7.
83. Troyer J, Beckett M, Wright G. Location of prostate-specific membrane antigen in the LNCaP prostate carcinoma cell line. *Prostate* 1997; 30: 232–42.
84. Chang SS, Reuter VE, Heston WD et al. Five different anti-prostate-specific membrane antigen (PSMA) antibodies confirm PSMA expression in tumor-associated neovasculature. *Cancer Res* 1999; 59: 3192–8.
85. Bander N, Nanus D, Bremer S. Phase I clinical trial targeting a monoclonal antibody (mAb) to the extracellular domain of prostate specific membrane antigen (PSMAext) in hormone-independent patients. *Urol* 2000; 163 (Suppl 4): 160.
86. Manyak MJ, Hinkle GH, Olsen JO et al. Immunoscintigraphy with indium-111-capromab pentetide: evaluation before definitive therapy in patients with prostate cancer. *Urology* 1999; 54: 1058–63.
87. Mundy GR. Metastasis to bone: causes, consequences and therapeutic opportunities. *Nat Rev Cancer* 2002; 2: 584–93.
88. de Jong IJ, Pruim J, Elsinga PH, Vaalburg W, Mensink HJ. Preoperative staging of pelvic lymph nodes in prostate cancer by ¹¹C-choline PET. *J Nucl Med* 2003; 44: 331–5.
89. Sabbatini P, Larson SM, Kremer A et al. Prognostic significance of extent of disease in bone in patients with androgen-independent prostate cancer. *J Clin Oncol* 1999; 17: 948–57.
90. Noguchi M, Kikuchi H, Ishibashi M, Noda S. Percentage of the positive area of bone metastasis is an independent predictor of disease death in advanced prostate cancer. *Br J Cancer* 2003; 88: 195–201.
91. Rigaud J, Tiguert R, Le Normand L et al. Prognostic value of bone scan in patients with metastatic prostate cancer treated initially with androgen deprivation therapy. *J Urol* 2002; 168: 1423–6.
92. Lund F, Smith PH, Suci S. Do bone scans predict prognosis in prostatic cancer? A report of the EORTC protocol 30762. *Br J Urol* 1984; 56: 58–63.
93. Oesterling JE, Martin SK, Bergstralh EJ, Lowe FC. The use of prostate-specific antigen in staging patients with newly diagnosed prostate cancer. *JAMA* 1993; 269: 57–60.
94. Sanz G, Rioja J, Zudaire JJ, Berian JM, Richter JA. PET and prostate cancer. *World J Urol* 2004; 22: 351–2.
95. Chybowski FM, Keller JJ, Bergstralh EJ, Oesterling JE. Predicting radionuclide bone scan findings in patients with newly diagnosed, untreated prostate cancer: prostate specific antigen is superior to all other clinical parameters. *J Urol* 1991; 145: 313–18.
96. Lee CT, Oesterling JE. Using prostate-specific antigen to eliminate the staging radionuclide bone scan. *Urol Clin North Am* 1997; 24: 389–94.
97. Cher ML, Bianco FJ Jr, Lam JS et al. Limited role of radionuclide bone scintigraphy in patients with prostate specific antigen elevations after radical prostatectomy. *J Urol* 1998; 160: 1387–91.
98. Kane CJ, Amling CL, Johnstone PA et al. Limited value of bone scintigraphy and computed tomography in assessing biochemical failure after radical prostatectomy. *Urology* 2003; 61: 607–11.
99. Terris MK, Klonecke AS, McDougall IR, Stamey TA. Utilization of bone scans in conjunction with prostate-specific antigen levels in the surveillance for recurrence of adenocarcinoma after radical prostatectomy. *J Nucl Med* 1991; 32: 1713–17.
100. Leo ME, Bilhartz DL, Bergstralh EJ, Oesterling JE. Prostate specific antigen in hormonally treated stage D2 prostate

- cancer: is it always an accurate indicator of disease status? *J Urol* 1991; 145: 802–6.
101. Cook GJ, Fogelman I. The role of nuclear medicine in monitoring treatment in skeletal malignancy. *Semin Nucl Med* 2001; 31: 206–11.
 102. Koizumi M, Matsumoto S, Takahashi S, Yamashita T, Ogata E. Bone metabolic markers in the evaluation of bone scan flare phenomenon in bone metastases of breast cancer. *Clin Nucl Med* 1999; 24: 15–20.
 103. Jacobson A, Fogelman I, Rosenthal L. In Collier BD, ed. *Skeletal Nuclear Medicine. Bonescanning in Metastatic Disease*. St Louis: Mosby, 1996: 87–123.
 104. O'Mara RE. Skeletal scanning in neoplastic disease. *Cancer* 1976; 37 (1 Suppl): 480–6.
 105. Horiuchi-Suzuki K, Konno A, Ueda M, et al. Skeletal affinity of Tc(V)-DMS is bone cell mediated and pH dependent. *Eur J Nucl Med Mol Imaging* 2004; 31: 388–98.
 106. Roland J, van den Weyngaert D, Krug B et al. Metastases seen on SPECT imaging despite a normal planar bone scan. *Clin Nucl Med* 1995; 20: 1052–4.
 107. Sedonja I, Budihna NV. The benefit of SPECT when added to planar scintigraphy in patients with bone metastases in the spine. *Clin Nucl Med* 1999; 24: 407–13.
 108. Schirrmeister H, Glatting G, Hetzel J et al. Prospective evaluation of the clinical value of planar bone scans, SPECT, and (18)F-labeled NaF PET in newly diagnosed lung cancer. *J Nucl Med* 2001; 42: 1800–4.
 109. Langsteger W, Heinisch M, Fogelman I. The role of fluoro-deoxyglucose, 18F-dihydroxyphenylalanine, 18F-choline, and 18F-fluoride in bone imaging with emphasis on prostate and breast. *Semin Nucl Med* 2006; 36: 73–92.
 110. Fricke E, Machtens S, Hofmann M et al. Positron emission tomography with 11C-acetate and 18F-FDG in prostate cancer patients. *Eur J Nucl Med Mol Imaging* 2003; 30: 607–11.
 111. Mathews D, Oz OK. Positron emission tomography in prostate and renal cell carcinoma. *Curr Opin Urol* 2002; 12: 381–5.
 112. Hara T, Kosaka N, Kishi H. PET imaging of prostate cancer using carbon-11-choline. *J Nucl Med* 1998; 39: 990–5.
 113. Roivainen A, Forsback S, Gronroos T, et al. Blood metabolism of [methyl-11C]choline; implications for in vivo imaging with positron emission tomography. *Eur J Nucl Med* 2000; 27: 25–32.
 114. Hara T, Kosaka N, Kishi H. Development of (18)F-fluoroethylcholine for cancer imaging with PET: synthesis, biochemistry, and prostate cancer imaging. *J Nucl Med* 2002; 43: 187–99.
 115. DeGrado TR, Coleman RE, Wang S et al. Synthesis and evaluation of 18F-labeled choline as an oncologic tracer for positron emission tomography: initial findings in prostate cancer. *Cancer Res* 2001; 61: 110–17.
 116. Bender H, Wiludda V, Matthies A et al. Use of 18F-fluoroethyl- and methyl-choline PET in prostate cancer: a comparative and feasibility study. Abstract presented at 44th Meeting of the German Society of Nuclear Medicine, 2006: P31.
 117. Pascali C, Bogni A, Iwata R, Cambie M, Bombardieri E. [11C]Methylation on a Sep-Pak cartridge: a convenient way to produce [N-methyl-11C]choline. *J Labelled Cpd Radiopharm* 2000; 43: 195–203.
 118. Iwata R, Pascali C, Bogni A et al. [18F]fluoromethyl triflate, a novel and reactive [18F]fluoromethylating agent: preparation and application to the on-column preparation of [18F]fluoro-choline. *Appl Radiat Isot* 2002; 57: 347–52.
 119. Nader M, Hoeppling A. Metamorphosis of a dedicated FDG disposable kit module to a multipurpose synthesizer. *Nuklearmedizin* 2005; 44: A192, 7.
 120. Costello LC, Franklin RB. Citrate metabolism of normal and malignant prostate epithelial cells. *Urology* 1997; 50: 3–12.
 121. Yoshimoto M, Waki A, Yonekura Y et al. Characterization of acetate metabolism in tumor cells in relation to cell proliferation: acetate metabolism in tumor cells. *Nucl Med Biol* 2001; 28: 117–22.
 122. Pike VW, Eakins MN, Allan RM, Selwyn AP. Preparation of [1-11C]acetate – an agent for the study of myocardial metabolism by positron emission tomography. *Int J Appl Radiat Isot* 1982; 33: 505–12.
 123. Pike V, Horlock P, Brown C, Clark J. The remotely controlled preparation of a carbon-11 labelled radiopharmaceutical—[11C]acetate. *Int J Appl Radiat Isot* 1984; 35: 623–7.
 124. Kruijper P, Linden T, Mooij R, Visser F, Herscheid J. A practical method for the preparation of [11C]acetate. *Appl Radiat Isot* 1995; 46: 317–21.
 125. Iwata R, Ito H, Hayashi T et al. Stable and general-purpose chemiluminescent detection system for horseradish peroxidase employing a thiazole compound enhancer and some additives. *Anal Biochemistry* 1995; 231: 170–4.
 126. Roeda D, Dolle F, Crouzel C. An improvement of 11C acetate synthesis – non-radioactive contaminants by irradiation-induced species emanating from the 11C carbon dioxide production target. *Appl Radiat Isot* 2002; 57: 857–60.
 127. Ishiwata K, Ishii S-I, Sasaki T, Senda M, Nozaki T. A distillation method of preparing C-11 labeled yields could be acetate for routine clinical use. *Appl Radiat Isot* 1993; 44: 761–3.
 128. Eison CT, Wickstrom M, Turck P, Wright G. A review of recent regulatory and environmental toxicology studies on 1080. *NZ J Ecol* 1999; 2: 129–37.
 129. Liebecq C, Peters RA. The toxicity of fluoroacetate and the tricarboxylic acid cycle. 1949. *Biochim Biophys Acta* 1989; 1000: 254–69.
 130. Clarke DD. Fluoroacetate and fluorocitrate: mechanism of action. *Neurochem Res* 1991; 16: 1055–8.
 131. Lear JL, Ackermann RF. Evaluation of radiolabeled acetate and fluoroacetate as potential tracers of cerebral oxidative metabolism. *Metab Brain Dis* 1990; 5: 45–56.
 132. Ponde D, Oyama N, Dence C, Welch M. [18F]fluoroacetate, an analog of C-11 acetate for tumor imaging. *J Nucl Med* 2003; 44: 1062P.
 133. Oyama N, Ponde D, Dence D et al. In vitro and in vivo assessment of F-18 fluoroacetate; a potential analog for tumor imaging. *J Nucl Med* 2004; 45: 331P.
 134. Sun LQ, Mori T, Dence CS et al. New approach to fully automated synthesis of sodium [18F]fluoroacetate – a simple and fast method using a commercial synthesizer. *Nucl Med Biol* 2006; 33: 153–8.
 135. Bonasera TA, O'Neil JP, Xu M et al. Preclinical evaluation of fluorine-18-labeled androgen receptor ligands in baboons. *J Nucl Med* 1996; 37: 1009–15.

136. Rogers BE, Bigott HM, McCarthy DW et al. MicroPET imaging of a gastrin-releasing peptide receptor-positive tumor in a mouse model of human prostate cancer using a ^{64}Cu -labeled bombesin analogue. *Bioconjug Chem* 2003; 14: 756–63.
137. Chen X, Park R, Hou Y et al. MicroPET and autoradiographic imaging of GRP receptor expression with ^{64}Cu -DOTA-[Lys3]bombesin in human prostate adenocarcinoma xenografts. *J Nucl Med* 2004; 45: 1390–7.
138. Schuhmacher J, Zhang H, Doll J et al. GRP receptor-targeted PET of a rat pancreas carcinoma xenograft in nude mice with a ^{68}Ga -labeled bombesin(6-14) analog. *J Nucl Med* 2005; 46: 691–9.
139. Zhang X, Cai W, Cao F et al. ^{18}F -labeled bombesin analogs for targeting GRP receptor-expressing prostate cancer. *J Nucl Med* 2006; 47: 492–501.
140. Cook GJ, Fogelman I. The role of positron emission tomography in the management of bone metastases. *Cancer* 2000; 88 (12 Suppl): 2927–33.
141. Valk PE, Pounds TR, Tesar RD, Hopkins DM, Haseman MK. Cost-effectiveness of PET imaging in clinical oncology. *Nucl Med Biol* 1996; 23: 737–43.
142. Gambhir SS, Shepherd JE, Shah BD et al. Analytical decision model for the cost-effective management of solitary pulmonary nodules. *J Clin Oncol* 1998; 16: 2113–25.
143. Bombardieri E, Aktolun C, Baum RP et al. FDG-PET: procedure guidelines for tumour imaging. *Eur J Nucl Med Mol Imaging* 2003; 30: BP115–24.
144. Even-Sapir E, Metser U, Flusser G et al. Assessment of malignant skeletal disease: initial experience with ^{18}F -fluoride PET/CT and comparison between ^{18}F -fluoride PET and ^{18}F -fluoride PET/CT. *J Nucl Med* 2004; 45: 272–8.
145. Fogelman I, Cook G, Israel O, Van der Wall H. Positron emission tomography and bone metastases. *Semin Nucl Med* 2005; 35: 135–42.
146. Minn H, Clavo AC, Wahl RL. Influence of hypoxia on tracer accumulation in squamous-cell carcinoma: in vitro evaluation for PET imaging. *Nucl Med Biol* 1996; 23: 941–6.
147. Paquet N, Albert A, Foidart J, Hustinx R. Within-patient variability of (^{18}F)-FDG: standardized uptake values in normal tissues. *J Nucl Med* 2004; 45: 784–8.
148. Keyes JW Jr. SUV: standard uptake or silly useless value? *J Nucl Med* 1995; 36: 1836–9.
149. Ramos CD, Erdi YE, Gonen M et al. FDG-PET standardized uptake values in normal anatomical structures using iterative reconstruction segmented attenuation correction and filtered back-projection. *Eur J Nucl Med* 2001; 28: 155–64.
150. Lucignani G, Paganelli G, Bombardieri E. The use of standardized uptake values for assessing FDG uptake with PET in oncology: a clinical perspective. *Nucl Med Commun* 2004; 25: 651–6.
151. Warburg O. On the origin of cancer cells. *Science* 1956; 123: 309–14.
152. Singh G, Lakkis CL, Laucirica R, Epner DE. Regulation of prostate cancer cell division by glucose. *J Cell Physiol* 1999; 180: 431–8.
153. Rossi F, Grzeskowiak M, Della Bianca V, Sbarbati A. De novo synthesis of diacylglycerol from glucose. A new pathway of signal transduction in human neutrophils stimulated during phagocytosis of beta-glucan particles. *J Biol Chem* 1991; 266: 8034–8.
154. Hofer C, Laubenbacher C, Block T et al. Fluorine-18-fluorodeoxyglucose positron emission tomography is useless for the detection of local recurrence after radical prostatectomy. *Eur Urol* 1999; 36: 31–5.
155. Effert PJ, Bares R, Handt S et al. Metabolic imaging of untreated prostate cancer by positron emission tomography with ^{18}F -labeled deoxyglucose. *J Urol* 1996; 155: 994–8.
156. Shreve PD, Grossman HB, Gross MD, Wahl RL. Metastatic prostate cancer: initial findings of PET with 2-deoxy-2-[^{18}F]fluoro-D-glucose. *Radiology* 1996; 199: 751–6.
157. Agus DB, Golde DW, Sgouros G et al. Positron emission tomography of a human prostate cancer xenograft: association of changes in deoxyglucose accumulation with other measures of outcome following androgen withdrawal. *Cancer Res* 1998; 58: 3009–14.
158. Seltzer MA, Barbaric Z, Beldegrun A et al. Comparison of helical computerized tomography, positron emission tomography and monoclonal antibody scans for evaluation of lymph node metastases in patients with prostate specific antigen relapse after treatment for localized prostate cancer. *J Urol* 1999; 162: 1322–8.
159. Oyama N, Akino H, Kanamaru H et al. ^{11}C -acetate PET imaging of prostate cancer. *J Nucl Med* 2002; 43: 181–6.
160. Hetzel M, Hetzel J, Arslanemir C, Nussle K, Schirrmeyer H. Reliability of symptoms to determine use of bone scans to identify bone metastases in lung cancer: prospective study. *BMJ* 2004; 328: 1051–2.
161. Schirrmeyer H, Arslanemir C, Glatting G et al. Omission of bone scanning according to staging guidelines leads to futile therapy in non-small cell lung cancer. *Eur J Nucl Med Mol Imaging* 2004; 31: 964–8.
162. Morris MJ, Akhurst T, Osman I et al. Fluorinated deoxyglucose positron emission tomography imaging in progressive metastatic prostate cancer. *Urology* 2002; 59: 913–18.
163. Shreve PD, Gross MD. Imaging of the pancreas and related diseases with PET carbon-11-acetate. *J Nucl Med* 1997; 38: 1305–10.
164. Shreve P, Chiao PC, Humes HD, Schwaiger M, Gross MD. Carbon-11-acetate PET imaging in renal disease. *J Nucl Med* 1995; 36: 1595–601.
165. Oyama N, Miller TR, Dehdashti F et al. ^{11}C -acetate PET imaging of prostate cancer: detection of recurrent disease at PSA relapse. *J Nucl Med* 2003; 44: 549–55.
166. Kotzerke J, Volkmer BG, Neumaier B et al. Carbon-11 acetate positron emission tomography can detect local recurrence of prostate cancer. *Eur J Nucl Med Mol Imaging* 2002; 29: 1380–4.
167. Dimitrakopoulou-Strauss A, Strauss LG. PET imaging of prostate cancer with ^{11}C -acetate. *J Nucl Med* 2003; 44: 556–8.
168. Albrecht S, Buchegger F, Soloviev D et al. (^{11}C)-acetate PET in the early evaluation of prostate cancer recurrence. *Eur J Nucl Med Mol Imaging* 2007; 34: 185–96.
169. Hara T, Kosaka N, Shinoura N, Kondo T. PET imaging of brain tumor with [^{11}C]choline. *J Nucl Med* 1997; 38: 842–7.

170. Hara T, Inagaki K, Kosaka N, Morita T. Sensitive detection of mediastinal lymph node metastasis of lung cancer with ¹¹C-choline PET. *J Nucl Med* 2000; 41: 1507–13.
171. Kobori O, Kirihara Y, Kosaka N, Hara T. Positron emission tomography of esophageal carcinoma using (11)C-choline and (18)F-fluorodeoxyglucose: a novel method of preoperative lymph node staging. *Cancer* 1999; 86: 1638–48.
172. Sutinen E, Nurmi M, Roivainen A et al. Kinetics of [(11)C]choline uptake in prostate cancer: a PET study. *Eur J Nucl Med Mol Imaging* 2004; 31: 317–24.
173. Reske SN, Blumstein NM, Neumaier B et al. Imaging prostate cancer with ¹¹C-choline PET/CT. *J Nucl Med* 2006; 47: 1249–54.
174. DeGrado TR, Baldwin SW, Wang S et al. Synthesis and evaluation of (18)F-labeled choline analogs as oncologic PET tracers. *J Nucl Med* 2001; 42: 1805–14.
175. DeGrado TR, Reiman RE, Price DT, Wang S, Coleman RE. Pharmacokinetics and radiation dosimetry of ¹⁸F-fluorocholine. *J Nucl Med* 2002; 43: 92–6.
176. Langsteger W, Beheshti M, Nader M et al. Evaluation of lymph node and bone metastases with Fluor Choline (FCH) PET–CT in the follow up of prostate cancer patients. *Eur J Nucl Med Mol Imaging* 2006; 33 (Suppl 2): 209.
177. Langsteger W, Beheshti M, Loidl W et al. Fluor Choline (FCH) PET–CT in preoperative staging of prostate cancer. *Eur J Nucl Med Mol Imaging* 2006; 33 (Suppl 2): 207–8.
178. Coleman R, DeGrado T, Wang S et al. Preliminary evaluation of F-18 fluorocholine (FCH) as a PET tumor imaging agent. *Clin Positron Imaging* 2000; 3: 147.
179. Beheshti M, Haim S, Nader M et al. Assessment of bone metastases in patients with prostate cancer by dual-phase F-18 Fluor Choline PET/CT. *Eur J Nucl Med Mol Imaging* 2006; 33 (Suppl 2): 208.
180. Heinisch M, Dirisamer A, Loidl W et al. Positron emission tomography/computed tomography with F-18-fluorocholine for restaging of prostate cancer patients: meaningful at PSA < 5 ng/ml? *Mol Imaging Biol* 2006; 8: 43–8.
181. Blau M, Nagler W, Bender MA. Fluorine-18: a new isotope for bone scanning. *J Nucl Med* 1962; 3: 332–4.
182. Wootton R, Dore C. The single-passage extraction of ¹⁸F in rabbit bone. *Clin Phys Physiol Meas* 1986; 7: 333–43.
183. Schirrmeister H, Rentschler M, Kotzerke J. Darstellung des normalen Skelettsystems mit ¹⁸F Na-PET im Vergleich zur konventionellen Skelettszintigraphie mit ^{99m}Tc-MDP. *Fortschr Röntgenstr* 1998; 168: 451–6.
184. Hawkins RA, Choi Y, Huang SC et al. Evaluation of the skeletal kinetics of fluorine-18-fluoride ion with PET. *J Nucl Med* 1992; 33: 633–42.
185. Schirrmeister H, Guhlmann A, Kotzerke J et al. Early detection and accurate description of extent of metastatic bone disease in breast cancer with fluoride ion and positron emission tomography. *J Clin Oncol* 1999; 17: 2381–9.
186. Beheshti M, Fitz F, Haim S et al. F-18 Fluor Choline PET/CT vs F-18 fluoride PET/CT in the detection of bone metastases in patients with prostate cancer. *Eur J Nucl Med Mol Imaging* 2006; 33 (Suppl 2): 208–9.
187. Hoegerle S, Juengling F, Otte A et al. Combined FDG and [F-18]fluoride whole-body PET: a feasible two-in-one approach to cancer imaging? *Radiology* 1998; 209: 253–8.

Ovarian cancer

Sandro Sironi, Maria Picchio, Luca Guerra, Cristina Messa, and Ferruccio Fazio

Primary ovarian cancer

Background

Ovarian carcinoma is the third most common cancer of the female genital tract, but it accounts for over half of all deaths related to gynecologic neoplasms. This is primarily because, unlike patients with other common malignant gynecologic tumors, most patients with ovarian cancer have an advanced stage of disease at the time of initial diagnosis.^{1–3}

The prognosis is considerably changed by the extent of spread: the 5-year survival rate is 85% if the cancer is confined to the ovaries (stage 1), 55% if the cancer has spread into the pelvis (stage 2), 14% for stage 3 abdominal spread, and 4% for stage 4 more distant spread.³ There are two major diagnostic challenges when an ovarian mass is detected: determination of malignancy and evaluation of tumor extent (staging). Diagnostic studies that allow accurate confirmation of benignity might reduce unnecessary surgery. On the other hand, diagnostic procedures that allow accurate cancer staging should help to determine surgical and chemotherapeutic planning.^{2,3} The current management of clinically suspected disease involves histological confirmation of the diagnosis, the identification of tumor spread, and debulking prior to chemotherapy, usually followed by second-look surgical procedures to assess the response.^{4,5} Because of the extremely poor prognosis for advanced ovarian cancer, suspicious ovarian masses need prompt attention. In fact, misleading symptoms of ovarian cancer often delay an early diagnosis. As a result, 75% of patients have stage 3 or 4 disease at the time of initial diagnosis.^{6–13} Accurate diagnosis of ovarian carcinoma is essential in the proper management of these patients. Measurement of the serum tumor marker CA125 may be used. However, its accuracy is limited because negative values do not rule out active disease, whereas elevated values cannot provide information on the site of tumor tissue.^{14–16} In the past decade, morphologic imaging modalities have played a major role in accurately delineating disease status: particularly, computed tomography (CT) and magnetic resonance imaging (MRI) have proved useful in evaluating the extent

of ovarian disease and evaluating the response to treatment in these patients.^{17–20}

Primary ovarian cancer: diagnostic modalities

Clinical pelvic examination and serum CA125 levels have failed to allow consistent detection of ovarian malignancy.^{14–16} As the sensitivities of these techniques are often below 50%, imaging modalities such as ultrasonography (US), CT, and MRI have become indispensable. US performed with transabdominal and endovaginal techniques has demonstrated accuracies of up to 80% in the evaluation of ovarian masses. US is better for the detection of masses than in the diagnosis of malignancy.¹⁷ Studies of contrast material-enhanced CT and MRI have shown accuracies of almost 80% in the diagnosis of cancer and 80–90% in the detection of abdominal spread.^{17–20} In general, comparative studies of US and MRI have shown MRI to be superior in the differentiation of benign from malignant masses.^{19,20} In previous reports, US, CT, and MRI were compared in diagnosing primary ovarian cancer.^{17,18} The three imaging modalities yielded similar estimated areas under the receiver operating characteristic (ROC) curve for discrimination between benign disease and cancer in all regions, with a mean area of 0.91 for all three modalities. Although the differentiation of benign from malignant disease is obviously clinically important, and these detection rates are higher than those previously reported, they are likely still not high enough for surgery to be avoided in most cases. The estimated areas under the ROC curve for each modality revealed that MRI and CT are superior to Doppler US for diagnosis of malignancy in the mass. It is unfortunate (but unavoidable) that the study design did not allow statistical evaluation of the performances of CT and MRI versus that of combined Doppler and conventional US. The relatively poor performance of Doppler US has been discussed without identification of a unifying cause. The neovascular response of ovarian cancer may be

incomplete or non-specific. Thus, when intratumoral arterial flow is detected with Doppler US, the differentiation of benign from malignant processes is often not possible. Therefore, whatever the reason, the present lack of specificity makes Doppler US a poor diagnostic tool. It is possible that different numerical cut-off values for the Doppler indices may provide more encouraging results, although the considerable overlap of the indices in benign and malignant tumors makes this possibility unlikely. Perhaps the use of intravenous contrast agents to enhance the tumor and its vascularity may improve diagnostic accuracy. Problems with both overstaging and understaging are also present with three morphologic imaging modalities.^{17–20} Overstaging leads to a wider surgical approach, but makes it more likely that malignancy will not be overlooked. Understaging causes extension of the originally planned pelvic surgery with the potential for a tumor to be overlooked. In most centers, the greater is the suspicion of abdominal spread, the more likely it is that a specialist in gynecologic oncology will perform the exploration. This point is important, because surgery by specialists leads to better staging and maximal debulking (cytoreduction) and to longer survival. Although one could argue that it is always better to overstage so that malignancy is not overlooked, it is more important to accurately distinguish malignancy that has spread into the abdomen (stage 3 or 4) from malignancy confined to the pelvis (stage 1 or 2).^{1–5} Because of the importance of not understaging abdominal malignancy as disease limited to the pelvis, if stage 3 cancer is not detected at initial abdominal US, CT or MRI should be performed because of their higher sensitivities in staging. Whatever the modality used, it is hoped that the correct staging of advanced disease will lead to appropriate referral to a specialist in gynecologic oncology.

Primary ovarian cancer: role of functional imaging

Positron emission tomography (PET) with [¹⁸F]-fluoro-2-deoxy-D-glucose (FDG) is a functional technique which can yield metabolic information, thus helping in the identification of cancer tissue. In contrast to CT and MRI, diagnoses with FDG-PET are made using functional rather than morphological criteria. In fact, FDG-PET is a method based on the increased glucose metabolism of malignant tumors. FDG-PET has been shown to be effective in the identification of different primary and metastatic tumor types. It can reveal the biochemical differences between normal and malignant tissues and has been used as a functional method of determining tumor viability in several cancer types.^{21–24} In particular, FDG-PET has been used for detecting malignancies in patients with an adnexal mass.

This diagnostic technique showed heterogeneous results in different studies, with sensitivities ranging from 58% to 90% and specificities ranging from 76% to 90%.^{24–31} Particularly the lower sensitivity value was due to the failure in detecting malignancies in a patient with early stage (1–2) tumors. In fact, due to the frequent small amount of solid tumor inside the cystic lesion, the presence of viable tumor tissue is too small to be clearly detected. Other cases of false negative (FN) results were observed in low malignant potential (LMP) tumors, also called ‘borderline’ tumors. In these cases the glucose metabolism is not highly increased, and FDG-PET may result in negative findings. Conversely, FDG-PET showed moderate-intense uptake in many non-malignant pathological conditions (false positive (FP) results), such as mucinous cystadenoma, serous cysts, endometrioma, inflammatory processes, corpus luteum cysts, dermoid cysts, and hydrosalpinx. In conclusion, FDG-PET accuracy in identifying malignancy in a patient with adnexal masses is not higher than that of conventional diagnostic techniques, such as US and MRI. FDG-PET should only be suggested in those cases where US and MRI are uncertain in the definition of adnexal masses.

PET shows a particular usefulness in staging, restaging, and follow-up of cancer patients. In particular, in ovarian cancer, the major role of the PET functional modality has been reported in the restaging and follow-up of these patients. However, based on the findings of several studies,^{24,32,33} FDG-PET may also become a tool for the initial staging of ovarian cancer patients. Preliminary data suggest that FDG-PET can effectively supplement clinical evaluation and CT or MRI information in the staging of ovarian cancer.²¹ In fact, although CT still remains the principal technique in staging ovarian cancer, the addition of FDG-PET seems to provide a better staging definition. As for pre-surgical staging, Yoshida et al.³⁴ enrolled 15 patients with suspected ovarian cancer and compared the results of CT alone with those of CT in addition to FDG-PET. Post-surgical histopathological findings were used as gold standard. Presurgical CT-alone staging was concordant with post-surgical histopathological findings in 8/15 (53%) patients, whereas presurgical CT plus FDG-PET staging was concordant in 13/15 (87%) patients. In particular, the additional information of FDG-PET increased the overall lesion-based sensitivity from 46% to 68%, specificity from 90% to 92%, and accuracy from 83% to 88%. A higher improvement in lesion detection was observed for extrapelvic locations (sensitivity from 24% to 63% and specificity from 85% to 93%).

Another diagnostic challenge in ovarian cancer staging is the definition of peritoneal involvement, as one of the principal ways of spread being one of the most important prognostic indicators of this neoplasm.³⁵ Early peritoneal disease may be limited to the ascitic fluid, but more advanced disease may invade the parietal peritoneum, omentum, mesenteric peritoneum, and surface of the bowel.

Macroscopic peritoneal involvement may have different aspects, including nodules of different size, flat plaque, and large sheets with little thickness.^{36,37} The heterogeneity of these findings may explain the difficulty in diagnosing peritoneal carcinomatosis. Surgical exploration and biopsies of suspected abdominal areas (subdiaphragmatic areas, lateral and paracolic gutters, scraping of the visceral and parietal surfaces, washing of the cul-de-sac, and cytological evaluation of peritoneal fluid) are the most common procedures for establishing peritoneal involvement. Conventional CT is currently the imaging procedure of choice to detect peritoneal carcinomatosis before surgery. However, it still remains inadequate^{37,38} with a sensitivity ranging from 17% to 54%.^{39,40}

Turlakow et al.⁴¹ analyzed CT and FDG-PET imaging in the detection of peritoneal carcinomatosis from different tumors, including ovarian cancer. The reported sensitivities for CT, FDG-PET, and CT combined with FDG-PET were 43%, 57%, and 78%, respectively. They concluded that FDG-PET helps in the diagnosis of peritoneal cancer involvement. A limitation of FDG-PET is the spatial resolution. In fact, of the ten reported FDG-PET FN cases, nine were due to small disease, as confirmed at histopathological findings (from 0.2 to 0.5 cm diameter). Examples of peritoneal neoplastic involvement as detected by FDG-PET are reported in Figures 9.1 and 9.2.

In staging neoplastic disease, PET images are usually qualitatively evaluated. However, quantitative evaluation of areas of increased activity can be performed on attenuation corrected scans. The quantification of FDG uptake in a lesion by means of measurement of the standardized uptake value (SUV) may be useful to determine whether the lesion is more likely to be benign or malignant. SUV is calculated as follows: $SUV = (\text{dose in tissue}/\text{injected dose}) \times \text{patient weight}$. SUV is dependent on many variables,

including body mass and the region of interest evaluated. Therefore it is not often used for diagnosis, but is commonly used to follow up treatment response. SUVs tend to be higher in tumor tissue as compared to corresponding normal tissue.

The value of PET, in comparison with conventional modalities, in diagnosis and staging primary ovarian cancer has been investigated by several authors, as reported in Table 9.1.

A potential advantage of PET is that lesions are conspicuous relative to minimal background activity, due to increased radiotracer uptake in tumor lesions. This phenomenon may help in detecting metastatic tumor on visceral surfaces and in normal-sized nodes. However, for lesions that are considered to be pathologic, accurate localization for surgical resection may be difficult, because of the lack of precise anatomic landmarks. In functional PET imaging, the evaluation of tracer distribution in the body without knowing its morphological substrate limits image interpretation. Different factors, including the kinetics and metabolism of tracers, may influence functional imaging. As an example, difficulties in image interpretation are encountered for lesions located in abdominal regions, as FDG physiological excretion is via the intestine and urinary tract. Therefore, in some cases, the characterization of a focal uptake cannot be definitively accomplished and the presence of disease cannot be excluded or confirmed. PET is, in fact, usually performed in conjunction with CT, the standard imaging technique for the majority of neoplasms.²¹ The combined use of CT and PET yields a diagnosis and staging of cancer in a very fast and accurate way. In clinical practice, PET is generally indicated when patients have already been assessed with CT (or MRI), in order to understand the nature of a suspected lesion or to look for lesions not detected at CT/MRI, but clinically

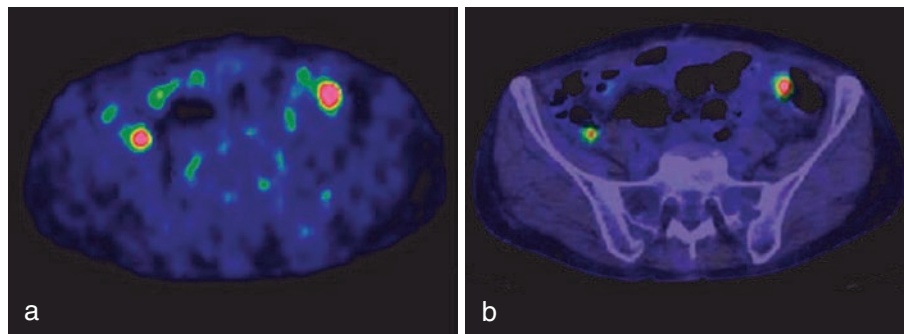


Figure 9.1

Peritoneal lesions in persistent carcinoma of the ovary. At positron emission tomography (PET) transaxial imaging (a), two circumscribed areas of intense focal [¹⁸F]fluro-2-deoxy-D-glucose (FDG) uptake are seen in the lower portion of the abdominal cavity, presumably in the peritoneal region. On related PET-computed tomography (CT) transaxial imaging (b), a correspondence between two small soft-tissue masses evident on CT imaging and the areas of abnormal FDG uptake at PET imaging is evident. These findings were judged as peritoneal persistent disease.

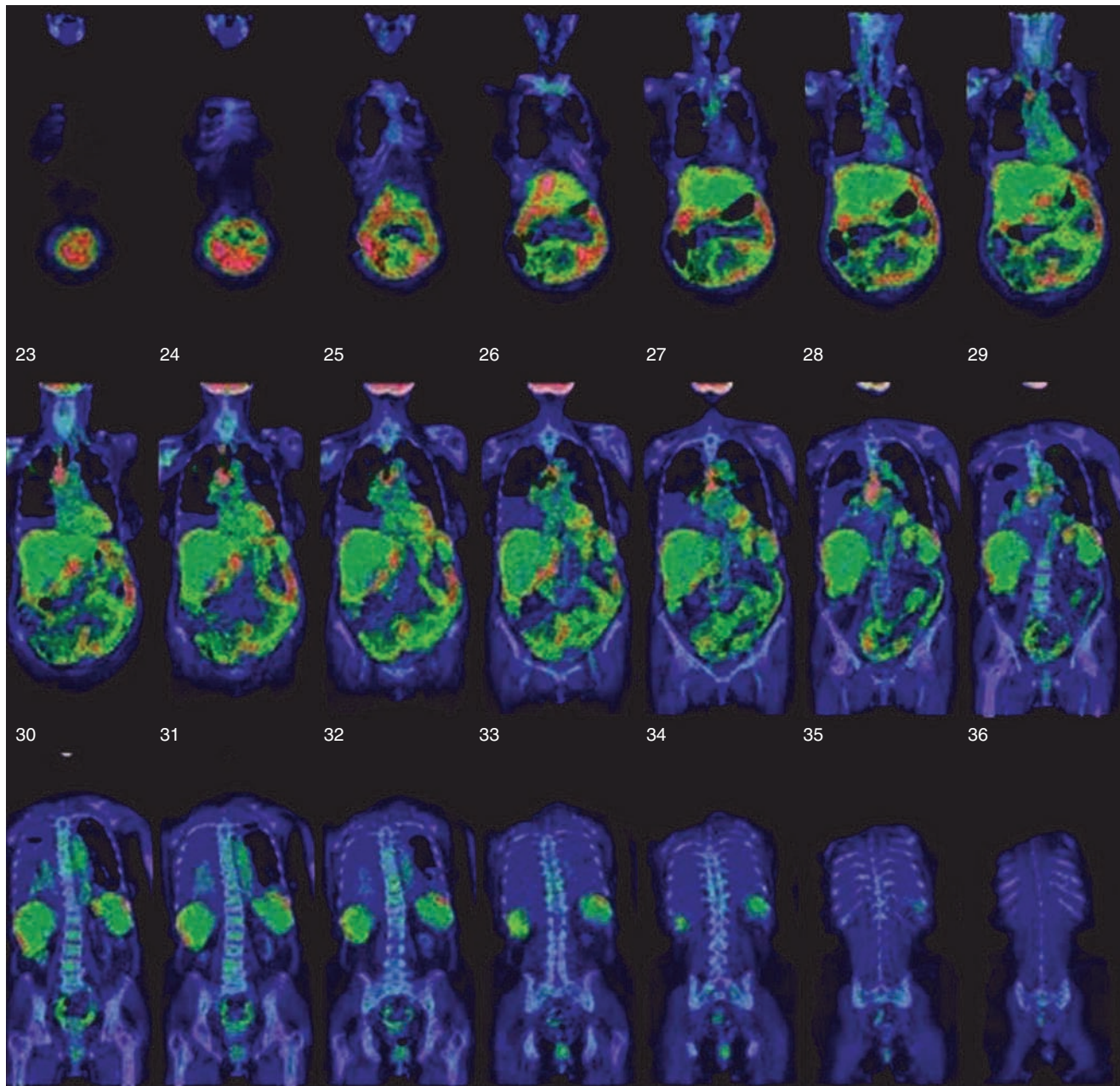


Figure 9.2

PET coronal images of a patient surgically operated for ovarian cancer. Diffuse abdominal FDG uptake is evident. This finding is representative of peritoneal involvement.

strongly suspected. The addition of CT imaging to PET is essential for PET image interpretation.^{21–24,32,33,42–46} However, in some cases, even when a previous CT study is available for visual comparison with PET data, such CT can be inadequate for the interpretation of PET images. In fact, the time spent between CT and PET examinations may be too long, and pathology can meanwhile change. Furthermore, the appropriate body section or the CT

window acquired (e.g. filtered for bone or soft tissue) is not always available for correct interpretation of PET images.

The introduction of PET–CT scanners overcomes these limitations.⁴⁷ The PET–CT device acquires PET and CT images that are contemporaneous and co-registered by means of the hardware arrangement. Increased FDG uptake may thus be localized with improved anatomic specificity.

Table 9.1 [¹⁸F]fluoro-2-deoxy-D-glucose-positron emission tomography (FDG-PET) and conventional imaging in ovarian cancer diagnosis and staging

Authors	Year	Patients (n)	Imaging modality	Sensitivity (%)	Specificity (%)	Accuracy (%)
Schroder et al. ²⁵	1999	40	PET	90	90	90
Grab et al. ²⁶	2000	101	US	92	60	63
			MRI	83	84	84
			PET	58	80	77
Rieber et al. ²⁷	2001	103	US	92	59	63
			MRI	83	84	83
			PET	58	78	76
			US + MRI + PET	92	84	85
Fenchel et al. ²⁸	2002	99	US	92	60	64
			MRI	83	84	84
			PET	58	76	74
			US + MRI + PET	92	85	86
Kawahara et al. ²⁹	2004	49	MRI	91	87	92
			PET	78	87	82
			MRI + PET	91	87	92
Yoshida et al. ³⁴	2004	15	CT	46	90	83
			CT + PET	68	92	88

US, ultrasonography; MRI, magnetic resonance imaging; CT, computed tomography.

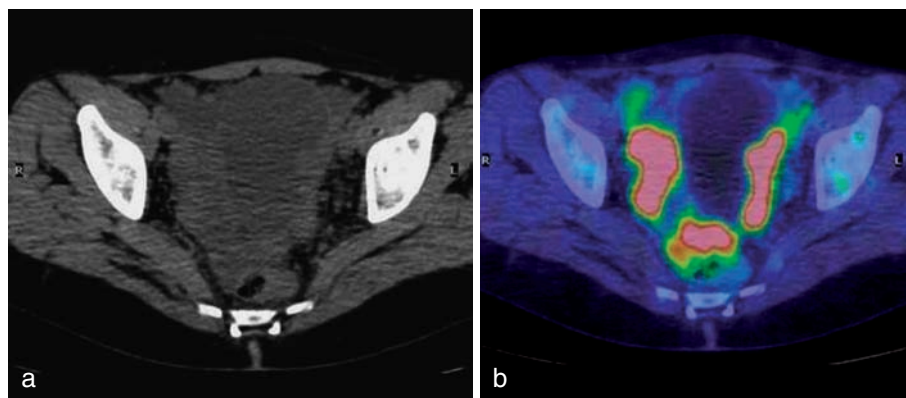
Potential advantages of PET–CT include increased lesion detectability, anatomic localization of lesions, and differentiation of a neoplastic disease process from inflammatory tissue (Figure 9.3).

PET–CT may provide a significant advantage in PET image interpretation in all cancers, including ovarian carcinoma, by accurately aligning whole-body anatomical and functional images in a single study session. The PET–CT technique and protocol will be described further in the second section of the present chapter.⁴⁷

Recurrent ovarian cancer

Background

Ovarian carcinoma has a propensity for either persistence or recurrence after primary surgery and chemotherapy, even in early-stage cases. In fact, after the completion of initial surgery, patients with ovarian cancer usually receive systemic chemotherapy for disease control. Despite the fact that ovarian cancer is very sensitive to platinum-based

**Figure 9.3**

Patient with adnexal mass suspected to be ovarian cancer. At CT imaging a hypodense area surrounded by a solid lesion is present (a). This area is clearly hypermetabolic at corresponding PET (b) where three areas of intense focal FDG uptake are seen in the pelvis, surrounding the central CT hypodense area. This finding is suggestive of neoplastic ovarian involvement.

chemotherapy, the majority of patients with advanced disease will die within 5 years of diagnosis.^{12,13} A second-look surgical procedure is performed in most institutions, as this is currently considered the most accurate method of assessing disease status in patients who have completed first-line treatment.^{7-9,12} For patients in whom recurrence is diagnosed, secondary cytoreductive surgery is beneficial if the largest tumor deposit is less than 5 cm; in other cases a second-line chemotherapeutic treatment is usually performed. Justification for the routine use of a second-look procedure has been questioned, and its role as a part of the standard treatment in the management of ovarian cancer is still discussed. Sijmons and Heintz⁹ reported that about 35% of patients with macroscopic or microscopic negative findings at second-look laparotomy will develop recurrent disease within 1 year of the procedure. In fact, accurately determining disease status is difficult when there are small, viable, neoplastic foci and when post-surgical adhesions are present. Currently, serial measurement of tumor-related antigen CA125 is the most common method used for monitoring clinical response after first-line treatment. However, its limited reliability is known, as CA125 elevation may indicate tumor persistence or recurrence but a negative value does not provide absolute assurance of the absence of disease.¹³⁻¹⁶

Recurrent ovarian cancer: diagnostic modalities

The traditional imaging modalities for evaluating patients with possible recurrence of ovarian cancer are CT and MRI. Two reports from the Radiology Diagnostic Oncology Group^{17,18} stated that CT and MRI are equally accurate, and either modality can be used for staging patients with ovarian cancer. However, correct assessment of persistent or recurrent disease using only these conventional imaging modalities can be difficult. MRI was found to be a useful adjunct to clinical examination to identify patients with recurrent disease, but it is limited in depicting small, calcified, peritoneal implants. In previous work,^{19,20} where findings at MRI and surgery were correlated, MRI showed an accuracy for lesions less than 2 cm of only 35%, which increased to 82% when the lesion diameter was greater than 2 cm. The overall accuracy rate was 59% for evaluating recurrent disease. Due to its wide availability and lower cost as compared to MRI, CT is currently the most common non-invasive imaging modality used to monitor patients with ovarian cancer after first-line treatment. Nevertheless, the effectiveness of CT scanning, even with the use of state of the art dynamic techniques, still remains unclear. This is mainly because CT has proved to have a low sensitivity for small lesions and hardly allows reliable differentiation between persistent disease and postoperative changes.

Recurrent ovarian cancer: role of functional imaging

Differently from CT and MRI, diagnoses with FDG-PET are made based on functional rather than morphological criteria. In fact, as previously reported, it may detect the presence of viable tumor tissue independent of its site and morphology.²¹⁻²³ FDG-PET is showing increasing usefulness in restaging and monitoring the therapeutic response of a variety of neoplasms, including gynecologic malignancies.⁵⁻⁸ In particular, there are several studies reporting the role of FDG-PET in the evaluation of ovarian cancer response after primary surgery and chemotherapy.^{24,32,33,42-49} Torizuka et al.⁴⁶ assessed the value of FDG-PET for the diagnosis of recurrent tumor in a series of 25 patients who had previously undergone surgery for ovarian cancer. FDG-PET showed a sensitivity of 80%, and an accuracy of 84%. In the same series, conventional imaging studies, including CT, showed lower sensitivity and accuracy rates of 55% and 64%, respectively. The results of that study confirmed that viable lesions in patients with treated ovarian cancer may become detectable due to metabolic changes before any morphological correlate. Nakamoto et al.⁴³ described the clinical value of FDG-PET in 24 patients with a suspicion of ovarian tumor recurrence. In their work, FDG-PET alone had a fairly good rate of diagnostic accuracy (79%). Interestingly, by adding information from conventional imaging modalities, including CT, the FDG-PET accuracy rate improved to 94%. Similar results were also obtained by Picchio et al.⁴⁹ In their series, where FDG-PET and CT images were co-registered using software, it was suggested that FDG-PET used in conjunction with CT improves the overall detection rate of residual ovarian carcinoma, compared to CT used alone. This study additionally indicated that the real advantage of PET in addition to CT is the possibility to exclude the presence of residual viable tumor after treatment, as shown by a high negative predictive value (NPV). However, a limitation of PET, as for morphological imaging modalities, is the misdetection of microscopic disease that can be depicted by histological analysis. In fact, it has been reported that PET may accurately detect tumors greater than 1.0 cm in diameter and that the sensitivity of FDG-PET for persistent lesions smaller than 0.5 cm in diameter is low. Lesions smaller than this size may be not visible, as it is smaller than the PET spatial resolution. Difficulties in identifying small tumors with FDG-PET were also reported in a study by Cho et al.,⁴⁵ in which the sensitivity for lesions smaller than 1.0 cm was about 50%. In addition, physiologic uptake observed in the stomach, colon, and bladder may occasionally mask the abnormal uptake of tiny disseminated lesions. Because of these circumstances, and of the reported FDG-PET limited sensitivity for small lesion detection, several authors have stated that it may be difficult to replace the second-look surgical procedure in the detection of persistent and recurrent

ovarian cancer. However, small, viable, neoplastic foci may be missed even at surgery, as suggested by Sijmons and Heintz.⁹ In their study, it was reported that when no tumor is found at second-look laparotomy, either macroscopically or microscopically, the persistence rate is about 35%.

In conclusion, FDG-PET may be a cost-effective, non-invasive imaging procedure for recurrent ovarian cancer. PET could replace, or at least postpone, some of the second-look operations in patients who have suspicious CT findings or rising tumor markers.

Recurrent ovarian cancer: integrated PET-CT, technique and preliminary results

As previously reported, a new imaging technique, combining a full-ring-detector clinical PET scanner and a multidetector row helical CT scanner in one machine, has been recently introduced into clinical practice.⁵⁰⁻⁵⁴ Both scanners are aligned so that patients can undergo imaging in either of two gantries by moving the one-system table. In this way, coverage of anatomically co-registered images from the head to the pelvic floor is obtained by means of the hardware, rather than by means of post-acquisition software. One of the advantages of integrated PET-CT over PET alone is the capability to localize foci of elevated tracer uptake with improved anatomical specificity.

The PET-CT standard protocol is as follows: patients fast for at least 6 hours before the intravenous administration of approximately 10 mCi (370 MBq) of FDG. In addition, patients are usually orally hydrated (500 ml of water) during the FDG uptake period, and are asked to empty their bladder before positioning for PET-CT study. Approximately 60 minutes after the injection of FDG, the combined examination starts. CT data are acquired first. An unenhanced CT image is generally obtained from the pelvic floor to the patient's head with the use of a standardized protocol. Several CT protocols are available, and one of the most used is the following: 140 kV, 80 mA (but adjusted for body thickness), a tube rotation time of 0.5 second per revolution, a pitch of 6, a section thickness of 5 mm to match the section thickness of PET images, and an acquisition time of 22 seconds. CT scans are acquired during shallow breathing. No oral or intravenous contrast agent is administered routinely, although intravenous injection of iodinated contrast media is feasible and can be useful for specific clinical questions, especially in cancer patients. Immediately after CT scanning, PET is performed, covering the identical axial field of view. The mean acquisition time for PET is usually 4 minutes per table position; as six incremental table positions are acquired, the PET study has a mean duration of 24 minutes. PET images are acquired

during quiet breathing. The PET component of the scanner has an in-plane spatial resolution which may range between 0.4 and 0.6 cm. Attenuation correction is performed by using CT images: the CT pixel values in Hounsfield units are transformed into linear attenuation coefficients for the 511-keV energy radiation. For fusion with PET data, images are reconstructed with a 128 × 128 matrix, an ordered subset expectation maximum iterative reconstruction algorithm, an 8-mm Gaussian filter, and a 50-cm field of view. Attenuation correction of the PET scans is needed for fusion with the CT scans. Attenuation correction compensates for differing activity in deep versus superficial lesions.

Image analysis for integrated PET-CT is performed as follows: attenuation-corrected PET images, CT images, and co-registered PET-CT images are displayed together on the monitor and the PET-CT examination analyzed as a single study. At PET-CT, regions of increased FDG activity seen at PET can be localized on CT scans, and lesions seen at CT can be evaluated for pathologic activity on PET scans. For peritoneal and pelvic recurrent lesions, PET-CT results are reported as whether or not abnormal FDG uptake is present in any abdominal region, and, when present, its exact anatomic site is indicated on the basis of CT findings. As for lymph node sites, the diagnosis of pathologic lymph nodes on PET-CT images is based on the presence of focal increased FDG uptake on PET images, whose location corresponded to lymph nodal chains on CT images. All data sets are analyzed at a workstation capable of providing interactively multiplanar reformations and any appropriate window and level settings: the images are reviewed in axial, coronal, and sagittal planes with a varying gray scale and rotating views.

Some pitfalls may be associated with PET-CT. Although the external anatomy is aligned, respiratory motion and bowel peristalsis can result in a mismatch between the location of a lesion at PET and its location at CT. A relatively common pitfall involves the gastrointestinal tract, where normal activity may be misinterpreted as pathologic or vice versa, especially if the activity is focal. Moreover, the size of lesions with intense radiotracer uptake can be overestimated on a PET scan relative to the lesion size at CT scan, due to the 'blooming' of intense activity that occurs at PET.

The value of PET and PET-CT in detecting ovarian cancer recurrence has been studied by several investigators in recent years (Table 9.2). Results of a recent investigation,⁵⁵ reporting a comparison of PET-CT and histopathologic findings, indicate that integrated PET-CT may be an effective means of detecting persistent or recurrent ovarian carcinoma, showing an overall accuracy of 77%. Results from that study also indicate that integrated PET-CT has a low (57%) NPV, and high (89%) positive predictive value (PPV), in detecting residual neoplastic lesions after first-line treatment. Interestingly, this is in agreement with previous results obtained with PET alone.^{44,46} The low NPV

Table 9.2 FDG-PET, PET-CT, and conventional imaging in ovarian cancer recurrence

Authors	Year	Patients (n)	Imaging modality	Sensitivity (%)	Specificity (%)	Accuracy (%)
Kubik-Huch et al. ¹⁹	2000	10	PET	100	50	90
			CT	40	50	43
			MRI	86	100	89
Nakamoto et al. ⁴³	2001	24	CT/MRI	73	75	73
			CT/MRI + PET	92	100	94
Zimny et al. ⁴⁴	2001	54	PET	83	83	—
Cho et al. ⁴⁵	2002	31	PET	45	100	91
			CT	54	100	92
Torizuka et al. ⁴⁶	2002	25	PET	80	100	84
			CT-MRI	55	100	64
Bristow et al. ⁴⁸	2002	22	PET-CT	83	—	82
Picchio et al. ⁴⁹	2003	25	CT	83	92	86
			CT + PET	83	92	86
Sironi et al. ⁵⁵	2004	31	PET-CT	78	75	77

seems to depend on the limited capability of PET-CT in depicting microscopic or small-volume lesions: such a limitation of PET-CT may make it difficult to identify patients with minimal tumor deposits. In those patients, therefore, the assessment of disease may still require a surgical second-look. On the other hand, integrated PET-CT presented a high PPV in revealing persistent disease: this could allow reliable identification of those patients with macroscopic disease who are candidates for salvage treatment.⁵⁵ PET-CT study has a potential role in evaluating patients for recurrent ovarian cancer, particularly those with negative CT or MRI findings and rising tumor marker levels.

PET-CT may be a valuable diagnostic investigation for the follow-up of ovarian cancer patients after first-line treatment, mainly because of its ability to depict macroscopic residual disease. Furthermore, integrated PET-CT could have a clear clinical impact on the therapeutic management of patients with ovarian cancer. In fact, following primary cytoreductive surgery and chemotherapy, a patient could be evaluated for persistence of disease by this imaging modality and then proceed to the most appropriate second-line treatment. Additional investigations with accurate histopathologic correlation are necessary to determine the benefits of lesion detectability at PET, and anatomic localization at CT, on combined PET-CT scans.

References

- Cannistra SA. Cancer of the ovary. *N Engl J Med* 1993; 329: 1550–9.
- American Cancer Society. Cancer facts and figures: 1998. Atlanta, GA: American Cancer Society, 1998.
- Landis SH, Murray T, Bolden S, Wingo PA. Cancer statistics. *CA Cancer J Clin* 1999; 49: 8–31.
- Hoskins WJ. Surgical staging and cytoreductive surgery of epithelial ovarian cancer. *Cancer* 1993; 71: 1534–40.
- Hoskins WJ. Epithelial ovarian carcinoma: principles of primary surgery. *Gynecol Oncol* 1994; 55: 91–6.
- McGuire WP, Hoskins WJ, Brady MF et al. Cyclophosphamide and cisplatin compared with paclitaxel and cisplatin in patients with stage III and stage IV ovarian cancer. *N Engl J Med* 1996; 334: 1–6.
- Friedman JB, Weiss NS. Second thoughts about second-look laparotomy in advanced ovarian cancer. *N Engl J Med* 1991; 322: 1079–81.
- Creasman WT. Second-look laparotomy in ovarian cancer. *Gynecol Oncol* 1994; 55: 122–7.
- Sijmons EA, Heintz AP. Second-look and second surgery: second chance or second best? *Semin Surg Oncol* 2000; 19: 54–61.
- Omura GA, Brady ME, Homesley HD et al. Long-term follow-up and prognostic factor analysis in advanced ovarian carcinoma: the Gynecologic Oncology Group experience. *J Clin Oncol* 1991; 9: 1138–50.
- NIH Consensus Development Panel on Ovarian Cancer. Ovarian cancer. Screening, treatment and follow-up. *JAMA* 1995; 273: 491–6.
- Rose PG. Surgery for recurrent ovarian cancer. *Semin Oncol* 2000; 27: 17–23.
- Thigpen JT, Vance RB, Khansur T. Second-line chemotherapy for recurrent carcinoma of the ovary. *Cancer* 1993; 71: 1559–64.
- Rubin SC, Hoskins WJ, Hakes TB et al. Serum CA 125 levels and surgical findings in patients undergoing secondary operations for epithelial ovarian cancer. *Am J Obstet Gynecol* 1989; 160: 667–71.

15. Pastner B, Orr JW, Mann WJ et al. Does serum CA125 level prior to second-look laparotomy for invasive ovarian carcinoma predict size of residual disease? *Gynecol Oncol* 1990; 38: 373–6.
16. Folk JJ, Botsford M, Musa AG et al. Monitoring cancer antigen 125 levels in induction chemotherapy for epithelial ovarian carcinoma and predicting outcome of second-look procedure. *Gynecol Oncol* 1995; 57: 178–82.
17. Kurtz AB, Tsimikas JV, Tempany CM et al. Diagnosis and staging of ovarian cancer: comparative values of Doppler and conventional US, CT, and MR imaging correlated with surgery and histopathologic analysis. Report of the Radiology Diagnostic Oncology Group. *Radiology* 1999; 212: 19–27.
18. Tempany CM, Zou KH, Silverman SG et al. Staging of advanced ovarian cancer: comparison of imaging modalities. Report from the Radiological Diagnostic Oncology Group. *Radiology* 2000; 215: 761–7.
19. Kubik-Huch RA, Dorffler W, von Schulthes GK et al. Value of FDG positron emission tomography, computed tomography, and magnetic resonance imaging in diagnosing primary and recurrent ovarian carcinoma. *Eur Radiol* 2000; 10: 761–7.
20. Forstner R, Hricak H, Powell CB et al. Ovarian cancer recurrence: value of MR imaging. *Radiology* 1995; 196: 715–20.
21. Ak I, Stokkel MP, Pauwels EK. Positron emission tomography with FDG in oncology. The clinical value in detecting and staging primary tumors. *J Cancer Res Clin Oncol* 2000; 126: 560–74.
22. Flamen P, Stroobants S, Cutsem EV et al. Additional value of whole-body positron emission tomography with FDG in recurrent colorectal cancer. *J Clin Oncol* 1999; 17: 894–901.
23. Schelling M, Avril N, Nahrig J et al. Positron emission tomography using FDG for monitoring primary chemotherapy in breast cancer. *J Clin Oncol* 2000; 18: 1689–95.
24. Hubner KE, McDonald TW, Niethammer JG et al. Assessment of primary and metastatic ovarian cancer by positron emission tomography (PET) using FDG. *Gynecol Oncol* 1993; 51: 197–204.
25. Schroder W, Zimny M, Rudolsky C et al. The role of 18F-fluoro-deoxyglucose positron emission tomography 18F-FDG PET in diagnosis of ovarian cancer. *Int J Gynecol Cancer* 1999; 9: 117–22.
26. Grab D, Flock F, Stohr I, et al. Classification of asymptomatic adnexal masses by ultrasound, magnetic resonance imaging and positron emission tomography. *Gynecol Oncol* 2000; 77: 454–9.
27. Rieber A, Nussle K, Stohr I et al. Preoperative diagnosis of ovarian tumors with MR imaging. Comparison with transvaginal sonography, positron emission tomography and histological findings. *AJR Am J Roentgenol* 2001; 177: 123–9.
28. Fenchel S, Grab D, Nuessle K et al. Asymptomatic adnexal masses: correlation of FDG PET and histopathological findings. *Radiology* 2002; 223: 780–8.
29. Kawahara K, Yoshida Y, Kurokawa T et al. Evaluation of positron emission tomography with tracer 18-fluoro-deoxyglucose in addition to magnetic resonance imaging in the diagnosis of ovarian cancer in selected woman after ultrasonography. *J Comput Assist Tomogr* 2004; 28: 505–16.
30. Romer W, Avril N, Dose J et al. Metabolic characterization of ovarian tumors with positron emission tomography and F-18 fluorodeoxyglucose. *Rofo Fortschr Geb Roentgenstr Neuen Bildgeb Verfahr* 1997; 36: 228–33.
31. Zimny M, Schroder W, Wolters S et al. 18F-fluorodeoxyglucose PET in ovarian carcinoma: methodology and preliminary results. *Nuklearmedizin* 1997; 36: 228–33.
32. Karlan BY, Howkins R, Hoh C et al. Whole-body positron emission tomography with FDG can detect recurrent ovarian carcinoma. *Gynecol Oncol* 1993; 51: 175–81.
33. Casey MJ, Gupta NC, Muths CK. Experience with positron emission tomography (PET) scans in patients with ovarian cancer. *Gynecol Oncol* 1994; 53: 331–8.
34. Yoshida Y, Kurokawa T, Kawahara K et al. Incremental benefits of FDG positron emission tomography over CT alone for preoperative staging of ovarian cancer. *AJR Am J Roentgenol* 2004; 182: 227–33.
35. Simojoki M, Santala M, Vuopala S et al. The prognostic value of peritoneal cytology in ovarian cancer. *Eur J Gynecol Oncol* 1999; 20: 357–60.
36. Kaste SC, Marina N, Fryrear R et al. Peritoneal metastases in children with cancer. *Cancer* 1998; 83: 85–9.
37. Raptopoulos V, Gourtsyiannis N. Peritoneal carcinomatosis. *Eur Radiol* 2001; 11: 2195–206.
38. Boudiaf M, Bedda S, Soyer P et al. Preoperative evaluation of gastric adenocarcinomas: comparison of CT results with surgical and pathological results. *Ann Chir* 1999; 53: 115–22.
39. Low RN, Barone RM, Lacey C et al. Peritoneal tumor: MR imaging with dilute oral barium and intravenous gadolinium-containing contrast agent compared with unenhanced MR and CT. *Radiology* 1997; 204: 513–20.
40. Gryspeerdt S, Clabout L, Van Hoet L et al. Intraperitoneal contrast material combined with CT for detection of peritoneal metastases of ovarian cancer. *Eur J Gynaecol Oncol* 1998; 19: 434–7.
41. Turlakow A, Yeung H, Salmon AS et al. Peritoneal carcinomatosis: role of FDG-PET. *J Nucl Med* 2003; 44: 1407–12.
42. Rose PG, Faulhaber P, Miraldi F, Abdul-Karim FW. Positron emission tomography for evaluating a complete clinical response in patients with ovarian or peritoneal carcinoma: correlation with second-look laparotomy. *Gynecol Oncol* 2001; 82: 17–21.
43. Nakamoto Y, Saga T, Ishimori T et al. Clinical value of positron emission tomography with FDG for recurrent ovarian cancer. *AJR Am J Roentgenol* 2001; 176: 1449–54.
44. Zimny M, Siggelkow W, Schroder W et al. FDG positron emission tomography in the diagnosis of recurrent ovarian cancer. *Gynecol Oncol* 2001; 83: 310–15.
45. Cho SM, Ha HK, Byun JY et al. Usefulness of FDG PET for assessment of early recurrent epithelial ovarian cancer. *AJR Am J Roentgenol* 2002; 179: 391–5.
46. Torizuka T, Nobezawa S, Kanno T et al. Ovarian cancer recurrence: role of whole-body positron emission tomography using FDG. *Eur J Nucl Med* 2002; 29: 797–803.
47. Makhija S, Howden N, Edwards R et al. Positron emission tomography-computed tomography imaging for the detection of recurrent ovarian and fallopian tube carcinoma: a retrospective review. *Gynecol Oncol* 2002; 85: 53–8.
48. Bristow ER, Simpkins F, Pannu HK, Fishman EK, Montz FJ. Positron emission tomography for detecting clinically occult

- surgically resectable metastatic ovarian cancer. *Gynecol Oncol* 2002; 85: 196–200.
49. Picchio M, Sironi S, Messa C et al. Advanced ovarian carcinoma: usefulness of FDG PET in combination with CT for lesion detection after primary treatment. *Q J Nucl Med* 2003; 47: 77–84.
 50. Beyer T, Townsend DW, Brun T et al. A combined PET-CT scanner for clinical oncology. *J Nucl Med* 2000; 41: 1369–79.
 51. Kluetz PG, Meltzer CC, Villemagne VL et al. Combined PET-CT imaging in oncology: impact on patient management. *Clin Positron Imaging* 2000; 3: 223–30.
 52. Townsend DW. A combined PET-CT scanner: the choices. *J Nucl Med* 2001; 42: 533–4.
 53. Hany FT, Steinert HC, Goerres GW, Buck A, von Schulthess GK. PET diagnostic accuracy: improvement with in-line PET-CT system: initial results. *Radiology* 2002; 225: 575–81.
 54. Lardinois D, Weder W, Hany TF et al. Staging of non-small-cell lung cancer with integrated positron emission tomography and computed tomography. *N Engl J Med* 2003; 348: 2500–7.
 55. Sironi S, Messa C, Mangili G, et al. Value of integrated FDG PET/CT for persistent ovarian cancer: correlation with histopathologic findings. *Radiology* 2004; 233: 433–40.

Breast cancer

*Emilio Bombardieri, Marco Maccauro,
Orazio Schillaci, and Flavio Crippa*

Background

The role of nuclear medicine in breast cancer has become very important. Different diagnostic approaches have been proposed to study breast tumors, and some of them have been adopted in the current work-up of patient management (Table 10.1). Sentinel lymph node biopsy (SLNB) after localization through lymphoscintigraphy has achieved large consensus among surgeons as a method for staging as well as enhancing the pathological analysis. The imaging of breast cancer and cancer metastases was studied initially with scintimammography, without a definitive satisfactory sensitivity, in spite of some improvement obtained by the use of single photon emission computed tomography (SPECT) and the recent development of dedicated breast γ cameras. There is no doubt that positron emission tomography (PET) and PET-computed tomography (CT) are the most reliable modalities for visualizing both primary and metastatic breast lesions. PET and PET-CT today can compete with conventional morphological tools in staging, detecting tumor relapses, evaluating tumor response to therapy, and giving useful prognostic indications. This chapter will summarize the most relevant advantages of nuclear medicine techniques, with particular attention to the diagnostic potential offered by PET.

Sentinel lymph node biopsy

SLNB has been proposed with the aim of staging breast cancer, to avoid axillary node dissection (ALD), which is not curative and is associated with a significant rate of complication.¹ In breast cancer patients, SLNB has been evaluated as an alternative method to routine axillary clearance to detect axillary node status. Today, many years after the first report from Krag et al., SLNB is considered in the majority of institutions to be the new standard method for axillary lymph node staging in breast cancer.² The efficacy

of SLNB has been widely demonstrated; the technique is considered very accurate and feasible, able to improve the staging and enhance the pathological analysis, and it shows less morbidity than axillary lymph node dissection. Several clinical studies have confirmed that lymphoscintigraphy in combination with γ probe-guided surgery is the best option for depicting and removing the sentinel lymph node (SLN).^{3,4} Nuclear medicine physicians are aware that the protocol for lymphoscintigraphy differs among Centers, and some controversies still exist:^{2,5-7}

- type of radiopharmaceutical: ^{99m}Tc -labeled sulfur colloids (size 15–5000 nm), ^{99m}Tc -labeled nanocolloids (size 4–100 nm), ^{99m}Tc -labeled antimony trisulfide colloids (size 3–30 nm)
- site of injection: intratumoral, intraparenchymal, periareolar/subareolar, intradermal/subdermal
- injected activity and volume of injection.

In spite of many discussions about and various experiences with the methods and optimal technique proposed, the general thought is that, whatever method is used, lymphoscintigraphy is always able to localize the axillary SLNs. It should be stressed that lymphoscintigraphy can also visualize the internal mammary chain in 2% of cases, when it is performed after subdermal/intradermal injection of radiocolloid.⁸ A deep injection under the tumor mass increases the rate of detection to 8%.⁹ The highest rate of visualization of the internal mammary chain has been described for tumors located in the inner quadrant. This finding leads to a change in the stage from N0 or N1 to N3.¹⁰

Despite the fact that SLNB is routinely performed in clinical practice, the clinical indications for SLNB nowadays still represent a matter of study. Many centers consider SLNB as standard practice in the treatment of patients with early breast cancer and clinically negative lymph nodes. Other proposals are under evaluation in order to extend and validate its indications. The available data derive mainly from retrospective studies. Many randomized prospective clinical trials have been designed to better evaluate SLNB, and most of them are still ongoing world wide.

Table 10.1 Current diagnostic work-up in patients for breast cancer

<i>Clinical problem</i>	<i>Tests</i>
Diagnosis of breast mass	Autopalpation Patient history Physical examination Mammography Ultrasonography (US) Magnetic resonance imaging (MRI) Scintimammography Cytology Biopsy
Follow-up	Physical examination Patient history Mammography (also for contralateral breast) US upper abdomen Chest X-ray Bone scan Computed tomography (CT) MRI Positron emission tomography (PET), PET-CT Tumor markers (CA15.3, AP)
Staging	Lymphoscintigraphy and sentinel node biopsy (locoregional staging) US upper abdomen Chest X-ray Bone scan CT MRI PET, PET-CT

The Medical Research Council in the UK has compared SLNB and axillary clearance in 1300 women with clinically negative nodes, randomized to either surgery or SLNB.¹⁰ Veronesi et al. have published the results of a prospective study in 517 women with breast cancer randomly assigned to undergo either SLNB and axillary dissection or SLNB followed by dissection only in the case of positive SLN. In patients who had routine axillary dissection, the sensitivity, specificity, and accuracy of SLN detection were 91.2%, 100%, and 96.6%, respectively. The false-negative results were 8.8% and the negative predictive value 95.4%.¹¹

Two studies were designed in the USA by the National Surgical Adjuvant Breast and Bowel Project Foundation in order to investigate whether SLNB alone was equivalent to

axillary dissection in terms of long-term control of regional disease, disease-free survival, and overall survival, in 5500 breast cancer patients with clinically negative axillae and pathologically negative SLNs.^{12,13}

The European Organization for Research and Treatment of Cancer (EORTC) is going to compare complete axillary dissection with radiotherapy in the axillae of women with positive SLNs. This trial has had an accrual of 3485 patients within 3 years.¹⁴ The International Breast Cancer Study Group has the goal of studying the prognostic value of SLN micrometastases or isolated tumor cells only in the SLN; patients are assigned randomly to either complete axillary clearance or no treatment.¹⁵

These large studies all demonstrate the extreme interest of clinicians in SLNB, and how the various issues are matters of much attention and investigation. Clinical trials and results deriving from clinical practice have led to changes in some concepts about the use of the SLNB technique. In fact, several situations were considered in the past to be contraindications to SLNB. Today, much clinical evidence has contributed to clarify several issues about: (1) the efficacy of SLNB in multifocal/multicentric breast cancer; (2) the effect of primary chemotherapy; and (3) the effect of previous breast biopsy. It has been demonstrated that SLN localization maintains its high negative predictive value also in multicentric/multifocal breast cancer, and in patients who have undergone breast biopsy SLNB can be a correct indication.^{16–18} Recent studies have concluded that SLNB in patients after neoadjuvant chemotherapy has demonstrated a certain rate of success in SLN identification and removal, with no significant differences compared to patients prior to chemotherapy; therefore, SLNB is also applicable following neoadjuvant chemotherapy.^{19–21} In the same way, it has been shown that SLNB can be performed accurately also after excisional biopsy, and is also effective in patients who have undergone partial mastectomy.^{22,23}

Other interesting questions, mainly in the area of pathology, are focused on the meaning of micrometastatic disease and occult metastases. Should the prognostic value of detected micrometastases in the SLN address the surgeon to perform axillary dissection or not?^{24,25} This is another subject of study where attention is transferred to new techniques of tissue and cell characterization using molecular biology analysis on pathological samples from the SLN.

Experience with SLNB is ongoing, and there is a continuous effort to better standardize and optimize all steps of this technique (surgery, nuclear medicine, pathology). This is the final goal of all investigations that are being carried out, also including prospective studies. We can say without any doubt that SLN localization and biopsy not only represents impressive progress in the area of nuclear medicine, but also is one of the most important developments in surgery.

Breast cancer imaging with planar scintigraphy and single photon emission computed tomography

[^{99m}Tc]sestamibi and [^{99m}Tc]tetrofosmin are the radiopharmaceuticals currently used to visualize breast lesions. They were introduced for myocardial perfusion imaging, and have been demonstrated to concentrate in cancer cells.²⁶ The mechanisms of uptake are similar, and both [^{99m}Tc]sestamibi and [^{99m}Tc]tetrofosmin are transport substrates for P-glycoprotein (Pgp), a plasma membrane protein encoded by the multidrug resistance (MDR) gene.^{26–31} [^{99m}Tc]sestamibi was the first radiopharmaceutical registered for this purpose in the USA, about 14 years ago. Scintimammography with [^{99m}Tc]sestamibi has been evaluated in single-center and multicenter trials in order to assess its sensitivity and specificity in both palpable and non-palpable breast lesions. The clinical data describe a good sensitivity for palpable lesions but poor sensitivity for non-palpable lesions.³² A large study in 673 patients was conducted, involving 42 clinical centers; randomized scintigraphic images were read by two groups of three, blinded readers. The sensitivity and specificity of [^{99m}Tc]sestamibi were strictly size-dependent, and were much higher when the lesions were >1cm in size (Figure 10.1). A meta-analysis was carried out by Hussain and Buscombe in 2424 breast cancer patients, and another meta-analysis was performed by Libermann et al. in 5340 patients.^{33,34} Both studies reported a maximum sensitivity of 85% and a maximum specificity of 86%; this means that in the diagnosis of tumor mass the authors had a not negligible ratio (15%)

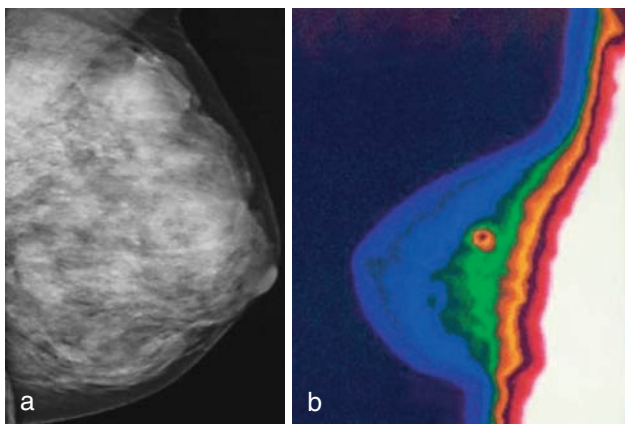


Figure 10.1

Forty-one-year-old patient with extremely dense breast on mammography (a) and a palpable mass on the left breast, which shows focal [^{99m}Tc]sestamibi uptake at scintimammography (b). Final diagnosis: invasive ductal breast carcinoma.

of false-negative results. A multicenter prospective clinical trial evaluated the diagnostic accuracy of scintimammography.³⁵ The results were a little better, since in 1243 evaluable patients the sensitivity was estimated to be 93% and the specificity 87%, with an overall diagnostic accuracy of 88%. The problem of correct diagnosis of small lesions remains critical. Lesions <1 cm in size are detectable in only 50% of cases.^{36,37} Also, results from a multicenter clinical trial involving 673 patients in North American institutions indicated that the sensitivity was 87% for palpable and 61% for non-palpable lesions.³⁸ The diagnostic specificity of scintimammography is usually better than the specificity, but several false-positive results have been described. These are due to areas of radiopharmaceutical uptake in local inflammation, fibroadenomas, and fibrocystic changes. [^{99m}Tc]sestamibi and [^{99m}Tc]tetrofosmin uptake in benign pathology is strongly correlated with the presence of proliferative changes.³⁹

Considering the worldwide experience in scintimammography, the results cannot be considered completely satisfactory for breast cancer diagnosis, since the low sensitivity, associated with the size of the lesions, cannot compete with the sensitivity of conventional radiological diagnostic imaging, such as mammography, ultrasound (US), and magnetic resonance imaging (MRI), which show higher spatial resolution⁴⁰ (Figure 10.2).

Scintimammography has also been used to evaluate tumor response to chemotherapy. The intensity of [^{99m}Tc]sestamibi in tumor lesions can change according to several biological factors, including the number and the activity of viable tumor cells. In this way it is possible to monitor the efficacy of anticancer treatments (Figure 10.3).

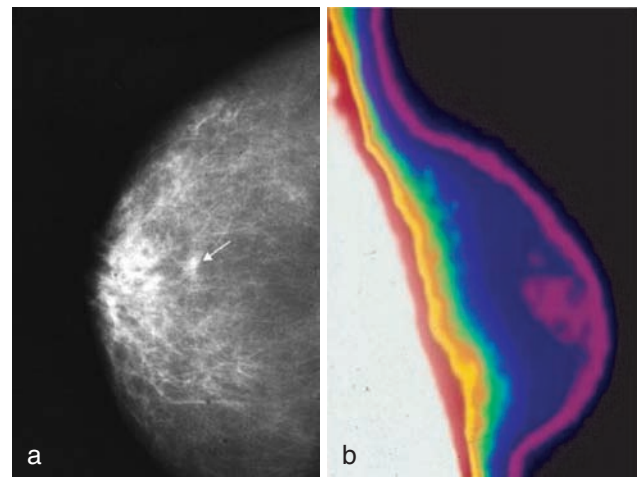


Figure 10.2

Sixty-four-year-old patient with a small highly suspicious lesion (arrow) on the right breast on mammography (a), which does not show [^{99m}Tc]sestamibi uptake at scintimammography (b), probably due to its limited size. Final diagnosis: invasive ductal breast carcinoma.

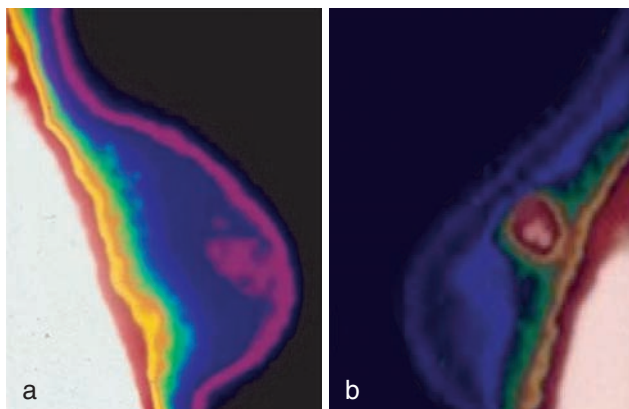


Figure 10.3

Patient with locally advanced left breast cancer. [^{99m}Tc]tetrofosmin imaging performed before (a) and after (b) neoadjuvant chemotherapy. Scintigraphy demonstrates only a partial response of the tumor to therapy.

Besides this, the [^{99m}Tc]sestamibi accumulation and release in tumors describe the MDR phenotype prior to any treatment. The evaluation of methoxyisobutylisonitrile (MIBI) kinetics as a MDR parameter includes: intensity of MIBI uptake, rapidity of tumor clearance, tumor/background ratio, etc., and according to several limited experiences it can predict success or failure of the treatment.

The acquisition of tomographic images, by means of SPECT, can enhance the sensitivity of planar scintimammography and reduce the number of false-negative results. An increasing number of SPECT studies have been reported in primary breast cancer detection in comparison with planar scintimammography. The accuracy of SPECT has proved higher than that observed in planar scintigraphy, in particular for the detection of small lesions.^{41–45} However, in this field, several technical problems can occur. Even if SPECT images provide better contrast resolution, in some cases it is difficult to obtain accurate localization. In this field the co-registration of SPECT with anatomical information obtained by radiological examination, or the commercial availability of a hybrid γ camera/CT scanner, can facilitate the fusion of morphological maps and SPECT images.⁴⁶ It should be remembered that SPECT images of good quality can be obtained only if the patient is in the supine position with arms raised above the head.^{47,48} The higher sensitivity of SPECT when compared to planar scintimammography was reported in a recent paper by Mathieu et al., who studied the impact of SPECT in a group of patients with discordant triple diagnosis (mammography, US, and fine-needle biopsy).⁴⁹ In a series of 104 patients (69 with proven breast cancer), SPECT showed a sensitivity of 88.4% and a specificity of 67%. Eleven cancers were diagnosed with SPECT, although planar images were negative.

The problem of detecting small tumors remains also with SPECT, and this is critical for the future application of conventional nuclear medicine modalities, considering that developments in oncology demand more and more the early identification of small, suspicious lesions. Today, scintimammography is carried out with a standard γ -camera (Anger camera), which has an intrinsically poor spatial resolution and limited detection geometry, because of the distance between the detector and the tumor mass. The design of the small field of view, high-resolution γ camera brings better flexibility in patient positioning, improving breast imaging without including the liver and heart, and giving breast compression. Some experimental dedicated γ cameras are also able to provide better intrinsic and extrinsic spatial resolution, and in very limited series of patients seem to improve the diagnostic performance.^{50,51} The dedicated camera LumaGEM® 3200S (Gamma Medica Inc. Northridge, USA), in a few studies of validation, gives high-resolution images that are able to visualize smaller and deeper breast cancer, overcoming the limitation of conventional scintimammography.^{52–54} In a study by Rhodes et al., the diagnostic sensitivity in tumors <1 cm was 86% (75% in T1a and 89% in T1b), while in tumors >1 cm in size it was 100%. These results are very preliminary; however, it seems that the availability of these new devices could partially improve the diagnostic value of scintimammography. Further studies are needed, and larger numbers of cases will allow a definite opinion to be drawn on the clinical impact of these devices.

SPECT, like planar scintimammography, can also simultaneously provide images of both breast and axillary regions. Furthermore, some comparative studies in breast cancer patients have shown that the performance of conventional SPECT is improved when a pinhole collimator is used for acquisition. Pinhole SPECT has a very high intrinsic spatial resolution, and is also able to describe the lymph node status with good accuracy.⁵⁵ In spite of some very interesting results obtained in certain qualified institutions, this method has been adopted in only a few centers, and is not of interest for routine staging.

In conclusion, the imaging of breast lesions with [^{99m}Tc]sestamibi and [^{99m}Tc]tetrofosmin, due to the facts that scintimammography does not reach an acceptable diagnostic sensitivity, the imaging protocol is fairly complex, patient positioning and image acquisition take time, compliance is not so good, and there is a current possibility to improve the diagnostic performance (tomography, collimators, dedicated breast cameras, etc.), at present does not give any satisfactory definitive perspective and remains an option of second choice in particular situations.⁵⁶ These have been described in the European Association of Nuclear Medicine (EANM) procedure guidelines for breast scintigraphy: (1) patients with equivocal mammograms; (2) patients with doubtful microcalcifications, or parenchymal distortions, in the presence of scarring following surgery

or biopsy; (3) patients with dense breasts; (4) patients with breast implants; (5) assessment of multicentric, multifocal, or bilateral disease; (6) monitoring response to neoadjuvant chemotherapy; and (7) evaluation and prediction of tumor response to chemotherapy for breast carcinoma. One should consider that all these indications, except for a few experimental applications that have been carried out using quantitative scintimammography to predict the chemoresistance of breast cancer prior to therapy (prediction of MDR), can be better covered by PET imaging.

Positron emission tomography imaging

Clinical diagnosis with PET in breast cancer patients is based mainly on the use of fluoro-2-deoxy-D-glucose labeled with fluorine-18 (^{18}F FDG). Breast cancer has been demonstrated to be particularly avid for FDG due to its elevated metabolic rate and the overexpression of some glucose transporters such as GLUT1 and GLUT3^{57–59} (Figure 10.4).

^{18}F FDG-PET was first used for breast imaging over 20 years ago by Beany et al., who studied tumor metabolism by measuring the blood flow and oxygen consumption in cancer.⁶⁰ The first diagnostic study of breast tumors was carried out by Wahl et al., who succeeded with FDG-PET to visualize primary breast cancer in a small group of patients with very large lesions.⁶¹ Many clinical trials have been carried out since these preliminary experiences, and today an impressive series of data confirm that PET plays an important role in the management of breast cancer patients.^{62,63} Clinical experience reports that FDG uptake is

higher in ductal carcinomas than in lobular carcinomas, in grade 3 carcinomas than in grade 1–2 carcinomas, and in carcinomas with a high level of p53 expression. Also, normal breast tissue shows a faint uptake of FDG: dense breast demonstrates higher FDG uptake than non-dense breast, and the lactating breast shows a high FDG uptake related to sucking. Acute mammary infections, inflammatory conditions, and post-surgical hemorrhagic mastitis may lead to FDG uptake.

When FDG-PET is used to evaluate a breast cancer patient, PET is able to: (1) detect whether a breast mass is benign or malignant; (2) determine the tumor extent (staging and restaging); (3) reveal local or distant recurrence; (4) assess response of the cancer to the treatment; and (5) prove the biological characterization of the tumor. The technological evolution of PET instrumentation has recently made available new integrated PET–CT systems, that combine a PET camera and CT scanner in a single session, providing both anatomical and functional information at the same time.⁶⁴ The functional and anatomic image fusion of ^{18}F FDG-PET–CT may improve the accuracy of cancer images, and clinical experience has demonstrated a diagnostic value superior to that of CT or PET alone.⁶⁵ Therefore, the introduction of PET in the diagnostic work-up of breast cancer patients is a great help in identifying malignant lesions and their metastases, and offers a higher accuracy in comparison to other conventional imaging modalities, such as US, mammography, CT, and MRI.^{66,67}

PET in the diagnosis of primary carcinoma

Clinical experience with PET in the diagnosis of primary carcinoma shows a good sensitivity for tumors > 0.8 cm in size, palpable, and with a high probability of malignancy (Figure 10.4). These tumors can often be visualized by other, conventional imaging modalities. For non-palpable tumors or for smaller breast lesions, the sensitivity and specificity are lower. The major factors limiting the accurate diagnosis of lesions < 0.5–0.6 mm in size by PET are the physical detection limits of the available scanners and the poor glucose utilization by some breast masses.^{68,69} A fundamental diagnostic issue is the differentiation between cancer and benign alterations. Among benign lesions, breast cysts are usually visualized by FDG-PET as a photopenic area.⁷⁰ The majority of fibroadenomas are negative. Fibrocystic changes and the inflammatory process often do not reveal any significant FDG uptake, even if some false-positive uptakes have been described with fibroadenoma, severe fibrocystic mastopathy, ductal ectasia, tubular angioepithelioma, and cystosarcoma phyllodes.^{68–71} A paper by Scheidhauer et al. on the use of FDG-PET in the primary diagnosis of suspicious breast

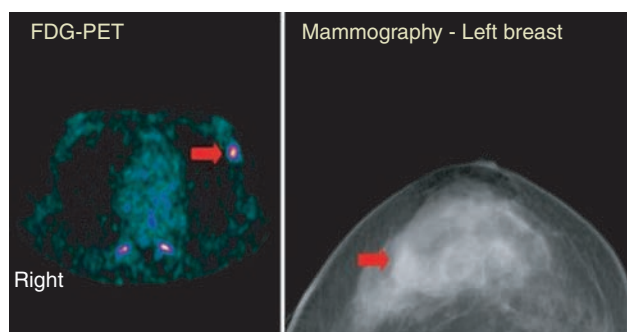


Figure 10.4

Patient with a malignant mass in the left breast shown on mammography. The focal uptake of fluoro-2-deoxy-D-glucose (FDG) visualized by FDG positron emission tomography (PET) in the transaxial slice confirms the mammographic findings. No other foci of FDG uptake were shown in the rest of the body by FDG-PET-whole-body scan.

lesions analyzes the experiences of different authors and summarizes a sensitivity ranging from 64 to 96%, a specificity from 73 to 100%, an accuracy from 70 to 97%, a positive predictive value from 81 to 100% and a negative predictive value from 52 to 89%.⁷² Of course the hybrid PET–CT system can increase the sensitivity of the test, enhancing the figures of merit. In the literature there are some reports of very small lesions detected by PET–CT; in these cases the hypermetabolism of cancer tissue could be a positive factor for its detection, in spite of the very small diameters of tumor masses.⁷³ Other clinical studies describe the occasional detection of unexpected areas of focal uptake in the breasts of patients undergoing PET–CT for reasons other than breast diagnosis or staging.⁷⁴ When evaluated, almost all of the abnormal foci that were seen in the breast subsequently proved to be breast carcinomas, and specifically infiltrating ductal carcinomas. In spite of such very interesting results with PET and PET–CT, there is a general agreement about the statement that FDG-PET should not be considered the first-choice modality for the diagnosis of any breast masses. In the study of breast lesions, mammography, in association with US, maintains excellent diagnostic efficacy with the advantage of lower cost. In the same way, mammography is the first diagnostic tool to be considered for screening breast cancer in the asymptomatic (Table 10.2). MRI has recently been proposed for screening women at high risk of breast cancer. Ultrasound should be considered an adjunctive tool for mammographically suspicious lesions, and as guidance for reliable histological diagnosis by percutaneous biopsy. Dynamic enhanced magnetic resonance mammography (MRM) shows a high sensitivity in detecting breast cancer and high resolution, but it has also a high rate of false-positive diagnosis.

FDG-PET can be very useful in some problematic cases, such as in women with breast prostheses where radiological modalities are not accurate, or in women with dense breasts or with breast alterations, who have already been exposed to morphological distortions (previous treatments, surgery, chemotherapy or radiotherapy).

PET in staging

Lymph node staging

While for the diagnosis of primary breast tumors oncologists have several different valid options (mammography, US, MRI), the diagnosis of axillary lymph node involvement is an area where nuclear medicine methods have obtained much consideration, because of the limits of the non-nuclear medicine techniques.⁷⁵ The relevance of SLNB in breast cancer patients after identification through lymphoscintigraphy has already been described.⁷⁶ It is known that clinical examination of the breast is not a reliable diagnostic tool, and conventional X-ray modalities are unable to solve the diagnostic problem. PET is able to visualize both the primary tumor and also axillary lymph nodes (Figure 10.5). Therefore, FDG-PET has been extensively evaluated for staging axillary lymph nodes in large series of patients, obtaining a sensitivity ranging from 30 to 80% and a specificity from 70 to 100%.^{71–82} In our experience at the nuclear medicine division of the Istituto Nazionale Tumori, we have obtained a negative predictive value in the group of patients with non-palpable lymph nodes equivalent to 95%. This large variability is due to the different

Table 10.2 Current non-nuclear medicine imaging modalities for studying a breast mass

Mammography	It has a relatively high sensitivity, good compliance, low cost; screening with mammography has resulted in a reduction of the breast cancer mortality rate by about 25–40% in females older than 40 years; digital mammography is superior (higher sensitivity, favorable dosimetry, better contrast resolution, high quality of imaging, image transmission); computed-aided detection (CAD) may reduce false-negative interpretations
Ultrasound (US)	Necessity for high-frequency devices (≥ 10 MHz); current work-up of questionable mammographic findings (second-level imaging); first-level imaging as evaluation in symptomatic women pregnant or younger than 30 years of age; guide for interventional procedures; second-level screening for high-risk women and for women with dense fibroglandular tissue
Magnetic resonance imaging (MRI)	High sensitivity (>90%) in most invasive cancers; sensitivity about 40% in ductal carcinoma in situ (DCIS); specificity generally moderate, with a wide range of results (50%–90%); useful for evaluation of women at genetic or familial high risk; search for multifocal or multicentric disease and bilateral tumors; localization of occult cancer in patients with axillary metastases from unknown primary (75% detection rate); study of women with breast implants or anatomical distortions after surgery, chemotherapy, radiotherapy

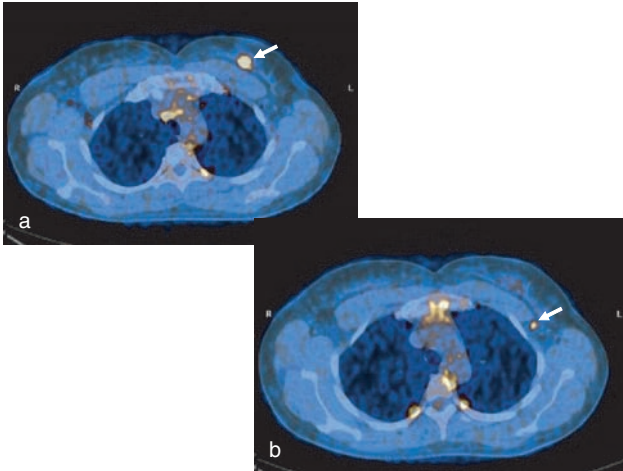


Figure 10.5

FDG-PET transaxial slices in a 40-year-old woman with a T2 malignant mass which was also visualized by mammography and US in the left breast (a). FDG-PET also revealed clear FDG uptake in the left axilla (b). FDG-PET can determine the local extent of cancer and regional lymph node involvement.

series of patients studied, the different technical protocols used for PET, and the individual conditions that can affect FDG uptake in lymphatic/cancer tissue. A large study was performed in the USA in 308 assessable patients who had FDG-PET and subsequent pathological diagnosis after surgery.⁸³ The mean and the range of diagnostic sensitivity and specificity, and positive and negative predictive values, for PET were 61% (54–67%), 80% (79–81%), 62% (60%–64%), and 79% (76–81%), respectively. Patients with PET false-negative axillae had significantly fewer tumor-positive lymph nodes (2.7%) than patients with PET true-positive axillae (5.1%). The authors concluded that FDG-PET revealed a moderate accuracy in detecting axillary metastases, and often failed to detect small and/or a few nodal metastases. Considering the overall experience with FDG-PET in detecting axillary lymph node metastases, there is no doubt that the detection of small lesions depends mainly on the PET resolution. At present, the maximum theoretical resolution for state-of-the-art PET is around 5 mm. It should be remembered that SLNB following lymphoscintigraphy has shown a very high sensitivity and has achieved general consensus for use in clinical management.^{76,84,85} Different studies have been carried out comparing SLNB and FDG-PET. Veronesi et al. evaluated 236 breast cancer patients clinically negative for axillary involvement.⁸⁶ FDG-PET was performed before surgery and sentinel node biopsy was carried out after identification through lymphoscintigraphy. Patients underwent lymph node dissection in the case of positive PET or positive sentinel node biopsy. All results were compared with histopathology. A total of 103 out of

236 patients (44%) had metastases in axillary nodes. The sensitivity of the FDG-PET scan was low (37%); however, the specificity and the positive predictive value were 96% and 88%, respectively. The high specificity of PET indicates that patients who have a PET-positive axilla should have an axillary lymph node dissection rather than a sentinel node biopsy for axillary staging. In contrast, FDG-PET showed poor sensitivity in the detection of axillary metastases, confirming the need for SLNB in cases where PET is negative for the axilla. Gil-Rendo et al. have confirmed this low sensitivity, but in the same way suggest that the high predictive value of PET (98.4%) could be an indication for a full axillary lymph-nodal dissection without previous SLNB.⁸⁷ In conclusion, FDG-PET, when positive in the axilla, could avoid sentinel node biopsy, but we cannot confirm that PET is able to substitute for SLNB in those patients with small breast tumors or negative axillae.

The problem of visualization of metastatic lymph nodes in the internal mammary chain is a matter for discussion, because this finding may alter the treatment. Conventional radiological imaging has limited diagnostic value because of its very low sensitivity in our experience and those of other authors. FDG-PET improves the detection of metastatic lymph nodes of the internal mammary chain and mediastinum. Positive lymph nodes can be observed mainly in 20–25% of patients with locally advanced breast cancer, before neoadjuvant chemotherapy. Due to non-systematic investigations, these diagnoses have not had pathological confirmation. However, the mammary chain involvement was usually associated with large tumors and inflammatory disease and a poor prognosis. There is a need for prospective studies, with pathological control, in this field.

Detection of distant metastases

FDG-PET has a role in staging patients with locally advanced breast cancer. van der Hoeven et al. demonstrated that the addition of FDG-PET to the standard work-up of this group of patients can lead to the detection of unexpected distant metastases. This may contribute to a more realistic stratification between patients with true stage III breast cancer and those who are in fact suffering from stage IV disease. The use of FDG-PET in this case prevents patients from being denied appropriate treatment.⁸⁸ Weir et al. demonstrated that in 165 patients with breast cancer, 5% were diagnosed with distant metastases and distant metastases were demonstrated in 30% of patients who were thought only to have locoregional recurrence.⁸⁹

There is evidence that FDG-PET has great potential in tumor staging (Figure 10.6). Data from the literature indicate that in breast cancer patients, FDG-PET permits complete tumor staging with a single whole-body investigation, even allowing the diagnosis of a significant number of metastases which would have been missed or non-correctly

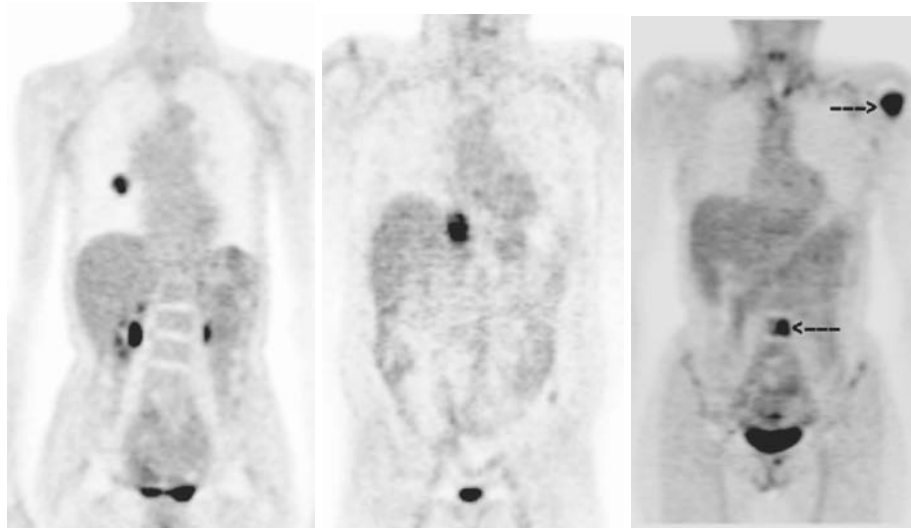


Figure 10.6

FDG-PET whole-body scan coronal slices in a patient with multiple bone lesions in shoulder and lumbar-spine (arrows), liver, and lung. FDG-PET can stage the disease, by depicting the involvement of the different structures, and sites of metastatic localization.

diagnosed by CT, US, MRI, and also bone scintigraphy, which is still widely used in breast cancer patients. In fact, clinical experience has demonstrated that FDG-PET is often superior to conventional imaging modalities in localizing tumor lesions, as significantly more lesions are detected in different sites. The role of PET in evaluating soft

tissue lesions appears to be important (liver, lung, distant lymph nodes). Also, bone metastases of breast carcinoma usually accumulate FDG (Figure 10.7). The availability of hybrid PET-CT allows better performance when compared with PET alone, and of course can improve the diagnostic accuracy in several situations.^{63–65,67}

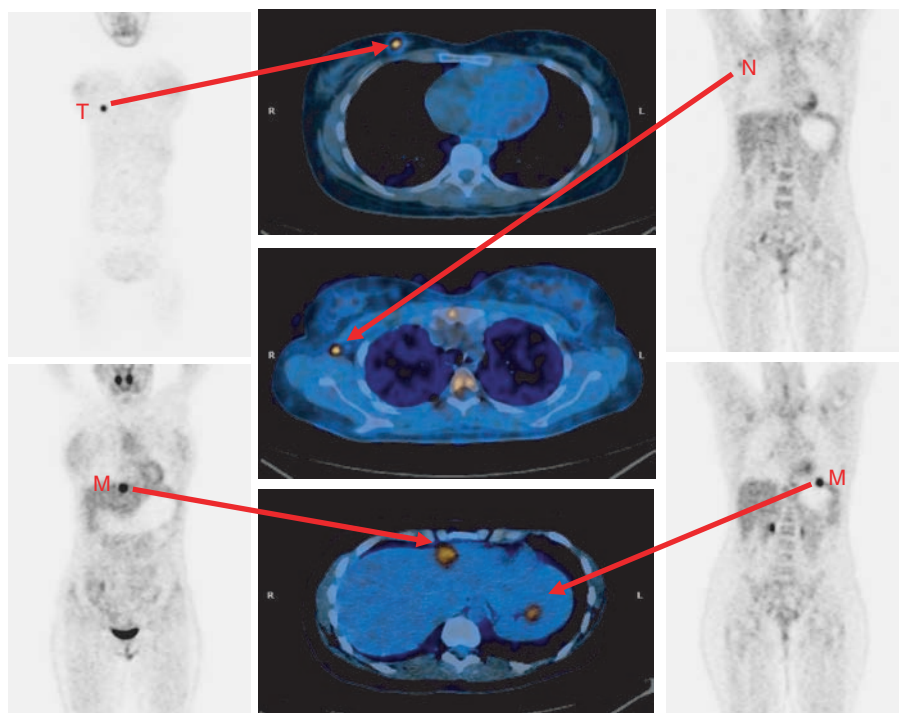


Figure 10.7

FDG-PET whole-body scan in a 50-year-old patient with breast cancer. The PET whole-body scan (coronal slices) indicates localizations in the left breast (T), in the left axilla (N), and in the liver and spleen (M). The fused PET-computed tomography images (PET-CT), transaxial slices, better localize the lesion by defining the relationships with the anatomical structures.

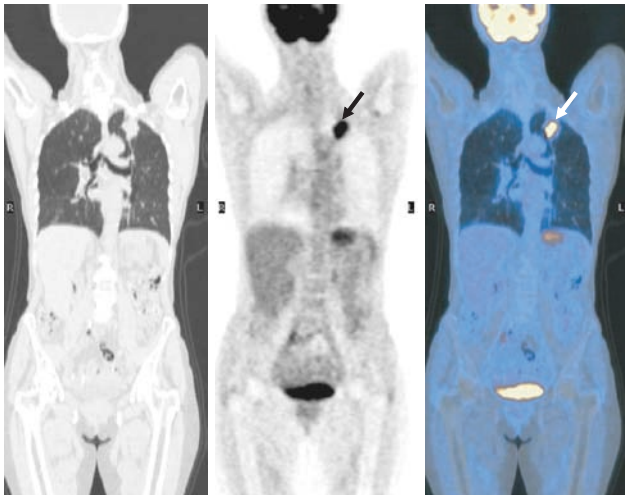


Figure 10.8
FDG-PET-CT whole-body scan coronal slices. Evidence of FDG uptake in a patient treated for breast cancer and with a single-site tumor relapse (arrow) in the left lung.

PET in the detection of tumor recurrences (follow-up and restaging)

Follow-up in patients with breast cancer has been, and remains, a subject of discussion. The current tendency to limit instrumental examinations as much as possible during follow-up in asymptomatic patients is known.^{90–94} Therefore, it is important to identify some categories of patients with a high risk of recurrence (with negative prognostic factors) in which an adequate program of diagnostic control could be acceptable. Besides this, it goes without saying that in symptomatic patients, detection of the sites

and extent of metastases is essential in order to plan the correct therapy. Without becoming too involved in a much debated problem, whole-body FDG-PET could limit the number of diagnostic tests to which asymptomatic patients at high risk of metastases could be exposed (Figure 10.8 and Figure 10.9). Apart from asymptomatic ones, patients with symptoms can benefit from FDG-PET. Whole-body PET becomes fundamental in the search for metastases, especially when a recurrence of disease is suspected because of the presence of clinical symptoms or a progressive increase of tumor markers. The major advantage of FDG-PET imaging when compared with conventional imaging is that PET is able to screen the body for local recurrence, lymph node metastases, and distant metastases, with a reported average sensitivity of 96% and a specificity of 77% (Figure 10.10 and Figure 10.11). The rather low specificity of FDG-PET can be increased by utilizing hybrid PET-CT systems.⁹⁵ A recent paper by Radan et al. reported that in patients with suspected recurrences of breast cancer and rising tumor markers, FDG-PET-CT had a better performance than CT for the diagnosis of tumor recurrence (overall accuracy of 81% vs. 59%), and led to changes in the subsequent clinical management of 51% of patients.⁹⁶ The high accuracy of FDG-PET to depict breast cancer recurrences in patients who were referred for clinical suspicion of tumor relapse has been described by Moon et al.⁹⁷ Patients were clinically followed for up to 2 years in order to assess the accuracy of PET diagnosis by biopsy, follow-up imaging, and other diagnostic tests. PET scans in 29 patients showed 41 sites indicating recurrent or metastatic disease, while in 28 patients there were 38 sites that showed no evidence for malignant disease. FDG-PET was able to detect cancer recurrence in bones, lymph nodes, breast, lung, chest wall, liver, and other sites. The FDG-PET performance on a per-patient basis was: sensitivity 93% and specificity 79%, and corresponding positive and negative predictive values 82% and 92%, respectively.

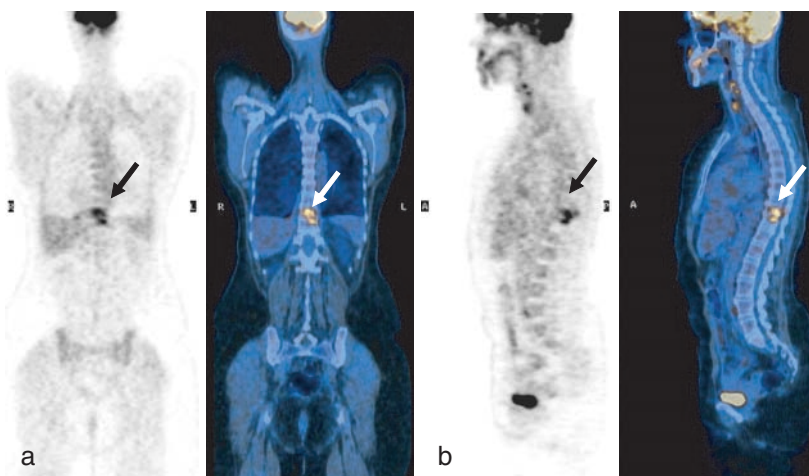


Figure 10.9

FDG-PET-CT of a patient treated for breast cancer with a history of pain in the spine. Coronal and sagittal views depict an intense focal area of FDG (a, b), uptake in the vertebral spine (D11). This is confirmed in the fused images. There are no other apparent areas of pathological uptake of FDG.

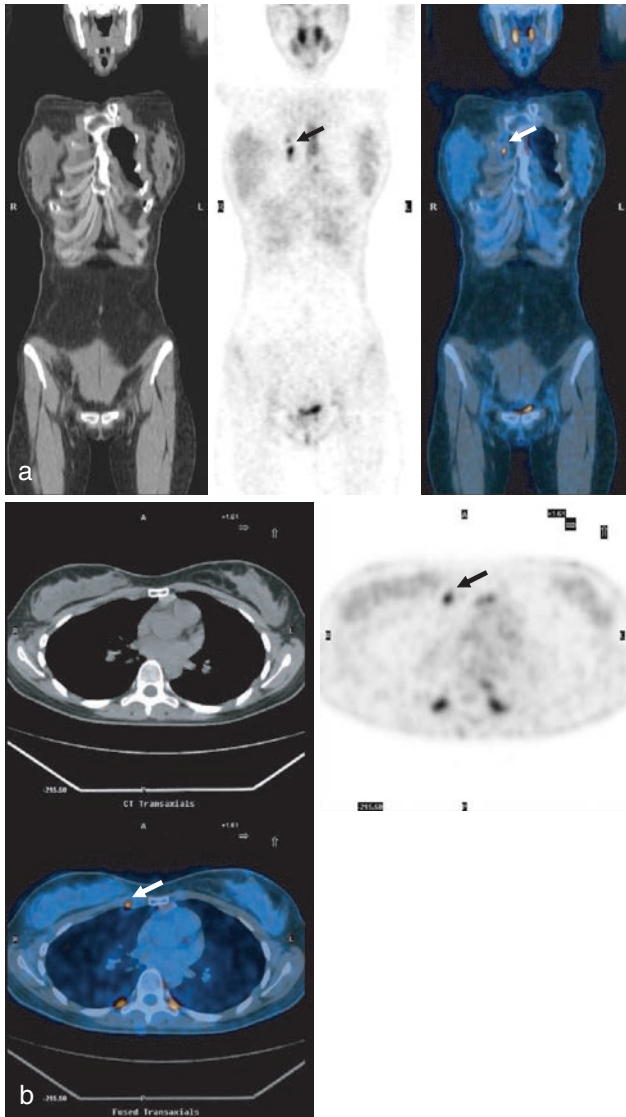


Figure 10.10
 (a) FDG-PET coronal slices in a patient treated for breast cancer. The images show a right para-sternal focal area of uptake; (b) Transaxial slices show an intense focal uptake (arrow) due to internal mammary chain metastatic involvement.

On a per-lesion basis, the sensitivity was 85% and specificity 79%. Whole-body FDG-PET seems to have a satisfactory accuracy in depicting bone lesions (Figure 10.12). However, in the literature, bone metastases are described to demonstrate a significantly larger proportion of false-negative lesions than other, non-osseous, malignant sites. False-positive lesions are due to muscle uptake, inflammation, blood pool activity in the great vessels, bowel uptake and other unknown causes. To improve the interpretation of

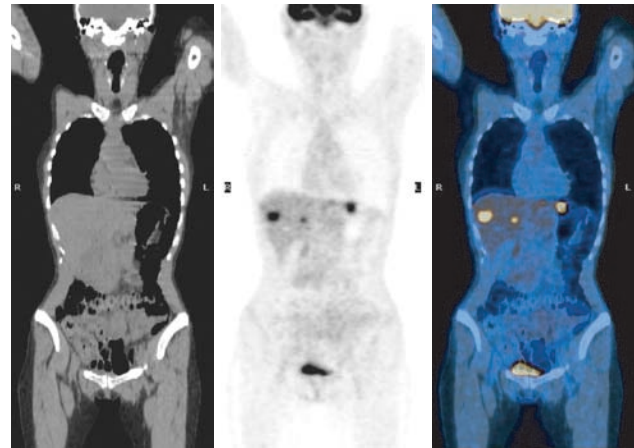


Figure 10.11
 FDG-PET-CT in a breast cancer patient in follow-up after a progressive increase of tumor markers. The coronal slices show multiple foci of FDG uptake in the liver, corresponding to multiple liver metastases (arrows).

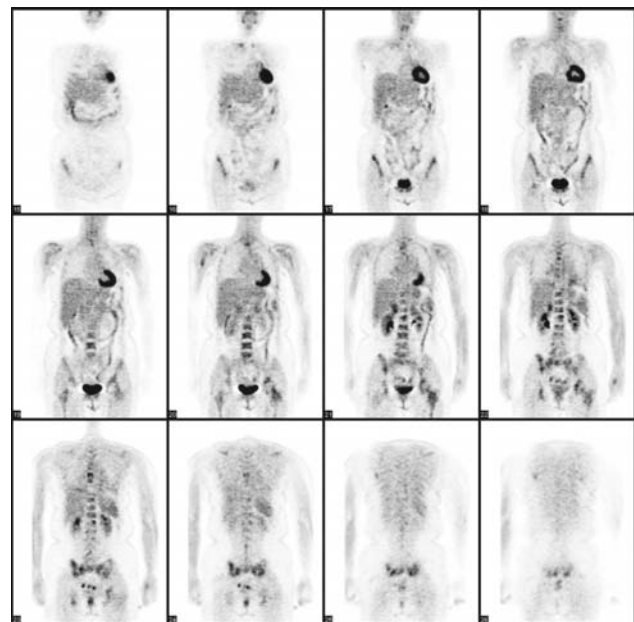


Figure 10.12
 FDG-PET whole-body scan in a 64-year-old breast cancer patient with multiple skeletal metastatic involvement, during follow-up. FDG uptake in the lesions is intense, and the scan excludes other localizations in the soft tissues or internal organs.

FDG-PET, the present authors suggest paying great attention to patient preparation, and accurately reading the FDG in skeletal muscles or in areas where artifactual images are more frequent. Wolford et al. studied the role of FDG-PET as an adjunct to localize recurrence in stage II and III breast cancer patients who present with clinical suspicion for recurrence.⁹⁸ Overall sensitivity, specificity, and accuracy were 81%, 100%, and 87% respectively; positive and negative predictive values were 100% and 83% for stage II and 100% and 50% for stage III, respectively.

A problem with FDG-PET includes some pitfalls described for the diagnosis of osteoblastic bone lesions. In this subset of lesions it seems that bone scintigraphy is still superior to PET, while FDG-PET has a good sensitivity for lytic lesions.^{99,100} Some authors propose using [¹⁸F]fluoride to study osteoblastic bone lesions showing a low avidity for FDG; however, [¹⁸F]fluoride scans do not discover metastases in soft tissues and organs¹⁰¹ (Figure 10.13). A very interesting review of this problem has been written by Fogelmann et al., who describe a different uptake of FDG in sclerotic lesions, in lytic lesions, and in lesions with a mixed pattern.¹⁰² Previous chemotherapy can influence the uptake of FDG in bone lesions, and the discrepancy often observed between the FDG-PET and CT patterns can have a prognostic value.

A specific condition in breast cancer patients is brachial plexopathy, which can cause pain and give a suspicion of tumor relapse. This disease is due to fibrosis secondary to treatment, and it is very difficult to assess on conventional



Figure 10.13

FDG-PET whole-body scan in a breast cancer patient with bone pain at the left shoulder. FDG-PET shows pathological uptake in the humerus and also in supraclavicular and axillary nodes (arrows). These indications cannot be provided by skeletal scintigraphy alone; such findings are very important for clinical management because the patient with soft tissue metastases can benefit from chemotherapy instead of hormone therapy, which is the standard treatment for postmenopausal patients with bone metastases.

anatomical imaging, as sometimes these patients have normal CT and MRI studies. FDG-PET is the best diagnostic tool to investigate patients with brachial plexopathy, as it is able to differentiate plexopathy induced by treatment from malignant relapse or progression.¹⁰³

PET in monitoring therapy response

FDG-PET is able to measure metabolic changes in tissues. Several papers have demonstrated that a reduction of FDG uptake occurs from 8 to 60 days after the beginning of therapy, while a significant morphological reduction in tumor size requires more time. The metabolic response of the tumor always precedes the dimensionally measurable response, because the effects of the anticancer treatment primarily influence the metabolism and only at a later stage are followed by a decrease of tumor mass. The usefulness of PET in the evaluation of all different types of therapy has been studied (chemotherapy, hormone therapy, and radiotherapy); however, only the therapy response in locally advanced breast cancer patients has been investigated thoroughly.¹⁰⁴ Histopathological response could be predicted with an accuracy of around 90%. A semiquantitative evaluation (through the standardized uptake value, SUV) is of course a prerequisite when PET is used for therapy monitoring. McDermott et al. evaluated FDG-PET for predicting tumor response to neoadjuvant chemotherapy.¹⁰⁵ SUV was measured after the first and the second cycle, at the midpoint, and at the end of chemotherapy. The best discrimination was measured for mean SUV at the midpoint of therapy, which correctly identified 77% of low-responding tumors, whilst identifying 100% of high-responding tumors. The predictive value of FDG-PET for the pathological response after completion of neoadjuvant chemotherapy was confirmed by Kim et al.¹⁰⁶ Rousseau et al. demonstrated that the pathologic response to neoadjuvant chemotherapy in stage II and III breast cancer patients can be predicted accurately by FDG-PET even after two courses of chemotherapy.¹⁰⁷ Many other studies have been carried out on the decline of FDG uptake in patients responsive to treatment. In contrast, any significant reductions in FDG uptake have not been observed in non-responsive patients.^{108–112} This finding should be used both to check the efficacy of therapy after the end of treatment and also to measure the subclinical response of the tumor mass during treatment, in order to predict the grade of clinical response (Table 10.3). FDG-PET study at the end of treatment can be also an index of prognostic stratification for survival. Cachin et al. demonstrated that FDG-PET study performed after the last cycle of high-dose chemotherapy before autologous stem cell transplantation can powerfully stratify for survival.¹¹³

Table 10.3 Use of fluoro-2-deoxy-D-glucose-positron emission tomography (FDG-PET) in the evaluation of tumor response

Evaluation of neoadjuvant chemotherapy for locally advanced disease	The aim of therapy is to reduce the size of the primary neoplasm in order to increase the success of surgical resection; anatomical changes are measurable only several weeks after the beginning of therapy and scar cannot be differentiated from viable tumor; FDG-PET is more effective than anatomic imaging in monitoring early treatment response, using serial SUV measurements; a rapid decrease in glucose metabolism in responders can be detected by PET as early as after 1–2 cycles of therapy
Treatment of metastatic disease	Monitoring therapy of metastatic disease is difficult, since tissue sampling is not feasible; earlier response assessment could be beneficial to guide further therapy and avoid prolonged treatment with ineffective drugs; CT or MRI is still the standard method to assess treatment, but anatomic changes occur too late in order to assess early treatment response (morphological changes shown by radiological methods take 2–3 months to show evidence); metabolic changes occur much earlier and can be easily assessed with PET

SUV, standardized uptake value.

Tumor characterization and radiopharmaceuticals other than [¹⁸F]FDG

At present, FDG remains the best tracer for breast cancer studies with PET. Its metabolic characteristics can also describe the aggressiveness of cancer. Inoue et al. studied a group of breast cancer patients for preoperative evaluation of prognosis.¹¹⁴ The SUV max-high group showed a significantly poorer prognosis than the SUV max-low group, and SUV was demonstrated to be a more accurate prognostic index than conventional TNM staging.

One of the strongest prognostic parameters for breast cancer is hormonal status, as knowledge of this condition allows the prediction of response to hormonal therapy and survival of the patient. Positron tracers for receptors are of great theoretical importance, and for this reason hormonal estrogens or progesterone derivatives have been studied for PET, such as fluoroestradiol (FES) and normoprogesterone (NPg) labeled with ¹⁸F.^{115–118} ¹⁸F-labeled estrogen analogs gave acceptable results in visualizing primary breast cancer and distant metastases. An overall sensitivity of 90% was described, and a good correlation between FES uptake in vivo and in vitro receptor status was observed. Nevertheless, in spite of intense radiochemistry research in this area, the clinical applications proposed by the literature have not yet been introduced into current clinical practice.

Another tracer, ¹¹C-labeled tyrosine, was successful in visualizing breast cancer, and was shown to correlate with the protein synthesis rate.¹¹⁹ ¹¹C-labeled methionine had some use in evaluating tumor response after chemotherapy. Comparative imaging prior to and post-therapy

demonstrated a decreasing uptake in stable or regressing tumors; in contrast an enhanced uptake was associated with cancer progression and non-response.^{120,121}

A very interesting new radiopharmaceutical is [¹⁸F] fluorothymidine (FLT), which has recently been proposed for the diagnosis of breast cancer and tumor characterization, since thymidine uptake is in vitro related to cell proliferation. Preliminary studies indicate that FLT-PET is suitable for the diagnosis of primary breast cancer and locoregional metastases.¹²²

Conclusions on FDG-PET and nuclear medicine modalities in breast cancer

Much clinical experience of FDG-PET in breast cancer has already been gained worldwide by studying a large number of patients and breast lesions. On the basis of data from the international literature and from our own experience, there is no doubt that FDG-PET has revealed good sensitivity and specificity in visualizing both primary and metastatic breast lesions. Considering all the diagnostic modalities currently available for this tumor type (primary breast cancer can be detected by mammography, digital mammography, US, MRI, scintimammography; metastatic breast cancer can be detected by conventional radiography, CT, US, bone scintigraphy), FDG-PET in clinical routine today finds its most important role in depicting tumor relapses, mainly in the presence of biochemical, clinical, or instrumental signs or symptoms of recurrence. In this

indication, much clinical evidence has shown that PET or PET–CT is so far more accurate than CT, MRI, and bone scintigraphy. Even if CT and MRI have a higher spatial resolution, it has been demonstrated that PET sometimes provides more useful information in discriminating lesions and differentiating viable tumors from benign conditions. FDG-PET also has an interesting role in establishing tumor extent and re-staging breast cancer, showing very good sensitivity in evaluating lymph node involvement, soft tissue lesions, and bone metastases. Some authors propose the use of whole-body FDG-PET–CT as the unique tool for staging, restaging, and monitoring follow-up, since they support the hypothesis that PET–CT is a reliable substitute for all other diagnostic imaging, excluding only the diagnosis of a breast mass at presentation. Besides this, the evaluation of tumor response has become another very important indication, in the different phases of chemotherapy. Strong clinical evidence shows that FDG-PET can predict early on whether cancer will respond to therapy, or, if PET is carried out at the end of treatment, can be useful to evaluate the metabolic response. It is easy to understand that this application is strategic in clinical oncology, since there is a need to measure the efficacy of the anticancer

therapy, both for evaluation of the current antineoplastic therapy and for the development of new drugs in experimental trials. The diagnosis of breast masses, in spite of the lower sensitivity of FDG-PET in comparison with conventional diagnostic modalities, can benefit from the use of FDG-PET in particular conditions. It goes without saying that in this indication, priority has to be given to mammography (alone or associated with US), which of course still remains the imaging of first choice at tumor onset. FDG-PET can be considered the second-choice examination, since it is effective in the study of patients with ambiguous mammographies. Finally, FDG uptake in the primary tumor correlates with the histological grade and potential aggressiveness of the breast cancer, and this may have prognostic consequences.

Considering all the abovementioned performances of PET and other nuclear medicine tools, we can confirm that the diagnosis of breast cancer today involves many diagnostic options based on the application of nuclear medicine procedures (Table 10.4). Not much more than 10 years ago, only the bone scan was suitable for studying breast cancer patients, and this confirms the impressive progress of this discipline in clinical practice.

Table 10.4 Nuclear medicine modalities for studying breast cancer

Sentinel node biopsy following lymphoscintigraphy	<p>Standard method for detection and analysis of the sentinel node (SLN); it improves preoperative staging and lymph node analysis; indication in patients with small primary breast cancer and non-palpable lymph nodes; precise and correct clinical indications are still under study in ongoing prospective multicentric trials</p> <p><i>Issues requiring further clarification:</i> standardization of methods, optimization of indications, standardization of pathological analysis, study of the meaning of micrometastases (in SLN)</p>
Scintimammography with [^{99m} Tc]sestamibi/tetrofosmin	<p>Second-choice examination to visualize primary breast cancer; indicated in cases where radiological methods cannot make diagnosis; limits due to its poor sensitivity in non-palpable/small breast tumor, non-optimal compliance with standard γ camera; possible diagnostic improvement by the use of SPECT, hybrid SPECT–CT, pinhole collimators, dedicated γ cameras</p> <p><i>Issues requiring further clarification:</i> proposed use in monitoring therapy and in predicting therapy response (MDR); proposed use in locoregional staging of breast cancer patients, with particular procedures (pinhole SPECT) only in a few centers</p>
[¹⁸ F]FDG-PET	<p>[¹⁸F]FDG-PET has only a complementary role in diagnosis of primary breast tumor, except for some particular conditions (anyhow more accurate than scintimammography); best indication in evaluating tumor extent (staging, restaging) and monitoring therapy (in many cases more accurate than conventional radiological modalities); appropriate indication in seeking distant metastases and tumor relapses (follow-up of symptomatic and non-symptomatic patients); hybrid PET–CT images improve the diagnostic accuracy, increasing the specificity and anatomical localization</p>

(cont'd)

Table 10.4 Nuclear medicine modalities for studying breast cancer (cont'd)

Bone scintigraphy with ^{99m} Tc-labeled diphosphonates	semiquantitative methods (SUV analysis) are valuable both as prognostic indicators of cancer aggressiveness and for monitoring therapy (early phases and at the end of treatment)
	<p><i>Issues requiring further clarification:</i> under study whether whole-body PET–CT alone can substitute for all other modalities in staging and follow-up of breast cancer patients; under development or under clinical validation, other radiopharmaceuticals as alternatives to FDG</p>
	<p>^{99m}Tc-labeled diphosphonate whole-bone scan has very high sensitivity, but low specificity to detect skeletal metastases in symptomatic patients. SPECT increases the specificity to study doubtful lesions in the spine; in asymptomatic patients bone scan has indication as staging modality in those patients at high risk of metastases or with clinically or biochemically suspected bone involvement; during follow-up bone scintigraphy has indication in those patients with suspected bone involvement, with symptoms or biochemical signs; [¹⁸F]FDG-PET has better accuracy for all types of bone metastases than bone scintigraphy; data on [¹⁸F]FDG-PET or PET–CT also indicate that [¹⁸F]FDG-PET is superior except for osteoblastic metastases</p>
	<p><i>Issues requiring further clarification:</i> can [¹⁸F]FDG-PET substitute for bone scan in clinical routine, considering that by means of a single test it is possible to study both skeleton and soft tissues and organs?</p>
SPECT, single photon emission computed tomography; MDR, multidrug resistance.	

References

- Giuliano AE, Jones RC, Brennan M et al. Sentinel lymphadenectomy and breast cancer. *J Clin Oncol* 1997; 15: 2345–50.
- Krag DN, Weaver DL, Alex JC et al. Surgical resection and radiolocalization of the sentinel lymph node in breast cancer using a gamma-probe. *Surg Oncol* 1993; 2: 335–40.
- Cody HS 3rd. Sentinel lymph node biopsy for breast cancer: does anybody not need one? *Ann Surg Oncol* 2003; 10: 1131–2.
- Veronesi U, Paganelli G, Galimberti V et al. Sentinel-node biopsy to avoid AD in breast cancer with clinically negative lymph-nodes. *Lancet* 1997; 349: 1864–7.
- Cody HS 3rd, Borgen PI. State of the art approaches to sentinel node biopsy for breast cancer: study design, patient selection, technique, and quality control at Memorial Sloan-Kettering Cancer Center. *Surg Oncol* 1999; 8: 85–91.
- Wilhelm AJ, Mijnhout GS, Franssen EJJ. Radiopharmaceuticals in sentinel lymph-node detection – an overview. *Eur J Nucl Med* 1999; 26: S36–42.
- Mariani G, Moresco L, Viale G et al. Radioguided sentinel lymph node biopsy in breast cancer surgery. *J Nucl Med* 2001; 42: 1198–215.
- Noguchi M, Tsugawa K, Miwa K. Internal mammary chain sentinel lymph node identification in breast cancer patient. *J Surg Oncol* 2000; 73: 75–80.
- Paganelli G, Galimberti V, Trifirò G et al. Internal mammary node lymphoscintigraphy and biopsy in breast cancer. *Q J Nucl Med* 2002; 46: 138–44.
- Clarke D, Khoni NI, Mansel ER. Sentinel node biopsy in breast cancer. AMLANAC trial. *World J Surg* 2001; 25: 819–22.
- Veronesi U, Paganelli G, Viale G et al. A randomized comparison of sentinel-node biopsy with routine axillary dissection in breast cancer. *N Engl J Med* 2003; 349: 546–53.
- Wilke LG, Giuliano AE. Sentinel lymph node biopsy in patients with early-stage breast cancer: status of the National Clinical Trials. *Surg Clin North Am* 2003; 83: 901–10.
- Krag DN, Julian T. Expert perspectives: update on NSABP B-32, a randomized phase III clinical trial to compare sentinel node resection to conventional axillary dissection for clinically node-negative breast cancer. *Breast Dis Year Book Q* 2002; 13: 113–14.
- Hurkmans CW, Borger JH, Rutgers EJ et al. Quality assurance of axillary radiotherapy in the EORTC AMAROS trial 10981/22023. *Radiother Oncol* 2003; 68: 233–40.
- Jin Kim H, Heerdt AS, Cody HS, Van Zee KJ. Sentinel node drainage in multicentric breast cancers. *Breast J* 2002; 8: 356–61.
- Kumar R, Jana S, Heiba SI et al. Retrospective analysis of sentinel node localization in multifocal, multicentric, palpable, or nonpalpable breast cancer. *J Nucl Med* 2003; 44: 7–10.

17. Tousimis E, van Zee KJ, Fey JV et al. The accuracy of sentinel lymph node biopsy in multicentric and multifocal invasive breast cancers. *J Am Coll Surg* 2003; 197: 529–35.
18. Knauer M, Konstantiniuk P, Haid A et al. Multicentric breast cancer: a new indication for sentinel node biopsy – a multi-institutional validation study. *J Clin Oncol* 2006; 24: 3374–80.
19. Schwartz GF, Meltzer AJ. Accuracy of axillary sentinel lymph node biopsy following neoadjuvant (induction) chemotherapy for carcinoma of the breast. *Breast* 2003; 9: 374–9.
20. Mamounas EP. Sentinel lymph node biopsy after neoadjuvant systemic therapy (review). *Surg Clin North Am* 2003; 83: 931–42.
21. Stearns V, Ewing CA, Slack R et al. Sentinel lymphadenectomy after neoadjuvant chemotherapy for breast cancer may reliably represent the axilla except for inflammatory breast cancer. *Ann Surg Oncol* 2002; 9: 235–42.
22. Wong SL, Edwards MJ, Chao C et al. The effect of prior breast biopsy method and concurrent definitive breast procedure on success and accuracy of sentinel lymph node biopsy. *Ann Surg Oncol* 2002; 9: 272–7.
23. Luini A, Galimberti V, Gatti G et al. The sentinel node biopsy after previous breast surgery: preliminary results on 543 patients treated at the European Institute of Oncology. *Breast Cancer Res Treat* 2005; 89: 159–63.
24. Viale G, Maiorano E, Mazzarol G et al. Histologic detection and clinical implications of micrometastases in axillary sentinel lymph nodes for patients with breast carcinoma. *Cancer* 2001; 92: 1378–84.
25. Turner RR, Chu KU, Qi K et al. Pathologic features associated with nonsentinel lymph node metastases in patients with metastatic breast carcinoma in a sentinel lymph node. *Cancer* 2000; 89: 574–81.
26. Schomacker K, Schicha H. Use of myocardial imaging agents for tumour diagnosis – a success story? *Eur J Nucl Med* 2000; 27: 1845–63.
27. Carvalho PA, Chiu ML, Kronauge JF et al. Subcellular distribution and analysis of Tc-99m MIBI in isolated perfused rat hearts. *J Nucl Med* 1992; 33: 1516–21.
28. Moublant J, Zhang Z, Rapp M et al. In vitro uptake of technetium-99m-teboroxime in carcinoma cell lines and normal cells: comparison with technetium-99m-sestamibi and thallium-201. *J Nucl Med* 1993; 34: 1949–52.
29. Pwinca-Worms D, Chiu ML, Budding M et al. Functional imaging of multidrug-resistant P-glycoprotein with an organotechnetium complex. *Cancer Res* 1993; 53: 977–84.
30. Arbab AS, Koizumi K, Toyama K et al. Uptake of technetium-99m-tetrofosmin, technetium-99m-MIBI and thallium-201 in tumor cell lines. *J Nucl Med* 1996; 37: 1551–6.
31. Ballinger JR. 99mTc-tetrofosmin for functional imaging of P-glycoprotein modulation in vivo. *J Clin Pharmacol* 2001 Suppl: 39S–47S.
32. Khalkhali I, Mena I, Jouanne E et al. Prone scintimammography in patients with suspicion of carcinoma of the breast. *J Am Coll Surg* 1994; 178: 491–7.
33. Liberman M, Sampalis F, Mulder DS et al. Breast cancer diagnosis by scintimammography: a meta-analysis and review of the literature. *Breast Cancer Res Treat* 2003; 80: 115–26.
34. Hussain R, Buscombe JR. A meta-analysis of scintimammography: an evidence-based approach to its clinical utility. *Nucl Med Commun* 2006; 27: 589–94.
35. Sampalis FS, Denis R, Picard D et al. International prospective evaluation of scintimammography with 99mTc-sestamibi. *Am J Surg* 2003; 185: 544–9.
36. Scopinaro F, Schillaci O, Scarpini M et al. Technetium-99m sestamibi: an indicator of breast cancer invasiveness. *Eur J Nucl Med* 1994; 21: 984–7.
37. Tolmos J, Cutrone JA, Wang B et al. Scintimammography analysis of nonpalpable breast lesions previously identified by conventional mammography. *J Natl Cancer Inst* 1998; 90: 846–9.
38. Khalkhali I, Villanueva-Meyer J, Edell SL et al. Diagnostic accuracy of 99mTc-sestamibi breast imaging: multicenter trial results. *J Nucl Med* 2000; 41: 1973–9.
39. Gupta P, Waxman A, Nguyen K et al. Correlation of Tc-99m sestamibi uptake with histopathologic characteristics in patients with breast diseases. *J Nucl Med* 1996; 37: 250–1.
40. Lumachi F, Ermani M, Marzola MC et al. Relationship between prognostic factors of breast cancer and 99m-Tc-sestamibi uptake in patients who underwent scintimammography: multivariate analysis of causes of false-negative results. *Breast* 2006; 15: 130–4.
41. Aziz A, Hashmi R, Ogawa Y et al. Tc-99m-MIBI scintimammography; SPECT versus planar imaging. *Cancer Biother Radiopharm* 1999; 14: 495–500.
42. Obwegeser R, Berghammer P, Rodrigues M et al. A head-to-head comparison between technetium-99m-tetrofosmin and technetium-99m-MIBI scintigraphy to evaluate suspicious breast lesions. *Eur J Nucl Med* 1999; 26: 1553–9.
43. Spanu A, Schillaci O, Meloni GB, et al. The usefulness of 99mTc-tetrofosmin SPECT scintimammography in the detection of small size primary breast carcinomas. *Int J Oncol* 2002; 21: 831–40.
44. Spanu A, Dettori G, Nuvoli S et al. 99mTc-tetrofosmin SPET in the detection of both primary breast cancer and axillary lymph node metastasis. *Eur J Nucl Med* 2001; 28:1781–94.
45. Spanu A, Schillaci O, Madeddu G. 99mTc labelled cationic lipophilic complexes in malignant and benign tumors: the role of SPET and pinhole-SPET in breast cancer, differentiated thyroid carcinoma and hyperparathyroidism. *Q J Nucl Med Mol Imaging* 2005; 49: 145–69.
46. Schillaci O, Scopinaro F, Danieli R et al. Scintimammography with technetium-99m-tetrofosmin in suspected breast cancer. *Anticancer Res* 1997; 17: 1623–6.
47. Waxman A, Nagaraj N, Kovalevsky M et al. Detection of primary breast malignancy with Tc-99m methoxyisobutylisonitrile in patients with non-palpable primary malignancies: the importance of lesion size. *J Nucl Med* 1995; 36: 194P.
48. Tiling R, Kessler M, Untch M et al. Initial evaluation of breast cancer using Tc-99m sestamibi scintimammography. *Eur J Radiol* 2005; 53: 206–12.
49. Mathieu I, Mazy S, Willermart B et al. Inconclusive triple diagnosis in breast cancer imaging: is there a place for scintimammography? *J Nucl Med* 2005; 46: 1574–81.
50. Brem RF, Schoonjans JM, Kieper DA et al. High-resolution scintimammography: a pilot study. *J Nucl Med* 2002; 43: 909–15.
51. Schillaci O, Manni C, Danieli R et al. Tc-99m sestamibi scintimammography with a hybrid SPECT/CT imaging system. *Eur J Nucl Med Mol Imaging* 2005; 32: S128.

52. Rhodes DJ, O'Connor MK, Philips SW et al. Molecular breast imaging: a new technique using technetium Tc scintimammography to detect small tumors of the breast. *Mayo Clin Proc* 2005; 80: 24–30.
53. Schillaci O, Cossu E, Romano P et al. High-resolution gamma-camera for molecular breast imaging: first clinical results. *Phys Med* 2006; 21: 113–16.
54. Brem RF, Rapelyea JA, Zisman G et al. Occult breast cancer: scintimammography with high-resolution breast-specific gamma camera in women at high risk for breast cancer. *Radiology* 2005; 237: 274–80.
55. Schillaci O, Scopinaro F, Spanu A et al. Detection of axillary lymph node metastases in breast cancer with Tc-99m tetrofosmin scintimammography. *Int J Oncol* 2002; 20: 483–7.
56. Bombardieri E, Aktolun C, Baum RP et al. Breast scintigraphy: procedure guidelines for tumour imaging. *Eur J Nucl Med Mol Imaging* 2003; 30: BP107–14.
57. Som P, Atkins HL, Bandoypadhyay D et al. A fluorinated glucose analog, 2-fluoro-2-deoxy-D-glucose (F-18): nontoxic tracer for rapid tumor detection. *J Nucl Med* 1980; 21: 670–5.
58. Brown RW, Wahl RL. Overexpression of GLUT-1 glucose transport in human breast cancer: an immunohistochemical study. *Cancer* 1993; 72: 2979–85.
59. Pauwels EKJ, Sturm EJ, Bombardieri E, Cleton FJ, Stokkel MPM. Positron-emission tomography with (18F)fluorodeoxyglucose. *J Cancer Res Clin Oncol* 2000; 126: 549–59.
60. Beaney RP, Lammertsma AA, Jones T, McKenzie CG, Halnan KE. Positron emission tomography for in vivo measurement of regional blood flow, oxygen utilization and blood volume in patients with breast carcinoma. *Lancet* 1984; 1: 131–4.
61. Wajl RL, Cody RL, Hutchins GD, Mudgett EE. Primary and metastatic breast carcinoma: initial clinical evaluation with PET with the radiolabeled glucose analogue 2-(F-18)-fluoro-2-deoxy-D-glucose. *Radiology* 1991; 179: 765–70.
62. Gambhir SS, Czernin J, Schwimmer J et al. A tabulated summary of the FDG PET literature. *J Nucl Med* 2001; 42: 1S–93S.
63. Kumar R, Alavi A. Fluorodeoxyglucose-PET in the management of breast cancer. *Radiol Clin North Am* 2004; 42: 1113–22.
64. Endo K, Oriuchi N, Higuchi T et al. PET and PET/CT using 18F-FDG in the diagnosis and management of cancer patients. *Int J Clin Oncol* 2006; 11: 286–96.
65. Zangheri B, Messa C, Picchio M et al. PET/CT and breast cancer. *Eur J Nucl Med Mol Imaging* 2004; 31: S135–42.
66. Adler LP, Bakale G. Positron emission tomography imaging. In: Khalkali I, Maublant JC, Goldsmith SJ, eds. *Nuclear Oncology. Diagnosis and therapy*. Philadelphia: Lippincott Williams & Wilkins, 2001: 289–95.
67. Rouesse J, Alberini JL, Wartski M et al. [FDG (18fluorodeoxyglucose) positron emission tomography and breast cancer]. *Bull Acad Natl Med* 2005; 189: 963–75. [in French]
68. Bender H, Palmedo H, Biersack HJ. Breast imaging with positron emission tomography. In: Taillefer R, Khalkhali I, Waxman AD, Biersack HJ, eds. *Radionuclide Imaging of the Breast*. New York: Marcel Dekker, 1998: 147–75.
69. Avril N, Dose J, Janicke F et al. Metabolic characterization of breast tumors with positron emission tomography using F-18 fluorodeoxyglucose. *J Clin Oncol* 1996; 14: 1848–57.
70. Palmedo H, Bender H, Grunwald F et al. Comparison of fluorine-18 fluorodeoxyglucose positron emission tomography and technetium-99m methoxysobutylisocyanide scintimammography in the detection of breast tumours. *Eur J Nucl Med* 1997; 24: 1138–45.
71. Avril N, Scheidhauer K, Kuhn W. Breast cancer. In: Helmut J, Wieler R, Coleman E, eds. *PET in Clinical Oncology*. New York: Springer, 2000: 355–72.
72. Scheidhauer K, Walter C, Seemann MD. FDG PET and other imaging modalities in the primary diagnosis of suspicious breast lesions. *Eur J Nucl Med Mol Imaging* 2004; 31: S170–9.
73. Owaki T, Kijima Y, Yoshinaka H et al. Ductal carcinoma in situ of the breast detected by F18 fluorodeoxyglucose positron emission tomography. *Breast Cancer* 2006; 13: 210–13.
74. Korn RL, Yost Am, May CC et al. Unexpected focal hypermetabolic activity in the breast: significance in patients undergoing 18F-FDG PET/CT. *AJR Am J Roentgenol* 2006; 187: 81–5.
75. Bombardieri E, Crippa F, Maffioli L et al. Nuclear medicine approaches for detection of axillary lymph node metastases. *Q J Nucl Med* 1998; 42: 54–65.
76. Sandrucci S, Casalegno PS, Percivale P et al. Sentinel lymph node mapping and biopsy for breast cancer: a review of literature relative to 4791 procedures. *Tumori* 1999; 85: 425–34.
77. Adler LP, Faulhaber PF, Schnur KC, Al-Kasi NL, Shenk RR. Axillary lymph node metastases: screening with (F-18) 2deoxy-2-fluoro-D-glucose (FDG) PET. *Radiology* 1997; 203: 323–7.
78. Smith I, Ogston K, Whitford P et al. Staging of the axilla in breast cancer: accurate in vivo assessment using positron emission tomography with 2-(fluorine-18)-fluoro-2-deoxy-D-glucose. *Ann Surg* 1998; 228: 220–7.
79. Greco M, Crippa F, Agresti R et al. Axillary lymph node staging in breast cancer by 2-fluoro-2-deoxy-D-glucose-positron emission tomography: clinical evaluation and alternative management. *J Natl Cancer Inst* 2001; 93: 630–5.
80. Crippa F, Agresti R, Seregini E et al. Prospective evaluation of fluoride-18-FDG PET in presurgical staging of the axilla in breast cancer. *J Nucl Med* 1998; 39: 4–8.
81. Utech CI, Young CS, Winter PF. Prospective evaluations of fluorine-18 fluorodeoxyglucose positron emission tomography in breast cancer for staging of the axilla related to surgery and immunocytochemistry. *Eur J Nucl Med* 1996; 23: 1588–93.
82. Fehr MK, Hornung R, Varga Z et al. Axillary staging using positron emission tomography in breast cancer patients qualifying for sentinel lymph node biopsy. *Breast J* 2004; 10: 89–93.
83. Wahl RL, Siegel BA, Coleman RE, Gatsonis CG; PET Study Group. Prospective multicenter study of axillary nodal staging by positron emission tomography in breast cancer: a report of the staging breast cancer with PET Study Group. *J Clin Oncol* 2004; 22: 277–85.
84. Veronesi U, Paganelli G, Galimberti V et al. Sentinel-node biopsy to avoid axillary dissection in breast cancer with clinically negative lymph-nodes. *Lancet* 1997; 349: 1864–7.
85. Krag D, Weaver D, Ashikaga T et al. The sentinel node in breast cancer. A multicentric validation study. *N Engl J Med* 1998; 339: 941–6.

86. Veronesi U, De Cicco C, Galimberti V et al. A comparative study on the value of FDG-PET and sentinel node biopsy to identify occult axillary metastases. *Ann Oncol* 2007; 18: 473–8.
87. Gil-Rendo A, Zornoza G, Garcia-Velloso MJ et al. Fluorodeoxyglucose positron emission tomography with sentinel lymph node biopsy for evaluation of axillary involvement in breast cancer. *Br J Surg* 2006; 93: 707–12.
88. van der Hoeven JJ, Krak NC, Hoekstra OS et al. 18F-2-fluoro-2-deoxy-D-glucose positron emission tomography in staging of locally advanced breast cancer. *J Clin Oncol* 2004; 22: 1253–9.
89. Weir L, Worsley D, Bernstein V. The value of FDG positron emission tomography in the management of patients with breast cancer. *Breast J* 2005; 11: 204–9.
90. Rosselli del Turco M, Palli D, Cariddi A et al. Intensive diagnostic follow up after treatment of primary breast cancer. A randomized trial. National Research Council Project on Breast Cancer Follow Up. *JAMA* 1994; 271: 1953–7.
91. Maffioli L, Zambetti M, Castellani MR, Bombardieri E. Role of bone scan in breast cancer follow-up. *Tumori* 1997; 83: 547–9.
92. Nicolini A, Ferrari P, Sacripanti A, Capri A. The role of tumour markers in predicting skeletal metastases in breast cancer patients with equivocal bone scintigraphy. *Br J Cancer* 1999; 79: 1443–7.
93. Bares R. Skeletal scintigraphy in breast cancer management. *Q J Nucl Med* 1998; 42: 43–8.
94. Eubank WB, Mankoff D, Bhattacharya M et al. Impact of FDG-PET on defining the extent of disease and on the treatment of patients with recurrent or metastatic breast cancer. *AJR Am J Roentgenol* 2004; 183: 479–86.
95. Lind P, Igerc I, Beyer T, Reinprecht P, Hausegger K. Advantages and limitations of FDG PET in the follow-up of breast cancer. *Eur J Nucl Med Mol Imaging* 2004; 31: S125–34.
96. Radan L, Ben-Haim S, Bar-Shalom R, Guralnik L, Israel O. The role of FDG-PET/CT in suspected recurrences of breast cancer. *Cancer* 2006; 107: 2545–51.
97. Moon DH, Maddahi J, Silverman DH et al. Accuracy of whole-body fluorine-18-FDG-PET for the detection of recurrent or metastatic breast carcinoma. *J Nucl Med* 1998; 39: 431–5.
98. Wolfort RM, Li BD, Johnson LW et al. The role of whole-body fluorine-18-FDG positron emission tomography in the detection of recurrence in symptomatic patients with stages II and III breast cancer. *World J Surg* 2006; 30: 1422–7.
99. Nakai T, Okuyama C, Kubota T et al. Pitfalls of FDG-PET for the diagnosis of osteoblastic bone metastases in patients with breast cancer. *Eur J Nucl Med Mol Imaging* 2005; 32: 1253–8.
100. Uematsu T, Yuen S, Yukisawa S et al. Comparison of FDG-PET and SPECT for detection of bone metastases in breast cancer. *AJR Am J Roentgenol* 2005; 184: 1266–73.
101. Langsteger W, Heinisch M, Fogelman I. The role of fluorodeoxyglucose, 18F-dihydroxyphenylalanine, 18F-choline, and 18F-fluoride in bone imaging with emphasis on prostate and breast. *Semin Nucl Med* 2006; 36: 73–92.
102. Fogelman I, Cook G, Israel O, Van der Wall H. Positron emission tomography and bone metastases. *Semin Nucl Med* 2005; 35: 135–42.
103. Ahmad A, Barrington S, Maisey M, Rubens RD. Use of positron emission tomography in evaluation of brachial plexopathy in breast cancer patients. *Br J Cancer* 1999; 79: 478–82.
104. Biersack HJ, Bender H, Palmedo H. FDG-PET in monitoring therapy of breast cancer. *Eur J Nucl Med Mol Imaging* 2004; 31: S112–17.
105. McDermott GM, Welch A, Staff RT et al. Monitoring primary breast cancer throughout chemotherapy using FDG-PET. *Breast Cancer Res Treat* 2006 Aug 9; [Epub ahead of print]
106. Kim SJ, Kim SK, Lee ES, Ro J, Kang S. Predictive value of 18F FDG-PET for pathological response of breast cancer to neo-adjuvant chemotherapy. *Ann Oncol* 2004; 15: 1352–7.
107. Rousseau C, Devillers A, Sagan C et al. Monitoring of early response to neoadjuvant chemotherapy in stage II and III breast cancer by 18F fluorodeoxyglucose positron emission tomography. *J Clin Oncol* 2006; 24: 5366–72.
108. Avril N, Schelling M, Naehrig J et al. Monitoring primary chemotherapy in advanced breast cancer using FDG-PET. *J Nucl Med* 2000; 41: 112P.
109. Smith IC, Welch AE, Hutcheon AW et al. Positron emission tomography using (18F)-fluorodeoxy-D-glucose to predict the pathologic response of breast cancer to primary chemotherapy. *J Clin Oncol* 2000; 18: 1676–88.
110. Schelling M, Avril N, Nahrig J et al. Positron emission tomography using (18F)fluorodeoxyglucose for monitoring primary chemotherapy in breast cancer. *J Clin Oncol* 2000; 18: 1689–95.
111. van der Hiel B, Pauwels EJK, Stokkel MP. Positron emission tomography with 2-(18F)-fluoro-2-deoxy-D-glucose in oncology. Part IIIA: therapy response monitoring in breast cancer, lymphoma and gliomas. *J Cancer Res Clin Oncol* 2001; 127: 269–77.
112. Nair N, Ali A, Dowlashahi K, Fan M, Lamonica G. Positron emission tomography with fluorine-18-fluorodeoxyglucose to evaluate response of early breast carcinoma treated with stereotaxic interstitial laser therapy. *Clin Nucl Med* 2000; 25: 505–7.
113. Cachin F, Prince HM, Hogg A, Ware RE, Hicks RJ. Powerful prognostic stratification by 18F fluorodeoxyglucose positron emission tomography in patients with metastatic breast cancer treated with high-dose chemotherapy. *J Clin Oncol* 2006; 24: 3026–31.
114. Inoue T, Yutani K, Taguchi T et al. Preoperative evaluation of prognosis in breast cancer patients by 18F 2-deoxy-2-fluoro-D-glucose positron emission tomography. *J Cancer Res Clin Oncol* 2004; 130: 273–8.
115. Dehdashti F, McGuire AH, van Brocklin HF et al. Assessment of 21-(18F)fluoro-16-alpha-ethyl-19-norprogesterone as a positron emitting radiopharmaceutical for the detection of progesterin receptors in human breast carcinoma. *J Nucl Med* 1991; 32: 1532–7.
116. McGuire AH, Dehdashti F, Siegel BA et al. Positron tomographic assessment of 16-alpha-[18F] fluoro-17 beta-estradiol uptake in metastatic breast carcinoma. *J Nucl Med* 1991; 32: 1526–31.

117. Katzenellenbogen JA, Welch MJ, Dehdashti F. The development of estrogen and progestin radiopharmaceuticals for imaging breast cancer. *Anticancer Res* 1997; 17: 1573–6.
118. Mintun MA, Welch MJ, Siegel BA et al. Breast cancer: PET imaging of estrogen receptors. *Radiology* 1988; 169: 45–8.
119. Kole AC, Nieweg OE, Prium J et al. Standardized uptake value and quantification of metabolism for breast cancer imaging with FDG and L-(1-11C)tyrosine PET. *J Nucl Med* 1997; 38: 692–6.
120. Leskinen Kallio S, Houvinen R, Nagren K et al. (11C)methionine quantitation in cancer PET studies. *J Comput Assist Tomogr* 1992; 16: 468–74.
121. Houvinen R, Leskinen Kallio S, Nagren K et al. Carbon-11-methionine and PET in evaluation of treatment response of breast cancer. *Br J Cancer* 1993; 67: 787–91.
122. Smyczek-Gargya B, Fersis N, Dittmann H et al. PET with 18F fluorothymidine for imaging of primary breast cancer: a pilot study. *Eur J Nucl Med Mol Imaging* 2004; 31: 720–4.

Thyroid cancer

Peter Lind and Susanne Kohlfürst

Background

The incidence of thyroid cancer (TC) ranges between 4 and 9/100 000/year. It increases with age and varies considerably in different countries, with the highest incidence rates being reported in areas with a normal or even high iodine supply. In addition, it has to be mentioned that, in former iodine-deficient countries which now belong to iodine-sufficient areas, mainly due to salt iodination, the incidence of TC has increased and the histopathology has changed from follicular to papillary TC.¹ Today, in countries with only moderate iodine deficiency, papillary thyroid cancer accounts for more than 75% of TC, and in iodine-sufficient areas more than 85%. The female to male ratio is reported to be 3:1 for papillary and 2:1 for follicular differentiated thyroid cancer (DTC). In general, DTC is known to have a good prognosis after radical primary treatment including total thyroidectomy and radioiodine ablation. However, mortality due to DTC is significantly higher in iodine-deficient regions than in areas with an adequate iodine supply, and higher in males than in females. Therefore it is very important to diagnose TC at a very early stage. Especially in areas with a sufficient iodine supply, clinical symptoms are rare. In most cases TC is detected by chance via small ultrasonographically hypoechoic thyroid nodules. Ultrasonography-guided fine needle aspiration biopsy (US-FNAB) of these small nodules is of great importance and should be performed early. Another tool that may be helpful in selected cases of thyroid nodules is scintigraphy using [^{99m}Tc]pertechnetate, or non-specific tumor searching tracers such as [^{99m}Tc]sestamibi or [^{99m}Tc]tetrofosmin. In recent years also the value of [¹⁸F] FDG (fluoro-2-deoxy-D-glucose)-positron emission tomography (PET) has been under consideration for the assessment of thyroid nodules.

After treatment, including total thyroidectomy, radioiodine remnant ablation, and thyroid hormone suppressive therapy, the follow-up of TC includes various tests. One has to consider that 50% of local recurrences appear in the first years but that distant metastases may occur after several years, sometimes decades, after initial therapy. Recombinant thyroid stimulating hormone (rhTSH) stimulated thyroglobulin (Tg) is the basis of following up TC. For the

localization of recurrences and metastases, several imaging methods are available today. Ultrasonography (US) is the method of choice for the detection of local recurrences and cervical lymph node metastases, ¹³¹I whole-body scintigraphy (¹³¹IWBS) for iodine-positive, and [¹⁸F] FDG-PET or PET-computed tomography (CT) for iodine-negative metastases. If [¹⁸F]FDG-PET or PET-CT is not available, whole-body scintigraphy and single photon emission computed tomography (SPECT) using non-specific tumor searching tracers such as [^{99m}Tc]sestamibi or [^{99m}Tc]tetrofosmin are alternatives. These tracers fall between ¹³¹I and [¹⁸F] FDG as they may demonstrate iodine-positive as well as iodine-negative metastases in some cases.

Diagnostic modalities

Preoperative assessment of thyroid nodules

Whereas in iodine-deficient areas TC may be symptomatic and is diagnosed often in huge, multinodular goiters, in iodine-sufficient areas TC is mostly diagnosed by chance. The best method to differentiate between benign and malignant changes of small thyroid nodules is US and US-FNAB, especially for the diagnosis of papillary TC.²⁻⁶

Sonography

Ultrasonography is a simple method that has become the basis of each morphological investigation of the thyroid. It allows assessment of the size of the gland, the detection of nodules, and evaluation of the echogenicity of the whole thyroid gland and the nodules (hypo-, hyper-, or isoechoic, echo-free structures, or calcifications). In addition, enlarged lymph nodes in the neck may be detected, localized, and investigated by US-guided FNAB. Modern systems usually provide algorithms to measure diameters of thyroid nodules

(cm) and to estimate volumes of each thyroid lobe according to an established formula: lobe volume (ml) = maximum depth (cm) \times breadth (cm) \times length (cm) \times 0.479.

Today, modern ultrasonography systems are equipped with high-resolution transducers (7.5–10 MHz). For routine use in most thyroid and/or nuclear medicine departments, transducers with 7.5 MHz are the standard armamentarium, allowing the detection of nodules below 5 mm. However, in special cases it might be necessary to reinvestigate the patient with a very high-resolution transducer (10–16 MHz), especially for the detection of lymph node pathology and assessment of the nodule margin and its relationship to surrounding structures. These small, high-resolution transducers also allow the detection and interpretation of substernal nodules to some extent. In most institutions the patient is examined in the supine position with the neck hyperextended. The thyroid gland can usually be well delineated from surrounding structures, especially the hypoechoic muscles. Nodules within the thyroid can easily be identified. Besides cystic lesions (that appear echo-free), calcifications, and degenerative nodules (mainly hyper- or isoechoic), the most important echo structure of a thyroid nodule, which should be further investigated, is the hypoechoic one. More than 90% of TCs are hypoechoic on ultrasonographic studies. On the other hand, echo-free, iso-, or hyperechoic nodules exclude TC in more than 90% of cases. However, it has to be stressed that no characteristic echo pattern has been found for TC. When the invasion of surrounding structures in the neck can be demonstrated, the diagnosis of thyroid cancer is obvious. With the exception of anaplastic thyroid cancer, this is seen very rarely in TC. Especially in nodules larger than 2 cm in diameter the performance of [^{99m}Tc]pertechnetate scintigraphy demonstrating the regional metabolism could be helpful in detecting hypofunctioning nodules that are suspicious for being malignant. In iodine-sufficient areas with a low prevalence of goiter, it is the goal to detect TC as early as possible. The detection of a small hypoechoic area, which is often not palpable, is a finding by chance. These hypoechoic, non-palpable nodules as small as <10 mm may further be investigated using US-FNAB.

In conclusion, ultrasound has an important role in the early detection of thyroid nodules, defining the echostructure of the nodule, giving a higher probability of malignancy in the case of hypoechoic nodules, and providing exact positioning of the needle for US-FNAB, also in nodules as small as 5 mm in diameter.

Fine needle aspiration biopsy

To detect TC at an early stage, even in non-palpable lesions, it can be demonstrated that US-guided FNAB has advantages over FNAB without US guidance.⁵ In most institutions,

US-guided FNAB is performed free-handed, with a 21-gauge needle attached to a 10- or 20-ml syringe. Nodules as small as < 10 mm can be investigated using this method (Figure 11.1). Cytological interpretation should be performed by experienced cytopathologists. For the interpretation of thyroid cytology the traditional classification by Papanicolaou is obsolete. Today the interpretation of FNAB is divided into three groups: A (non-neoplastic lesion), B (suspicious lesion), and C (malignant lesion). Using US-guided FNAB, the sensitivity is reported to be > 80% and specificity > 70%.^{5,6} However, it is important that the pathologist receives not only cytological material but also clinical, sonographic, and scintigraphic information. A variety of functional mechanisms as well as antithyroid drug therapy or previous [^{131}I] therapy can grossly distort the cytological pattern and therefore lead to a wrong interpretation.

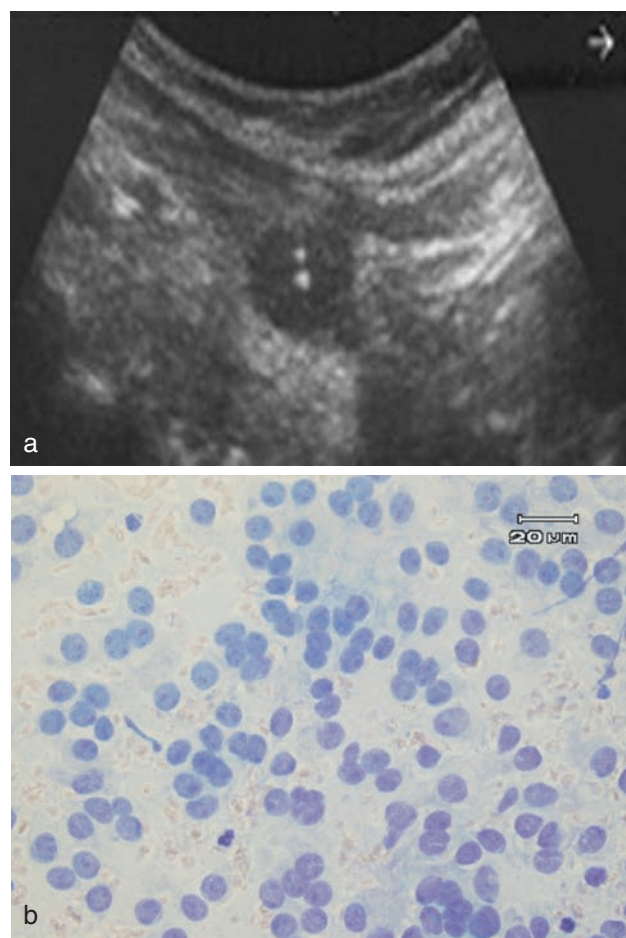


Figure 11.1

Ultrasonography-guided fine needle aspiration biopsy. Hypoechoic nodule with the the tip of the needle in the center of the nodule (a). Cytology with follicular proliferation (b).

In contrast to follicular TC, papillary TC can be diagnosed very accurately using US-FNAB. One major advantage of US-FNAB is that the negative predictive value (NPV) is as high as 95%, increasing to 99% for solitary thyroid nodules, as reported by Mikosch et al.^{6,7} This means that non-suspicious US-FNAB excludes TC at a very high degree. Still unresolved is the problem of rather low specificity and poor positive predictive value (PPV) due to the fact that follicular proliferation has to be interpreted as suspicious for malignancy. Although US-FNAB is a very valuable procedure to determine the nature of thyroid nodules, in cases of follicular proliferation or inconclusive cytological results, further methods such as ^{201}Tl , [$^{99\text{m}}\text{Tc}$]sestamibi, or [$^{99\text{m}}\text{Tc}$]tetrofosmin scintigraphy or [^{18}F] FDG-PET may be helpful in the finding of hypofunctioning thyroid nodules in conventional [$^{99\text{m}}\text{Tc}$]pertechnetate or ^{123}I scintigraphy. It has to be mentioned that the sensitivity of these conventional thyroid scintigraphic methods regarding hypofunctioning nodules depends on the size of the nodule. In some cases, however, a definitive diagnosis can only be obtained by surgery and postoperative histological results.

Scintigraphy using $^{99\text{m}}\text{Tc}$ pertechnetate or ^{123}I

Scintigraphy using [$^{99\text{m}}\text{Tc}$]pertechnetate or ^{123}I demonstrates the metabolic activity of the thyroid gland.⁸ Therefore, scintigraphy is able to show the regional iodine metabolism, including hyperfunctional as well as hypofunctional areas or nodules. With respect to the probability of malignancy, hypofunctioning nodules are more suspicious than hyperfunctioning (Figure 11.2). However, hypofunction of a thyroid nodule does not mean malignancy in all cases. The reasons for such a decrease in iodine metabolism are regressive changes in pre-existing adenomas and cystic degeneration. However, also inflammatory destruction of thyrocytes, and most important of all malignant growth, produce a functional decrease of thyroid tissue visible as a hypofunctional area in scintigraphy. The incidence of TC in hypofunctioning nodules is almost proportional to the iodine supply in a given population. The better is the iodine supply, the higher is the likelihood of a hypofunctioning nodule to be malignant. The highest rate of malignancy in hypofunctioning nodules (38%) is described by Molitch et al.⁹ In most reports, malignancy of hypofunctioning nodules, depending on iodine supply and age of the patient, is reported to be between 5 and 15%.^{10,11} However, eufunctional or hyperfunctional nodules cannot be considered as benign in each case, especially when scans were obtained with [$^{99\text{m}}\text{Tc}$]pertechnetate and the nodule is very small. One problem of planar scintigraphy is the fact that

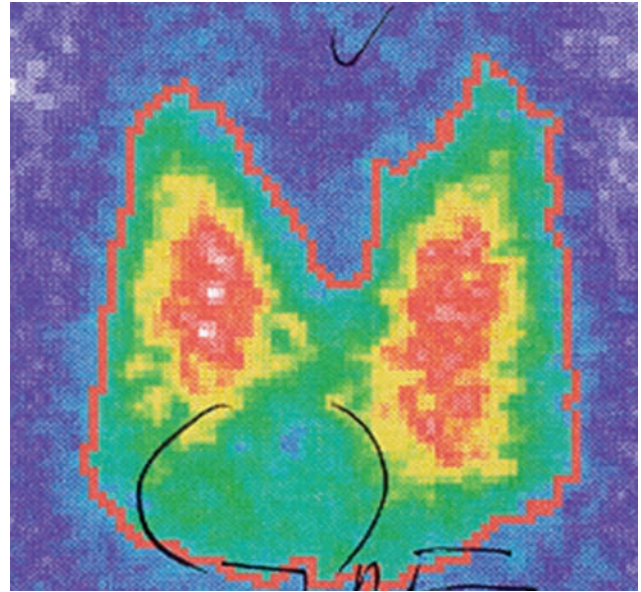


Figure 11.2

Hypofunctioning nodule (right lower pole) in [$^{99\text{m}}\text{Tc}$]pertechnetate scintigraphy (size > 1.5 cm).

the scintigraphic pattern of a nodule depends also on the size and the location of the nodule. Kresnik et al. noted that most hypofunctioning nodules that turned out to be thyroid cancers were larger than 2 cm in diameter. In contrast, nodules below 1 cm demonstrated normal radionuclide distribution on planar scintigraphy, despite being malignant at final histological evaluation.¹² The reason for this pattern is mainly due to overlapping of normally functioning thyroid tissue in front of the (hypofunctional) nodule. Therefore, it can be concluded that the value of the scintigraphic pattern for the probability of malignancy of a thyroid nodule smaller than 1 cm is to be questioned, and in nodules between 1 and 2 cm the scintigraphic result has to be interpreted with caution. However, together with ultrasonography, especially in cases of multiple hypoechogenic nodules, scintigraphy can help to select lesions for FNAB.

Today [$^{99\text{m}}\text{Tc}$]pertechnetate is the tracer of choice for functional thyroid scanning. [$^{99\text{m}}\text{Tc}$]pertechnetate is administered intravenously (37–74 MBq). Scans are obtained 20 minutes post-injection, usually as planar images in anterior–posterior projection. [$^{99\text{m}}\text{Tc}$] is rapidly trapped into thyroid cells, but then washed out from the cells as no organification occurs in thyroid tissue. Due to the low γ energy of $^{99\text{m}}\text{Tc}$ (140 keV), the demonstration of tracer uptake in retrosternal/mediastinal goiter can be impaired by attenuation in the sternum.¹³ The technique usually produces excellent images of cervical thyroid

activity, with a radiation dose of only 0.05–0.1/mSv effective equivalent dose. [^{99m}Tc]pertechnetate is cheap, and always available in any nuclear medicine department. It seems obvious that SPECT studies, especially using pin-hole collimators, would improve the anatomical assessment of nodular changes within the thyroid gland.¹⁴ Iodine-123 was proposed as an ideal substitute (γ radiation only, 160 keV, 13 h half-life), but its widespread use has been impaired by its high cost and logistic difficulties arising from the short half-life. Wherever obtainable, however, it would be the best radiotracer for thyroid studies (7.4–18.5 MBq per os or intravenously, scanning after 6–8 h, low-energy high-resolution collimators on cameras).

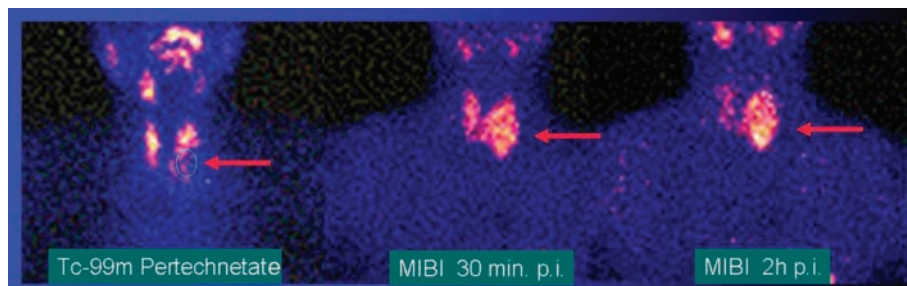
[^{99m}Tc]sestamibi, [^{99m}Tc]tetrofosmin scintigraphy and [^{18}F]-FDG-PET

Preoperative diagnosis of follicular TC remains difficult. In cases of unclear cytology or the cytological diagnosis of follicular proliferation, multitracer imaging may play a helpful role in the clinical assessment.¹⁴ Due to the low diagnostic specificity of functional imaging for TC with [^{99m}Tc]pertechnetate or ^{123}I scintigraphy, other radionuclides and radiotracers with affinity to malignant lesions such as [^{201}Tl] chloride, [^{99m}Tc]sestamibi, or [^{99m}Tc]tetrofosmin were used to assess the probability of malignancy of thyroid nodules.^{15–19} Neither ^{201}Tl nor cationic complexes such as [^{99m}Tc]sestamibi or [^{99m}Tc]tetrofosmin were able to clearly differentiate between benign and malignant sonographically hypoechoogenic, scintigraphically hypofunctioning thyroid nodules (Figure 11.3). Nevertheless the results of such studies can be important for therapy planning, especially in a case of inconclusive cytology from US-FNAB or multinodular goiter. Recently, the value of [^{18}F]FDG-PET was investigated not only for the follow-up of TC but also

for the preoperative assessment of hypoechoogenic and/or hypofunctioning thyroid nodules.^{20–24} Joensuu et al. found clearly elevated [^{18}F] FDG uptake only in one patient with anaplastic thyroid cancer and in one with oxyphilic thyroid carcinoma out of five patients investigated.²⁰ Three patients with papillary TC demonstrated only moderate [^{18}F]FDG uptake. In contrast to this study, Uematsu et al. could demonstrate in 11 patients investigated that all malignant nodules could be separated from benign ones using a standardized uptake value (SUV) cut-off of 5 and time activity curves.²² Mitchell et al. performed FNAB and [^{18}F]FDG-PET-CT before surgery in 31 patients with 48 lesions. Fifteen out of 48 lesions were malignant, and 33 were benign. Nine of the 15 malignant lesions demonstrated [^{18}F]FDG uptake (sensitivity: 60%). Thirty of 33 benign lesions were [^{18}F]FDG-negative (specificity 91%). The authors conclude that [^{18}F]FDG-PET-CT with a high NPV of 83% for malignancy may be a useful tool in the evaluation of thyroid nodules with indeterminate fine needle aspiration biopsy.²³ Our own experience in 43 patients with hypoechoogenic and/or hypofunctioning thyroid nodules (11 papillary DTC, three follicular TC, two anaplastic carcinomas, 11 microfollicular adenomas, 10 oxyphilic adenomas and two macrofollicular adenomas, four regressive goiters) demonstrates that all patients with TC and oxyphilic adenomas had an elevated [^{18}F]FDG uptake²⁵ (Figure 11.4). Using a SUV threshold of 2 for differentiating benign from malignant nodules, sensitivity, specificity and NPV were 100%, 63%, and 100% respectively. In a subgroup of 24 patients with cytological diagnosis follicular proliferation, [^{18}F]FDG-PET was able to differentiate between follicular adenoma and carcinoma. From these studies it may be concluded that tumor-seeking agents including [^{18}F]FDG are not able to differentiate 100% benign from malignant thyroid nodules. However, in a case of non-diagnostic cytology or a cytological diagnosis of follicular proliferation, [^{18}F]FDG-PET seems to be the method of choice to decide whether surgery or a wait and watch strategy should be recommended.

Figure 11.3

[^{99m}Tc]sestamibi dual-phase scintigraphy with tracer uptake in a case of indeterminate cytology in hypoechoogenic, hypofunctional thyroid nodule. Histology revealed microfollicular adenoma. p.i., post-injection.



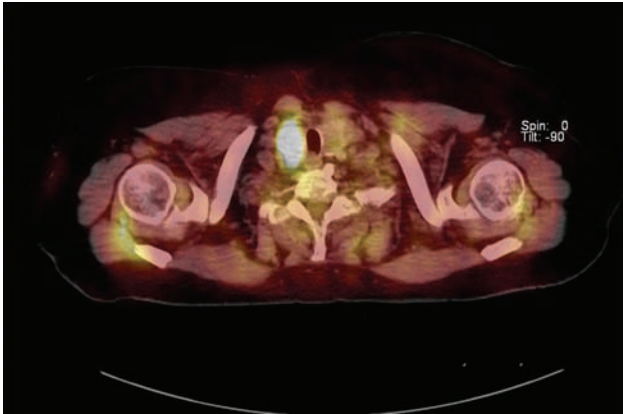


Figure 11.4

$[^{18}\text{F}]$ fluoro-2-deoxy-D-glucose (FDG)-positron emission tomography–computed tomography (PET–CT) in a case of hypofunctioning thyroid nodule and undetermined cytology. The nodule demonstrates a clear FDG uptake. Histology revealed follicular thyroid cancer.

Follow-up of thyroid cancer after treatment

The radicality of treatment of TC depends on the TNM classification after surgery. With the exception of papillary microcarcinoma (pT1a according to TNM 2003 supplement), total thyroidectomy, followed by radioiodine therapy, and TSH suppressive thyroid hormone therapy is the standard treatment of differentiated TC, at least in Europe. Radioiodine therapy is indicated not only to destroy any microscopic cells remaining after surgery, but also to increase the specificity of the tumor marker Tg. TSH stimulated Tg should be negative (< 0.5 ng/ml) after surgery and radioiodine therapy. In these cases, each increase of Tg over time in the follow-up means recurrent or metastatic disease. To localize recurrence and metastases US of the neck, radioiodine imaging, scintigraphy using non-specific tracers such as $[^{99\text{m}}\text{Tc}]$ sestamibi or tetrofosmin and $[^{18}\text{F}]$ FDG-PET (better, PET–CT) as whole-body modalities for distant metastases are the methods of choice.

Thyroglobulin as tumor marker

Serum Tg is a very sensitive tumor marker for following TC if determined by immunoradiometric assays, and also has a high specificity after total thyroidectomy and radioiodine remnant ablation.^{26–29} After total thyroidectomy and radioiodine remnant ablation, Tg should be undetectable in cases of complete remission. However, it has to be mentioned that the value of Tg is only reliable if Tg-antibodies are undetectable and recovery of Tg is within the normal

range between 70 and 130%. In the presence of Tg-antibodies, serum Tg can be falsely lowered if determined by an immunoradiometric assay.³⁰ It has also to be mentioned that in the case of measurable Tg-antibodies more than a year after surgery and radioiodine therapy, persistent thyroid tissue or recurrence has to be suspected. In a case of increasing Tg, recurrence, lymph node metastases, or distant metastases are likely. The serum Tg level under TSH elevation (either after withdrawal of thyroid hormone over 4–6 weeks or after recombinant TSH given intramuscularly) is thought to be the most reliable indicator for persistent or recurrent disease.³¹ However, there are some case reports with proven recurrent or metastatic disease but negative Tg.³² Sometimes this may be due to an oxyphilic subtype of DTC, in which not only Tg levels remain negative in the case of recurrent disease but also ^{131}I WBS is negative. Therefore, metastatic disease can only be detected by non-specific tracers.³³ With the exception of these rare cases Tg is an excellent tumor marker for TC. The sensitivity of Tg, however, depends on the TSH serum level and is much higher under TSH elevation > 30 mU/l (98%) than under TSH suppressive thyroid hormone therapy (80%). A negative TSH stimulated Tg level is highly predictive for the absence of disease. In two retrospective studies it could be demonstrated that in the case of negative TSH stimulated Tg, routine diagnostic ^{131}I WBS does not add any further information.^{34,35} For the most sensitive (TSH stimulated) measurement of Tg, the withdrawal of thyroid hormone over a period of 4–6 weeks and hypothyroidism is now substituted by intramuscular injection of recombinant TSH: twice 0.9 mg rhTSH intramuscularly on two subsequent days.³⁶ With the introduction of rhTSH it has been shown that the sensitivity of rhTSH stimulated Tg is as high as after the withdrawal of thyroid hormone after several weeks, although the values are somewhat lower.³⁷ Against this background, the question arises whether rhTSH stimulated Tg alone is sufficient for the follow-up of patients with TC. In two studies it is concluded that in general, TSH stimulated Tg alone is not sufficient to screen unselected patients.^{38–40} However, a recently published consensus paper that differentiates between high- and low-risk patients concludes that for low-risk patients in whom initial work-up after treatment has demonstrated complete remission (negative radioiodine scanning, negative ultrasonography, and non-detectable TSH stimulated Tg), ultrasonography of the neck and rhTSH stimulated Tg is sufficient for further follow-up.⁴¹ Ultrasensitive Tg assays measuring Tg levels as low as 0.07 ng/ml are now available. Whether these supersensitive assays add clinical information in the follow-up of TC or even substitute TSH stimulation of Tg is not clear up to now, but it is unlikely. It may be concluded that serum Tg under elevated TSH conditions plays a major role in the follow-up of TC, either in combination with ultrasonography alone for low-risk

patients or with the complete armamentarium of nuclear medicine methods, including radioiodine scanning and [^{18}F]FDG-PET or, better, PET-CT.

Ultrasonography

Ultrasonography of the neck should be performed at any visit in the follow-up of TC. It is the most sensitive method to detect local recurrence and lymph node metastases at an early stage, although it is not specific.⁴² In a case of any pathologic US findings in the neck, US-FNAB should be performed to obtain cytological diagnosis and to be able to plan the further management and treatment of the patient. For low-risk patients a combination of rhTSH stimulated Tg and US may be sufficient in most cases, as described above.⁴¹ Figure 11.5 demonstrates a hypoechoogenic lymph node metastasis in a case of increasing serum Tg after surgery and radioiodine ablation due to papillary thyroid cancer pT3bN1M0 (TNM 2003 supplement).

Radioiodine whole-body scintigraphy and SPECT

Iodine-131 or ^{123}I WBS was performed periodically over several years for the follow-up of TC, either under thyroid hormone withdrawal or under rhTSH. However, it could be demonstrated that two negative ^{131}I WBSs within 1 year in combination with negative TSH stimulated Tg had a very good predictive value for the absence of recurrent or

metastatic disease.^{43–46} On the other hand, in a study by Robbins et al., 13% of patients with negative TSH stimulated Tg (< 2 ng/ml) had evidence of disease.³⁸ In this light, the question of a correct value for negative Tg arises. In our center, after surgery and radioiodine therapy, a TSH stimulated Tg < 0.5 ng/ml is claimed to designate a patient free of disease.⁴⁷ In a consensus paper by Schlumberger et al., for low-risk patients, rhTSH stimulated Tg and ultrasonography were described to be sufficient for following up TC.⁴¹ This is not true for high-risk patients, and many centers are still performing radioiodine scanning in connection with TSH stimulated serum Tg. Radioiodine ($^{131}\text{I}/^{123}\text{I}$) is the most specific radionuclide to image recurrences or distant metastases of TC. However, the sensitivity is rather low, and depends on the activity administered.⁴⁸ There are several preconditions that have to be fulfilled before WBS using radioiodine can be performed.⁴⁹ To image patients with radioiodine in the follow-up of TC, TSH suppressive L-thyroxine therapy has to be withdrawn for several weeks to achieve a TSH of at least 30 mU/l, and a low iodine diet is recommended. Several authors claim that a TSH of more than 50 mU/l is required before radioiodine should be administered.^{50,51} This, however, leads to transient hypothyroidism with all the known disadvantages for the patient: reduced quality of life, emotional dysfunction, tiredness, increase in weight, possible cardiac failure, possible growth of local recurrence and distant metastases, and disruption in work life, with its possible negative economic and professional consequences. Considering these facts it is no surprise that the administration of rhTSH has such a high compliance among patients. Due to this fact, today, many thyroid centers use rhTSH (0.9 mg twice intramuscularly) instead of withdrawing L-thyroxine to achieve elevated TSH. During this procedure, the patient remains in euthyroidism, without symptoms of hypothyroidism. Before the administration of radioiodine, contamination due to contrast media or iodine-containing drugs has to be excluded. In this context, the determination of urinary iodine excretion is recommended. If these preconditions are fulfilled, ^{131}I (mostly given orally) or ^{123}I (injected intravenously) is administered. The advantage of ^{123}I includes a favorable γ energy of 159 keV with good quality γ camera imaging and the lack of β energy, and therefore lack of thyroid stunning.⁴⁶ However, ^{123}I is expensive and not readily available. The short half-life of 13 hours may also be a disadvantage in imaging recurrent and metastatic disease. Furthermore, the ^{123}I activity administered and the time of acquisition are still a matter of debate. Concerning the diagnostic accuracy, ^{123}I is not superior to ^{131}I scanning, and post-therapy ^{131}I WBS demonstrates sometimes more lesions when compared to a diagnostic ^{123}I WBS. Therefore, most thyroid centers remain using ^{131}I for diagnostic WBS. After surgery and radioiodine remnant ablation therapy, the first ^{131}I WBS is performed post-therapy, 5–7 days after radioiodine. In the majority of patients this post-therapy



Figure 11.5

Hypoechoogenic lymph node metastasis in a patient with recurrent papillary thyroid cancer pT4N1M0, 1 year after surgery and radioiodine therapy.

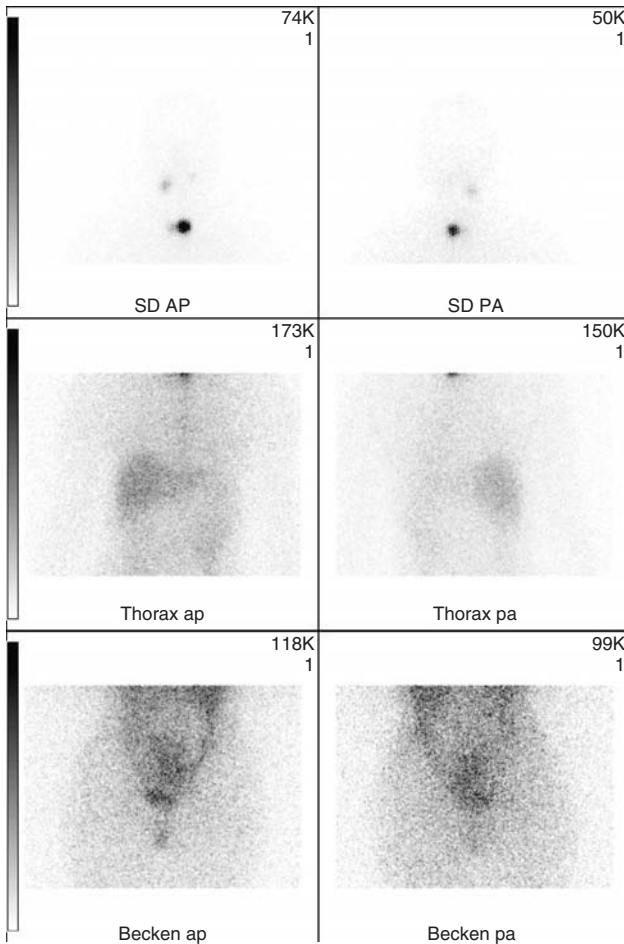


Figure 11.6

Post-therapy ^{131}I whole-body scintigraphy after 2960 MBq ^{131}I remnant ablation demonstrates uptake in the thyroid bed and physiologic iodine distribution in the salivary glands, liver, gut and urinary bladder.

^{131}I WBS demonstrates some activity in the remnants, depending on the surgical radicality, and non-specific uptake in the salivary glands, the stomach, intestine and urinary bladder (Figure 11.6). Sometimes in this post-therapeutic ^{131}I WBS, additional metastases that are not known before can be detected (Figure 11.7). Four to six months after radioiodine remnant ablation the first diagnostic ^{131}I WBS is performed to evaluate the success of the initial treatment. At this time, M-staging of the disease is possible. Under endogenous (4–6-week withdrawal of thyroid hormones) or exogenous TSH elevation (0.9 mg rhTSH intramuscularly on two subsequent days), ^{131}I is administered orally, and diagnostic WBS is performed 48–72 hours later. In most studies, 185 MBq ^{131}I is recommended. Due to the possibility of thyroid stunning, in the case of elevated Tg and planned radioiodine treatment the administered activity for the diagnostic scan should not exceed 74 MBq. The specificity of ^{131}I WBS ranges between 96 and 100%.^{52,53}

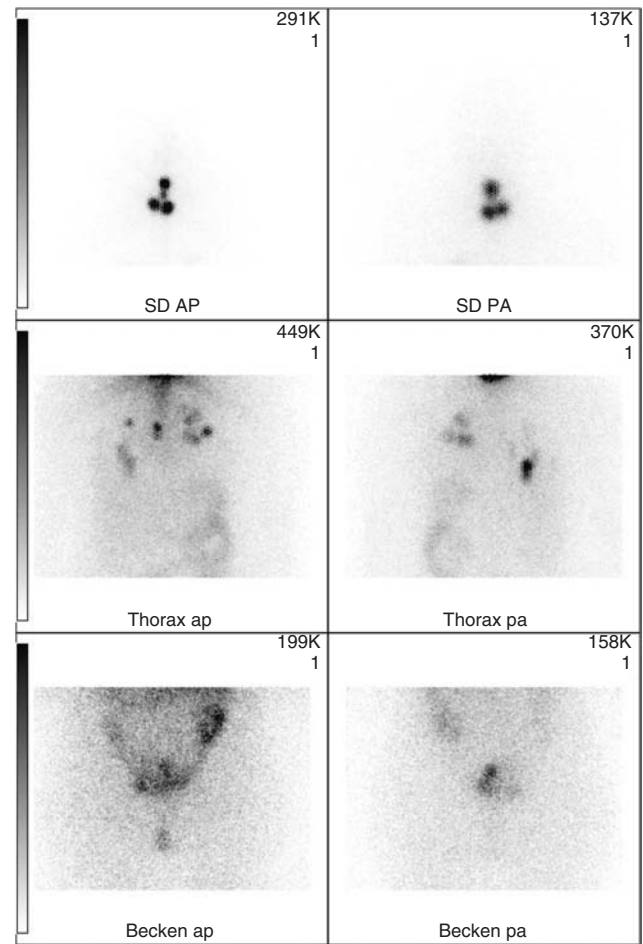


Figure 11.7

Post-therapy ^{131}I whole-body scintigraphy after 2960 MBq ^{131}I remnant ablation demonstrates uptake in the thyroid bed but also multiple metastases in the lung.

Besides physiological uptake, some pitfalls of false positive ^{131}I WBS results have to be considered.⁵⁵ The sensitivity of ^{131}I WBS, however, is low, and depends on the administered activity and the type of histology. According to the literature, the sensitivity of a diagnostic ^{131}I WBS ranges between 45 and 75%, and is somewhat lower for papillary compared to follicular DTC.^{51,52,54,56,57} Due to the low impact of diagnostic ^{131}I WBS in low-risk patients with negative TSH stimulated Tg (no evidence of residual disease), some doubts regarding the value of this procedure have emerged in recent years. In addition, due to the low sensitivity of a low-dose diagnostic ^{131}I WBS with the possibility of stunning in a case of elevated Tg, the performance is also questioned in a case of planned ^{131}I therapy.^{58,59} For the future, it may be recommended that in low-risk patients, rhTSH stimulated Tg is sufficient, and in patients with elevated Tg with evidence of disease, high-dose radioiodine therapy and a post-therapy scan should be performed.^{60,61} The place

for a low dose-diagnostic ^{131}I WBS may remain in the follow-up of high-risk patients. However, the role of a low-dose radioiodine scan even in these patients is increasingly a matter of discussion. There are several papers demonstrating that radioiodine therapy due to increasing Tg has a therapeutic effect, and post-therapy ^{131}I WBS has a higher sensitivity compared to a low-activity diagnostic scan.^{54,62} Therefore, some centers prefer, in a case of elevated or increasing Tg, radioiodine therapy and post-therapy ^{131}I WBS only, without performing a diagnostic scan (Figure 11.8). An additional problem arises if TSH stimulated Tg is elevated or increases over time (e.g. > 3 ng/ml) and diagnostic ^{131}I is negative. The reason for this false negative ^{131}I WBS may be insufficient TSH stimulation, iodine contamination, small tumor volume, or iodine-negative metastases.^{46,63} If the first and second reasons are excluded, the patient should be scheduled for [^{18}F] FDG-PET (PET-CT without contrast media), and should be treated with radioiodine followed by

a post-therapy ^{131}I WBS. In a study by Ruf et al., 25 patients with inconclusive findings in planar scanning after ablative radioiodine therapy underwent SPECT-CT of the questionable region.⁶⁴ Forty-one lesions were observed in the 25 patients. In 17/41 lesions uptake was due to remnant tissue, 13/41 lesions were caused by metastases, and 11/41 lesions were not malignant. In 44% of lesions, improved anatomical assignment was seen by SPECT-CT. In patients with strongly elevated Tg, but only faint uptake in the ^{131}I WBS, a combination with ^{18}F FDG-PET-CT is able to demonstrate the complete extent of the disease, with exact anatomical localization of iodine-positive and iodine-negative lesions.⁶⁵ This is not only important for exact staging and restaging of metastasizing thyroid cancer, but also for individually based multimodality treatment of these patients, including radioiodine treatment, surgery, external radiotherapy, retinoic acid, and somatostatin receptor therapy.

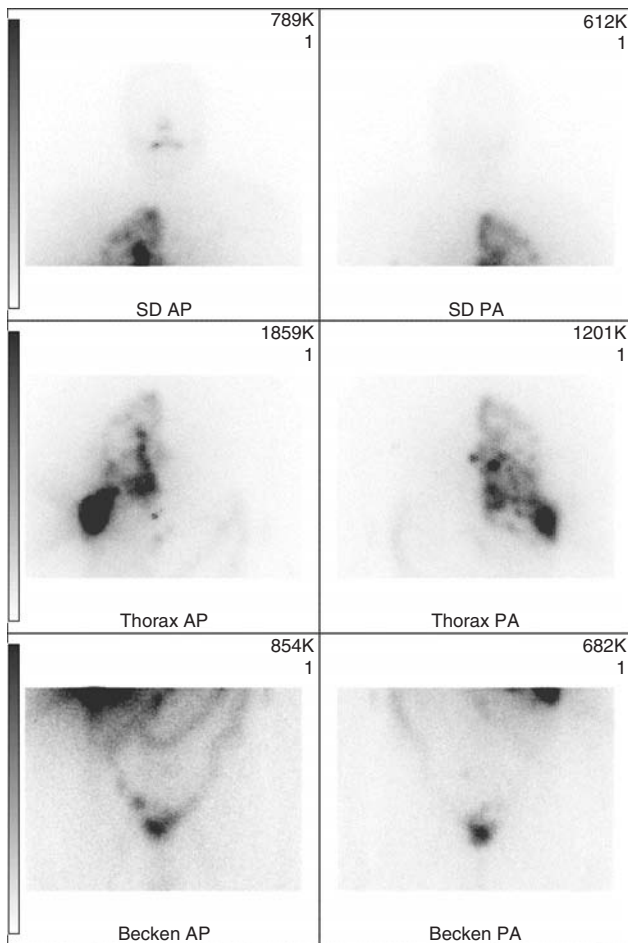


Figure 11.8

Post-therapy ^{131}I whole-body scintigraphy after 7400 MBq ^{131}I due to increasing serum thyroglobulin (Tg) in a patient with follicular thyroid cancer. Multiple mediastinal, lung (pleural), and rib metastases.

Whole-body scintigraphy and SPECT using non-specific tracers

Due to the fact that only two-thirds of recurrences and metastases store iodine, and due to the low sensitivity of diagnostic ^{131}I WBS, additional methods are necessary to detect early (iodine-negative) recurrences and metastases. Several years ago, ^{201}Tl was used to give additional information to ^{131}I WBS in patients with elevated Tg, and several studies in the literature reported that ^{201}Tl is superior to ^{131}I WBS in the follow-up of TC.^{54,66,67} ^{201}Tl has a high affinity to Na^+/K^+ adenosine triphosphatase (ATPase), and is therefore stored in the intracellular compartment. One of the main advantages of ^{201}Tl WBS is the fact that ^{201}Tl is taken up by tumor cells without the need for withdrawal of thyroid hormone to achieve elevated TSH levels. In a study by Hoefnagel et al., ^{201}Tl WBS was performed in 326 patients (301 TC, six anaplastic thyroid carcinomas, one giant cell carcinoma, 18 medullary thyroid carcinomas) after total thyroidectomy for thyroid carcinoma.⁶⁶ As in most of the centers ^{201}Tl WBS was performed 20 minutes after intravenous injection of 74 MBq ^{201}Tl . In this study, it was found that ^{201}Tl WBS had a sensitivity of 94%, compared to 48% for the diagnostic ^{131}I WBS. Charkes et al. reported a detection rate for metastases of 60% using planar ^{201}Tl scintigraphy, which however increased to 85% when SPECT imaging was performed.⁶⁷ Like ^{201}Tl , [$^{99\text{m}}\text{Tc}$]sestamibi and [$^{99\text{m}}\text{Tc}$]tetrofosmin are mainly used for myocardial perfusion scintigraphy. With the introduction of these $^{99\text{m}}\text{Tc}$ -labeled cationic complexes, they were also evaluated as imaging modalities in the follow-up of TC. The most likely mechanism for cellular uptake of both tracers is diffusion of the lipophilic cation across the mitochondrial (and sarcolemmal)

membranes in response to an electrical potential.⁶⁸ After an intravenous injection of 555 MBq [^{99m}Tc]sestamibi, WBS is performed 20 minutes post-injection. As with ²⁰¹Tl, withdrawal of thyroid hormone is not necessary. In an early study, Briele et al. compared ²⁰¹Tl and [^{99m}Tc]sestamibi in 12 patients with suspicion of recurrent DTC.⁶⁹ They found that, except in one case, the findings concerning tumor localization and extension were identical. Whereas locoregional lymph node metastases and bone metastases could be imaged very well, this was not the case for lung metastases. Sundram et al. found that [^{99m}Tc]sestamibi was less sensitive compared to ¹³¹I WBS in patients after surgery before radioiodine in detecting thyroid remnants, but superior to ¹³¹I WBS to detect lymph node metastases.⁷⁰ Alam et al. reported in a retrospective study that [^{99m}Tc]sestamibi can be proposed as a first-line diagnostic agent to follow up patients with TC, with some limitation in small lung metastases. They found a sensitivity of 94.4% for neck, 78.4% for lung, and 92.8% for bone metastases.⁷¹ For all sites together, PPV and NPV were 96.1% and 86.5% respectively. All together, studies performed up to now using [^{99m}Tc]sestamibi in the follow-up of TC have demonstrated quite different results with sensitivities between 45 and 94%.^{69–72} In a preliminary study comparing ²⁰¹Tl, [^{99m}Tc]sestamibi, and [^{99m}Tc]tetrofosmin in 15 patients in the follow-up of TC with elevated Tg levels, we found that [^{99m}Tc]tetrofosmin had significantly higher in vivo target/background (T/Bg) ratios (1.76 ± 0.345) and detection rates compared to [^{99m}Tc]sestamibi (1.51 ± 0.31). For ²⁰¹Tl (1.59 ± 0.396) the in vivo T/Bg ratio was slightly but not significantly lower compared to [^{99m}Tc]tetrofosmin.⁷³ In a subsequent study in 114 patients, we found that the overall detection rate of metastatic disease for [^{99m}Tc]tetrofosmin was 86%⁷⁴ (Figure 11.9).

[¹⁸F]FDG-PET and PET-CT

In less- or dedifferentiated thyroid cancer patients recurrences or metastases may lose the ability to concentrate iodine. Iodine-131 WBS may therefore be negative or not able to demonstrate the complete extent of the disease. In former years, ²⁰¹Tl, [^{99m}Tc]tetrofosmin, or [^{99m}Tc]sestamibi were introduced to image iodine-negative metastases from TC. Due to the limited spatial resolution of single photon emitters, up to 15–25% of recurrences and metastases were missed by these methods. To overcome this problem [¹⁸F]FDG-PET was introduced in the follow-up of TC patients.⁷⁵ Whereas the role of [¹⁸F]FDG-PET in the preoperative assessment of thyroid nodules is not yet fully evaluated, its use in the follow-up of TC belongs to the 1a indications for [¹⁸F]FDG-PET in oncology.⁷⁶ In most centers [¹⁸F]FDG-PET is performed after overnight fasting, with blood glucose below 140 mg/dl. Sixty to 90 minutes

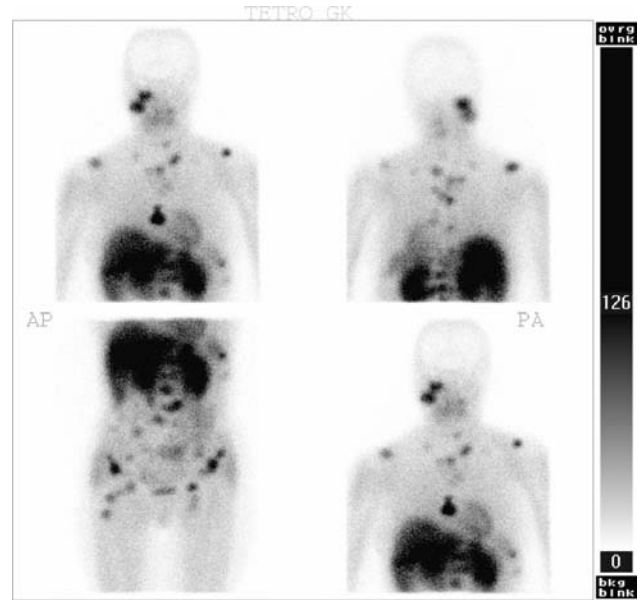


Figure 11.9

[^{99m}Tc]tetrofosmin whole-body scintigraphy in a patient with clearly elevated thyroglobulin but only faint uptake in ¹³¹I whole-body scintigraphy demonstrates multiple tetrofosmin-positive metastases.

after the intravenous injection of 200–500 MBq [¹⁸F]FDG (depending on the PET system, two-dimensional (2D), 3D acquisition), emission scanning is started. Transmission scanning is performed either before FDG injection (cold transmission) or after FDG injection (hot transmission). Recently, CT transmission has become available in combined PET-CT machines, where morphology and metabolism will be imaged during one investigation. Already, the first investigations using [¹⁸F]FDG-PET in the follow-up of TC have demonstrated that [¹⁸F]FDG uptake represents less-differentiated thyroid cancer cells or the dedifferentiation of cells. Feine et al. investigated 41 patients, comparing [¹⁸F]FDG-PET and ¹³¹I WBS in the follow up of differentiated thyroid cancer.⁷⁷ Combined imaging resulted in a sensitivity of about 95% in detecting recurrences and metastases. Alternating uptake (¹³¹I negative but [¹⁸F]FDG positive or ¹³¹I positive and [¹⁸F]FDG negative) was found in 90% of patients. The authors conclude that besides an increase of sensitivity using ¹³¹I WBS and [¹⁸F]FDG-PET, the uptake of [¹⁸F]FDG seems to be an indicator of poor differentiation. In a multicenter trial, Grünwald et al. compared the sensitivity and specificity of [¹⁸F]FDG-PET, ¹³¹I WBS, and [^{99m}Tc]sestamibi/²⁰¹Tl WBS.⁷⁸ The sensitivity of [¹⁸F]FDG-PET, ¹³¹I WBS, and [^{99m}Tc]sestamibi/²⁰¹Tl was 75%, 50%, and 53% and specificity 90%, 99%, and 92% respectively. The sensitivity of [¹⁸F]FDG-PET increased to 85% in a subgroup of patients with ¹³¹I negative WBS. In a recent study by Iwata et al., [¹⁸F]FDG-PET was compared

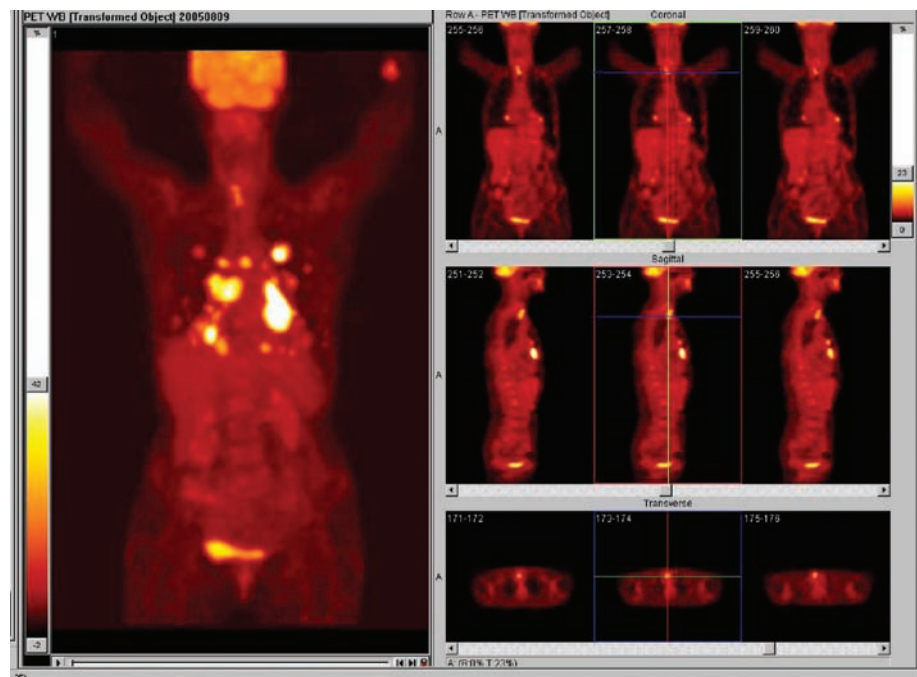
with [^{99m}Tc]sestamibi and ^{131}I post-therapy whole-body scintigraphy.⁷⁹ In 19 patients, a total of 32 lesions were diagnosed as metastases. [^{18}F]FDG-PET, [^{99m}Tc]sestamibi WBS, and post-therapy ^{131}I WBS respectively revealed a total of 26 (81%), 20 (62.5%), and 22 (68.8%) lesions. Similar results were obtained by our group comparing [^{18}F]FDG-PET, [^{99m}Tc]tetrafosmin WBS, and post-therapy ^{131}I WBS in the follow-up of TC in 35 patients.⁸⁰ In a retrospective study by Conti et al., 30 patients with TC, 24 with rising or elevated thyroglobulin, and six with elevated calcitonin had a [^{18}F]FDG-PET investigation.⁸¹ In all 24 patients with papillary/follicular thyroid carcinoma and in all six patients with medullary cancer, [^{18}F]FDG-PET was able to detect recurrent or metastatic disease, which was confirmed directly by surgery or indirectly by changes or persistence of laboratory findings in 17/24 patients with papillary/follicular and 4/6 patients with medullary TC. From a group of 32 TC patients with elevated thyroglobulin but negative ^{131}I WBS, Altevorder et al. performed [^{18}F]FDG-PET in 12 patients.⁸³ In 6/12 patients [^{18}F]FDG-PET was positive. The Tg level was much higher in [^{18}F]FDG-PET positive patients (23–277 ng/ml) compared to [^{18}F]FDG-PET negative patients (1.5–17 ng/ml). According to a German consensus conference in 2000, the sensitivity and specificity of [^{18}F]FDG-PET in detecting ^{131}I negative metastases in cases of elevated thyroglobulin were 85–94% and 90–95% respectively.⁷⁶ In a study by Schluter and co-workers, a total of 118 [^{18}F]FDG-PET studies in 64 patients with elevated thyroglobulin but negative ^{131}I WBS with respect to change of therapy due to the outcome of [^{18}F]FDG-PET were performed.⁸³ Forty-four patients had positive

[^{18}F]FDG-PET (34 true positive, seven false positive, two with secondary malignancy, one non-evaluable), and 20 patients had negative PET scans (five true negative, 15 false negative). According to these results the PPV was 83%, and the NPV only 25%. Treatment strategy was changed in 19 of 34 patients with true positive PET scans. It has to be mentioned that the sensitivity of [^{18}F]FDG-PET is higher under endogenous or exogenous TSH stimulation.^{84,85} Moog et al. investigated ten TC patients under TSH suppressive L-thyroxine therapy and after withdrawal of L-thyroxine (TSH > 22 mU/l),⁸⁴ they could demonstrate that the T/Bg ratio increased after TSH stimulation from 3.85 to 5.84 ($p < 0.001$). Similar preliminary results with an increase of the SUV from 1.3 to 4.4 are reported by Petrich et al. using recombinant TSH before [^{18}F]FDG-PET.⁸⁵ In our own series we performed 221 [^{18}F]FDG-PET studies in 161 TC patients. Of the 122 follow-up patients, 96 had differentiated (33 papillary and 63 follicular), 15 medullary, and 11 anaplastic histology of thyroid cancer.⁸⁰ Among the 96 patients with differentiated histology, in 81 patients Tg was elevated and in a group of 15 patients [^{18}F]FDG-PET was performed due to positive Tg-polymerase chain reaction (PCR) but normal serum Tg. The sensitivity of [^{18}F]FDG-PET for the detection of metastases in cases of elevated Tg for all patients was 77%, and in cases of elevated Tg but negative ^{131}I WBS it increased to 88%. [^{18}F]FDG-PET is a valuable tool to detect recurrences and metastases of TC, especially in cases of elevated Tg and negative ^{131}I WBS (Figure 11.10).

Although the introduction of PET has improved the follow-up of TC, the localization of FDG-positive lesions is

Figure 11.10

[^{18}F]FDG-PET in dedifferentiated thyroid cancer with elevated serum Tg but negative ^{131}I whole-body scintigraphy.



sometimes difficult using PET alone. This is also true for other malignancies, especially head and neck cancer. As early as 1998, Beyer and Townsend developed a combination of a (partial ring) PET and CT machine, and published their first 100 clinical cases in the year 2000.⁸⁷ This prototype of PET–CT was followed by the development of second- and third-generation machines, culminating in a combination of high-end PET (LSO/GSO (lutetium oxyorthosilicate/gadolinium oxyorthosilicate crystals)) and high-end CT (64 slices) scanners (Figure 11.11). PET–CT is available from all major companies of PET imaging equipment: Siemens, CTI, GE, and Philips. All these systems have in common that a commercial CT scanner is in conjunction with a commercial PET scanner. This construction creates the possibility to gather data from CT and PET and fuse them without having to register the images manually. For daily routine in the clinical environment, a standard acquisition protocol was generated. First a topogram is taken by CT. After defining the region of interest to scan, a diagnostic – or low-dose – CT is recorded. Finally, data from PET are collected. The whole procedure takes from 15 to 45 minutes depending on the scanner, the activity injected, and the crystal. The CT and PET images can be merged automatically. Because of the time difference between CT and PET, movement artifacts can occur and must be taken into consideration. The construction of the PET–CT device implies also the possibility of reconstruction errors due to the low physical integration. Nevertheless, the number of worldwide ordered PET–CT devices is increasing greatly compared to the number of ordered PET standalone solutions. With the introduction of this new modality of imaging in oncology, the question arises whether PET–CT is superior to PET and CT alone, and, if so, can PET–CT affect patient management better than both modalities alone. PET can assess, for example, metabolism, protein



Figure 11.11
Today's modern PET–CT scanner.

synthesis, gene expression, and tissue hypoxia depending on the tracer used, whereas CT mainly reflects anatomy and to some degree perfusion.⁸⁷ In the combined modality, CT data are used for the calculation of attenuation correction as well as for anatomic information. The question whether CT should be performed as contrast-enhanced diagnostic CT or only as low-dose CT for anatomic correlation is not yet answered. There is also some debate on the use of oral contrast media for PET–CT imaging.⁸⁸ First clinical results of PET–CT in oncology reveal that in general there is much better reliability of the results and higher diagnostic confidence using PET–CT compared to each modality alone.^{87,89,90} Due to the fusion of anatomy and metabolism, exact localization of hypermetabolic spots (e.g. osseous versus soft tissue lesions) on the one hand and metabolic evaluation of anatomic lesions on the other hand can be achieved. The combination of PET and CT is most helpful in the cervical and abdominal regions. Our own experience in the first 2000 patients using PET–CT for staging and restaging of various tumors confirms that there is additional information in about 45% of patients and a change of management in 15% of patients. In addition, it could be demonstrated that the pitfalls of PET (e.g. normal structures in the head and neck region that are positive on FDG-PET, bowel activity, muscle activity, excretion via the kidneys, and subsequent sometimes circumscribed ureter activity, brown fat tissue, etc.) can be reduced using PET–CT (Figure 11.12). An overview regarding the hardware, software, and current clinical role of PET–CT was published from a symposium ‘PET–CT: the holy grail of multi-modality imaging?’^{91–93} There are only few data about PET–CT in TC. In a study by Ong et al., 17 patients with elevated Tg but negative ¹³¹I WBS underwent FDG-PET–CT.⁹⁴ Fifteen out of 17 PET–CT scans revealed lesions consistent with metastases, giving a sensitivity of 88.2%. Unfortunately this paper gives little information on the additional value of PET/CT compared to PET alone. Nahaz et al. investigated the impact of PET–CT on the management of 33 patients with recurrent papillary thyroid cancer.⁹⁵ In 67% of patients, PET–CT supplied additional information that altered or confirmed the management plan. Twenty of the 33 patients underwent surgery, with an accuracy for PET–CT of 70%, comparing the results with histopathology. The sensitivity of PET–CT in identifying recurrent disease was found to be 66%, with a specificity of 100% and a PPV of 100%. When PET–CT is positive it is a powerful tool for predicting the exact location of recurrent papillary TC. The authors conclude that PET–CT is most useful in the detection and management of recurrent papillary TC in patients with average Tg >10 ng/ml. In our own first series, 33 [¹⁸F]FDG-PET–CT investigations in 27 TC patients were performed (follicular TC: 14; papillary TC: 10; medullary TC: 2, anaplastic TC: 1). In six of the 27 patients a second investigation was done after treatment (surgery, external radiotherapy, etc.). Most of them had already-known iodine-negative

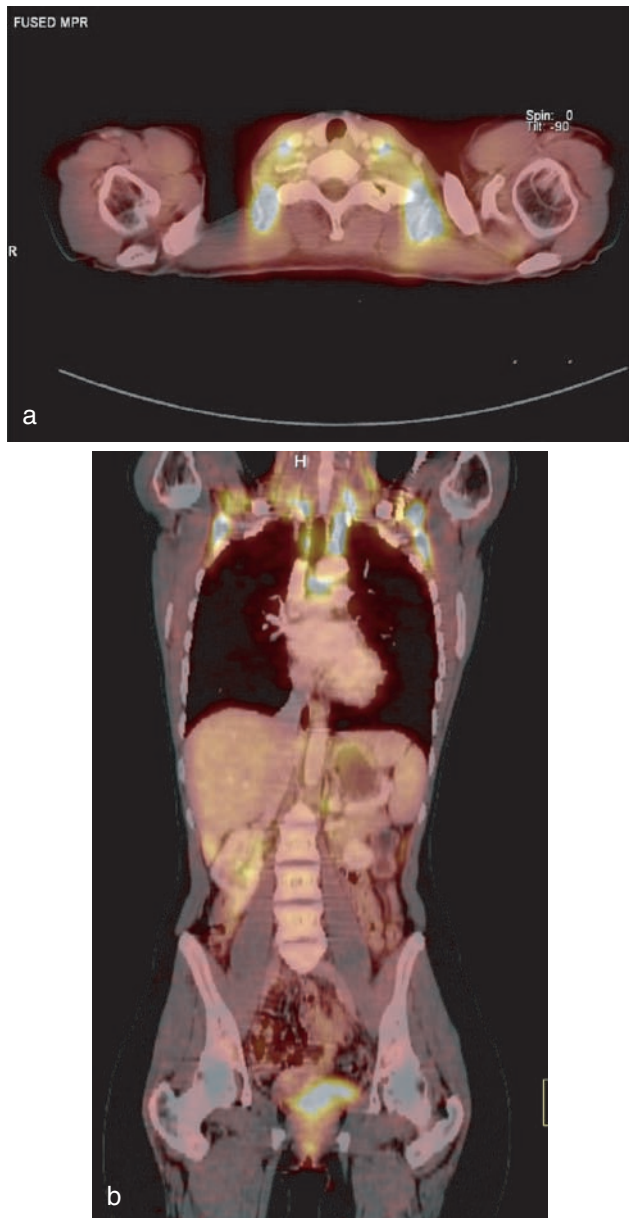


Figure 11.12

Brown fat tissue as possible pitfall in following up thyroid cancer: (a) transaxial slice; (b) coronal slice. Due to image fusion, FDG uptake can easily be correlated with fatty tissue in CT.

metastases or elevated Tg levels but negative post-therapy ^{131}I WBS (Figure 11.13). In 67% of patients, PET-CT was more accurate than PET or CT alone, and in 17%, PET-CT results led to a change of treatment (change of radiation field, radiation instead of surgery, surgery due to exact localization of recurrence, heparin treatment instead of surgery due to tumor thrombosis) (Figure 11.14).⁶⁵ The first results of PET-CT in TC provide increased diagnostic confidence, reduction of equivocal results in PET and CT alone,

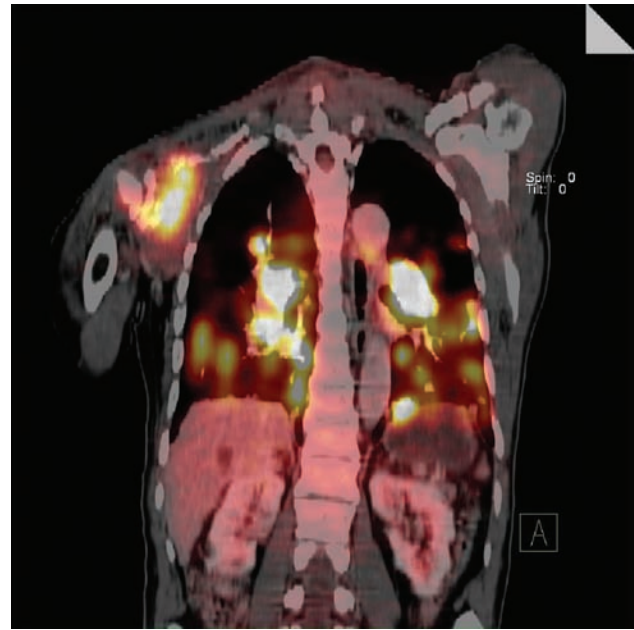


Figure 11.13

^{18}F FDG-PET-CT: ^{18}F FDG activity in the lung and right subscapular soft tissue due to metastases from low differentiated follicular thyroid cancer.

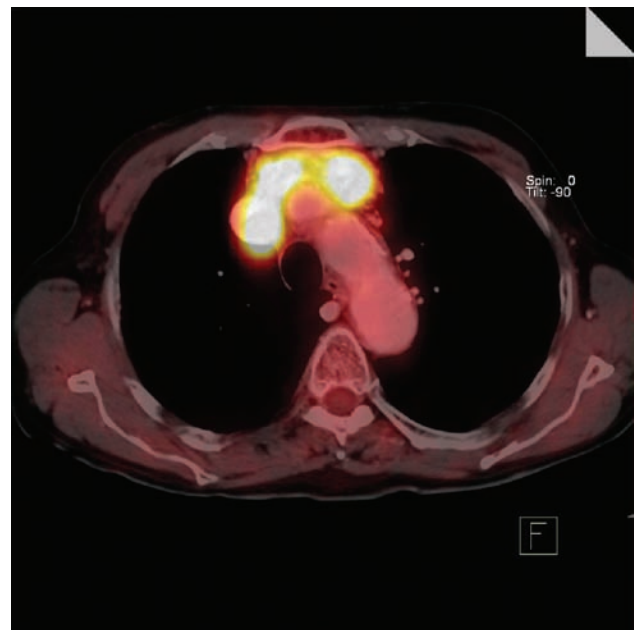


Figure 11.14

^{18}F FDG-PET-CT: ^{18}F FDG activity in the mediastinum. Due to image fusion with CT the mediastinal ^{18}F FDG could be localized as metastatic thrombosis which changed treatment from surgery to antithrombotic heparin therapy.

additional information in about 45%, and a change of therapeutic management in about 10–15% of patients.

Despite that rhTSH stimulated Tg and ultrasonography are the basis for following up thyroid cancer patients, and are probably sufficient for low-risk patients, the whole armamentarium of modern nuclear medicine investigations may be necessary for individual treatment planning of high-risk patients with elevated serum thyroglobulin.^{96–97}

References

- Lind P, Kumnig G, Heinisch M et al. Iodine supplementation in Austria: methods and results. *Thyroid* 2002; 12: 903–7.
- Rojewski MT, Gharib H. Nodular thyroid disease. Evaluation and management. *N Engl J Med* 1985; 313: 428–36.
- Watters DAK, Ahuya AT, Evans RM et al. Role of ultrasound in the management of thyroid nodules. *Am J Surg* 1992; 164: 654–657.
- Gharib H, Goellner JR, Johnson DA. Fine needle aspiration cytology of the thyroid: a 12 year experience with 11,000 biopsies. *Clin Lab Med* 1993; 13: 699–709.
- Carmeci C, Jeffrey RB, McDougall IR et al. Ultrasound-guided fine-needle aspiration biopsy of thyroid masses. *Thyroid* 1998; 8: 283–9.
- Mikosch P, Gallowitsch HJ, Kresnik E et al. Value of ultrasound-guided fine needle aspiration biopsy of thyroid nodules in an endemic goitre area. *Eur J Nucl Med* 2002; 27: 62–9.
- Mikosch P, Wartner U, Kresnik E et al. Results from preoperative ultrasound guided fine needle aspiration biopsy of solitary thyroid nodules as compared with the histology. *Nuklearmedizin* 2001; 40: 148–54.
- Pfannenstiel P, Hotze LA, Saller B. *Schilddrüsenkrankungen: Diagnose und Therapie*. Berlin: Berliner Medizinische Verlagsanstalt, 1997: 86–94.
- Molitch ME, Beck JR, Dreisman M et al. The cold thyroid nodule: an analysis of diagnostic and therapeutic option. *Endocr Rev* 1984; 5: 185–99.
- Belfiore A, Giuffrida D, La Rosa GL et al. High frequency of cold thyroid nodules occurring at young age. *Acta Endocrinol (Copenh)* 1989; 121: 565–9.
- Belfiori A, La Rosa GL, Padova G. The frequency of cold thyroid nodules and thyroid malignancies in patients from an iodine deficient area. *Cancer* 1987; 60: 3096–112.
- Kresnik E, Gallowitsch HJ, Mikosch P et al. Scintigraphic and ultrasonographic appearance in different tumor stages of thyroid carcinoma. *Acta Med Austriaca* 2000; 27: 716–21.
- Park H, Tarver RD, Siddiqui AR et al. Efficacy of thyroid scintigraphy in the diagnosis of intrathoracic goiter. *AJR Am J Roentgenol* 1987; 148: 527–9.
- Lind P. Multi-tracer imaging of thyroid nodules: is there a role in the preoperative assessment of nodular goiter? Editorial? *Eur J Nucl Med* 1999; 26: 795–7.
- El-Desouki M. Tl 201 thyroid imaging in differentiating benign from malignant thyroid nodules. *Clin Nucl Med* 1991; 16: 225–30.
- Sundran FX, Mack P. Evaluation of thyroid nodules for malignancy using T-99m-sestamibi. *Nucl Med Commun* 1995; 16: 687–93.
- Mezosi E, Bajnok I, Gyory F et al. The role of Tc-99m methoxy-isobutyl-isonitrile (MIBI) scintigraphy in the differential diagnosis of cold thyroid nodules. *Eur J Nucl Med* 1999; 26: 798–803.
- Kresnik E, Gallowitsch HJ, Mikosch P et al. Tc-99m MIBI scintigraphy of thyroid nodules in an endemic goiter area. *J Nucl Med* 1997; 38: 62–5.
- Kresnik E, Gallowitsch HJ, Mikosch P et al. Evaluation of thyroid nodules with Tc-99m tetrofosmin dual phase scintigraphy. *Eur J Nucl Med* 1997; 4: 716–21.
- Joensuu H, Ahonen A, Klemi PJ. 18F-fluorodeoxyglucose imaging in the preoperative diagnosis of thyroid malignancy. *Eur J Nucl Med* 1988; 13: 502–6.
- Bloom AD, Adler LP, Shuck JM. Determination of malignancy of thyroid nodules with positron emission tomography. *Surgery* 1993; 114: 728–34.
- Uematsu H, Sadato N, Ohtsubo T et al. Fluorine-18-fluorodeoxyglucose PET versus thallium-201 scintigraphy evaluation of thyroid tumors. *J Nucl Med* 1998; 39: 453–9.
- Mitchell JC, Grant F, Evenson AR et al. Preoperative evaluation of thyroid nodules with (18)FDG-PET/CT. *Surgery* 2005; 138: 1166–75.
- Sasaki M, Ichiya Y, Kuwabara Y et al. An evaluation of FDG PET in the detection and differentiation of thyroid tumors. *Nucl Med Commun* 1997; 18: 957–63.
- Kresnik E, Gallowitsch HJ, Mikosch P et al. Fluorine-18-fluorodeoxyglucose positron emission tomography in the preoperative assessment of thyroid nodules in an endemic goiter area. *Surgery* 2003; 133: 294–9.
- Van Herle AJ, Uller RP. Elevated thyroglobulin: a marker of metastases in differentiated thyroid carcinoma. *J Clin Invest* 1975; 56: 272–6.
- Pacini F, Lari R, Mazzeo S et al. Diagnostic value of single serum thyroglobulin determination on and off thyroid suppressive therapy in the follow-up of patients with differentiated thyroid cancer. *Clin Endocrinol (Oxf)* 1985; 23: 405–8.
- Ronga G, Fiorentino A, Paserio E et al. Can iodine-131 whole body scan be replaced by thyroglobulin measurement in the postsurgical follow up of differentiated thyroid carcinoma? *J Nucl Med* 1985; 31: 1766–71.
- Ozata M, Suzuki S, Miyamoto T et al. Serum thyroglobulin in the follow-up of patients with treated differentiated thyroid cancer. *J Clin Endocrinol Metab* 1994; 79: 98–105.
- Spencer CA, Takeuchi M, Kazarosyan M et al. Serum thyroglobulin autoantibodies: prevalence, influence on serum thyroglobulin measurement, and prognostic significance in patients with differentiated thyroid carcinoma. *J Clin Endocrinol Metab* 1998; 83: 1121–7.
- Pacini F. Follow-up of differentiated thyroid cancer. *Eur J Nucl Med Mol Imaging* 2002; 29 (Suppl 2): S492–6.
- Westbury C, Vini L, Fisher C, Harmer C. Recurrent differentiated thyroid cancer without elevation of thyroglobulin. *Thyroid* 2000; 10: 171–6.
- Harder W, Lind P, Mollnar M et al. Thallium-201 uptake with negative I-131 scintigraphy and serum thyroglobulin in metastatic oxyphilic papillary thyroid carcinoma. *J Nucl Med* 1997; 39: 236–8.
- Cailaux AF, Baudin E, Travagli JP et al. Is diagnostic iodine-131 scanning useful after total thyroid ablation for differentiated thyroid cancer? *J Clin Endocrinol Metab* 2000; 85: 175–8.

35. Pacini F, Cappezone M, Elisei R et al. Diagnostic 131-iodine whole body scan may be avoided in thyroid cancer patients who have undetectable stimulated thyroglobulin levels after initial treatment. *J Clin Endocrinol Metab* 2002; 87: 1492–5.
36. Kohlfuerst S, Igerc I, Lind P. Recombinant thyrotropin is helpful in the follow up and I-131 therapy of patients with thyroid cancer: a report of the results and benefits using recombinant human thyrotropin in clinical routine. *Thyroid* 2005; 15: 371–6.
37. Pacini F, Lippi F. Clinical experience with recombinant human thyroid-stimulating hormone (rhTSH): serum thyroglobulin measurement. *J Endocrinol Invest* 1999; 22 (Suppl): 25–9.
38. Robbins RJ, Chon JT, Fleisher M et al. Is the serum thyroglobulin response to recombinant human thyrotropin sufficient, by itself, to monitor for residual thyroid carcinoma. *J Clin Endocrinol Metab* 2002; 87: 3242–7.
39. Wartofsky L. Management of low-risk well differentiated thyroid cancer based only on thyroglobulin measurement after recombinant human thyrotropin. *Thyroid* 2002; 12: 583–90.
40. Menzel C, Zaplatnikov K, Diel M et al. The influence of functional imaging in differentiated thyroid cancer. *Nucl Med Commun* 2004; 25: 239–43.
41. Schlumberger M, Berg G, Cohen O et al. Follow-up of low risk patients with differentiated thyroid carcinoma: a European perspective. *Eur J Endocrinol* 2004; 150: 105–12.
42. Haber RS. Role of ultrasonography in the diagnosis and management of thyroid cancer. *Endocr Pract* 2000; 6: 396–400.
43. Mazzaferri E, Robbins RJ, Spencer CA et al. A consensus report of the role of serum thyroglobulin as a monitoring method for low-risk patients with papillary thyroid carcinoma. *J Clin Endocrinol Metab* 2003; 88: 1433–41.
44. Fatourech V, Hay ID. Treating the patient with differentiated thyroid cancer with thyroglobulin-positive, iodine-131 diagnostic scan negative metastases: including comments on the role of serum thyroglobulin monitoring in tumor surveillance. *Semin Nucl Med* 2000; 30: 107.
45. Mazzaferri E, Kloos RT. Is diagnostic iodine-131 scanning with recombinant human TSH useful in the follow-up of differentiated thyroid cancer after thyroid ablation? *J Clin Endocrinol Metab* 2002; 87: 1490–8.
46. Intenzo CM, Jabbour S, Dam HQ et al. Changing concepts in the management of differentiated thyroid cancer. *Semin Nucl Med* 2005; 35: 257–65.
47. Lind P, Igerc I, Kohlfuerst S. Diagnosis, treatment and follow-up in case of differentiated thyroid cancer. *Wien Med Wschr* 2005; 19/20: 429–35.
48. Waxman A, Ramanna L, Chapman N et al. The significance of I-131 scan dose in patients with thyroid cancer: determination of ablation. Concise communication. *J Nucl Med* 1981; 22: 861–5.
49. Lind P. I-131 whole body scintigraphy in thyroid cancer patients. *Q J Nucl Med* 1999; 43: 188–94.
50. Dadparvar S, Krishna L, Slizofski WJ et al. The role of iodine-131 and thallium-201 imaging and serum thyroglobulin in the management of differentiated thyroid carcinoma. *Cancer* 1993; 11: 3767–73.
51. Franceschi M, Kusic Z, Franceschi D et al. Thyroglobulin determination, neck ultrasonography and iodine-131 whole-body scintigraphy in differentiated thyroid carcinoma. *J Nucl Med* 1996; 37: 446–51.
52. Filesi M, Signore A, Ventroni G et al. Role of initial iodine-131 whole-body scan and serum thyroglobulin in differentiated thyroid carcinoma metastases. *J Nucl Med* 1998; 39: 1542–6.
53. Spies WG, Wojtowicz CH, Spies SM et al. Value of post-therapy whole-body 131-I imaging in the evaluation of patients with thyroid carcinoma having undergone high-dose 131-I therapy. *Clin Nucl Med* 1989; 14: 793–800.
54. Van-Sorge-Van Boxtel RA, Van Eck-Smit BL, Goslings BM. Comparison of serum thyroglobulin, I-131 and Tl-201 scintigraphy in the postoperative follow up of differentiated thyroid cancer. *Nucl Med Commun* 1993; 14: 365–72.
55. Sutter CW, Masilungan BG, Stadalnic RC. False positive results of 131-I whole-body scan in patients with thyroid cancer. *Semin Nucl Med* 1995; 25: 279–82.
56. Lubin E, Mechlis-Frish S, Zatz S et al. Serum thyroglobulin and iodine-131 whole-body scan in the diagnosis and assessment of treatment for metastatic differentiated thyroid carcinoma. *J Nucl Med* 1994; 35: 257–62.
57. Simpson WJ, Panzarella T, Curruthers JS et al. Papillary and follicular thyroid cancer; impact of treatment in 1578 patients. *Int J Rad Oncol Biol Phys* 1988; 14: 1063–75.
58. Leger FA, Izembart M, Dagousset F et al. Decreased uptake of therapeutic doses of iodine-131 after 185 MBq iodine-131 diagnostic imaging for thyroid remnants in differentiated thyroid carcinoma. *Eur J Nucl Med* 1988; 25: 242–6.
59. Coakey AJ. Thyroid stunning. *Eur J Nucl Med* 1998; 25: 203–4.
60. Pineda JD, Lee T, Ain K et al. I-131 therapy for thyroid cancer patients with elevated thyroglobulin and negative diagnostic scan. *J Clin Endocrinol Metab* 1995; 80: 1488–92.
61. Lind P. Should high hTg levels in the absence of iodine uptake be treated. *Eur J Nucl Med* 2003; 30: 157–60.
62. Pace L, Klain M, Albanese C et al. Short-term outcome of differentiated thyroid cancer patients receiving a second iodine-131 therapy on the basis of a detectable serum thyroglobulin level after initial treatment. *Eur J Nucl Med Mol Imaging* 2006; 33: 179–83.
63. Ma C, Kuang A, Xie J et al. Possible explanations for patients with discordant findings of serum thyroglobulin and 131I whole-body scanning. *J Nucl Med* 2005; 46: 1473–80.
64. Ruf J, Lehmkuhl L, Bertram H et al. Impact of SPECT and integrated low-dose CT after radioiodine therapy on the management of patients with thyroid carcinoma. *Nucl Med Commun* 2004; 25: 1177–82.
65. Lind P, Igerc I. PET and PET/CT in the following up of thyroid cancer patients. In: Langsteger W, Sungler P, Lind P, Niederle B, eds. *Thyroid Cancer 4 2004*. Vienna: KOOP, 2004 [CD ROM].
66. Hoefnagel CA, Delprat CC, Marcuse HR, de Vijlder JJM. Role of thallium-201 total body scintigraphy in follow up of thyroid carcinoma. *J Nucl Med* 1986; 27: 1854–7.
67. Charkes ND, Vitti RA, Brooks K. Thallium-201 SPECT increases detectability of thyroid cancer metastases. *J Nucl Med* 1990; 31: 147–53.

68. Patts EA, North TL, Pickert RD et al. Mechanism of uptake of technetium tetrofosmin. I. Uptake into isolated rat ventricular myocytes and subcellular localization. *J Nucl Cardiol* 1995; 2: 317–26.
69. Briele B, Hotze A, Kropp J et al. Vergleich von Tl-201 und Tc-99m MIBI in der Nachsorge des differenzierten Schilddrüsencarcinoms. *Nuklearmedizin* 1991; 30: 115–24.
70. Ng DC, Sundram FX, Sin AE. Tc-99m sestamibi and I-131 whole-body scintigraphy and initial serum thyroglobulin in the management of differentiated thyroid carcinoma. *J Nucl Med* 2000; 41: 631–5.
71. Alam MS, Kasagi K, Misaki T et al. Diagnostic value of technetium-99m methoxyisobutylisonitril (99mTc-MIBI) scintigraphy in detecting thyroid cancer metastases. *Thyroid* 1998; 8: 1091–100.
72. Sundram FX, Goh AS, Ang ES. Role of technetium-99m sestamibi in localisation of thyroid cancer metastases. *Ann Acad Med Singapore* 1993; 22: 557–9.
73. Gallowitsch HJ, Kresnik E, Mikosch P et al. Tc-99m tetrofosmin scintigraphy: an alternative scintigraphic method for following up differentiated thyroid carcinoma – preliminary results. *Nuklearmedizin* 1996; 35: 230–5.
74. Lind P, Gallowitsch HJ, Langsteger W et al. Technetium-99m-tetrofosmin whole-body scintigraphy in the follow up of differentiated thyroid carcinoma. *J Nucl Med* 1997; 38: 348–52.
75. Joensuu H, Ahonen A. Imaging of metastases of thyroid carcinoma with fluorine-18-fluorodeoxyglucose. *J Nucl Med* 1987; 28: 910–14.
76. Reske SN, Kotzerke J. FDG PET for clinical use. Results of the 3rd German Interdisciplinary Consensus Conference, Onko PET III, 21 July and 19 September 2000. *Eur J Nucl Med* 2001; 28: 1707–23.
77. Feine U, Lizenmayer R, Hanke JP et al. Fluorine-18 FDG and iodine-131 uptake in thyroid cancer. *J Nucl Med* 1996; 37: 1468–72.
78. Grünwald F, Menzel C, Bender H et al. Comparison of 18FDG-PET with 131-iodine and 99m Tc-sestamibi scintigraphy in differentiated thyroid cancer. *Thyroid* 1997; 7: 327–35.
79. Iwata M, Kasagi K, Misaka T et al. Comparison of whole body F-18 FDG PET, Tc-99m MIBI SPET, and post-therapeutic I-131 scintigraphy in the detection of metastatic thyroid cancer. *Eur J Nucl Med Mol Imaging* 2004; 31: 491–8.
80. Lind P, Kresnik E, Kumnig G et al. F-18-FDG PET in following up thyroid cancer. *Acta Med Austriaca* 2003; 30: 17–21.
81. Conti PS, Durski JM, Bacqai F et al. Imaging of locally recurrent and metastatic thyroid cancer with positron emission tomography. *Thyroid* 1999; 9: 797–804.
82. Altenvoerde G, Lerch H, Kuwert T et al. Positron emission tomography with F-18-deoxyglucose in patients with differentiated thyroid carcinoma, elevated thyroglobulin levels and negative iodine scans. *Langenbecks Arch Surg* 1998; 383:160–3.
83. Schluter B, Bohuslavizki KH, Beyer W et al. Impact of FDG PET on patients with well differentiated thyroid cancer who present with elevated thyroglobulin and negative I-131 scan. *J Nucl Med* 2001; 42: 71–6.
84. Moog F, Linke R, Manthey N et al. Influence of thyroid-stimulating hormone levels on uptake of FDG in recurrent and metastatic differentiated thyroid carcinoma. *J Nucl Med* 2000; 41: 1989–95.
85. Petrich T, Börner AR, Weckesser E. Follow up of thyroid cancer patients using rhTSH – preliminary results. *Nuklearmedizin* 2001; 40: 7–14.
86. Beyer T, Townsend DW, Brun T et al. A combination of PET/CT scanner for clinical oncology. *J Nucl Med* 2000; 41: 1369–79.
87. Schöder H, Erdi YE, Larson SM, Yeung HWD. PET/CT: a new imaging technology in nuclear medicine. *Eur J Nucl Med Mol Imaging* 2003; 30: 1419–37.
88. Hausegger K, Reinprecht P, Kau T et al. Clinical experience with a commercially available negative oral contrast medium in PET/CT. *Fortschr Roentgenstr* 2005; 177: 796–9.
89. Lardinois D, Weder W, Hany TF et al. Staging of non-small-cell lung-cancer with integrated positron-emission tomography and computed tomography. *N Engl J Med* 2003; 348: 2500–7.
90. Burger I, Görres G, von Shulthess G et al. PET/CT: diagnostic improvement in recurrent colorectal carcinoma compared to PET alone. *Radiology* 2002; 225: 424.
91. Beyer T. Towards truly integrated hardware fusion with PET/CT. *Nuklearmedizin* 2005; 44S (suppl 1): S5–12.
92. Pietrzyk U. Does PET/CT render software registration obsolete? *Nuklearmedizin* 2005; 44 (suppl 1): S13–17.
93. Czernin J, Auerbach MA. Clinical PET/CT imaging. *Nuklear-Mmedizin* 2005; 44 (suppl 1): S18–23.
94. Ong SC, Ng DC, Sundram FX. Initial experience in use of fluorine-18-fluorodeoxyglucose positron emission tomography/computed tomography in thyroid carcinoma patients with elevated thyroglobulin but negative iodine-131 whole body scans. *Singapore Med J* 2005; 46: 297–301.
95. Nahas Z, Goldenberg D, Fakhry C et al. The role of positron emission tomography-computed tomography in the management of recurrent papillary thyroid carcinoma. *Laryngoscope* 2005; 115: 237–43.
96. Lind P. Differentiated thyroid cancer. In: Ell, PJ, Gabhir SS, ed. *Nuclear Medicine in Clinical Diagnosis and Treatment*. Edinburgh: Churchill Livingstone, 2004; 1: 145–64.
97. Lind P, Kohlfürst S. Respective roles of Tg, radioiodine imaging and PET in the assessment of thyroid cancer. *Semin Nucl Med* 2006; 36: 194–205.

Adrenal tumors

Christiane Franzius and Otmar Schober

Background

The adrenal glands are two small retroperitoneal organs composed of a cortex and a medulla. These components are of entirely different tissue embryologically, histologically, and functionally. The cortex is responsible for the synthesis and excretion of adrenal steroid hormones and is divided into three histological and functional zones. The outer zone produces the principal mineralocorticoid aldosterone, the middle zone produces glucocorticoids, primarily cortisol, and the inner zone the androgenic hormones androstenedione and dehydroepiandrosterone (DHEA, and the sulfate DHEAS). Growth and secretory functions of cortisol and adrenal androgenic hormones are controlled by the anterior pituitary adrenocorticotrophic hormone (ACTH). Aldosterone secretion is controlled by extracellular sodium concentration, blood volume, and the renin–angiotensin–aldosterone system (RAAS) via angiotensin 2. Cholesterol is the principal metabolic precursor of the adrenocortical steroids. Consequently, cholesterol analogs are used for adrenal scintigraphy.^{1–3}

The adrenal medulla is embryologically derived from the neural crest, and is a part of the sympathetic nervous system. The adrenal medulla secretes the catecholamines epinephrine and norepinephrine. Radiolabeled catecholamine analogs are used for scintigraphic imaging of tumors deriving from the sympathetic nervous system.^{2–4}

Adrenocortical tumors

The hypersecretion of different steroid hormones leads to different clinical symptoms and syndromes.¹

Cushing's syndrome is caused by excess glucocorticoids, usually cortisol. The clinical signs are hypertension, obesity, purple striae, and virilization. The hypercortisolism

results from excessive ACTH secretion from the pituitary, from ectopic sources stimulating adrenal cortisol secretion (ACTH dependent), or directly from an adrenal adenoma or bilateral nodular adrenal hyperplasia (ACTH independent).

Primary aldosteronism is caused by adrenal adenoma or bilateral hyperplasia excessively producing aldosterone. The correct treatment of patients depends upon distinguishing these two possibilities. Because aldosterone does not suppress ACTH secretion, dexamethasone medication is used during adrenal scintigraphy for the suppression of tracer uptake in normal adrenocortical tissue. Thus, the detection and lateralization of aldosterone-producing adenomas is enhanced.

In hyperandrogenism the excess androgens may originate from the ovaries, the adrenals, or through peripheral conversion of androstenedione to testosterone. Androgen secretion by the adrenal gland is controlled by ACTH, and androgen secretion by the ovaries is controlled by pituitary luteinizing hormone (LH). Usual suppression and stimulation tests of the ovaries and adrenals, however, do not reliably identify the origin of excess androgen production. Dexamethasone suppression scintigraphy with cholesterol analogs is used to evaluate patients in whom an adrenal source of androgen hypersecretion is suspected.

Adrenocortical carcinoma is an extremely rare disease. Only 60% of the carcinomas produce hormones, most of them aldosterone. Diagnosis is usually late. Metastases occur in the liver, lungs, and bones. Lymph node metastases are also common. Most adrenocortical carcinomas do not show an increased tracer uptake in adrenal scintigraphy with cholesterol analogs, but there are exceptions. These highly aggressive tumors may show an increased glucose metabolism, and therefore [¹⁸F]fluoro-2-deoxy-D-glucose (FDG) may be used for imaging with positron emission tomography (PET).⁵

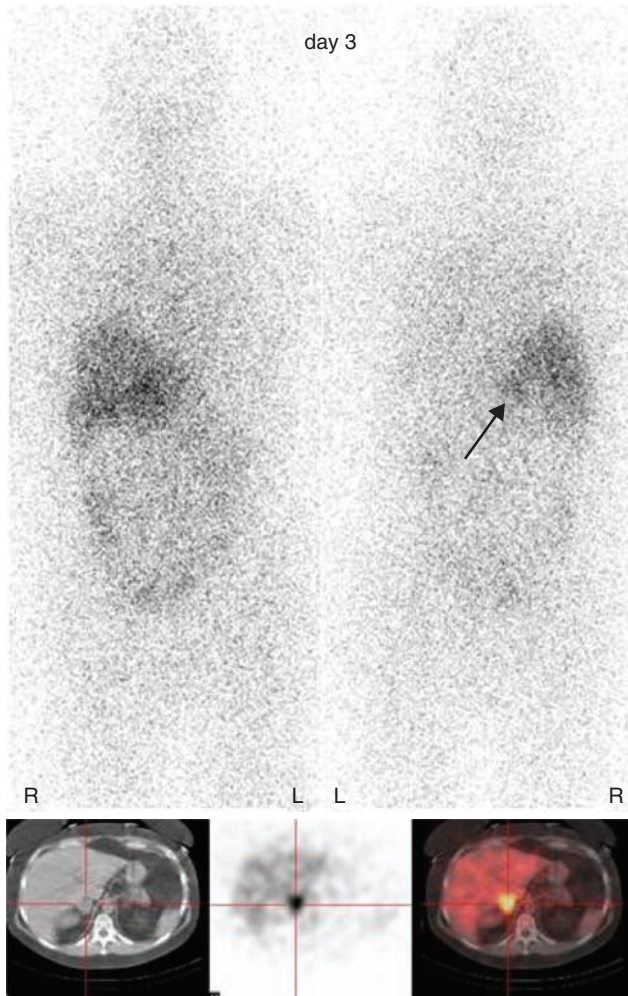


Figure 12.1

A 50-year-old female patient presenting with Cushing's syndrome, enlargement of the right adrenal gland, decreased adrenocorticotropic hormone (ACTH), and increased cortisol. Planar [^{131}I]norcholesterol scintigraphy (views from ventral and dorsal) demonstrates slightly increased tracer uptake of the right adrenal gland on day 3 (arrow). Single photon emission computed tomography (SPECT) with low-dose computed tomography (CT) (left CT, middle SPECT, right SPECT–CT fusion) clearly shows focal tracer uptake of the endocrine active adenoma in the right adrenal gland.

Tumors of the adrenal medulla and other tumors deriving from the sympathetic nervous system

Tumors deriving from the sympathetic nervous system are pheochromocytomas, neuroblastomas, paragangliomas, and ganglioneuromas/ganglioneuroblastomas. These tumors

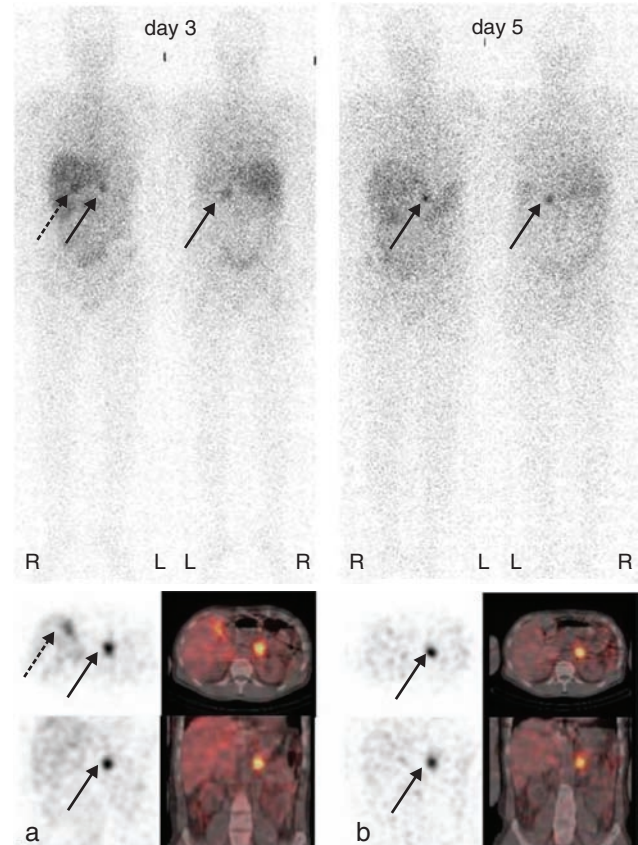


Figure 12.2

A 34-year-old male patient presenting with hypertension and hypokalemia. Magnetic resonance imaging (MRI) shows normal-sized adrenal glands but a mass ventral and medial of the left renal pelvis. Planar [^{131}I]norcholesterol dexamethasone suppression scintigraphies (views from ventral and dorsal) demonstrate increased tracer uptake ventral of the left kidney on day 3 (a) and even more intense on day 5 (b, arrow). The focus on the right hand side on day 3 (a, dotted arrow) fades on the following days. SPECT with low-dose CT (left SPECT, right SPECT–CT fusion) clearly shows focal tracer uptake in the mass ventral and medial of the left renal pelvis on days 3 and 5 (arrows), which was revealed to be an aldosterone-producing adenoma. The focus on the right hand side on the day 3 SPECT is unequivocally physiological gall bladder activity (dotted arrow).

occur in the adrenals and in other tissues of the sympathetic nervous chain. Pheochromocytomas are rare; 85% are benign, and 15% are malignant. The sole criterion for malignancy is the presence of metastases. Some 90% of pheochromocytomas are unilateral, and 10% are bilateral; 85% are localized in the adrenal glands; 10% are recognized within the multiple endocrine syndrome (MEN) type 2, von Hippel–Lindau disease, or neurofibromatosis (von Recklinghausen's disease). The clinical signs

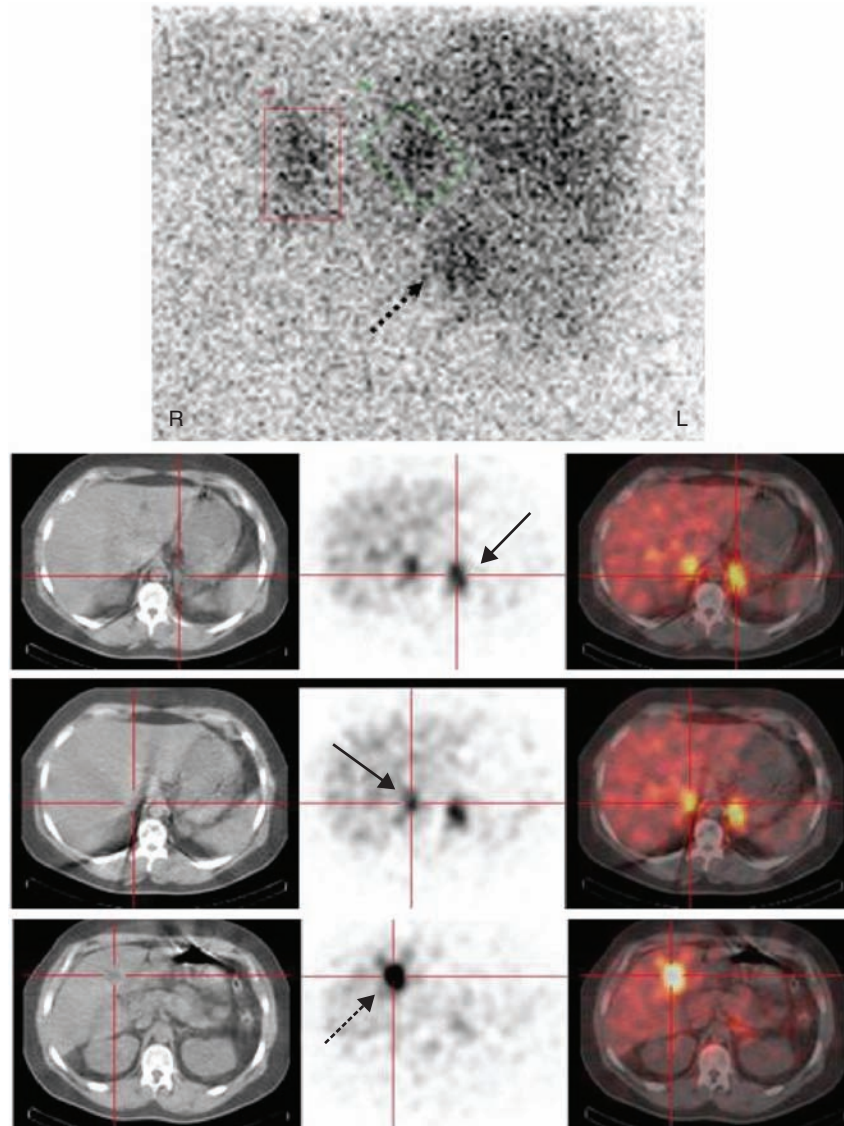


Figure 12.3

A 37-year-old female patient with an enlargement of the left adrenal gland and increased dehydroepiandrosterone (DHEA). Planar [^{131}I]norcholesterol dexamethasone suppression scintigraphy (view from dorsal, day 3) demonstrates increased tracer uptake in both adrenal gland and physiological gall bladder activity (dotted arrow) on day 3. SPECT with low-dose CT (left CT, middle SPECT, right SPECT–CT fusion) clearly shows focal tracer uptake in both adrenal glands (arrows) and uptake in the gall bladder (dotted arrow). This is the typical pattern of bilateral adrenal hyperplasia.

of pheochromocytoma include headache, palpitations, hyperhidrosis, and hypertension. Paroxysms may be triggered by emotional stress, physical exercise, and palpation of the tumor.⁴

Neuroblastoma is the most common solid tumor in childhood. Most primary tumors arise in the adrenal gland, but they can arise anywhere along the sympathetic chain.

Some 15–20% of primary tumors are located in the thorax. At presentation, about 60% of patients have metastases in cortical bones, bone marrow, lymph nodes, and liver. The most common presenting signs and symptoms include a palpable mass and the secondary conditions associated with bone marrow involvement which are anemia, thrombocytopenia, and leukopenia.⁶

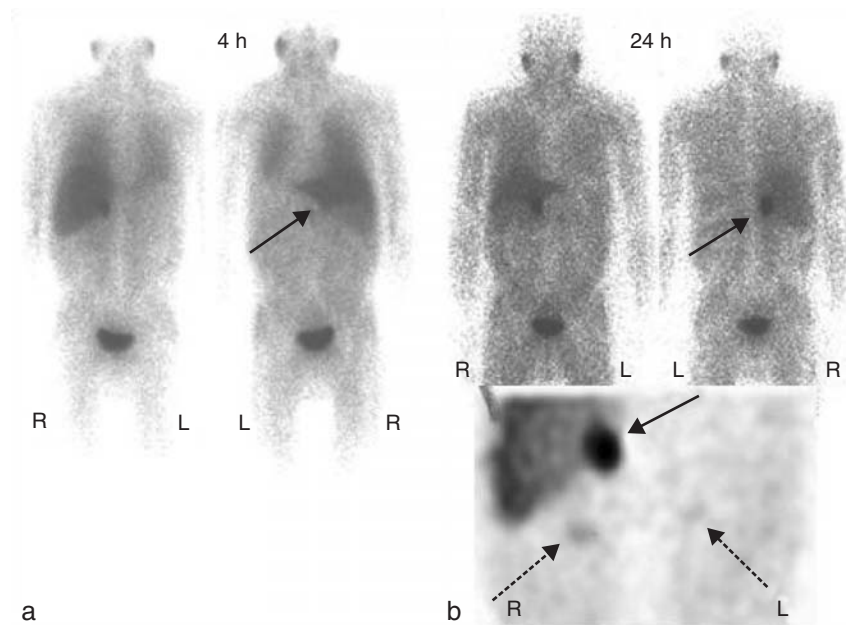


Figure 12.4

A 58-year-old male patient with hypertensive crises, increased urinary catecholamines, and an enlarged right adrenal gland. Planar [^{123}I]meta-isomer of iodobenzylguanidine (MIBG) scintigraphies (view from dorsal) demonstrate increased tracer uptake in the right adrenal gland 4 h after injection (a, arrow) and even more intense 24 h after injection (b, arrow). SPECT shows focal tracer uptake in the right adrenal gland (arrow) and slightly increased tracer retention in both renal pelvises (dotted arrows). The pheochromocytoma of the right adrenal gland was confirmed histologically.

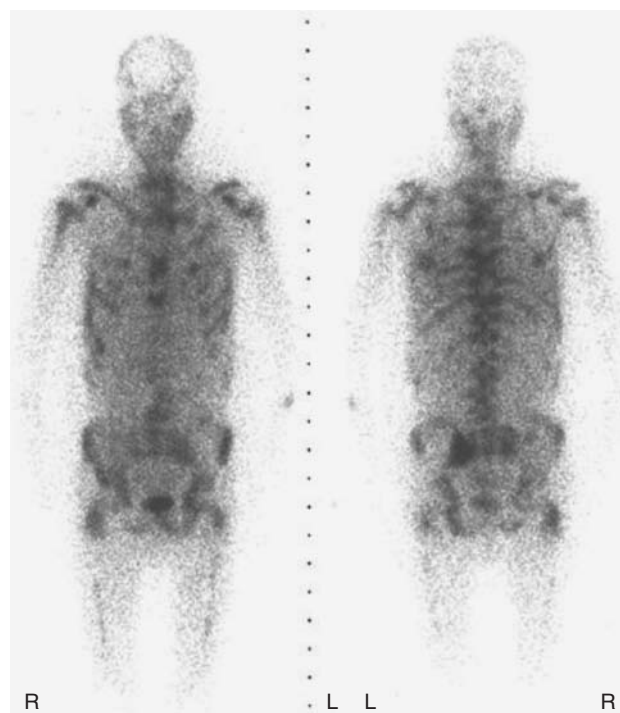


Figure 12.5

A 43-year-old male patient with a metastasized pheochromocytoma. Planar [^{123}I]MIBG scintigraphy (views from ventral and dorsal) 24 h after injection shows increased bone marrow uptake due to an extended bone marrow infiltration.

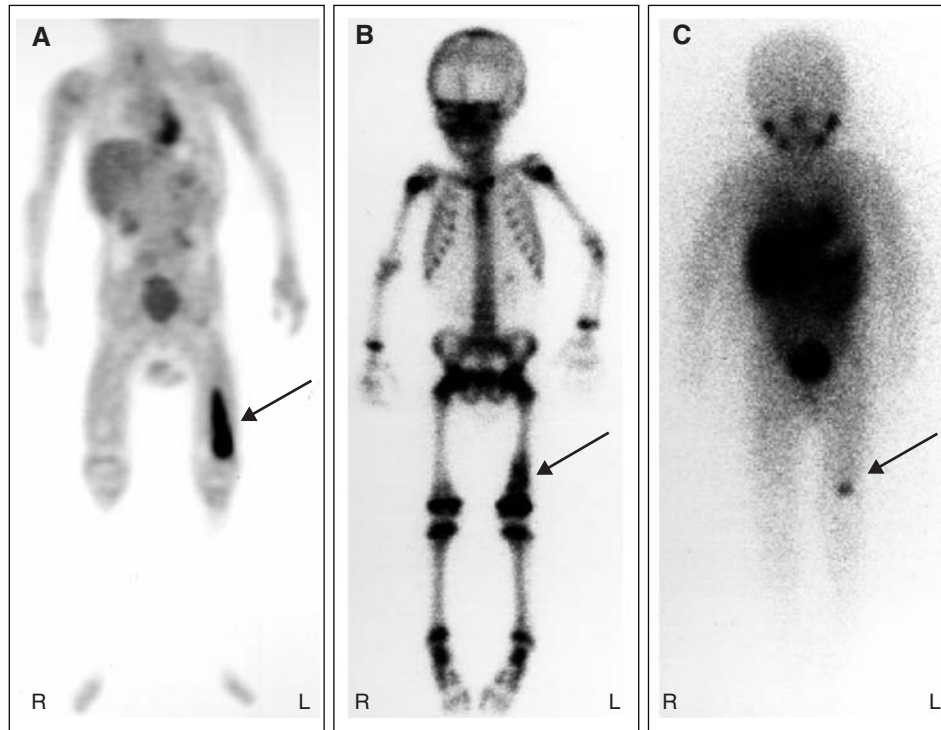


Figure 12.6

A 3-year-old boy with a neuroblastoma relapse in the left femur. [^{18}F]fluoro-2-deoxy-D-glucose-positron emission tomography (FDG-PET) (a), [$^{99\text{m}}\text{Tc}$] methylene diphosphonate (MDP) bone scintigraphy (b), and [^{123}I]MIBG scintigraphy (c) clearly demonstrate increased tracer uptake in the left femur (arrows). No other metastases are visible.

Other adrenal tumors

Adrenal metastases deriving from extra-adrenal malignomas are rare conditions. The most common malignoma producing adrenal metastases is lung cancer (Figure 12.10).⁷

Diagnostic modalities

Adrenocortical scintigraphy

Conventional scintigraphy and single photon emission computed tomography (SPECT)

Adrenocortical scintigraphy is based on radiolabeled cholesterol, as cholesterol is the principal precursor in the synthesis of adrenocortical steroid hormones. ^{131}I - or ^{75}Se labeled norcholesterol analogs with high affinity to the adrenal cortex and great *in vivo* stability are used, e.g. ^{131}I -labeled 6 β -iodomethyl-19-norcholesterol (NP-59). After slow intravenous injection, NP-59 is transported by low-density lipoproteins (LDLs), and uptake in the adrenocortical cell is via LDL-receptors. Once located within the adrenal cortex, NP-59 is esterified, but it does not enter the steroid

metabolic pathway. Esterified NP-59 is metabolically inert and cannot be converted back to free NP-59. Thus, it is trapped irreversibly within the cell. Adrenocortical cellular uptake of NP-59 is increased with an increased adrenocortical steroid hormone synthesis and increased plasma ACTH level. A high serum cholesterol level can reduce NP-59 uptake.^{2,3}

Preparation of patients

Prior to NP-59 application the iodine uptake of the thyroid should be blocked, e.g. with perchlorate, which blocks the sodium iodide symporter. The treatment is continued for 2 weeks after NP-59 application. In addition, all patients studied for hyperaldosteronism or hyperandrogenism receive 5 mg of oral dexamethasone daily, starting 7 days prior to injection and ending on the last day of imaging, to suppress pituitary ACTH secretion. Medication that influences the renin-angiotensin-aldosterone system has to be paused (Table. 12.1).

Imaging

NP-59 is administered intravenously with an activity of 20–40 MBq. Sufficient time must be allowed between NP-59 injection and imaging for the clearance of

Table 12.1 Most important drugs that are known or may be expected to interfere with 6β -iodomethyl-19-norcholesterol (NP-59) uptake and/or storage

Diuretics

ACE inhibitors, e.g. captopril and enalapril

Vasodilative drugs, e.g. minoxidil

Calcium antagonists, e.g. verapamil

Central α -sympathomimetics such as clonidine and methyl-DOPA

Peripheral α_1 -receptor-blockers, e.g. prazosin

β -Receptor blockers

Aldosterone antagonists, e.g. spironolactone

ACE, angiotensin converting enzyme; DOPA, 3,4-dihydroxy-2-phenylalanine.

background activity. The usual imaging interval is 3–5 (or 7) days after injection. Planar scintigraphy is performed in posterior view with a high-energy collimator. An acquisition time of 10 min is usually sufficient. Using a double-head γ camera, the additional anterior projection should be acquired for the assessment of bowel activity. Because of biliary elimination, activity within the gall bladder or bowel can superimpose the adrenal region. Therefore, it is recommended to give laxatives the day before the first scan. For exact anatomical orientation and unequivocal judgment, lateral views, SPECT(–CT), or comparison with computed tomography (CT) or magnetic resonance imaging (MRI) is helpful.⁸

In some patients, the right adrenal gland shows a physiologically higher intensity on planar images in the posterior view because of the dorsal location of the right gland. In planar dexamethasone suppression scintigraphy, visible adrenal activity before day 5 after injection is pathological. A normal scan demonstrates bilateral adrenal activity on day 5.³

Adverse reactions and radiation exposure

Even with slow injection of NP-59, in about 8% of patients there are side-effects such as hypertensive crisis, flush, headache, and nausea. The radiation exposure of the examination is relatively high. The effective dose in adults is 1.5 mSv/MBq [^{131}I]NP-59, which is about 30 mSv after application of 20 MBq [^{131}I]NP-59. The adrenal dose is up to 4 mSv/MBq, and lower in dexamethasone-suppression scintigraphy.²

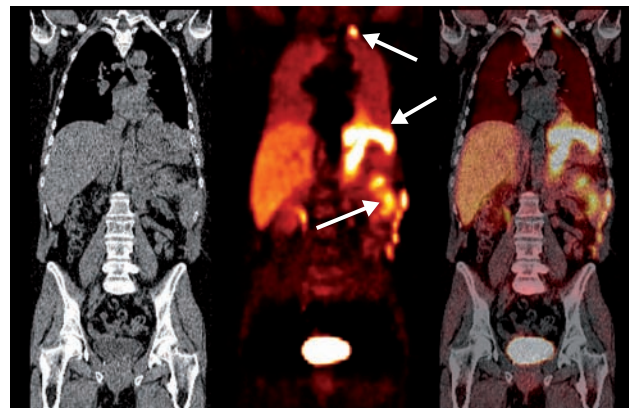
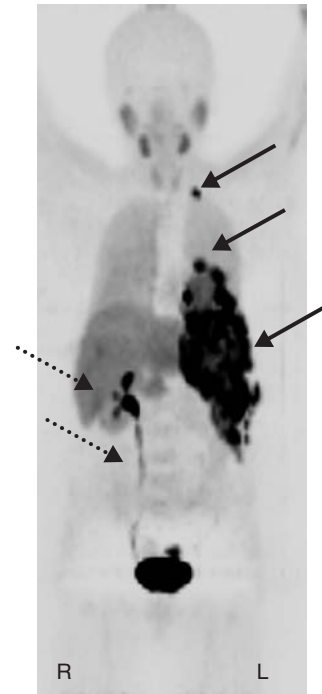


Figure 12.7

A 52-year-old female patient with a metastatic pheochromocytoma relapse in the left adrenal region, spleen, pulmonary, and pleural (apex and base of the left lung). [^{11}C]hydroxyephedrine-PET (HED-PET)–CT with low-dose CT (maximum intensity projection (MIP) and coronal slices, left CT, middle PET, right PET–CT fusion) demonstrates increased tracer accumulation in all tumor manifestations (arrows). Furthermore, there is high HED accumulation in the right renal pelvis and the right ureter (dotted arrows).

Interpretation

In ACTH-dependent hypercortisolism, excessive ACTH secretion from the pituitary gland or ectopic ACTH production from an occult neoplasm leads to bilateral adrenal hyperplasia. Usually, in this situation there is no need for adrenal scintigraphy. If performed, scans demonstrate a symmetrical increased adrenal NP-59 uptake. The classical pattern of a glucocorticoid-producing adrenal adenoma (ACTH independent) is increased NP-59 uptake in the

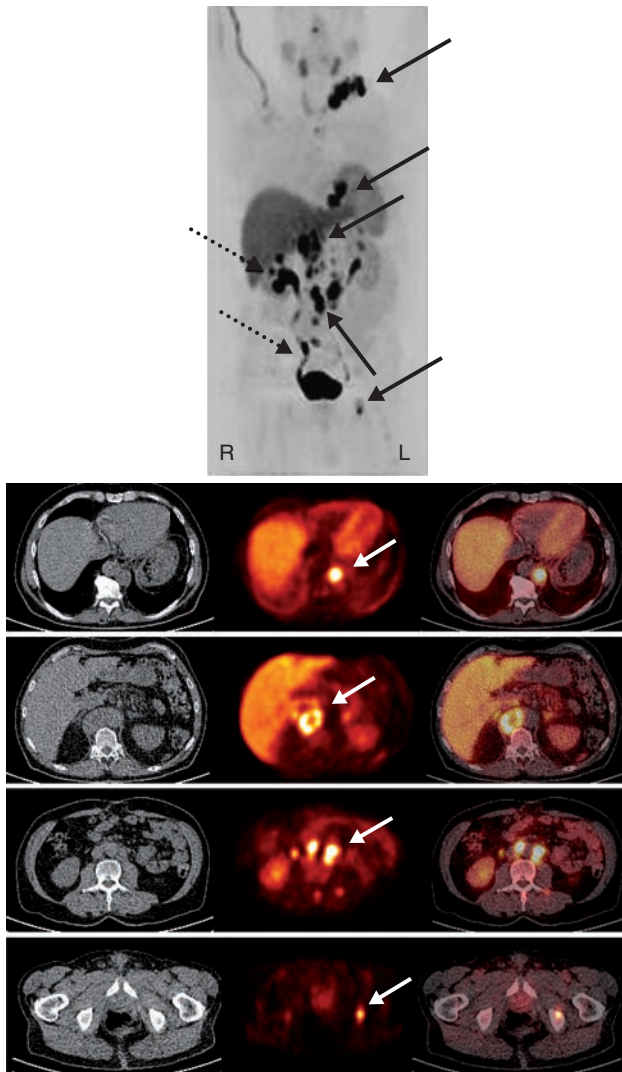


Figure 12.8

A 57-year-old male patient with a metastatic pheochromocytoma and multiple tumor manifestations in soft tissue and bones. [^{11}C]-HED-PET-CT with low-dose CT (MIP and transverse slices, left CT, middle PET, right PET-CT fusion) demonstrates an increased tracer accumulation in all tumor manifestations. Furthermore, there is high HED accumulation in the right renal pelvis and the right ureter.

affected gland and absent uptake in the contralateral gland (Figure 12.1). The decreased or absent uptake in normal tissue is caused by the suppression of ACTH. Unilateral NP-59 uptake can also be present in unilateral carcinoma. However, as carcinomas function poorly, there can also be no uptake in the adrenal glands in the rare case of carcinoma.

In aldosteronomas, dexamethasone suppression imaging is used to enhance detection and localization of aldosterone-producing adenomas. Usually there is an early (day 3 or 4) unilateral uptake, with absent or poor visualization

of the contralateral gland (Figure 12.2). This is a very specific sign for adenomas. Because of the small size of many adenomas, the sensitivity is limited. In patients with hyperplasia, uptake is usually symmetrical and is visualized before day 5 (Figure 12.3).

The same patterns as shown in hyperaldosteronism can be found in hyperandrogenism. After adrenalectomy, NP-59 can be used to visualize functioning remnants that cannot be depicted by morphological imaging or selective hormone sampling.⁸⁻¹¹

Positron emission tomography with FDG-PET

There is no indication for FDG-PET in adrenocortical hyperplasia or adenoma, as these benign conditions usually do not show an increased glucose metabolism.^{12,13} FDG-PET publications in adrenocortical carcinoma are limited. Reports of single cases suggest a high sensitivity in the detection of recurrences of adrenocortical carcinoma.

FDG-PET may be extremely helpful in the detection of adrenal metastases deriving from other tumor entities such as lung cancer. The sensitivity of FDG-PET is reported to be between 93% and 100% in patients with non-adrenal cancer; the specificity is reported to be between 90% and 100%.^{7,14,15}

Scintigraphy of tumors deriving from the sympathetic nervous system

Conventional scintigraphy and SPECT

Scintigraphic imaging of tumors deriving from the adrenal medulla is based on radiolabeled catecholamine analogs or precursors. The commercially available ^{123}I - or ^{131}I -labeled meta-isomer of iodobenzylguanidine (MIBG) is the most widely applied tracer. The cellular uptake mechanism is the norepinephrine reuptake (so called uptake one) into the presynaptic sympathetic neuron and thus into the adrenomedullary cells, neuroblastoma, and pheochromocytoma cells.¹⁶ About 90–95% of tumors deriving from the sympathetic nervous system demonstrate an increased MIBG uptake. Pharmacological intervention studies and clinical observations show that MIBG uptake is blocked by uptake- one inhibitors such as tricyclic antidepressants, cocaine, and reserpine. Most α and β blocking drugs are without any effect on the MIBG uptake. The usual MIBG distribution includes uptake in the salivary glands, myocardium, and liver, and excretion via the urinary tract. Colon activity may also be observed; uptake in the thyroid gland may be seen, if it is inadequately blocked. In renal

Table 12.2 Most important drugs that are known or may be expected to interfere with the uptake and/or storage of the norepinephrine analogs [¹²³I]meta-isomer of iodobenzylguanidine (MIBG), [¹¹C]hydroxyephedrine (HED)

Opioids, cocaine, tramadol

Tricyclic antidepressants, e.g. amitriptyline and derivatives, imipramine and derivatives, amoxapine, loxapine, doxepine

Sympathomimetics, e.g. dopamine, salbutamol, terbutaline, xylometazoline

Antihypertensive and cardiovascular agents, e.g. labetalol, metoprolol, amiodarone, reserpine, calcium channel blockers, ACE inhibitors

Antipsychotics, e.g. phenothiazines, thioxanthenes, butyrophenones

failure the image quality is severely impaired by high background activity and increased colon excretion.

Preparation of patients

Before imaging, any interfering medication has to be stopped early enough (Table 12.2). Thyroid uptake of free radioiodine should be blocked, e.g. with perchlorate.

Imaging

[¹²³I]MIBG is used for diagnostic purposes. The application of [¹³¹I]MIBG is applied only in the case of MIBG therapy. [¹²³I]MIBG is administered by slow intravenous injection of 400 MBq in adults, with appropriate downscaling in children. Planar whole-body imaging in anterior and posterior views and lateral views of the head are performed 4 h, 24 h, and in some cases 48 h post-injection. Additional SPECT (or even better SPECT–CT with low-dose CT) is extremely helpful, and therefore recommended.¹⁷

Adverse reactions and radiation exposure

Adverse effects of MIBG such as tachycardia, pallor, vomiting, and abdominal pain are very rare when slow injection is used. Rapid injection is contraindicated since it can induce these effects. The estimated effective doses following administration of [¹²³I]MIBG are 0.013 mSv/MBq (adult), 0.017 mSv/MBq (15 years old), and 0.037 mSv/MBq (5 years old).

Interpretation

The sensitivity of [¹²³I]MIBG scintigraphy is about 90% in the detection of neuroblastoma and pheochromocytoma

and their metastases (Figures 12.4 and 12.5). The diagnosis of these tumors is established biochemically by measuring the level of urinary and plasma catecholamines and their metabolites. Today there are several morphological and functional imaging methods available that predict tumor localization and tumor extent and give anatomic information. CT and MRI are the morphological imaging modalities of choice in localizing these tumors. Both provide excellent anatomical details and the sensitivity is very high. Both lack in specificity, as difficulties may occur in distinguishing between tumors deriving from the sympathetic nervous system and other tumor entities. The major advantages of [¹²³I]MIBG imaging are high sensitivity, especially in the depiction of extra-adrenal tumors and metastases, very high specificity, and the routine use of whole-body scanning. Furthermore, in follow-up examinations functional imaging is not influenced by postoperative artifacts such as scar tissue or metallic clips. Therefore, [¹²³I]MIBG imaging is used for characterization of adrenal lesions and for staging of tumors deriving from the sympathetic nervous system. The MIBG avidity influences the choice of follow-up examinations. Usually, [¹²³I]MIBG scintigraphy is necessary before [¹³¹I]MIBG therapy of these tumor entities, and is excellent for monitoring therapy.^{6,16,17}

Positron emission tomography

PET with [¹¹C] hydroxyephedrine (HED-PET)

HED is a catecholamine analog that has been specifically developed for imaging the sympathetic nervous system using PET.¹⁸ Comparable to MIBG, HED uptake reflects catecholamine transport, storage, and catecholamine recycling. For imaging, patients receive an intravenous injection of 370 MBq with adaptation of activity to lower body weight in children. Medication that interferes with uptake one has to be stopped in advance (Table 12.2). Whole-body PET acquisition is started 3–5 min after the injection. Because of the short half-life of ¹¹C, PET–CT scanners with no need for time-consuming radioactive source-based transmission measurement are preferred. Kinetic studies show a rapid accumulation and high retention of HED in localized neuroblastomas and pheochromocytomas.^{19,20} Due to the favorable physical conditions of positron emitters, HED-PET enables higher spatial resolution than does [¹²³I]MIBG scintigraphy. First clinical whole-body HED-PET studies demonstrate that the high image quality results in the detection of more lesions and even small lesions (Figures 12.7, 12.8 and 12.9).^{21,22} Whereas [¹²³I]MIBG scintigraphy requires at least 18–24 h to achieve tumor-to-background ratios adequate for imaging, whole-body HED-PET is completed in one examination within 30 minutes after injection. [¹²³I]MIBG scintigraphy requires at least two, and in the case of SPECT, up to four, acquisition sessions. This advantage of HED-PET is especially beneficial

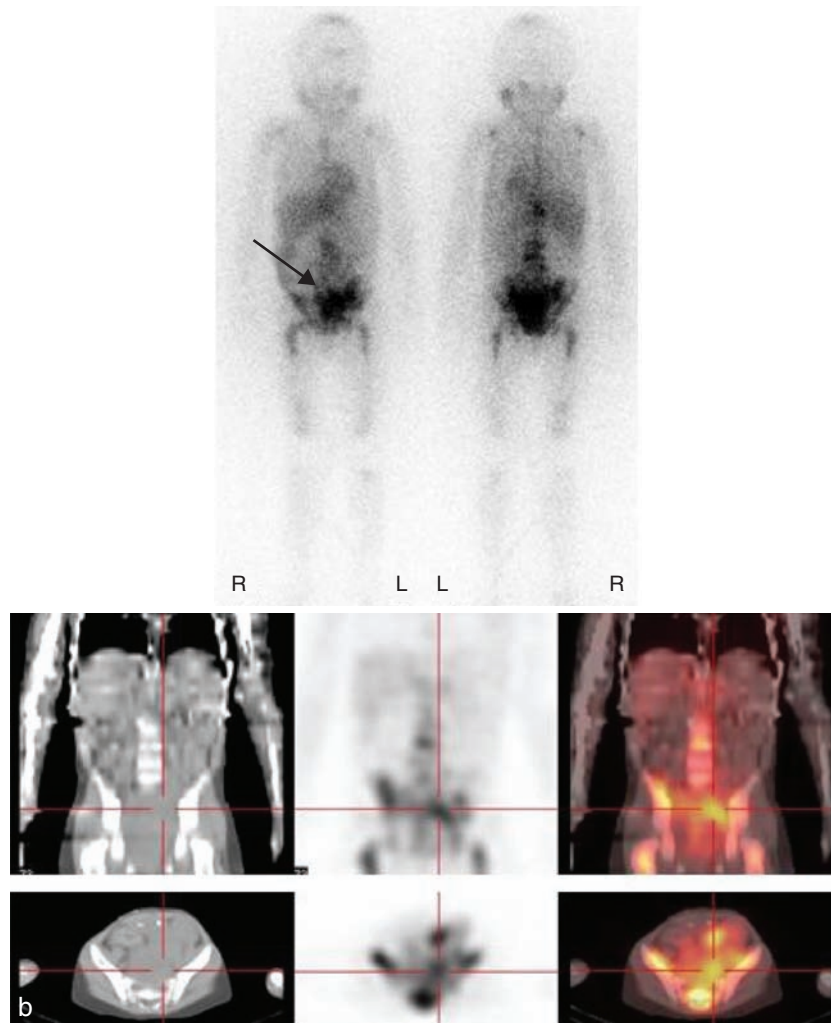


Figure 12.9

A 4-year-old boy with a large neuroblastoma in the lower abdomen and bone marrow infiltration. (a) Planar [^{123}I]MIBG scintigraphies (view from ventral and dorsal) and SPECT (left CT, middle SPECT, right SPECT–CT fusion) demonstrate increased tracer uptake in the neuroblastoma in the lower abdomen (arrow) and in the bone marrow.

in children, where the shorter scanning time improves compliance and reduces sedation (or anesthesia) time.²³ Because of the short half-life of ^{11}C , whole-body radiation exposure is considerably lower using HED-PET as compared with [^{123}I]MIBG scintigraphy. However, due to the short half-life of ^{11}C , an on-site cyclotron is necessary. Therefore the availability is limited. Furthermore, the on-site production for every patient is time-consuming and cost intensive. Due to the renal excretion during imaging, tumor manifestations next to the kidney or ureter may be missed using HED-PET.

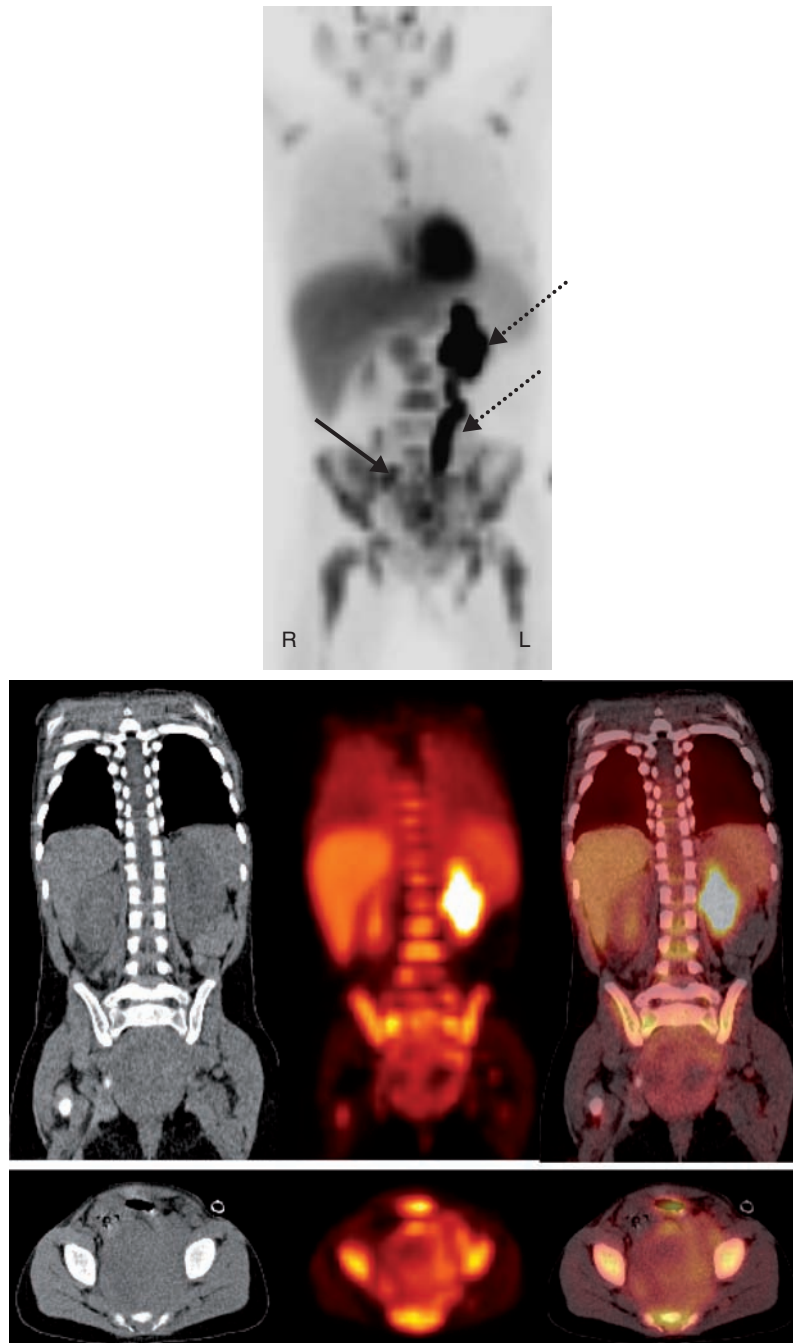
PET with L3,4-dihydroxy-2-phenylalanine (L-DOPA-PET)

Both [^{18}F] L-DOPA-PET and [^{11}C] L-DOPA-PET, show higher sensitivities in the detection of pheochromocytoma manifestations than [^{123}I]MIBG scintigraphy with and

without SPECT.^{24–26} The specificities of radiolabeled L-DOPA-PET and [^{123}I]MIBG scintigraphy are comparably high. Additionally, PET with radiolabeled L-DOPA can be used for other neuroendocrine tumors such as carcinoids or gastrinomas, with high performance characteristics. Up to now there are no studies comparing PET with HED and radiolabeled L-DOPA in neuroblastoma and pheochromocytoma patients.

PET with [^{18}F]FDG (FDG-PET)

The published experience on tumors of the sympathetic nervous system and FDG-PET is limited. In one large study in patients with high-risk neuroblastoma, FDG-PET was found to be sensitive in the detection of soft-tissue and extracranial osseous neuroblastoma lesions (Figure 12.6).⁶

**Figure 12.9, cont'd**

(b) [^{11}C]HED-PET-CT with low-dose CT (MIP, coronal and transverse slices, left CT, middle PET, right PET-CT fusion) demonstrates increased tracer accumulation in the neuroblastoma in the lower abdomen (arrow) and in the bone marrow. Furthermore, there is high HED accumulation in the left renal pelvis and the left ureter (dotted arrows).

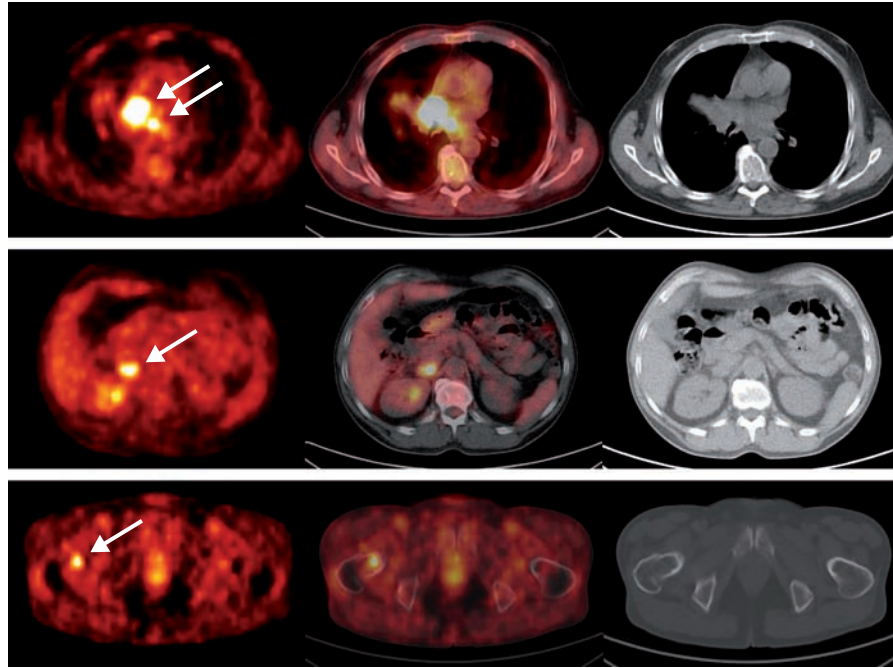


Figure 12.10

A 59-year-old patient with non-small-cell lung cancer in the middle lobe. FDG-PET-CT with low-dose CT (transverse slices, left PET, middle PET-CT fusion, right CT) shows clearly increased FDG uptake in the primary tumor and metastases in the mediastinum, right adrenal gland, and right femur.

FDG-PET is recommended in neuroblastoma and pheochromocytoma with negative $[^{123}\text{I}]$ MIBG scintigraphy, negative $[^{11}\text{C}]$ HED-PET, or negative $[^{18}\text{F}]$ I-DOPA-PET.^{27–29} FDG uptake is particularly high in patients with aggressive pheochromocytoma.³⁰

Further studies are required to elucidate the role of PET with various tracers in imaging tumors deriving of the sympathetic nervous system.

References

- Williams GH, Dluhy RG. Disorders of the adrenal cortex. In: Braunwald E, Fauci A, Kasper D, et al., eds. *Harrison's Principles of Internal Medicine*, 16th edn. New-York: McGraw-Hill, 2005: 2127–48.
- Gross MD, Shapiro B, Thrall JH. Adrenal scintigraphy. In: Gottschalk A, Hoffer PB, Potchen EJ, eds. *Diagnostic Nuclear Medicine*. Baltimore: Williams & Wilkins, 1988: 815–829.
- Harbert JC. The adrenal glands and neural crest tumors. In: Harbert JC, Eckelman WC, Neumann RD, eds. *Nuclear Medicine. Diagnosis and Therapy*. Stuttgart: Georg Thieme Verlag, 1996: 745–58.
- Landberg L, Young JB. Pheochromocytoma. In: Braunwald E, Fauci A, Kasper D, et al., eds. *Harrison's Principles of Internal Medicine*, 16th edn. New-York: McGraw-Hill, 2005: 2149–51.
- Ng L, Libertino JM. Adrenocortical carcinoma: diagnosis, evaluation and treatment. *J Urol* 2003; 169: 5–11.
- Kushner BH. Neuroblastoma: a disease requiring a multitude of imaging studies. *J Nucl Med* 2004; 45: 1172–88.
- Kumar R, Xiu Y, Yu JQ et al. F-18-FDG-PET in evaluation of adrenal lesions in patients with lung cancer. *J Nucl Med* 2004; 45: 2058–62.
- La Cava G, Imperiale A, Olianti C, et al. SPECT semiquantitative analysis of adrenocortical I-131-6 beta iodomethylnorcholesterol uptake to discriminate subclinical and preclinical functioning adrenal incidentaloma. *J Nucl Med* 2003; 44: 1057–64.
- Moreira SGJ, Pow-Sang JM. Evaluation and management of adrenal masses. *Cancer Control* 2002; 9: 326–34.
- Maurea S, Klain M, Caraco C, Ziviello M, Salvatore M. Diagnostic accuracy of radionuclide imaging using I-131 nor-cholesterol or meta-iodobenzylguanidine in patients with hypersecreting or non-hypersecreting adrenal tumors. *Nucl Med Commun* 2002; 23: 951–60.
- Rubello D, Bui C, Casara D, et al. Functional scintigraphy of the adrenal gland. *Eur J Endocrinol* 2002; 147: 13–28.
- Bagheri B, Maurer AH, Cone L, Doss M, Adler L. Characterization of the normal adrenal gland with F-18-FDG PET/CT. *J Nucl Med* 2004; 45: 1340–43.
- Yun M, Kim W, Alnafisi N, et al. F-18-FDG PET in characterizing adrenal lesions detected on CT or MRI. *J Nucl Med* 2001; 42: 1795–9.
- Frilling A, Tecklenborg K, Weber F et al. Importance of adrenal incidentaloma in patients with a history of malignancy. *Surgery* 2004; 136: 1289–96.

15. Jana S, Zhang T, Milstein DM, Isasi CR, Blaufox MD, FDG-PET and CT characteristics of adrenal lesions in cancer patients. *Eur J Nucl Med Mol Imaging* 2005; 33: 29–35.
16. Hoefnagel CA, Metaiodobenzylguanidine and somatostatin in oncology: role in the management of neural crest tumors. *Eur J Nucl Med* 1994; 21: 561–81.
17. Bombardieri E, Aktolun C, Baum RP et al. I-131/I-123-metaiodobenzylguanidine (MIBG) scintigraphy: procedure guidelines for tumour imaging. *Eur J Nucl Med Mol Imaging* 2003; 30: BP132–9.
18. Langer O, Halldin C, PET and SPET tracers for mapping the cardiac nervous system. *Eur J Nucl Med* 2002; 29:416–34.
19. Shulkin BL, Wieland DM, Schwaiger M et al. PET scanning with hydroxyephedrine: an approach to the localization of pheochromocytoma. *J Nucl Med* 1992; 33: 1125–31.
20. Shulkin BL, Wieland DM, Baro ME et al. PET hydroxyephedrine imaging of neuroblastoma. *J Nucl Med* 1996; 37: 16–21.
21. Trampal C, Engler H, Juhlin C, Bergström M, Langström B. Pheochromocytomas: Detection with C-11 hydroxyephedrine PET. *Radiology* 2004; 230: 423–8.
22. Franzius C, Hermann K, Weckesser M, et al. Whole-body PET/CT with ¹¹C meta-hydroxyephedrine in tumors of the sympathetic nervous system: feasibility study and comparison with ¹²³I-MIBG SPECT/CT. *J Nucl Med* 2006; 47: 1635–42.
23. Franzius C, Juergens KJ, Schober O. Is PET necessary in pediatric oncology? *Eur J Nucl Med Mol Imaging* 2006; 33: 960–5.
24. Ilias I, Yu J, Carrasquillo JA et al. Superiority of 6-[F-18]-fluorodopamine positron emission tomography versus [I-123]-metaiodobenzylguanidine scintigraphy in the localization of metastatic pheochromocytoma. *J Clin Endocrinol Metab* 2003; 88: 4083–7.
25. Hoegerle S, Nitzsche E, Althoefer C et al. Pheochromocytomas: detection with F18-DOPA whole-body PET – initial results. *Radiology* 2002; 222: 507–12.
26. Becherer A, Szabó M, Karanikas G et al. Imaging of advanced neuroendocrine tumors with F-18-FDOPA PET. *J Nucl Med* 2004; 45: 1161–7.
27. Shulkin BL, Hutchinson RJ, Castle VP et al. Neuroblastoma: positron emission tomography with 2-[fluorine-18]-fluoro-2-deoxy-D-glucose compared with metaiodobenzylguanidine scintigraphy. *Radiology* 1996; 199: 743–50.
28. Shulkin BL, Koeppe RA, Francis IR et al. Pheochromocytomas that do not accumulate metaiodobenzylguanidine: localization with PET and administration of FDG. *Radiology* 1993; 186: 711–15.
29. Shulkin BL, Thompson NW, Shapiro B, Francis IR, Sisson JC. Pheochromocytomas: imaging with 2-[fluorine-18]fluoro-2-deoxy-D-glucose PET. *Radiology* 1999; 212: 35–41.
30. Mamede M, Carrasquillo JA, Chen CC et al. Discordant localization of 2-[F-18]-fluoro-2-deoxy-D-glucose in 6-[F-18]-fluorodopamine- and [I-123]-metaiodobenzylguanidine-negative metastatic pheochromocytoma sites. *Nucl Med Commun* 2006; 27: 31–6.

Neuroendocrine gastroenteropancreatic (GEP) tumors

Emilio Bombardieri, Angela Coliva, Marco Maccauro, Ettore Seregni, and Irene Virgolini

Background

In recent years, nuclear medicine has become strategic in the diagnosis of neuroendocrine tumors, thanks to the good diagnostic performance of somatostatin radiolabeled analogs used for scintigraphic imaging.¹⁻³ Other radiopharmaceuticals are proposed for use in this area. Some precursors of the catecholamine metabolism, such as metaiodobenzylguanidine (MIBG), find their main indication for tumors of sympathoadrenal lineage, while different peptides with affinities for various receptors have been studied in many experimental clinical trials.⁴⁻⁶

The peculiarity of nuclear medicine imaging is that it allows functional information to be obtained based on the kinetics and biodistribution of particular radiolabeled substances, providing images of cellular structures involved in metabolic processes. In recent years, tremendous technological progress has been obtained in scintigraphic imaging, using both γ cameras and positron emission tomography (PET). One of the most relevant achievements is image fusion using dedicated software and hybrid instrumentation (single photon emission computed tomography–computed tomography (SPECT–CT, PET–CT) that allow the combination of both functional and morphologic information. Nowadays, nuclear medicine diagnostic modalities can be divided into two fields of application, according to the detection technique: (1) scintigraphy with γ emitting radiopharmaceuticals (planar scintigraphy and SPECT) and (2) PET.

Neuroendocrine tumors are a heterogeneous group of tumors that have recently been reconsidered in terms of biology and classification. Today it is universally accepted that they derive from pluripotent stem cells or differentiated neuroendocrine cells and the term ‘neuroendocrine’ defines cells and tumors with a characteristic pattern of histology (particular pathological staining, secretory products, and presence of specific cytoplasmic proteins). Therefore, the neuroendocrine cell system includes all neuronal and endocrine elements that share a common phenotypic

program characterized by the simultaneous expression of specific marker proteins (neuroendocrine markers) and cell type-specific hormonal products. These peptides are contained within membrane-bound vesicles from which they are released by exocytosis in response to external stimuli. On the basis of the above definition and their anatomical and clinical features, neuroendocrine tumors can be classified into different types: (1) neuroendocrine tumors from the gastroenteropancreatic (GEP) tract (pancreatic endocrine tumors; neuroendocrine tumors of the stomach; duodenum; jejunum, appendix, and cecum; colon and rectum); (2) tumors of sympathoadrenal lineage (pheochromocytoma, paraganglioma, neuroblastoma); (3) medullary carcinoma of the thyroid gland; (4) multiple neuroendocrine neoplasia (MEN 1, MEN 2A, MEN 2B); neuroendocrine tumors of the lung; and (5) pituitary tumors (Table 13.1). In this chapter we will discuss nuclear medicine applications in only neuroendocrine gastroenteropancreatic tumors, since they constitute about 2% of gastrointestinal malignancies and their clinical impact is increasing more and more.

Diagnostic approaches

Neuroendocrine GEP tumors include the so-called carcinoid tumors and endocrine pancreatic tumors. The carcinoid tumors can be divided into three groups: (1) foregut tumors (50–60% of total), mainly located in the gastric mucosa, duodenum, lung, and thymus; (2) midgut carcinoids (20–25%), located in the distal ileum and the jejunum; and (3) hindgut tumors (15–30%), located in the distal colon and rectum. The typical carcinoid syndrome (flushing, diarrhea, heart disease, bronchial constriction, and high levels of 5-hydroxyindole acetic acid in the urine), when present, is mainly related to midgut carcinoids;

Table 13.1 Classification of neuroendocrine tumors

Neuroendocrine tumors of the gastroenteropancreatic tract (GEP)	Pancreatic endocrine tumors (gastrinomas, insulinomas, VIPomas, glucagonomas, somatostatinomas) Neuroendocrine tumors of the stomach Neuroendocrine tumors of the duodenum Neuroendocrine tumors of the jejunum, appendix, and cecum Neuroendocrine tumors of the colon and rectum
Tumors of sympathoadrenal lineage	Pheochromocytoma Paraganglioma Neuroblastoma
Medullary carcinoma of the thyroid gland (MTC)	
Multiple neuroendocrine neoplasia (MEN)	MEN 1 (hyperplasia or neoplasia of anterior pituitary, parathyroid gland, duodenopancreatic endocrine system, adenomas or hyperplastic nodules of adrenal and thyroid glands, multiple lipomas) MEN 2A syndrome (MTC, pheochromocytoma, hyperplasia of parathyroid gland) FMTC (MTC) MEN 2B (rare parathyroid involvement; neurinomas, musculoskeletal abnormalities, disturbances of intestinal motility)
Neuroendocrine tumors of the lung	
Pituitary tumors	
FMTC, familial MTC; VIP, vasoactive intestinal peptide.	

however, it can also be observed in patients with lung carcinoids.^{7,8}

The diagnosis of neuroendocrine tumor is based on different approaches, starting with the physical examination (Table 13.2). Endocrine pancreatic tumors are located in the pancreas and can be classified as functioning (about 60%) and non-functioning tumors (about 40%). The clinical syndrome depends on the circulating levels of secretory products. High blood levels of glucagon cause hyperglycemic glucagonoma syndrome, hyperinsulinemia determines the hypoglycemic syndrome, elevated levels of vasoactive intestinal peptide (VIP) are related to Verner–Morrison syndrome, and the hypersecretion of gastrin is associated with Zollinger–Ellison syndrome. Non-functioning tumors produce different substances such as chromogranin A, pancreatic polypeptide (PP), and also hormones, but they do not induce clinical syndrome.

The diagnosis is always based on histopathology, which is fundamental, since it also has a prognostic value. Immunohistochemistry, using antibodies targeting several specific neuroendocrine markers, such as chromogranin A, neuron-specific enolase (NSE), and synaptophysin, can be helpful. Staining for hormones can help diagnosis in patients with clinical syndrome. Proliferation markers (Ki67 or MIB-1 antigen) give information about biological aggressiveness. The World Health Organization (WHO)

has established new criteria for classification, taking into account both the classical structural criteria and the proliferation index (PI) ki67 expression. Three groups of tumors can be identified: well-differentiated endocrine tumors (PI < 2%), well-differentiated endocrine carcinomas (2% < PI < 15%), poorly differentiated endocrine carcinomas (PI > 15%), and mixed exocrine–endocrine tumors.

Tests for circulating tumor markers such as chromogranin A or NSE can give some useful information; their diagnostic value is satisfactory in the presence of a large tumor mass, and also for monitoring therapy. Some false-negative results can be described in the case of small tumors or in poorly differentiated carcinoma. Other tumor markers such as VIP, PP, and carcinoembryonic antigen (CEA) have, at present, only experimental value. When a clinical syndrome is observed and symptoms are present, the measurement of specific hormones or metabolites reveals great value for diagnosis.

Radiological diagnosis can be performed by ultrasonography (US), CT, or magnetic resonance imaging (MRI). Data from the literature indicate that these modalities are able to depict 65–75% of lesions; however, the sensitivity changes according to the size of the lesion and location of the tumor. Of course, the diagnostic sensitivity of MRI and CT is higher in visualizing lesions larger than 1–2 cm in size. Endoscopic ultrasonography (EUS) has great diagnostic

Table 13.2 Diagnostic work-up of neuroendocrine tumors

Physical examination	Medical history, signs and symptoms
Laboratory tests	Circulating tumor markers (chromogranin A, NSE, specific hormones)
Pathology	Histology, specific histological staining (silver and argyrophil, electron microscopy: large dense-core granules, vesicles); immunohistochemistry (cytosolic: NSE, PGP 9.5, p/B2; granule associated: chromogranin A, B, C; vesicle associated: synaptophysin, synapsin, etc.; receptor expression; mRNA in situ hybridization; markers of proliferation)
Endoscopy	
Morphologic imaging	X-rays Ultrasonography (US) Endoscopic ultrasonography (EUS) Computed tomography (CT) Magnetic resonance imaging (MRI)
Nuclear medicine imaging	Planar scintigraphy/single photon scintigraphy (SPECT) with γ -emitting somatostatin analogs and other radiolabeled radiopharmaceuticals such as MIBG Positron emission tomography (PET) with positron-emitting radiopharmaceuticals (glucose analogs, catecholamine precursors, somatostatin analogs)
Image fusion modalities	SPECT-CT PET-CT

NSE, neuron-specific enolase; PGP, protein gene product; MIBG, metaiodobenzylguanidine.

value for certain tumors with a particular anatomical localization. EUS allows the examination to be performed using a flexible endoscopic probe, which can reach the area including and surrounding the cancer, increasing the accuracy of the test. EUS for tumors of the duodenum and pancreas shows a sensitivity and a specificity of around 90%.

Several radiopharmaceuticals have shown great affinity for these neoplasms, and they are used in visualization of the lesions by nuclear medicine modalities (Table 13.3). Molecular studies have revealed the existence of five distinct somatostatin receptor types (SSTR) with different tissue distributions. These receptors have been cloned, and are termed SSTR1, SSTR2 (with two splice variants, SSTR

and SSTRB), SSTR3, SSTR4 and SSTR5. Of the five major subtypes, SSTR2 and SSTR5 are the ones most commonly expressed in GEP tumors, which express receptors in 80–90% of cases. However, there is a considerable variation in somatostatin receptor expression in different tumor types and among tumors of the same type. The somatostatin analogs bind somatostatin receptors, and the most widely used radiolabeled somatostatin analog for planar scintigraphy and SPECT is [¹¹¹In]DTPA-octreotide (pentetreotide), (where DTPA is diethylenetriaminepentaacetic acid), commercially available. Other analogs labeled with γ emitting radiopharmaceuticals can be used, such as [^{99m}Tc]EDDA/HYNIC-TOC (ethylenediaminediacetic acid/hydrazynicotinyl-Tyr³-octreotide) [^{99m}Tc]P829 (depreotide), [¹¹¹In]DOTA-lanreotide (where DOTA is tetraazacyclododecanetetracetic acid), [¹¹¹In]DOTA-NOC-ATE (1-Nal³-Thr⁸-octreotide), and [¹¹¹In]DOTA-BOC-ATE, (Bz Thi³-Thr⁸-octreotide).^{9–14} However, at present these compounds have importance only for limited studies, since they are not available on the market. Other non-somatostatin analog peptides labeling receptors expressed by neuroendocrine tumors and suitable for SPECT scintigraphy are of potential interest, such as [¹²³I]VIP and [¹¹¹In]GLP-1 (glucagon-like pancreatic peptide).^{15,16} Metaiodobenzylguanidine (MIBG) labeled with ¹²³I or ¹³¹I accumulates in neuroendocrine tissues, in particular those of sympathoadrenal lineage, while its sensitivity for other neuroendocrine types is so far lower than that of somatostatin analogs such as [¹¹¹In] pentetreotide. In fact, MIBG is still considered the radiopharmaceutical of first choice to image neuroblastoma and pheochromocytoma, but its use in patients with other neuroendocrine tumors is justified only in those without somatostatin receptors and to select candidates for therapy with high doses of [¹³¹I]MIBG.

An alternative modern nuclear medicine approach to imaging neuroendocrine tumors is to use radiopharmaceuticals labeled with PET radioisotopes, using PET or PET-CT technology. The most common PET examination in oncology is PET with [¹⁸F]FDG (fluoro-2-dexy-D-glucose). However, the accuracy of [¹⁸F]FDG-PET for neuroendocrine tumors is not very high, since these neoplasms are often well differentiated and have a low metabolism. For this reason the FDG uptake is limited in many tumors, and this affects the overall PET sensitivity. A great avidity for FDG is shown only for poorly differentiated tumors, but this kind of neoplasia represents only a small number of examined patients.^{17,18} Better results can be obtained today with [⁶⁸Ga]DOTA-TOC or [⁶⁸Ga]DOTA-NOC, which show a sensitivity and a specificity similar to that of [¹¹¹In]pentetreotide, and in some clinical studies even higher sensitivity and etter specificity.^{19–22} This radioreceptor-PET approach is very interesting, since tumor localization remains based on somatostatin receptor imaging but its diagnostic performance lies in the great efficacy of PET systems. The current trend in nuclear oncology is to substitute,

Table 13.3 Radiopharmaceuticals used to visualize gastroenteropancreatic (GEP) tumors

<i>Group</i>	<i>Acquisition modality</i>	<i>Radioisotope</i>	<i>Radiopharmaceutical</i>
Somatostatin analogs			
DTPA-octreotide	Planar, SPECT	¹¹¹ In	[¹¹¹ In]DTPA-OCT
DOTA-Tyr ³ -octreotide	Planar, SPECT	¹¹¹ In	[¹¹¹ In]DOTA-TOC
DOTA-Tyr ³ -octreotide	PET	¹⁸ F	[¹⁸ F]DOTA-TOC
DOTA-Tyr ³ -octreotate	Planar, SPECT	¹¹¹ In	[¹¹¹ In]DOTA-TATE
DOTA-Tyr ³ -octreotate	PET	¹⁸ F	[¹⁸ F]DOTA-TATE
DOTA-Nal ³ -octreotide	Planar, SPECT	¹¹¹ In	[¹¹¹ In]DOTA-NOC
DOTA-Nal ³ -octreotide	PET	¹⁸ F	[¹⁸ F]DOTA-NOC
DOTA-Nal ³ -octreotate	Planar, SPECT	¹¹¹ In	[¹¹¹ In]DOTA-NOC-ATE
DOTA-BzThi ³ -octreotate	Planar, SPECT	¹¹¹ In	[¹¹¹ In]DOTA-BOC-ATE
EDDA/HYNIC-Tyr ³ -octreotide	Planar, SPECT	^{99m} Tc	[^{99m} Tc]HYNIC-TOC
EDDA/HYNIC-Tyr ³ -octreotate	Planar, SPECT	^{99m} Tc	[^{99m} Tc]HYNIC-TATE
Depreotide	Planar, SPECT	^{99m} Tc	
Other peptides			
Vasoactive intestinal peptide (VIP)	Planar, SPECT	¹²³ I	[¹²³ I]VIP
Vasoactive intestinal peptide (VIP)	Planar, SPECT	^{99m} Tc	[^{99m} Tc]P3654
Glucagon-like pancreatic peptide (GLP)	Planar, SPECT	¹¹¹ In	[¹¹¹ In]GLP-1R
Catecholamine metabolism			
Metaiodobenzylguanidine (MIBG)	Planar, SPECT	¹³¹ I	[¹³¹ I]MIBG
Metaiodobenzylguanidine (MIBG)	Planar, SPECT	¹²³ I	[¹²³ I]MIBG
L-DOPA	PET	¹¹ C	[¹¹ C]L-DOPA
L-DOPA	PET	¹⁸ F	[¹⁸ F]L-DOPA
5-HTP	PET	¹¹ C	[¹¹ C]HTP
Other metabolism			
Fluoro-2-deoxy-D-glucose (FDG)	PET	¹⁸ F	[¹⁸ F]FDG
DTPA, diethylenetriaminepentaacetic acid; DOTA, tetraazacyclododecanetetraacetic acid; EDDA, ethylenediaminediacetic acid; HYNIC, hydrazinonicotiny; DOPA, dihydroxyphenylalanine; 5-HTP, 5-hydroxy-L-tryptophan; OCT, octreotide; TOC, Tyr ³ -octreotide; TATE, Tyr ³ -octreotate; NOC, 1-Nal ³ -octreotide; NOC-ATE, 1-Nal ³ -Thr ⁸ -octreotide; BOC-ATE, BzThi ³ -Thr ⁸ -octreotide.			

progressively, traditional scintigraphy by γ camera with PET, even if at present the clinical availability of PET systems is still a problem in several countries.

Scintigraphy with γ -emitting radiopharmaceuticals and single photon emission computed tomography

Imaging with radiolabeled octreotide

Octreotide is a somatostatin analog with high affinity for receptor subtypes 2 and 5, and it has been the first tracer

applied in the imaging of GEP tumors. This peptide was initially labeled with [¹²³I] (¹²³I-Tyr³-octreotide), but, because of the high cost of the reagent, the short half-life of radioisotope, and the rapid biliar clearance hampering the abdominal localization, its clinical use was not successful. ¹¹¹In-labeled octreotide, [¹¹¹In]DTPA-octreotide, or [¹¹¹In]pentetreotide), commercially available as Octreo-Scan®, became immediately popular.^{23–25} The relatively long radioisotope half-life and its pharmacokinetics are more suitable for diagnostic purposes; the diagnostic procedure is well tolerated by patients and the irradiation is similar to that of traditional radiological tests (effective dose for adults 0.054 mSv/MBq). The uptake of [¹¹¹In]pentetreotide is usually very elevated in tumor lesions, and this is the reason why, by using high doses, it is also possible to carry out successful radioreceptor therapy. However, at the moment, trials on the therapeutic application of [¹¹¹In]pentetreotide are limited in number, in spite of some interesting results.^{26–29}

Clinical evidence in the diagnostic use of OctreoScan® scintigraphy in GEP tumors reports high accuracy, better than that of traditional radiological examinations (CT and MRI). The diagnostic sensitivity ranges between 80 and 100% in the localization of primary lesions and in the evaluation of disease extent.^{30,31} These characteristics are particularly evident for carcinoids and pancreatic neoplasias (except for insulinomas which express somatostatin receptors in fewer than 70% of cases), and remain the same for both functioning and non-functioning forms. Other instrumental examinations (in particular US, spiral CT, and echoendoscopy in some cases) associated with [¹¹¹In]pentetreotide scintigraphy improve the diagnostic accuracy.^{32,33} In a multicentric study performed in our institute together with the nuclear medicine divisions of Careggi Hospital (Florence) and the S. Orsola Malpigli Hospital (Bologna), the diagnostic efficacy of planar scintigraphy and of SPECT has been evaluated in 253 patients bearing neuroendocrine tumours (112 carcinoids), and data obtained were of high diagnostic value.³⁰ The accuracy was 82% for primary lesions in abdominal sites, 94% for hepatic lesions, 91% for soft tissue, and 98% for bone localizations (Table 13.4). The results reported by other authors in the literature confirm these findings. Moreover, in our experience, the possibility of analyzing the images also considering semiquantitative evaluation of the uptake intensity contributed to improving the global accuracy from 90 to 93% and the accuracy for primary tumors and hepatic metastases up to 99% (Table 13.5).

So, currently [¹¹¹In]pentetreotide scintigraphy has been widely adopted in the clinical management of GEP tumors, where this functional and morphological information is essential in order to plan the subsequent therapy.^{33–36} In healthy subjects different organs weakly express somatostatin receptors, including the thyroid, spleen, liver, kidneys and, in some patients, also the pituitary. Other organs can be visualized in scintigraphy as a result of excretion of the radiopharmaceutical by the urinary tract, the bladder, the gall bladder, and the colon. Any uptake in a

non-physiologic area reflects the presence of somatostatin receptor-expressing lesions: this can be a sign of neoplasia, but also of benign lesions.²⁴

Cellular differentiation seems to be associated with intense receptor expression, and so pretreatment scintigraphic positivity can be considered predictive for subsequent therapy with somatostatin analog. On the other hand, poorly differentiated neoplasias do not express somatostatin receptors and are not shown by scintigraphy. It is important to note that highly intense areas of uptake can be observed also in different tumors (lymphomas, melanomas, sarcomas, breast cancer, thyroid tumors, etc.), in inflammatory disease such as granulomas and in autoimmune disease.^{24,25}

The diagnostic sensitivity of scintigraphy with OctreoScan® is elevated for all neuroendocrine tumors, but in particular for GEP tumors such as carcinoids, gastrinomas, glucagonomas, and VIPomas, which show high expression of somatostatin receptors.³³ Whole-body images are able to describe the extent of the disease and to give the oncologist information about the resectability of the primary tumor (Figures 13.1–13.4). Scintigraphy shows distant metastases as areas of focal uptake of the radiopharmaceutical in soft tissue, in lymph nodes, and in bones (Figure 13.2). SPECT should be performed in association with planar scintigraphy in order to better define the relationships of the lesions with the anatomical structures (Figure 13.3). In the presence of symptoms or biochemical signals such as an increase of tumor markers or hormone levels, radioreceptor scintigraphy can discover the relapse of disease (Figure 13.4). On the basis of clinical experience, the use of radioreceptor scintigraphy is consolidated worldwide, especially for GEP tumors, and the clinical usefulness has been demonstrated in the following indications:^{33,37–39} (1) staging and restaging (study of primary tumor and detection of distant metastases); (2) monitoring/evaluation of treatment response; (3) patient selection for treatment with ‘cold’ or radiolabeled analogs; (4) prognostic indications on the basis of lesion receptor expression; and

Table 13.4 Results of somatostatin receptor imaging in group according to qualitative evaluation. Data are expressed on a per-lesion basis, the lesions being subdivided into four major groups

Sites	TP	FP	FN	TN	SN (%)	SP (%)	ACC (%)	PPV (%)	NPV (%)
Primary	41	1	29	100	59	99	82	98	78
Liver	86	3	8	74	91	96	94	97	90
Soft tissue	47	6	9	109	84	95	91	89	92
Bone	12	2	2	155	86	99	98	86	99

TP, true-positive result; FP, false-positive result; FN, false-negative result; TN, true-negative result; SN, sensitivity; SP, specificity; ACC, accuracy; PPV, positive predictive value; NPV, negative predictive value.

Table 13.5 Results of somatostatin receptor imaging in group 2 (qualitative and semiquantitative evaluation). Data are expressed on a per-lesion basis, the lesions being subdivided into four major groups

Sites	TP	FP	FN	TN	SN (%)	SP (%)	ACC (%)	PPV (%)	NPV (%)
Primary	46	3	1	32	98	91	99	94	97
Liver	20	0	1	61	95	100	99	100	98
Soft tissue	3	0	0	79	–	–	–	–	–
Bone	1	0	0	0	–	–	–	–	–

(5) search for tumor with primary unknown origin in patients with metastasis or elevated levels of circulating markers.

It has been observed that the elevated diagnostic sensitivity of [¹¹¹In]pentetreotide scintigraphy allows finding some occult lesions not demonstrated by other conventional diagnostic procedures. This is very helpful in the

management of patients, and sometimes can modify the therapeutic strategy.⁴⁰

Scintigraphy with OctreoScan® is performed following a standard protocol; 220 MBq (6 mCi, 5–6 µg of peptide) of the radiopharmaceutical are injected intravenously^{8,9} and whole-body images are acquired after 24 and 48 hours.

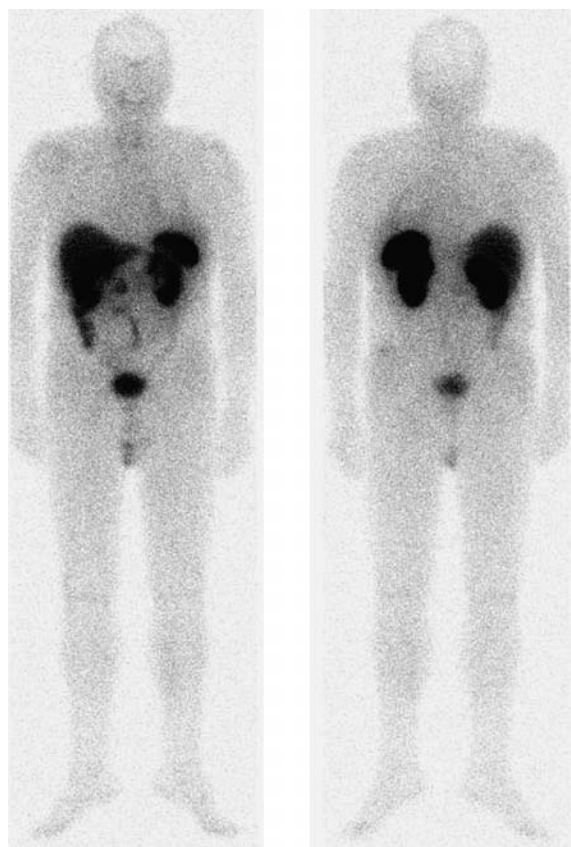


Figure 13.1

Whole-body scan with [¹¹¹In]pentetreotide of a patient with a pancreatic mass (neuroendocrine pancreatic cancer). No other foci of uptake are depicted in the extrapancreatic regions. The patient underwent surgery.

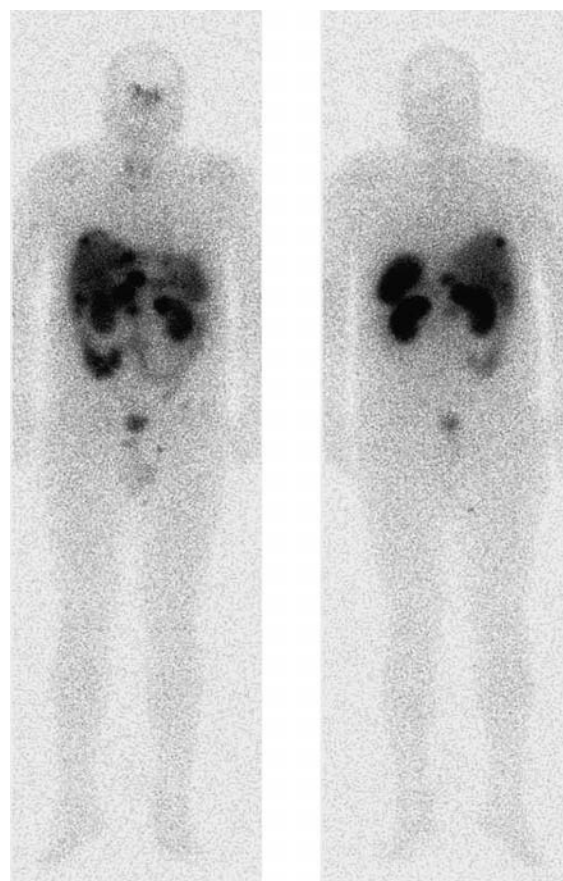


Figure 13.2

Staging with [¹¹¹In]pentetreotide scintigraphy of a patient with neuroendocrine pancreatic cancer at presentation. Visualization of the primary tumor and multiple localizations. The patient had systemic treatment with somatostatin analogs.

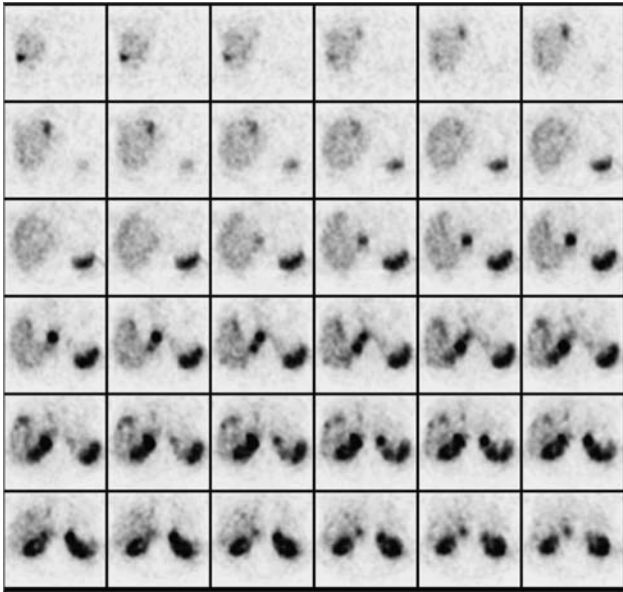


Figure 13.3

[¹¹¹In]pentetreotide single photon emission computed tomography (SPECT) of the same patient as described in Figure 13.2. The transaxial sections better define the sites of metastases as foci of intense uptake in the liver (segment 4 and 6), the epigastic region, and the adrenal gland.

For some specific sites also tomographic images can be acquired. The radiopharmaceutical has a rapid plasma clearance: only 1% of the activity remains in the blood 24 hours after administration. Excretion is mostly renal: at 24 hours after administration, 85% of the activity has been eliminated with the urine. The hepatobiliary or fecal elimination is less than 2%. Uptake in the lesions is quite slow, and needs at least 4 hours; for this reason images should be acquired at 24 and 48 hours, and, in some particular cases, at 72 hours after injection. A semiquantitative measurement of the radiopharmaceutical uptake based on the tumor/background ratio can be calculated on SPECT images acquired at 4 and 24 hours post-injection; this parameter seems to be correlated with the intensity of receptor expression and thus can have a prognostic role.²⁴

Recent technological developments have made available several hybrid instrumentations that combine both nuclear medicine and radiological detectors (SPECT-CT). This approach improves the overall diagnostic accuracy because morphological and functional data deriving from the two detector systems can be acquired at the same time in the same patient.⁴¹⁻⁴³

Another interesting application of [¹¹¹In]pentetreotide is radioguided surgery by using dedicated γ probes during the operation to directly localize somatostatin receptors in the lesions, define the tumor extent, search local and lymph-node

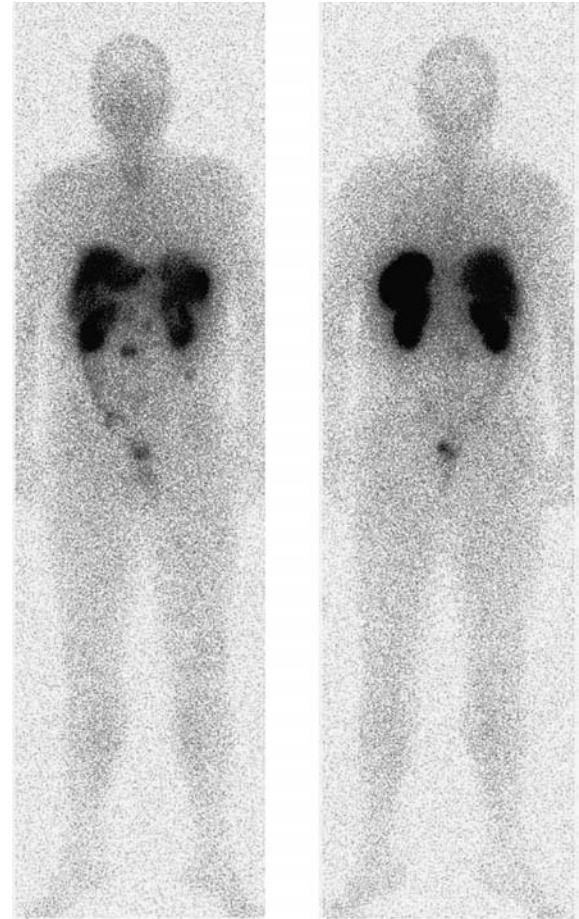


Figure 13.4

Patient with carcinoid already treated with surgery. After a progressive increase of chromogranin A levels during follow-up, [¹¹¹In]pentetreotide scintigraphy showed a focus of uptake in the mesogastric region. This diagnosis was confirmed with surgery and following pathology.

occult metastases, define the margins of surgery, and facilitate their radical resection.⁴⁴⁻⁴⁷ Experience in this field is limited; nevertheless, the reported results are encouraging.

Imaging with other somatostatin analogs and other radiolabeled peptides

Many somatostatin analogs have been synthesized and developed in order to obtain higher affinity for the various receptor subtypes in comparison with native somatostatin. Several differences in the chemical structure have led to related differences also in the affinity of the molecule for

the five receptor subtypes. Some of these reagents (DOTA-Tyr³-octreotide, DOTA-TOC; DOTA-lanreotide, DOTA-LAN; DOTA-Tyr³-octreotate, DOTA-TATE; DOTA-Nal³-octreotide, DOTA-NOC) have raised the interest of physicians also for their potential application as therapeutic agents.^{2,28,47} Radiopharmaceuticals labeled with ^{99m}Tc seemed to bring some advantages. The biodistribution of [^{99m}Tc]EDDA/HYNIC-TOC shows high physiological uptake in the kidneys, moderate uptake in the liver and spleen, and little uptake in the gut, with predominant renal and negligible hepatobiliary excretion.⁴⁸ Tumors expressing somatostatin receptors demonstrate a high and rapid [^{99m}Tc]EDDA/HYNIC-TOC uptake in imaging acquisition within the first hours after injection; this shortens the time for examination. In a similar way it is possible to use [^{99m}Tc]EDDA/HYNIC-TATE, which allows images of high quality to be obtained a few hours after injection (Figure 13.5). In clinical application, this scintigraphy has sometimes revealed more metastases than by using [¹¹¹In]pentetreotide imaging. The radiopharmaceutical has also been used for radioguided surgery.⁴⁹ On the basis of clinical experience, this radiopharmaceutical seems to be a good tracer for imaging tumors expressing somatostatin receptors, thanks to several interesting clinical characteristics. In particular, the tracer shows a high specificity for receptors, good biodistribution, and a high quality of imaging, and allows earlier diagnosis (from 15 minutes to 4 hours after injection).⁹ This is not always an advantage, since tumors expressing somatostatin receptors with low intensity are sometimes visualized after days, due to the slow kinetics of the tracer biodistribution and uptake. Other advantages of [^{99m}Tc]labeled compounds should be low radiation exposure for the patient and favorable cost-effectiveness. The literature reports experience with image fusion analysis combining [^{99m}Tc]EDDA/HYNIC-TOC-SPECT with diagnostic CT (Figure 13.6). In this way it is possible to obtain better accuracy in patients with known or suspected endocrine tumors, since image fusion reduces false-positive results and can detect additional lesions.⁵⁰

Among other peptides that recognize other receptors expressed by GEP neuroendocrine tumors, [^{99m}Tc]TP3654 has been evaluated. This tracer images cancer cells through its affinity for VIP receptors, and has been studied also for tumors of the gastrointestinal tract. The available data are very few, and [^{99m}Tc]TP3654 still has to demonstrate its usefulness in current diagnosis of this kind of neoplasia.^{51–53}

A number of clinical experiences have been gained with [^{99m}Tc]depreotide, a somatostatin analog, that visualizes tumors overexpressing somatostatin receptors. This radiopharmaceutical has been Food and Drug Administration (FDA)-approved for use in the diagnosis of indeterminate solitary pulmonary nodules and to discriminate malignant from benign lung lesions. Therefore, it has been rarely used in patients with GEP tumors, since the majority of studies have been carried out on lung cancer. Even the reported overall diagnostic accuracy is acceptable, although clinical

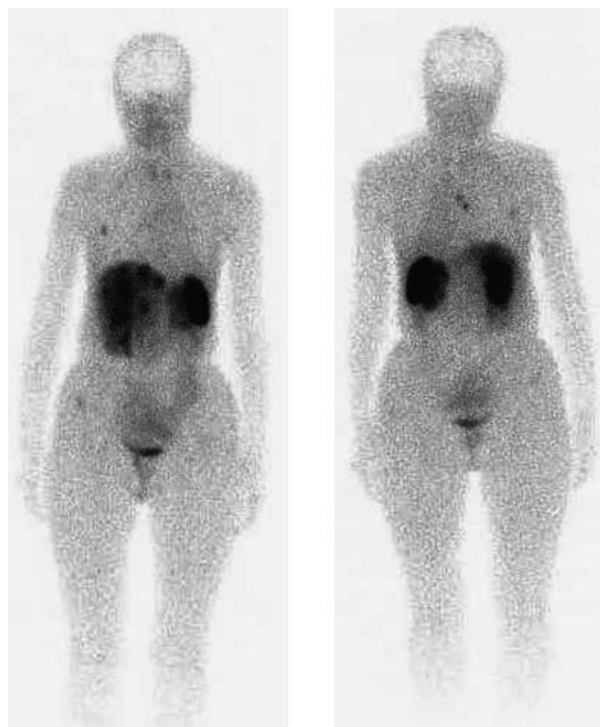


Figure 13.5

[^{99m}Tc]EDDA/HYNIC-TOC (ethylenediaminediacetic acid/hydrazinonicotinil-Tyr³-octreotide) scintigraphy in a patient with carcinoid syndrome (unknown primary). Somatostatin receptor scintigraphy was able to identify liver metastases and multiple skeletal lesions, but not depicted the primary tumor.

data demonstrate that [^{99m}Tc]depreotide-SPECT is less sensitive than [¹⁸F]FDG-PET for the diagnosis of lung malignancies. At present, [^{99m}Tc]depreotide-SPECT cannot substitute PET in lung cancer staging, and it remains a second-choice tracer in this indication.^{54–56}

Imaging with radiolabeled metaiodobenzylguanidine

MIBG is a derivative of guanethidine and acts as an analog of norepinephrine. MIBG labeled with ¹²³I or ¹³¹I can be used as an index of the integrity and function of the adrenergic nervous system, especially in the heart. MIBG shows the same cellular transport system as norepinephrine, and accumulates in neuroendocrine tumors, mainly in pheochromocytoma, neuroblastoma, and paraganglioma.^{57–59} [¹²³I]MIBG, due to the physical characteristics of the radioisotope and the favorable dosimetry, represents the radiopharmaceutical of choice for SPECT. Nevertheless, the elevated cost and limited availability are negative factors for extensive clinical use. [¹³¹I]MIBG, however, due to the longer half-life of ¹³¹I that allows also dosimetric studies, its low cost, and easy

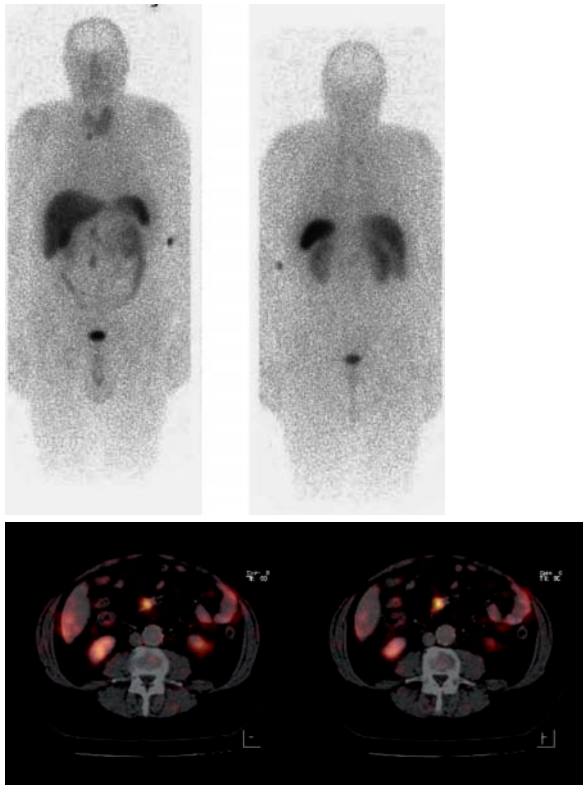


Figure 13.6

Patient who presented with liver and lymph node metastases from unknown neuroendocrine primary. [^{99m}Tc]EDDA/HYNIC-TOC scintigraphy demonstrated at whole-body scan (upper panel) liver and lymph node metastases. SPECT-computed tomography (CT) image fusion (lower panel) localized the primary tumor in the lower duodenal tract.

availability, is nowadays the radiopharmaceutical most used in clinical routine, except for pediatric patients.

Before the scintigraphic examination, the patient has to be prepared by the oral administration of potassium iodide or potassium perchlorate to block the thyroid uptake of free iodine. Moreover, patients should withdraw from some treatments (α and β blockers) that could interfere with MIBG uptake, for a time depending on the individual drug.³² 37–74 MBq (1–2 mCi) of the radiopharmaceutical is administered by slow intravenous injection (1–2 minutes). Using [¹³¹I]MIBG, images should be acquired at 24 and 48 hours post-injection (in some cases 72 hours). Using [¹²³I]MIBG, the administered activity for adults is about 370 MBq; images should be acquired at 24 hours and only in some exceptional cases at 48 hours post-injection. SPECT studies must be carried out at 24 hours post-injection. The effective dose in adults is 0.013 mSv/MBq for [¹²³I]MIBG and 0.14 mSv/MBq for [¹³¹I]MIBG.⁶⁰

The biodistribution of MIBG is characterized by uptake in the normal liver, myocardium, salivary glands, intestines,

spleen, bladder, and thyroid. The adrenal medulla can sometimes be visualized with [¹²³I]MIBG and more rarely with [¹³¹I]MIBG. In pediatric patients the cardiac uptake can be elevated, and sometimes uptake in the shoulder and neck region can be observed. A neuroendocrine tumor can be evidenced by a non-physiologic area of uptake. False-positive cases are very rare because of the high specificity of the tracer, but are possible in the presence of an obstruction in the urinary tract or hyperplasia of the adrenal glands after a monolateral adrenalectomy.

MIBG scintigraphy has a limited role in the management of carcinoids and in GEP tumors, while it has found a large application for the diagnosis of neoplasia of sympatho-adrenal lineage (Figure 13.7).⁵⁸ A review of the literature regarding MIBG scintigraphy reports that about 60–70% of carcinoids are visualized using this radiopharmaceutical.^{60–65} MIBG uptake is shown both in primary lesions and in metastatic sites; the best results can be obtained with SPECT in hepatic metastasis. A comparison of the diagnostic sensitivity of MIBG scintigraphy and that of somatostatin analogs indicates that the latter are better in depicting both the primary tumor and its metastases. This indication

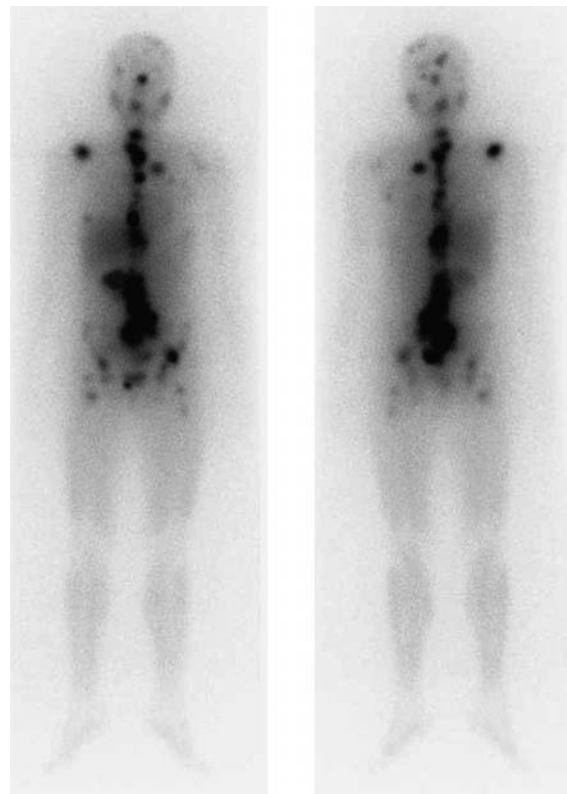


Figure 13.7

[¹³¹I]MIBG (metaiodobenzylguanidine) whole-body scan of a patient with multiple metastases from pheochromocytoma. Scintigraphy shows various pathologic areas of intense uptake in bone, lung, abdomen, and lumbo-aortic lymph nodes.

remains true also for the study of solitary metastasis or for the diagnosis of unknown primary tumor site in the presence of metastasis. Nevertheless, there are some carcinoids that are not visualized by scintigraphy with OctreoScan®, and in contrast are shown by MIBG scan. Scintigraphy with MIBG is compulsory before the administration of high therapeutic activity of [¹³¹I]MIBG, in order to assess the potential efficacy of this radiopharmaceutical at high doses, such as in the case of nuclear medicine therapy of patients with neuroendocrine tumors that do not express somatostatin receptors.

Positron emission tomography

PET is a scintigraphic technique based on the use of positron-emitting radioisotopes, such as ¹¹C, ¹⁵O, ¹³N, and ¹⁸F. Some biological molecules can be labeled with these radioisotopes without compromising their structure, and so they can be useful as radiopharmaceuticals for PET technology. PET is commonly used in clinical applications for the diagnosis of neoplasia, since it has been shown to be a very powerful tool for staging, restaging, diagnosis of hidden lesions during follow-up, monitoring therapy response, and therapeutic planning.^{66,67} Hybrid instruments, such as PET–CT, are able to increase the accuracy of tumor detection, giving both morphological and metabolic information.^{65,68} [¹⁸F]FDG is today the most important radiopharmaceutical used in oncology both for its physical characteristics (favorable half-life of ¹⁸F) and for the reason that FDG is the most reliable general tracer for cancer (the tumor uptake reflects an elevated anaerobic glycolysis which is common in all neoplastic processes). Nowadays PET with [¹⁸F]FDG is included in many diagnostic protocols for different tumors, because it is a non-invasive method and highly effective, often capable of giving information that, in 30% of cases, contributes to a modification of the therapeutic strategy.^{69,70} Moreover, in spite of the relative high cost of PET instrument and facilities, studies of technological assessment have demonstrated that [¹⁸F]FDG-PET has a favorable cost/effectiveness balance in oncology. [¹⁸F]FDG-PET has been employed also for the diagnosis of neuroendocrine tumors, but the results in this area are not completely satisfactory in terms of diagnostic sensitivity. In fact, neuroendocrine tumors often have a well-differentiated histology and show a very slow metabolism; this leads to a poor uptake of FDG. This characteristic can be used as a prognostic index, because an intense uptake of [¹⁸F]FDG signifies a parameter of elevated proliferation and high biological aggressiveness.^{17,18} In fact, an intense uptake of [¹⁸F]FDG is usually accompanied by weak positive or negative imaging with somatostatin analogs; this happens for poorly differentiated tumors that scarcely express somatostatin receptors.

GEP tumors metabolize L-dihydroxyphenylalanine (L-DOPA) and 5-hydroxy-L-tryptophan (5-HTP) by transforming these substances in dopamine and serotonin, respectively. For this reason, ¹¹C-on ¹⁸F-labeled L-DOPA and ¹¹C-labeled 5-HTP have been used as PET radiopharmaceuticals. Interesting results were obtained in some studies with ¹¹C-5-HTP, even if in a limited number of patients. An overall sensitivity of 84% has been obtained, and this result is better than that obtained with conventional radiology.^{71,72} [¹⁸F]DOPA-PET was used to investigate the activity of aromatic L-amino acid decarboxylase in the brain and to assess in vivo the integrity of the dopaminergic system in patients. Neuroendocrine tumors demonstrate an increased activity of L-DOPA decarboxylase, and for this reason they show a high uptake of ¹⁸F-DOPA. Several studies have reported that [¹⁸F]DOPA-PET is a good procedure for detecting neuroendocrine lesions (including carcinoids).^{73,74} When PET–CT is used, the hybrid system increases the spatial resolution and allows more accurate localization of the focal uptake, thanks to the anatomical map obtained by CT.⁷⁵

Nowadays the major interest in this field is represented by somatostatin analogs radiolabeled with positron-emitting isotopes, such as ⁶⁸Ga. ⁶⁸Ga (half-life 68.3 minutes) is produced by the ⁶⁸Ge generator (half-life 2070.8 days) available on the market which allows a constant and continuous production of the radioisotope.⁷⁶ Peptides DOTA-TOC, DOTA-NOC, and DOTA-TATE can be easily labeled with ⁶⁸Ga without the need for a cyclotron. ⁶⁸Ga-radiolabeled peptides show a brief renal clearance and are rapidly accumulated in tumors (about 30 minutes). Administered activities in adults are 100–150 MBq (2.7–4 mCi) and images are acquired 60–90 minutes after injection, so the procedure is straightforward. Clinical studies with [⁶⁸Ga]DOTA-TOC, [⁶⁸Ga]DOTA-NOC, and [⁶⁸Ga]DOTA-TATE are still limited; however, the available clinical results are very interesting and they encourage the use of this diagnostic procedure in the management of GEP tumors.^{19–22,77,78} ⁶⁸Ga-labeled somatostatin analogs for PET show several advantages in comparison with [¹¹¹In]pentetreotide: PET has very good spatial resolution, and the advantage of carrying out a whole-body scan in a short time (about 1 hour from injection), and produces high-quality images. The diagnostic sensitivity of ⁶⁸Ga-labeled somatostatin analogs PET leads to very interesting results (Figures 13.8 and 13.9). The available data suggest that the diagnostic efficacy of ⁶⁸Ga-labeled somatostatin analogs PET is higher than that obtained with [¹¹¹In]pentetreotide. For example, comparison of PET with [⁶⁸Ga]DOTA-NOC and SPECT with [¹¹¹In]pentetreotide has shown that the former has better diagnostic accuracy. PET with [⁶⁸Ga]DOTA-NOC is particularly sensitive in imaging small-dimension lesions, above all in lymph nodes, and lesions in the liver and in bones, as well as in finding unknown primary tumor sites in patients with metastasis.^{79–82}

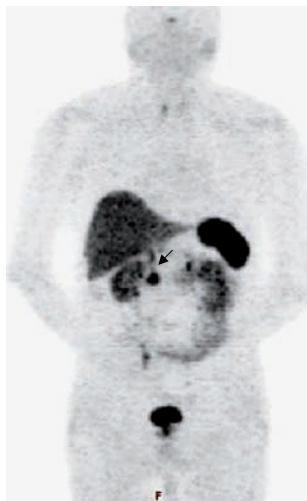


Figure 13.8

Patient with neuroendocrine primary of unknown origin detected by [^{68}Ga]DOTA-TOC-PET (tetraazacyclododecanetetraacetic acid-Tyr³-octreotide positron-emission tomography) in the pancreatic head (arrow).

Conclusions

Nuclear medicine imaging of GEP tumors has become more and more important over time, with the evolution of technology and increasing knowledge of the biology and natural history of these tumors. The impressive pharmacological research in the area of somatostatin analogs has



Figure 13.9

Patient with neuroendocrine primary of unknown origin localized by [^{68}Ga]DOTA-TOC-PET in the jejunum (arrow). Clear hyperfixation in multiple liver metastases. The primary was not revealed by conventional radiological imaging.

obtained several substances that have achieved a very important role in tumor targeting. Somatostatin analogs radiolabeled with γ and positron emitters are one of the best examples of the impact of radioreceptor imaging on patient management. The qualitative and quantitative imaging of receptor expression and distribution is essential not only for diagnosis but mainly for the characterization of lesions (prognostic value) and the selection of patients candidate for somatostatin analog therapy (prediction therapy response). At present it is not possible to approach the different steps of management in patients with GEP tumors without the support of nuclear medicine, and in the near future we should expect further improvements in this area. For many reasons nuclear medicine still remains the most fertile field of discovery and new developments.

References

1. Bombardieri E, Maccauro M, de Deckere E, Savelli G, Chiti A. Nuclear medicine imaging of neuroendocrine tumours. *Ann Oncol* 2001; 12: S51–61.
2. Rufini V, Calcagni ML, Baum RP. Imaging of neuroendocrine tumors. *Semin Nucl Med* 2006; 36: 228–47.
3. Oberg K, Eriksson B. Nuclear medicine in the detection, staging and treatment of gastrointestinal carcinoid tumours. *Best Pract Res Clin Endocrinol Metab* 2005; 19: 265–76.
4. Kolby L, Bernhardt, P, Levin-Jakobsen AM et al. Uptake of metaiodobenzylguanidine in neuroendocrine tumors is mediated by vesicular monoamine transporters. *Br J Cancer* 2003; 89: 1383–8.
5. Kurtaran A. Receptor imaging in oncology. In: Aktolun C, Tauxe WN eds. *Nuclear Oncology*; New York: Springer 1999; 333–43.
6. Kwekkboom DJ, Krenning EP. Somatostatin receptor imaging in oncology. In: Aktolun C, Tauxe WN (Eds), *Nuclear Oncology*, New York: Springer 1999, 345–57.
7. Seregni E, Chiti A, Bombardieri E. Radionuclide imaging of neuroendocrine tumors: biological basis and diagnostic results. *Eur J Nucl Med* 1998; 25: 639–58.
8. Arnold R, Goke R, Behr T. Neuroendocrine gastro-enteropancreatic (GEP) tumours. In: Scheppach W, Bresalier RS, Tytgat GNJ (Eds), *Gastrointestinal and Liver Tumors*, New York: Springer 2004, 195–233.
9. Maecke HR, Behe M. New octreotide derivatives labeled with technetium-99m. *J Nucl Med* 1996; 37: 1144 (abstrt).
10. Gabriel M, Muehllechner P, Decristoforo C et al. 99mTc-EDDA/HYNIC-Tyr(3)-octreotide for staging and follow-up of patients with neuroendocrine gastro-enteropancreatic tumors. *Q J Nucl Med Mol Imaging* 2005; 49: 237–44.
11. Lebtahi R, Le Cloirec J, Houzard C et al. Detection of neuroendocrine tumors: 99mTc-P829 scintigraphy compared with 111In-pentetreotide scintigraphy. *J Nucl Med* 2002; 43: 889–95.
12. Blum J, Handmaker H, Lister-James J, Rinne N. A multicenter trial with a somatostatin analog (99m)Tc depreotide in

- the evaluation of solitary pulmonary nodules. *Chest* 2000; 117: 1232–8.
13. Reubi JC, Schar JC, Waser B et al. Affinity profiles for human somatostatin receptor subtypes SST1–SST5 of somatostatin radiotracers selected for scintigraphic and radiotherapeutic use. *Eur J Nucl Med* 2000; 27: 273–82.
 14. Ginj M, Chen J, Walter MA et al. Preclinical evaluation of new and highly potent analogues of octreotide for predictive imaging and targeted radiotherapy. *Clin Cancer Res* 2005; 11: 1136–45.
 15. Virgolini I, Traub-Weidinger T, Decristoforo C. Nuclear medicine in the detection and management of pancreatic islet-cell tumours. *Best Pract Res Clin Endocrinol Metab* 2005; 19: 213–27.
 16. Behe M, Behr TM, Schmalor W et al. Indium-111-labeled GLP-1 for in vivo diagnostic of insulinomas. *J Nucl Med* 2002; 43: (Suppl): 92P (abstr).
 17. Adams S, Baum RP, Rink T et al. Limited value of fluorine-18 fluorodeoxyglucose positron emission tomography for the imaging of neuroendocrine tumours. *Eur J Nucl Med* 1998; 25: 79–83.
 18. Eriksson B, Bergstrom M, Orlefors H et al. Use of PET in neuroendocrine tumors. In vivo applications and in vitro studies. *Q J Nucl Med* 2000; 44: 68–76.
 19. Hofmann M, Maecke H, Borner R et al. Biokinetics and imaging with the somatostatin receptor PET radioligand (68)Ga-DOTATOC: preliminary data. *Eur J Nucl Med* 2001; 28: 1751–7.
 20. Baum RP, Schmucking M, Niesen A et al. Receptor-PET/CT of neuroendocrine tumors using the gallium-68 labelled somatostatin analog DOTA-NOC: first clinical results. *Eur Radiol* 2005; 15 (suppl 1): C-0409 (abstr).
 21. Kowalski J, Henze M, Schuhmacher J et al. Evaluation of positron emission tomography imaging using [68Ga]-DOTA-D-Phe(1)-Tyr(3)-octreotide in comparison to [111In]-DTPAOC SPECT. First results in patients with neuroendocrine tumors. *Mol Imaging Biol* 2003; 5(1): 42–8.
 22. Hofmann M, Boemer A, Krause T et al. Clinical applications of Ga-68-DOTATOC in 132 patients with neuroendocrine tumors. *Eur J Nucl Med Mol Imaging* 2005; 32: S53 (abstr).
 23. Westlin JE, Janson ET, Arnberg H et al. Somatostatin receptor scintigraphy of carcinoid tumours using the ¹¹¹In-DTPA-D-Phe1-octreotide. *Acta Oncol* 2003; 32: 783–6.
 24. Bombardieri E, Aktolun C, Baum RP et al. ¹¹¹In-pentetreotide scintigraphy: procedure guidelines for tumour imaging. *Eur J Nucl Med Mol Imaging* 2003; 30: BP140–7.
 25. Krenning EP, Kwekkeboom DJ, Bakker WH et al. Somatostatin receptor scintigraphy with [¹¹¹In-DTPA-D-Phe1] and [¹²³I-Tyr3] octreotide: the Rotterdam experience with more than 1000 patients. *Eur J Nucl Med* 1993; 20: 716–31.
 26. McCarthy KE, Wolteing EA, Anthony LB. In situ radiotherapy with ¹¹¹In-pentetreotide. State of the art and perspectives. *Q J Nucl Med* 2000; 44: 88–95.
 27. Valkema R, De Jong M, Bakker WH et al. Phase I study of peptide receptor radionuclide therapy with (In-DTPA)octreotide: the Rotterdam experience. *Semin Nucl Med* 2002; 32: 110–22.
 28. Kaltas GA, Papadogias D, Markas P, Grossman AB. Treatment of advanced neuroendocrine tumours with radiolabelled somatostatin analogues. *Endocr Relat Cancer* 2005; 12: 683–99.
 29. Kwekkeboom DJ, Mueller-Brand J, Paganelli G et al. Overview of results of peptide receptor radionuclide therapy with 3 radiolabeled somatostatin analogs. *J Nucl Med* 2005; 46: 62S–6S.
 30. Chiti A, Briganti V, Fanti S. Results and potential in neuroendocrine gastro-entero-pancreatic tumors. *Q J Nucl Med* 2000; 44: 42–9.
 31. Briganti V, Matteini M, Ferri P. Octreoscan SPET evaluation in the diagnosis of pancreas neuroendocrine tumors. *Cancer Biother Radiopharm* 2001; 16: 515–24.
 32. Warner RP, O'Dorisio T. Radiolabeled peptides in diagnosis and tumor imaging: clinical overview. *Semin Nucl Med* 2002; 32: 79–83.
 33. Bombardieri E, Seregini E, Villano C, Chiti A, Bajetta E. Position of nuclear medicine techniques in the diagnostic work-up of neuroendocrine tumors. *Q J Nucl Med* 2004; 48: 150–63.
 34. Bajetta E, Procopio G, Ferrari L et al. Update on the treatment of neuroendocrine tumors. *Expet Rev Anticancer Ther* 2003; 3: 631–42.
 35. Lebtahi R, Cadiot G, Sarda L et al. Clinical impact of somatostatin receptor scintigraphy in the management of patients with neuroendocrine gastroenteropancreatic tumors. *J Nucl Med*, 1997; 38: 853–8.
 36. Jensen RT. Carcinoid and pancreatic endocrine tumors: recent advances in molecular pathogenesis, localization and treatment. *Curr Opin Oncol* 2000; 12: 368–77.
 37. Reubi JC. Somatostatin and other peptide receptors as tools for tumor diagnosis and treatment. *Neuroendocrinology* 2004; 80: 51–6.
 38. Schillaci O, Spanu A, Scopinaro F et al. Somatostatin receptor scintigraphy in liver metastasis detection from gastroenteropancreatic neuroendocrine tumors. *J Nucl Med* 2003; 44: 359–68.
 39. Schillaci O, Spanu A, Scopinaro F et al. Somatostatin receptor scintigraphy with ¹¹¹In-pentetreotide in non-functioning gastroenteropancreatic neuroendocrine tumors. *Int J Oncol* 2003; 23: 1687–95.
 40. Savelli G, Lucignani G, Seregini E et al. Feasibility of somatostatin receptor scintigraphy in the detection of occult primary gastro-entero-pancreatic (GEP) neuroendocrine tumours. *Nucl Med Commun* 2004; 25: 445–9.
 41. Schillaci O. Hybrid SPET/CT: a new era for SPET imaging? *Eur J Nucl Med Mol Imaging* 2005; 32: 521–4.
 42. Krausz Y, Keidar Z, Kogan I et al. SPECT/CT hybrid imaging with ¹¹¹In-pentetreotide in assessment of neuroendocrine tumours. *Clin Endocrinol* 2003; 59: 565–73.
 43. Ingui CJ, Shah NP, Oates ME. Endocrine neoplasm scintigraphy: added value of fusing SPECT/CT images compared with traditional side-by-side analysis. *Clin Nucl Med* 2006; 31: 665–72.
 44. Filippi L, Valentini FB, Gossetti B et al. Intraoperative gamma probe detection of head and neck paragangliomas with ¹¹¹In-pentetreotide: a pilot study. *Tumori* 2005; 91: 173–6.
 45. Grossrubatscher E, Vignati F, Dalino P et al. Use of radioguided surgery with [¹¹¹In]-pentetreotide in the management of an ACTH-secreting bronchial carcinoid causing ectopic Cushing's syndrome. *J Endocrinol Invest* 2005; 28: 72–8.
 46. Adams S, Acker P, Lorenz M et al. Radioisotope-guided surgery in patients with pheochromocytoma and recurrent

- medullary thyroid carcinoma: a comparison of preoperative and intraoperative tumor localization with histopathologic findings. *Cancer* 2001; 92: 263–70.
47. Virgolini I, Traub T, Leimer M et al. New radiopharmaceuticals for receptor scintigraphy and radionuclide therapy. *Q J Nucl Med* 2000; 44: 50–8.
 48. Decristoforo C, Melendez-Alafort L, Sosabowski JK, Mather SJ. ^{99m}Tc-HYNIC-[Tyr3]-octreotide for imaging somatostatin-receptor-positive tumors: preclinical evaluation and comparison with ¹¹¹In-octreotide. *J Nucl Med* 2000; 41: 1114–19.
 49. Hubalewska-Dydejczyk A, Fross-Baron K, Mikolajczak R et al. ^{99m}Tc-EDDA/HYNIC-octreotate scintigraphy, an efficient method for the detection and staging of carcinoid tumours: results of 3 years' experience. *Eur J Nucl Med Mol Imaging* 2006; 33: 1123–33.
 50. Gabriel M, Hausler F, Bale R et al. Image fusion analysis of (^{99m}Tc)-HYNIC-Tyr(3)-octreotide SPECT and diagnostic CT using an immobilization device with external markers in patients with endocrine tumours. *Eur J Nucl Med Mol Imaging* 2005; 32: 1440–51.
 51. Reubi JC. Peptide receptors as molecular targets for cancer diagnosis and therapy. *Endocr Rev* 2003; 24: 389–427.
 52. Virgolini I, Raderer M, Kurtaran A et al. Vasoactive intestinal peptide (VIP) receptor imaging in the localization of intestinal adenocarcinomas and endocrine tumors. *N Engl J Med* 1994; 331: 1116–21.
 53. Hassenius C, Bader M, Meinhold H et al. Vasoactive intestinal peptide receptor scintigraphy in patients with pancreatic adenocarcinomas or neuroendocrine tumors. *Eur J Nucl Med* 2000; 27: 1684–93.
 54. Menda Y, Kahn D. Somatostatin receptor imaging of non-small cell lung cancer with ^{99m}Tc depreotide. *Semin Nucl Med* 2002; 32: 92–6.
 55. Baath M, Kolbeck KG, Danielsson R. Somatostatin receptor scintigraphy with ^{99m}Tc depreotide (NeoSpect) in discriminating between malignant and benign lesions in the diagnosis of lung cancer: a pilot study. *Acta Radiol* 2004; 45: 833–9.
 56. Halley A, Hugentobler A, Icard P et al. Efficiency of ¹⁸F-FDG and ^{99m}Tc depreotide SPECT in the diagnosis of malignancy of solitary pulmonary nodules. *Eur J Nucl Med Mol Imaging* 2005; 32: 1026–32.
 57. Shapiro B. Ten years of experience with MIBG applications and the potential of new radiolabeled peptides: a personal overview and concluding remarks. *Q J Nucl Med* 1995; 39: 150–5.
 58. Troncone L, Rufini V: MIBG in diagnosis of neuroendocrine tumors. In: Ell PJ, Gambhir SS (Eds): *Nuclear Medicine in Clinical Diagnosis and Treatment*. Edinburgh. Churchill Livingstone 2004; 1: 83–95.
 59. Bombardieri E, Aktolun C, Baum RP et al. ¹³¹I/¹²³I-Metaiodobenzylguanidine (MIBG) scintigraphy: procedure guidelines for tumor imaging. *Eur J Nucl Med Mol Imaging* 2003; 30: BP132–9.
 60. Bonnin F, Lumbroso J, Tenebaum F et al. Refining interpretation of MIBG scans in children. *J Nucl Med* 1994; 35: 803–10.
 61. Ramage JK, Williams R, Buxton-Thomas M. Imaging secondary neuroendocrine tumours of the liver: comparison of ¹²³I metaiodobenzylguanidine (MIBG) and ¹¹¹In-labelled octreotide (Octreoscan). *Q J Med*, 1996; 89: 539–42.
 62. Nocaudite-Calzada M, Huglo D, Carnaille B et al. Comparison of somatostatin analogue and metaiodobenzylguanidine scintigraphy for the detection of carcinoid tumours. *Eur J Nucl Med* 1996; 23: 1448–54.
 63. Taal BG, Hoefnagel CA, Valdes Olmos RA et al. Combined diagnostic imaging with ¹³¹I-metaiodobenzylguanidine and ¹¹¹In-pentetreotide in carcinoid tumours. *Eur J Cancer* 1996; 32A: 1924–32.
 64. Kaltas G, Korbonits M, Heintz E et al. Comparison of somatostatin analog and meta-iodobenzylguanidine radionuclides in the diagnosis and localization of advanced neuroendocrine tumors. *J Clin Endocrinol Metab* 2001; 86: 895–902.
 65. Macfarlane D, Gonin J, Wieland D et al. Successful and unsuccessful approaches to imaging carcinoids: comparison of a radiolabelled tryptophan hydroxylase inhibitor with a tracer of biogenic amine uptake and storage, and a somatostatin analogue. *Eur J Nucl Med* 1996; 23: 131–40.
 66. Bamberg M, Diehl V, Herrmann T et al. Positron emission tomography (PET) in oncology: a part of medical therapeutic expertise. *Dtsch Med Wochenschr* 2006; 131: 512–15.
 67. Shields AF. Positron emission tomography measurement of tumor metabolism and growth: its expanding role in oncology. *Mol Imaging Biol* 2006; 8: 141–50.
 68. von Schulthess GK, Steinert HC, Hany TF. Integrated PET/CT: current applications and future directions. *Radiology* 2006; 238: 405–22.
 69. Bombardieri E, Aktolun C, Baum RP et al. FDG-PET: procedure guidelines for tumour imaging. *Eur J Nucl Med Mol Imaging* 2003; 30: BP115–24.
 70. Reske SN, Kotzerke J. FDG-PET for clinical use. Results of the 3rd German interdisciplinary consensus conference 'Onko-PET III', 21 July and 19 September 2000. *Eur J Nucl Med* 2001; 28: 1707–23.
 71. Orlefors H, Sundin A, Garske U et al. Whole-body ¹¹C-5-hydroxytryptophan positron emission tomography as a universal imaging technique for neuroendocrine tumors: comparison with somatostatin receptor scintigraphy and computed tomography. *J Clin Endocrinol Metab* 2005; 90: 3392–400.
 72. Sundin A, Eriksson B, Bergstrom M et al. Demonstration of ¹¹C-5-hydroxy-L-tryptophan uptake and decarboxylation in carcinoid tumors by specific positioning labeling in positron emission tomography. *Nucl Med Biol* 2000; 27: 33–41.
 73. Becherer A, Stabo M, Karanikas G et al. Imaging of advanced neuroendocrine tumours with ¹⁸F-DOPA PET. *J Nucl Med* 2004; 45: 1161–7.
 74. Hoegerle S, Althoefer C, Ghanem N et al. Whole-body ¹⁸F-DOPA PET for detection of gastrointestinal carcinoid tumors. *Radiology* 2001; 220: 373–80.
 75. Nanni C, Rubello D, Fanti S. ¹⁸F-DOPA PET/CT and neuroendocrine tumours. *Eur J Nucl Med Mol Imaging* 2006; 33: 509–13.
 76. Maecke HR, Hofmann M, Haberkorn U. (⁶⁸Ga)-labeled peptides in tumor imaging. *J Nucl Med* 2005; 46: 172S–8S.
 77. Wild D, Macke HR, Waser B et al. ⁶⁸Ga-DOTANOC: a first compound for PET imaging with high affinity for somatostatin receptor subtypes 2 and 5. *Eur J Nucl Med Mol Imaging* 2005; 32: 724.
 78. Win Z, Rahman L, Murrell J et al. The possible role of ⁶⁸Ga-DOTATATE PET in malignant abdominal paraganglioma. *Eur J Nucl Med Mol Imaging* 2006; 33: 506.

79. Baum RP, Niesen A, Leonhardi J et al. Receptor PET/CT imaging of neuroendocrine tumors using the Ga-68 labelled, high affinity somatostatin analogue DOTA-1-Nal3-octreotide (DOTA-NOC): clinical results in 327 patients. *Eur J Nucl Med Mol Imaging* 2005; 32: 54S.
80. Oksuz MO, Aschoff P, Kemke B et al. Imaging of somatostatin-receptor expressing neuroendocrine tumours with ⁶⁸Ga-DOTATOC-PET/CT versus ¹¹¹In-DTPA-octreotide SPECT/CT. *Eur J Nucl Med Mol Imaging* 2005; 32: 109S.
81. Milker-Zabel S, Zabel-du Bois A, Henze M et al. Improved target volume definition for fractionated stereotactic radiotherapy in patients with intracranial meningiomas by correlation of CT, MRI, and [68Ga]-DOTATOC-PET. *Int J Radiat Oncol Biol Phys* 2006; 65: 222–7.
82. Henze M, Dimitrakopoulou-Strauss A, Milker-Zabel S et al. Characterization of ⁶⁸Ga-DOTA-D-Phe1-Tyr3-octreotide kinetics in patients with meningiomas. *J Nucl Med* 2005; 46: 763–9.

Lymphoma

Simona Ben-Haim and Ora Israel

Background

Lymphoma was initially described by Thomas Hodgkin in 1832. It includes Hodgkin's disease (HD) and non-Hodgkin's lymphoma (NHL), and is characterized by transformations of normal lymphoid cells at different stages of their development. Lymphoma may present as the involvement of one or more lymph node groups or of an isolated organ, or as widely disseminated disease. In general, enlarged lymph nodes displace other structures, but large-cell high-grade NHL may also be locally invasive.

Lymphomas represent about 8% of adult malignancies and 10% of childhood tumors.^{1,2} Histological classifications of HD were first introduced in 1947, and were finalized in the revised European–American lymphoma classification in 1994.^{3–5} Over the past 60 years there have been several reclassifications of NHL, until the World Health Organization (WHO) adopted an official classification.^{6–9}

The goals of the diagnostic work-up of a patient with lymphoma include establishing the precise histological subtype, the localization and extent of the disease, and the performance status of the patient. Assessment for B-symptoms, whole-body computed tomography (CT), bone marrow biopsy, and lymph node biopsy with histological, immunological, and molecular biologic assessment are required for precise diagnosis. Functional imaging, mainly with ⁶⁷Ga, in the past had an important role in the assessment of lymphoma patients.^{10–12} ⁶⁷Ga scintigraphy has been proved to be superior to CT to define the response to therapy,^{13–15} to characterize a residual mass post-therapy,¹⁶ in the early detection of disease recurrence,¹⁷ and as a predictor of long-term prognosis in HD and NHL.^{18–21} [¹⁸F]fluoro-2-deoxy-D-glucose-positron emission tomography (FDG-PET) and PET–CT are being increasingly used in the evaluation of lymphoma, and have an established role for staging, evaluation of response to therapy, routine follow-up, and early detection of recurrence.^{22–27} In addition to these well-established indications, PET may also have a role in radiotherapy planning, by defining functional tumor target volumes.²⁸ Owing to a more accurate definition of the extent of disease, PET–CT can define the radiation field arrangements and dose distributions in order to minimize radiation exposure to normal tissues.²⁸

Hodgkin's disease

There are about 7500 new HD cases yearly in the USA. This incidence has been stable for the past 50 years. HD is more common in the third and seventh decades and in men,^{29,30} and accounts for 7% of lymphoma deaths.²⁹ The most common histological type is nodular sclerosis (65%), usually involving the mediastinum.³¹ The mixed cellularity type is present in 25%, while lymphocyte-predominant and lymphocyte-depletion types each account for 5%.³² Cervical lymph nodes are the most commonly involved site in HD (60–80%), and two-thirds of newly diagnosed HD present with intramediastinal disease involvement. Fewer than 10% of patients present with isolated infradiaphragmatic lymphadenopathy. HD spreads contiguously to adjacent lymph nodes.³² Extranodal involvement is uncommon in HD³³ and is caused mainly by direct extension from nodal disease. Hematogenous spread, reported in 10–15% of patients, is associated with a less favorable outcome.³⁴

Histologic classification is not of major importance in the management of patients with HD. The prognosis is directly related to the stage of disease and presence of systemic symptoms.^{35,36} At presentation, 85% of patients have stage I or II disease, with lymphadenopathy confined to one or a few sites on one side of the diaphragm. In patients with stage III or IV disease lymphadenopathy is present both above and below the diaphragm, with or without involvement of organs such as the liver, spleen, lung, and bone marrow.³⁰ Nodular sclerosis type HD stage I or II has the most favorable prognosis. The recurrence rate in HD ranges between 10 and 40% and occurs mainly during the first 3 years after the initial diagnosis.²⁹

Currently HD is cured in over 80% of patients.^{29,37,38} However, treatment-related mortality has increased dramatically over recent decades, mainly due to MOPP chemotherapy (mechlorethamine, vincristine, procarbazine, prednisone).³⁹ Major research goals in HD are therefore directed at present towards defining novel therapeutic regimens for the 20% of patients who are not cured with currently used treatment regimens, as well as towards maintaining high cure rates while reducing the treatment-related toxicities in the remaining 80% of patients.

Non-Hodgkin's lymphoma

NHL is more frequent in patients over the age of 50 years, with a similar incidence in men and women. There are about 50 000 new cases yearly in the USA, and approximately 23 000 patients die yearly of NHL.⁴⁰

Lymph nodes involved by NHL are usually larger than those involved by HD. NHL commonly arises in nodal sites; however, extranodal disease is more common than with HD and may occur in extranodal lymphatic tissue, such as Waldeyer's ring, the thymus, and spleen, and in non-lymphatic organs, such as the liver, the gastrointestinal tract, region of the head and neck, the orbit, central and peripheral nervous system, lung and pleura, skeleton, bone marrow, skin, breast, testis, thyroid, and genitourinary system.⁴¹

NHL is classified using the modified working formulation.⁹ The classification of I–IV stages is applied also in NHL, but the prognosis of NHL depends less on this classification. Histology and cellular origin, the presence of bulky disease, and specific organ involvement determine the clinical and radiographic presentation of NHL, and are important in risk stratification with an impact on the clinical management and outcome of patients.⁴⁰ High-grade NHL (HG-NHL) represents about 25% of tumors,⁴⁰ is the most aggressive type of disease, and without therapy has a short survival. Most patients have localized disease at initial diagnosis. Low-grade NHL (LG-NHL) is an indolent type of disease with slow progression, but often associated with large-volume disseminated nodal stage III or IV disease at presentation.^{40,42,43} Intermediate-grade NHL (of the follicular and diffuse types) is often associated with rapidly enlarging lymph nodes and with extranodal disease.⁴⁰

The treatment of NHL is less successful as compared to HD. In HG-NHL, 50–70% of patients achieve complete response with first-line chemotherapy, cure is obtained in about a third of patients, and the annual relapse rate is 7%.⁴⁰ Early diagnosis of treatment failure and early detection of recurrence determine the results of salvage therapy.

Anatomic imaging modalities of lymphoma

Computed tomography

CT is one of the major imaging modalities for detection, staging, and follow-up of lymphoma.⁴⁴ The extent of disease is a main factor affecting the choice of appropriate therapy in HD. In both HD and NHL the disease bulk and the presence of extranodal disease provide prognostic information. Accurate imaging enables radiotherapy planning for localized disease. CT has replaced the need for staging laparotomy and lymphangiography for the detection

of lymph node involvement.^{44,45} A major limitation of CT is represented by the use of size-related criteria for the diagnosis of nodal disease, which makes the detection of lymphoma in normal-sized nodes very difficult. In addition, CT cannot distinguish between lymphadenopathy caused by reactive hyperplasia and lymphoma involvement.⁴⁴ Extranodal involvement, which occurs primarily in NHL, is an adverse prognostic factor. In the abdomen, focal liver and spleen involvement can be easily detected by CT, whereas diffuse infiltration of either organ cannot be reliably diagnosed.^{44–51} Extranodal disease in organs such as the lung, breast, and gastrointestinal tract can be easily identified on CT.⁴⁴ Bone marrow involvement, which indicates stage IV disease with poor prognosis, cannot be defined by CT.⁴⁴

For the purpose of assessment of the response to therapy and definitions for complete or partial response, as well as stable or progressive disease, CT imaging is based on assessing interval changes in nodal or organ size.⁵² CT enables accurate and reproducible measurements, mainly in regularly shaped tumors, although with up to 15% interobserver variability, higher in cases of irregular masses or poor lesion to background contrast.^{52–54} The structural changes of the mass following therapy may also be helpful to determine tumor viability. Low attenuation may indicate cystic degeneration and calcifications which are seen in response to therapy.⁵⁵ Furthermore, dynamic contrast-enhanced CT may be used to obtain perfusion measurements, which are higher in the case of active disease.⁵⁶

Residual masses occur in 50–64% of patients with HD, mainly in the mediastinum,^{57–59} and in 20–60% of patients treated for NHL.^{52,60} Residual masses seen on CT following treatment may indicate fibrosis or necrosis, but in some cases may represent viable tumor. In large-cell NHL, while 30–50% of patients will have a residual mass post-therapy, only 5% of these lesions will represent active disease.⁶⁰ The change in size cannot be used as an indicator, and therefore CT cannot differentiate residual tumor from a fibrotic mass. CT attenuation values are also not reliable in this differentiation, showing similar levels in fibrosis and in active lymphoma.⁵²

Routine follow-up of patients with lymphoma is performed in order to assess the response to therapy, to differentiate patients in complete response (CR) from other clinical settings, in order to make decisions with respect to further clinical management. CT is therefore performed at the time of diagnosis, during treatment, and after completion of therapy. In patients during continuous clinical remission (CCR), early detection of recurrent disease is important in order to institute salvage therapy as soon as possible. In patients with a residual mass, CT is only of limited value in the detection of a recurrence in the same region, since there may be some time lag until the volume of the viable tumor is large enough to be recognized by CT.⁵²

Magnetic resonance imaging

As for CT, lymph node assessment on magnetic resonance imaging (MRI) is also based on nodal size. The accuracy of MRI for the detection of lymph node involvement is similar to that of CT and is hampered by the same limitations. Superparamagnetic iron oxide is taken up by nodal reticuloendothelial cells and leads to a decrease in signal on T₂-weighted images. In the presence of malignancy, iron oxide is not taken up in the specific node, and the signal does not decrease. However, in cases of only partial replacement by tumor, iron oxide may still be taken up and micrometastases may therefore be missed.⁶¹

MRI has a major role in the evaluation of meningeal or spinal cord involvement, and in diagnosis of bone marrow involvement, scenarios where CT cannot provide information. Infiltration of the bone marrow occurs in 20–40% of NHL at presentation and is an indicator of poor prognosis.⁵⁰ Intramedullary infiltration is often patchy, and therefore bilateral iliac crest biopsies are routinely performed, to increase the diagnostic yield. MRI is the most sensitive imaging modality for the detection of bone marrow involvement, with affected areas showing a low T₁ and high STIR (short T₁ inversion recovery) signal.⁴⁴ MRI can result in the upstaging of up to 33% of patients with negative bone marrow biopsies, and may be useful in guiding biopsy.⁴⁴ False-negative studies can occur in cases with microscopic infiltration, such as with LG-NHL. In patients with lymphoma involving the skeleton, MRI shows the extent of bone marrow and soft tissue invasion, while CT is better in predicting bone destruction.⁴⁴

MRI may have a role in monitoring the response to therapy, and may be able to differentiate active tumor from fibrosis or necrosis, due to excellent contrast resolution, changes in signal intensity, and enhancement after therapy. Active disease contains an excess of free water, and has a low signal on T₁-weighted sequence and an intermediate to high signal on T₂-weighted sequence.⁵² Following successful therapy, the collagen and fibrotic stroma show a low signal on T₂-weighted sequence. However, there still may be active tumor within the low signal areas, and also inflammatory changes and edema due to a successful response may be falsely related to as active disease.^{52,62} Radiotherapy can cause false-positive readings.⁵² As with CT, MRI cannot precisely diagnose whether there is viable tumor within a residual mass; however, MRI may sometimes be helpful in cases with a residual mass on CT. If the mass decreases in size and if there is also a rapid decrease in T₂-weighted signal and uniform low signal intensity, this may indicate a good response.⁵² False-positive results have been reported with this same pattern in cases of inflammation and necrosis, most commonly within 4 months post-therapy. New high signal abnormalities suggest recurrence of lymphoma, and may precede symptoms by 8–12 weeks.⁵² Contrast-enhanced MRI may also be useful in predicting the

recurrence of lymphoma. A significant decrease in the amount of enhancement on MRI was reported in patients showing residual masses during CCR as compared with patients who had recurrence, with sensitivity and specificity of 40–90% and 80–90%, respectively.⁶³

Ultrasound

Ultrasound (US) is useful for the assessment of superficial lymph nodes and the genitourinary tract. It is also useful for US-guided biopsies of focal lesions.⁶⁴

Functional imaging modalities of lymphoma: single photon emission computed tomography Gallium-67

Before the growth of oncologic PET indications, gallium-67 (Ga) was widely used for the assessment of HD and NHL. The precise mechanism of Ga localization in lymphoma is not fully understood, and many different factors are likely to be involved.^{65–67} Normal physiologic Ga activity is present in the liver, spleen, bone marrow, bone and growth plates, lacrimal and salivary glands, and breast tissue, and is due to transport by transferrin receptors. Ga is excreted via the kidneys and bowel. In tumors, specifically lymphoma, the mechanism of Ga uptake is more complex. Increased permeability of tumor blood vessels as compared to the normal vasculature enhances intracellular delivery of transferrin-bound Ga into the tumor cells.⁶⁸ In cells that are rapidly proliferating, transferrin receptors are upregulated, enhancing Ga uptake.⁶⁹ The Ga–transferrin complex is bound to the CD71 transferrin receptor on the surface of lymphoma cells. This mechanism contributes to over 70% of the Ga uptake by the tumor.⁷⁰ There is also a slower transferrin-independent pathway, which contributes 10–25% of tumor uptake.^{71,72} Intracellular Ga has also been found in lysosomes and in the rough endoplasmic reticulum bound to macromolecules, including ferritin and lactoferrin.^{66,71,73} The cellular tumoral uptake of Ga is linked to the metabolic activity of cells. Iosilevsky et al. showed in an animal model that Ga uptake correlates with the amount of viable tumor tissue.⁷⁴

Ga imaging protocol

High doses of Ga (260–370 MBq) and single photon emission computed tomography (SPECT) imaging are prerequisites

for high-end Ga imaging.¹⁰ SPECT, performed 48–72 hours after radiotracer injection, offers the greatest gain in contrast and in disease detection. Iterative reconstruction algorithms improve image quality. Due to bowel excretion of Ga, planar images of the abdomen and pelvis should be repeated at 7–10 days after the injection, when the physiologic bowel activity has cleared and disease can become more apparent.¹⁰ With the use of SPECT–CT, which includes CT imaging for attenuation correction and anatomic localization of abnormal Ga foci, SPECT image quality is further improved, as well as diagnostic accuracy, and there is no need for delayed imaging.⁷⁵

Ga-SPECT for staging of lymphoma

In centers using Ga-SPECT for functional assessment of lymphoma, staging is done primarily with CT. Ga has a lower sensitivity as compared with CT. For HD, Ga-SPECT has a reported sensitivity of 86–97% and a specificity of 100% (Figure 14.1). For NHL the sensitivity is 86–92% and

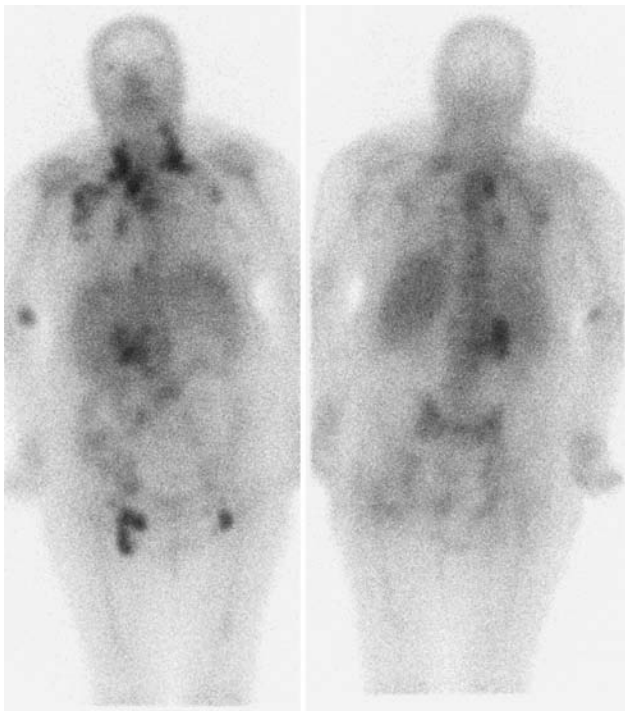


Figure 14.1

Gallium-67 scan at diagnosis in a 77-year-old female patient with Hodgkin's disease, nodular sclerosing type, showing extensive nodal disease above and below the diaphragm: bilateral cervical, supraclavicular and axillary, superior mediastinal, right hilar, mesenteric, para-aortic, para-iliac, bilateral inguinal, and left femoral lymphadenopathy. (Courtesy Department of Nuclear Medicine, Carmel Medical Center, Haifa, Israel.)

the specificity is 100%.^{68,76} The sensitivity is mainly reduced in patients with abdominal involvement, ranging from 69% for planar imaging to 85% for SPECT. The specificity is likewise improved with SPECT in the chest from 66% to 100% and in the abdomen from 87% to 100%.^{13,77} At the time of presentation, Ga imaging is performed to determine whether a specific tumor is tracer-avid, and will thus benefit in the future from Ga imaging for monitoring response to therapy and follow-up.

Ga avidity varies among the different subtypes of HD and NHL. In general, HD and HG-NHL have intense Ga uptake.^{12,78,79} In patients with LG-NHL, early studies reported a low sensitivity, related in part to the use of suboptimal planar imaging. Later studies indicate better results, with sensitivity ranging between 79 and 89% at initial staging and 89% for detection of recurrent disease.^{79,80} Among LG-NHL, low Ga-SPECT sensitivity has been mainly reported for MALT (mucosa-associated lymphoid tissue) (50%) and small lymphocytic lymphoma (64%), as compared to 84% in follicular, types mixed small-cleaved cell and 91% in follicular, mixed small-cleaved and large cell types.⁸⁰ It has been demonstrated that patients with LG-NHL and a high degree of Ga uptake had worse prognosis as compared to patients with low or absent Ga uptake.⁸¹

Ga-SPECT for extranodal lymphoma

Extranodal disease, mainly NHL, may arise along the gastrointestinal tract, head and neck, central and peripheral nervous system, lung and pleura, bone, and skin, and is more common in LG-NHL.^{41,82} In primary extranodal disease of the skin, gastrointestinal tract, and testis, Ga (planar studies only) has very low sensitivity,⁸² but sensitivity is higher, reaching 88%, in other locations, comparable to nodal disease.

Bone involvement occurs in 4–15% of patients with HD or NHL during the course of disease.^{83,84} Ga has a sensitivity of 93% and specificity of 91% for the diagnosis of skeletal involvement, and is superior to bone scintigraphy and CT in the follow-up of skeletal lesions.⁸⁵ In the diagnosis of bone marrow involvement, Ga has poor results, while MRI and bone marrow biopsy are currently utilized for the diagnosis of bone marrow involvement.

Liver involvement, either focal or diffuse, occurs in 3% of patients with HD and in 15% of patients with NHL. The spleen is frequently involved, in 30–40% of HD and 22% of NHL. Due to physiologic uptake of Ga in the liver and spleen, it is suboptimal for the detection of disease involvement in these organs.^{86–88}

The gastrointestinal tract is the most common site of primary extranodal lymphoma, mainly B-cell origin NHL, of which gastric lymphoma is the most common (50%), followed by the small bowel (30%). Ga imaging is useful in staging the extent of gastric involvement, with a reported

sensitivity of 92%,⁸⁹ but has significantly lower sensitivity in MALT lymphoma (50%).⁸⁰ One should be cautious in the interpretation of gastric Ga uptake, as it has been reported to occur in 10% of patients without disease involvement,⁹⁰ likely due to reflux of biliary contents into the stomach.

Ga-SPECT for restaging, assessing response to therapy, and evaluation of a residual mass

One of the major dilemmas after therapy is assessment of the residual mass, and whether this mass is due to fibrosis, associated with a good prognosis and no need for further therapy,^{58,91–93} or whether it is due to residual or progressive disease, which is associated with poor prognosis and necessitates further treatment. Residual masses are present in 20–60% of NHL^{92,94} and 50–64% in HD.^{91,95–97} Of these residual masses, 59% disappear without further treatment and 45% disappear within 1 year.⁵⁸ Disease activity in a residual mass was correlated with the presence of Ga uptake, which predicted poor clinical outcome.^{95,96} In 25 lymphoma patients, Ga became negative in 95%, compared to 57% in CT.¹⁶ Post-therapy Ga had a positive predictive value of 73% in 43 patients with HD and 80% in 56 patients with NHL, compared with 35% and 29% respectively for CT.¹³ Disease-free survival of patients with negative post-therapy Ga was significantly better than that of patients with positive post-therapy Ga, whereas there was no significant difference in the disease-free survival of patients with positive or negative post-therapy CT.¹⁴ In HD patients with suspected residual mediastinal disease who had biopsy confirmation, Ga-SPECT had a sensitivity and specificity of 96% and 80% respectively,^{81,98} as compared with 68% and 60% for CT. Twenty-seven percent of patients with positive biopsies had a non-conclusive CT. Normal Ga post-therapy indicates remission, whereas positive Ga in a residual mass on CT implies disease progression.⁹⁹ This is supported by other studies, showing a 100% 4-year survival rate of patients with negative Ga compared to 51% in patients with positive Ga.^{100,101} It has been shown that abnormalities in patients who respond to therapy tend to persist on MRI for up to 6 months, due to inflammatory changes, fibrosis, and necrosis, whereas Ga normalizes more rapidly.¹⁰²

Ga-SPECT for assessment of prognosis

In patients with aggressive NHL, follow-up Ga can predict outcome better than can CT.¹⁰³ When abnormalities on Ga persist, or a negative scan turns positive, the outcome is poor. At the end of chemotherapy, patients with persistent

Ga-positive scans are likely to have local relapse, whereas when Ga is negative they remain disease-free despite a positive CT.⁹³ In HD, Ga has a positive predictive value of 85% and a negative predictive value of 87% at the end of therapy. When Ga is negative at the end of therapy the relapse rate is 19.7%, compared to 84.6% in patients with positive Ga.¹⁰⁰ Similarly, Salloum et al. found a high negative predictive value of Ga in stages I and II, but relapse had occurred in this series in 34% of patients with stage III and IV disease, despite negative Ga.¹⁰⁴ This finding can be explained by the failure of Ga to detect small-volume viable tumor, mainly if surrounded by a large volume of fibrosis and/or necrosis.

Ga-SPECT evaluation of rapidity of response to therapy

Early response to therapy and achievement of an early CR predicts a favorable outcome.^{18–20,22,105} Israel et al. found, in patients with aggressive NHL, that Ga after one course of chemotherapy and at mid-treatment was a significant variable and a better indicator of response rate and failure-free survival compared to pretreatment risk factors.²¹ Similar findings were reported by the same group for HD and NHL patients.^{19,20} Kaplan et al. found a 3-year disease-free survival rate of 70% of patients with aggressive NHL and negative Ga at mid-treatment, compared to 24% when Ga was positive.¹⁰⁶ Other studies have demonstrated that the prediction of outcome is more accurate when Ga imaging is performed early during treatment. The relapse rate of patients with early CR was significantly lower as compared to patients who achieved late CR (20% vs. 60%).¹⁰⁵ In patients with bulky NHL, Janicek et al. found that Ga after two cycles of chemotherapy is a better predictor of response compared to Ga at the end of four cycles.¹⁸ A positive Ga early during treatment can identify patients who will not respond and may benefit from early modification of their treatment.

Ga-SPECT for early detection of recurrence

Early detection of recurrent lymphoma is critical, as treatment is more effective in patients with minimal disease. In 139 patients with large-cell NHL who were in CR, Weeks et al.¹⁰⁷ found that Ga was the most sensitive technique with a sensitivity of 90% to detect early recurrence in 36 patients. Front et al. found that follow-up Ga can detect recurrent disease 8.6 months before clinical symptoms and other diagnostic tests.¹⁷ About 25% of relapses occur only in new sites;^{17,107} therefore, whole-body imaging and serial follow-up studies are important in patients in CR.

Other SPECT agents

Additional SPECT agents have been assessed as lymphoma-seeking tracers. In comparison with Ga, ^{201}Tl (Tl) is more specific in differentiating lymphoma from inflammatory lesions, and its uptake is not affected by steroid administration, or by prior chemo- or radiotherapy. The uptake appears to be higher in low-grade than in high-grade lymphoma, and in low-grade lymphoma T₁ appears to be more sensitive than Ga.¹⁰⁸ A sensitivity of 100% for HD, low-grade, and intermediate-grade NHL, and 75% in high-grade NHL, was reported.¹⁰⁸ Tl may solve causes for false-positive Ga results, such as benign thymic hyperplasia and benign hilar uptake, where it appears to be more accurate than Ga in ruling out the presence of active lymphoma.^{12,109}

[$^{99\text{m}}\text{Tc}$]methoxyisobutylisonitrile (MIBI) has a lower sensitivity and specificity for the assessment of lymphoma as compared to Tl: 71% and 76%, respectively.¹¹⁰ However, studies in cell cultures have shown that the uptake of MIBI is higher in malignant cells that do not develop multidrug resistance following chemotherapy.^{111,112} MIBI was positive in most patients with complete or partial response, and was negative in patients who did not respond to therapy or had tumor progression.¹¹³ The potential role for MIBI in the evaluation of multidrug resistance in treated lymphoma is unclear, although it has been suggested that a positive scan in a residual tumor may suggest the need to use non-cross-resistant chemotherapeutic drugs.¹²

Somatostatin receptors have been demonstrated in HD and NHL; however, their density is low.¹¹⁴ In a prospective study in 126 patients with HD, somatostatin-receptor scintigraphy (SRS) had a site-based sensitivity of 98% for lesions above the diaphragm and 67% below the diaphragm.¹¹⁵ In NHL an inverse correlation has been demonstrated between the expression of somatostatin receptors and the degree of lymphoma differentiation. In a prospective study in 50 patients with low-grade NHL, SRS was positive in 84%.¹¹⁶ In 20% of patients, SRS revealed unsuspected lesions, but in 38% lesions were missed. SRS is not used routinely in the management of patients with lymphoma.

Different monoclonal antibodies (mAb) were evaluated for the imaging of lymphoma, but have not gained widespread acceptance, possibly because of cost and availability, but also due to the evolving role of PET in lymphoma patients. Lymphomas are radiosensitive and also have easy access via the blood; therefore, B-cell lymphomas and HD appear to be good targets for radioimmunotherapy (RIT). As treatment strategies include mAb, scintigraphy performed prior to RIT may gain new clinical significance.¹¹⁷ Uptake in the specific lymphoma at hand should first be confirmed by imaging with mAb, which could also be used for dosimetry calculations.¹¹⁸

Metabolic imaging modalities of lymphoma

The use of FDG-PET in lymphoma and other tumors is based on the concentration and metabolic trapping of the glucose analog, FDG, in malignant cells.¹¹⁹ The glycolytic metabolic rate of malignant cells is higher than in normal tissues. This metabolic imaging modality detects changes in tumor biology, allowing for early detection of disease as compared to conventional anatomical imaging modalities, which can only detect morphological changes.¹²⁰ Over the past decade PET has become the most important nuclear medicine technique in the assessment of lymphoma. Recently, the use of combined PET-CT scanners has resulted in an improved resolution of approximately 3.5 mm, automatic co-registration of FDG-PET and CT images, reduced scanning time, and improved signal-to-noise ratio.¹²¹ With attenuation corrected PET images it is also possible to quantify the degree of FDG uptake in treated and untreated lymphoma by the use of standardized uptake values (SUVs) (ratio of activity per volume unit over injected activity per body mass).

Imaging protocol

Imaging is performed about 60–90 minutes after the injection of 370 MBq of FDG. When using PET-CT, CT images are acquired first and are used for attenuation correction and for precise anatomical localization of PET findings. Intravenous and sometimes also oral contrast can be used, and some centers apply standardized breathing protocols during acquisition of the CT component. In follow-up studies during or after the completion of treatment, PET should be performed at least 10 days after the last treatment cycle. Early after treatment, false-negative studies as well as false-positive findings may occur, due to an inflammatory response to chemo- or radiotherapy.¹²²

Knowledge of the normal biodistribution of FDG is of major importance in lymphoma, a multifocal disease that can be located in any region of the body and affect all organs. Intense physiologic FDG uptake is seen in the brain. Urinary excretion of FDG accounts for activity in the collecting systems of the kidneys, variable visualization of the ureters and urinary bladder, and low-level renal parenchymal activity. Myocardial uptake is variable and increases in the presence of high insulin blood levels. In an attempt to minimize myocardial activity, patients are instructed to fast for 4–6 hours. Mildly intense activity is seen throughout the liver, and may limit FDG-PET sensitivity for small liver lesions. Normal bowel activity, usually of low intensity, can be seen in the esophagus (mainly the gastroesophageal junction), stomach, small bowel,

and colon. The correct localization of sites of increased activity is facilitated by the use of integrated PET–CT. Differentiating normal bowel activity from pathological, clinically significant uptake can occasionally be difficult. Focally intense activity should be interpreted with suspicion, and can be related to inflammatory processes, or pre-malignant or malignant lesions. Muscular FDG activity varies with insulin level, and is also higher following strenuous exercise. The neck is a frequent site for benign muscular activity, but physiologic uptake can occur even in small muscles such as the vocal cords. Physiologic low-level FDG uptake is noted in the oropharynx, tonsils, salivary glands, thyroid, breast, and bone marrow. Focal increased bone marrow activity is suspicious for malignancy, although it can also occur due to benign reasons. Diffusely increased bone marrow activity can be seen in patients with activated bone marrow secondary to treatment with colony-stimulating factor or anemia.¹²³

In recent years, FDG studies have been reviewed with attenuation correction provided by PET–CT systems. Non-attenuation corrected images may be useful in evaluation of the lung fields, to better localize lesions in the periphery of the lung vs. pleura, skin lesions in cutaneous lymphoma, or the liver in large patients to decrease the incidence and severity of reconstruction artifacts.¹²³

There are many causes of benign FDG activity on PET scans. False-positive results may be related to the presence of inflammatory processes showing significant FDG uptake, sites of prior surgery or biopsy causing low-grade activity, and recent chemo- or radiation therapy. Recent trauma can also cause false-positive results of FDG-PET. Children and young adults may show increased FDG uptake in the anterior mediastinum due to thymic hyperplasia, more frequent after treatment.¹²³

Tumor biology

Preliminary studies showed that higher-grade lymphomas tend to have higher FDG uptake than that of low-grade tumors.^{124–128} Most large B-cell NHL, mantle cell, follicular lymphoma, and HD are FDG-positive,¹²⁹ and only 6% of these tumors have non FDG-avid disease. However, the sensitivity of FDG-PET is lower in marginal zone lymphoma,¹³⁰ mainly in extranodal sites,¹³¹ and is only 50% in small lymphocytic lymphoma.^{132,133} In 42 patients with NHL, Jerusalem et al.¹³² report that PET identified 40% more abnormal sites compared to conventional imaging modalities in 24 patients with follicular histology, but fewer than 58% of CT abnormalities in 11 patients with small lymphocytic lymphoma. There are contradictory data about the relationship between FDG uptake in tumors measured as SUV and the grade of malignancy. Some authors report that patients with lymphomas with a high

glycolytic rate had a higher mitotic rate, a higher-grade malignancy, and poor prognosis,^{124,126,134} whereas others found no significant differences between low-grade and high-grade lymphoma,¹³⁵ and report a good performance of FDG-PET in low-grade lymphoma.^{132,133,136}

FDG-PET for initial staging of lymphoma

The prognosis of both HD and NHL and the therapeutic strategy depend on the histological type and disease stage. Correct staging is an important factor for selection of the most appropriate treatment. Staging is performed using conventional imaging studies including CT or MRI, in addition to the clinical history, physical examination, and laboratory data. FDG-PET imaging is more accurate than Ga-SPECT, and has therefore replaced it, where available.^{137,138} Because of concerns about the long-term toxicity of high-dose irradiation and alkylating agent chemotherapy, such as MOPP,¹³⁹ combined modality protocols now include low-dose radiotherapy and chemotherapy with non-alkylating agents, such as ABVD (doxorubicin, bleomycin, vinblastine, dacarbazine). Patients with bulky (< 10 cm) stage I or II disease and patients with advanced disease are treated with 6–8 cycles of chemotherapy followed by radiotherapy to the initial site of bulky disease. The detection of more extensive disease at initial staging using PET rather than conventional imaging can upstage disease and alter management. For example, the detection of more extensive disease in patients previously considered to have limited stage I or II HD will lead to chemotherapy or combined modality treatment instead of only radiotherapy. Due to the fact that lymphoma is a systemic disease and usually not treated surgically, it is problematic to obtain pathologic validation for each suspected site on PET or CT. The true accuracy of anatomic and metabolic imaging modalities cannot therefore be precisely assessed, except for selected cases in which a change in stage will occur and will cause a change in treatment. An alternative strategy to confirm the presence or absence of disease is long-term clinical follow-up.

Several studies have shown superior sensitivity of FDG-PET compared to CT for the staging of lymphoma^{28,140–143} (Figure 14.2). In 60 consecutive patients with HD and NHL, Moog et al. showed that PET is superior to CT in the initial staging. FDG-PET correctly identified all abnormalities seen on CT, detected additional CT-negative lesions, and excluded disease in one false-positive CT lesion.¹⁴⁴ In a prospective study in 45 patients with newly diagnosed and four patients with relapsed HD, including 38 patients who had pathological validation of all abnormalities detected on CT and PET, PET was superior to CT with a sensitivity, specificity, positive predictive value, and negative predictive value of 100%,

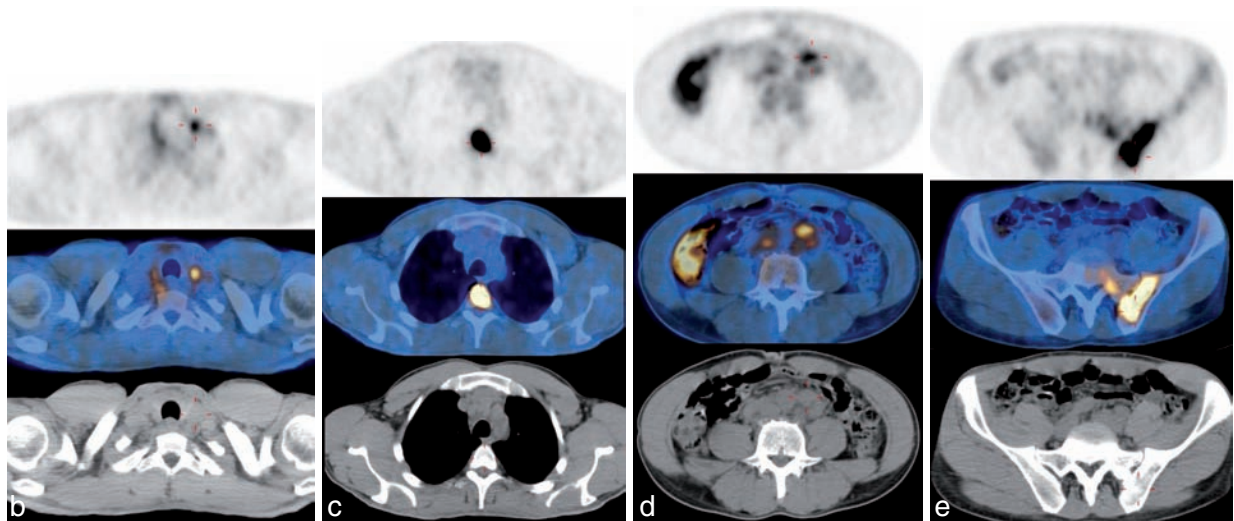
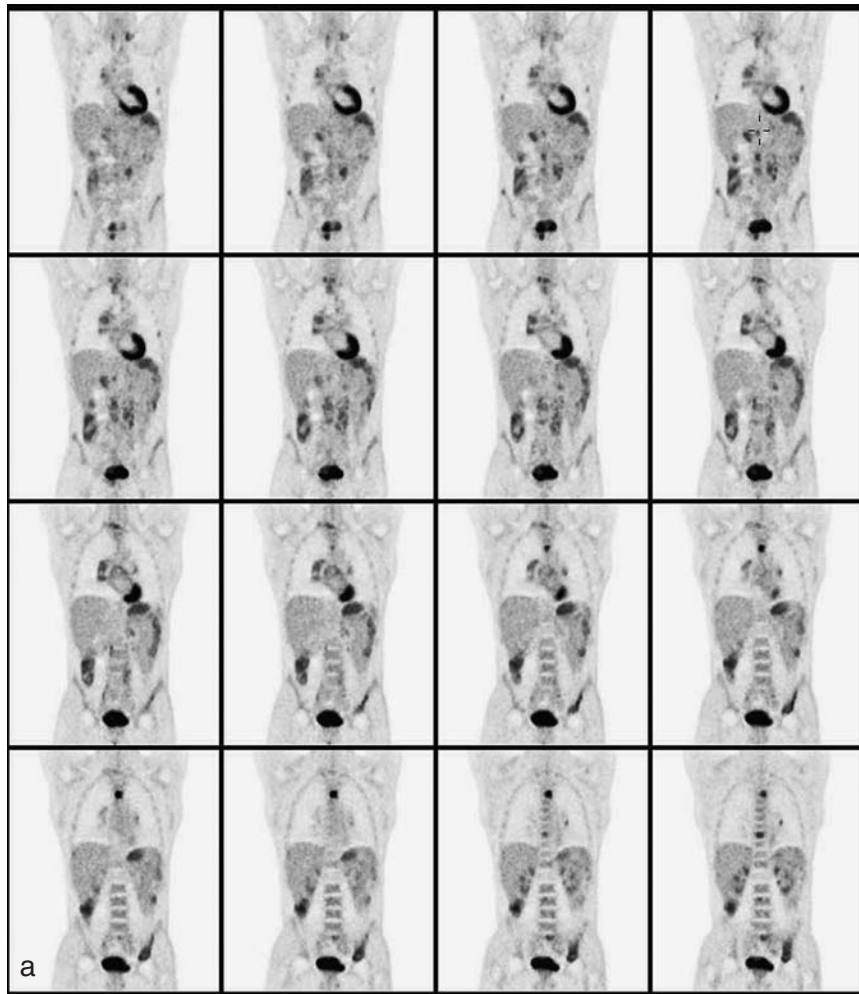


Figure 14.2

[¹⁸F]fluoro-2-deoxy-D-glucose-positron emission tomography-computed tomography (FDG-PET-CT) at diagnosis: initial staging of Hodgkin's disease with nodal and extranodal (skeletal) involvement, in a 41-year-old man. (a) PET study, coronal slices show foci of abnormal FDG uptake involving disease sites above and below the diaphragm: bilateral supraclavicular, hilar, para-aortic and para-iliac lymphadenopathy, as well as additional foci of unclear location. (b) Transaxial PET (top), PET-CT (center), and CT (bottom) images show the precise localization of abnormal FDG uptake to an enlarged left supraclavicular lymph node. (c) Transaxial PET (top), PET-CT (center), and CT (bottom) images show the precise localization of abnormal FDG uptake to the T9 vertebral body. (d) Transaxial PET (top), PET-CT (center), and CT (bottom) images show the precise localization of abnormal FDG uptake to an enlarged left para-iliac lymph node. (e) Transaxial PET (top), PET-CT (center), and CT (bottom) images show the precise localization of abnormal FDG uptake to a sclerotic lesion in the left iliac bone.

compared to 20%, 83%, 50%, and 56% respectively for CT. PET changed the stage of HD in 59% of the patients.¹⁴⁵ In 45 patients with newly diagnosed HD and NHL, where discordant lesions on CT and FDG-PET were verified by biopsy or clinical follow-up, Delbeke et al.¹⁴⁶ report that FDG-PET correctly changed the initial staging in 16% of patients, followed by a change in therapy in 13% of patients, but also understaged 7% of patients. The authors therefore conclude that FDG-PET can be used efficiently for staging lymphoma in conjunction with conventional imaging modalities. Hueltschmidt et al.¹⁴⁷ report that PET had an accuracy of 96% in the initial staging of HD compared to 56% for the conventional imaging modalities, including CT, and in some cases MRI and US. FDG-PET resulted in a change in stage in 40% of these patients. In another prospective study PET changed the staging in 8% of patients with 1297 nodal, extranodal, and bone marrow sites. PET was significantly more accurate than CT in all sites and was comparable to bone marrow biopsy for intramedullary involvement.¹⁴³ Since no attenuation correction was used, PET and CT were found to have similar accuracy in the abdomen, but PET was significantly more accurate for sites above the diaphragm. Wirth et al.¹⁴⁸ found a sensitivity of 95% for PET and 90% for CT, clinical examination, and bone marrow biopsy. The improved site sensitivity of PET (82% vs. 68%) led to a change in staging in 14% and change in management in 18% of patients, including altered radiation fields in 4% of cases. A summary of recent studies shows an improved sensitivity of PET compared to CT (79–99% vs. 65–90%), and similar specificities of 99–100%.¹³⁴

Overall, it has been shown that FDG-PET has a higher sensitivity for disease detection compared to conventional imaging.^{23,137,140,144,149} It changes the staging in 10–14% of patients, and may also lead to a modification of treatment. It should be noted, however, that most literature data currently available analyzed studies performed using first-generation PET scanners, with no attenuation correction and inaccurate anatomical localization of lesions. PET–CT may have a further impact on the staging of lymphoma, overcoming pitfalls which are due to physiological FDG uptake.^{121,150–152}

FDG-PET in extranodal lymphoma

FDG-PET was shown to be superior to CT also in the detection of extranodal involvement of lymphoma^{149,153–156} (Figure 14.2). In 81 patients with HD and NHL, Moog et al. found that PET modified staging by either detection of spleen, liver, and bone involvement or by excluding sites falsely reported as disease on CT.¹⁵³ Schaefer et al. showed in 60 lymphoma patients better sensitivity of PET–CT compared to CT for detection of extranodal involvement (88% vs. 50%). The specificity of PET–CT was also better (100% vs. 90%).¹⁵¹ In 103 patients with HD and NHL,

PET–CT changed the staging of patients considered to have stage I and II, detecting involvement in small, normal-sized lymph nodes, and in extra-nodal sites, including the spleen, liver, thymus, cortical bone, bone marrow, lung, and pleura, which were all missed on CT.¹⁵⁵

Mucosa-associated lymphoid tissue (MALT) lymphoma involves mainly the gastric mucosa and less commonly may involve the skin, thyroid, breast, thymus, orbit, liver, kidney, prostate, urinary bladder, and gall bladder.^{41,157,158} Twenty-five percent of patients may have multiple sites of disease, including the bone marrow.¹⁵⁹ Initially MALT lymphoma was considered to be non-FDG-avid.¹⁶⁰ However, a study in 175 patients with MALT lymphoma reported a sensitivity of PET–CT of 81%, which may potentially be related, although this is not proven, to technological improvement.¹⁶¹

The gastrointestinal tract is the most common extranodal site in NHL, and gastrointestinal lymphoma occurs in 10–15% of NHL and 30–40% of the extranodal NHL.⁴¹ Physiological FDG uptake may cause false-positive and false-negative results.¹⁵³ The use of PET–CT and of oral contrast appears, however, to improve the performance of the study.^{162,163}

Hepatic or splenic lymphomatous involvement may present as diffuse or mass-forming disease. Liver involvement is present in 3% of newly diagnosed HD and 15% of newly diagnosed NHL. Splenic involvement is present in 30–40% of patients with HD^{34,164} and 22% of patients with NHL.¹⁵³ Only limited data are available on the role of FDG-PET in the evaluation of splenic lymphoma, suggesting better accuracy for PET compared to CT.^{165,166}

Bone marrow involvement occurs in 10% and 25% of newly diagnosed HD and NHL, respectively.¹⁵³ It has been previously shown that FDG-PET can accurately demonstrate bone marrow lymphoma infiltration. Carr et al.¹⁶⁷ showed an accuracy of 93% of PET for the detection of bone marrow involvement, while Moog et al. reported an accuracy of 95%, superior to bone marrow biopsy and CT.¹⁶⁸ However, Jerusalem et al.¹³² found that FDG-PET is not reliable for the exclusion of bone marrow involvement in low-grade lymphoma, probably due to a lower sensitivity of FDG-PET in LG-NHL, or to a diffuse rather than focal pattern of involvement, and therefore more difficult to diagnose. Treatment with granulocyte colony-stimulating factors can cause increased FDG uptake by the bone marrow, which may be difficult to differentiate from active marrow disease.¹⁶⁹

In the region of the head and neck there is physiologic FDG uptake in the buccal region, nasopharynx, tonsils, and nasal cavity. Increased FDG uptake can also be related to an inflammatory or infectious process in this region. Corresponding CT findings may assist in the diagnosis. Focal or diffusely increased FDG uptake may be observed in thyroid lymphoma. These findings are, however, non-specific, and may also be caused by benign lesions, such as goiter, thyroiditis, adenoma, or thyroid cancer.¹⁷⁰

Lymphoma of the central nervous system (CNS) accounts for 2–4% of extranodal lymphomas and 1–4% of

malignant brain tumors.⁴¹ However, this incidence increases in immunocompromised patients.¹⁷¹ Because of physiological FDG uptake in the cortex, diagnosis of lymphoma in this area is problematic. FDG-PET is also unable to differentiate between primary CNS lymphoma and other malignancies or infectious processes.¹⁷²

FDG-PET for restaging, assessing response to therapy, and evaluation of a residual mass

The role of FDG-PET in assessing response to treatment has been evaluated in heterogeneous patient populations, including HD and NHL. Cremerius et al.¹⁷³ reported a better specificity and positive predictive value for FDG-PET

compared to CT (92% and 94% for PET vs. 17% and 60% for CT, respectively). In 44 patients with residual abdominal masses reported by Zinzani et al.,¹⁷⁴ none of the seven patients who had negative PET and CT relapsed. In the remaining 37 patients with positive CT findings, 13 patients with a positive PET relapsed, as compared to only one of 24 patients with a negative PET. The majority of relapses occurred at sites showing persistent FDG uptake at the time of therapy completion. The 2-year relapse-free survival was 95% for the PET-negative group and 0% for the PET-positive group.¹⁷⁴ Jerusalem et al.¹⁷⁵ evaluated post-treatment PET and CT at completion of treatment in 54 patients with HD and NHL. PET had a positive predictive value for relapse of 100% compared to 42% for CT ($p > 0.05$), and patients with a positive PET scan had a 1-year progression-free survival rate of 0% compared to 86% in cases with negative PET after treatment ($p > 0.0001$). In 848 patients with NHL and HD, Castellucci et al.²⁷



Figure 14.3

Negative FDG-PET at the end of treatment: assessment of complete response and good prognosis. (a) Baseline PET study of a 76-year-old woman with immunoblastic T-cell non-Hodgkin's lymphoma, shows abnormal FDG uptake in left cervical, supraclavicular, and anterior mediastinal lymph nodes.

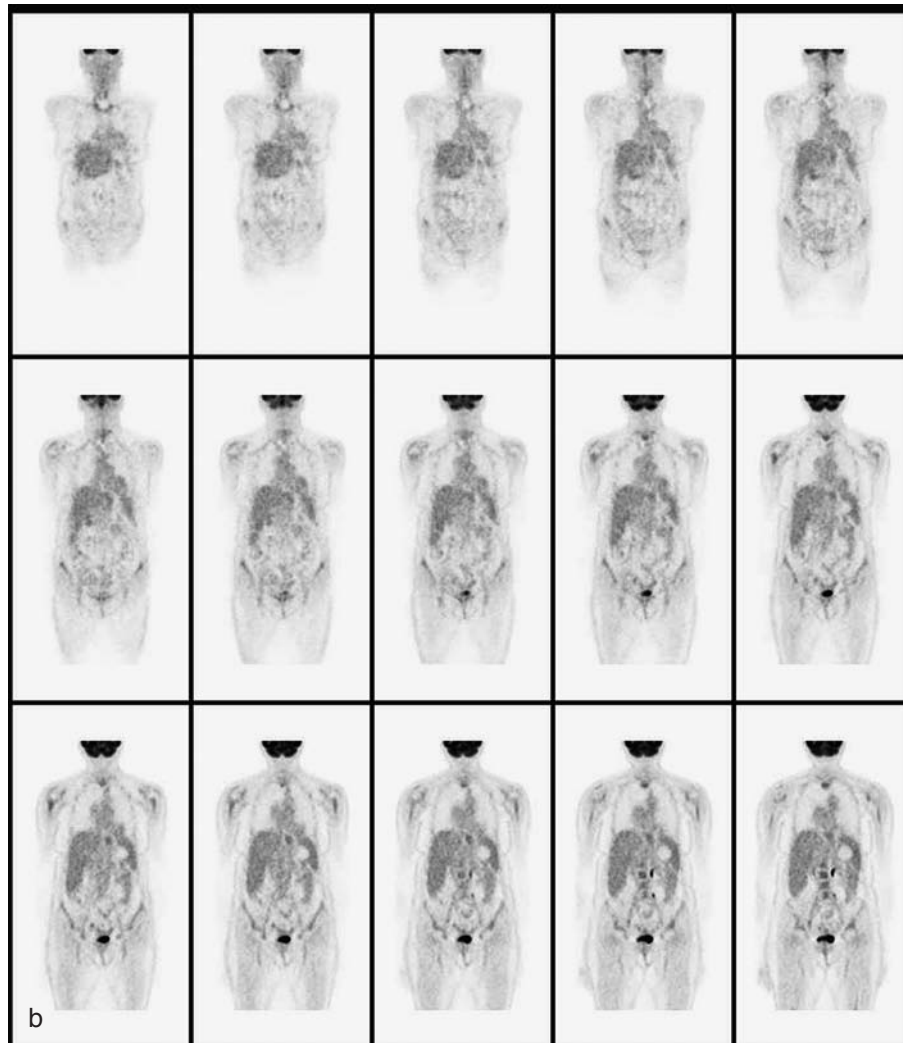


Figure 14.3, cont'd

(b) Repeat FDG-PET, performed at the end of chemotherapy (CHOP (cyclophosphamide, doxorubicin, vincristine, prednisone) protocol), is negative, showing no evidence of active disease. The patient achieved a complete response.

reported a true-negative rate for PET of 100%, and a false-positive rate of only 5%, mainly due to inflammation. In patients with NHL, Mikhael et al.¹⁷⁶ found FDG-PET to be more accurate than CT in the assessment of achieving a remission after treatment (Figure 14.3). PET-positive patients had a relapse rate of 100%, as compared to 17% in PET-negative patients, whereas the relapse rate for patients with positive and negative CT at the end of treatment was 41% and 25%, respectively. The 1-year progression-free survival was 0% for the PET-positive and 83% for the PET-negative group.¹⁷⁶ Spaepen et al.¹⁷⁷ report a high predictive value of FDG-PET for the detection of residual or recurrent lymphoma. All patients with persistent FDG uptake had a recurrence. The 2-year progression-free survival was 85% for PET-negative and 4% for PET-positive patients.¹⁷⁷ Jerusalem et al.¹³² found 0% 1-year progression-free survival in patients with a positive PET compared to 86% in

patients with a negative study ($p > 0.0001$), as well as a significantly lower overall survival at 1 year of PET-positive patients (50% vs. 92%, $p > 0.001$). Based on the combination of PET and CT results, the authors identified three prognostic groups: low-risk patients (CT negative, PET negative), intermediate-risk patients (CT positive, PET negative), and high-risk patients (CT positive, PET positive), showing significant differences between progression-free and overall survival rates.¹³² Juweid et al.¹⁷⁸ also reported higher positive and negative predictive values for 1-year progression-free survival of FDG-PET as compared to CT (92% and 88% vs. 47% and 85%, respectively).

Similar results were reported in HD patients.^{147,179–183} In 37 HD patients with 50 studies, de Wit et al.¹⁸² report a sensitivity, specificity, positive predictive value (PPV), negative predictive value (NPV), and accuracy of 91%, 69%, 46%, 96%, and 74%, respectively for the prediction of disease-free

survival for FDG-PET. They found a relatively high number of false-positive studies, causing the lower specificity and positive predictive value. In 28 HD patients with a residual mass at the end of therapy, Weihrauch et al.¹⁷⁹ report 1-year progression-free survival of 95% of patients with PET-negative studies, compared to 40% for the patients with PET-positive studies, again noting the number of false-positive results. In 60 HD patients after first-line therapy reported by Spaepen et al.,¹⁸¹ 55 patients had a negative PET after treatment and 50 of these remained in complete remission. All five patients with a positive PET relapsed. The 2-year progression-free survival was 0% in patients with a positive PET, compared with 91% in patients with a negative PET.

Discrepant results were reported regarding the predictive performance of FDG-PET after treatment. Most authors report a high negative predictive value of 90–100%, with lower values of 80–83% only infrequently presented.^{175,184} However, there is a much larger variability in positive predictive values for FDG-PET prediction of outcome, ranging from 25% to 100%, due to a relatively high false-positive rate.^{176,179,182–184} False-positive findings were due to post-irradiation inflammatory processes, mainly radiation pneumonitis, thymic hyperplasia, and muscular uptake. False-negative PET results were caused by minimal residual disease. It has been suggested that in LG-NHL, FDG-PET may be less valuable, because of a lower sensitivity on the pre-therapy study.

Overall, in NHL patients, a persistently abnormal FDG study in the initially involved disease sites is predictive of residual or recurrent disease.²⁴ FDG uptake in other sites may suggest the presence of infection, inflammation, or thymic hyperplasia. A negative study cannot exclude the presence of minimal residual disease, and therefore a relapse after a negative PET, although rare, may occur.

HD patients usually have a higher response rate, and therefore, mainly in early-stage disease, a negative FDG-PET correlates with prolonged CR. This is due mainly to the excellent prognosis of these patients, as well as to the high predictive value of a negative scan. The clinical value of the FDG-PET in HD at the end of treatment is therefore somewhat controversial.²⁴ However, in HD patients with a residual mass on CT, defining CR based only on the conventional modalities may not be possible. Positive PET at the end of therapy in HD patients is infrequent, and the chance of it being false-positive is relatively high, causing the lower positive predictive value of PET compared to its negative predictive value.^{147,179–182} Naumann et al.¹⁸⁴ reported that one of six HD patients with a positive PET relapsed (none with equivocal or low-grade FDG uptake relapsed), compared to all NHL patients with an FDG abnormality and two of three NHL patients with an equivocal study who relapsed.

It has been suggested that different algorithms should be applied for the use of post-treatment PET in different types of lymphoma.^{177,181} In NHL and high-stage HD a positive PET at the end of first-line therapy is highly suggestive of active disease, and requires intensive confirmatory investigations. A negative PET does not exclude the presence of

minimal residual disease and future relapse and requires close follow-up. On the other hand, in early-stage HD a negative PET can be used to define CR despite the presence of a residual mass on CT. A positive PET, especially if located in a site different from the original tumor or the residual mass may also be due to a benign or inflammatory etiology.

In addition to the prognostic information following standard chemotherapy, FDG-PET has also been used to predict outcome following autologous stem cell transplantation and radioimmunotherapy for recurrent lymphoma. Becherer et al.¹⁸⁵ studied 16 patients who relapsed and had FDG-PET before autologous stem cell transplantation. One-year progression-free survival and overall survival were 100% for the PET-negative patients and only 18% and 55%, respectively, for the PET-positive patients. Similar results in small numbers of patients were reported by other groups.^{186–188} Spaepen et al.¹⁸⁸ evaluated the predictive value of FDG-PET for post-transplant prognosis in 60 patients and showed a significant difference in overall and progression-free survival after high-dose chemotherapy with autologous bone marrow transplantation between patients with negative PET and those with positive PET before transplant. Twenty-five of 30 patients with negative PET achieved prolonged CR, whereas 26 of 30 patients with positive PET relapsed. PET performed 2–5 weeks after the initiation of salvage therapy was shown to predict outcome of transplantation better than CT.¹⁸⁹

In a small group of patients who received radioimmunotherapy after one or more failures of chemotherapy, Torizuka et al.¹⁹⁰ showed that FDG-PET results correlated with the response of NHL to this treatment. Patients showed a slower pattern of metabolic response to radioimmunotherapy in comparison with the response pattern to first-line chemotherapy. Delayed FDG-PET, performed 1–2 months after therapy, had a better predictive value than early PET.¹⁹⁰ Recently, Hart et al.¹⁹¹ described 15 patients who received radioimmunotherapy and showed that FDG-PET–CT provided additional information to CT in 73% of patients, influenced the administration of donor lymphocyte infusions in nine patients, and documented a graft-versus-lymphoma effect in five patients. The authors conclude that a large prospective study is needed to clarify the role of FDG-PET–CT in this clinical setting.

Evaluation of rapidity of response to therapy

Long-term prognosis of lymphoma depends not only on the pre-therapy clinical risk factors but also on the sensitivity of the individual tumor to the chemotherapeutic regimen.¹⁴⁹ Since more aggressive but also more toxic treatment modalities are available, therapy monitoring of lymphoma patients is of clinical significance. Prognostic assessment early during treatment, leading to a rapid change in therapy, might improve

outcome and survival.²⁴ Rapidity of response during treatment appears to be an accurate predictor, with early tumor regression indicating higher cure rates.¹⁰⁵ Accurate early assessment of response allows the timely institution of aggressive second-line protocols in the presence of a smaller resistant tumor load, and can also avoid treatment-related toxicity.¹⁴⁹

As previously demonstrated with Ga after one or two cycles of chemotherapy,²⁰ FDG-PET performed early during treatment allows the assessment of early response and the prediction of long-term prognosis.^{113,154,192} Initial data in small groups of patients showed significantly reduced FDG activity even after one cycle of chemotherapy.^{154,192,193} SUVs decreased by 60% at 7 days and by 76% after 42 days. A cut-off SUV of 2.5 differentiated responders from non-responders.¹⁹² Jerusalem et al. found visual assessment of FDG-PET predictive of therapy response in 28 NHL patients evaluated after 2–5 cycles of chemotherapy.¹⁹⁴ Twenty-one of 23 patients with negative PET achieved CR, whereas four of five PET-positive patients did not respond to treatment. The 2-year progression-free survival was 0% for PET-positive patients and 81% for PET-negative patients. Mikhaeel et al.¹⁷⁶ evaluated 23 NHL patients after 2–4 chemotherapy cycles. PET-positive patients had a relapse rate of 87%, compared with 0% in PET-negative patients. The same group evaluated 32 HD patients after two or three cycles of chemotherapy and found a relapse rate of 100% for the PET-positive group compared with 8% for the PET-negative group.¹⁹⁵ In a prospective study in 70 patients with aggressive NHL who had FDG-PET after three or four cycles of chemotherapy, Spaepen et al.¹⁹⁶ reported that 33 patients had persistent FDG uptake, and none of them achieved a durable CR. Of the 37 patients with a negative scan, 31 remained in CR, as compared with six who achieved only partial response (PR) or had relapse.

Kostakoglu et al.¹⁹³ evaluated response during therapy using FDG-PET with a dual-head coincidence camera after one cycle of chemotherapy in 30 patients with HD and NHL, and compared this with the post-therapy scan. The progression-free survival correlated better with FDG-PET after the first cycle than with imaging results at the end of therapy. FDG-PET had a greater sensitivity and positive predictive value after the first cycle (82% vs. 45% and 90% vs. 83%, respectively) and a lower false-positive rate (13% vs. 35%). Lowe and Wiseman¹⁹⁷ analyzed these data in a related editorial, and suggested that the less optimal post-therapy assessment could be related to the histological type of disease and the treatment protocols of these patients as well as use of the low-performance coincidence scanners.

Early detection of recurrence

Early diagnosis of relapse and early administration of salvage therapy may improve patient outcome.¹⁴⁹ FDG-PET can detect early recurrence,¹⁹⁸ and was found to be superior to conventional imaging for diagnosis and

restaging of recurrent HD and NHL (83% vs. 56%).¹⁴⁷ In 27 patients with HD and NHL, Freudenberg et al.¹⁹⁹ showed the incremental value of FDG-PET–CT imaging, which significantly improved the sensitivity and specificity for restaging lymphoma compared with CT alone (96% and 99% vs. 61% and 89%, respectively). In 36 HD patients, routine follow-up FDG-PET was positive in all five patients with recurrence, and preceded other imaging modalities by 1–9 months. Negative FDG-PET excluded relapse. However, six of the 11 positive findings were false-positive, due to hyperplastic thymus, gastrointestinal activity, and an inflammatory lung lesion.¹⁹⁴

Limitations and pitfalls of FDG-PET

FDG is not tumor-specific, and can be taken up by anti-inflammatory cells such as macrophages, leukocytes, or granulation tissue.²⁴ Common causes of false-positive studies in patients with lymphoma include radiation pneumonitis, non-specific nodal inflammatory reaction after radiotherapy, and pleural and pulmonary inflammatory lesions.¹²² In addition, physiologic uptake in thymic hyperplasia, urinary or colonic artifacts due to physiologic tracer excretion, uptake in tense muscles, and non-specific brown-fat uptake above and below the diaphragm may also cause false-positive results.²⁴

The experience of the reporting physicians with the patterns of physiologic biodistribution, artifacts, and benign FDG-avid findings unrelated to lymphoma, correlation and comparison of post-therapy with pre-therapy studies, and knowledge of clinical data and results of other imaging modalities can all reduce the incidence of false-positive results. Co-registration of PET and CT data allows for the identification of non-specific uptake, and the use of integrated PET–CT scanners will further reduce the numbers of false studies.

The limited spatial resolution of PET instrumentation may reduce the sensitivity of this modality, mainly for the detection of minimal residual or small-volume disease. The performance of FDG-PET in some LG-NHL is probably limited. Data regarding monitoring response to treatment are mainly available for HG-NHL, and these may not necessarily apply to the low-grade types of lymphoma.²⁴

Comparison of FDG-PET and Ga-SPECT imaging

In a first report of FDG uptake in lymphoma, Paul²⁰⁰ compared FDG and Ga planar imaging in five patients with NHL. FDG was positive in four, while Ga was positive in two, suggesting the potential superiority of FDG.

Both scans were negative in all patients after therapy, suggesting that both tracers can be used for monitoring response to therapy. Shen et al.²⁰¹ evaluated 25 HD and NHL patients at diagnosis and relapse. The sensitivity of FDG-PET was better as compared to Ga (96% vs. 73%), mainly due to falsely negative Ga in low-grade lymphoma, bone and bone marrow involvement, and small lesions, less than 12 mm in diameter. PET was falsely negative in only one patient with low-grade gastric NHL.

As detailed above, FDG is taken up with high avidity by LG-NHL, particularly follicular-cell lymphoma. FDG-PET and Ga were incongruent in six of 16 patients.²⁰² Kostakoglu et al. studied 50 patients with HD and NHL¹³⁷ using camera-based FDG-PET, Ga, and CT. The sensitivity of FDG-PET was superior to that of Ga for both site-based (100% vs. 72%) and patient-based (100% vs. 80%) analysis. In 84 patients who had camera-based PET and Ga and had 219 suspected disease sites, Bar-Shalom et al.²⁰³ reported a higher sensitivity of FDG-PET as compared to Ga (83% vs. 63% in patient-based analysis, and 87% vs. 33% in site-based analysis). A higher detection rate was reported for the camera-based FDG-PET compared to Ga for both nodal and extranodal lymphoma sites, and mainly for the accurate assessment of bone and bone marrow disease. In 50 patients, Wirth et al.¹⁴⁸ reported a sensitivity of 95% for PET vs. 88% for Ga on a patient-based analysis and 82% vs. 61% on the site-based analysis. Both modalities altered staging in 14% of patients, compared to CT. Clinical management was modified in 18% of patients based on PET and in 14% based on Ga, again compared to CT. In 32 HD patients with splenic involvement, FDG-PET was superior to Ga, with sensitivity, specificity, and accuracy of 92%, 100%, and 97% vs. 50%, 95%, and 78%, respectively.¹⁶⁵ FDG-PET was also found to be superior to Ga for early monitoring of response to treatment in 26 NHL patients evaluated after two cycles of chemotherapy.²⁰⁴

Other PET agents

Amino-acid utilization is increased in malignant lymphoma.²⁰⁵ Methionine is an essential amino acid, and its tissue uptake and tracer kinetics reflect the metabolism of essential amino acids. [¹¹C]-labeled methionine was compared with FDG-PET in 14 patients with head and neck NHL,²⁰⁶ and was positive in 13/14 patients compared to 8/14 for FDG. In 17 patients with HD and NHL, Sutinen et al. reported comparable sensitivities of FDG-PET and [¹¹C]methionine-PET.²⁰⁷ Due to unfavorable biodistribution in the abdomen and the short half-life of ¹¹C, this tracer is not widely used. However, to avoid some of the pitfalls related to the reduced specificity of FDG-PET, and as data suggest comparable sensitivity to that of FDG-PET, it

may be of use in selected cases, such as hyperglycemic patients.

Thymidine is incorporated into DNA in correlation to cellular proliferation. [³H]thymidine has been used in experimental tumor models to measure proliferation rates. 3'-[¹⁸F]thymidine (FLT) was developed as a PET imaging agent to evaluate tissue proliferation in vivo.^{206,208} FLT showed comparable detection rates to those of FDG in nine patients with NHL.²⁰⁹ In another report of the same group there was excellent separation between aggressive and indolent lymphoma types using FLT as a measure of malignancy grade.²¹⁰ As a marker of proliferation, this tracer may prove suitable for monitoring response to therapy.

Receptors for somatostatin are expressed in relatively low density on lymphoma cells.^{211,212} Octreotide derivatives were labeled with positron emitters ⁶⁴Cu, ⁶⁸Ga, and ⁸⁶Yr. These could represent potential tracers for the imaging of lymphomas for diagnostic purposes as well as for targeting internal radiation therapy.

Conclusion

FDG-PET is considered at present to be more sensitive than conventional imaging modalities for the staging of lymphoma patients, leading mainly to upstaging and, in smaller numbers, to downstaging of the disease. PET further plays an important role in monitoring response to treatment and in restaging of disease, and is therefore routinely used for post-therapy evaluation in patients with nodal and extranodal lymphoma. Persistent FDG uptake during and after chemotherapy indicates a poor prognosis and high likelihood of relapse, while a negative study indicates a good prognosis. Therefore, FDG-PET may be used to guide and follow therapy and to improve the outcome of patients. The use of integrated PET-CT scanners with radiotherapy, planning CT to better define radiation fields and to minimize radiation exposure, may improve the management of lymphoma patients in the future.

Nuclear medicine techniques have for decades played a significant role in the evaluation of lymphoma patients along the course of their disease. The concept of using nuclear medicine procedures as functional indices of the presence of viable tumor tissue and for monitoring the success or resistance to treatment has evolved from the use of this modality in lymphoma. The incremental value of the metabolic information provided by nuclear medicine procedures in general and specifically by PET in the assessment of lymphoma is well established. PET and CT are not competing but rather complementing techniques, and therefore the integrated PET-CT devices are widely accepted by the imaging community and by the referring clinical teams.

References

1. Boring C, Squires T, Tong T et al. Cancer statistics. *Cancer J Clin* 1994; 44: 7–26.
2. Smith SD, Rubin CM, Horvath A et al. Non-Hodgkin's lymphoma in children. *Semin Oncol* 1990; 17: 113–19.
3. Lukes RJ, Butler JJ. The pathology and nomenclature of Hodgkin's disease. *Cancer Res* 1966; 26: 1063–83.
4. Rosenberg SA. Report of the committee on staging of Hodgkin's disease. *Cancer Res* 1966; 26: 1310.
5. Harris NL, Jaffe ES, Stein H et al. A revised European-American classification of lymphoid neoplasms: a proposal from the International Lymphoma Study Group. *Blood* 1994; 84: 1361–92.
6. Gall EA, Mallory TB. Malignant lymphoma: a clinico-pathological survey of 618 cases. *Am J Pathol* 1942; 18: 1341–429.
7. Aisenberg AC. Historical review of lymphomas. *Br J Haematol* 2000; 109: 466–76.
8. Hicks EB, Rappaport H, Winter WJ. Follicular lymphoma: a re-evaluation of its position in the scheme of malignant lymphoma, based on a survey of 253 cases. *Cancer* 1956; 9: 792–821.
9. Non-Hodgkin's Lymphoma Classification Project: National Cancer Institute study of classifications of non-Hodgkin's lymphomas: summary and description of a working formulation for clinical usage. *Cancer* 1982; 49: 2112–35.
10. Front D, Bar-Shalom R, Israel O. Role of gallium 67 and other radiopharmaceuticals in the management of patients with lymphoma. In: Freeman LM, ed. *Nuclear Medicine Annual*, 1998. New-York: Raven Press, 1998: 247–64.
11. Bar-Shalom R, Mor M, Yefremov N, Goldsmith SJ. The value of Ga-67 scintigraphy and F-18 fluorodeoxyglucose positron emission tomography in staging and monitoring the response of lymphoma to treatment. *Semin Nucl Med* 2001; 31: 177–90.
12. Even-Sapir E, Israel O. Gallium-67 scintigraphy: a cornerstone in functional imaging of lymphoma. *Eur J Nucl Med Mol Imaging* 2003; 30 (Suppl 1): S65–81.
13. Front D, Israel O, Epelbaum R et al. Ga-67 SPECT before and after treatment of lymphoma. *Radiology* 1990; 175: 515–19.
14. Front D, Ben-Haim S, Israel O et al. Lymphoma: predictive value of Ga-67 scintigraphy after treatment. *Radiology* 1992; 182: 359–63.
15. Gasparini M, Bombardieri E, Castellani M et al. Gallium-67 scintigraphy evaluation of therapy in non-Hodgkin's lymphoma. *J Nucl Med* 1998; 39: 1586–90.
16. Israel O, Front D, Lam M et al. Gallium 67 imaging in monitoring lymphoma response to treatment. *Cancer* 1988; 61: 2429–43.
17. Front D, Bar-Shalom R, Epelbaum R et al. Early detection of lymphoma recurrence with gallium-67 scintigraphy. *J Nucl Med* 1993; 34: 2101–4.
18. Janicek M, Kaplan W, Neuberg D et al. Early restaging gallium scans predict outcome in poor-prognosis patients with aggressive non-Hodgkin's lymphoma treated with high-dose CHOP chemotherapy. *J Clin Oncol* 1997; 15: 1631–7.
19. Front D, Bar-Shalom R, Mor M et al. Hodgkin disease: prediction of outcome with ⁶⁷Ga scintigraphy after one cycle of chemotherapy. *Radiology* 1999; 210: 487–91.
20. Front D, Bar-Shalom R, Mor M et al. Aggressive non-Hodgkin lymphoma: early prediction of outcome with ⁶⁷Ga scintigraphy. *Radiology* 2000; 214: 253–7.
21. Israel O, Mor M, Epelbaum R et al. Clinical pre-treatment risk factors and Ga-67 scintigraphy early during treatment for prediction of outcome of patients with aggressive non-Hodgkin lymphoma. *Cancer* 2002; 94: 873–8.
22. Reske SN. PET and restaging of malignant lymphoma including residual masses and relapse. *Eur J Nucl Med Mol Imaging* 2003; 30 (Suppl 1): S89–96.
23. O'Doherty MJ, Hoskin PJ. Positron emission tomography in the management of lymphomas: a summary. *Eur J Nucl Med Mol Imaging* 2003; 30 (Suppl 1): S128–30.
24. Spaepen K, Stroobants S, Verhoef G, Mortelmans L. Positron emission tomography with [¹⁸F]FDG for therapy response monitoring in lymphoma patients. *Eur J Nucl Med Mol Imaging* 2003; 30 (Suppl 1): S97–105.
25. Torizuka T, Nakamura F, Kanno T et al. Early therapy monitoring with FDG-PET in aggressive non-Hodgkin's lymphoma and Hodgkin's lymphoma. *Eur J Nucl Med Mol Imaging* 2004; 31: 22–8.
26. Hicks RJ, MacManus MP, Seymour JF. Initial staging of lymphoma with positron emission tomography and computed tomography. *Semin Nucl Med* 2005; 35: 165–75.
27. Castellucci P, Zinzani PL, Pourdehnad M et al. ¹⁸F-FDG in malignant lymphoma: significance of positive findings. *Eur J Nucl Med Mol Imaging* 2005; 32: 749–56.
28. Hoskin PJ. PET in lymphoma: what are the oncologist's needs? *Eur J Nucl Med Mol Imaging* 2003; 30 (Suppl 1): S37–41.
29. Hagemester FB. Hodgkin's disease: the next decade. *Leuk Lymph* 1996; 21: 53–61.
30. Sandrasegaran K, Robinson PJ, Selby P. Staging of lymphoma in adults. *Clin Oncol* 1994; 94: 149–61.
31. Marglin SI, Castellino RA. Selection of imaging studies for the initial staging of patients with Hodgkin's disease. *Semin US CT MR* 1985; 6: 380–93.
32. De Vita VY, Hellman S, Jaffe ESW. Hodgkin's disease. In: DeVita VT, Hellman S, Rosenberg S, eds. *Cancer Principles and Practice of Oncology*. Philadelphia: JB Lippincott 1993; 1819–59.
33. Freeman C, Berg JW, Cutler SJ. Occurrence and prognosis of extranodal lymphoma. *Cancer* 1972; 29: 252–60.
34. Guermazi A, Brice P, de Kerviler EE et al. Extranodal Hodgkin disease: spectrum of disease. *Radiographics* 2001; 21: 161–79.
35. Carbonne PP, Kaplan HS, Musshof K et al. Report of the committee on Hodgkin's disease staging. *Cancer Res* 1971; 31: 1860–1.
36. Jotti G, Bonadonna G. Prognostic factors in HD: implications for modern treatment. *Anticancer Res* 1988; 8: 749–60.
37. Devesa SS, Fears T. Non-Hodgkin's lymphoma time trends. *Cancer Res* 1992; 52: S5432–40.
38. Canellos GP. Current strategies for early Hodgkin's disease. *Ann Oncol* 1996; 7: S91–3.
39. Connors JM. Hodgkin's lymphoma: the hazards of success. *J Clin Oncol* 2003; 21: 3388–90.
40. Aisenberg AC. Coherent view of non-Hodgkin's lymphoma. *J Clin Oncol* 1995; 13: 2656–75.
41. Zucca E, Conconi A, Cavalli F. Treatment of extranodal lymphomas. *Best Pract Res Clin Haematol* 2002; 15: 533–47.

42. Grogan TM. New classification of low-grade lymphoma. *Ann Oncol* 1996; 7: S3–12.
43. Vose JM. Classification and clinical course of low-grade non-Hodgkin's lymphomas with overview of therapy. *Ann Oncol* 1996; 7: S13–19.
44. Vinnicombe SJ, Reznick RH. Computerized tomography in the staging of Hodgkin's disease and non-Hodgkin's lymphoma. *Eur J Nucl Med Mol Imaging* 2003; 30 (Suppl 1): S42–55.
45. Moskovic E, Fernando I, Blake P, Parsons C. Lymphography – current role in oncology. *Br J Radiol* 1991; 64: 422–7.
46. Redman HC, Glatstein E, Castellini RA, Federal WA. Computed tomography as an adjunct in the staging of Hodgkin's disease and non-Hodgkin's lymphoma. *Radiology* 1977; 124: 381–5.
47. Alcorn FS, Mategrano VC, Petasnick JP, Clark JW. Contributions of computed tomography in the staging and management of malignant lymphoma. *Radiology* 1977; 125: 717–23.
48. Best JK, Blackledge G, Forbes WS et al. Computed tomography of abdomen in staging and clinical management of lymphoma. *Br Med J* 1978; 2: 1675–7.
49. Blackledge GM, Best JKK, Crowther D, Isherwood I. Computed tomography (CT) in staging of patients with Hodgkin's disease: a report on 136 patients. *Clin Radiol* 1980; 31: 143–7.
50. Kaplan HS. Essentials of staging and management of the malignant lymphomas. *Semin Roentgenol* 1980; 15: 219–26.
51. Jonsson K, Karp W, Landberg T et al. Radiologic evaluation of subdiaphragmatic spread of Hodgkin's disease. *Acta Radiol* 1983; 24: 153–9.
52. Rankin SC. Assessment of response to therapy using conventional imaging. *Eur J Nucl Med Mol Imaging* 2003; 30 (Suppl 1): S56–64.
53. Husband JE. Diagnostic techniques: their strength and weaknesses. *Br J Cancer* 1980; 41: 21.
54. Hopper KD, Kasales CJ, van Slyke MA et al. Analysis of interobserver and intraobserver variability in CT tumor measurements. *Am J Roentgenol* 1996; 167: 851–4.
55. Apter S, Avigdor A, Gayer G et al. Calcification in lymphoma occurring before therapy: CT features and clinical correlation. *Am J Roentgenol* 2002; 178: 935–8.
56. Dugdale PE, Miles KA, Bunce I, Kelley BB, Leggatt DA. CT measurement of perfusion and permeability within lymphoma masses and its ability to assess grade, activity and chemotherapeutic response. *J Comput Assist Tomogr* 1999; 23: 540–7.
57. Jochelson M, Mauch P, Balikian J et al. The significance of the residual mediastinal mass in treated Hodgkin's disease. *J Clin Oncol* 1985; 3: 637–40.
58. Radford JA, Cowan RA, Flanagan M et al. The significance of residual mediastinal abnormality on the chest radiograph following treatment for Hodgkin's disease. *J Clin Oncol* 1988; 6: 940–6.
59. Thomas F, Cosset JM, Cherel P et al. Thoracic CT-scanning follow up of residual mediastinal masses after treatment of Hodgkin's disease. *Radiother Oncol* 1988; 11: 119–22.
60. Surbone A, Longo DL, De Vita VT, et al. Residual abdominal masses in aggressive non-Hodgkin's lymphoma after combination chemotherapy: significance and management. *J Clin Oncol* 1988; 6: 1832–7.
61. Mack MG, Balzer JO, Straub R, Eichler K, Vogl TJ. Supermagnetic iron oxide-enhanced MR imaging of head and neck lymph nodes. *Radiology* 2002; 1: 239–44.
62. Nyman RS, Rehn SM, Glimelius BL et al. Residual mediastinal masses in Hodgkin disease: prediction of size with MR imaging. *Radiology* 1989; 170: 435–40.
63. Rahmouni A, Divine M, Lepage E et al. Mediastinal lymphoma: quantitative changes in gadolinium enhancement at MR imaging after treatment. *Radiology* 2001; 219: 621–8.
64. Lieberman S, Libson E, Maly B et al. Imaging-guided percutaneous splenic biopsy using a 20- or 22-gauge cutting-edge core biopsy needle for the diagnosis of malignant lymphoma. *Am J Roentgenol* 2003; 181: 1025–7.
65. Hoffer P. Gallium: mechanisms. *J Nucl Med* 1980; 21: 282–5.
66. Nejmeddine F, Raphael M, Martin A et al. ⁶⁷Ga scintigraphy in B-cell non-Hodgkin's lymphoma: correlation of ⁶⁷Ga uptake with histology and transferrin receptor expression. *J Nucl Med* 1999; 40: 40–5.
67. Sohn MH, Jones BJ, Whiting JH et al. Distribution of gallium-67 in normal and hypo-transferrinemic tumor-bearing mice. *J Nucl Med* 1993; 34: 2135–43.
68. Van der Wahl H, McLaughlin AF, Southee AE. In: Ell PJ, Gambhir SS, eds. *Nuclear Medicine in Clinical Diagnosis and Treatment*. Philadelphia, PA: Churchill Livingstone, 2004, 53–69.
69. Kiratli PO, Canpinar H, Ruacan S, Kansu E. Correlation of flow cytometric parameters and transferring receptors with gallium-67 scintigraphic images in lymphoma patients. *Nucl Med Commun* 2000; 21: 925–31.
70. Van Leeuwen-Stock AE, Drager AM, Scuurhuis GJ et al. Gallium 67 in the human lymphoid cell line U-715: uptake, cytotoxicity and intracellular localization. *Int J Radiat Biol* 1993; 64: 749–59.
71. Chitambar CR, Zivkovic Z. Uptake of gallium 67 by human leukemic cells: demonstration of transferring receptor-dependent and transferring receptor-independent mechanisms. *Cancer Res* 1987; 47: 3929–34.
72. Chan SM, Hoffer PB, Maric N, Duray P. Inhibition of gallium-67 uptake in melanoma by an anti-human transferring receptor monoclonal antibody. *J Nucl Med* 1987; 28: 1303–7.
73. Larson SM, Rasey JS, Allen DR et al. Common pathway for tumor cell uptake of gallium-67 and iron-59 via a transferring receptor. *J Natl Cancer Inst* 1980; 64: 41–53.
74. Iosilevsky G, Front D, Bettman L, Hardoff R, Ben Arieh Y. Uptake of gallium-67 citrate and [2-³H] deoxyglucose in the tumor model following chemotherapy and radiotherapy. *J Nucl Med* 1985; 26: 278–82.
75. Keidar Z, Israel O, Krausz Y. SPECT/CT in tumor imaging: technical aspects and clinical applications. *Semin Nucl Med* 2003; 33: 205–18.
76. Jochelson MS, Herman TS, Stomper PC, Mauch PM, Kaplan WD. Planning mantle radiation therapy in patients with Hodgkin's disease: role of gallium 67 scintigraphy. *Am J Roentgenol* 1988; 151: 1229–31.
77. Tumei SS, Rosenthal DS, Kaplan WD. Lymphoma: evaluation with Ga-67 SPECT. *Radiology* 1987; 164: 111–14.
78. Anderson KC, Leonard RCF, Canellos GP et al. High dose gallium imaging in lymphoma. *Am J Med* 1983; 75: 327–31.
79. Sandrock D, Lastoria S, Magrath IT et al. The role of gallium-67 tumor scintigraphy in patients with small, non-cleaved cell lymphoma. *Eur J Nucl Med* 1993; 20: 119–22.

80. Ben-Haim S, Bar-Shalom R, Israel O et al. Utility of gallium-67 scintigraphy in low-grade non-Hodgkin's lymphoma. *J Clin Oncol* 1996; 14: 1936–42.
81. Gallamini A, Biggi A, Fruttero A et al. Revisiting the prognostic role of gallium scintigraphy in low-grade non-Hodgkin's lymphoma. *Eur J Nucl Med* 1997; 24: 1499–506.
82. Hussain R, Christie DR, GebSKI V, Barton MB, Gruenwald SM. The role of the gallium scan in primary extranodal lymphoma. *J Nucl Med* 1998; 39: 95–8.
83. Orzel JA, Sawaf NW, Richardson ML. Lymphoma of the skeleton: scintigraphic evaluation. *Am J Roentgenol* 1988; 150: 1095–9.
84. Bar-Shalom R, Israel O, Epelbaum R et al. Gallium-67 scintigraphy in lymphoma with bone involvement. *J Nucl Med* 1995; 36: 446–50.
85. Israel O, Mekel M, Bar-Shalom R et al. Bone lymphoma: Ga-67 scintigraphy and CT for prediction of outcome after treatment. *J Nucl Med* 2002; 43: 1295–303.
86. Castellino RA. Diagnostic imaging evaluation of Hodgkin's disease and non-Hodgkin's lymphoma. *Cancer* 1991; 67: 1177–80.
87. Stomper PC, Choleweinsky SP, Park J et al. Abdominal staging of thoracic Hodgkin's disease: CT-lymphangiography–Ga-67 scanning correlation. *Radiology* 1993; 187: 381–6.
88. Ben-Haim S, Bar-Shalom R, Israel O et al. Liver involvement in lymphoma: the role of gallium-67 scintigraphy. *J Nucl Med* 1995; 36: 900–4.
89. Katoka M, Kawamura M, Tsuda T et al. The role of gallium-67 imaging in non-Hodgkin lymphoma of the gastrointestinal tract. *Eur J Nucl Med* 1990; 17: 142–7.
90. MacMahon H, Vyborny C, Sephardari S, Kirchner P, Ryan J. Gallium accumulation in the stomach. A frequent incidental finding. *Clin Nucl Med* 1985; 10: 719–23.
91. Canellos GP. Residual mass in lymphoma may not be residual disease [Editorial]. *J Clin Oncol* 1988; 6: 931–3.
92. Hagemester FB. Treatment of relapsed aggressive lymphomas: regimens with and without high-dose therapy and stem cell rescue. *Cancer Chemother Pharmacol* 2002; 49: S13–20.
93. Zinzani PL, Monetti N, Zompatori M et al. Importance of gallium scan restaging for curative treatment of mediastinal lymphomas. *Haematologica* 2001; 86: 1229–30.
94. Coiffier B, Gisslebrecht C, Vose JM et al. Prognostic factors in aggressive malignant lymphomas: description and validation of a prognostic index that could identify patients requiring a more intensive therapy. *J Clin Oncol* 1991; 9: 211–19.
95. Southee AE, Wylie BR, McLaughlin AF et al. Gallium scintigraphy in the management of mediastinal Hodgkin disease. *Aust NZ J Med* 1988; 18: 508.
96. Wylie BR, Southee AE, Joshua DE et al. Gallium scanning in the management of mediastinal Hodgkin disease. *Eur J Haematol* 1989; 42: 344–7.
97. Cooper DL, Caride VJ, Zloty M et al. Gallium scans in patients with mediastinal Hodgkin's disease treated with chemotherapy. *J Clin Oncol* 1993; 11: 1092–8.
98. Kostakoglu L, Yeh SD, Portlock C et al. Validation of gallium-67 citrate single-photon emission computed tomography in biopsy-confirmed residual Hodgkin disease in the mediastinum. *J Nucl Med* 1992; 33: 345–50.
99. Zinzani PL, Martelli M, Magagnoli M et al. Treatment and clinical management of primary mediastinal large B-cell lymphoma with sclerosis: MACOP-B regimen and mediastinal radiotherapy monitored by ⁶⁷gallium scan in 50 patients. *Blood* 1999; 94: 3289–93.
100. King SC, Reiman RJ, Prosnitz LR. Prognostic importance of restaging gallium scans following induction chemotherapy for advanced Hodgkin's disease. *J Clin Oncol* 1994; 12: 306–11.
101. Brenot-Rossi I, Bouabdallah R, Do Stefano D et al. Hodgkin's disease: prognostic role of gallium scintigraphy after chemotherapy. *Eur J Nucl Med* 2001; 28: 1482–8.
102. Abrahamsen AF, Lien HH, Aas M et al. Magnetic resonance imaging and 67-gallium scan in mediastinal malignant lymphoma: a prospective pilot study. *Ann Oncol* 1994; 5: 433–6.
103. Vose JM, Bierman PJ, Anderson JR et al. Single-photon emission computed tomography gallium imaging versus computed tomography: predictive value in patients undergoing high-dose chemotherapy and autologous stem-cell transplantation for non-Hodgkin's lymphoma. *J Clin Oncol* 1996; 14: 2473–9.
104. Salloum E, Brandt DS, Claride VJ et al. Gallium scans in the management of patients with Hodgkin's disease: a study of 101 patients. *J Clin Oncol* 1997; 15: 518–27.
105. Armitage JO, Weisenburger DD, Hutchins M et al. Chemotherapy for diffuse large-cell lymphoma – rapidly responding patients have more durable remissions. *J Clin Oncol* 1986; 4: 160–4.
106. Kaplan WD, Jochelson MS, Herman TS et al. Gallium-67 imaging: a predictor of residual tumor viability and clinical outcome in patients with diffuse large-cell lymphoma. *J Clin Oncol* 1990; 8: 1966–70.
107. Weeks JC, Yeap BY, Canellos GP, Shipp MA. Value of follow-up procedures in patients with large-cell lymphoma who achieve a complete remission. *J Clin Oncol* 1991; 9: 1196–203.
108. Waxman AD, Eller D, Ashok G et al. Comparison of gallium-67 citrate and thallium-201 scintigraphy in peripheral and intrathoracic lymphoma. *J Nucl Med* 1996; 37: 46–50.
109. Israel O, Front D. Benign mediastinal and parahilar uptake of gallium-67 in treated lymphoma: do we have all the answers? *J Nucl Med* 1993; 34: 1330–2.
110. Kapuco OL, Skyuz C, Vural G et al. Evaluation of therapy response in children with untreated lymphoma using technetium-99m sestamibi. *J Nucl Med* 1997; 38: 243–7.
111. Piwnicka-Worms D, Chiu ML, Budding M et al. Functional imaging of multidrug resistant P-glycoprotein with an organotechnetium complex. *Cancer Res* 1993; 53: 977–84.
112. Tsai SC, Shiau YC, Wang JJ et al. Comparison of the uptake and clearance of Tc-99m MIBI, Tl-201 and Ga-67 in drug-resistant lymphoma cell lines. *Cancer Lett* 2001; 171: 147–52.
113. Dimitrakopoulou-Strauss A, Strauss LG, Goldschmidt H et al. Evaluation of tumour metabolism and multidrug resistance in patients with treated malignant lymphoma. *Eur J Nucl Med* 1995; 22: 434–42.
114. Reubi JC, Waser B, Vanhagen M et al. In vitro and in vivo detection of somatostatin receptors in human malignant lymphomas. *Int J Cancer* 1992; 50: 895–900.
115. Lugtenberg PJ, Krenning EP, Valkems R et al. Somatostatin receptor scintigraphy useful in stage I–II Hodgkin disease:

- more extended disease identified. *Br J Haematol* 2001; 112: 936–44.
116. Lugtenberg PJ, Krenning EP, Valkema R et al. Somatostatin receptor scintigraphy in the initial staging of low-grade non-Hodgkin lymphomas. *J Nucl Med* 2001; 42: 222–9.
 117. Zuckier LS, DeNardo GL. Trials and tribulations: oncological antibody imaging comes to the fore. *Semin Nucl Med* 1997; 25: 10–29.
 118. Kaminski MS, Zasadny KR, Francis IR et al. Iodine-131-anti-B1 radioimmunotherapy for B-cell lymphoma. *J Clin Oncol* 1996; 14: 1974–81.
 119. Som P. A fluorinated glucose analog, 2-fluoro-2-deoxy-D-glucose (F-18): non-toxic tracer for rapid tumour detection. *J Nucl Med* 1980; 21: 670–5.
 120. Bomanji JB, Ell PJ. The role of PET scanning in lymphoma assessment. *Br J Cancer Manag* 2005; 2: 7–11.
 121. Visvikis D, Ell PJ. Impact of technology on the utilization of positron emission tomography in lymphoma: current and future perspectives. *Eur J Nucl Med Mol Imaging* 2003; 30 (Suppl 1): S89–91.
 122. Barrington SF, O'Doherty MJ. Limitations of PET for imaging lymphoma. *Eur J Nucl Med Mol Imaging* 2003; 30 (Suppl 1): S117–27.
 123. Kipper MS, Tartar M. Approach to PET image interpretation, normal variants and benign processes. In: Kipper MS, Tartar M, eds. *Clinical Atlas of PET with Imaging Correlations*. Philadelphia: Saunders, 2004: 5–74.
 124. Okada J, Yoshikawa K, Itami M et al. Positron emission tomography using fluorine-18-fluorodeoxyglucose in malignant lymphoma: a comparison with proliferative activity. *J Nucl Med* 1992; 33: 325–9.
 125. Goldberg MA, Lee MJ, Fischman AJ et al. Fluorodeoxyglucose PET of abdominal and pelvic neoplasms: potential role in oncologic imaging. *Radiographics* 1993; 13: 1047–62.
 126. Lapela M, Leskinen S, Minn HR et al. Increased glucose metabolism in untreated non-Hodgkin lymphoma: a study with positron emission tomography and fluorine-18-fluorodeoxyglucose. *Blood* 1995; 86: 3522–7.
 127. Rodriguez M, Rehn S, Ahlstrom H, Sunstrom C, Grimelius B. Predicting malignancy grade with PET in non-Hodgkin lymphoma. *J Nucl Med* 1995; 36: 1790–6.
 128. Rodriguez M, Ahlstrom H, Sundin A et al. [¹⁸F] FDG PET in gastric non-Hodgkin lymphoma. *Acta Oncol* 1997; 36: 577–84.
 129. Elstrom R, Guan L, Baker G et al. Utility of FDG-PET scanning in lymphoma by WHO classification. *Blood* 2003; 101: 3875–6.
 130. Hoffman M, Kletter K, Diemling M et al. Positron emission tomography with fluorine-18-2-fluoro-2-deoxy-D-glucose (F-18 FDG) does not visualize extranodal B-cell lymphoma of the mucosa-associated lymphoid-tissue (MALT) type. *Ann Oncol* 1999; 10: 1185–9.
 131. Hoffman M, Kletter K, Becherer A et al. 18-F-fluorodeoxyglucose positron emission tomography (18-F FDG-PET) for staging and follow-up of marginal-zone B-cell lymphoma. *Oncology* 2003; 64: 336–40.
 132. Jerusalem G, Beguin Y, Najjar F et al. Positron emission tomography (PET) with 18F-fluorodeoxyglucose (18F-FDG) for the staging of low-grade non-Hodgkin's lymphoma (NHL). *Ann Oncol* 2001; 12: 825–30.
 133. Najjar F, Hustinx R, Jerusalem G et al. Positron emission tomography (PET) for staging low-grade non-Hodgkin's lymphomas (NHL). *Cancer Biother Radiopharm* 2001; 16: 297–304.
 134. Schiepers C, Filmont JE, Czernin J. PET for staging of Hodgkin's disease and non-Hodgkin's lymphoma. *Eur J Nucl Med Mol Imaging* 2003; 30 (Suppl 1): S82–8.
 135. Newman JS, Francis IR, Kaminski KS, Wahl RL. Imaging of lymphoma with PET with 2-[F-18]-fluoro-2-deoxy-D-glucose: correlation with CT. *Radiology* 1994; 190: 111–16.
 136. Jerusalem GH, Beguin YP. Positron emission tomography in non-Hodgkin's lymphoma (NHL): relationship between tracer uptake and pathological findings, including preliminary experience in the staging of low-grade NHL. *Clin Lymphoma* 2002; 3: 56–61.
 137. Kostakoglu L, Leonard JP, Kuji I, Vallabhajosula S, Goldmith SJ. Comparison of fluorine-18 fluorodeoxyglucose positron emission tomography and Ga-67 scintigraphy in evaluation of lymphoma. *Cancer* 2002; 94: 879–88.
 138. Sasaki M, Kuwabara Y, Koga H et al. Clinical impact of whole-body FDG-PET on the staging and therapeutic decision making for malignant lymphoma. *Ann Nucl Med* 2002; 16: 337–45.
 139. Armitage JO. Long-term toxicity of the treatment of Hodgkin's disease. *Ann Oncol* 1998; 9: S133–6.
 140. Bangerter M, Moog F, Buchmann I et al. Whole-body 2-[¹⁸F]-fluoro-2-deoxy-D-glucose positron emission tomography (FDG-PET) for accurate staging of Hodgkin's disease. *Ann Oncol* 1998; 9: 1117–22.
 141. Shah N, Hoskin P, McMillan A et al. The impact of FDG positron emission tomography imaging on the management of lymphomas. *Br J Radiol* 2000; 73: 482–7.
 142. Partridge S, Timothy A, O'Doherty MJ et al. 2-Fluorine-18-fluoro-2-deoxy-D-glucose positron emission tomography in the pre-treatment staging of Hodgkin's disease: influence on patient management in a single institution. *Ann Oncol* 2000; 11: 1273–9.
 143. Buchmann I, Reinhardt M, Elsner K et al. 2-(Fluorine-18) fluoro-2-deoxy-D-glucose positron emission tomography in the detection and staging of malignant lymphoma. A bicenter trial. *Cancer* 2001; 91: 889–99.
 144. Moog F, Bangerter M, Diederichs CG et al. Lymphoma: role of 2-deoxy-2-[F-18] fluoro-D-glucose (FDG) PET in nodal staging. *Radiology* 1997; 203: 795–800.
 145. Young CS, Young BL, Smith SM. Staging Hodgkin's disease with 18-FDG PET: comparison with CT and surgery. *Clin Pos Imaging* 1998; 1: 161–4.
 146. Delbeke D, Martin WH, Morgan DS et al. 2-deoxy-2-[F-18]fluoro-D-glucose imaging with positron emission tomography for initial staging of Hodgkin's disease and lymphoma. *Mol Imaging Biol* 2002; 4: 105–14.
 147. Hueltenschmidt B, Sautter-Bihl M, Lang O et al. Whole body positron emission tomography in the treatment of Hodgkin disease. *Cancer* 2001; 91: 302–10.
 148. Wirth A, Seymour JE, Hicks RJ, et al. Fluorine-18 fluorodeoxyglucose positron emission tomography, gallium-67 scintigraphy and conventional staging for Hodgkin disease and non-Hodgkin lymphoma. *Am J Med* 2002; 112: 262–8.
 149. Israel O, Keidar Z, Bar-Shalom R. Positron emission tomography in the evaluation of lymphoma. *Semin Nucl Med* 2004; 34: 166–79.

150. Schoder H, Larson SM, Yeung HWD. PET/CT in oncology: integration into clinical management of lymphoma, melanoma and gastrointestinal malignancies. *J Nucl Med* 2004; 43: 72S–81S.
151. Schaefer NG, Hany TF, Taverna C et al. Non-Hodgkin lymphoma and Hodgkin disease: coregistered FDG PET and CT at staging and restaging – do we need contrast-enhanced CT? *Radiology* 2004; 233: 823–9.
152. Hutchings M, Eigtved AI, Specht L. FDG-PET in the clinical management of Hodgkin lymphoma. *Crit Rev Oncol Hematol* 2004; 52: 19–32.
153. Moog F, Bangerter M, Diederichs CG, et al. Extranodal malignant lymphoma: detection with FDG PET versus CT. *Radiology* 1998; 206: 475–81.
154. Wiedmann E, Baican B, Hertel A et al. Positron emission tomography (PET) for staging and evaluation of response to treatment in patients with Hodgkin's disease. *Leuk Lymphoma* 1999; 34: 545–51.
155. Raanani P, Shasha Y, Perry C et al. Is CT scan still necessary for staging in Hodgkin and non-Hodgkin lymphoma patients in the PET/CT era? *Ann Oncol* 2006; 17: 117–22.
156. Even-Sapir E, Lievshitz G, Perry C et al. ¹⁸F-FDG-PET/CT patterns of extranodal involvement with non-Hodgkin's lymphoma and Hodgkin's disease. *PET Clin North Am* 2006; 1: 251–64.
157. Maes B, De Wolf-Peeters C. Marginal zone cell lymphoma – an update on recent advances. *Histopathology* 2002; 40: 117–26.
158. Bertoni F, Zucca E. State-of-the-art therapeutics: marginal-zone lymphoma. *J Clin Oncol* 2005; 23: 6415–20.
159. Nakamura S, Aoyagi K, Furuse M, et al. B-cell monoclonality precedes the development of gastric MALT lymphoma in *Helicobacter pylori*-associated chronic gastritis. *Am J Pathol* 1998; 152: 1271–9.
160. Hoffmann M, Kletter K, Becherrer A et al. ¹⁸F-fluorodeoxyglucose positron emission tomography (¹⁸F-FDG PET) for staging and follow-up of marginal zone B-cell lymphoma. *Oncology* 2003; 64: 336–40.
161. Beal KP, Yeung HW, Yahalom J. FDG-PET scanning for detection and staging of extranodal marginal zone lymphomas of the MALT type: a report of 42 cases. *Ann Oncol* 2005; 16: 473–8.
162. Metser U, Goor O, Lerman H et al. PET-CT of extranodal lymphoma. *Am J Roentgenol* 2004; 182: 1579–86.
163. Wahl RL. Why nearly all PET of abdominal and pelvic cancers will be performed as PET/CT. *J Nucl Med* 2004; 45 (Suppl 1): 82S–95S.
164. Shirkhoda A, Ros PR, Farah J et al. Lymphoma of the solid abdominal viscera. *Radiol Clin North Am* 1990; 28: 785–99.
165. Rini JN, Leonidas JC, Tomas MB et al. ¹⁸F-FDG PET versus CT for evaluating the spleen during initial staging of lymphoma. *J Nucl Med* 2003; 44: 1072–4.
166. Metser U, Miller E, Kessler A et al. Solid splenic masses: evaluation with ¹⁸F-FDG PET/CT. *J Nucl Med* 2005; 46: 52–9.
167. Carr R, Barrington SF, Madan B et al. Detection of lymphoma in bone marrow by whole-body positron emission tomography. *Blood* 1998; 91: 3340–6.
168. Moog F, Bangerter M, Kotzerke J et al. ¹⁸F-fluorodeoxyglucose positron emission tomography as a new approach to detect lymphomatous bone marrow. *J Clin Oncol* 1998; 16: 603–9.
169. Gundlapalli S, Ojha B, Mountz JM. Granulocyte colony-stimulating factor: confounding F-18 FDG uptake in outpatient positron emission tomographic facilities for patients receiving ongoing treatment of lymphoma. *Clin Nucl Med* 2002; 27: 140–1.
170. Cohen MS, Arslan N, Dehdashti F et al. Risk of malignancy in thyroid incidentalomas identified by fluorodeoxyglucose-positron emission tomography. *Surgery* 2001; 130: 941–6.
171. Palmedo H, Urbach H, Bender H et al. FDG-PET in immunocompetent patients with primary central nervous system lymphoma: correlation with MRI and clinical follow-up. *Eur J Nucl Med Mol Imaging* 2006; 33: 164–8.
172. Roelcke U, Leenders KL. Positron emission tomography in patients with primary CNS lymphomas. *J Neurooncol* 1999; 43: 231–6.
173. Cremerius U, Fabri U, Neuerburg J et al. Positron emission tomography with ¹⁸F-FDG to detect residual disease after therapy for malignant lymphoma. *Nucl Med Commun* 1998; 19: 1055–63.
174. Zinzani PL, Magagnoli M, Chierichetti F et al. The role of positron emission tomography (PET) in the management of lymphoma patients. *Ann Oncol* 1999; 10: 1181–4.
175. Jerusalem G, Beguin Y, Fassotte MF et al. Whole body positron emission tomography using ¹⁸F-fluorodeoxyglucose for post-treatment in Hodgkin disease and non-Hodgkin lymphoma has higher diagnostic and prognostic value than classical computed tomography scan imaging. *Blood* 1999; 94: 429–33.
176. Mikhaeel NG, Timothy AR, O'Doherty MJ, Hain S, Maisey MN. ¹⁸F-FDG-PET as a prognostic indicator in the treatment of aggressive non-Hodgkin's lymphoma, comparison with CT. *Leuk Lymphoma* 2000; 39: 543–53.
177. Spaepen K, Stroobants S, Dupont P et al. The prognostic value of positron emission tomography (PET) with ¹⁸F-fluorodeoxyglucose (¹⁸FDG) after first-line chemotherapy in non-Hodgkin's lymphoma: ¹⁸FDG-PET, a valid alternative to conventional diagnostic methods. *J Clin Oncol* 2001; 19: 414–19.
178. Juweid ME, Weisman GA, Menda Y et al. FDG-PET in the prediction of progression-free survival at 1-year of patients with aggressive non-Hodgkin's lymphoma following anthracycline-based first-line chemotherapy [Abstract]. *Eur J Nucl Med* 2002; 20 (Suppl 1): S264.
179. Weihrauch MR, Re D, Scheidhauer K et al. Thoracic positron emission tomography using ¹⁸F-fluorodeoxyglucose for the evaluation of residual mediastinal Hodgkin disease. *Blood* 2001; 98: 2930–4.
180. Dittman H, Sokler M, Kollmannsberger C et al. Comparison of ¹⁸F-FDG-PET with CT scans in the evaluation of patients with residual and recurrent Hodgkin's lymphoma. *Oncol Rep* 2001; 8: 1393–9.
181. Spaepen K, Stroobants S, Dupont P et al. Can positron emission tomography with [(18)F]-fluorodeoxyglucose after first-line treatment distinguish Hodgkin's disease patients who need additional therapy from others in whom additional therapy would mean avoidable toxicity? *Br J Haematol* 2001; 115: 272–8.

182. de Wit M, Bohuslavizki KH, Buchert R et al. 18-FDG-PET following treatment as valid predictor for disease-free survival in Hodgkin's lymphoma. *Ann Oncol* 2001; 12: 29–37.
183. Montravers F, McNamara D, Landman-Parker J et al. [(18)F] FDG in childhood lymphoma: clinical utility and impact on management. *Eur J Nucl Med Mol Imaging* 2002; 29: 1155–65.
184. Naumann R, Vaic A, Beuthien-Baumann B et al. Prognostic value of positron emission tomography in the evaluation of post-treatment residual mass in patients with Hodgkin's disease and non-Hodgkin's lymphoma. *Br J Haematol* 2001; 115: 793–800.
185. Becherer A, Mitterbauer M, Jaeger U et al. Positron emission tomography with [18F]2-fluoro-D-2-deoxyglucose (FDG-PET) predicts relapse of malignant lymphoma after high-dose therapy with stem-cell transplantation. *Lukemia* 2002; 16: 260–7.
186. Friedberg JW, Neuberger D, Monson E et al. The impact of external beam radiation therapy prior to autologous bone marrow transplantation in patients with non-Hodgkin's lymphoma. *Biol Blood Marrow Transplant* 2001; 7: 446–73.
187. Cremerius U, Fabry U, Wildberger JE et al. Pre-transplant positron emission tomography (PET) using fluorine-18 fluoro-deoxyglucose (FDG) predicts outcome in patients treated with high-dose chemotherapy and autologous stem cell transplantation for non-Hodgkin's lymphoma. *Bone Marrow Transplant* 2002; 30: 103–11.
188. Spaepen K, Stroobants S, Dupont P et al. Prognostic value of pretransplantation positron emission tomography using fluorine-18 fluorodeoxyglucose in patients with aggressive lymphoma treated with high-dose chemotherapy and stem cell transplantation. *Blood* 2003; 102: 53–9.
189. Filmont JE, Czernin G, Yap C et al. Value of F-18 fluoro-deoxyglucose positron emission tomography for predicting the clinical outcome of patients with aggressive lymphoma prior to and after autologous stem-cell transplantation. *Chest* 2003; 124: 608–13.
190. Torizuka T, Zasadny KR, Kison PV et al. Metabolic response of non-Hodgkin's lymphoma to ¹³¹I-anti-B1 radioimmunotherapy: evaluation with FDG-PET. *J Nucl Med* 2000; 41: 999–1005.
191. Hart DP, Avivi I, Thomson KJ et al. Use of 18F-FDG positron emission tomography following allogeneic transplantation to guide adoptive immunotherapy with donor lymphocyte infusions. *Br J Haematol* 2005; 128: 824–9.
192. Romer W, Hanauske AR, Ziegler S et al. Positron emission tomography in non-Hodgkin's lymphoma: assessment of chemotherapy with fluorodeoxyglucose. *Blood* 1998; 91: 4464–71.
193. Kostakoglu L, Coleman M, Leonard JP et al. PET predicts prognosis after 1 cycle of chemotherapy in aggressive lymphoma and Hodgkin's disease. *J Nucl Med* 2002; 43: 1018–27.
194. Jerusalem G, Beguin Y, Fassotte MF, et al. Persistent tumor 18F-FDG uptake after a few cycles of polychemotherapy is predictive of treatment failure in non-Hodgkin's lymphoma. *Haematologica* 2000; 85: 613–18.
195. Mikhaeel NG, Mainwaring P, Nunan T, Timothy AR. Prognostic value of interim and post treatment FDG-PET scanning in Hodgkin lymphoma [Abstract]. *Ann Oncol* 2002; 13 (Suppl 2): 21.
196. Spaepen K, Stroobants S, Dupont P et al. Early restaging positron emission tomography with ¹⁸F-fluorodeoxyglucose predicts outcome in patients with aggressive non-Hodgkin's lymphoma. *Ann Oncol* 2002; 13: 1356–63.
197. Lowe VJ, Weisman GA. Assessment of lymphoma therapy using ¹⁸F-FDG-PET. *J Nucl Med* 2002; 43: 1028–30.
198. Alavi JB, Benard F, Alavi A. Detection of unsuspected recurrent lymphoma with fluorodeoxyglucose-positron emission tomographic imaging after induction chemotherapy: a case study. *Am J Clin Oncol* 1998; 21:126–8.
199. Freudenberg LS, Antoch G, Schutt P et al. FDG-PET/CT in re-staging of patients with lymphoma. *Eur J Nucl Med Mol Imaging* 2004; 31: 325–9.
200. Paul R. Comparison of fluorine-18-2-fluorodeoxyglucose and gallium-67 citrate imaging for detection of lymphoma. *J Nucl Med* 1987; 28: 288–92.
201. Shen YY, Kao A, Yen RF. Comparison of 18F-fluoro-2-deoxyglucose positron emission tomography and gallium-67 citrate scintigraphy for detecting malignant lymphoma. *Oncol Rep* 2002; 9: 321–5.
202. Van Den Bossche B, Lambert B, De Winter F et al. 18FDG PET versus high-dose Ga-67 scintigraphy for restaging and treatment follow up of lymphoma patients. *Nucl Med Commun* 2002; 23: 1079–83.
203. Bar-Shalom R, Yefremov N, Haim N et al. Camera-based FDG-PET and Ga-67 SPECT in evaluation of lymphoma: comparative study. *Radiology* 2003; 227: 353–60.
204. Zijlstra JM, Hoekstra O, Raijmakers PGH et al. 18-FDG positron emission tomography versus Ga-67 scintigraphy as prognostic test during chemotherapy for non-Hodgkin's lymphoma. *Br J Haematol* 2003; 123: 454–62.
205. Chillaron J, Roca R, Valencia A et al. Heteromeric amino acid transporters: biochemistry, genetics, and physiology. *Am J Physiol Renal Physiol* 2001; 281: 995–1018.
206. Toyohara J, Hayashi A, Sato M et al. Development of radioiodinated nucleoside analogs for imaging tissue proliferation: comparisons of six 5-iodonucleosides. *Nucl Med Biol* 2003; 30: 687–96.
207. Sutinen E, Jyrkkio S, Varpula M et al. Nodal staging of lymphoma with whole-body PET: comparison of [¹¹C]methionine and FDG. *J Nucl Med* 2000; 12: 1980–8.
208. Been LB, Suurmeijer AJ, Cobben DC et al. [¹⁸F]FLT-PET in oncology: current status and opportunities. *Eur J Nucl Med Mol Imaging* 2004; 31: 1659–72.
209. Buchmann I, Neumaier B, Schreckenberger M et al. (18F)3'-deoxy-3'-fluorothymidine PET in NHL patients. Whole-body biodistribution and imaging of lymphoma manifestations – a pilot study. *Cancer Biother Radiopharm* 2004; 19: 436–42.
210. Juweid ME, Cheson BD. Role of positron emission tomography in lymphoma. *J Clin Oncol* 2005; 23: 4577–80.
211. Reubi JC, Waser B, Schaer JC et al. Somatostatin receptor sst1-sst5 expression in normal and neoplastic human tissues using receptor autoradiography with subtype-selective ligands. *Eur J Nucl Med* 2001; 28: 836–46.
212. Ferone D, Semino C, Boschetti M et al. Initial staging of lymphoma with octreotide and other receptor imaging agents. *Semin Nucl Med* 2005; 35: 176–85.

Bone and soft tissue tumors

*Gopinath Gnanasegaran, Gary Cook,
Sanjay Vijayanathan, and Ignac Fogelman*

Background

Diagnosis of bone and soft tissue tumors is generally difficult, as they have heterogeneous biologic behavior patterns.¹ Early detection and accurate grading or classification of these tumors can improve the overall outcome and prognosis. The classification and staging of soft-tissue and bone neoplasms is evolving and depends on multiple factors and staging methods including clinical, radiographic, and histological features² (Table 15.1). The American Joint Committee on Cancer and the Musculoskeletal Tumor Society systems are the most commonly used staging methods for bone and soft tissue tumors.²⁻⁷ High-grade tumors with evidence of metastases are reported to be associated with a poor prognosis for all bone and soft tissue neoplasms regardless of the staging system that is used.² The size of the tumor, the anatomical compartment, and the depth of tumor invasion are also considered to be important variables.² However, determination of the anatomical extent, characteristics, and histopathological features of bone tumors and soft-tissue sarcomas involves a diagnostic strategy in which a biopsy is the final step.² In general, histology remains the most reliable method for establishing a diagnosis but depends on the site, quality, and size of the biopsy specimen.¹ In some tumor types, the diagnosis can be difficult even for the experienced pathologist. In these clinical dilemmas, diagnosis can be established with the complementary aid of conventional and radionuclide imaging techniques.^{1,8,9} Conventional and radionuclide imaging provide important information with regard to the appearance, extent, and characteristics of this group of tumors.

Conventional and radionuclide imaging

The main role of conventional and radionuclide imaging in the management of bone and soft tissue tumors is to

differentiate between benign and malignant masses, to assess local tumor extent/invasion, to screen for metastases, to assess the effect of chemotherapy, and finally to evaluate residual tumor or recurrence^{10,11} (Table 15.2). However, no single modality can be used to complete all these tasks.¹¹

The radiological assessment of bone tumors is based on multiple parameters such as its location, rate of growth, tumor margin, periosteal reaction, and mineralization of the matrix. In general, magnetic resonance imaging (MRI)

Table 15.1 Summary of TNM classification and histological grading of bone and soft tissue sarcomas²⁻⁷

Bone tumors

Tx: primary tumor cannot be assessed
T0: No evidence of primary tumor
T1: Tumor within the cortex
T2: Tumor beyond the cortex

N0: No regional lymph node metastases
N1: Regional lymph nodes

Soft tissue tumors

T1: < 5cm, T1a superficial, T1b deep
T2: > 5cm, T2a superficial, T2b deep

N0: No regional lymph node metastases
N1: Regional lymph nodes

Grading and differentiation (bone and soft tissue tumors)

GX: Grade and differentiation cannot be assessed
G1: Well differentiated
G2: Moderately differentiated
G3: Poorly differentiated
G4: Undifferentiated

Table 15.2 Role of conventional radiological and radionuclide imaging in bone and soft tissue tumors

Differentiate benign and malignant tumors
 Evaluation of tumor extent and invasion
 Screen for distant metastases
 Assessment of treatment response
 Evaluation of residual tumor or recurrence
 Follow-up

and [¹⁸F]fluoro-2-deoxy-D-glucose positron emission tomography ([¹⁸F]FDG-PET) are able to detect marrow involvement early in the course of the disease, often before identifiable bone destruction/osteoblastic changes occur. These modalities may also precede computed tomography (CT) and [^{99m}Tc] methylene diphosphonate ([^{99m}Tc]MDP) bone scintigraphy in identifying the presence of malignant bone involvement.¹² In general, CT is used for the assessment of bone structure/morphology and MRI for detecting early marrow infiltration and epidural masses.

Currently a wide range of radiopharmaceuticals are available for the diagnosis and management of primary bone and soft tissue tumors. However, they are not widely utilized, although this may change with the development of newer single photon and PET related tracers. Compared to conventional nuclear medicine imaging, PET has an inherent advantage, as tomography is performed routinely and the spatial resolution of resultant images is relatively superior. PET also has the advantage of superior quantitative accuracy, which may be useful for following the effects of therapy. The improved sensitivity reported with PET is partly explained by the fact that the direct imaging of tumor metabolism is possible with [¹⁸F]FDG.

Recent advances in conventional imaging techniques such as CT and MRI as well as technological advances in nuclear medicine including the use of single photon emission computed tomography (SPECT)-CT and PET-CT, may provide a better localization of scintigraphic findings and may improve the overall diagnostic accuracy.¹² Currently, with wider availability of PET-CT, the clinical applications are likely to increase. In general, all these modalities have advantages and limitations and their role may vary in patients in different clinical settings or with different tumors (Tables 15.3–15.6).^{10,12–19} However, these techniques can be used to full potential only when they are used in a complementary fashion.

Table 15.3 Advantages and limitations of plain radiography in imaging bone and soft tissue tumors^{12–19}**Advantages**

Non-invasive method to establish differential diagnosis
 Readily available
 May be useful in evaluating location of lesion
 May be useful in evaluating type of bone destruction
 May be useful in evaluating presence of soft tissue mass

Limitations

Only five densities such as air, fluid, fat, calcium, and metal are demonstrated
 Diagnosis of lesions is limited primarily to evaluation of tumor mineralization or documentation of lesions with a high fat content

Radiopharmaceuticals: mechanism, advantages, and limitations

Various specific and non-specific radiopharmaceuticals including [^{99m}Tc]MDP, (⁶⁷Ga) citrate [⁶⁷Ga], [²⁰¹Tl]chloride

Table 15.4 Advantages and limitations of ultrasonography in imaging bone and soft tissue tumors^{12–19}**Advantages**

Lack of ionizing radiation
 Readily available
 Identifies size and extent of soft tissue lesions
 Useful in differentiating cystic from solid masses
 Combined with color and power Doppler may enable assessment of vascular architecture and altered blood flow
 Vascular architecture analysis can be helpful in differentiating benign from malignant tumors
 Under ultrasound guidance biopsy or aspiration can be easily performed

Limitations

Rarely used as the primary modality for evaluation of a soft tissue mass
 Operator dependent
 Limited specificity

Table 15.5 Advantages and limitations of computed tomography (CT) in imaging bone and soft tissue tumors^{12–19}**Advantages**

Useful in both diagnosis and staging

Good anatomic resolution, soft-tissue contrast, and detailed morphology

Accurate assessment of size of the tumor

Accurate assessment of extent and anatomic margin of disease

Assessment of integrity of adjacent bones

Identifies complications in the bone and soft tissues

In hybrid or fusion imaging it is useful for attenuation correction

Identifies extrinsic osseous erosions, subtle areas of mineralization, or soft tissue gas

Useful in assessing anatomic landmarks and localizing lesion seen on scintigraphy

Sensitivity for detecting sclerotic lesions is high

Useful as a guide for tissue sampling

More sensitive than MRI in the detection of metastatic disease to the lungs

Useful in planning surgical resection and radiation therapy

Limitations

Unable to differentiate between disease and scar, necrosis, when monitoring response to therapy

CT is not sensitive for assessment of malignant marrow infiltration

MRI, magnetic resonance imaging.

Table 15.6 Advantages and limitations of MRI in imaging bone and soft tissue tumors^{12–19}**Advantages**

Useful in both diagnosis and staging

Optimal imaging modality for bone marrow assessment

Detects malignant marrow involvement/infiltration early in course of the disease

Able to differentiate hematopoietic marrow from non-hematopoietic marrow

Identifies anatomical changes

Critical role in planning surgical resection and radiation therapy

Soft tissue contrast to delineate tumor relationship to muscle, fat, fibrous tissue, and adjacent blood vessels is relatively superior to CT

Identifies skip lesions

Limitations

Less sensitive than CT for detecting cortical bone destruction

May be contraindicated in the presence of cardiac pacemakers and cerebral aneurysm clips

Unable to differentiate between disease and scar, necrosis, when monitoring response to therapy

Limited sensitivity in detecting soft tissue calcification

(²⁰¹Tl), [^{99m}Tc]hexakis-2-methoxyisobutylisonitrile ([^{99m}Tc] MIBI (sestamibi)), [^{99m}Tc]tetrofosmin ([^{99m}Tc] MyoviewTM), and [^{99m}Tc]pentavalent dimercaptosuccinic acid (DMSA) ([^{99m}Tc]DMSA) are used in imaging bone and soft tissue tumors (Table 15.7).^{20–24} [^{99m}Tc]MDP is the most widely used bone agent, giving optimal contrast between normal and diseased bone but, similar, alternative [^{99m}Tc]diphosphonate tracers exist.²⁰ The uptake of diphosphonates depends on local blood flow, osteoblastic activity, and extraction efficiency. The actual mechanism of uptake is still not fully understood, but diphosphonates are probably incorporated into the hydroxyapatite crystal on the mineralizing bone surface.

²⁰¹Tl, an analog of potassium, enters tumor cells via the Na⁺/K⁺ adenosine triphosphatase (ATPase) pump, but as

well as reflecting the metabolic status of the cell, uptake also depends on blood flow. The accumulation of ²⁰¹Tl indicates viability and metabolic activity of the tumor cell.^{21,22}

^{99m}Tc-labeled sestamibi has a different mechanism of accumulation, and is thought to reflect cell viability, being mainly associated with mitochondria intracellularly. [^{99m}Tc]DMSA uptake has also been described in soft tissue tumors, the exact mechanism of uptake being uncertain.²³

The ⁶⁷Ga uptake mechanism is not fully understood, but its uptake probably reflects metabolic activity or tumor viability, and it is known to be transported protein-bound, predominantly to transferrin, in the circulation. Tumor localization of ⁶⁷Ga is multifactorial, and various mechanisms include neovascularity and uptake in the inflammatory portion of the tumor.²⁴

In general, these radiopharmaceuticals are used to improve the specificity in differentiating benign from malignant lesions. However, reported results are variable, and suggest that there may only be a limited role for nuclear medicine techniques in clinical situations, where

Table 15.7 Advantages and limitations of common conventional planar and single photon emission computed tomography (SPECT) pharmaceuticals in imaging bone and soft tissue tumors^{15,20–28}

<i>Advantages</i>	<i>Limitations</i>
<p>[^{99m}Tc]MDP bone scan High sensitivity Easy availability Less expensive</p>	<p>Lower specificity in differentiating benign and malignant tumors/lesions Distinguishing a healing process from other active metabolic processes (tumor recurrence or metastases) is limited Differentiating 'flare' phenomenon from residual/recurrent tumor is difficult</p>
<p>⁶⁷Ga Reliable in predicting malignancy of soft tissue masses Useful in staging accurately (can detect occult non-pulmonary metastases) in childhood rhabdomyosarcoma, epithelioid sarcoma, and synovial sarcomas Sensitivity is highest in intermediate- and high-grade tumors and lower in low-grade tumors</p>	<p>Not used routinely in the evaluation of bone and soft-tissue tumors Uptake mechanism is not fully understood Utility in diagnosis of abdominal and pelvic pathologies is limited due to its physiological excretion into the bowel Physical characteristics are suboptimal for imaging Delayed imaging protocol post-injection makes it less popular Non-specific uptake in inflammation limits its use in assessment of tumor response Poor uptake in myxoid tumors</p>
<p>²⁰¹Tl High positive predictive value Uptake in inflammatory and non-tumorous lesions is negligible Defines the extent of soft tissue tumor accurately Serial quantitative of uptake in malignant bone tumors post-chemotherapy predicts histological response and prognosis Differentiates recurrent or residual tumor and post-treatment changes Imaging can be performed soon after injection</p>	<p>Poor uptake in chondroid lesions and myxoid tumors Physical and biological characteristics limit imaging quality and the radiation burden is also relatively high Biological excretion makes it less ideal for abdominal, lung, or pelvic imaging Uptakes in myositis ossificans, chronic granulomatous synovitis, in highly cellular and vascular benign lesions are the reported pitfalls</p>
<p>[^{99m}Tc]MIBI and [^{99m}Tc]tetrofosmin Sensitive and has high negative predictive value Useful in diagnosis as well as assessment of multidrug-resistant tumors Differentiates active tumors from post-treatment changes Evaluates therapeutic response and prognosis</p>	<p>Tumors located near the heart, kidney, and bladder are difficult to localize Chronic granulomatous synovitis and benign lesions are reported false positive The role of [^{99m}Tc]tetrofosmin has not been studied extensively</p>
<p>[^{99m}Tc](5)DMSA Useful in detecting progressive and hypervascular soft tissue tumors (low-grade sarcomas, tenosynovial giant cell tumours, etc.) Accumulates in chondrogenic and myxoid tumors</p>	<p>Low specificity in diagnosing malignant chondrogenic tumor</p>

MDP, methylene diphosphonate; MIBI, methoxyisobutylisonitrile; DMSA, dimercaptosuccinic acid

conventional techniques are equivocal or unavailable.^{25–29} In recent years there has been increasing interest in the use of PET tracers in the investigation of bone and soft tissue sarcomas. Currently, [¹⁸F]FDG (a tumor specific tracer) and [¹⁸F]fluoride ion (non-specific bone tracer) have been assessed, and early results suggest that both agents may have a role to play in the clinical management

of musculoskeletal tumors. Most malignant tumors are known to exhibit increased glucose membrane transporters and a high glycolytic rate due to increased hexokinase activity, which may be reflected in enhanced accumulation of [¹⁸F]FDG, but other mechanisms such as tumor hypoxia may also play a part in the uptake of this radiopharmaceutical.³⁰

Bone tumors: etiology, pathogenesis, and scintigraphy

Primary bone tumors may arise from any element indigenous to bone.¹⁵ Malignant bone tumors represent 0.2% of all new cancers.^{15,31–3} The role of nuclear medicine techniques is limited except in specific tumor types and certain clinical situations. Bone scintigraphy is the initial investigation of choice when a bone lesion is seen incidentally on a radiograph and cannot be characterized accurately. The lesion is more likely to be benign when not visualized on a radionuclide bone scan.³³ The converse is not true, and an area of increased metabolic activity does not help in differentiating benign from malignant lesions. Scintigraphy is a sensitive but non-specific technique for the assessment of bone tumors. Malignant tumors are characteristically very vascular, and dynamic scintigraphy with the three-phase bone scan may be useful but not sufficient to make a diagnosis, as there are a number of vascular benign bone tumors such as osteoid osteoma or aneurysmal bone cyst with similar appearances.³⁴ A characteristic pattern of uptake in some primary bone tumors^{35,36} has been reported by various authors, but in practice there is too much overlap of features on the radionuclide bone scan to differentiate tumor types. The differential diagnosis depends on conventional imaging techniques such as plain X-ray, CT, or MRI, and a specific diagnosis depends on histopathology.

The role of radionuclide imaging in the initial evaluation of primary bone tumors prior to intervention or surgery varies. However, it plays a role in the post-therapy evaluation of primary bone tumors and in the detection of skeletal metastases.³⁷

Radionuclide scintigraphy of benign bone tumors

The role of radionuclide scintigraphy in the diagnosis and management of benign tumors is limited. However, scintigraphy of benign bone tumors such as osteochondroma, osteoid osteoma, osteofibrous dysplasia, enchondroma, chondroblastoma, and aneurysmal bone cyst has been reported in the literature^{38–44} (Table 15.8) (Figure 15.1). The findings noted in these tumors are not consistent or specific (Table 15.9). Generally a negative bone scan may be useful in excluding malignancy, but it is not always the case. Benign tumors usually demonstrate clearly delineated margins. In general bone islands are not visualized on scintigraphy, but occasionally low-grade focal uptake may be seen.^{39,61}

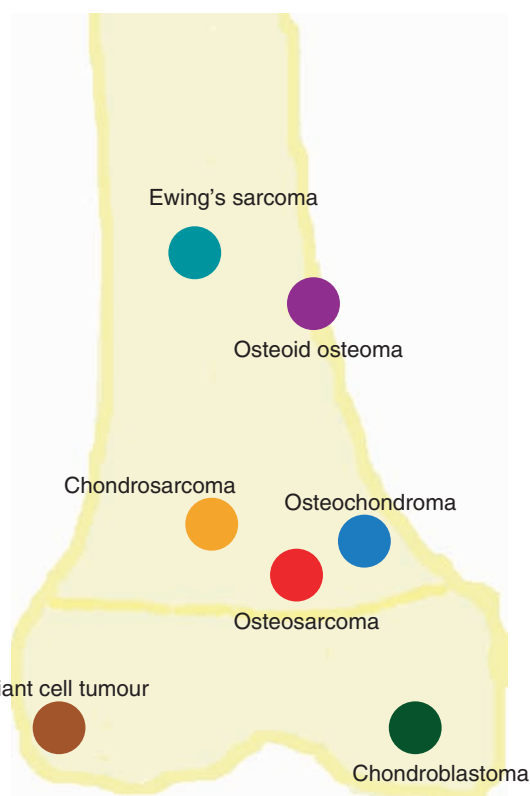


Figure 15.1

Schematic representation of the common sites of some major primary bone tumors.

Osteoid osteoma

These benign bone tumors commonly present in adolescents with a classical history of night pain relieved by non-steroidal anti-inflammatory drugs. They are often small, and may not be detected with conventional radiography,⁵² the commonest areas of occurrence being the long bones (meta-diaphysis) and the posterior elements of vertebral bodies in the spine. Bone scintigraphy plays an important role in localizing these tumors, as it is extremely sensitive.³³ The typical appearances on a bone scan are of an intense focus of uptake within an area of abnormal osteoblastic activity, often called the 'double density sign'⁵³ (Table 15.9). Once located, further imaging, e.g. with CT, may lead to a specific diagnosis as an appearance of sclerotic cortical thickening, and a radiolucent area within the sclerosis is a typical appearance. The high avidity for [^{99m}Tc]MDP in osteoid osteomas can be used to accurately locate the tumor during surgery by the use of a probe, and ensuring complete excision.⁵⁴ A negative study virtually excludes the diagnosis.³⁹

Table 15.8 Classification of benign bone tumors and their common sites^{2,7,9,38-51}

<i>Benign tumors</i>	<i>Age range and sex</i>	<i>Common sites</i>
<i>Chondroid origin</i>		
Chondroma	10–80 years Peak in 2nd–4th decade M:F equal	Hands (40%), appendicular skeleton
Osteochondroma	2–60 years (common in 2nd decade) M:F 1.4:1	Long bones (especially around knee joint)
Chondroblastoma	2nd decade (80%) M:F 2:1	Epiphysis (most common), metaphysis
Chondromyxoid fibroma	10–30 years (75%) Peak in 2nd decade M:F slight male predominance	Metaphyseal
<i>Osteoid origin</i>		
Osteoid osteoma	2nd–3rd decade M:F 2.5:1	No skeletal site is exempt Common in appendicular skeleton
Osteoblastoma	Under 30 years (80%) Peak in 2nd decade M:F 2:1	Spine (vertebral arch), diaphysis and metaphysis of long bones
<i>Bone cysts</i>		
Simple bone cyst	4–10 years (70%) Under 20 years (90%) M:F 2:1	Proximal third of femur, calcaneum, ilium
Aneurysmal bone cyst	5–20 years (70%) M:F equal (slight female predominance)	Any bone but usually arises from the metaphysis of the long bones and posterior elements of vertebral bodies
Giant cell tumor/osteoclastoma	18–45 years (80%) M:F 2:3	Knee joint, distal end of femur
<i>Fibrous origin</i>		
Non-ossifying fibroma	2nd decade M:F male predominance	Lower limb (90%)
Benign fibrous histiocytoma	20–50 years Peak 3rd decade M:F equal	Knee
Desmoplastic fibroma	10–30 years (70%) M:F equal	Metaphyseal region of long bones, pelvis, scapula, humerus, femur, forearm
<i>Other tumors</i>		
Angioma, cystic angiomatosis, massive osteolysis	—	—
<i>Tumor-like disorders</i>		
Implantation dermoid, fibrous dysplasia, osteofibrous dysplasia	—	—

Table 15.9 [^{99m}Tc]MDP bone scan findings in some primary benign and malignant bone tumors^{15,39,46,52–60}

<i>Tumor</i>	<i>[^{99m}Tc]MDP bone scan findings</i>
Osteogenic sarcoma	Markedly increased uptake with some patchy areas of decreased accumulation with ill-defined margins/distortions. In some, uniform and increased uptake is noted. Rarely photopenia has also been reported
Ewing's sarcoma	Markedly increased accumulation with a homogeneous distribution. Distortion is less marked than with osteogenic sarcoma. Tumor margins are poorly delineated
Chondrosarcoma	Moderately increased throughout the tumor with some scattered areas of focal intense uptake. The tumor margins are well defined with mild distortion
Non-ossifying fibroma	Mild increase in the delayed images only or no increase in uptake
Simple bone cyst	Non-traumatized bone cysts may be indiscernible, as they typically show a slight reactive margin surrounding a photopenic center
Unicarmel bone cyst	Normal or cold (unless there is complicating fracture)
Monostotic fibrous dysplasia	Markedly increased uptake on all three phases of the bone scan (intense homogeneous uptake pattern in the delayed phase)
Aneurysmal bone cyst	Hypervascularity with a ring-like pattern (non-specific). (Moderate to intense tracer accumulation at the periphery of the lesion with little activity at its center (doughnut sign))
Osteochondroma	Normal vascular phase and increased uptake in delayed phases
Chondroblastoma	Mild uniform uptake
Enchondroma	Unremarkable first and second phases and the delayed phase shows mild to moderate uptake
Osteoid osteoma	Intense focus of uptake with area of abnormal osteoblastic activity. Negative study excludes diagnosis
Giant cell tumor	Rim of moderately increased uptake surrounding a photopenic area/doughnut pattern
Langerhans cell histiocytosis	Early phase may show intense vascularity, delayed phase often shows centrally reduced uptake

Osteoclastoma/giant cell tumor (GCT)

Osteoclastoma may arise anywhere in the skeleton. The common sites include the lower end of the femur, upper tibia, and distal radius. The distinction between a benign and a malignant lesion is often difficult based only on clinical and radiological findings. Approximately 10% of these tumors are malignant. The scintigraphic findings are increased tracer uptake in all three phases of a bone scan, and accumulation of the tracer around the tumor periphery is more than in its center (doughnut sign)^{55–58} (Figure 15.2). However, this feature is non-specific, and can also be seen in tumors such as telangiectatic osteosarcoma, chondrosarcoma, and aneurysmal bone cyst.^{55–58} The bone scan is useful in detecting local recurrence. Although several groups have investigated the role of bone scintigraphy in assessing the true extent of this tumor,

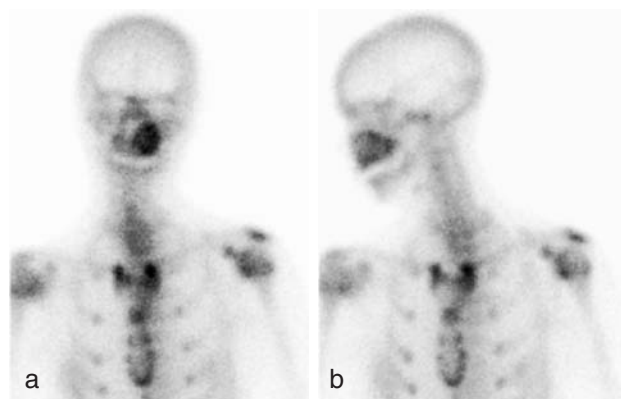


Figure 15.2

(a, b) Giant cell tumor: increased uptake around the left maxilla as seen on anterior and left lateral images.

they concluded that the bone scan was less useful than conventional radiological imaging in planning surgical margins.^{56–58} Further, ⁶⁷Ga, was also reported to have a very limited role in these tumors.

Aneurysmal bone cyst (ABC)

Aneurysmal bone cyst is an expansile lesion of bone containing thin-walled blood-filled cystic cavities, and patients often present with pain or pathologic fracture.^{29,39,55,59} In general, primary ABC is more common than secondary ABC. The secondary ABC arises from pre-existing benign or malignant bone lesions.^{29,39,55,59} The scintigraphic appearances of this tumor are similar to chondrosarcoma and GCT, and thus lack specificity and radiography is often helpful in excluding GCT (18–45 years of age) and chondrosarcoma (metaphyseal/diaphyseal). The telangiectatic osteosarcoma is difficult to differentiate from ABC as it can present as a lytic lesion with fluid levels and also have a ‘doughnut’ appearance on a bone scan.⁵⁹

Fibrous dysplasia of bone

Fibrous dysplasia is a skeletal developmental anomaly in which mesenchymal osteoblasts fail to undergo normal morphologic differentiation and maturation.²⁹ Patients are usually asymptomatic, although pathologic fracture resulting from fibrous dysplasia can cause pain. Approximately 70–80% of cases are monostotic and 20–30% are polyostotic. In general, amorphous or irregular calcification is seen on CT scans, and MRI is also useful in accurately defining the full extent of the lesion. The bone scan shows increased uptake on all three phases, with an intense homogeneous uptake pattern in the delayed phase. In some cases, only minimal uptake or even no uptake is noted on a bone scan. The main use of the bone scan in fibrous dysplasia is to demonstrate polyostotic involvement⁶⁰ (Figure 15.3).

Other miscellaneous benign bone lesions

Osteochondroma is the commonest benign bone tumor and may present as solitary or as multiple lesions. The bone scan appearances may vary from moderately increased uptake to no focal increased uptake, and scintigraphy has been reported to have no value in predicting sarcomatous changes in these tumors.³⁹

Bone islands consist of foci of compact lamellar bone in a normal cancellous bone, and 50% of these show increased uptakes on a bone scan and the remainder may show no abnormal uptake. Bone islands and osteoblastic metastases



Figure 15.3

Fibrous dysplasia. [^{99m}Tc] methylene diphosphonate (MDP) bone scan shows increased uptake in the right hemipelvis, right knee joint, right tibia, and right foot. Right total hip replacement (THR) is noted with increased uptake around the acetabular component and the tip.

may have similar radiological appearances and a normal bone scan can help to exclude a malignant lesion.^{61,62}

Chondroblastoma appears as a lytic lesion in the epiphyseal ossification center of long bones, and may also invade the adjacent bone. The bone scan appearances vary from normal to markedly increased uptake.⁶³

Benign cortical irregularity of the distal femur (BCIDF) is a condition that usually mimics malignancy on radiography but the bone scan is normal. The bone scan distinguishes it from primary lesions of bone.⁶⁴

Increased uptake of bone scanning agents has also been reported in conditions such as intraosseous ganglion,

cholesteatoma, ameloblastoma, periosteal leiomyoma, non-ossifying fibroma, osteoblastoma, Langerhan's cell histiocytosis, etc.⁶⁵

Radionuclide scintigraphy of malignant bone tumors

Malignant bone tumors can occur at any age. There are several types of malignant bone tumors and the most common are osteosarcoma, Ewing's sarcoma, and chondrosarcoma (Table 15.10).^{2,45,66–69} Excluding multiple myeloma,

osteosarcoma is reported to be the most common primary tumor of bone and accounts for 36% of primary bone malignancies.¹⁵

Osteosarcoma

Osteosarcoma is a high-grade, malignant spindle cell tumor that arises within a bone, and it typically occurs during childhood and adolescence.⁶⁶ It can occur in the elderly as a rare complication of Paget's disease. In general, 80–90% of these tumors occur in the long bones, and are usually metaphyseal, and pain is the most common complaint (Figure 15.4).⁶⁶

Table 15.10 Classification of malignant bone tumors and their common sites^{2,7,9,40,45,47–51,66–68}

<i>Malignant tumors</i>	<i>Age range and sex</i>	<i>Common sites</i>
Chondroid origin		
Chondrosarcoma (central and peripheral)	Over 40 years (>50%) M:F 1.5:1	Pelvis, proximal femur, proximal humerus
Other varieties of chondrosarcoma (juxtacortical, mese-chymal, clear cell)	—	—
Osteoid origin		
Osteosarcoma (central)	Under 30 years (> 80%) M:F 2:1	Metaphyseal region of growing bones. 75% are found in distal femur or proximal tibia
Other varieties of osteosarcoma (telangiectatic, low-grade intramedullary, surface, parosteal, periosteal, high grade)	—	—
Fibrous origin		
Malignant fibrous histiocytoma	All ages with a predilection for 4th decade (rare in children) M:F 1.5:1	Metaphyses of long bones (particularly around knee)
Fibrosarcoma	20–50 years M:F equal	Long bones, diaphyses of femur and tibia
Marrow tumors		
Ewing's sarcoma	Under 20 years (75%); under 30 years (90%) M:F 2:1	Diaphysis, femur, tibia, and humerus
Primary lymphoma of bone (lymphosarcoma of bone, reticulum cell sarcoma of bone)	2nd–8th decade (mean age 50 years) M:F 1.6:1	Diaphysis of long bones (femur, tibia, and humerus)
Metastatic neuroblastoma	Under 5 years	Any bone, skull (50%), long bones (metaphyseal)
Notochordal in origin		
Chordoma	All decades (max. 50–70 years) M:F equal below 40 years (later M > F)	Basisphenoid, sacrum
Other tumors		
Angiosarcoma (hemangioendothelioma, hemangioendothelial sarcoma)	All ages M:F 2:1	Any bone, long bones predominate, tibia, humerus, femur

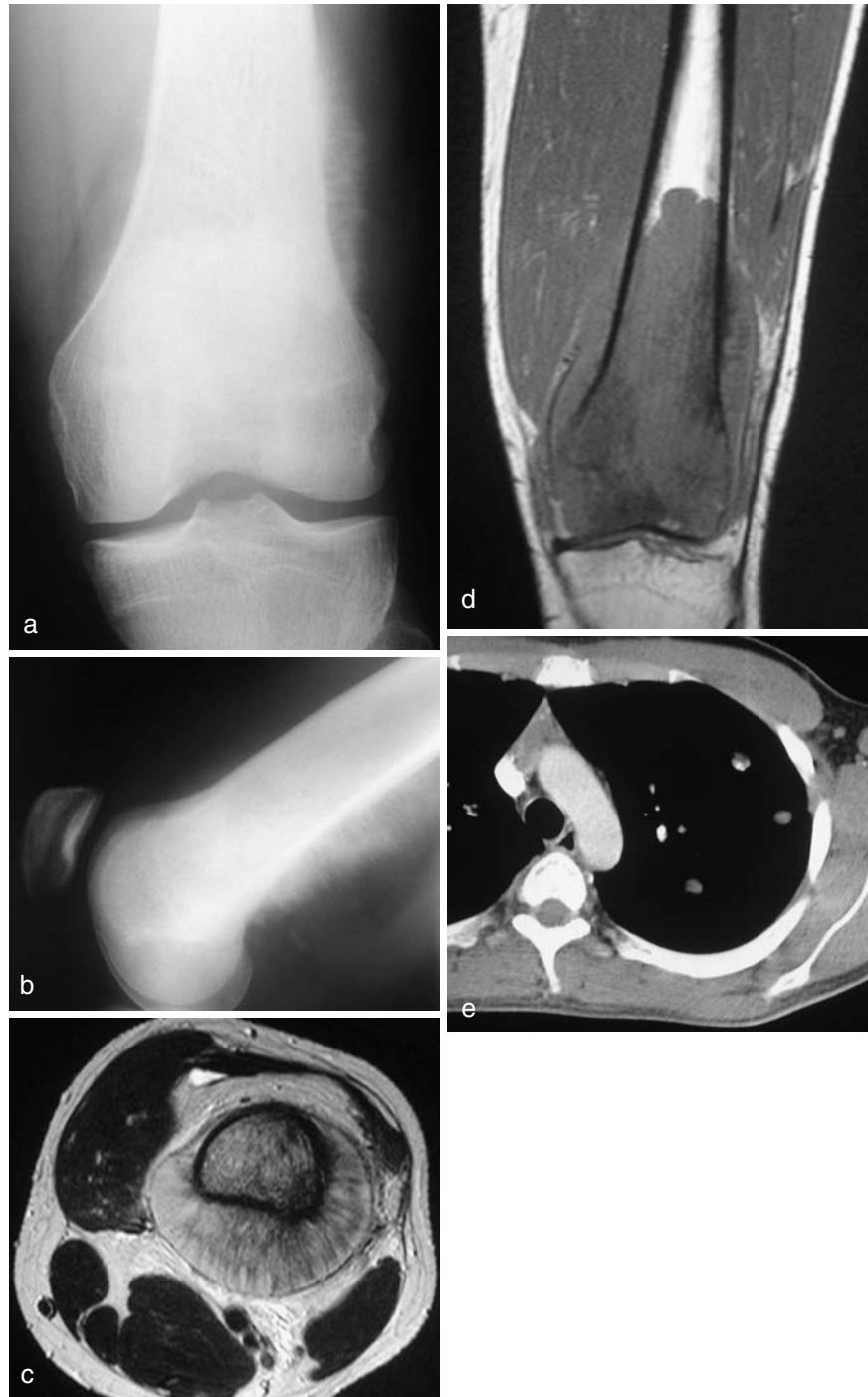


Figure 15.4

Osteogenic sarcoma. (a,b) Radiograph demonstrating metaphyseal osteosarcoma with ill-defined increased density and 'sunburst' spiculation. (c) T₂-weighted transaxial magnetic resonance imaging (MRI) demonstrating perpendicular spiculation into the soft tissue mass. (d) Coronal unenhanced T₁-weighted MRI showing intermediate signal tumor invading the marrow. (e) Computed tomography (CT) scan showing pulmonary metastases, some of which are calcified. (Image courtesy Dr Richard Hughes.)

Table 15.11 Clinical staging of osteosarcoma based on tumor grade and TNM^{2-8,73}

Clinical stage	Tumor grade	TNM
Stage 1A	G1	T1N0M0
Stage 1B	G1	T2N0M0
Stage 2A	G2	T1N0M0
Stage 2B	G2	T2N0M0
Stage 3A	G3	T1N0M0
Stage 3B	G3	T2N0M0
Stage 4A	Any G	Any T N1M0
Stage 4B	Any G	Any T any N M1

T, Tumor; N, nodes; M, metastasis.

The diagnosis is made by an initial biopsy, and standard treatment involves the use of multiagent chemotherapy and definitive surgery of the primary tumor, followed by postoperative chemotherapy.⁶⁹ In recent years aggressive adjuvant and neoadjuvant treatment has improved the treatment outcome.^{70,71} These tumors commonly metastasize to the lungs, other bones, and lymph nodes,⁷² and accurate preoperative staging and evaluation of response to chemotherapy are therefore important aspects of patient management (Tables 15.11 and 15.12).²⁻⁹ The bone scan is markedly abnormal in osteosarcoma, and the typical findings include markedly increased uptake, patchy tracer distribution within the lesion, marked distortion of the bony outline, and a moderately well defined margin (Figure 15.5). In parosteal osteosarcoma tracer distribution is more uniform within the lesion. Radionuclide scintigraphy has been used to detect osseous metastases at the time of diagnosis and during follow-up.

The use of bone scintigraphy in assessing local tumor extent is controversial and remains an area of debate, but is

a technique which can readily be used to assess the rest of the skeleton for metastatic sites. At presentation, skeletal metastases are relatively rare, only appearing in 2–6% of patients.^{46,74} This technique may be even more useful in the post-treatment follow-up of such patients, because it is at this stage that skeletal metastases are commoner.⁷⁴ Bone metastases from osteosarcoma characteristically show increased uptake, but cold lesions (photopenic) have also been reported. The lungs are a common site of metastatic spread, and although uptake of bone seeking tracers has been recorded in the chest this is not a sufficiently reliable technique for staging. Currently CT is the preferred technique both at presentation and as a follow-up investigation.

A good preoperative response to chemotherapy correlates with relapse-free and overall survival.^{75,76} The assessment of response to preoperative chemotherapy is of particular interest in functional nuclear medicine imaging as the degree of tumor necrosis may be related to the prognosis.⁷⁷ Recent reports indicate that patients with more than 90% necrosis have a better prognosis than those with less than 90% necrosis. Conventional imaging modalities have been used to assess response after preoperative treatment. These techniques provide the size of the tumor after preoperative treatment, but these seem to correlate poorly with histological necrosis of the tumor.^{76,78-80}

For bone scintigraphy, initial studies reported an overall accuracy of 88–96% for assessing tumor regression prior to surgery.⁸¹⁻⁸⁵ However, further studies do not recommend using bone scintigraphy for assessing tumor response.⁸¹⁻⁸⁵ Kobayashi et al. reported a method to assess the effects of preoperative chemotherapy using bone scintigraphy.⁸⁶ In his method the uptake was calculated as tumor-to-background ratio (TBR), and the changes in TBR before and after chemotherapy were calculated as the alteration ratio. However, this technique is limited by the fact that increased osseous uptake may reflect both tumor viability and healing.^{76,87} In general bone, scintigraphy overestimates the extent of the tumor, and post-therapeutic bone scintigraphy has difficulty in differentiating tumor viability and healing response.^{81,88-92}

Radionuclide scintigraphy with ²⁰¹Tl is useful in the assessment of response to chemotherapy in osteosarcoma. Many studies have confirmed that the changes in accumulation of ²⁰¹Tl in the tumor are effective for evaluating the response to preoperative treatment.^{22,90,93-99} A marked decrease in ²⁰¹Tl uptake by the tumor indicates a favorable response to chemotherapy. A change in therapy may be needed when ²⁰¹Tl uptake by the tumor does not decrease within weeks of chemotherapy.⁹⁹ Kunisada et al. compared thallium scintigraphy and angiography in the assessment of preoperative treatment response, and suggested that thallium scintigraphy was more useful than angiography in categorizing responders and non-responders to preoperative chemotherapy.⁷⁶

Table 15.12 surgical staging system by Enneking et al.^{2-9,73}

Grade	Tumor site	Stage
Low	Intracompartmental	1A
Low	Extracompartmental	1B
High	Intracompartmental	2A
High	Extracompartmental	2B
Low or high	Metastasis (regional or distant)	3

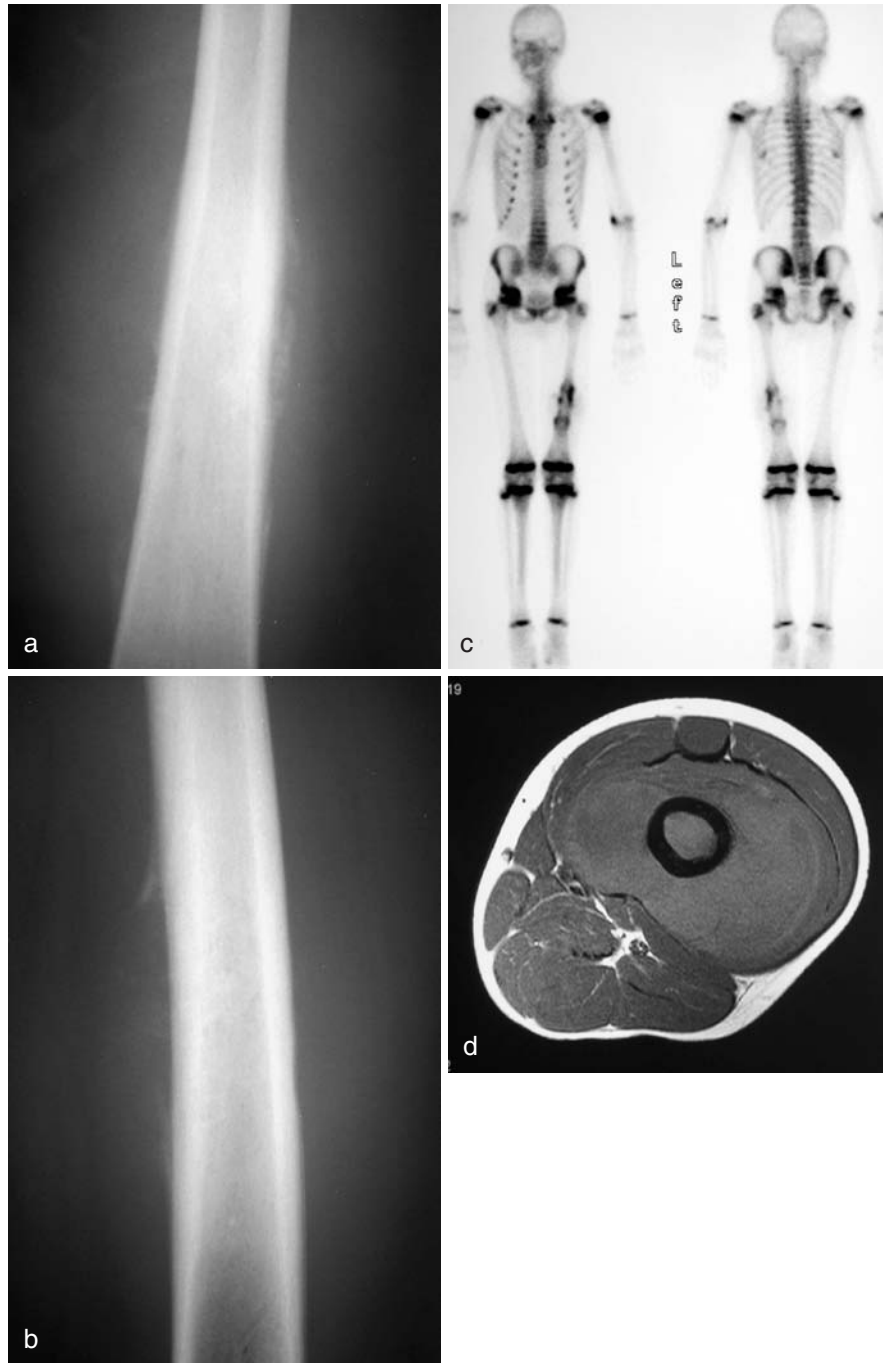


Figure 15.5

Osteogenic sarcoma. (a) Radiograph showing a less common diaphyseal osteosarcoma with periosteal reaction and spiculation. (b) Radiograph demonstrating Codman's triangle of periosteal elevation by the tumor at the peripheries. (c) ^{99m}Tc MDP bone scan demonstrating irregular, predominantly cortical uptake seen in the left femoral diaphysis. (d) Unenhanced transaxial T₁-weighted MRI showing intermediate tumor signal in the bone marrow and a soft tissue mass encircling the femur.

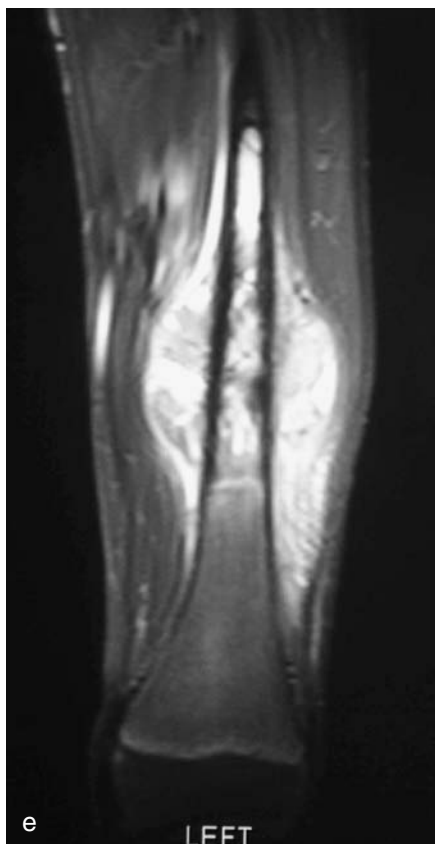


Figure 15.5, cont'd

(e) Coronal short time inversion recovery (STIR) MRI showing high signal within the marrow and the extraosseous soft tissue component of the tumor. (Image courtesy Dr Richard Hughes.)

Radionuclide scintigraphy with [^{99m}Tc]MIBI has also been reported to be useful in the imaging evaluation of osteosarcoma, and it also identifies non-responders earlier during chemotherapy, which would then help in deciding on alternative chemotherapeutic agents or surgery.^{27, 100–103} [^{99m}Tc]MIBI has also been assessed in a series of predominantly bone sarcomas post-therapy.^{100–104} It was found to accurately differentiate active sarcoma from post-treatment changes.

Paget's sarcoma

In fewer than 1% of patients with Paget's disease a sarcoma may develop. The tumor characteristically shows relatively reduced uptake compared with the benign pagetic bone,^{105,106} but in active Paget's disease it may be difficult to identify superimposed osteosarcoma. Smith et al. described a series with a variety of imaging tests in patients with Paget's sarcoma. ^{67}Ga showed a slight increase in tracer

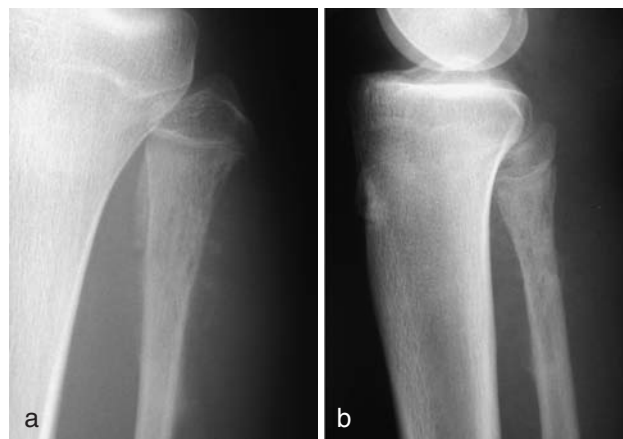


Figure 15.6

(a,b) Ewing's sarcoma: radiograph showing permeative destruction and periosteal reaction with multilaminar 'onion peel' appearance on the medial aspect of the fibula on the frontal view. (Image courtesy Dr Richard Hughes.)

uptake in benign pagetic bone compared to normal bone, and in the pagetic sarcoma the uptake was markedly increased (where MDP was cold).^{105,106} In general, pagetic sarcoma can be confirmed by conventional radiological imaging; however, in equivocal cases a combination of [^{99m}Tc]MDP bone scan and ^{67}Ga may be helpful in identifying a site for biopsy.

Ewing's sarcoma

These tumors occur primarily in children and adolescents, and they arise in the diaphysis of long bones (Figure 15.6). The primary lesion usually shows avid uptake of [^{99m}Tc]MDP (Figure 15.7), which is more uniform and shows less irregularity of contours than with osteosarcoma,³⁵ but similarly may not accurately demonstrate the true extent of tumor due to marrow involvement. ^{67}Ga also avidly accumulates into primary lesions,¹⁰⁷ but surprisingly Caner et al. noted absent uptake in a number of Ewing's tumors using [^{99m}Tc]MIBI.²⁷ Skeletal metastases are considerably more common (> 10%)^{108–110} than with osteosarcoma, and so routine bone scintigraphy has a role in the initial staging of these patients. Bone scintigraphy also has a role in routine surveillance of patients, as more than one-third subsequently develop skeletal metastases.^{103,110} Unlike osteosarcoma, extraskeletal metastases from Ewing's sarcoma will not accumulate bone-scanning agents.¹¹¹ [^{18}F]FDG-PET is also reported to be superior to bone scintigraphy in the detection of bone metastases of Ewing's tumors.¹¹² In general, ^{201}Tl and [^{18}F]FDG imaging are more reliable than a bone scan in monitoring tumor response to treatment.

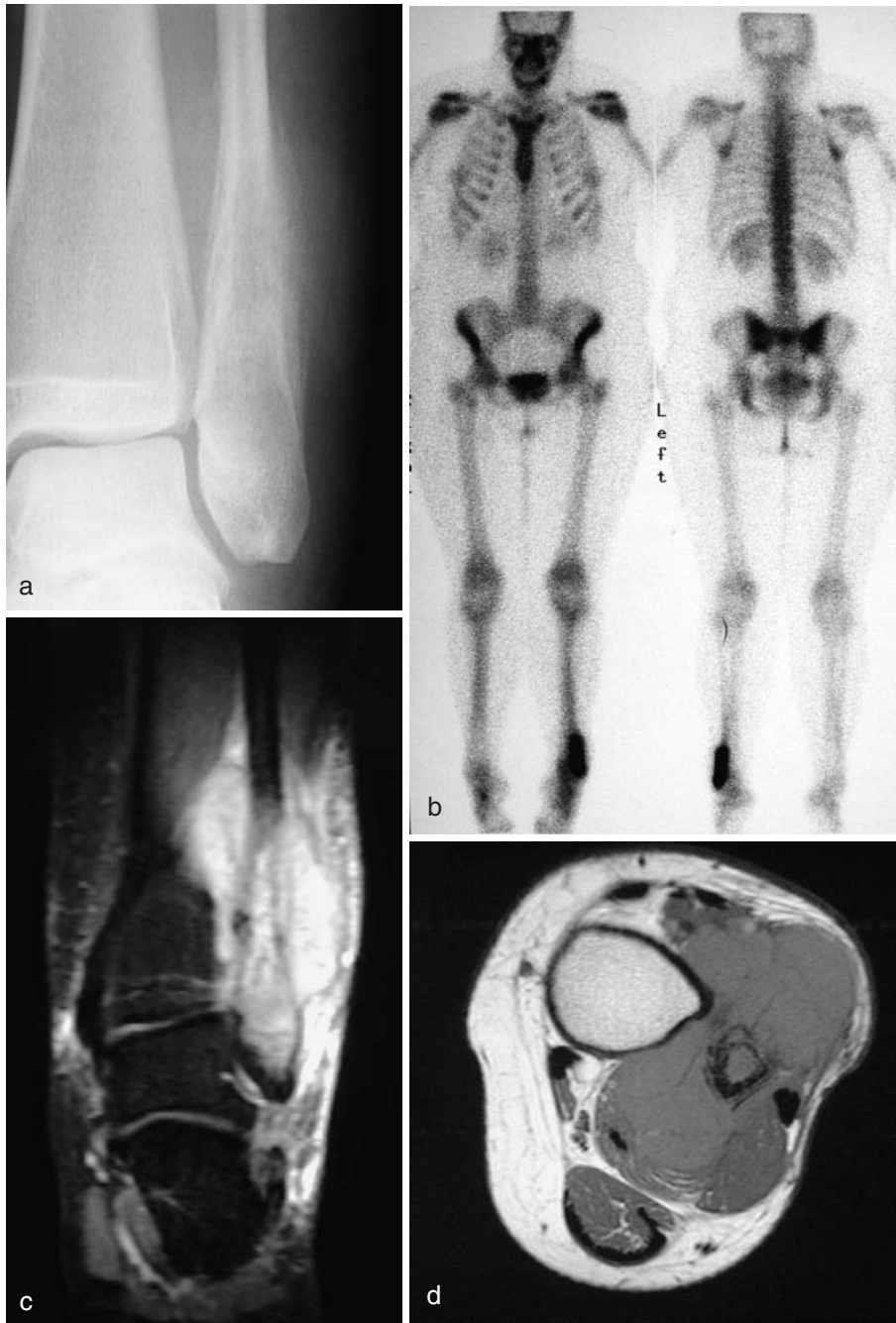


Figure 15.7

Ewing's sarcoma. (a) Radiograph showing a permeative destructive lesion of the distal fibula with periosteal reaction. (b) Increased uptake at left distal fibula on bone scintigraphy but no skeletal metastases. (c) Coronal STIR MRI showing a high signal soft tissue mass involving the distal fibula. (d) Transaxial unenhanced T₁-weighted MRI showing the large intermediate signal soft tissue component surrounding the distal fibula with infiltration of the marrow. (Image courtesy Dr Richard Hughes.)

Chondrosarcoma

Chondrosarcoma is the second most common primary malignant spindle cell tumor of bone.³⁹ These are a heterogeneous group of tumors whose basic neoplastic tissue is cartilaginous.⁴⁷ Five types of chondrosarcomas have been described (central, peripheral, mesenchymal, differentiated, and clear cell).^{48,49,113} These tumors are broadly classified as primary and secondary (often arising from benign cartilage tumors). The most common primary sites of chondrosarcomas are the pelvis, femur, and shoulder girdle.

These tumors are also the most common malignant tumors of the sternum and scapula. Metastatic potential correlates with the histological grade of the tumor.^{64,113,114} The role of radionuclide bone scan is limited, and the typical appearances show moderately increased uptake throughout the tumor with some focal areas of intense uptake. Distortion of the bone outline is usually slight, and the scintigraphic margin is well defined. The scintigraphic appearances do not correlate with histological grading of the tumor.^{36,115,116} If serial scans are available, the bone scan may play a role in screening the sarcomatous transformation of enchondroma

into chondrosarcoma. Further, [^{99m}Tc]DMSA scintigraphy can also be used in distinguishing benign and malignant chondrogenic tumors, and in predicting malignant transformation of chondrogenic tumors.^{28,117}

Lymphoma of bone

Lymphomas of bone are rare, and constitute 5–8% of primary malignant bone tumors.^{118–121} The most common forms of primary bone lymphomas are large cell or mixed small and large cell lymphomas of B-cell lineage. The femur is the most common site, and other sites include the pelvis, humerus, head and neck, and tibia.¹²² Involvement of the skeleton occurs in up to 20% of patients with Hodgkin's (HD), and 3–5% of all cases of non-Hodgkin's lymphoma (NHL) are primary disease of the skeleton (secondary involvement occurs in up to 25% of patients).^{119–121} Bone involvement upgrades disease to stage, and is indicative of an aggressive disease with a poor outcome¹² (Figure 15.8). Extension of disease from adjacent disease in the soft tissue to bone, however, does not alter staging.¹² The radiographic features of bone lymphomas are non-specific.^{122,123} Radionuclide scintigraphy using ⁶⁷Ga scintigraphy is reported to be useful in diagnosis and for assessing the treatment response. However, its role in the assessment of tumor response is debatable. Some studies have demonstrated that ⁶⁷Ga scintigraphy is of value in assessing bone lymphoma, whereas others have suggested that ⁶⁷Ga uptake in skeletal lesions after treatment may preferentially reflect bone healing.^{90,124–127} However, the hypothesis is that ⁶⁷Ga uptake is seen in both osteosclerotic and osteolytic lymphoma. The lymphoma-seeking properties, rather than the bone-seeking properties of ⁶⁷Ga, play the primary role in uptake in sites of active bone involvement.¹¹⁹ ⁶⁷Ga scintigraphy may be used as a predictor of long-term outcome in patients with lymphoma of the skeleton, as CT scans do not become negative even 1 year after treatment.¹²² PET using [¹⁸F]FDG has proven accurate for the initial diagnosis and staging of bone lymphoma.^{128–131} In general, [¹⁸F]FDG-PET has the potential for predicting treatment outcome early during the treatment. However, it may be limited by bone marrow uptake and other conditions affecting the bone, particularly in the axial skeleton.^{128,129} The CT images of PET-CT may be helpful in detecting soft-tissue paravertebral masses as well as epidural masses and neural foramen invasion in patients with lymphomas.¹² In general, the pattern of marrow involvement by lymphoma is often patchy, and a blind marrow sampling technique could result in false-negative results if the biopsy site is not infiltrated by lymphoma.¹² It is reported that [¹⁸F]FDG-PET could be used to guide the biopsy site, and can also identify patients with HD who are at high risk of having marrow involvement.¹² However, we should be cautious in assessing the marrow involvement in lymphoma, as reactive changes

following chemotherapy and granulocyte colony-stimulating factors may cause increased bone marrow activity.^{130,131} The role of [¹⁸F]FDG-PET and PET-CT imaging for monitoring the treatment response still needs to be assessed.¹³¹

Myeloma/plasmacytoma

Myeloma is a plasma cell tumor, and in general patients may present with symptoms such as persistent, unexplained backache, impaired renal function, hypercalcemia, and anemia.^{132–134} The diagnosis is confirmed by bone marrow aspirate ± trephine biopsy. Further, to estimate tumor burden and prognosis, bone marrow cytogenetics is used.¹³⁴ The skeletal survey remains the standard method for radiological screening at diagnosis,¹³⁴ but plain radiography has a low sensitivity and specificity. CT has a higher sensitivity than plain radiographs at detecting small lytic lesions.^{135–137} MRI is useful for the assessment of the extent and nature of soft tissue disease, and in patients with cord compression it provides an accurate assessment of the level and extent of cord or nerve root compression. Further, MRI provides information about bone marrow infiltration.¹³⁸ The role of radionuclide bone scintigraphy is limited by its low sensitivity in myeloma, owing to the lack of osteoblastic activity. Reported sensitivities for [^{99m}Tc]MDP bone scan range from 40% to 60%.¹³⁹

[^{99m}Tc]MIBI imaging has been reported to be useful and to have higher sensitivity and specificity in the detection of bone marrow involvement than radiography.^{139–141} Both focal and diffuse bone marrow uptake patterns have been reported as evidence for active myeloma,^{139–141} although a diffuse pattern may also be seen in normal individuals.¹⁴¹ Nandurkar et al. have reported that focal uptake of MIBI is a better indicator of active myeloma than diffuse uptake.¹³⁹ [¹⁸F]FDG-PET is reported to be useful in accurate staging and evaluation of therapy response.^{142,143} Schirrmeister et al. reported that [¹⁸F]FDG-PET is accurate in detecting multiple myeloma, and revealed a greater extent of disease than routine radiographs in 60% of patients who had osteolytic bone lesions.¹⁴⁴ Further, a focal or mixed focal/diffuse [¹⁸F]FDG-PET uptake pattern exhibited a higher positive predictive value for active disease compared with a diffuse uptake pattern (100% and 75% respectively).¹⁴⁴ In detecting myelomatous involvement by [¹⁸F]FDG-PET, Bredella et al. reported a sensitivity and specificity of 85% and 92% respectively.^{142,143,145} Mileschkin et al. compared the utility of MIBI with [¹⁸F]FDG-PET in the evaluation of bone disease in myeloma and they found that in the patients investigated by both [^{99m}Tc]MIBI and [¹⁸F]FDG-PET, MIBI not only detected additional sites to those detected by [¹⁸F]FDG-PET in 52% of cases, but also demonstrated a positive correlation with plasma cell infiltrate in the bone marrow.¹⁴⁶ In general, both [^{99m}Tc]MIBI and [¹⁸F]FDG-PET are useful in the diagnosis and management of myeloma.

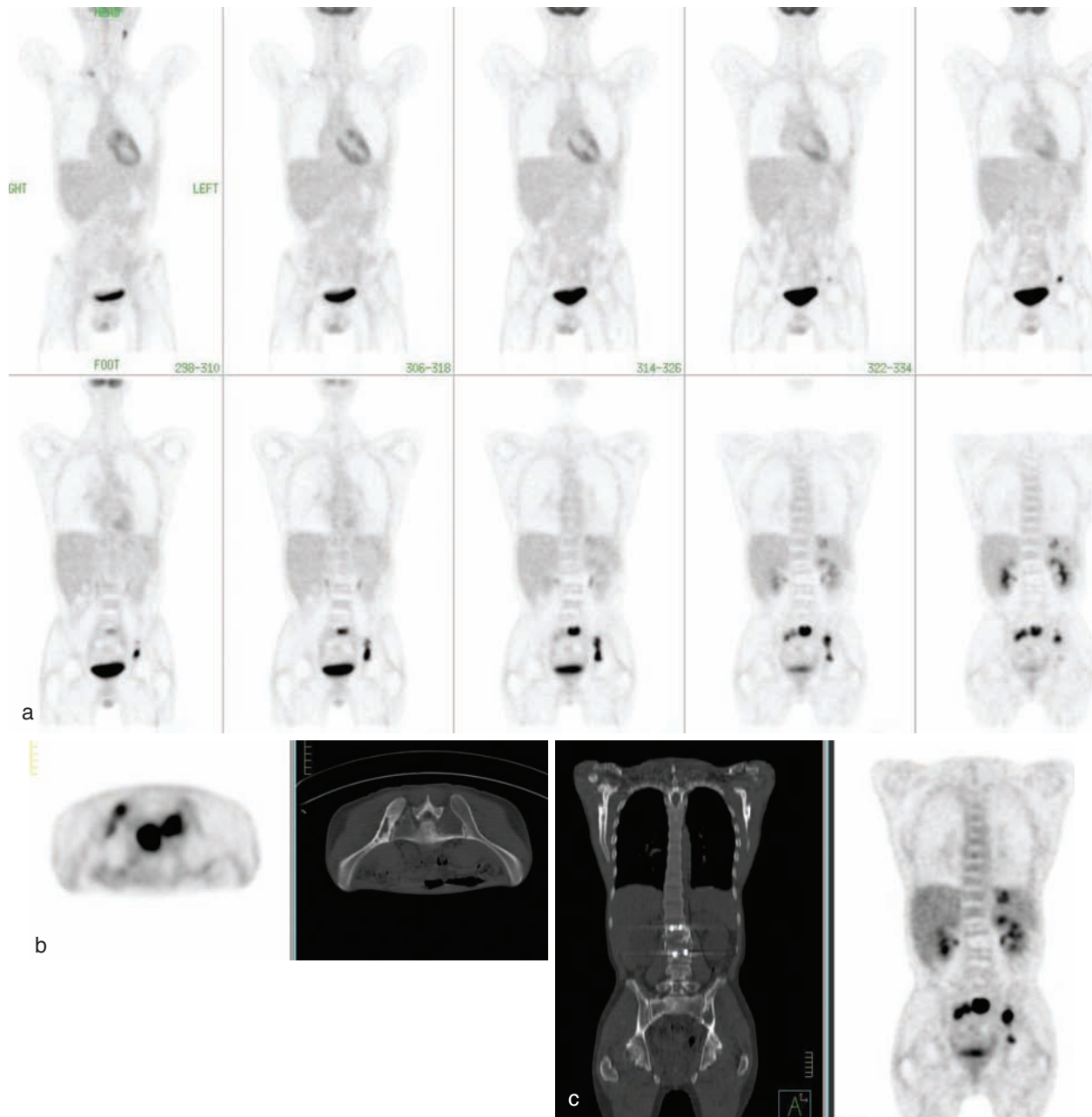


Figure 15.8

Bone lymphoma. (a) Coronal [^{18}F]fluoro-2-deoxy-D-glucose-positron emission tomography (FDG-PET) scan showing active disease in left cervical and right supraclavicular nodes as well as focal disease within the spleen. There is also evidence of bone disease affecting the pelvis. (b, c) Transaxial PET-CT images of the pelvis showing active bone disease appearing both lytic and sclerotic on CT bone windows.

Bone tumors: PET and PET-CT

The exact role of [^{18}F]FDG-PET in osteosarcoma is unclear. Most reports using PET have investigated soft tissue sarcomas rather than bone tumors. However, current literature suggests that in patients with bone sarcomas, [^{18}F]FDG-PET

may play an important role in guiding biopsy, detecting recurrence in amputation stumps, evaluating metastatic disease, and assessing treatment response and prognosis.^{73,103,147,148} The possible role of [^{18}F]FDG-PET in differentiating benign and malignant bone tumors by using standardized uptake values (SUVs) has been studied by

Aoki et al., and they found that [^{18}F]FDG-PET may be of limited value in distinguishing malignant from benign bone tumors accurately because of the high accumulation of [^{18}F]FDG in some benign bone lesions.¹⁴⁹ However, [^{18}F]FDG-PET SUV analysis may be helpful in histologic grading and guiding biopsy (most metabolically active regions).^{73,103,147,148}

In the detection of local recurrence in the amputation stump, the role of [^{18}F]FDG-PET may be limited by increased uptake seen in the postoperative period, which can last up to 18 months post-surgery.¹⁵⁰ However, in the absence of local inflammatory or reactive changes, one should suspect recurrence, and confirmation with biopsy is necessary.^{147,148}

Franzius et al. compared [^{18}F]FDG-PET and bone scintigraphy for detecting osseous metastases, and concluded that the sensitivity, specificity, and accuracy of [^{18}F]FDG-PET in the detection of osseous metastases from Ewing's sarcomas are superior to those of bone scintigraphy.¹⁵¹ However, in the detection of osseous metastases from osteosarcoma, [^{18}F]FDG-PET seems to be less sensitive than bone scintigraphy.¹⁵¹ Further studies from other groups reported that [^{18}F]FDG-PET, when compared to CT, is reported to have lower sensitivity but increased specificity in detecting lung metastases from osteosarcoma.^{148,152,153} The sensitivity of [^{18}F]FDG-PET in detecting bone metastases is also limited.¹⁵⁴

Currently it is difficult to comment on the role of PET-CT technology in detecting metastases, and results are awaited. In the assessment of treatment response in bone tumors, [^{18}F]FDG-PET using the SUV and tumor-to-background analysis is reported to be useful in predicting response and responders.^{81,147,148,155–157} [^{18}F]FDG-PET is also reported to be a useful adjunct to MRI in distinguishing viable tumor from post-treatment changes in patients with bone and soft-tissue sarcomas.^{143,158} Finally, in judging the prognosis in patients with osteosarcoma, [^{18}F]FDG-PET is reported to be useful and complementary.¹⁵⁹ Franzius et al. have reported that overall and event-free survivals were significantly better in patients with low [^{18}F]FDG uptake in the tumor than in patients with high [^{18}F]FDG accumulation in the tumor at the time of diagnosis.¹⁵⁹

Soft tissue sarcomas: etiology, pathogenesis, and scintigraphy

Soft tissue sarcomas are a heterogeneous group of tumors that arise from tissue of mesenchymal origin and account for approximately 1% of all malignant tumors.^{160,161} The etiology of these tumors is not well defined, but multiple associated and predisposing factors have been reported.¹⁶² Tumor suppressor genes play a critical role in cell growth

inhibition and can suppress the growth of cancer cells, and the retinoblastoma (Rb) gene and the p53 tumor suppressor gene are reported to be relevant to soft tissue sarcomas.¹⁶³ Imaging of soft tissue sarcomas requires a multimodality approach, no single imaging modality being ideal for every tumor.^{14,164,165} In general, following radiography, MRI is usually considered as a first line for the evaluation of a soft tissue mass, followed by CT, [^{18}F]FDG-PET, ultrasonography (US), and magnetic resonance angiography (MRA), depending on the availability and the clinical scenario.^{14,164}

Soft tissue sarcomas can occur in any site in the body, and approximately 50% of them appear in the extremities.⁵⁰ These tumors generally grow in a centrifugal fashion, compressing the surrounding normal structures.¹⁶⁶ Different types of soft tissue sarcomas have been described and have distinguishing histological characteristics, although many of them have common clinical and pathological features^{50,51,167} (Table 15.13). These tumors also have numerous grading criteria and grading scales. Unfortunately the grading criteria are neither specific nor standardized.^{50,168–170} The tumor grade, size, and depth in relation to the muscle fascia are important determinants of disease recurrence and the development of metastases.^{16,171–176} The overall 5-year survival rate in patients with soft tissue sarcomas of all stages remains only 50–60%. In general the dominant pattern of metastasis is hematogenous and is site specific.^{161,162} In patients with lesions in the extremities, most metastasize primarily to the lungs (70%), and in those with retroperitoneal or visceral lesions, the more common site would be the liver, with lung a secondary site.^{50,177}

Radionuclide scintigraphy in diagnosis, staging, and management

The role of nuclear medicine in the detection and staging of soft tissue sarcomas is uncertain. However, the advantage of being a functional imaging modality will be useful in differentiating viable from non-viable tumor and in assessing the response to therapy. ^{67}Ga is reported to have high sensitivities for the detection of soft tissue sarcomas and metastases,^{178,179} but uptake depends on tumor grade, and this makes it less sensitive for some tumors.¹⁶⁷ The reported results are equally good before or after therapy, with 52/56 (93%) of patients having true positive studies prior to treatment and 8/9 (89%) post-treatment, in a study by Southee et al.¹⁷⁸ Approximately 85% of disease sites were correctly located, although liver metastases were poorly identified presumably due to physiological gallium accumulation in the liver, making lesions obscure. One tumor that is consistently negative with ^{67}Ga imaging is Kaposi's sarcoma. This finding is diagnostically useful, as gallium

Table 15.13 Classification of soft tissue sarcomas^{2–9,14,50,51,160,161}

<i>Histology subtype</i>	<i>Age range (years)</i>	<i>Common site of primary</i>
Liposarcoma	40–60	Majority lower extremities and retroperitoneum
Angiosarcoma	50–70	Cutis/subcutis of head, lower extremities
Ewing's sarcoma (extraskelatal)	10–30	Lower extremities, paravertebral, chest wall
Fibrosarcoma	30–50	Extremities, trunk
Leiomyosarcoma	50–60	Retroperitoneum, cutis/subcutis of lower extremities
Primitive neuroectodermal tumor (PNET)	15–35	Trunk, lower extremities
Malignant fibrous histiocytoma	50–70	Proximal extremities, retroperitoneum
Malignant schwannoma	25–30	Proximal extremities, trunk
Embryonal rhabdomyosarcoma	7–11	Head, neck, urogenital
Alveolar rhabdomyosarcoma	15–20	Extremities, head, neck
Pleomorphic rhabdomyosarcoma	40–60	Extremities, urogenital
Synovial sarcoma	20–35	Extra-articular joints of lower extremities

imaging may then differentiate Kaposi's sarcoma from infective abnormalities such as atypical mycobacterial infections, which are gallium positive, in patients with acquired immunodeficiency syndrome (AIDS).¹⁷⁹ In general, thallium imaging has been shown to be more accurate than gallium in both soft tissue sarcomas and bone tumors in assessment of chemotherapy response.

PET and PET–CT in diagnosis, staging, and management

Diagnosis and staging

[¹⁸F]FDG–PET is recommended for the diagnosis and staging as well as for the detection of recurrence in patients with malignant soft-tissue sarcomas (Table 15.14). The reported results vary from visual evaluation to semiquantitative evaluation using SUVs.¹⁸² The sensitivity and specificity reported in the literature using a dedicated PET scanner is 91–100% and 65–88% respectively,^{183–187} with a close correlation between tumor grade and degree of uptake.^{8,188–191} Common false negatives are in low-grade sarcomas and false positive in some benign tumors and inflammatory lesions.^{183,187,190–192} In detecting local disease, Lucas et al. have reported a sensitivity of 73% and specificity of 94%, and the results for MRI were 88% and 96% respectively.¹⁹³ A number of studies have reported the ability of [¹⁸F]FDG–PET to grade tumors, although the differentiation of low-grade from benign lesions is more difficult.^{8,185,187,193–196} In a systematic review and meta-analysis (17 studies), Bastiaannet

et al. found that [¹⁸F]FDG–PET has the potential to discriminate between sarcomas and benign tumors, as well as between low- and high-grade sarcomas.¹⁸⁰ The pooled sensitivity, specificity, and accuracy of PET for the detection of sarcomas were 91%, 85%, and 88%, respectively.¹⁸⁰ Further reports suggest that evaluating full FDG kinetics may provide superior information for discriminating grade I and grade II tumors (positive predictive value of 80%).^{147,183,180} The differentiation of benign lesions from high-grade tumors is improved by delayed scanning (as high-grade tumors may not reach peak activity until 4 hours, whereas benign lesions plateau as early as 30 minutes).¹⁸⁰ Intermediate-grade and high-grade sarcomas are reported to accumulate and metabolize FDG to a greater extent than in normal tissues, many benign tumors, and low-grade sarcomas,^{161,181,187,190,196} and grading of low-grade tumors and benign lesions may not be adequate and accurate.

Guiding biopsies

Sarcomas are often heterogeneous and may contain areas of inflammation, fibrosis, and necrosis in addition to viable tumor cells. By demonstrating the most metabolically active sites within a primary sarcoma, [¹⁸F]FDG–PET may be helpful in guiding biopsies to ensure a representative sample.¹⁹³ Hain et al. reported that benign lesions showed low or no FDG uptake, and in malignant masses the biopsy site suggested based on the [¹⁸F]FDG–PET scan was found to be representative of the most malignant site on histology.¹⁹⁷ With the availability of PET–CT, localization of the most active metabolic site will become easier and will

Table 15.14 Summary of [¹⁸F]fluoro-2-deoxy-D-glucose (FDG)-PET in bone and soft tissue tumors^{12,73,98,150,161,180,181}**1. Non-invasive****2. Diagnosis and staging**

Useful in the evaluation of both primary and recurrent soft-tissue lesions

Clinically helpful in tumor grading

Accurate in differentiating low- from high-grade tumors

Preoperative analysis of glucose metabolism may help in selecting appropriate treatment regimen

Superior to [^{99m}Tc]MDP bone scintigraphy in detecting bone tumors

3. Assessment of treatment response and prognosis

Detects early responses to therapy

SUV is useful in predicting patient outcomes

Change in the maximum accumulation of FDG in sarcomas closely relates with survival

Differentiates scar from viable tumor

4. Guiding biopsies

Helpful in guiding biopsies

Helpful in localization of the most active metabolic site

5. Limitations

[¹⁸F]FDG-PET may not be quite as sensitive as CT for lung metastases

[¹⁸F]FDG-PET may not be quite as sensitive as MRI for local recurrence

It may not discriminate between low-grade tumors and benign lesions

Probable lower sensitivity in detecting osteosclerotic bone metastases from extraskeletal malignancies

Epiphyseal growth plates in children show moderate uptake and must not be misinterpreted as tumors

Intense uptake may be noted in patients using crutches (shoulder, axilla, etc.)

The cost-effectiveness needs to be delineated

Further evaluation and comparison against other newer radiopharmaceuticals is required

SUV, standardized uptake value

help the surgeon to plan an appropriate approach to reach the biopsy site.

Detection of metastases

In detecting metastases, [¹⁸F]FDG-PET may not be quite as sensitive as CT for lung metastases or as sensitive as MRI for local recurrence, although it demonstrates good specificity and is able to detect other distant metastases.¹⁵⁰ It has therefore been suggested that all three imaging procedures may be required to accurately stage patients. For the identification of lung metastases, the sensitivity and specificity of [¹⁸F]FDG-PET were 86% and 100%, respectively, and those of chest CT were 100% and 96%, respectively. However, [¹⁸F]FDG-PET is reported to be helpful in identifying other unexpected sites of metastases.^{198,199}

Assessment of local recurrence

In earlier studies, Lucas et al. reported [¹⁸F]FDG-PET to be not as satisfactory as conventional imaging for the identification of local recurrence (MRI is better) in patients with

surgically excised tumors.¹⁶¹ However, further study by Hian et al. and others was reassuring, and they concluded that, in the absence of localized clinical changes (pressure areas with skin breakdown), these areas represented a recurrence and needed a biopsy.^{150,199,200} Schuetze et al., with a median patient follow-up of 46 months, reported that the sarcoma SUV_{max} is a strong predictor of local and distant disease recurrence.¹⁷¹ The risk of distant recurrence of disease was reported to be higher in patients with a baseline tumor SUV_{max} ≥ 6.¹⁷¹

Assessment of treatment response

In general, it has not been well established whether a significant change in the tumor size is a meaningful surrogate of patient outcome.^{73,201} More recently there has been much interest in the use of [¹⁸F]FDG-PET to assess response to therapy.^{73,171,202–203} Successful treatment results in a sharp decline in tumor glucose metabolism, in comparison with the high level of glucose metabolism in the tumor before therapy.^{205–207} The results from Schuetze et al. show that with pre-treatment tumor SUV_{max} and change in SUV_{max} after neoadjuvant chemotherapy it is possible to identify

patients who may be at high risk of tumor recurrence.¹⁷¹ In a retrospective analysis, the ability of pre-therapy [¹⁸F]FDG-PET was determined in predicting patient survival and disease-free interval in patients with sarcoma.^{180,201} Further, multivariate analysis showed that SUV_{max} was a statistically significant independent predictor of patient survival, such that tumors with larger SUV_{max} had a significantly poorer prognosis. [¹⁸F]FDG-PET is also reported to be a useful adjunct to MRI in distinguishing viable tumor from post-therapeutic changes in patients with bone and soft-tissue sarcomas, especially when MRI is equivocal.¹⁵⁸ However, a definitive value of [¹⁸F]FDG-PET in the evaluation of therapy is still unclear, and needs further investigation and clarification.

Specific tumor types

Rhabdomyosarcoma

Rhabdomyosarcoma is the commonest soft tissue tumor of childhood, and is a highly malignant tumor (Figure 15.9). The tumor usually presents as a mass, and metastasizes to the lungs, bones, and lymph nodes. Radionuclide imaging with ⁶⁷Ga, [^{99m}Tc]MDP, and thallium are reported to be useful. In a retrospective study by Cogswell et al., ⁶⁷Ga scans had a sensitivity of 84% and specificity of 95%, and [^{99m}Tc]MDP bone scans had a sensitivity of 70% and specificity of 95% for detection of metastatic disease in all tissues. In the detection of skeletal metastases, bone scan sensitivity and specificity of 100% and 95% were reported, respectively.²⁰⁸ The bone scan was sensitive in detecting bone metastases, and ⁶⁷Ga was better for the detection of soft tissue metastasis. Similar sensitivities were reported between ²⁰¹Tl and ⁶⁷Ga in localizing the sites of rhabdomyosarcoma.²⁰⁹

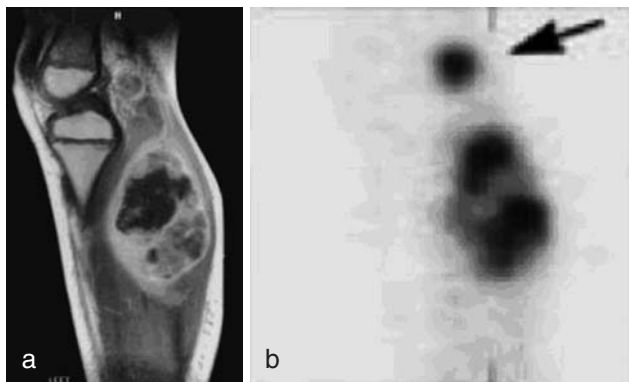


Figure 15.9

Alveolar rhabdomyosarcoma. Sagittal MRI (a) and localized [¹⁸F]FDG image (b) show the tumor with a satellite lesion (arrow). (Reproduced with permission, from reference 185.)

Further, Menedez et al., in a small group of patients, reported that thallium was useful in assessing treatment response in patients with high-grade sarcomas.²¹⁰ Nine of their ten patients showed reduced thallium uptake after chemotherapy, and also marked histological response.²¹⁰ [¹⁸F]FDG-PET imaging may be useful in detecting the primary and monitoring therapeutic response (Figure 15.9). Peng et al., in a small group of pediatric patients, showed that a decreased [¹⁸F]FDG uptake by the tumor was associated with a favorable response to therapy and prolonged remission of the disease. In contrast, persistent abnormal FDG was associated with early relapse.²¹¹

Gastrointestinal stromal tumors

Gastrointestinal stromal tumors (GISTs) constitute approximately 0.1–3.0% of all gastrointestinal tract neoplasms and 6% of all sarcomas. Nearly 70% of GISTs are benign, and 30% are malignant. Malignant GIST is reported to recur and metastasize, often to the liver and peritoneum. It can metastasize less frequently to other sites such as the lungs, pleura, retroperitoneum, bone, and subcutaneous tissues.^{202,212,213} GISTs are reported to be chemoresistant and insensitive to irradiation.²¹⁴ Recent studies show promising results by treating GIST tumors with imatinib (tyrosine kinase inhibitor).^{215–217} CT and [¹⁸F]FDG-PET are reported to have comparable sensitivity and positive predictive values in staging malignant recurrent GISTs. In predicting early response to therapy, [¹⁸F]FDG-PET is reported to be superior.^{201,214–217} (Figure 15.10). However, in treatment planning, PET-CT is reported to

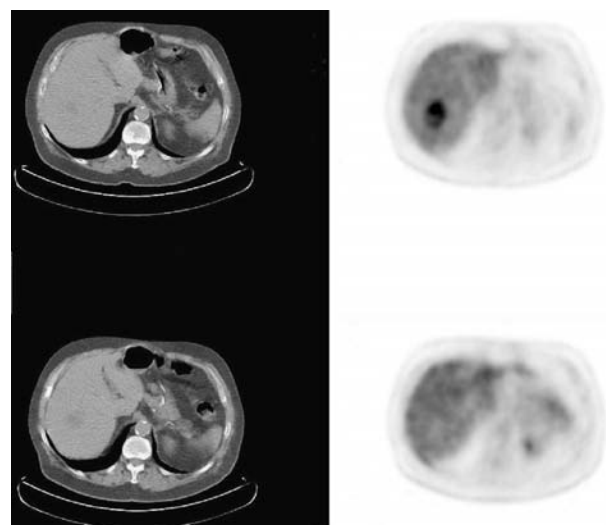


Figure 15.10

Gastrointestinal stromal tumors. Liver metastases pretreatment (top row) show good response after 2 weeks of Glivec[®] (on [¹⁸F]FDG-PET) (bottom row).

be more useful than PET alone, as it precisely delineates lesions and aids in the correct planning of surgical interventions.²¹⁸

Malignant peripheral nerve sheath tumor

Neurofibromas are benign skin tumors with typical histological features.²¹⁹ Some 4% of patients with neurofibromatosis type 1 (NF1) develop malignant peripheral nerve sheath tumors.²²⁰ Malignant peripheral nerve sheath tumor (MPNST) represents approximately 10% of all soft tissue sarcomas. Its diagnosis is often difficult, and the survival rates are low. The prognosis is not well correlated with the histopathology and tumor grading²²¹ (Figure 15.11). The tumors may metastasize to the lung, brain, liver, bone, soft tissue, regional lymph nodes, skin, and retroperitoneum.²²²



Figure 15.11
Neurofibromatosis. [¹⁸F]FDG images show tumor on the right is low grade and that on the left thigh is high grade with heterogeneous uptake. (Reproduced with permission, from reference 185.)

Ferner et al., using SUV, have reported that [¹⁸F]FDG-PET is helpful in determining malignant change in plexiform neurofibromas in NF1.²²³ They have also concluded that, by calculating the SUV at about 200 minutes post-injection of [¹⁸F]FDG (peak activity in malignant tumors), it may be possible to differentiate benign and malignant tumors.²²⁴ Brenner et al. have also reported that tumor SUVs help in the prediction of survival in NF1 patients with MPNSTs.²²¹

Primitive neuroectodermal tumor (peripheral neuroepithelioma, extraosseous Ewing's sarcoma)

Primitive neuroectodermal tumor (PNET) is a soft tissue sarcoma, and there is considerable clinical and histological overlap between this tumor and Ewing's sarcoma. In general, Ewing's sarcoma arises within the bone, while PNET arises within soft tissues. MRI is useful in the assessment of the extent of disease. [¹⁸F]FDG-PET imaging may be useful in detecting the primary and metastatic lesions of PNET.

Recent advances and future trends

SPECT-CT and PET-CT imaging

Recently, integrated or hybrid imaging systems composed of SPECT or PET with CT have been used in clinical practice. Acquisition of both the SPECT or PET and CT is performed without changing the patient's positioning. The limitations of using only scintigraphic techniques in localizing lesions in the vicinity of physiological uptake may be overcome using these hybrid techniques. The CT part of the SPECT-CT or PET-CT is reported to be valuable for attenuation correction and anatomical localization of the abnormality. Further, because routine radiopharmaceuticals used for the detection of malignant bone involvement are generally not tumor-specific, false-positive benign lesions may also show increased tracer uptake and, thus, correlation, mainly with CT, is often indicated and may prove to be useful.

Newer tracers

Currently, PET imaging with newer tracers such as ¹⁸F-labeled Fab fragment of TP3 (animal study), [¹⁸F]fluoride, and [¹¹C]choline are being investigated for the evaluation of bone tumors.^{152,161,224} In brain, head and neck, bone, and soft tissue tumors, [¹¹C]choline is reported to show higher contrast than FDG.²²⁵ Reports comparing [¹⁸F]FDG-PET

with [^{11}C]choline-PET found [^{11}C]choline to be advantageous because of its shorter examination time and minimal urine retention in the bladder.²²⁶ [^{11}C]choline also has lower muscle uptake, and is thereby expected to provide a higher contrast tumor image than [^{18}F]FDG-PET.²²⁷ Further, [^{11}C]aminoisobutyric acid (AIB) and ^{15}O labeled water are reported to be suitable for functional imaging of soft tissue sarcomas and the detection of sarcoma recurrence.¹⁹⁷ These tracers were found to accumulate in primary and recurrent soft tissue sarcomas of different histological type. Suzuki et al. have reported that ^{18}F labeled α methyl tyrosine ([^{18}F]FMT) is superior to FDG in the differentiation between benign and malignant tumors.^{228,229} However, they were unable to establish a cut-off SUV for benign and malignant tumor differentiation. Finally, there are few reports on the use of [^{18}F]FDG-PET in bone tumors.⁷³ However, these results are preliminary, and further studies are awaited.

Conclusion

Functional imaging using radiotracers, imaged using a conventional γ camera or PET scanner, provides unique and complementary information in the overall diagnosis and management of bone and soft tissue tumors. Although there is a limited role in initial staging of primary bone and soft tissue tumors and in differentiating benign from malignant masses, in specific tumor types conventional planar and SPECT techniques have proven useful in diagnosis, staging, assessment of treatment response, and differentiating responders and non-responders. PET imaging using [^{18}F]FDG, acquired either on a dedicated PET system or by using hybrid PET-CT, plays an important role in the diagnosis and management of soft tissue tumors. However, the definitive role in various stages of the disease process needs further evidence and clarification. Finally, with the advent of newer state-of-the-art hybrid technology and tracers, there may be a more definitive role for radionuclide imaging in the near future.

Acknowledgment

We thank Dr Richard Hughes, Consultant, Department of Radiology, Royal National Orthopaedic Hospital, London, for letting us use some of his valuable images.

References

- van Ginkel RJ, Hoekstra HJ, Pruijm J et al. FDG-PET to evaluate response to hyperthermic isolated limb perfusion for locally advanced soft-tissue sarcoma. *J Nucl Med* 1996; 37: 984–90.
- Peabody TD, Gibbs CD, Simon MA. Current concepts review – evaluation and staging of musculoskeletal neoplasms. *J Bone Joint Surg Am* 1998; 80: 1204–18.
- American Joint Committee on Cancer: Soft tissues. In: Fleming ID, Cooper JS, Henson DE, eds. *AJCC Cancer Staging Manual*, 5th edn. Philadelphia: Lippincott-Raven, 1997; 149–156.
- Enneking WF. Staging musculoskeletal tumors. In: Enneking WF, ed. *Musculoskeletal Tumor Surgery*. New York: Churchill Livingstone, 1983; 87–8.
- Enneking WF, Spanier SS, Goodman MA. A system for the surgical staging of musculoskeletal sarcoma. *Clin Orthop* 1980; 153: 106–20.
- Hajdu SI. *Pathology of Soft Tissue Tumors*. Philadelphia: Lea and Febiger, 1979.
- Sobin LH, Wittekond Ch. Tumours of bone and soft tissue tumours. In: Sobin LH, Wittekond Ch, eds. *UICC TNM Classification of Malignant Tumors*, 5th edn. New York: John Wiley and Sons, 1997: 101–10.
- Nieweg OE, Pruijm J, van Ginkel RJ et al. Fluorine-18-fluorodeoxyglucose PET imaging of soft-tissue sarcoma. *J Nucl Med* 1996; 37: 257–61.
- Unni KK. *Dahlin's Bone Tumors: General Aspects and Data on 11,087 Cases*, 5th edn. Philadelphia: Lippincott-Raven, 1996.
- Massengill AD, Seeger LL, Ehardt JJ. The role of plain radiography, computed tomography and magnetic resonance imaging in sarcoma evaluation. *Hematol Oncol Clin North Am* 1995; 9: 571–603.
- Hicks RJ. Functional imaging techniques for evaluation of sarcomas. *Cancer Imaging* 2005; 21: 58–65.
- Even-Sapir E. Imaging of malignant bone involvement by morphologic, scintigraphic, and hybrid modalities. *J Nucl Med* 2005; 46: 1356–67.
- Vogler JB 3rd, Murphy WA. Bone marrow imaging. *Radiology* 1998; 168: 679–93.
- Knapp EL, Kransdorf MJ, Letson GD. Diagnostic imaging update: soft tissue sarcoma. *Cancer Control* 2005; 12: 22–6.
- Ho YY. Review of non-positron emission tomography functional imaging of primary musculoskeletal tumours: beyond the humble bone scan. *Australas Radiol* 2005; 49: 445–59.
- Elias DA, White LM, Simpson DJ. Osseous invasion by soft-tissue sarcoma: assessment with MR imaging. *Radiology* 2003; 229: 145–52.
- Panicek DM, Gatsonis C, Rosenthal DI et al. CT and MR imaging in the local staging of primary malignant musculoskeletal neoplasms: report of the Radiology Diagnostic Oncology Group. *Radiology* 1997; 202: 237–46.
- Bodner G, Schocke MF, Rachbauer F et al. Differentiation of malignant and benign musculoskeletal tumors: combined color and power Doppler US and spectral wave analysis. *Radiology* 2002; 223: 410–16.
- Lin J, Fessel DP, Jacobson JA et al. An illustrated tutorial of musculoskeletal sonography: part 4, musculoskeletal masses, sonographically guided interventions, and miscellaneous topics. *AJR Am J Roentgenol* 2000; 175: 1711–9.
- Fogelman I. Diphosphonate bone scanning agents – current concepts. *Eur J Nucl Med* 1982; 7: 506–9.

21. Salvatore M, Carratolo L, Porta E. Thallium-201 as a positive indicator for lung neoplasms: preliminary experiments. *Radiology* 1976; 121: 487–8.
22. Lin J, Leung W, Ho SKW et al. Quantitative evaluation of thallium-201 uptake in predicting chemotherapeutic response of osteosarcoma. *Eur J Nucl Med* 1995; 22: 553–5.
23. Lam AS, Kettle AG, O'Doherty MJ et al. Pentavalent ⁹⁹Tcm-DMSA imaging in patients with bone metastases. *Nucl Med Commun* 1997; 18: 907–14.
24. Weiner RE. The mechanism of ⁶⁷Ga localization in malignant disease. *Nucl Med Biol* 1996; 23: 745–51.
25. Simon MA, Kirchner PT. Scintigraphic evaluation of primary bone tumours. Comparison of technetium ^{99m} phosphate and gallium citrate imaging. *J Bone Joint Surg Am* 1980; 62: 758–64.
26. Van der Wall H, Murray IPC, Huckstep RL, Philips RL. The role of thallium scintigraphy in excluding malignancy in bone. *Clin Nucl Med* 1993; 18: 551–7.
27. Caner B, Kitapel M, Unlu M et al. Technetium-^{99m}-MIBI uptake in benign and malignant bone lesions: a comparative study with technetium-^{99m}-MDP. *J Nucl Med* 1992; 33: 319–24.
28. Kobayashi H, Kotoura Y, Hosono M et al. Diagnostic value of Tc-^{99m} (V) DMSA for chondrogenic tumours with positive Tc-^{99m} HMDP uptake on bone scintigraphy. *Clin Nucl Med* 1995; 20: 361–4.
29. Tateishi U, Gladish GW, Kusumoto M et al. Chest wall tumors: radiologic findings and pathologic correlation: part 1. Benign tumors. *Radiographics* 2003; 23: 1477–90.
30. Clavo AC, Brown RS, Wahl RL. Fluorodeoxyglucose uptake in human cancer cell lines is increased by hypoxia. *J Nucl Med* 1995; 36: 1625–32.
31. Malawer MM, Link MP, Donaldson SS. Sarcomas of bone. In: De Vita VT Jr, Hellman S, Rosenberg SA, eds. *Cancer: Principles and Practice of Oncology*, 5th edn. Philadelphia: Lippincott-Raven, 1997; 1731–852.
32. Warburg O. *The Metabolism of Tumors*. New York: Richard R Smith, 1931.
33. Cook GJ, Fogelman I. The role of nuclear medicine in monitoring treatment in skeletal malignancy. *Semin Nucl Med* 2001; 31: 206–11.
34. Caluser CI, Abdel-Dayem HM, Macapinlac HA et al. The value of thallium and three-phase bone scans in the evaluation of bone and soft tissue sarcomas. *Eur J Nucl Med* 1994; 21: 1198–205.
35. McLean RG, Murray IP. Scintigraphic patterns in certain primary bone tumours. *Clin Radiol* 1984; 35: 379–83.
36. Goodgold HM, Chen DC, Majd M, Nolan NG. Scintigraphy of primary bone neoplasia. *J Nucl Med* 1983; 24: 57.
37. Wang K, Allen L, Fung E et al. Bone scintigraphy in common tumors with osteolytic components. *Clin Nucl Med* 2005; 30: 655–71.
38. Dobernt N, Menzel C, Ludwig R et al. Enchondroma: a benign osseous lesion with high F-18 FDG uptake. *Clin Nucl Med* 2002; 27: 695–7.
39. Van der Wall H, Clarke S, Andrew MS, Murray IPC. Evaluation of primary bone tumours. In: Ell PJ, Gambhir SS, eds. *Nuclear Medicine in Clinical Diagnosis and Treatment*. New York: Churchill Livingstone 2004; 623–39.
40. Stoker DJ, Saifuddin A. Bone tumours (1) General characteristics, benign lesions. In: Grainger RG, Allison DJ, Adam A, Dixon AK, eds. *Grainger & Allison's Diagnostic Radiology: A Text Book of Medical Imaging*, 4th edn. New York: Churchill Livingstone, 2002; 1835–68.
41. Cerase A, Priolo F. Skeletal benign bone-forming lesions. *Eur J Radiol* 1998; 27: S91–7.
42. Taconis WK, Schutte HE, van der Heul RO. Desmoplastic fibroma of bone: a report of 18 cases. *Skeletal Radiol* 1994; 23: 283–8.
43. Vergel De Dios AM, Bond JR, Shives TC et al. Aneurysmal bone cyst: a clinicopathologic study of 238 cases. *Cancer* 1992; 69: 2921–31.
44. Fukumitsu N, Dohi M, Mida K et al. Bone scintigraphy in polyostotic fibrous dysplasia. *Clin Nucl Med* 1999; 24: 446–7.
45. Stoker DJ, Saifuddin A. Bone tumours (2) Malignant lesions. In: Grainger RG, Allison DJ, Adam A, Dixon AK, eds. *Grainger & Allison's Diagnostic Radiology: A Text Book of Medical Imaging*, 4th edn. New York: Churchill Livingstone, 2002; 1869–900.
46. Murray IPC, Elison BS. Radionuclide bone imaging for primary bone malignancy. *Clin Oncol* 1986; 5: 141–58.
47. Marcove RC. *The Surgery of Tumours of Bone and Cartilage*, 2nd edn. New York:
48. Dahlm DC. *Bone Tumours, General Aspects and Data on 6221 Cases*, 3rd edn. Springfield, IL: Charles C Thomas, 1978.
49. Lichtenstein I. *Bone Tumors*, 5th ed. St Louis: Mosby, 1977.
50. Brennan MF, Alektiar KM, Maki RG. Sarcomas of the soft tissue and bone. In: DeVita V, Hellman S, Rosenberg SA, eds. *Cancer: Principles and Practice of Oncology*. Philadelphia: Lippincott Williams & Wilkins 2001; 1841–91.
51. Fletcher DM, Unni KK, Mertens F, (2002) *WHO Classification of Tumours, Pathology and Genetics, Tumours of Soft Tissue and Bone*. Lyon: IARC Press.
52. Smith FW, Gilday DL. Scintigraphic appearance of osteoid osteoma. *Radiology* 1980; 137: 191–5.
53. Helms CA. Osteoid osteoma. The double density sign. *Clin Orthop Relat Res* 1987; (222): 167–73.
54. Ghelman B, Thompson FM, Arnold WD. Intraoperative localisation of an osteoid osteoma. *J Bone Joint Surg* 1981; 63: 826–7.
55. Peimer CA, Sciller AL, Mankin HJ, Smith RJ. Multicentric giant cell tumour. *J Bone Joint Surg Am* 1980; 62: 652–6.
56. Goodgold HM, Chen DC, Majd M, Nolan NG, Malawer M. Scintigraphic features of giant cell tumour. *Clin Nucl Med* 1984; 9: 526–30.
57. O'Reilly M, Chew FS. The scintigraphic features of giant-cell tumors in relation to other imaging modalities. *Clin Nucl Med* 1996; 21: 43–8.
58. Levine E, De Smet AA, Neff JR, Martin NL. Scintigraphic evaluation of giant cell tumor of bone. *AJR Am J Roentgenol* 1984; 143: 343–8.
59. Makhija MC. Bone scanning in aneurysmal bone cyst. *Clin Nucl Med* 1981; 6: 500–1.
60. Johns WD, Gupta SM, Kayani N. Scintigraphic evaluation of polyostotic fibrous dysplasia. *Clin Nucl Med* 1987; 12: 627–31.
61. Greenspan A. Bone island (enostosis): current concept. *Skeletal Radiol* 1995; 24: 111–5.
62. Greenspan A, Stadalnik RC. Bone island: scintigraphic findings and their clinical application. *Can Assoc Radiol J* 1995; 46: 368–79.

63. Humphry A, Gilday DL, Brown RG. Bone scintigraphy in chondroblastoma. *Radiology* 1980; 137: 497–9.
64. Velchik MG, Heyman S, Makler PT Jr, Goldstein HA, Alavi A. Bone scintigraphy: differentiating benign cortical irregularity of the distal femur from malignancy. *J Nucl Med* 1984; 25: 72–4.
65. Gilday DL, Ash JM, Reilly BJ. Radionuclide skeletal survey for pediatric neoplasms. *Radiology* 1977; 123: 399–406.
66. Malawer MM, Link MP, Donaldson SS. Sarcomas of the soft tissue and bone. 1891–935.
67. Brien EW, Mirra JM, Luck JV Jr. Benign and malignant cartilage tumors of bone and joint: their anatomic and theoretical basis with an emphasis on radiology, pathology and clinical biology. II. Juxtacortical cartilage tumors. *Skeletal Radiol* 1999; 28: 1–20.
68. Link TM, Haeussler MD, Poppek S et al. Malignant fibrous histiocytoma of bone: conventional X-ray and MR imaging features. *Skeletal Radiol* 1998; 27: 552–8.
69. Man TK, Chintagumpala M, Visvanathan J et al. Expression profiles of osteosarcoma that can predict response to chemotherapy. *Cancer Res* 2005; 65: 8142–50.
70. Link MP, Goorin AM, Miser AW et al. The effect of adjuvant chemotherapy on relapse-free survival in patients with osteosarcoma of the extremity. *N Engl J Med* 1986; 314: 1600–6.
71. Goorin AM, Andersen JW. Experience with multiagent chemotherapy for osteosarcoma: improved outcome. *Clin Orthop* 1991; 270: 22–8.
72. Longhi A, Errani C, De Paolis M, Mercuri M, Bacci G. Primary bone osteosarcoma in the pediatric age: state of the art. *Cancer Treat Rev* 2006; 32: 423–36.
73. Brenner W, Bohuslavizki KH, Eary JF. PET imaging of osteosarcoma. *J Nucl Med* 2003; 44: 930–42.
74. McKillop JH, Etcubanas E, Goris ML. The indications for and the limitations of bone scintigraphy in osteogenic sarcoma. 1981; 48: 1133–8.
75. Bacci G, Sprnigfield D, Capanna R et al. Neoadjuvant chemotherapy for osteosarcoma of the extremity. *Clin Orthop* 1987; 224: 268–76.
76. Kunisada T, Ozaki T, Kawai A et al. Imaging assessment of the responses of osteosarcoma patients to preoperative chemotherapy angiography compared with thallium-201 scintigraphy. *Cancer* 1999; 86: 949–55.
77. Raymond AK, Chawla SP, Carrasco Ch et al. Osteosarcoma chemotherapy effect: a prognostic factor. *Semin Diagn Pathol* 1987; 4: 212–36.
78. Wellings RM, Davies AM, Pynsent PB, Carter SR, Grimer RJ. The value of computed tomographic measurements in osteosarcoma as a predictor of response to adjuvant chemotherapy. *Clin Radiol* 1994; 49: 19–23.
79. Holscher HC, Bloem JL, Van der Woude HJ et al. Can MRI predict the histopathological response in patients with osteosarcoma after the first cycle of chemotherapy? *Clin Radiol* 1995; 50: 384–90.
80. Siegel BA, Donovan RL, Alderson PO, Mack GR. Skeletal uptake of 99mTc-diphosphonate in relation to local bone blood flow. *Radiology* 1976; 120: 121–3.
81. Franzius C, Sciuk J, Brinkschmidt C, Jurgens H, Schober O. Evaluation of chemotherapy response in primary bone tumors with F-18 FDG positron emission tomography compared with histologically assessed tumor necrosis. *Clin Nucl Med* 2000; 25: 874–81.
82. Riebel T, Knop J, Winkler K, Delling G. Comparative x-ray and nuclear medical studies of osteosarcomas to evaluate the effectiveness of preoperative chemotherapy. *Rofo* 1986; 145: 365–72.
83. Bielack S, Knop J, Delling G, Winkler K. Scintigraphic follow-up of osteosarcoma during neoadjuvant chemotherapy. Results of the cooperative osteosarcoma study of the Society for Pediatric Oncology. *Nuklearmedizin* 1988; 27: 237–41.
84. Knop J, Delling G, Salzer-Kuntschik M et al. [Nuclear medicine prediction of histologic tumor response of osteosarcoma]. *Klin Padiatr* 1989; 201: 285–92.
85. Knop J, Delling G, Heise U et al. Scintigraphic evaluation of tumor regression during preoperative chemotherapy of osteosarcoma. *Skeletal Radiol* 1990; 19: 165–72.
86. Kobayashi Y, Ozaki T, Takeda Y, Kawai A, Inoue H. Evaluation of the effect of preoperative chemotherapy in bone sarcomas. 99mTc-HMDP scintigraphy in 34 cases. *Acta Orthop Scand* 1998; 69: 611–16.
87. Genant HK, Bautovich GJ, Singh M, Lathrop KA, Harper PV. Bone-seeking radionuclides: an in vivo study of factors affecting skeletal uptake. *Radiology* 1974; 113: 373–82.
88. Ilhan IE, Vural G, Berberoglu S et al. Quantitative thallium-201 scintigraphy in childhood osteosarcoma: comparison with technetium-99m MDP and magnetic resonance imaging in the evaluation of chemotherapeutic response. *Pediatr Hematol Oncol* 2005; 22: 153–62.
89. Estes DN, Magill HL, Thompson EI, Hayes FA. Primary Ewing sarcoma: follow-up with Ga-67 scintigraphy. *Radiology* 1990; 177: 449–53.
90. Ramanna L, Waxman A, Binney G, et al. Thallium-201 scintigraphy in bone sarcoma: comparison with gallium-67 and technetium-MDP in the evaluation of chemotherapeutic response. *J Nucl Med* 1990; 31: 567–72.
91. Caluser CI, Abdel-Dayem HM, Macapinlac HA et al. The value of thallium and three-phase bone scans in the evaluation of bone and soft tissue sarcomas. *Eur J Nucl Med* 1994; 21: 1198–205.
92. Chew FS, Hudson TM. Radionuclide bone scanning of osteosarcoma: falsely extended uptake patterns. *Am J Roentgenol* 1982; 139: 49–54.
93. Ohtomo K, Terui S, Yokoyama R et al. Thallium-201 scintigraphy to assess effect of chemotherapy in osteosarcoma. *J Nucl Med* 1996; 37: 1444–8.
94. Imbriaco M, Yeh SDJ, Yeung H et al. Thallium-201 scintigraphy for the evaluation of tumor response to preoperative chemotherapy in patients with osteosarcoma. *Cancer* 1997; 80: 1507–12.
95. Menendez LR, Fideler BM, Mirra J. Thallium-201 scanning for the evaluation of osteosarcoma and soft tissue sarcoma. *J Bone Joint Surg* 1993; 75: 526–31.
96. Kostakoglu L, Panicek DM, Divgi CR et al. Correlation of the findings of thallium-201 chloride scans with those of other imaging modalities and histology following therapy in patients with bone and soft tissue sarcomas. *Eur J Nucl Med* 1995; 22: 1232–7.
97. Abdel-Dayem HM. The role of nuclear medicine in primary bone and soft tissue tumors. *Semin Nucl Med* 1997; 27: 355–63.

98. Jadvar H, Gamie S, Ramanna L, Conti PS. Musculoskeletal system. *Semin Nucl Med* 2004; 34: 254–61.
99. Ilhan IE, Vural G, Berberoglu S et al. Quantitative thallium-201 scintigraphy in childhood osteosarcoma: comparison with technetium-99m MDP and magnetic resonance imaging in the evaluation of chemotherapeutic response. *Pediatr Hematol Oncol* 2005; 22: 153–62.
100. Ishiyama K, Tomura N, Okada K et al. Evaluating benign and malignant musculoskeletal lesions with radionuclide angiography and SPECT using Tc-99m MIBI. *Clin Nucl Med* 2005; 30: 598–603.
101. Garcia R, Kim EE, Wong FC et al. Comparison of fluorine-18-FDG PET and technetium-99m-MIBI SPECT in evaluation of musculoskeletal sarcomas. *J Nucl Med* 1996; 37: 1476–9.
102. Aoki J, Inoue T, Tomiyoshi K et al. Nuclear imaging of bone tumors: FDG-PET. *Semin Musculoskelet Radiol* 2001; 5: 183–7.
103. Moustafa H, Riad R, Omar W, Zaher A, Ebied E. 99mTc-MIBI in the assessment of response to chemotherapy and detection of recurrences in bone and soft tissue tumours of the extremities. *Q J Nucl Med* 2003; 47: 51–7.
104. Pinkas L, Robinson D, Halperin N et al. 99mTc-MIBI scintigraphy in musculoskeletal tumors. *J Nucl Med* 2001; 42: 33–7.
105. Yeh SD, Rosen G, Benua RS. Gallium scans in Paget's sarcoma. *Clin Nucl Med* 1982; 7: 546–52.
106. Smith J, Botet JF, Yeh SD. Bone sarcomas in Paget disease: a study of 85 patients. *Radiology* 1984; 152: 583–90.
107. Frankel RS, Jones AE, Cohen JA et al. Clinical correlations of 67-gallium and skeletal whole body radionuclide studies with radiography in Ewing's sarcoma. *Radiology* 1974; 110: 597–603.
108. Jones GR, Miller JH, White L, Laug WE, Shore NA. Improved detection of metastatic Ewing's sarcoma with the use of bone marrow scintigraphy. *Med Pediatr Oncol* 1987; 15: 78–81.
109. Goldstein H, McNeil BJ, Zufall E, Treves S. Is there a place for bone scanning in Ewing's sarcoma? *J Nucl Med* 1980; 1: 10–12.
110. Nair N. Bone scanning in Ewing's sarcoma. *J Nucl Med* 1985; 26: 349–52.
111. McNeil BJ, Cassady JR, Geiser CF et al. Fluorine-18 bone scintigraphy in children with osteosarcoma or Ewing's sarcoma. *Radiology* 1973; 109: 627–31.
112. Gyorke T, Zajic T, Lange A et al. Impact of FDG PET for staging of Ewing sarcomas and primitive neuroectodermal tumours. *Nucl Med Commun* 2006; 27: 17–24.
113. Shives TS, Wold LE, Dahlin DC, Beabout JW. Chondrosarcoma and its variants. In: Sim FH, ed. *Diagnosis and treatment of Bone Tumours: A Team Approach*. Mayo Clinic Monograph. Thorofare, NJ: Slack. 1983; 211.
114. Pritchard DJ, Lunke RJ, Taylor WF, Dahlin DC, Medley BE. Chondrosarcoma: clinicopathologic statistical analysis. *Cancer* 1980; 45: 149–57.
115. Maclean RG, Murray IP. Scintigraphic features of certain primary malignant bone tumours. *Clin Radiol* 1984; 35: 379–83.
116. Hudson TM, Chew FS, Manaster BJ. Radionuclide bone scanning in medullary chondrosarcoma. *AJR Am J Roentgenol* 1982; 139: 1071–6.
117. Kobayashi H, Sakahara H, Hosono M et al. Soft-tissue tumors: diagnosis with Tc-99m (V) dimercaptosuccinic acid scintigraphy. *Radiology* 1994; 190: 277–80.
118. Kirsch J, Ilaslan H, Bauer TW, Sundaram M. The incidence of imaging findings, and the distribution of skeletal lymphoma in a consecutive patient population seen over 5 years. *Skeletal Radiol* 2006; 35: 590–4.
119. Ozdemirli M, Mankin HJ, Aisenberg AC et al. Hodgkin's disease presenting as a solitary bone tumour: a report of four cases and review of the literature. *Cancer* 1996; 77: 79–88.
120. Vincent JM, Ng YY, Norton AJ, Armstrong P. Case report: primary lymphoma of bone – MR imaging appearances with pathological correlation. *Clin Radiol* 1992; 45: 407–9.
121. Krishnan A, Shirkhoda A, Tehranzadeh J et al. Primary bone lymphoma: radiographic-MR imaging correlation. *Radiographics* 2003; 23: 1371–83.
122. Israel O, Mekel M, Bar-Shalom R et al. Bone lymphoma: 67Ga scintigraphy and CT for prediction of outcome after treatment. *J Nucl Med* 2002; 43: 1295–303.
123. Pires de Camargo O, Machado TMS, Croci AT et al. Primary bone lymphoma in 24 patients treated between 1955 and 1999. *Clin Orthop* 2002; 397: 271–80.
124. Bar-Shalom R, Israel O, Epelbaum R et al. Gallium-67 scintigraphy in lymphoma with bone involvement. *J Nucl Med* 1995; 36: 446–50.
125. Moon TY, Kim E, Kim YC et al. Comparison of nuclear bone and gallium scans in the therapeutic evaluation of bone lymphoma. *Clin Nucl Med* 1995; 20: 721–4.
126. Roach PJ, Janicek MJ, Kaplan WD. Bone lymphoma, comparison of Tl-201 and Ga-67 scintigraphy in assessment of treatment response. *Clin Nucl Med* 1996; 21: 689–94.
127. Moon TY, Kim EE, Kim YC et al. Comparison of nuclear bone and gallium scans in the therapeutic evaluation of bone lymphoma. *Clin Nucl Med* 1995; 20: 721–4.
128. Moog F, Bangerter M, Diederichs CG et al. Extra nodal malignant lymphoma: detection with FDG PET versus CT. *Radiology* 1998; 206: 475–81.
129. Moog F, Kotzerke J, Reske SN. FDG PET can replace bone scintigraphy in primary staging of malignant lymphoma. *J Nucl Med* 1999; 40: 1407–13.
130. Hollinger EF, Alibazoglu H, Ali A, Green A, Lamonica G. Hematopoietic cytokine-mediated FDG uptake simulates the appearance of diffuse metastatic disease on whole-body PET imaging. *Clin Nucl Med* 1998; 23: 93–8.
131. Chiang SB, Rebenstock A, Guan L, Alavi A, Zhuang H. Diffuse bone marrow involvement of Hodgkin lymphoma mimics hematopoietic cytokine-mediated FDG uptake on FDG PET imaging. *Clin Nucl Med* 2003; 28: 674–6.
132. Dvorak C. Common complaints, difficult diagnosis: multiple myeloma. *J Am Acad Nurse Pract* 2006; 18: 190–4.
133. Blade, J, Kyle, RA. Multiple myeloma in young patients: clinical presentation and treatment approach. *Leuk Lymphoma* 1998; 30: 493–501.
134. Smith A, Wisloff F, Samson D; UK Myeloma Forum; Nordic Myeloma Study Group; British Committee for Standards

- in Haematology. Guidelines on the diagnosis and management of multiple myeloma 2005. *Br J Haematol* 2006; 132: 410–51.
135. Kyle RA, Schreiman JS, McaLeod RA, Beabout JW. Computed tomography in diagnosis and management of multiple myeloma and its variants. *Arch* 1985; 145: 1451–2.
 136. Walker MP, Yaszemski MJ, Kim CW, Talac R, Bradford LC. Metastatic disease of the spine: evaluation and treatment. *Clin Orthop Relat Res* 2003; 415: S165–75.
 137. Tirovola EB, Biassoni L, Britton KE et al. The use of ^{99m}Tc-MIBI scanning in multiple myeloma. *Br J Cancer* 1996; 74: 1815–20.
 138. Joffe J, Williams MP, Cherryman GR et al. Magnetic resonance imaging in myeloma. *Lancet* 1988; 1: 1162–3.
 139. Nandurkar D, Kalf V, Turlakow A et al. Focal MIBI uptake is a better indicator of active myeloma than diffuse uptake. *Eur J Haematol* 2006; 76: 141–6.
 140. Alper E, Gurel M, Evrensel T et al. ^{99m}Tc-MIBI scintigraphy in untreated stage III multiple myeloma: comparison with X-ray skeletal survey and bone scintigraphy. *Nucl Med Commun* 2003; 24: 537–42.
 141. Wakasugi S, Teshmina H, Nakamura H et al. Tc-^{99m} MIBI localisation in bone-marrow: a marker of bone marrow malignancy. *Clin Nucl Med* 1998; 10: 664–71.
 142. Durie BG, Waxman AD, D'Agnolo A, Williams CM. Whole-body (18)F-FDG PET identifies high-risk myeloma. *J Nucl Med* 2002; 43: 1457–63.
 143. Bredella MA, Steinbach L, Caputo G, Segall G, Hawkins R. Value of FDG PET in the assessment of patients with multiple myeloma. *AJR Am J Roentgenol* 2005; 184: 1199–204.
 144. Schirrmeyer H, Bommer M, Buck AK et al. Initial results in the assessment of multiple myeloma using ¹⁸F-FDG PET. *Eur J Nucl Med Mol Imaging* 2002; 29: 361–6.
 145. Jadvar H, Conti PS. Diagnostic utility of FDG PET in multiple myeloma. *Skeletal Radiol* 2002; 31: 690–4.
 146. Milesshkin L, Blum R, Seymour JF et al. A comparison of fluorine-18 fluoro deoxyglucose PET and technetium-^{99m} sestamibi in assessing patients with multiple myeloma. *Eur J Haematol* 2004; 72: 32–7.
 147. Schulte M, Brecht-Krauss D, Heymer B et al. Fluorodeoxyglucose positron emission tomography of soft tissue tumours: is a non-invasive determination of biological activity possible? *Eur J Nucl Med* 1999; 26: 599–605.
 148. Hawkins DS, Rajendran JG, Conrad EU 3rd, Bruckner JD, Eary JE. Evaluation of chemotherapy response in pediatric bone sarcomas by [¹⁸F]-fluorodeoxy-D-glucose positron emission tomography. *Cancer* 2002; 94: 3277–84.
 149. Aoki J, Watanabe H, Shinozaki T et al. FDG PET of primary benign and malignant bone tumors: standardized uptake value in 52 lesions. *Radiology* 2001; 219: 774–7.
 150. Hain SF, O'Doherty MJ, Lucas JD et al. Fluorodeoxyglucose PET in the evaluation of amputations for soft tissue sarcoma. *Nucl Med Commun* 1999; 20: 845–8.
 151. Franzius C, Sciuk J, Daldrup-Link HE, Jurgens H, Schober O. FDG-PET for detection of osseous metastases from malignant primary bone tumours: comparison with bone scintigraphy. *Eur J Nucl Med* 2000; 27: 1305–11.
 152. Tse N, Hoh C, Hawkins R et al. Positron emission tomography diagnosis of pulmonary metastases in osteogenic sarcoma. *Am J Clin Oncol* 1994; 17: 22–5.
 153. Franzius C, Daldrup-Link HE, Sciuk J et al. FDG-PET for detection of pulmonary metastases from malignant primary bone tumors: comparison with spiral CT. *Ann Oncol* 2001; 12: 479–86.
 154. Franzius C, Daldrup-Link HE, Wagner-Bohn A et al. FDG-PET for detection of recurrences from malignant primary bone tumors: comparison with conventional imaging. *Ann Oncol* 2002; 13: 157–60.
 155. Jones DN, McCowage GB, Sostman HD et al. Monitoring of neoadjuvant therapy response of soft-tissue and musculoskeletal sarcoma using fluorine-18-FDG PET. *J Nucl Med* 1996; 37: 1438–44.
 156. Dehdashti F, Siegel BA, Griffeth LK et al. Benign versus malignant intraosseous lesions: discrimination by means of PET with 2-[¹⁸F]fluoro-2-deoxy-D-glucose. *Radiology* 1996; 200: 243–7.
 157. Nair N, Ali A, Green AA et al. Response of osteosarcoma to chemotherapy. Evaluation with F-18 FDG-PET scans. *Clin Positron Imaging* 2000; 3: 79–83.
 158. Bredella MA, Caputo GR, Steinbach LS. Value of FDG positron emission tomography in conjunction with MR imaging for evaluating therapy response in patients with musculoskeletal sarcomas. *AJR Am J Roentgenol* 2002; 179: 1145–50.
 159. Franzius C, Bielack S, Flege S et al. Prognostic significance of (18) FFDG and (99m)Tc-methylene diphosphonate uptake in primary osteosarcoma. *J Nucl Med* 2002; 43: 1012–7.
 160. Souhami R, Tobias J. Bone and soft tissue sarcomas. In: *Cancer and its Management*. 4th edn. Malden, MA: Blackwell Publishing, 2003: 344–62.
 161. Buck AK, Schirrmeyer H, Reske SN. Musculoskeletal tumours. In: *Oehr P, Beirsack H-J, Coleman E, eds. PET and PET-CT in Oncology*. Berlin: Springer, 2003; 275–84.
 162. Dimitrakopoulou-Strauss A, Strauss LG, Schwarzbach M et al. Dynamic PET ¹⁸F-FDG studies in patients with primary and recurrent soft-tissue sarcomas impact: on diagnosis and correlation with grading. *J Nucl Med* 2001; 42: 713–20.
 163. Cormier JN, Pollock RE. Soft tissue sarcomas. *CA Cancer J Clin* 2004; 54: 94–109.
 164. Israel-Mardirosian N, Adler LP. Positron emission tomography of soft tissue sarcomas. *Curr Opin Oncol* 2003; 15: 327–30.
 165. Brennan MF, Casper ES, Harrison LB et al. The role of multimodality therapy in soft-tissue sarcoma. *Ann Surg* 1991; 214: 328–36.
 166. Pisters P. Staging and prognosis. In: *Pollock RE, ed. American Cancer Society Atlas of Clinical Oncology: Soft Tissue Sarcomas*. Hamilton, Ont. :BC Decker, 2002: 80–8.
 167. Greene FL, Page DL, Fleming ID et al, eds. *American Joint Committee on Cancer: Cancer Staging Manual*, 6th edn. New York: Springer 2002; 221–6.
 168. Costa J, Wesley RA, Glatstein E, Rosenberg SA. The grading of soft tissue sarcomas. Results of a clinicohistopathologic correlation in a series of 163 cases. *Cancer* 1984; 53: 530–41.
 169. Guillou L, Coindre JM, Bonichon F, et al. Comparative study of the National Cancer Institute and French Federation of Cancer Centers Sarcoma Group grading systems in a population of 410 adult patients with soft tissue sarcoma. *J Clin Oncol* 1997; 15: 350–62.

170. Ramanathan RC, A'Hern R, Fisher C, Thomas JM. Modified staging system for extremity soft tissue sarcomas. *Ann Surg Oncol* 1999; 6: 57–69.
171. Schuetze SM, Rubin BP, Vernon C et al. Use of positron emission tomography in localized extremity soft tissue sarcoma treated with neoadjuvant chemotherapy. *Cancer* 2005; 103: 339–48.
172. Singer S, Corson JM, Gonin R et al. Prognostic factors predictive of survival and local recurrence for extremity soft tissue sarcoma. *Ann Surg* 1994; 219: 165–73.
173. Collin C, Godbold J, Hajdu S, Brennan M. Localized extremity soft tissue sarcoma: an analysis of factors affecting survival. *J Clin Oncol* 1987; 5: 601–12.
174. Tehranzadeh J, Mnaymneh W, Ghavam C, Morillo G, Murphy BJ. Comparison of CT and MR imaging in musculoskeletal neoplasms. *J Comput Assist Tomogr* 1989; 13: 466–72.
175. Slominski A, Wortsman J, Carlson A. Molecular pathology of soft tissue and bone tumors. *Arch Pathol Lab Med* 1999; 123: 1246–59.
176. Kempson RL, Fletcher CDM, Evans HL, Hendrickson MR, Sibley RK. Tumors of the soft tissues. In: *Atlas of Tumor Pathology, 3rd Series*. Washington, DC: Armed Forces Institute of Pathology.
177. Gadd M, Casper E, Woodruff JM, McCormack PM, Brennan MF. Development and treatment of pulmonary metastases in adult patients with extremity soft tissue sarcoma. *Ann Surg* 1993; 218: 705–12.
178. Southee AE, Kaplan WD, Jochelson MS et al. Gallium imaging in metastatic and recurrent soft tissue sarcoma. *J Nucl Med* 1992; 33: 1594–9.
179. Lee VW, Fuller JD, O'Brien MJ et al. Pulmonary Kaposi sarcoma in patients with AIDS: scintigraphic diagnosis with sequential thallium and gallium scanning. *Radiology* 1991; 180: 409–12.
180. Bastiaannet E, Groen H, Jager PL et al. The value of FDG-PET in the detection, grading and response to therapy of soft tissue and bone sarcomas; a systematic review and meta-analysis. *Cancer Treat Rev* 2004; 30: 83–101.
181. Ioannidis JP, Lau J. 18F-FDG PET for the diagnosis and grading of soft-tissue sarcoma: a meta-analysis. *J Nucl Med* 2003; 44: 717–24.
182. Eary JF, Conrad EU, Bruckner JD et al. Quantitative [F-18]fluorodeoxyglucose positron emission tomography in pretreatment and grading of sarcoma. *Clin Cancer Res* 1998; 4: 1215–20.
183. Zhang H, Tian M, Oriuchi N. 11C-choline PET for the detection of bone and soft tissue tumors in comparison with FDG PET. *Nucl Med Commun* 2003; 24: 273–9.
184. Schuetze SM. Utility of positron emission tomography in sarcomas. *Curr Opin Oncol* 2006; 18: 369–73.
185. Lucas JD, O'Doherty MJ, Cronin BF et al. Prospective evaluation of soft tissue masses and sarcomas using fluorodeoxyglucose positron emission tomography. *Br J Surg* 1999; 86: 550–6.
186. Kole AC, Nieweg OE, van Ginkel RJ et al. Detection of local recurrence of soft-tissue sarcoma with positron emission tomography using [18F]fluorodeoxyglucose. *Ann Surg Oncol* 1997; 4: 57–63.
187. Schwarzbach M, Dimitrakopoulou-Strauss A, Willeke F et al. Clinical value of [18F]fluorodeoxyglucose positron emission tomography imaging in soft tissue sarcomas. *Ann Surg* 2000; 231: 380–6.
188. Hoh CK, Hawkins RA, Glaspy JA et al. Cancer detection with whole-body PET using 2-[18F]fluoro-2-deoxy-D-glucose. *J Comput Assist Tomogr* 1993; 17: 582–9.
189. Adler LP, Blair HF, Makley JT et al. Noninvasive grading of musculoskeletal tumors using PET. *J Nucl Med* 1991; 32: 1508–12.
190. Schwarzbach MH, Dimitrakopoulou-Strauss A, Mechtersheimer G et al. Assessment of soft tissue lesions suspicious for liposarcoma by F18-deoxyglucose (FDG) positron emission tomography (PET). *Anticancer Res* 2001; 21: 3609–14.
191. Kern KA, Brunetti A, Norton JA et al. Metabolic imaging of human extremity musculoskeletal tumors by PET. *J Nucl Med* 1988; 29: 181–6.
192. Shields AF, Mankoff DA, Link JM et al. Carbon-11-thymidine and FDG to measure therapy response. *J Nucl Med* 1998; 39: 1757–62.
193. Lucas JD, O'Doherty MJ, Wong JC et al. Evaluation of fluorodeoxyglucose positron emission tomography in the management of soft-tissue sarcomas. *J Bone Joint Surg Br* 1998; 80: 441–7.
194. Lodge MA, Lucas JD, Marsden PK et al. A PET study of 18FDG uptake in soft tissue masses. *Eur J Nucl Med* 1999; 26: 22–30.
195. Eary JF, Conrad EU, Bruckner JD et al. Quantitative [F-18] fluorodeoxyglucose positron emission tomography in pretreatment and grading of sarcoma. *Clin Cancer Res* 1998; 4: 1215–20.
196. Folpe AL, Lyles RH, Sprouse JT, Conrad EU, Eary JF. (F-18) fluorodeoxyglucose positron emission tomography as a predictor of pathologic grade and other prognostic variables in bone and soft tissue sarcoma. *Clin Cancer Res* 2000; 6: 1279–87.
197. Hain SF, O'Doherty MJ, Bingham J, Chinyama C, Smith MA. Can FDG PET be used to successfully direct preoperative biopsy of soft tissue tumors? *Nucl Med Commun* 2003; 24: 1139–43.
198. Schulte M, Brecht-Krauss D, Werner M et al. Evaluation of neoadjuvant therapy response of osteogenic sarcoma using FDG PET. *J Nucl Med* 1999; 40: 1637–43.
199. Johnson GR, Zhuang H, Khan J, Chiang SB, Alavi A. Roles of positron emission tomography with fluorine-18-deoxyglucose in the detection of local recurrent and distant metastatic sarcoma. *Clin Nucl Med* 2003; 28: 815–20.
200. Schwarzbach M, Willeke F, Dimitrakopoulou-Strauss A et al. Functional imaging and detection of local recurrence in soft tissue sarcomas by positron emission tomography. *Anticancer Res* 1999; 19: 1343–9.
201. Eary JF, O'Sullivan F, Powitan Y et al. Sarcoma tumor FDG uptake measured by PET and patient outcome: a retrospective analysis. *Eur J Nucl Med Mol Imaging* 2002; 29: 1149–54.
202. Gayed I, Vu T, Iyer R et al. The role of 18F-FDG PET in staging and early prediction of response to therapy of recurrent gastrointestinal stromal tumors. *J Nucl Med* 2004; 45: 17–21.

203. Conti PS, Menendez LR, Ramanna L et al. Use of positron emission tomography in the evaluation of cryosurgical treatment of musculoskeletal tumors. *Radiology* 1999; 213: 118.
204. Vernon CB, Eary JF, Rubin BP et al. FDG PET imaging guided reevaluation of histopathologic response in a patient with high-grade sarcoma. *Skeletal Radiol* 2003; 32: 139–42.
205. Stroobants S, Goeminne J, Seegers M et al. 18FDG-Positron emission tomography for the early prediction of response in advanced soft tissue sarcoma treated with imatinib mesylate (Glivec). *Eur J Cancer* 2003; 39: 2012–20.
206. Van den Abbeele AD, Badawi RD. Use of positron emission tomography in oncology and its potential role to assess response to imatinib mesylate therapy in gastrointestinal stromal tumors (GISTs). *Eur J Cancer* 2002; 38: S60–5.
207. Antoch G, Kanja J, Bauer S et al. Comparison of PET, CT, and dual modality PET/CT imaging for monitoring of imatinib (STI571) therapy in patients with gastrointestinal stromal tumors. *J Nucl Med* 2004; 45: 357–65.
208. Cogswell A, Howman-Giles R, Bergin M. Bone and gallium scintigraphy in children with rhabdomyosarcoma: a 10-year review. *Med Pediatr Oncol* 1994; 22: 15–21.
209. Howman-Giles R, Uren RF, Shaw PJ. Thallium-201 scintigraphy in pediatric soft-tissue tumors. *J Nucl Med* 1995; 36: 1372–6.
210. Menendez LR, Fideler BM, Mirra J. Thallium-201 scanning for the evaluation of osteosarcoma and soft-tissue sarcoma. A study of the evaluation and predictability of the histological response to chemotherapy. *J Bone Joint Surg Am* 1993; 75: 526–31.
211. Peng F, Rabkin G, Muzik O. Use of 2-deoxy-2-[F-18]-fluoro-D-glucose positron emission tomography to monitor therapeutic response by rhabdomyosarcoma in children: report of a retrospective case study. *Clin Nucl Med* 2006; 31: 394–7.
212. Burkill GJ, Badran M, Al-Muderis O et al. Malignant gastrointestinal stromal tumor: distribution, imaging features, and pattern of metastatic spread. *Radiology* 2003; 226: 527–32.
213. Demetri G. Identification and treatment of chemoresistant inoperable or metastatic GIST: experience with the selective tyrosine kinase inhibitor imatinib mesylate (STI571). *Eur J Cancer* 2002; 38: S52–9.
214. Plaat BE, Hollema H, Molenaar WM et al. Soft tissue leiomyosarcomas and malignant gastrointestinal stromal tumors: differences in clinical outcome and expression of multidrug resistance proteins. *J Clin Oncol* 2000; 18: 3211–20.
215. van Oosterom AT, Judson I, Verweij J et al. Safety and efficacy of imatinib (STI571) in metastatic gastrointestinal stromal tumors: a phase I study. *Lancet* 2001; 358: 1421–3.
216. Joensuu H. Treatment of inoperable gastrointestinal stromal tumor (GIST) with imatinib (Glivec, Gleevec). *Med Klin* 2002; 97: 28–30.
217. Jager PL, Gietema JA, van der Graaf WT. Imatinib mesylate for the treatment of gastrointestinal stromal tumors: best monitored with FDG PET. *Nucl Med Commun* 2004; 25: 433–8.
218. Goerres GW, Stupp R, Barghouth G et al. The value of PET, CT and in-line PET/CT in patients with gastrointestinal stromal tumors: long-term outcome of treatment with imatinib mesylate. *Eur J Nucl Med Mol Imaging*. 2005; 32: 153–62.
219. Cardona S, Schwarzbach M, Hinz U et al. Evaluation of F18-deoxyglucose positron emission tomography (FDG-PET) to assess the nature of neurogenic tumors. *Eur J Surg Oncol* 2003; 29: 536–41.
220. Ducatman BS, Scheithauer BW, Piepgras DG et al. Malignant peripheral nerve sheath tumors, a clinicopathologic study of 120 cases. *Cancer* 1986; 57: 2006–21.
221. Brenner W, Friedrich RE, Gawad KA et al. Prognostic relevance of FDG PET in patients with neurofibromatosis type-1 and malignant peripheral nerve sheath tumors. *Eur J Nucl Med Mol Imaging* 2006; 33: 428–32.
222. Lawrence W, Donegan WL, Natarajan N et al. Adult soft-tissue sarcomas: a pattern of care survey by the American College of Surgeons. *Ann Surg* 1987; 205: 349–59.
223. Ferner RE, Lucas JD, O'Doherty MJ et al. Evaluation of (18) fluorodeoxyglucose positron emission tomography ((18) FDG PET) in the detection of malignant peripheral nerve sheath tumors arising from within plexiform neurofibromas in neurofibromatosis 1. *J Neurol Neurosurg Psychiatry* 2000; 68: 353–7.
224. Page RL, Garg PK, Garg S et al. PET imaging of osteosarcoma in dogs using a fluorine-18-labeled monoclonal antibody Fab fragment. *J Nucl Med* 1994; 35: 1506–13.
225. Tian M, Zhang H, Oriuchi N, Higuchi T, Endo K. Comparison of 11C-choline PET and FDG PET for the differential diagnosis of malignant tumors. *Eur J Nucl Med Mol Imaging* 2004; 31: 1064–72.
226. Yanagawa T, Watanabe H, Inoue T et al. Carbon-11 choline positron emission tomography in musculoskeletal tumors: comparison with fluorine-18 fluorodeoxyglucose positron emission tomography. *J Comput Assist Tomogr* 2003; 27: 175–82.
227. Khan N, Oriuchi N, Ninomiya H et al. Positron emission tomographic imaging with 11C-choline in differential diagnosis of head and neck tumors: comparison with 18F-FDG PET. *Ann Nucl Med* 2004; 18: 409–17.
228. Watanabe H, Inoue T, Shinozaki T et al. PET imaging of musculoskeletal tumors with fluorine-18 alpha-methyl-tyrosine: comparison with fluorine-18 fluorodeoxyglucose PET. *Skeletal Radiol* 2003; 32: 201–8.
229. Suzuki H, Watanabe H, Shinozaki T et al. Positron emission tomography imaging of musculoskeletal tumors in the shoulder girdle. *J Shoulder Elbow Surg* 2004; 13: 635–47.

Bibliography and further reading

- DeVita V, Hellman S, Rosenberg SA, eds. *Cancer: Principles and Practice of Oncology*. Philadelphia: Lippincott Williams & Wilkins, 2001.
- Enneking WF, ed. *Musculoskeletal Tumor Surgery*. New York: Churchill Livingstone, 1983.
- Fleming ID, Cooper JS, Henson DE, eds. *AJCC Cancer Staging Manual*, 5th edn. Philadelphia: Lippincott-Raven, 1997.

-
- Grainger RG, Allison OJ, Dixon AK, eds. Grainger & Allison's Diagnostic Radiology: A Textbook of Medical Imaging, 4th edn. New York: Churchill Livingstone, 2002.
- Greene FL, Page DL, Fleming ID, et al., eds. American Joint Committee on Cancer: Cancer Staging Manual, 6th edn. New York: Springer, 2002.
- Hajdu SI. Pathology of Soft Tissue Tumors. Philadelphia: Lea & Febiger, 1979.
- Oehr P, Beirsack H-J, Coleman E, eds. PET and PET-CT in Oncology. Berlin: Springer, 2003.
- Souhami R, Tobias J. Cancer and its management, 4th edn. Malden, MA: Blackwell Publishing, 2003.
- Unni KK. Dahlin's Bone Tumors: General Aspects and Data on 11,087 Cases. 5th edn. Philadelphia: Lippincott-Raven, 1996.

Malignant melanoma

*Ehab M Kamel and Angelika Bischof
Delaloye*

Background

Malignant melanoma (MM) is the most common fatal skin cancer. It usually stems from dermic or epidermic neural-crest derived melanocytes. However, melanocytes located in other regions of the body such as the meninges, the choroidal tissue of the eye, the digestive tract, the mucosal surfaces, and the lymph nodes can also give rise to MM.¹ Currently, there are no proven causes of MM, but the most likely associated factor is episodic exposure to the ultraviolet (UV) component of sun rays.² The risk of melanoma is relatively higher in fair-skinned individuals, particularly those with blond or red hair who sunburn and freckle easily in contrast to those with darker complexions. The sites of predilection for MM are primarily related to the areas of intermittent exposure to the sun, such as the back in men and the lower leg in women, with relative sparing to the more frequently exposed sites such as the face, hand, and forearms.² Despite the continuous advances in prevention, early detection, and treatment, the worldwide incidence and mortality rate of MM are increasing dramatically. The National Cancer Institute Surveillance, Epidemiology, and End Results (SEER) database documents increases of 619% in annual diagnosis of cutaneous melanoma and of 165% in annual mortality from 1950 to 2000.³ Malignant melanoma has four histogenetic types: superficial spreading, lentigo maligna, nodular, and acral lentiginous melanoma. Clinical signs that may be indicative of possible MM are asymmetry, border irregularity, color variegation, increase in diameter, elevation, ulceration, and bleeding of pigmented lesions.¹ Histologic findings (tumor thickness, tumor invasion), surface ulceration, spread to regional lymph nodes, and distant metastases are interchangeably applied to predict disease course and patient outcome.

Staging of malignant melanoma

According to the American Joint Committee on Cancer (AJCC), the staging criteria for MM include lesion

thickness, surface ulceration, number of involved lymph nodes, pattern of nodal involvement (microscopic, macroscopic), and the presence or absence of distant metastases.⁴ Currently, there are four stages that are derived from the TNM status of each individual lesion (Table 16.1). It is generally agreed that patients with stage I–II are categorized as low risk, whereas stage III–IV are portending high risk of disease relapse and poor outcome, respectively. Since precise tumor (T) staging can only be obtained after surgical resection, diagnostic imaging has no significant role in this regard. Based upon the Breslow microstaging method, which estimates the total vertical height of the melanoma, thin MMs, measuring < 1 mm thickness, have a very favorable prognosis, with a 10-year survival of > 90%.^{4,5} Increasing Breslow thickness is associated with a significant decrease in the overall disease-free survival, since both locoregional disease recurrence and the incidence of distant metastases augment steadily. For MM thicker than 4 mm, a 5-year survival of 67% has been reported.⁴

The role of diagnostic imaging in MM is to accurately identify potential disease spread to the locoregional lymph basin or to distant sites. Accurate disease staging is a prerequisite for choosing the appropriate therapeutic approach and to extrapolate the forthcoming disease course and patient outcome. For now, a group of non-invasive and invasive tests have been recommended for initial staging of MM. However, understanding the advantages and limitations of each of them can help in offering the best healthcare service in a cost-effective manner without any loss in the overall diagnostic accuracy.

Nodal staging

Since MM cells usually spread to regional nodal basins before metastasizing widely,¹ accurate nodal staging is of paramount importance, since immediate lymphadenectomy in patients with subclinical sentinel-node metastases has been shown to significantly increase the melanoma-specific 5-year survival rate, as compared with

Table 16.1 Currently applied melanoma staging algorithm according to final version of the American Joint Committee on Cancer^{1,4}

<i>Pathological and TNM stage</i>	<i>Thickness of lesion</i>	<i>Ulceration</i>	<i>No. of involved lymph nodes</i>	<i>Nodal involvement</i>	<i>Distant metastasis</i>
IA	mm ≤ 1.0	No	0	————	No
IB					
T1b	≤ 1.0	Yes or Clark level IV or V	0	————	No
T2a	1.01-2.0	No	0	————	No
IIA					
T2b	1.01-2.0	Yes	0	————	No
T3a	2.01-4.0	No	0	————	No
IIB					
T3b	2.01-4.0	Yes	0	————	No
T4a	> 4.0	No	0	————	No
IIC	> 4.0	Yes	0	————	No
IIIA					
N1a	Any	No	1	Microscopic	No
N2a	Any	No	2 or 3	Microscopic	No
IIIB					
N1a	Any	Yes	1	Microscopic	No
N2a	Any	Yes	2 or 3	Microscopic	No
N1b	Any	No	1	Microscopic	No
N2b	Any	No	2 or 3	Microscopic	No
IIIC					
N1b	Any	Yes	1	Macroscopic	No
N2b	Any	Yes	2 or 3	Macroscopic	No
N3	Any	Yes or No	4	Macroscopic or microscopic	No
IV					
M1a	Any	Yes or No	Any	Any	Skin, subcutaneous
M1b	Any	Yes or No	Any	Any	Lung
M1c	Any	Yes or No	Any	Any	Other visceral site

delayed lymphadenectomy for clinically detected nodal relapse (72% vs. 52%).⁶ Anatomic imaging studies such as computed tomography (CT) and magnetic resonance imaging (MRI) that rely on morphologic alterations at secondary tumor sites are neither sensitive nor specific in identifying occult metastatic tumor nests.⁷ In contradiction, functional imaging studies using both lymphoscintigraphy with sentinel lymph node biopsy (SLNB) and [¹⁸F]fluoro-2-deoxy-D-glucose-positron emission tomography ([¹⁸F]FDG-PET) have enriched the process of nodal staging in MM, provided that certain 'patient selection criteria' are considered. In fact, SLNB and [¹⁸F]FDG-PET have a reciprocal role in nodal staging of MM, which is directly related to the tumor burden at the time of initial presentation.

Lymphoscintigraphy and SLNB

Lymphoscintigraphy with small particle radiocolloids and SLNB provide the road map to identify the nodes to study, even if these lymph nodes lie outside habitual node fields or are interval nodes lying between the primary tumor site and the lymphatic basin. This technique is based on the hypothesis that lymphatic drainage from the primary tumor follows an orderly progression through afferent lymphatic vessels into sentinel node(s) before flowing into non-sentinel node(s). Sentinel lymph node evaluation has the potential to separate patients without nodal metastases, who can avoid nodal basin dissection with its known risk of chronic lymphedema and nerve injury, from those with

metastatic involvement, who may benefit from alternative therapeutic pathways such as radical lymphadenectomy and adjuvant therapy. The incidence of sentinel lymph node metastasis is around 5% for MM with thickness between 0.76 and 1.5 mm; however, it increases to about 20% for lesions with thickness between 1.5 and 4 mm.⁸ Consequently, patients with lesion thickness ≤ 4 mm represent the population who are most likely to benefit from elective lymph node dissection in case SLNB demonstrates metastatic deposits.

Using a colloidal particle size of 2.5–100 nm, which is essential for efficient uptake of radiolabeled particles by macrophages, an intradermal/subdermal injection of small volume (0.05–0.2 ml depending on skin thickness) of 7–20 MBq ^{99m}Tc-labeled sulfur or rhenium colloid or albumin nanocolloid is performed. Injection should be 0.5–1 cm away from the scar or the tumor margin, and one or two injections are sufficient to imitate the pattern of lymphatic drainage of any potential tumor emboli leaving the MM (Figures 16.1 and 16.2). It is recommended to start with a dynamic acquisition (20–30 s/frame over 20–30 min) after radiotracer injection to better identify any eventual in-transit nodes (nodes along the channel from primary site to regional basin) such as cubital and popliteal lymph nodes, and to precisely separate first (sentinel) from second (non-sentinel) order nodes in the basin. Subsequently, anterior, posterior, and oblique static (300 s) images are acquired in order to localize the nodes in three dimensions.⁸ To facilitate spatial localization of the detected nodes, a ⁵⁷Co flood source can be used to silhouette the patient during the 5-min image acquisition, or a radioactive point/rode source can be moved along the contour of the patient body during the scan. In case a single photon emission computed

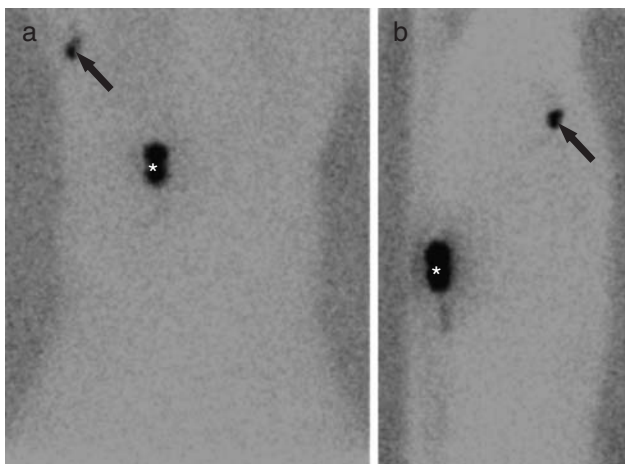


Figure 16.1 Lymphoscintigram, (a) anterior and (b) right lateral views, in a 30-year-old patient with melanoma of the trunk. The arrows depict a sentinel lymph node in the right axilla as confirmed by surgical exploration. (*) Injection site.

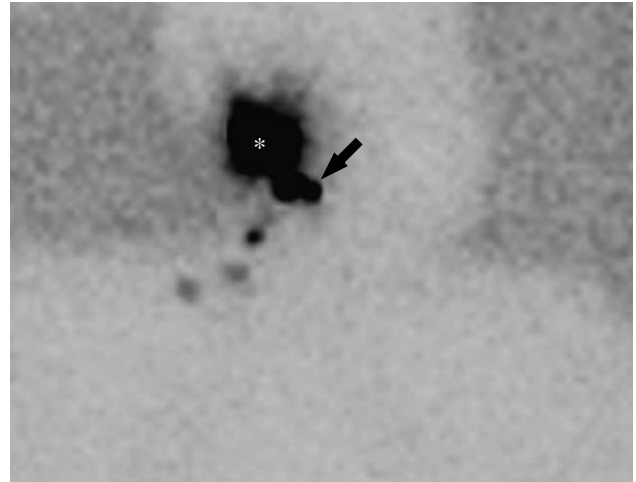


Figure 16.2 Lymphoscintigram, right lateral view, in a 63-year-old patient with right auricular melanoma. The arrow depicts a sentinel lymph node that was located in the parotid gland upon surgical exploration. (*) Injection site.

tomography–computed tomography (SPECT–CT) camera is available, image fusion can be used to precisely localize each individual lymph node, for a relatively rapid intraoperative recognition, with a detection rate that reaches 100% in some series.⁹ The study is completed by applying a handheld γ probe detector in order to draw guiding marks for the surgeon on the overlying skin.

Lymphoscintigraphy for sentinel node detection has a success rate of about 98%,⁸ and failure is primarily related to the existence of diffuse metastatic spread in the lymph node of advanced MM, which can certainly interfere with adequate retention of the radiocolloid, or to the masking of the sentinel node by neighboring activity in the injection site, as seen in some MMs of the head and neck that are in close proximity to the draining nodal basin. The negative predictive value of SLNB is very high owing to the low (2%) incidence of skip metastases (involvement of second- or third-order lymph nodes while escaping the sentinel node) in MM.⁸ The specificity of SLNB is 100%, since thorough ultrathin sections, histopathological and immunohistochemical examinations are usually performed for the resected node(s).

[¹⁸F]fluoro-2-deoxy-D-glucose-positron emission tomography

Since the sensitivity of [¹⁸F]FDG-PET is directly proportionate to the patient's tumor burden at the scan time, [¹⁸F]FDG-PET is generally considered for the metastatic

work-up of high-risk patients (melanoma of the trunk and upper arm, Breslow thickness of >4 mm, surface ulceration, and high mitotic index) who are expected to harbor potential disease manifestations within the detection capability of PET. In fact, applying [^{18}F]FDG-PET for early stage MM (AJCC stage I–II), where the challenge is to detect microscopic disease spread, has yielded quite disappointing results in nodal staging, with an overall sensitivity ranging from 14% to 21%.^{10–12} Consequently, it has been concluded that [^{18}F]FDG-PET neither is a sensitive indicator of occult regional lymph node metastases nor provides a significant impact on the care of patients with early stage MM. However, the situation can be reversed substantially when [^{18}F]FDG-PET is considered for staging high-risk (AJCC stage III–IV) patients (Figures 16.3 and 16.4). Among 70 foci of locoregional or distant nodal/soft

tissue metastases in 103 patients with stage III–IV, [^{18}F]FDG-PET was successful in identifying 55 (78%) lesions.¹³ Similar encouraging results were reported in another study comprising 92 patients with advanced MM.¹⁴

Distant metastases

Malignant melanoma can metastasize anywhere in the human body. This is primarily attributed to the rapid proliferation potential and the high rate of tumor angiogenesis that characterize MM. However, some types of MM such as choroidal melanoma and head and neck melanoma tend to metastasize to selective body organs such as the liver and the brain, respectively.^{15–17} Early identification of occult

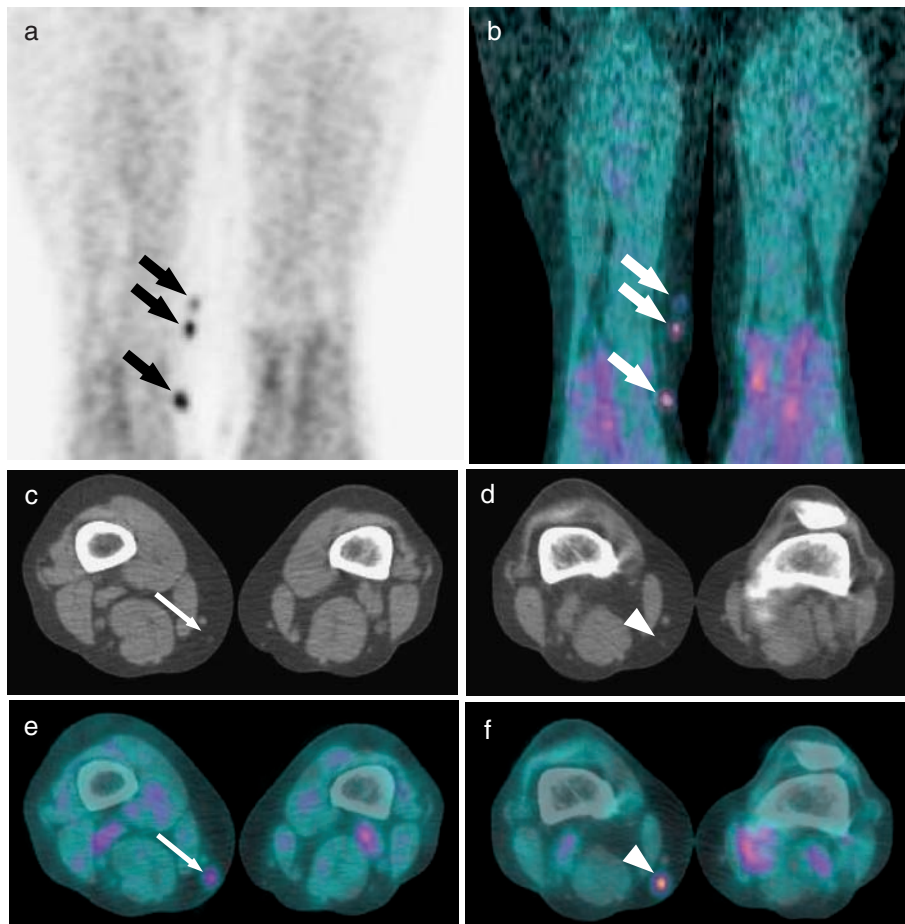


Figure 16.3

Millimetric in-transit metastases of malignant melanoma and the negative contribution of partial volume effect. (a) Coronal ^{18}F -FDG PET and (b) coronal PET/CT reveal 3 millimetric focal hot spots (arrows) consistent with in transit metastases in a 62-year-old patient with melanoma of the right leg. (c and d) Transverse CT and (e and f) correlative transverse PET/CT show the aforementioned lesions with significant underestimation of ^{18}F -FDG activity in the smallest (3 mm) nodule due to partial volume effect (small arrows) in comparison with a relatively larger (5 mm) one (arrowheads).

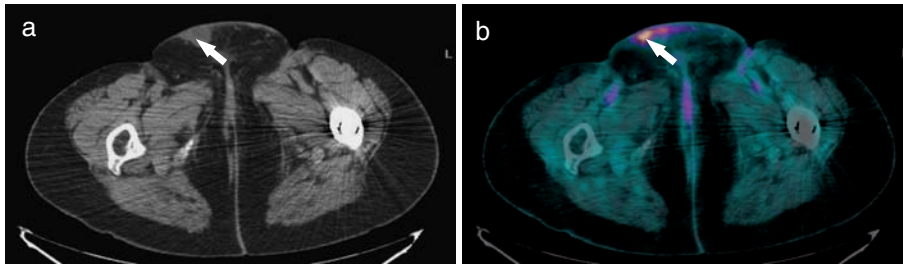


Figure 16.4

Cutaneous melanoma metastasis in the upper thigh. (a) Transverse CT and (b) co-registered transverse ¹⁸F-FDG PET/CT display cutaneous metastasis in the upper thigh (arrows) of a 74-year-old patient previously treated for malignant melanoma of the right foot.

distant metastases derives its importance from the fact that curative surgical resection of locoregional tumor burden or even isolated distant metastatic focus is invariably precluded in patients who harbor widely disseminated melanoma manifestations. Based upon the hematogenous nature of disease spread in advanced MM, a battery of imaging tests is performed, such as CT of the chest and abdomen, CT or MRI of the brain, bone scan, and ultrasonography of soft tissues. Some investigators have advocated the use of gallium-67 whole body scan and immunoscintigraphy using monoclonal antibodies directed against specific melanoma-associated antigens; however, these attempts did not offer any significant advantage in diagnostic accuracy over that obtained from cross-sectional imaging modalities.^{18–20} A single diagnostic test that can cover the whole body in one session for the detection of distant metastasis in MM would be of great benefit.

[¹⁸F]fluoro-2-deoxy-D-glucose-positron emission tomography

Whole body [¹⁸F]FDG-PET was extensively investigated for the detection of distant metastatic disease spread in advanced (AJCC stage III–IV) MM. Aside from small (< 80 mm³) tumor volumes, which are often missed, PET has not only yielded high sensitivity (84% to 92%) in identifying occult metastatic disease (Figures 16.5 and 16.6), but also affected the clinical decision-making process in at least one-third of the studied patient populations.^{14,21} Furthermore, two recent reports have advocated the usage of [¹⁸F]FDG-PET–CT in the metastatic work-up of a patient with choroidal melanoma (Figure 16.7), since PET–CT precisely identified distant disease spread in many organs of the studied patient cohort.^{15,16}

These promising results can be explained in light of the known avidity of MM to [¹⁸F]FDG as well as the whole body mode of PET scan that maximizes the chance of identifying any macroscopic distant disease spread. However, it has to be noted that the high sensitivity figures of [¹⁸F]FDG-PET may be thwarted by a non-negligible rate of false positives owing to the non-specificity of the [¹⁸F]FDG molecule to human malignancies.²² [¹⁸F]FDG is known to

be taken up by both acute and chronic active inflammatory cells.^{23–25} Correlating PET findings with those obtained from cross-sectional structural modalities such as CT and MRI, especially using hybrid PET–CT scanners, has been recommended to improve the specificity of lesion categorization. In a recent report comprising 250 melanoma patients,²⁶ the diagnostic performance of [¹⁸F]FDG-PET–CT in detecting both visceral and non-visceral metastases was significantly better than that of PET alone and CT alone (97%, 93%, and 79%, respectively). This is not surprising, since the morphologic data derived from the CT part of PET–CT represent a cornerstone in identifying the

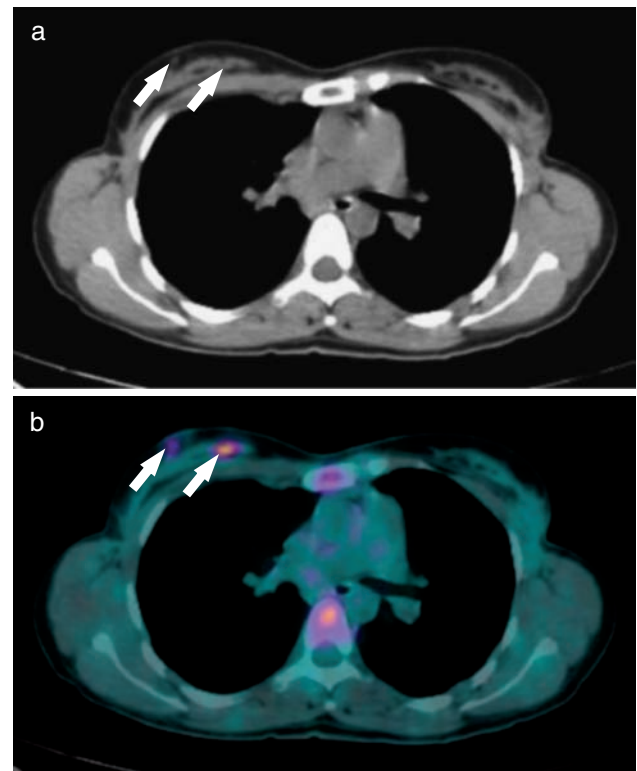


Figure 16.5

Melanoma metastases in the mammary gland. (a) Transverse CT and (b) co-registered transverse ¹⁸F-FDG PET/CT show infracentimetric melanoma metastases in the parenchyma of the right breast of 29-year-old patient with melanoma (arrows).

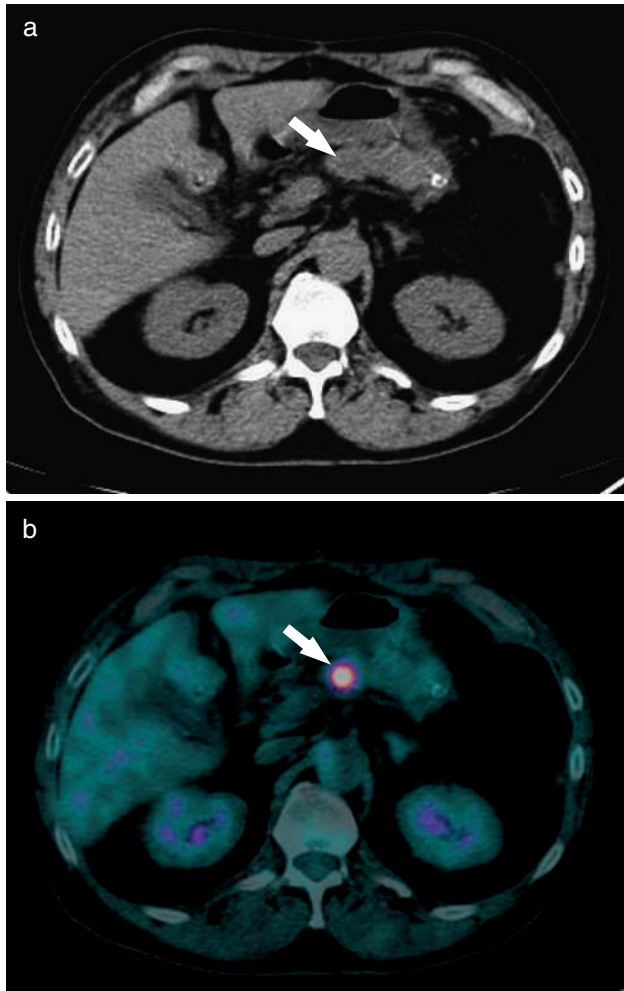


Figure 16.6

Melanoma metastasis in the pancreatic parenchyma. (a) Transverse CT and (b) co-registered transverse ^{18}F -FDG PET/CT display focal metabolically active melanoma metastasis in the pancreatic body of a 64-year-old patient (arrows).

true origin of ^{18}F FDG signals. However, it has to be emphasized that ^{18}F FDG-PET is known by its limited yield (~60%) in the detection of brain metastases, owing to the high physiologic accumulation of ^{18}F FDG in the cerebral cortex (Figure 16.8), suggesting that MRI with gadolinium enhancement should remain the method of choice in this regard.²⁷

Detection of recurrence

In MM, patients initially identified with AJCC stage IIB, IIC, or III have risks of relapse, and death exceeds 40% at 5 years.²⁸ Interestingly, 10–60% of patients with locoregional or solitary distant metastasis have additional lesions

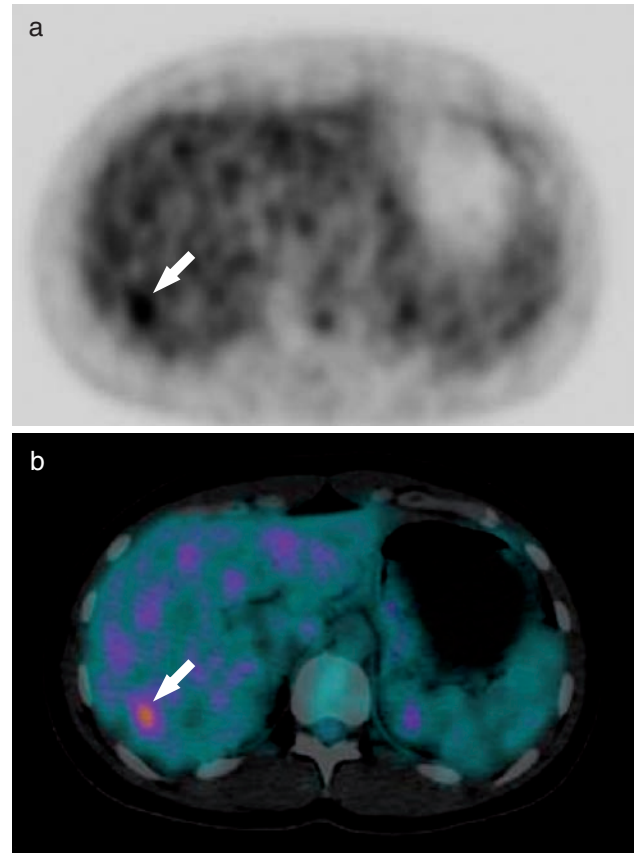


Figure 16.7

Melanoma metastasis in the hepatic parenchyma. (a) Transverse ^{18}F -FDG PET and (b) co-registered transverse PET/CT reveal solitary melanoma metastasis in segment VII of the liver in a 30-year-old patient with ocular melanoma (arrows).

at occult sites;^{29,30} consequently, an accurate non-invasive diagnostic test for melanoma metastases is strongly warranted. Several studies have demonstrated that ^{18}F FDG-PET can detect and localize disease recurrence in MM even in clinically asymptomatic patients.^{31–33} Identifying the exact recurrent tumor burden may avert futile surgery in patients with unresectable disease and target those with isolated distant tumor manifestation to benefit from surgical enucleation aiming at achieving long-term remission. With a range of sensitivity between 85% and 92% and specificity between 90% and 94%,^{31,32} ^{18}F FDG-PET performs better than conventional imaging modalities in the detection of relapsing melanoma (Figure 16.9), with an overall impact on management of 14–36%.^{33,34} However, the high performance of ^{18}F FDG-PET in detecting distant treatment failure in MM may be compromised in certain body regions. For instance, it is known that small (≤ 6 mm) lung metastases are hardly detected by the currently available PET scanners; this is primarily attributed, in part, to the partial volume effect (PVE) that tends to underestimate

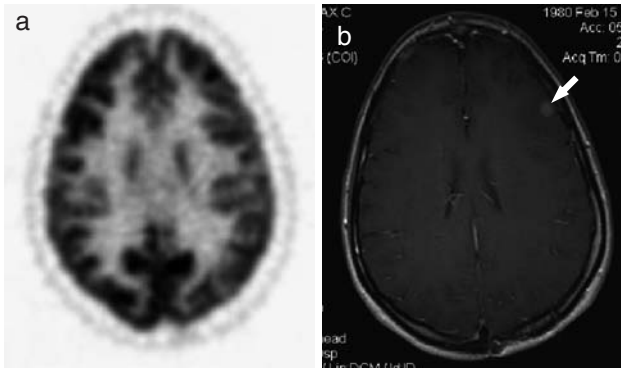


Figure 16.8

Small cortical metastasis that resulted in a false-negative PET scan. (a) Transverse ^{18}F -FDG PET scan in a 27-year-old patient with melanoma shows normal tracer distribution with no evidence of cerebral metastasis. Even at retrospective review, no abnormal ^{18}F -FDG activity could be appreciated against the background activity of the cerebral cortex. (b) Transverse T1-weighted MR image display an 8-mm metastatic lesion (arrow) in the left frontal region.

the ^{18}F FDG concentration of small sized lesions, as well as to activity smearing by virtue of the respiratory movements during PET data acquisition. In fact, the sensitivity of ^{18}F FDG-PET in detecting pulmonary metastases in MM has been shown to be ~70%, in comparison with 93% for CT.^{32,33} Combining both functional and morphological data in hybrid systems is potentially capable of resolving the aforementioned shortcoming of PET. However, it has to be recognized that the currently applied CT acquisition protocols (free breathing or post-normal expiration) may not allow full expansion of the caudal end of both lungs.³⁵ Consequently, for ^{18}F FDG-PET-CT negative studies, a dedicated, full inspiration, chest CT is still needed if small pulmonary metastases in the lower lobe of both lungs are to be excluded.^{36,37} Likewise, since high signal intensity on T₁-weighted MRI can be obtained from melanoma metastases to the brain (especially those that have both melanin

and hemorrhagic components), no currently available imaging modality performs better than MRI in this regard.³⁸

In contrast to locoregional nodal and distant recurrence, there are no adequate studies that specifically investigate the role of ^{18}F FDG-PET in evaluating patients with satellite or in-transit metastases of MM (Figure 16.3). Satellite metastasis refers to skin metastasis within 2 cm of the primary site, whereas in-transit metastasis refers to that from 2 cm to the regional lymphatic basin. Both, indeed, are lymphogenous metastases. Preliminary results, however, have shown a possible role for ^{18}F FDG-PET in this domain. Among 65 skin or subcutaneous sites containing tumor, PET detected 56 (86%) lesions, which led to a change of management in 17% of the studied patient cohort.³¹ Noteworthy, however, is the reported low (25%) specificity that may be related to the chronic post-therapy inflammatory reactions and/or to the process of skin and soft tissue remodeling after surgical interference, radiotherapy, and isolated limb perfusion therapy. Future applications of ^{18}F FDG-PET-CT will certainly reduce this relatively high incidence of false positive results.

Therapy monitoring

Since surgical intervention with curative intent is the standard care for patients with early stage (AJCC stage I–II) MM, systemic therapy (chemotherapy/immunotherapy) and radiotherapy are usually reserved for patients with relatively advanced disease stage or for those who harbor unresectable tumor burden. Unfortunately the role of functional imaging in therapy monitoring of metastatic melanoma is not fully established, potentially due to the suboptimal therapeutic effect of the currently available modalities. However, it has to be recognized that ^{18}F FDG-PET was proven to be of great benefit in monitoring the response of other tumor types to systemic therapy or radiation treatment.³⁹ Adding ^{18}F FDG-PET to future clinical trials that concern advanced MM may offer

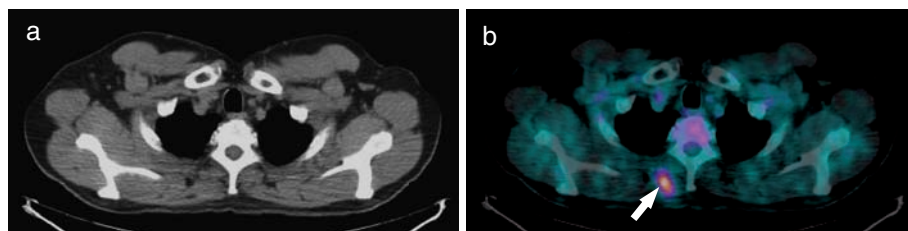


Figure 16.9

Melanoma metastasis in the skeletal muscle. (a) Transverse CT and (b) co-registered transverse ^{18}F -FDG PET/CT in a 63-year-old patient with melanoma. Please note the normal appearance of the right paravertebral muscle on CT that proved to harbor a metabolically active melanoma metastasis (arrow).

non-responders the opportunity to have alternative therapies before developing further tumor progression, and, thereby, spare them unnecessary toxicity burden.

Risk stratification/ outcome prediction

Since [^{18}F]FDG-PET is known for its unique ability to resume the global metabolic state of each individual tumor, numerous studies have reported a frank correlation between the tumor's avidity to [^{18}F]FDG and the overall disease-free survival and patient outcome. Using different cut-off values for SUV, these postulations have been validated for brain, head and neck, pulmonary, breast, and pancreatic tumors in addition to lymphoma and sarcoma.^{40–46} In a recent study, a SUV_{mean} cut-off value of 5.2 could predict disease-free survival (DFS) in 38 melanoma patients who presented with palpable, [^{18}F]FDG avid, lymph node metastases.⁴⁷ Patients who presented with a SUV_{mean} of ≤ 5.2 had a mean DFS of 790 days, whereas those who expressed higher values had a mean DFS of only 377 days. Similarly, among 14 patients with choroidal melanoma, the highest SUV_{max} was observed in two (14%) patients who developed distant metastases along their disease course.⁴⁸ These concordant results are of paramount importance, since identifying high-risk groups may allow adjuvant radiation treatment or chemotherapy to be applied, aiming at an optimal DFS.

Imaging pitfalls

Pitfalls of [^{18}F]FDG-PET data interpretation in MM can be classified into three main categories: (1) secondary pitfalls that result from the insufficient topographic resolution of PET, (2) false positives that are frequently related to the lack of appropriate clinical data, and (3) incidental findings that stem from other pathological processes distinct from the primary one for which PET is considered.

The first category includes [^{18}F]FDG accumulation that mimics active disease foci, such as segmental muscular uptake in the head and neck region, uptake in the salivary glands, excreted saliva in the pharynx, [^{18}F]FDG-avid brown adipose tissue (Figure 16.10), uptake in recent rib fractures and scars, uptake in degenerative joint diseases, accumulation in vascular abnormalities (atheromatosis or venous thrombosis), stagnant [^{18}F]FDG activity in the ureters, and [^{18}F]FDG accumulation along the gastrointestinal tract.^{49–55} In fact, resolving the vast majority of these pitfalls can easily be accomplished by virtue of PET–CT image fusion,^{56,57} where the location of any

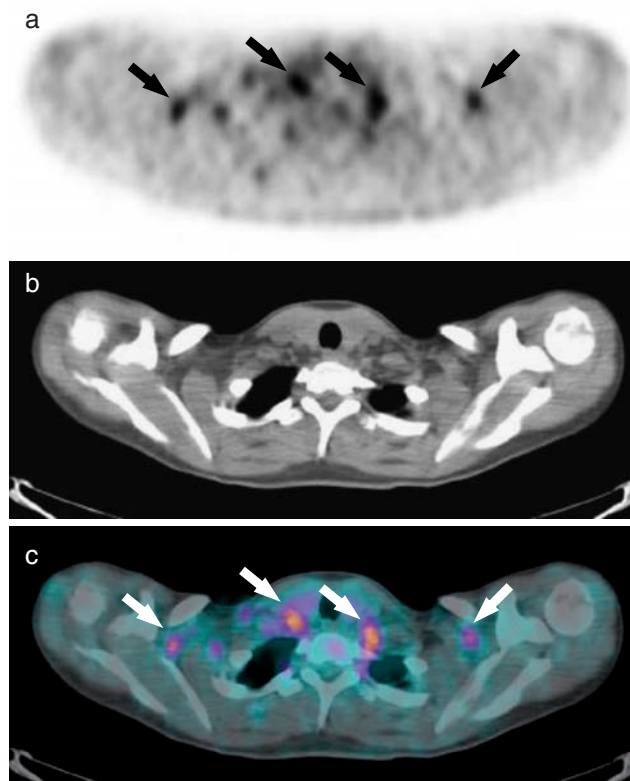


Figure 16.10

^{18}F -FDG accumulation in brown adipose tissue mimicking lymph node metastases. (a) Transverse PET in a 30-year-old patient with melanoma shows multiple focal ^{18}F -FDG uptake in the lower cervical and supraclavicular regions on either side mimicking bilateral metastatic lymph node involvement (black arrows). (b) Correlative transverse CT and (c) co-registered transverse ^{18}F -FDG PET/CT confirm that the aforementioned focal hot spots stem from the brown adipose tissue and not the lymph nodes (white arrows).

abnormal [^{18}F]FDG uptake can be precisely identified. Especially for MM, the integration of the patient's clinical information in the process of [^{18}F]FDG-PET reading has been shown to optimize the overall specificity.⁵⁸ In the case of blind data interpretation, reactive lymph nodes secondary to recent biopsy, or subcutaneous injection of interferon (Figure 16.11), can easily be mistaken for active metastatic foci or in-transit metastases, and the same holds true for patients undergoing melanoma vaccination. It should be emphasized, however, that some non-specific [^{18}F]FDG accumulation in lymph nodes remains inevitable, and may lead to unnecessary biopsy in up to 8% of patients.⁵⁹ For the third category, many incidental [^{18}F]FDG-avid lesions, which mimic active manifestations of MM, can be detected anywhere in the human body. For instance, some active granulomatous lung diseases such as tuberculosis and sarcoidosis have been shown to accumulate considerable amounts of [^{18}F]FDG.⁶⁰

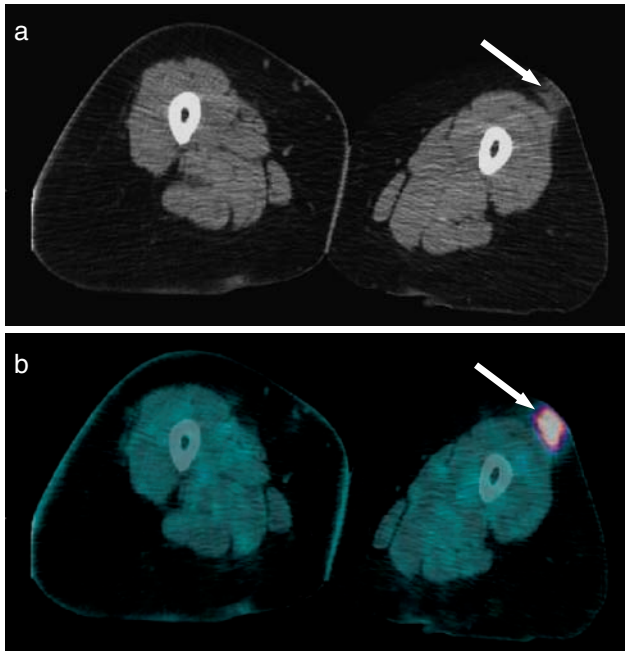


Figure 16.11

Post immunotherapy cutaneous reaction mimicking melanoma metastasis. (a) Transverse CT and (b) co-registered transverse ^{18}F -FDG PET/CT show cutaneous and subcutaneous thickening along with pathological ^{18}F -FDG accumulation in a 62-year-old patient with melanoma after adjuvant treatment with subcutaneous interferon injection in the left thigh (arrows).

Likewise, synchronous tumors in the head and neck, breast, lung, and lymph nodes may be easily mistaken for melanoma metastasis on ^{18}F -FDG-PET.^{61,62} Furthermore, some precancerous lesions such as advanced colonic adenomas, which are known for high ^{18}F -FDG avidity, may be confounded with gastrointestinal metastases of MM.^{55,63} Despite the fact that these incidental pathologic findings are likely to deteriorate the specificity of ^{18}F -FDG-PET, their early detection may have a major positive impact on patient management and consequently outcome.

Future directions

The development trials of alternative radiotracers and diagnostic tools for MM are of great clinical importance. For instance, N-isopropyl-p- ^{123}I iodoamphetamine (^{123}I IMP), which is known to be incorporated into the melanin producing melanocytes, has recently been investigated using SPECT for the detection of primary uveal MM.⁶⁴ In fact, ^{123}I IMP-SPECT revealed better sensitivity than ^{18}F -FDG-PET. Another radiopharmaceutical of potential prognostic benefit is $^{99\text{m}}\text{Tc}$ interleukin-2 ($^{99\text{m}}\text{Tc}$ IL-2). This agent traces the IL-2 receptors that may be expressed

in the melanoma-infiltrating lymphocytes. Since IL-2 immunotherapy potentiates the action of IL-2 receptor positive lymphocytes, a positive $^{99\text{m}}\text{Tc}$ IL-2 scintigraphy indicates that the lesions under investigation are prone to a successful IL-2 immunotherapy.⁶⁵ The proliferation potential of MM can be assessed *in vivo* using tracers that target the process of DNA synthesis such as 3'- ^{18}F fluoro-3'-deoxy-L-thymidine (^{18}F FLT). Except for those lesions that stem from the liver or the skeleton, where ^{18}F FLT normally accumulates, a sensitivity of 88% has been reported for ^{18}F FLT in the detection of locoregional melanoma metastases.⁶⁶ Accordingly, this tracer may have a complementary role to that of ^{18}F FDG in characterizing indeterminate lesions that may be mistaken for melanoma metastasis. The recent introduction of the high-energy γ photon probe into the clinical environment has facilitated intraoperative detection of some challenging (non-palpable or non-visualized) ^{18}F FDG-avid lesions, especially those that locate in areas where the anatomy is perturbed by virtue of surrounding scar tissue or previous surgical interference.⁶⁷ Despite a high specificity figure, a positron detecting probe revealed a moderate sensitivity for some melanoma lesions due to signal loss within the background activity.⁶⁸ Future developments will certainly overcome these shortcomings to allow an ideal performance of the positron detecting probe.

Conclusions

As MM is categorized as the most common fatal skin cancer, the primary care of MM patients represents one of the major clinical priorities. For the initial tumor (T) stage, excisional biopsy and pathological examination remain the standard of reference against which accurate T-staging can be established. For nodal (N) staging of early (AJCC stage I–II) MM, lymphoscintigraphy and SLNB have far surpassed ^{18}F -FDG-PET; this latter, however, has an established role in excluding the existence of extracranial metastasis in patients with high-risk (primary lesion of the trunk and upper arm, Breslow thickness of > 4 mm, surface ulceration, and high mitotic index) or advanced (AJCC stage III) MM. For patients who present with a suspicion of local or distant treatment failure, the application of whole body ^{18}F -FDG-PET–CT may allow rapid identification of any potential disease relapse and, thus, spare additional radiological or invasive diagnostic procedures. Furthermore, PET–CT image fusion has the potential to dramatically reduce the rate of false positives, since it has the capability to relate each individual ^{18}F -FDG signal to its true origin. Besides a possible role in the evaluation of melanoma response to systemic therapy, PET can offer reliable prognostic information for *de novo* MM patients since the ^{18}F -FDG avidity of some primary lesions/nodal metastases has been shown to predict disease-free survival.

In the near future, further brilliant horizons are awaited, since the development trials of other radiotracers that target certain pathophysiological processes in MM are advancing steadily.

References

1. Tsao H, Atkins MB, Sober AJ. Management of cutaneous melanoma. *N Engl J Med* 2004; 351: 998–1012.
2. Gilchrist BA, Eller MS, Geller AC, Yaar M. The pathogenesis of melanoma induced by ultraviolet radiation. *N Engl J Med* 1999; 340: 1341–48.
3. National Cancer Institute. 51-Year trends in US cancer death rates. In: SEER cancer statistics review, 1975–2000. Accessed August 9, 2004, at http://seer.cancer.gov/csr/1975_2000/results_merged/topic_inc_mor_trends.pdf.
4. Balch CM, Buzaid AC, Soong SJ et al. Final version of the American Joint Committee on Cancer staging system for cutaneous melanoma. *J Clin Oncol* 2001; 19: 3635–48.
5. Balch CM, Soong SJ, Smith T et al. Long-term results of a prospective surgical trial comparing 2 cm vs 4 cm excision margins for 740 patients with 1–4 mm melanomas. *Ann Surg Oncol* 2001; 8: 101–8.
6. Morton DL, Thompson JF, Cochran AJ et al. Sentinel-node biopsy or nodal observation in melanoma. *N Engl J Med* 2006; 355: 1307–17.
7. Kuvshinoff BW, Kurtz C, Coit DG. Computed tomography in evaluation of patients with stage III melanoma. *Ann Surg Oncol* 1997; 4: 252–8.
8. Mariani G, Erba P, Manca G et al. Radioguided sentinel lymph node biopsy in patients with malignant cutaneous melanoma: the nuclear medicine contribution. *J Surg Oncol* 2004; 85: 141–51.
9. Ishihara T, Kaguchi A, Matsushita S et al. Management of sentinel lymph nodes in malignant skin tumors using dynamic lymphoscintigraphy and the single-photon-emission computed tomography/computed tomography combined system. *Int J Clin Oncol* 2006; 11: 214–20.
10. Wagner JD, Schauwecker D, Davidson D et al. Inefficacy of F-18 fluorodeoxy-D-glucose-positron emission tomography scans for initial evaluation in early-stage cutaneous melanoma. *Cancer* 2005; 104: 570–9.
11. Wagner JD, Schauwecker D, Davidson D et al. Prospective study of fluorodeoxyglucose-positron emission tomography imaging of lymph node basins in melanoma patients undergoing sentinel node biopsy. *J Clin Oncol* 1999; 17: 1508–15.
12. Belhocine T, Pierard G, de Labrassinne M, Lahaye T, Rigo P. Staging of regional nodes in AJCC stage I and II melanoma: 18FDG PET imaging versus sentinel node detection. *Oncologist* 2002; 7: 271–8.
13. Brady MS, Akhurst T, Spanknebel K et al. Utility of preoperative [(18)F] fluorodeoxyglucose-positron emission tomography scanning in high-risk melanoma patients. *Ann Surg Oncol* 2006; 13: 525–32.
14. Harris MT, Berlangieri SU, Cebon JS, Davis ID, Scott AM. Impact of 2-deoxy-2[F-18]fluoro-D-glucose positron emission tomography on the management of patients with advanced melanoma. *Mol Imaging Biol* 2005; 7: 304–8.
15. Finger PT, Kurli M, Reddy S, Tena LB, Pavlic AC. Whole body PET/CT for initial staging of choroidal melanoma. *Br J Ophthalmol* 2005; 89: 1270–4.
16. Kurli M, Reddy S, Tena LB, Pavlick AC, Finger PT. Whole body positron emission tomography/computed tomography staging of metastatic choroidal melanoma. *Am J Ophthalmol* 2005; 140: 193–9.
17. Daryanani D, Plukker JTh, de Jong MA et al. Increased incidence of brain metastases in cutaneous head and neck melanoma. *Melanoma Res* 2005; 15: 119–24.
18. Kagan R, Witt T, Bines S, Mesleh G, Economou S. Gallium-67 scanning for malignant melanoma. *Cancer* 1988; 61: 272–4.
19. Böni R, Huch-Böni R, Steinert H et al. Antimelanoma monoclonal antibody 225.28S immunoscintigraphy in metastatic melanoma. *Dermatology* 1995; 191: 119–23.
20. Divigi CR, Larson SM. Radiolabeled monoclonal antibodies in the diagnosis and treatment of malignant melanoma. *Semin Nucl Med* 1989; 19: 252–61.
21. Swetter SM, Carroll LA, Johnson DL, Segall GM. Positron emission tomography is superior to computed tomography for metastatic detection in melanoma patients. *Ann Surg Oncol* 2002; 9: 646–53.
22. Rosenbaum SJ, Lind T, Antoch G, Bockisch A. False-positive FDG PET uptake—the role of PET/CT. *Eur Radiol* 2006; 16: 1054–65.
23. Kaim AH, Weber B, Kurrer MO et al. Autoradiographic quantification of 18F-FDG uptake in experimental soft-tissue abscesses in rats. *Radiology* 2002; 223: 446–51.
24. Wyss MT, Honer M, Spath N et al. Influence of ceftriaxone treatment on FDG uptake—an in vivo [18F]-fluorodeoxyglucose imaging study in soft tissue infections in rats. *Nucl Med Biol* 2004; 31: 875–82.
25. Kamel EM, McKee TA, Calcagni ML et al. Occult lung infarction may induce false interpretation of 18F-FDG PET in primary staging of pulmonary malignancies. *Eur J Nucl Med Mol Imaging* 2005; 32: 641–6.
26. Reinhardt MY, Joe AY, Jaeger U et al. Diagnostic performance of whole body dual modality 18F-FDG PET/CT imaging for N- and M-staging of malignant melanoma: Experience with 250 consecutive patients. *J Clin Oncol* 2006; 24: 1178–87.
27. Rohren EM, Provenzale JM, Barboriak DP, Coleman RE. Screening for cerebral metastases with FDG PET in patients undergoing whole-body staging of non-central nervous system malignancy. *Radiology* 2003; 226: 181–7.
28. Balch CM, Soong SJ, Gershenwald JE et al. Prognostic factors analysis of 17,600 melanoma patients: validation of the American Joint Committee on Cancer melanoma staging system. *J Clin Oncol* 2001; 19: 3622–34.
29. Buzaid A, Tinoco L, Ross M, Legha S, Benjamin R. Role of computed tomography in the staging of patients with local-regional metastases of melanoma. *J Clin Oncol* 1995; 13: 2104–8.
30. Ryan L, Kramar A, Borden E. Prognostic factors in metastatic melanoma. *Cancer* 1993; 71: 2995–3005.
31. Stas M, Stroobants S, Dupont P et al. 18-FDG PET scan in the staging of recurrent melanoma: additional value and therapeutic impact. *Melanoma Res* 2002; 12: 479–90.

32. Rinne D, Baum RP, Hor G, Kaufmann R. Primary staging and follow-up of high risk melanoma patients with whole-body 18F-fluorodeoxyglucose positron emission tomography: results of a prospective study of 100 patients. *Cancer* 1998; 82: 1664–71.
33. Fuster D, Chiang S, Johnson G et al. Is 18F-FDG PET more accurate than standard diagnostic procedures in the detection of suspected recurrent melanoma? *J Nucl Med* 2004; 45: 1323–7.
34. Tyler DS, Onaitis M, Kherani A et al. Positron emission tomography scanning in malignant melanoma. *Cancer* 2000; 89: 1019–25.
35. Goerres GW, Kamel E, Heidelberg TN et al. PET-CT image co-registration in the thorax: influence of respiration. *Eur J Nucl Med Mol Imaging* 2002; 29: 351–60.
36. Allen-Auerbach M, Yeom K, Park J, Phelps M, Czernin J. Standard PET/CT of the chest during shallow breathing is inadequate for comprehensive staging of lung cancer. *J Nucl Med* 2006; 47: 298–301.
37. Aquino SL, Kuester LB, Muse VV, Halpern EF, Fischman AJ. Accuracy of transmission CT and FDG-PET in the detection of small pulmonary nodules with integrated PET/CT. *Eur J Nucl Med Mol Imaging* 2006; 33: 692–6.
38. Healy ME, Hesselink JR, Press GA, Middleton MS. Increased detection of intracranial metastases with intravenous Gd-DTPA. *Radiology* 1987; 165: 619–24.
39. Juweid ME, Cheson BD. Positron-emission tomography and assessment of cancer therapy. *N Engl J Med* 2006; 354: 496–507.
40. Padma MV, Said S, Jacobs M et al. Prediction of pathology and survival by FDG PET in gliomas. *J Neurooncol* 2003; 64: 227–37.
41. Allal AS, Dulguerov P, Allaoua M et al. Standardized uptake value of 2-[(18)F] fluoro-2-deoxy-D-glucose in predicting outcome in head and neck carcinomas treated by radiotherapy with or without chemotherapy. *J Clin Oncol* 2002; 20: 1398–404.
42. Downey RJ, Akhurst T, Gonen M et al. Preoperative F-18 fluoro-deoxyglucose-positron emission tomography maximal standardized uptake value predicts survival after lung cancer resection. *J Clin Oncol* 2004; 22: 3255–60.
43. Cachin F, Prince HM, Hogg A, Ware RE, Hicks RJ. Powerful prognostic stratification by [18F]fluorodeoxyglucose positron emission tomography in patients with metastatic breast cancer treated with high-dose chemotherapy. *J Clin Oncol* 2006; 24: 3026–31.
44. Lyshchik A, Higashi T, Nakamoto Y et al. Dual-phase 18F-fluoro-2-deoxy-D-glucose positron emission tomography as a prognostic parameter in patients with pancreatic cancer. *Eur J Nucl Med Mol Imaging* 2005; 32: 389–97.
45. Spaepen K, Stroobants S, Dupont P et al. Prognostic value of pretransplantation positron emission tomography using fluorine 18-fluorodeoxyglucose in patients with aggressive lymphoma treated with high-dose chemotherapy and stem cell transplantation. *Blood* 2003; 102: 53–9.
46. Hawkins DS, Schuetze SM, Butrynski JE et al. [18F]Fluoro-deoxyglucose positron emission tomography predicts outcome for Ewing sarcoma family of tumors. *J Clin Oncol* 2005; 23: 8828–34.
47. Bastiaannet E, Hoekstra OS, Oyen WJ et al. Level of fluoro-deoxyglucose uptake predicts risk for recurrence in melanoma patients presenting with lymph node metastases. *Ann Surg Oncol* 2006; 13: 919–26.
48. Finger PT, Chin K, Jacob C. 18-Fluorine-labelled 2-deoxy-2-fluoro-D-glucose positron emission tomography/computed tomography standardised uptake values: a non-invasive biomarker for the risk of metastasis from choroidal melanoma. *Br J Ophthalmol* 2006; 90: 1263–6.
49. Blodgett TM, Fukui MB, Snyderman CH et al. Combined PET-CT in the head and neck: Part 1. Physiologic, altered physiologic, and artifactual FDG uptake. *Radiographics* 2005; 25: 897–912.
50. Hany TF, Gharehpapagh E, Kamel EM et al. Brown adipose tissue: a factor to consider in symmetrical tracer uptake in the neck and upper chest region. *Eur J Nucl Med Mol Imaging* 2002; 29: 1393–8.
51. Shon IH, Fogelman I. F-18 FDG positron emission tomography and benign fractures. *Clin Nucl Med* 2003; 28: 171–5.
52. Dunphy MP, Freiman A, Larson SM, Strauss HW. Association of vascular 18F-FDG uptake with vascular calcification. *J Nucl Med* 2005; 46: 1278–84.
53. Miceli M, Atoui R, Walker R et al. Diagnosis of deep septic thrombophlebitis in cancer patients by fluorine-18 fluoro-deoxyglucose positron emission tomography scanning: a preliminary report. *J Clin Oncol* 2004; 22: 1949–56.
54. Kamel EM, Jichlinski P, Prior JO et al. Forced diuresis improves the diagnostic accuracy of ¹⁸F-FDG PET in abdominopelvic malignancies. *J Nucl Med* 2006; 47: 1803–7.
55. Kamel EM, Thumshirn M, Truninger K et al. Significance of incidental 18F-FDG accumulations in the gastrointestinal tract in PET/CT: correlation with endoscopic and histopathologic results. *J Nucl Med* 2004; 45: 1804–10.
56. Kostakoglu L, Hardoff R, Mirtcheva R, Goldsmith SJ. PET-CT fusion imaging in differentiating physiologic from pathologic FDG uptake. *Radiographics* 2004; 24: 1411–31.
57. von Schulthess GK, Steinert HC, Hany TF. Integrated PET/CT: current applications and future directions. *Radiology* 2006; 238: 405–22.
58. Steinert HC, Huch Boni RA, Buck A et al. Malignant melanoma: staging with whole-body positron emission tomography and 2-[F-18]-fluoro-2-deoxy-D-glucose. *Radiology* 1995; 195: 705–9.
59. Crippa F, Leutner M, Belli F et al. Which kinds of lymph node metastases can FDG PET detect? A clinical study in melanoma. *J Nucl Med* 2000; 41: 1491–4.
60. Asad S, Aquino SL, Piyavisetpat N, Fischman AJ. False-positive FDG positron emission tomography uptake in non-malignant chest abnormalities. *AJR Am J Roentgenol* 2004; 182: 983–9.
61. Agress H Jr, Cooper BZ. Detection of clinically unexpected malignant and premalignant tumors with whole-body FDG PET: histopathologic comparison. *Radiology* 2004; 230: 417–22.
62. Ishimori T, Patel PV, Wahl RL. Detection of unexpected additional primary malignancies with PET/CT. *J Nucl Med* 2005; 46: 752–7.
63. Gutman F, Alberini JL, Wartski M et al. Incidental colonic focal lesions detected by FDG PET/CT. *AJR Am J Roentgenol* 2005; 185: 495–500.

64. Kato K, Kubota T, Ikeda M et al. Low efficacy of 18F-FDG PET for detection of uveal malignant melanoma compared with 123I-IMP SPECT. *J Nucl Med* 2006; 47: 404–9.
65. Signore A, Annovazzi A, Barone R et al. 99mTc-interleukin-2 scintigraphy as a potential tool for evaluating tumor-infiltrating lymphocytes in melanoma lesions: a validation study. *J Nucl Med* 2004; 45: 1647–52.
66. Cobben DC, Jager PL, Elsinga PH et al. 3'-18F-fluoro-3'-deoxy-L-thymidine: a new tracer for staging metastatic melanoma? *J Nucl Med* 2003; 44: 1927–32.
67. Higashi T, Saga T, Ishimori T et al. What is the most appropriate scan timing for intraoperative detection of malignancy using 18F-FDG-sensitive gamma probe? Preliminary phantom and preoperative patient study. *Ann Nucl Med* 2004; 18: 105–14.
68. Franc BL, Mari C, Johnson D, Leong SP. The role of a positron- and high-energy gamma photon probe in intraoperative localization of recurrent melanoma. *Clin Nucl Med* 2005; 30: 787–91.

Cancer of unknown primary

Emilio Bombardieri, Stefano Fanti, Arturo Chiti, Cristina Nanni, Angela Coliva, Enrico Pelosi, and Gianni Bisi

Background

Cancer of unknown primary (CUP) is defined as a biopsy-proven secondary lesion with no detectable primary tumor after physical examination and conventional imaging tests (X-ray imaging, computed tomography (CT), and ultrasound (US)). The primary site of some cancers may eventually be found by additional tests, and in this case they are no longer considered CUP. The reasons why the primary tumor sometimes is not found can be different: (1) sometimes the secondaries have grown very quickly while the primary remains very small or below the resolution of the diagnostic modalities; (2) some immunitary reactions can cause the spontaneous disappearance of the primary tumor; and (3) the diagnostic imaging methods are not able to depict the primary because it is hidden.¹ The frequency of CUP in cancer varies from 2–3 to 4.2%, depending on geographical area, and represents the eighth most frequently occurring malignancy in the world. CUP prognosis is poor: fewer than 25% and 10% of patients are alive at 1 and 5 years respectively.^{2,3} The histological types have been classified according to the World Health Organization (WHO) into: adenocarcinoma (well to moderately differentiated and poorly or undifferentiated), squamous cell carcinoma (undifferentiated and not specified), neuroendocrine tumors, lymphomas, germ cell tumors, melanomas, sarcomas, and embryonal malignancies.⁴ The diagnosis of CUP can be made on the basis of symptoms, which depend on the organ the CUP has spread to.

The conventional diagnostic work-up for CUP syndrome consists of two distinct phases: the first includes detailed history, physical examination, laboratory tests, chest radiography, contrast-enhanced (ce)-CT of the abdomen and pelvis, and mammography. Should these procedures not be sufficient, the following examinations are ce-CT of the chest, endoscopic procedures, magnetic resonance imaging (MRI), and even exploratory surgery.^{1,5}

Unfortunately, at completion of both phases of the traditional work-up, the rate of identification of the primary site does not exceed 10–35%, thus leaving us with actual CUP syndrome.⁶

Imaging studies are therefore very important (Table 17.1) and can sometimes be guided by progressively increasing levels of tumor markers (Table 17.2).⁷

Of course, pathologic analysis, including microscope morphological examination, immunohistochemistry, electron microscopy, and cytogenetic and molecular genetic testing (polymerase chain reaction, PCR), can contribute to clarify the origin of a lesion from an unknown primary. Also, the pathology sometimes does not succeed in giving a correct diagnosis even if the search for immunoperoxidase markers (e.g. cytokeratin, vimentin, desmin, cutaneous lymphocyte-associated antigen (CLA), epithelial membrane antigen (EMA), thyroid transcription factor 1 (TTF-1), S-100 protein, melanocytic marker HMB-45, etc.) contributes towards identifying the characteristic pattern

Table 17.1 Most common imaging studies for cancer of unknown primary (CUP)

Chest X-ray
X-ray of the gastrointestinal tract
Mammography
Computed tomography (CT)
Magnetic resonance imaging (MRI)
Ultrasound (US)
Endoscopy
Nuclear medicine (planar scintigraphy/SPECT/PET)
SPECT, single photon emission computed tomography; PET, positron emission tomography.

Table 17.2 Most relevant tumor markers guiding the diagnosis of CUP*Markers with high tissue specificity*

PSA
Tg
hCG and other hormones
AFP
CgA

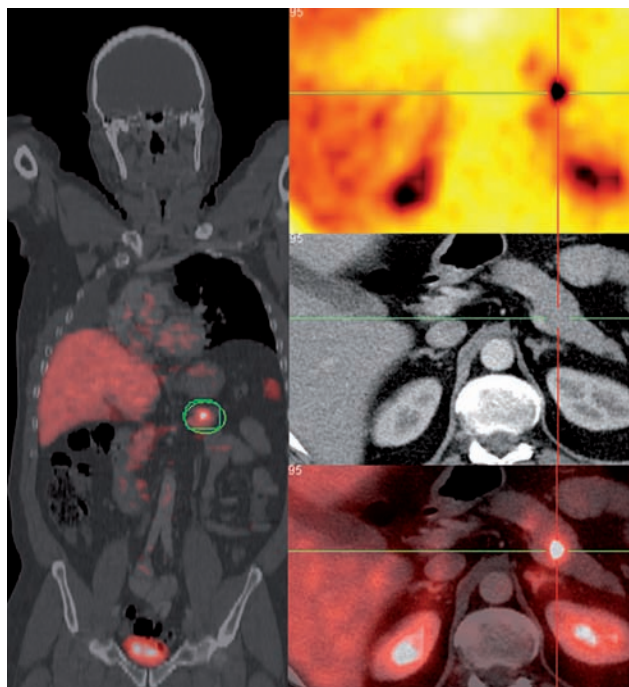
Markers with moderate tissue specificity

CA125
Enolase (NSE)

Markers with low tissue specificity

CEA
CA15.3, CA19.9, and other mucin markers
Enzymes (LDH, BAP, etc.)

PSA, prostate specific antigen; Tg, thyroglobulin; hCG, human chorionic gonadotropin; AFP, α -fetoprotein; CgA, chromogranin A; NSE, neuron-specific enolase; CEA, carcinoembryonic antigen; LDH, lactate dehydrogenase; BAP, bone alkaline phosphatase.

**Figure 17.1**

^{68}Ga DOTA (tetraazacyclododecanetetraacetic acid) positron emission tomography–computed tomography (PET–CT): patient with 6-mm neuroendocrine tumor (NET) of the pancreas confirmed by surgery (cancer of unknown primary, CUP). (Courtesy of Prof. essor Baum, Zentralklinik Bad Berka.)

associated with a single organ or tissue.⁸ Recently, after using a gene-based algorithm reverse transcriptase-polymerase chain reaction (RT-PCR), Talantov et al. published some interesting results for identifying the tissue of origin of metastatic carcinoma. However, this approach still has only experimental value, and further studies are needed to validate this method.⁹ Among the imaging modalities, nuclear medicine examinations have a very important impact on making an accurate diagnosis, due to the widespread use of positron emission tomography (PET) and PET/CT in oncology, and to the high diagnostic efficacy of this new technology. In this area, the most important experience has been gained with ^{18}F FDG fluoro-2-deoxy-D-glucose. Whole-body PET and PET/CT using ^{18}F FDG have demonstrated good accuracy in identifying CUP for the most common histologies, namely adenocarcinoma, squamous cell carcinoma, and poorly differentiated carcinoma.¹⁰ However, it is well known that ^{18}F FDG is of limited value in tumors that do not usually show enhanced FDG uptake, such as some neuroendocrine tumors. Alternative PET tracers have been proposed for studying these types of tumors, but unfortunately no large experience is reported in the literature for radiopharmaceuticals other than FDG.¹¹ At the same time, we would like to point out that also several single photon emission computed tomography (SPECT) tracers have demonstrated their diagnostic value in detecting CUP. This review will discuss the most relevant results obtained with the different γ emitting tracers (SPECT radiopharmaceuticals) and those with positron-emitting tracers (PET radiopharmaceuticals) (Table 17.3).

Table 17.3 Proposed radiopharmaceuticals for detecting cancer of unknown origin *γ -emitting radiopharmaceuticals (SPECT tracers)*

$^{99\text{m}}\text{Tc}$ pertechnetate
 $^{99\text{m}}\text{Tc}$ MDP
 $^{99\text{m}}\text{Tc}$ sestamibi
 ^{67}Ga citrate
 ^{111}In pentetreotide
 $^{99\text{m}}\text{Tc}$ EDDA/HYNIC-octreotate

Positron-emitting radiopharmaceuticals (PET tracers)

^{18}F FDG
 ^{18}F DOPA
 ^{18}F DOPA-NOC

MDP, methylene diphosphonate; EDDA, ethylenediaminediacetic acid; HYNIC, hydrazinonicotinyl; FDG, fluoro-2-deoxy-D-glucose; DOPA, dihydroxyphenylalanine; NOC, 1-Nal³-octreotide.

Planar and SPECT scintigraphy

$[^{67}\text{Ga}]$ citrate scintigraphy

Gallium-67 has been used in recent decades as a radiopharmaceutical for oncology, and due to its uptake in many tumor types this radiopharmaceutical has been suggested for cases presenting with metastases without a known primary. Gallium scintigraphy, for a long period, has been used in patients with lymphoma, malignant melanoma, and lung malignancies, and it has been a usual indication in tumor staging, restaging, monitoring, and prediction of tumor response to therapy.^{12,13}

The results of ^{67}Ga scintigraphy in occult tumor detection were not satisfactory.¹⁴ However, in patients with lymphoma and melanoma, the primary sites can sometimes be detected by whole-body scan scintigraphy when metastases are evident at diagnostic imaging. The limitations in using the gallium scan are well known, such as its poor cancer specificity, the slow biokinetics requiring at least 2–3 days for good image acquisition, interference of its physiological uptake in the gastrointestinal system, and relatively high irradiation of patients. All these factors have progressively limited the wide use of gallium in oncology, and today this tracer has almost been abandoned. Therefore, gallium-67 at present is not used to identify an unknown primary.¹¹

$[^{99m}\text{Tc}]$ Pertechnetate scintigraphy

In the presence of metastasis of unknown origin, the demonstration of a thyroid nodule by means of ultrasonography or scintigraphy suggests the possibility of thyroid cancer, and requires fine needle aspiration biopsy (FNAB). The risk of cancer is higher if the nodule does

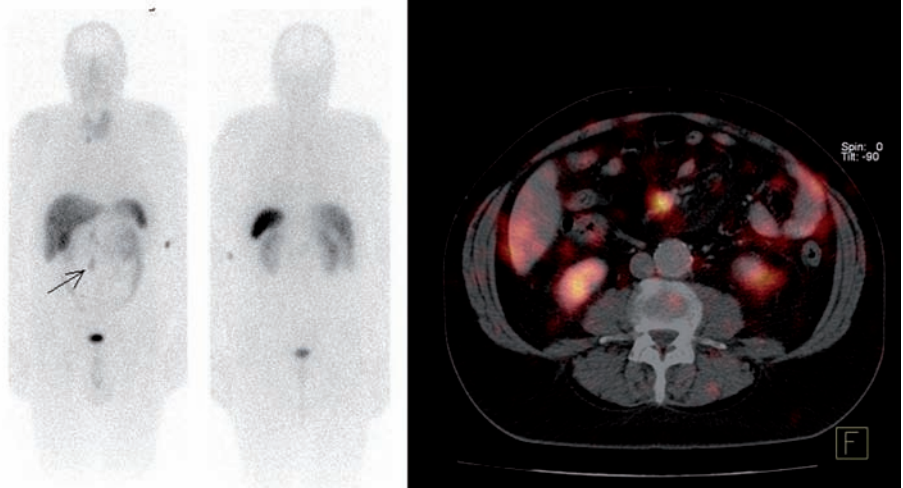
not concentrate $[^{99m}\text{Tc}]$ pertechnetate ('cold nodule').¹⁵ According to some authors, the $[^{99m}\text{Tc}]$ pertechnetate scan finds indication when metastases from an unknown primary are first depicted in the perithyroidal cervical lymph nodes. FNAB of the nodules is required to confirm or rule out the possibility of primary tumor in this gland.¹⁶ It should be stressed that in this area there is no general agreement, since many authors suggest that echography combined with FNAB is sufficient to obtain a correct diagnosis; therefore, the thyroid scan has to be considered redundant.^{17,18} However, scintigraphy can be of help in describing the function of the nodule, and the examination, especially in the presence of multiple nodules, could guide the biopsy that should be performed on non-functioning nodules.¹⁹ In conclusion, thyroid scintigraphy with $[^{99m}\text{Tc}]$ pertechnetate ought to be considered in patients with CUP of suspect thyroid origin, in association with echotomography and FNAB.

$[^{99m}\text{Tc}]$ MDP bone scintigraphy

$[^{99m}\text{Tc}]$ MDP (methylene diphosphonate) whole-body scan is able to examine the entire skeleton, but the published data on its use in detecting CUP are only anecdotal. A bone scan may be useful to detect unknown skeletal metastases. For this reason, bone scintigraphy is in current use for staging patients with prostate cancer, and lung and breast carcinomas, at high risk of distant metastases.^{20–22} Besides this, the bone scan is important in studying primary bone tumors. Nonetheless, the application of the bone scan to depict CUP is very limited. Some bone scan metastatic patterns are associated with a particular cancer type. However, they are not specific for diagnosing the origin of the cancer, and can only give a general orientation. Therefore $[^{99m}\text{Tc}]$ MDP bone scan at present has no role in depicting CUP.

Figure 17.2

$[^{99m}\text{Tc}]$ EDDA/HYNIC-TATE (ethylenediaminediacetic acid/hydrazinonicotinyl-octreotate): secondary hepatic lesions in a patient with unknown primary carcinoid that is demonstrated by $[^{99m}\text{Tc}]$ EDDA/HYNIC-TOC (duodenum). Unknown primary carcinoid of duodenum is indicated by the arrow. (Courtesy of Professor Chiti, Humanitas Institute)



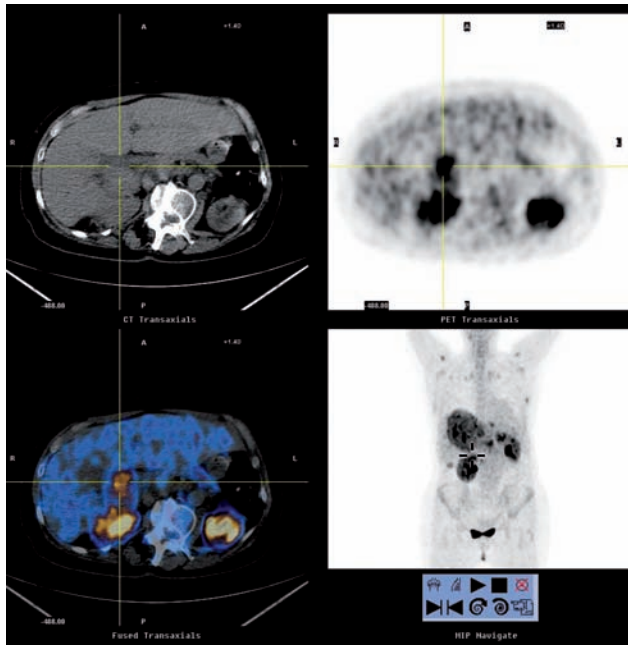


Figure 17.3

[¹⁸F]DOPA-PET/CT (dihydroxyphenylalanine): secondary hepatic and bone lesions in a patient with unknown primary carcinoid that is demonstrated by [¹⁸F]DOPA-PET–CT (head of the pancreas).

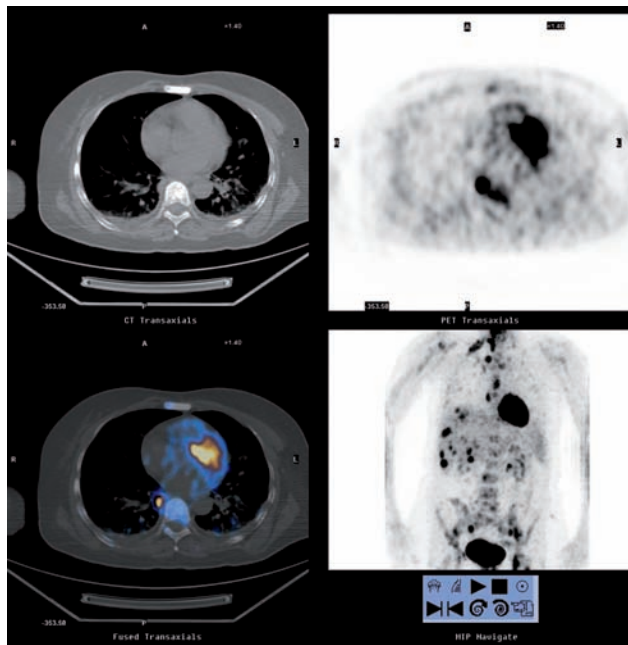


Figure 17.4

[¹⁸F]FDG-PET/CT (fluoro-2-deoxy-D-glucose): secondary hepatic and bone lesions in a patient with unknown primary adenocarcinoma that is demonstrated by [¹⁸F]FDG-PET–CT (hilum of the right lung).

[^{99m}Tc]sestamibi scintigraphy

Apart from cardiologic applications, [^{99m}Tc]sestamibi has demonstrated success in oncology, and in particular for studying breast cancer. It has been registered by the Food and Drug Administration (FDA) as the radiopharmaceutical for scintimammography, and has been indicated as the examination of second choice when other diagnostic imaging modalities are not conclusive.^{23,24} One of the most important limitations of scintimammography is the resolution of detection, which, using the current γ cameras, is around 8 mm. This resolution should be improved by adopting particular collimators (pin-hole) or dedicated detectors.^{25,26} Few studies in the literature describe the use of [^{99m}Tc]sestamibi for depicting occult breast carcinoma. Coover et al. evaluated 37 patients with dense breast tissue and a family/personal history of breast neoplasms but without any evidence of cancer. Scintimammography with a dedicated breast camera was carried out in association with a clinical examination and mammography. The pathologic examination of a biopsy from five patients who showed a focal uptake yielded three carcinomas that were undetectable by clinical breast examination or mammography, even on retrospective review.²⁷ [^{99m}Tc]sestamibi scintigraphy has also been used in different tumor types as a tumor-seeking agent.²⁸ The literature describes only a case report where an occult phosphaturic mesenchymal tumor was discovered by scintigraphy.²⁹ From the theoretic point of view, [^{99m}Tc]sestamibi scintigraphy could be useful for the diagnosis of CUP with suspected breast origin, especially in the case of patients with locoregional or distant metastases, dense breast tissue, and a history of breast cancer. However, the clinical use of [^{99m}Tc]sestamibi scintigraphy in this indication is very limited.

[¹¹¹In]pentetreotide scintigraphy

The use of functional imaging with [¹¹¹In]DTPA-octreotide [¹¹¹In]pentetreotide or OctreoScan® (where DTPA is diethylenetriaminepentaacetic acid) is based on the observation of an enhanced expression of somatostatin receptors in neuroendocrine tumors (NETs), demonstrated in a high percentage of tumors. Somatostatin receptor scintigraphy (SRS) has gained widespread acceptance in the past decade, and SRS is routinely used in NET evaluation (mainly in patients with carcinoids and pancreatic NETs) with a major clinical role. The main localizations of primary gastroenteropancreatic (GEP) tumors are: 35% appendix, 15% ileum, 10% rectum, 10% pancreas, and 7% colon. For the finding of 35% of NETs present with functional syndrome, 38% showed local invasion and 42% were metastatic at staging.³⁰

Due to the good results in identifying NETs, [^{111}In]pentetreotide has been suggested for detecting CUP of neuroendocrine origin. Our group assessed the feasibility of SRS for the detection of the site of unknown primary neuroendocrine neoplasms in patients in whom clinical examination and conventional radiological imaging were not successful. According to this study in 14 patients, it was concluded that SRS was able to modify the management in six patients, who had surgery, i.e. prompted surgical management in 17% of cases.³¹ This paper indicates a good capability of SRS in localizing the site of the primary lesion (14/36 cases = 3%), suggesting a useful role for this approach.

[^{111}In]OctreoScan has also been used to study a group of women presenting with metastatic carcinoma in axillary nodes and suspect occult primary breast cancer. The rationale of this application relies on the frequent expression of somatostatin receptors in breast cancer; this issue, however, has not been extensively studied.³² On the basis of these clinical experiences, [^{111}In]pentetreotide scintigraphy can be useful to detect clinically occult tumors of neuroendocrine origin or other kinds of cancer expressing somatostatin receptors.

[$^{99\text{m}}\text{Tc}$]EDDA/HYNIC-octreotate scintigraphy

Recent papers suggested the use of a new tracer, [$^{99\text{m}}\text{Tc}$]EDDA/HYNIC-octreotate (ethylenediaminediacetic acid/hydrazinonicotinyl), for SRS.³³ In comparison with [^{111}In]pentetreotide, [$^{99\text{m}}\text{Tc}$]EDDA/HYNIC-octreotate should improve the diagnosis of carcinoids owing to the better affinity for somatostatin receptor type SST2, the higher count rate due to [$^{99\text{m}}\text{Tc}$]emission, the short time to obtain imaging, and the lower irradiation of patients.³⁴ On the basis of clinical experience it seems that [$^{99\text{m}}\text{Tc}$]EDDA/HYNIC-octreotate may be usefully applied for detection of the primary focus in patients with metastases from an unknown primary tumor of neuroendocrine origin.

[$^{99\text{m}}\text{Tc}$]EDDA/HYNIC-octreotate may have the same indications as [^{111}In]pentetreotide, but further studies in this area are compulsory.

Positron emission tomography

[^{18}F]FDG-PET

[^{18}F]fluoro-2-deoxy-D-glucose-positron emission tomography (FDG-PET) has become one of the most reliable

examinations when the majority of diagnostic tests have failed to identify the primary site. A complete evaluation of the diagnostic value of FDG-PET is not easy, since the patient population described in the literature is still too small, and very heterogeneous (patients with cervical and extracervical lymph node metastases are often mixed, and also the paraneoplastic syndromes are included). Besides this, the diagnostic work-up before PET is variable, and therefore several conflicting or non-conclusive results have been described. However, it must be pointed out that in this setting FDG-PET can reach a very high added value, since it is a single-step whole-body study able to identify the primary site and at the same time stage the disease.

As far as primary tumor detection is concerned, several studies have demonstrated that PET with [^{18}F]FDG can be useful for localizing primaries both in patients with tumor metastases within the head and neck region,³⁵⁻³⁷ and in patients with extracervical metastases,³⁸⁻⁴¹ with a detection rate ranging between 24 and 53%.^{42,43} In the year 2000, these findings led to a German Consensus Conference to recognize the whole-body FDG-PET study as a class I-a diagnostic technique (with scientifically proven benefit and established clinical use) in patients with CUP syndrome, irrespective of the site of metastatic disease. However, it is important to stress that the diagnostic work-up is not the same when a patient presents with cervical lymph node or with extracervical metastases, since the involvement of upper and middle cervical lymph nodes is usually related to cancers of the head and neck region, while, on the other hand, the involvement of lower laterocervical, supraclavicular, and other visceral stations can be the expression of neoplasms from any region.

In 2004, Rusthoven et al. carried out a meta-analysis in patients presenting with CUP with cervical lymph node metastases, pooling data from 16 studies, giving a total of 302 patients. The identification rate for the primary site was 24.5%. Furthermore, they considered the false-positive and -negative rates in this setting: tonsil and base of the tongue were the more critical regions due to the possible physiologic or parapsiologic uptake of FDG, while the regions with higher accuracy were the larynx and the hypopharynx.⁴⁴ Considering patients who presented with extracervical metastases, in a study by Joshi et al. in 62 patients, the identification rate was exactly the same as for the laterocervical region, i.e. 25%.⁴⁵

Finally, in a comprehensive meta-analysis by Delgado-Bolton et al. who examined 15 studies and 298 patients, the identification rate of the primary was determined to be 43% (54 lung cancer, 37 oropharynx, nine nasopharynx, six breast, four colorectal, two esophagus, 17 other).⁴³ With the clinical introduction of combined PET/CT instrumentation, which allows the simultaneous acquisition of accurately aligned whole-body anatomical and functional images, the study is more accurate than PET alone in assessing the presence and location of tumor foci and

therefore in tumor staging. Similar benefits can be expected in metastatic cancer of unknown primary origin. Recently, three different papers^{46–48} studying heterogeneous populations with CUP syndrome, including patients with cervical lymph node metastases and extracervical metastases, agreed on the concept that dual-modality PET/CT is ‘a promising alternative to separate acquisition of morphologic and functional data when assessing patients with cancer of an unknown primary tumor’, showing that the whole-body FDG-PET/CT technique has an interesting sensitivity associated with a high positive predictive value. Gutzeit et al. with fused PET/CT images depicted primary tumor in 15 of 45 patients (33% sensitivity), versus 67% (8/12) for CT and 28% (11/39) for PET alone. PET and CT side by side evaluation depicted 13 of 45 tumors (29%). PET alone revealed the primary in 11 (24%) while CT alone helped in correct diagnosis in 8 of 45 patients (18%).¹⁶ In a study carried out by the nuclear medicine division of the University of Bologna, an identification rate for the primary tumor of 57% is described.⁴⁷

Clinical trials of CUP depiction have given another important result. PET provides the opportunity to obtain a complete evaluation of disease extent. In a meta-analysis of a subgroup with cervical lymph node metastases, Rusthoven et al. focused attention on the detection of eventual, not previously known, additional metastases, and reported an identification rate of 27.1% for additional sites of disease, both regional and distant metastases.⁴⁴ Considering the subgroup of patients with extracervical lymph node involvement, Joshi et al. reported an identification rate for additional secondary sites of 40%.⁴⁵ Even though we are discussing small numbers, this difference is not a surprise, since extracervical metastases are expected to be often associated with other involved sites.

It goes without saying that any detection of a known site of the primary can lead to a change in the management of patients. The meta-analysis of Rusthoven et al. demonstrated a change in management, related to the PET study, in about 25% of patients. In fact, in the presence of cervical lymph node metastases, when the primary origin is not known, the current treatment consists of comprehensive mucosal irradiation (which can lead to heavy post-actinic side-effects). In contrast, identification of the lesion can allow more specific and even curative therapy, sparing peritumoral organs. On the other hand, the eventual discovery of unexpected metastases obviously shifts the therapeutic approach from curative to palliative.

In the experience of the nuclear medicine department of the University of Turin, 72 patients^{48,49} were studied with FDG-PET and divided into two groups: those with cervical metastases ($n = 18$) and those with extracervical metastases ($n = 54$). All of them had a negative diagnostic work-up which included detailed history, physical examination, laboratory tests, chest radiography, ce-CT of the abdomen/pelvis, and mammography, followed by

whole-body FDG-PET/CT scan. Patients with positive PET/CT scans were further evaluated with biopsy, or alternatively with further diagnostic imaging modalities during an adequate follow-up. Patients with negative PET/CT scans were followed for a minimum period of 3 months. In the group of 18 patients with biopsy-proven laterocervical metastases, the identification rate for the primary site was 44% and that for additional secondary sites was 16.6%. This result allowed rational clinical management in 61.1% of cases (data not published). It must be pointed out that in two cases with involvement of the lower laterocervical nodes, the primary site was found in the lung and the pancreas. In the group of 54 patients with biopsy-proven extracervical metastases the identification rate for the primary site was 35.2%, with a positive predictive value of 90% (most frequent primaries were in the lung and pancreas).

Regarding possible changes in patient management due to the use of FDG-PET, in this second group we adopted three different strategies: (1) the identification of some additional metastatic sites, independent of the diagnosis of the presence of the primary tumor, leads us to consider the disease as being at an extended stage, and all locoregional therapeutic approaches are prevented; (2) identification of the primary site without any distant localizations shifts the strategy from systemic treatment to locoregional and potentially curative therapy; and (3) when, after PET/CT, the biopsy does not confirm the presence of cancer in the positive-imaged primary site, the patient should be considered free of disease, but in this case it is mandatory to monitor the patient with prolonged and strict follow-up. Our results suggest the concept that, in CUP syndrome, the FDG-PET/CT scan has a high clinical impact and should be performed early in the work-up of the patient.

^[18F]DOPA-PET

Neuroendocrine tumors have shown an increased uptake and metabolism of [^{18F}]DOPA (dihydroxyphenylalanine). [^{18F}]DOPA-PET has demonstrated better sensitivity compared to that of [^{131I}]MIBG (metaiodobenzylguanidine) and [^{111In}]pentetreotide scintigraphy in the diagnosis of several neuroendocrine malignancies.^{50,51} We recently reported our experience of the use of [^{18F}]DOPA for studying the unknown primary of demonstrated tumors of neuroendocrine origin: our population consisted of five patients with at least one biopsied secondary lesion, and all examinations and imaging procedures were negative for the detection of CUP.⁵² In two out of five cases, [^{18F}]DOPA-PET/CT detected the primary occult lesion. In a patient with diffuse abdominal secondary lesions the primary cancer was correctly identified at pancreatic level; in a patient with doubtful findings at CT and SRS the primary

cancer was confirmed to be located in the ileum, and unsuspected bone lesions were documented. In the remaining three cases, [¹⁸F]DOPA-PET/CT did not identify the CUP; in one case, however, unknown bone and lymph node lesions were demonstrated. Although very preliminary, these data indicate the feasibility of detecting occult primary tumors of neuroendocrine origin by using [¹⁸F]DOPA-PET/CT. Therefore, in our opinion, [¹⁸F]DOPA-PET may have a role in detecting clinically occult gastroenteropancreatic tumors of neuroendocrine origin.

[⁶⁸Ga]DOTA-NOC and [⁶⁸Ga]DOTA-TOC

In recent years, [⁶⁸Ga]DOTA-NOC and [⁶⁸Ga]DOTA-TOC (tetraazacyclododecanetetraacetic acid-1-NaI³-octreotide and -Tyr³-octreotide) was introduced as an effective tracer for NETs, due to the high affinity for SST2, SST3, and SST5 receptors.⁵³ The uptake is based on a receptorial mechanism, and, although not yet demonstrated by a large series of cases, it seems to have higher sensitivity for this kind of neoplastic disease.⁵⁴ The clinical evidence demonstrates that ⁶⁸Ga-labeled somatostatin analogs are increasingly being used in specialized centers in Europe for PET and PET/CT imaging and show very promising results, with high diagnostic accuracy. New somatostatin analogs with different receptor affinities as well as other peptides are currently under investigation, and will further improve our diagnostic and therapeutic capabilities in the future, in our opinion, due to the high diagnostic sensitivity of PET and PET/CT, the very high quality of imaging, and the high specificity of the mechanism of uptake of the radiopharmaceutical. The use of ⁶⁸Ga-labeled somatostatin analogs may be a valuable tool for revealing unknown primaries of neuroendocrine nature. There is a need for clinical validation by means of large prospective studies.

Conclusions

Cancer of unknown origin has recently been reconsidered, and has been classified according to particular clinicopathological entities, taking into consideration the organ involved by secondaries and the histology.⁵⁵ The treatment strategies of CUP are different because oncologists consider two different groups of diseases: (1) favorable subsets: poorly differentiated carcinoma with mid-line distribution; women with papillary adenocarcinoma of the peritoneal cavity; women with adenocarcinoma involving only axillary lymph nodes; squamous cell carcinoma involving cervical lymph nodes; isolated inguinal adenopathy; poorly

differentiated neuroendocrine carcinomas; men with blastic bone metastases and elevated prostate specific antigen (PSA); patients with a single, small, potentially resectable tumor; (2) unfavorable subsets: adenocarcinoma metastatic to the liver and other organs; non-papillary malignant ascites; multiple cerebral metastases; multiple lung/pleural metastases; multiple metastatic bone disease. This classification is carried out according to some prognostic parameters. The overall results of treatment at present are not satisfactory. Treatment of favorable subsets is well identified, and sometimes it is possible to obtain complete response. In fact, complete responses are reported and a satisfactory rate of long-term disease-free survival can be described. In contrast, the treatment of the unfavorable group, presenting with disseminated bone, liver, or multi-organ metastases, is not effective at all. Median survival is still in the range of 8–9 months.

Therefore, there is a need to implement the diagnostic potential of CUP, and PET technology seems at present to be the nuclear medicine tool more adequate to improve the detectability of CUP. Until now, FDG-PET/CT has often been considered only at the end of an unsuccessful conventional diagnostic approach, and not in the early phases of diagnostic work-up, with a considerable waste of time and money. In spite of the limitations of the available clinical trials, the low number of patients included in each individual study, and the extremely heterogeneous cohort of patients presenting with CUP, FDG-PET/CT scan has been revealed to be a very important tool for studying CUP syndrome, allowing the identification of primary tumors in one out of three cases and modifying the stage of the disease and oncological treatment in about 50% of cases. These results suggest the use of PET/CT with FDG in an early phase of the diagnostic work-up in order to optimize the management of these patients.

References

1. Pavlidis N, Briasoulis E, Hainsworth J, Greco FA. Diagnostic and therapeutic management of cancer of unknown primary. *Eur J Cancer* 2003; 39: 1990–2005.
2. van de Wouw AJ, Janssen-Heijnen ML, Coebergh JW, Hillen HF. Epidemiology of unknown primary tumors; incidence and population-based survival of 1285 patients in Southeast Netherlands, 1984–1992. *Eur J Cancer* 2002; 38: 409–13.
3. Levi F, Te VC, Erler G, Randimbison L, La Vecchia C. Epidemiology of unknown primary tumors. *Eur J Cancer* 2002; 38: 1810–12.
4. Fritz A, Percy C, Jack A et al., eds. *International Classification of Diseases for Oncology (ICD-O)*, 3rd edn. Geneva: World Health Organization, 2000.
5. Abbruzzese JL, Abbruzzese MC, Lenzi R, Hess KR, Raber MN. Analysis of a diagnostic strategy for patients with

- suspected tumors of unknown origin. *J Clin Oncol* 1995; 13: 2094–103.
6. Chorost MI, Lee MC, Yeoh CB, Molina M, Ghosh BC. Unknown primary. *J Surg Oncol* 2004; 87: 191–203.
 7. Seregini E, Bombardieri E. Tumor markers in oncology. In: Aktolun C, Tauxe WN, eds. *Nuclear Oncology*. New York: Springer, 1999: 415–32.
 8. Tot T. Cytokeratins 20 and 7 as biomarkers: usefulness in discriminating primary from metastatic adenocarcinomas. *Eur J Cancer* 2002; 38: 758–63.
 9. Talantov D, Baden J, Jatkoa T et al. A quantitative reverse transcriptase-polymerase chain reaction assay to identify metastatic carcinoma tissue of origin. *J Mol Diag* 2006; 8: 320–9.
 10. Sève P, Billotey C, Broussolle C, Dumointet C, Mackey JR. The role of FDG-PET in disseminated carcinoma of unknown primary site. *Cancer* 2007; 109: 292–99.
 11. Demir H, Berk F, Raderer M et al. The role of nuclear medicine in the diagnosis of cancer of unknown origin. *Q J Nucl Med Mol Imaging* 2004; 48: 164–73.
 12. Bombardieri E, Aktolun C, Baum RP et al. ⁶⁷Ga scintigraphy: procedure guidelines for tumor imaging. *Eur J Nucl Med Mol Imaging* 2003; 30: BP125–31.
 13. Even-Sapir E, Israel O. Gallium-67 scintigraphy: a cornerstone in functional imaging of lymphoma. *Eur J Nucl Med Mol Imaging* 2003; 30 (Suppl 1): S65–81.
 14. Gaber AO, Rice P, Eaton C et al. Metastatic malignant disease of unknown origin. *Am J Surg* 1983; 145: 493–7.
 15. Didolker MS, Fanous N, Elias EG, Moore RH. Metastatic carcinomas from occult primary tumors. A study of 254 patients. *Ann Surg* 1997; 186: 625–30.
 16. Chorost MI, McKinley B, Tschoi M, Glosch BC. The management of the unknown primary. *J Am Coll Surg* 2001; 193: 666–77.
 17. Singer PA, Cooper DS, Daniels GH et al. Treatment guidelines for patients with thyroid nodules and well-differentiated thyroid cancer. *Arch Intern Med* 1996; 156: 2165–72.
 18. Castro MR, Gharib H. Continuing controversies in the management of thyroid nodules. *Ann Intern Med* 2005; 142: 926–31.
 19. Mansi L, Moncayo R, Cucurullo V et al. Nuclear medicine in diagnosis, staging and follow-up of thyroid cancer. *Q J Nucl Med Mol Imaging* 2004; 48: 82–95.
 20. Bombardieri E, Aktolun C, Baum RP et al. Bone scintigraphy: procedure guidelines for tumor imaging. *Eur J Nucl Med Mol Imaging* 2003; 30: BP99–106.
 21. O'Sullivan JM, Cook GJ. A review of the efficacy of bone scanning in prostate and breast cancer. *Q J Nucl Med* 2002; 46: 152–9.
 22. Cook GJ, Fogelman I. The role of nuclear medicine in monitoring treatment in skeletal malignancy. *Semin Nucl Med* 2001; 31: 206–11.
 23. Bombardieri E, Aktolun C, Baum RP et al. Breast scintigraphy: procedure guidelines for tumor imaging. *Eur J Nucl Med Mol Imaging* 2003; 30: BP107–14.
 24. Horne T, Pappo I, Cohen-Pour M et al. ⁹⁹Tc(m)-tetrofosmin scintimammography for detecting breast cancer: a comparative study with ⁹⁹Tc(m)-MIBI. *Nucl Med Commun* 2001; 22: 807–11.
 25. Madeddu G, Spanu A. Use of tomographic nuclear medicine procedures, PECT and pinhole SPECT, with cationic lipophilic radiotracers for the evaluation of axillary lymph node status in breast cancer patients. *Eur J Nucl Med Mol Imaging* 2004; 31 (Suppl 1): S23–34.
 26. Spanu A, Dettori G, Nuvoli S et al. ⁹⁹mTc-tetrofosmin SPET in the detection of both primary breast cancer and axillary lymph node metastasis. *Eur J Nucl Med* 2001; 28: 1781–94.
 27. Coover LR, Caravaglia G, Kuhn P. Scintimammography with dedicated breast camera detects and localizes occult carcinoma. *J Nucl Med* 2004; 45: 553–8.
 28. Schillaci O, Spanu A, Madeddu G. [^{99m}Tc]sestamibi and [^{99m}Tc]tetrofosmin in oncology: SPET and fusion imaging in lung cancer, malignant lymphomas and brain tumors. *Q J Nucl Med Mol Imaging* 2005; 49: 133–44.
 29. Siegel HJ, Rock MG. Occult phosphaturic mesenchymal tumor detected by Tc-^{99m} sestamibi scan. *Clin Nucl Med* 2002; 27: 608–9.
 30. Bombardieri E, Aktolun C, Baum RP et al. ¹¹¹In-pentetreotide scintigraphy: procedure guidelines for tumor imaging. *Eur J Nucl Med Mol Imaging* 2003; 30: BP140–7.
 31. Savelli G, Lucignani G, Seregini E et al. Feasibility of somatostatin receptor scintigraphy in the detection of occult primary gastro-entero-pancreatic (GEP) neuroendocrine tumors. *Nucl Med Commun* 2004; 25: 445–9.
 32. Lenzi R, Kim EE, Raber MN, Abbruzzese JL. Detection of primary breast cancer presenting as metastatic carcinoma of unknown primary origin by ¹¹¹In-pentetreotide scan. *Ann Oncol* 1998; 9: 213–16.
 33. Decristoforo C, Mather SJ, Cholewinski W et al. ^{99m}Tc-EDDA/HYNIC-TOC: a new ^{99m}Tc-labelled radiopharmaceutical for imaging somatostatin receptor-positive tumors; first clinical results and intra-patient comparison with ¹¹¹In-labelled octreotide derivatives. *Eur J Nucl Med* 2000; 27: 1318–25.
 34. Hubalewska-Dydejczyk A, Fross-Baron K, Mikolajczak R, et al. ^{99m}Tc-EDDA/HYNIC-octreotate scintigraphy, an efficient method for the detection and staging of carcinoid tumors: results of 3 years' experience. *Eur J Nucl Med Mol Imaging* 2006; 33: 1123–33.
 35. Braams JW, Pruim J, Kole AC et al. Detection of unknown primary head and neck tumors by positron emission tomography. *Int J Oral Maxillofac Surg* 1997; 26: 112–15.
 36. Assar OS, Fischbein NJ, Caputo GR et al. Metastatic head and neck cancer: role and usefulness of FDG PET in locating occult primary tumors. *Radiology* 1999; 210: 177–81.
 37. Hanasono MM, Kunda LD, Segall GM et al. Uses and limitations of FDG positron emission tomography in patients with head and neck cancer. *Laryngoscope* 1999; 109: 880–5.
 38. Kole AC, Nieweg OE, Pruim J et al. Detection of unknown occult primary tumors using positron emission tomography. *Cancer* 1998; 82: 1160–6.
 39. Lassen U, Daugaard G, Eigtved A et al. ¹⁸F-FDG whole body positron emission tomography (PET) in patients with unknown primary tumors (UPT). *Eur J Cancer* 1999; 35: 1076–82.
 40. Bohuslavizki KH, Klutmann S, Kroger S et al. FDG PET detection of unknown primary tumors. *J Nucl Med* 2000; 41: 816–22.

41. Lonneux M, Reffad AM. Metastases from unknown primary tumor: PET-FDG as initial diagnostic procedure? *Clin Positron Imaging* 2000; 3: 137–41.
42. Reske SN, Kotzerke J. FDG PET for clinical use: results of the 3th German Interdisciplinary Consensus Conference, 'Onko PET III'. *Eur J Nucl Med* 2001; 28: 1707–23.
43. Delgado-Bolton RC, Fernandez-Perez C, Gonzalez-Mate A, Carreras JL. Meta-analysis of the performance of 18F-FDG PET in primary tumor detection in unknown primary tumors. *J Nucl Med* 2003; 44: 1301–14.
44. Rusthoven KE, Koshy M, Paulino AC. The role of fluorodeoxyglucose positron emission tomography in cervical lymph node metastases from an unknown primary tumor. *Cancer* 2004; 101: 2641–9.
45. Joshi U, Van Der Hoeven JJ, Comans EF et al. In search of an unknown primary tumor presenting with extracervical metastases: the diagnostic performance of FDG-PET. *Br J Radiol* 2004; 77: 1000–6.
46. Gutzeit A, Antoch G, Kuhl H et al. Unknown primary tumors: detection with dual-modality PET/CT—initial experience. *Radiology* 2005; 234: 227–34.
47. Nanni C, Rubello D, Castellucci P et al. Role of 18F-FDG PET-CT imaging for the detection of an unknown primary tumor: preliminary results in 21 patients. *Eur J Nucl Med Mol Imaging* 2005; 32: 589–92.
48. Pelosi E, Pennone M, Deandreis D et al. Role of whole body positron emission tomography/computed tomography scan with ¹⁸F-fluorodeoxyglucose in patients with biopsy proven tumor metastases from unknown primary site. *Q J Nucl Med Mol Imaging* 2006; 50: 15–22.
49. Deandreis D, Pelosi E, Douroukas A et al. Role of FDG-PET/CT in the management of patients with CUP syndrome (cancer of unknown primary site) and extra cervical biopsy proven metastases. *J Nucl Med* 2006; 47 (Suppl1): 223P.
50. Hoegerle S, Nitzsche E, Althoefer C et al. Pheochromocytomas: detection with 18-F DOPA whole body PET – initial results. *Radiology* 2002; 222: 507–12.
51. Koopmans KP, de Vries EG, Kema IP et al. Staging of carcinoid tumors with 18F-DOPA PET: a prospective, diagnostic accuracy study. *Lancet Oncol* 2006; 7: 728–34.
52. Fanti S, Tomassetti P, Campana D et al. Whole-body ¹⁸F-DOPA PET-CT for the detection of unknown primary cancer of neuroendocrine nature. Abstract presented at EANM 2006, Athens.
53. Wild D, Schmitt JS, Ginj M et al. DOTA-NOC, a high-affinity ligand of somatostatin receptor subtypes 2, 3 and 5 for labelling with various radiometals. *Eur J Nucl Med Mol Imaging* 2003; 30: 1338–47.
54. Rufini V, Calcagni ML, Baum RP. Imaging of neuroendocrine tumors. *Semin Nucl Med* 2006; 36: 228–47.
55. Pavlidis N, Fizaki K. Cancer of unknown primary (CUP). *Crit Rev Oncol Haematol* 2005; 54: 243–50.

Therapy of differentiated thyroid cancer

Martin Biermann and Otmar Schober

Background

Thyroid cancer (TC) is a generic term for cancer arising in the thyroid gland.

More than 90% of TC originates from the follicular cells, whose task it is to produce thyroid hormone. Follicular-cell-derived tumors are: (1) differentiated thyroid carcinoma (DTC; ~90%), which includes the papillary (PTC; ~80%) and the follicular (FTC; ~10%) subtypes, and (2) dedifferentiated, so-called anaplastic thyroid carcinoma (ATC; ~5%). C-cell carcinoma or medullary thyroid carcinoma (MTC) is derived from the calcitonin-producing C-cells and constitutes 5% of all cases of TC. MTC is distinguished from DTC by the absence of iodide uptake, the production of calcitonin as a tumor marker, and its frequent association with multiple endocrine neoplasia type II. Because of many special aspects in the management of MTC, including genetic testing, it will not be discussed in the present chapter.

DTC has unique properties. Cancer cells resemble the normal follicular cells in their ability to actively accumulate iodine, an advanced cell function needed for thyroid hormone production. This unique property, normally found only in the healthy thyroid gland, can be used diagnostically and therapeutically, as will be discussed in the present chapter. Advances in the treatment of DTC include: (1) improved methods for pre-surgical diagnosis of TC, most importantly, ultrasound-guided fine-needle aspiration cytology (FNAC), (2) systematic compartment-oriented microdissection of the cervical viscera, (3) improved follow-up methods, including [¹³¹I]SPECT-CT (single photon emission computed tomography-computed tomography), [¹⁸F]FDG-PET-CT (fluro-2-deoxy-D-glucose-positron emission tomography-computed tomography), high-resolution ultrasound, and highly sensitive assays for the tumor marker human thyroglobulin (hTg), and (4) the strive towards evidence-based interdisciplinary guidelines^{1,2} for the therapy and follow-up of TC.

Therapeutic approaches

The therapy of DTC includes the following modalities: surgery, radioiodine therapy (RIT), thyroid stimulating hormone (TSH)-suppressive thyroid hormone therapy,³ and – in selected advanced cases – external beam radiotherapy⁴ (Figure 18.1). The tumor is generally very slow-growing. This has two consequences: (1) the prognosis is excellent,^{5,6} with further improvements in the last decade (Figure 18.2),^{7,8} and (2) recurrences are possible, long after initial diagnosis and therapy.⁹ Long-term follow-up is therefore mandatory. Because of the rarity of the disease, follow-up should be restricted to specialized centers.¹⁰

There are many guidelines on thyroid cancer.¹ In the following discussion we will focus on the newly published guidelines of the European Thyroid Association (ETA),¹¹ the current interdisciplinary German guidelines of the German Cancer Society (DKG),³ which form the basis for our own therapeutic practice at Münster University,⁸ and the current North American guidelines from the National Comprehensive Cancer Network (NCCN).¹²

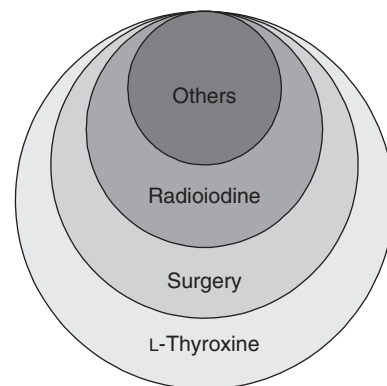
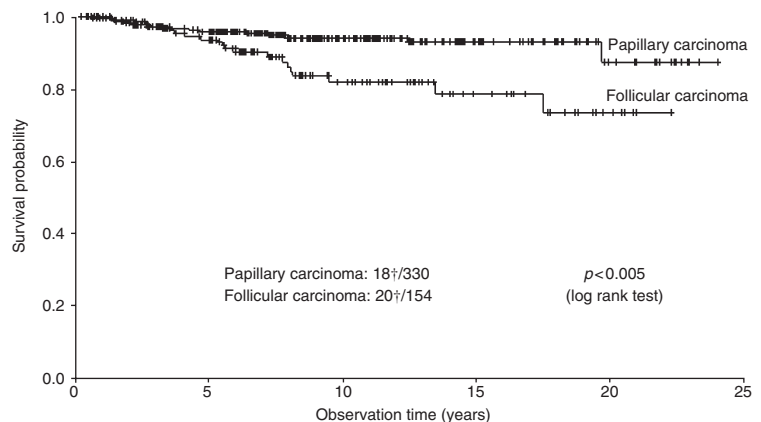


Figure 18.1

Multimodal therapy of differentiated thyroid carcinoma.

Figure 18.2

Prognosis of differentiated thyroid carcinoma. The 10-year cancer-specific survival for papillary and follicular cancer was 97% and 89% for low-risk patients and 85 and 75% for high-risk patients (local invasion or distant metastases).⁷



Surgery

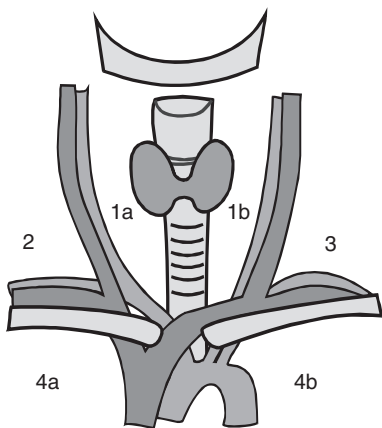
The object of surgery is to remove the primary tumor as well as regional metastases (Figure 16.3), and to prepare ablative radioiodine therapy.

Guideline recommendations

The guidelines of the European Thyroid Association explicitly recommend thyroid cancer surgery only in specialized centers. Preoperative staging must include ultrasound of the cervical lymph node chains, and FNAC^{14–16} of any solitary thyroid nodule ≥ 1 cm that is not proven to be hyperfunctioning, and of suspicious cervical lymph nodes.¹¹ If FNAC gives rise to the suspicion of PTC, total

(or near-total) thyroidectomy is recommended, as the false-positive rate of FNAC suspicious for PTC is only about 2%. If FNAC shows a follicular neoplasm,¹⁷ hyperfunctioning nodules are to be excluded by means of thyroid scintigraphy. A near-total thyroidectomy is recommended if there is clinical suspicion of malignancy or if the patient wants to avoid a two-stage operation.¹¹ The only situation in which thyroid cancer does not require a (near) total thyroidectomy is solitary well-differentiated TC less than 1 cm without evidence for nodal or distant metastases (N0M0) and no history of previous radiation exposure.¹¹ The German DKG guidelines developed together with the German Society of Surgery likewise recommend (near) total thyroidectomy in all tumors over 1 cm with multifocality or lymph node metastases. Total thyroidectomy is recommended in FTC regardless of size. In addition to total thyroidectomy, the German guidelines advocate routine systematic lymph node dissection in the central compartment (Figure 18.3) of the neck between the jugulum and hyoid bone and medial to the large vessels.³

The North American NCCN base their treatment algorithm primarily on the results of a preoperative FNAC.¹² In suspected PTC, they recommend total thyroidectomy in any patient who is younger than 15 or older than 45 years, or with a tumor that is bilateral, larger than 4 cm, or locally invasive (pT3a/b), or has cervical lymph node (N1) or distant metastases (M1), or has had previous radiation therapy or a positive family history of papillary or follicular thyroid cancer.¹² In cases that do not meet any of the above-named conditions, a choice is given between lobectomy with isthmusectomy or a total thyroidectomy. If histology then shows an aggressive variant of TC, macroscopic multifocal disease, positive margins (R1/2), or cervical lymph node metastases, total (completion) thyroidectomy is recommended. In FTC, total thyroidectomy is recommended if the tumor is widely invasive or has metastasized (N1 or M1), or if this is preferred by the patient; otherwise a lobectomy with isthmusectomy is

**Figure 18.3**

Thyroid cancer surgery. The central compartment 1a + b reaches from the brachiocephalic vein to the hyoid bone between the trachea and the carotid sheath. The vascular sheath is part of the lateral compartments 2 and 3.¹³

considered adequate. For Hürthle cell (oxyphilic) carcinoma total thyroidectomy is recommended in all cases.¹² In patients with a follicular neoplasm on FNAC¹⁷ and a low TSH, thyroid scintigraphy is recommended. If the suspect nodule is hot, radioiodine is the preferred mode of therapy because the risk of malignancy is minimal.^{12,18}

The guidelines of the DKG and German Society of Surgery have recommended routine systematic dissection of the central cervical compartment (perithyroidal, pretracheal, and prelaryngeal) since 1996,^{3,19} and similarly the guidelines of the Austrian Society of Surgery.²⁰ The British Thyroid Association recommends routine dissection of lymph nodes in the vicinity of the recurrent laryngeal nerve in patients with PTC.²¹ The current guidelines of the American Association of Endocrine Surgeons²² and the British Association of Endocrine Surgeons²³ recommend removal of all enlarged lymph nodes (so-called berry-picking) but no prophylactic dissection, and the NCCN guidelines recommend regional lymph node dissection only for Hürthle-cell carcinoma.¹² The ETA guidelines consider prophylactic 'en bloc' central node dissection in the absence of pre- or intraoperative evidence for nodal disease to be 'controversial'.¹¹ There is consensus between all the major guidelines that lateral lymph node dissection for DTC is only indicated when there is clear evidence for metastatic involvement.

Commentary

The rationale of thyroid surgery – lobectomy and lymph node dissection – is to remove all locoregional tumor manifestations. The rationale underlying *total* thyroidectomy is (1) to prevent recurrences in the contralateral lobe or remaining thyroid gland and (2) to prepare ablative radioiodine therapy. The potential benefits of the more radical surgery have to be balanced against the risks. Unfortunately, there are no randomized prospective trials on the benefits of thyroid ablation,²⁴ and experiences with other randomized trials on DTC such as our own Multicenter Study Differentiated Thyroid Carcinoma (MSDS) trial²⁵ teach us not to expect any such trials in the foreseeable future.

All current guidelines attempt to draw a line between low-risk cases that are adequately treated with a less than total thyroidectomy – lobectomy or subtotal resection – and cases with higher risk, which warrant more radical surgery. In this they have to take into account the biological heterogeneity of DTC and integrate evidence from a large number of retrospective series from different institutions with a plethora of different treatment protocols.

PTC

PTC is multifocal in approximately 20% of cases if the thyroid is examined routinely²⁶ and up to 80% if with very

great care.²⁷ The majority of multifocal cancer lesions in PTC arise from different somatic mutations.²⁸ Seemingly normal follicular cells may therefore have the potential for malignant transformation, which may explain the sometimes very late tumor recurrences.²⁹ This argues for total thyroidectomy in PTC. Indeed, this is the line taken by most guidelines.

The controversy lies in which criteria distinguish low-risk patients from patients who require radical thyroidectomy. At one end of the disease spectrum, papillary microcarcinomas – PTC \leq 10 mm, as defined by the World Health Organization (WHO)³⁰ – are very frequent. This has been documented in autopsy series, with a prevalence up to 30%,³¹ as well as epidemiologically.³² The risk for extrathyroid growth and lymph node metastases then rises continuously with the diameter of the primary tumor.³³ This extends to clinical events. In a retrospective cohort of 403 patients from the University of Vienna with pT1/pT2 DTC and up to 10 years of follow-up, all of the 163 patients with PTC \leq 10 mm survived but 3/80 with PTC between 11 and 20 mm and 4/76 with PTC between 21 and 40 mm died of thyroid cancer.³⁴ All patients in this series received total thyroidectomy and central lymphadenectomy as the preferred mode of therapy, except patients with unifocal PTC \leq 10 mm N0. In the light of this and other recent series,³⁵ ETA and the German interdisciplinary guidelines continue to recommend that PTC over 1 cm should be treated with total thyroidectomy and subsequent ablative radioiodine therapy, and the decision of the International Union against Cancer (UICC) to raise the threshold between pT1 and pT2 tumors from 1 to 2 cm without new published evidence supporting this change has been widely criticized.^{36,37}

In a number of circumstances, PTC smaller than 1 cm can also carry a significant risk for subsequent complications. These include the presence of lymph node metastases,³⁸ multifocality,³⁸ a positive family history,³⁹ or previous external beam radiotherapy in the head or neck.⁴⁰ In these circumstances total thyroidectomy is also recommended by most authorities,^{29,41} if not in all the guidelines themselves.

FTC

Follicular cancers are a biologically heterogeneous group that are relatively more frequent in iodine-depleted regions of the world.^{36,42,43} Minimally invasive FTC is an encapsulated tumor that is very rarely multifocal (2.3% in one recent study)⁴⁴ and rarely associated with lymph node metastases.⁴⁴ The problem lies in the potential for distant hematogenous metastases, predominantly bone and lung. Some authorities²⁹ and a number of guidelines^{12,45} advocate total thyroidectomy only in tumors larger than 4 cm. Considering that this cancer is rare in countries with good iodine supplementation, and very few series have

distinguished between minimally invasive and widely invasive FTC, we doubt that there are adequate data to quantify the risk reliably. In a series from Hong Kong with 52 patients with minimally invasive FTC, the 10-year cancer-specific survival was 97.6% and freedom from distant metastases 90.6%, with local control in 100%. The association between tumor diameter and prognosis did *not* reach statistical significance.⁴⁶ In the abovementioned series from the University of Vienna, cancer mortality was 1/7 for FTC \leq 10 mm, 2/25 for FTC between 11 and 20 mm, and 3/37 for FTC between 21 and 40 mm (effect of tumor size not significant).³⁴ Petrich et al. reported on patients who presented with primary distant metastases at the University of Hannover.⁴⁷ Of 102 patients with FTC, 40% had locally invasive disease, which implies the diagnosis of widely invasive FTC. Some 20% had tumors larger than 4 cm (pT3), 33% tumors between 1 and 4 cm (pT2), and 5% FTC smaller than 1 cm.⁴⁸ Lin et al. reported 70 patients with FTC and pulmonary metastases, out of the institution's cohort of 2003 TC patients, who had 5-year survival of 69%; 28/70 cases had a history of prior thyroid surgery.⁴⁹ Also in our experience, prior thyroid surgery is not uncommon in patients presenting with newly diagnosed metastases of TC, often with histological diagnosis of a 'follicular adenoma'. Treatment for bone metastases is rarely curative unless instituted very early.⁵⁰ Only total thyroidectomy with subsequent ablative RIT allows a timely diagnosis and treatment of distant metastases. We therefore conclude that subtotal resection without RIT is not adequate treatment for minimally invasive FTC, and agree with the ETA recommendation to perform total thyroidectomy for all minimally invasive FTC larger than 1 cm.

Widely invasive FTC is essentially an aggressive tumor entity with the tendency for local invasion and regional lymph node metastases. In one series the relative risk of recurrence was 2.2 if the FTC was not encapsulated, and 6.8 if the grading was aggressive.⁵¹ Other series confirm these observations.^{46,52} Widely invasive FTC warrants radical surgery as well as ablative RIT.

Completion thyroidectomy

Often the diagnosis of TC can only be established after paraffin embedding of serial slices through the tumor, especially if the aim is to document, or exclude, capsular or vascular invasion in the differential diagnosis between follicular adenoma and minimally invasive FTC. If the final histological diagnosis is cancer, thyroidectomy needs to be completed within a few days.³ Completion thyroidectomy is associated with risk if the ipsilateral thyroid bed has been explored as a part of the initial procedure. Many endocrine surgeons therefore prefer total hemithyroidectomy with ipsilateral central lymph node dissection as the primary procedure if there is suspicion of TC, so that re-exploration of the thyroid bed is avoided. The risk for surgical

complications rises steeply after the first postoperative week, and completion thyroidectomy is recommended only in the first few days or 3–6 months after the initial operation.

Currently, about 60% of all TC patients in Germany receive two operations as their primary surgical therapy.⁵³ One important reason is that FNAC is only used in about 30% of all cases, and that ultrasound examination of the thyroid gland does not always include cervical lymph nodes.⁵³ Few studies have addressed whether a delay in instituting primary therapy has an effect on prognosis. In Mazzaferri's series, a delay in cancer diagnosis imparted a risk comparable to that of old age.⁹ In Scheumann's series, delaying completion thyroidectomy by more than 30 days was also associated with an adverse prognosis.²⁷

Central lymph node dissection

Lymph node dissection as part of the primary surgical procedure for thyroid cancer has long been a subject of debate.⁵⁴

Proponents of the more aggressive strategy point out that in the hands of an experienced endocrine surgeon the procedure entails limited extra risk,²⁰ but that recurrences in the pre- and paratracheal region are highly dangerous and very difficult to operate.

Only a limited number of studies have examined the effect of prophylactic systematic lymph node dissection on recurrence rates and/or survival.⁵⁵ Tisel's series from Göteborg, also mostly without subsequent radioiodine therapy,⁵⁶ lacked a control group. Noguchi et al. reported 2859 patients operated on at a single center in Japan between 1946 and 1991.⁵⁷ Prophylactic lymph node dissection improved survival in patients with locally invasive DTC (pT4) or patients with lymph node metastases (N1).⁵⁷ However, patients did not receive routine radioiodine therapy, which limits the applicability of the results to current therapeutic practice in the Western world. Scheumann et al. demonstrated improved local control and survival in 342 patients operated on at Hannover University Hospital in Germany before and after 1986 without, and with, systematic lymphadenectomy, respectively. The second group included many patients from the former group who had had locoregional recurrence.¹³ Results from the ongoing MSDS trial may provide further evidence,⁵³ but so far recurrence rates in the trial have been generally lower than expected.⁵⁸ In the light of a recent prospective cohort survey, which demonstrated a clear correlation between complications and the radicality of the thyroid surgery (subtotal vs. total lobectomy),⁵⁹ the stipulation of the German guidelines to perform a central lymph node dissection has been questioned.⁶⁰

Based on our clinical experience we caution against well-intentioned but overaggressive surgery outside specialized centers which have sufficient patient numbers, optimal diagnostic resources, and stringent quality control.

Complications from overambitious surgery are generally irreversible, while recurrences of thyroid cancer can usually be cured in a multimodal approach without undue iatrogenic morbidity.

Surgical complications

The main complications specific to thyroid cancer surgery are recurrent laryngeal nerve palsy (RLNP), and hypoparathyroidism. Both conditions can be transitory due to irritation of the nerve on preparation of the thyroid bed, or a temporarily disturbed blood supply to the parathyroid glands, or permanent. Most data on complication rates have been published by specialized centers and may not reflect results under real-world conditions. In a prospective quality assurance study with 7617 patients operated on at 50 centers in the five East-German states, RLNP occurred transiently in 12.8% and permanently in 6.8% of patients, and hypoparathyroidism in 23.8% and 7.1%, respectively.⁶¹ These figures correspond to documented – presumably transient – rates for RLNP and hypoparathyroidism of 15.9% and 12.9% in the Patient Care Evaluation Study of thyroid cancer (PCES)⁶² and 20% and 22% in the MSDS trial.⁶³ In the MSDS trial the risk for RLNP increased to 42% in patients receiving three or more operations.⁶³ This underlines the need for optimal preoperative diagnostics including FNAC, which was underused in the trial. In a continuation of the cited quality assurance study, the risk of permanent RLNP was correlated to radicality of surgery (subtotal vs. total lobectomy) as well as the experience of the center.⁶⁴ This underlines the recommendation of the ETA to have thyroid cancer surgery performed only in centers of excellence.¹¹

Radioiodine therapy

Radioactive iodine-131 (¹³¹I) is generally applied orally in the form of gelatin capsules or, less frequently, as a liquid solution in water. Iodine is rapidly absorbed in the upper intestine and actively concentrated in the follicular epithelial cells by means of the sodium iodide symporter. Depending on the preservation of thyroid architecture, ¹³¹I is then stored as preformed thyroid hormone in the thyroid follicles (Figure 18.4). The physical half-life is 8 days. When ¹³¹I disintegrates radioactively, it emits both β and γ radiation. β radiation is a particle radiation consisting of rapid electrons. These have a maximum reach of 2 mm in tissue. The therapeutic effect is therefore confined to sites with ¹³¹I uptake. The effected tissue damage is apoptosis and/or necrosis of thyroid cells. γ radiation is an electromagnetic radiation similar to X-rays, and can be used diagnostically to image the distribution of ¹³¹I in the body (Figure 18.5).

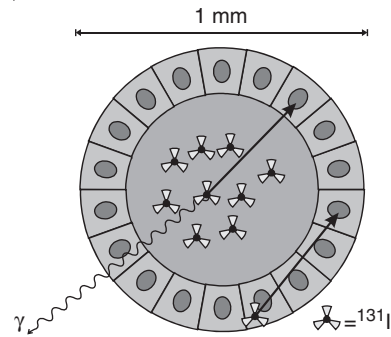


Figure 18.4

Radioiodine therapy. Radioactive iodine is taken up by the follicular cells and stored in the follicular lumen. As ¹³¹I disintegrates it emits β particles (solid arrows), which have a maximum reach in tissue of 2 mm.

Guideline recommendations

Ablative RIT

The ETA guidelines stratify their recommendations for RIT and follow-up into three risk categories at the time of initial treatment:¹¹

1. Very low risk – no indication for RIT:⁶⁵ unifocal TC ≤ 1 cm with no extension beyond the thyroid capsule and without lymph node or distant metastases and complete resection (T1N0M0R0) and a favorable histological type.¹¹
2. Medium risk – probable indication for RIT: TC > 1 cm N0M0R0. This includes also patients with less than total thyroidectomy, no lymph node dissection, age < 18 years, or unfavorable histology: PTC tall-cell, columnar cell, diffuse sclerosing; FTC widely invasive or poorly differentiated.¹¹
3. High risk – definitive indication for RIT: tumor extension beyond the thyroid capsule, lymph node metastases, incomplete tumor resection, or distant metastases (T3/4 or N1 or R1 or M1).¹¹

For high-risk patients therapy is recommended with high activity (≥ 3.7 GBq) of ¹³¹I following prolonged withdrawal of thyroid hormone.¹¹ For low-risk patients ETA guidelines leave a choice between 1.1 or 3.7 GBq of ¹³¹I, and a withdrawal of thyroxine or stimulation with recombinant human TSH (rhTSH).¹¹ The ETA guidelines explicitly do not recommend a diagnostic scan before thyroid ablation because of its low clinical utility compared to a post-therapeutic scan and because of a possible stunning^{66,67} during the subsequent therapeutic activity of ¹³¹I.¹¹ If a diagnostic scintigraphy is required, ¹²³I or a very low activity of ¹³¹I (4 MBq) is recommended.¹¹

German DKG guidelines recommend ablative RIT in all cases of thyroid cancer except papillary microcarcinoma (pT1a N0; < 1 cm) without radical surgery, medullary TC,

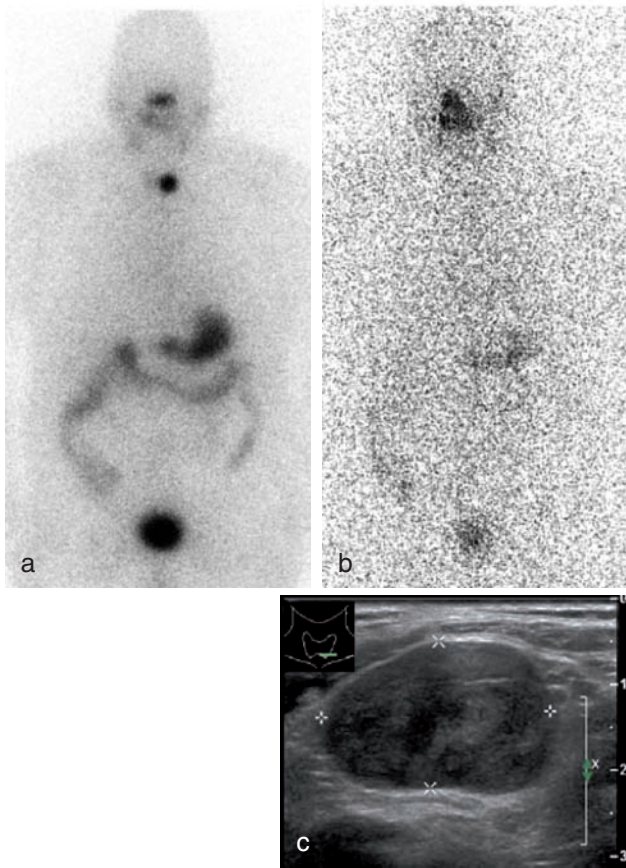


Figure 18.5

Radioiodine therapy. This 45-year-old man was diagnosed with papillary carcinoma pT3 (m) (4.6 cm) pN1 Mx in July 2005. Post-ablation scintigraphy 9/2005 (panel (a), 4 days after 5.6 GBq ^{131}I) showed focal uptake in the left thyroid bed, but otherwise physiological tracer distribution in stomach, colon, and urinary bladder. The diagnostic scintigraphy 1/2006 (panel (b), 48 h after 200 MBq ^{131}I) is negative. The corresponding ultrasound examination from 1/2006 showed a 2.7 cm large lymph node metastasis. The diagnosis has since been confirmed histologically. This case illustrates the inferior image quality of low activities of ^{131}I (b) and underlines the necessity for routine cervical ultrasound as an adjunct to ^{131}I imaging.

and anaplastic TC.³ A radioiodine test with 10–20 MBq over 24 h is recommended. When the uptake is >20% a completion thyroidectomy is to be considered.³ The recommended activity is 1–3 GBq ^{131}I , or based on individual dosimetry aiming for an absorbed dose of >300 Gy.³

The American NCCA guidelines recommend a diagnostic whole-body radioiodine scan off thyroid hormone 4–12 weeks after thyroidectomy. If the diagnostic radioiodine scan is negative *and* serum thyroglobulin (Tg) is lower than 1 ng/ml, no indication for RIT is seen.¹² The NCCA guidelines do not specify the activity of ^{131}I to be used or the time interval for scanning (24, 48, or 72 h).¹²

Preparation for RIT

ETA guidelines recommend that the patient be seen by a nuclear medicine specialist or endocrinologist for an assessment and full discussion about the rationale and side-effects of RIT.¹¹ Practice at our own center is that a nuclear medicine specialist sees the patient in the outpatient clinic some 10–14 days after thyroidectomy before thyroid hormone withdrawal interferes with the patient's intellectual capabilities and coping mechanisms. Our department's website contains detailed information for patients, including a special brochure.

A sufficient level of TSH is necessary in order to increase uptake in the thyroid remnant. Thyroid hormone is withdrawn 4 weeks^{3,68} to 5 weeks¹¹ before RIT in order to increase TSH to levels above 25⁶⁹ to 30 mU/L.⁷⁰ Alternatively, exogenous stimulation with rhTSH has been shown to be effective with a fixed activity of 3700 MBq ^{131}I .⁷¹ rhTSH has been approved for ablative therapy by the European Medicines Agency (EMA) for use in low-risk patients.¹¹ The patient should receive an intramuscular injection of 0.9 mg on two consecutive days and receive ^{131}I the day after.¹¹

RIT must only be given in centers suitably equipped for that purpose,¹¹ which should include a γ camera with high-energy collimators capable of performing SPECT and ideally SPECT–CT. In all Western countries, radioprotection legislation requires patients to be isolated in approved units under high-dose RIT. Before patient discharge the dose rate of the remaining ^{131}I activity must be measured and documented.¹¹

Pregnancy must be excluded.¹¹ A low-iodine diet is recommended 10 days⁷² to 3 weeks¹¹ before RIT. In cases of doubt, urinary iodine excretion should be measured.¹¹

hTg should be measured immediately before administration of RIT in patients under thyroid hormone withdrawal or on the third day following the last application of rhTSH.¹¹ If the patient has stopped thyroid hormone, oral thyroid hormone is begun on the second or third day after ^{131}I administration.¹¹

A whole-body ^{131}I scintigraphy is performed 3–5 days after ^{131}I application¹¹ when the residual ^{131}I activity is sufficiently low that the maximum count rate of the γ camera is not exceeded.

Commentary

The rationale underlying ablative RIT includes (1) the sterilization of occult cancer foci, or residual normal follicular cells destined to become malignant, in or near the thyroid remnant, (2) the sterilization of metastatic foci in cervical lymph nodes, (3) detection of lymph node and distant metastases in the post-therapeutic ^{131}I whole-body scintigraphy, and (4) elimination of serum hTg to (almost) undetectable levels so that it can be used as a highly

sensitive tumor marker.¹¹ Tumor foci in the thyroid remnant need not take up ¹³¹I as they receive radiation from the surrounding thyroid tissue ('bystander effect').

A number of retrospective series have documented an impressive benefit in terms of freedom of recurrence and survival. Mazzaferri and Jhiang were able to document a reduction in the 10-year rate of recurrence from 28% to 6% in medium-risk patients ($p < 0.001$) that extended over the whole follow-up period, and an elimination of tumor-related deaths.⁹ In Samaan's study, RIT was the single most powerful predictor for increased disease-free interval with a concomitant survival benefit.⁷³ Data from our own institution document a 97% 5-year survival rate among patients with TC limited to the thyroid and without distant metastases.⁸ A prospective cohort study in high-risk patients with TC showed a survival benefit due to RIT.⁷⁴ A recent meta-analysis showed a significant 10-year risk reduction for locoregional recurrence (relative risk 0.31, 95%-confidence interval 0.2–0.49) and for distant metastases (absolute decrease in risk 3%; 1–4%). The incremental benefit of remnant ablation in low-risk patients treated with total thyroidectomy and thyroid hormone suppressive therapy was unclear.⁷⁵ Unfortunately, there are no randomized trials on the effectiveness of ablative RIT.²³

The optimum activity for thyroid remnant ablation has been addressed by a number of retrospective series⁷⁶ and at least four randomized trials.^{77–80} The latter include two trials by Bal et al.^{79,80} In the original 1996 trial, activities over 1.9 GBq (50 mCi) did not increase the efficacy of ablation beyond 77%.⁷⁹ Based on 19 studies, a recent meta-analysis has concluded that high-dose remnant ablation 2.7–3.7 GBq is more effective than low-dose with 1 GBq or less.⁸¹

An important area of controversy between the various guidelines is whether a diagnostic ¹³¹I scintigraphy should precede ablative RIT. We agree with the ETA guidelines that a diagnostic ¹³¹I scintigraphy preceding RIT has very limited utility, and should be discouraged for the following reasons:

1. Activities of ¹³¹I as low as 40 MBq can stun subsequent ¹³¹I uptake under RIT by 50%.⁸² The effect sets in after a couple of days and is maximal after 3 weeks.⁶⁶
2. The sensitivity of 'diagnostic' ¹³¹I scintigraphy with activities of a few hundred MBq is limited compared to post-therapeutic scintigraphy after RIT. In a series of 81 patients studied by Fatourehchi et al., post-therapeutic scans revealed a new site with abnormal uptake not seen on a diagnostic scan with 111 MBq in 13% of the scans, which changed management in 9% of the patients.⁸³ This is also a well documented phenomenon in the evaluation of hTg-positive patients with negative 'diagnostic' ¹³¹I scintigraphy. In an early series by Pacini et al., scintigrams with a therapeutic activity revealed tumor tissue previously undiagnosed with 185 MBq ¹³¹I

in 16/17 patients.⁸⁴ In de Keizer's series of 16 Tg-positive patients, ¹³¹I-scintigraphy with 7.4 GBq revealed pathologic uptake not seen on scintigraphy with 370 MBq ¹³¹I a week before in 11/16 patients (69%; neck in seven, mediastinum in three, lung in one patient).⁸⁵ In Koh's series the corresponding fraction was 12/28 cases (43%),⁸⁶ in Pineda's series 16/17,⁸⁷ and in van Tol's 28/54.⁸⁸ One explanation for these findings is that contrast in ¹³¹I scintigraphy is optimal only after 3–5 days, due to both the slow uptake of tracer in the tumor tissue and the slow elimination of background activity. With 'diagnostic' ¹³¹I activities the count rate after 48–72 h is suboptimal. A ¹³¹I scan with a 'diagnostic' activity has therefore insufficient sensitivity to be able to exclude distant metastases also in cases of newly diagnosed TC.

The ideal diagnostic tracer with respect to stunning is ¹²³I, a pure γ emitter. When scintigraphy with ¹²³I is positive, a subsequent RIT will show uptake.⁸⁹ However, ¹²³I is vulnerable to the same pre-therapy staging inaccuracies as is low-dose diagnostic imaging with ¹³¹I.^{90–92} Alzahrani et al. compared ¹²³I scintigraphies 24 h after oral ingestion of 185–555 MBq ¹²³I with post-therapeutic ¹³¹I scans 4–5 days after RIT. In 166 patients receiving their first ablative RIT, six post-therapeutic ¹³¹I scans showed extra foci in the thyroid bed, three extra foci in cervical lymph nodes, one in the lung, and one new bone metastasis.⁹² A single study reported that ¹²³I was more sensitive for imaging thyroid remnants.⁹³ Also, with ¹²³I, contrast improves over time: a scan after 24 h is more sensitive than after 4 h.⁹⁴ Compared with other tracers, ¹²³I is more costly and needs to be delivered on the day of the study.

Radioiodine uptake over 24 h with ¹²³I or a tracer dose of ¹³¹I is a good observer-independent way to quantify thyroid remnant tissue.⁹⁵ In line with the German guidelines, the latter method is in routine use at our institution in Münster. Because we apply ablative RIT the following day, stunning of subsequent ¹³¹I uptake is presumably not relevant. If the only intention is to prove or exclude the presence of a large remnant that precludes ablative RIT without completion thyroidectomy, thyroid scintigraphy with [^{99m}Tc] pertechnetate is a readily available and cheap alternative to ¹²³I. This is a technique which we routinely use in the postoperative evaluation of patients with subtotal or partial thyroid resections.

¹³¹I scintigraphy has a very high specificity if one takes care to avoid a number of pitfalls.^{96–98} Patients should receive a laxative the day before and empty the bladder, suck lemon, and drink some water immediately before scintigraphy in order to reduce ¹³¹I activity in the colon, urinary bladder, salivary gland, and esophagus. Scanning with diagnostic activities should be performed at a slow speed for optimal statistics.¹¹ Since the anatomic information contained in ¹³¹I scintigrams is limited, SPECT–CT

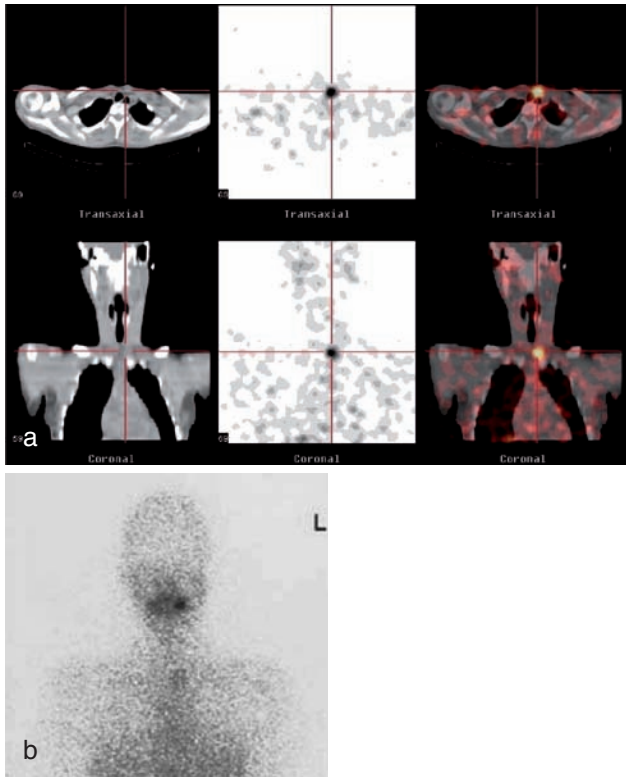


Figure 18.6

^{131}I -single photon emission computed tomography–computed tomography (SPECT–CT). This 27-year-old woman had papillary thyroid cancer pT3b (5 cm; locally invasive) pN1 Mx. 3 months after ablation with 3 GBq ^{131}I the planar scan (370 MBq; not shown) was negative. Human thyroglobulin (hTg) was 18.6 ng/ml, which indicated tumor tissue. ^{131}I scintigraphy with a therapeutic activity (panel (b); 3 GBq, 72 h) shows a weak focus to the left of the midline. The corresponding ^{131}I -SPECT (panel (a); center column) shows weak focal uptake, but contains no anatomic information. CT (left column) was done as part of the same examination. When CT was fused with the ^{131}I -SPECT the focus could be localized in the jugulum to the left of the trachea. Sonographically the focus corresponded to two lymph node metastases, which had not been diagnosed before. [^{18}F]fluoro- 2-deoxy-D-glucose-positron emission tomography (FDG-PET) was negative. Operation 11/2003 confirmed the diagnosis. Laryngeal nerve function was intact. The patient has since been in complete remission; hTg under stimulation was <0.2 ng/ml 2/2004.

increases diagnostic accuracy considerably (Figure 18.6),⁹⁹ especially when combined with high-resolution ultrasound. Dual-isotope scanning may be an alternative for institutions that lack SPECT–CT.¹⁰⁰

Harmful effects of RIT

Radiation thyroiditis is frequent in patients with large remnants, and can usually be controlled with an ice bag. Abnormalities of taste are frequent but transient.¹⁰¹

Standard practice is to have the patient lick lemon juice or a sour sweet and/or chew gum in order to induce a steady flow of saliva that transports ^{131}I out of the salivary gland.¹⁰² Diagnostic salivary gland scintigraphy demonstrates that these maneuvers effectively reduce the levels of radioactivity in the salivary gland.¹⁰³ Amifostin is effective for radioprotection, but has side-effects.¹⁰⁴ Whether Nakada's recommendation to delay sucking of lemon candies until 24 h after ^{131}I administration, which is based on historical controls,¹⁰³ is to be followed without further validation is a matter of debate.¹⁰⁵

Hypospermia has been observed but is usually transient.¹⁰⁶ Pretreatment sperm-banking should be offered to male patients if multiple high-dose RIT is planned.^{11,107} Conception should be avoided for 4¹¹ to 6–12³ months in males and 6¹¹ to 12 months³ in females. Pregnancy is safe.^{108,109} However, there is a slight increase in miscarriage if pregnancy occurs between 6 and 12 months after treatment.¹⁰⁹ Breast-feeding should be stopped before RIT,¹¹ also for radioprotection of the mammary gland. An earlier onset of menopause has been reported after repeated RIT.¹¹⁰ Transient thrombocytopenia and leukopenia are normal after RIT for TC. They may be chronic above cumulative activities > 18.5 GBq.¹¹¹

An increase in secondary primary malignancies has been documented, especially with RIT with activities exceeding 20–30 GBq.^{112–114} Therefore, the indication for high-dose therapy should be established with diligence.¹¹ Pulmonary fibrosis can be a problem after high-dose therapy for pulmonary metastases.¹¹⁵ For a further discussion of side-effects of RIT we refer to Mazzaferri's review.²⁹

Hormone therapy

The aim for therapy with thyroid hormone in TC is two-fold: (1) to treat hypothyroidism by providing normal levels of thyroid hormone, and (2) to inhibit TSH-dependent growth of residual cancer cells by suppressing TSH below normal levels.¹¹

Guideline recommendations

The guidelines of the European Thyroid Association recommend suppression of TSH below 0.1 mU/l in all patients with persistent disease, including patients with detectable hTg.¹¹ In high-risk patients (see above) who have achieved complete remission, TSH-suppressive therapy is recommended for 3–5 years. In low-risk patients in complete remission, TSH should be between 0.5 and 1.0 mU/l.¹¹ L-Thyroxine should be taken once a day in the morning on an empty stomach.¹¹ Dose adjustments should be in steps of 25 $\mu\text{g}/\text{day}$ with a control of TSH 3 months later.¹¹ In pregnancy more frequent dose adjustments are necessary.¹¹

Treatment is best supervised by an endocrinologist or other member of the multidisciplinary team.¹¹

For the USA, the NCCA guidelines recommend a risk-stratified approach, but do not define explicitly which degree of TSH-suppression is to be aimed for.¹² The American Association of Clinical Endocrinologists (AACE) guidelines recommend a TSH goal between 0.1 and 0.4 mU/l.⁶⁹ The interdisciplinary German guidelines recommend TSH suppression to 0.1–0.2 mU/l without risk stratification.³ Current German nuclear medicine guidelines recommend TSH suppression below 0.2 mU/l and 0.3–0.5 mU/l for papillary microcarcinoma.⁷²

Commentary

A number of retrospective series were able to demonstrate an effect of TSH-suppressive therapy in patients without RIT¹¹⁶ or with RIT.¹¹⁷ A recent meta-analysis concluded that TSH-suppressive therapy had an effect on reducing recurrence rates.¹¹⁸ However, compared with surgery and RIT, the effect is weak. At the same time there is an increasing body of published evidence on the deleterious effects of even subclinical hyperthyroidism, especially atrial fibrillation and stroke¹¹⁹ and bone loss.¹²⁰ This has induced the authors of most guidelines to relax the aims for TSH-suppressive therapy in recent years.

External beam radiotherapy

Both the European and the German guidelines see an indication for external beam radiotherapy (RTx) only in undifferentiated TC or in cases of residual tumor (R1 or R2) that is not treatable by surgical resection and/or RIT.^{3,11} The NCCN guidelines recommend that RTx be considered for patients older than 45 years with gross extrathyroidal invasion.¹²

There is inconclusive evidence from a large number of retrospective series. A prospective randomized multicenter trial which was coordinated by the authors had to be terminated because of lack of acceptance of randomization.²⁴ We recently conducted a comprehensive meta-analysis and concluded that there is no longer an indication for adjuvant RTx in patients with locally invasive TC under the prevailing conditions in the industrialized world.⁴

Follow-up

Follow-up is primarily based on the following methods: clinical examination, cervical high-resolution ultrasound, determination of serum hTg with and without TSH stimulation, and ¹³¹I scintigraphy.¹¹

Guideline recommendations

The ETA's recommendations can be briefly summed up as follows. Very-low-risk patients not submitted to ablative RIT are followed up by hTg under L-thyroxine treatment and neck ultrasound.¹¹ Patients without evidence for metastases are seen under ongoing L-thyroxine therapy at 3 months with control of TSH, free thyroxine (FT4), and free triiodothyronine (FT3). At 6–12 months hTg is determined under rhTSH stimulation, and neck ultrasonography is performed. If the hTg is undetectable and there are no other abnormalities, patients are followed up yearly with neck ultrasonography and a determination of TSH, FT3, FT4, and hTg. If the hTg is larger than an institutional cut-off or there are other abnormalities, L-thyroxine is withdrawn and the patient receives a large activity of ¹³¹I with whole-body scintigraphy (WBS). Follow-up should be lifelong.¹¹ The role of supersensitive hTg assays^{121,122} has not yet been established.¹¹

The current German guidelines give the following recommendations. The success of RIT is documented with two diagnostic WBSs with 100–300 MBq ¹³¹I under endogenous or exogenous TSH stimulation 3–4 months and 1 year after RIT.³ If there is demonstrable thyroid bed uptake, RIT is repeated until WBS is negative. Patients with local invasion or distant metastases receive a WBS every 2 years. All patients are followed-up with a half-yearly examination that includes determination of hTg and cervical ultrasonography until year 5, and thereafter at yearly intervals.³

The NCCN guidelines¹² recommend regular diagnostic WBS with 150 MBq ¹³¹I over 48 h¹²³ every 12 months until the scan is negative. WBS is performed under endogenous TSH stimulation if a repeat RIT is likely, or under endogenous or exogenous TSH stimulation. Thereafter the patient is controlled half-yearly, and yearly after year 2, with a physical examination, serum TSH, hTg and hTg-antibodies, and periodic ultrasound.¹²

Commentary

The chief controversy between current guidelines is the role of diagnostic ¹³¹I WBS. A number of studies have tried to shed light on the issue.

In a classical report from 1970, Varma et al. reported a 20-fold increase in mortality from DTC when RIT was discontinued short of total ablation of functioning thyroid tissue.¹²⁴

Grigsby et al. reported on 76 patients after ablative RIT with at least one negative WBS 1 year after RIT. WBS was repeated at years 1 and 2 and then every 3–5 years. Seven patients had a positive ¹³¹I WBS 1 year after the first negative WBS, and two patients 1 year after two consecutive WBSs. None of these patients had measurable hTg.

The authors concluded that a single negative WBS after complete ablation has a lower predictive value than two consecutive negative studies.¹²⁵

Cailleux et al. evaluated ¹³¹I WBS in 256 consecutive patients with DTC 6–12 months after ablative RIT.¹²⁶ A total of 113 patients were nodal positive (N1). Surgery included lymph node dissection in 228 patients. Ablative RIT was performed with 3.7 GBq. Therapeutic uptake was <1% in 189 patients and 1–2% in 67 patients. Patients with extrathyroidal uptake in the post-therapeutic WBS or with interference in the hTg assay were excluded. Diagnostic WBS was performed 72 h after 74 MBq (in low-risk patients) or 185 MBq (in high-risk patients) under TSH stimulation (TSH > 30 mU/l). WBS showed no uptake in 92% of the patients and thyroid bed uptake <1% in the remaining eight patients. A ¹³¹I WBS with 3.7 GBq was additionally performed in nine of 15 patients with a hTg >10 ng/ml. It showed uptake corresponding to lymph node metastases in two patients and chest uptake corresponding to lung metastases in one patient. Of the six ¹³¹I-negative patients one had lymph node and one had lung metastases. Of the remaining patients in the cohort, three were diagnosed with lymph node metastases 3–4 years after the initial surgery over a mean follow-up period of 5 years. The authors conclude that WBS with 74–185 MBq ¹³¹I has no incremental value over serum hTg under TSH stimulation and neck ultrasound, and that if hTg exceeds a certain value, diagnostic scanning with ¹³¹I should be performed with an activity of 3.7 GBq or more.¹²⁶

Pacini et al. described 662 consecutive patients undergoing the first control WBS 6–12 months after ablative RIT with 1.1–3.7 GBq between 1980 and 1990. Follow-up was a mean of 12 years, with yearly hTg and ultrasonography and periodic ¹³¹I WBS. A total of 315 patients had undetectable hTg (<3 ng/ml). WBS was performed with 148–185 MBq after 48–72 h with a rectilinear scanner. The post-RIT scan showed uptake in the thyroid bed in 100%, in lymph node metastases in 10.5%, and in the lung in 1.3%. In the diagnostic WBS, uptake was found in the thyroid bed in 90 patients (28.6%); 54 patients received one extra RIT, and seven patients received two. Of the 315 patients, two relapsed with lymph node metastases after 2 and 9 years respectively, both discovered by cervical ultrasound. Twenty-nine patients with persistent thyroid bed uptake had no clinical events. None died of TC.¹²⁷

Taylor et al. reported 153 consecutive patients treated between 1990 and 2000. RIT was performed with 1.1–3 GBq ¹³¹I. Post-therapeutic WBS showed thyroid bed uptake with or without extrathyroid uptake in all. The diagnostic scan 6 months after RIT with 185 MBq over 48–72 h was positive in 20 and faintly positive in another 16 patients. Of the former 20, 16 received RIT with 5.5 GBq ¹³¹I. WBS became negative in nine and remained positive in seven

(thyroid bed uptake in six, lymph nodes in one). Of the latter seven, six had elevated hTg and one had hTg-antibodies. At follow-up all seven are alive and disease-free. Of the 117 patients with negative WBS, ten had recurrences which were always detected clinically or by a rising hTg.¹²⁸

Serum hTg may be falsely negative. Schlumberger and Baudin estimate that hTg under L-thyroxine is not measurable in fewer than 1% of patients with distant metastases visible on X-ray, 5% of patients with lung metastases not visible on X-ray and 20% of patients with isolated lymph node metastases. Patients with negative hTg under TSH stimulation in patients with recurrences are rare,¹²⁹ but are occasionally observed (Figure 18.7).

We agree with the European guidelines that determination of hTg under TSH stimulation and cervical ultrasonography¹³⁰ are the two most sensitive tests for recurrence. However, Cailleux' data, which provide the strongest evidence against routine diagnostic WBS, cannot be generalized. That lymph node dissection was performed in 89% of patients and ¹³¹I uptake was less than 2% indicates that patients were exceptionally well operated. This in no way reflects the prevailing conditions in Germany, where centers receive patients from many surgical departments. In the MSDS trial, a systematic lymph node dissection was performed in only 32% of patients,¹³¹ and radioiodine uptake was over 3% in half the study patients.¹ Also as Cailleux et al. point out, large thyroid remnants interfere with the detection of metastatic ¹³¹I uptake. We therefore argue against abandoning diagnostic WBS after ablation without evaluating the concept in large multicenter studies. The ETA guidelines rely heavily on ultrasound of the neck. The diagnosis of recurrences especially in the thyroid bed is a challenge (Figure 18.8). It is very important to perform ultrasound in direct correlation with all scintigraphic studies. We perform ultrasound routinely at each visit in the follow-up of all our TC patients, and we encourage every nuclear physician specializing in the treatment and follow-up of TC to learn the technique, as the diagnostic gain often lies in the combination of the different imaging modalities.

Recurrent and metastatic cancer

All guidelines recommend [¹⁸F]FDG-PET in patients with suspected recurrence.^{3,11,12,132–136} The value of other scintigraphic methods such as [^{99m}Tc]MIBI (methoxyisobutylisonitrile), [^{99m}Tc]tetrofosmin, [¹¹¹In]octreotide, and [²⁰¹Tl] is comparatively limited.^{136,137}

In patients with suspected recurrence, we routinely use the following work-up:¹³⁸ endogenous or exogenous TSH stimulation with determination of serum hTg, ¹³¹I WBS including a SPECT-CT of the neck⁹⁹ (Figure 18.6) with a 'therapeutic' activity ≥3 GBq, and [¹⁸F]FDG-PET-CT following the therapeutic ¹³¹I application, including a diagnostic

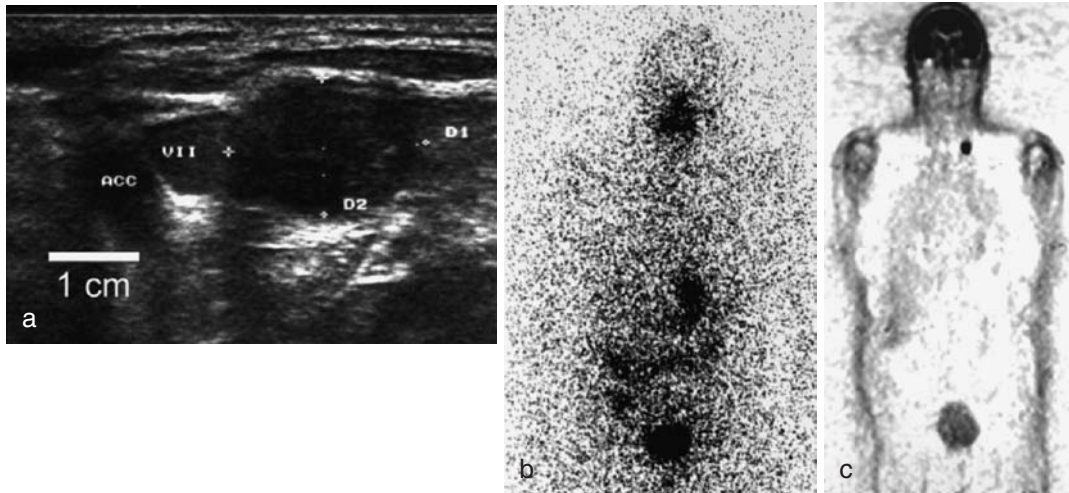


Figure 18.7

Recurrence with negative hTg. This 77-year-old woman had papillary thyroid cancer pT3b (4 cm; locally invasive) (1 cm) pN1 Mx. She received ablative radioiodine therapy 3/1997. In 1999 sonography discovered an echo-depleted lesion behind the left clavicle in contact with the left internal jugular (VII) and subclavian veins. ^{131}I scintigraphy off thyroxine (panel (b); 1 GBq ^{131}I , 72 h) was negative, but ^{18}F FDG-PET (panel (c); in 1999 without attenuation correction) highly positive. Thyroid stimulating hormone (TSH) was 34 mU/l, hTg 0.8 $\mu\text{g/l}$, hTg-recovery 91%, anti-Tg-antibodies negative. Histology was positive. The patient was event-free until another regional recurrence 6 years later.

CT of the neck and – if there is suspicion of pulmonary metastases – of the chest. The last examination is ultrasound of the neck in the light of all other imaging studies. Rarely, both ^{131}I scintigraphy and FDG-PET may both be negative (Figure 18.9).

We routinely perform ^{18}F FDG-PET under TSH stimulation. The sensitivity is best under rhTSH, because lesional FDG uptake is promoted by TSH¹³⁹ and the elimination of background activity is not delayed as in the hypothyroid state. Endogenous TSH stimulation is more sensitive than TSH suppression¹⁴⁰ (Figure 18.8). The observation in the German multicenter study that FDG-PET was seemingly more sensitive than under endogenous TSH stimulation is probably not valid,¹³⁶ since this was a comparison between two unrelated historical groups.

It is estimated that remission can be obtained in two-thirds of patients with a neck recurrence and one-third of patients with distant metastases.¹¹ Remission is more frequently achieved in patients with a limited tumor burden.¹¹ The therapeutic strategy is primarily surgical.¹¹ Lesions that are not operable but take up ^{131}I are treated with repeated high-dose RIT.¹¹ ^{131}I negative, inoperable lesions may be treated with RTx, especially when there is risk for local complications.¹¹ Disseminated lung metastases can be cured by repeated high-dose RIT.^{141–143} Bone metastases should be treated surgically whenever possible.^{11,50,144} Bone metastases of TC are difficult to diagnose in conventional skeletal scintigraphy because lesions are mostly cold. They are heavily vascularized and

may require preoperative embolization. Metastases in the pelvis and spine can only rarely be completely resected. A combination of surgery with repeated high-dose RIT is therefore the rule. External RTx should be delayed as long as there is the option for RIT, as RTx may stun subsequent therapeutic ^{131}I uptake. TSH stimulation and RIT entail a chance of transitory tumor swelling with the risk of compressive symptoms. In this situation we prefer short-term TSH stimulation with rhTSH under prophylactic therapy with corticosteroids.⁹⁸ Diagnostic WBS with ^{131}I before RIT is to be discouraged because of stunning therapeutic ^{131}I uptake.¹¹

Cytotoxic therapy

There is consensus among guidelines that cytotoxic chemotherapy¹⁴⁵ has no role in the routine management of DTC. Its use is restricted to patients with progressive disease uncontrolled by surgery, ^{131}I , TSH suppression, and RTx.¹¹

Therapy with derivatives of vitamin A can reinduce expression of the sodium iodide symporter in dedifferentiated, iodine-negative tumor manifestations of DTC.¹⁴⁶ The therapy has only moderate side-effects, mostly dryness of the skin, which is reversible.¹⁴⁷ Uncontrolled series document that ^{131}I uptake may be reinduced in 30%¹⁴⁸ to 40%^{149–151} of patients, and partial remissions may be

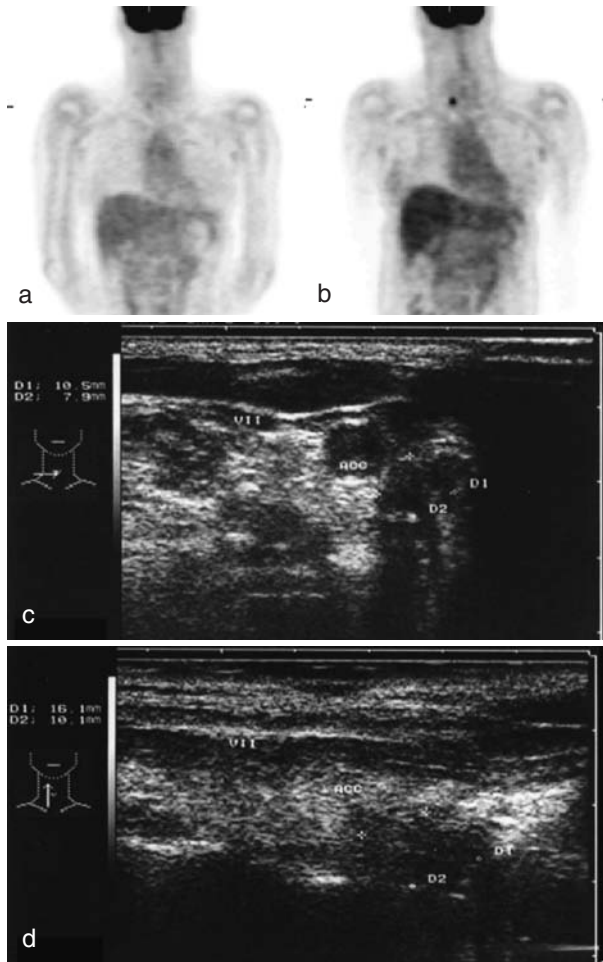


Figure 18.8

Local FDG-positive recurrence only under TSH stimulation. This 28-year-old woman had right-sided papillary thyroid cancer pT3b (2.5 cm; locally invasive) pN1 Mx. The patient received radioiodine therapy at another institution (3 GBq 5/02, 8/02, and 12/02 under L-thyroxine withdrawal). ^{131}I scintigraphy showed minimal thyroid bed uptake 8/2002.

At this time hTg was 40 $\mu\text{g/l}$. We saw the patient 2/2003 while she was under TSH suppression. Initial sonography and FDG-PET (a) were negative. Only when the patient was TSH-stimulated after 4 weeks' cessation of L-thyroxine therapy was FDG-PET positive (b), and we were at last able to diagnose a $10 \times 10 \times 16$ mm large local recurrence in the thyroid bed (c,d). Reoperation confirmed the diagnosis. Recurrent laryngeal nerve function remained intact. Stimulated hTg after surgery was 4 $\mu\text{g/l}$. The patient has been free of recurrence since.

induced in 20%¹⁴⁹ to 40%¹⁵¹ of patients. It is important to note that hTg may rise even if lesions regress, since redifferentiation may increase hTg production of dedifferentiated tissue.¹⁴⁷ It is not clear whether redifferentiation by itself or RIT utilizing reinduction of ^{131}I uptake induces remission. As with other treatment modalities for DTC, there is a lack of prospective randomized trials.

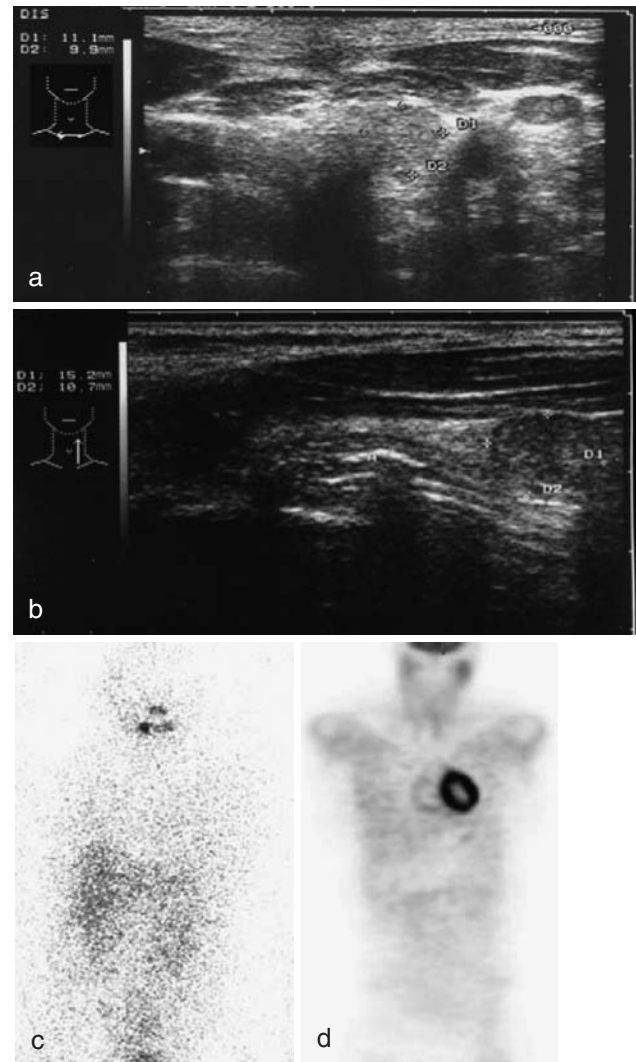


Figure 18.9

^{131}I - and FDG-negative recurrence. This 28-year-old woman had bilateral papillary thyroid cancer pT1 (m) (17 cm) pNx Mx. After ablative radioiodine therapy, hTg off L-thyroxine was 6.4 ng/ml. Cervical ultrasound showed a lesion ($11 \times 11 \times 15$ mm) in the left thyroid bed (a,b). ^{131}I scintigraphy (panel (c); 3 GBq, 72 h) and [^{18}F]FDG-PET (d) were both negative. Fine-needle aspiration cytology yielded papillary structures. Surgery revealed a lymph node metastasis. Recurrent laryngeal nerve function remained intact. The patient has since been in complete remission.

Conclusions

DTC is an example of a disease where improvements in multiple diagnostic and therapeutic modalities and interdisciplinary cooperation have almost eliminated cancer-related mortality for the vast majority of patients.

References

1. Biermann M, Pixberg MK, Dörr U et al. Guidelines on radioiodine therapy for differentiated thyroid carcinoma. Impact on clinical practice. *Nuklearmedizin* 2005; 44: 229–37.
2. Belin RM, Ladenson PW, Robinson KA, Powe NR. Development and use of evidence-based clinical practice guidelines for thyroid disease. *Endocrinol Metab Clin North Am* 2002; 31: 795–817.
3. Deutsche Krebsgesellschaft. Concise interdisciplinary guidelines on thyroid cancer, 2002. <http://www.uni-duesseldorf.de/AWMF/ll/032-014.htm>.
4. Biermann M, Pixberg M, Schuck A et al. External beam radiotherapy. In: Biersack H-J, Grünwald F, eds. *Thyroid Cancer*, 2nd edn. Heidelberg: Springer 2005; 139–61.
5. Akslen LA, Haldorsen T, Thoresen SO, Glatte E. Survival and causes of death in thyroid cancer: a population-based study of 2479 cases from Norway. *Cancer Res* 1991; 51: 1234–41.
6. Salvesen H, Njolstad PR, Akslen LA et al. Thyroid carcinoma: results from surgical treatment in 211 consecutive patients. *Eur J Surg* 1991; 157: 521–6.
7. Eichhorn W, Tabler H, Lippold R et al. Prognostic factors determining long-term survival in well-differentiated thyroid cancer: an analysis of four hundred eighty-four patients undergoing therapy and aftercare at the same institution. *Thyroid* 2003; 13: 949–58.
8. Lerch H, Schober O, Kuwert T, Saur HB. Survival of differentiated thyroid carcinoma studied in 500 patients. *J Clin Oncol* 1997; 15: 2067–75.
9. Mazzaferri EL, Jhiang SM. Long-term impact of initial surgical and medical therapy on papillary and follicular thyroid cancer. *Am J Med* 1994; 97: 418–28.
10. Biermann M, Schober O. How many high-risk patients with differentiated thyroid cancer needs a ‘Tumor Center’ per year Editorial? *Nuklearmedizin* 2002; 41: 61–2.
11. Pacini F, Schlumberger M, Dralle H et al. European consensus for the management of patients with differentiated thyroid carcinoma of the follicular epithelium. *Eur J Endocrinol* 2006; 154: 787–803.
12. National Comprehensive Cancer Network. Clinical practice guidelines in oncology. *Thyroid Carcinoma v. 1.2006*, 2006. http://www.nccn.org/professionals/physician_gls/PDF/thyroid.pdf.
13. Scheumann GF, Gimm O, Wegener G, Hundeshagen H, Dralle H. Prognostic significance and surgical management of locoregional lymph node metastases in papillary thyroid cancer. *World J Surg* 1994; 18: 559–67.
14. Yang GC, Liebeskind D, Messina AV. Ultrasound-guided fine-needle aspiration of the thyroid assessed by Ultrafast Papanicolaou stain: data from 1135 biopsies with a two- to six-year follow-up. *Thyroid* 2001; 11: 581–9.
15. Cochand-Priollet B, Prat JJ, Polivka M et al. Thyroid fine needle aspiration: the morphological features on ThinPrep slide preparations. Eighty cases with histological control. *Cytopathology* 2003; 14: 343–9.
16. Berner A, Pradhan M, Jorgensen L, Heilo A, Groholt KK. Fine needle cytology of the thyroid gland. *Tidsskr Nor Lægeforen* 2004; 124: 2359–61.
17. Yang GC, Liebeskind D, Messina AV. Should cytopathologists stop reporting follicular neoplasms on fine-needle aspiration of the thyroid? *Cancer* 2003; 99: 69–74.
18. Hegedüs L. Clinical practice. The thyroid nodule. *N Engl J Med* 2004; 351: 1764–71.
19. Junginger T, Hartel W. Leitlinien der Therapie maligner Schilddrüsentumoren. *Mitt Dtsch Ges Chir* 1996; 3.
20. Österreichische Gesellschaft für Chirurgie, ACO-Manual, 2006. <http://www.aco-asso.at/main/manual.html>.
21. British Thyroid Association. Guidelines for the management of thyroid cancer in adults, 2002. <http://www.british-thyroid-association.org/guidelines.htm>.
22. American Association of Clinical Endocrinologists, American College of Endocrinology. AACE/AAES medical/surgical guidelines for clinical practice: management of thyroid carcinoma. *Endocr Pract* 2001; 7: 202–20.
23. British Association of Endocrine Surgeons. Surgical treatment of diseases of the thyroid gland, 2001. <http://www.baes.info/>.
24. Mazzaferri E. A randomized trial of remnant ablation – in search of an impossible dream? *J Clin Endocrinol Metab* 2004; 89: 3662–4.
25. Biermann M, Pixberg MK, Schuck A et al. Multicenter Study Differentiated Thyroid Carcinoma (MSDS): diminished acceptance of adjuvant external beam radiotherapy for differentiated thyroid carcinoma. *Nuklearmedizin* 2003; 42: 244–50.
26. Mazzaferri E. Carcinoma of follicular epithelium. Radioiodine or other treatment and outcomes. In: Braverman LE, Utiger RD, eds. *The Thyroid*, 9th edn. Lippincott Williams & Williams: Philadelphia; 2005, 934–66.
27. Scheumann GF, Seeliger H, Musholt TJ. Completion thyroidectomy in 131 patients with differentiated thyroid carcinoma. *Eur J Surg* 1996; 162: 667–84.
28. Sugg SL, Ezzat S, Rosen IB, Freeman JL, Asa SL. Distinct multiple RET/PTC gene rearrangements in multifocal papillary thyroid neoplasia. *J Endocrinol Metab* 1998; 83: 4116–22.
29. Mazzaferri EL, Kloos RT. Current approaches to primary therapy for papillary and follicular thyroid cancer. *J Endocrinol Metab* 2001; 86: 1447–63.
30. Hedinger CE, Williams ED, Sobin LH. *Histological Typing of Thyroid Tumors*. Springer: Berlin, 1988.
31. Harach HR, Franssila KO, Wasenius VM. Occult papillary carcinoma of the thyroid. A ‘normal’ finding in Finland. A systematic autopsy study. *Cancer* 1985; 56: 531–8.
32. Leenhardt L, Grosclaude P, Cherie-Challine L. Increased incidence of thyroid carcinoma in France: a true epidemic or thyroid nodule management effects? Report from the French Thyroid Cancer Committee. *Thyroid* 2004; 14: 1056–60.
33. Machens A, Holzhausen HJ, Dralle H. The prognostic value of primary tumor size in papillary and follicular thyroid carcinoma. *Cancer* 2005; 103: 2269–73.
34. Passler C, Scheuba C, Asari R et al. Importance of tumour size in papillary and follicular thyroid cancer. *Br J Surg* 2005; 92: 184–9.
35. Dobert N, Menzel C, Oeschger S, Grünwald F. Differentiated thyroid carcinoma: the new UICC 6th edition TNM classification system in a retrospective analysis of 169 patients. *Thyroid* 2004; 14: 65–70.

36. Schmid KW, Sheu S-Y, Tötsch M et al. Pathology of thyroid cancer. *Onkologie* 2005; 11: 29–39.
37. Paschke R, Reiners C, Führer D et al. Recommendations and unanswered questions in the diagnosis and treatment of thyroid nodules. Opinion of the Thyroid Section of the German Society for Endocrinology. *Dtsch Med Wochenschr* 2005; 130: 1831–6.
38. Chow SM, Law SC, Chan JK et al. WH. Papillary microcarcinoma of the thyroid – prognostic significance of lymph node metastasis and multifocality. *Cancer* 2003; 98: 31–40.
39. Lupoli G, Vitale G, Caraglia M et al. Familial papillary thyroid microcarcinoma: a new clinical entity. *Lancet* 1999; 353: 637–9.
40. Mihailescu D, Shore-Freedman E, Mukani S et al. Multiple neoplasms in an irradiated cohort: pattern of occurrence and relationship to thyroid cancer outcome. *J Clin Endocrinol Metab* 2002; 87: 3236–41.
41. Schlumberger M, Pacini F, Wiersinga WM et al. Follow-up and management of differentiated thyroid carcinoma: a European perspective in clinical practice. *Eur J Endocrinol* 2004; 151: 539–48.
42. Reiners C, Geling M, Farahati J, Mäder U. Epidemiology of thyroid cancer. *Onkologie* 2005; 11: 11–19.
43. Schmid K, Böcker W, Schilddrüse. In: Remmele W, ed. *Pathologie*. Springer-Verlag: Berlin; 1997, 579–616.
44. Thompson LD, Wieneke JA, Paal E et al. A clinicopathologic study of minimally invasive follicular carcinoma of the thyroid gland with a review of the English literature. *Cancer* 2001; 91: 505–24.
45. Dansk Selskab for Klinisk Fysiologi og Nuklearmedicin. Guidelines for behandling af thyreoideacancer i Danmark, 2005. <http://www.dskfnm.dk/Fagligt/fagligt.htm>.
46. Chow SM, Law SC, Mendenhall WM et al. Follicular thyroid carcinoma: prognostic factors and the role of radioiodine. *Cancer* 2002; 95: 488–98.
47. Petrich T, Widjaja A, Musholt TJ et al. Outcome after radioiodine therapy in 107 patients with differentiated thyroid carcinoma and initial bone metastases: side-effects and influence of age. *Eur J Nucl Med* 2001; 28: 203–8.
48. Petrich T. Das differenzierte Schilddrüsenkarzinom mit initialer Fernmetastasierung (M1). *Diagnose, Therapie, Nachsorge und Prognose*. Gladbeck KFVR: 2000.
49. Lin JD, Chao TC, Hsueh C. Follicular thyroid carcinomas with lung metastases: a 23-year retrospective study. *Endocr J* 2004; 51: 219–25.
50. Schlumberger M, Challeton C, De Vathaire F et al. Radioactive iodine treatment and external radiotherapy for lung and bone metastases of differentiated thyroid carcinoma. *J Nucl Med* 1996; 37: 398–605.
51. Müller-Gärtner H-W, Brzac HT, Rehpenning W. Prognostic indices for tumor relapse and tumor mortality in follicular thyroid carcinoma. *Cancer* 1991; 67: 1903–11.
52. Lo CY, Chan WF, Lam KY, Wan KY. Follicular thyroid carcinoma: the role of histology and staging systems in predicting survival. *Ann Surg* 2005; 242: 708–15.
53. Biermann M, Pixberg M, Schober O, MSDS Study Group. The multicentric study differentiated thyroid carcinoma (MSDS): First results [Abstract]. *Ann Endocrinol* 2003; (suppl 4): 4.
54. Cady B. Lymph node metastases: indicators but not governors of survival. *Arch Surg* 1984; 199: 1067–72.
55. Thomusch O, Dralle H. Endocrine surgery and evidence-based medicine. *Chirurg* 2000; 71: 635–45.
56. Tisell LE, Nilsson B, Molne J et al. Improved survival of patients with papillary thyroid cancer after surgical microdissection. *World J Surg* 1996; 20: 854–9.
57. Noguchi S, Murakami N, Yamashita H, Toda M, Kawamoto H. Papillary thyroid carcinoma: modified radical neck dissection improves prognosis. *Arch Surg* 1998; 133: 276–80.
58. Biermann M, Pixberg MK, Schuck A et al. Clinical outcomes in the Multicenter Study Differentiated Thyroid Carcinoma (MSDS): interim report after 784 patient-years of follow-up [Abstract]. *Nuklearmedizin* 2006; 45: 26.
59. Dralle H, Sekulla C, Haerting J et al. Risk factors of paralysis and functional outcome after recurrent laryngeal nerve monitoring in thyroid surgery. *Surgery* 2004; 136: 1310–22.
60. Dralle H, Machens A, Brauckhoff M et al. Surgery of thyroid cancer: should the surgical guidelines be revised following the introduction of the new TNM classification? *Onkologie* 2005; 11: 58–69.
61. Thomusch O, Sekulla C, Ukkat J et al. Qualitätssicherungsstudie benigne und maligne Struma. Prospektive multizentrische Erhebungsstudie mit 7617 Patienten. *Zentralbl Chir* 2001; 126: 664–71.
62. Hölzer S, Reiners C, Mann K et al. Patterns of care for patients with primary differentiated carcinoma of the thyroid gland treated in Germany during 1996. *Cancer* 2000; 89: 192–201.
63. Biermann M, Pixberg MK, Schober O. Complications due to treatment for locally invasive differentiated thyroid carcinoma (DTC) [Abstract]. *Nuklearmedizin* 2005; 44: A59–60.
64. Dralle H, Sekulla C, Haerting J et al. Risk factors of paralysis and functional outcome after recurrent laryngeal nerve monitoring in thyroid surgery. *Surgery* 2004; 136: 1310–22.
65. Pacini F, Schlumberger M, Harmer C et al. Post-surgical use of radioiodine (131I) in patients with papillary and follicular thyroid cancer and the issue of remnant ablation: a consensus report. *Eur J Endocrinol* 2005; 153: 651–9.
66. Hilditch TE, Dempsey MF, Bolster AA, McMenemin RM, Reed NS. Self-stunning in thyroid ablation: evidence from comparative studies of diagnostic 131I and 123I. *Eur J Nucl Med Mol Imaging* 2002; 29: 783–8.
67. Lassmann M, Luster M, Hanscheid H, Reiners C. Impact of 131I diagnostic activities on the biokinetics of thyroid remnants. *J Nucl Med* 2004; 45: 619–25.
68. Dietlein M, Dressler J, Eschner W et al. Procedure guideline for radioiodine test (version 2). *Nuklearmedizin* 2003; 42: 116–19.
69. Thyroid Carcinoma Task Force. AACE/AAES medical/surgical guidelines for clinical practice: management of thyroid carcinoma. *Endocr Pract* 2001; 7: 203–18.
70. Dietlein M, Dressler J, Eschner W et al. Procedure guideline for iodine-131 whole-body scintigraphy for differentiated thyroid cancer (version 2). *Nuklearmedizin* 2003; 42: 123–5.
71. Pacini F, Ladenson PW, Schlumberger M et al. Radioiodine ablation of thyroid remnants after preparation with recombinant human thyrotropin in differentiated thyroid carcinoma: results of an international, randomized, controlled study. *J Clin Endocrinol Metab* 2006; 91: 926–32.

72. Dietlein M, Dressler J, Farahati J et al. Procedure guidelines for radioiodine therapy of differentiated thyroid cancer (version 2). *Nuklearmedizin* 2004; 43: 115–20.
73. Samaan NA, Schultz PN, Hickey RC et al. The results of various modalities of treatment of well differentiated thyroid carcinomas: a retrospective review of 1599 patients. *J Clin Endocrinol Metab* 1992; 75: 714–20.
74. Taylor T, Specker B, Robbins J et al. Outcome after treatment of high-risk papillary and non-Hurthle-cell follicular thyroid carcinoma. *Ann Intern Med* 1998; 129: 622–7.
75. Sawka AM, Thephamongkhon K, Brouwers M et al. Clinical review 170: a systematic review and metaanalysis of the effectiveness of radioactive iodine remnant ablation for well-differentiated thyroid cancer. *J Clin Endocrinol Metab* 2004; 89: 3668–76.
76. Beierwaltes WH, Rabbani R, Dmuchowski C et al. An analysis of ‘ablation of thyroid remnants’ with I-131 in 511 patients from 1947–1984: experience at University of Michigan. *J Nucl Med* 1984; 25: 1287–93.
77. Johansen K, Woodhouse NJ, Odugbesan O. Comparison of 1073 MBq and 3700 MBq iodine-131 in postoperative ablation of residual thyroid tissue in patients with differentiated thyroid cancer. *J Nucl Med* 1991; 32: 252–4.
78. Creutzig H. High or low dose radioiodine ablation of thyroid remnants? *Eur J Nucl Med* 1987; 12: 500–2.
79. Bal C, Padhy AK, Jana S, Pant GS, Basu AK. Prospective randomized clinical trial to evaluate the optimal dose of 131 I for remnant ablation in patients with differentiated thyroid carcinoma. *Cancer* 1996; 77: 2574–80.
80. Bal CS, Kumar A, Pant GS. Radioiodine dose for remnant ablation in differentiated thyroid carcinoma: a randomized clinical trial in 509 patients. *J Clin Endocrinol Metab* 2004; 89: 1666–73.
81. Doi SA, Woodhouse NJ. Ablation of the thyroid remnant and 131I dose in differentiated thyroid cancer. *Clin Endocrinol (Oxf)* 2000; 52: 765–73.
82. Yeung HW, Humm JL, Larson SM. Radioiodine uptake in thyroid remnants during therapy after tracer dosimetry. *J Nucl Med* 2000; 41: 1082–5.
83. Fatourehchi V, Hay ID, Mullan BP et al. Are posttherapy radioiodine scans informative and do they influence subsequent therapy of patients with differentiated thyroid cancer? *Thyroid* 2000; 10: 573–7.
84. Pacini F, Lippi F, Formica N et al. Therapeutic doses of iodine-131 reveal undiagnosed metastases in thyroid cancer patients with detectable serum thyroglobulin levels. *J Nucl Med* 1987; 28: 1888–91.
85. de Keizer B, Koppeschaar HP, Zelissen PM et al. Efficacy of high therapeutic doses of iodine-131 in patients with differentiated thyroid cancer and detectable serum thyroglobulin. *Eur J Nucl Med* 2001; 28: 198–202.
86. Koh JM, Kim ES, Ryu JS et al. Effects of therapeutic doses of 131I in thyroid papillary carcinoma patients with elevated thyroglobulin level and negative 131I whole-body scan: comparative study. *Clin Endocrinol (Oxf)* 2003; 58: 421–7.
87. Pineda JD, Lee T, Ain K, Reynolds JC, Robbins J. Iodine-131 therapy for thyroid cancer patients with elevated thyroglobulin and negative diagnostic scan. *J Endocrinol Metab* 1995; 80: 1488–92.
88. van Tol KM, Jager PL, de Vries EG et al. Outcome in patients with differentiated thyroid cancer with negative diagnostic whole-body scanning and detectable stimulated thyroglobulin. *Eur J Endocrinol* 2003; 148: 589–96.
89. Ali N, Sebastian C, Foley RR et al. The management of differentiated thyroid cancer using 123I for imaging to assess the need for 131I therapy. *Nucl Med Commun* 2006; 27: 165–9.
90. Cohen JB, Kalinyak JE, McDougall IR. Clinical implications of the differences between diagnostic 123I and post-therapy 131I scans. *Nucl Med Commun* 2004; 25: 129–34.
91. de Geus-Oei LF, Oei HY, Hennemann G, Krenning EP. Sensitivity of 123I whole-body scan and thyroglobulin in the detection of metastases or recurrent differentiated thyroid cancer. *Eur J Nucl Med Mol Imaging* 2002; 29: 768–74.
92. Alzahrani AS, Bakheet S, Al Mandil M et al. 123I isotope as a diagnostic agent in the follow-up of patients with differentiated thyroid cancer: comparison with post 131I therapy whole body scanning. *J Clin Endocrinol Metab* 2001; 86: 5294–300.
93. Mandel SJ, Shankar LK, Benard F, Yamamoto A, Alavi A. Superiority of iodine-123 compared with iodine-131 scanning for thyroid remnants in patients with differentiated thyroid cancer. *Clin Nucl Med* 2001; 26: 6–9.
94. Shankar LK, Yamamoto AJ, Alavi A, Mandel SJ. Comparison of 123I scintigraphy at 5 and 24 hours in patients with differentiated thyroid cancer. *J Nucl Med* 2002; 43: 72–6.
95. Rosario PW, Maia FF, Cardoso LD et al. Correlation between cervical uptake and results of postsurgical radioiodine ablation in patients with thyroid carcinoma. *Clin Nucl Med* 2004; 29: 358–61.
96. Shapiro B, Rufini V, Jarwan A et al. Artifacts, anatomical and physiological variants, and unrelated diseases that might cause false-positive whole-body 131-I scans in patients with thyroid cancer. *Semin Nucl Med* 2000; 30: 115–32.
97. Leitha T, Staudenherz A. Frequency of diagnostic dilemmas in 131I whole body scanning. *Nuklearmedizin* 2003; 42: 55–62.
98. Biermann M, Pixberg M, Riemann B et al. Radioiodine therapy of thyroid carcinoma. *Onkologie* 2005; 11: 70–7.
99. Tharp K, Israel O, Hausmann J et al. Impact of 131I-SPECT/CT images obtained with an integrated system in the follow-up of patients with thyroid carcinoma. *Eur J Nucl Med Mol Imaging* 2004; 31: 1435–42.
100. Schönberger J, Männer P, Fuchs E, Eilles C. Doppelisotopszintigraphie zur verbesserten anatomischen Lokalisierbarkeit Iod-positiver Metastasen beim schilddrüsenkarzinom. *Nuklearmedizin* 2004; 43: A54.
101. Alexander C, Bader JB, Schaefer A, Finke C, Kirsch CM. Intermediate and long-term side effects of high-dose radioiodine therapy for thyroid carcinoma. *J Nucl Med* 1998; 39: 1551–4.
102. Mandel SJ, Mandel L. Radioactive iodine and the salivary glands. *Thyroid* 2003; 13: 265–71.
103. Nakada K, Ishibashi T, Takei T et al. Does lemon candy decrease salivary gland damage after radioiodine therapy for thyroid cancer? *J Nucl Med* 2005; 46: 261–6.
104. Bohuslavizki KH, Klutmann S, Brenner W et al. Radioprotection of salivary glands by amifostine in high-dose radioiodine treatment. Results of a double-blinded,

- placebo-controlled study in patients with differentiated thyroid cancer. *Strahlenther Onkol* 1999; 175 (Suppl 4): 6–12.
105. Lam MG, van Isselt JW, Nakada K. Re: does lemon candy decrease salivary gland damage after radioiodine therapy for thyroid cancer? *J Nucl Med* 2005; 46: 2118–19.
 106. Pacini F, Gasperi M, Fugazzola L et al. Testicular function in patients with differentiated thyroid carcinoma treated with radioiodine. *J Nucl Med* 1994; 35: 1418–22.
 107. Mazzaferri EL. Gonadal damage from ¹³¹I therapy for thyroid cancer. *Clin Endocrinol (Oxf)* 2002; 57: 313–14.
 108. Pomorski L, Bartos M, Narebski J. Pregnancy following operative and complementary treatment of thyroid cancer. *Zentralbl Gynakol* 2000; 122: 383–6.
 109. Schlumberger M, De Vathaire F, Ceccarelli C et al. Exposure to radioactive iodine-131 for scintigraphy or therapy does not preclude pregnancy in thyroid cancer patients. *J Nucl Med* 1996; 37: 606–12.
 110. Ceccarelli C, Bencivelli W, Morciano D, Pinchera A, Pacini F. ¹³¹I therapy for differentiated thyroid cancer leads to an earlier onset of menopause: results of a retrospective study. *J Clin Endocrinol Metab* 2001; 86: 3512–15.
 111. Schober O, Günter H-H, Schwarzrock R, Hundeshagen H. Hämatologische Langzeitveränderungen bei der Radioiodtherapie des Schilddrüsenkarzinoms. I. Periphere Blutbildveränderungen. *Strahlenther Onkol* 1987; 163: 464–74.
 112. Rubino C, de Vathaire F, Dottorini ME et al. Second primary malignancies in thyroid cancer patients. *Br J Cancer* 2003; 89: 1638–44.
 113. de Vathaire F, Schlumberger M, Delisle MJ et al. Leukaemias and cancers following iodine-131 administration for thyroid cancer. *Br J Cancer* 1997; 75: 734–9.
 114. Günter H-H, Schober O, Schwarzrock R, Hundeshagen H. Hämatologische Langzeitveränderungen nach Radiojodtherapie des Schilddrüsenkarzinoms. II. Knochenmarkveränderungen einschließlich Leukämien. *Strahlenther Onkol* 1987; 163: 475–85.
 115. Biko J, Demidchik YE, Reiners C. Spontanverlauf des pulmonal metastasierten kindlichen Schilddrüsenkarzinoms nach nicht vollständiger Elimination der Metastasen durch die hochdosierte Radiojodtherapie. Abstractband der 40 Jahrestagung der Deutschen Gesellschaft für Nuklearmedizin. Berlin: Blackwell 2002: 62.
 116. Cooper DS, Specker B, Ho M et al. Thyrotropin suppression and disease progression in patients with differentiated thyroid cancer: results from the National Thyroid Cancer Treatment Cooperative Registry. *Thyroid* 1998; 8: 737–44.
 117. Pujol P, Daures JP, Nsakala N et al. Degree of thyrotropin suppression as a prognostic determinant in differentiated thyroid cancer. *J Clin Endocrinol Metab* 1996; 81: 4318–23.
 118. McGriff NJ, Csako G, Gourgiotis L et al. Effects of thyroid hormone suppression therapy on adverse clinical outcomes in thyroid cancer. *Ann Med* 2002; 34: 554–64.
 119. Sawin CT, Geller A, Wolf PA et al. Low serum thyrotropin concentrations as a risk factor for atrial fibrillation in older persons. *N Engl J Med* 1994; 331: 1249–52.
 120. Biondi B, Palmieri EA, Klain M et al. Subclinical hyperthyroidism: clinical features and treatment options. *Eur J Endocrinol* 2005; 152: 1–9.
 121. Persoon AC, Van Den Ouweland JM, Wilde J et al. Clinical utility of an automated immunochemiluminometric thyroglobulin assay in differentiated thyroid carcinoma. *Clin Chem* 2006; 52: 686–91.
 122. Biermann M, Nofer JR, Riemann B et al. Clinical evaluation of a new highly sensitive thyroglobulin assay (Nichols Advantage®) in 99 patients with differentiated thyroid cancer (DTC) after total thyroidectomy [Abstract]. *Clin Chem* 2004; 50: A73.
 123. Haugen BR, Pacini F, Reiners C et al. A comparison of recombinant human thyrotropin and thyroid hormone withdrawal for the detection of thyroid remnant or cancer. *J Clin Endocrinol Metab* 1999; 84: 3877–85.
 124. Varma VM, Beierwaltes WH, Nofal NM, Nishiyama RH, Copp JE. Treatment of thyroid cancer. Death rates after surgery and after surgery followed by sodium iodide I ¹³¹. *JAMA* 1970; 214: 1437–42.
 125. Grigsby PW, Baglan K, Siegel BA. Surveillance of patients to detect recurrent thyroid carcinoma. *Cancer* 1999; 85: 945–51.
 126. Cailleux AF, Baudin E, Travagli JP, Ricard M, Schlumberger M. Is diagnostic iodine-131 scanning useful after total thyroid ablation for differentiated thyroid cancer? *J Clin Endocrinol Metab* 2000; 85: 175–8.
 127. Pacini F, Capezzone M, Elisei R et al. Diagnostic ¹³¹-iodine whole-body scan may be avoided in thyroid cancer patients who have undetectable stimulated serum Tg levels after initial treatment. *J Clin Endocrinol Metab* 2002; 87: 1499–501.
 128. Taylor H, Hyer S, Vini L et al. Diagnostic ¹³¹I whole body scanning after thyroidectomy and ablation for differentiated thyroid cancer. *Eur J Endocrinol* 2004; 150: 649–53.
 129. Schlumberger M, Baudin E. Serum thyroglobulin determination in the follow-up of patients with differentiated thyroid carcinoma. *Eur J Endocrinol* 1998; 183: 249–52.
 130. Alzahrani AS, Alsuhaibani H, Salam SA et al. Diagnostic accuracy of high-resolution neck ultrasonography in the follow-up of differentiated thyroid cancer: a prospective study. *Endocr Pract* 2005; 11: 165–71.
 131. Biermann M, Pixberg MK, Schober O. Changing patterns of care for locally advanced differentiated thyroid carcinoma (DTC) in German-speaking Europe since 1996 [abstract]. *Eur J Nucl Med* 2003; 30: S155.
 132. Chung JK, So Y, Lee JS et al. Value of FDG PET in papillary thyroid carcinoma with negative ¹³¹I whole-body scan. *J Nucl Med* 1999; 40: 986–92.
 133. Wang W, Macapinlac H, Larson SM et al. [¹⁸F]-2-fluoro-2-deoxy-D-glucose positron emission tomography localizes residual thyroid cancer in patients with negative diagnostic (¹³¹)I whole body scans and elevated serum thyroglobulin levels. *J Clin Endocrinol Metab* 1999; 84: 2291–302.
 134. Altenvoerde G, Lerch H, Kuwert T et al. Positron emission tomography with F-18-deoxyglucose in patients with differentiated thyroid carcinoma, elevated thyroglobulin levels, and negative iodine scans. *Langenbecks Arch Surg* 1998; 383: 160–3.
 135. Alnafisi NS, Driedger AA, Coates G, Moote DJ, Raphael SJ. FDG PET of recurrent or metastatic ¹³¹I-negative papillary thyroid carcinoma. *J Nucl Med* 2000; 41:1010–15.
 136. Grünwald F, Kalicke T, Feine U et al. Fluorine-18 fluoro-deoxyglucose positron emission tomography in thyroid cancer: results of a multicentre study. *Eur J Nucl Med* 1999; 26: 1547–52.

137. Wu HS, Huang WS, Liu YC et al. Comparison of FDG-PET and technetium-99m MIBI SPECT to detect metastatic cervical lymph nodes in well-differentiated thyroid carcinoma with elevated serum hTg but negative I-131 whole body scan. *Anticancer Res* 2003; 23: 4235–8.
138. Biermann M, Schober O. Should high hTg levels in absence of iodine uptake be treated? *Eur J Nucl Med* 2003; 30: 160–3.
139. Deichen JT, Schmidt C, Prante O et al. Influence of TSH on uptake of [18F]fluorodeoxyglucose in human thyroid cells in vitro. *Eur J Nucl Med Mol Imaging* 2004; 31: 507–12.
140. van Tol KM, Jager PL, Piers DA et al. Better yield of (18)fluorodeoxyglucose-positron emission tomography in patients with metastatic differentiated thyroid carcinoma during thyrotropin stimulation. *Thyroid* 2002; 12: 381–7.
141. Casara D, Rubello D, Saladini G et al. Different features of pulmonary metastases in differentiated thyroid cancer: natural history and multivariate statistical analysis of prognostic variables. *J Nucl Med* 1993; 34: 1626–31.
142. Dottorini ME, Vignati A, Mazzucchelli L, Lomuscio G, Colombo L. Differentiated thyroid carcinoma in children and adolescents: a 37-year experience in 85 patients. *J Nucl Med* 1997; 38: 669–75.
143. Reiners C. Radioiodine therapy in patients with pulmonary metastases of thyroid cancer: when to treat, when not to treat? *Eur J Nucl Med Mol Imaging* 2003; 30: 939–42.
144. Zettinig G, Fueger BJ, Passler C et al. Long-term follow-up of patients with bone metastases from differentiated thyroid carcinoma – surgery or conventional therapy? *Clin Endocrinol (Oxf)* 2002; 56: 377–82.
145. Mann K, Möller LC, Bockisch A et al. Chemotherapy for thyroid cancer. *Onkologie* 2005; 11: 78–86.
146. Schmutzler C, Kohrle J. Retinoic acid redifferentiation therapy for thyroid cancer. *Thyroid* 2000; 10: 393–406.
147. Simon D, Koehrlé J, Reiners C et al. Redifferentiation therapy with retinoids: therapeutic option for advanced follicular and papillary thyroid carcinoma. *World J Surg* 1998; 22: 569–74.
148. Grüning T, Tiepolt C, Zophel K et al. Retinoic acid for redifferentiation of thyroid cancer – does it hold its promise? *Eur J Endocrinol* 2003; 148: 395–402.
149. Simon D, Korber C, Krausch M et al. Clinical impact of retinoids in redifferentiation therapy of advanced thyroid cancer: final results of a pilot study. *Eur J Nucl Med* 2002; 29: 775–82.
150. Grünwald F, Menzel C, Bender H et al. Redifferentiation therapy-induced radioiodine uptake in thyroid cancer. *J Nucl Med* 1998; 39: 1903–6.
151. Börner AR, Petrich T, Weckesser E et al. Monitoring isotretinoin therapy in thyroid cancer using F18-FDG PET. *Eur J Nucl Med* 2002; 29: 231–6.

Therapy of medullary thyroid cancer

Aurore Oudoux, Catherine Ansquer, Jacques Barbet, David M Goldenberg, Jean-François Chatal, and Françoise Kraeber-Bodéré

Background

Epidemiology

Medullary thyroid carcinoma (MTC) is a neoplasm of the parafollicular C cells and belongs to the neuroendocrine tumor group. MTC represents 5–10% of thyroid cancers.¹ C cells secrete calcitonin (Ct), other polypeptides and glycoproteins, such as carcinoembryonic antigen (CEA), vasoactive intestinal polypeptide, and somatostatin. MTC may occur sporadically or in a hereditary form as familial MTC that includes multiple endocrine neoplasia type IIA, type IIB, and isolated familial MTC.² Germline mutations in the RET protooncogene have been identified in families with these syndromes, and genetic screening has become integrated to the clinical management.¹ Both sporadic and familial MTC are characterized by relatively slow tumor growth but early lymphatic metastatic spread. Metastases are already present in 35% of patients at the time of initial diagnosis.³

Prognosis

The prognosis of MTC varies from long-term survival to a much shorter duration in patients with poor prognostic factors, including age, initial stage, and biochemical markers (pre- and postoperative serum concentrations of Ct and CEA).⁴ After initial surgery, Saad et al. observed that the slope of the curve for serum CEA concentrations over time and its doubling time (DT) correlate well with the course of the disease.⁵ Recently, we confirmed this observation in a retrospective study performed on 65 MTC patients (6–75 years of age) after initial surgery:⁶ when Ct DT was < 6 months, 5- and 10-year survivals were 3/12 (25%) and 1/12 (8%), respectively; when Ct DT was between 6 months and 2 years, 5- and 10-year survivals were 11/12 (92%) and 3/8 (37%), respectively, whereas all 41 patients with Ct DT > 2 years were alive at the end of the study (Figure 19.1). TNM stage, European Organization for Research and Treatment of Cancer (EORTC) score, and Ct DT were significant predictors of

survival by univariate analysis, but only Ct DT remained an independent predictor of survival by multivariate analysis ($p=0.002$). Ct DT was a better predictor than CEA DT.

Imaging

One study performed in 35 patients with progressive MTC showed neck metastases in 81% of patients, mediastinal metastases in 54%, lung metastases in 34%, liver metastases in 43%, and bone involvement in 74%.⁷ Several imaging methods should be proposed for a patient with abnormal residual Ct level persisting after complete surgery: ultrasonography and computed tomography (CT) for neck exploration, and CT for chest, abdomen, and pelvis. Magnetic resonance imaging (MRI) seems to have an edge over CT for the detection of liver metastases from endocrine tumors.⁸ Moreover, MRI appears to be a sensitive imaging technique for detecting the spread of MTC to bone/bone marrow.⁷ It has a higher sensitivity than bone scintigraphy, which detects bone involvement at a relatively advanced stage of tumor infiltration, when an osteoblastic reaction has occurred. The advantage of bone scintigraphy is the evaluation of the whole skeleton. [¹⁸F]fluoro-2-deoxy-D-glucose-positron emission tomography or [¹⁸F]FDG-PET also appears to be of interest for the detection of disease throughout the body.⁹ [¹⁸F]dihydroxyphenylalanine(DOPA)-PET is another functional imaging procedure that seems to provide interesting results in neuroendocrine tumors.¹⁰

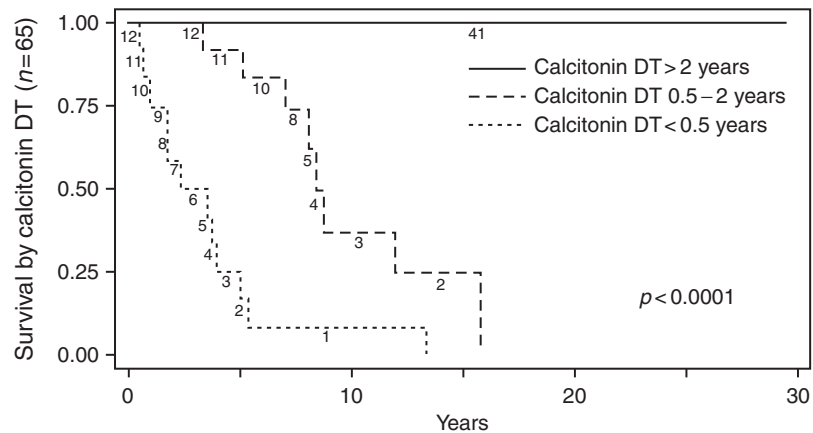
Therapeutic approaches

Conventional treatments

Surgery can cure patients with a localized tumor. However, MTC is often diagnosed at an advanced stage, resulting in a low cure rate. Indeed, 48–80% of patients are operated on with a stage-3 or -4 TNM; i.e. with lymph node involvement

Figure 19.1

Prognostic value of calcitonin doubling time (DT). Prognosis of patients with calcitonin DT <2 years was significantly worse than prognosis of patients with DT >2 years. (Reprinted with permission from reference 6.)



or extrathyroidal invasion.¹¹⁻¹³ In the management of this group, some investigators have recommended repeated lymph node dissection in the neck and mediastinum.^{14,15} The rate of postoperative normalization of serum Ct is low, ranging from 6 to 38%.^{16,17} Because of the relative scarcity of MTC, few prospective studies have investigated the efficacy of systemic treatments of metastatic disease. A review of several studies indicates that chemotherapy is associated with a partial response rate lower than 30%, with severe morbidity.^{18,19} An in vitro study using a human MTC cell line attributed resistance to chemotherapy to the association of overexpression of the *mdr* gene (multidrug resistance gene) and low proliferation fraction.²⁰ The analogs of somatostatin or interferon only have an effect on the symptoms induced by the hormones secreted by the tumor.²¹ The efficacy of internal radiotherapy using [¹³¹I]MIBG (metaiodobenzylguanidine), which can only be performed in about 35% of patients with a moderate to high tumor uptake, is generally limited to a symptomatic effect.²² Thus, new therapeutic strategies are needed. MTC cells express high amounts of CEA,²³ and thus this tumor appears to be a candidate for radioimmunotherapy (RIT) with anti-CEA monoclonal antibodies (mAb).

Radioimmunotherapy

Pre-targeting strategies

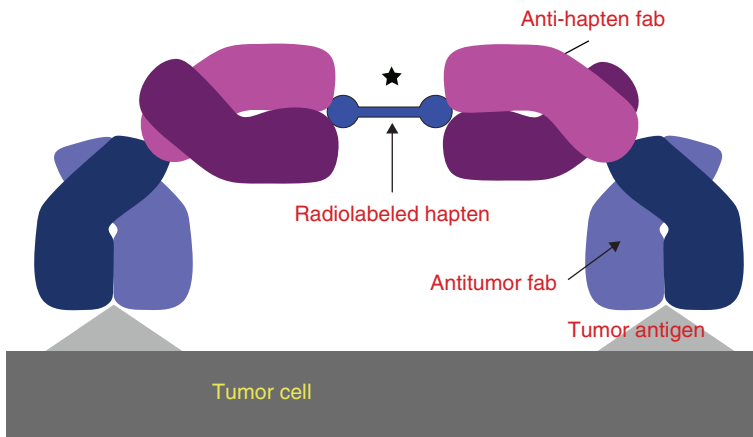
RIT is a new therapeutic modality using radiolabeled mAb targeting tumor antigens, and which has been validated for the treatment of non-Hodgkin's lymphoma. Several clinical studies have shown high response rates with both myeloablative and non-myeloablative doses, and improved survival with myeloablative activity in patients with recurrent or refractory lymphoma.^{24,25} In the more radioresistant solid tumors, RIT has not yet shown sufficient antitumor effects

in metastatic disease to suggest that it could be considered as a new therapeutic option.^{26,27} This is mainly due to a low therapeutic index with the current one-step RIT using directly labeled mAb.

Pre-targeting strategies have been proposed to overcome this problem.^{28,29} In the first step, an unlabeled antitumor immunoconjugate is injected. In a later step, when the immunoconjugate has sufficiently cleared from the circulation, the radionuclide is injected, coupled to a rapidly clearing effector with a high affinity for the immunoconjugate pre-localized in the tumor. Interesting clinical results have been obtained with the avidin-biotin system, using one or several chase steps to clear excess high-affinity ($K_d = 10^{-15}$ mol/l) antibody-avidin complexes.³⁰ The affinity enhancement system (AES) is another pre-targeting technique that uses a bispecific antibody (BsmAb) and a radiolabeled bivalent hapten (Figure 19.2). In this system, the hapten's affinity for the BsmAb is limited ($K_d = 10^{-8}$ mol/l), but the bivalent hapten binds avidly to the immunoconjugate bound to the surface of target cells, whereas hapten-BsmAb complexes in the circulation can dissociate and excess hapten is cleared, at least in part, through the kidneys. Increased tumor-to-normal tissue ratios and reduced toxicity have been demonstrated in animal RIT studies³¹⁻³⁴ and improved by adding a chase step.³⁵

Pre-targeted RIT in MTC

Two-step AES RIT using anti-CEA × anti-DTPA (diethylenetriaminepentaacetic acid) BsmAb and di-DTPA-[¹³¹I] bivalent hapten has been evaluated in MTC with interesting results. A study in CEA-producing MTC xenograft, comparing toxicity and efficacy of [¹³¹I]-labeled F(ab')₂ and pre-targeted bivalent hapten, showed that two-step RIT was as efficient as the one-step system and markedly less toxic.³⁴ Repeated treatments with AES agents increased efficacy without increasing toxicity.³⁶ These data allowed us to

**Figure 19.2**

Pre-targeted affinity enhancement system (AES). A bispecific antitumor (anti-carcinoembryonic antigen (CEA))/anti-hapten antibody is injected first and binds to the tumor antigen (CEA). A few days later the radiolabeled divalent hapten is injected and binds to the prelocalized bispecific antibody.

implement a clinical evaluation of this new therapeutic approach.

A first feasibility study was carried out in five patients with persistent disease or recurrence of MTC.³⁷ The purpose of this study was to estimate the dose delivered to tumor targets and normal tissues after two-step injections of a BsmAb anti-CEA \times anti-DTPA (F6-734) and a di-DTPA-^[131I]hapten. All patients showed positive immunoscintigraphy. Dosimetric results showed that small lesions received potentially tumoricidal irradiation (up to 174 cGy/mCi), a dose comparable with that delivered by iodine-131 internal radiotherapy to cervical metastases of differentiated thyroid carcinoma (43–140 cGy/mCi for lesions of 8–40 g).³⁸

A phase I/II clinical trial with escalating doses began, in 1996, to evaluate toxicity, pharmacokinetics, dosimetry, and antitumor activity of AES, using murine anti-CEA \times anti-DTPA (F6-734) BsmAb and di-DTPA-^[131I]hapten, in 26 patients with recurrence of MTC.³⁹ Twenty to 50 mg of BsmAb and 1.5–3.7 GBq of di-DTPA-^[131I] were injected 4 days apart. Clinical, biological, and morphological follow-up was carried out for 1 year after treatment. Immunoscintigraphy showed a good targeting of tumor sites suspected by conventional imaging (Figure 19.3). The biological half-life in tumors ranged from 3 to 95 days, and tumor doses ranged from 2.91 to 184 cGy/mCi. The estimated tumor-to-non-tumor dose ratios were 43.8 ± 53.4 , 29.6 ± 35.3 , 10.9 ± 3.6 , and 8.4 ± 10.0 for total body, red marrow, liver, and kidney, respectively. Dose limiting toxicity was hematological, and maximum tolerated activity was estimated at 48 mCi/m² in the group of patients with suspected bone marrow involvement. Preliminary data analysis showed a significant analgesic effect in five cases, five minor tumor responses, and four biological responses. The therapeutic responses were observed mainly in patients with a small tumor burden and after repeated courses of RIT. Nine patients developed human anti-mouse antibody (HAMA).

Because hematological toxicity was relatively high and immune responses frequent, further optimization of the

**Figure 19.3**

Immunoscintigraphy in medullary thyroid cancer (MTC) patient. Anterior view recorded 10 days after injection of ^[131I]hapten in a MTC patient, showing excellent targeting of multiple lung metastases.

treatment including the development of chimeric or humanized BsmAb became necessary. A prospective phase I optimization study was designed to determine optimal BsmAb dose, hapten activity, and pre-targeting interval.^{40,41} Thirty-four patients with CEA-expressing tumor were enrolled (non-MTC: 25 patients, MTC: nine patients). These patients received escalating doses of BsmAb hMN-14 (humanized anti-CEA antibody) \times m734 (murine anti-DTPA antibody) and escalating activities of radiolabeled di-DTPA-^[131I], 5 or 7 days later. Targeting, pharmacokinetics, dosimetry, toxicity, and efficacy were studied. A BsmAb dose of 40 mg/m² with a pre-targeting interval of 5 days appeared to be a good compromise between toxicity and efficacy. The rate of tumor stabilization was 45% in the 1-year assessment. HAMA elevation was observed in 8% of patients and HAHA (human anti-human antibody) in 33%. Accordingly, fully humanized BsmAb constructs have been produced for future clinical trials.

Increased hematological toxicity risk in MTC patients

The risk of severe hematological toxicity was higher in MTC patients than in patients with other CEA-expressing tumors, limiting the maximum activity that would be administered to 1.8 GBq/m².⁴⁰ Bone involvement (BI) is known to increase the hematological toxicity of internal radiotherapy, and could thus explain the toxicity observed with moderate radiation doses administered by RIT. Indeed we evaluated, retrospectively, the prevalence of BI using MRI and post-RIT immunoscintigraphy in 35 MTC patients enrolled in the two phase 1/2 clinical pre-targeted RIT trials.⁷ Bone scintigraphy, MRI, and immunoscintigraphy detected bone/bone-marrow involvement in 74.3% of MTC patients (Figure 19.4).

RIT and effect on survival

Six years after the first pre-targeted RIT study and 3 years after the second, long-term disease stabilization was observed in 53% of the MTC patients, as documented by morphological imaging (CT, MRI) and serial Ct and CEA serum measurements. The survival of 29 patients given pre-targeted RIT has been compared to that of 39 contemporaneous untreated patients for whom data were collected by the French Tumor Endocrine Group (GTE).⁴² A second objective was to examine whether post-pre-targeted RIT variations of Ct DT could be used as a surrogate marker for survival by comparing, among treated patients, the survival of biological responders and non-responders, defining a responder as showing at least a 100% increase in Ct DT. Overall survival (OS) was significantly longer in high-risk (Ct DT <2 years) treated than in high-risk untreated



Figure 19.4

Bone/bone-marrow involvement in a MTC patient.

(a) Immunoscintigraphy image (posterior view) recorded 7 days after injection of ^[131I]hapten shows high bone-marrow uptake; (b) magnetic resonance imaging (MRI) confirms bone marrow metastases.

patients (median OS, 110 vs. 61 months; $p < 0.030$). Forty-seven percent of patients, defined as biological responders, experienced significantly longer survival than did non-responders (median OS, 159 vs. 109 months; $p < 0.035$) or untreated patients (median OS, 159 vs. 61 months; $p < 0.010$) (Figure 19.5). Treated patients with bone/bone marrow disease had a longer survival than patients without such involvement (10-year OS of 83% vs. 14%; $p < 0.023$). Toxicity was mainly hematological and related to bone/bone-marrow tumor spread.

Procedure of pre-targeted radioimmunotherapy

A French phase 2 pre-targeted RIT study is ongoing, with the aim to evaluate the response rate, time to progression, and overall survival as endpoints in two separate groups of MTC patients: those with minimum residual disease (elevated Ct without imaging evidence of disease) and those with measurable disease. In this study, patients receive 40 mg/m² of BsmAb and 1.8 GBq/m² of radiolabeled di-DTPA-^[131I], 4–6 days apart. They are kept in lead-shielded rooms for 5–7 days, until the exposure rate decreases to less

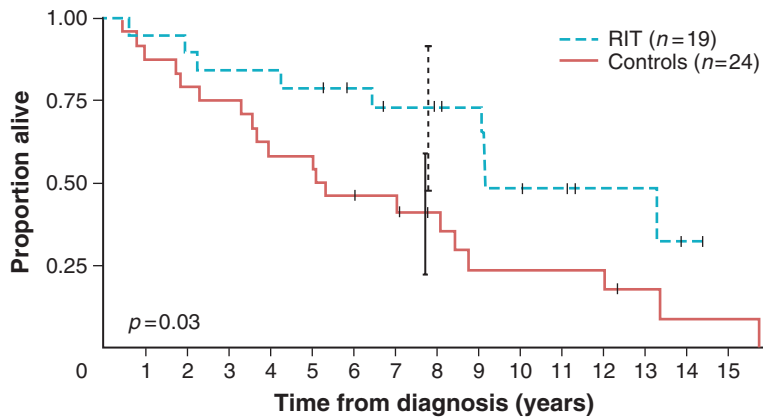


Figure 19.5

Survival of MTC patients treated by pre-targeted radioimmunotherapy (RIT). Overall survival in patients with calcitonin doubling time less than 2 years (high-risk group) was significantly longer after pre-targeted radioimmunotherapy than in the untreated control group. Vertical bars correspond to 95% confidence interval for survival rate at median follow-up. (Reprinted with permission from reference 42.)

than 25 $\mu\text{Sv/h}$. Whole body immunoscintigraphy is recorded 5–7 days after hapten infusion to document tumor targeting. The toxicity is monitored by clinical examination 15 and 30 days after RIT and at 3, 6, and 12 months; complete peripheral blood cell counts every week during 2 months and at 3, 6, and 12 months after therapy; and by performing renal and hepatic function evaluations at 15, 30, 45, and 60 days and again at 3, 6, and 12 months after therapy. Human anti-BsmAb immune response is evaluated by HAMA and HAHA levels. Tumor response is assessed at 3 and 6 months after RIT and every 6 months during 36 months. This evaluation is performed by physical examination, determining serum biomarker levels and DT (Ct and CEA), and CT, MRI, and [^{18}F]FDG-PET studies.

Conclusion

If the efficacy of pre-targeted RIT in progressive MTC patients is confirmed in the ongoing phase 2 study, this treatment modality could become a standard in the post-surgery treatment of high-risk patients with progressing disease. Since synergistic antitumor effects between RIT and chemotherapy, especially using paclitaxel, have been demonstrated in animal studies, this combination should be evaluated in future clinical trials of pre-targeted RIT.^{43,44}

References

1. Marsh DJ, Learoyd DL, Robinson BG. Medullary thyroid carcinoma: recent advances and management update. *Thyroid* 1995; 5: 407–24.
2. Grauer A, Raue F, Gagel RF. Changing concepts in the management of hereditary and sporadic medullary thyroid carcinoma. *Endocrinol Metab Clin North Am* 1990; 19: 613–35.
3. Lairmore TC, Wells SA Jr. Medullary carcinoma of the thyroid: current diagnosis and management. *Semin Surg Oncol* 1991; 7: 92–9.

4. Van Heerden JA, Grant CS, Gharib H et al. Long term course of patients with persistent hypercalcitoninemia after apparent curative primary surgery for medullary thyroid carcinoma. *Ann Surg* 1990; 212: 395–400.
5. Saad MF, Fritsche HA, Samaan NA. Diagnostic and prognostic values of carcinoembryonic antigen in medullary carcinoma of the thyroid. *J Clin Endocrinol Metab* 1984; 58: 889–94.
6. Barbet J, Campion L, Kraeber-Bodéré F et al. Prognostic impact of serum calcitonin and carcinoembryonic antigen doubling-times in patients with medullary thyroid carcinoma. *J Clin Endocrinol Metab* 2005; 90: 6077–84.
7. Mirallié E, Vuillez JP, Bardet S et al. High frequency of bone/bone marrow involvement in advanced medullary thyroid cancer. *J Clin Endocrinol Metab* 2005; 90: 779–88.
8. Dromain C, de Baere T, Lumbroso J et al. Detection of liver metastases from endocrine tumors: a prospective comparison of somatostatin receptor scintigraphy, computed tomography, and magnetic resonance imaging. *J Clin Oncol* 2005; 23: 70–8.
9. Oudoux A, Salaun PY, Ansquer C et al. Positron emission tomography with F-18-fluorodeoxyglucose (PET-FDG) in patients with rapidly progressing medullary thyroid carcinoma (MTC). *J Nucl Med* 2006; 47 (Suppl 1): 328 (abstr).
10. Hoegerle S, Althoefer C, Ghanem N et al. 18F-DOPA positron emission tomography for tumour detection in patients with medullary thyroid carcinoma and elevated calcitonin levels. *Eur J Nucl Med* 2001; 1: 64–71.
11. Machens A, Gimm O, Ukkat J et al. Improved prediction of calcitonin normalization in medullary thyroid carcinoma patients by quantitative lymph node analysis. *Cancer* 2000; 88: 1909–15.
12. Fleming J, Lee J, Bouvet M et al. Surgical strategy for the treatment of medullary thyroid carcinoma. *Ann Surg* 1999; 230: 697–707.
13. Weber T, Schilling T, Franck-Raue K et al. Impact of modified radical neck dissection on biochemical cure in medullary thyroid carcinomas. *Surgery* 2001; 130: 1044–9.
14. Dralle H, Damm I, Scheumann GF, Kotzerke J, Kupsch E. Frequency and significance of cervicomediastinal lymph node metastases in medullary thyroid carcinoma: results of a compartment-oriented microdissection method. *Henry Ford Hosp Med J* 1992; 40: 264–7.
15. Machens A, Gimm O, Ukkat J, Dralle H. Repeat mediastinal lymph node dissection for palliation in advanced medullary thyroid carcinoma. *Langenbecks Arch Surg* 1999; 384: 271–6.

16. Vitale G, Caraglia M, Ciccarelli A et al. Current approaches and perspectives in the therapy of medullary thyroid carcinoma. *Cancer* 2001; 91: 1798–808.
17. Moley JF, Dilley W, DeBenedetti M. Improved results of cervical re-operation for medullary thyroid carcinoma. *Ann Surg* 1997; 225: 734–43.
18. Schlumberger M, Abdelmouene N, Delisle MJ, Couette JE. Treatment of advanced medullary thyroid cancer with an alternating combination of 5 FU-streptozocin and 5 FU-dacarbazine. The Groupe d'Etude des Tumeurs à Calcitonine (GETC). *Br J Cancer* 1995; 71: 363–5.
19. Wu LT, Averbuch SD, Ball DW et al. Treatment of advanced medullary thyroid carcinoma with a combination of cyclophosphamide, vincristine, and dacarbazine. *Cancer* 1994; 73: 432–6.
20. Yang KP, Liang YF, Samaan NA. Intrinsic drug resistance in a human medullary thyroid carcinoma cell line: association with overexpression of mdrl gene and low proliferation. *Anticancer Res* 1991; 11: 1065–8.
21. Lupoli G, Cascone E, Arlotta F et al. Treatment of advanced medullary thyroid carcinoma with a combination of recombinant interferon α -2b and octreotide. *Cancer (Phila)* 1996; 78: 1114–18.
22. Hoefnagel CA. Metaiodobenzylguanidine and somatostatin in oncology: role in management of neural crest tumours. *Eur J Nucl Med* 1994; 21: 561–81.
23. Ishikawa N, Hamada S. Association of medullary carcinoma of the thyroid with carcinoembryonic antigen. *Br J Cancer* 1976; 34: 111–15.
24. Press OW, Eary JF, Gooley T et al. A phase I/II trial of iodine-131-tositumomab (anti-CD20), etoposide, cyclophosphamide, and autologous stem cell transplantation for relapsed B-cell lymphomas. *Blood* 2000; 96: 2934–42.
25. Gopal AK, Gooley TA, Maloney DG et al. High-dose radioimmunotherapy versus conventional high-dose therapy and autologous hematopoietic stem cell transplantation for relapsed follicular non-Hodgkin lymphoma: a multivariable cohort analysis. *Blood* 2003; 102: 2351–7.
26. Chatal JF, Mahé M. Therapeutic use of radiolabeled antibodies. In: Murray P, Ell P, eds. *Nuclear Medicine in Clinical Diagnosis and Treatment*. Edinburgh: Churchill Livingstone, 1998: 1101–14.
27. Goldenberg DM. Targeted therapy of cancer with radiolabeled antibodies. *J Nucl Med* 2002; 5: 693–713.
28. Barbet J, Kraeber-Bodéré F, Vuillez JP et al. Pretargeting with the affinity enhancement system for radioimmunotherapy. *Cancer Biother Radiopharm* 1999; 14: 153–66.
29. Chang CH, Sharkey RM, Rossi EA et al. Molecular advances in pretargeting radioimmunotherapy with bispecific antibodies. *Mol Cancer Ther* 2002; 1: 553–63.
30. De Santis R, Anastasi AM, D'Alessio et al. Novel antitenascin antibody with increased tumour localisation for Pretargeted Antibody-Guided RadioImmunoTherapy (PAGRIT). *Br J Cancer* 2003; 88: 996–1003.
31. Le Doussal JM, Martin M, Gautherot E, Delaage M, Barbet J. In vitro and in vivo targeting of radiolabeled monovalent and divalent haptens with dual specificity monoclonal antibody conjugates: enhanced divalent hapten affinity for cell-bound antibody conjugate. *J Nucl Med* 1989; 30: 1358–66.
32. Le Doussal JM, Gruaz-Guyon A, Martin M et al. Targeting of indium-111-labeled bivalent hapten to human melanoma mediated by bispecific monoclonal antibody conjugates: imaging of tumors hosted in nude mice. *Cancer Res* 1990; 50: 3445–52.
33. Hosono M, Hosono M, Kraeber-Bodéré F et al. Biodistribution and dosimetry study in medullary thyroid cancer xenograft using bispecific antibody and iodine-125-labeled bivalent hapten. *J Nucl Med* 1998; 39: 1608–13.
34. Kraeber-Bodere F, Faivre-Chauvet A, Sai-Maurel C et al. Bispecific antibody and bivalent hapten radioimmunotherapy in CEA-producing medullary thyroid cancer xenograft. *J Nucl Med* 1999; 40: 198–204.
35. Mirallié E, Sai-Maurel C, Faivre-Chauvet et al. Improved pre-targeted delivery of radiolabelled hapten to human tumour xenograft in mice by avidin chase of circulating bispecific antibody. *Eur J Nucl Med Mol Imaging* 2005; 32: 901–9.
36. Kraeber-Bodere F, Faivre-Chauvet A, Sai-Maurel C et al. Toxicity and efficacy of radioimmunotherapy in carcinoembryonic antigen-producing medullary thyroid cancer xenograft: comparison of iodine 131-labeled F(ab')₂ and pretargeted bivalent hapten and evaluation of repeated injections. *Clin Cancer Res* 1999; 5: 3183s–9s.
37. Bardies M, Bardet S, Faivre-Chauvet A et al. Bispecific antibody and iodine-131-labeled bivalent hapten dosimetry in patients with medullary thyroid or small-cell lung cancer. *J Nucl Med* 1996; 37: 1853–9.
38. Thomas SR, Maxon MR, Kereiakes JG, Saenger EL. Quantitative external counting techniques enabling improved diagnostic and therapy decisions in patients with well-differentiated thyroid cancer. *Radiology* 1977; 122: 731–7.
39. Kraeber-Bodere F, Bardet S, Hoefnagel CA et al. Radioimmunotherapy in medullary thyroid cancer using bispecific antibody and iodine 131-labeled bivalent hapten: preliminary results of a phase I/II clinical trial. *Clin Cancer Res* 1999; 5: 3190–8.
40. Kraeber-Bodere F, Faivre-Chauvet A, Ferrer L et al. Pharmacokinetics and dosimetry studies for optimisation of carcinoembryonic antigen x anti-hapten bispecific antibody mediated pretargeting of iodine-131-labeled hapten in a phase I radioimmunotherapy trial. *Clin Cancer Res* 2003; 9: 3973–81.
41. Kraeber-Bodere F, Rousseau C, Bodet-Millin C et al. Targeting, toxicity and efficacy of 2-step, pretargeted radioimmunotherapy using a chimeric bispecific antibody and 131-I-labeled bivalent hapten in a phase I optimisation clinical trial. *J Nucl Med* 2006; 47: 247–55.
42. Chatal JF, Campion L, Kraeber-Bodéré F et al.; for the French GTE Group. Survival improvement in medullary thyroid carcinoma patients given pretargeted CEA radioimmunotherapy. *J Clin Oncol* 2006; 24: 1705–11.
43. Kraeber-Bodere F, Sai-Maurel C, Campion L et al. Enhanced antitumor activity of combined pretargeted radioimmunotherapy and paclitaxel in medullary thyroid cancer xenograft. *Mol Cancer Ther* 2002; 1: 267–74.
44. Stein R, Juweid M, Zhang CH et al. Assessment of combined radioimmunotherapy and chemotherapy for treatment of medullary thyroid cancer. *Clin Cancer Res* 1999; 5: 3199–206.

Therapy of lymphoma

Tim Illidge and Yong Du

Background

Lymphomas represent abnormal proliferations of B or T cells and are currently classified on the basis of the histological appearance into Hodgkin's lymphoma (HL) and non-Hodgkin's lymphoma (NHL). HL is now curable in the majority of patients with modern treatment approaches which usually involve chemotherapy, or in combination with radiotherapy. Radionuclide therapy does not play a part of the established approach, although clinical investigations are ongoing.¹ In contrast, impressive clinical progress has been made in the last decade with radiolabeled antibody therapy or radioimmunotherapy (RIT) applied to NHL. Following the recent approval of two radioimmunoconjugates (Zevalin[®] and Bexxar[®]) by the United States Food and Drug Administration (US FDA) and the European authorities (Zevalin[®]), RIT has become established as a new therapeutic modality for NHL. This chapter will thus focus on the scientific background and development of RIT, the current clinical and potential future clinical indications, a review of the efficacy data, and the practicalities of RIT delivery.

Non-Hodgkin's lymphoma

NHL encompasses many heterogeneous different histological subtypes. NHL is largely a disease of older adults, with peak incidence in individuals greater than 60 years of age (the average diagnosis age is 60). It is the fifth and sixth most common malignancy in females and males, respectively, and NHL is responsible for 4% of all cancers and 4% of cancer deaths seen in the United States.² The incidence of NHL has been continuously on the rise over the past 25 years, and the reasons for this are largely unknown. Data collected from the Survival, Epidemiology, and End Results (SEER) project demonstrated a two-fold rise in incidence (8/100 000 to 16/100 000) between 1973 and 1995. A majority (85%) of NHLs are of B-lymphocyte origin, while T-lymphocytes, natural killer cells, or unknown cell

type origins form the rest (15%).^{3,4} Although observational data have demonstrated an association between NHL and several toxic exposures, immune defects, or infectious diseases, the cause of NHL in most individuals is unknown, however.

The NHLs have in the past been divided into the clinical entities of 'low grade' and 'high grade', reflecting the biological behavior of the disease and the type of treatment approach that was generally adopted. Paradoxically, high-grade lymphomas are potentially curable, such as Burkitt's lymphoma, whereas low-grade lymphomas are still generally considered to be incurable with conventional therapy, although patients may live for a number of years and respond to treatment several times.⁵ The recognition and description of such heterogeneous lymphoma types has evolved over many years. Currently, the World Health Organization classification scheme for non-Hodgkin's lymphoma (Table 20.1)^{6,7} is widely accepted, and is a largely successful attempt to integrate clinical and new pathological information into one classification.

Antibody-targeted therapy in NHL

Despite the sensitivity of most lymphomas to initial therapy with chemotherapy or radiotherapy, the majority of patients with advanced NHL eventually relapse and die of their disease.⁵ Furthermore, patients with advanced low-grade lymphomas remain incurable, and their survival has not altered since the early 1960s. The introduction of monoclonal antibody (mAb) based therapy and more recently radioimmunotherapy (RIT) has provided fresh hope for NHL patients that their prognosis can be improved.

Following the advent of monoclonal antibody technology in the 1970s,⁸ there was a great expectation that mAb would provide effective targeted therapy for cancer. Over the past three decades, there has been intense therapeutic evaluation of a wide spectrum of mAb recognizing different tumor-specific or tumor-associated antigens. Finally in 1997, rituximab, a mAb directed at the CD20 antigen on the

Table 20.1 World Health Organization classification scheme of the more common non-Hodgkin's lymphomas

	<i>Frequency (%)</i>
<i>Mature B-cell neoplasms</i>	
B-cell chronic lymphocytic leukemia/small lymphocytic lymphoma	7
Lymphoplasmacytic lymphoma	1.5
Extranodal marginal zone B-cell lymphoma of MALT type	10
Follicular lymphoma	25
Mantle cell lymphoma	5–7
Diffuse large B-cell lymphoma	31
Burkitt's lymphoma	2
Other rarer lymphomas	
<i>T-cell and NK-cell neoplasms</i>	
	15

HTLV-1, human T-cell leukemia virus 1; MALT, mucosa-associated lymphoid tissue; NK, natural killer.

surface of B cells, was approved by the US FDA for the treatment of cancer, and this provided a very significant milestone in the history of targeted therapy. Rituximab has subsequently been successfully used in a wide variety of B-cell malignancies.⁹ The single agent response rates of rituximab, however, remain rather modest, with overall response rates in the order of around 50% and complete response rates usually in single figures for previously treated patients with follicular lymphoma.^{10,11}

The principles of radioimmunotherapy

Radioimmunotherapy (RIT) refers to the therapeutic administration of radionuclides chemically conjugated to mAb or mAb-derived constructs. It is a conceptually appealing approach for cancer treatment, where the conjugation of radioisotope to mAb enables the delivery of targeted radiotherapy in addition to the specific cytotoxic effects of the mAb. mAb can be generated to recognize and bind to either tumor-specific antigens or antigens that are highly expressed on tumor cells. mAb were initially regarded only to serve as direct carriers for the radionuclide, which delivers systemically targeted radiation to areas of disease with relative sparing of normal tissue. It is, however, becoming clearer that the mAb effector mechanisms may also play an important additional role in killing lymphoma cells. RIT therefore holds potential advantages of enhanced therapeutic effect over conventional external

beam radiation therapy (EBRT). The efficacy of RIT depends on a number of factors, including properties of the targeted antigen (specificity, density, availability, shedding, and heterogeneity of expression), the tumor (vascularity, blood flow, and permeability), and the mAb (specificity, immunoreactivity, stability, and affinity) and the properties of chosen radionuclides (emission characteristics, half-life, and availability).¹²

Over the past few years RIT has demonstrated vastly superior clinical responses to unlabeled anti-CD20 mAb.^{13,14} A variety of different mAb, delivery schedules, radioisotopes, and doses of radioactivity have been used in RIT and have resulted in impressive durable partial and complete responses in the treatment of non-Hodgkin's lymphoma (NHL).^{13,15,16} It now seems highly likely that RIT will play a significant role in the treatment of some NHLs following the US FDA approval of [⁹⁰Y]ibritumomab tiuxetan (Zevalin®) and [¹³¹I]tositumomab (Bexxar®).

Therapeutic approaches

The choice of target antigen

The pursuit of 'tumor-specific antigens' has been difficult, and most targets are in fact tumor-associated antigens that are more highly expressed on tumor cells than on normal cells. The exception is the 'tumor-specific' idiotype or cell surface immunoglobulin present on the B-cell lymphomas. Although anti-idiotype mAb can be prepared and appear

clinically efficacious, such a patient-specific approach is not feasible for large-scale production. Furthermore, another disadvantage of idiotype antigens is that these immunoglobulins on the B-cell surface are commonly shed into the circulation. Thus, high levels of idiotype are often present in the circulation and can interfere with administered radiolabeled mAb and prevent it from reaching the tumor.¹⁷

Therefore, although tumor-specific antigens sound the ideal targets, that degree of specificity is unusual, and in practice tumor-associated antigens, expressed abundantly on tumor cells as well as some normal tissues, represent the majority of potential targets. During the process of B- and T-cells developing from marrow stem cells, a variety of lymphocyte differentiation markers are expressed at different stages. These antigens are not tumor-specific but are generally B- or T-cell-specific. As most NHLs are of B-cell origin, the pan-B-cell antigens such as human leukocyte antigen DR (HLA-DR), CD19, CD20, CD22, CD37, and CD52 have been extensively evaluated as targets for RIT.^{18–26} Among them, CD20 has many of the characteristics thought to be important for an ideal target (Table 20.2)²⁷ which does not internalize or shed from the cell surface and initiates signal transduction that triggers apoptosis through a caspase-dependent pathway.^{28,29} CD20 is highly expressed on the majority of B-cell lymphomas but not expressed on stem cells or plasma cells, so that after treatment the B-cell pool is replenished. Currently, anti-CD20 directed approaches are dominating the clinical RIT of NHL, although other antigens such as CD22 are still being actively investigated.^{30,31}

The selection of radionuclide

The optimal radionuclide delivers the maximal dose of ionizing radiation to tumor sites whilst minimizing the radiation dose to normal tissue and to medical personnel.

Table 20.2 The characteristics of an ideal target antigen

Tumor cell specific
Highly expressed on tumor cells
No tendency to mutation
Not secreted or shed
Not rapidly modulated on antibody binding
Critical for target cell survival
Not expressed on critical or non-renewable host cells

The physical characteristics considered important for a radionuclide in RIT include half-life, type of radioactive emissions (α , β , or γ), and ionization path length. Particle energy and mean path length in tissue are important determinants of therapeutic efficacy. The emission profile of the radionuclide determines not only its suitability for therapy, but also the toxicological profile.

Animal studies have consistently indicated that the major dose-limiting organ for RIT is the bone marrow.³² With the advent of bone marrow and peripheral blood stem cell transplantation, the upper limit of the amount of tolerable radiation dose is likely to increase, and, in the mean time, also the wider choice of radionuclides.³⁰

The availability of radiolabeling techniques is another factor which limits the RIT application of radionuclides. The most frequently used radionuclides and their physical characteristics are listed in Table 20.3.

In practice, the choice of the optimal isotope for RIT remains controversial, with proponents advocating the relative merits of iodine-131, yttrium-90, rhenium-186, copper-67, and α emitters such as astatine-211.³⁰ Comparative studies are difficult to conduct, and scientifically sound randomized human trials have not been performed.

The vast majority of clinical trials so far have been conducted with either ¹³¹I or ⁹⁰Y because of their favorable emission characteristics, availability, and well documented radiochemistry that permits reliable and stable attachment to mAb. ¹³¹I has the advantage of a long history of successful use in the management of thyroid cancer and a well documented safety profile. It is readily available, inexpensive, and easily conjugated, and emits both β particles with a path length of 0.8 mm and penetrating γ emissions. The γ emissions enable uncomplicated imaging using a γ camera for dosimetry purposes, but result in a significant non-targeted normal tissue radiation dose, as well as radiation protection issues for visitors and medical/nursing staff.

⁹⁰Y offers a number of theoretical advantages over ¹³¹I, although the radioisotopes have not been directly compared, conjugated to the same mAb. ⁹⁰Y is a pure β emitter, delivering higher energy radiation (2.3 MeV vs. 0.6 MeV) at a longer path length (5.3 mm vs. 0.8 mm). This increased path length would be expected to enhance the ‘crossfire effect’ and could therefore potentially be advantageous in treating larger, poorly vascularized tumor nodules or tumors with heterogeneous antigen expression.³³ This longer path length will, however, increase the normal tissue dose when targeting microscopic disease, for which the shorter path length of ¹³¹I may be preferable. The half-life of 64 hours matches the biological half-life of murine monoclonal antibodies, and the absence of penetrating γ emissions enables delivery as an outpatient.³⁰ In addition, if a cell internalizes ⁹⁰Y, it is likely to be retained within the cell.³⁴ In contrast, if ¹³¹I conjugates are internalized by a cell they will be rapidly dehalogenated and the small ¹³¹I products rapidly released into the bloodstream, reducing

Table 20.3 Physical characteristics of radionuclides used in radioimmunotherapy

<i>Radioisotope</i>	<i>Half-life</i>	<i>Emission (MeV)</i>	<i>Path length (mm)</i>
Iodine-131	8.1 days	β , 0.6 γ (81%), 0.37	0.8
Yttrium-90	2.5 days	β , 2.3 γ , nil	5.3
Rhenium-186	3.7 days	β , 1.1 (γ (9%), 0.14	1.8
Iodine-125	60.1 days	Electron capture, 7.45 γ , 0.027	0.001
Copper-67	2.5 days	β , 0.4–0.6 γ , 0.185	0.6
Astatine-211	7 hours	α , 6.8 Electron capture, 7.45	0.065
Bismuth-213	1 hour	α , 7.8 γ , 0.72	0.07

desired tumor absorbed radiation dose and increasing normal tissue exposure to radiation.³⁵

The major disadvantages of ⁹⁰Y relate to its greater expense, relatively limited availability, and complicated chelation radiochemistry, making radiolabeling more difficult. In addition, as ⁹⁰Y is a pure β emitter, in the absence of γ emissions, there is a need to use a surrogate isotope, indium-111, to obtain images for biodistribution and dosimetry studies. Rhenium-186 and copper-67 have physical and chemical properties that make them attractive alternatives; however, their current limited availability has meant that these radioisotopes have received limited clinical use.³⁶

Astatine-211 is an α emitter producing a particle of very high energy but with a very short path length. The high linear energy transfer (LET) radiation of α emitters may be lethal to cells with a single hit; however, the very short path length means that the isotope must be internalized to be effective and is likely to have little or no 'crossfire effect'. The suitability of α emitters therefore appears limited to readily accessible tumors such as leukemia cells in blood or bone marrow. The short half-life of around 7 hours complicates administration, meaning that such radioisotopes are likely to require generation on the same site as delivery in the clinic. Despite this logistical hurdle, early clinical data in the treatment of leukemia appear extremely promising.^{37,38} Recent experimental RIT studies involving animal leukaemia models have also demonstrated the therapeutic potential of another α emitter, bismuth-213.^{39,40} Recently, Oh et al. reported impressive therapeutic effects using an Auger emitter, ²⁵I-labeled mAb targeting on a tumor blood vessel (endothelial cell) specific protein, anti-annex A1, to treat lung tumor bearing rats.⁴¹

The evolution of radioimmunotherapy

Initially, radiolabeled antibodies were assessed in radioimmunodetection (RID) or radioimmunoimaging (RII) using a γ camera to localize and identify tumor-specific binding. Early RIT trials dating back to the 1960s used ¹³¹I-labeled polyclonal antibodies, but these antibodies lacked homogeneity in specificity and affinity and resulted in tremendous in vivo variability.⁴² Accelerated by the availability of mAb technology, RIT attracted wide interest and led to extensive preclinical and clinical investigations in the 1980s. However, by the end of the 1980s many investigators had become increasingly despondent with the realization of some of the obstacles of using mAb in RIT: (1) the insufficient penetration of tumor tissue by mAb; (2) the low radiation doses delivered to tumors in patients via mAb being insufficient to have significant effects on tumor growth; (3) the prolonged retention of the radiolabeled mAb in the blood leading to increased myelotoxicity; and (4) the development of human anti-murine Ab (HAMA) to the administered murine origin mAb, which subsequently compromises repeated administration. These problems appeared to be related to the biological features of mAb molecules. Therefore, most investigators have since focused on manipulating the mAb itself in an effort to improve its performance in radionuclide delivery. A variety of different approaches have been investigated including mAb fragments, single chain Fv (scFv), bispecific mAb, and pre-targeting techniques.^{12,39,40,42–46}

In order to deliver a therapeutic dose of radiation to all tumor cells, the penetration of the radiolabeled mAb is crucial, especially for solid tumors. A variety of physical parameters are known to influence the penetration of protein molecules such as mAb into tumors. These include the infused protein dose of mAb, the circulating half-life of the mAb, the abundance of blood vessels perfusing tumor sites, the permeability of the tumor vessels, the interstitial fluid pressure and intratumoral pressure impeding mAb penetration of tumors, the binding avidity of mAb for tumor antigens, and the specificity of Ab binding.⁴⁷ One of the easiest ways to increase the penetration seems to be by using mAb fragments such as F(ab)₂, Fab, or scFv constructs, which are smaller than the intact mAb. Experimental data indicated that these fragments penetrate into tumors faster and have a shorter circulating half-life, which may have the benefit of less radiation exposure to normal organs.^{48,49} However, clinical trials revealed that these fragments have high renal retention, and the monovalent reagents (Fab and scFv) have lower avidities and much shorter tumor retention times and, therefore, reduced radiation dose delivered to the tumor. Besides the above disadvantages, the difficulty of producing a large enough quantity of these fragments, and the inability of such fragments to recruit host immune effectors which require Fc segments, also contribute to outweigh their penetration advantage. Although currently there are still investigators using bioengineering techniques to improve the features of radiolabeled mAb fragments, intact mAb are preferred for clinical RIT studies.³⁰

Most of the early antibody vectors used for RIT were murine in origin, and the development of a human anti-mouse antibody (HAMA) has been another significant challenge in the development of clinical RIT.⁵⁰ The development of a HAMA response is itself dependent on the integrity of the host immunity. Most cancer patients, greater than 80%, usually develop an immune response against a therapeutically administered murine or other species antibody even after a single injection. Such an immune response can occur with small protein doses of 1 mg of antibody fragments or smaller constructs, though with less frequency than found after the administration of intact immunoglobulin G (IgG).^{12,51} Repeated administration of antibody in a patient with a HAMA response can result in a severe immune reaction and rapid blood clearance, which may substantially reduce tumor uptake of radiolabeled mAb.¹² Patients treated in the majority of clinical RIT trials to date have been mainly relapsed 'low grade lymphoma', many of whom have been heavily pretreated and chemotherapy 'refractory'. As a consequence primarily of the previous chemotherapy exposure, in addition to a background of a probably impaired host immune system, these patients are observed to be less prone to develop an immune response to the given antibody, occurring among 10–30% patients after [¹³¹I]tositumomab or [¹³¹I]Lym-1.^{50,52}

Interestingly, Kaminski et al. observed that in 76 stage III and stage IV previously untreated NHL patients, after a single dosimetric dose in the course of treatment with [¹³¹I]tositumomab therapy, 48 (63%) developed a HAMA reaction. They also observed a reduced therapeutic effect in patients who developed a HAMA reaction. In this study, among 23 patients in whom antibody levels were more than five times the lowest level of detection within the first 7 weeks, the 5-year rate of progression-free survival was 35%, as compared with 70% for the remaining 53 patients ($p = 0.003$). The authors did not, however, discuss whether the potential mechanisms behind this compromised therapeutic effect in HAMA-positive patients was related to different biodistribution patterns of the infused therapeutic radiolabeled mAb.¹⁶

The use of recombination DNA technology to produce humanized or chimeric murine mAb has contributed effectively in overcoming the HAMA problem. These mAb are much less immunogenic, and allow for repeated mAb administration. Rituximab is one such chimeric mAb, and a variety of others are under investigation.⁹ In a study to assess the safety and efficacy of rituximab treatment, a multicenter, phase II study of eight consecutive weekly infusions of 375 mg/m² rituximab in patients with low-grade or follicular B-cell NHL who had relapsed or had failed primary chemotherapy was conducted. Among the 37 patients with a median age of 55 years who were treated, none developed human anti-chimeric antibody (HACA).⁵³ Interestingly, in a recently conducted phase I/II dose-escalation trial of rituximab in the treatment of systemic lupus erythematosus (SLE), although the amount of infused rituximab was much less, six out of 17 (35%) patients developed human anti-chimeric antibodies (HACA) at a level ≥ 100 ng/ml. In this study, rituximab was administered as a single infusion of 100 mg/m² (low dose), a single infusion of 375 mg/m² (intermediate dose), or four infusions (1 week apart) of 375 mg/m² (high dose). These HACA titers were observed to be associated with African-American ancestry, reduced B-cell depletion, and lower levels of rituximab at 2 months after initial infusion.⁵⁴

The humanized or chimeric mAb had been found to have longer circulating half-lives, which is thought to be secondary to their human Fc portion which is believed to be more compatible with human tissues. This prolonged circulating half-life may theoretically cause excessive radiation exposure to normal organs, and this initially led to concerns that humanized mAb may be less favorable for RIT.³⁰ However, recent RIT studies using [¹³¹I]-labeled rituximab have demonstrated favorable therapeutic results, and data suggest that radiolabeled chimeric mAb may not in fact have increased myelotoxicity.^{55–57} More importantly, the substantially reduced immunogenicity of rituximab makes it suitable for repeated administration, and therefore to deliver increased radiation doses to refractory or relapsed tumors.

Recent preclinical work using syngeneic murine B-cell lymphoma models has demonstrated that RIT is not simply targeted radiation therapy, and the mAb effector mechanisms played an important role in the success of RIT.^{58,59} In another recent report, Sharkey et al. have also postulated that the possible interaction between mAb and host immune effectors may have contributed significantly to the otherwise inexplicable therapeutic responses of ⁹⁰Y-labeled humanized anti-CD22 IgG ([⁹⁰Y]epratuzumab) in NHL patients.⁶⁰ These important insights may have an important impact on the future selection of mAb in RIT, with the possible use of combinations of mAb and radioimmunoconjugates.

Newer RIT approaches include pre-targeting RIT. Here, instead of labeling the vector mAb with radionuclides, the initial infused mAb is labeled with streptavidin and subsequently followed 1–2 days later by a clearing agent that binds to unbound mAb in the circulation before the therapeutic radionuclide-labeled biotin is administered. This radiolabeled biotin rapidly conjugates with the streptavidin, ensuring rapid targeting of the radiation to the lymphoma cells and minimizing exposure of non-antigen bearing cells to radiation. In animal models this technique has been shown to improve the ratio of tumor-to-normal tissue-absorbed radioactivity by a factor of 9, enabling safer dose escalation and improved responses.^{40,43,44,61} Limited numbers of patients have been treated by this pre-targeting approach thus far. Pilot clinical studies of this approach are now under way.^{61–63} Most recently, Forero et al. reported an impressive phase I clinical study of pre-targeted RIT for B-cell NHL in 15 patients. In this study, the ratio of average tumor to whole-body radiation dose reached 49. At the fixed low dose of ⁹⁰Y administered (555 MBq/m²), 21% (3/14) of patients achieved an objective response, and no RIT-induced hematological toxicity was observed.⁶⁴

Clinical progress of RIT for non-Hodgkin's lymphoma

Although clinical RIT trials in NHL differ in terms of eligibility criteria, antibody, and radioisotopes used, dose, number of treatments, doses of unlabeled mAb pre-infused or co-infused, and the biodistribution or dosimetry estimations required for the administration of a therapeutic dose of radiolabeled Ab, virtually all clinical studies performed to date have shown promising results.^{12,14,16,26,46,61,65}

Non-myeloablative RIT

DeNardo et al. pioneered RIT for NHL.^{24,66} In their early studies, patients were given fractionated doses (30–60 mCi) of ¹³¹I-labeled anti-HLA-DR mAb (Lym-1) at 2–6-week intervals.²⁴ Thirty patients with relapsed NHL or chronic

lymphocytic leukemia were treated. Three (10%) achieved complete remission (CR) and 14 (47%) achieved partial remission (PR) for an overall response rate of 57%. A subsequent trial investigating the efficacy of escalating doses of ¹³¹I-labeled Lym-1 (40–100 mCi/m²) achieved an overall response rate of 52% in 21 treatment courses administered to 20 patients, with seven patients (33%) achieving CR and four patients (19%) achieving PR.²⁴ Goldenberg et al. used ¹³¹I-labeled anti-CD22 Ab (LL2) to treat B-cell lymphomas. In one of their trials, four out of 17 patients achieved objective remission, including one CR.¹⁹ In another trial, ⁹⁰Y-labeled LL2 was administered to seven patients with B-cell lymphomas, two of whom achieved PR.⁶⁷ In a recent dose escalation trial using ⁹⁰Y-labeled humanized anti-CD22 mAb, among 16 treated patients the objective response rate was 62% and complete response rate 25%.⁶⁸

The majority of clinical trials of B-cell lymphomas and the most impressive clinical results to date have used radiolabeled anti-CD20 mAb. Kaminski and colleagues have conducted a series of trials at the University of Michigan using ¹³¹I labeled tositumomab (Bexxar®) for the treatment of relapsed follicular lymphoma.^{16,25,69,70} On the basis of these clinical trials, Bexxar® was approved by the US FDA in June, 2003.⁷¹

The Bexxar® therapeutic regimen is completed in four visits over 1–2 weeks, as shown in Table 20.4. This regimen involves an initial biodistribution/dosimetry study followed by a therapeutic infusion given 7–14 days later.

Each infusion of radiolabeled mAb is preceded by an infusion of 450 mg per patient of unlabeled 'cold' tositumomab as a pre-dose. Whole-body γ imaging is performed three times over the week following the trace labeled infusion to calculate the whole body half-time and the dose required for the therapeutic infusion to deliver 65–75 cGy of whole body irradiation (usually 100–150 mCi).⁷² In the study to evaluate the therapeutic efficacy of ¹³¹I-labeled tositumomab, a single course of [¹³¹I]tositumomab has shown to provide far unreachable disease-free survival over the last qualifying chemotherapy (LQC) received by 60 extensively pretreated patients with chemotherapy-refractory low-grade, or transformed low-grade NHL. In this study, the 60 patients acted as their own internal controls.²⁵

Myelosuppression was found to be the dose-limiting toxicity. Since 1990, over 800 patients with 'low grade' and transformed lymphoma have been treated with [¹³¹I]tositumomab. Long-term follow-up data were presented at the American Society of Hematology (ASH) Annual Meeting 2002 for 250 of these patients, indicating a response rate of 56%, with 30% of patients achieving a complete response (CR). Perhaps the most impressive fact was that 70% of the patients who achieved a CR are alive and remain in CR at up to 7.8 years, with a median follow-up of almost 4 years.⁷³ An analysis of prognostic factors has confirmed that this remarkable durability of response cannot be accounted for by patient selection in the reported trials.⁷⁴ Of the patients

Table 20.4 Bexxar® (^{131}I tositumomab) therapeutic regimen

*Dosimetric step**
beginning on day 0

Tositumomab
(450 mg, 60 min IV infusion)

^{131}I tositumomab
(35 mg mAb labeled with 185 MBq
 ^{131}I , 20 min IV infusion)

→

*Therapeutic step**
1 day between days 7 and 14

Tositumomab
(450 mg, 60 min IV infusion)

^{131}I tositumomab
(35 mg mAb labeled with patient-specific dose of ^{131}I to deliver
65–75 cGy total body dose, 20 min IV infusion)

Three total body scans for **dosimetry and biodistribution:**

day 0

day 2, 3 or 4

day 6 or 7

*Thyroid protection medication at least 24 hours prior to dosimetric dose and continuing for 14 days after therapeutic dose.
IV, intravenous; mAb, monoclonal antibody.

who achieved CR, 89% had stage III/IV disease, 32% had no response to their last therapy, 45% had > 4 prior therapies, 50% had bulky disease, and 43% had bone marrow involvement.

Impressive response rates have also been seen in patients who were refractory to rituximab. Horning and colleagues have treated 40 patients with low-grade NHL, 72% of whom had received four or more previous lines of therapy and 60% of whom had failed to respond to rituximab. An overall response rate of 68% with a CR rate of 30% was noted, and a median duration of response of 14.7 months reported. Nine of the 12 complete responders remained in CR at the time of presentation, with a range of 12–26 months.⁷⁵ More recently, an analysis including 230 patients treated with ^{131}I tositumomab was made. Independently assessed durable CRs were noted with similar frequency in patients with rituximab-refractory disease (28%) and rituximab-naïve patients, all of whom had chemotherapy-refractory disease (23%). With a median follow-up of 4.6 years, 75% of patients with durable CR continue in complete remission.⁷⁶

Highly promising results have also been seen in the frontline treatment of previously untreated low-grade lymphomas using ^{131}I tositumomab. The most recent update included 76 patients with a median follow-up of 5.1 years. An encouraging overall response rate of 95% was seen, with 75% achieving CR. The actuarial 5-year progression-free survival for all patients was 59%, with a median progression-free survival of 6.1 years. Hematological toxicity was moderate, with no patient requiring transfusion or hematopoietic growth factors.^{16,73,77} In a recent multicenter, randomized study comparing treatment outcomes for

^{131}I -labeled tositumomab and an equivalent total dose of unlabeled tositumomab, involving 78 patients with refractory/relapsed NHL (median follow-up 42.6 months), Davis et al. reported the following responses in ^{131}I -labeled tositumomab versus unlabeled tositumomab groups: overall response 55% vs. 19% ($p = 0.002$); complete response 33% vs. 8% ($p = 0.012$); median duration of overall response not reached vs. 28.1 months; median duration of complete response not reached in either arm; and median time to progression 6.3 vs. 5.5 months ($p = 0.031$), respectively. Although hematological toxicity was more severe and non-hematological adverse events were more frequent after ^{131}I -labeled tositumomab than after tositumomab alone, there were no serious infectious or bleeding complications. The frequency of developing HAMA was similar in the two arms at 27% (^{131}I -labeled tositumomab group) vs. 19% (tositumomab alone group), respectively. This study demonstrated that although unlabeled tositumomab showed single agent activity, the conjugation of ^{131}I to tositumomab significantly enhanced the therapeutic efficacy.¹⁴

A parallel series of clinical trials has also been conducted by investigators using ^{90}Y -labeled ibritumomab tiuxetan (Zevalin®), which was the first radioimmunoconjugate to be granted US FDA approval in February, 2002.¹³ The studies included in the FDA submission were a randomized controlled trial comparing ^{90}Y -labeled ibritumomab tiuxetan with rituximab in relapsed or refractory low-grade B-cell NHL.¹³ Seventy-three patients received two doses of rituximab 250 mg/m² a week apart as pre-dosing followed by a single dose of ^{90}Y -labeled ibritumomab tiuxetan 0.4 mCi/kg body weight. Seventy patients in the control

arm received rituximab 375 mg/m² weekly for 4 weeks. The overall response rate was 80% for the labeled antibody group versus 56% for the rituximab alone group ($p = 0.002$). Complete responses were 30% and 16% in the ⁹⁰Y-labeled ibritumomab tiuxetan and rituximab groups, respectively.

Myelosuppression was found to be the dose-limiting toxicity of RIT. An analysis of all patients treated in ⁹⁰Y-labeled ibritumomab tiuxetan trials ($n = 261$) indicated that 28% will experience grade 4 neutropenia and 8% will experience grade 4 thrombocytopenia.⁷⁸ ⁹⁰Y-labeled ibritumomab tiuxetan also appeared to be able to deliver durable remissions, and for those patients who achieved a CR, a median duration of response approaching 2 years and ongoing responses of more than 4 years have been reported.⁷⁹ These highly promising results demonstrated for the first time that RIT can lead to superior overall and complete response rates compared to those seen with 'naked' mAb. Clinical responses have also been observed for ⁹⁰Y-labeled ibritumomab tiuxetan in transformed follicular and relapsed diffuse large B-cell lymphoma (DLBC). A phase I/II study reported a response rate of 58% with a 33% CR rate in a group of patients who had relapsed following two previous chemotherapy regimens that included

CHOP (cyclophosphamide, doxorubicin, vincristine, prednisolone).⁷⁸

Table 20.5 compares the characteristics of ⁹⁰Y-labeled ibritumomab tiuxetan (Zevalin®) and ¹³¹I-labeled tositumomab (Bexxar®).

Myeloablative RIT

In contrast to most of the other investigators, the Seattle group has investigated high-dose 'myeloablative' RIT for patients with relapsed lymphomas, supported by autologous stem-cell transplantation (ASCT).^{15,22} The use of ASCT has allowed dose escalation to at least three-fold the dose delivered in the non-myeloablative approach, although the established approach of delivering 75 cGy to the whole body with ¹³¹I-labeled tositumomab (anti-B1) has proved to be extremely well tolerated, with predictable grade 4 thrombocytopenia or neutropenia occurring in fewer than 10%, and rarely manifested clinically.^{52,69}

Press and colleagues in Seattle, using [¹³¹I]anti-B1, have pioneered the myeloablative approach and have arguably achieved the best results thus far reported in clinical RIT,

Table 20.5 Characteristics of [¹³¹I]tositumomab (Bexxar®) and [⁹⁰Y]ibritumomab tiuxetan (Zevalin®)

	¹³¹ I]tositumomab	⁹⁰ Y]ibritumomab tiuxetan
US trade name	Bexxar	Zevalin
Monoclonal antibody	Tositumomab (anti-B1) – murine	Ibritumomab (2B8) – murine
Chelation	Simple	More complex
Isotope	¹³¹ I	⁹⁰ Y
Isotope emissions	γ and β	β only
β Energy	0.606 MeV	2.293 MeV
β Particle path length	0.8 mm	5.3 mm
Isotope half-life	8 days	2.6 days
γ Energy	0.364 MeV	None
Radiation protection measures	4–6-day inpatient stay in shielded room	Outpatient
Isotope excretion	Renal (variable)	Limited
Normal tissue uptake	Thyroid (blocked with potassium iodate)	Bone
Pre-dose (unlabeled antibody)	Tositumomab (450 mg/patient)	Rituximab (250 mg/m ²) × 2
Dose	65–75 cGy whole body dose Dosimetric dose obligatory	11.1–14.8 MBq/kg depending on patient platelet count Dosimetric dose not required Dose reduction for thrombocytopenia

albeit in a highly selected group of patients. In a group of multiply relapsed patients with low-grade lymphoma, a durable CR rate of 73% was reported,⁸⁰ and outcomes have been shown to be superior to conventional high-dose chemotherapy and stem cell transplantation in a non-randomized cohort analysis.⁸¹ Following this success, the same group have reported a CR rate of 91% and a progression-free survival of 61% at 3 years in poor-prognosis mantle cell lymphoma using high-dose RIT with cyclophosphamide and etoposide chemotherapy followed by ASCT.⁸² In Germany, Behr et al. reported their initial myeloablative RIT study using high-dose (261–495 MBq) ¹³¹I-labeled rituximab, treating seven mantle cell NHL patients. In this study, six patients achieved CR and one PR.⁵⁷ Nevertheless, the much higher dose of administered radioimmunoconjugate does impose bigger safety problems, and currently there are very few centers in the world that have the necessary facilities to reproduce this type of approach. This makes the more widespread establishment of this approach seem unlikely at the current time; however, the data are sufficiently compelling to demand further investigation.

Although the high CR rates and prolonged remissions are encouraging, more than half of patients eventually relapse with single-agent RIT, even when given at maximal doses with stem-cell support. In an attempt to further increase the percentage of patients with durable remission, RIT is currently being investigated as a component of high-dose therapy, and both [¹³¹I]tositumomab and ⁹⁰Y-labeled ibritumomab tiuxetan have been added to high-dose chemotherapy with BEAM (BCNU, etoposide, Ara-C, melphalan). The early results have confirmed the feasibility of this approach and studies are ongoing.⁸³

Procedures

Clinical indications

[⁹⁰Y]ibritumomab tiuxetan (Zevalin®) was the first of this class of drugs to be licensed by the United States FDA, and is currently the only radioimmunoconjugate to be licensed within the European Union (EU). However both [⁹⁰Y]ibritumomab tiuxetan (Zevalin®) and [¹³¹I]tositumomab (Bexxar®) are approved for the treatment of adult patients with relapsed CD20+ follicular or transformed B-cell NHL within the USA. Bexxar® can be given in most (but not all) of the states in the USA on an outpatient basis, while Zevalin®, using pure β emitter ⁹⁰Y, can be used throughout the USA on an outpatient basis. The license for [⁹⁰Y]ibritumomab tiuxetan (Zevalin®) within the EU is restricted to relapsed follicular lymphoma which is refractory to or relapsed after rituximab, and it can be given on an outpatient basis. As these are currently the only RIT drugs to have a licensed indication for NHL, this section will focus on the delivery of these two treatments, which differ substantially in their mode of dosimetry and requirements for hospital stay. The characteristics of both [⁹⁰Y]ibritumomab tiuxetan (Zevalin®) and [¹³¹I]tositumomab (Bexxar®) are shown in Table 20.4. Table 20.6 is the Zevalin® administration schedule. The most noticeable difference is regarding the 4–5-day inpatient stay within the EU required for [¹³¹I]tositumomab (Bexxar®), which contrasts with a single outpatient visit required for the delivery of [⁹⁰Y]ibritumomab tiuxetan (Zevalin®).

No comparative clinical trial has ever been performed between [⁹⁰Y]ibritumomab tiuxetan and [¹³¹I]tositumomab,

Table 20.6 Administration schedules for Zevalin®

*Dosimetric step beginning on day 0
(not required in the EU)*

Rituximab

(250 mg/m², 50 mg/h IV infusion)

Dosimetric dose: [¹¹¹In]ibritumomab tiuxetan

1.6 mg ibritumomab tiuxetan labeled with 185 MBq ¹¹¹In, IV injection over 10 minutes, given within 4 h of rituximab infusion

Assess biodistribution

Required scan: day 2 or 3
Optional: other time points

Therapeutic step day 7–9

Rituximab

(250 mg/m², 50 mg/h IV infusion)

Therapeutic dose: [⁹⁰Y]ibritumomab tiuxetan

3.2 mg ibritumomab tiuxetan labeled with ⁹⁰Y, IV injection over 10 min within 4 h of rituximab infusion as follows:*

14.8 MBq/kg for patients with normal platelet count

11.1 MBq/kg for patients with platelet count 100–150 × 10⁹/l

*The maximum allowable dose of [⁹⁰Y]ibritumomab is 1184 MBq (32.0 mCi).

and is unlikely ever to be. However, it appears reasonable to surmise that the two drugs have very similar response rates and response durations, from the published results. The integration of [⁹⁰Y]ibritumomab tiuxetan and [¹³¹I]tositumomab into routine clinical practice seems therefore more likely to depend on the cost and convenience of each therapy rather than perceived differences in clinical efficacy. [¹³¹I]tositumomab remains licensed in the USA only, and if an EU license is eventually gained, the radiation protection issues with the necessity for 5–6 days of inpatient stay for patients (within the EU) receiving [¹³¹I]tositumomab may influence clinicians on health economic grounds in favor of [⁹⁰Y]ibritumomab tiuxetan. The removal of the dosimetric dose, within the EU, further simplifies the delivery of [⁹⁰Y]ibritumomab tiuxetan, making the whole regimen very easy for the patient. Notably, in the US license for Zevalin®, pretherapy imaging using ¹¹¹In-labeled ibritumomab tiuxetan as surrogate is required to ensure a suitable mAb distribution pattern.

Patients with an increased likelihood of developing hematological toxicity or patients with impaired bone marrow reserve as defined by the following criteria should be excluded from RIT with [¹³¹I]tositumomab or [⁹⁰Y]ibritumomab:

- presence of > 25% infiltration of lymphoma cells within the bone marrow
- prior history of external beam radiation therapy to > 25% of the bone marrow
- baseline platelet counts < 100 000/μl or neutrophil counts < 1500/μl
- patients with a platelet count between 100 000 and 150 000/μl should be given a dose reduction of 0.3 mCi/kg (11.1 MBq/kg) for [⁹⁰Y]ibritumomab.

All patients require a bone marrow trephine examination within 4–6 weeks prior to treatment with RIT. Patients should be excluded if pregnant or breast-feeding, or if known to have hypersensitivity to mouse antibodies or chelating agents such as tiuxetan or serum human anti-murine antibody (HAMA). Patients with known active infection with the human immunodeficiency virus, or lymphoma of the central nervous system, should also be excluded, as there are currently no data to confirm the safety of this approach in these groups of patients. Patients who have progressed within 1 year of radiation in a field that has previously been irradiated, or who are receiving other anticancer drugs or biologics, are not eligible. Thyroid blockade with potassium iodide or Lugol's solution is required prior to the administration of Bexxar® therapy. It is recommended that prior chemotherapy must have been discontinued ≥ 4 weeks (6 weeks for nitrosourea compounds) before RIT.

Despite initial concerns, preliminary data suggest that patients after prior bone marrow transplant or stem cell

support can be safely treated as long as a significant dose reduction is made. For the [⁹⁰Y]ibritumomab tiuxetan regimen, the published data at present suggest 0.2 mCi/kg, and for [¹³¹I]tositumomab around 65 cGy whole-body dose (WBD).^{84,85} It should be emphasized that the delivery of either reagent post-autologous stem cell transplantation (ASCT) is outside the current licensed indication.

Treatment dosing schedule

Radioimmunotherapy with [⁹⁰Y]ibritumomab tiuxetan is completed within 1 week, and consists of a single dose of the therapeutic radioimmunoconjugate. The treatment schedule includes intravenous infusion of rituximab (250 mg/m²) on days 1 and 8.⁸⁶ As yttrium-90 is a pure β emitter, to facilitate γ camera imaging, indium-111 (¹¹¹In) is used as a surrogate, and chelated to ibritumomab tiuxetan for dosimetry. Imaging was done as part of the registration studies on day 1 (at a dose of 185 MBq (5 mCi)) following rituximab infusion, with imaging done at 2–24 hours, at 48–72 hours, and at 90–120 hours post-injection, and two scans still form part of the approved schedule within the USA.⁸⁷ [⁹⁰Y]ibritumomab tiuxetan is administered within 4 hours after the second rituximab infusion via slow intravenous push over a period of 10 minutes, provided that a 0.2- or 0.22 μm low protein binding filter is in place.

An initial phase I dose escalation study of [⁹⁰Y]ibritumomab tiuxetan up to a myeloablative activity of 1850 MBq (50 mCi), which included 14 patients with relapsed or refractory low- or intermediate-grade B-cell NHL, established that predosing with unlabeled ibritumomab (murine antibody) improved the tumor dose and also demonstrated that the hematological toxicity was correlated most closely with body weight, rather than body surface area.⁸⁸ A further phase I/II study was subsequently performed, and this demonstrated that the biodistribution of the radioimmunoconjugate can be improved by predosing with rituximab (chimeric antibody), and no difference was found between 125 mg/m² or 250 mg/m² dosing. Myelotoxicity was found to be the dose-limiting toxicity, and the maximum tolerated dose (MTD) was identified as 14.8 MBq/kg or 0.4 mCi/kg (to a maximum dose of 1184 MBq or 32 mCi) for patients with a baseline platelet count of ≥ 150 000 × 10⁹/l and 11.1 MBq/kg or 0.3 mCi/kg for patients with baseline platelet counts of < 150 000 × 10⁹/l but ≥ 100 000 × 10⁹/l.⁸⁶ Another study specifically examined the tolerability of a reduced dose in patients with mild thrombocytopenia (baseline platelet count of 100–150 000 × 10⁹/l). This study demonstrated that such patients can be safely treated with [⁹⁰Y]ibritumomab tiuxetan at a dose of 11.1 MBq/kg or 0.3 mCi/kg.⁸⁹ The recommended maximal dose for Zevalin® is no more than 1184 MBq per patient.

The [¹³¹I]tositumomab (Bexxar®) therapeutic regimen differs from [⁹⁰Y]ibritumomab tiuxetan (Zevalin®) and is completed in four visits over 1–2 weeks as shown in Table 20.6. For Bexxar®, the therapeutic dose is calculated based on the pre-therapy dosimetric data using the MIRDOSE 3 software program, and the recommended total body dose is 65 cGy to 75 cGy.¹⁶ This regimen involves an initial biodistribution/dosimetry study followed by a therapeutic infusion given 7 days later.

Each infusion of [¹³¹I]tositumomab is preceded by an infusion of a predose of 450 mg ‘cold’ or unlabeled tositumomab. Whole-body γ camera imaging is performed three times over the week following the trace labeled infusion to calculate the whole body half-time and the dose required for the therapeutic infusion to deliver 65–75 cGy of whole body irradiation (usually 100–150 mCi).⁷² A therapeutic total body dose (TBD) of 75 cGy is preceded by a dosimetric step. Dose adjustments to 65 cGy are made for a baseline platelet count of 100 000/mm³ to < 150 000/mm³ and for obesity.

Integration into treatment algorithms for NHL

The high response rates and durable remissions achieved with either [⁹⁰Y]ibritumomab (Zevalin®) or [¹³¹I]tositumomab (Bexxar®) make single-agent RIT an attractive treatment option for many patients with relapsed follicular lymphoma. Furthermore, the impressive duration of response seen after achieving a complete response is achieved with a treatment that is completed within a week, is very well tolerated, and has minimal non-myelotoxicity toxicity and easily manageable myelotoxicity. There is no doubt that RIT drugs are highly active, but considerable uncertainty remains as to when and how best to integrate RIT into clinical practice even within the licensed indication of relapsed low grade (US) or relapsed rituximab failure or refractory follicular lymphoma (within the EU).

Although the results for single-agent RIT are encouraging and make RIT an attractive treatment option for relapsed follicular lymphoma, the future is likely to involve integrating RIT into chemotherapy treatment protocols in an attempt to increase relapse-free and overall survival. The current challenge for clinical investigators is to determine the optimal approach of integrating RIT into chemotherapy schedules. The emerging data using both [¹³¹I]tositumomab and [⁹⁰Y]ibritumomab tiuxetan as consolidation following shortened or full course chemotherapy look extremely promising and suggest that the quality of response can be substantially increased by this type of approach.^{90–92} Future randomized clinical trials will define whether this type of approach offers similar or perhaps even superior relapse-free survival over rituximab–chemotherapy regimens followed

by maintenance rituximab. Future clinical studies will indicate whether the ability of RIT to improve the quality of response from partial to complete will add to relapse-free survival and perhaps even overall survival.

In the education session on follicular lymphoma at the 2004 American Society of Hematologists an algorithm was suggested whereby RIT was recommended upon first relapse after a rituximab–chemotherapy combination (Figure 20.1). Currently, this seems a very reasonable strategy as it does not exclude transplantation options at a later date, especially if, as recommended, progenitor stem cell collection is performed at the time of the initial remission. Further clinical trials will need to be performed to further define the integration of RIT into treatment protocols for other NHL.

Precautions and side-effects in use

Successful implementation of RIT requires a multidisciplinary approach which ideally includes hematologists/oncologists, nuclear medicine physicians, physicists, radiopharmacists, and trained nursing staff. Regular communication between the hematology/oncology department and the nuclear medicine department is essential throughout treatment. For the successful delivery of RIT a coordinator is required to organize the logistics of delivering RIT. Good practice should involve patients who are being considered for treatment consulting with the nuclear medicine physician or radiation oncologist (radioisotope delivery

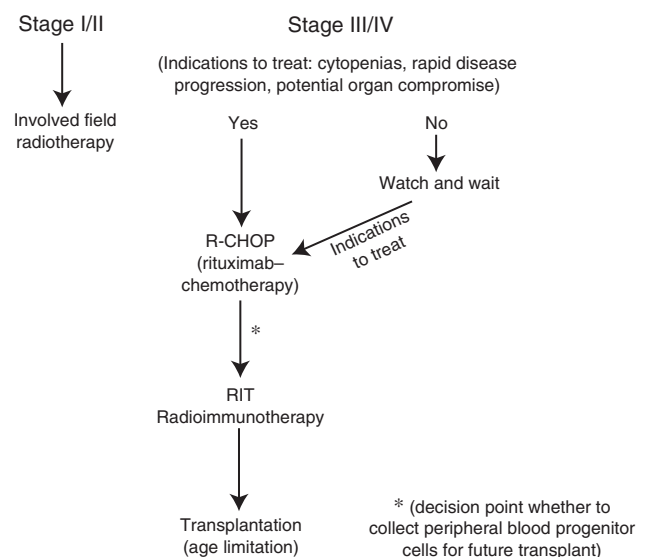


Figure 20.1

Proposed treatment algorithm for follicular lymphoma patients. R-CHOP, rituximab–cyclophosphamide, doxorubicin, vincristine, prednisolone.

certificate holder) prior to treatment, to confirm that all safety criteria for treatment are met and to provide the patient with additional information regarding radiation safety issues and the practicalities of RIT. The certificate holder (nuclear medicine physician/radiation oncologist) is responsible for the preparation and administration of RIT.

For the preparation of [⁹⁰Y]ibritumomab tiuxetan (Zevalin®), only trained personnel should perform the labeling of ibritumomab tiuxetan with radiopharmaceutical grade ⁹⁰Y, with appropriate facilities for shielding, calibration, and quality control. Emitted β particles are absorbed completely by plastic or acrylic pots with a thickness of 1 cm. To ensure the accuracy of results, all quality control testing should be performed in duplicate, and the [⁹⁰Y]ibritumomab tiuxetan preparation should not be administered if radiochemical purity is < 95%.

[¹³¹I]tositumomab is delivered radiolabeled, and the appropriate quality control including labeling efficiency and immunoreactivity will have been performed at the production facility prior to dispatch. The patient-specific dose is calculated from the whole body dosimetry and pre-ordered, and therefore the required activity of [¹³¹I]tositumomab requires measurement prior to administration.

Both [¹³¹I]tositumomab and [⁹⁰Y]ibritumomab tiuxetan should be administered through a patent indwelling cannula, with a 0.20–0.22-μm in-line filter placed between the injection port and the patient. Acute side-effects during infusion of the radioimmunoconjugates are extremely rare, but steroids and antihistamines should be readily available during [¹³¹I]tositumomab and [⁹⁰Y]ibritumomab tiuxetan administration. If extravasation occurs, the infusion should be stopped immediately, and the arm should be elevated and massaged to facilitate lymphatic drainage.

Safety data for [⁹⁰Y]ibritumomab tiuxetan from four clinical trials were reviewed retrospectively in an integrated analysis⁹³ encompassing 349 patients, of whom 345 (99%) completed treatment. Although 80% of patients reported non-hematological adverse events, those were generally mild to moderate in severity with asthenia, nausea, and chills being the most common events that were considered probably or possibly related to treatment. Only 11% (39 patients) of all patients experienced grade 3–4 non-hematological toxicity.

The primary and dose-limiting toxicity associated with [⁹⁰Y]ibritumomab tiuxetan was transient, reversible myelosuppression, typically developing delayed by week 4–6, reaching a nadir by week 7–9. Of note, thrombocytopenia grade 1–2 and 3–4 occurred in 37% and 63% of patients, respectively. Some 87% of patients with grade 3–4 thrombocytopenia recovered to ≥ 50 000/μl by week 12 following therapy. Neutropenia grade 3–4 was observed in 30% of patients, with 90% recovering to > 1000/μl within 12 weeks post-treatment.

Incidences of severe thrombocytopenia and neutropenia correlated significantly with the degree of bone marrow

involvement and platelet counts at baseline, underscoring the importance to exclude patients with ≥ 25% bone marrow infiltration and inadequate bone marrow reserve. Patients who had more than two prior chemotherapies were twice as likely to develop grade 4 thrombocytopenia, whereas number of prior chemotherapies did not correlate with longer median duration of neutropenia, thrombocytopenia, and anemia.

For [¹³¹I]tositumomab (Bexxar®) the short-term non-hematological adverse events are also generally mild, and include typically fatigue, nausea, fever, vomiting, pruritus, and rash, which usually respond well to antihistamines. Hypothyroidism appears to be one of the most notable long-term adverse effects after ¹³¹I-labeled mAb treatment, which can however be easily managed with thyroid hormone replacement. Most recently, Zelenetz reviewed the multicenter RIT trials using [¹³¹I]tositumomab in NHL patients, and reported that elevated thyroid stimulating hormone (TSH) was observed in five out of 59 patients in the phase I study.⁵² However, Liu et al. observed elevated TSH in 59% of patients treated in Seattle with a myeloablative dose of [¹³¹I]tositumomab.⁸⁰

HAMA reactions appear to be substantially lower in previously treated NHL patients compared to the rates experienced in solid tumor RIT.¹² DeNardo et al. analyzed 617 samples from 112 subjects, including 85 patients with B-cell malignancies. They found that 77% of B-cell malignancy patients developed no response or a weak response after multiple doses of mouse Lym-1 antibody.⁵⁰ In a separate study, Zelenetz observed similar results, with approximately 10% of [¹³¹I]tositumomab-treated patients developing a positive HAMA reaction.⁵² However, in a most recent study involving previously untreated patients, Kaminski et al. reported that 48 out of 76 (63%) patients developed detectable HAMA after a single course of treatment with ¹³¹I-labeled tositumomab.¹⁶

Secondary malignancy following RIT has fortunately proved to be rare.^{16,52} In a very recent study, 1071 RIT-treated patients were assessed for treatment-related myelodysplastic syndromes (MDS) and acute myeloid leukemia (AML). Among them, 995 patients with low-grade and transformed low-grade NHL had been treated with a median of three previous therapies (range 1–13 therapies) prior to RIT. Seventy-six patients received RIT as their initial therapy for follicular NHL. For the previously treated patients, the median follow-up from the diagnosis of NHL and RIT was 6 years and 2 years, respectively; for the patients who received RIT as their initial therapy, the corresponding median follow-up times were 5.6 years and 4.6 years, respectively. Of the 995 previously treated patients, 35 (3.5%) cases of treatment-related MDS/AML were reported and 13 cases were confirmed to have developed MDS/AML following RIT. This incidence was found to be consistent with that expected on the basis of patients' prior chemotherapy for NHL. With a median follow-up approaching

5 years, no case of treatment-related MDS/AML has been reported in the 76 patients receiving [¹³¹I]tositumomab as their initial therapy.⁹⁴

It is strongly recommended that the hematologist/oncologist is responsible for the post-treatment evaluation of the patient, keeping the nuclear medicine physician informed about the patient's progress. Follow-up involves weekly full blood count from 3 weeks following radioimmunotherapy until hematological recovery. Response to treatment should be assessed no earlier than 3 months after treatment, and even at this point clinicians should be aware that the quality of response may continue to improve beyond this time, with the conversion of partial to complete response occurring many weeks and months later in some patients.

Conclusions

Despite more than two decades of expectation since the introduction of RIT, it has only been in the last few years that this technology has begun to gain a role in the treatment of cancer because of its successful application in lymphoma patients. Following US FDA (Zevalin® and Bexxar®) and European Union (Zevalin®) approval, RIT is likely to contribute substantially to the future treatment of non-Hodgkin's lymphoma.

Although RIT has emerged as an effective treatment for NHL, the underlying mechanisms of action, such as the interaction of irradiation and mAb in RIT, the existence of radiation dose response, and the role of radiation dose rate effect in the overall therapeutic outcome, are still poorly understood.^{30,95,96} These issues are probably better investigated through preclinical experiments, and recently results from our group have provided some new insights into some of them, which could be helpful for the design of future clinical RIT protocols.^{58,59} Clinically, the optimal integration of RIT into other therapeutic modalities needs to be further clarified. Future randomized clinical trials will define whether this type of approach offers similar or perhaps even superior relapse-free survival over rituximab-chemotherapy regimens followed by maintenance rituximab. Long-term observation will elucidate whether the ability of RIT to improve the quality of response from partial to complete will add to relapse-free survival and perhaps even overall survival.

References

1. Kelsey SM, Gallagher GJ, Tata T. Medical oncology including haematological malignancy. In: Kumar P, Clark M, eds. *Clinical Medicine*, 5th ed. Philadelphia: WB Saunders 2002: 496–500.
2. Wingo PA, Tong T, Bolden S. Cancer statistics, 1995. *CA Cancer J Clin* 1995; 45: 8–30.
3. Wingo PA, Ries LA, Rosenberg HM, Miller DS, Edwards BK. Cancer incidence and mortality, 1973–1995: a report card for the US. *Cancer* 1998; 82: 1197–207.
4. Weir HK, Thun MJ, Hankey BF et al. Annual report to the nation on the status of cancer, 1975–2000, featuring the uses of surveillance data for cancer prevention and control. *J Natl Cancer Inst* 2003; 95: 1276–99.
5. Fisher RI. Overview of non-Hodgkin's lymphoma: biology, staging, and treatment. *Semin Oncol* 2003; 30 (2 Suppl 4): 3–9.
6. Armitage JO, Weisenburger DD. New approach to classifying non-Hodgkin's lymphomas: clinical features of the major histologic subtypes. Non-Hodgkin's Lymphoma Classification Project. *J Clin Oncol* 1998; 16: 2780–95.
7. Harris NL, Jaffe ES, Diebold J et al. World Health Organization classification of neoplastic diseases of the hematopoietic and lymphoid tissues: report of the Clinical Advisory Committee meeting—Airlie House, Virginia, November 1997. *J Clin Oncol* 1999; 17: 3835–49.
8. Kohler G, Milstein C. Continuous cultures of fused cells secreting antibody of predefined specificity. *Nature* 1975; 256: 495–7.
9. Avivi I, Robinson S, Goldstone A. Clinical use of rituximab in haematological malignancies. *Br J Cancer* 2003; 89: 1389–94.
10. McLaughlin P. Rituximab: perspective on single agent experience, and future directions in combination trials. *Crit Rev Oncol Hematol* 2001; 40: 3–16.
11. Coiffier B. Monoclonal antibodies in the treatment of indolent lymphomas. *Best Pract Res Clin Haematol* 2005; 18: 69–80.
12. Knox SJ, Meredith RF. Clinical radioimmunotherapy. *Semin Radiat Oncol* 2000; 10: 73–93.
13. Witzig TE, Gordon LI, Cabanillas F et al. Randomized controlled trial of yttrium-90-labeled ibritumomab tiuxetan radioimmunotherapy versus rituximab immunotherapy for patients with relapsed or refractory low-grade, follicular, or transformed B-cell non-Hodgkin's lymphoma. *J Clin Oncol* 2002; 20: 2453–63.
14. Davis TA, Kaminski MS, Leonard JP et al. The radioisotope contributes significantly to the activity of radioimmunotherapy. *Clin Cancer Res* 2004; 10: 7792–8.
15. Press OW, Leonard JP, Coiffier B, Levy R, Timmerman J. Immunotherapy of Non-Hodgkin's lymphomas. *Hematology (Am Soc Hematol Educ Program)* 2001: 221–40.
16. Kaminski MS, Tuck M, Estes J et al. 131I-tositumomab therapy as initial treatment for follicular lymphoma. *N Engl J Med* 2005; 352: 441–9.
17. White CA, Halpern SE, Parker BA et al. Radioimmunotherapy of relapsed B-cell lymphoma with yttrium 90 anti-idiotype monoclonal antibodies. *Blood* 1996; 87: 3640–9.
18. Dyer MJ, Hale G, Hayhoe FG, Waldmann H. Effects of CAM-PATH-1 antibodies in vivo in patients with lymphoid malignancies: influence of antibody isotype. *Blood* 1989; 73: 1431–9.
19. Goldenberg DM, Horowitz JA, Sharkey RM et al. Targeting, dosimetry, and radioimmunotherapy of B-cell lymphomas with iodine-131-labeled LL2 monoclonal antibody. *J Clin Oncol* 1991; 9: 548–64.

20. Hekman A, Honselaar A, Vuist WM et al. Initial experience with treatment of human B cell lymphoma with anti-CD19 monoclonal antibody. *Cancer Immunol Immunother* 1991; 32: 364–72.
21. Kaminski MS, Fig LM, Zasadny KR et al. Imaging, dosimetry, and radioimmunotherapy with iodine 131-labeled anti-CD37 antibody in B-cell lymphoma. *J Clin Oncol* 1992; 10: 1696–711.
22. Press OW, Eary JE, Appelbaum FR et al. Radiolabeled-antibody therapy of B-cell lymphoma with autologous bone marrow support. *N Engl J Med* 1993; 329: 1219–24.
23. Brown RS, Kaminski MS, Fisher SJ, Chang AE, Wahl RL. Intratumoral microdistribution of [¹³¹I]MB-1 in patients with B-cell lymphoma following radioimmunotherapy. *Nucl Med Biol* 1997; 24: 657–63.
24. DeNardo GL, DeNardo SJ, Goldstein DS et al. Maximum-tolerated dose, toxicity, and efficacy of (¹³¹I)-Lym-1 antibody for fractionated radioimmunotherapy of non-Hodgkin's lymphoma. *J Clin Oncol* 1998; 16: 3246–56.
25. Kaminski MS, Zelenetz AD, Press OW et al. Pivotal study of iodine I 131 tositumomab for chemotherapy-refractory low-grade or transformed low-grade B-cell non-Hodgkin's lymphomas. *J Clin Oncol* 2001; 19: 3918–28.
26. Press OW. Radioimmunotherapy for non-Hodgkin's lymphomas: a historical perspective. *Semin Oncol* 2003; 30 (2 Suppl 4): 10–21.
27. Grossbard ML, Press OW, Appelbaum FR, Bernstein ID, Nadler LM. Monoclonal antibody-based therapies of leukemia and lymphoma. *Blood* 1992; 80: 863–78.
28. Shan D, Ledbetter JA, Press OW. Apoptosis of malignant human B cells by ligation of CD20 with monoclonal antibodies. *Blood* 1998; 91: 1644–52.
29. Shan D, Ledbetter JA, Press OW. Signaling events involved in anti-CD20-induced apoptosis of malignant human B cells. *Cancer Immunol Immunother* 2000; 48: 673–83.
30. Press OW, Rasey J. Principles of radioimmunotherapy for hematologists and oncologists. *Semin Oncol* 2000; 27 (6 Suppl 12): 62–73.
31. Goldenberg DM. The role of radiolabeled antibodies in the treatment of non-Hodgkin's lymphoma: the coming of age of radioimmunotherapy. *Crit Rev Oncol Hematol* 2001; 39: 195–201.
32. Vriesendorp HM, Quadri SM, Stinson RL et al. Selection of reagents for human radioimmunotherapy. *Int J Radiat Oncol Biol Phys* 1992; 22: 37–45.
33. DeNardo GL, O'Donnell RT, Shen S et al. Radiation dosimetry for ⁹⁰Y-2IT-BAD-Lym-1 extrapolated from pharmacokinetics using ¹¹¹In-2IT-BAD-Lym-1 in patients with non-Hodgkin's lymphoma. *J Nucl Med* 2000; 41: 952–8.
34. Sharkey RM, Behr TM, Mattes MJ et al. Advantage of residualizing radiolabels for an internalizing antibody against the B-cell lymphoma antigen, CD22. *Cancer Immunol Immunother* 1997; 44: 179–88.
35. Press OW, Shan D, Howell-Clark J et al. Comparative metabolism and retention of iodine-125, yttrium-90, and indium-111 radioimmunoconjugates by cancer cells. *Cancer Res* 1996; 56: 2123–9.
36. DeNardo GL, Kukis DL, Shen S et al. ⁶⁷Cu-versus ¹³¹I-labeled Lym-1 antibody: comparative pharmacokinetics and dosimetry in patients with non-Hodgkin's lymphoma. *Clin Cancer Res* 1999; 5: 533–41.
37. McDevitt MR, Sgouros G, Finn RD et al. Radioimmunotherapy with alpha-emitting nuclides. *Eur J Nucl Med* 1998; 25: 1341–51.
38. Jurcic JG, Larson SM, Sgouros G et al. Targeted alpha particle immunotherapy for myeloid leukemia. *Blood* 2002; 100: 1233–9.
39. Zhang M, Yao Z, Garmestani K et al. Pretargeting radioimmunotherapy of a murine model of adult T-cell leukemia with the alpha-emitting radionuclide, bismuth 213. *Blood* 2002; 100: 208–16.
40. Zhang M, Zhang Z, Garmestani K et al. Pretarget radiotherapy with an anti-CD25 antibody-streptavidin fusion protein was effective in therapy of leukemia/lymphoma xenografts. *Proc Natl Acad Sci USA* 2003; 100: 1891–5.
41. Oh P, Li Y, Yu J et al. Subtractive proteomic mapping of the endothelial surface in lung and solid tumours for tissue-specific therapy. *Nature* 2004; 429: 629–35.
42. Milenic DE. Radioimmunotherapy: designer molecules to potentiate effective therapy. *Semin Radiat Oncol* 2000; 10: 139–55.
43. Yao Z, Zhang M, Axworthy DB et al. Radioimmunotherapy of A431 xenografted mice with pretargeted B3 antibody-streptavidin and (⁹⁰Y)-labeled 1,4,7,10-tetraazacyclododecane-N,N',N'',N'''-tetraacetic acid (DOTA)-biotin. *Cancer Res* 2002; 62: 5755–60.
44. Yao Z, Zhang M, Garmestani K et al. Pretargeted alpha emitting radioimmunotherapy using (²¹³Bi) 1,4,7,10-tetraazacyclododecane-N,N',N'',N'''-tetraacetic acid-biotin. *Clin Cancer Res* 2004; 10: 3137–46.
45. Sharkey RM, Karacay H, Chang CH et al. Improved therapy of non-Hodgkin's lymphoma xenografts using radionuclides pretargeted with a new anti-CD20 bispecific antibody. *Leukemia* 2005; 19: 1064–9.
46. Sharkey RM, Goldenberg DM. Perspectives on cancer therapy with radiolabeled monoclonal antibodies. *J Nucl Med* 2005; 46 (Suppl 1): 115S–27S.
47. Sharkey RM, Blumenthal RD, Hansen HJ, Goldenberg DM. Biological considerations for radioimmunotherapy. *Cancer Res* 1990; 50 (3 Suppl): 964s–9s.
48. Thomas GD, Chappell MJ, Dykes PW et al. Effect of dose, molecular size, affinity, and protein binding on tumor uptake of antibody or ligand: a biomathematical model. *Cancer Res* 1989; 49: 3290–6.
49. Yokota T, Milenic DE, Whitlow M, Schlom J. Rapid tumor penetration of a single-chain Fv and comparison with other immunoglobulin forms. *Cancer Res* 1992; 52: 3402–8.
50. DeNardo GL, Mirick GR, Kroger LA et al. Characterization of human IgG antimouse antibody in patients with B-cell malignancies. *Clin Cancer Res* 2003; 9: 4013S–21S.
51. Khazaeli MB, Conry RM, LoBuglio AF. Human immune response to monoclonal antibodies. *J Immunother* 1994; 15: 42–52.
52. Zelenetz AD. A clinical and scientific overview of tositumomab and iodine I 131 tositumomab. *Semin Oncol* 2003; 30 (2 Suppl 4): 22–30.
53. Piro LD, White CA, Grillo-Lopez AJ et al. Extended Rituximab (anti-CD20 monoclonal antibody) therapy for relapsed

- or refractory low-grade or follicular non-Hodgkin's lymphoma. *Ann Oncol* 1999; 10: 655–61.
54. Looney RJ, Anolik JH, Campbell D et al. B cell depletion as a novel treatment for systemic lupus erythematosus: a phase I/II dose-escalation trial of rituximab. *Arthritis Rheum* 2004; 50: 2580–9.
 55. Illidge TBMZMDYLVJP. Phase I/II study of fractionated radioimmunotherapy in relapsed low grade non-Hodgkin's lymphoma. *Blood* 2004; 104: 131.
 56. Behr TM, Wormann B, Gramatzki M et al. Low- versus high-dose radioimmunotherapy with humanized anti-CD22 or chimeric anti-CD20 antibodies in a broad spectrum of B cell-associated malignancies. *Clin Cancer Res* 1999; 5 (10 Suppl): 3304s–14s.
 57. Behr TM, Griesinger F, Riggert J et al. High-dose myeloablative radioimmunotherapy of mantle cell non-Hodgkin lymphoma with the iodine-131-labeled chimeric anti-CD20 antibody C2B8 and autologous stem cell support. Results of a pilot study. *Cancer* 2002; 94 (4 Suppl): 1363–72.
 58. Du Y, Honeychurch J, Bayne M et al. Antibody-induced intracellular signaling works in combination with radiation to eradicate lymphoma in radioimmunotherapy. *Blood* 2004; 103: 1485–94.
 59. Illidge TM, Cragg MS, McBride HM, French RR, Glennie MJ. The importance of antibody-specificity in determining successful radioimmunotherapy of B-cell lymphoma. *Blood* 1999; 94: 233–43.
 60. Sharkey RM, Brenner A, Burton J et al. Radioimmunotherapy of non-Hodgkin's lymphoma with 90Y-DOTA humanized anti-CD22 IgG (90Y-Epratuzumab): do tumor targeting and dosimetry predict therapeutic response? *J Nucl Med* 2003; 44: 2000–18.
 61. Sharkey RM, Goldenberg DM. Advances in radioimmunotherapy in the age of molecular engineering and pre-targeting. *Cancer Invest* 2006; 24: 82–97.
 62. Press OW, Corcoran M, Subbiah K et al. A comparative evaluation of conventional and pretargeted radioimmunotherapy of CD20-expressing lymphoma xenografts. *Blood* 2001; 98: 2535–43.
 63. Pagel JM, Hedin N, Subbiah K et al. Comparison of anti-CD20 and anti-CD45 antibodies for conventional and pre-targeted radioimmunotherapy of B-cell lymphomas. *Blood* 2003; 101: 2340–8.
 64. Forero A, Weiden PL, Vose JM et al. Phase I trial of a novel anti-CD20 fusion protein in pretargeted radioimmunotherapy for B-cell non-Hodgkin's lymphoma. *Blood* 2004; 104: 227–36.
 65. Wilder RB, DeNardo GL, DeNardo SJ. Radioimmunotherapy: recent results and future directions. *J Clin Oncol* 1996; 14: 1383–400.
 66. DeNardo GL, DeNardo SJ, O'Grady LF et al. Fractionated radioimmunotherapy of B-cell malignancies with 131I-Lym-1. *Cancer Res* 1990; 50 (3 Suppl): 1014s–16s.
 67. Juweid ME, Stadtmauer E, Hajar G et al. Pharmacokinetics, dosimetry, and initial therapeutic results with 131I- and (111)In-/90Y-labeled humanized LL2 anti-CD22 monoclonal antibody in patients with relapsed, refractory non-Hodgkin's lymphoma. *Clin Cancer Res* 1999; 5 (10 Suppl): 3292s–303s.
 68. Linden O, Hindorf C, Cavallin-Stahl E et al. Dose-fractionated radioimmunotherapy in non-Hodgkin's lymphoma using DOTA-conjugated, 90Y-radiolabeled, humanized anti-CD22 monoclonal antibody, epratuzumab. *Clin Cancer Res* 2005; 11: 5215–22.
 69. Kaminski MS, Zasadny KR, Francis IR et al. Radioimmunotherapy of B-cell lymphoma with [131I]anti-B1 (anti-CD20) antibody. *N Engl J Med* 1993; 329: 459–65.
 70. Kaminski MS, Zasadny KR, Francis IR et al. Iodine-131-anti-B1 radioimmunotherapy for B-cell lymphoma. *J Clin Oncol* 1996; 14: 1974–81.
 71. Friedberg JW, Fisher RI. Iodine-131 tositumomab (Bexxar®): radioimmunoconjugate therapy for indolent and transformed B-cell non-Hodgkin's lymphoma. *Expert Rev Anticancer Ther* 2004; 4: 18–26.
 72. Hohenstein MA, Augustine SC, Rutar F, Vose JM. Establishing an institutional model for the administration of tositumomab and iodine I 131 tositumomab. *Semin Oncol* 2003; 30 (2 Suppl 4): 39–49.
 73. Kaminiski MS, Zelenetz A, Leonard J, Saleh M, Jain V. Bexxar radioimmunotherapy produces a substantial number of durable complete responses in patients with multiply relapsed or refractory low grade or transformed low grade non-Hodgkin's lymphoma. 2002; 100: 357a (abstr).
 74. Gregory S, Kaminiski MS, Zelenetz A, Jain V. Characteristics of patients with relapsed and refractory low grade non-Hodgkin's lymphoma who sustained durable responses following treatment with tositumomab and iodine-131 tositumomab (Bexxar). *Blood* 2002; 100: (abstr).
 75. Horning S, Younes A, Lucas J, Podoloff DA, Jain V. Rituximab treatment failures: tositumomab and iodine-131 tositumomab (Bexxar) can produce meaningful durable responses. *Blood* 2002; 100: (abstr).
 76. Coleman M, Kaminiski MS, Knox SJ, Zelenetz A, Vose J. The Bexxar therapeutic regimen (tositumomab and iodine I 131 tositumomab) produced durable complete remissions in heavily pretreated patients with non-Hodgkin's lymphoma (NHL), rituximab-relapsed/refractory disease, and rituximab-naive disease. *Blood* 2003; 102: (abstr).
 77. Koral KF, Dewaraja Y, Li J et al. Update on hybrid conjugate-view SPECT tumor dosimetry and response in 131I-tositumomab therapy of previously untreated lymphoma patients. *J Nucl Med* 2003; 44: 457–64.
 78. Gordon LI, Witzig TE, Wiseman GA et al. Yttrium 90 ibritumomab tiuxetan radioimmunotherapy for relapsed or refractory low-grade non-Hodgkin's lymphoma. *Semin Oncol* 2002; 29(1 Suppl 2): 87–92.
 79. Gordon LI, Molina A, Witzig T et al. Durable responses after ibritumomab tiuxetan radioimmunotherapy for CD20+ B-cell lymphoma: long-term follow-up of a phase 1/2 study. *Blood* 2004; 103: 4429–31.
 80. Liu SY, Eary JF, Petersdorf SH et al. Follow-up of relapsed B-cell lymphoma patients treated with iodine-131-labeled anti-CD20 antibody and autologous stem-cell rescue. *J Clin Oncol* 1998; 16: 3270–8.
 81. Gopal AK, Gooley TA, Maloney DG et al. High-dose radioimmunotherapy versus conventional high-dose therapy and autologous hematopoietic stem cell transplantation

- for relapsed follicular non-Hodgkin lymphoma: a multivariable cohort analysis. *Blood* 2003; 102: 2351–7.
82. Rajendran J, Gopal A, Durack L et al. Comparison of radiation dose estimation for myeloablative radioimmunotherapy for relapsed or recurrent mantle cell lymphoma using (131)I tositumomab to that of other types of non-Hodgkin's lymphoma. *Cancer Biother Radiopharm* 2004; 19: 738–45.
 83. Nademanee A, Forman S, Molina A et al. A phase 1/2 trial of high-dose yttrium-90-ibritumomab tiuxetan in combination with high-dose etoposide and cyclophosphamide followed by autologous stem cell transplantation in patients with poor-risk or relapsed non-Hodgkin lymphoma. *Blood* 2005; 106: 2896–902.
 84. Wagner HN Jr, Wiseman GA, Marcus CS et al. Administration guidelines for radioimmunotherapy of non-Hodgkin's lymphoma with (90)Y-labeled anti-CD20 monoclonal antibody. *J Nucl Med* 2002; 43: 267–72.
 85. Wahl RL. Tositumomab and (131)I therapy in non-Hodgkin's lymphoma. *J Nucl Med* 2005; 46 (Suppl 1): 128S–40S.
 86. Witzig TE, White CA, Wiseman GA et al. Phase I/II trial of IDEC-Y2B8 radioimmunotherapy for treatment of relapsed or refractory CD20(+) B-cell non-Hodgkin's lymphoma. *J Clin Oncol* 1999; 17: 3793–803.
 87. Wiseman GA, Kornmehl E, Leigh B et al. Radiation dosimetry results and safety correlations from 90Y-ibritumomab tiuxetan radioimmunotherapy for relapsed or refractory non-Hodgkin's lymphoma: combined data from 4 clinical trials. *J Nucl Med* 2003; 44: 465–74.
 88. Wiseman GA, White CA, Witzig TE et al. Radioimmunotherapy of relapsed non-Hodgkin's lymphoma with zevalin, a 90Y-labeled anti-CD20 monoclonal antibody. *Clin Cancer Res* 1999; 5 (10 Suppl): 3281s–6s.
 89. Schilder R, Molina A, Bartlett N et al. Follow-up results of a phase II study of ibritumomab tiuxetan radioimmunotherapy in patients with relapsed or refractory low-grade, follicular, or transformed B-cell non-Hodgkin's lymphoma and mild thrombocytopenia. *Cancer Biother Radiopharm* 2004; 19: 478–81.
 90. Press OW, Unger JM, Brazier RM et al. A phase 2 trial of CHOP chemotherapy followed by tositumomab/iodine I 131 tositumomab for previously untreated follicular non-Hodgkin lymphoma: Southwest Oncology Group Protocol S9911. *Blood* 2003; 102: 1606–12.
 91. Dosik AD, Coleman M, Kostakoglu L et al. Subsequent therapy can be administered after tositumomab and iodine I-131 tositumomab for non-Hodgkin lymphoma. *Cancer* 2006; 106: 616–22.
 92. Leonard JP, Coleman M, Kostakoglu L et al. Abbreviated chemotherapy with fludarabine followed by tositumomab and iodine I 131 tositumomab for untreated follicular lymphoma. *J Clin Oncol* 2005; 23: 5696–704.
 93. Witzig TE, White CA, Gordon LI et al. Safety of yttrium-90 ibritumomab tiuxetan radioimmunotherapy for relapsed low-grade, follicular, or transformed non-Hodgkin's lymphoma. *J Clin Oncol* 2003; 21: 1263–70.
 94. Bennett JM, Kaminski MS, Leonard JP et al. Assessment of treatment-related myelodysplastic syndromes and acute myeloid leukemia in patients with non-Hodgkin lymphoma treated with tositumomab and iodine I131 tositumomab. *Blood* 2005; 105: 4576–82.
 95. Zelenetz AD. Radioimmunotherapy for lymphoma. *Curr Opin Oncol* 1999; 11: 375–80.
 96. Illidge TM, Johnson PW. The emerging role of radioimmunotherapy in haematological malignancies. *Br J Haematol* 2000; 108: 679–88.

Recommended internet links

<http://www.zevalin.com>
<http://www.bexxar.com>

Therapy of neuroendocrine tumors

Irene Virgolini, Ulrich Andergassen, Tatjana Traub-Weidinger, Dirk Heute, Elisabeth von Guggenberg, Dorota Kendler, Margarida Rodrigues, Georg Dobrozemsky, Boris Warwitz, Daniel Putzer, Roy Moncayo, Clemens Decristoforo, and Michael Gabriel

Background

The family of neuroendocrine tumors

Neuroendocrine tumors (NETs) are relatively rare disease entities derived from the diffuse endocrine system, and found anywhere in the body. They often present as a bizarre diagnostic puzzle.¹ The fact that these malignancies arise from hormonally active cells explains the wide variety of symptoms encountered in NET patients of various origin. The different manifestations are related to the release of hormones or other biologically active substances produced in excessive amounts, such as insulin, gastrin, vasoactive intestinal peptide (VIP), glucagon, or serotonin.²

NETs are classified according to their site of origin and whether they are functioning (hormone secreting) or non-functioning (non-hormone secreting). There are many types of NETs, including the most common gastroenteropancreatic (GEP) tumors which encompass gastrointestinal carcinoid tumors originating in the foregut, midgut, or hindgut as well as pancreatic islet cell tumors (e.g. insulinoma, gastrinoma, VIPoma, glucagonoma, and non-functional tumors), medullary thyroid cancer (MTC), paraganglioma, pheochromocytoma, and bronchial carcinoid tumors, among others. NETs may present at different stages of the disease. Functioning tumors are usually detected in earlier stages, due to hormone secretion, rather than detected as tumor bulk, along with distant metastases.

NETs constitute a group of relatively slow-growing malignancies, which are sometimes diagnosed after years of symptoms in affected patients. This is related to the fact that the amount of hormones secreted does not necessarily correlate with tumor size, whereas small cancers tend to escape clinical detection by conventional radiological imaging.

Thus, the start of successful therapy or symptomatic palliation is often delayed. A multidisciplinary approach for therapeutic intervention is necessary.

Once metastasized, the therapeutic options for patients with NETs are limited. Treatment with long-acting somatostatin (SST) analogs results in reduced hormonal (over)production and thus relief of symptoms.^{2,3} Surgery is the therapy of choice in localized disease. Chemoembolization of primary tumor/liver metastases can be attempted in order to reduce the tumor mass for subsequent therapy with radiolabeled peptide analogs in patients with slow-growing tumors. In patients with poorly differentiated tumors, chemotherapy may be considered. However, the management options are manifold. There are few evidence-based controlled studies available. Furthermore, formal guidelines are required. One should be aware that not all centers have the same treatment approach. For example, some believe that the long-acting SST analogs exert a beneficial effect even when the patient does not appear to have a carcinoid syndrome. In addition, there is no general agreement as to the scope and timing of tumor debulking surgery and/or chemoembolization.³

For the optimal management of NETs, the following strategy has been suggested:⁴ (1) suspect the diagnosis; (2) perform appropriate biochemistry profile including 24-hour urine 5-hydroxyindole acetic acid (5-HIAA) and serum hormone including chromogranin A measurements; (3) assessment of histopathology to confirm diagnosis and determine aggressiveness of the disease, e.g. features of tumor differentiation, invasion, and proliferation index; (4) determine the presence of inherited disorders such as multiple endocrine neoplasia type 1 (MEN-1) or the von Hippel–Lindau syndrome; (5) determine the site and extent of disease using, for example, contrast-enhanced computed tomography (CT) or magnetic resonance imaging (MRI) as well as the most sensitive modality, OctreoScan®; (6) treat the symptoms or excessive hormonal state; (7) treat

the disease if possible with curative surgery otherwise consider surgical debulking; non-surgical treatments of metastatic disease include SST analogs, interferon α , chemotherapy, hepatic artery embolization, and radionuclide therapies (see below); and (8) all patients will require long-term follow-up, preferably within treatment protocols.

Peptide receptor expression on neuroendocrine tumors

The expression of peptide receptors on various tumor cells including NETs was shown to be significantly higher as compared to normal tissues or cells.^{5,6} Over the past decade such receptors have become recognized targets for molecular imaging and therapy, because they are expressed on the cell surface and, upon binding of a ligand, the receptor–ligand complex is internalized. Receptor scintigraphy using radiolabeled peptide ligands, in particular with long-acting SST analogs, is nowadays established in clinical practice.

The 14 amino acid peptide SST is a multifunctional peptide mediator which is involved in the regulation of diverse biological processes. Most significantly, SST and its analogs inhibit the growth of normal as well as of neoplastic cells.^{7,8} The effects of SST are mediated via specific cell surface receptors expressed in abundant numbers on human tumors. Five different human SST receptors (hSSTR)^{9–15} have been characterized in detail and have been cloned. The vast majority of human tumor entities seem to overexpress one or another of these receptor subtypes (hSSTR1–5).

However, the expression of hSSTR on tumors seems to be very individual and varies from tumor entity to tumor entity. In initial studies only hSSTR2 was identified frequently in primary human tumors.⁵ Over the years, other hSSTR have frequently been described.^{16–30} The data published vary from research group to research group, most probably due to the different techniques applied and also to the various tumor entities investigated. We and others have identified hSSTR3 as another peptide receptor expressed on, or in, human tumor cells.³⁰ hSSTR3 may be responsible for binding both VIP and SST/octreotide (common binding site), and for the observed cross-competition between these peptides in primary human tumors as well as a variety of human tumor cell lines.⁶ Whereas NETs frequently overexpress hSSTR2, intestinal adenocarcinomas and a variety of other tumor types seem to overexpress mainly hSSTR3 and/or hSSTR4.^{30–38}

Not only SST receptors have been implemented as targets for molecular imaging and therapy of NETs. VIP receptor subtypes regularly found^{5,6} in high numbers on tumor cells have also been targets for NET tumor imaging.³⁹ Interestingly, many tumors appear to co-express binding sites for VIP and SST.^{6,40} However, due to instability, radiolabeled

VIP analogs have so far not been used for therapeutic approaches.

Similar to VIP receptor subtypes, bombesin receptor subtypes have also been found in high numbers on a variety of more frequently appearing tumor types, rather than on NETs where they are also expressed.⁴¹ More recently, radiolabeled bombesin analogs have also been implemented for radionuclide therapy of tumors expressing bombesin subtype receptors.^{42,43} Furthermore, substance P⁴⁴ and neurotensin receptors⁴⁵ have been suggested as possible molecular targets.

Radiolabeled peptides as molecular agents

With the spreading idea of molecular targeting on the basis of SSTR expression, a variety of SSTR radioligands (Table 21.1) have been synthesized and comparatively investigated for their *in vitro* binding properties. The SSTR subtype receptor binding profile of various radiolabeled SST analogs is depicted in Table 21.2.

Native SST exists in two forms (14 or 28 amino acids), but it is readily attacked by aminopeptidases and endopeptidases, and has a short *in vivo* half-life. Consequently, synthetic SST analogs, which incorporate a Phe-D-Trp-Lys-Thr (or similar sequence) and which are metabolically stabilized, at both the N- and C-terminals, were developed for clinical applications. In the past, three commercially available SST analogs, i.e. octreotide,⁵⁰ lanreotide,⁵¹ and vapreotide,⁵² have been shown to be effective in controlling the growth of some human tumors. These SST analogs all have similar binding profiles for four of the five hSSTR subtypes (i.e. a high affinity for hSSTR2 and hSSTR5, moderate affinity for hSSTR3, and very low affinity for hSSTR1), but lanreotide and vapreotide have a moderate affinity for hSSTR4, whereas octreotide has little or no affinity for this hSSTR.⁵³

Octreotide-based ligands

In initial studies, [¹²³I]Tyr³-octreotide was used to demonstrate the feasibility of detecting and localizing human neuroendocrine tumors.^{54,55} However, labeling with [¹²³I]sodium iodide of high specific activity is expensive, and hardly available worldwide. Furthermore, iodination of peptides requires technology and skills which are usually restricted to larger nuclear medicine institutions. Due to substantial accumulation of [¹²³I]Tyr³-octreotide in the gut as a result of hepatobiliary clearance of the agent, interpretation of the abdominal images is sometimes troublesome. Similar high abdominal accumulation was also found with [¹²³I]octreotide.⁵⁶ Some of the aforementioned problems

Table 21.1 Overview of selected imaging agents

Name	Abbreviation	Structure	Labeling with
Tyr ³ -octreotide	TOC		¹²³ I
DTPA-octreotide	DTPA-OC		¹¹¹ In
DOTA-Tyr ³ -octreotide	DOTA-TOC		¹¹¹ In, ⁹⁰ Y, ⁶⁸ Ga
DOTA-Tyr ³ -Thr ⁸ -octreotate	DOTA-TATE		¹¹¹ In, ⁹⁰ Y, ¹⁷⁷ Lu, ⁶⁸ Ga
DOTA-NaI ³ -octreotide	DOTA-NOC		¹¹¹ In, ⁹⁰ Y, ¹⁷⁷ Lu, ⁶⁸ Ga
DOTA-lanreotide	DOTA-LAN		¹¹¹ In, ⁹⁰ Y, ¹⁷⁷ Lu, ⁶⁸ Ga

DTPA, diethylenetriaminepentaacetic acid; DOTA, tetraazacyclododecanetetraacetic acid.

have successfully been overcome by the introduction of [¹¹¹In]DTPA-DPhe¹-octreotide [¹¹¹In]DTPA-OC (where DTPA is diethylenetriaminepentaacetic acid) which was the first receptor radiopharmaceutical available on the market (OctreoScan; Mallinckrodt Medical, St Louis, MO). In this molecule a DTPA group is coupled to the αNH₂ group of the N-terminal DPhe residue.⁵⁷ As opposed to [¹²³I]Tyr³-octreotide, [¹¹¹In]DTPA-OC shows minor accumulation in the liver and is predominantly excreted via the kidneys.⁵⁸ Therefore, the interpretation of scintigrams of the abdominal region is less affected by intestinal background radioactivity.

Clinical studies with [¹¹¹In]DTPA-OC have clearly shown that this receptor radiopharmaceutical is effective in diagnosing and staging tumors and their metastases, due to binding to hSSTR2.^{56,59}

Another analog of octreotide, [¹¹¹In]DOTA-DPhe¹-Tyr³-octreotide [¹¹¹In]DOTA-TOC (where DOTA is tetraazacyclododecanetetraacetic acid), shows similar in vivo accumulation as compared with [¹¹¹In]DTPA-OC.⁶⁰ The purpose of this development was to create a ligand which

could be stably labeled with ⁹⁰Y for receptor-mediated radiotherapy.^{61–64} In this molecule the Phe³ was replaced with Tyr to increase the hydrophilicity of the radiolabeled peptide. DOTA is a universal ligand for labeling with trivalent metal ions, which made feasible also the creation of the positron emission tomography (PET) tracer [⁶⁸Ga]DOTA-Tyr³-octreotide ([⁶⁸Ga]DOTA-TOC^{65,66}) and labeling with ⁶⁷Ga for therapy.⁶⁷

First data for [⁶⁴Cu]TETA-octreotide (where TETA is triethylenetetramine) have recently described a high rate of lesion detection, sensitivity, favorable dosimetry, and pharmacokinetics in a small cohort of NET patients.⁶⁸ Furthermore, several efforts have been made to label octreotide with ^{99m}Tc. [^{99m}Tc]N-α-(6-hydrazinonicotinoyl)-octreotide (HYNIC-octreotide) shows excellent image quality.^{69–71}

Improvements to octreotide itself included the replacement by octreotate, thereby increasing the internalization rate and subsequently the in vivo uptake by hSSTR2-expressing tumor cells.⁶⁸ The change from octreotide to octreotate analogs – differing only in that the C-terminal

Table 21.2 Somatostatin receptor subtype binding of peptides

<i>Radioligand</i>	<i>1</i>	<i>2</i>	<i>3</i>	<i>4</i>	<i>5</i>	<i>Reference</i>
Somatostatin 14	0.1–2.26	0.2–1.3	0.3–1.6	0.3–1.8	0.2–0.9	46
Somatostatin 28	0.1–2.2	0.2–4.1	0.3–6.1	0.3–7.9	0.05–0.4	46
Octreotide (OCT)	200	0.6	10	1000	7	6
	290–1140	0.4–2.1	4.4–34.5	> 1000	5.6–32	46
Lanreotide (LAN)	500–2330	0.5–1.8	43–107	66–2100	0.6–14	46
DTPA-OCT	> 10 000	12	376	> 1000	299	36
[In]-DTPA-OCT	> 1000	1.5	30	> 1000	1	36
	> 10 000	22	182	> 1000	237	
DOTA-Tyr ³ -TOC	> 100	0.9	15	> 1000	700	47
	> 10 000	14	880	> 1000	393	36
[In]DOTA-TOC	> 1000	0.1	250	> 1000	1.0	48
	> 10 000	4.6	120	230	130	
[Y]DOTA-TOC	> 10 000	11	389	> 10 000	114	36
[Ga]DOTA-TOC	> 10 000	2.5	600	> 1000	70	36
	> 10 000	2.5	613	> 1000	73	
DOTA-LAN	154	0.3	15	2.5	0.4	47
	> 10 000	26	771	> 10 000	73	36
[In]/[Y]DOTA-LAN	215	4.3	5.1	3.8	10	47
[Y]DOTA-LAN	> 10 000	23	290	> 10 000	16	36
DOTA-Tyr ³ -octreotate (TATE)	> 10 000	1.5	> 1000	453	547	36
[Y]DOTA-TATE	> 10 000	1.6	> 1000	523	187	36
[Ga]DOTA-TATE	> 10 000	0.2	> 1000	300	377	36
[In]DOTA-1-NaI ³ -octreotide (NOC)	> 10 000	2.9	8	227	11.2	49
[Y]DOTA-NOC	> 10 000	3.3	26	> 1000	10.4	49
[Tc]Depreotide (P829)	> 1000	1	1.5	> 1000	2	37
[In]DOTA-NOC	> 10 000	2.9	8	227	11.2	1
DOTA-NOC-ATE	> 1000	3.6	302	260	16.7	4
DOTA-BOC-ATE	> 1000	0.8	33	80	3.6	4

All values are in nmol/l, indicating the binding affinity constant K_d .

threoninol is replaced with threonine – not only increased the binding affinity, internalization rate, and selectivity of hSSTR2, but clinical studies with Tyr³-octreotate derivatives have shown considerable improvement of SSTR scintigraphy.⁷² Recently, a new octreotate derivatized with the tetramine chelator has been introduced for clinical studies.⁷³ DOTA-1-NaI³-octreotide (DOTA-NOC) shows a 3–4 times higher binding affinity to hSSTR2 than that of DOTA-TOC, together with a good affinity for hSSTR3 and hSSTR5, leading

to an improved tumor uptake and kidney-to-tumor ratio in animal biodistribution studies.⁴⁹ In clinical studies performed with the ¹¹¹In and ⁶⁸Ga-radiolabel, more lesions could be detected with [⁶⁸Ga]DOTA-NOC in comparison to [¹¹¹In]DOTA-NOC and [^{99m}Tc]EDDA-HYNIC-TOC (where EDDA is ethylenediamineacetic acid).⁷⁴ DOTA-NOC-ATE (1-NaT³-Thr²-octreotide) and DOTA-BOC-ATE (B2 Thi³-Thr³-octreotide) also show high affinity to hSSTR2, hSSTR3, and hSSTR5, and some intermediate

Table 21.3 Comparative positron emission tomography (PET) data from the University of Innsbruck: tumor uptake of [⁶⁸Ga]DOTA-lanreotide compared with [⁶⁸Ga]DOTA-TOC in selected patients

Patient no	Diagnosis	Age (years)	Sex	[⁶⁸ Ga]DOTA-lanreotide	[⁶⁸ Ga]DOTA-TOC
1	MTC	52	M	+	–
2	Carcinoid–bowel	60	M	–	++
3	NET	64	F	++	++
4	NET	64	M	–	–
5	Hemangiopericytoma	31	M	–	+
6	NET–VIPoma	40	M	–	++
7	Thyroid CA–poorly differentiated	55	M	–	–
8	Urothelial cell CA	76	M	++	+
9	Hypernephroma	64	M	+	+
10	NET	32	F	++	–
11	Carcinoid–lung	43	F	++	–
12	Adeno-CA–parotid gland	27	M	+	+

MTC, medullary thyroid carcinoma; NET, neuroendocrine tumor; VIP, vasoactive intestinal peptide; CA, carcinoma.

affinity to hSSTR4. Both ¹¹¹In radiopeptides internalize much more efficiently than [¹¹¹In]DOTA-TOC into AR4-2J cells, and show a two-fold higher tumor uptake and significantly lower kidney uptake in animal biodistribution studies compared with [¹¹¹In]DOTA-TOC.⁴⁸ The enhanced tumor uptake of these ligands seems to be related to improved hSSTR2 and hSSTR3 internalization, as it has been shown recently that even highly potent hSSTR5 agonists such as KE108, BIM-23244, and L-817,818 are not able to induce hSSTR5 internalization.⁷⁵

All together, it has to be mentioned that the different chemical structures, different charges, and different hydrophilicities of the SST analogs lead to marked changes in the subtype receptor affinity profiles (Table 21.2).

Lanreotide-based ligands

[¹¹¹In]DOTA-lanreotide ([¹¹¹In]DOTA-LAN; MAURITIUS (Multicenter Analysis of a Universal Receptor Imaging and Treatment Initiative: a eUropean Study)) is a SST analog which is a conjugate of DOTA coupled directly to the N-terminus of lanreotide.⁴⁷ The substance can be stably labeled with a variety of radionuclides. [¹¹¹In]/[⁹⁰Y]DOTA-lanreotide (LAN) binds with high affinity (dissociation

constant K_d 1–12 nmol/l) to numerous primary human tumors. When expressed in COS7 cells, [¹¹¹In]/[⁹⁰Y]DOTA-LAN binds with high affinity to hSSTR2 (K_d ~5 nmol/l), hSSTR3 (K_d 5 nmol/l), hSSTR4 (K_d 3.8 nmol/l), and hSSTR5 (K_d 10 nmol/l), and with lower affinity to hSSTR1 (K_d ~200 nmol/l). A direct comparison of [¹¹¹In]DOTA-LAN with [¹¹¹In]DTPA-OC and [¹¹¹In]DOTA-TOC has resulted in discrepancies in the scintigraphic imaging pattern in one-third of tumor patients concerning both tumor uptake and detection of tumor lesions.⁷⁶ Similar discrepancies were found for the ⁶⁸Ga-labeled analogs, as depicted for selected patients in Table 21.3.

Depreotide-based ligands (P829; NeoTect[®], NeoSpect[™])

Although clinical results with ¹¹¹In- and ¹²³I-labeled peptides have been excellent, extensive efforts have been made in preparing and evaluating peptides labeled with ^{99m}Tc. [^{99m}Tc]P829 has been identified as a suitable hSSTR ligand which binds to hSSTR2, 3, and 5 with high affinity.³⁷ The cyclic hexapeptide domain of the peptide component of [^{99m}Tc]P829 contains the pharmacophore L-tyrosine-D-tryptophan-L-lysine-L-valine, which binds to the SSTR of tumor cells. The therapeutic compound analog P2045 can

be stably labeled with rhenium,⁷⁷ but larger patient studies are missing.

VIP-based analogs

Vasoactive intestinal peptide (VIP) is a 28 amino acid neuropeptide with a broad range of biological activities. VIP receptor scintigraphy uses naturally occurring VIP labeled with ¹²³I in positions 10 and 22 of the amino acids.^{39,78,79}

Although the results obtained suggested [¹²³I]VIP to be a promising tumor tracer with the potential to provide additional information to that of conventional imaging, there are some shortcomings which hamper widespread clinical use of the compound. Attempts have been made to label VIP with ^{99m}Tc, since [¹²³I]VIP is difficult and costly to produce. In developing such a radiopharmaceutical, the ^{99m}Tc-labeled VIP analog TP3654 showed promising results for imaging VIP receptor-positive cancer.⁸⁰ Consequently, Re-labeled products have been suggested for therapy.

Radiolabeled neurotensin analogs

In the periphery, neurotensin (NT) acts as a local hormone, exerting a paracrine and endocrine modulation of the digestive tract.⁸¹ The pharmacological effects of NT result from the specific interaction of the peptide with the cell surface. To date there are three known NT subtype receptors (NTRs). NTR1 is a well documented receptor, including Ca²⁺ release after inositol-1,4,5-triphosphate stimulation,⁸⁷ and activation of mitogen-activated protein kinases (MAPKs)⁸³ via protein kinase C, leading to its role in cell proliferation, and whereas the levocabastine sensitive NTR2 is still a matter of controversy.⁸⁴ NTR3 is non-G protein-coupled and capable of binding the peptide with high affinity.⁸⁵

The prevalence of NT receptors (NTRs) in several human tumors makes it an attractive target for the delivery of cytotoxic drugs and imaging agents^{45,86} which bind to NTRs and induce tumor growth.⁸⁷

The short plasma half-life of NT hinders its clinical application. Some effort has been undertaken to develop NT derivatives for possible clinical application.^{88–90} With the development of Tc(CO)₃-technology, NT analogs are currently being used in clinical trials.^{91,92}

Radiolabeled bombesin/gastrin releasing peptides

Bombesin and gastrin releasing peptide (GRP) are members of a family of brain–gut peptides.⁹³ The 14 amino acid peptide bombesin (BN) has a high affinity for GRP receptors expressed in a variety of tumors. Stimulation of

proliferation by BN was reported for lung, breast, and pancreatic cancer.^{94,95} BN and GRP mediate their action through membrane-bound, G protein-coupled receptors, which include at least four different subtypes, namely the neuromedin B receptor subtype (BB1), the GRP receptor subtype (BB2), the BB3, and BB4 subtypes.⁹⁶ With the exception of the GRP receptor⁹⁷ these have been poorly investigated with regard to their subtypes and function in human tissue. High densities of GRP receptors were identified by in vitro receptor autoradiography in human prostate, breast, and gastrointestinal cancer.^{98,99} Accordingly, interest in developing radiometal labeled BN derivatives was generated.^{100–102} First data show promising results for tumor imaging: [^{99m}Tc]BN,¹⁰³ [^{99m}Tc]RP527,¹⁰⁴ [¹¹¹In]DTPA-Pro¹-Tyr⁴-BN,¹⁰⁵ and [⁶⁴Cu]DOTA-Aoc-BN(7–14) (where Aoc is 8-aminooctanoic acid).¹⁰⁶ Radiolabeled bombesin analogs for radionuclide therapy have recently been postulated.^{42,43}

Radiolabeled cholecystokinin/gastrin analogs

The gastrointestinal peptides cholecystokinin (CCK) and gastrin exist in different molecular forms. Pro-CCK and pro-gastrin can be processed to peptides of variable length, but, as biologically active peptides, they have the same five terminal amino acids at their carboxyl terminus. Both act as neurotransmitters in the brain, and as regulators of various functions of the gastrointestinal tract (i.e. stomach, pancreas, and gall bladder).⁹³ Besides their physiological role as growth factors in the gastrointestinal tract, they can also act as growth factors in some tumor entities, such as colonic, gastric, and brain carcinomas.^{107–109} To date, three CCK receptor subtypes are known. CCK1 (formerly CCK-A) and CCK2 (formerly CCK-B) subtypes are well described,¹¹⁰ distinguishable pharmacologically by their low CCK1- versus high CCK2-affinity for gastrin. CCK2 receptors have been described in small-cell lung carcinomas, medullary thyroid carcinoma, astrocytomas, in sex cord stromal ovarian carcinomas, in some neuroendocrine gastroenteropancreatic tumors, especially insulinomas, in breast and endometrial adenocarcinomas, and in soft tissue tumors, in particular leiomyosarcomas.^{111–113} CCK1 were expressed in neuroendocrine lung and gastroenteropancreatic tumors, and meningiomas.^{113,114} For CCK2 receptor imaging [¹¹¹In]DTPA-DGlu¹-minigastrin has recently been developed and clinically investigated.^{115,116}

Substance P

Substance P, a neuropeptide involved in a variety of functions of the central and peripheral nervous systems, is able to stimulate proliferation of malignant tumor cells.¹¹⁷

One of the substance P receptor subtypes is the neurokinin-1 (NK1) receptor frequently expressed in glial tumors, medullary thyroid cancer, small-cell lung cancer, and pancreatic as well as breast cancer.⁴⁴ However, to date there is only one report of visualization of the thymus in autoimmune disease using an ¹¹¹In-labeled-DTPA derivate of substance P.¹¹⁸

Impact of receptor-mediated imaging

Since its implementation in the late 1980s, SSTR scintigraphy^{54,55} has improved the ability to diagnose, detect, stage, and review the response to therapy in patients with NETs.

The biodistribution of [¹¹¹In]DTPA-OC as well as of [¹¹¹In]/[⁹⁰Y]DOTA-TOC differs from that of [¹¹¹In]/[⁹⁰Y]DOTA-LAN in terms of higher liver and kidney and less bone marrow uptake. Based on this hSSTR binding profile, [¹¹¹In]DOTA-LAN may be a more powerful radioligand for other tumor entities, and [⁹⁰Y]DOTA-LAN for SST-mediated radionuclide therapy.

When directly compared in patients with NETs, discrepancies concerning both the tumor uptake and the detection of tumor lesions were found between [¹¹¹In]DOTA-LAN and [¹¹¹In]DTPA-D-OC or [¹¹¹In]DOTA-TOC in about one-third of patients.¹¹⁹ This divergence is most probably based on the different SSTR binding profiles.

Similar to lanreotide, the newer analog NOC shows a broader receptor binding profile with higher binding affinities for hSSTR3 and hSSTR4 (Table 21.2).

In about two-thirds of patients with NET, [¹¹¹In]DOTA-LAN tumor uptake was found to be lower than that with other octreotide derivatives such as [¹¹¹In]DOTA-TOC.¹¹⁹

This holds true also for patients investigated with the PET ligands [⁶⁸Ga]DOTA-TOC and [⁶⁸Ga]DOTA-LAN (Table 21.3). Therefore, [⁹⁰Y]DOTA-TOC should be considered the first choice radiopharmaceutical for experimental SSTR-based therapy in patients with NETs. Evaluation of the type of radiotracer to be used for SSTR-targeted radiotherapy, based on scintigraphic pattern and dosimetric studies, should, however, always be performed for the individual patient, because of the discrepancies concerning both the tumor uptake and the detection of tumor lesions between the different radiopharmaceuticals available.

Potential *first-choice indications* for [⁹⁰Y]DOTA-LAN remain neuroendocrine carcinoma, radioiodine-negative thyroid cancer, hepatocellular cancer, small- and non-small-cell lung cancer, brain tumors, and possibly malignant melanomas.

Therapeutic approaches

So far, several radionuclides have been used for peptide therapy (Table 21.4). The first nuclide used for this purpose is ¹¹¹In. However, ¹¹¹In has a low β energy and therefore a short particle range. Several mechanisms may contribute to the therapeutic effect of SSTR therapy. Among these is the internalization of the receptor ligand complex.⁷² This binds the radiopharmaceutical to the targeted cells and will be indispensable when using Auger emitters such as ¹¹¹In as radionuclide. On the other hand, the so called ‘crossfire’ of β -particles will affect not only the cell that the radiopharmaceutical is bound to, but also a number of cells in the vicinity. In this case, lower tissue penetration (e.g. ¹⁷⁷Lu versus ⁹⁰Y) may be an important feature for small-sized tumors. (Radio)nuclides that show a small fraction of

Table 21.4 Physical properties of radionuclides used for peptide receptor radionuclide therapy

Radionuclide	$t_{1/2}$ (days)	E_{max} (keV)	Path length (mm)	γ (keV)
¹⁷⁷ Lu	6.7	498	2.1	113 (6.6%) 208 (11%)
⁹⁰ Y	2.7	2280	12	No γ
¹¹¹ In	2.8	14.7 (AE)	<0.01	172 (90%) 247 (94%)
⁶⁷ Ga	3.3	8.6 (AE)	<0.01	93 (39%) 185 (21%)
⁶⁴ Cu	0.53	1673 (β^+) 7, 4; (AE) 578 (β^-)	10 2	1346 (< 1%) No γ

$T_{1/2}$, half-life E_{max} , maximum energy of emitted electrons (β^- particles) and Auger electrons (AE; $K\alpha$ energy of daughter nuclide); branch ratio for ⁶⁴Cu is 61% β^+ electron capture (EC), and 39% β^- decay, γ , γ energies from decay of daughter nuclides to ground state (most prominent only).

Table 21.5 Innsbruck – somatostatin analogs for diagnosis today

1. [⁶⁸Ga]DOTA-Tyr³-octreotide-PET
tracer of choice for staging and restaging
2. [¹¹¹In]DOTA-Tyr³-octreotide-SPECT
tracer of choice for dosimetry preceding radionuclide therapy with [⁹⁰Y]DOTA-Tyr³-octreotide
3. [⁶⁸Ga]DOTA-lanreotide-PET/[¹¹¹In]DOTA-lanreotide-SPECT
tracer of choice for staging and restaging if octreotide is negative or unfavorable/dosimetry preceding therapy with [⁹⁰Y]DOTA-lanreotide
4. [¹⁷⁷Lu]DOTA-Tyr³-octreotate–scintigraphy and dosimetry following high-dose radionuclide therapy
5. [^{99m}Tc]HYNIC-octreotide, [^{99m}Tc]NeoTect®, OctreoScan®

SPECT, single photon emission computed tomography; HYNIC, hydrazinonicotinoyl.

γ emission such as ¹⁷⁷Lu may further be useful for dosimetry, as they allow intratherapeutic imaging. The approaches for diagnostic and therapeutic work-up used at the Innsbruck Medical University are presented in Tables 21.5 and 21.6, respectively.

[¹¹¹In]DTPA-D-Phe¹-octreotide (OctreoScan®)

The Rotterdam group pioneered radionuclide treatment with [¹¹¹In]DTPA-OC (OctreoScan®). Initial results published for the first time in 1994, and later in a small cohort of patients in 1996 using high amounts of [¹¹¹In]DTPA-OC, indicated a significant therapeutic potential for patients with SSTR-expressing tumors.^{61,62} In a follow-up the Rotterdam group¹²⁰ reported that 2/26 patients with GEP tumors who had received cumulative doses of more than 20 GBq had decreases in tumor size by 25–50%, as

evidenced by CT. In a similar NET patient group, Anthony et al.¹²¹ from New Orleans reported prolonged survival in this cohort of patients with a poor clinical prognosis. Despite improved clinical status and a low rate of side-effects at both study centers, CT-measurable tumor load was rare.

In a more recent study,¹²² the Melbourne group reported in 21 GEP tumor patients a 67% stabilization rate on CT and improvement or stabilization on scintigraphy in 77% of patients using a combined scheme of high-dose OctreoScan® plus 5-fluorouracil chemotherapy as radiosensitizing agent.

The Toulouse group¹²³ came up with a report on 19 patients in whom 6.6 GBq was administered in 3-month intervals. Patients were followed for up to 3.8 years. In a single patient a partial remission (PR) was seen, eight patients had stable disease (SD), and the other patients were progressive. The results are in line with other observations that the overall response to treatment correlates with the extent of tumoral disease. Many patients could gain more benefit from peptide-mediated radionuclide therapy if treated earlier.

Table 21.6 Innsbruck – somatostatin analogs for therapy today

1. [⁹⁰Y]DOTA-Tyr³-octreotide for patients with larger NET (crossfire effect)
2. [¹⁷⁷Lu]DOTA-Tyr³-octreotate for patients with smaller NET (Auger electrons)
3. [⁹⁰Y]/[¹⁷⁷Lu]DOTA-lanreotide – broader spectrum of SSTR binding, thus higher soft tissue and bone marrow dose; if octreotide analogs show no satisfactory tumor accumulation

SSTR, somatostatin receptor.

[⁹⁰Y]DOTA-D-Phe¹-Tyr³-octreotide ([⁹⁰Y]DOTA-TOC)

Despite differences in the protocols used since its first application, complete remissions (CRs) were rarely reported. PRs in most studies were around 25% and the stabilization rate was around 50%, which gave an overall response to therapy of about 75% (Table 21.7).

The Basel group was the first to report the *in vivo* administration of [⁹⁰Y]DOTA-D-Phe¹-Tyr³-octreotide in patients with NETs.^{63,64,124,131,132} In their first group of patients a dose-escalating treatment scheme was applied with a cumulative dose of 6 GBq/m².¹³¹ Later, in four treatment

Table 21.7 Representative treatment results in patients with NETs using [⁹⁰Y]DOTA-D-Tyr³-octreotide ([⁹⁰Y]DOTA-TOC)

<i>Basel</i> ¹²⁴	39 GEP and bronchial carcinoids	Up to a cumulative dose of 7.4 GBq/m ² in four cycles	5% CR, 18% PR, 69 % PR
<i>Milano</i> ¹²⁵	114/141 NET, 59/141 GEP	7.4–26.4 GBq in 2–16 cycles, administered 4–6 weeks apart	76% overall clinical benefit, 26% overall objective response (CR, PR)
<i>Rotterdam and Tampa</i> ¹²⁶	54 GEP	Up to a cumulative dose of 14.8 GBq in four cycles	7% PR, 13% MR, 61% SD
<i>Iowa City</i> ¹²⁷	21 GEP	Up to 13.3 GBq in three cycles	66% overall response
<i>Vienna</i> ¹²⁸	10	4 × 1.8 GBq, 28 Gy	25% PR, 50% CR
<i>Innsbruck</i> ¹²⁹	98 GEP	2-4 GBq per cycle until tumor progression (see also Figure 21.1)	22% PR, 50% SD
<i>Bad Berka</i> ¹³⁰	57	Up to a max. cumulative dose of 3.5 GBq in up to six cycles	20% PR (60% SD)

GEP, gastroenteropancreatic; CR, complete remission; PR, partial remission; MR, minor response; SD, stable disease

cycles¹³² or two treatment cycles¹³³ the treatment substance was given up to a cumulative dose of 7.4 GBq/m². Tumor response was found in 23%¹³² and 33%,¹²⁶ respectively. Whereas the first applications were done without renal protection, all later studies were performed under amino acid infusion.

The Milan group injected up to 5.2 GBq per cycle, which they defined as maximum tolerated dose per cycle.^{125,134} The group reported a response rate of 29% in patients with 21 GEP tumors after two treatment cycles with a cumulative dose of 5.9–11.1 GBq.¹²⁶ The Milan summary¹²⁷ includes 141 patients, among whom 114 patients were affected by NETs, and 59 patients had GEP tumors. An overall objective response was observed in 26% (PR, CR) of patients. Considering the progressive status of disease in 80% of patients, an overall clinical benefit was observed in 76% (CR, PR, SD). Stable patients showed a response (CR, PR) in 32%. The duration of response was 2–59 months with a median of 18 months overall, and a median of 13 months in progressing patients and 16 months in stable patients.

The Rotterdam group together with centers in Brussels, Belgium, and Tampa (Florida) injected escalating doses up to 14.8 GBq in four cycles, or up to 9.3 GBq in a single administration.¹³⁰ These administrations were done up to a cumulative radiation dose to the kidneys limited to 27 Gy, and all 54 patients received amino acids concomitantly for kidney protection. In 7% PR and in 13% minor response (MR) was measured. The median time to progression in 44 patients who had stable disease was 30 months.

Recently, the Iowa City group¹³⁵ reported an overall clinical response of 66% in 21 patients with GEP, allowing a total cumulative dose of 13.3 GBq in three cycles.

The Bad Berka group¹³⁶ summarized results from 57 patients treated with 3.25 GBq up to six times with a 3–6-month time interval between each treatment cycle. Despite that, no CR was seen, 20% of patients had PR, and 60% had SD, providing an overall response of 80%.

Since 1997 we have treated more than 100 patients with [⁹⁰Y]DOTA-TOC.¹²⁹ In general, our current treatment schedule (Figure 21.1) foresees 3–4 cycles with 3.7 GBq, given under kidney protection with amino acids, up to a cumulative kidney dose of 28 Gy. If the patient shows response to therapy in terms of MR, PR, or SD, a further 1–3 treatment cycles are added individually according to the clinical status of the patient. Radioactive treatment is usually applied every 10 weeks with long-acting octreotide (two injections) between the radioactive treatments (Figure 21.2). Restaging is done in all patients with [⁶⁸Ga]DOTA-TOC-PET and repeated dosimetry with [¹¹¹In]DOTA-TOC. A representative case is shown in Figure 21.3. All patients also undergo repeated [¹⁸F]FDG-PET (FDG is fluoro-2-deoxy-D-glucose) scanning.

[¹⁷⁷Lu]DOTA-Tyr³-octreotate **([¹⁷⁷Lu]DOTA-TATE)**

Reports with larger numbers of patients in treatment protocols using [¹⁷⁷Lu]DOTA-TATE (Tyr³-octreotate) are limited to the Rotterdam group,¹³⁷ who also initiated this kind of treatment. In 131 patients, cumulative doses of 22.2–29.8 GBq were applied, and CR was observed in 2%, PR in 26%, MR in 24%, and SD in 35% of patients. Most significantly, median time to progression of more than

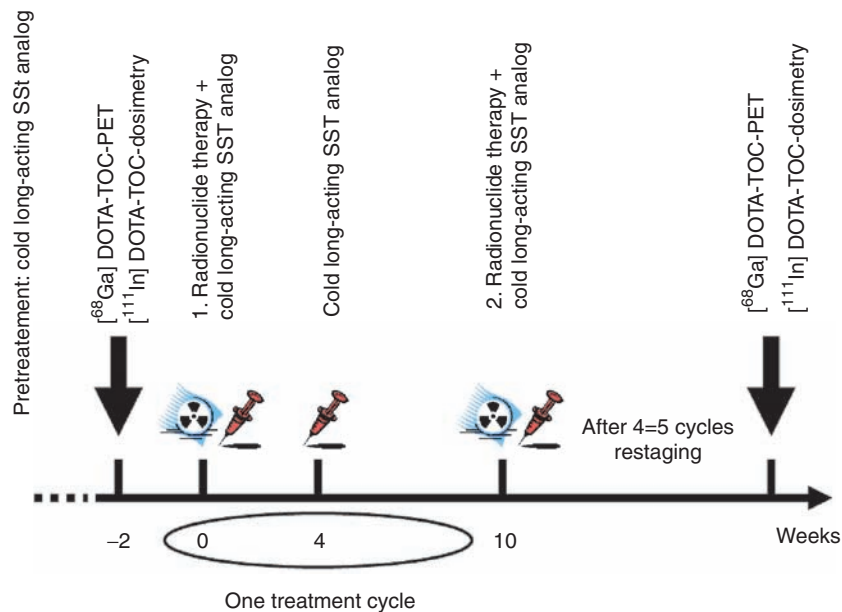


Figure 21.1

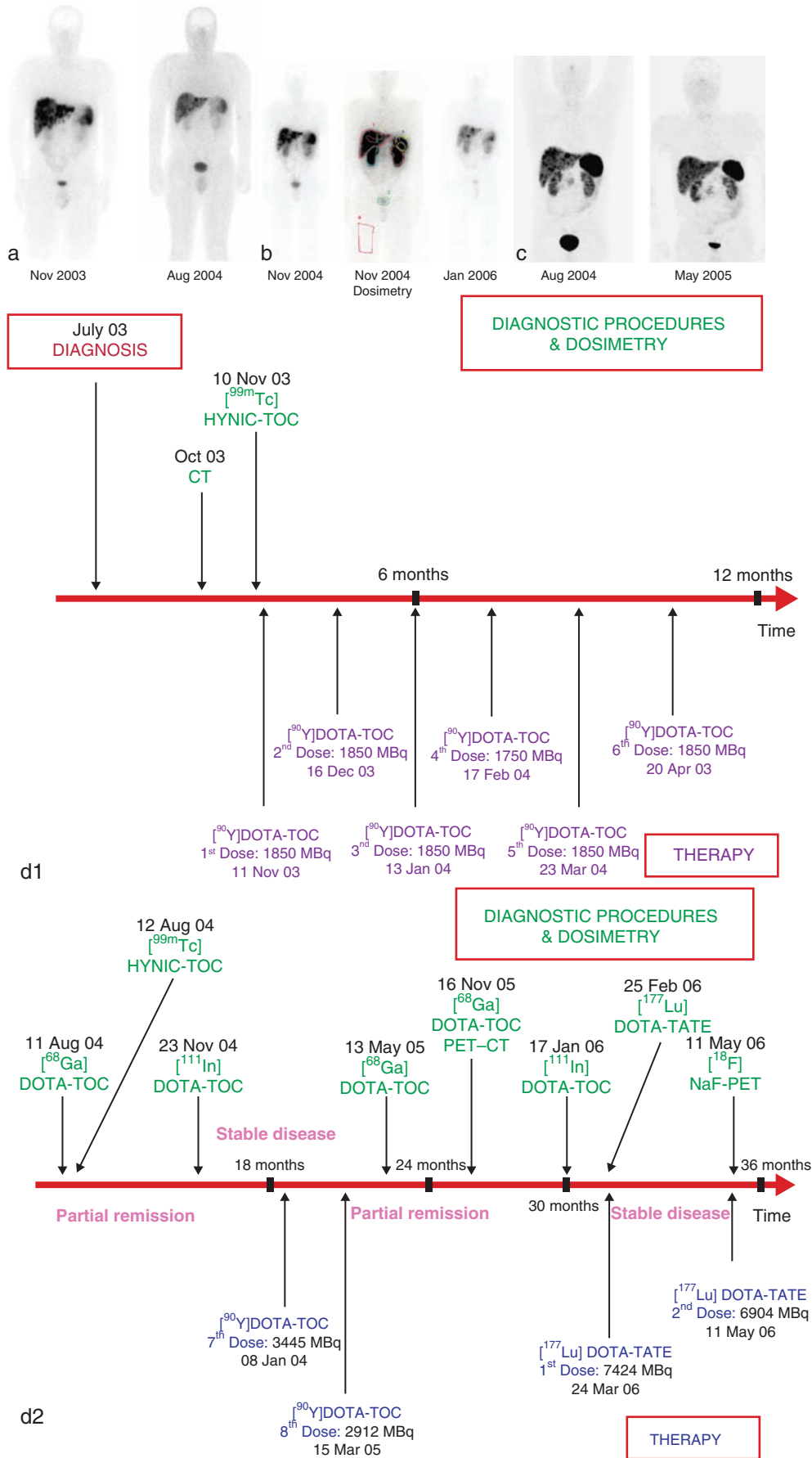
Current treatment scheme used at the University of Innsbruck. Initial evaluation for treatment is done by ^{68}Ga DOTA-TOC. (where DOTA is tetraazacyclododecanetetraacetic acid and TOC is Tyr³-octreotide). A highly positive positron emission tomography (PET) scan predicts high somatostatin receptor (SSTR) expression and response to treatment with ^{90}Y DOTA-TOC. Dosimetry with ^{111}In DOTA-TOC is then performed for tumor dose and critical organ dose estimation. Treatment is started with a fixed dose of 3.7 GBq ^{90}Y DOTA-TOC under kidney protection with amino acids. The patient is dismissed from hospital with an intramuscular injection of long-acting octreotide (dose 20–30 mg). A second long-acting octreotide injection is given after 4 weeks, and after 6 weeks the next radionuclide therapy cycle is applied. Such a treatment cycle is repeated 4–5 times until restaging.

36 months was seen in 103 patients who had either SD or tumor progression. Remission rates were higher in patients with high pre-therapeutic SST agent uptake and a limited number of liver metastases, whereas PD was more frequent in patients with a low performance score and extensive disease.

At Innsbruck, we have so far involved in this kind of treatment only patients who had previously already undergone treatments with the ^{90}Y -labeled derivatives. One of 20 patients treated to date is depicted as an example in Figure 21.4.

Figure 21.2

Follow-up in a patient with pancreatic carcinoid aged 50 years treated with ^{90}Y DOTA-TOC (cumulative dose 18.5 GBq) by $^{99\text{m}}\text{Tc}$ HYNIC-TOC (where HYNIC is hydrazinonicotinoyl (a), ^{111}In DOTA-TOC (b), and ^{68}Ga DOTA-TOC (c). The images indicate partial remission of liver metastases in all three imaging modalities over the treatment years. The treatment schedule since 2003 is depicted in (d). $^{99\text{m}}\text{Tc}$ -HYNIC-TOC (a) scan at 4 hours post-injection of 400 MBq. ^{111}In DOTA-TOC dosimetry (b). After injection of 200 MBq, serial whole-body images were acquired up to 48 hours post-injection (the images depict the 24-hour acquisition). The estimated tumor dose was 10 Gy/GBq for representative liver lesions, the dose to the kidneys 4.5 Gy/GBq, the liver dose 1.52 Gy/GBq, the bone marrow dose 0.06 Gy/GBq, and the spleen dose 8.85 Gy/GBq. The effective dose was 0.41 Sv. ^{68}Ga DOTA-TOC whole-body PET (c) was performed at 90 minutes post-injection of 200 MBq. (d) Reviewing the treatment schedule of the patient from November 2003 until May 2006, the patient had received a cumulated total dose of 31.7 GBq. The estimated total tumor dose was 130 Gy for the representative liver lesions, the cumulated total dose to the kidneys 77.7 Gy, the liver dose 28.8 Gy, the bone marrow dose 1.3 Gy and the spleen dose 160.5 Gy. The effective dose was 7.7 Sv. The treatment response was partial remission, and no toxicity was noted. In particular, hematological parameters and kidney function remained in the normal range over the whole treatment and follow-up period since 2003. Creatinine clearance was slightly decreased, but remained within the normal range.



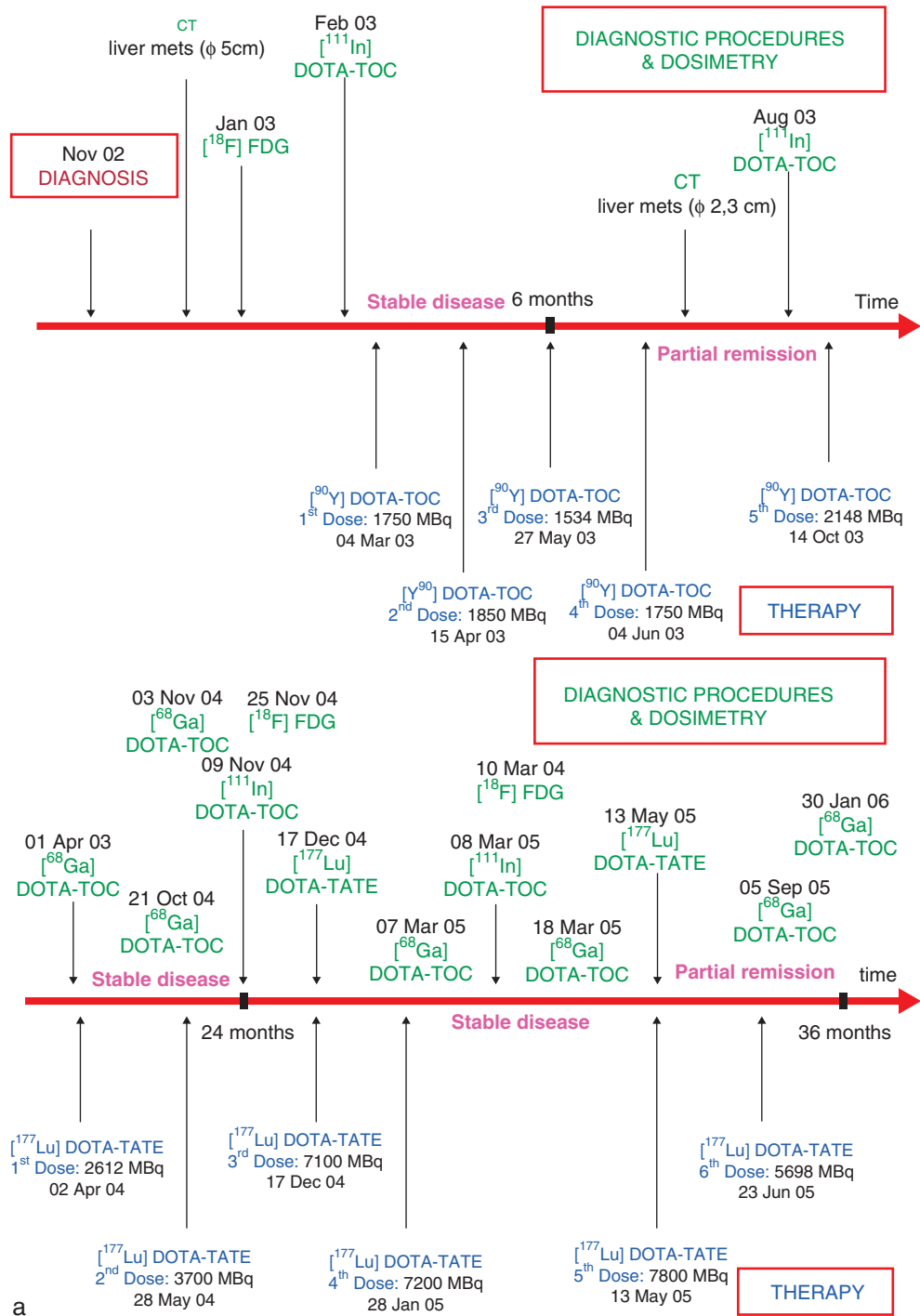


Figure 21.3

Follow-up in a patient aged 62 years with a neuroendocrine tumor (NET) (primary unknown) treated with [⁹⁰Y]DOTA-TOC and [¹⁷⁷Lu]DOTA-TOC. (a) Treatment schedule since 2002. In the patient, the diagnosis was established in 2002 with high-grade NET of unknown origin and liver, lymph node, and bone metastases. Following diagnosis, chemoembolization of liver metastases was performed. Later, the patient was referred for possible therapy with radioactive analogs to our center in Vienna, Lainz Vienna City Hospital, where he received on an outpatient basis treatments with [⁹⁰Y]DOTA-TOC. After stabilization, further treatment with [¹⁷⁷Lu]DOTA-TATE (where TATE is Tyr³-octreotate) was given at the University of Innsbruck as depicted.

Reviewing the treatment schedule of the patient from March 2003 to June 2005, the patient had received a cumulated total dose of 43.1 GBq. The estimated total tumor dose was 150 Gy for the representative tumor lesions, the cumulated total dose to the kidneys 40.9 Gy, the liver dose 8.4 Gy, the bone marrow dose 1.7 Gy, and the spleen dose 32.5 Gy. The effective dose was 3.9 Sv. The treatment response was partial remission, and no toxicity was noted. In particular, hematological parameters and kidney function remained in the normal range over the whole treatment and follow-up period since 2003. Creatinine clearance remained stable and within the normal range.

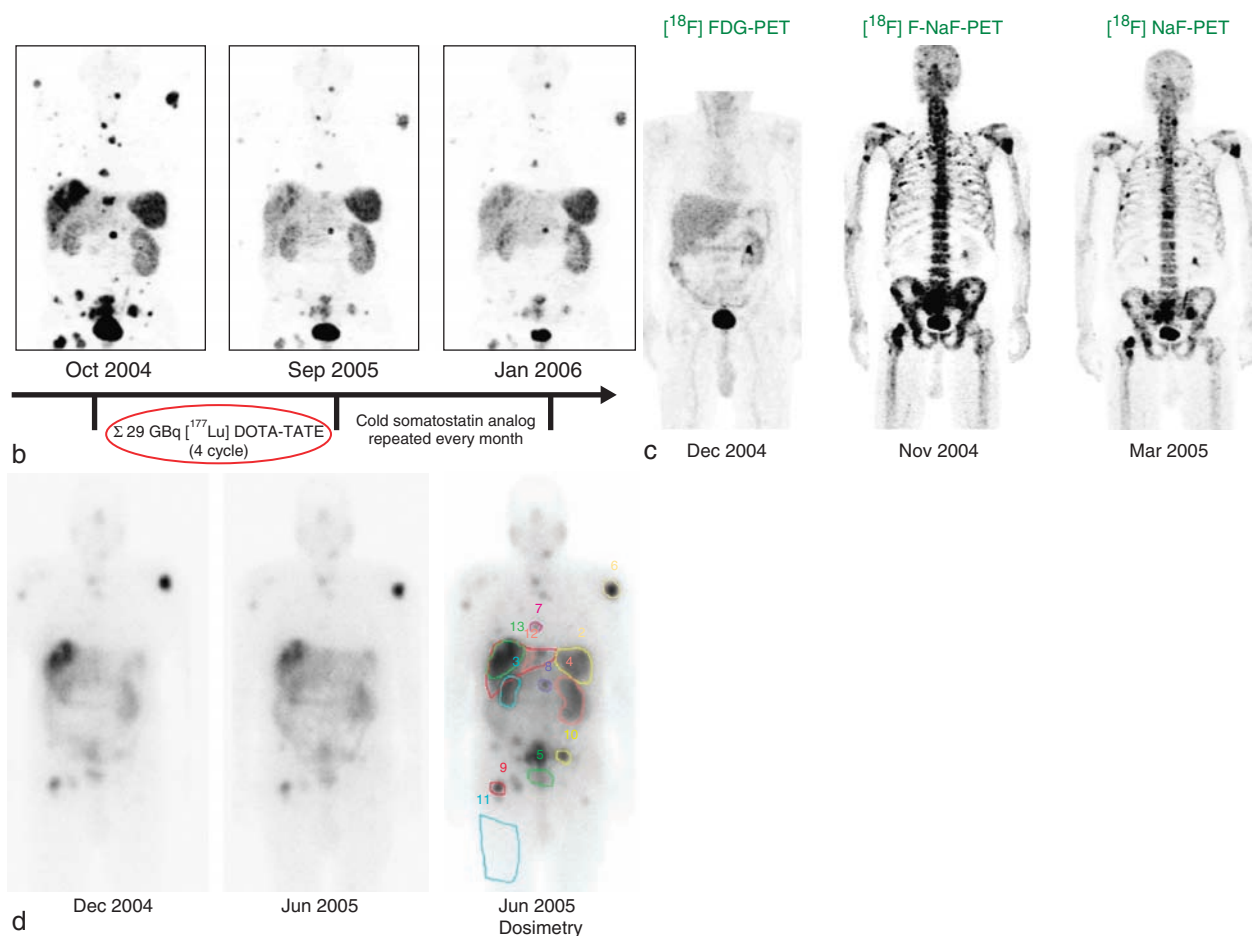


Figure 21.3—cont'd

(b) ^{68}Ga]DOTA-TOC-PET scans indicated partial remission of liver, lymph node, and bone metastases following treatment with ^{177}Lu]DOTA-TATE. The images were acquired at 90 minutes post-injection of 200 MBq. (c) ^{18}F]FDG-PET (where FDG is fluoro-2-deoxy-D-glucose) was negative, whereas ^{18}F]NaF-PET (where NaF is sodium fluoride) bone scanning was highly positive at the time of treatment initialization. Following treatment, a partial response for the bone metastases was observed as well. (d) ^{177}Lu]DOTA-TATE whole-body scan and dosimetry during the first treatment cycle and after four treatment cycles as depicted in (a). After treatment with 7.4 MBq, serial whole-body images were acquired up to 96 hours post-injection (the images depict the 24-hour acquisition of the geometric mean with the regions of interest set for dosimetry). The estimated tumor dose was 25 Gy/GBq for representative lesions, the dose to the kidneys 0.49 Gy/GBq, the liver dose 0.10 Gy/GBq, the bone marrow dose 0.03 Gy/GBq, and the spleen dose 0.48 Gy/GBq. The effective dose was 0.06 Sv.

Also, the Basel group¹³⁸ reports 27 patients pretreated with ^{90}Y]DOTA-TOC. Patients received a fixed dose of 7.4 MBq ^{177}Lu]DOTA-TATE. Restaging after 8–12 weeks showed PR in two patients, MR in five patients, and SD in 12 patients, suggesting a safe and efficacious form of retreatment modality. The time of remission ranged from 4 to 13 months. These authors suggested that obviously a positive prognostic factor for further radionuclide treatment with ^{177}Lu]DOTA-TATE exists in a good response to ^{90}Y]DOTA-TOC.

^{90}Y]DOTA-Tyr³-octreotate (^{177}Lu]DOTA-TATE)

The Bad Berka group¹³⁹ reported in 75 patients a rate of 37% PR and SD in 52%; thus, objective tumor response was seen in 85% of the patients. In this study the mean activity applied was 3.6 GBq, and the time between cycles ranged from 3 to 6 months. Besides tumor shrinkage, significant clinical response was seen in terms of symptom reduction, low toxicity, and few adverse effects.

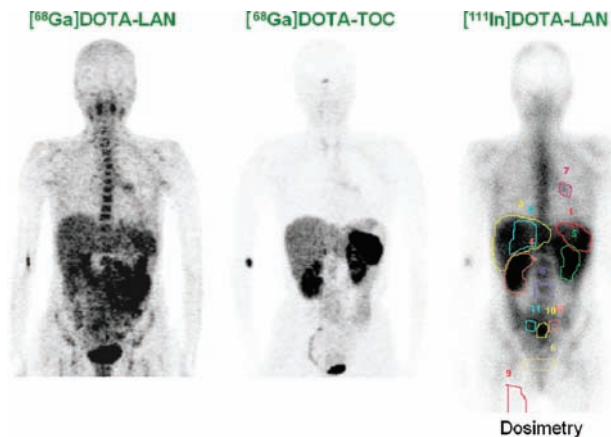


Figure 21.4

Treatment evaluation with $[^{68}\text{Ga}]\text{DOTA-LAN}$ (where Lan is lanreotide) versus $[^{68}\text{Ga}]\text{DOTA-TOC}$. In this patient age 42 years with lung carcinoid/neuroendocrine carcinoma, $[^{68}\text{Ga}]\text{DOTA-TOC}$ -PET scanning as first choice modality was negative. Therefore, therapy evaluation was performed with $[^{68}\text{Ga}]\text{DOTA-LAN}$, which indicated sufficient accumulation in the tumor lesions. Following dosimetry, the patient is currently treated with $[^{90}\text{Y}]\text{DOTA-LAN}$. The estimated tumor dose was 15 Gy/GBq, the dose to the kidneys 1 Gy/GBq, the liver dose 0.22 Gy/GBq, the bone marrow dose 0.09 Gy/GBq, and the spleen dose 0.56 Gy/GBq. The effective dose was 0.09 Sv.

$[^{67}\text{Ga}]\text{DOTA-Tyr}^3\text{-octreotide}$ ($[^{67}\text{Ga}]\text{DOTA-TOC}$)

^{67}Ga -labeled radiopeptides may become a new class of labeled peptides for radionuclide therapy, based on the high microdosimetric effect of Augerelectrons produced by the electron-capture decay of ^{67}Ga . In first clinical applications the Hannover group⁷² reports promising results in a series of ten patients with high $[^{68}\text{Ga}]\text{DOTA-TOC}$ uptake.

$[^{177}\text{Lu}]\text{DOTA-Nal}^3\text{-octreotide}$ ($[^{177}\text{Lu}]\text{DOTA-NOC}$)

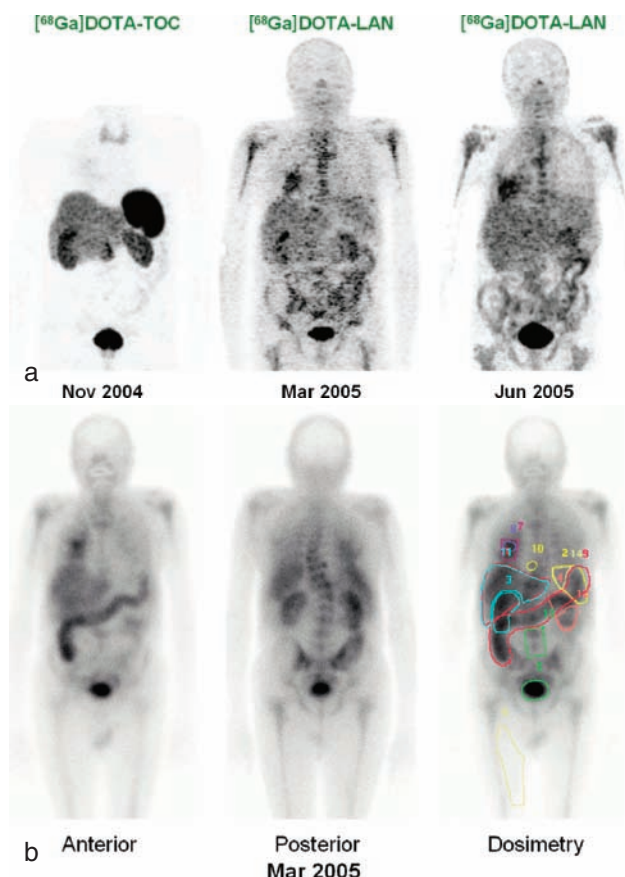
This new SST analog was recently used for the first time for treatment in patients in whom a higher $[^{111}\text{In}]\text{DOTA-Nal}^3\text{-octreotide}$ uptake as compared to OctreoScan was measured.¹⁴⁰ As with lanreotide analogs (see below), due to the binding to a broader spectrum of SSTR, especially hSSTR3, a higher background activity is observed, as well as higher doses to normal organs. In line with this observation, despite higher tumor uptake, the Bad Berka group¹⁴¹ discontinued treatment with this substance.

$[^{90}\text{Y}]\text{DOTA-lanreotide}/[^{177}\text{Lu}]\text{DOTA-lanreotide}$

The first data (phase I/IIa trial) that suggested a significant potential for $[^{90}\text{Y}]\text{DOTA-LAN}$ for SST receptor-positive tumors were obtained in the Vienna–Innsbruck Multicenter Study which was initiated in 1997. Subsequently, the results of the European study MAURITIUS (Multicenter Analysis of a Universal Receptor Imaging and Treatment Initiative, an eUropean Study) confirmed the potential usefulness of $[^{111}\text{In}]/[^{90}\text{Y}]\text{DOTA-LAN}$ for diagnosis/therapy in 154 patients with different tumor entities expressing hSSTR.⁷⁶ A further review of the MAURITIUS trial was presented in May 2003, after 5 years of follow-up¹⁴² (Figures 21.4 and 21.5). The data analyzed included those for 235 patients with neuroendocrine tumors, thymoma, thyroid cancer, brain tumors, lymphoma, intestinal adenocarcinoma and some rare tumors.⁷⁶ Patients had received up to an accumulated dose of 8.5 GBq of $[^{90}\text{Y}]\text{DOTA-LAN}$ which was applied in up to seven treatment applications. $[^{90}\text{Y}]\text{DOTA-LAN}$ was given either intravenously (121 patients), intra-arterially (21 patients), or by local intratumoral injection (93 patients). Patients were at a stage of progressive disease when entering treatment. During the follow-up period, disease was evaluated by repeated scintigraphy and computer tomography/magnetic resonance imaging, documenting the response to therapy (in terms of stable tumor disease, progressive disease, partial remission, or complete remission), as well as by documenting the time of progression of disease and quality of life parameters. Overall results indicate that beneficial effects can be suspected from therapy with $[^{90}\text{Y}]\text{DOTA-LAN}$. The 5-year follow-up period indicated that 37% (40/109) of the patients treated with $[^{90}\text{Y}]\text{DOTA-LAN}$ had stable disease and 18% (18/109) had partial remission of tumor lesions. Objective response of quality of life measurements was documented in 10–20% of patients, and subjective response was found in 30–50% of patients. So far, results of the MAURITIUS trial indicate that radiolabeled SST analogs may be considered in patients with SSTR-positive tumors for size reduction and improvement of quality of life parameters. Furthermore, the new tracer $[^{68}\text{Ga}]\text{DOTA-LAN}$ may provide helpful information in the pretherapeutic work-up of patients suitable for therapy with $[^{90}\text{Y}]\text{DOTA-LAN}$.¹⁴³

$[^{131}\text{I}]\text{MIBG}$ and $[^{90}\text{Y}]\text{DOTA-Tyr}^3\text{-octreotide}$

A potential advantage of combined $[^{131}\text{I}]\text{MIBG}$ (metaiodobenzylguanidine) and $[^{90}\text{Y}]\text{DOTA-TOC}$ therapy was recently proposed by the Iowa group¹⁴⁴ on the basis of

**Figure 21.5**

Patient with small-cell lung cancer and only weak positive $[^{68}\text{Ga}]\text{DOTA-TOC}$ binding to the recurrent lung tumor mass followed by $[^{68}\text{Ga}]\text{DOTA-LAN-PET}$ prior to and after therapy (a) with 7.4 GBq $[^{177}\text{Lu}]\text{DOTA-lanreotide}$ (b). The estimated tumor dose was 10 Gy/GBq, the dose to the kidneys 4.8 Gy/GBq, the liver dose 6.6 Gy/GBq, the bone marrow dose 2.24 Gy/GBq, and the spleen dose 1.85 Gy/GBq. The effective dose was 0.47 Sv.

an analysis of published data. Because of the differences in biodistribution and critical organ targeted therapy in NET patients, such combined targeted therapy in NET patients could provide a significant increase in the delivered tumor dose over either agent alone. The magnitude of increase depends on the relative dose delivered by each agent. The optimal tumor dose for the combined agent will occur when the dose per activity delivered to the tumor by the $[^{90}\text{Y}]\text{DOTA-TOC}$ is 2–3 times that of $[^{131}\text{I}]\text{MIBG}$.

Procedures

Selection of patients for radiopeptide therapy

The various response rates reported for radiopeptide therapy may at least be in part due to differences in patient selection. In principle, all patients with tumors known to express hSSTR are eligible for the application of high-dose radiolabeled SST analogs, provided that the tumors demonstrate sufficient uptake of the radiolabeled peptide on scintigraphy.

It is still a matter of discussion at which stage of the disease we should start treatment with radiopeptides.

Most patients treated so far with radiolabeled peptides had no other treatment option, were refractory to conventional treatment strategies, and/or were at a progressive stage at the time of the first treatment application. In fact, a ‘wait and see’ attitude is not justified any longer, as results from larger trials are nowadays available. Results from those centers who have treated larger numbers of patients point to the fact that one can expect better treatment results, the earlier therapy is initiated. Furthermore, the better is the Karnofsky score the better also is the therapeutic outcome.

Another important parameter seems to be the uptake of radiolabeled SST analog by the tumor. Therefore, a highly positive scintigraphic study and a proceeding dosimetric evaluation are prerequisite for the initiation of treatment with radiolabeled peptides (Figure 21.1, Tables 21.5 and 21.6). Usually, patients who were included in therapeutical trials had multiple sites of disease, as evidenced by scintigraphic and dosimetric evaluation with $^{111}\text{In}/^{99\text{m}}\text{Tc}$ -labeled peptides and/or by imaging with PET performed with $^{86}\text{Y}/^{68}\text{Ga}$ -labeled peptide analogs. Patients with less liver involvement seem to respond better than those with extensive liver burden.

In general, the clinical protocols available are designed such that tumor uptake is controlled by dosimetry, or at least by repeated scintigraphic studies which score the tumor uptake prior to, and during the whole treatment and

follow-up period. The MAURITIUS study⁶¹ included an extensive dosimetry protocol, as also did the studies by the Rotterdam Group together with the group in Brussels.^{130,137}

Substances known to block hSSTRs such as octreotide or lanreotide are usually withdrawn at least 7 days prior to a planned dosimetric study and prior to each treatment cycle. However, there are conflicting data on the withdrawal of pre-existing therapy with long-acting SST analogs (see below).

Discontinuation of treatment

Usually, treatment is discontinued if the patient shows progressive disease under treatment with the radiolabeled peptide, or in the case of dose-limiting toxicity. Dose-limiting toxicity is mostly regarded as the failure of kidney function.

Diagnostic and dosimetric evaluation

There is no standard dosimetry protocol available. At Innsbruck, the protocol for each patient follows standard nuclear medicine procedures and includes serial whole-body scintigraphies. For organ and tumor dose calculation, regions of interest (ROIs) are drawn on every whole-body scintigram at each acquisition time up to 72 hours. The mean of the anterior and posterior counts is calculated for large ROIs of the liver, spleen, kidneys, and urinary bladder. In addition, ROIs are drawn for all tracer accumulations regarded as tumor sites and background regions using the software written for the camera analyzing system. The background and decay are corrected to the time of injection. The derived residence times are used for organ dose calculation on the basis of the Medical Internal Radiation Dose (MIRD) concept for the organ dose calculation, and the 'nodule module' option of the program for estimating the self-s values of spherical tumors for tumor dose calculation, as described previously.¹⁴⁵ The effective dose, as defined by the International Commission on Radiological Protection (ICRP), is also calculated. For the assessment of tumor volume, conventional radiological techniques such as CT and/or MRI are used.

The primary critical organ with radiopeptide therapy is the kidney, because small peptides are filtered through the glomerular capillaries and are reabsorbed by the proximal tubular cells. In external beam radiation, the critical dose to the kidneys is set in most protocols to about 30 Gy (or below) accumulative dose of the radiopeptide. Some groups have thus recommended infusion of positively charged amino acids such as L-lysine or L-arginine to reduce renal uptake of peptide radiotracers (see below).

There has been some debate on the type of tracer used for diagnostic calculations, i.e. estimations. Adequate dosimetry prior to peptide therapy is mandatory and the most effective surrogate should be used, i.e. for instance [⁸⁶Y]DOTA-TOC for [⁹⁰Y]DOTA-TOC therapy. However, such isotopes are limited to only a few centers, and a more widely feasible method should be used. In our opinion we agree with the Basel group¹⁴⁶ that dosimetry should be performed with the same peptide used for therapy, and not with OctreoScan® as a first choice tracer. Recent data have also pointed out that there exist only minimal differences in the pharmacokinetics of [¹¹¹In]DOTA-TOC and [¹⁷⁷Lu]DOTA-TATE.¹⁴⁷ Practically, if individual dosimetry is performed in every patient and if several treatment cycles are planned, dosimetry would be most adequate when being performed during the first treatment cycle by adding the ¹¹¹In-labeled substance. It has been the attitude that kidney toxicity is the dose-limiting parameter. But no clear data are available on the relation between absorbed dose and irreversible renal toxicity in internal radiotherapy. Therefore, the patient should not be excluded from beneficial treatment due to strict settings which are not proven and can be overcome.

Dose and administration of radiolabeled peptide

The administration of radiolabeled peptides was done either intravenously, intra-arterially, or intratumorally, for example in the MAURITIUS trial.^{76,142,148} For intravenous injections, many different regimens were used with either radiopeptide. Starting with escalating doses in the early phase 1 trials with [⁹⁰Y]DOTA-TOC, fixed doses are given in most of the clinical applications nowadays. A single 3.7–5.2-GBq dose of [⁹⁰Y]DOTA-TOC per cycle can be regarded as tolerable if the individual dosimetry data are in favor of radionuclide therapy. With cumulative doses up to 15 GBq, usually the kidney dose of about 30 Gy is reached. However, we have given cumulated kidney doses of 80 Gy in individual patients treated first with [⁹⁰Y]DOTA-LAN and/or with [⁹⁰Y]DOTA-TOC and/or [¹⁷⁷Lu]DOTA-TOC, over years, without seeing notable kidney toxicity (see also Figures 21.3 and 21.4). Dosing of radiopeptides, in our point of view, is more complex than limiting the maximal tolerable dose to be applied to the estimation of tolerable kidney dose that has only empirically been adapted from external beam radiation to around 30 Gy. Therefore, the calculated absorbed kidney dose can only be a guideline for our therapy decision. The fact that NET patients usually have no other treatment option makes their exclusion from radiopeptide treatment ethically unacceptable. The therapeutic situation is best displayed by the reality that most of our patients have already undergone

potentially nephrotoxic or hematotoxic therapies such as [¹³¹I]MIBG, or cisplatin.

In most centers, therapeutic applications are repeated only if the patient does not have dose-limiting toxic reactions (i.e. World Health Organization (WHO) grade 4 hematological toxicity or grade 3 non-hematological toxicity), has stable disease or tumor regression with measurable persistent disease, and if the blood count, levels of hepatic and renal function, and performance status in the ranges originally required for patient entry into the study.

Evaluation of therapeutic response

Tumor burden

Evaluation of the tumor disease response is performed according to WHO standard criteria. Accordingly, disease is classified as complete remission, CR (disappearance of all tumor masses for a minimum of 4 weeks), partial remission, PR (decrease of all tumor masses by at least 50% without appearance of new lesions for a duration of at least 4 weeks), stable disease, SD (no significant regression (i.e. > 50% of all lesions) or increase (i.e. < 25% of measurable tumor masses, no new lesions), or progressive disease, PD (increase of known tumour masses by > 25%, or appearance of any new lesions).

As with other treatment modalities, CT and/or MRI are performed repeatedly to measure tumor burden and to document response to therapy. A tumor size dose–response relationship is documented in most centers. In general, the smaller are the tumor lesions in patients treated with radiolabeled peptides, the better is the response observed for these particular lesions.

Time of regression/progression of disease

In addition to the evaluation of tumor disease response to treatment, the time to disease progression and the survival time are usually recorded. There are long-term data now available.

Under therapy with [¹⁷⁷Lu]DOTA-TATE, the median time to progression in 103 patients who had either SD or tumor regression was more than 36 months and thus this was more beneficial as compared with chemotherapy.¹³⁷ Also cardiac adverse effects, as well as vomiting and hematological toxicity, are much more frequent with chemotherapy than with treatment with radiopeptides. Randomized trials have not established a standard chemotherapy protocol, and most evaluated chemotherapies have had response rates of < 20%.¹⁴⁹

For [⁹⁰Y]DOTA-TOC, the Rotterdam group, in 44 patients with MRs, PRs, or SD documented a median time to progression of 30 months.¹³¹ The Milan group reported a median duration of response of 9 months for a group of 21 patients.¹²⁶

Long-term and survival statistics for patients treated with [⁹⁰Y]DOTA-LAN therapy are available in the form of a 5-year follow-up in patients with radioiodine-negative thyroid cancer including MTC.¹⁴² Improved progression-free and overall survival was also reported by the London group.¹⁵⁰

Biochemical parameters

Tumor markers most commonly used for following the treatment of respective tumor entities are measured before and under therapy. Changes in laboratory parameters such as in serotonin, gastrin, chromogranin, neuron-specific enolase (NSE), or thyroglobulin serum levels have frequently been found. However, no conclusions can be drawn on the general behavior of hormone values in hormone-producing tumor patients under ongoing therapy. However, an early decline of the specific tumor markers reflects response to radionuclide therapy, and therefore these parameters are regularly measured before each therapy cycle.

Quality of life parameters

In symptomatic patients, treatment with long-acting SST analogs is the therapy of choice and is highly effective in these patients for symptom reduction.¹⁵¹

Following treatment with radiolabeled SST analogs in patients with metastasized tumors, with or without systemic therapy with long-acting SST analogs (see below), regardless of its effects on tumor shrinkage, improved quality of life was repeatedly reported.

In line with the generally accepted European Organization for Research and Treatment of Cancer (EORTC) QLQ-C30 questionnaire,¹⁵² we have evaluated the impact of radionuclide treatment in patients undergoing therapy with [¹¹¹In]DOTA-LAN. Improvement in quality of life for some months, sometimes over years, was reported for patients in all MAURITIUS centers.⁷⁶ Objective response of quality of life measurement documented an improvement in the quality of life in 10–20% of patients, and subjective improvement was reported in 30–50% of patients. A reduction of general pain, bone pain reduction or relief, reduction of headache, and improvement of sleeping behavior, appetite, weight, and general well-being were found. Most patients with subjective improvement reported this after single injections of therapy. The response of improved quality of life was not dependent on the tumor response, and was observed also in patients with progressive disease.

In a more recent study, significantly improved global health and quality of life parameters were also reported for treatment with [¹⁷⁷Lu]DOTA-TATE in patients with metastasized GEP tumors.¹⁵³ The score was significantly increased 6 weeks after therapy. Furthermore, significant improvement was observed in role, emotional, and social function scales. The symptom scores for fatigue, insomnia, and pain were significantly decreased. Most significantly, patients with progressive disease also indicated an improvement in their global health score.

In our patients we evaluate the pain intensity by quantitative measurement of a visual analog score prior to and during each therapy cycle with either [¹¹¹In]DOTA-LAN or [⁹⁰Y]DOTA-TOC, and by recording the use of analgesics. The Karnofsky score and vegetative symptoms such as appetite, weight, bowel movement, miction, and sleep are also recorded. The general well-being (from comfortable feeling to discomfort) is evaluated by interviewing the patient.

Side-effects of treatment with radiolabeled peptide analogs

Side-effects of receptor-mediated radionuclide therapy concern mainly the critical organs, which are the kidney and bone marrow (for review see also reference 154). Possible toxicity may be divided into acute and delayed. Acute toxicity consists of a transient reduction in blood cells, with the nadir occurring 3–5 weeks after therapy. Acute effects such as nausea and vomiting appear to be related to the coadministration of renal protective agents.

Renal toxicity

In the kidney, radiolabeled SST analogs are efficiently reabsorbed by cells in the proximal tubule of the nephron, where a significant amount of activity is retained. Using octreotide derivatives ([⁹⁰Y]DOTA-TOC or [¹⁷⁷Lu]DOTA-TATE) a few patients were seen with renal problems, reduced renal function, and over the years chronic renal failure. After [⁹⁰Y]DOTA-LAN, a reduced creatinine clearance was seen in 2% of patients.

A recent long-term follow-up after therapy with [⁹⁰Y]DOTA-TOC and [¹⁷⁷Lu]DOTA-TATE¹⁵⁵ showed that the time course of creatinine clearance after therapy was compatible with the pattern of sustained loss in progressive kidney disease. The infusion of large amounts of amino acids reduces renal exposure during peptide-based radiotherapy and allows higher absorbed doses to tumors.¹⁵⁶ Several alternative amino acid regimens have been investigated, and reduction of kidney dose reported was extremely variable, with large interpatient variation amounting to

roughly 25–50%.^{126,127,155,156} It is difficult to derive from the available studies a clear relationship between cumulative or per-cycle radiation dose and renal damage. Obviously, there is substantial variation in the kidney uptake of the radiopeptide, which leads to different accumulated activities. With the assessment of renal toxicity by the commonly used National Cancer Institute (NCI) grades 0–4 for serum creatinine and blood urea nitrogen, it is difficult to predict which patient will develop nephrotoxicity after radiopeptide therapy. There are several improvements. One, for instance, was recently demonstrated by the Greek group,¹⁵⁷ who showed a beneficial effect of DTPA co-infusion. DTPA gravely decreased the blood pool indium-free (ionic) fraction, and consequently the bone marrow and whole body burden.

Bone marrow toxicity

Using octreotide derivatives ([⁹⁰Y]DOTA-TOC or [¹⁷⁷Lu]DOTA-TATE), grades 3 and 4 hematological toxicity were reported in a small number of patients (roughly 10% of all patients treated) throughout the various clinical trials. Single patients developed a myelodysplastic syndrome (MDS), whereas with [¹¹¹In]DTPA-OC also acute myeloid leukemia was seen (for review see reference 154).

None of the patients treated with [⁹⁰Y]DOTA-LAN developed any severe acute or chronic hematological side-effect, or had significant changes in renal or liver function parameters caused by this type of radiopeptide therapy under the doses administered. Transient thrombocytopenia or lymphocytopenia grade 1–2 was found in roughly 10% of patients.

Impact of concomitant therapy with long-acting analogs

According to the results obtained so far, there can be no doubt about the wide therapeutic index and the high efficacy of SST analogs in the symptomatic management of NETs. Symptomatic improvements have been obtained in about 60% of patients, and biochemical responses in 40–60%. The use of SST analogs as antineoplastic agents outside of clinical trials is still questionable, as the optimal dose and schedule of application has not been defined for the currently used agents.¹⁵⁸ Most of the reported side-effects are gastrointestinal in nature and include minor nausea, bloating, diarrhea, constipation, and steatorrhea. The observation that SST inhibits the release of various peptide hormones and therefore reverses many symptoms attributable to NETs has also stimulated interest in its use as an antiproliferative agent. From the studies reported so far, several important conclusions can be drawn for the future.

Following therapy with long-acting analogs, tumor shrinkage was reported in many studies (for review see reference 158). However, the doses used in many of the trials seem to be too small to exert a marked tumor response. High-dose treatment with SST analogs has given significant antitumor responses in patients resistant to standard doses of SST analog treatment. A combination α -interferon and SST analogs in patients resistant to single treatment with either compound has generated significant tumor reduction in about 25% of patients, with a median duration of almost 2 years and further stabilization in 60% of patients.

In our patients, we are following a treatment schedule (Figure 21.1) that changes between cold and hot SST analog. In fact, recent studies¹⁵⁹ have indicated that chronic octreotide does not influence the upregulation of SSTR on tumor cells. Furthermore, no desensitization of SSTR, tachyphylaxis, has been observed. This observation is very important, as in patients on long-term octreotide treatment, whether by frequent short-acting subcutaneous injection, by continuous pump delivery, or by monthly subcutaneous long-acting release, the efficacy of radioactive therapy would be expected to decrease over time. This study also suggested that cessation of the aqueous octreotide for 48 hours before a diagnostic SSTR scan or therapy is not required.

Conclusions

The overall results of receptor therapy with radiolabeled SST analogs indicate that these molecular therapies have their place in patients with SSTR-positive tumors for size reduction, improvement of quality of life, and overall prognosis. Serious side-effects are rare, especially in combination with amino acids for kidney protection. Patients should always be evaluated by preceding SSTR scanning and dosimetry using respective octreotide or lanreotide analogs, preferably those used for PET. At the University of Innsbruck the current evaluation procedure includes a [⁶⁸Ga]DOTA-TOC- and/or [⁶⁸Ga]DOTA-LAN-PET scan, followed by dosimetry with the ¹¹¹In-labeled analog. This procedure is repeated during therapy with the therapeutic yttrium or lutetium analog.

Results with [⁹⁰Y]DOTA-LAN therapy have pointed out the clinical potential of SSTR-targeted radiotherapy in patients with tumor sites expressing hSSTR. In particular, the MAURITIUS trial documented the possibility of imaging and treating specifically (receptor-mediated) cancer patients in an advanced stage of the disease, with only mild side-effects.⁷⁶ Although all patients included in this trial started [⁹⁰Y]DOTA-LAN therapy when tumor disease was progressive, disease control at a cost much less than that of conventional chemotherapy was achieved in several patients.

A reduction of tumor size and improvement of quality of life was found in a significant number of patients. It was most notable that also in patients with progressive disease, improved quality of life was observed. More recent long-term data on [¹⁷⁷Lu]DOTA-TATE, in a large number of patients, evidenced significant tumor shrinkage, improved quality of life, and prolonged survival.¹³⁷

Clinical improvement can be observed with [¹⁷⁷Lu]DOTA-TATE in patients pretreated with [⁹⁰Y]DOTA-TOC or [⁹⁰Y]DOTA-LAN after relapse. It is most notable that only a small number of serious adverse events occurred in those centers retreating patients who already had previously undergone a radioactive treatment phase. In fact, in our patients, accumulated kidney doses over 5–10 years were in the range as high as 50–80 Gy, without a decrease in creatinine clearance over time. A good response to any radioactive peptide therapy obviously is a positive prognostic factor for further treatment with radiopeptides.

Therapy might be improved by combining both radionuclides, ¹⁷⁷Lu and ⁹⁰Y. The ⁹⁰Y gives high doses to tumors and also to areas with low SSTR expression and heterogeneous tumor tissue. Because of the strong crossfire effect, parts of the tumor that are either poorly differentiated and therefore have a low density of SSTR2 subtype receptors, and are poorly vascularized, can thus be reached.

The future treatment of NETs will be more individualized, whereby the tumor biology and molecular genetics play a major role. It is a general understanding that patients with low proliferating tumors with a Ki-67 level < 3% should receive biotherapy, SST analogs, α interferon, or combinations of both. Patients with high proliferating tumors with a Ki-67 above 10% are usually first treated with cytotoxic treatment, streptozotocin plus 5-fluorouracil, or cisplatin plus etoposide. At progression, tumor-targeted radiotherapy is considered. In fact, so far, mostly patients with an advanced stage of tumor disease have been treated with peptide receptor-mediated radionuclide therapy. Future therapeutic trials should discuss the possibility of inclusion of patients at an earlier stage of disease and therefore be able to evaluate the possible potential of radiopeptide therapy at an earlier stage of tumor disease.

There is also a need for randomized trials in order to establish which treatment scheme and which radiolabeled SST analog, or combination of analogs, is optimal for radiopeptide therapy.

Our early results¹⁶⁰ have indicated that chemotherapeutic agents may modulate SSTR expression on tumor cells. Targeted therapy combinations have demonstrated unique promise, and also provide challenges related to timing, and the dosage necessary to enhance efficacy and reduce overlapping toxicities. Enhancement of immunotherapy and radioimmunotherapy has recently been demonstrated by the use of combined molecular targeting. Regarding the SST signaling pathway, the use of two biologic agents to

achieve therapeutic synergy by coactivation or blockade of cancer cell signaling pathways was recently postulated by the Rotterdam group.¹⁶¹ In particular, they linked octreotate with RGD (Arg-Gly-Asp) peptides that are antagonists of the $\alpha_v\beta_3$ integrin receptors found on neovascular cells and epithelial tumors. These peptides induce apoptosis in vascular endothelium in only newly sprouting vessels. Whereas an enhanced apoptosis was observed with this bifunctional compound, the uptake of the radiolabeled agent by the kidneys was considered not appropriately safe for therapy. Members of our group¹⁶² have recently introduced [¹⁸F]galacto-RDG-PET for non-invasive determination of integrin receptor expression, with the goal of providing important dose and time sequence information for the development of effective therapy and clinical monitoring of these therapies. Anyway, such combinations provide new scientific dimensions for radionuclide peptide or cancer therapy in general, as part of molecular targeted regimens.

The incorporation of radionuclide therapy into clinical protocols in combination with chemotherapy, immunotherapy, or external beam radiation is an evolving new treatment option for future targeted therapy protocols. The concomitant benefit of radionuclide therapy (⁸⁹Sr) and chemotherapy (doxorubicin) in the treatment of patients with painful metastases from advanced prostate carcinoma was recently demonstrated.¹⁶³ Similar beneficial effects were reported for low-dose cisplatin in combination with ⁸⁹Sr.¹⁶⁴ Radiosensitization with gemcitabine after high-dose [¹⁵³Sa]EDTMP (ethylenediaminetetramethylenephosphonic acid) with stem cell support pointed out a significant response in patients with osteosarcoma.¹⁶⁵ In the field of neuroblastoma¹⁶⁶ the feasibility of [¹³¹I] MIBG (metaiodobenzylguanidine) in combination with chemotherapy or myeloablative chemotherapy has been demonstrated. Many other combination possibilities are nowadays evolving and find their way towards clinical trials. There exists emerging interest in the oncological community and industry in combining therapeutic radiopharmaceuticals with other modalities such as immunotherapy, radiotherapy, or chemotherapy. This trend is illustrated by the fact that recognized organizations – such as the International Atomic Energy Agency (IAEA) – are currently setting up clinical protocols of such combinations for the treatment of malignancies with a higher incidence such as lymphoma or prostate cancer. Recently, experts in ‘radiopeptides’ met in Innsbruck¹⁶⁷ to discuss the current status of clinical applications. It was agreed that several aspects of information on trial conduction, and the definition of response to treatment, should be brought together into a common documentation file.

When we look towards radiation therapy, which is nowadays widely applied in combination with other modalities for malignancies, the combination of peptide receptor therapy with chemotherapy could aim at chemosensitization of

the antitumor effect of therapeutic peptides for internal radiation.¹⁶⁵ The synergistic antitumor effect could be explored. The majority of NETs display tyrosine kinase receptors, and new tyrosine kinase inhibitors might play an important role in future treatment. Other molecules are angiogenesis inhibitors (such as bevacizumab), which may alone or in combination with cytotoxic agents have some significance. Rapamycin (RAD001), an inhibitor on the mTOR (mammalian target of rapamycin) signaling pathway, alone or in combination with cytotoxic treatment, might be of value for treatment in NET patients.

Of course, there is great demand for multi-institutional trials on the concomitant use of therapeutics. The availability of adequate facilities, and legislation, are restricting progress. One of the major problems still is the availability of these radiopeptides in general, and the request for new and cheaper therapeutic radionuclides in particular.

Acknowledgments

We wish to thank all our technologists (Angelika Hutter and her team) as well as our nursing staff (Martin Jeller and his team), and Drs Amir Kurtaran, Shuren Li, Markus Raderer, Maria Leimer, Ernst Havlik, and Peter Angelberger from The University of Vienna, among many others, for helpful and fruitful cooperation throughout the past decade.

References

1. Moertel C. Karmofsky Memorial Lecture: an odyssey in the land of small tumours. *J Clin Oncol* 1987; 5: 1503–22.
2. Kvols L. Medical oncology considerations in patients with metastatic neuroendocrine tumours. *Semin Oncol* 1994; 21: 56–60.
3. Ruzsniowski P, Ducreux M, Chavaille JA et al. Treatment of the carcinoid syndrome with long acting somatostatin analogue lanreotide: a prospective study in 39 patients. *Gut* 1996; 39: 279–83.
4. Plöckinger U, Rindi G, Arnold R et al. Guidelines for the diagnosis and treatment of neuroendocrine gastrointestinal tumours. *Neuroendocrinology* 2004; 80: 394–424.
5. Reubi JC. In vitro identification of vasoactive peptide receptors in human tumours: implications for tumour imaging. *J Nucl Med* 1995; 36: 1846–53.
6. Virgolini I, Yang Q, Li S et al. Cross-competition between vasoactive intestinal peptide and somatostatin for binding to tumour cell membrane receptors. *Cancer Res* 1994; 54: 690–700.
7. Liebow C, Reilly C, Serrano M, Schally A. Somatostatin analogues inhibit growth of pancreatic cancer by stimulating tyrosine phosphatase. *Proc Natl Acad Sci USA* 1989; 86: 2003–7.

8. Schally A. Oncological applications of somatostatin analogues. *Cancer Res* 1988; 15: 6977–85.
9. Yamada Y, Post S, Wang K et al. Cloning and functional characterization of a family of human and mouse somatostatin receptors expressed in brain, gastrointestinal tract and kidney. *Proc Natl Acad Sci USA* 1992; 89: 251–5.
10. Yamada Y, Reisine S, Law S et al. Somatostatin receptors, an expanding gene family: cloning and functional characterization of human SSTR3, a protein coupled to adenylate cyclase. *Mol Endocrinol* 1992; 6: 2136–42.
11. Yasuda K, Res-Domiano S, Breder C et al. Cloning of a novel somatostatin receptor, SST3, coupled to adenylate cyclase. *J Biol Chem* 1992; 267: 20422–28.
12. Demchyschyn L, Srikant C, Sunahara R et al. Cloning and expression of a human somatostatin-14-selective receptor variant (somatostatin receptor 4) located on chromosome 20. *Mol Pharmacol* 1993; 43: 894–901.
13. Corness J, Demchyschyn L, Seeman P. A human somatostatin receptor (SSTR3), located on chromosome 22, displays preferential affinity for somatostatin-14 like peptides. *FEBS Lett* 1993; 321: 279–84.
14. Rohrer L, Raulf F, Bruns C et al. Cloning and characterization of a fourth human somatostatin receptor. *Proc Natl Acad Sci USA* 1993; 90: 4196–200.
15. Bell GI, Yasuda K, Kong H. Molecular biology of somatostatin receptors. *Ciba Found Symp* 1995; 190: 65–88.
16. Greenman Y, Melmed S. Heterogeneous expression of two somatostatin receptor subtypes in pituitary tumours. *J Clin Endocrinol Metab* 1994; 78: 398–403.
17. Greenman Y, Melmed S. Expression of three somatostatin receptor subtypes in pituitary adenomas: evidence for preferential SSTR5 expression in the mammosomatotroph lineage. *J Clin Endocrinol Metab* 1994; 79: 724–9.
18. Kubota A, Yamada Y, Kagimoto S et al. Identification of somatostatin receptor subtypes and an implication for the efficacy of somatostatin analogue SMS 201-995 in treatment of human endocrine tumours. *J Clin Invest* 1994; 93: 1321–5.
19. Panetta R, Patel Y. Expression of mRNA for all five human somatostatin receptors (hSSTR-1–5) in pituitary tumours. *Life Sci* 1994; 56: 333–42.
20. Vikić-Topić S, Raisch KP, Kvols L, Vuk-Pavlović S. Expression of somatostatin receptor subtypes in breast carcinoma, carcinoid tumours, and renal cell carcinoma. *J Clin Endocrinol Metab* 1995; 80: 2974–9.
21. Miller G, Alexander J, Bikkal H et al. Somatostatin receptor subtype gene expression in pituitary adenomas. *J Clin Endocrinol Metab* 1995; 80: 2974–9.
22. John M, Meyerhof W, Richter D et al. Positive somatostatin receptor scintigraphy correlates with the presence of somatostatin receptor subtype 2. *Gut* 1996; 38: 33–9.
23. Buscail L, Saint-Laurent N, Chastre E et al. Loss of SSTR2 somatostatin receptor gene expression in human pancreatic and colorectal cancer. *Cancer Res* 1996; 54: 1823–7.
24. Janson E, Gobl A, Kalkner K, Ölber K. A comparison between the efficacy of somatostatin receptor scintigraphy and that of in situ hybridization of somatostatin receptor subtype 2 messenger RNA to predict therapeutic outcome in carcinoid patients. *Cancer Res* 1996; 56: 2561–5.
25. Schaefer JC, Waser B, Mengold G, Reubi JC. Somatostatin receptor subtypes sst1, sst2, sst5 expression in human pituitary, gastroentero-pancreatic and mammary tumours: comparison of mRNA analysis with receptor autoradiography. *Int J Cancer* 1997; 70: 530–7.
26. Laws S, Gough A, Evans A, Bains M, Primrose J. Somatostatin receptor subtype mRNA expression in human colorectal cancer and normal colonic mucosa. *Br J Cancer* 1997; 75: 360–6.
27. Jais P, Terris B, Ruzsniowski P et al. Somatostatin receptor subtype gene expression in human endocrine gastroenteropancreatic tumours. *Eur J Clin Invest* 1997; 27: 639–44.
28. O'Nilsson L, Kölbly L, Wängberg B et al. Comparative studies on the expression of somatostatin receptor subtypes, outcome of octreotide scintigraphy and response to octreotide treatment in patients with carcinoid tumours. *Br J Cancer* 1998; 77: 632–7.
29. Fisher W, Doran T, Muscarella P II et al. Expression of somatostatin receptor subtype 1–5 genes in human pancreatic cancer. *J Natl Cancer Inst* 1998; 90: 322–4.
30. Pangerl T, Peck-Radosavljević M, Kaserer K et al. Somatostatin (SST) and VIP receptor subtype gene expression in human tumours. *Eur J Nucl Med* 1997; 24: 995 (abstr).
31. Virgolini I, Pangerl T, Bischof C, Smith-Jones P, Peck-Radosavljević M. Somatostatin receptor subtype expression in human tissues: a prediction for diagnosis and treatment of cancer? *Eur J Clin Invest* 1997; 27: 645–7.
32. Reubi JC, Maurer K, von Werder K et al. Somatostatin receptors in human endocrine tumours. *Cancer Res* 1989; 47: 551–8.
33. Reubi JC, Maurer K, von Werder K et al. Somatostatin receptors in human endocrine tumours. *Cancer Res* 1987; 47: 551–8.
34. Reubi JC, Schaefer JC, Waser B. Cholecystokinin (CCK)-A and CCK-B/gastrin receptors in human tumours. *Cancer Res* 1997; 60: 3105–12.
35. Reubi JC, Schaefer JC, Waser B, Mengold G. Expression and localization of somatostatin receptor SSTR1, SSTR2 and SSTR3 mRNAs in primary human tumours using in situ hybridization. *Cancer Res* 1994; 54: 3455–9.
36. Reubi JC, Schar JC, Waser B et al. Affinity profiles for human somatostatin receptor subtypes SST1–5 of somatostatin radiotracers selected for scintigraphic and radiotherapeutic use. *Eur J Nucl Med* 2000; 27: 273–82.
37. Virgolini I, Leimer M, Hirschmacker H et al. Somatostatin receptor subtype specificity and in vivo binding of a novel tumour tracer, ^{99m}Tc-P829. *Cancer Res* 1998; 58: 1850–9.
38. Raderer M, Pangerl T, Leimer T et al. Expression of human somatostatin receptor subtype 3 in pancreatic cancer in vitro and in vivo. *J Natl Cancer Inst* 1998; 90: 1666–8.
39. Virgolini I, Raderer M, Kurtaran A et al. Vasoactive intestinal peptide (VIP) receptor imaging for the localisation of intestinal adenocarcinomas and endocrine tumours. *N Engl J Med* 1994; 331: 1116–21.
40. Virgolini I, Traub T, Novotny C et al. New trends in peptide receptor radioligands. *Q J Nucl Med* 2001; 45: 153–9.
41. Reubi JC, Wenger S, Schmuckli-Maurer J, Schaefer JC, Gugger M. Bombesin receptor subtypes in human cancer; detection with the universal radioligand ¹²⁵I-[D-Tyr⁶-beta-Ala¹¹, Phe¹³, Nle¹⁴] bombesin (6–14). *Clin Cancer Res* 2002; 8: 1139–46.
42. Breeman WA, de Jong M, Erion JL et al. Preclinical comparison of ¹¹¹In-labelled DTPA- or DOTA-bombesin analogues

- for receptor-targeted scintigraphy and radionuclide therapy. *J Nucl Med* 2002; 43: 1650–6.
43. Zhang H, Chen J, Waldherr C et al. Synthesis and evaluation of bombesin derivatives on the basis of pan-bombesin peptides labelled with ¹¹¹Indium, ¹⁷⁷Lutetium, and ⁹⁰Yttrium for targeting bombesin receptor-expressing tumours. *Cancer Res* 2004; 64: 6707–15.
 44. Henning I, Laissue J, Horisberger U, Reubi JC. Substance P receptors in human primary neoplasms: tumoural and vascular localisation. *Int J Cancer* 1995; 61: 786–92.
 45. Reubi JCC, Waser B, Friess H, Buchler M, Laissue J. Neurotensin receptors: a new marker for human ductal pancreatic adenocarcinoma. *Gut* 1998; 42: 546–50.
 46. Patel YC. Somatostatin and its receptor family. *Front Neuroendocrinol* 1999; 20: 157–98.
 47. Smith-Jones P, Bischof C, Leimer M et al. 'MAURITIUS': a novel tumour diagnostic and therapeutic somatostatin analogue. *Endocrinology* 1999; 140: 5136–48.
 48. Ginj M, Chen J, Walter MA et al. Preclinical evaluation of new and highly potent analogues of octreotide for predictive imaging and targeted radiotherapy. *Clin Cancer Res* 2005; 11: 1136–45.
 49. Wild D, Schmitt JS, Ginj M et al. DOTA-NOC, a high-affinity ligand of somatostatin receptor subtypes 2, 3 and 5 for labelling with various radiometals. *Eur J Nucl Med Mol Imaging* 2003; 30: 1338–47.
 50. Rosenberg L, Brown R. Sandostatin in the management of nonendocrine gastrointestinal and pancreatic disorders: a preliminary study. *Cancer J Surg* 1991; 34: 223–9.
 51. Giusti M, Ciccarelli, Dallabonzana D et al. Clinical results of long term slow release lanreotide treatment of acromegaly. *Eur J Clin Invest* 1997; 27: 277–84.
 52. Stiefel F, Morant R. Vapreotide, a new somatostatin analogue in the palliative management of obstructive ileus in advanced cancer. *Support Care Cancer* 1993; 1: 57–8.
 53. Lamberts S, van der Lely A, de Herder W, Hofland L. Drug therapy: octreotide. *N Engl J Med* 1996; 334: 246–54.
 54. Lamberts S, Bakker W, Reubi JC, Krenning E. Somatostatin receptor imaging in the localization of endocrine tumours. *N Engl J Med* 1990; 323: 1246–9.
 55. Krenning E, Bakker W, Breeman W et al. Localization of endocrine-related tumours with radioiodinated analogue of somatostatin. *Lancet* 1989; 1: 242–4.
 56. Virgolini I, Angelberger P, Li S et al. In vitro and in vivo studies of three radiolabelled somatostatin analogues: ¹²³I-octreotide (OCT), ¹²³I-Tyr³-OCT and ¹¹¹In-DTPA-D-Phe¹-OCT. *Eur J Nucl Med* 1996; 23: 1388–99.
 57. Bakker W, Alberts R, Bruns C et al. [¹¹¹In-DTPA-D-Phe¹]-octreotide, a potential radiopharmaceutical for imaging of somatostatin receptor-positive tumours: synthesis, radiolabelling and in vitro validation. *Life Sci* 1991; 49: 1583–91.
 58. Krenning E, Bakker W, Kooij P et al. Somatostatin receptor scintigraphy with [¹¹¹In-DTPA-D-Phe¹]-octreotide in man: metabolism, dosimetry and comparison with [¹²³I-Tyr³]-octreotide. *J Nucl Med* 1992; 33: 652–8.
 59. Krenning E, Kwekkeboom DJ, Bakker WH et al. Somatostatin receptor scintigraphy with [¹¹¹In-DTPA-D-Phe¹]- and [¹²³I-Tyr³]-octreotide: the Rotterdam experience with more than 1000 patients. *Eur J Nucl Med* 1993; 20: 716–31.
 60. Krenning E, Bakker W, Kwekkeboom D et al. Biodistribution of a new chelated somatostatin analogue, [¹¹¹In-DOTA-D-Phe¹-Tyr³]-octreotide; comparison with [¹¹¹In-DTPA-D-Phe¹]-octreotide in humans. *J Nucl Med* 1997; 38: 103 (abstr).
 61. Krenning EP, Kooij PP, Bakker WH et al. Radiotherapy with a radiolabelled somatostatin analogue, ¹¹¹In-DTPA-D-Phe¹-octreotide. A case history. *Ann NY Acad Sci* 1994; 733: 496–504.
 62. Krenning E, Kooij P, Pauwels S et al. Somatostatin receptor: scintigraphy and radionuclide therapy. *Digestion* 1996; 57: 57–61.
 63. Otte A, Jermann E, Behe M et al. DOTATOC: a powerful new tool for receptor-mediated radionuclide therapy. *Eur J Nucl Med* 1997; 24: 792–5.
 64. Otte A, Mueller-Brand J, Dellas S et al. ⁹⁰Yttrium labelled somatostatin-analogue for cancer treatment. *Lancet* 1998; 351: 417–18.
 65. Hofmann M, Maecke H, Borner R et al. Biokinetics and imaging with the somatostatin receptor PET radioligand ⁶⁸Ga-DOTATOC: preliminary data. *Eur J Nucl Med* 2001; 12: 1751–7.
 66. Gabriel M, Decristoforo C, Kendl D et al. PET imaging of NETs using ⁶⁸Ga-DOTA-TOC: comparison with somatostatin receptor scintigraphy and CT. *Nuclear Medicine/Nuklearmedizin* 2006; 44: 18 (abstr).
 67. Meyer GJ, Gielow P, Börner AR, Hofmann M, Knapp WH. ⁶⁷Ga- and ⁶⁸Ga-labelled DOTA-derivatised peptide-ligands. *Nucl Med* 2006; 6: 20 (abstr).
 68. Anderson C, Dehdeshi F, Cutler P et al. ⁶⁴Cu-TETA-octreotide as a PET imaging agent for patients with neuroendocrine tumours. *J Nucl Med* 2001; 42: 213–21.
 69. Gabriel M, Mühllechner P, Decristoforo C et al. ^{99m}Tc-EDDA/HYNIC-Tyr³-octreotide for staging and follow-up of patients with neuroendocrine gastro-entero-pancreatic tumours. *J Nucl Med Mol Imaging* 2005; 49: 237–44.
 70. Decristoforo C, Mather S, Cholewinski W et al. ^{99m}Tc-EDDA/HYNIC-TOC: a new ^{99m}Tc-labelled radiopharmaceutical for imaging somatostatin receptor-positive tumours: first clinical results and intra-patient comparison with ¹¹¹In-labelled octreotide derivatives. *Eur J Nucl Med* 2000; 27: 1318–25.
 71. Gabriel M, Decristoforo C, Donnemiller E et al. An intra-patient comparison of ^{99m}Tc-EDDA/HYNIC-TOC with ¹¹¹In-DTPA-octreotide for diagnosis of somatostatin receptor-expressing tumours. *J Nucl Med* 2003; 44: 708–16.
 72. De Jong M, Bernard B, De Bruin E et al. Internalization of radiolabelled [DTPA⁰]octreotide and [DOTA⁰,Tyr³]octreotide: peptides for somatostatin receptor-targeted scintigraphy and radionuclide therapy. *Nucl Med Commun* 1998; 19: 283–8.
 73. Maina T, Nock B, Nikolopoulou A et al. [^{99m}Tc]demotate, a new ^{99m}Tc-based [Tyr³]octreotate analogue for the detection of somatostatin receptor-positive tumours: synthesis and preclinical results. *Eur J Nucl Med Mol Imaging* 2002; 29: 742–53.
 74. Baum RP, Niesen A, Leonhardi J et al. Receptor PET/CT imaging of neuroendocrine tumours using the Ga-68 labelled, high affinity somatostatin analogue DOTA-1-NaI3-octreotide (DOTA-NOC): clinical results in 327 patients. *Eur J Nucl Med Mol Imaging* 2005; 32: (Suppl): 54–5.

75. Cescato R, Schulz S, Waser B et al. Internalization of sst2, sst3, and sst5 receptors: effects of somatostatin agonists and antagonists. *J Nucl Med* 2006; 47: 502–11.
76. Virgolini I, Britton K, Buscombe J et al. ¹¹¹In- and ⁹⁰Y-DOTA-lanreotide: results and implications of the MAURITIUS trial. *Semin Nucl Med* 2002; 32: 148–55.
77. Zinn KR, Chaudhuri TR, Krasnykh VN et al. Gamma camera dual imaging with a somatostatin receptor and thymidine kinase after gene transfer with a bicistronic adenovirus in mice. *Radiology* 2002; 223: 417–25.
78. Virgolini I, Kurtaran A, Leimer M et al. Location of a VIPoma by ¹²³Iodine-vasoactive intestinal peptide scintigraphy. *J Nucl Med* 1998; 39: 1575–9.
79. Virgolini I, Kurtaran A, Raderer M et al. Vasoactive intestinal peptide receptor scintigraphy. *J Nucl Med* 1995; 36: 1732–9.
80. Thakur L, Marcus C, Saed S. ^{99m}Tc-labelled vasoactive intestinal peptide analog for rapid localization of tumours in humans. *J Nucl Med* 2000; 41: 107–10.
81. Vincent J, Mazella J, Kitabgi P. Neurotensin and neurotensin receptors. *Trends Pharmacol Sci* 1999; 20: 302–9.
82. Chabry J, Labbe-Julie C, Gilly D et al. Stable expression at the cloned rat brain neurotensin receptor into fibroblasts: binding properties, photoaffinity labelling, transduction mechanisms, and internalization. *J Neurochem* 1994; 63: 19–27.
83. Poinot-Chazel C, Portier M, Bouaboula M et al. Activation of mitogen-activated protein kinase couples neurotensin receptor stimulation to induction of the primary response gene Krox-24. *Biochem J* 1996; 320: 145–55.
84. Yamada M, Yamada M, Lombet A, Forgez P, Rostène W. Distinct function characteristics of levobastine sensitive rat neurotensin NT2 receptor expressed in Chinese hamster ovary cells. *Life Sci* 1998; 62: 375–80.
85. Mazella J, Zsurger N, Navarro V et al. The 100-kDa neurotensin receptor id gp95/sortilin, a non-G protein-coupled receptor. *J Biol Chem* 1998; 273: 26273–6.
86. Reubi JC, Walser B, Schaer JC, Laissue JA. Neurotensin receptors in human neoplasms: high incidence in Ewing's sarcomas. *Int J Cancer* 1999; 82: 213–18.
87. Moody T, Chiles J, Casibang M et al. SR48692 is a neurotensin receptor antagonist which inhibits the growth of small cell lung cancer cells. *Peptides* 2001; 22: 109–15.
88. Akilefu S, Srinivasan A, Schmidt M et al. Novel bioactive and stable neurotensin peptide analogue capable of delivering radiopharmaceuticals and molecular beacons to tumour. *J Med Chem* 2003; 46: 3403–11.
89. Garcia-Garayoa E, Allemann-Tannahill L, Blauenstein P et al. In vitro and in vivo evaluation of new radiolabelled neurotensin(8-13) analogues with high affinity for NT1 receptors. *Nucl Med Biol* 2001; 28: 75–84.
90. Hillairet De Boiferon M, Raguin O, Thiercelin C et al. Improved tumour selectivity of radiolabelled peptides by receptor and antigen dual targeting in the neurotensin receptor model. *Bioconjug Chem* 2002; 13: 654–62.
91. Buchegger F, Bonvin F, Kosinski M et al. Radiolabelled neurotensin analogue, ^{99m}Tc-NT-XI, evaluated in ductal pancreatic adenocarcinoma patients. *J Nucl Med* 2003; 44: 1649–54.
92. Gabriel M, Decristoforo C, Woell E et al. Pilot/Phase I study of a new technetium-labelled neurotensin analogue ([^{99m}Tc]Demotensin VI). *Eur J Nucl Med* 2004; 31 (Suppl 2): P315 (abstr).
93. Walsh J. Gastrointestinal hormones. In: Johnson LR, ed. *Physiology of the Gastrointestinal Tract*. New York: Raven Press, 1994; 3: 1–28.
94. Alexander R, Upp J Jr Poston G et al. Effects of bombesin on human small cell carcinoma in vivo. *Cancer Res* 1988; 48: 1439–41.
95. Nelson J, Donnelly M, Walker B et al. Bombesin stimulates proliferation of human breast cell cancer cells in culture. *Br J Cancer* 1991; 63: 933–6.
96. Spindel ER, Giladi E, Brehm P et al. Cloning and functional characterization of a complementary DANN encoding the murine fibroblast bombesin/gastrin-releasing peptide receptor. *Mol Endocrinol* 1990; 4: 1956–63.
97. Ferris HA, Carroll RE, Creswick KC, Banya RV. Location and characterization of the human GRP receptor expressed by gastrointestinal epithelial cells. *Peptides* 1997; 18: 663–72.
98. Gugger M, Reubi JC. Gastrin-releasing peptide receptors in non-neoplastic and neoplastic human breast. *Am J Pathol* 1999; 155: 2067–76.
99. Carroll RE, Carroll R, Benya R. Characterization of gastrin-releasing peptide receptors aberrantly expressed by non-antral gastric adenocarcinomas. *Peptides* 1999; 20: 229–37.
100. Nock B, Nikolopoulou A, Chiotellis E et al. ^{99m}Tc-Demobesin1, a novel potent bombesin analogue for GRP receptor-targeted tumour imaging. *Eur J Nucl Med Mol Imaging* 2003; 30: 247–58.
101. Hoffmann T, Gali H, Smith C et al. Novel series of ¹¹¹In-labelled bombesin analogues as potential radiopharmaceuticals for specific targeting of gastrin-releasing peptide receptors expressed on human prostate cancer cells. *J Nucl Med* 2003; 44: 823–31.
102. La Bella R, Garcia-Garayoa E, Bahler M et al. A ^{99m}Tc (I)-postlabelled high affinity bombesin analogue as a potential tumour imaging agent. *Bioconjug Chem* 2002; 13: 599–604.
103. Scopinaro F, Varvarigou A, Ussof W et al. Technetium labelled bombesin-like peptide: preliminary report on breast cancer uptake in patients. *Cancer Biother Radiopharm* 2002; 17: 327–35.
104. Van der Wiele C, Dumont F, Vanden Broecke R et al. ^{99m}Technetium-RP527, a GRP analogue for visualisation of GRP receptor expressing malignancies: a feasibility study. *Eur J Nucl Med* 2000; 27: 1694–9.
105. Breeman W, de Jong M, Erion J et al. Preclinical comparison of ¹¹¹In-labelled DTPA- or DOTA-bombesin analogues for receptor-targeted scintigraphy and radionuclide therapy. *J Nucl Med* 2002; 43: 1650–6.
106. Rogers B, Bigott H, McCarthy D et al. MicroPET imaging of a gastrin-releasing peptide receptor-positive tumour in a mouse model of human prostate cancer using a ⁶⁴Cu labelled analogue. *Bioconjug Chem* 2003; 14: 756–63.
107. Dockray G. Gastrin, growth, and colonic neoplasia. *Gut* 2000; 47: 747–8.
108. Rehfeld J, van Solinge W. The tumour biology of gastrin and cholecystokinin. *Adv Cancer Res* 1994; 3: 295–347.
109. Camby I, Salmon I, Oiry C et al. The influence of gastrin and/or cholecystokinin antagonists on the proliferation of three human astrocytic tumour cell lines. *Neuropeptides* 1996; 433–7.

110. Wank S, Pisegna J, de Weerth A. Brain and gastrointestinal cholecystochinin receptor family: structure and functional expression. *Proc Natl Acad Sci USA* 1992; 89: 8691–5.
111. Behe M, Behr TM. Cholecystokinin-B (CCK.B)/gastrin receptor targeting for staging and therapy of medullary thyroid cancer and other CCK-B receptor expressing malignancies. *Biopolymers* 2003; 66: 399–418.
112. Blaker M, de Weerth A, Tomettem M et al. Expression of cholecystokinin-2 receptor in normal human thyroid gland and medullary thyroid carcinoma. *Eur J Endocrinol* 2002; 146: 89–96.
113. Reubi JC, Waser B. Concomittant expression of several peptide receptors in neuroendocrine tumours: molecular basis for in vivo multireceptor tumour targeting. *Eur J Nucl Med Mol Imaging* 2003; 30: 781–93.
114. Mailleux P, Vanderhaeghen J. Cholecystokinin receptors of A type in the human dorsal medulla oblongata and meningiomas, and of B type in small cell lung cancer. *Nature* 1990; 316: 823–5.
115. Behr T, Behe M, Angerstein C et al. Cholecystokinin-B/gastrin receptor binding peptides: preclinical development and evaluation of their diagnostic and therapeutic potential. *Clin Cancer Res* 1999; 5: 3124–38s.
116. Behr T, Behe M. Cholecystokinin-B/gastrin receptor-targeting peptides for staging and therapy of medullary thyroid cancer and other cholecystokinin-B receptor-expressing malignancies. *Semin Nucl Med* 2002; 32: 97–109.
117. Hökfelt T, Pernow B, Wahren J. Substance P: a pioneer among neuropeptides. *J Intern Med* 2001; 249: 27–40.
118. van Hagen P, Breeman W, Reubi JC et al. Visualization of the thymus by substance P receptor scintigraphy in man. *Eur J Nucl Med* 1996; 23: 1508–13.
119. Rodrigues M, Traub-Weidinger T, Li S, Ibi B, Virgolini I. Comparison of ^{111}In -DOTA-D-Phe 1 -Tyr 3 -octreotide and ^{111}In -DOTA-Ianreotide scintigraphy and dosimetry in patients with neuroendocrine tumours. *Eur J Nucl Med Mol Imaging* 2006; 33: 532–40.
120. Valkema R, de Jong M, Bakker WH et al. Phase I study of peptide receptor radionuclide therapy with [^{111}In -DTPA 0]octreotide: the Rotterdam experience. *Semin Nucl Med* 2002; 32: 110–22.
121. Anthony L, Woltering E, Espanan G et al. ^{111}In ium-pentetreotide prolongs survival in gastroenteropancreatic malignancies. *Semin Nucl Med* 2002; 32: 123–32.
122. Kong G, Lau S, Ramdave S, Hicks R. High-dose ^{111}In -octreotide therapy in combination with radiosensitizing 5-Fu chemotherapy for treatment of SSR-expressing neuroendocrine tumours. *J Nucl Med* 2005; 64: 437(abstr).
123. Gancel M, Girault S, Zerdoud S et al. ^{111}In -pentetreotide radionuclide therapy in patients with unresectable progressive malignant endocrine and nonendocrine tumours: clinical results in 20 consecutive cases. *Eur J Nucl Med Mol Imaging* 2005; 32 (Suppl 1): 378 (abstr).
124. Otte A, Hermann R, Heppeler A et al. ^{90}Y trium DOTA-DOC; first clinical results. *Eur J Nucl Med* 1999; 26: 1439–47.
125. Paganelli G, Bodei L, Hankiewicz Junak D et al. ^{90}Y -DOTA-D-Phe 1 -Tyr 3 -octreotide in therapy of neuroendocrine malignancies. *Biopolymers* 2002; 66: 393–8.
126. Bodei L, Cremonesi M, Zoboli S et al. Receptor-mediated radionuclide therapy with ^{90}Y -DOTA-TOC in association with amino acid infusion: a phase I study. *Eur J Nucl Med Mol Imaging* 2003; 30: 207–16.
127. Chinol M, Bodei L, Cremonesi M, Paganelli G. Receptor-mediated radiotherapy with Y-DOTA-D-Phe-Tyr-octreotide; the experience of the European Institute of Oncology Group. *Semin Nucl Med* 2002; 32: 141–7.
128. Virgolini I, Traub T, Novotny C et al. Experience with ^{111}In dium and ^{90}Y trium-labelled somatostatin analogues. *Curr Pharm Design* 2002; 8: 1781–807.
129. Virgolini I. Radionuclide therapy of GEP tumours. *Eur J Nucl Med Mol Imaging* 2005; (Suppl): 25–6.
130. Valkema R, Pauwels S, Kvols L et al. Long-term follow-up of a phase I study of peptide receptor radionuclide therapy (PRRT) with [^{90}Y -DOTA 0 , Tyr 3]-octreotide in patients with somatostatin receptor positive tumours. *Eur J Nucl Med Mol Imaging* 2003; 30 (Suppl 2): 232(abstr).
131. Waldherr C, Pless M, Maecke H, Haldemann A, Mueller-Brand J. The clinical value of [^{90}Y -DOTA]-D-Phe 1 -Tyr 3 -octreotide (^{90}Y -DOTATOC) in the treatment of neuroendocrine tumours: a clinical phase II study. *Ann Oncol* 2001; 12: 941–5.
132. Waldherr C, Pless M, Maecke H et al. Tumour response and clinical benefit in neuroendocrine tumours after 7.4 GBq ^{90}Y -DOTATOC. *J Nucl Med* 2002; 43: 610–16.
133. Waldherr C, Schumacher T, Maecke H et al. Does tumour response depend on the number of treatment sessions at constant injected dose using ^{90}Y trium-DOTA-DOC in neuroendocrine tumours? *Eur J Nucl Med Mol Imaging* 2002; 29 (Suppl): 100 (abstr).
134. Chinol M, Bodei L, Cremonesi M, Paganelli G. Receptor-mediated radiotherapy with Y-DOTA-D-Phe-Tyr 3 -octreotide; the experience of the European Institute of Oncology group. *Semin Nucl Med* 2002; 32: 141–7.
135. Rushnell D, O'Dorisio T, Menda Y et al. Evaluating the clinical effectiveness of ^{90}Y -SMT 487 in patients with neuroendocrine tumours. *J Nucl Med* 2003; 44: 1556–60.
136. Baum R, Soeldner J, Schmuecking M. Clinical results of peptide receptor radionuclide therapy (PRRT) with Ytrium 90 -DOTA-Tyr 3 -Octreotate (Y 90 DOTA-TATE) in patients with neuroendocrine tumours. *J Nucl Med* 2004; 45 (Suppl): 441(abstr).
137. Kwekkeboom D, Teunissen J, Bakker W et al. Radiolabelled somatostatin analog [^{177}Lu -DOTA 0 , Tyr 3]octreotate in patients with endocrine gastroenteropancreatic tumours. *J Clin Oncol* 2005; 23: 2762.
138. Forrer F, Uusijärvi H, Storch D, Maecke H, Mueller-Brand J. Treatment with ^{177}Lu -DOTATOC of patients with relapse of neuroendocrine tumours after treatment with ^{90}Y -DOTA-TOC. *J Nucl Med* 2005; 46: 1310–16.
139. Baum R, Söldner J, Schm,cking M, Niesen A. Intravenous and intraarterial peptide receptor radionuclide therapy (PRRT). Using ^{90}Y -DOTA-Tyr 3 -octreotoate (^{90}Y -DOTA-TATE) in patients with metastatic neuroendocrine tumours. *Eur J Nucl Med Mol Imaging* 2004; 31: (Suppl 2): 155 (abstr).
140. Valkema R Froberg A, Bakker W et al. Peptide receptor radionuclide therapy (PRRT) with ^{177}Lu -DOTA-NOC and ^{68}Ga -DOTA-NOC. *J Nucl Med* 2005; 64: 435 (abstr).
141. Handkiewicz Junak D, Baum RP, Jarzak B. Toxicity of peptide receptor radiotherapy (PRRT) using the somatostatin

- analogue DOTA-NOC labelled with Y-90 or Lu-177. *Eur J Nucl Med Mol Imaging* 2005; 32 (Suppl 1): 202.
142. Virgolini I. Overview on ⁹⁰Yttrium-DOTA-lanreotide therapy. *Cancer Biotherapy & Radiopharm* 2003; 18: 276–7.
 143. Traub-Weidinger T, Guggenberg E, Kendler D et al. First experience with ⁶⁸Ga-DOTA-lanreotide in tumour patients. *Nuklearmedizin* 2005; 44: 24 (abstr).
 144. Madsen M, Bushnell D, Menda Y, Dosirisio T. Potential therapeutic advantage with combined ¹³¹I MIBG and ⁹⁰Y-DOTA-D-Phe¹-Tyr³-Octreotide (DOTATOC) for treating neuroendocrine tumours. *J Nucl Med* 2005; 65: 1449 (abstr).
 145. Stabin MG. MIRdose. Personal computer software for internal dose assessment in nuclear medicine. *J Nucl Med* 1996; 37: 538–46.
 146. Forrer F, Mueller-Brand J. Pre-therapeutic dosimetry with radiolabelled somatostatin analogues in patients with advanced neuroendocrine tumours. *Eur J Nucl Med Mol Imaging* 2005; 32: 511–12.
 147. Forrer F, Uusijarvi H, Waldherr C et al. A comparison of ¹¹¹In-DOTA-TOC and ¹¹¹In-DOTA-TATE; biodistribution and dosimetry in the same patients with metastatic neuroendocrine tumours. *Eur J Nucl Med Mol Imaging* 2004; 31: 1257–62.
 148. Buscombe R, Caplin ME, Hepplewhite J et al. Use of radiolanreotide to treat somatostatin receptor positive tumours. *Eur J Nucl Med* 2001; 28: 1198.
 149. Oeberg K. Advances in chemotherapy and biotherapy of endocrine tumours. *Curr Opin Oncol* 1998; 10: 58–65.
 150. Buscombe J, Rourke E, Chaplin M, Croasdale J, Hilson A. Minimum 1 year progression and overall survival data in patients treated with ⁹⁰Y-lanreotide. *J Nucl Med* 2004; 45 (Suppl): 446 (abstr).
 151. Kuhlke M, Mayer R. Carcinoid tumours. *Eng J Med* 1999; 340: 858–68.
 152. Aaronson N, Ahmedzai S, Bergman B et al. The European Organization for Research and Treatment of Cancer QLQ-C30; a quality of life instrument for use in international clinical trials in oncology. *J Natl Cancer Inst* 1993; 85: 365–76.
 153. Teunissen J, Kwekkeboom D, Krenning E. Quality of life in patients with gastroenteropancreatic tumours treated with [¹⁷⁷Lu-DOTA⁰, Tyr³]octreotate. *J Clin Oncol* 2004; 22: 2724–8.
 154. Kwekkeboom D, Mueller-Brand J, Paganelli G et al. Overview of results of peptide receptor radionuclide therapy with 3 radiolabelled somatostatin analogues. *J Nucl Med* 2005; 46 (Suppl 1): 62–6.
 155. Valkema R, Pauwels S, Kvols L et al. Long term follow-up of renal function after peptide receptor radiation therapy with ⁹⁰Y-DOTA⁰-Tyr³-octreotide and ¹⁷⁷Lu-DOTA⁰-Tyr³-octreotate. *J Nucl Med* 2005; 46 (Suppl 1): 83–91s.
 156. Jamar F, Barone R, Mathieu I et al. ⁸⁶Y-DOTA⁰-D-Phe¹-Tyr³-octreotide (SMT487) – a phase 1 clinical study: pharmacokinetics, biodistribution and renal protective effect of different regimes of amino acid co-infusion. *Eur J Nucl Med Mol Imaging* 2003; 30: 510–16.
 157. Limouris G, Kontogeorgakos D, Koutoulidis V et al. Diethylenetriaminepentaacetic acid (DTPA) co-infusion with ¹¹¹In-DTPA-Phe-octreotide decreases trivalent ionic (free) ¹¹¹Indium and ^{114m}Indium during peptide receptor radionuclide therapy (PRRT) in man. *J Nucl Med* 2004; 45 (Suppl): 445 (abstr).
 158. Henja M, Schmidinger M, Raderer M. The clinical role of somatostatin analogues as antineoplastic agents; much ado about nothing? *Ann Oncol* 2002; 13: 653–68.
 159. Gunn S, Schwimer J, Cox M et al. In vitro modeling of the clinical interactions between octreotide and ¹¹¹In-pentetreotide; is there evidence of somatostatin receptor down-regulation? *J Nucl Med* 2006; 47: 354–9.
 160. Fueger B, Hamilton G, Raderer M et al. Effects of chemotherapeutic agents on expression of somatostatin receptors in pancreatic tumour cells. *J Nucl Med* 2001; 42: 1856–62.
 161. Capello A, Krenning EP, Bernard BF et al. Anticancer activity of targeted proapoptotic peptides. *J Nucl Med* 2006; 47: 122–9.
 162. Haubner R, Weber WA, Beer AJ et al. Non-invasive visualization of the activated $\alpha v \beta 3$ integrin in cancer patients by positron emission tomography and ¹⁸F-galacto-RGD. *Plos&Med* 2005; 2: 244–52.
 163. Tu SM, Millikan RE, Menigistu B et al. Bone-targeted therapy for advanced androgen-independent carcinoma of the prostate: a randomized phase II trial. *Lancet* 2001; 357: 336–41.
 164. Sciuto R, Festa A, Rea S et al. Effects of low-dose cisplatin on ⁸⁹Sr therapy for painful bone metastases from prostate cancer: a randomized clinical trial. *J Nucl Med* 2002; 43: 79–86.
 165. Anderson PM, Wiseman GA, Erlandson L et al. Gemcitabine radiosensitization after high-dose samarium for osteoblastic osteosarcoma. *Clin Cancer Res* 2005; 11: 6895–900.
 166. Yanik GA, Levine JE, Matthay KK et al. Pilot study of iodine-131-metaiodobenzylguanidine in combination with myeloablative chemotherapy and autologous stem-cell support for the treatment of neuroblastoma. *J Clin Oncol* 2002; 20: 2142–9.
 167. www.uibk.ac.at/nuklearmedizin

Therapy of bone metastases

Holger Palmedo

Background

Radionuclide therapy of bone metastases represents a systemic therapy administering open radioactive agents intravenously. It is the aim of each radiation therapy to apply a maximal dose to the target – in this case bone metastases – and a minimal dose to the rest of the whole body. The dose to the rest of the body determines the frequency and intensity of side-effects and limits treatment efficacy.

Bone metastases are frequent, and will occur for every physician treating oncologic patients.¹ Many solid tumors generate bone metastases. Mainly, patients with breast, prostate, and lung cancer are concerned. Over 60% of all breast cancer patients develop osseous metastases of the osteolytic or combined osteolytic/osteoblastic type during the course of disease.² A half of prostate cancer and a third of lung cancer patients will show metastatic bone disease. In prostate cancer, bone metastases are predominantly osteoblastic.³

Once bone metastases are diagnosed, the disease must be classified as incurable.⁴ At this stage, quality of life and prolongation of survival are the important parameters that constitute the basis of further medical decision-making.

Although bone metastases are rarely the cause of cancer-related death, they lead to serious complications:⁵ (1) 30–60% of patients develop pain symptoms of diverse intensity; (2) predominantly the osteolytic type has the tendency to develop fractures, resulting in important morbidity; (3) a hypercalcemic syndrome due to increased bone resorption of osteolytic metastases can occur, and this can also appear as a paraneoplastic syndrome; and (4) if there is extensive metastatic disease the bone marrow can be destroyed, and clinically relevant alterations to blood counts can be observed.

A chronic pain syndrome is the most important complication of bone metastases, having a negative impact on quality of life and the social environment of the patient. These patients represent the main indication for radionuclide therapy. Up to one-half of the patients do not receive adequate pain treatment.⁶ About two-thirds of pain patients complain about breakthrough pain, meaning a contemporary appearance of strong pain in spite of the

intake of analgesics. It is therapeutically relevant that, in most patients with breakthrough pain, optimization of pain therapy is possible.⁶

From a pathophysiologic point of view, it is important to differentiate nociceptor pain from neuropathic pain (nerve pain). Nociceptor pain is mediated by free sensoric nerve endings of the nociceptor cells that can be found throughout the body.⁷ A large amount of nociceptors are located in the skin, the skeleton musculature, the tendons, the joints, and the intestine.⁸ Depending on their location, we differentiate somatic and visceral or superficially and deeply located nociceptor pain. Visceral excitations are frequently projected to special skin regions, the so-called dermatoma. While nociceptor pain is generally described by the patient as being of a stinging, drilling, or dull character, neuropathic pain is described as burning, and suddenly appearing (e.g. in the case of nerve plexus infiltration).⁹ Therefore, already patient interrogation leads to a differentiation between the two pain entities. This is extremely important, because radionuclide therapy is useful in nociceptor pain patients but not for neuropathic pain.

Physiologically, the nociceptor is not activated unless strong mechanical or thermal influences are present.¹⁰ This makes sense as, for example, a warm object should not cause painful sensations. However, the nociceptor can be sensitized by the production of endogenous algescic agents: an arthritis patient will suffer from pain even if smallest movements and the slightest pressure are applied to an affected joint. In these cases, substances such as prostaglandin E, bradykinin, histamine, and interleukin act as pain mediators, changing the microcirculation and permeability of the vessels and leading to a decrease of the excitation level.^{11,12} Lymphocytes and macrophages assist in this process. The simultaneous excretion of different pain mediators can lead to an exponential increase of their effect. This principle is known in the field of pharmacological pain treatment, and therefore agents inhibiting the production of, for example, prostaglandin E are successfully administered to pain patients.

The nociceptor cell also can self-regulate its excitation level. By secretion of the so-called substance P, vasodilatation and

consequently an invasion of inflammatory cells and enhanced secretion of pain mediators will occur. This process is often called neurogenic inflammation.¹¹

Bone metastases can generate pain either by a strong mechanical impact to the nociceptor or by an osteoblastic- and osteoclastic-induced excretion of pain mediators that results in the described sensitization of the nociceptor.¹³

Therapeutic approaches

Radionuclide therapy of bone metastases was begun decades ago, with the administration of phosphorus-32.¹⁴ ³²P is incorporated in the DNA of rapidly proliferating cells of the bone marrow as well as in the trabecular and cortical structures of the bone. The ratio of ³²P in normal bone to that in metastatic tissue was calculated to be 1:2, and therefore relatively low.¹⁵ This inappropriate ratio and the frequently observed strong myelosuppression were the reasons for abandoning phosphorus-32.

Since that time, a variety of β emitters have been investigated for therapy of bone metastases (Table 22.1). The maximal β -energy lies between 0.8 and 2.3 MeV, and the average β -energy between 0.27 and 0.8 MeV. The electrons deposit their radiation energy in a field of a few millimeters around the place of decay. The physical half-life of the nuclides in Table 22.2 differs importantly in the range 2–52 days. Therefore, the energy per time unit transferred to the tissue varies from nuclide to nuclide, although the total amount of radiation energy may be the same for two radionuclides. Principally, the radiation dose can be applied over a very short period necessitating a high dose rate, or over a longer time period administering a radionuclide with a low dose rate. Since the aspect of killing tumor cells has gained more and more importance, new treatment schemes that use repeated radionuclide applications and

that administer radionuclides combined with low-dose chemotherapy are increasingly favored.

The two calcium analogs strontium-89 chloride and yttrium-90 are taken up by bone to an extent dependent on the intensity of the osseous metabolism.^{16–18} Strontium-89 is excreted renally to 70–90%, and is eliminated from the vascular compartment within a few hours.¹⁹ Except for bone uptake and excretion via the urinary system, there is no accumulation in any organ system. Depending on the extension of metastatic disease the tracer uptake in the skeletal system ranges between 12 and 90% of the administered activity. The more extensive are the bone metastases, the quicker is the blood clearance into the skeleton. The accumulation of strontium-89 chloride in metastatic lesions is 5–20 times as high as the accumulation in normal bone tissue. Ninety days after administration, 20–88% of the injected strontium-89 activity was found in metastatic bone lesions.²⁰ The effective half-life was calculated to be over 50 days, and thus strontium-89 chloride delivers a low dose-rate radiation.

A different radiopharmaceutical option is to label radionuclides to phosphonates that are known to have a high osteoaffinity. In the diagnostic field, this principle was realized by introducing bone scintigraphy into clinical routine, and transferred to therapy after the development of radiopharmaceuticals such as samarium-153 ethylenediaminetetramethylenephosphonate (¹⁵³Sm]EDTMP) and rhenium-186 hydroxyethylidenediphosphonate (¹⁸⁶Re]HEDP).^{21,22} Also, these agents are excreted mainly by the kidneys, and they disappear rapidly from the vascular compartment.^{23,24} Twelve hours after administration, 50% of the administered activity of [¹⁸⁶Re]HEDP and [¹⁵³Sm]EDTMP has been eliminated renally. The uptake in the skeleton is in the range 20–30% and 30–50% of the injected dose for [¹⁸⁶Re]HEDP and [¹⁵³Sm]EDTMP, respectively. Depending on the intensity of bone metabolism, the radio-labeled phosphonates are accumulated via adhesion to bone and bone metastases. The accumulation in metastatic lesions is between 3 and 20 times as high as in normal bone. The effective half-life of [¹⁸⁶Re]HEDP and [¹⁵³Sm]EDTMP lies in the range of 2–3 days.

All commercially available radiopharmaceuticals for bone palliation (⁸⁹Sr]chloride, [¹⁸⁶Re]HEDP, and [¹⁵³Sm]EDTMP) do not accumulate in the tumor cell itself but they are deposited in close vicinity in the bone, emitting radiation to the tumor and pain mediator cells. The higher is the β -energy of the radionuclide, the longer is the range of electrons into the tissue. Since bone is characterized by high-energy absorption, the range of therapeutic electrons emitted by osteotropic radionuclides does not reach more than a few millimeters at maximum.

The creation of bone tissue takes place around conglomerations of tumor cells in primitive tumor bone or osteoid.²⁵ If osteolytic metastases are present, a broad line of resorption lacunes is found at a distance of 80–100 μ m

Table 22.1 Nuclide and carrier of the radiopharmaceutical

Nuclide	Carrier
Strontium-89	Chloride
Samarium-153	EDTMP
Rhenium-186/188	HEDP
Yttrium-90	Citrate
Phosphorus-32	Orthophosphate

EDTMP, ethylenediaminetetramethylenephosphonate; HEDP, hydroxyethylidenediphosphate.

Table 22.2 Physical properties of radionuclides used for treatment of bone metastases

Nuclide	⁸⁹ Sr	¹⁵³ Sm	¹⁸⁶ Re	¹⁸⁸ Re	³² P	⁹⁰ Y	¹¹⁷ Sn
Half-life (days)	52	2.1	3.8	0.7	14	2.7	13.6
β _{max} energy (MeV)	1.4	0.8	1.1	2.1	1.7	2.27	CE
Maximum range (mm) (soft tissue)	6.6	3.7	4.6	10.0	8.1	10.9	0.9
CE, conversion electrons.							

from the tumor borders.²⁶ In the case of osteoblastic metastases, resorption lacunes are rarely found. Typically, the trabeculae are covered by freshly produced bone tissue and the agent is integrated deeply in the bone structure. Therefore, the accumulation of radiopharmaceuticals is much higher in osteoblastic than in osteolytic metastases, with ratios of 1:15 and 1:3, respectively. The uptake of the radionuclide determines the therapeutic dose in the bone metastases, and, thus, the predictive value of bone scintigraphy previous to treatment is indispensable, even if osseous metastases have already been diagnosed by other imaging modalities.

To calculate the radiation dose applied to tumor tissue and organs, different methods are used,^{27–29} showing a deviation in the calculated to the real dose of up to 50%. Generally, a time–activity curve is generated over the region of interest (ROI), e.g. a reference metastasis, by ROI analysis of multiple whole-body scintigrams. The area under the curve represents the accumulated activity, which has to be normalized to the target volume and must be multiplied by the S-value. The S-value contains nuclide- and tissue-specific parameters such as the average

energy per decay and radiation sensitivity of the concerned tissue.

Using different models of dosimetry, the dose to bone metastases was calculated for [⁸⁹Sr]chloride and [¹⁸⁶Re]HEDP to be 60–600 mGy and 11–108 mGy per MBq administered activity, respectively (Table 22.3).^{27–29} If a standard dose of 4 mCi [⁸⁹Sr]chloride, 70 mCi [¹⁵³Sm]EDTMP, and 35 mCi [¹⁸⁶Re]HEDP is taken into account, the radiation dose to bone metastases lies between 8 and 90 Gy, 10 and 70 Gy, and 14 and 140 Gy, respectively (Table 22.3). Normal bone tissue receives a dose between 1 and 2.5 Gy, which is significantly below that of metastatic lesions. The variation of radiation dose in osseous metastases can be explained by the different intensities of radionuclide accumulation in the metastases. This stresses the importance of pre-therapeutic scintigraphy to perform at least a visual estimation of the tumor uptake and to predict therapy response.

The organ doses are also listed in Table 22.3, demonstrating that the kidneys and bladder receive non-critical doses. Obviously, the critical organ is the bone marrow that is exposed to doses between 1 and 1.5 Gy. At this level, first alterations to blood counts can be expected.^{27–29}

Table 22.3 Organ doses and whole-body dose for commercially available radiopharmaceuticals using standard amount of applied radioactivity

Organ	Radiation dose (Gy/Sv)		
	[⁸⁹ Sr]chloride (4 mCi)	[¹⁵³ Sm]EDTMP (70 mCi)	[¹⁸⁶ Re]HEDP (35 mCi)
Kidneys	0.9	0.8	1.4
Bladder	0.2	0.6	0.63
Bone	2.5	1.5	1.05
Bone marrow	1.6	1.2	0.97
Metastases	8–90	10–70	14–140
Whole body	0.43	0.23	0.105

Procedures

Pain therapy

The application of radionuclides for the treatment of painful bone metastases has been investigated for some decades. Beginning in the 1960s, the first nuclide administered for pain therapy of multiple osseous metastases was phosphorus-32.¹⁴ Since that time many different radiopharmaceuticals including [⁸⁹Sr]chloride, [⁹⁰Y]citrate, [¹⁸⁶Re]HEDP, [¹⁵³Sm]EDTMP, [^{177m}Sn]DTPA (where DTPA is diethylenetriaminepentaacetic acid), and [¹⁸⁸Re]HEDP have been investigated. Even this list is not complete, and therefore this chapter can only be confined to the most important agents.

First [⁸⁹Sr]chloride (⁸⁹Sr) must be mentioned, with which the nuclear medicine community has gained the largest experience. Laing et al.³⁰ treated 119 prostate cancer patients with painful metastatic bone disease, who did not respond to conventional therapy, by application of ⁸⁹Sr. A total of 75% of the patients demonstrated a marked improvement of pain status, and every fifth patient was almost completely pain-free. The effect of ⁸⁹Sr treatment began 10–20 days post-injection, and reached a maximum after 6 weeks. Pain improvement lasted for 6 months on average, with a variation between 4 and 15 months. This group evaluated the efficiency of treatment by pain intensity, change of pain medication, the patient's mobility, and a score for the patient's general condition. The authors could not find a significant advantage of a dosage of 3.0 MBq per kilogram body weight over that of 1.5 or 2.2 MBq per kilogram, resulting in a recommended dose of 150 MBq or 4 mCi of ⁸⁹Sr. This dose has been considered the standard dosage since that time. Lewington et al.³¹ performed a randomized, placebo-controlled, double-blind study in prostate cancer patients who were refractory to hormonal treatment and external radiation therapy. The patients treated with ⁸⁹Sr showed significantly better pain reduction than did patients of the placebo group. Also in this study, the evaluation of efficacy comprised all the abovementioned parameters of Laing's study. Considering that these patients were end-stage patients who had failed all conventional therapy, the effect of ⁸⁹Sr treatment is impressive. Further studies confirmed the beneficial effect of ⁸⁹Sr for pain treatment in prostate cancer patients. Quilty et al.³² could demonstrate in 284 prostate cancer patients that one injection of ⁸⁹Sr is as efficient as hemibody irradiation, which frequently shows intolerable side-effects.

Among the group of the new radiopharmaceuticals, [¹⁵³Sm]EDTMP (¹⁵³Sm) and [¹⁸⁶Re]HEDP (¹⁸⁶Re) are the most studied and also commercially available agents. In a double-blind and placebo-controlled study, Serafini et al.³³ investigated the effect of ¹⁵³Sm in 80 prostate cancer patients. Four weeks after the injection of a single dose of

1.0 mCi per kilogram body weight, an improvement of the pain situation was observed in 72% of the patients. In 31% of cases, almost complete pain reduction could be found. Four months after the treatment, 43% of the patients showed a continuing improvement of pain symptoms. In this study, a visual analog scale for different regions of the body, the consumption of analgesics, and a pain scoring system performed by the physician served as criteria for treatment response. The response rate of the ¹⁵³Sm group was significantly better than that of the placebo group, who showed a response rate of 40% and 2% after 4 weeks and 4 months, respectively. Furthermore, the study delivered evidence that a dose of 1.0 mCi per kilogram body weight results in pain reduction more frequently and for a longer period than a dose of 0.5 mCi per kilogram body weight. However, Tian et al.³⁴ could not confirm in their multicenter trial that the two different doses of ¹⁵³Sm had different effects in pain palliation. Collins et al.³⁵ reported that the beginning of pain alleviation can be expected after 7–14 days. Also, for ¹⁸⁶Re Maxon et al.²⁹ could demonstrate in a group of 20 patients that a significant improvement of pain could be achieved in 80% of cases after a single injection. The investigated parameters were a special pain and analgesic index. They used a standard dose of 30–35 mCi per patient. Our own experience in 30 patients with osseous metastases due to different tumor types revealed a response rate of 70% and an average time of 4 weeks for pain relief, beginning 1 week after injection of ¹⁸⁶Re.³⁶ The main criterion of treatment response was the visual analog scale. Also, the follow-up study published by Schoeneich et al.³⁷ in 44 patients confirmed these results. In all cited studies, treatment consisted of a single injection of 35 mCi ¹⁸⁶Re. Quirijnen et al.³⁸ performed a dose escalation study in 43 prostate cancer patients, investigating the effect of ¹⁸⁶Re in dosage groups of 35 mCi, 50/65 mCi, and 80/95 mCi. The authors used a multimodality score to determine the pain situation, consisting of the parameters pain intensity, analgesic consumption, and general activity of patients. The development of the single parameters, scored accordingly, was then transferred to a total overall score using a special algorithm. Referring to these very strict criteria, the groups with an activity of 35 mCi, 50/65 mCi, and 80/95 mCi showed a response rate of 33%, 78%, and 70%, respectively. Although the correlation of response rate and dosage was not statistically significant, there is a clear tendency favoring the dose of 50–65 mCi. Unfortunately, the commercially available standard dose of 35 mCi (1.3 GBq) ¹⁸⁶Re was not increased to 65 mCi (2.4 GBq). Han et al.³⁹ conducted a double-blind, placebo-controlled, randomized trial testing ¹⁸⁶Re in hormone-resistant prostate cancer patients with painful bone metastases (Placorhen (placebo-controlled rhenium) study). They included 111 patients and assessed pain relief using an electronic pain diary, containing questions reflecting the multidimensional character of chronic pain. The total response of patients treated with

^{186}Re was statistically significantly better than that of the placebo group. Also, the rate of patients requesting additional radiotherapy was lower in the ^{186}Re group at 44% than that in the placebo group at 67%. Amazingly, the overall response rate to ^{186}Re was only 30% on average. One reason for this might be the aforementioned low-dose activity of ^{186}Re that was also used in the Placorhen trial. In summary, there are sufficient evidence-based data to confirm the benefit of radionuclide therapy as an effective treatment modality of painful osseous metastases in hormone-refractory prostate cancer patients.

These radiopharmaceuticals have not been exclusively used to treat prostate cancer patients, but also other tumors such as breast cancer and lung cancer. The tumor most frequently studied after prostate cancer is carcinoma of the breast. Robinson⁴⁰ reported a response rate of 81% in breast cancer patients with multiple bone metastases, investigating 500 patients with different tumors retrospectively after injection of ^{89}Sr at a standard dose. Baziotis et al.⁴¹ treated 64 breast cancer patients by a single injection of 2 MBq per kilogram body weight of ^{89}Sr . They found an improvement of the pain situation in 80% of cases, including 35% of patients demonstrating almost complete pain relief. The average time of response was 3 months.

In the case of the radiopharmaceutical [^{153}Sm]EDTMP, the already mentioned studies by Serafini et al. and Tian et al. also investigated breast cancer patients.^{33,34} They report effective pain therapy in 72–85% of metastatic bone disease, with a mean duration of 1–2 months. After 4 months, the response rate was still at a level of 43%. Hauswirth et al.⁴² prospectively investigated 17 breast cancer patients receiving 35 mCi ^{186}Re , and found a response rate of 60% and a mean duration of response of 5 weeks. Our follow-up study in 30 patients confirmed these data, and showed that repetition of treatment could prolong the duration of pain relief.⁴³ Han et al.³⁹ investigated 24 breast cancer patients in a dose-escalation study, administering doses between 35 mCi and 80 mCi, and assessed therapeutic effect by a multimodality pain evaluation scoring system. They also found a response rate of 60%, and a mean duration of 1 month. In summary, also in breast cancer patients, there is evidence that radionuclide therapy is effective in palliating painful bone metastases.

Antitumor therapy

In a randomized, placebo-controlled phase III study, Porter et al.⁴⁴ investigated the efficacy of ^{89}Sr treatment for hormone-refractory prostate cancer patients as an adjunct to radiation therapy. They irradiated 126 patients with multiple osseous metastases, progressive disease, and a significant pain syndrome by external beam therapy, and administered additionally either placebo or ^{89}Sr . Besides the pain

documentation, the authors registered the frequency of newly appearing painful bone metastases and also the overall survival. Three months after radiation therapy, the rate of new osseous metastases was 66% and 41% in the placebo group and the ^{89}Sr group, respectively. This difference was statistically significant. Also, the time interval between ^{89}Sr or placebo injection and a second external beam irradiation, due to recurrent pain symptoms, was significantly longer for the ^{89}Sr group at 35 weeks than for the placebo group at 20 weeks. This tumoricidal effect was confirmed by laboratory testing of prostate specific antigen (PSA) and alkaline phosphatase. More patients in the ^{89}Sr group demonstrated a reduction in pain of over 50% within the first 4 months after treatment. These results were confirmed by a different study performed by Quilty et al.³² in 284 prostate cancer patients with bone metastases. In this study, one patient group received either local radiation therapy or hemibody irradiation depending on the site and extent of metastases. The other patient group underwent a single injection treatment with ^{89}Sr . Comparing both groups it was observed that pain reduction was equivalent; however, new pain foci were significantly less frequent in the ^{89}Sr group, even when compared to hemibody irradiation. The necessity of new radiation therapy due to these new pain sites was also less frequent in the ^{89}Sr group when compared to local radiation therapy, but not when compared to hemibody irradiation.

Both cited studies give evidence that radionuclide therapy with ^{89}Sr is more than pure pain palliation, and certainly has a tumoricidal effect. This favors an earlier rather than late-stage administration of ^{89}Sr in prostate cancer patients, ideally combined with external radiotherapy. In the cited studies, no prolongation of overall survival could be proved for ^{89}Sr . To enhance survival, it seems that an additional antitumor effect is necessary (see 'New treatment strategies' below).

Looking at the dosimetric data (Table 22.3) it becomes quite clear that the organ limiting therapeutic dosage is the blood cell generating system. No other organs are affected by side-effects. It is known that blood cell counts can change if a dose of 1 Gy or more is applied. Therefore, the most relevant side-effect of radionuclide therapy of bone metastases is thrombo- and leukopenia. If the mentioned standard doses are applied for the different radionuclides and if pretreatment blood counts are normal, changes of blood counts are moderate. However, for patients who have received chemotherapy, it may be necessary to take into account that the bone marrow reserve is limited. In these cases, blood counts must be considered more critical, and a certain time interval (generally the time to the expected nadir of thrombo- or leukopenia) must be accepted before a new myelosuppressive treatment can be started. Also, it may be necessary to reduce the dosage of the radionuclide for treatment.

In the British multicenter study, Quilty et al.³² describe that leuko- and thrombocyte counts demonstrated an average

decrease of 30–40% compared to baseline values after the injection of 200 MBq (5.4 mCi). The average interval of the maximal decrease (nadir) of thrombo- and leukocytes was 6 weeks (4–8 weeks). In the follow-up, blood counts increased again but at week 12 after injection, baseline levels were not yet reached. Significant toxicity (World Health Organization (WHO) grades III and IV) of blood count was observed in only 7% of patients. In the cited study, only one patient needed a thrombocyte concentrate due to treatment-related toxicity. The erythrocyte count and hemoglobin levels were not altered by radionuclide therapy. In comparison to ^{89}Sr therapy, hemibody irradiation resulted in twice as many blood transfusions. Also nausea, vomiting, and diarrhea were observed four times more frequently after hemibody irradiation. Laing et al.³⁰ confirmed in their study that the main side-effect was thrombocytopenia, with an average decrease of 25% and a nadir at week 6. No patient showed a toxicity of more than grade II.

Also, [^{153}Sm]EDTMP and [^{186}Re]HEDP led to mild hematotoxicity if a dose of 1.0 mCi/kg body weight and of 35 mCi were administered, respectively. The nadir of the 20–30% decrease of thrombo- and leukocytes was found to be at week 4–5. In contrast to ^{89}Sr , after injection of these newer radionuclides, baseline levels were reached at week 8 post-injection. Erythrocyte counts and hemoglobin did not change, and toxicity was maximally grade II. If higher doses of [^{153}Sm]EDTMP (>2.0 mCi/kg body weight) and [^{186}Re]HEDP (>70 mCi) were used, grade III or higher toxicity could occur.

The patient must be informed that pain syndromes might be aggravated for some days (flare effect), and return to the initial level afterwards. Rarely, it is necessary to increase the pain medication in this situation. In the author's experience, the flare phenomenon is less frequent than described (up to 30% of cases).

There are some cases in the literature describing temporary paresis and paresthesia for [^{186}Re]HEDP in patients with extensive metastatic disease of the skull base and of the vertebral column. However, this might also be caused by progressive bone metastases. After more than 400 treatments with rhenium-labeled HEDP, we could not observe any patient who developed temporary paresis and paresthesia due to radionuclide therapy. Conversely, one patient with pre-therapeutic, unilateral hypoglossus paresis showed a significant improvement of tongue movement after [^{188}Re]HEDP treatment. Eight weeks after radionuclide therapy, paresis had completely disappeared.

New treatment strategies

To enhance the effect of radionuclide therapy on cancer cells, the following new strategies have recently been investigated: combined radionuclide and chemotherapy, high-dose radionuclide therapy, and repeated radionuclide therapy.

It is known that special cytotoxic agents such as cisplatin work as radiosensitizers.⁴⁵ This means that the addition of chemotherapy and radiation therapy not only has an accumulative effect on tumor cells, but should result in an exponentially increased cell killing. If both treatment modalities are applied simultaneously, however, also the side-effects will increase. Therefore, the administration of a reduced-dosage protocol for chemotherapy would mean that side-effects could be kept on a stable level, but efficiency would grow due to a higher tumoricidal effect of the combination therapy.

Yet in 1992 Mertens et al.⁴⁶ investigated 18 hormone-refractory prostate cancer patients who received a combination of 4 mCi ^{89}Sr and a low-dose cisplatin infusion (35 mg/m²). They observed good pain palliation and an improvement in hemoglobin, tumor markers, and bone scans in some patients. Sciuto et al.⁴⁷ randomized 70 patients with painful bone metastases either to group A receiving 148 MBq ^{89}Sr and 50 mg/m² cisplatin or to group B receiving 148 MBq ^{89}Sr plus placebo. The follow-up was until death, to evaluate outcome. Overall pain relief occurred in 91% of patients in arm A and 63% of patients in arm B, with a median duration of 120 days in arm A and 60 days in arm B. New painful sites on previously asymptomatic bone metastases appeared in 14% of patients in arm A and in 30% of patients in arm B. The median survival without new painful sites was 4 months in arm A and 2 months in arm B. Sciuto et al.⁴⁷ observed a progression of bone disease in 27% and 64% of patients in groups A and B, respectively. This shows quite clearly that the progression of bone metastases is slowed down by combined therapy, and that, therefore, new painful sites are significantly less frequent. This improves, importantly, quality of the remaining life, especially because hematologic toxicity is moderate. Between both arms of the cited study, there was no significant difference in side-effects. Median global survival was better at 9 months for combined therapy (only 6 months for ^{89}Sr alone), but this was not statistically significant. That also overall survival can be improved by combined chemo- and radionuclide therapy was demonstrated by a study of Tu et al.⁴⁸ They investigated 103 patients with advanced, hormone-refractory prostate cancer, and performed induction chemotherapy consisting of ketoconazole (400 mg orally thrice daily for 7 days) and doxorubicin (20 mg/m² at weeks 1, 3, and 5) alternating with estramustine (140 mg orally thrice daily for 7 days) and vinblastine (4 mg/m² intravenously on the first day of every week). After two or three cycles of induction chemotherapy, 72 patients who were clinically stable or responders were randomized to one group receiving chemotherapy with doxorubicin and ^{89}Sr or to a second group receiving chemotherapy alone. Chemotherapy with doxorubicin was administered weekly for 6 weeks and ^{89}Sr was given at week 1 at a dose of 2.035 MBq per kilogram body weight (approximately 4 mCi for a 70-kg person). A substantial (more than 80% from baseline) and continued

(for at least 8 weeks) decrease of PSA values was observed in 72% and 36% of the combined (doxorubicin plus ^{89}Sr) and of the doxorubicin-alone treatment group, respectively. The median time to progression was significantly longer after combined therapy at 13.9 months in contrast to 7.0 months after pure chemotherapy. The median survival of patients also increased from 16.8 months (chemotherapy alone) to 27.7 months after additional injection of ^{89}Sr . Moreover, 52% of patients with bone pain showed a complete resolution of pain. The authors hypothesize that ^{89}Sr not only is responsible for an additional tumoricidal effect but also has an impact on the microenvironment of the bone (e.g. paracrine growth factors), leading to an increasing resistance against metastatic tumor cells.

Akerley et al.⁴⁹ performed a multicenter study in hormone-refractory prostate cancer patients using estramustine (600 mg/m² daily in weeks 1–4 and 7–10) and vinblastine (4 mg/m² intravenously, each week, in weeks 1–4 and 7–10) combined with ^{89}Sr 2.2 MBq per kilogram bodyweight (equaling 4 mCi for a 70-kg individual). Courses were repeated every 12 weeks, meaning that repeated doses of ^{89}Sr were applied. The authors assessed treatment response based on a change in the serum PSA level. A greater than or equal to 50% decline of PSA for at least 6 weeks was observed in 21 of 44 patients (48%), with a mean duration of response of 23 weeks. Hematologic toxicity was within the expected range. This study is interesting because it shows that the addition of ^{89}Sr to chemotherapy and its repeated administration is safe and effective. Furthermore, also this study confirms that there is a tumoricidal effect on the prostate cancer cells. Repeated injections of radionuclide seem to enhance the treatment efficacy. However, clinicians are often concerned about hematological toxicity when radionuclide therapy is repeated or administered simultaneously with chemotherapy. Tu and colleagues⁵⁰ investigated, in a subgroup analysis, 34 prostate cancer patients who had undergone combined chemotherapy with doxorubicin and a single ^{89}Sr injection. Subsequently, they assessed hematotoxicity in terms of bone marrow failure and the ability to tolerate additional treatments during a median of 25 months follow-up after ^{89}Sr administration. Within the 6 months after receiving ^{89}Sr , no patient developed bone marrow failure. Five of 34 patients developed bone marrow failure at a median of 23 months after ^{89}Sr treatment. Bone marrow biopsy performed in two of these five patients showed complete replacement of the marrow by tumor cells. In the remaining three (9%) patients, differentiation could not be made between tumor cell invasion and bone marrow aplasia originated by β irradiation. However, these data show that bone marrow failure, even after simultaneously applied chemotherapy and radionuclide treatment, is rather unlikely, and if suspected also aplasia induced by diffuse bone marrow infiltration must be considered. This has to be kept in mind when clinicians blame radionuclide therapy predominantly for bone marrow failure. This seems not to be justified.

Furthermore, it is evident that a therapeutic regimen applying chemotherapy and radionuclide therapy separated by a time interval of 4–8 weeks or more is substantially less toxic for the bone marrow than a treatment affecting simultaneously the hematopoietic system. In the therapy tolerance study of Tu et al.,⁵⁰ 91% of patients received subsequent cytotoxic treatments at a median of 11 months after ^{89}Sr injection. In their analysis, the authors state that a single dose of ^{89}Sr combined with chemotherapy did not affect the delivery of subsequent courses of chemotherapy in a selected patient group.

As a further cytotoxic agent, gemcitabine has been investigated in combination with ^{89}Sr in patients with androgen independent prostate carcinoma and bone metastases. Pagliaro et al.⁵¹ performed a phase I/II study applying gemcitabine at a dosage of 600 mg or 800 mg/m² on days 1, 8, 15, 43, 50, and 57, and a single dose of ^{89}Sr (55 $\mu\text{Ci}/\text{kg}$, equaling almost 4 mCi for 70 kg body weight) on day 8. The authors treated 15 patients, but there was no response measured by PSA concentration. However, six patients had stable disease. The authors conclude that 800 mg/m² gemcitabine is the maximal tolerated dose for the combination, and that a response rate over 10% cannot be expected. Therefore, further studies with gemcitabine at the indicated dosage and schedule are not warranted.

Another new approach to enhance the efficacy of radionuclide therapy is to repeat the injection, aiming at a higher radiation dose. Rhenium-188 hydroxyethylidenediphosphonate (^{188}Re]HEDP) is a new radiopharmaceutical that we have previously investigated for pain palliation of bone metastases.⁵² We have shown that the application of ^{188}Re]HEDP in humans is safe, and that pain palliation can be achieved in about 70% of patients. A major advantage is that rhenium-188 is inexpensively available on demand from a $^{188}\text{W}/^{188}\text{Re}$ generator, and a kit is available for easy radiolabeling of the bone-seeking hydroxyethylidenediphosphonate (HEDP). The most important physical characteristics of ^{188}Re are its emission of high-energy β particles with a maximal energy of 2.1 MeV and a relatively short physical half-life of 17 hours. Therefore ^{188}Re is readily available, and due to its high dose constant it offers the possibility of repeated therapy without additional costs, compared to those of a single injection. We performed a prospective phase II trial in 64 hormone-refractory prostate carcinoma patients who were randomly assigned to one of two groups.⁵³ One group (group A) received a single injection of ^{188}Re]HEDP, and patients in the other group (group B) received two injections (interval 8 weeks). After therapy, patients were followed up by assessment of pain palliation and clinical outcome until death. In both groups, toxicity was low, with moderate thrombo- and leukopenia (maximum common toxicity criteria (CTC) grade II). The effectiveness of ^{188}Re]HEDP for pain palliation with repeated treatment (group B) was significantly better, with a response rate and time of response of 92% and 5.66 months, respectively. In this group, 11 (39%) of

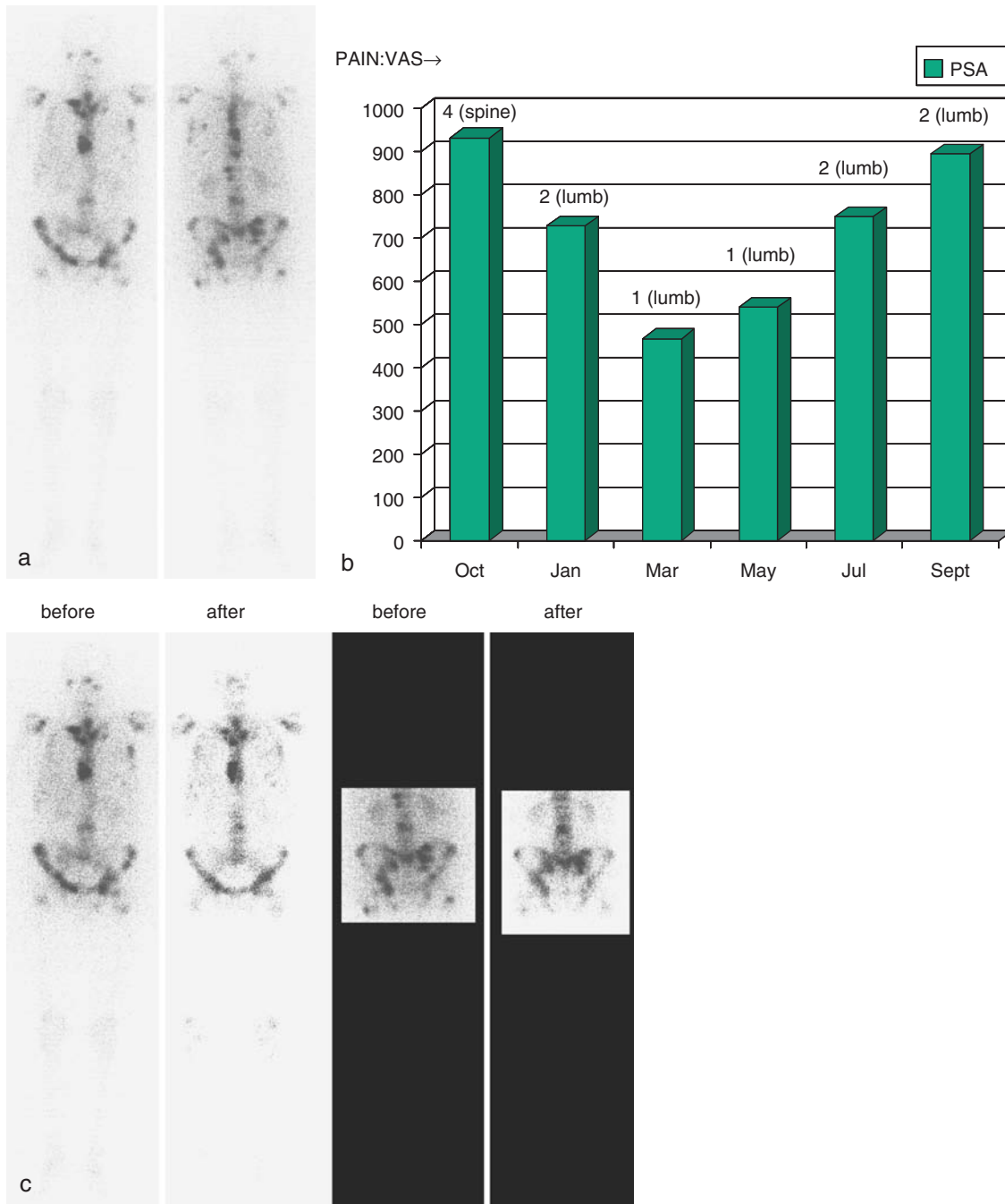


Figure 22.1

Post therapy Rhenium-188 HEDP scintigraphy from ventral and dorsal view (a). The patient had prostate cancer diagnosed 4 years ago (initially pT3 N0 M1, PSA 1570 ng/ml). Under antiandrogenic treatment, the PSA value was decreased to 30 ng/ml and kept stable at this level for 2 years. In the following 2 years, PSA value rose to 930 ng/ml despite different hormonal treatment regimens. The patient complained about pain in the entire vertebrae (visual analog scale 4) although he was taking pain medication. We applied a total of five rhenium-188 HEDP injections over almost one year. The pain medication could be discontinued after pain was reduced significantly (VAS 1 only lumbar spine). PSA-value decreased to a minimum of 466 ng/ml after the second therapy cycle. The pain situation could be kept stable for almost one year (b). Post-therapy scintigraphy with rhenium-188 HEDP only showed minor regression of metastatic sites in the lumbar spine and the pelvis (c).

28 patients had a PSA decrease of more than 50% for at least 8 weeks, in comparison to two (7%) of 30 patients in the single-injection group (group A). The median times to progression of group A and group B were 2.3 and 7.0 months, respectively, and the median overall survival times of group A and group B were 7.0 months and 12.7 months, respectively. These differences were statistically significantly different. Our data confirm that bone-targeted therapy with high-energy [^{188}Re]HEDP has an antitumor effect in prostate cancer patients, resulting in a better clinical outcome. One advantage of a short-living radionuclide such as [^{188}Re]HEDP is that it can deliver a high dose rate, meaning a high radiation dose within a relatively short time interval. Moreover, we think that the high electron energy (2.1 MeV) of [^{188}Re]HEDP is an important factor. This results in electrons ranging from approximately 3 to 5 mm in osseous tissue. We suppose that the high-energy radiation of [^{188}Re]HEDP reaches the tumor tissue, which is surrounded by bone trabeculae. This would lead to cytotoxic effects in the outer layers of the tumor. By repeating treatment with [^{188}Re]HEDP within an interval short enough to avoid new tumor growth, the following tumor layer could be eradicated (onion peeling). We believe that a time interval even shorter than 6–8 weeks would be more effective, and that therapy might be repeated several times to enhance the cytostatic effect. This seems to be possible because toxicity, which was limited to the bone marrow, was very moderate after repeated treatment with [^{188}Re]HEDP. Recently, we have been evaluating our experience in patients treated with up to six cycles of radionuclide therapy. In our experience, it seems that patients can significantly benefit from multiple injections of [^{188}Re]HEDP without increasing the rate of bone marrow failure and without inhibiting further chemotherapy.

A third new approach is the application of high-dose radionuclide therapy necessitating bone marrow support. Anderson et al.⁵⁴ administered different doses of [^{153}Sm]EDTMP (1, 3, 4.5, 6, 12, 19, and 30 mCi per kilogram body weight; standard dose of [^{153}Sm]EDTMP for pain palliation is 1.0 mCi/kg body weight) in 30 patients with locally recurrent or metastatic osteosarcoma or skeletal metastases. Patients received peripheral-blood progenitor cell (PBPC) or bone marrow support. The authors found that marrow radiation doses corresponded linearly to the injected amount of [^{153}Sm]EDTMP. Also, the grade of cytopenia was dose-related. After PBPC or marrow infusion on day 14 after [^{153}Sm]EDTMP injection, recovery of hematopoiesis was problematic in two patients who had received 30 mCi/kg body weight and who were infused with less than 2×10^6 CD34/kg. However, in the remaining patients, no complications were observed. A reduction or elimination of opiates for pain was seen in all patients, and there was no adverse change in appetite or performance status. The authors conclude that high-dose irradiation (39–241 Gy) by bone-targeted therapy with [^{153}Sm] EDTMP is feasible, and that non-hematologic side-effects are minimal.

References

1. Cserhati P. Metastatic disease in breast cancer. *J Clin Oncol* 1987; 21: 1235–41.
2. Paterson AHG. Bone metastases in breast cancer, prostate cancer and myeloma. *Bone* 1987; 8 (Suppl 1): 17–22.
3. Jacobs SC. Spread of prostatic cancer to bone. *Urology* 1983; 21: 337–44.
4. Eisenberger MA, Simon R, O'Dwyer PJ, Wittes RE, Friedman MA. A reevaluation of nonhormonal cytotoxic chemotherapy in the treatment of prostatic carcinoma. *J Clin Oncol* 1985; 3: 827–41.
5. Nielsen OS, Munro AJ, Tannock IF. Bone metastases: pathophysiology and management policy. *J Clin Oncol* 1991; 9: 509–24.
6. Strumpf M. Krebsschmerz. In: Zenz J, Jurna I, eds. *Lehrbuch der Schmerztherapie*. Stuttgart: Wissenschaftliche Verlagsgesellschaft, 1993: 427–36.
7. Zimmermann M. Physiologie von Nozizeption und Schmerz. In: Zimmermann M, Handwerker HO, eds. *Schmerz—Konzepte und ärztliches Handeln*. Berlin: Springer-Verlag, 1984: 1–43.
8. Besson JM, Chaouch A. Peripheral and spinal mechanisms of nociception. *Physiol Rev* 1987; 67: 67–186.
9. Willis WD. *The Pain System*. Basel: Karger-Verlag, 1985: 341–88.
10. Resch K. Der entzündliche Gelenkschmerz. In: Zimmermann M, Zeidler H, Ehlers H, eds. *Rheuma und Schmerz*. *Der Schmerz* 1991; 5: (Suppl 1) 3–12.
11. Mense S. Sensitization of group IV muscle receptors to bradykinin by 5-hydroxytryptamine and prostaglandin E2. *Brain Res* 1981; 225: 95–105.
12. Schmidt RF. Physiologie und Pathophysiologie der Schmerzentscheidung und Schmerzverarbeitung im Bewegungssystem. In: Zimmermann M, Zeidler H, Ehlers H, eds. *Rheuma und Schmerz*. *Der Schmerz* 1991; 5: (Suppl 1) 13–28.
13. Mundy GR, Martin TJ. Pathophysiology of skeletal complications of cancer. In: Mundy GR, Martin TJ, eds. *Physiology and Pharmacology of Bone*. Berlin: Springer-Verlag, 1989: 641–4.
14. Kaplan E, Fels IG, Kotlowski BR. Therapy of carcinoma of the prostate metastatic to bone with P-32 labeled condensed phosphate. *J Nucl Med* 1960; 1: 1–13.
15. Lewington VJ. Targeted radionuclide therapy for bone metastases. *Eur J Nucl Med* 1993; 20: 66–74.
16. Kutzner J, Dähnert W, Schreyer T et al. Yttrium-90 zur Schmerztherapie von Knochenmetastasen. *Nuklearmedizin* 1981; 20: 229.
17. Blake GM, Zivanovic MA, Lewington VJ. Measurements of the strontium plasma clearance rate in patients receiving Sr89 radionuclide therapy. *Eur J Nucl Med* 1989; 15: 780–3.
18. Blake GM, Wood JE, Wood PJ, Zivanovic MA, Lewington VJ. 89Sr therapy: strontium plasma clearance in disseminated prostatic carcinoma. *Eur J Nucl Med* 1989; 15: 49–54.
19. Blake GM, Zivanovic MA, McEwan AJ, Batty VB, Ackery DM. 89Sr radionuclide therapy: dosimetry and haematological toxicity in two patients with metastasising prostatic carcinoma. *Eur J Nucl Med* 1987; 13: 41–46.
20. Blake GM, Zivanovic MA, McEwan AJ, Ackery DM. Sr-89 therapy: strontium kinetics in disseminated carcinoma of the prostate. *Eur J Nucl Med* 1986; 12: 447–54.

22. Ketrings AR. ¹⁵³Sm-EDTMP and ¹⁸⁶Re-HEDP as bone therapeutic radiopharmaceuticals. *Nucl Med Biol* 1987; 14: 223–32.
23. Singh A, Holmes RA, Farhangi M. Human pharmacokinetics of Samarium-153 EDTMP in metastatic cancer. *J Nucl Med* 1989; 30: 1814–18.
24. de Klerk JMH, van Dijk A, van het Schip AD, Zonnenberg BA, van Rijk PP. Pharmacokinetics of Rhenium-186 after administration of Rhenium-186-HEDP to patients with bone metastases. *J Nucl Med* 1992; 33: 646–51.
25. Gerson BD, Dorfman HD, Norman A, Mantius HJ. Patterns of localization in osteosarcoma. *J Bone Joint Surg* 1972; 54: 817–27.
26. Baud C, Boivin G. Periosteocytic remodelling in the vicinity of bone metastases. In: Donath A, Courvoisier B, eds. *Bone and Tumours*. Bern: 1980: 280–98.
27. Blake GM, Zivanovic MA, Blaquiére RM et al. Strontium-89 therapy: measurement of absorbed dose to skeletal metastases. *J Nucl Med* 1988; 29: 549–57.
28. Eary JF, Collins C, Stabin M et al. Samarium-153-EDTMP biodistribution and dosimetry estimation. *J Nucl Med* 1993; 34: 1031–6.
29. Maxon HR, Deutsch EA, Thomas SR. Re-186 (Sn)HEDP for treatment of multiple metastatic foci in bone: human biodistribution and dosimetric studies. *Radiology* 1988; 166: 501–7.
30. Laing AH, Ackery DM, Bayly RJ et al. Strontium-89 chloride for pain palliation in prostatic skeletal malignancy. *Br J Radiol* 1991; 64: 816–22.
31. Lewington VJ, McEwan AJ, Ackery DM et al. A prospective, randomised double-blind crossover study to examine the efficacy of Strontium-89 in pain palliation in patients with advanced prostate cancer metastatic to bone. *Eur J Cancer* 1991; 27: 954–8.
32. Quilty PM, Kirk D, Bolger JJ et al. A comparison of the palliative effect of strontium 89 and external beam radiotherapy in metastatic prostate cancer. *Radiother Oncol* 1993; 31: 33–40.
33. Serafini AN, Houston SJ, Resche I et al. Palliation of pain associated with metastatic bone cancer using Samarium-153 Lexidronam: a double blind placebo-controlled trial. *J Clin Oncol* 1998; 16: 1574–81.
34. Tian J, Zhang J, Hou Q et al. Multicentre trial on the efficacy and toxicity of single dose samarium-153 EDTMP as a palliative treatment for painful skeletal metastases in China. *Eur J Nucl Med* 1999; 26: 2–7.
35. Collins C, Eary JF, Donaldson G et al. Samarium-153-EDTMP in bone metastases of hormone refractory prostate carcinoma: a phase I/II trial. *J Nucl Med* 1993; 34: 1839–44.
36. Palmedo H, Bender H, Schomburg A et al. Schmerztherapie mit Rhenium-186 HEDP bei multiplen Knochenmetastasen. *Nuklearmedizin* 1996; 35: 63–7.
37. Schoeneich G, Palmedo H, Dierke-Dzierzon C, Müller SC, Biersack HJ. Palliative radionuclide therapy of painful bone metastases. *Scand J Urol Nephrol* 1997; 31: 445–8.
38. Quirijnen JMSP, Han SH, Zonnenberg BA et al. Efficacy of Rhenium-186-HEDP in prostate cancer patients with metastatic bone pain. *J Nucl Med* 1996; 37: 1511–15.
39. Han S, Zonnenberg B, De Klerk J et al. Re-186 HEDP in breast cancer patients with metastatic bone pain. *J Nucl Med* 1999; 40: 639–42.
40. Robinson RG. Strontium-89 precursor targeted therapy for pain relief of blastic metastatic disease. *Cancer* 1993; 72: 3433–5.
41. Baziotis N, Yakoumakis E, Zissimopoulos A et al. Sr-89 chloride in the treatment of bone metastases from breast cancer. *Oncology* 1998; 55: 377–81.
42. Hauswirth AE, Palmedo H, Dierke-Dzierzon C et al. Pain therapy in multiple bone metastases in breast carcinoma. *Zentralbl Gynäkol* 1998; 120: 83–6.
43. Palmedo H, Bender H, Dierke-Dzierzon C et al. Pain palliation with Rhenium-186 HEDP in breast cancer patients with disseminated bone metastases. *Clin Nucl Med* 1999; 24: 643–8.
44. Porter AT, McEwan AJB, Powe JE et al. Results of a randomized phase-III trial to evaluate the efficacy of Strontium-89 adjuvant to local field external beam irradiation in the management of endocrine resistant metastatic prostate cancer. *Int J Radiat Oncol Biol Phys* 1993; 25: 805–13.
45. Geldof AA, de Rooij L, Versteegh RT, Newling DW, Teule GJ. Combination ¹⁸⁶Re-HEDP and cisplatin supra-additive treatment effects in prostate cancer cells. *J Nucl Med* 1999; 40: 667–71.
46. Mertens WC, Porter AT, Reid RH, Powe JE. Strontium-89 and low-dose infusion cisplatin for patients with hormone refractory prostate carcinoma metastatic to bone: a preliminary report. *J Nucl Med* 1992; 33: 1437–43.
47. Sciuto R, Festa A, Rea S et al. Effects of low-dose cisplatin on ⁸⁹Sr therapy for painful bone metastases from prostate cancer: a randomized clinical trial. *J Nucl Med* 2002; 43: 79–86.
48. Tu S, Millikan RE, Mengistu B et al. Bone targeted therapy for advanced androgen-independent carcinoma of the prostate: a randomised phase II trial. *Lancet* 2001; 357: 336–41.
49. Akerley W, Butera J, Wehbe T et al. A multiinstitutional, concurrent chemoradiation trial of strontium-89, estramustine, and vinblastine for hormone refractory prostate carcinoma involving bone. *Cancer* 2002; 94: 1654–60.
50. Tu SM, Kim J, Pagliaro LC et al. Therapy tolerance in selected patients with androgen-independent prostate cancer following strontium-89 combined with chemotherapy. *J Clin Oncol* 2005; 23: 7904–10.
51. Pagliaro LC, Delpassand ES, Williams D et al. A phase I/II study of strontium-89 combined with gemcitabine in the treatment of patients with androgen independent prostate carcinoma and bone metastases. *Cancer* 2003; 97: 2988–94.
52. Palmedo H, Gohlke S, Bender H et al. Dose escalation study with rhenium-188 HEDP in prostate cancer patients with osseous metastases. *Eur J Nucl Med* 2000; 27: 123–30.
53. Palmedo H, Manka-Waluch A, Albers P et al. Repeated bone-targeted therapy for hormone-refractory prostate carcinoma: randomized phase II trial with the new, high-energy radiopharmaceutical rhenium-188 hydroxyethylidenediphosphonate. *J Clin Oncol* 2003; 21: 2869–75.
54. Anderson PM, Wiseman GA, Dispenzieri A et al. High-dose samarium-153 ethylene diamine tetramethylene phosphonate: low toxicity of skeletal irradiation in patients with osteosarcoma and bone metastases. *J Clin Oncol* 2002; 20: 189–96.

Therapy of liver tumors

John Buscombe

Background

The liver plays host to both primary and secondary tumors. However, the scope of this chapter is to concentrate on those tumors which have their primary origin within the liver. These tumors are unusual in that they can be limited to a single organ, grow, metastasize, and then kill their host, still within their organ of origin. In addition, unlike most other tumors, the host organ is normally sick before the tumor develops, and successful treatment of the tumor can be followed by death from liver failure. It is also unusual in that the radionuclide therapies that have been developed are local in nature.

Hepatocellular carcinoma: definitions

Hepatocellular carcinoma (HCC) can also be called a hepatoma, but the term hepatoma is misleading as it suggests a benign disease, which is not the case. Within the rest of this chapter, the term HCC will be used.

Epidemiology

The incidence of HCC varies widely throughout the world. In Northern Europe and North America it tends to be seen as a rarity, maybe representing only 1% of all cancers, whilst in East Asia and sub-Saharan Africa it is the most common tumor, causing 20–30% of all cancers.^{1,2} This epidemiology is important, as it enabled the etiology to be determined, leading to steps to prevent disease development and early diagnosis through targeted screening.³ However, it has been noted that even with the same risk factors the rate of disease still differs with different ethnic groups, as does the way the disease spreads. For example, the Japanese have a higher incidence and a more diffuse type of HCC than that seen in North America.⁴

Causative agents

The liver is an amazing organ: it can regenerate itself after much tissue has been destroyed, so that if half the liver is removed, within months the liver will return to its normal volume. This, however, is the Achilles heel of the liver. If, instead of a single injury, there are small repeat injuries, then the liver will be continuously trying to repair itself. This rapid regrowth becomes disorganized, leading to a condition known as cirrhosis. The theory is that continued cell division leads to an increased chance of a fatal DNA error to be replicated, and then cancer can develop. However, this could be going on throughout the liver (the so-called field change), which means that multiple spontaneous or sequential cancers can develop.⁵

The most common cause of cirrhosis leading to HCC is viral hepatitis B and C. The peak incidence of HCC in East Asia and Africa is from 20 to 40%, suggesting that HCC resulted from hepatitis B contracted at birth, from the mother, or in childhood.⁶ The time from infection with hepatitis C to HCC is about 30 years,⁷ with 3–8% of infected patients converting each year.

Other agents which have been suggested include aflatoxins, which occur in rice infected with *aspergillus*, the oral contraceptive, and alcohol. These can all be linked to cirrhosis, but the link to HCC is less clear.⁸

Staging of the disease

Again, HCC is different from other tumors in that the pattern of disease is to grow or spread within the organ of origin. Small solitary tumors of less than 2 cm are stage 1 up to stage 4, with disease disseminated throughout the liver. The added complication is that HCC has the same density as that of liver, and is not easily distinguished even on contrast computed tomography (CT). Magnetic resonance imaging (MRI) is much better, but again small daughter tumors may not be seen. Some tumors grow as lumps, and others just spread as lines of individual cells

growing through the liver.⁹ Because the primary cause is normally cirrhosis, multiple synchronous tumors may develop within the liver. Metastases are rare, but are known within the lung and bones. A more common manifestation is that the tumor, still taking its blood supply from the liver, grows up the inferior vena cava into the right atrium. The most useful staging systems are those that combine information about tumor size with information as to how the rest of the liver is working, such as the Okuda and Child–Pugh staging systems.^{10,11}

Natural history

As the disease progresses, the common problems are related to loss of functioning liver tissue; this will include a raised bilirubin, reduced albumin, and a reduction in clotting factors. The portal vein may become occluded, leading to signs of portal hypertension. It is this progressive liver failure which will kill the patient. Confusingly, the same could be due to the underlying cirrhosis, so the patient may die with their tumor size unchanged, but the surrounding liver has just failed. If the HCC is slow growing and the rest of the liver can remain well, then the patient may live several years, even without treatment.

Measuring hepatocellular carcinoma

As stated, CT, even triple-phase, may not identify the disease correctly. MRI may be better, and still not see small tumors. Ultrasound is sensitive to tumors that are superficial, but is less useful when they are deeper in the liver. Most HCCs (> 90%) excrete the α -fetoprotein (AFP), and in an individual patient levels of AFP map changes in tumor size quite precisely. Many of these tumors are very vascular, and on angiography multiple nests of angiogenic vessels are seen. Most metastases into the liver are hypoperfused, and so the HCC stands out as unusually vascular; only neuroendocrine tumors tend to be that vascular.

When looking for metastatic disease, CT and bone scan seem to be of most use. [¹⁸F]FDG (fluoro-2-deoxy-D-glucose) is of variable use, but could monitor those patients who are FDG-positive.

Because these tumors occur in patients with underlying disease, Okuda et al.¹⁰ have devised a method of staging using the tumor size and the state of the liver to determine prognosis. First, each factor is graded, then the grades added to form the Okuda score (Tables 23.1 and 23.2).

Though we have more sophisticated measures such as the Child–Pugh index, they use a system similar to the

Table 23.1 Scoring of factors for Okuda staging¹⁰

<i>Predictive factor</i>	<i>Score</i>
Tumor > 50% of liver volume	1
Tumor < 50% of liver volume	0
Ascites present	1
Ascites absent	0
Albumin < 30 g/l	1
Albumin > 30 g/l	0
Bilirubin > 30 mg/l	1
Bilirubin < 30 mg/l	0

Okuda system, and as the established system, nuclear medicine papers often refer to the Okuda system.

Confirming the diagnosis

If there is any chance of cure, it is not normal practice to biopsy the lesion, as seeding along a biopsy route has been reported. The diagnosis is made by the fact that there are risk factors present, a hepatic mass, and rising AFP.

Other liver cancers

The other most common liver cancer is the cholangiocarcinoma, arising from the biliary tract lining. The outlook for these patients is grim, and no therapy, let alone with radionuclides, appears to make any difference.

Another is the fibrolamellar variant of HCC. This arises mainly in male Caucasians, and the peak incidence is 15–25%. It is slowly metastatic, spreading to the lungs, myocardium, and bones. It can be controlled by repeat surgery. It has a unique tumor marker, the B12 binding protein.¹² It is not related to hepatitis infection. The tumors often have somatostatin receptors, but the use of radionuclide therapy using radiolabeled somatostatins has been disappointing.¹³

Table 23.2 Calculation of Okuda grading¹⁰

<i>Total grade from Table 23.1</i>	<i>Okuda score</i>
0	1
1–2	2
3–4	3

Treating hepatocellular carcinoma

If the tumor is single (or limited to one or two segments), then surgery is ideal, especially in the non-cirrhotic. Wedge resection or lobectomy can be curative. Success depends on finding the tumor when it is small, which normally occurs in patients on active screening with risk factors such as known hepatitis C. Those who are resected live longer, but the non-cirrhotic do best with a 50% 3-year survival, compared to no survivors without resection.¹⁴ As patients may die of cirrhosis despite a successful cancer operation, another strategy is to use a liver transplant. This will remove both the tumor and any abnormal tissue likely to develop into cancer. The initial mortality is higher than with resection, but if the patient survives the operative period their outlook is good. However, this treatment is not common due to the low number of donors.

Chemotherapy

There has been no convincing evidence that any chemotherapy-alone regimen has any effect on survival in either local or systemic disease.¹⁵

Local treatments

As stated earlier, HCC is unusual in that as a cancer it can start, grow, metastasize, and kill the patient all whilst staying in the liver. It would appear logical then to treat the tumor. This should maximize efficacy but reduce systemic side-effects. Simplest treatments include ultrasound or CT-guided alcohol injections and radiofrequency (RF) ablation.¹⁵ These are best suited to those lesions easily punctured by the skin and not too close to a major blood vessel, or the lesion should not be too large. However, alcohol will be absorbed, as one of our patients found out after he drove home from the procedure and there were many difficult explanations to the court!

HCCs are vascular tumors, but their blood supply is normally from the hepatic artery (the normal hepatocytes are fed from both hepatic artery and portal vein (which is really an artery!)). Therefore, embolization via the hepatic artery should affect the HCC more than the liver. This can be done with Gelfoam®, coils, or iodinated poppy seed oil, lipiodol, either on its own or mixed with a chemotherapy agent such as cisplatin. Whilst cure is not possible, these treatments are generally well tolerated and can be repeated. However, if it is possible to treat HCC locally with these techniques, could they not be used to deliver therapeutic radiopharmaceuticals?

Radionuclide therapy

Initial attempts to treat HCC concentrated on the use of radionuclide therapy in disseminated disease, probably as outlooks with other treatments remained grim. Order et al. in Baltimore produced antibodies against human α -fetoprotein labeled with ¹³¹I.¹⁶ Though this work has continued intermittently since about 1980 there has been little advance, partly as it is difficult to deliver sufficient radioactivity to the tumor using a systemically injected radiolabeled antibody. Repeat treatments were difficult because of the immune reaction caused from repeat use of animal-based antibodies. In the author's experience, ¹³¹I-labeled anti-AFP has always failed to have any significant impact on disease,¹⁷ but a properly engineered antibody with appropriate radionuclide could still offer some hope to patients with disseminated HCC.

Local treatments

The most successful strategy for the treatment of HCC with radionuclides has been to use a combination of radiopharmaceutical and the local approach to ensure that treatment is delivered to the tumor. As stated previously, the HCC has a single blood supply, and the normal liver a dual supply. Cannulization of the hepatic artery either by surgical placement of a 'portocath' into the gastroduodenal artery or angiographically via the femoral artery and aorta will allow the radiopharmaceutical to be administered via the catheter in the right, left, or common hepatic artery, to ensure that the agent bathes the site of the tumor and maximizes uptake. The catheter must be placed so that no activity passes through the gastroduodenal artery and hence damage the stomach wall or the duodenum (Figures 23.1 and 23.2). This may mean, as the anatomy is variable, that a direct visual approach is the best.¹⁸ The procedure requires local anesthesia over the femoral artery, and then a 5-French catheter is passed into the celiac trunk and an angiogram performed to map out the main arteries. This may also be the first time that the full extent of the tumor and its intrahepatic metastases will be seen as areas of tumor flush. The patency of the portal vein is also checked. In addition, a superior mesenteric angiogram is done so that it can be seen whether any tumor is fed from this artery in addition to the celiac trunk. When it is confirmed that the site of the tumor is known, a catheter is advanced into the right or left hepatic artery, depending whether it is a right- or left-sided tumor, or the common hepatic artery if bilobar (though a preferred strategy is to treat the side with the larger tumor first then treat the other side 6 weeks later). Though a '5-French' catheter is optimal for delivery of lipiodol, the vessels near an HCC can be thin and tortuous, and thin, stiff catheters such as a microcatheter may

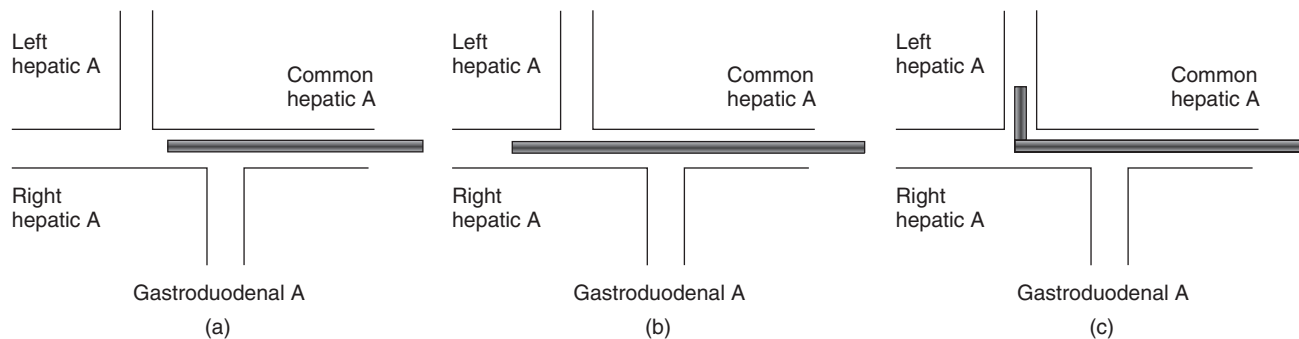


Figure 23.1

Placement of catheter for treating both lobes (a), right lobe (b), and left lobe (c). A, artery.

need to be used. Once the catheter is placed correctly the radionuclide therapy can be infused, and the line is then fully flushed to ensure that, as the catheter is withdrawn, there is no leakage into the systemic circulation.

$[^{131}\text{I}]$ lipiodol

The first candidate for such therapy was lipiodol; as mentioned previously, it had been used for localizing HCC. It is a viscous brown liquid which is mixed with chemotherapy agents for the local treatment of HCC. Work with lipiodol in animal models shows that there is preferential uptake into HCC cells compared to normal hepatocytes by a ratio of 9:1,¹⁹ with electron microscopy finding that the lipiodol localizes close to the nucleus. Also, using cell cultures, it was found that though non-radioactive lipiodol and ^{131}I have

little action on HCC cells, combined $[^{131}\text{I}]$ lipiodol has a significant cytotoxic effect.¹⁹ To obtain calculated tumor doses of 30 Gy, then 1 GBq of $[^{131}\text{I}]$ lipiodol in a volume of 1–1.5 ml is infused over 5 minutes (any longer and the catheters start to dissolve in the lipiodol). The substance does not mix with water, so during administration it forms little globules; these are radio-opaque so can be seen if the patient undergoes fluoroscopy. This is useful because if the lipiodol is given too fast it could reflux into the gastroduodenal artery; therefore, the rate of infusion can be adjusted so that this does not happen. Also, it is possible, where the lipiodol is moving in a direction that is not wanted, to readjust the catheter tip and redirect the flow. Confirmation of residency of $[^{131}\text{I}]$ lipiodol at the site of the tumor is determined by planar X-ray at the time of infusion, a radionuclide image 2 days later (Figure 23.3), and CT at 10 days. If more than 15% of activity has shunted into the lungs, repeat treatment should be avoided.



Figure 23.2

Image taken during catheterization of the right hepatic artery. During this procedure multiple tumors not seen on computed tomography (CT) can be seen by their vascular blush.

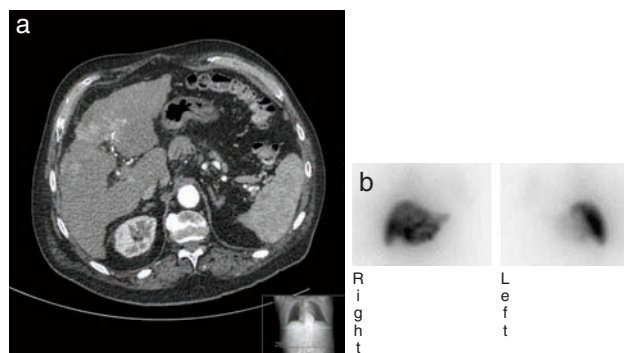


Figure 23.3

CT (a) of patient with unresectable hepatocellular carcinoma (HCC) in the right lobe seen as areas of increased contrast in the upper right lobe. Imaging 48 hours post-infusion of $[^{131}\text{I}]$ lipiodol (b) shows focal uptake in multiple tumors including those not seen on CT. There is no lung shunting.

First results

The group with the greatest experience of this technique is from Rennes, France.²⁰ Their first publications showed that the technique was safe, and there was evidence of efficacy in terms of both radiologically reduced tumor size and reduced AFP. There followed a randomized controlled trial comparing the results of [¹³¹I]lipiodol and chemo-lipiodol²¹ (Table 23.3).

Results showed a similar response rate between the two techniques, but the [¹³¹I]lipiodol was better tolerated than chemo-lipiodol, with shorter hospital stay and less severe side-effects. With [¹³¹I]lipiodol, the patient typically had 2–3 days of mild pain and low-grade fever after administration of 1 GBq, and discharge was related to radiation protection issues normally on day 3 or 4. With chemo-lipiodol, discharge was 3–4 days later, and was determined by the need for symptom control. These findings were confirmed by those from the UK²¹ (Table 23.3). Unfortunately, there is no evidence for improved survival, partly as the patients may have died from their background liver disease and not their cancer. It was also clear that the outcome in Okuda-1 patients was poor, with survival beyond 6 months unlikely; however, they were treated. The only peri-treatment deaths occurred in Okuda stage-2 patients, and no form of radionuclide therapy should be considered in these patients. Radiation hepatitis was rare, and systemic side-effects non-existent. One important fact, however, was that [¹³¹I]lipiodol was safe in patients with a blocked portal vein, and, in this group, it remains the primary anticancer therapy in HCC. We have found that lipiodol contains so much elemental iodine that thyroid blockage is not needed, but other centers still do this.

The advantages of [¹³¹I]lipiodol compared with other treatments in terms of reduced side-effects for similar efficacy means that it remains the method of choice for the

treatment of non-resectable HCC with or without a blocked portal vein.²²

Extended use of [¹³¹I]lipiodol

Because many HCCs are multifocal, either because they arise at different points in the liver or because multiple micrometastases are common, about 50% of patients having a curative resection with all known HCC removed have recurrent disease within 2 years. This would be an excellent indication for adjuvant treatment. The point of adjuvant treatment is to treat disease that cannot be seen, and therefore prevent or slow recurrent disease. It would also be ideal if such a treatment were to be relatively non-toxic and easily tolerated. It has been postulated that [¹³¹I]lipiodol would fit this role perfectly. It is also postulated that the growth factors released after liver resection, which stimulate liver growth, and also liver cancer growth, are at their most active 6 weeks post-surgery.²³ This would therefore be an ideal time for adjuvant therapy. The Hong Kong group studied 43 patients; 21 were randomized to treatment with a single activity of 1.8 GBq of ¹³¹I or best supportive care. The median progression-free survival in the [¹³¹I]lipiodol-treated group was 57 months, compared to 14 months in the untreated group. At 3 years, 86% of treated patients were alive, but only 46% in the untreated group. These results have been confirmed by other groups^{24,25} (Figure 23.4).

An extension of the idea would be the use of [¹³¹I]lipiodol before operation to try and shrink the tumor to a size where it becomes operable. This is described as neo-adjuvant therapy. This has been tried in both France and Belgium, and early results suggest that up to 50% of tumors may undergo a significant reduction in size,^{26,27} and that

Table 23.3 Summary of results of randomized controlled trials of [¹³¹I]lipiodol and chemotherapy-based lipiodol regimens

Trial	Treatment (n)	Survival (%)			Comments
		6 months	12 months	24 months	
Battacharya, 1995 ²¹	[¹³¹ I]lipiodol (11)	58	29	0	Hospital stay shorter for [¹³¹ I]lipiodol; NS
	Epirubicin–lipiodol (17)	40	25	6	
Raoul, 1997 ²⁰	[¹³¹ I]lipiodol (65)	69	39	22	Life-threatening toxicity 39%, death 9% of cisplatin arm, none for [¹³¹ I]lipiodol; NS
	Cisplatin–lipiodol (64)	66	42	22	

NS, no significant difference between treatments.

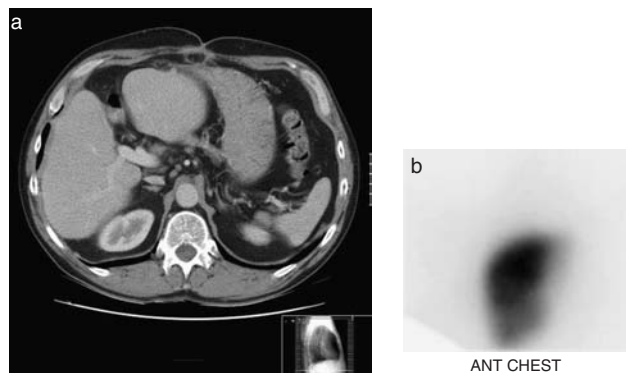


Figure 23.4

CT (a) of a patient who has undergone left lobe resection for surgically treatable HCC. Note the reduced liver volume. The $[^{131}\text{I}]$ lipiodol image (b) performed 6 weeks after surgery shows equal distribution throughout the liver remnant, confirming no focal residual HCC.

CT is a poor arbiter of response, and patients may still have a lesion on their CT after $[^{131}\text{I}]$ lipiodol. However, pathological examination of the explants only finds fibrosis at resection. This again raises the problem of how to image HCC and the need for a good positron emission tomography (PET) agent. Often the only reliable source of data about response is the AFP level.

$[^{188}\text{Re}]$ lipiodol

Whilst HCC shows a good level of response to $[^{131}\text{I}]$ lipiodol, there are some problems, namely:

1. The long half-life limits the activity that can be administered, so the dose rate immediately after administration is not ideal. As there is good initial uptake into the HCC, a high initial dose rate would be desirable.
2. The long half-life and high-energy γ emissions of the ^{131}I mean that radiation protection precautions are required for a significant period.
3. All $[^{131}\text{I}]$ lipiodol comes from France (Europe); most patients with HCC are in East Asia and sub-Saharan Africa, so logistics are difficult.
4. The cost of $[^{131}\text{I}]$ lipiodol at 1000 euros is not high for the developed world, but may not be affordable in the less rich countries with a high incidence of HCC.

There was therefore a need to develop an alternative. One of these still uses a lipiodol carrier, but the radioisotope is no longer ^{131}I but ^{188}Re . ^{188}Re is available from a $^{188}\text{W}/^{188}\text{Re}$ generator. Each generator costs about 10 000 Euros, but can produce a therapeutic dose of ^{188}Re every day for 6 months, bringing the cost down to about 100 euros per patient. The half-life is only 17 hours, allowing a higher initial activity

(5–7 GBq vs. 1–2 GBq for ^{131}I). This will hopefully deliver a higher radiation dose rate to the tumor. However, whilst iodine freely associates with lipiodol and substitutes for a non-radioactive iodine in the fatty acid, ^{188}Re does not do this. Therefore, some pharmaceuticals have been developed that will allow the ^{188}Re to associate with the lipiodol. The one most commonly used comes from Korea and is based on a substance called 4-hexadecyl 1-2,9,9-tetramethyl-4,7-diaza-1,10-decanethiol, fortunately also known as HDD.²⁸ After initial mixing, the mixture is centrifuged and the $[^{188}\text{Re}]$ HDD will transfer to the lipiodol layer.

As shunting could occur into the lungs, a low activity ‘scout’ dose is performed first. This is imaged, and the activity that will allow a maximum of 12 Gy to the lungs, 30 Gy to the liver, and 1.5 Gy to the bone marrow is calculated.²⁹ Up to 7.4 GBq can be administered. It is possible for all this to occur in one long sitting, with the patient moving from the fluoroscopy suite to nuclear medicine and then back to fluoroscopy, though it is more normal for this to be done in two sittings.

The project was initially funded and organized through the International Atomic Energy Agency, and both early phase I results and an extended phase II study showed high levels of efficacy with little toxicity. As toxicity occurred much sooner after administration than with $[^{131}\text{I}]$ lipiodol (12–24 hours), and because of the short half-life of ^{188}Re a 1–2-day admission was more normal than the 3–4-day admission for the ^{131}I product.³⁰

Confirmatory studies from Belgium have shown that activities of 7 GBq are easily tolerated, and that the treatment is safe in patients with advanced cirrhosis.^{31,32}

$[^{166}\text{Ho}]$ chitosan

Chitosan is a derivative of chitin, and has been found to have high levels of retention within HCC. In Korea and China it has been complexed to holmium (^{166}Ho), another β emitting isotope more commonly available in East Asia. The product has been injected both intra-arterially and directly into the tumor.^{33,34} In addition, ^{166}Ho has been complexed to small plastic beads in the same way as ^{90}Y microspheres.³⁵ Early results are encouraging, but most of the patients treated had fairly small tumors for which a good prognosis is normally expected. At present these agents are not available outside of East Asia.

^{90}Y microspheres

Life sometimes seems to go round in circles: 25 years ago there were attempts to treat HCC with ^{32}P and ^{90}Y particulates passed into the liver, but these were abandoned when

¹³¹Ilipiodol was used. However, the combination of modern interventional radiology and advances in ⁹⁰Y labeling has meant that this technique is being reconsidered. The latest study uses a commercial preparation of ⁹⁰Y resin spheres called 'SIRSpheres' or ⁹⁰Y in irradiated glass balls called 'Theraspheres'.^{36,37} These are small glass balls of 25–35 µm. The ⁹⁰Y has a much longer path length than ¹³¹I, and as a consequence may be better for treating bigger tumors. The method of administration differs slightly from lipiodol. In this case, a scout dose of [⁹⁹Tc]MAA macro-aggregated albumin is given via an angiographic catheter; the patient is then taken to nuclear medicine, and if good flow to the tumor and shunting of less than 15% is demonstrated, the patient returns to the fluoroscopy suite and 1 GBq of ⁹⁰Y SIRSpheres mixed with saline to form an emulsion is then administered via the catheter.³⁶ Whilst originally used in metastatic carcinoma of the colon in Hong Kong, it has been administered to 71 patients with HCC; 1 GBq was given in each administration, with some patients receiving a total of five treatments, and hence accumulated activity of 5 GBq of ⁹⁰Y SIRSpheres. It has been calculated that this method will deliver 750 Gy to the tumor. In 94% of patients there was a drop of 90% in AFP to normal. However, only 27% of patients had > 50% reduction in the liver tumor size on CT. In addition, where it has been used as a neoadjuvant treatment, it has been found that whilst the lesions were present on CT at surgery, no live HCC cells were found again, showing that CT is not the best way to monitor tumor response. There is an issue of cost, as this method may cost as much as 10 000 euros per treatment.

Conclusions

Though primarily used by departments which are enthusiasts, there is solid evidence from a variety of radiopharmaceuticals that there is a role for radionuclide therapy (delivered to the liver by intra-arterial catheter) in the palliative treatment of non-resectable HCC, and in adjuvant therapy after potentially curative resection. In a recent review of 44 randomized trials of available treatments for nonresectable HCC, two American authors conclude that: 'Hepatic artery infusion of I-131 Lipiodol appears safe; initial trials suggest a survival benefit and efficacy comparable to more toxic embolization-based therapies'.³⁸

References

1. Bosch FX, Ribes J, Cleries R, Diaz M. Epidemiology of hepatocellular carcinoma. *Clin Liver Dis* 2005; 9: 191–211.
2. Srivatanakul P, Sriplung H, Deerasamee S. Epidemiology of liver cancer: an overview *Asian Pac J Cancer Prev* 2004; 5: 118–25.
3. Mima S, Sekiya C, Kanagawa H et al. Mass screening for hepatocellular carcinoma: experience in Hokkaido, Japan. *J Gastroenterol Hepatol* 1994; 9: 361–5.
4. Okuda K. Identification and localisation of resectable tumours in the liver *Trop Gastroenterol* 1990; 11: 119–29.
5. Chu CM, Liaw YF. Hepatitis B virus-related cirrhosis: natural history and treatment. *Semin Liver Dis* 2006; 26: 142–52.
6. Beasley RP, Hwang LY, Lin CC, Chien CS. Hepatocellular carcinoma and hepatitis B virus. A prospective study of 22 707 men in Taiwan. *Lancet* 1981; 8256: 1129–33.
7. Tong MJ, el-Farra NS, Reikes AR, Co RL. Clinical outcomes after transfusion-associated hepatitis C. *N Engl J Med* 1995; 332: 1463–6.
8. Johnson PJ. The epidemiology of hepatocellular carcinoma. *Eur J Gastroenterol Hepatol* 1996; 8: 845–9.
9. Qazi FM, Khan M, Geisinger KR. Diffuse type of hepatocellular carcinoma. *J Pak Med Assoc* 1990; 40: 69–71.
10. Okuda K, Ohtsuki T, Obata H et al. Natural history of hepatocellular carcinoma and prognosis in relation to treatment. Study of 850 patients. *Cancer* 1985; 56: 918–28.
11. Pugh RNH, Murray-Lyon IM, Dawson JL et al. Transection of the oesophagus for bleeding oesophageal varices *Br J Surg* 1973; 60: 646–64.
12. Sheppard KJ, Bradbury DA, Davies JM, Ryrie DR. High serum vitamin B12 binding capacity as a marker of the fibro-lamellar variant of hepatocellular carcinoma *Br Med J* 1983; 286: 57.
13. Buscombe JR, Caplin ME, Hilson AJ. Long-term efficacy of high-activity ¹¹¹In-pentetreotide therapy in patients with disseminated neuroendocrine tumors. *J Nucl Med* 2003; 44: 1–6.
14. Okuda K, Tanaka M, Kanazawa N et al. Evaluation of curability and prediction of prognosis after surgical treatment for hepatocellular carcinoma by lens culinaris agglutinin-reactive alpha-fetoprotein. *Int J Oncol* 1999; 14: 265–71.
15. Cormier JN, Thomas KT, Chari RS, Pinson CW. Management of hepatocellular carcinoma. *J Gastrointest Surg* 2006; 10: 761–80.
16. Order SE, Klein JL, Ettinger D et al. Phase I-II study of radiolabeled antibody integrated in the treatment of primary hepatic malignancies. *Int J Radiat Oncol Biol Phys* 1980; 6: 703–10.
17. Lechner PK, Klein JL, Fishman EK et al. Comparative tumor dose from ¹³¹I-labeled polyclonal anti-ferritin, anti-AFP, and anti-CEA in primary liver cancers. *Cancer Drug Deliv* 1984; 1: 321–8.
18. Buscombe JR. Iodine-131 Lipiodol therapy. In: Padhy A, Solanki KK, eds. *Nuclear Medicine Resource Manual* Vienna: International Atomic Energy Agency 2006: 310–23.
19. Towu E, Al-Mufti R, Winslet M. Uptake of lipiodol-cytotoxic conjugates by hepatocellular carcinoma cells *J Pediatr Surg* 2004; 39: 203–6.
20. Raoul JL, Guyader D, Bretagne JF et al. Prospective randomized trial of chemoembolization versus intra-arterial injection of ¹³¹I-labeled-iodized oil in the treatment of hepatocellular carcinoma. *Hepatology* 1997; 26: 1156–61.
21. Bhattacharya S, Novell JR, Dusheiko GM et al. Epirubicin-Lipiodol chemotherapy versus ¹³¹Iodine-Lipiodol radiotherapy in the treatment of unresectable hepatocellular carcinoma. *Cancer* 1995; 76: 2202–10.

22. Raoul JL, Guyader D, Bretagne JF et al. Randomized controlled trial for hepatocellular carcinoma with portal vein thrombosis: intra-arterial iodine-131-iodized oil versus medical support *J Nucl Med* 1994; 35: 1782–7.
23. Lau WY, Leung TW, Ho SK et al. Adjuvant intra-arterial iodine-131-labelled lipiodol for resectable hepatocellular carcinoma: a prospective randomised trial. *Lancet* 1999; 353: 797–801.
24. Boucher E, Corbinais S, Rolland Y et al. Adjuvant intra-arterial injection of iodine-131-labeled lipiodol after resection of hepatocellular carcinoma. *Hepatology* 2003; 38: 1237–41.
25. Partensky C, Sassolas G, Henry L, Paliard P, Maddern GJ. Intra-arterial iodine 131-labeled lipiodol as adjuvant therapy after curative liver resection for hepatocellular carcinoma: a phase 2 clinical study *Arch Surg* 2000; 135: 1298–300.
26. Brans B, De Winter F, Defreyne L et al. The anti-tumoral activity of neoadjuvant intra-arterial 131I-lipiodol treatment for hepatocellular carcinoma: a pilot study. *Cancer Biother Radiopharm* 2001; 16: 333–8.
27. Raoul JL, Messner M, Boucher E et al. Preoperative treatment of hepatocellular carcinoma with intra-arterial injection of 131I-labelled lipiodol. *Br J Surg* 2003; 90: 1379–83.
28. Lee YS, Jeong JM, Kim YJ et al. Synthesis of 188 Re-labelled long chain alkyl diaminedithiol for therapy of liver cancer. *Nucl Med Commun* 2002; 23: 237–42.
29. Sundram FX, Jeong JM, Zanzonico P et al. Trans-arterial rhenium-188 lipiodol in the treatment of inoperable hepatocellular carcinoma – an IAEA sponsored multi-centre phase I study. *World J Nucl Med* 2002; 1: 5–11.
30. Sundram F, Chau TC, Onkhuudai P, Bernal P, Padhy AK. Preliminary results of transarterial rhenium-188 HDD lipiodol in the treatment of inoperable primary hepatocellular carcinoma. *Eur J Nucl Med Mol Imaging* 2004; 31: 250–7.
31. Lambert B, Bacher K, Defreyne L et al. Re-188-HDD/lipiodol therapy for hepatocellular carcinoma: a phase I clinical trial. *J Nucl Med* 2005; 46: 60–6.
32. Lambert B, Bacher K, De Keukeleire K et al. 188Re-HDD/lipiodol for treatment of hepatocellular carcinoma: a feasibility study in patients with advanced cirrhosis. *J Nucl Med* 2005; 46: 1326–32.
33. Cho BC, Kim EH, Choi HJ et al. A pilot study of trans-arterial injection of 166Holmium–Chitosan complex for treatment of small hepatocellular carcinoma. *Yonsei Med J* 2005; 46: 799–805.
34. Kim JK, Han KH, Lee JT et al. Long-term clinical outcome of phase IIB clinical trial of percutaneous injection with holmium-166/chitosan complex (Milican) for the treatment of small hepatocellular carcinoma. *Clin Cancer Res* 2006; 12: 543–8.
35. Seppenwoolde JH, Nijsen JF, Bartels LW et al. Internal radiation therapy of liver tumors: qualitative and quantitative magnetic resonance imaging of the biodistribution of holmium-loaded microspheres in animal models. *Magn Reson Med* 2005; 53: 76–84.
36. Lau WY, Ho S, Leung TW et al. Selective internal radiation therapy for nonresectable hepatocellular carcinoma with intraarterial infusion of 90yttrium microspheres. *Int J Radiat Oncol Biol Phys* 1998; 40: 583–92.
37. Salem R, Lewandowski R, Roberts C et al. Use of yttrium-90 glass microspheres (TheraSphere) for the treatment of unresectable hepatocellular carcinoma in patients with portal vein thrombosis. *J Vasc Interv Radiol* 2004; 15: 335–45.
38. Schwartz JD, Beutler AS. Therapy for unresectable hepatocellular carcinoma: review of the randomized clinical trials-II: systemic and local non-embolization-based therapies in unresectable and advanced hepatocellular carcinoma. *Anti-cancer Drugs* 2004; 15: 439–52.

Therapy of colorectal cancer

John Buscombe

Background

Colorectal cancer remains one of the most common cancers worldwide. There are over 875 000 sufferers per year, and it accounts for 8.5% of all cancers and 7.2% of all cancer deaths.¹ The incidence rises with age, with slightly more women suffering than men, but this may just reflect that in many societies women live 10 years more than men and therefore are more likely to suffer this age-related disease. The disease is curable if found early, and may yet be treatable or controllable in more advanced cases. Because of the presence of carcinoembryonic antigen (CEA) on most colorectal cancer cells, the main strategy has been based on the development of radiolabeled anti-CEA antibodies.

Etiology

A higher incidence of colorectal cancer has been linked to low-fiber diets, where reduced gut transit may lead to potential carcinogens being in touch with the bowel for longer. As a consequence there is some suggestion that the disease is commoner in the developed world, but part of this will be because as a person lives longer the chance of colorectal cancer increases. There is an increased incidence in patients with colonic polyps, in particular if they are familial. In patients with multiple polyps, it is possible for there to be more than one primary at one time in about 5% of cases.² In familial adenomatous polyposis it has been found that the genetic defect is a deletion of the short arm of chromosome 5.³

Staging

The primary staging of colorectal cancer is by direct vision and biopsy via endoscopy, and imaging normally relying on

computed tomography (CT). The main method of staging was described by Dukes in 1932, as seen in Table 24.1.⁴ In terms of prognosis, the Dukes staging method has proved to be very robust.

The TNM staging system is similar to the Dukes method with stage 1 equaling Dukes A; there is in addition a stage 4 in patients with distant metastasis.

The prognosis for stage 1 and 2 disease is good, and should be considered curable. In patients suffering from stage 4 there are few survivors over 5 years.

Treatment

Early treatment by surgery is normally curative for Dukes A and B (stages 1 and 2); for stage 3 disease extended lymph node resection may prevent later metastasis. In stage 4 disease, surgery may still be considered for symptom relief such as removing an obstruction. If surgery is not possible then radical radiotherapy, with 50 Gy in 25 fractions, may be curative, though with high levels of morbidity.⁵ Chemotherapy has been used as both adjuvant therapy and palliative treatment in disseminated disease. Until very recently all the successful regimens have been based on 5-fluorouracil (5-FU).⁶ Irinotecan has shown some improved results, but has still not become routine.⁷

If these methods fail, then effective options are very limited, and it is in these patients that nuclear medicine methods have been directed. There is a unique target in the CEA, which is overexpressed in colorectal cancer, and there have been attempts to develop antibodies against CEA for the past 30 years. However, success has eluded the nuclear medicine community. It has been said that if there was a mouse with colon cancer we would know how to treat that mouse with ten different agents, yet, after 30 years, we have not really progressed in our management of patients with colorectal cancer. Though this is a gross simplification, there remains an element of truth, and it is this frustrating journey that this chapter will map.

Table 24.1 Dukes staging of colorectal cancer

Stage	Pathological/radiological characteristics
A	Tumor confined to gut wall
B	Tumor through muscularis propia
C	Spread to regional lymph nodes

Early use of radiolabeled antibodies

It has been known for 30 years that there is variation in the CEA antigen; this is not unexpected, as other systems such as the adrenergic receptor or the somatostatin receptor system also show some natural variation. In 1975, a group from Yale obtained different forms of purified CEA from different sources and originating from different countries.⁸ Looking at binding profiles they were able to show very different kinetics for a single anti-CEA antibody, with up to three times variation in affinity between different formulations of CEA. Therefore, this group suggested that CEA was not a single antigen but a family of antigens. This may help to explain some of the different results obtained from different centers. There has also been much refinement of the antibodies so that they may recognize particular domains within the CEA molecule.

¹³¹I-labeled anti-CEA antibodies

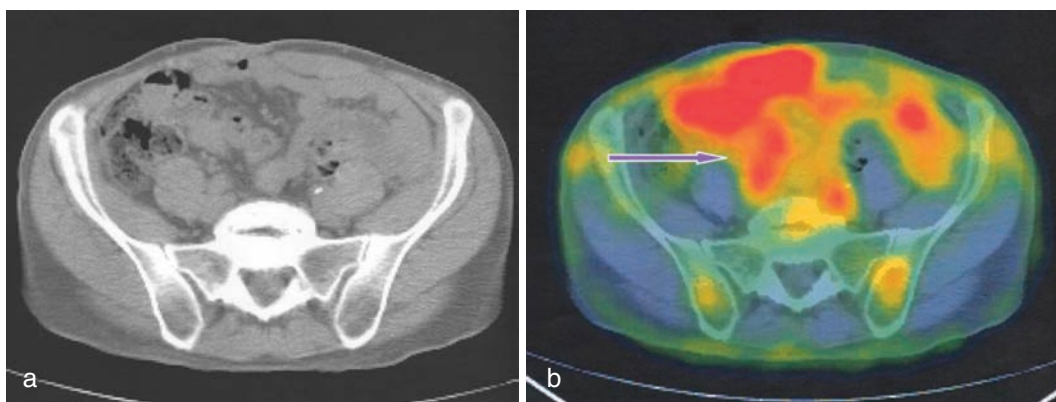
The era of radioimmunotherapy in colon cancer started with the first reported successful localization of colon

cancer with an ¹³¹I-labeled murine anti-CEA antibody by Goldenburg et al.⁹ Imaging per se is not the topic of this chapter, but the development of imaging has proceeded therapy, and until recently CEA-positive tumors have been visualized using ^{99m}Tc-labeled antibody fragments (arctimomab)¹⁰ (Figure 24.1).

Though most radioimmunotherapy has used the CEA target, an alternative has been the tumor-associated glycoprotein 72 (TAG72). In a short series, 15 patients with metastatic colon cancer were treated with 2.8 GBq/m² [¹³¹I]CC49 directed to TAG72.¹¹ The antibody was a non-engineered mouse protein, and 12/13 patients tested developed human anti-mouse antibody. Bone marrow toxicity was common, with 7/15 patients having reversible grade III and grade IV toxicity. Despite calculated radiation doses to the tumors of 0.19–6.67 Gy there was no tumor response.

Overall there have been three main studies in humans with some mixed results, and an overall response rate of 0% with the antibody on its own to 45% when combined with chemotherapy (Table 24.2). As can be seen fewer than 40 patients have been studied, and only in one series was ¹³¹I-labeled anti-CEA antibody used on its own. In others there were cofactors. The use of heat to improve blood flow and penetration would seem to improve the response from the antibody alone. In the third study reported, the ¹³¹I-labeled antibody was combined with 5-FU and leucovorin, and it is unclear whether the chemotherapy or the radiolabeled antibody resulted in the reported response rate.

One of the limitations affecting radioimmunotherapy is the poor distribution of the antibody within the tumor, with antibody penetrating the tumor edge but little passing into the main tumor mass. Using a mouse model and ¹¹¹In-labeled anti-CEA antibody F33-104 for imaging and ¹³¹I-labeled antibody for autoradiography, it was shown that once the tumor had a diameter greater than 0.5 cm there

**Figure 24.1**

Computed tomography (CT) scan in patient with previous history of colon cancer resected 2 years previously. The carcinoembryonic antigen (CEA) level is rising but CT (a) is unhelpful. ^{99m}Tc-labeled arctimomab (b) however shows accumulation on the serosal surface of the small bowel (arrowed) due to cancer infiltration.

Table 24.2 Results of human studies using ^{131}I -labeled antibodies in human colorectal cancers^{11–13}

Study	Year	n	mAb	Activity	ORR (%)	PR (%)	CR (%)	Comments
Murray et al. ¹¹	1994	15	CC49	75 mCi/m ²	0	0	0	GIII and GIV toxicity in 12 patients, HAMA 67%
Mittal et al. ¹²	1996	6	IMMU-4	30, 60 mCi/m ²	17	17	0	Combined with hyperthermia, 50% GIII and GIV toxicity, 83% drop in CEA
Behr et al. ¹³	1999	12	MN-14	50–70 mCi/m ²	45	5	0	Combined with 5-FU and leucovorin, MTD 70 mCi/m ²

MAB, monoclonal antibody; ORR, objective response rate; PR, partial response; CR, complete response; G, grade; HAMA, human anti-murine antibodies; CEA, carcinoembryonic antigen; MTD, maximal tolerated dose.

was a rim of antibody uptake around the edge of the tumor with little penetration into the center of the tumor.¹⁴ This would suggest that ^{131}I -labeled monoclonal antibodies are best suited to clearance of tumors of 0.5 cm and below, i.e. as adjuvant therapy only.

This lack of success in treating colon cancer metastases is even more frustrating in view of the fact that both radioimmunotherapy and chemotherapy induce similar changes in cellular mucin-1 (MUC1) and colon specific antigen-p (CSAp), which are seen as markers of cell damage.¹⁵

^{90}Y -labeled antibodies

Wong et al. have successfully undertaken a phase I trial using ^{90}Y linked via DOTA (tetraazacyclododecanetetraacetic acid) to a chimeric anti-CEA antibody termed T84.66.¹⁶ The use of the DOTA linker comes primarily from work with ^{90}Y peptides in neuroendocrine tumors and the hLL2 antibody used in lymphoma. In these cases the complex remained stable, which is important, as free ^{90}Y is bone-seeking and will lead to significant bone marrow toxicity. An initial imaging study was performed using 185 MBq labeling on 5 mg of T84.66. This was used to identify active accumulation at the tumor site and estimate dosimetry with imaging up to 7 days post-injection of the tracer dose. The dose-ranging stage of the trial started with 444 MBq/m² [^{90}Y]DOTA nT84.66 up to 1147 MBq/m². In the first few patients, grade II and grade III hematological toxicity was noted, so a co-infusion of Ca-DTPA (diethylenetriamene-pentaacetic acid) was given 3 days post-treatment to mop up any free ^{90}Y . Mild to moderate bone marrow toxicity was seen in nine patients. There was no recorded liver or kidney toxicity. In eight patients a human anti-chimeric antibody reaction was induced; in four of these patients it was of sufficient strength to prevent retreatment. Though there were

no cases of partial or complete response, in four patients with previously progressive disease there was stability after treatment for 3–5 months. A phase II study is now planned.

Other isotopes

An alternative β emitting isotope is ^{188}Re . This has the advantage of being available from a tungsten generator. The chemistry is related to technetium, but there are some significant differences, and its use in labeled biomolecules has been limited. It has been attached to a bispecific antibody using complex chemistry, but uptake in the tumor was less than using an ^{125}I -labeled antibody.¹⁷

The radiation dose that can be delivered even with β radiation is limited, and if good targeting can be achieved then α emitters may be able to deliver a higher linear energy transfer. Behr et al. have compared ^{90}Y - and ^{213}Bi -labeled antibodies in an animal model. The α emitter was more active in tumor destruction with similar toxicity; however, it was not known whether this can be translated to the larger tumors in the human where the short path length of the α may be a disadvantage.¹⁸

Bispecific antibodies

This is a strategy to try and optimize localization of the radioisotope at the site of the tumor but reduce uptake elsewhere, especially in the bone marrow, which is often the dose-limiting organ. Two main methods have been developed, first using pre-targeting techniques such as the biotin–avidin system or the antibody-directed enzyme pro-drug therapy (ADEPT) system.^{19,20}

With bispecific antibodies, the 'two arms' of the antibody have different antigenic properties. The first is like a traditional anti-CEA antibody able to attach to a colon cancer cell. The other 'arm' is directed towards a specific antigen such as a peptide or another antibody which contains the radioisotope. The first antibody is given, and when enough time has elapsed to allow clearance from the blood, the second radiolabeled antibody or peptide is given, acting as a hapten, and will only attach to the antibody which is itself attached to the cancer cell, allowing delivery of the radioactive dose to the tumor. By their very nature these bispecific antibodies are heavily engineered and normally also humanized, so that repeat administrations can be given.

An example of this is the work by Karacay et al.²¹ They have used an antibody directed against CEA and a hapten which is a ⁹⁰Y peptide (defined as di-HSG (histamine-succinyl glycine) with ⁹⁰Y attached via a DOTA linker). In initial animal studies there was rapid clearance of the ⁹⁰Y peptide from the blood over the first few hours. There was a tumor to blood ratio of about 24:1 at 24 hours post-injection, and a tumor to liver ratio of 31:1. By 48 hours the ratio of tumor uptake to liver uptake had risen to 80:1, and that of the blood had risen less, but was still 33:1. When the bispecific method was compared with the antibody directly labeled with ⁹⁰Y, the 96% injected dose in the tumor was greater by a factor of 2.6 times.

Combination with physical factors

A group from Chicago used hyperthermia as a method to improve the blood flow and hence delivery of antibodies into the tumor. They used the IMMU-4 anti-CEA antibody labeled with ¹³¹I in activities of 1.1 GBq/m² to 2.2 GBq/m². This was combined with local hyperthermia to liver colonic cancer metastasis, raising the local temperature to an average 42.5°C.¹² There was a good improvement in symptoms in 2/6 patients and a drop in CEA in 5/6 patients, though only one patient had a radiological response; this could suggest that radiology may not be ideal in determining response in these patients. Toxicity was very limited and easily reversed.

A more conventional physical therapy is to combine targeted radioimmunotherapy with external beam radiotherapy. In a Swiss study, six patients with liver metastases were treated with 20 Gy external beam radiotherapy to the liver, combined with 7.4 GBq of ¹³¹I-labeled anti-CEA antibody.²² There was bone marrow toxicity in all patients, but in addition there was grade I–III liver toxicity. One of the patients imaged had disease regression, and three others disease stability, on CT. This work should be repeated in a larger study.

Combination with chemotherapy

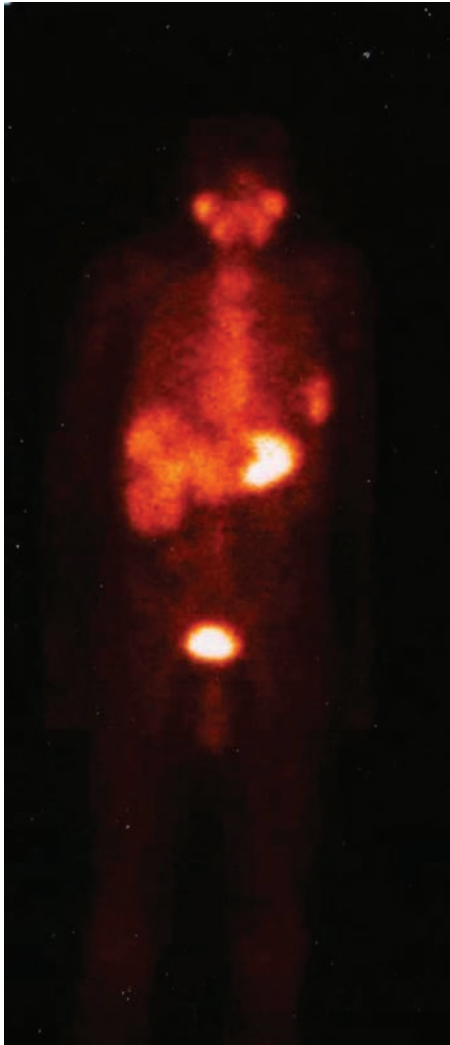
One unique method is to use less toxic substances which still have anti-colon cancer action, such as the cyclooxygenase-2 (COX-2) inhibitor parecoxib. In a nude mouse model, however, it was found that the addition of a COX-2 inhibitor did not improve uptake of ¹²⁴I-labeled MN-14 anti-CEA antibody into tumor xenografts or result in increased tumor kill.²³

Work with more conventional chemotherapy agents has also been carried out using a high-affinity antibody MN-14. In an animal model, the antibody was given with coadministration of 5-FU and leucovorin, with clearance of small vessel disease.¹³ An extended study in humans using 5-FU, leucovorin, and increasing activities of ¹³¹I-labeled MN-14 from 1.1 GBq/m² up to a maximal tolerated dose of 2.2 GBq/m² was then performed. In these patients who had small volume disease, there was some reduction in tumor size in 7/12 patients, with 2/12 having a formal partial response (PR).

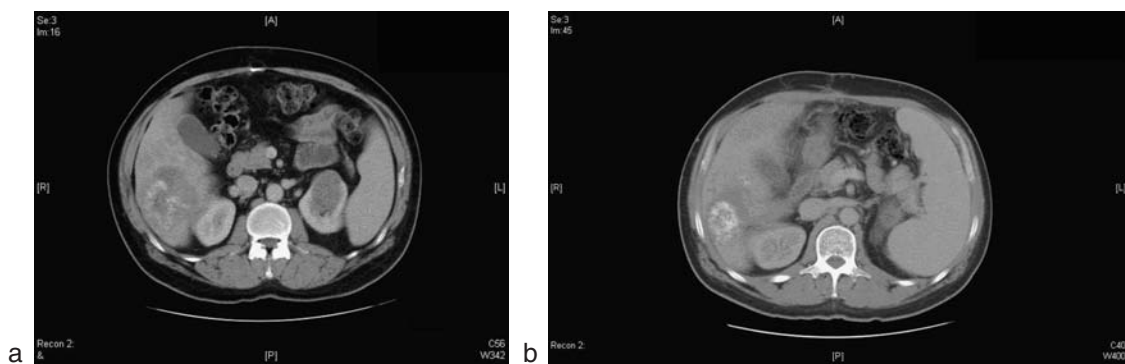
There have been attempts to use radiosensitizers in addition to radioimmunotherapy. In a mouse model, the hypoxic cell radiosensitizer misonidazole was combined with ¹³¹I-labeled A5B7 (an anti-CEA antibody).²⁴ More recently, newer agents such as the anti-angiogenic drug combretastatin have been combined with ¹³¹I-labeled A5B7 (Figure 24.2). The hypothesis is that combretastatin will turn hypoxic tumor into infarcted tumor, and the ¹³¹I-labeled A5B7 will attack the viable tumor around the edge. Phase I studies are progressing.

⁹⁰Y-labeled SIRSpheres™

The primary site for metastatic colorectal cancer is the liver. Though a single metastasis can be removed with improved survival, many patients will present with multiple liver metastases either at diagnosis or with recurrent disease later. Despite nearly 30 years of research into radiolabeled antibodies in metastatic colorectal cancer, the first licensed radioactive product for the treatment of metastatic colorectal cancer is not an antibody but a ⁹⁰Y-labeled resin. Using the same principle as used in the treatment of liver cancer, this is given directly into the liver via the hepatic artery. The technique involves cannulization of the hepatic artery via a surgically placed 'portocath' or radiologically via a transarterial route. Then, up to 2.5 GBq of ⁹⁰Y resin spheres is instilled over about 10 minutes (Figures 24.3 and 24.4). The method appears to be safe.²⁵ In a phase II trial, a combination of ⁹⁰Y resin spheres (SIRSpheres™) and 5-FU–leucovorin chemotherapy was compared with chemotherapy alone. To have an expected effect, all or nearly all of the sites of known tumor were in the liver, and

**Figure 24.2**

Whole body anti-CEA antibody (^{131}I -labeled A5B7) image at 72 hours showing some focal accumulation within the liver. (Courtesy of R Begent, T Meyer, B Pedley, K Chester, and A Green, UCL.)

**Figure 24.3**

Patient with metastatic colon cancer in the liver. CT (a) and ^{18}F -FDG-PET (fluoro-2-deoxy-D-glucose-positron emission tomography) (b) show a large amount of cancer within the liver. After treatment with 1 GBq of ^{90}Y SIRSpheresTM there is improvement seen on both the CT scan (c) and ^{18}F -FDG-PET (d). (Images courtesy of Dr Adil Al-Nahaas, Hammersmith Hospital.)

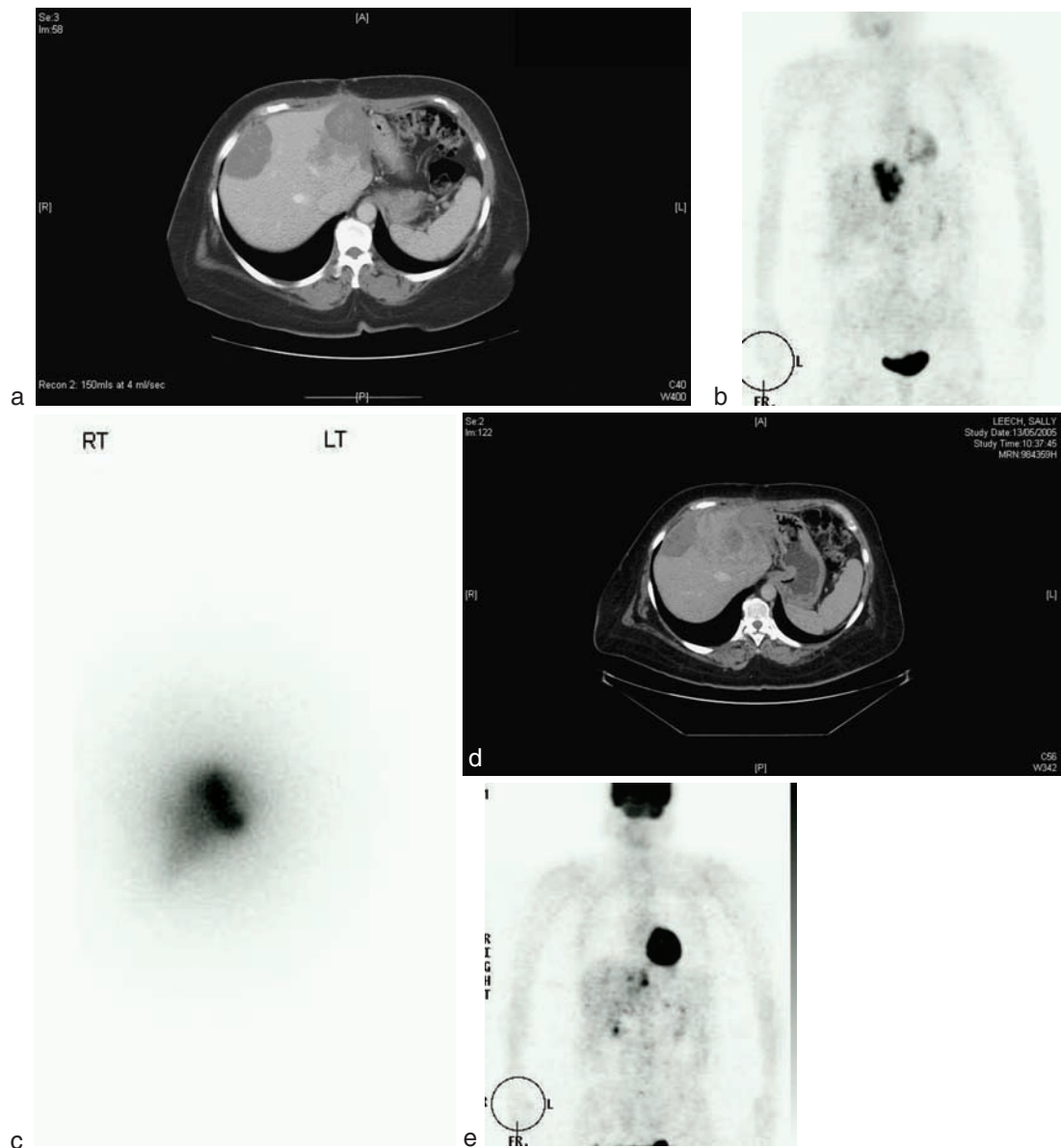


Figure 24.4

Patient with metastatic colon cancer in the liver. CT (a) and [^{18}F]FDG-PET (b) show a large amount of cancer within the liver. After treatment with 1 GBq of ^{90}Y SIRSpheres with good localization seen on brehmsstrahlung imaging in the left lobe lesions (c), there is improvement seen on both the CT scan (d) and more clearly on [^{18}F]FDG-PET (e). (Images courtesy of Dr Adil Al-Nahaas, Hammersmith Hospital.)

of the 21 patients enrolled 11 received the chemotherapy and the ^{90}Y resin spheres.

Though assessment of response was limited to the liver by necessity, six patients demonstrated disease stability and four with progressive disease with chemotherapy alone, compared with ten partial responses and one with disease stability when both chemotherapy and ^{90}Y resin spheres were used. This translated to improved survival, with a mean of 3.6 months with chemotherapy alone and 18.6 months when the combination therapy was used.²⁶

As a consequence, registration approval has now been given in Australia, Hong Kong, the European Union, and North America, though use is still limited possibly by the high cost of 15 000 euros per dose.

Conclusion

The long search for radioimmunotherapy in colorectal cancer has been frustrating. There is no clear consensus

regarding the best strategy: should bispecific antibodies be used, or should radioimmunotherapy be combined with chemotherapy, and if so which agent should be used? ^{131}I has been the most commonly used isotope, but there is no evidence that this or any alternative is the best radiolabel.

There is an approved and licensed method using radioisotopes to treat colorectal metastasis as long as it is in the liver, where intra-arterial ^{90}Y -labeled resin (SIRspheres) in combination with common chemotherapy has prolonged survival, but as yet this is not widely used.

References

- Potter JD. Food, nutrition and the prevention of cancer a global perspective. Washington: World Cancer Research Fund, 1992.
- Eide T. The age-, sex-, and site-specific occurrence of adenomas and carcinomas of the large intestine within a defined population. *Scand J Gastroenterol* 1986; 21: 1083–8.
- Groden J, Thliveris A, Samowitz W et al. Identification and characterization of the familial adenomatous polyposis coli gene. *Cell* 1991; 66: 589–600.
- Dukes CE. The classification of cancer of the rectum. *J Path Bacteriol* 1932: 323–2.
- Taylor RE, Kerr GR, Arnott SJ. External beam radiotherapy for rectal adenocarcinoma. *Br J Surg* 1987; 74: 455–9.
- Buyse M, Zeleniuch-Jacquotte A, Chalmers TC. Adjuvant therapy of colorectal cancer. Why we still don't know. *JAMA* 1988; 259: 3571–8.
- Becouarn Y, Gamelin E, Coudert B et al. Randomized multicenter phase II study comparing a combination of fluorouracil and folinic acid and alternating irinotecan and oxaliplatin with oxaliplatin and irinotecan in fluorouracil-pretreated metastatic colorectal cancer patients. *J Clin Oncol* 2001; 19: 4195–201.
- Vrba R, Alpert E, Isselbacher KJ. Carcinoembryonic antigen: evidence for multiple antigenic determinants and isoantigens. *Proc Natl Acad Sci USA* 1975; 72: 4602–6.
- Goldenberg DM, DeLand F, Kim E et al. Use of radiolabeled antibodies to carcinoembryonic antigen for the detection and localization of diverse cancers by external photoscanning. *N Engl J Med* 1978; 298: 1384–6.
- Moffat FL Jr, Pinsky CM, Hammershaimb L et al. Clinical utility of external immunoscintigraphy with the IMMU-4 technetium-99m Fab' antibody fragment in patients undergoing surgery for carcinoma of the colon and rectum: results of a pivotal, phase III trial. The Immunomedics Study Group. *J Clin Oncol* 1996; 14: 2295–305.
- Murray JL, Macey DJ, Kasi LP et al. Phase II radioimmunotherapy trial with ^{131}I -CC49 in colorectal cancer. *Cancer* 1994; 73 (Suppl): 1057–66.
- Mittal BB, Zimmer MA, Sathiaseelan V et al. Phase I/II trial of combined ^{131}I anti-CEA monoclonal antibody and hyperthermia in patients with advanced colorectal adenocarcinoma. *Cancer* 1996; 78: 1861–70.
- Behr TM, Memtsoudis S, Vougioukas V et al. Radioimmunotherapy of colorectal cancer in small volume disease and in an adjuvant setting: preclinical evaluation in comparison to equitoxic chemotherapy and initial results of an ongoing phase-I/II clinical trial. *Anticancer Res* 1999; 19: 2427–32.
- Sato N, Saga T, Sakahara H et al. Intratumoral distribution of radiolabeled antibody and radioimmunotherapy in experimental liver metastases model of nude mouse. *J Nucl Med* 1999; 40: 685–92.
- Modrak DE, Gold DV, Goldenberg DM, Blumenthal RD. Colonic tumor CEA, CSAP and MUC-1 expression following radioimmunotherapy or chemotherapy. *Tumor Biol* 2003; 24: 32–9.
- Wong JC, Chu DZ, Williams LE et al. A phase I trial of ^{90}Y -DOTA-Anti-CEA Chimeric T84.66 (cT84.66) radioimmunotherapy in patients with metastatic CEA producing malignancies. *Cancer, Biother Radiopharm* 2006; 21: 88–100.
- Gestin JF, Loussouarn A, Bardies M et al. Two-step targeting of xenografted colon carcinoma using a bispecific antibody and ^{188}Re -labeled bivalent hapten: biodistribution and dosimetry studies. *J Nucl Med* 2001; 42: 146–53.
- Behr TM, Sgouros G, Stabin MG et al. Studies on the red marrow dosimetry in radioimmunotherapy: an experimental investigation of factors influencing the radiation-induced myelotoxicity in therapy with beta-, Auger/conversion electron-, or alpha-emitters. *Clin Cancer Res* 1999; 5: 3031s–43s.
- Martin J, Stribbling SM, Poon GK et al. Antibody-directed enzyme prodrug therapy: pharmacokinetics and plasma levels of prodrug and drug in a phase I clinical trial. *Cancer Chemother Pharmacol* 1997; 40: 189–201.
- Francis RJ, Sharma SK, Springer C et al. A phase I trial of antibody directed enzyme prodrug therapy (ADEPT) in patients with advanced colorectal carcinoma or other CEA producing tumors. *Br J Cancer* 2002; 87: 600–7.
- Karacay H, Brard PY, Sharkey RM et al. Therapeutic advantage of pretargeted radioimmunotherapy using a recombinant bispecific antibody in a human colon cancer xenograft. *Clin Cancer Res* 2005; 11: 7879–85.
- Buchegger F, Roth A, Allal A et al. Radioimmunotherapy of colorectal cancer liver metastases: combination with radiotherapy. *Ann NY Acad Sci* 2000; 910: 263–9.
- Koppe MJ, Oyen WJ, Bleichrodt RP et al. Combination therapy using the cyclooxygenase-2 inhibitor Parecoxib and radioimmunotherapy in nude mice with small peritoneal metastases of colonic origin. *Cancer Immunol Immunother* 2006; 55: 47–55.
- Pedley RB, Begent RH, Boden JA et al. The effect of radiosensitizers on radio-immunotherapy, using ^{131}I -labelled anti-CEA antibodies in a human colonic xenograft model. *Int J Cancer* 1991; 47: 597–602.
- Moroz P, Anderson JE, Van Hazel G, Gray BN. Effect of selective internal radiation therapy and hepatic arterial chemotherapy on normal liver volume and spleen volume. *J Surg Oncol* 2001; 78: 248–52.
- Van Hazel G, Blackwell A, Anderson J et al. Randomised phase 2 trial of SIR-Spheres plus fluorouracil/leucovorin chemotherapy versus fluorouracil/leucovorin chemotherapy alone in advanced colorectal cancer. *J Surg Oncol* 2004; 88: 78–85.

Therapy of brain tumors

*Chiara Maria Grana, Mirco Bartolomei, Mahila Ferrari,
and Giovanni Paganelli*

Background

Tumors of the central nervous system (CNS) include a number of different difficult-to-treat neoplasms.

In the United States alone, more than 17 000 new cases of primary malignant brain tumor are diagnosed per year, and the incidence appears to be increasing.

Studies using data from the Surveillance, Epidemiology, and End Results (SEER) registry report that the incidence of primary tumors of the CNS is between 2 and 19 per 100 000 per year depending on age.¹ From birth to age 4 years the incidence of primary brain tumors is approximately 3.1 per 100 000, and then slowly declines to a nadir of 1.8 per 100 000 in persons aged 15–24 years. The incidence then rises again to a relative plateau at around age 65 years, with an incidence of approximately 18 cases per 100 000 persons. The most common and serious malignant neoplasm is glioblastoma multiforme (GBM), which accounts for 23% of cases, and is among the most lethal and difficult-to-treat cancers: median survival is less than 1 year from the time of diagnosis.²

The great majority of glioma patients experience local recurrence, and the management of recurrent disease is even less effective, with a median survival of only 16–24 weeks being reported.³

The epidemiology of primary brain tumors is complex, because a large number of histologic subtypes of tumor arise within the CNS, reflecting the diversity of cell types found there. Nevertheless, based on informal reviews of the literature and case series from the neuropathologic literature, an estimate of the approximate frequency of 15 major subgroups of CNS tumors can be made (Table 25.1). Such percentages can be misleading, because the frequency of particular subtypes of tumor is highly dependent on age. For example, although gliomas are the most common type of primary brain tumor – accounting for nearly 50% of all primary CNS neoplasms – gliomas represent a minority of primary brain tumors in children. By contrast, primitive neuroectodermal tumors (PNETs) represent the most common primary brain tumor in the pediatric population,

but are relatively uncommon in adults. Estimating the incidence and prevalence for any given tumor subtype is further complicated because age is a continuous variable, not truly separable into discrete categories such as childhood and adulthood. Similarly, the frequency of glioma subtypes is age dependent: low-grade tumors are much more prevalent in children and young adults, whereas malignant tumors (particularly glioblastomas) are increasingly more common in elderly populations.

Given the problems in determining the true prevalence of CNS tumors, it is not surprising that it has been difficult to estimate whether the incidence of CNS tumors is changing. A 1990 study reported a very large increase in the incidence of malignant gliomas in the elderly.⁴ These and other similar findings have been partially attributed to the greater availability of diagnostic imaging tests such as computed tomography (CT) and magnetic resonance imaging (MRI) over the past two decades, which potentially causes screening artifact.

Pathological classification

The pathological classification of CNS tumors reflects the many cell types that constitute the CNS, any of which can transform into a neoplastic phenotype. The frequency of individual tumor types roughly parallels the relative frequency of cell types within the CNS and their normal proliferative capacity. Astrocytes are among the most common cell types in the CNS and are mitogenically competent; thus, astrocytomas are the most common primary CNS tumor. In contrast, although neurons are also numerous in the CNS, they are postmitotic, and therefore neuronally derived tumors are uncommon.

CNS tumors can be divided into tumors derived from glial cells, neuronal cells, cells that surround or insulate the CNS, and cells that form specialized anatomic structures. Glial cells that are thought to give rise to specific tumor types include astrocytes (astrocytomas), oligodendrocytes

Table 25.1 Frequency of primary intracranial central nervous system (CNS) tumor

Histopathology	Primary brain tumors (%)	Gliomas (%)
Glioblastoma multiforme	21.7	47
Malignant astrocytomas	16.6	36
All oligodendrogliomas	3.1	6.7
All ependymomas	2.3	5.1
Low-grade astrocytoma	1.8	3.9
Meningiomas and other mesenchymal tumors	26.7	—
Pituitary tumors	9.7	—
Nerve sheath tumors (e.g. schwannomas)	7.3	—
CNS lymphomas	3.5	—
Medulloblastomas and other primitive neuroectodermal tumors	1.7	—
All neuron and neuron/glioma tumors	1.0	—
Craniopharyngiomas	1.0	—
Germ cell tumors	0.5	—
Choroid plexus tumors	0.3	—
Other tumors	2.7	—

CNS, central nervous system.

(oligodendrogliomas), and ependymal cells (ependymomas). Neuronal cells identified as the precursors for specific tumors include the cerebellar external granular cells (medulloblastoma) and neuroblasts (PNETs). Transformation of cells lining the CNS causes meningiomas (derived from arachnoid cells) and schwannomas (derived from Schwann cells). Specialized anatomic structures within the CNS and the tumors arising there include the pituitary gland (pituitary adenomas), pineal gland (pineocytomas), notochord remnants (chordomas), endothelial or stromal vascular cells (hemangioblastomas), primitive germ cells (all subtypes of germ cell tumors), and choroidal epithelial cells (choroid plexus papillomas and carcinomas).

Although the classical description of the cell of origin depicted previously is satisfyingly straightforward, this schema remains speculative, sometimes based on scanty phenotypical and immunohistochemical evidence.

Thus, it is possible that the long-accepted dogma that specific CNS tumor types are derived from specific normal differentiated cell types within the CNS may in fact

be incorrect. An alternative view is that because all neuroepithelial cells are derived from a common precursor cell (i.e. a multipotent neural stem cell), all neuroepithelial tumors are derived from neural stem cells or their committed progen. This theory holds that tumors of neural stem cell origin might exhibit phenotypic characteristics of a terminally differentiated cell because the neural stem cell of origin had undergone partial differentiation either before the transforming event(s) or through partial induction of the differentiation process through genetic perturbations responsible for transformation itself.

A complete and proper classification of tumors is important, because tumor subtyping can affect prognosis and treatment recommendations as much as does the general tumor category. Tumor location and patient age are also relevant in tumor classification. For instance, astrocytomas of the spine, brainstem, and cortex may portend very different prognoses. Whether the different natural histories reflect different neuroanatomic constraints or diverse biologic properties of these tumors in various locations, or both, is not known. Finally, patient age not only may influence prognosis but may actually predict a totally different tumor type. For example, tumors in many young adults with glioblastomas (the most aggressive type of astrocytoma) have the genetic and behavioral characteristics of tumors derived from lower-grade gliomas ('secondary glioblastomas'), whereas almost all older patients have de novo ('primary') glioblastomas.

There has been significant controversy over the pathologic classification of astrocytic tumors. Generally speaking, slower growing and less aggressive tumors have been designated as low grade, and faster growing, more aggressive tumors have been designated as high grade. The first widely used system was devised by Kernohan and co-workers, who proposed a four-tier system with grades 1 and 2 defined as lower-grade tumors and grades 3 (*anaplastic astrocytoma*) and 4 (*glioblastoma multiforme*) as high-grade gliomas.

A more useful approach was suggested by Daumas-Duport and co-workers, who developed a four-tier system based on a small set of objective criteria: nuclear pleomorphism, mitoses, endothelial proliferation, and necrosis. Grade 1 tumors had none of these features, grade 2 tumors had one feature, grade 3 tumors had two features, and grade 4 tumors had three or four. Although the classification initially appeared to demonstrate good separation in survival among patients with all four grades of tumor, the system did not adequately differentiate between prognoses of patients with tumors designated as grades 2 and 3 in one single-center validation study.

To resolve these controversies, in 1999 the World Health Organization (WHO) convened an international consensus panel of neuropathologists to define a new classification system, which has since garnered worldwide acceptance. The WHO ratified a new comprehensive classification (Table 25.2) of neoplasms affecting the central nervous system.

In recognition of the emerging role of molecular diagnostic approaches to tumor classification, genetic profiles

Table 25.2 The new World Health Organization (WHO) classification of tumors of the central nervous system

1 Neuroepithelial tumors of the CNS:

- Astrocytic tumors: Astrocytoma (WHO grade II) *variants*: protoplasmic, gemistocytic, fibrillary, mixed
Anaplastic (malignant) astrocytoma (WHO grade III)
Glioblastoma multiforme (WHO grade IV) *variants*: giant cell glioblastoma, gliosarcoma
Pilocytic astrocytoma (non-invasive, WHO grade I)
Subependymal giant cell astrocytoma (non-invasive, WHO grade I)
Pleomorphic xanthoastrocytoma (non-invasive, WHO grade I)
- Oligodendroglial tumors: Oligodendroglioma (WHO grade II)
Anaplastic (malignant) oligodendroglioma (WHO grade III)
- Ependymal cell tumors: Ependymoma (WHO grade II)
Anaplastic ependymoma (WHO grade III)
Myxopapillary ependymoma
Subependymoma (WHO grade I)
- Mixed gliomas: Mixed oligoastrocytoma (WHO grade II)
Anaplastic (malignant) oligoastrocytoma (WHO grade III)
Others (e.g. ependymo-astrocytomas)
- Neuroepithelial tumors of uncertain origin: Polar spongioblastoma (WHO grade IV)
Astroblastoma (WHO grade IV)
Gliomatosis cerebri (WHO grade IV)
- Tumors of the choroid plexus: Choroid plexus papilloma
Choroid plexus carcinoma (anaplastic choroid plexus papilloma)
- Neuronal and mixed neuronal-glial tumors: Gangliocytoma
Dysplastic gangliocytoma of cerebellum (Lhermitte-Duclos)
Ganglioglioma
Anaplastic (malignant) ganglioglioma
Desmoplastic infantile ganglioglioma
Central neurocytoma
Dysembryoplastic neuroepithelial tumor
Olfactory neuroblastoma (esthesioneuroblastoma)
- Pineal parenchyma tumors: Pineocytoma
Pineoblastoma
Mixed pineocytoma/pineoblastoma
- Tumors with neuroblastic or glioblastic elements (embryonal tumors): Medulloepithelioma
Primitive neuroectodermal tumors with multipotent differentiation medulloblastoma
cerebral primitive neuroectodermal tumor
Neuroblastoma
Retinoblastoma
Ependymoblastoma

2 Other CNS neoplasms:

- Tumors of the sellar region
- Hematopoietic tumors
- Germ cell tumors
- Tumors of the meninges
- Non-meningothelial tumors of the meninges
- Tumors of cranial and spinal nerves
- Local extensions from regional tumors
- Metastatic tumours
- Unclassified tumors
- Cysts and tumor-like lesions

have been emphasized, as in the distinct subtypes of glioblastoma and the already clinically useful 1p and 19q markers for oligodendroglioma and 22q/INI1 for atypical teratoid/rhabdoid tumors. The classification of brain tumors is based on the premise that each type of tumor results from the abnormal growth of a specific cell type. To the extent that the behavior of a tumor correlates with basic cell type, tumor classification dictates the choice of therapy and predicts prognosis. In this revised WHO schema, astrocytic tumors are divided into three categories: astrocytoma (including fibrillary, gemistocytic, and protoplasmic), anaplastic astrocytoma, and glioblastoma (including giant cell glioblastoma and gliosarcoma). Juvenile pilocytic astrocytomas and pleomorphic xanthoastrocytomas, two tumors with unique histologic and clinical features, are considered as separate entities in this schema.

Oligodendrogliomas tend to occur in young to middle-aged adults. They are quite uncommon in the very young or the elderly. Grossly, oligodendrogliomas are often well demarcated, with 20% being cystic. Like astrocytomas, oligodendrogliomas display various degrees of clinical aggressiveness, although they are more likely to spread along cerebrospinal fluid (CSF) pathways. Although multi-level grading systems for oligodendrogliomas have been proposed, a two-level classification of differentiated (grade 2) or anaplastic (grade 3) appears to be as useful. Oligodendrogliomas often display areas of astrocytic or, much more rarely, ependymal differentiation. Such tumors, referred to as oligoastrocytomas or mixed gliomas, are also classified as low grade (grade 2) or high grade (grade 3 or anaplastic). Clinically, oligodendrogliomas present in a fashion typical of cortical astrocytomas, but with a more indolent course, a longer antecedent history of symptoms (often over many years), and a higher frequency of seizures. Many are calcified on CT scan. Patients with well-differentiated tumors survive much longer than those with anaplastic tumors (median survival of 9.0 vs. 2.2 years for low-grade and high-grade oligodendrogliomas, respectively).⁹ Most data suggest that patients with pure oligodendrogliomas have better prognoses than those with mixed gliomas. Shaw and colleagues found that the 5- and 10-year survival rates for patients with oligodendrogliomas were 72% and 46%, respectively, whereas the survival rates for mixed oligoastrocytomas were 63% and 33%.¹⁰

Therapeutic approaches and procedures

Surgery

An accurate tumor diagnosis requires surgery. With current stereotactic procedures, tissue samples should be obtainable

from any location in the brain with few exceptions. In most cases, a surgical resection should be considered and recommended: there is a possible sampling error when only biopsy is performed, and the improvement of symptoms is related to the mass effect of the tumor.

For high-grade glioma, the extent of tumor resection and survival are related, favoring any degree of resection beyond biopsy.

The major objective of brain tumor surgery is to resect and potentially cure the tumor.

There are several reasons for performing a resection of gliomas in adults whenever it is thought to be safe. First, resection (rather than stereotactic biopsy) provides the best opportunity to obtain an accurate diagnosis. Gliomas are notoriously heterogeneous, and therapy is guided by the most aggressive histologic type detected in the specimen. Studies have shown that more complete resections are more likely to provide a high-grade diagnosis¹¹ and to detect an oligodendroglial component in the tumor.¹² Second, resection relieves symptoms from the mass effect in many patients, and more extensive resections are associated with greater chances of neurologic improvement; however, it may happen that neurological impairment can derive from a large resection. Third, response to postoperative radiation therapy is more favorable and deterioration during treatment is less likely after resection.¹³ Finally, it is likely that resection has a modest survival benefit through cytoreduction. Only one randomized trial of resection of malignant gliomas has been published; survival was approximately twice as long with resection.¹⁴ Many retrospective studies of both low-grade¹⁵ and high-grade glioma¹⁶ have shown longer survival with resection, after adjustment for age, performance score, tumor histologic type, and other prognostic factors. Although selection bias accounts for some of the difference in survival, most surgeons believe that resection is beneficial, especially in patients who have a mass effect at presentation.

For deeply situated intrinsic tumors, or for diffuse non-focal tumors, resection is not practical. In these situations, needle biopsy is used for diagnosis. Open biopsy is reserved for unusual situations, such as a lesion abutting a large blood vessel or the brainstem; such lesions are often simply resected. Although tissue can be obtained through a needle directed by hand through a burr hole under ultrasonographic, CT, or MRI guidance, nothing is as simple or as accurate as CT- or MRI-directed stereotactic biopsy.

Radiotherapy

Most common brain tumors, such as low-grade and malignant astrocytomas, are infiltrative into surrounding normal brain tissue, many centimeters from the

primary lesion. Radiation treatment volumes for these tumors generally include the enhancing volume (which contains solid tumor tissue), surrounding edema (which comprises normal brain infiltrated by microscopic tumor), and a margin of normal brain. Thus, even with the use of very conformal techniques, a substantial amount of 'normal' brain is included in the full-dose volume. The tolerance of normal brain (and spinal cord in the case of cord tumors) is a major limiting factor in achieving local control and cure.

The tolerance of the brain depends on the size of the dose per fraction, total dose given, overall treatment time, volume of brain irradiated, host factors, and adjunctive therapies. The probability of injury increases with larger daily doses (2.2 Gy/fraction), and doses in excess of 60 Gy are delivered in 30 fractions over approximately 6 weeks.

Approximately 4–9% of patients treated with 50–60 Gy using conventional fractionated radiation for brain tumors develop clinically detectable focal radiation necrosis, but this form of injury may be found in as many as 10–22% of patients at autopsy.

The appropriate volume to encompass within the radiation treatment portal varies with the specific histopathologic tumor type, and, with certain histologies, is controversial. Benign tumors typically do not infiltrate beyond the lesional borders seen by MRI. Certain tumors, such as benign meningiomas, pituitary adenomas, cranio-pharyngiomas, and acoustic neuromas, may be treated with narrow margins of surrounding normal tissue. In contrast, the astrocytic gliomas require larger margins because of their tendency to infiltrate beyond the imaged tumor border.

The across-target volume is defined as a three-dimensional reconstruction of the tumor contour based on operative findings and data from CT and MRI studies. The planning target volume consists of the volume of tissue that must be irradiated to encompass the tumor volume, with a margin of surrounding tissue considered to be at risk for microscopic tumor spread and to account for patient movement and daily set-up uncertainties. Three-dimensional conformal radiation therapy and the advanced technique of intensity-modulated radiation therapy are new methods of treatment planning and delivery designed to enhance conformation of the dose to the target volume, while maximally restricting the dose delivered to the normal tissue outside the treatment volume.

Radiosurgery is a method of highly focal, closed-skull external irradiation that uses an imaging-compatible stereotactic device for precise target localization. It is being used to treat other intracranial lesions, including small arteriovenous malformations, pituitary adenomas, acoustic neuromas, meningiomas, gliomas, and brain metastases. The relationship between the stereotactic coordinate system and the radiation source(s) allows accurate delivery

of radiation to the target volume. Radiosurgery can be administered by γ knife units, made up of multiple cobalt beams, and by modified linear accelerators. This technique is designed to give a high radiation dose to an intracranial target in a single session without delivering significant radiation to adjacent normal tissues. Stereotactic radiotherapy may be delivered in a fractionated dose schedule using stereotactic radiosurgery hardware and software and head frames that can be relocalized daily in a reproducible fashion.

Temozolomide is a novel oral alkylating agent with known activity in patients with malignant gliomas. A pilot phase II trial demonstrated the feasibility of the concomitant administration of temozolomide with fractionated radiotherapy, followed by up to six cycles of adjuvant temozolomide, and suggested that this treatment had promising clinical activity (2-year survival rate 31%).¹⁷

The European Organization for Research and Treatment of Cancer (EORTC) Brain Tumor and Radiotherapy Groups and the National Cancer Institute of Canada (NCIC) Clinical Trials Group therefore initiated a randomized, multicenter, phase III trial to compare radiotherapy plus continuous daily temozolomide (followed by six cycles of adjuvant temozolomide) with radiotherapy alone in patients with newly diagnosed GBM. A total of 573 patients from 85 centers underwent randomization. At a median follow-up of 28 months, the median survival was 14.6 months with radiotherapy plus temozolomide and 12.1 months with radiotherapy alone. The 2-year survival rate was 26.5% with radiotherapy plus temozolomide and 10.4% with radiotherapy alone. The addition of temozolomide to radiotherapy for newly diagnosed glioblastoma resulted, therefore, in a clinically meaningful and statistically significant survival benefit with minimal additional toxicity.¹⁸

Another way to increase the radiation dose is with interstitial brachytherapy. Iodine-125 and iridium-192 sources have been used in clinical practice in well-circumscribed, peripheral, solitary supratentorial lesions of limited volume. Early phase II studies showed promising survival in patients with glioblastoma multiforme treated with external irradiation combined with brachytherapy. However, two randomized trials did not succeed in demonstrating any statistically significant results in terms of survival, comparing the use of interstitial implantation (60 Gy at 10 Gy/day) preceding external irradiation (60.2 Gy at 1.72 Gy/fraction) and BCNU (carmustine) versus external irradiation and BCNU alone.^{19,20} Thus, despite the survival advantage suggested in early trials, these randomized trials do not support the use of brachytherapy to treat newly diagnosed glioblastoma. Brachytherapy has also been suggested to improve the survival and quality of life of patients with recurrent malignant gliomas who meet criteria for implantation.²¹ The use of less invasive highly conformal radiation

techniques (i.e. radiosurgery) appears to provide results equivalent to those of brachytherapy in patients with recurrent gliomas, and this has become the radiation treatment of choice for patients with small recurrences.²²

Chemotherapy

Although there have been advances in intraoperative imaging and other neurosurgical techniques, many tumors still remain only partially resectable or non-resectable because of their location in important areas of the brain (i.e. brainstem, base of the skull), or because of their highly infiltrative nature (glial tumors), or their tendency to disseminate along CSF pathways (embryonal tumors). Although most CNS tumors are partially responsive to radiotherapy, neural tissue toxicity usually prevents the administration of curative doses of radiation. Thus, there is a significant need for additional treatment modalities.

Chemotherapy offers the theoretical advantage of reaching all tumor cells, regardless of their gross or microanatomic location within the CNS, because all tumor cells must be within the perfusion zone of pre-existing or tumor-associated microvasculature. Furthermore, many chemotherapeutic agents have minimum neurotoxic effects, so toxicity concerns are largely confined to systemic toxicity. Finally, because the vast majority of normal cells within the CNS are postmitotic, chemotherapeutic agents that are preferentially toxic to dividing cells should have a high therapeutic index within the CNS. Despite these theoretical arguments, the fact is that chemotherapy is used as primary therapy for few types of CNS tumor (i.e. primary CNS lymphoma), is at most an adjunct to surgery and radiation for some CNS tumors, and is totally ineffective for others.

There are several reasons for the largely disappointing results of chemotherapy. As with systemic tumors, intrinsic and acquired drug resistance at doses attainable with acceptable systemic toxicity remains a primary reason for chemotherapy failure. The challenges for successful use of chemotherapy for CNS tumors, however, are even greater than they are for systemic tumors. Central to this difference is the issue of drug delivery. The CNS is protected from toxic substances in the blood by the blood–brain barrier (BBB).

Ever since the blush of dye extravasation was first seen in tumors on cerebral angiography, it was appreciated that the blood–tumor barrier (BTB) was different from the BBB. The microvascular differences between the BTB and the normal BBB range from a subtle increase in endothelial fenestrations to a dramatic breakdown of tight junctions, enlargement of the perivascular space, and swelling of the basal lamina.^{23,24} Different tumors display different degrees of disruption of the BTB. For example,

most low-grade gliomas do not have contrast enhancement on CT or MRI scans and have BTBs that are quite similar to the normal BBB. In contrast, highly malignant tumors such as glioblastoma may have nearly total disruption of most barrier functions within the avidly contrast-enhancing portion of the tumor. Even in these tumors, however, drug delivery is not normal, because the tumor-induced neovasculature is often poorly perfused or not patent, and there is a relatively long distance between tumor-induced angiogenic vessels and individual tumor cells. Furthermore, even in these highly malignant and angiogenic tumors, the leading front of infiltrating tumor cells is located in normal brain parenchyma with a relatively intact BBB. The limited access of most chemotherapeutic drugs to the tumor decreases the chance that cytotoxic concentrations of the drug will be delivered to all or even most of the infiltrating tumor cells, and results in tumor cell exposure to sublethal concentrations of the drug, which increases the chances of acquired drug resistance.

Physicochemical characteristics largely determine a drug's ability to cross the BBB. Smaller, ionically neutral, lipophilic drugs, with a high octanol/water coefficient, are more likely to penetrate the BBB and BTB.²⁵ Unfortunately, most drugs lack these characteristics and are excluded by the barrier. For this reason, and because only a tiny portion of any systemically delivered drug finds its way into a relatively small tumor regardless of permeability issues, there are significant problems both in obtaining homogeneous, pharmacologically active concentrations of drugs throughout a brain tumor and in limiting systemic toxicity. This has led to the development of alternative drug administration techniques that either disrupt the BBB and BTB or deliver drugs directly to the region. One way to do this is the surgical placement of biodegradable synthetic polymers impregnated with a drug. The prototype implantable polymer is the Gliadel® wafer, which contains BCNU.²⁶ After surgical debulking of a malignant glioma, the surgeon lines the surgical cavity with Gliadel wafers that are left in place. Over the next several weeks the BCNU diffuses out of the wafers into the surrounding brain, providing very high local concentrations of BCNU with little systemic exposure to the drug. Although theoretically attractive, this approach has pharmacologic constraints. BCNU is highly lipid soluble and crosses the BBB readily in both directions. BCNU that diffuses out of the polymer therefore passes into the local bloodstream, where the BCNU concentration is low. This carries the drug away from the brain, a phenomenon known as the *sink effect*. Another limitation is that drug penetrates the surrounding brain only by passive diffusion, a slow and inefficient process. High concentrations of BCNU are thus found only within a few millimeters of the wafers, which makes it unlikely that cytotoxic drug concentrations will reach distant infiltrating tumor cells.²⁷

Despite the large number of trials of chemotherapy for glioma conducted in the past 30 years, relatively little can be said about the proven benefit of individual agents or even of chemotherapy in general because of discrepancies and inconsistencies in clinical trial design, interpretation, and reporting.

Although there is growing consensus on the benefit of adjuvant chemotherapy for high-grade astrocytomas at diagnosis, the evidence favoring chemotherapy use in the recurrent setting is much less compelling. To date there is no convincing demonstration of a survival benefit for patients with recurrent astrocytomas treated with chemotherapy, although few controlled trials have examined the question.

Clearly, the agent with the most proven activity against recurrent astrocytomas is temozolomide, an orally administered, second-generation imidazotetrazine pro-drug with excellent bioavailability; wide tissue distribution, including the ability to cross the BBB; and alkylating activity principally at the O⁶ position of guanine.²⁸ After phase I trials revealed activity in glioma patients, a pivotal open-label multicenter phase II trial of temozolomide in patients with anaplastic gliomas at first relapse was conducted.²⁹ There were 97 evaluable patients with anaplastic astrocytoma and 14 patients with anaplastic oligoastrocytoma. The overall objective radiographic response rate was 35% (8% complete response and 27% partial response); 26% had stable disease. Unfortunately, median progression-free survival was relatively short (5.4 months), and 12-month progression-free survival was only 12%. A parallel trial accrued 225 patients with glioblastoma at first relapse to a multicenter randomized phase II trial of temozolomide versus procarbazine.³⁰ Patients treated with temozolomide had statistically significantly longer median progression-free survival than patients treated with procarbazine (12.4 vs. 8.3 weeks; $p < 0.006$). Radiographic response rates were disappointing: 5.4% in temozolomide-treated patients and 5.3% in procarbazine-treated patients.

A new standard of care for patients with newly diagnosed glioblastoma may be now on the horizon. Stupp and co-workers treated 64 patients with newly diagnosed glioblastoma in a phase II trial of low-dose temozolomide (75 mg/m²/day for 7 days) given during conventional fractionated radiotherapy, followed by six cycles of standard-dose temozolomide (200 mg/m²/day for 5 days every 28 days) after radiotherapy.¹⁷ Treatment was well tolerated, and the median survival of the group was an impressive 16 months, with 1- and 2-year survival rates of 58% and 31%, respectively. An EORTC randomized trial is currently comparing this treatment regimen to radiation alone. If the promising findings of the phase II study are confirmed by this trial, then low-dose temozolomide during radiotherapy followed by standard-dose adjuvant temozolomide will become the new standard of care

for glioblastoma. However, alkylating agents such as temozolomide are highly reactive molecules that cause cell death by binding to DNA. The most frequent site of alkylation in DNA is the O⁶ position of guanine. Alkylation here forms cross-links between adjacent strands of DNA, which explains how the nitrosoureas, tetrazines, and procarbazine kill cells. The cross-linking of double-stranded DNA by alkylating agents is inhibited by the cellular DNA-repair protein O⁶-methylguanine-DNA methyltransferase: the DNA-repair enzyme O⁶-methylguanine-DNA methyltransferase (MGMT) inhibits the killing of tumor cells by alkylating agents. MGMT activity is controlled by a promoter; methylation of the promoter silences the gene in cancer, and the cells no longer produce MGMT. Esteller et al. examined gliomas to determine whether methylation of the MGMT promoter is related to the responsiveness of the tumor to alkylating agents. They analyzed the MGMT promoter in tumor DNA by a methylation-specific polymerase chain reaction assay. The molecular data were correlated with the clinical outcome. They found that MGMT promoter was methylated in gliomas from 19 of 47 patients (40%). This finding was associated with regression of the tumor and prolonged overall and disease-free survival. It was an independent and stronger prognostic factor than age, stage, tumor grade, or performance status. In this paper they concluded that methylation of the MGMT promoter in gliomas is a useful predictor of the responsiveness of the tumors to alkylating agents.³¹

Radioimmunotherapy

Despite the modest benefits afforded by radiation therapy and alkylating agent chemotherapy, it is clear that more effective treatments are desperately needed.

Monoclonal antibodies (mAb) against tumor-associated antigens can be used therapeutically as delivery systems for chemotherapeutic agents, toxins, and radionuclides. In particular, the utility of mAb (molecular weight 150 kDa) for targeting radioactive agents to tumor cells, for diagnostic (radioimmunoscinigraphy and radioimmunoguided surgery) and therapeutic purpose (radioimmunotherapy, RIT), has been extensively studied.³²⁻³⁵

Because of its potential for more selectively irradiating tumor cells than conventional radiotherapy, radioimmunotherapy is an attractive strategy for brain tumors. Its antitumor effect is primarily due to the associated radioactivity of the radiolabeled antibody, which emits continuous slowing-down, low dose-rate irradiation.^{36,37} One of the main therapeutic advantages of radiolabeled mAb is their potential to overcome the problem of tumor heterogeneity. Because the radionuclides can penetrate up to several millimeters of tissue, radioemission can kill

Table 25.3 Isotope characteristics

Isotope	$t_{1/2}$ (days)	$E_{\max\beta}$ (MeV)	R_{\max} (mm)	E_{γ} (keV)
^{131}I	8.0	0.81	3.3	360 (81%)–630 (7%)
^{90}Y	2.7	2.27	11.9	—
^{177}Lu	6.7	0.50	2.2	113 (6%)–208 (11%)

$t_{1/2}$, half-life; $E_{\max\beta}$, maximum energy of β particles;
 R_{\max} , maximum range; E_{γ} , γ energy.

those antigen-negative tumor cells which have no specific radiolabeled antibody localized on their surface (crossfire effect).

The range of radioisotopes available for the production of radiolabeled compounds is ever increasing. Although damaging DNA represents the main mechanism for killing tumor cells, the choice of suitable radioisotopes needs appropriate consideration in order to match their decay properties with the characteristics of the tumor (Table 25.3).

Among the radionuclides used in clinical practice, ^{90}Y has physical and radiobiological features suitable for the RIT approach, due to its high-energy β^- particles (maximum energy 2.27 MeV). Moreover, ^{90}Y penetration (maximum particle range in tissue 12 mm, range in tissue after which 50% of particles are stopped 4 mm) allows high radiation doses to the target area, while sparing surrounding tissues and normal organs and maximizing the tumor to non-tumor dose ratio.

Besides, the radiochemistry procedures apt to conjugate an antibody with a radioisotope can be varied according to different chemical reactions: several isotopes, in particular ^{131}I and ^{125}I , can be directly conjugated to the antibodies. In contrast, the use of radiometals such as ^{90}Y , ^{177}Lu , and ^{186}Re requires more complex reactions, involving first the binding of a chelator with the antibody and subsequently conjugation with the isotope.^{38,39} The attractive feature of RIT is the prospect that most normal tissues are spared from a high radiation burden. Unfortunately, RIT has thus far failed to fulfill this expectation mainly because only a very small amount of tagged mAb localizes per gram of tumor (<0.001%), while the remainder stays in the circulation conjugated to the radioisotope with toxic effects on tissues, especially bone marrow.⁴⁰

Tumor pre-targeting

One of the limitations of directly labeled antibodies for targeted radiotherapy is that, as a consequence of their

macromolecular size, they diffuse slowly through tissue, hampering their delivery to tumor cells distant from their site of injection. In an attempt to overcome this problem and the low uptake of radiolabeled mAb by the tumor, various studies have examined the concept of tumor pre-targeting, consisting of the administration of a modified mAb (first conjugate) that permits a second component (second conjugate) to bind specifically to it.⁴¹ Conceptually, the modified mAb is administered first and allowed to distribute throughout the body, to bind to the cells expressing antigen, and to clear substantially from other tissues. Then the radiolabeled second component is administered and, ideally, it localizes at sites where the modified mAb has accumulated. If the second component has higher permeation, clearance, and diffusion rates than those of the mAb, more rapid radionuclide localization to the tumor and higher tumor selectivity are possible, thus achieving a higher tumor to non-tumor ratio.⁴²

The avidin–biotin model

One of the most clinically used pre-targeting techniques is the avidin–biotin system (Figure 25.1). This pre-targeting approach takes advantage of the extremely high affinity between avidin and biotin. Avidin (molecular weight 66 kDa) is a small oligomeric protein made up of four identical subunits, each bearing a single binding site for biotin (vitamin H, molecular weight 244 Da). They can therefore bind up to four moles of biotin per mole of protein. The affinity of avidin for biotin is extremely high, with a dissociation constant of the avidin–biotin complex in the order of 10^{-15} mol/l. For practical purposes, their binding can be regarded as irreversible.^{43,44} Briefly, pre-targeted antibody-guided radioimmunotherapy (PAGRIT®) is based on intravenous or locoregional sequential administration of a specific biotinylated antibody, avidin, and radioactive biotin (^{90}Y -biotin).⁴⁵ The first clinical experience with the avidin–biotin pre-targeting system in cancer therapy was performed almost a decade ago at the European Institute of Oncology in Milan, in patients affected by recurrent high-grade glioma (HGG).⁴⁶

Clinical applications

Theoretically, the radioimmunotherapy approach could be exploited in all those tumors for which a specific monoclonal antibody is available to target its specific antigen.

However, malignant gliomas represent the most favorable model since they are refractory to conventional treatments, and a suitable marker, the glycoprotein tenascin-C, is overexpressed in the extracellular matrix of gliomas, but not in normal cerebral tissues⁴⁷ (Figure 25.2). The level

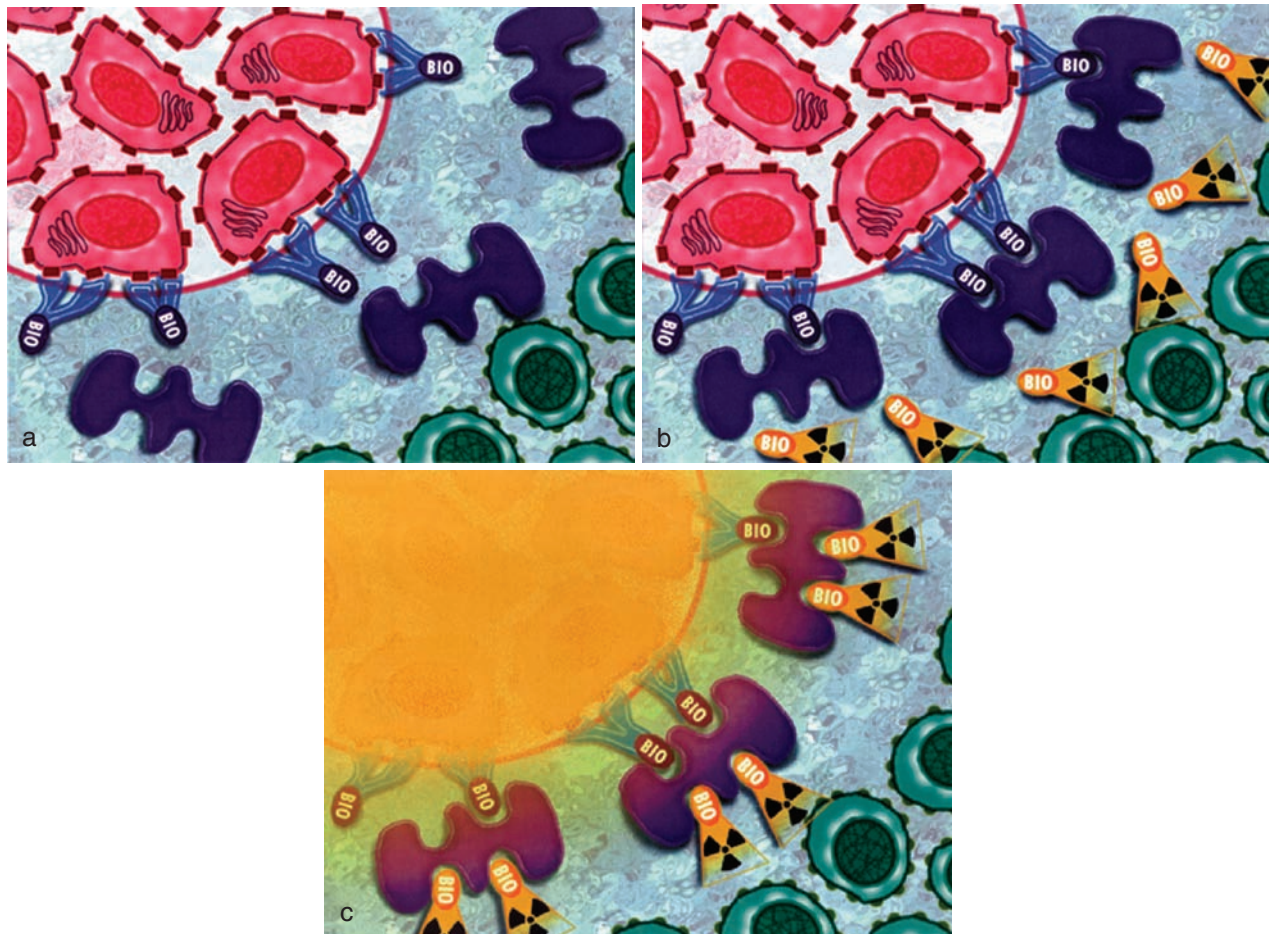


Figure 25.1

Three-step radioimmunotherapy: (a) binding of biotinylated monoclonal antibodies to the antigen tenascin; (b) binding of avidin to biotinylated monoclonal antibodies; (c) binding of radioactive biotin to avidin.

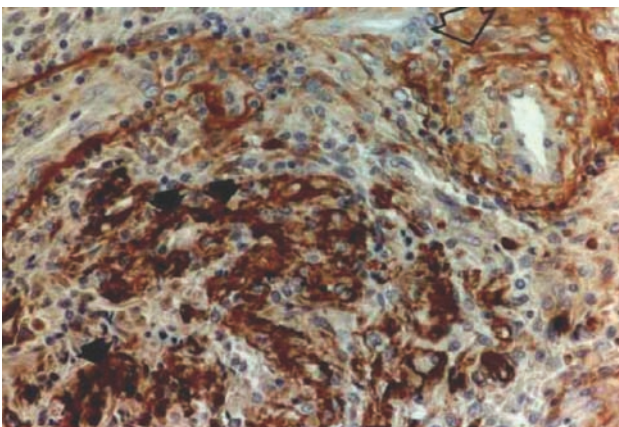


Figure 25.2

Example of immunohistochemistry for tenascin.

of tenascin expression increases with tumor grade.⁴⁸ Important for its role as a target for radioimmunotherapy is the fact that more than 90% of glioblastomas exhibit high levels of tenascin expression.⁴⁹ In addition, tenascin is located primarily around tumor blood vessels, with this feature becoming more predominant with advancing tumor grade.⁵⁰

The hope of therapy for brain tumors and, in particular, for high-grade gliomas lies in the potential to extend functional life-span with little additional, and possibly reduced, morbidity, as compared with current aggressive treatment modalities. In fact, protocols including aggressive combined therapies, such as surgical debulking, external beam radiotherapy, and chemotherapy, usually provide time-limited results, and local recurrence is a common event, occurring within a few months. Surgical resection could potentially represent the only curative option, but, in clinical practice, it is impossible to remove

the microscopic tumor foci, which constantly spread into the brain adjacent tissue (BAT) giving rise to recurrence. The efficacy of conventional external radiotherapy has been demonstrated, but no more than 60 Gy can be delivered, due to unacceptable risks of neurological toxicity.

Radioimmunotherapy, as systemic or locoregional application, has the potential to become a well-tolerated therapeutic option in the management of HGG, complementing traditional regimens.

Systemic PAGRIT® in high-grade glioma

In a phase I–II study the toxicity and therapeutic efficacy of the avidin–biotin pre-targeting approach in a group of 48 eligible patients were evaluated. All patients had histologically confirmed grade III or IV glioma and documented residual disease or recurrence after conventional treatment.⁴⁶ Three-step radioimmunotherapy was performed by intravenous administration of biotinylated anti-tenascin monoclonal antibody (BC2 and BC4 epitopes), followed 36 hours later by avidin and streptavidin (a non-glycosylated analog of avidin), and 18–24 hours later by ⁹⁰Y labeled biotin. The injected activity, calculated on the basis of previous studies and dosimetry calculation, ranged from 2.22 to 2.97 GBq/m² per cycle. Three major conclusions emerged from this study. First, three-step radionuclide therapy with high-dose ⁹⁰Y produced acceptable toxicity at the dose of 2.22 GBq/m² due to the extremely favorable biodistribution of ⁹⁰Y-DOTA-biotin (where DOTA is tetraazacyclododecanetetraacetic acid) with the majority of the non-tumor-bound activity eliminated in the first 24 hours. MTD was determined at the level of 2.96 GBq/m². Second, an objective therapeutic response was documented in an encouraging fraction of our patients, who were no longer responsive to conventional treatments: 52% did not progress any further (the majority suspended steroid consumption, had a reduction in epileptic seizure rate and an improved quality of life), while significant tumor reduction occurred in 25%. Third, immune response to the murine monoclonal antibody, known to interfere with localization in subsequent administrations, was less frequent than in patients treated with the directly labeled mAb used in other studies, possibly because of its shorter residence time in the circulation with our procedure.

The encouraging results obtained in this phase I–II study prompted us to apply the same approach in an adjuvant setting, to evaluate: (1) the time to relapse and (2) the overall survival.⁵¹ We studied 37 high-grade glioma patients, 17 with grade III glioma and 20 with glioblastoma, in a controlled, open, non-randomized study. All patients received surgery and radiotherapy and were disease-free by neuroradiological examination. Nineteen patients (treated)

received adjuvant treatment with radioimmunotherapy. In the treated glioblastoma patients, the median disease-free interval was 28 months (range 9–59); median survival was 33.5 months and one patient is still without evidence of disease. All 12 control glioblastoma patients (non-treated) died after a median survival from diagnosis of 8 months. In the treated grade III glioma patients, the median disease-free interval was 56 months (range 15–60) and survival cannot be calculated as only two, within this group, died.

A number of points arose from the results of this second study. First, three-step radioimmunotherapy was confirmed as highly active against malignant glioma, yet did not cause major adverse events, as previously described. Second, the effect of RIT on glioblastoma was interesting: it considerably prolonged the disease-free interval and overall survival relative to the untreated group.

Locoregional PAGRIT® in high-grade glioma

The principal advantages of a locally delivered compound (chemotherapeutic agent or radiopharmaceutical) consist mainly of bypassing the blood–brain barrier, minimizing systemic toxicity, and achieving prolonged local drug concentration.

Several studies demonstrated that the locoregional (LR) infusion of ¹³¹I- or ⁹⁰Y-labeled anti-tenascin mAb in glioma patients provided a favorable safety profile and the possibility to control the growth of the tumor in the long-term.^{52,53} Riva et al.⁵⁴ evaluated the efficacy of ¹³¹I-labeled and ⁹⁰Y-labeled BC2 and BC4 moAb for the locoregional treatment of malignant gliomas. The phase 2 study with ¹³¹I involved 91 patients, including 74 with GBM and nine with anaplastic astrocytoma (AA). The study population consisted of 47 newly diagnosed and 44 recurrent tumors. Patients received 3–10 cycles of ¹³¹I-labeled moAb, at intervals of either 1 or 3 months, with a cumulative administered activity of up to 20.35 GBq (550 mCi). The median survival was >46 months in AA and 19 months in GBM, with no distinction between newly diagnosed and recurrent patient groups. The response rate was better in those with small volume (56.7%) compared with larger tumors. A subsequent study was performed using ⁹⁰Y in order to investigate the potential effects of a radionuclide emitting β particles with greater tissue penetration. Patients received between three and five cycles of ⁹⁰Y-labeled moAb with a cumulative activity of 3.145 GBq (85 mCi). The median survival for patients with AA and GBM was 90 months and 20 months, respectively.

In a more recent study, the therapeutic potential of ¹³¹I- and ⁹⁰Y-labeled BC4 moAb was evaluated in 37 patients, consisting of 13 with AA and 24 with GBM.⁵⁵ Multiple cycles of labeled moAb were administered (mean, three per patient) at various activity levels. The median

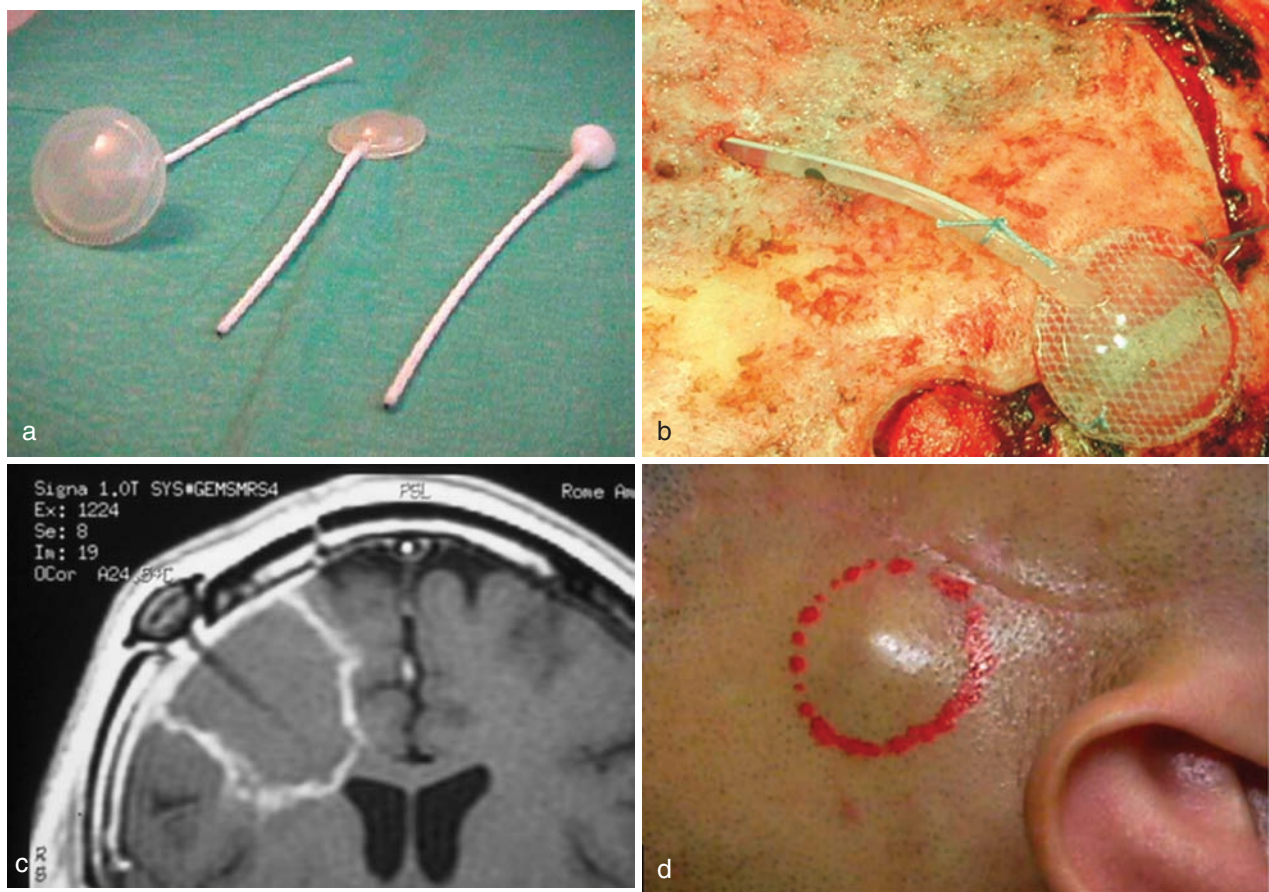


Figure 25.3

Different models of reservoirs connected with catheter (a) and placed into the surgical cavity (b). The subcutaneous reservoir is well tolerated by the patient (c). In locoregional radioimmunotherapy, all reagents are injected through the reservoir (d).

survival for GBM was 17 months. No attempt was made to stratify analyses according to the radionuclide used or whether the patients had recurrent or newly diagnosed lesions.

The three-step pre-targeting approach, described above and applied in a systemic fashion, has also been validated in the locoregional treatment of glioma. In a phase I–II study we investigated the safety profile and antitumor efficacy of the three-step method, employing [^{90}Y]biotin in the locoregional therapy of recurrent high-grade glioma.⁵⁶ Twenty-four patients with recurrent glioma (eight anaplastic astrocytoma and 16 GBM) underwent second surgical debulking with implantation of an indwelling catheter (connected with a subcutaneous reservoir) (Figure 25.3) into the surgical cavity in order to receive the radioimmunotherapeutic agent.

Biotinylated anti-tenascin mAb (BC2 or BC4), avidin, and, finally, ^{90}Y -biotin were subsequently injected through

the catheter. Each patient received two of these treatments 8–10 weeks apart, and the injected activity ranged from 0.5 to 1.1 GBq. Dosage was escalated by 0.2 GBq in four consecutive groups. Bremsstrahlung images were acquired to confirm the correct localization of the ^{90}Y -biotin (Figure 25.4). The treatment was well tolerated without acute side-effects up to 0.7 GBq. The maximum tolerated activity was 1.1 GBq, limited by neurologic toxicity. None of the patients developed hematological toxicity. In three patients infection occurred around the catheter, and was promptly treated. The average absorbed dose to the normal brain was minimal compared with that received at the surgical resection cavity interface.

This study assessed that with activity ranging from 0.7 to 0.9 GBq per cycle, three-step locoregional radioimmunotherapy was safe, and produced an objective response (partial and stable disease in 75% of patients).

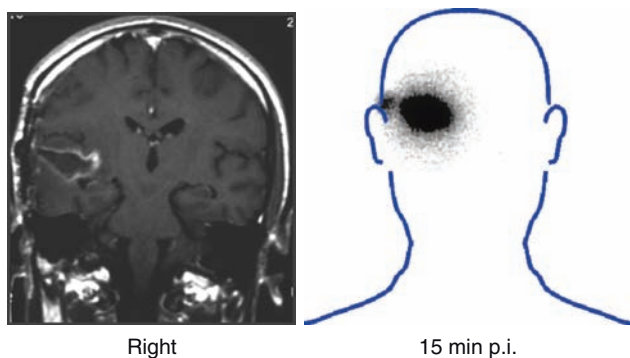


Figure 25.4

Pre-targeted antibody-guided radioimmunotherapy (PAGRIT®) biodistribution: after locoregional injection of reagents. p.i., post-injection.

Multimodal approach: locoregional PAGRIT® in association with chemotherapy

From the beginning of 1999, in our department, temozolomide (TMZ) was proposed in association with LR RIT to the newly enrolled patients. In our opinion, the basis for combining LR RIT and TMZ includes toxicity independence (the two treatments have different toxicity profiles) and the possibility to eliminate microscopic disease outside the radiation LR RIT field with TMZ. This hypothesis is supported by a retrospective analysis performed in a group of 73 patients with histologically proven recurrent GBM and immunohistochemical demonstration of tenascin expression in the tumor.⁵⁷ All patients had a catheter implanted at second surgery and underwent at least two cycles of locoregional radioimmunotherapy (range 2–7) with 2 month's interval. Thirty-five out of 73 patients were also treated with oral chemotherapy (TMZ). Two cycles of TMZ (200 mg/m²/day, for 5/28 days) were administered between each course of LR RIT.

Radiological objective response occurred in nine patients (3 partial response, 6 minor response). In a large number of patients (63%) a stabilization of disease was obtained.

In the 38 patients treated with LR RIT alone, median overall survival and progression-free survival were respectively 17.5 months (95% confidence interval (CI) 17–20) and 5 months (95% CI 4–8), while in the 35 treated with the combined treatment (LR RIT + TMZ) respective values were 25 months (95% CI 23–30) and 10 months (95% CI 9–18, $p < 0.01$). The addition of TMZ to LR RIT did not increase neurological toxicity, and no major hematological toxicity was observed.

This study confirmed the efficacy and safety of locoregional radioimmunotherapy in recurrent glioblastoma patients, with a significant increase in survival compared

to that obtained with surgery and external radiotherapy alone. In particular, this study shows that this improvement in survival can be further increased by the multimodal approach of combining LR RIT with TMZ.

More recently, our group has assessed another multimodal therapeutic strategy in cooperation with the Neuro-Oncology Department of the National Neurological Institute 'C Besta' in Milan.⁵⁸ Twenty-six recurrent GBM patients sequentially treated at the 'C Besta' Institute were enrolled for a second surgery in order to remove recurrent tumor and to place the indwelling catheter into the surgical cavity, to allow local delivery of chemotherapy and pre-targeted RIT. All patients had partial tumor resection and 75% of them had a residual tumor mass after excision larger than 2 cm. After surgery all patients were managed with second-line systemic chemotherapy (PCV; procarbazine, CCNU, vincristine). Moreover, the protocol scheduled two cycles of locoregional RIT, according to the 'three-step' method, with an activity ranging from 0.2 to 1.0 GBq (depending on the cavity volume), with a 10-week interval. Mitoxantrone chemotherapy was also locally delivered as a single dose of 4 mg every 20 days. Responses to treatment were assessed by monthly neurological examination and by MRI or contrast-enhanced CT scan performed every 2 months. For the whole group of patients the progression-free survival after second surgery at 6 and 12 months was 61% and 22%, respectively, and survival after recurrence at 6, 12, and 18 months was 80%, 53%, and 42%, respectively. Major side-effects occurred neither systemically nor related to the site of local injections. The percentage of long-term survivors was very high: 42% of patients were still alive at 18 months.

Radiation dosimetry evaluation

The challenge for internal therapy is to deliver the highest possible dose to the tumor while sparing normal organs from damage. Response and toxicity prediction are essential to the rational implementation of cancer therapy.

The appropriate term for the quantity of interest in dosimetry, however, is absorbed dose (D), expressed in units of Gray. This is defined as the energy (E) absorbed in a particular mass of tissue, divided by the tissue mass (M):

$$D = \frac{E}{M}$$

In particular, in radionuclide therapy: E = number of radionuclide disintegrations in a particular volume × energy emitted per disintegration of the radionuclide × fraction of emitted energy that is absorbed by a particular (target) mass.

The biologic effects of radionuclide therapy are mediated via the absorbed dose.

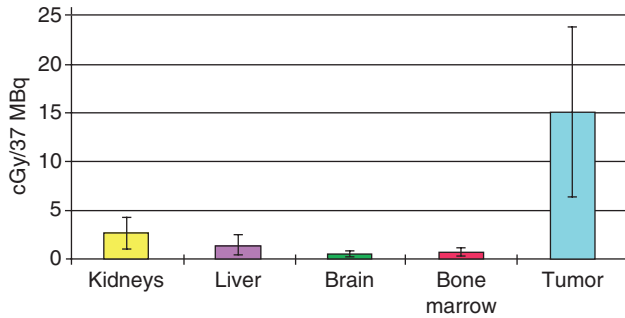


Figure 25.5

Absorbed dose (cGy/37 MBq) in critical organs and in tumor. Mean values are calculated in 12 patients. Note higher uptake in tumor compared with non-targeted organs. Reproduced from *European Journal of Nuclear Medicine*, 1999, 26(4): 348–57, Antibody-guided three-step therapy for high grade glioma with yttrium-90 biotin, Paganelli G, Grana C, Chinol M, Cremonesi M, De Cicco C, De Braud F, Robertson C, Zurrida S, Casadio C, Soboli S, Siccardi AG, Veronesi U, Figure no. 2, © With kind permission of Springer Science and Business Media (reference 46).

Thus, an accurate dosimetry method that would provide reliable dose estimates to critical organs and to tumors before therapy would allow the clinician to plan a specific therapeutic regimen and also to select those patients who would benefit the most from treatment.

In radionuclide treatment, different from external beam radiotherapy, dosimetry is strongly time and space dependent. Radiopharmaceuticals may in fact show different distribution patterns.

The normal brain is the critical organ for external beam radiotherapy, as it is inevitably included in the field of treatment. In contrast, during radioimmunotherapy, the normal brain receives negligible doses. The mean absorbed dose in normal brain was 0.16 ± 0.08 mGy/MBq and 0.015 ± 0.005 mGy/MBq in systemic and in locoregional treatments, respectively.^{59,60}

Compared to systemic treatment,⁵⁹ local administration has been demonstrated to be advantageous in the minimization of systemic toxicity. The adsorbed dose to red marrow was 0.22 mGy/MBq in systemic treatment compared to 0.03 mGy/MBq in locoregional treatment.

In the systemic treatment, the biodistribution images showed rapid clearance of the radiocompound. The normal organs mainly involved in the biodistribution of the ⁹⁰Y-biotin were the liver (1.5 ± 1.0 cGy/37 MBq) and kidneys (2.7 ± 1.6 cGy/37 MBq); $65\% \pm 28\%$ of the injected activity was eliminated via the kidneys in the first 24 h after the treatment (Figure 25.5).

Scintigraphic images acquired up to 48 h after LR RIT with ⁹⁰Y-biotin showed the radiolabeled compound to be well localized within the injection site and minimal activity in the remainder of the body. Low ⁹⁰Y activities

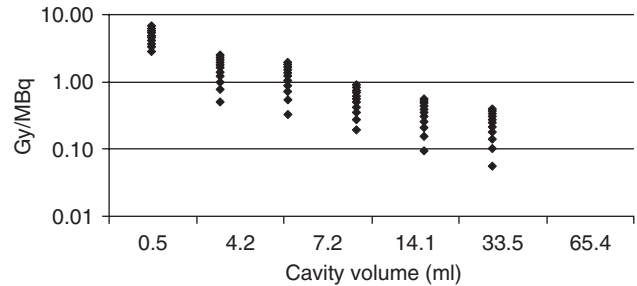


Figure 25.6

Mean dose to a cuff of tissue 6 mm thick around the cavity.

were found in the bloodstream. The activity in other normal organs was negligible in most cases, as confirmed by imaging.

After injection into the surgical resection cavity, the radiocompound diffuses into the brain adjacent tissue (BAT) to target the neoplastic cells scattered throughout this region, or remains localized in the cavity, depending on tumor cell distribution and on the amount of binding to the tumor cells.

Considering a cavity of 7.2 ml (radius 1.2 cm), the mean dose to a cuff of tissue 6 mm thick around the cavity (BAT) ranged from 130 to 1300 mGy/MBq, considering different degrees of binding to the cavity wall for ⁹⁰Y-biotin: from lack of binding (all the radiopharmaceutical remains uniformly distributed inside the cavity) to complete binding (all the radiopharmaceutical is bound to the cavity wall) (Figure 25.6).

The LR approach, whenever feasible, guarantees a higher irradiation of the tumor-resected cavity, while sparing normal brain.⁶⁰

Considerations and future directions

The combined modality approach to treating brain tumors was introduced about 30 years ago; it remains the most effective approach we have. The promise is that the combination of surgery, radiotherapy, chemotherapy, new targeted small molecules (as inhibitors of growth factor receptors), and RIT may provide, at last, a way of increasing life expectancy in high-grade glioma patients.

Acknowledgments

We thank Mrs Deborah Console for editing the manuscript.

References

- Davis FG, Preston-Martin S. Epidemiology. Incidence and survival. In: Bigner DD, McLendon RE, Bruner JM, eds. *Russell and Rubinstein's Pathology of Tumors of the Central Nervous System*. London: Arnold 1999; 5–46.
- Stewart LA. Chemotherapy in adult high-grade glioma: a systematic review and meta-analysis of individual patient data from 12 randomised trials. *Lancet* 2002; 359: 1011–18.
- Wong ET, Hess KR, Gleason MJ et al. Outcomes and factors in recurrent glioma patients enrolled onto phase II trials. *J Clin Oncol* 1999; 17: 2572–8.
- Greig NH, Ries LG, Yancik R, Rapoport SI. Increasing annual incidence of primary malignant brain tumors in the elderly. *J Natl Cancer Inst* 1990; 82: 1621–4.
- Maher EA, Furnari FB, Bachoo RM et al. Malignant glioma: genetics and biology of a grave matter. *Genes Dev* 2001; 15: 1311–33.
- Daumas-Duport C, Scheithauer BW, O'Fallon J, Kelly P. Grading of astrocytomas, a simple and reproducible method. *Cancer* 1988; 62: 2152–65.
- Kim TS, Halliday AL, Hedley-Whyte ET, Convery K. Correlates of survival and the Daumas-Duport grading system of astrocytomas. *J Neurosurg* 1991; 74: 27–37.
- Kleihues P, Louis DN, Scheithauer BW et al. The WHO classification of tumors of the nervous system. *J Neuropathol Exp Neurol* 2002; 61: 215–25.
- Berger MS, Leibel SA, Bruner JM. Primary central nervous system tumors of the supratentorial compartment. In: Levin VA, ed. *Cancer in the Nervous System*. New York: Churchill Livingstone, 1995.
- Shaw EG, Scheithauer BW, O'Fallon JR, Tazelaar HD, David DH. Oligodendrogliomas: the Mayo Clinic Experience. *J Neurosurg* 1992; 76: 428–34.
- Jackson RJ, Fuller GN, Abi-Said D et al. Limitations of stereotactic biopsy in the initial management of gliomas. *Neuro-oncol* 2001; 3: 193–200.
- Perry A, Jenkins RB, O'Fallon JR et al. Clinicopathologic study of 85 similarly treated patients with anaplastic astrocytic tumors. An analysis of DNA content (ploidy), cellular proliferation, and p53 expression. *Cancer* 1999; 86: 672–83.
- Barker FG 2nd, Chang SM, Larson DA et al. Age and radiation response in glioblastoma multiforme. *Neurosurgery* 2001; 49: 1288–98.
- Vuorinen V, Hinkka S, Farkkila M et al. Debulking or biopsy of malignant glioma in elderly people—a randomised study. *Acta Neurochir Wien* 2003; 145: 5–10.
- Keles GE, Lamborn KR, Berger MS. Low-grade hemispheric gliomas in adults: a critical review of extent of resection as a factor influencing outcome. *J Neurosurg* 2001; 95: 735–45.
- Hess KR. Extent of resection as a prognostic variable in the treatment of gliomas. *J Neurooncol* 1999; 42: 227–31.
- Stupp R, Dietrich PY, Ostermann Kraljevic S et al. Promising survival for patients with newly diagnosed glioblastoma multiforme treated with concomitant radiation plus temozolomide followed by adjuvant temozolomide. *J Clin Oncol* 2002; 20: 1375–82.
- Stupp R, Mason WP, van den Bent MJ et al. European Organisation for Research and Treatment of Cancer Brain Tumor and Radiotherapy Groups; National Cancer Institute of Canada Clinical Trials Group. Radiotherapy plus concomitant and adjuvant temozolomide for glioblastoma. *N Engl J Med* 2005; 352: 987–96.
- Selker RG, Shapiro WR, Burger P et al. The Brain Tumor Cooperative Group NIH Trial 87-01: a randomized comparison of surgery, external beam radiotherapy, and carmustine versus surgery, interstitial radiotherapy boost, external radiation therapy, and carmustine. *Neurosurgery* 2002; 51: 343–55.
- Laperriere NJ, Leung PM, McKenzie S et al. Randomized study of brachytherapy in the initial management of patients with malignant astrocytoma. *Int J Radiat Oncol Biol Phys* 1998; 41: 1005–111.
- Leibel SA, Gutin PH, Wara WM et al. Survival and quality of life after interstitial implantation of removable high-activity iodine-125 sources for the treatment of patients with recurrent malignant gliomas. *Int J Radiat Oncol Biol Phys* 1989; 17: 1129–39.
- Shrieve DC, Alexander E, Wen PY et al. Comparison of stereotactic radiosurgery and brachytherapy in the treatment of recurrent glioblastoma multiforme. *Neurosurgery* 1995; 36: 275–82.
- Groothuis DR. The blood–brain and blood–tumor barriers: a review of strategies for increasing drug delivery. *Neuro-oncol* 2000; 2: 45–59.
- Dropcho EJ, Rosenfeld SS, Vitek J, Guthrie BL, Morawetz RB. Phase II study of intracarotid or selective intracerebral infusion of cisplatin for treatment of recurrent anaplastic gliomas. *J Neurooncol* 1998; 36: 191–8.
- Greig NH, Yu QH, Utsuki T et al. Optimizing drugs for brain action. In: Kobiler D, ed. *Blood–Brain Barrier*. New York: Kluwer Academic/Plenum Publishers, 2001: 281–311.
- Brem H, Mahaley MS Jr, Grossman SA, Saltzman WM. Interstitial chemotherapy with drug polymer implants for the treatment of recurrent gliomas. *J Neurosurg* 1991; 74: 441–6.
- Strasser JF, Fung LK, Eller S, Grossman SA, Saltzman WM. Distribution of 1,3-bis(2-chloroethyl)-1-nitrosourea and tracers in the rabbit brain after interstitial delivery by biodegradable polymer implants. *J Pharmacol Exp Ther* 1995; 275: 1647–55.
- Clark AS, Deans B, Stevens MF et al. Antitumor imidazotetrazines: 32. Synthesis of novel imidazotetrazinones and related dicyclic heterocycles to probe the mode of action on the antitumor drug temozolomide. *J Med Chem* 1995; 38: 1493–504.
- Yung WK, Prados MD, Yaya-Tur R et al. Multicenter phase II trial of temozolomide in patients with anaplastic astrocytoma or anaplastic oligoastrocytoma at first relapse. *Temodal Brain Tumor Group*. *J Clin Oncol* 1999; 17: 2762–71.
- Yung WK, Albright RE, Olson J et al. A phase II study of temozolomide vs. procarbazine in patients with glioblastoma multiforme at first relapse. *Br J Cancer* 2000; 83: 588–93.
- Esteller M, Gargia-Foncillas J, Andion E et al. Inactivation of the DNA-repair gene MGMT and the clinical response of gliomas to alkylating agents. *N Engl J Med* 2000; 343: 1350–4.
- Epenetos AA, Munro AJ, Stewart S et al. Antibody-guided irradiation of advanced ovarian cancer with intraperitoneally

- administered radiolabelled monoclonal antibodies. *J Clin Oncol* 1987; 5: 1890–9.
33. Larson SM. Radiolabelled monoclonal anti-tumor antibodies and therapy. *J Nucl Med* 1985; 26: 538–45.
 34. Buraggi GL, Callegaro L, Mariani G et al. Imaging with ¹³¹I-labeled monoclonal antibodies to a high-molecular-weight melanoma-associated antigen in patients with melanoma: efficacy of whole immunoglobulin and its F(ab')₂ fragments. *Cancer Res* 1985; 45: 3378–87.
 35. Kim JA, Triozzi PL, Martin EW Jr. Radioimmunoguided surgery for colorectal cancer. *Oncology* 1993; 7: 55–64.
 36. Fazio F, Paganelli G. Antibody-guided scintigraphy: targeting of the 'magic bullet'. *Eur J Nucl Med* 1993; 20: 1138–40.
 37. Hazra DK, Britton KE, Lahiri VL et al. Immunotechnological trend in radioimmuno-targeting: from 'magic bullet' to 'smart bomb'. *Nucl Med Commun* 1995; 16: 66–75.
 38. Wessels BW, Rogus RD. Radionuclide selection and model absorbed dose calculations for radiolabeled tumor associated antibodies. *Med Phys* 1984; 11: 638–45.
 39. Chinol M, Hnatowich DJ. Generator-produced yttrium-90 for radioimmunotherapy. *J Nucl Med* 1987; 28: 1465–70.
 40. Goldenberg DM, Griffiths GL. Radioimmunotherapy of cancer: arming the missiles. *J Nucl Med* 1992; 33: 1110–12.
 41. Chetanneau A, Barbet J, Peltier P et al. Pretargeted imaging of colorectal cancer recurrences using an In-111-labelled bivalent hapten and a biospecific antibody conjugate. *Nucl Med Commun* 1994; 15: 972–80.
 42. Magnani P, Paganelli G, Modorati G et al. Quantitative comparison of direct antibody labeling and tumor pretargeting in uveal melanoma. *J Nucl Med* 1996; 37: 967–71.
 43. Wilchek M, Bayer EA. The avidin biotin complex in bioanalytical applications. *Anal Biochem* 1988; 171: 1–32.
 44. Paganelli G, Magnani P, Zito F et al. Three-step monoclonal antibody tumor targeting in carcinoembryonic antigen-positive patients. *Cancer Res* 1991; 51: 5960–6.
 45. Paganelli G, Chinol M, Grana C et al. Optimization of the three-step pretargeting approach for diagnosis and therapy in cancer patients. *J Nucl Med* 1995; 36: 225P (abstr).
 46. Paganelli G, Grana C, Chinol M et al. Antibody-guided three-step therapy for high grade glioma with yttrium-90 biotin. *Eur J Nucl Med* 1999; 26: 348–57.
 47. Zagzag D, Friedlander DR, Dosik J et al. Tenascin-C expression by angiogenic vessels in human astrocytomas and by human brain endothelial cells in vitro. *Cancer Res* 1996; 56: 182–9.
 48. Leins A, Riva P, Lindstedt R et al. Expression of tenascin-C in various human brain tumors and its relevance for survival in patients with astrocytoma. *Cancer* 2003; 98: 2430–9.
 49. Wilkstrand CJ, Zalutsky MR, Bigner DD. Therapy of brain tumors with radiolabeled antibodies. In: Liau LM, Becker DP, Cloughsey TE, Bigner DD, eds. *Brain Tumor Immunotherapy*. Totowa, NJ: Humana Press, 2001: 205–29.
 50. Herold-Mende C, Mueller MM, Bonsanto MM et al. Clinical impact and functional aspects of tenascin-C expression during glioma progression. *Int J Cancer* 2002; 98: 362–9.
 51. Grana C, Chinol M, Robertson C et al. Pretargeted adjuvant radioimmunotherapy with yttrium-90-biotin in malignant glioma patients: a pilot study. *Br J Cancer* 2002; 86: 207–12.
 52. Riva P, Franceschi G, Frattarelli M. Loco-regional radioimmunotherapy of high-grade malignant gliomas using specific monoclonal antibodies labeled with ⁹⁰Y: a phase I study. *Clin Cancer Res* 1999; 5: 3275–80.
 53. Cokgor I, Akabani G, Kuan CT. phase I trial results of iodine-131-labeled antitenascin monoclonal antibody 81C6 treatment of patients with newly diagnosed malignant gliomas. *J Clin Oncol* 2000; 18: 3862–72.
 54. Riva P, Franceschi G, Riva N et al. Role of nuclear medicine in the treatment of malignant gliomas: the loco-regional radioimmunotherapy approach. *Eur J Nucl Med* 2000; 27: 601–9.
 55. Goetz C, Riva P, Poepperl G et al. Locoregional radioimmunotherapy in selected patients with malignant gliomas: experiences, side effects and survival times. *J Neurooncol* 2003; 62: 321–8.
 56. Paganelli G, Bartolomei M, Ferrari M et al. Pre-targeted locoregional radioimmunotherapy with ⁹⁰Y-biotin in glioma patients: phase I study and preliminary therapeutic results. *Cancer Biother Radiopharm* 2001; 16: 227–35.
 57. Bartolomei M, Mazzetta C, Handkiewicz-Junak D et al. Combined treatment of glioblastoma patients with locoregional pre-targeted ⁹⁰Y-biotin radioimmunotherapy and temozolomide. *Q J Nucl Med Mol Imaging* 2004; 48: 220–8.
 58. Boiardi A, Bartolomei M, Silvani A et al. Intratumoral delivery of mitoxantrone in association with ⁹⁰Y radioimmunotherapy (RIT) in recurrent glioblastoma. *J Neurooncol* 2005; 72: 125–31.
 59. Cremonesi M, Ferrari M, Chinol M et al. Three-step radioimmunotherapy with yttrium-90 biotin: dosimetry and pharmacokinetics in cancer patients. *Eur J Nucl Med* 1999; 26: 110–20.
 60. Ferrari M, Cremonesi M, Bartolomei M et al. Dosimetric modeling for locoregional treatment of brain tumors with ⁹⁰Y-Biotin. *J Nucl Med* 2006; 47: 105–12.

Therapy of ovarian cancer

Angela Coliva, Ettore Seregni, Mariangela Figini, Alberto Zacchetti, Rosanna Fontanelli, Francesco Raspagliesi, Silvana Canevari, and Emilio Bombardieri

Background

Ovarian cancer is the fifth leading cause of cancer death in the USA. This is due mainly to the advanced stage of disease at diagnosis and the non-curative responses often achieved with standard treatments. The therapeutic management of ovarian cancer today is dependent on early diagnosis, exquisitely exhaustive surgical treatment, and platinum/paclitaxel-based chemotherapy. However, the majority of patients are diagnosed in advanced stages. Although cures can be achieved in the primary treatment of stage III disease, the rate of complete response to the conventional anticancer treatments is very low. Moreover, the main problem is that also those patients who achieve a complete remission show an elevated ratio of recurrent disease. Monoclonal antibody (mAb) therapies have recently had a positive impact and become standard elements in the treatment of both hematologic and certain solid malignancies. Such advances have shown only a marginal value in the treatment of ovarian cancer; however, novel antibodies and different approaches, now in development, could impact on therapeutic standards for ovarian cancer in the coming years.¹

Ovarian cancer is a very heterogeneous disease and a variety of tumor types, including mucinous, clear cell, and serous cell types, are associated with the variable expression of different tumor markers including mucins (MUC16/CA125, MUC1), and tumor-associated glycoproteins (TAG72, folate receptor). Since antibodies can be raised against a wide range of macromolecules, they represent an ideal targeting vehicle for detecting antigenic structures expressed in neoplastic tissues. The prospect of utilizing mAb to deliver radiopharmaceuticals precisely to tumor targets has raised the interest and investigative effort of many researchers.

An antibody is a tetramer composed of a pair of identical heavy and light chains linked by disulfide bonds. Each chain is composed of domains of constant size

(100–110 amino acid residues) characterized by a loop defined by the presence of intrachain disulfide bonds. The N-terminal domain of each chain is termed the variable (V) region and is followed by one (light chain) or three (heavy chain) constant (C) domains. The antigen binding sites are determined by the association of V regions of light and heavy chains and depend on specific hypervariable sequences named CDR (complementarity-determining region), while the biological activities of the immunoglobulins (i.e. complement fixation, antibody-dependent cellular cytotoxicity, and the possibility to be reabsorbed and recirculate) are associated with the heavy constant regions (Figure 26.1).

The first developed and most widely used technology for the generation of monoclonal antibodies (mAb) is the use of mouse hybridomas generated from the stable fusion of immortalized myeloma cells with B cells from immunized mice. These reagents, due to their heterologous origin, are highly immunogenic, limiting their *in vivo* utilization. Several different modifications of mAb have been proposed in order to decrease the immunogenicity of these molecules. Accordingly, mAb were modified by protein engineering to be chimeric (V regions of murine origin and C regions of human origin) or humanized (CDR of murine origin and the majority of the residual sequence of human origin). More recently, fully human mAb have been obtained by phage display technology, from transgenic mice, or by immortalization of human B lymphocytes.²

The efficacy of mAb in cancer treatment is limited by different factors (antibody structure and size, target antigen, antibody affinity, immunogenicity, biodistribution, kinetics) as summarized in Table 26.1.

The level of antigen expression by the neoplastic cells represents one of the most important factors affecting the uptake of antibodies in solid tumors, and several studies indicate that the choice of antigen for antibody targeting should be guided by the level of their expression *in vivo*.

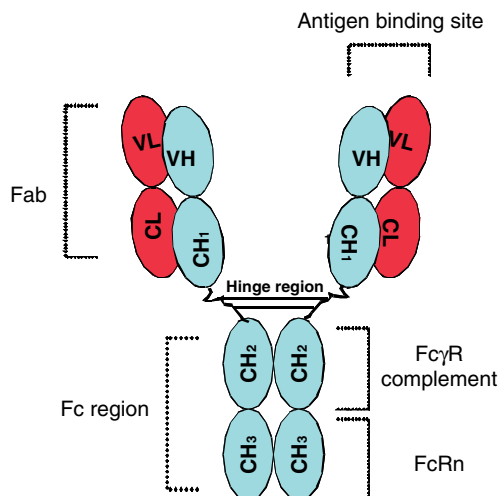


Figure 26.1

Immunoglobulin G (IgG) structure and function. The heavy (H) chains (in gray) contain a variable (V) domain and three constant (C) domains; the light (L) chains (in purple) contain a V domain and a single C domain.

Relatively lower relevance could be attributed to the other factors, although a relevant issue is the mAb relative inability to reach their target *in vivo* in adequate quantities.^{3,4} Besides the levels of antigen expression, other issues are also critical for a satisfactory mAb accretion in neoplastic lesions. In fact, low and/or heterogenic expression of tumor antigen alone cannot account for the poor penetration of antibodies in tumors and their inability to reach all regions of a tumor in adequate quantities.^{5,6}

Table 26.1 Principal parameters conditioning application of antibodies in the clinical setting

Characteristics	Parameter
Antigen	<ul style="list-style-type: none"> ● Localization: extracellular (microenvironment), membrane, intracellular ● Level of expression ● Metabolism of the antigen–antibody complex: internalization, release ● Function ● Clinical correlation
Antibody	<ul style="list-style-type: none"> ● Origin of species: homologous, heterologous ● Dimension: whole antibody, fragments ● Specificity ● Affinity
Pathology	<ul style="list-style-type: none"> ● Vascularization ● Interstitial pressure

Only recently have the peculiarities of tumor physiology been recognized as determinants in antibody distribution. Three physiological barriers responsible for the poor localization of macromolecules in tumors have been identified: (1) heterogeneous blood supply; (2) elevated interstitial pressure; and (3) long transport distances in the interstitium. The first barrier limits the delivery of molecules to well-perfused regions of a tumor; the second barrier reduces extravasation of fluid and macromolecules in the high interstitial pressure regions and also leads to a radially outward convection in the tumor periphery, which opposes the inward diffusion; and the third barrier increases the time required for slowly moving macromolecules to reach distal regions of a tumor. Binding of antibody to an antigen further lowers the effective diffusion rate by reducing the amount of mobile antibody. Due to micro- and macroscopic heterogeneities in tumors, the relative magnitude of each of these barriers will vary from one location to another, from one day to the next in the same tumor, and from one tumor to another.⁷ In the specific case of ovarian cancer, Choi et al.⁸ suggest that poor antibody penetration is due to the intratumoral collagen content. Experiments performed in athymic rats bearing human ovarian tumors (SKOV-3 and OVCAR-3) in the abdominal wall were designed to study the influence of tumor interstitial pressure on the penetration of an antibody. They concluded that the elevation of interstitial pressure might not be the sole explanation for the transport barrier to immunoglobulin G (IgG) in tumor tissue; nevertheless, measurement of tumor interstitial pressures showed a peak pressure of 30 mmHg at the center of the tumor and an average pressure of 10–12 mmHg, which were greater than the maximum pressure attainable in the peritoneal cavity (8–10 mmHg). They hypothesized that the tumor interstitial matrix (tumor cell microenvironment) was a major barrier to intraperitoneal macromolecular delivery. From histologic observations, a similar pattern of distribution of collagen and hyaluronic acid in the experimental tumors in that rat model was shown. Both hyaluronan and collagen were located mainly at the periphery, in the layer of proliferating cells surrounding the tumor cell mass. An analogous configuration for the interstitial structure has been reported in human ovarian tumors that have metastasized to the abdominal wall. The findings of Choi et al.⁸ indicated that collagen but not hyaluronic acid contributes resistance to the transport of antibody. This suggests that the nature of a potential transport barrier is as important as its structural location. Also, the influence of electrostatic repulsion between negative charges on the glycosaminoglycans and the protein was minimized, as similar transport profiles were found for two different antibodies with different net charge, a non-specific IgG with isoelectric point of 7.6 and the monoclonal antibody trastuzumab with isoelectric point of 9.2. They concluded that, while the high interstitial pressure is a

deterrent to convective penetration of macromolecules into the tumor parenchyma, there is also an inherent resistance in the structure of the interstitial matrix that must be overcome before effective delivery of an antibody. The physical presence of the collagen microfibrillar network could thus be the primary barrier to transport.

Furthermore, the structure of mAb is very important, since the most common subclass of mAb used in immunotherapy is IgG, characterized by a long circulatory half-life in plasma. This determines a tumor-to-background ratio that is usually low. In order to improve the tumor uptake, other immunoreagents have been constructed and investigated, such as antibody fragments obtained by enzymatic digestion of the intact IgG antibodies or protein engineering. Thus, the tumor-to-non-tumor ratio increases, even if the tumor retention time tends to be shorter than that of intact mAb, and the kidney excretion increases.⁹

Radioimmunotherapy

Radioimmunotherapy (RIT) has two major advantages over the application of mAb alone or conjugated with drugs or toxins.¹⁰ First, radionuclides can irradiate not only the specifically targeted tumor cells, but also the surrounding area, including tumor cells not expressing the target antigen (crossfire phenomenon). Second, the mechanism of action of radionuclides is not dependent on multidrug resistance.

Whereas RIT of hematopoietic neoplasms is gaining attention as a future therapy modality, solid tumors have been less responsive, and targeting minimal or micrometastatic disease appears at present to be the optimal approach in solid tumor therapy. The challenge of treating solid tumors has stimulated several approaches to improve the radiation dose delivered and to achieve a more uniform distribution of ionizing radiation, with the ultimate goal being the delivery of tumoricidal doses while sparing normal tissues.¹¹

Since ovarian cancer has a high propensity to stay confined to the peritoneal cavity until very late in the course of the disease, radiolabeled antibodies have been administered intraperitoneally in many trials (see Table 26.3). Authors' opinion about the advantage of such a route of administration is somewhat conflicting. It is suggested that possible peritoneal implants will more likely benefit from intraperitoneal injection, whereas non-implants (i.e. those metastases in the peritoneal cavity resulting from hematologic spread) are more likely to have higher uptake following intravenous injection.¹¹ It has furthermore been suggested that intravenous administration may result in a more homogeneous uptake in intraperitoneal tumors, as compared to intraperitoneal administration.¹² However, it is evident that in spite of many different targets located

in ovarian cancer cells and the number of mAb raised against the tumor-associated antigens of ovarian cancer, the clinical applications of radiolabeled mAb are still limited to a small number of clinical studies. This does not correspond to the huge number of experimental data obtained in cell lines and animal models, where the potential effectiveness of RIT has been well demonstrated. The general opinion is that the intraperitoneal route has several advantages for achieving an optimal tumor/non-tumor ratio of radioconjugates, allowing the administration of a high activity of radioisotope and at the same time limiting the myelotoxicity, compared to the systemic route. However, it should be borne in mind that the intravenous route of administration may result in a wider distribution of mAb in the bloodstream, and this can be an advantage because it allows the targeting of distant metastases and the potential treatment of metastatic disease, such as that in extraperitoneal lymph nodes.

Radiolabeling techniques

The most commonly used radionuclides in RIT are β emitters, although Auger electron emitting radionuclides and α emitters can also be used. Efficient labeling of monoclonal antibodies depends on a large number of factors, including the physicochemical properties of the radionuclide and the methods of its incorporation into the protein. A wide variety of nuclides with different physical, chemical, and biological properties are now available for experimental and clinical evaluation. Table 26.2 reports

Table 26.2 Radioisotopes most commonly used in radioimmunotherapy of ovarian cancer

Radionuclide	Half-life	Decay mode (MeV)	Particle maximum range in soft tissue (mm)
¹³¹ I	8.0 days	β^- (0.192), γ (0.364)	3.0
⁹⁰ Y	64 hours	β^- (0.935)	12.0
¹⁷⁷ Lu	6.7 days	β^- (0.149), γ (0.208)	2.5
¹⁸⁶ Re	3.72 days	β^- (0.362), γ (0.137)	5.1
¹⁸⁸ Re	17 hours	β^- (0.795), γ (0.155)	11
²¹¹ At	7.2 hours	α (5.9), γ (0.687)	0.065

the isotopes generally used for the labeling of monoclonal antibodies.

The most commonly used radioisotopes for therapy are the β emitters iodine-131 (^{131}I) and yttrium-90 (^{90}Y). Other interesting β emitters are rhenium-186 (^{186}Re), rhenium-188 (^{188}Re), and lutetium-177 (^{177}Lu). Iodine-125 (^{125}I) has been used as an Auger electron emitter and astatine-211 (^{211}At) as an α -emitter. These radioisotopes differ with respect to their radioactive emission, energy, physical half-life, absence or presence of γ rays, and range of particles in the tissues. These parameters affect the radiation dose delivered to the tumor, which can be estimated by dosimetric analysis. For instance, the medium-energy β emitters such as ^{131}I and ^{177}Lu are more effective for smaller tumor nodules since the radiation energy is deposited mainly inside the diameter of a small tumor. On the other hand, high-energy β emitters such as ^{90}Y are more suitable for larger tumors due to the high penetration of their radiation through large tumor masses. The α emitting radionuclides emit particles of higher energy than β particles, with a much shorter range (less than 100 μm) and considerably higher linear energy transfer. mAb radiolabeled with α emitters or Auger electron emitters need to be internalized into the cancer cells, because the very short range of these radiations require almost a contact with proteins or nucleic acids in order to be effective in killing cells.

The most widely used isotope in clinical practice for radioimmunotherapy is iodine-131, due to its well established protein iodination chemistry, availability, and cost. However, its long half-life and abundance of 364-keV photons (81%) results in less attractive tumor/non-tumor target ratios. An important limitation of iodinated antibodies is the high degree of dehalogenation which occurs in vivo. Free iodine leads to misplaced radiation to non-target organs such as the thyroid and gut. The dehalogenation is attributed to deiodinases unable to distinguish between thyroxine and the iodinated tyrosine on antibodies. The most extensively adopted procedure of antibody iodination includes an electrophilic substitution reaction on the aromatic ring of specific amino-acid residues, such as tyrosine. Electrophilic reactions require the production of an electrophilic radiohalogenation reagent through oxidation of iodine. The most used oxidants are chloramine T, Iodogen[®], lactoperoxidase, and indirect conjugation methods such as the classic Bolton–Hunter method.¹³ mAb were also labeled with ^{211}At , using the intermediate labeling reagent N-succinimidyl-3-(trimethylstannyl)benzoate (m-MeATE) and N-iodosuccinimide.¹⁴ The possibility of labeling immunoproteins with metallic radioisotopes represents a further improvement in tumor therapy. Radiometal labeling protocols make use of bifunctional chelating agents to obtain stable radiometal antibody conjugates. Bifunctional chelating agents possess the correct stereochemistry for radiometal binding and a reactive

functional group for covalent attachment to antibodies. The most used chelator for indirect labeling is called DOTA (tetraazacyclododecanetetraacetic acid) and is able to bind many radiometals, such as ^{90}Y and ^{177}Lu , in a very stable way, also in vivo.¹⁵ A direct approach is feasible for radiometals such as ^{188}Re . The radiometal binds the protein residues containing free sulfhydryl groups generated by the reduction of disulfide bridges. Commonly employed reducing agents include dithiothreitol, 2-mercaptoethanol, ascorbic acid, and tin chloride.¹⁶

Targets and reagents

The more important antigens expressed on ovarian carcinoma cells and their associated antibodies, already evaluated at preclinical and clinical levels, are listed in Table 26.3.

Mucins

Mucins are a family of large, heavily glycosylated proteins. The major targets used in radioimmunotherapy are MUC16 and MUC1.

Table 26.3 Most commonly used monoclonal antibodies in radioimmunotherapy

<i>Target antigen</i>	<i>Antibody</i>	<i>Radioisotopes utilized</i>
<i>Mucins</i>		
MUC16/ CA125 ^{17,18}	OC125 B43.13 776.1	^{131}I , ^{111}In $^{99\text{m}}\text{Tc}$, ^{188}Re ^{90}Y
MUC1 ^{19,20}	HMFG1, HMFG2, AUA	^{131}I , ^{90}Y
<i>Glycoproteins</i>		
CEA ²¹	MN-14	^{131}I
aFR/gp38 ^{22,23}	MOv18	^{131}I , ^{90}Y , ^{177}Lu , ^{211}At
TAG72 ²⁴	B72.3 CC49	^{90}Y ^{90}Y , ^{177}Lu
gp95 ²⁵	MX35	^{211}At
<i>Oligosaccharides</i>		
Lewis Y ^{26,27}	hu3S193	^{90}Y

Antigen: MUC16/CA125

CA125, first identified in 1981,¹⁷ is a large membrane-bound glycoprotein whose biological function remains unknown. CA125 appears to function as a calcium-dependent protease with autoprolytic activity, its release is regulated by phosphorylation, and its binding to mesothelin appears to contribute to epithelial ovarian cancer (EOC) invasion.¹⁸

This antigen is present in fetal celomic epithelia derivatives, serous ovarian carcinoma cell lines, and serous adenocarcinoma tissue. The antigen is also found in several adult tissues such as the epithelium of the fallopian tubes, the endometrium, the endocervix, the pleura, and the peritoneum.

Antibody: OC125

The monoclonal antibody OC125 was developed by conventional hybridoma technology using as immunogen the OVCA 433 cell line derived from a human serous cystadenocarcinoma.

In several reports this antibody or its F(ab')₂ fragment were used in diagnostic immunoscintigraphic studies after labeling with ¹¹¹In,^{28–30} and the encouraging results led to its evaluation in intraperitoneal radioimmunotherapy.

In 1999, Mahe et al.³¹ reported the results of a phase II study designed to evaluate the efficacy of intraperitoneal radioimmunotherapy in patients with minimal residual disease after primary treatment with surgery and chemotherapy (see Table 26.3). Six patients with minimal residual disease received intraperitoneal RIT performed with 60 mg of OC125 F(ab')₂ monoclonal antibody labeled with 4.44 GBq of ¹³¹I injected 5–10 days after the surgical procedure. Systematic laparoscopy or laparotomy with multiple biopsies was performed 3 months after RIT in five patients, and showed no change in three patients, and progression in two patients (clinical progression was seen in one patient). Toxicity was mainly hematological, with grade 3 neutropenia and thrombocytopenia in two patients. Human anti-mouse antibody production was demonstrated in all six patients. This study showed little therapeutic benefit from intraperitoneal RIT in patients with residual ovarian carcinoma.

Antibody: B43.13

B43.13 is another monoclonal murine antibody which was produced by immunizing mice with a partially purified CA125 antigen. McQuarrie et al.³² demonstrated that B43.13 radiolabeled with ^{99m}Tc had a tumor uptake and showed a pharmacokinetic profile similar to that of the unlabeled antibody. The dosimetric study indicated that

target organs are liver, spleen, kidneys, and heart. The same group published the radiolabeling protocol with ¹⁸⁸R,³³ but no clinical study based on this radiopharmaceutical has yet been published.

Antibody: 776.1

776.1 mAb is a murine monoclonal antibody directed to the antigen CA125 that has the unique property of preferential binding to the cell-associated form of the antigen. Studies performed using a subcutaneous OVCAR-3 xenograft mouse model demonstrated a peak uptake of 17.7%ID/g (where ID is injected dose) in tumors at 72 hours post-injection. Little uptake in other organs was observed. DOTA-776.1 was labeled with ⁹⁰Y and used in efficacy studies. [⁹⁰Y]DOTA-776.1 at a single dose of 555 kBq was able to mediate an efficient reduction of tumor growth, with regression observed in a subset of animals for a period ranging from 3 to 48 days. No significant regression was observed in animals treated with control antibody.³⁴ These results suggest that 776.1 mAb may be a promising radioimmunotherapeutic agent for the treatment of human ovarian cancer.

Antigen: MUC1

The antigen MUC1 is a 300-kDa molecular weight glycoprotein expressed by over 90% of epithelial ovarian tumors and is antigenically distinct from normal tissue mucin, as a result of underglycosylation or aberrant glycosylation of this protein in cancerous tissue.¹⁹ The antigen is expressed by the lactating breast and weakly by some normal epithelial tissues. The extracellular portion of the MUC1 protein mainly consists of a variable number of highly conserved 20 amino acid repeats. In malignancy, the complex carbohydrate side chains are truncated, leading to exposure of cryptic epitopes within these amino acid repeats.²⁰

Antibody: HMFG1

HMFG1 is a murine monoclonal antibody developed against a delipidated preparation of the human milk fat globule.³⁵ One of the very first clinical trials of RIT in patients with ovarian cancer was carried out by Epenetos et al.,³⁶ who treated 24 patients with stage III ovarian cancer, after cytoreductive surgery and first line platinum-based chemotherapy, with escalating activity doses of ¹³¹I-labeled mAb HMFG1, HMFG2, AUA1, or H17E2. The radiolabeled antibodies were administered alone or, when immunohistochemical staining showed the strong presence of more

than one antigen, as a mixture. Clinical responses were limited to those 16 patients with minimal residual or small volume disease (< 2 cm). Four patients experienced complete responses for up to 3 years, whereas five patients showed stable disease for up to 20 months. In a second trial, Nicholson et al.³⁷ tested the efficacy of 666 MBq/m² of ⁹⁰Y-labeled HMFG-1 mAb in 21 patients with stage IIC–IV ovarian cancer who had no macroscopic disease after cytoreductive surgery and completion of platinum-based chemotherapy. Sixteen patients were still alive 10 years after treatment, which was significantly better than the median survival of less than 4 years of a matched historical control group. Epenetos et al.³⁸ reported later that, within the subgroup of 21 patients who experienced complete remission, the median survival had not yet been reached at a follow-up of > 12 years.

Janssen et al.³⁹ studied the therapeutic efficacy of RIT using HMFG1 labeled with ⁹⁰Y, ¹³¹I, or ¹⁸⁶Re in nude mice with intraperitoneally growing OVCAR-3 ovarian carcinoma xenografts. Each of the three regimens caused a delay in ascites formation and mortality as compared with the control groups. They also concluded that [⁹⁰Y]HMFG1 is more effective in inhibiting tumor growth when administered intraperitoneally than intravenously. Based on these promising results a multicenter phase III trial was initiated, comparing the efficacy of [⁹⁰Y]DOTA-HMFG1 to no treatment in a total of 447 patients with ovarian cancer with no evidence of disease following cytoreductive surgery and platinum- or taxol-based chemotherapy, as confirmed by diagnostic laparoscopy. Results of the study indicated that a single intraperitoneal administration to patients who showed no evidence of disease after first line therapy did not extend survival or time to relapse.⁴⁰ Several factors including dose, pharmacokinetics, and the absence of microscopic disease, may theoretically have hampered the efficacy of RIT. Other potentially confounding variables include the use of different consolidation strategies adopted in this multicenter trial.

Glycoproteins

Antigen: CEA

Carcinoembryonic antigen (CEA) is a glycoprotein involved in cell adhesion. It can be found in many types of cells associated with tumors and the developing fetus. CEA, first identified in human colon cancer tissue, was then found associated with many other types of tumors, such as pancreas, stomach, breast, lung, and certain types of thyroid and ovarian cancer.²¹ The antigen is normally secreted into the circulation, but a high CEA content, ranging from 115 to 17 800 ng/g, was reported in malignant ovarian tumors even when the plasma CEA level was normal.

Antibody: MN-14

Murine mAb MN-14 (mMN-14) is a high-affinity anti-CEA antibody produced by a hybridoma cell line. In 1997 Juweid et al. published a case report of a patient with advanced ovarian cancer refractory to paclitaxel therapy. The patient received radioimmunotherapy with 2.7 GBq of [¹³¹I]MN-14, followed 4 months later by a similar dose. A partial remission was seen by computed tomography (CT) 1 month after the first radioimmunotherapy, and a further objective response was documented after the second radioimmunotherapy.⁴¹

A humanized version of MN-14 (hMN-14) was selected from several clones that differed slightly in their framework composition. Targeting studies using ¹³¹I-labeled humanized MN-14 showed excellent tumor uptake and tumor/non-tumor ratios, similar to the mMN-14. A pilot clinical imaging trial was initiated to determine the targeting, pharmacokinetics, and dosimetry for ¹³¹I-labeled hMN-14 IgG. An antibody response to hMN-14 was not detected in patients who received only the hMN-14 (as many as three injections). With similar, excellent targeting properties to those of the mMN-14 and the potential for reduced immunogenicity, hMN-14 is an attractive candidate for further clinical imaging and therapy applications.⁴²

Antigen: gp38 (aFR)

gp38 is a tumor-associated glycoprotein of 38 kDa identified as the α isoform of the folate receptor.²² On ovarian cancer cells the antigen is expressed on the whole cellular surface; in contrast, normal cells express it only on the apical portion that is not accessible by the injected antibodies. Different studies have demonstrated the high correlation between aFR and ovarian carcinoma, as it is absent on the superficial epithelial ovarian cells, and the highly correlated expression with malignancy.²³ Furthermore, the antigen is not internalized after interaction with specific antibodies and its expression is not modulated by chemotherapeutic agents.

Antibody MOv18

MOv18 is a murine monoclonal antibody with a high affinity constant for the antigen gp38, selected for its positive reactivity towards non-mucinous malignant ovarian carcinoma and the negative reactivity in other non-epithelial tumors or normal tissues, except for very faint staining on kidney and lung specimens.⁴³

Radiolabeled MOv18 in its chimeric form was applied in the radioimmunotherapy of ovarian carcinoma.

After demonstrating preferential uptake of intraperitoneally or intravenously administered ^{131}I -labeled murine MOv18 in tumors in 30 patients with ovarian cancer, Crippa et al. tested the efficacy of high-dose intraperitoneal RIT using ^{131}I MOv18 (3700 MBq) in 16 patients with minimal or small volume ovarian cancer.⁴⁴ Clinical follow-up and/or third-look evaluation performed 90 days after RIT showed complete response in five patients, stable disease in six patients, and progressive disease in the remaining five patients. Of the five patients who experienced complete remission, one patient remained clinically disease-free for 34 months, whereas the remaining four patients relapsed after a mean disease-free period of 10.5 months. With the aim of reducing the immunogenicity of the treatment, van Zanten-Przybysz et al.⁴⁵ studied the pharmacokinetics and efficacy of RIT using ^{131}I -labeled chimeric MOv18 (3 GBq) in three patients with ovarian cancer. The tumor-absorbed radiation dose was estimated by means of dosimetric analysis of repeated radioimmunoscintigraphic images. All patients experienced stabilization of disease for 2–6 months, as assessed by CT scans and serum CA125 measurements. Tumor absorbed radiation doses varied from 600 to 3800 cGy. None of the patients developed a human anti-chimeric antibody (HACA) response.

Andersson et al.⁴⁶ studied the feasibility of labeling MOv18 with ^{211}At and assessed it in nude mice with intraperitoneally growing human ovarian cancer xenografts. The antibody was injected intraperitoneally when the cancer growth was microscopic. The injected activity was 485–555 kBq. The median survival for treated mice was 213 days, compared to 138 days for untreated mice. No obvious toxicity was seen. Thirty-three percent of the mice were apparently free of cancer after 7 months and were probably cured. In the second part of the study, mice with macroscopic cancer and signs of ascites were injected intraperitoneally with the same ^{211}At -labeled antibody (377–389 kBq). This treatment delayed the production of ascites. No transfer to a clinical setting has yet been reported.

Coliva et al. reported the possibility of labeling MOv18 with ^{90}Y via the bifunctional chelator DOTA.⁴⁷ The radiopharmaceutical was assessed in a preclinical setting in nude mice bearing a subcutaneous human ovarian cancer xenograft. Biodistribution studies indicated a significant uptake of the radiolabeled antibody in the tumor, while a normal distribution was observed in the other target organs (Figure 26.2). Despite the good preclinical results, a pilot trial in a woman bearing ovarian cancer evidenced a quite high bone marrow toxicity.

To overcome this toxicity the antibody was labeled with ^{177}Lu (Figure 26.3). In the animal model the radiopharmaceutical has been demonstrated to be effective in decreasing tumor volume without any toxicity at the doses injected (5,55–9,25 kBq). A clinical trial will assess the capacity to localize in tumor, the biodistribution, and the dosimetry of ^{177}Lu MOv18.

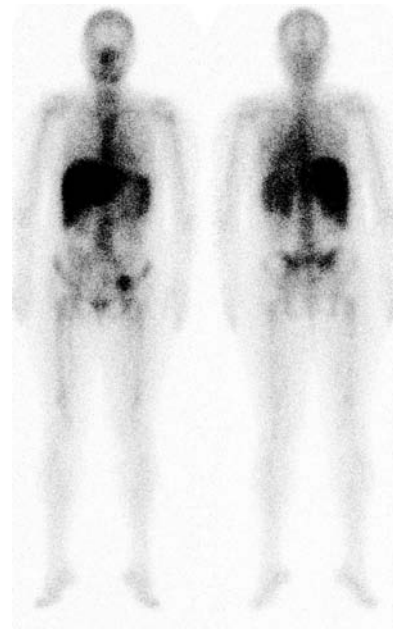


Figure 26.2

A representative scintigraphic image acquired 48 hours post-injection of ^{111}In MOv18 in a woman with pelvic lymph node recurrence.

Antigen: TAG72

TAG72 is a high molecular weight (>200 kDa) tumor-associated oncofetal antigen, expressed by a wide variety of human adenocarcinomas. This antigen is expressed by 50% of primary breast carcinomas, in 85% of primary colon carcinomas, in 71% of metastatic ovarian cancers, and in several other carcinomas.²⁴ It is not expressed by leukemia, lymphomas, sarcomas, mesotheliomas, melanomas, or

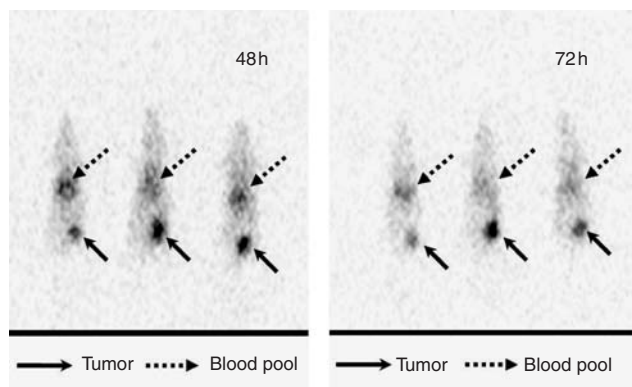


Figure 26.3

Scintigraphic images of mice bearing subcutaneous human ovarian cancer xenografts expressing the folate receptor (aFR) injected with a diagnostic dose of ^{177}Lu MOv18 and acquired at different time points.

benign tumors. TAG72 is also expressed on normal secretory endometrium, but not on other normal tissues.

Antibody: B72.3

Murine monoclonal antibody B72.3 recognizes the surface domain of the glycoprotein complex TAG72, and was developed using a membrane-enriched fraction of human metastatic mammary carcinoma tissue as immunogen.⁴⁸ It was used by several investigators for immunohistochemical staging of ovarian carcinoma and to perform scintigraphy of various human tumors. It has been coupled with ¹¹¹In and ⁹⁰Y via the ligand DTPA (diethylenetriaminepentaacetic acid). After studying the clinical pharmacology, metabolism, and tissue distribution and confirming preferential uptake of ⁹⁰Y-labeled B72.3 in tumors in nine patients with ovarian cancer, Rosenblum et al.⁴⁹ performed a dose-escalating, phase I study of radioimmunotherapy using [⁹⁰Y]DTPA-B72.3 administered intraperitoneally in a total of 38 patients with ovarian cancer. Accumulation in the bone had limited the maximal tolerated dose because of hematological toxicity and platelet suppression. To suppress the bone uptake of ⁹⁰Y and therefore overcome the myelotoxicity, patients were treated with a continuous intravenous infusion of EDTA (ethylenediaminetetraacetic acid) immediately before administration of the radiolabeled antibody. This modification to the protocol allowed the administration of higher activity doses. Dose-limiting toxicity was thrombocytopenia and neutropenia. Four responses 2 complete responses (CR), 2 partial responses (PR) were observed in patients who received 555–1110 MBq of ⁹⁰Y-labeled B72.3, with response durations of 1–12 months. These results encouraged an expanded phase II trial in patients with minimal residual disease after standard chemotherapy or for the palliation of refractory ascites, but no results have yet been published.

Antibody: CC49

Murine CC49 mAb has a higher affinity and more rapid plasma clearance than B72.3, recognizes a distinct epitope, and exhibits higher reactivity to gastric, colonic, and pancreatic adenocarcinomas. Preclinical studies in athymic mice bearing human tumor xenografts showed improved targeting and 3–5-fold greater therapeutic efficacy of mAb CC49 labeled with either ¹³¹I or ⁹⁰Y compared with similarly labeled B72.3.⁵⁰

Alvarez et al. conducted two phase I/II trials in which they investigated the toxicity and efficacy of CC49 labeled with either ⁷⁷Lu or ⁹⁰Y via the bifunctional chelator PA-DOTA. In their first trial,⁵¹ 27 patients with ovarian cancer, who failed conventional chemotherapy, were treated with [¹⁷⁷Lu]CC49. The maximum tolerated activity

dose was established to be 1665 MBq/m², at which dose-limiting myelosuppression was encountered. Radio-immunoscintigraphic imaging revealed intraperitoneal tumors in 19 out of 27 patients. Of the 13 patients with measurable disease, one showed a partial response. Of the nine patients with <1 cm tumor nodules, two patients showed stable disease for 4 and 5 months, respectively, whereas the other seven patients progressed within 21 months. Five patients had only microscopic disease upon study entry. Of these, one showed evidence of progression at 10 months, whereas the remaining four patients remained disease-free at 6–35 months post-treatment.

Meredith et al.⁵² subsequently tested the feasibility and efficacy of the combination of intraperitoneal RIT using [¹⁷⁷Lu]CC49 and intraperitoneal paclitaxel (100 mg/m²) in 34 patients with ovarian cancer. Chemotherapy was given 48 hours prior to the administration of the radiolabeled antibodies. In addition, patients received subcutaneous injections of interferon (IFN) α_{2b} in order to enhance the expression of TAG72. The maximal tolerated dose (MTD) of [¹⁷⁷Lu]CC49 within this combination treatment regimen was reached at 1480 MBq/m², above which dose-limiting bone marrow toxicity occurred. Four out of 17 patients with measurable disease on CT had partial responses, whereas four out of 27 patients with non-measurable disease experienced progression-free time intervals of >18 months. After showing the feasibility of the combination of RIT using [¹⁷⁷Lu]CC49 and paclitaxel in a phase I trial, Alvarez et al.⁵³ treated 20 patients with persistent or recurrent ovarian cancer after conventional cytoreductive surgery and chemotherapy, with a combination of RIT using ⁹⁰Y-labeled CC49 and chemotherapy using paclitaxel. Patients received subcutaneous injections of IFN α_{2b} as well. The MTD of [⁹⁰Y]CC49 was reached at 895 MBq/m², with hematological toxicity being dose-limiting. Of nine patients with measurable disease, two had partial responses for up to 4 months. Eleven patients had non-measurable disease. Of these, four patients remained disease free, three of whom for longer than 18 months post-treatment.

Antigen: gp95

gp95 is a cell surface antigen of about 95 kDa, initially identified on OVCAR-3 ovarian cancer cells. This antigen is a glycoprotein, stabilized by disulfide bonds, with a large protease-resistant region that carries the MX35 epitopes.²⁵

Antibody: MX35

Monoclonal antibody MX35 reacts with approximately 90% of ovarian epithelial cancers, and has been studied in

localization and biodistribution trials in ovarian cancer patients. Rubin et al.⁵⁴ performed a clinical trial using ¹²⁵I- or ¹³¹I-labeled MX35. Twenty-five patients with advanced ovarian cancer entered the study and were administered intravenously or intraperitoneally with the radiolabeled antibody. They observed a specific localization of mAb in tumor. The tumor/normal tissue ratios were not significantly related to mAb dose, the level of immunohistochemical antigen expression, or the interval between mAb injection and surgery.

In the search for increased efficacy and lower toxicity for normal tissues, α emitters may play an important role in the treatment of micrometastases and small tumors.

Elgqvist et al. investigated the therapeutic efficacy of radioimmunotherapy in an ovarian cancer model using the α particle emitting nuclide ²¹¹At labeled to MX35.⁵⁵ Dosimetric evaluations based on assumed tumor cluster sizes and on studies of the binding kinetics of the radioimmunocomplexes in vitro, indicated that, for tumor clusters smaller than 71 μ m (maximum path length of the α particle emitted by ²¹¹At), the mean absorbed dose is surprisingly high (15 Gy), and effective also if mAb do not penetrate the tumor. These conclusions indicate that the high-LET (linear energy transfer), short-range, α particle emitter ²¹¹At, labeled to the mAb MX35 and intraperitoneally injected, exhibits a high efficacy when treating micrometastatic growth of the ovarian cancer cell line OVCAR-3 on the peritoneum of nude mice.

From the whole murine monoclonal antibody the F(ab')₂ fragment was derived. Studies performed by Finstad et al.⁵⁶ demonstrated that mAb MX35 F(ab')₂ localizes to the micrometastatic ovarian carcinoma deposits within the peritoneal cavity. Back et al.⁵⁷ determined the relative biological effectiveness in vivo of [²¹¹At]MX35 F(ab')₂ in a human ovarian cancer xenograft in nude mice. The slow diffusion in combination with the short particle range may result in a heterogeneous dose distribution, reducing the overall tumor cell eradication effect.

Saccharide antigens

Antigen: Lewis Y

The Lewis Y (Le^Y) antigen is a family member of the blood group-related difucosylated oligosaccharides associated with 60–90% of human carcinomas of epithelial cell origin, including breast, colon, gastric, ovarian, and lung cancer.²⁶ The high frequency of Le^Y-expressing tumors, high density of Le^Y on the tumor cell surface, and relatively homogeneous expression in primary and metastatic lesions have led to its selection as an antigenic target. Its presence in normal tissues is limited to the surface of the epithelium of

the esophagus, gastric mucosa, proximal small intestine, acinar cells of the pancreas, ciliated epithelium of the trachea, and the bronchus and type II pneumocytes.²⁷

However, because Le^Y is located on the epithelial surface of these tissues, the antigen should have restricted accessibility to administered antibodies.

Antibody: hu3S193

During recent decades, several antibodies that recognize Le^Y have been generated. Most of these, however, show cross-reactivity with Le^X and type II H-antigen structures. 3S193 is a murine monoclonal antibody with exceptional specificity for Le^Y.⁵⁸ The humanized version of this antibody, hu3S193, has been generated by CDR grafting. hu3S193 not only retains the specificity of 3S193 for Le^Y but also has gained the capability to mediate complement dependent cytotoxicity (CDC) and antibody dependent cellular cytotoxicity (ADCC). This antibody targets Le^Y-expressing xenografts in nude mice as demonstrated by biodistribution studies with hu3S193 labeled with ¹²⁵I, ¹¹¹In, or ⁹⁰Y.⁵⁹ Greater tumor uptake and retention of ¹¹¹In-labeled hu3S193 and similar blood clearance compared with ¹²⁵I-labeled hu3S193, suggest that radiometals are the preferred radioisotope for this antibody–antigen system. A phase I/II clinical trial is ongoing at the Memorial Sloan-Kettering Cancer Center to evaluate humanized 3S193 labeled with ⁹⁰Y and administered intraperitoneally.

Other antigens and alternative radioimmunotherapy approaches

Antigen: HER2/neu

The HER2/neu proto-oncogene encodes a tyrosine kinase growth factor receptor involved in the development and progression of the majority of cancers. Initial studies have shown that HER2/neu oncogene is overexpressed in approximately 15–30% of ovarian carcinomas.⁶⁰ However, findings regarding the overexpression and prognosis are still conflicting.

Antibody: AE1

The tumor-specific anti-HER2/neu monoclonal antibody AE1 was tested for specificity, toxicity, and efficacy after labeling with ²¹²Pb in nude mice bearing the SKOV-3 human ovarian tumor cell line expressing the HER2/neu proto-oncogene. The therapeutic agent used was conjugated to ²¹²Pb whose decay generates ²¹²Bi, an α and

β emitter. A derivative of DOTA was used to couple ^{212}Pb to the anti-HER2/neu monoclonal antibody AE1. The radiopharmaceutical as an intact radiolabeled monoclonal antibody may be of only modest value in the therapy of bulky solid tumors due to the short physical half-life of ^{212}Pb and the time required to achieve a useful tumor-to-normal-tissue ratio of radionuclide after administration. However, the radiolabeled monoclonal antibody may be useful in the therapy of tumors in the adjuvant setting.⁶¹

IgM antibody

IgM antibody can also be used as a radioimmunotherapeutic agent.

Antibody: AC6C3-2B12

An IgM λ human tumor cell-reactive monoclonal antibody was developed that reacts with cells of ovarian cancer, colorectal cancer, breast cancer, and certain other malignancies. The monoclonal antibody AC6C3-2B12, obtained from a recent recloning, was conjugated to isothiocyanato-2-benzyl-3-methyl-diethylenetriamine-pentaacetic acid and labeled with either ^{111}In or ^{90}Y . Borhardt et al.⁶² studied the therapeutic efficacy in nude mice bearing intraperitoneal nodules of SKOV-3 NMP2 of intraperitoneal administration of [^{90}Y]2B12 as a single or fractionated administration. Untreated mice and mice treated with unlabeled immunoconjugates served as controls. The controls had a mean survival time of 20 and 17 days, respectively. Treatment with [^{90}Y]2B12 increased median survival by 11–12 days per 3.7 MBq for a single administration (1.8–14.8 MBq) and fractionated administrations (5.6–18.9 MBq).

Three-step strategy

A method to improve the tumor targeting of mAb and reduce bone marrow toxicity is the so-called pre-targeting method, where the radionuclide is administered separately from the tumor targeting mAb. This approach using the (strept)avidin–biotin or bispecific antibody methodology has been applied in preclinical and clinical research.⁶³ In an attempt to improve tumor-to-tissue ratios of anticancer agents in radioimmunotherapy, Xiao et al. studied a three-step strategy for targeting drug carriers to human ovarian carcinoma cells in vitro.⁶⁴ The approach consists of prelabeling target cells with biotinylated anti-CA125 antibody and streptavidin prior to administration of biotinylated liposomes. Biotinylated, conventional liposomes were

specifically and effectively delivered to OVCAR-3 cells prelabeled with biotinylated B43.13.1 and streptavidin. The slow internalization and shedding properties of these antibodies are useful for multistep pre-targeting methods. Thus, a modified targeting strategy, utilizing a bispecific antibody and liposomes, may be feasible for radioimmunoliposomal therapy of ovarian cancer.⁶⁵

Most important clinical radioimmunotherapy studies

The most important clinical trials are summarized in Table 26.4. Since access to the tumor site is a limiting factor in targeting solid tumors, the locoregional routes of administration show several advantages. The efficacy of the treatment can be affected by several variables; however, the intraperitoneal route has been chosen by the majority of investigators for their clinical trials in order to obtain optimal delivery of the radioconjugates. Even if several issues affect tumor targeting with the intraperitoneal approach (penetration of mAb, clearance from cavity, local biodistribution of radioimmunoconjugates), there is evidence that the intraperitoneal route allows the administration of high activities of radioisotopes with relatively low toxicity. ^{131}I -labeled immunoconjugates have been used without limiting problems of toxicity; in fact, the predictable myelotoxic effects are correlated to the radiation dose, and activities up to 3.7–5.55 GBq can be administered with negligible toxicity. Also, the myelotoxicity consequent to ^{90}Y -labeled radioimmunoconjugate treatment was limited at activities ranging from 555 to 740 MBq when DOTA was used as chelating agent. Radioimmunoconjugates as alternatives to ^{131}I and ^{90}Y have been actively investigated for clinical applications in order to explore the possibility of optimizing the therapeutic efficacy of RIT. ^{177}Lu -labeled radioimmunoconjugates seem to be very promising due to the physical characteristics of this radioisotope, which emits both β and γ radiation, and the reliable radiolabeling procedure.

Reviewing the clinical trials it is evident that intraperitoneal RIT offers great benefits to patients with small-volume disease. All investigations demonstrate that patients with limited residual tumor burden (nodules <2 cm in diameter) showed a prolonged disease-free period when compared with historical controls.^{51,66} Furthermore, patients with minimal residual disease have achieved complete response after RIT.^{44,67} In contrast, clinical effects are limited in patients with tumors larger than 2 cm in diameter, and the non-success could be mainly attributed to the poor penetration of mAb in cancer masses and to the range of irradiation penetration.⁶⁸ Some clinical trials in patients with negative second-look laparotomy who

Table 26.4 Most important clinical trials using radiomunotherapy

<i>Author</i>	<i>Year</i>	<i>Antibody</i>	<i>Isotope and activity (GBq)</i>	<i>Via, patients (n)</i>	<i>Stage</i>	<i>Residual disease</i>	<i>Response</i>
<i>MUC1</i>							
Epenetos ³⁶	1987	Murine IgG, HMFG1	¹³¹ I up to 7.4 (dose-escalating)	ip, 24	III after CT	Small volume	4 CR, 5 SD
Nicholson ³⁷	1998	Murine IgG, HMFG1	⁹⁰ Y 0.67/m ²	ip, 25	IC–IV after CT	Complete clinical remission	70% 10-year OS
Epenetos ³⁸	2000	Murine IgG, HMFG1	⁹⁰ Y 0.67/m ²	ip, 52	III–IV after CT	Complete clinical remission	15/21 longer OS
Verheijen ⁴⁰	2006	Murine IgG, HMFG1	⁹⁰ Y 0.67/m ²	ip, 447	IC–IV after CT	Complete clinical remission	No difference
<i>Folate receptor</i>							
Crippa ⁴⁴	1995	Murine IgG, MOv18	¹³¹ I 3.7	ip, 16	III	Minimal	5 CR, 6 SD
van Zanten-Przybysz ⁴⁵	2000	Chimeric IgG, MOv18	¹³¹ I 3	iv, 3	III	Minimal	3 SD
<i>TAG72</i>							
Alvarez ⁵¹	1997	Murine IgG, CC49	¹⁷⁷ Lu up to 1.665/m ² (dose-escalating)	ip, 27	IC–IV	Gross disease, small nodules < 1 cm	1 PR, 2 SD, 4 DFS 6–35 months
Rosenblum ⁴⁹	1999	Murine IgG, B72.3	⁹⁰ Y up to 1.48/m ² (dose-escalating)	ip, 38	III–IV after CT	Minimal refractory ascites	2CR, 2MR
Meredith ⁵²	2001	Murine IgG, CC49	¹⁷⁷ Lu up to 1.48/m ² (dose-escalating)	ip, 34	III after CT	Recurrent, persistent	4PR, 4 PFS 18–37 months
Alvarez ⁵³	2002	Murine IgG, CC49	⁹⁰ Y up to 0.895/m ² (dose-escalating)	ip, 20	III after CT	Persistent, delayed recurrence	2PR, 2 DFS 18 months
<i>CA125</i>							
Mahe ³¹	1999	Murine IgG, OC125, F(ab') ₂	¹³¹ I 4.44	ip, 6	III after CT	Minimal	3 SD

IgG, immunoglobulin G; ip, intraperitoneal; iv, intravenous; CT, computed tomography; CR, complete response; SD, stable disease; OS, overall survival; PR, partial response; DFS, disease-free survival; MR, minor response; PFS, progression-free survival.

received intraperitoneal RIT as an adjuvant treatment demonstrated an increased disease-free survival.^{53,66} Intraperitoneal RIT can have also a palliative effect on recurrent and symptomatic chemotherapy-resistant ascites.⁶⁹

Twenty-seven patients who failed chemotherapy entered a phase I/II trial of intraperitoneal [¹⁷⁷Lu]CC49 mAb. Patients had disease confined to the abdominal cavity, and retroperitoneal lymph nodes.⁵¹ The maximum tolerated activity was 1.67 GBq/m². The most common side-effects were delayed transient arthralgia (ten out of 27 patients) and bone marrow suppression at the maximum tolerated dose. One of 13 patients with gross disease

had >50% tumor reduction after therapy, while most others progressed (one had stable disease and went off study). Two of nine patients with small nodules (<1 cm) progressed in 21 months, and two of nine remained without evidence of disease at 4–5 months. Among patients with microscopic occult disease, one relapsed at 10 months and four of five remained without evidence of disease at 6–35 months.

Some attempts to increase the antigen expression on cancer cells have also been made with the combined administration of interferon.⁵³ Another phase I/II trial with [¹⁷⁷Lu]CC49 mAb has been carried out to assess

the feasibility of combining interferon and Taxol with intraperitoneal RIT.⁵² Patients with recurrent or persistent ovarian cancer after first line chemotherapy were enrolled. IFN was administered as four subcutaneous injections before RIT to increase the expression of TAG72, and this increased hematological toxicity. Taxol was given intraperitoneally 48 hours before RIT. A subsequent group of patients were treated with IFN, 100 mg/m² Taxol®, and escalating doses of [¹⁷⁷Lu]CC49. The maximum tolerated dose was 1.48 GBq/m² given with IFN plus 100 mg/m² Taxol. Therapy was well tolerated with the expected reversible hematological toxicity. IFN increased the effective whole body radiation dose. Four of 17 patients with measurable disease had a partial response, and four of 27 patients with non-measurable disease had progression-free intervals of 18–37 months.

Concluding remarks

At present, is not clear what is the most effective RIT for ovarian cancer, since many immunoreagents have been studied and the different results depend on the mAb type used, the protocol of administration, and the characteristics of the radioisotope. Also, the choice of optimal radionuclide for RIT still remains an open problem, depending upon its efficacy on physical characteristics, availability and cost, specific activity, method of radiolabeling, and biokinetics, which is related to the radiopharmaceutical bioavailability. The route generally used is the intraperitoneal one since ovarian cancer disease, in the majority of patients, involves the abdominal cavity. Looking at papers published in the literature, the radioisotopes mostly investigated are iodine-131 and yttrium-90. Much experience has been gained with the ¹³¹I-labeled radioimmunoconjugates, and recently great progress has been achieved in labeling yttrium-90 to some stable chelating agents, such as DOTA.

As already mentioned above, the intraperitoneal route does not guarantee the efficient targeting of retroperitoneal, lymph node, and hematogenous metastases, even if the spread of ovarian cancer is often limited to the abdomen. Investigations using RIT via the intravenous route, using the same mAb as utilized intraperitoneally or other radiopharmaceuticals (chimeric antibodies, immunoreactive fragments, or radiolabeled peptides), can provide further information about the real efficacy of this approach.

The data collected to date and the ongoing clinical trials do not give sufficient evidence in order to draw any reliable conclusions about these treatments.

Speaking about toxicity, it should be noted that intraperitoneal administration gives a very low toxicity, in spite of the fact that it is possible to reach a high activity of the injected radiolabeled mAb. The

dose-limiting organ is the bone marrow, with myelosuppression that arises about 1 month after injection. Hypersensitivity reactions to human anti-mouse antibodies (HAMA) are sometimes described and generally well tolerated, and occur from 1 to 3 weeks after the treatment. Anaphylaxis is rare and some elevations of hepatic enzymes have also been described, but without clinical importance.

The overall data emerging from evaluations of clinical trials of RIT through the intraperitoneal route support the concept that RIT can have a role in the treatment of small lesions of ovarian cancer and minimal residual disease. Our opinion is that indications for RIT should be moved from advanced disease after first and second line therapy to earlier phases of therapy, in those patients not radically operated, in order to eliminate residual disease, or in patients already treated and with second look negative, as adjuvant therapy. Other possible applications of RIT are in combination with chemotherapy, as biological response modifiers, or with radiotherapy in order to enhance its anticancer effectiveness.

Acknowledgment

The Editors are grateful to the 'Fondazione CARIPLO, Milano', for having partially supported the activities described in this chapter and the research in the field.

References

1. Nicodemus CF, Berek JS. Monoclonal antibody therapy of ovarian cancer. *Expert Rev Anticancer Ther* 2005; 5: 87–96.
2. Carter PJ. Potent antibody therapeutics by design. *Nature Rev Immuno* 2006; 6: 343–57.
3. Shockley T, Lin K, Sung C et al. A quantitative analysis of tumour specific monoclonal antibody uptake by human melanoma xenografts: effects of antibody immunological properties and tumour antigen expression levels. *Cancer Res* 1992; 52: 357–66.
4. Kennel S. Effects of target antigen competition on distribution of monoclonal antibody to solid tumours. *Cancer Res* 1992; 52: 1284–90.
5. Kennel S, Falcioni R, Wesley J. Microdistribution of specific rat monoclonal antibodies to mouse tissue and human tumour xenografts. *Cancer Res* 1991; 51: 1529–39.
6. Shockley T, Lin K, Nagy S et al. Spatial distribution of tumour-specific monoclonal antibodies in human melanoma xenografts. *Cancer Res* 1992; 52: 367–76.
7. Jain RK. Physiological barriers to delivery of monoclonal antibodies and other macromolecules in tumors. *Cancer Res* 1990; 50: 814s–19s.
8. Choi J, Credit K, Henderson K et al. Intraperitoneal immunotherapy for metastatic ovarian carcinoma: resistance of intratumoral collagen to antibody penetration. *Clin Cancer Res* 2006; 12: 1906–12.

9. Goldenberg DM. Targeted therapy of cancer. *J Nucl Med* 2002; 43: 693–713.
10. Ross J, Gray K, Schenkein D et al. Antibody-based therapeutics in oncology. *Expert Rev Anticancer Ther* 2003; 3: 107–21.
11. Sharkey RM, Goldenberg DM. Perspectives on cancer therapy with radiolabeled monoclonal antibodies. *J Nucl Med* 2005; 46: 115s–27s.
12. Koppe MJ, Postema EJ, Aarts F et al. Antibody guided radiation therapy of cancer. *Cancer Metastasis Rev* 2005; 24: 539–67.
13. Wilbur DS. Radiohalogenation of proteins: an overview of radionuclides, labeling methods, and reagents for conjugate labeling. *Bioconjug Chem* 1992; 3: 433–70.
14. Zalutsky MR, Garg PK, Narula AS. Labeling monoclonal antibodies with halogen nuclides. *Acta Radiol* 1990; 374 (Suppl): 141–5.
15. Volkert WA, Hoffman TJ. Therapeutic radiopharmaceuticals. *Chem Rev* 1999; 99: 2269–92.
16. Iznaga-Escobar N. Direct radiolabeling of monoclonal antibodies with rhenium-188 for radioimmunotherapy of solid tumors—a review of radiolabeling characteristics, quality control and in vitro stability studies. *Appl Radiat Isot* 2001; 54: 399–406.
17. Bast RC Jr, Feeney M, Lazarus H et al. Reactivity of a monoclonal antibody with human ovarian carcinoma. *J Clin Invest* 1981; 68: 1331–7.
18. Whitehouse C, Solomon E. Current status of the molecular characterization of the ovarian cancer antigen CA125 and implications for its use in clinical screening. *Gynecol Oncol* 2003; 88: S152–7.
19. Mukherjee P, Madsen CS, Ginardi AR. Mucin 1-specific immunotherapy in a mouse model of spontaneous breast cancer. *J Immunother* 2003; 26: 47–62.
20. Miles DW, Taylor-Papadimitriou J. Therapeutic aspects of polymorphic epithelial mucin in adenocarcinoma. *Pharmacol Ther* 1999; 82: 97–106.
21. Sarandakou A, Phocas I, Botsis D et al. Tumour-associated antigens CEA, CA125, SCC and TPS in gynaecological cancer. *Eur J Gynaecol Oncol* 1998; 19: 73–7.
22. Coney LR, Tomassetti A, Carayannopoulos L et al. Cloning of a tumor associated antigen: MOv18 and MOv19 antibodies recognize a folate-binding protein. *Cancer Res* 1991; 51: 6125–32.
23. Toffoli G, Cernigoi C, Russo A et al. Overexpression of folate binding protein in ovarian cancers. *Int J Cancer* 1997; 74: 193–8.
24. Thor A, Gorstein F, Ohuchi N. Tumor-associated glycoprotein (TAG-72) in ovarian carcinomas defined by monoclonal antibody B72.3. *J Natl Cancer Inst* 1986; 76: 995–1006.
25. Welshinger M, Yin BW, Lloyd KO. Initial immunochemical characterization of MX35 ovarian cancer antigen. *Gynecol Oncol* 1997; 67: 188–92.
26. Scott AM, Geleick D, Rubira M et al. Construction, production, and characterization of humanized anti-Lewis Y monoclonal antibody 3S193 for targeted immunotherapy of solid tumors. *Cancer Res* 2000; 60: 3254–61.
27. Zhang S, Zhang HS, Cordon-Cardo C et al. Selection of tumor antigens as targets for immune attack using immunohistochemistry: II. Blood group-related antigens. *Int J Cancer* 1997; 73: 50–6.
28. Thedrez P, Saccavini JC, Nolobe D et al. Biodistribution of indium-111-labeled OC 125 monoclonal antibody after intraperitoneal injection in nude mice intraperitoneally grafted with ovarian carcinoma. *Cancer Res* 1989; 49: 3081–6.
29. Jimenez-Vicioso A, Torres M, Jimenez-Heffernan A et al. Immunoscintigraphy with ¹³¹I or ¹¹¹In labelled OC 125 F(ab')₂ fragments in patients with ovarian carcinoma. *Int J Biol Markers* 1990; 5: 159–65.
30. Peltier P, Dutin JP, Chatal JF et al. Usefulness of imaging ovarian cancer recurrence with In-111-labeled monoclonal antibody (OC 125) specific for CA 125 antigen. The INSERM Research Network (Nantes, Rennes, Reims, Villejuif, Saclay). *Ann Oncol* 1993; 4: 307–11.
31. Mahe MA, Fumoleau P, Fabbro M et al. A phase II study of intraperitoneal radioimmunotherapy with iodine-131-labeled monoclonal antibody OC-125 in patients with residual ovarian carcinoma. *Clin Cancer Res* 1999; 5 (10 Suppl): 3249s–53s.
32. McQuarrie SA, Baum RP, Niesen A et al. Pharmacokinetics and radiation dosimetry of ^{99m}Tc-labelled monoclonal antibody B43.13 in ovarian cancer patients. *Nucl Med Commun* 1997; 18: 878–86.
33. Sykes TR, Somayaji VV, Bier S. Radiolabeling of monoclonal antibody B43.13 with rhenium-188 for immunoradiotherapy. *Appl Radiat Isot* 1997; 48: 899–906.
34. Berger MA, Masters GR, Singleton J et al. Pharmacokinetics, biodistribution, and radioimmunotherapy with monoclonal antibody 776.1 in a murine model of human ovarian cancer. *Cancer Biother Radiopharm* 2005; 20: 589–602.
35. Arklie J, Taylor-Papadimitriou J, Bodmer WF et al. Differentiation antigens expressed by epithelial cells in lactating breast are also detectable in breast cancer cells. *Int J Cancer* 1981; 28: 23–9.
36. Epenetos AA, Munro AJ, Stewart S et al. Antibody-guided irradiation of advanced ovarian cancer with intraperitoneally administered radiolabeled monoclonal antibodies. *J Clin Oncol* 1987; 5: 1890–9.
37. Nicholson S, Gooden CS, Hird V et al. Radioimmunotherapy after chemotherapy compared to chemotherapy alone in the treatment of advanced ovarian cancer. A matched analysis. *Oncol Rep* 1998; 5: 223–6.
38. Epenetos AA, Hird V, Lambert H et al. Long term survival of patients with advanced ovarian cancer treated with intraperitoneal radioimmunotherapy. *Int J Gynecol Cancer* 2000; 10 (Suppl 1): 44–6.
39. Janssen ML, Pels W, Massuger LF et al. Intraperitoneal radioimmunotherapy in an ovarian carcinoma mouse model: effect of the radionuclide. *Int J Gynecol Cancer* 2003; 13: 607–13.
40. Verheijen RH, Massuger LF, Benigno B et al. Phase III trial of intraperitoneal therapy with Yttrium-90-labeled HMFG1 murine monoclonal antibody in patients with epithelial ovarian cancer after a surgically defined complete remission. *J Clin Oncol* 2006; 24: 571–8.
41. Juweid M, Sharkey RM, Alavi A. Regression of advanced refractory ovarian cancer treated with ¹³¹I-labeled anti-CEA monoclonal antibody. *J Nucl Med* 1997; 38: 257–60.

42. Sharkey RM, Juweid M, Shevitz J et al. Evaluation of a complementarity-determining region-grafted (humanized) anti-carcinoembryonic antigen monoclonal antibody in preclinical and clinical studies. *Cancer Res* 1995; 55: 5935s–45s.
43. Miotti S, Canevari S, Menard S. Characterization of human ovarian carcinoma-associated antigens defined by novel monoclonal antibodies with tumor-restricted specificity. *Int J Cancer* 1987; 39: 297–303.
44. Crippa F, Bolis G, Seregini E et al. Single dose intraperitoneal radioimmunotherapy with the murine monoclonal antibody ¹³¹I-MOv18: clinical results in patients with minimal residual disease of ovarian cancer. *Eur J Cancer* 1995; 31A: 686–90.
45. van Zanten-Przybysz I, Molthoff CF, Roos JC et al. Radioimmunotherapy with intravenously administered ¹³¹I-labeled chimeric monoclonal antibody MOv18 in patients with ovarian cancer. *J Nucl Med* 2000; 41: 1168–76.
46. Andersson H, Lindgren S, Back T et al. Radioimmunotherapy of nude mice with intraperitoneally growing ovarian cancer xenograft utilizing ²¹¹At-labelled monoclonal antibody MOv18. *Anticancer Res* 2000; 20: 459–62.
47. Coliva A, Zacchetti A, Luison E et al. ⁹⁰Y labeling of monoclonal antibody MOv18 and preclinical validation for radioimmunotherapy of human ovarian carcinomas. *Cancer Immunol Immunother* 2005; 54: 1200–13.
48. Colcher D, Horn Hand P, Nuti M. A spectrum of monoclonal antibodies reactive with human mammary tumor cells. *Proc Natl Acad Sci USA* 1981; 78: 3199–203.
49. Rosenblum MG, Verschraegen CF, Murray JL et al. Phase I study of ⁹⁰Y-labeled B72.3 intraperitoneal administration in patients with ovarian cancer: effect of dose and EDTA coadministration on pharmacokinetics and toxicity. *Clin Cancer Res* 1999; 5: 953–61.
50. Tempero M. High dose therapy with ⁹⁰-Yttrium labelled monoclonal antibody CC49: a phase I trial. *Clin Cancer Res* 2000; 6: 3095–102.
51. Alvarez RD, Partridge EE, Khazaeli MB et al. Intraperitoneal radioimmunotherapy of ovarian cancer with ¹⁷⁷Lu-CC49: a phase I/II study. *Gynecol Oncol* 1997; 65: 94–101.
52. Meredith RF, Alvarez RD, Partridge EE et al. Intraperitoneal radioimmunotherapy of ovarian cancer: a phase I study. *Cancer Biother Radiopharm* 2001; 16: 305–15.
53. Alvarez RD, Huh WK, Khazaeli MB, A phase I study of combined modality (⁹⁰)yttrium-CC49 intraperitoneal radioimmunotherapy for ovarian cancer. *Clin Cancer Res* 2002; 8: 2806–11.
54. Rubin SC, Kostakoglu L, Divgi C et al. Biodistribution and intraoperative evaluation of radiolabeled monoclonal antibody MX35 in patients with epithelial ovarian cancer. *Gynecol Oncol* 1993; 51: 61–6.
55. Elgqvist J, Andersson H, Bäck T. Therapeutic efficacy and tumor dose estimations in radioimmunotherapy of intraperitoneally growing OVCAR-3 cells in nude mice with ²¹¹At-labeled monoclonal antibody MX35. *J Nucl Med* 2005; 46: 1907–15.
56. Finstad CL, Lloyd KO, Federici MG et al. Distribution of radiolabeled monoclonal antibody MX35 F(ab')₂ in tissue samples by storage phosphor screen image analysis: evaluation of antibody localization to micrometastatic disease in epithelial ovarian cancer. *Clin Cancer Res* 1997; 3: 1433–42.
57. Back T, Andersson H, Divgi CR. ²¹¹At radioimmunotherapy of subcutaneous human ovarian cancer xenografts: evaluation of relative biologic effectiveness of an alpha-emitter in vivo. *J Nucl Med* 2005; 46: 2061–7.
58. Hellstrom I, Garrigues HJ, Garrigues U, Hellstrom KE. Highly tumor reactive, internalizing, mouse monoclonal antibodies to Le^y-related cell surface antigens. *Cancer Res* 1990; 50: 2183–90.
59. Clarke K, Lee F, Brechbiel MW et al. In vivo biodistribution of a humanized anti-lewis Y monoclonal antibody (hu3S193) in MCF-7 xenografted BALB/c nude mice. *Cancer Res* 2000; 60: 4804–11.
60. Verri E, Guglielmini P, Puntoni M et al. HER2/neu oncoprotein overexpression in epithelial ovarian cancer: evaluation of its prevalence and prognostic significance. Clinical study. *Oncology* 2005; 68: 154–61.
61. Horak E, Hartmann F, Garmestani K et al. Radioimmunotherapy targeting of HER2/neu oncoprotein on ovarian tumor using lead-212-DOTA-AE1. *J Nucl Med* 1997; 38: 1944–50.
62. Borchardt PE, Quadri SM, Freedman RS, Vriesendorp HM. Intraperitoneal radioimmunotherapy with human monoclonal IGM in nude mice with peritoneal carcinomatosis. *Cancer Biother Radiopharm* 2000; 15: 53–64.
63. Boerman OC, van Schaijk FG, Oyen WJ et al. Pretargeted radioimmunotherapy of cancer: progress step by step. *J Nucl Med* 2003; 44: 400–11.
64. Xiao Z, McQuarrie SA, Suresh MR, A three-step strategy for targeting drug carriers to human ovarian carcinoma cells in vitro. *J Biotechnol* 2002; 94: 171–84.
65. McQuarrie SA, Xiao Z, Miller GG, Mercer JR, Suresh MR. Modern trends in radioimmunotherapy of cancer: pretargeting strategies for the treatment of ovarian cancer. *Q J Nucl Med* 2001; 45: 160–6.
66. Hird V, Maraveyas A, Snook D et al. Adjuvant therapy of ovarian cancer with radioactive monoclonal antibody. *Br J Cancer* 1993; 68: 403–6.
67. Maraveyas A, Snook D, Hird V et al. Pharmacokinetics and toxicity of an yttrium-90-CITC-DTPA-HMFG1 radioimmunocjugate for intraperitoneal radioimmunotherapy of ovarian cancer. *Cancer* 1994; 73: 1067–75.
68. Ward B, Mather S, Shepherd J et al. The treatment of intraperitoneal malignant disease with monoclonal antibody guided ¹³¹I radiotherapy. *Br J Cancer* 1988; 58: 658–62.
69. Buckman R, De Angelis C, Shaw P et al. Intraperitoneal therapy of malignant ascites associated with carcinoma of ovary and breast using radioiodinated monoclonal antibody 2G3. *Gynecol Oncol* 1992; 47: 102–9.

New instrumentation

Jörg Eckardt, Klaus Schäfers, and Lars Stegger

Background

Recent years have seen tremendous advancements in nuclear imaging technology. These include the development of new detector materials for both single photon and positron emission imaging, the development of devices dedicated to single-organ imaging, and the development of devices that combine single photon emission computed tomography (SPECT) or positron emission tomography (PET) with computed tomography (CT) in one gantry. Many of these inventions have already been deployed in commercially available scanners and have found widespread clinical acceptance. In this chapter, an overview of these new technologies, either already used in clinical routine or under investigation, is provided, with a focus on oncological imaging.

Detector technology

Imaging in nuclear medicine is based on the tracer principle, which was first applied by Hevesy in 1911. A radioactive pharmaceutical is injected into a living organism and tracked by a detection system. By following the radioactivity from the outside, the distribution of the pharmaceutical can be measured over time. Gamma (γ) radiation-emitting isotopes with well defined γ energies such as technetium-99m (emitting a single γ photon with an energy of 140 keV) are commonly used as radioactive markers for planar and SPECT imaging. For PET, two γ photons with an energy of 511 keV each are produced secondary to a β^+ decay (positron–electron annihilation). A great variety of detectors for γ radiation have been developed over recent decades to allow sensitive and exact measurement of the radioactivity distribution. Camera systems are equipped with such γ photon sensitive detectors for generating projection images by using planar detectors or for generating three-dimensional images by using tomographic devices. No matter which system design has been chosen, the performance of a single detector is the core part of good image quality.

Great effort has been made over recent decades to construct the optimal γ -ray detector for nuclear imaging. The performance characteristics of γ -ray detectors have been constantly improved and optimized for their respective fields of application, resulting in a group of devices with different strengths and weaknesses. Detectors can be based on various principles, such as gas amplification chambers, semiconductors, or inorganic scintillators. However, scintillators using crystalline materials are the most commonly employed for nuclear imaging today. γ photon energy is converted into scintillation light, which can then be converted into free electrons suitable for electronic readout circuits after amplification by devices such as photomultipliers (Figure 27.1). The development of new inorganic crystals with improved performance is one of the major fields in γ detector development.

Inorganic scintillators

In 1948, Robert Hofstadter discovered that inorganic crystalline sodium iodide doped with thallium (NaI(Tl)) is an

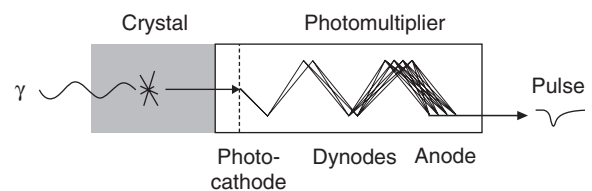


Figure 27.1

Principle of γ photon detection by a scintillation crystal and a photomultiplier tube. The scintillation light is converted into a photoelectron at the photomultiplier entrance window which is then further accelerated towards the first dynode to produce secondary electrons. A dynode cascade multiplies the number of electrons until a measurable signal reaches the anode. The resulting electrical signal pulse is directly proportional to the number of scintillation photons and the absorbed γ photon energy.

excellent scintillator since it produces a very large light output when absorbing γ photons.¹ This discovery established the basis for the development of many imaging modalities, and contributed importantly to the success of modern nuclear medicine. It is remarkable that NaI(Tl) is still the crystal of choice for many imaging devices, although efforts have been made to develop crystals with improved characteristics (Table 27.1). An ideal scintillator would be described by the following properties: a high density and high atomic number for a high detection efficiency for γ photons; good energy resolution to allow precise characterization of the photon energy which can be used to separate scattered from true events; a short decay constant for exact coincidence timing and high count-rate capability; and a high light yield (the number of photons produced per absorbed γ photon) to improve the data readout and to lower the noise level. Other factors such as the refraction index, hygroscopic properties, the presence or absence of natural radioactivity, or the ruggedness of the material may also be important for construction of an ideal detector.

The dominant decay time of the scintillation pulse for sodium iodine is 230 ns. This time is comparatively long, and leads to a significant dead time in which no other event can be detected. As the count rate becomes higher, the detector is no longer able to collect and adequately process all events, effectively limiting the amount of injectable radiotracer. Additionally, a fast scintillator allows for a short coincidence time window in PET, decreasing random coincidences. However, the speed of the scintillator is often not a critical factor for a γ camera intended for lower

γ energies (e.g. 140 keV for ^{99m}Tc). Owing to its low cost, NaI(Tl) is still the crystal of choice for most present day γ camera designs.

In 1970, a new crystal material became commercially available, bismuth germanate (BGO). Its main advantage over NaI(Tl) is its higher density (7.13 g/cm³), which results in an increased absorption probability for high energy γ photons. This is of major interest for the design of PET devices, since it allows for the construction of smaller crystals, resulting in a higher spatial resolution without sacrificing sensitivity. One of the drawbacks of BGO is the quite long decay time of 300 ns. Again, this limits the high count rate capability and precludes a narrow coincidence time window. Cerium-doped gadolinium oxyorthosilicate (GSO) is as dense as BGO but with a significantly shorter decay time (60 ns). It is therefore an excellent PET detector. It cleaves easily, which makes fabrication more difficult. Both BGO and GSO suffer from a relatively low light yield compared to NaI(Tl). Cerium-doped lutetium oxyorthosilicate (LSO) offers a significantly better light yield compared to BGO and GSO. Together with a fast decay time (40 ns) and high density (7.4 g/cm³), this attribute characterizes this crystal. In fact, many newly developed PET scanners are equipped with LSO crystals today. Time-of-flight information of the traveling photons becomes measurable in PET with faster crystals such as LSO or LYSO (with yttrium). This can effectively improve the signal-to-noise properties of the reconstructed images. Several PET scanner prototypes equipped with alternative crystals are currently under construction.

Table 27.1 Properties of scintillator crystals for γ photon detection.²⁻⁹ Values are approximations and can vary depending on crystal impurities, growing conditions, etc.

Name	Density (g/cm ³)	Energy resolution (%)	Decay time (ns)	Light yield (ph/MeV)
NaI (Tl)	3.7	6	230	38 000
BGO	7.1	9	300	8200
GSO:Ce	6.7	8	60	10 000
LSO:Ce	7.4	10	40	28 000
LYSO:Ce	5.4	10	40	28 000
LuAP:Ce	8.3	7	17	12 000
LuYAP:Ce	7.1	10	24	10 000
LaBr ₃	5.3	3	25	60 000

BGO, bismuth germanate; GSO, gadolinium oxyorthosilicate; LSO, lutetium oxyorthosilicate; LYSO, yttrium containing LSO; LuAp, lutetium orthoaluminate; LuYAp, yttrium containing LuAp.

Photomultiplier tubes

The conversion of scintillation light into a measurable electrical current is commonly performed by photomultiplier tubes (PMTs). A high gain (leading to a high signal-to-noise ratio), a high speed, ruggedness and stability are the main advantages of PMTs. The basic principle is the conversion of the incoming photon into a photoelectron (photoelectric effect) directly at the PMT entrance window, which is then further accelerated towards the first dynode to produce secondary electrons which are likewise accelerated to produce a measurable electrical signal at the end of the dynode cascade (Figure 27.1). The electrical signal pulse is directly proportional to the number of scintillation photons and in turn the absorbed γ photon energy.

Avalanche photodiodes

Photodiodes are alternative elements for converting the scintillation light into an electrical signal.^{10–13} In semiconductor layers, light can be used to generate electron–hole pairs. The detection principle is characterized by the junction (depletion layer) between n-type and p-type materials, which is generated by doping. Electron–hole pairs that are created near the junction cause an electrical signal by moving out of the depletion layer due to an intrinsic electric field. An external voltage is applied to increase this effect. For higher quantum efficiency the thickness of the depletion layer is increased in positive intrinsic negative (PIN) diodes with a wide, undoped intrinsic semiconductor region between the p-type semiconductor and n-type semiconductor (Figure 27.2). PIN diodes have no internal gain. Therefore, energy resolution is determined by electronic noise rather than photoelectron statistics, as in the case of PMTs.

To overcome this limitation, a new class of photodiodes with internal gain has been developed – avalanche

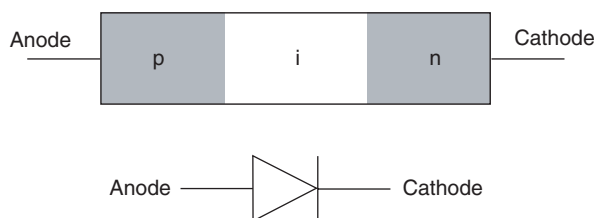


Figure 27.2

Scheme of a positive intrinsic negative (PIN) diode. The detection principle is characterized by the junction (depletion layer) between n-type and p-type materials, which are generated by doping. Electron–hole pairs that are created near the junction cause an electrical signal by moving out of the depletion layer.

photodiodes (APDs).^{14,15} The basic idea is that a specially designed semiconductor-based photodiode is operated with a relatively high reverse voltage. If an electron is created after light absorption, the electron is accelerated in the electric field, causing further electron–hole pairs by impact ionization. This avalanche process effectively amplifies the photocurrent, which is helpful in producing very sensitive detectors. The main advantages of APDs compared to PMTs are their compactness, insensitivity to magnetic fields, and their low price, even with large active areas.

SPECT developments

Most commercial γ cameras available today are still based on the original design by Hal Anger, who combined a single flat NaI(Tl) scintillator crystal with a number of photomultiplier tubes for highly sensitive and position-encoded count detection (Figure 27.3).¹⁶ The detector has to be combined with a collimator that serves to focus the γ radiation onto the detector. The most widely applied design is that of a parallel-hole collimator that allows only photons with a trajectory path that is nearly perpendicular to the detector to reach the scintillator; all others are absorbed. Collimators are optimized with respect to photon energy, sensitivity, and resolution, depending on the radiotracer and the clinical protocol. Modern γ cameras offer a vastly improved image quality owing to many technical advancements in the fields of electronics and digitization. Therefore, much present-day development still focuses on image enhancement, e.g. by scatter and attenuation correction, for traditional Anger cameras. New camera designs

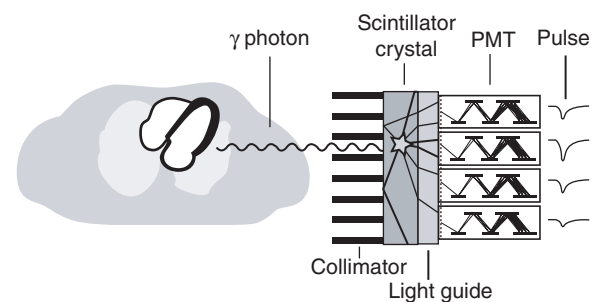


Figure 27.3

Principle of an Anger γ camera. A large flat scintillator crystal is combined with a light guide and an array of photomultiplier tubes (PMTs). A collimator (depicted is a parallel-hole collimator) is attached to the detector head to absorb photons with an oblique trajectory path. During event detection, all PMTs produce differently shaped electrical signal pulses dependent on their positions relative to the locus position of γ photon impact. Electronic circuitry is used to calculate the locus of γ photon impact from the pulses.

based on semiconductor detectors are currently under development and are likely to become commercially viable in the foreseeable future. A completely new concept of a γ camera is that of a 'Compton' camera. This design obviates the need for collimators and consequently leads to a significant increase in sensitivity.

Attenuation and scatter correction

Scatter and attenuation are known to degrade the image quality in emission imaging significantly.

Scatter correction

Inelastically (Compton) scattered photons lose energy to the surrounding tissue and may change their trajectory path considerably. Compton scatter deserves particular attention since it can lead to image blur. An effective way to correct for scatter is to optimize the energy resolution of the imaging system. The energy of unscattered photons is close to the photo peak, whereas the energy of scattered photons is lower. By defining an energy window around the photo peak, many scattered photons with an energy outside of this window can be excluded from image generation. This approach to scatter correction has been successfully implemented for many years. More advanced correction techniques that also strive to eliminate scattered photons with energies within the acceptance window do not only record counts with an energy deposition near the photo peak. They also utilize count rate information from additional energy windows. In the *Compton-windows subtraction technique* all counts from an energy window below the photo peak are also recorded, multiplied by a constant factor k , and subtracted from the photo peak image.¹⁷ The *split photo peak method* estimates the amount of scattered events from the fraction of counts in a bisected photo peak window.¹⁸ For imaging of isotopes that emit photons of different energies such as iodine-123 or gallium-67, down-scatter from higher energy photons into the photopeak window occurs. Ogawa and coworkers have proposed a triple window technique where the amount of scatter is estimated from counts acquired in energy windows above and below the photo peak window.¹⁹

In addition to these long established windowing techniques, newer software based methods for scatter elimination have been developed. The image of a point source (point spread function, PSF) surrounded by tissue is degraded by the limited intrinsic resolution of the imaging device, by photon attenuation, and also by scatter. The long tails of the PSF are mainly due to scatter, so that scatter causes an effect on the original activity distribution that is similar to that of a low-pass filter. Knowledge about how

scatter degrades the image of a point source can be used to correct images of a complex activity distribution encountered in clinical nuclear medicine. To understand the ideas behind these techniques it is important to know that the image of a complex activity distribution can be exactly described as the 'convolution' of the original activity distribution and the PSF, where convolution is a special mathematical calculation. This means that the image of a scan can be exactly calculated if the original activity distribution and the PSF are known (in practice only approximations for the PSF are feasible). In nuclear imaging we are confronted with the inverse problem. Hence it should, in theory, be possible to measure the PSF, correct the PSF for scatter, and calculate the images by deconvolution (the inverse of convolution). However, data quality is not good enough for direct deconvolution, so equivalent numerical algorithms are used. These scatter correction techniques can be incorporated into the process of image reconstruction in SPECT imaging, together with techniques for attenuation correction.

Attenuation correction

Emitted γ photons may be absorbed by the surrounding tissue without reaching the detector, a process called attenuation. Since the magnitude of attenuation depends on the shape and density of tissue that the photons travel through, attenuation is not isotropic in the body and is also patient specific. Therefore, for best results, attenuation must be measured individually using an external radiation source ('transmission scan'). Different types of attenuation measurements have been implemented using rotating point, line, or flat panel sources of radioactive material with known activity, or, for newer camera designs, using X-ray sources in combined SPECT-CT devices (see Chapter 27 for a more detailed description of CT-based attenuation correction in combined SPECT-CT and PET-CT). Simultaneous transmission and emission scanning is possible when using radioactive sources. A more detailed description of the available attenuation correction methodologies can be found elsewhere.²⁰

Compton camera

One of the major limitations in all traditional single photon emission cameras is the need for mechanical apertures (collimators) to restrict the incoming photon pathways. This decreases the sensitivity of the camera system substantially.

Compton cameras overcome this limitation by avoiding mechanical apertures altogether. Instead, they use the physical principle of Compton scattering to obtain information

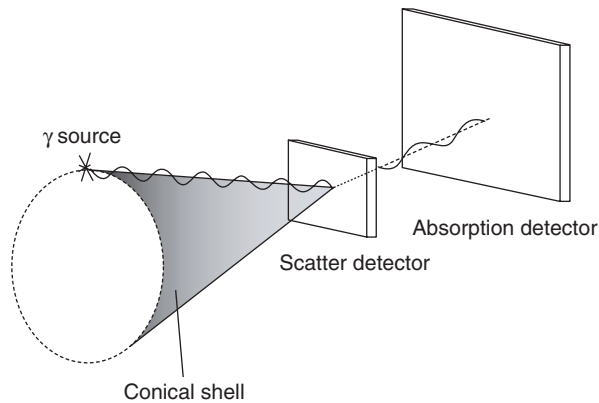


Figure 27.4

Principle of a Compton camera. The emitted γ photon of a radiation source Compton-scatters within a first detector (scatter detector) while the deposited energy and the exact position is recorded. A second detector (absorption detector) located directly behind the scatter detector absorbs the scattered γ photon and registers position and energy. By using all the acquired information, the possible origin of the γ photon can be restricted to lie on a well defined conical shell.

about the γ photon's trajectory path. Although the theoretical concept of a Compton camera was described many years ago,^{21,22} the immense technical challenges have hampered a direct translation of this idea into a commercial product.

In principle, the emitted γ photon of a radiation source Compton-scatters within a first detector (scatter detector), and the deposited energy and the exact position of the scatter event is recorded (Figure 27.4). A second detector (absorption detector) located directly behind the scatter detector absorbs the scattered γ photon, and, again, both position and energy are registered. Using all the acquired information, the possible origin of the γ photon can be restricted to lie on a well defined conical shell. Sophisticated reconstruction algorithms have been developed to obtain a three-dimensional (3D) distribution image.²³ At present, the obtainable spatial resolution is still not good enough to be usable for routine applications.

PET developments

Basic principle

Positron emission tomography is a powerful imaging technology. It utilizes the liberation of positrons in β^+ -decay events and their interaction with the surrounding tissue. A positron is emitted and rapidly loses its kinetic energy in dense material such as body tissue. If most of its kinetic energy is lost, it can interact with an electron, leading to positron–electron annihilation, since positrons are the

antimatter particles of electrons. The mass-equivalent energy of the two particles is converted into electromagnetic energy. Most often two γ photons with an energy of 511 keV each will be produced that fly in nearly 180°-opposing directions at the speed of light. Ideally, both annihilation photons are detected by the detectors commonly arranged in a ring system (Figure 27.5). If two photons are measured within a certain time frame (coincidence time window), they will be accepted as a coincidence pair which stem from one annihilation process. The annihilation process is known to have occurred on the line between the two photon detectors (line of response, LOR) in the case of non-scattered γ photons. Since the locus of the β^+ -decay event is very close to the locus of the annihilation process, the coincidence detection principle in PET acts like an electronic collimation. This obviates the need for physical collimation as in SPECT imaging. Each detector is connected to a fan of detectors on the opposite side of the ring by means of coincidence detection circuitry. For all other detector pairs the associated LORs do not traverse the scanner's field of view, and can therefore be ignored. Usually a number of detector rings are combined to improve sensitivity and to increase the axial field of view.

Ideally, only true non-scattered coincidence events would be recorded by PET. However, certain detector limitations as well as interactions of the 511-keV photons with tissue lead to other types of events such as random, scattered, or multiple coincidences. Random coincidences

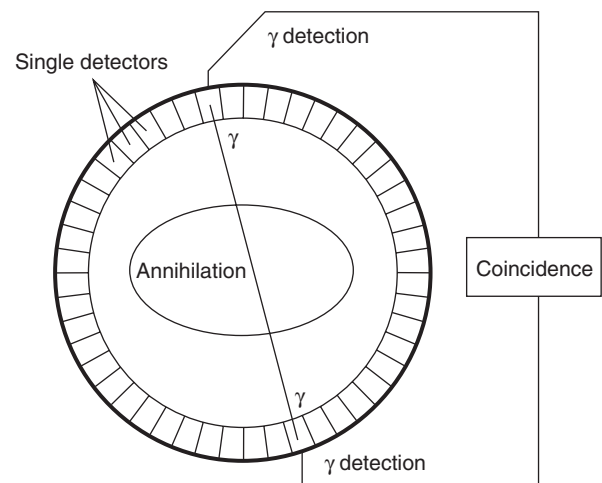


Figure 27.5

Principle of positron emission tomography (PET) coincidence detection. Two annihilation photons are recognized by the detectors commonly arranged in a ring system. If two photons are measured within a certain time frame (coincidence time window) they will be accepted as a coincidence pair (except for random coincidences) that stem from one annihilation process. The annihilation process is assumed to have occurred on the line between the two photon detectors in the case of non-scattered γ photons.

are recorded, if two photons that stem from two different annihilation processes are detected within the coincidence time window. They are then mistaken for photons that stem from the same annihilation event, leading to a wrong LOR assignment. If a 511-keV photon interacts with the body tissue it may be Compton scattered, with a loss of energy and a change in traveling direction. If the redirected photon is then detected with its partner photon in coincidence (scattered coincidence), a misplaced LOR will be recorded. Multiple coincidences may occur at high count rates when three or more events are detected simultaneously. They are commonly rejected.

All of these effects impair image quality. Corrections need to be applied to produce acceptable images. One other major factor that needs to be addressed is the attenuation of emitted photons in the surrounding tissue. Most often attenuation correction is performed by using an additional transmission scan with an external radiation source. For brain imaging, simple model-based approaches may be adequate. In combined PET-CT scanners attenuation correction is based on a CT-derived attenuation map.

2D versus 3D

2D data acquisition used to be the standard in PET for a long time, since it reduces random events and scattered coincidences. By inserting tungsten septa between the detector planes, only the in-plane LORs can reach the scintillators; photons with oblique LORs are absorbed (Figure 27.6).

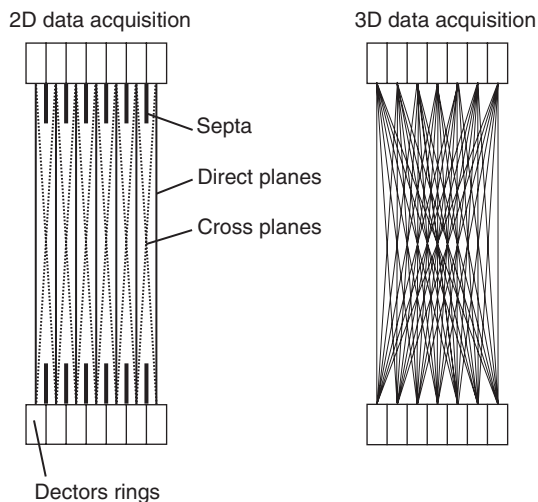


Figure 27.6

Two-dimensional (2D) versus 3D data acquisition. In 2D data acquisition only lines of response (LORs) lying on 'direct planes' or 'cross planes' are detected. Photon pairs on oblique LORs are absorbed by tungsten septa. In 3D-PET also detector pair combinations that represent oblique LORs are accepted.

Most designs accept coincidence events recorded by detectors located in the same detector ring (direct planes), and also events recorded by detectors located in adjacent detector rings (cross planes). By removing the septa between the detector rings (3D data acquisition), also detector pair combinations that represent oblique LORs are possible. Compared to 2D acquisition this leads to a significantly improved sensitivity. This improved sensitivity may yield better signal-to-noise properties, reduced acquisition time, or less radiation exposure. However, this comes at the expense of a higher scatter fraction. Today, 3D imaging has evolved into the standard acquisition mode for brain and whole-body PET imaging. In many combined PET-CT designs septa have been eliminated in favor of a wider gantry opening.

Depth of interaction

The spatial resolution in PET is limited by a number of factors such as positron range, scanner geometry, and detector shape and size. The invention of new technologies to improve spatial resolution is among the major challenges in PET development. One solution is obviously to miniaturize the size of a single detector. While simple in concept, an implementation of this idea without losing sensitivity requires sophisticated approaches. Crystals with a high density, and consequently high stopping power for 511-keV photons, are required. With currently available crystals (BGO, LSO, etc.), the potential for miniaturization is limited. One option is to reduce the width of a single detector while keeping the depth unchanged. The reduced crystal width allows for more precise spatial localization of photons with a trajectory path parallel to the detector (Figure 27.7). For photons with an oblique trajectory path, the relatively large depth may cause a parallax error. When a photon is interacting at the edge of a detector element, the true LOR may not correspond to the assigned LOR, which is defined to intersect the detector's center-of-mass. The parallax error is a typical problem of ring PET scanners, and increases from the center towards the edges of the transaxial field of view (FOV). One technical solution to correct for this effect is the depth-of-interaction (DOI) measurement.²⁴⁻²⁸ Thereby some information about the location of the γ photon interaction within a crystal element can be derived. This is achieved by splitting up a single detector element into several regions with separate data readouts. Although not a standard feature of modern scanners, it has seen first implementation in some PET scanner designs.

Time of flight

The two photons of a coincidence pair may reach the detectors at discrepant time points, dependent on their origin

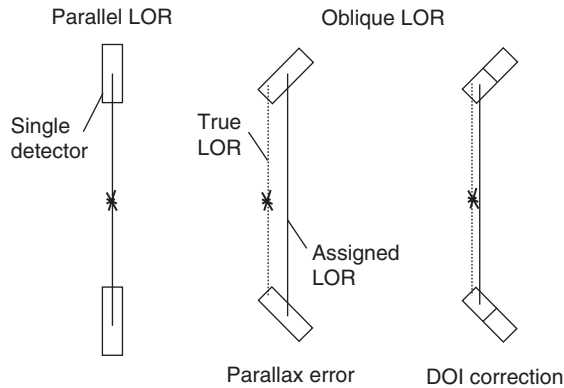


Figure 27.7 Depth-of-interaction (DOI) correction. Photons with an oblique trajectory path may cause a parallax error. The true LOR may not correspond to the assigned LOR, which is defined to intersect the detector’s center-of-mass. DOI measurements can partially correct for this error by deriving information about the location of the γ photon interaction within a crystal element. This can be achieved by splitting up a single detector element into several regions with separate data readouts.

from the respective detectors. Time-of-flight (TOF) PET utilizes this time difference to improve image quality, especially the signal-to-noise ratio, due to a reduction of scattered and random coincidences. Using the additional time information the annihilation point can be restricted to certain sections of the LOR (Figure 27.8), which can be used in specialized reconstruction algorithms.^{29–33} The new generation of fast scintillators such as LSO, LYSO, or LaBr₃ (Table 27.1) have reinvigorated the TOF concept originally developed in the 1970s and 1980s.^{34–42}

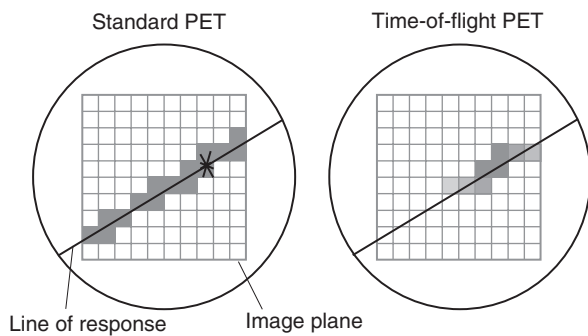


Figure 27.8 Time-of-flight PET (TOF-PET). Two photons of a coincidence pair may reach the detectors at discrepant time points. TOF-PET utilizes this time difference to restrict the possible annihilation point to a certain section of the LOR. This can improve image quality when using sophisticated reconstruction algorithms.

Dedicated imaging devices

The all-purpose γ cameras used today in clinical routine diagnostics allow for manifold acquisition modes, including planar and tomographic (SPECT) scintigraphy, partial-body and whole-body scans, static and dynamic imaging, and, in hybrid systems, also coincidence imaging of positron-emitting radiotracers. This is similar for PET scanners. Although adequate for many clinical applications, the image quality of these all-purpose cameras is likely to be inferior to that of cameras dedicated to single-organ imaging (Table 27.2). One important advantage of dedicated devices is that their geometry is adapted to the organ of interest (Figure 27.9). The organ–detector distance is reduced for better image quality. Additionally, random and scattered coincidences can be reduced in PET.

Nuclear mammographic imaging

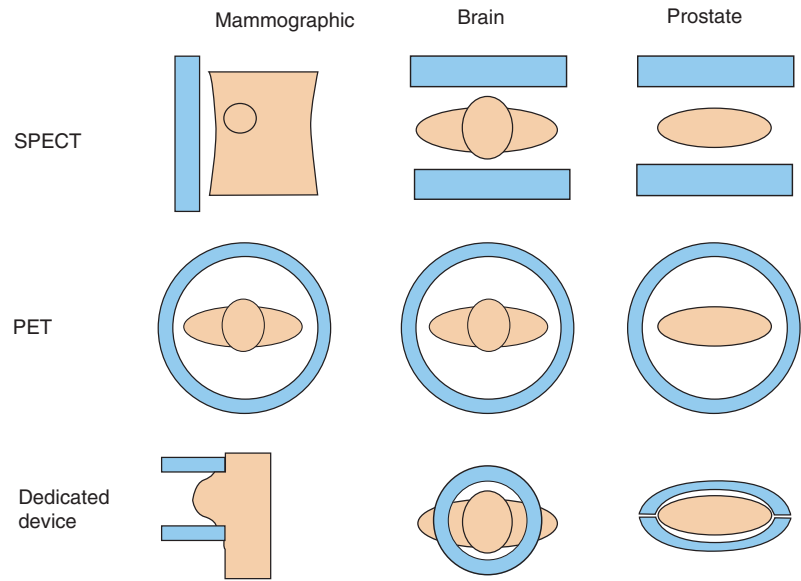
Dedicated devices for molecular imaging are most likely to be deployed in areas with a strong and broad clinical or scientific interest. A prime example is the field of mammographic imaging. Breast cancer is one of the most relevant types of cancer in women. A huge number of imaging procedures, mostly X-ray mammography and ultrasound, are performed every year. In many cases the results obtained are equivocal, and additional molecular imaging is desired. It has been shown that imaging of the breast using an all-purpose γ camera and the technetium-99m labeled radiotracer methoxyisobutylisonitrile ([^{99m}Tc] MIBI) can identify breast cancer.^{43,44} Unlike other imaging modalities, nuclear imaging is not hampered by dense breast tissue and

Table 27.2 Advantages (+) and (–) disadvantages of dedicated devices in comparison to all-purpose systems

	<i>Dedicated</i>	<i>All-purpose</i>
Time needed for patient positioning	+	–
Time needed for camera preparation (collimator change, detector configuration)	+	–
Total cost	+	–
Sensitivity	+	–
Spatial resolution	+	–
Whole-body information	–	+
Variability	–	+

Figure 27.9

Schematic drawing of organ–detector distance for all-purpose single photon emission computed tomography (SPECT) and PET cameras as well as for dedicated devices, depicted for mammographic, brain, and prostate imaging. The human body is displayed in orange, the detectors in blue.

**Figure 27.10**

Photograph of a mammoscintigraphy device (LumaGEM®; Gamma Medica-Ideas, Fornebu, Norway). (Reproduced with kind permission from Gamma Medica-Ideas.)

breast implants. However, lesions with a size of less than 1 cm regularly evade detection.^{45,46} Although whole-body PET systems offer higher spatial resolution than SPECT, the resolution may still be not good enough to detect small lesions. Therefore, dedicated single photon emission (scintimammography) and positron emission (positron mammography, PEM) cameras have been constructed and evaluated.

Dedicated mammographic camera systems are usually equipped with small detector heads in a quadratic or rectangular shape (dimensions of 10×10 up to 20×20 cm²) for imaging of a single breast. For planar image acquisition, compression of the breast during imaging similar to X-ray mammography can be useful to improve image quality (Figure 27.10).⁴⁷ Additionally, this geometry allows for software fusion with X-ray mammography.⁴⁸

Single photon emission mammography

Several detector designs have been developed for optimized resolution. While in a small number of scanner designs a single crystal is coupled to a number of photomultiplier tubes (PMTs), most designs deviate from this Anger set-up.⁴⁹ Some designs are based on an array of very small scintillator crystals made of NaI(Tl) or CsI(Tl), coupled to one or more position-sensitive PMTs (PS-PMTs). Coover et al. showed an improved detectability of small lesions with a dedicated camera using an array of $2 \times 2 \times 6$ -mm NaI(Tl) scintillators.⁵⁰ Pani et al. used an array of $2 \times 2 \times 3$ -mm CsI(Tl) scintillators to achieve an intrinsic resolution of less than 2 mm in a 10×10 -cm detector.⁵¹ They were also able to show an improved sensitivity for small malignant

breast lesions compared to an Anger camera.⁵² Some designs have replaced the photomultiplier tubes by photodiodes to obtain a better energy resolution, usually a problem for multicrystal/PMT designs.^{53,54} Other designs are based on semiconductor detectors that can achieve an energy resolution of less than 4% for ^{99m}Tc-based radiotracers.⁵⁵ Mueller and co-workers have evaluated a camera with 2.5 × 2.5-mm cadmium zinc telluride (CZT) detector elements and a total detector size of 20 × 20 cm.⁵⁶ They showed that the sensitivity was 76% of that for an equivalent NaI(Tl) system, the energy resolution was 6.5% for ^{99m}Tc-based tracers, and the resolution was excellent. Brzymialkiewicz and colleagues successfully combined a CZT-based detector with a 3D positioning system for mammothography.⁵⁷ They optimized the rotation orbit and camera tilt.

Positron emission mammography

Positron emission mammography (PEM) is based on coincident γ photon detection following positron–electron annihilation. Planar systems use two adjacent detectors and electronic circuitry for coincidence detection (Figure 27.11). Again, several different designs are used. Thompson et al. proposed and simulated a PEM device in 1994 that was later implemented using 2 × 2 pixelized BGO detector blocks with a size of 36 × 36 × 20 mm (effective single detector size 2 mm) connected to PS-PMTs.^{58,59} Spatial resolution was measured to be 2.8 mm FWHM (full width half maximum) with a system sensitivity of 3%. The system was successfully tested in patients.⁶⁰ Weinberg and co-workers integrated two detectors into a standard mammography system.⁶¹ They used a 1 cm thick slab of a BGO crystal coupled to a PS-PMT to achieve a detector with a FOV of 6 × 6 cm and a spatial resolution of 3.1 mm FWHM. This early PEM

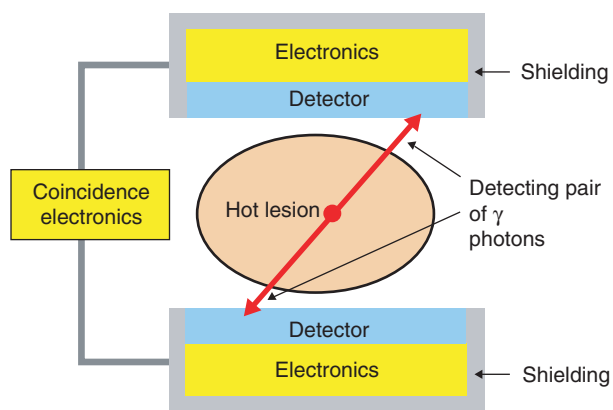


Figure 27.11
Principle of a positron emission mammography device. It consists of two detectors and electronic circuitry for coincidence detection.

system was also successfully used in patients. Doshi et al. developed modular detectors based on LSO scintillators (9 × 9 array of size 3 × 3 × 20 mm) coupled to PS-PMTs for sensitive and fast coincidence imaging.⁶² Raylman and colleagues used GSO crystals (30 × 30 array of size 3.1 × 3.1 × 10 mm) coupled to PS-PMTs for stereotactic biopsies.⁶³ Modern PEM systems can achieve an intrinsic resolution in the order of 1.5 mm FWHM.⁶⁴ Tomographic imaging is possible with PEM when using a rotating set-up.⁶⁵ Rosen and co-workers used a PEM system with large area detectors (size 15–20 cm) using 3 × 3 × 10 mm lutetium gadolinium oxyorthosilicate (LGSO) scintillators to obtain tomographic images without detector rotation.⁶⁶

Several clinical studies using [¹⁸F]fluoro-2-deoxy-D-glucose (FDG) have shown the clinical applicability of modern PEM systems and the improvement of diagnostic accuracy over conventional PET for breast imaging.^{64,67}

Positron emission prostate imaging

PET imaging of the prostate with the radiotracer [¹¹C]choline has become increasingly important for evaluation of prostate carcinomas.⁶⁸ A prototype design of a PET scanner dedicated for prostate imaging has been developed and evaluated.⁶⁹ Scanner geometry allows for a reduced distance between prostate and detector head compared to a conventional full-ring PET scanner, for favorable signal-to-background characteristics.

Intraoperative probes

Non-imaging radiation probes have found widespread clinical application in recent years. They have been used for the intraoperative detection of sentinel lymph nodes (SLNs) in patients with skin or breast cancer, and numerous other malignant tumors. The targeted removal of SLNs by help of radioguided surgery instead of systematic lymphadenectomy can prevent many side-effects without reducing the staging accuracy.⁷⁰

Several hours or 1 day before surgery, radiolabeled colloid is injected at the site of the tumor. The drainage of the radiotracer and its accumulation in SLNs can be imaged with a conventional γ camera after injection. Often the locations of the SLNs are marked on the body surface to guide the surgeon. The γ radiation probe is used intraoperatively to identify and remove the SLNs. The radiation probe should have a high sensitivity and a defined photon acceptance angle for good spatial resolution. Probes for detecting positron-emitting nuclides or small transportable camera systems extend this concept.^{71,72}

Combined molecular–morphological imaging

One of the most exciting developments in the field of nuclear imaging in oncology has been combined molecular–morphological imaging technologies such as SPECT–CT and PET–CT. These combine a SPECT or PET scanner with a CT in one device (Figure 27.12). Imaging can be performed within one session and without repositioning of the patient.

Images from nuclear imaging procedures reflect physiological and biochemical processes within the body and provide only limited information about anatomy and morphology. Therefore, nuclear physicians have always made use of additional morphological imaging for anatomic correlation and image interpretation. In the majority of cases, SPECT or PET images have been correlated with images from ultrasound, X-ray, CT, and magnetic resonance imaging (MRI) by means of visual side by side interpretation. Additionally, computer programs have been developed that assist in the alignment of different studies.^{73–75} Some computer programs only implement simple rigid body transformations, while others use more sophisticated non-linear transformations for even better co-registration. While these techniques work rather well for rigid structures, e.g. the brain, they are in many cases inadequate for whole body imaging. In whole body imaging there is a far greater variability of body part and organ position between different scans. As an example, PET whole body imaging has most

often been acquired with arms positioned next to the body, and CT scanning has most often been performed with arms elevated over the head, resulting in a non-linearly changed body configuration between PET and CT. In addition, off-line computer-based image co-registration tends to be laborious and time-consuming.

Contrary to off-line image fusion, the combined imaging with SPECT–CT and PET–CT devices produces spatially co-registered images without additional user interaction. Co-registration is optimized since the patient is scanned in one image session and without patient repositioning. Combined molecular–morphological imaging will likely be obligatory for future clinical applications of highly specific radiotracers that may accumulate, for instance, only in cancer cells, without providing enough background information for anatomic orientation. However, even though image co-registration is optimized by the integrated imaging approach, the achievable image fusion is still not perfect. With the present generation of devices, image acquisition of molecular and morphological data is not simultaneous but sequential. Moreover, movement due to respiration and heart contraction as well as accidental patient movement leads to misalignment, especially given the different imaging time required for SPECT or PET on one side (several minutes) compared to CT on the other side (seconds). Additionally, misalignment also adversely affects SPECT or PET image generation itself since the CT data are also used for attenuation correction in most devices. It is important to know about these limitations for adequate image interpretation.

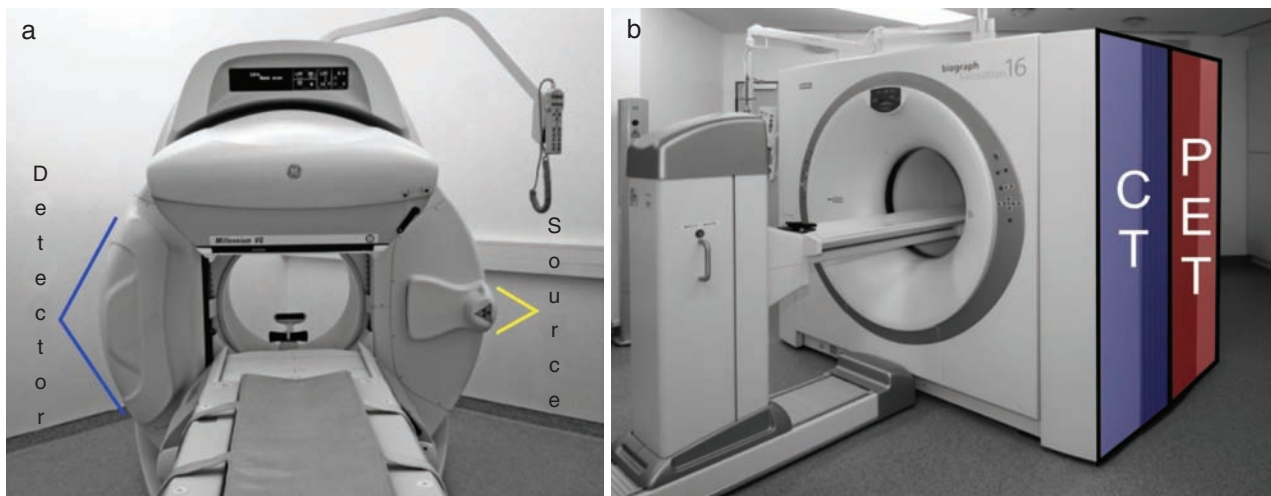


Figure 27.12

SPECT–computed tomography (CT) and PET–CT devices. (a) Photograph of a combined SPECT–CT system VG Millenium (Hawkeye®; GE Medical Systems) that combines a two-head SPECT camera with a simple CT component used for attenuation correction and anatomical landmarking. The X-ray source and detectors are attached to the rotating SPECT camera head support system. (b) Photograph of a combined PET–CT system (Biograph® Sensation 16; Siemens Medical Solutions) that combines a state-of-the-art 3D-only LSO-PET system with a diagnostic 16-slice CT. Basic operation of the PET and CT systems is largely independent of one another. They are arranged sequentially within the gantry, the CT at the front, the PET at the rear.

CT technology

Widely used in medical imaging since the early 1970s as a stand-alone device for morphological imaging, CT utilizes an X-ray tube together with one or more opposing detectors for signal generation. In the most widely used (third generation) design, the tube and a small arc of opposing detectors rotate together around the patient on a circular orbit. A large number of the produced X-ray photons directed at the opposing detectors are absorbed on their way through the patient without reaching the detector, reflecting the body tissue density with respect to X-ray photons along the trajectory path. From a large number of such projections transaxial tomographic images through the patient's body are reconstructed by help of a computer.

Achievable image quality and imaging speed vary widely across the range of available CT scanners; state of the art imaging requires a sophisticated technical design. Simple scanners use a single beam that allows for acquisition of a single slice at a time. More sophisticated multislice CT designs, developed in the late 1990s, use a fan-shaped beam with four, 16, 64, or more detector rows to acquire a corresponding number of slices simultaneously. In modern high-performance designs rotation speed can be very fast at one-third of a second and less for a 360° orbit. Some tomographs use two tube/detector configurations with 90° angular offset, effectively reducing the necessary scanning orbit from 180° to 90°. Future designs will probably use a cone beam approach with flat panel detectors for volumetric imaging. Another technique to improve imaging speed that was introduced in the late 1980s and is implemented in all modern scanners is spiral CT acquisition, where bed motion, tube/detector rotation, and image acquisition are continuous, resulting in projections on a spiral trajectory path around the patient.

Image quality is also dependent on the tube voltage and the tube current. These values can be arbitrarily chosen within the technical limits of the scanner. Often an inverse relationship exists between image quality and

radiation exposure. Sometimes a suboptimal image quality is chosen in order to limit radiation exposure to the patient. Another way to improve the diagnostic accuracy of CT imaging is the use of a contrast agent. Intravenously administered contrast agent improves the assessment of blood vessels and well perfused organs. Orally administered contrast agents can enhance the visibility of gastrointestinal structures.

CT as a component within a combined SPECT–CT or PET–CT scanner can be of very different quality according to requirements. For attenuation correction and coarse anatomic orientation a low-quality (low-dose) scan is usually adequate. Simple CT designs can then be used, and radiation exposure can be kept at a minimum. For the assessment of subtle disease-related changes in morphology, the quality of the CT component has to be comparable to that of dedicated stand-alone CT scanners, and contrast-enhanced imaging is usually desirable. Technically, all available CT scanner designs can be incorporated into a SPECT–CT or PET–CT system. Most technical features from stand-alone CT scanners, with the exception of oblique scanning, can be used.

SPECT–CT

Combined SPECT–CT was introduced in the early 1990s, followed by the technical implementation of CT-derived attenuation correction.^{76–79} The first commercially available systems use low-resolution and low-dose CT devices for attenuation correction and anatomic orientation (Figure 27.12a). Acquisition speed is slow, since the X-ray tube and the CT detector are attached to the same rotation mechanisms as the scintigraphic camera heads. Image acquisition is performed without breath-holding, similarly to SPECT data acquisition. Although this CT component is unable to deliver diagnostic image quality, it is ideally suited for SPECT attenuation correction and anatomical landmarking (Figure 27.13). No difference in breathing

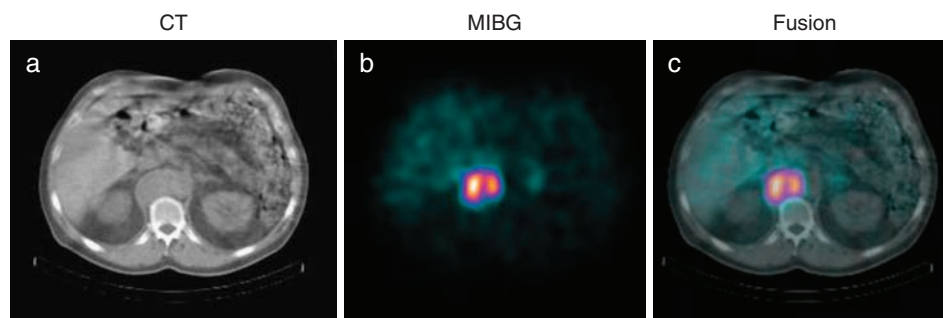


Figure 27.13

SPECT–CT example. Images of a transaxial slice located in the region of the upper abdomen showing [metastatic uptake of [¹²³I]-metaiodobenzylguanidine ([¹²³I]MIBG)] (a), the morphology by low-quality CT for attenuation correction and anatomical landmarking (b), and the fused molecular–morphological information (c) of a patient with malignant paraganglioma.

pattern between SPECT and CT image acquisition exists. Two-head camera systems with thick NaI(Tl) crystals for adequate 511-keV photon detection efficiency and an attached coincidence unit are used in some designs to allow coincidence imaging with positron emitting radionuclides.

SPECT–CT systems with a diagnostic quality CT component have been introduced into the market, offering the possibility to replace a separate CT scan on a stand-alone device.

PET–CT

The first prototype scanner was developed in the mid- to late 1990s and was successfully applied in a large number of oncology patients.⁸⁰ Today, a number of integrated PET–CT designs are commercially available from several manufacturers (Figure 27.12b). Most scanners combine state-of-the-art PET and diagnostic-quality CT (Figure 27.14). PET components with long-established BGO detectors or with newer and faster LSO or GSO detectors are available. Especially cardiovascular imaging requires the fastest multislice CT available. The speed demand for oncological imaging is usually lower, so that intermediate-quality CT scanners suffice.

Attenuation correction for PET imaging is in the majority of cases performed by using a CT-derived attenuation map. Additionally, most scanners are 3D-only scanners without retractable septa for additional 2D imaging, so that a large gantry opening in the order of 70 cm is possible. This facilitates the use of PET–CT for radiotherapy planning.

CT-based attenuation correction for SPECT and PET

The use of CT for SPECT and PET attenuation correction has some important advantages over external positron

emitting sources: (1) a CT scan is very fast compared to a traditional transmission scan, thus reducing required scanning time considerably; and (2) a CT scan offers less noisy attenuation maps, effectively increasing image quality.

However, there are also several challenges associated with CT-based attenuation correction: (1) attenuation (and scatter) is energy dependent: the energy range of photons produced by an X-ray tube (peak at ~70 keV) is very different from the energies for most isotopes used in nuclear imaging; this is especially true for the high-energy 511-keV photons in PET, and therefore, processing of the CT-derived attenuation map is required; (2) spatial resolution is much lower in SPECT and PET compared to CT; (3) spatial co-registration of SPECT or PET and CT is limited due to respiratory, cardiac, and involuntary movement between the sequentially acquired scans; additionally, functional changes such as bladder filling and peristaltic movement of gastrointestinal and urogenital organs can further hamper co-registration; (4) contrast agent application leads to different attenuation maps during CT and SPECT/PET imaging; and (5) metal objects such as hip implants and cardiac pacemakers lead to artifacts in the CT-based attenuation map which are then transferred into SPECT/PET images.

Several technical solutions have been found for the above problems.

Energy scaling of attenuation map

The CT-derived attenuation map for PET attenuation correction (principles are similar for SPECT attenuation correction) has to be scaled to 511-keV photons. Adequate scaling can be achieved when using a common scaling factor for air, water, blood, and soft tissue, and a second scaling factor for bone. Either a bilinear combination of these two scaling factors can be applied on a pixel by pixel basis to account for a mixture of soft tissue and bone, or segmentation of bone and soft tissue can be combined with scaling.^{78,81,82}

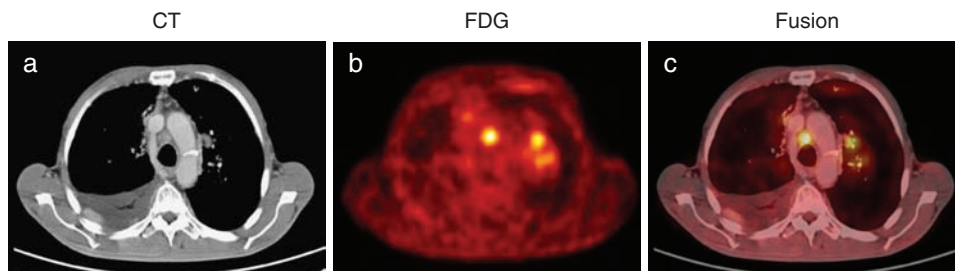


Figure 27.14

PET–CT example. Images of a transaxial slice located cranially to the heart showing [metastatic uptake of [¹⁸F]-fluoro-2-deoxy-D-glucose ([¹⁸F]FDG)] (a), the morphology by contrast-enhanced diagnostic-quality CT (b), and the fused molecular–morphological information (c) of a patient with poorly differentiated thyroid carcinoma.

Resolution scaling

Resolution of the CT-based attenuation map can be adapted to the SPECT or PET resolution by simple low-pass filtering. This eliminates higher frequencies representing sharp edges so that resolution is effectively reduced.

Motion artifacts

The largest contribution to motion-related misalignment of SPECT or PET and CT data normally stems from respiratory movement. This effect is especially aggravated near the diaphragm and near the anterior chest wall. However, many other thoracic and abdominal organs may also be affected.⁸³ Since SPECT or PET requires several minutes of acquisition time per bed position, data acquisition during breath-holding is impossible. On the other hand, CT acquisition using modern equipment is very fast, so that imaging of the chest and upper abdomen is usually possible during a single breath-hold. To make things worse, the diagnostic accuracy of CT chest imaging is highest when acquired in near-maximal inspiration. This respiratory position is very different from that during the usually shallow tidal breathing during SPECT or PET data acquisition. Several breathing protocols have been proposed, but no single standard protocol has yet emerged. To better match the respiration pattern during CT and SPECT or PET acquisition, either CT acquisition with shallow tidal breathing or during a breath-hold in the non-forced expiratory position seems best.^{84,85} An additional CT scan in full inspiration might be required for optimal diagnostic accuracy. In many cases this additional scan can be performed with reduced radiation exposure for accurate lung imaging.⁸⁶ In the future, computer algorithms are likely to be clinically useful for movement-adapted attenuation correction.⁸⁷ Nevertheless, the additional assessment of uncorrected SPECT and PET images is of paramount importance to assess equivocal findings in the attenuation corrected images and to increase sensitivity for small lesions, especially in the lung.

Effect of contrast agents

Contrast agents for intravenous application are positive contrast agents that increase attenuation compared to the surrounding tissue. The attenuation map measured during contrast-enhanced CT reflects the contrast agent density at exactly this time. During the SPECT or PET scan the contrast agent has redistributed to a large degree so that the effect of the contrast agent on 511-keV photon attenuation is considerably different. The attenuation map acquired during contrast-enhanced CT therefore does not reflect the true attenuation during the SPECT/PET scan so that errors

are being introduced. This effect is even aggravated if the regional contrast agent density makes local attenuation indistinguishable from bone, so that a wrong factor is used for energy scaling. Fortunately, in real-world applications, the effect of intravenously administered contrast agents on PET quality was found to be small, and is not considered to be a grave problem in most cases.⁸⁸

Oral contrast agents can either be positive or negative (e.g. cellulose). As the amount of local contrast agent deposition can be very high compared to intravenously applied contrast agents, a noticeable effect on SPECT or PET image quality can result. For that reason the use of negative contrast agents is preferred by some centers. Again, assessment of non-attenuation-corrected SPECT or PET images can help to distinguish true positive findings from attenuation artifacts.

SPECT/PET and CT have to be acquired in the same position. Scanning with both arms elevated over the head is optimal for attenuation correction, since for some CT scanners the attenuation map is truncated because the chest with both arms next to the trunk is too wide for complete imaging. However, not all patients tolerate this position well enough for acquisition times of 20 minutes and longer for whole-body SPECT-CT or PET-CT data acquisition.

PET-MRI

The integration of PET with magnetic resonance imaging (MRI) into a single PET-MRI device is feasible, as several prototypes have shown. The complexity of developing an integrated PET-MRI device is magnitudes higher compared to SPECT-CT or PET-CT technologies. The static magnetic field precludes the use of classic photomultiplier tubes for radiation detection, so that the design of the PET component has to be fundamentally changed. Fiberoptic cables can be used to transport the scintillation light from the detector crystals inside the magnet to photomultiplier tubes outside.^{89,90} Modern MRI scanners use active shielding so that the magnetic field drops to low values within a short distance. Another promising development is to replace photomultiplier tubes by semiconductor converters that are compatible with strong magnetic fields.^{13,15}

MRI yields unique morphological and functional information, especially for soft tissue characterization, unobtainable by other imaging modalities. The possibility of additional magnetic resonance spectroscopy (MRS) adds to the diagnostic possibilities of this imaging modality. A very important advantage of PET-MRI over SPECT-CT or PET-CT is that simultaneous and not only sequential imaging is possible. The MRI component may be used to monitor movement during the PET acquisition, so that accurate motion correction in PET can be performed for better delineation of small lesions such as pulmonary nodules.

MRI-derived anatomical information may also be used for partial volume correction and region of interest (ROI) definition in quantitative PET. Moreover, the usage of MRI is not limited by ionizing radiation. The future will show whether this new technique can find its way into clinical practice.

Conclusion

Many exciting new technologies developed for radionuclide imaging have begun to emerge in recent years. Some of them have already seen widespread clinical application. In many ways these new technologies have contributed to better diagnostic quality, albeit, in some cases, at the expense of increased methodological complexity.

With the rapidly increasing knowledge about the genetic aberrations underlying malignant diseases and the associated changes on a molecular and cellular level, the need for adequate molecular imaging devices will equally increase. Nuclear imaging methods are uniquely suitable owing to their high sensitivity, molecular target specificity, and whole-body imaging capability. It is therefore likely that the pace of technological progress in the field of radionuclide imaging will be maintained on a high level in the foreseeable future.

References

- Hofstadter R. Alkali halide scintillation counters. *Phys Rev* 1948; 74: 100–1.
- Dahlbom M, Cherry SR. PET: physics, instrumentation and scanners. In: Phelps ME, ed. *PET: Molecular imaging and its Biological Applications*. Heidelberg: Springer, 2004: 101–4.
- Melcher CL. Scintillation crystals for PET. *J Nucl Med* 2000; 41: 1051–5.
- Wilkinson F. Scintillators. In: Wernick MN, Aarsvold JN, eds. *Emission Tomography: The Fundamentals of PET and SPECT*. Amsterdam, Elsevier, 2004: 229–54.
- Chen JM, Zhang LY, Zhu RY. Large size LYSO crystals for future high energy physics experiments. *IEEE Trans Nucl Sci* 2005; 52: 3133–40.
- Balcerzyk M, Moszynski M, Galazka Z et al. Perspectives for high resolution and high light output LuAP: Ce crystals. *IEEE Trans Nucl Sci* 2005; 52: 1823–9.
- Pepin CM, Berard P, Perrot AL et al. Properties of LYSO and recent LSO scintillators for phoswich PET detectors. *IEEE Trans Nucl Sci* 2004; 51: 789–95.
- Kuhn A, Surti S, Karp JS et al. Design of a lanthanum bromide detector for time-of-flight PET. *IEEE Trans Nucl Sci* 2004; 51: 2550–7.
- Kuntner C, Auffray E, Bellotto D et al. Advances in the scintillation performance of LuYAP:Ce single crystals. *Nucl Instr Meth* 2005; 537: 295–301.
- Blancar G, Dietl H, Dobbins J et al. Photo-diode readout for scintillating crystals of BGO and NaI(Tl). *Nucl Instr Meth* 1982; 203: 213–21.
- Pichler B, Ziegler S. Photodetectors. In: Wernick MN, Aarsvold JN, eds. *Emission Tomography: The Fundamentals of PET and SPECT*. Amsterdam: Elsevier, 2004: 255–267.
- Fiorini C, Longoni A, Perotti F. New detectors for gamma-ray spectroscopy and imaging, based on scintillators coupled to silicon drift detectors. *Nucl Instr Meth* 2000; 454: 241–6.
- Huber JS, Moses WW, Derenzo SE et al. Characterization of a 64 channel PET detector using photodiodes for crystal identification. *IEEE Trans Nucl Sci* 1997; 44: 1197–201.
- Pichler BJ, Bernecker F, Boning G et al. A 4×8 APD array, consisting of two monolithic silicon wafers, coupled to a 32-channel LSO matrix for high-resolution PET. *IEEE Trans Nucl Sci* 2001; 48: 1391–6.
- Pichler BJ, Judenhofer MS, Catana C et al. Performance test of an LSO-APD detector in a 7-T MRI scanner for simultaneous PET/MRI. *J Nucl Med* 2006; 47: 639–47.
- Anger HO. Scintillation camera. *Rev Sci Instrum* 1958; 29: 27–33.
- Jaszczak RJ, Greer KL, Floyd CE Jr, Harris CC, Coleman RE. Improved SPECT quantification using compensation for scattered photons. *J Nucl Med* 1984; 25: 893–900.
- King MA, Hademenos GJ, Glick SJ. A dual-photopeak window method for scatter correction. *J Nucl Med* 1992; 33: 605–12.
- Ogawa K, Harata, Y, Ichihara T, Kubo A, Hashimoto S. A practical method for position-dependent Compton-scatter correction in single photon emission CT. *IEEE Trans Med Imaging* 1991; 10: 408–12.
- Zaidi H, Hasegawa B. Determination of the attenuation map in emission tomography. *J Nucl Med* 2003; 44: 291–315.
- Todd RW, Nightingale JM, Everett DB. A proposed gamma-camera. *Nature* 1974; 25: 132.
- Everett DB, Todd RW, Nightingale JM. Gamma-radiation imaging system based on Compton effect. *PROC IEEE* 124: 995–1000.
- Rogers WL, Clinthorne NH, Bologzyna A, Compton cameras for nuclear medicine imaging. In: Wernick MN, Aarsvold JN, eds. *Emission Tomography: The Fundamentals of PET and SPECT*. Amsterdam: Elsevier, 2004: 383–419.
- Yang Y, Dokhale PA, Silverman RW et al. Depth of interaction resolution measurements for a high resolution PET detector using position sensitive avalanche photodiodes. *Phys Med Biol* 2006; 51: 2131–42.
- Sánchez-Crespo A, Larsson SA. The influence of photon depth of interaction and non-collinear spread of annihilation photons on PET image spatial resolution. *Eur J Nucl Med Mol Imaging* 2006; 33: 940–7.
- Moehrs S, Del Guerra A, Herbert DJ, Mandelkern MA. A detector head design for small-animal PET with silicon photomultipliers (SiPM). *Phys Med Biol* 2006; 51: 1113–27.
- McCallum S, Clowes P, Welch A. A four-layer attenuation compensated PET detector based on APD arrays without discrete crystal elements. *Phys Med Biol* 2005; 50: 4187–207.
- Dokhale PA, Silverman RW, Shah KS et al. Performance measurements of a depth-encoding PET detector module based on position-sensitive avalanche photodiode read-out. *Phys Med Biol* 2004; 49: 4293–304.

29. Vandenberghe S, Daube-Witherspoon ME, Lewitt RM, Karp JS. Fast reconstruction of 3D time-of-flight PET data by axial rebinning and transverse mashing. *Phys Med Biol* 2006; 51: 1603–21.
30. Defrise M, Casey ME, Michel C, Conti M. Fourier rebinning of time-of-flight PET data. *Phys Med Biol* 2005; 50: 2749–63.
31. Mallon A, Grangeat P. Three-dimensional PET reconstruction with time-of-flight measurement. *Phys Med Biol* 1992; 37: 717–29.
32. Bendriem B, Soussaline F, Campagnolo R et al. A technique for the correction of scattered radiation in a PET system using time-of-flight information. *J Comput Assist Tomogr* 1986; 10: 287–95.
33. Mullani NA, Markham J, Ter-Pogossian MM. Feasibility of time-of-flight reconstruction in positron emission tomography. *J Nucl Med* 1980; 21: 1095–7.
34. Budinger TF. Time-of-flight positron emission tomography: status relative to conventional PET. *J Nucl Med* 1983; 24: 73–8.
35. Ter-Pogossian MM, Mullani NA, Ficke DC, Markham J, Snyder DL. Photon time-of-flight-assisted positron emission tomography. *J Comput Assist Tomogr* 1981; 5: 227–39.
36. Ter-Pogossian MM, Ficke DC. Re: Time-of-flight positron-emission tomography status relative to conventional PET. *J Nucl Med* 1984; 25: 136–8.
37. Budinger TF. PET instrumentation: what are the limits? *Semin Nucl Med* 1998; 28: 247–67.
38. Lewellen TK. Time-of-flight PET. *Semin Nucl Med* 1998; 28: 268–75.
39. Surti S, Karp JS, Muehlethner G. Image quality assessment of LaBr₃-based whole-body 3D PET scanners: a Monte Carlo evaluation. *Phys Med Biol* 2004; 49: 4593–610.
40. Conti M, Bendriem B, Casey M et al. First experimental results of time-of-flight reconstruction on an LSO PET scanner. *Phys Med Biol* 2005; 50: 4507–26.
41. Lucignani G. Time-of-flight PET and PET/MRI: recurrent dreams or actual realities? *Eur J Nucl Med Mol Imaging* 2006; 33: 969–71.
42. Surti S, Karp JS, Popescu LM, Daube-Witherspoon ME, Werner M. Investigation of time-of-flight benefit for fully 3-D pet. *IEEE Trans Med Imaging* 2006; 25: 529–38.
43. Palmedo H, Schomburg A, Grunwald F et al. Scintimammography with Tc-99m MIBI in patients with suspicion of primary breast cancer. *Nucl Med Biol* 1996; 23: 681–4.
44. Mekhmandarov S, Sandbank J, Cohen M, Lelcuk S, Lubin E. Technetium-99m-MIBI scintimammography in palpable and nonpalpable breast lesions. *J Nucl Med* 1998; 39: 86–91.
45. Scopinaro F, Schillaci O, Ussof W et al. A three center study on the diagnostic accuracy of 99mTc-MIBI scintimammography. *Anticancer Res* 1997; 17: 1631–4.
46. Scopinaro F, Mezi S, Ierardi M et al. 99mTc MIBI prone scintimammography in patients with suspicious breast cancer: relationship with mammography and tumor size. *Int J Oncol* 1998; 12: 661–4.
47. Pani R, Scopinaro F, Pellegrini R et al. The role of Compton background and breast compression on cancer detection in scintimammography. *Anticancer Res* 1997; 17: 1645–9.
48. Bergman AM, Thompson CJ, Murthy K et al. Technique to obtain positron emission mammography images in registration with x-ray mammograms. *Med Phys* 1998; 25: 2 119–29.
49. Kim JH, Choi Y, Joo KS et al. Development of a miniature scintillation camera using an NaI(Tl) scintillator and PSPMT for scintimammography. *Phys Med Biol* 2000; 45: 3481–8.
50. Coover LR, Caravaglia G, Kuhn P. Scintimammography with dedicated breast camera detects and localizes occult carcinoma. *J Nucl Med* 2004; 45: 553–8.
51. Pani R, Pellegrini R, Scopinaro F et al. Scintillating array gamma camera for clinical use. *Nucl Instrum Meth* 1997; A392: 295–8.
52. Scopinaro F, Pani R, De Vincentis G et al. High-resolution scintimammography improves the accuracy of technetium-99m methoxyisobutylisonitrile scintimammography: use of a new dedicated gamma camera. *Eur J Nucl Med* 1999; 26: 1279–88.
53. Gruber GJ, Moses WW, Derenzo SE et al. A discrete scintillation camera module using silicon photodiode readout of CsI(Tl) crystals for breast cancer imaging. *IEEE Trans Nucl Sci* 1998; 45: 1063–8.
54. Patt BE, Iwaczyk JS, Rossington Tull C et al. High resolution CsI(Tl)/Si-PIN detector development for breast imaging. *IEEE Trans Nucl Sci* 1998; 45: 2126–31.
55. Butler JF, Lingren CL, Friesenhahn SJ et al. CdZnTe solid-state gamma camera. *IEEE Trans Nucl Sci* 1998; 45: 359–63.
56. Mueller B, O'Connor MK, Blevins I et al. Evaluation of a small cadmium zinc telluride detector for scintimammography. *J Nucl Med* 2003; 44: 602–9.
57. Brzymialkiewicz CN, Tornai MP, McKinley RL, Bowsher JE. Evaluation of fully 3-D emission mammothomography with a compact cadmium zinc telluride detector. *IEEE Trans Med Imaging* 2005; 24: 868–77.
58. Thompson CJ, Murthy K, Weinberg IN, Mako F. Feasibility study for positron emission mammography. *Med Phys* 1994; 21: 529–38.
59. Murthy K, Aznar M, Bergman AM et al. Positron emission mammographic instrument: initial results. *Radiology* 2000; 215: 280–5.
60. Murthy K, Aznar M, Thompson CJ et al. Results of preliminary clinical trials of the positron emission mammography system PEM-I: a dedicated breast imaging system producing glucose metabolic images using FDG. *J Nucl Med* 2000; 41: 1851–8.
61. Weinberg I, Majewski S, Weisenberger A et al. Preliminary results for positron emission mammography: real-time functional breast imaging in a conventional mammography gantry. *Eur J Nucl Med* 1996; 23: 804–6.
62. Doshi NK, Shao Y, Silverman RW, Cherry SR. Design and evaluation of an LSO PET detector for breast cancer imaging. *Med Phys* 2000; 27: 1535–43.
63. Raylman RR, Majewski S, Weisenberger AG et al. Positron emission mammography-guided breast biopsy. *J Nucl Med* 2001; 42: 960–6.
64. Berg WA, Weinberg IN, Narayanan D et al. Positron Emission Mammography Working Group. High-resolution fluorodeoxyglucose positron emission tomography with compression ('positron emission mammography') is highly accurate in depicting primary breast cancer. *Breast J* 2006; 12: 309–23.
65. Smith MF, Raylman RR, Majewski S, Weisenberger AG. Positron emission mammography with tomographic

- acquisition using dual planar detectors: initial evaluations. *Phys Med Biol* 2004; 49: 2437–52.
66. Rosen EL, Turkington TG, Soo MS, Baker JA, Coleman RE. Detection of primary breast carcinoma with a dedicated, large-field-of-view FDG PET mammography device: initial experience. *Radiology* 2005; 234: 527–34.
 67. Tafra L, Cheng Z, Uddo J et al. Pilot clinical trial of 18F-fluorodeoxyglucose positron-emission mammography in the surgical management of breast cancer. *Am J Surg* 2005; 190: 628–32.
 68. Jana S, Blaurox MD. Nuclear medicine studies of the prostate, testes, and bladder. *Semin Nucl Med* 2006; 36: 51–72.
 69. Huber JS, Choong WS, Moses WW et al. Characterization of a PET camera optimized for prostate imaging. *IEEE Nucl Sci Symp Conf Rec* 2005; 3: 1556–9.
 70. Morton DL, Cochran AJ, Thompson JF et al. Multicenter Selective Lymphadenectomy Trial Group. Sentinel node biopsy for early-stage melanoma: accuracy and morbidity in MSLT-I, an international multicenter trial. *Ann Surg* 2005; 242: 302–11.
 71. Franc BL, Mari C, Johnson D, Leong SP. The role of a positron- and high-energy gamma photon probe in intraoperative localization of recurrent melanoma. *Clin Nucl Med* 2005; 30: 787–91.
 72. Kojima T, Kumita S, Yamaguchi F et al. Radio-guided brain tumorectomy using a gamma detecting probe and a mobile solid-state gamma camera. *Surg Neurol* 2004; 61: 229–38.
 73. Pelizzari CA, Chen GTY, Spelbring DR, Weichselbaum RR, Chen CT. Accurate three-dimensional registration of CT, PET and MR images of the brain. *J Comp Assist Tomogr* 1989; 13: 20–6.
 74. Pietrzyk U, Herholtz K, Heiss W-D. Three-dimensional alignment of functional and morphological tomograms. *J Comput Assist Tomogr* 1990; 14: 51–9.
 75. Wahl RL, Quint LE, Cieslak RD et al. 'Anatomometabolic' tumor imaging: fusion of FDG PET with CT or MRI to localize foci of increased activity. *J Nucl Med* 1993; 34: 1190–7.
 76. Hasegawa BH, Stebler B et al. A prototype high-purity germanium detector system with fast photon-counting circuitry for medical imaging. *Med Phys* 1991; 18: 900–9.
 77. Hasegawa BH, Lang TE, Brown EL et al. Object-specific attenuation correction of SPECT with correlated dual-energy x-ray CT. *IEEE Trans Nucl Sci* 1993; NS-40: 1242–52.
 78. Blankespoor SC, Xu X, Kaiki K et al. Attenuation correction of SPECT using x-ray CT on an emission-transmission CT system: myocardial perfusion assessment. *IEEE Trans Nucl Sci* 1996; 43: 2263–74.
 79. Patton JA, Delbeke D, Sandler MP. Image fusion using an integrated, dual-head coincidence camera with X-ray tube-based attenuation maps. *J Nucl Med* 2000; 41: 1364–8.
 80. Beyer T, Townsend DW, Brun T et al. A combined PET/CT scanner for clinical oncology. *J Nucl Med* 2000; 41: 1369–79.
 81. Burger C, Goerres G, Schoenes S et al. PET attenuation coefficients from CT images: experimental evaluation of the transformation of CT into PET 511-keV attenuation coefficients. *Eur J Nucl Med Mol Imaging* 2002; 29: 922–7.
 82. Kinahan PET, Townsend DW, Beyer T, Sashin D. Attenuation correction for a combined 3D PET/CT scanner. *Med Phys* 1998; 25: 2046–53.
 83. Weckesser M, Stegger L, Juergens KU et al. Correlation between respiration-induced thoracic expansion and a shift of central structures. *Eur Radiol* 2006; 16: 1614–20.
 84. Goerres GW, Burger C, Schwitter MR et al. PET/CT of the abdomen: optimizing the patient breathing pattern. *Eur Radiol* 2003; 13: 734–9.
 85. Beyer T, Antoch G, Blodgett T et al. Dual-modality PET/CT imaging: the effect of respiratory motion on combined image quality in clinical oncology. *Eur J Nucl Med Mol Imaging* 2003; 30: 588–96.
 86. Juergens KU, Weckesser M, Stegger L et al. Tumor staging using whole-body high-resolution 16-channel PET-CT: does additional low-dose chest CT in inspiration improve the detection of solitary pulmonary nodules? *Eur Radiol* 2006; 16: 1131–7.
 87. Dawood M, Lang N, Jiang X, Schafers KP. Lung motion correction on respiratory gated 3-D PET/CT images. *IEEE Trans Med Imaging* 2006; 25: 476–85.
 88. Delbeke D, Coleman RE, Guiberteau MJ et al. Procedure guideline for tumor imaging with 18F-FDG PET/CT 1.0. *J Nucl Med* 2006; 47: 885–95.
 89. Christensen NL, Hammer BE, Heil BG, Fetterly K. Positron emission tomography within a magnetic field using photomultiplier tubes and lightguides. *Phys Med Biol* 1995; 40: 691–7.
 90. Shao Y, Cherry SR, Farahani K et al. Simultaneous PET and MR imaging. *Phys Med Biol* 1997; 44: 1167–71.

New radiopharmaceuticals for cancer diagnosis

Jane K Sosabowski, Matthias Glaser, and Stephen J Mather

Background

Problems and opportunities in developing new radiopharmaceuticals

In the past decade, no new radiopharmaceuticals have been approved by the regulatory authorities in Europe or the USA for use in the diagnosis of cancer. The reasons for this stem almost totally from a rapid escalation in costs for developing and licensing new drugs.¹ However, this state of affairs has not inhibited the rate of academic research into the field, and this has continued unabated throughout this period of time. The increasing availability of positron emission tomography (PET) technology means that the distinct separation between PET and single photon emission computed tomography (SPECT) radiopharmaceutical development which used to be present is starting to disappear. Although different research groups continue to specialize in their own fields, an increasing number are working across both disciplines.

Radiopharmaceuticals currently under development for cancer imaging fall into two main categories – those that are targeted towards peptide hormone receptors or antibody epitopes that show enhanced levels of expression in malignancy and those that interact with metabolic pathways which are important in the response of cancer to therapy. For a detailed discussion of these pathways readers are referred to Chapter 1. The pathways that have been most extensively explored in radiopharmaceutical development are glucose transport, proliferation, apoptosis, angiogenesis, and hypoxia.

These two groups are, however, not entirely distinct, and there is a significant degree of overlap between them. In many cases, therefore, the same targets are being pursued for both PET and SPECT imaging, as described below.

Perspectives for new SPECT radiopharmaceuticals

Apoptosis

Two quite different mechanisms are responsible for cell death – the relatively rapid and uncontrolled process of necrosis, and the much slower, highly controlled system of apoptosis. Apoptosis can be the outcome in a number of different therapeutic interventions, and there is therefore an interest in imaging this process using a variety of imaging modalities, including radionuclide imaging.² The different stages of apoptosis can each present possible targets for radiopharmaceutical development. These stages include: (1) induction of apoptosis, e.g. through p53 signaling; (2) nuclear condensation, endonuclease and caspase activation, and fall in intracellular pH; (3), phospholipid and cytoskeleton reorganization, and cell shrinkage; and (4) production of apoptotic bodies and phagocytosis. By far the most widely explored is stage (3), which results among other things in the switch of intracellular phosphatidylserine (PS) to the external surface of the dying cell. Several proteins bind to PS, of which annexin v (recently given the nomenclature anxA5) has been the most widely used.³ anxA5 can be produced in *Escherichia coli* using recombinant techniques to provide a suitable source of pharmaceutical grade material for clinical application. anxA5 has been labeled with a number of radionuclides, including ¹²³I, ¹¹¹In, and ¹⁸F, but a major impetus for clinical research was the development of technetium-99m labeling kits by Theseus Imaging Corp. The first generation of ‘Apomate™’ employed a pre-labeling approach developed by NeoRx Corp. to label antibody fragments for the imaging of small-cell lung cancer.⁴ This approach had two problems. The first was that the labeling procedure was

rather complex and took up to 2 hours to perform. Yields were also relatively low. Second, metabolism of the protein conjugate *in vivo* resulted in the production of lipophilic metabolites which were excreted by the hepatobiliary tract resulting in high non-specific accumulation in the abdomen.⁵ The second generation of kits produced by Theseus Corp. used hydrazinonicotinate (HYNIC) (Figure 28.1) as a bifunctional chelating agent. anxA5–HYNIC conjugate was formulated along with stannous ions and the tricine coligand in a freeze-dried kit, which can simply be labeled in one step by the addition of sodium pertechnetate.⁶

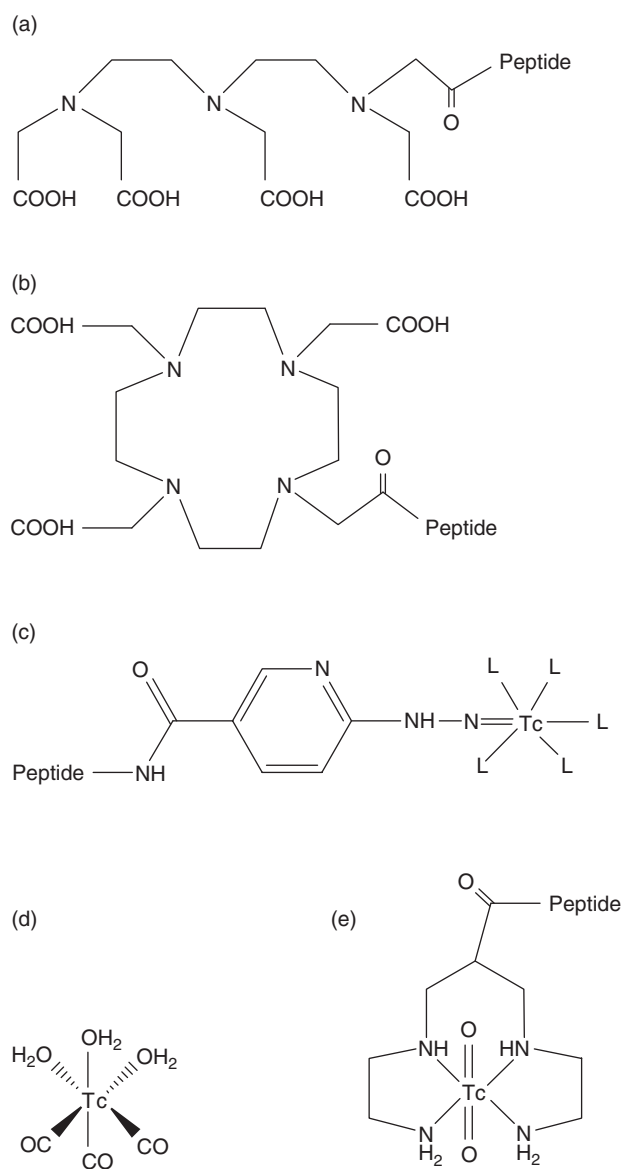


Figure 28.1

Structures of some commonly used chelating systems for peptide radiopharmaceuticals: (a) diethylenetriaminepentaacetic acid (DTPA), (b) 1,4,7,10-tetraazacyclododecane-*N,N',N'',N'''*-tetraacetic acid (DOTA), (c) Tc-HYNIC core where L = coligand (HYNIC = 6-hydrazinopyridine-3-carboxylic acid), (d) Tc tricarbonyl precursor, and (e) N_4 Tc chelating system.

The great majority of the preclinical and clinical research undertaken with radiolabeled annexin has been performed with this formulation, although, unfortunately, financial issues forced Theseus to withdraw the product from late-phase clinical trials. The results of these studies are summarized elsewhere,³ but it can be concluded that, although [^{99m}Tc]-anxA5 does show promise for imaging apoptosis, its use is complicated by two distinct factors. The first is that this tracer is not an ideal radiopharmaceutical. Although its distribution and clearance are more rapid than those of larger proteins such as monoclonal antibodies, it is still cleared too slowly for optimal imaging, and this, together with normal uptake in the kidney, spleen, and bone marrow, provides a high background against which to image 'pathological' sites of apoptosis. The second complicating factor relates to the kinetics of the apoptotic process itself. This is essentially a transient process which occurs in a subpopulation of cells within a tissue. The best time for imaging is therefore uncertain, and likely to vary from one indication to another.

The second feature of apoptosis that has been most extensively pursued as a target for radiopharmaceutical development is caspase activation, although this approach is currently at a much earlier stage. Induction of apoptosis results in a cascade of events in which intracellular enzymes known as caspases are involved. The activation of early caspases such as caspase-8 results in a number of intracellular events, including the activation of late caspases such as caspase-9 and caspase-3 that implement the later stages of cell destruction. Radiolabeled substrates for caspases that are retained by the cell after enzyme cleavage are therefore an interesting means for imaging apoptosis. This approach has been pursued by Haberkorn et al. Initial studies used radioiodinated Z-VAD-fmk (where VAD is Val-Ala-Asp and fmk is fluoromethylketone), a pan-caspase inhibitor. These showed that cells undergoing apoptosis accumulated more radioiodine than normal cells, but the absolute level of uptake of the tracer was relatively low.⁷ More recent studies have employed radiolabeled peptide substrates for caspase-3. Cellular uptake of these peptides was also low, but could be enhanced by conjugation with tat-sequences while still retaining a level of discrimination between cells undergoing apoptosis and those not.⁸

Angiogenesis

Angiogenesis, or the production of a new blood supply, is a prerequisite for tumor growth and progression. Consequently, drugs that interfere with this process could be useful therapeutic agents, and radiotracers that monitor the efficacy of such drugs could be useful.⁹ The angiogenic process follows a series of steps beginning with the secretion of growth factors such as vascular endothelial growth factor (VEGF) triggered by hypoxia within the tumor.

Contributions are also made by normal tissues including stromal and endothelial cells, which secrete proteolytic enzymes such as matrix metalloproteinases (MMPs) and serine proteases to break down the structure of the tissue. Activated endothelial cells express integrin ligands such as $\alpha_v\beta_3$ that allow them to migrate through the extracellular matrix, and new proteins such as laminin and collagen type IV are produced to form a basement membrane on which the endothelial cells can organize to form new blood vessels. Each of these steps can form a target for therapeutic drug and also radiopharmaceutical development; however, focus has been concentrated on three main targets – MMPs, integrins, especially $\alpha_v\beta_3$, and extracellular matrix proteins.

MMPs are zinc-containing peptidases that degrade a number of proteins that form the extracellular matrix. A number of radiolabeled substrates for MMPs have been explored. They include fragments of naturally occurring inhibitors (TIMPs),¹⁰ artificial peptides generated by phage-display,¹¹ and small synthetic non-peptide inhibitors.¹² These have been labeled with a variety of radionuclides including ^{99m}Tc , ^{123}I , ^{111}In , ^{64}Cu , ^{11}C , and ^{18}F . Encouraging results have been obtained in animal models, but these compounds have not yet been extensively explored in clinical studies.

Integrins

$\alpha_v\beta_3$ and other integrins are expressed by activated endothelial cells to aid their migration through the extracellular matrix, and may also be expressed by the tumor cells themselves. $\alpha_v\beta_3$ is not, however, expressed by normal vascular endothelium other than during pregnancy or wound healing. $\alpha_v\beta_3$ acts by binding to the sequence Arg-Gly-Asp (RGD), which is present in many extracellular matrix proteins such as fibronectin or fibrinogen. Consequently the RGD sequence has formed the basis for many drug and radiopharmaceutical candidates. Short linear peptides containing this sequence have only low binding affinity for the $\alpha_v\beta_3$ and are also rapidly degraded by serum proteases in vivo. Consequently, cyclic peptides, which contain a number of artificial substitutions, have formed the basis of the most promising radioligands. Cyclo(-Arg-Gly-Asp-DPhe-Val-), first introduced by Kessler et al., has been the lead structure for ligand development.¹³ Tracers initially labeled with ^{125}I showed high non-specific uptake in the intestines as a result of hepatobiliary excretion,¹⁴ but Haubner et al. were able to improve the pharmacokinetics by conjugation of sugars such as glucose and galactose.¹⁵ An improvement in affinity and selectivity can be achieved by linking together several $\alpha_v\beta_3$ binding sequences. Thus, a homodimer of cyclo(-Arg-Gly-Asp-DPhe-Val-) conjugated by either DOTA (tetraazacyclododecanetetraacetic acid) for group III radiometal labeling or HYNIC for ^{99m}Tc labeling showed increased uptake in animal tumor models compared to the monomer.¹⁶ This approach has been further extended by making tetrameric

and even octameric constructs. Such compounds were studied in animal models and showed improving tumor uptake in the order of tetramer > dimer > monomer.¹⁷ Most recently the use of water-soluble N-(2-hydroxypropyl)methacrylamide (HPMA) copolymers bearing up to 15 doubly cyclized $\alpha_v\beta_3$ binding peptide ligands labeled with ^{99m}Tc using the carbonyl precursor also showed improved tumor uptake compared to the unconjugated peptide.¹⁸

Extracellular matrix proteins

Fibronectin is a widely distributed matrix protein that exists in a variety of isoforms, depending on alternative splicing in different regions of the molecule. One such isoform contains the ED-B domain, a 91-residue sequence that has been shown to be important in angiogenesis. This protein is widely expressed in fetal and malignant tissues but shows a highly restricted pattern of expression in normal adult tissues. Neri et al. have developed a number of conventional and single-chain antibodies that show high-affinity binding to the ED-B sequence, and several constructs have been engineered for molecular imaging or therapeutic approaches.¹⁹ Among the radioactive ligands produced is one labeled with ^{211}At , which could potentially be used for targeted radionuclide therapy.²⁰ Clinical studies with a ^{123}I -labeled F(ab')₂ fragment of the L19 anti-ED-B antibody showed selective localization in tumor lesions in aggressive types of lung cancer and colorectal cancer. This approach, therefore, deserves further evaluation to determine its possible clinical application for imaging and monitoring of antiangiogenic therapies.²¹

Hypoxia

Hypoxia has long been recognized as playing a major role in mediating resistance to external-beam radiotherapy. However, recent identification of the molecular basis of the relationship between hypoxia and angiogenesis has raised the possibility that hypoxia may also have a prognostic influence in other treatment modalities such as chemotherapy with mitomycin C or porfiromycin.²² In addition, the cellular response to hypoxia is controlled through a complex gene expression pattern. This includes, for instance, the expression of growth factor genes for adaptive cellular response, leading to increased tumor cell vascularization.²² Classically, tissue hypoxia is measured either by the use of pH-sensitive electrodes or by immunohistochemistry of nitroimidazole adducts on tissue sections removed at biopsy. However, both techniques are necessarily relatively invasive and also provide only an indication of hypoxia at monitored positions in the tumor, even though the oxygen concentrations in tumor are known to be extremely heterogeneous.

They can only be used for tumors that are accessible to biopsy or needle placement. For this reason, a non-invasive procedure that could provide whole-body information on the regional distribution of oxygen levels throughout the tumor would be very valuable.

Radiopharmaceuticals for imaging hypoxia fall into two types, those based on nitroimidazoles that are trapped in hypoxic tissues due to irreversible reduction of the nitrogroup to reactive species that bind to intracellular macromolecules, and those based on metal complexes that show enhanced bioreduction in hypoxic tissues leading to selective retention of the radiometal (for review see reference 23).

Nitroimidazoles

The most well-established hypoxia tracer is 1H-1-(3-[^{18}F]fluoro-2-hydroxypropyl)-2-nitroimidazole (^{18}F FMISO), described below in the 'PET radiopharmaceuticals' section. Because of the limited (although currently increasing) availability of PET imaging, single photon nitroimidazole tracers have also been developed. The most widely explored is [^{123}I]IAZA (iodoazomycin arabinoside)²⁴ (Figure 28.2), a nitroimidazole conjugated nucleoside which lacks the metabolic instability and high lipophilicity of simple iodo-nitroimidazoles. Both FMISO and IAZA have undergone extensive clinical evaluation.

A number of technetium-labeled compounds have also been developed. One of the first to be studied was BMS181,321²⁵ (Figure 28.2), in which a 2-nitroimidazole

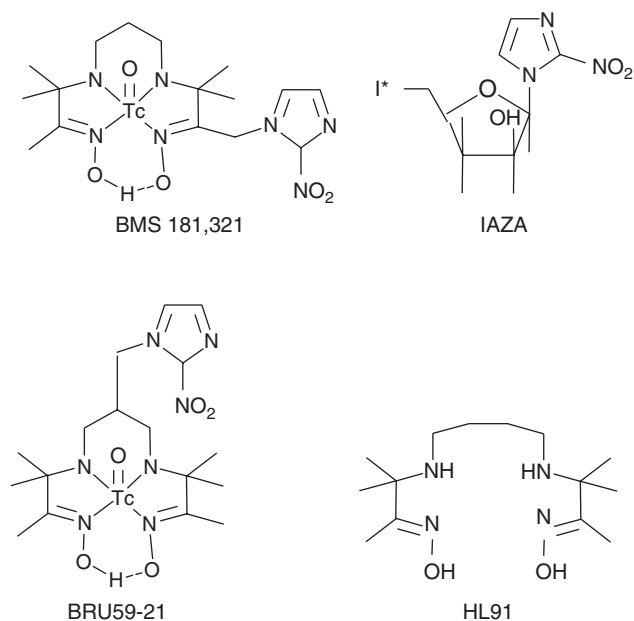


Figure 28.2

Chemical structures of some single photon emission computed tomography (SPECT) imaging agents for hypoxia. IAZA, iodoazomycin arabinoside.

was coupled to a propylene amine oxime (PnAO) chelator, similar to that employed in exametazime (CeretekTM). This tracer shows relatively high selective uptake in hypoxic tumors in animal models, but owing to its very high lipophilicity blood clearance is slow, resulting in poor tumor/blood ratios and high intestinal excretion which severely limits imaging in the abdomen. A second-generation tracer is BRU59-21²⁶ (Figure 28.2), in which the nitroimidazole group is moved to a different point in the chelator. This small change reduces the lipophilicity of the molecule and improves its metabolic stability. Clinical studies with [$^{99\text{m}}\text{Tc}$]BRU59-21 showed good correlation with staining for pimonidazole adducts.

Bioreductive metal complexes

The best-explored bioreductive systems are the copper–semicarbazone complexes PTSM and ATSM, which are discussed in the 'PET radiopharmaceuticals' section below. During the development of technetium-labeled nitroimidazole–chelate complexes, a control compound consisting of a technetium-labeled butylene amine oxime (BnAO, HL91), but lacking a nitroimidazole moiety, surprisingly showed high and selective uptake in hypoxic cells²⁷ (Figure 28.2). This hydrophilic compound shows generally lower tumor uptake than BMS181,321 and BRU59-21, but the rapid clearance and predominantly renal route of excretion engender high tumor to background ratios. The mechanism of retention of [$^{99\text{m}}\text{Tc}$] BnAO has not been elucidated.

Receptor-binding peptide-based radiopharmaceuticals

In the past decade, *in vivo* peptide receptor scintigraphy has become a reality. The successful use of the somatostatin analog, [^{111}In]DTPA-octreotide (OctreoScan[®]) (where DTPA is diethylenetriaminepentaacetic acid) for imaging neuroendocrine tumors has led the way in a field that is rapidly expanding. In oncology, the use of these small radiolabeled biological molecules is based upon the overexpression of their receptors in various tumor types²⁸ (Table 28.1). Tumor imaging with radiolabeled peptides that target these receptors may lead to radionuclide therapy using the same targeted peptide carrying a therapeutic isotope. Therefore, in addition to tumor localization information, the diagnostic scan also provides a measure of whether the receptors are sufficiently dense for peptide receptor radionuclide therapy. It is not uncommon for the development of diagnostic and therapeutic peptide radiopharmaceuticals to proceed hand in hand. For instance, the same chelating systems can be used for indium, yttrium, and lutetium, and therefore the development of many

Table 28.1 Peptide receptor proteins found in some human tumors. Adapted from reference 28

<i>Tumor type</i>	<i>Receptor type (subtype)</i>	<i>Tumor type</i>	<i>Receptor type (subtype)</i>
GH-producing pituitary adenoma	Somatostatin (SST2 , SST5)	Neuroblastoma	Somatostatin (SST2) CCK (CCK-1)
Non-functioning pituitary adenoma	Somatostatin (SST3 > SST2)	Medulloblastoma	Somatostatin (SST2) Neurotensin (NTR1)
Gut carcinoid	Somatostatin (SST2 > SST1 , SST5) CCK (CCK-1) GRP/bombesin (NMB-R)	Astrocytoma	Somatostatin CCK/gastrin (CCK-2) Neurotensin (NTR1)
Gastrinoma	Somatostatin (SST2) GRP/bombesin (GRP)	Exocrine pancreatic tumor	Neurotensin (NTR1)
Insulinoma	Somatostatin CCK/gastrin (CCK-2)	Gastric carcinoma	Somatostatin
Paraganglioma	Somatostatin (SST2)	Hepatocellular carcinoma	Somatostatin
Pheochromocytoma	Somatostatin (SST2)	Renal cell carcinoma	Somatostatin GRP/bombesin (GRP)
Medullary thyroid carcinoma	Somatostatin CCK/gastrin (CCK-2) Neurotensin (NTR1)	Prostate carcinoma	Somatostatin (SST1) GRP/bombesin (GRP)
Small-cell lung cancer	Somatostatin (SST2) CCK/gastrin (CCK-2) GRP/bombesin (BB3) Neurotensin (NTR1)	Breast carcinoma	Somatostatin GRP/bombesin (GRP)
Meningioma	Somatostatin (SST2) Neurotensin (NTR1) CCK (CCK-1)	Ovarian carcinoma	Somatostatin
		Lymphoma	Somatostatin
		Ewing sarcoma	Neurotensin (NTR1)
		Leiomyoma	Somatostatin

Subtype in bold indicates receptor of high density and incidence; preferentially expressed subtype in parentheses only when shown by immunohistochemistry or autoradiography.

CCK, cholecystokinin; GRP, gastrin releasing peptide.

¹¹¹In-labeled peptide diagnostic agents is followed closely by that of the ⁹⁰Y or ¹⁷⁷Lu analogs for radionuclide therapy. Similarly, studies of ^{99m}Tc labeled peptide diagnostic imaging agents are often coupled with development of ^{186/188}Re therapeutic analogs. This section will focus primarily on the diagnostic applications of peptide receptor imaging, while peptide receptor radionuclide therapy will be dealt with in a later chapter. Radiolabeled analogs of minigastrin, cholecystokinin, bombesin, and neurotensin are among the more promising peptide diagnostics emerging in the field, and these will be covered in detail.

Peptides are small proteins consisting of anything from two up to 50 amino acids. In general, the peptides being used for receptor targeting in nuclear medicine are in a group of naturally occurring peptides known as regulatory peptides. Regulatory peptides have a wide range of functions, acting as hormones, neurotransmitters, neuromodulators, vasodilators, and growth factors, to name a few.

They have membrane-bound receptors (mainly G protein-coupled receptors) through which they control or modulate the function of major organs and metabolic processes. In general, the peptides are small and hydrophilic, and therefore localize rapidly to the tumor site, binding to the receptor at the cell membrane. Since most peptides used for radionuclide imaging are agonists, the receptor–ligand complex usually internalizes into the cell. This agonist internalization is desirable as it causes accumulation of radioisotope at the tumor site, with little washout over the period of time required for imaging. Any unbound peptide is rapidly excreted through the hepatobiliary or renal route, depending on the peptide. Although these peptides can have side-effects due to their pharmacological activity, these can be minimized by administering extremely low doses, as is usual for radiotracer studies. Peptides are relatively easy to synthesize and radiolabel, and as they are widely conserved through species, have no antigenicity.

However, due to their natural structures, they are rapidly degraded *in vivo* by peptidases. Therefore, one of the greatest challenges in developing new peptide radiopharmaceuticals is to synthesize metabolically stable analogs which maintain the high affinity binding shown by the native peptide.

The somatostatin analogs

The most notable success in the field of peptide receptor scintigraphy has been in the use of radiolabeled somatostatin analogs for diagnosis of somatostatin receptor-positive tumors. Somatostatin is a cyclic 14-mer peptide for which five main receptor subtypes have been identified and cloned (SST1–SST5). As is the case with most native peptides, somatostatin is metabolically unstable, having a circulatory half-life of only 3 minutes.²⁹ This problem was overcome by the incorporation of D-amino acids (to reduce enzymatic degradation) and shortening of the molecule to the core sequence required for receptor binding. This resulted in stabilized analogs (Figure 28.3), some of which are used for conventional therapy of acromegaly and neuroendocrine tumors³⁰ as well as for radionuclide imaging and targeted therapy.

The most widely used of these somatostatin analogs is octreotide. Initially, a tyrosine containing analog, Tyr³-octreotide (TOC) (Figure 28.3) was developed for radiolabeling with isotopes of iodine. However, the use of diethylenetriaminepentaacetic acid (DTPA, see Figure 28.1) conjugated octreotide analogs for labeling with ¹¹¹In greatly improved the biodistribution, shifting the gastrointestinal

excretion of the iodinated compound to a predominantly renal excretion pathway.³¹ This led to commercialization of [¹¹¹In]DTPA-DPhe¹-octreotide (OctreoScan®), the first ever licensed peptide radiopharmaceutical, for the imaging of neuroendocrine tumors. The only other peptide radiopharmaceutical to receive regulatory approval for oncological applications since then is a ^{99m}Tc-labeled somatostatin analog, [^{99m}Tc]Depreotide (NeoTect®), for imaging pulmonary tumors. The clinical use of OctreoScan® and NeoTect® has been extensively covered in the literature, and does not fall within the scope of this chapter.^{32,33} However, work on other somatostatin analogs has continued, and various DTPA and DOTA (Figure 28.1) conjugated analogs have been radiolabeled with radioisotopes of indium, gallium (for PET imaging), yttrium and lutetium (for therapy of neuroendocrine tumors, covered in Chapter 29). Some workers have sought to identify ligands with increased affinity for SST2, the receptor most commonly found in human tumors. Tyr³-octreotate (TATE), an octreotide derivative which lacks the threonine alcohol moiety, shows higher affinity for SST2 than octreotide, and changing the radiometal also has an effect.³⁴ Reubi et al. showed that [Ga]DOTA-Tyr³-octreotate displayed the highest affinity for SST2, followed by [In]-DTPA-Tyr³-octreotate and [Y]DOTA-Tyr³-octreotate. The affinity of [Ga]DOTA-Tyr³-octreotate was two orders of magnitude greater than that of [In]DTPA-octreotide.³⁴ Analogs with different SST receptor affinity profiles have also been investigated. Somatostatin-14 binds to all five of the receptors with high affinity, but the stabilized analogs have varying affinity profiles. Octreotide binds with high affinity to SST2, and with intermediate and moderately high affinity to SST3

Figure 28.3

Some somatostatin analogs which have been radiolabeled with various radioisotopes, usually through bifunctional chelators. Nal, naphthylalanine; Hcy, L-homocysteine; β-Dap, β-(L-1,2-diaminopropionic acid).

Somatostatin-14	Ala-Gly-Cys-Lys-Asn-Phe-Phe-Trp-Lys-Thr-Phe-Ser-Cys
Octreotide	D-Phe-Cys-Phe-D-Trp-Lys-Thr-Cys-Thr(ol)
Lanreotide	β-D-Nal-Cys-Tyr-D-Trp-Lys-Val-Cys-Thr-NH ₂
Tyr ³ -octreotide (TOC)	D-Phe-Cys-Tyr-D-Trp-Lys-Thr-Cys-Thr(ol)
RC-160 (Vapreotide)	D-Phe-Cys-Tyr-D-Trp-Lys-Val-Cys-Trp-NH ₂
Tyr ³ -octreotate (TATE)	D-Phe-Cys-Tyr-D-Trp-Lys-Thr-Cys-Thr
Depreotide (P829)	(N-Me)Phe-Tyr-D-Trp-Lys-Val-Hcy-(CH ₂ CO-(β-Dap)-Lys-Cys-Lys-NH ₂)
Nal ³ -octreotide (NOC)	D-Phe-Cys-Nal-D-Trp-Lys-Thr-Cys-Thr(ol)
Nal ³ -octreotate (NOC-ATE)	D-Phe-Cys-Nal-D-Trp-Lys-Thr-Cys-Thr

and SST5, respectively. A more recently developed compound, (^{111}In -DOTA-1-Nal³-octreotide (^{111}In -DOTA-NOC) (Nal is naphthylalanine), binds SST2, SST3, and SST5, all with high affinity, and has higher binding affinity than all other somatostatin-based radiopeptides.³⁵ The internalization rate of [^{111}In]-DOTA-NOC into AR4-2J rat pancreatic tumor cells was twice that of [^{111}In]-DOTA-TOC, and three times higher than that of [^{111}In]-DOTA-octreotide.³⁵ Furthermore, the uptake of [^{111}In]-DOTA-NOC-ATE into somatostatin receptor positive tissues and AR4-2J tumors in Lewis rats was at least twice that of [^{111}In]-DOTA-TOC, with lower kidney uptake.³⁶ In a study in a single patient with an advanced neuroendocrine tumor [^{68}Ga]-DOTA-NOC showed better imaging characteristics than did [^{111}In]-DOTA-TOC, with some bone metastases being better visualized, perhaps due to expression of SST5 receptors.³⁷

To take advantage of the shorter half-life and superior imaging characteristics of $^{99\text{m}}\text{Tc}$, mixed ligand ethylenediaminediacetic acid (EDDA)/tricine-HYNIC, tricarbonyl, and N_4 (see Figure 28.1) chelating systems (amongst others) have been used to label somatostatin analogs. Of these, the most developed are the [$^{99\text{m}}\text{Tc}$]HYNIC-TOC compounds.^{38,39} It was shown by Decristoforo et al. that the use of EDDA rather than tricine or tricine/nicotinic acid as co-ligand in the labeling of HYNIC-derivatized somatostatin analogs gave higher stability, lower protein binding, and higher tumor/organ ratios.⁴⁰ These findings were supported by a comparison of the results of clinical studies of [$^{99\text{m}}\text{Tc}$]tricine/HYNIC-TOC,³⁹ and [$^{99\text{m}}\text{Tc}$]EDDA/HYNIC-TOC.^{38,41} Since then, [$^{99\text{m}}\text{Tc}$]EDDA/HYNIC-TOC has been evaluated in a number of clinical studies with promising results.^{42–46} In a preclinical study, Storch et al. have recently compared a number of [$^{99\text{m}}\text{Tc}$]EDDA/HYNIC-TOC octreotide derivatives with [^{111}In]DOTA-TATE and [^{111}In]-DTPA-octreotide, showing that [$^{99\text{m}}\text{Tc}$]HYNIC/EDDA-TATE and [^{111}In]-DOTA-TATE had the highest internalization rates and tumor uptakes.⁴⁷ Other workers in the field have been developing Tyr³-octreotate analogs derivatized with a tetraamine chelator (Figure 28.1) (Demotate-1 and -2).^{48–50} One of these (Demotate-1) has been evaluated clinically alongside [$^{99\text{m}}\text{Tc}$]EDDA/HYNIC-TOC, and shows faster pharmacokinetics, providing images as early as 1 hour after injection.^{51,52} In a different approach, octreotide analogs have also been labeled using $^{99\text{m}}\text{Tc}$ -tricarbonyl complexes^{53,54} (Figure 28.1). However, despite the good specific uptake seen in CA20948 pancreatic tumor-bearing Lewis rats of some of the analogs, and commercial availability of the IsoLink[®] kit (Mallinckrodt, Petten, The Netherlands) for preparation of the [$^{99\text{m}}\text{Tc}(\text{H}_2\text{O})_3(\text{CO})_3$]⁺ precursor, none of these compounds has yet progressed to studies in man.

In summary, a number of studies of new somatostatin receptor imaging agents have shown that the octreotate derivatives are generally superior to the octreotide

compounds such as OctreoScan[®], and it remains to be seen whether any of these compounds will undergo commercialization to become licensed radiopharmaceuticals.

Peptide receptor scintigraphy of CCK-2 receptor expressing tumors

The success of peptide receptor scintigraphy with somatostatin analogs has been tempered by the fact that somatostatin receptors are only overexpressed in sufficient quantities in tumor types that are relatively uncommon. Therefore, many workers are seeking to repeat this success using a variety of peptides that have receptors in a wide range of malignancies, especially those that are more common such as lung, colon, or prostate carcinomas. Investigations of a number of other peptide radiopharmaceuticals have been carried out, with perhaps the most advanced and promising being the minigastrin/CCK-8 analogs. The gastrin/CCK-2 receptor has been shown to be present in a number of tumor types, including medullary thyroid carcinoma (MTC) (92%), small-cell lung cancer, astrocytomas (65%), stromal ovarian cancers (100%), and others.^{55,56} Increased expression of CCK-2 mRNA has also been seen in colorectal cancers.⁵⁷ The peptide ligands for this receptor are analogs of either gastrin or cholecystokinin (CCK), both of which are 34 amino acid peptides, and share a C-terminal sequence that confers binding affinity, i.e. Trp-Met-Asp-Phe-NH₂ (Figure 28.4). One of the several shorter forms of CCK is CCK-8, the sulfated form of which binds with high affinity to the CCK-1 receptor as well as CCK-2. Non-sulfated CCK-8, like gastrin, has only low affinity for the CCK-1 receptor, but binds with high affinity to CCK-2.

Behr et al. have looked at a variety of these CCK-2 receptor binding peptides in vivo, either iodinated or labeled with ^{111}In through a DTPA moiety.⁵⁸ They showed that the non-sulfated CCK-8 analogs gave the lowest tumor and CCK-2 receptor positive tissue uptakes in nude mice bearing human medullary thyroid tumors (TT). The sulfated analogs had higher receptor positive tissue uptake, but were also taken up in normal CCK-1 receptor expressing tissues. The gastrin analogs (containing the Glu⁵ sequence) had the highest tumor uptake and highest tumor-to-non-tumor ratios, but also high kidney uptake. [^{111}In]DTPA-minigastrin was used to visualize normal CCK-B receptor expressing

Minigastrin	Leu-(Glu) ⁵ -Ala-Tyr-Gly-Trp-Met-Asp-Phe-NH ₂
MG0	DTPA-DGlu-(Glu) ⁵ -Ala-Tyr-Gly-Trp-Met-Asp-Phe-NH ₂
CCK-8	Asp-Tyr-Met-Gly-Trp-Met-Asp-Phe-NH ₂

Figure 28.4

The amino acid sequences of some CCK-2 (cholecystokinin receptor) ligands.

organs as well as all known tumor sites. This group then went on to develop a [^{111}In]DTPA-DGlu-minigastrin derivative (MG0), which had improved metabolic stability in comparison to the conventional [^{111}In]DTPA-minigastrin conjugate, with corresponding improved background signal.⁵⁹ This radiolabeled minigastrin analog was used to look at MTC in 75 patients, with a sensitivity of 91%.^{60,61} Since the thrust of this work was to combine imaging with peptide receptor radionuclide therapy, eight patients were treated with [^{90}Y]DTPA-D-Glu-minigastrin. Although this treatment had some therapeutic efficacy, some rather severe nephrotoxicity was also seen due to the high renal uptake of this compound.

Other groups working in this field have developed some DTPA- and DOTA-linked non-sulfated CCK analogs.^{62,63} In particular, Reubi and co-workers identified conjugates of DAsp-Tyr-Nle-Gly-Trp-Nle-Asp-Phe-NH₂ as high affinity CCK-2 receptor binders.⁶³ In vivo, the [^{111}In]DOTA conjugate showed specific uptake into receptor positive tissues in CA20948 tumor bearing rats.⁶⁴ On the basis of these findings, an imaging study using the [^{111}In]DTPA analog in seven MTC patients was carried out. Although some of the lesions were visualized, uptake in the strongly receptor positive stomach was low, and the peptide underwent rapid in vivo degradation.⁶⁵

Although most of the work on CCK-2 receptor scintigraphy has been carried out using ^{111}In , a few groups have focused on imaging with $^{99\text{m}}\text{Tc}$ due to its more suitable β emission and half life.⁶⁶⁻⁶⁹ Von Guggenberg et al. have demonstrated very high uptake of a [$^{99\text{m}}\text{Tc}$]EDDA/HYNIC-minigastrin compound in AR4-2J tumors in nude mice,⁶⁹ while Nock and co-workers have evaluated minigastrin analogs modified with N-terminal open chain tetraamines in the same animal model.⁶⁸ Imaging with their lead compound, Demogastrin-2, in one MTC patient detected all known lesions in lymph node, lung, and bone. $^{99\text{m}}\text{Tc}$ -labeled analogs of CCK have also been developed using HYNIC⁶⁷ and diphenylphosphinopropionyl⁶⁶ as chelators. However, these studies have yet to be followed up in humans.

The area of CCK-2 receptor scintigraphy with radiolabeled gastrin/CCK analogs is expanding rapidly, and there are some promising new agents being developed. Although a number of clinical studies have been carried out in MTC, this approach has yet to be evaluated in other CCK-2 receptor expressing tumor types such as small-cell lung carcinoma or (possibly) cancers of the colon.

Receptor scintigraphy with radiolabeled bombesin analogs

Several groups have recently made progress in the development of radiolabeled bombesin analogs for receptor scintigraphy. Bombesin is a 14 amino acid peptide of

amphibian origin, and gastrin releasing peptide (GRP) is its 27 amino acid human counterpart. Apart from one amino acid, the ten C-terminal amino acids of GRP and bombesin are the same. There are three human receptor subtypes, namely the neuromedin B receptor (BB1, NMB, for which neuromedin B is a high affinity ligand), the GRP receptor subtype (BB2, for which GRP is a high affinity ligand), and the orphan receptor, BB3, for which the native ligand has yet to be identified. The GRP receptor is the subtype most frequently expressed in tumors,⁷⁰ and is overexpressed in some common tumor types such as carcinomas of the prostate and breast,²⁸ as well as gastrointestinal stromal tumors.⁷¹ For this reason, research effort has focused on the GRP receptor.

The tendency of Tc/Re-labeled peptides to be somewhat lipophilic and to clear via the hepatobiliary pathway (thus hindering imaging in the abdominal region)⁷² has been a recurrent theme in the development of $^{99\text{m}}\text{Tc}$ -labeled bombesin analogs for SPECT imaging of GRP receptors. Baidoo et al. have described the synthesis of [$^{99\text{m}}\text{Tc}$]diaminodithiol (DADT) conjugates of Lys³-BN.⁷³ Subsequent work by this group involved modifications of this compound to reduce the lipophilicity of these analogs in order to decrease hepatobiliary clearance and allow scintigraphy of the abdominal region.^{74,75} The group of Volkert have used P₂S₂^{76,77} and N₃S BN(7-14) conjugates⁷⁸ using different carbon chain spacers between the Tc binding moiety and the peptide. They showed that between 3 and 8 spacer carbon atoms could be used without compromising the agonist binding affinity.⁷⁹ Van de Wiele and co-workers have demonstrated the clinical utility of these compounds using [$^{99\text{m}}\text{Tc}$]N₃S-Gly-5-Ava-BN(7-14) ([$^{99\text{m}}\text{Tc}$]RP527) in patients, where specific uptake was seen in 4/6 breast and 1/4 androgen-resistant bone-metastasized prostate carcinomas, with good tumor to normal ratios,⁸⁰ but again, hepatobiliary excretion of this compound makes imaging in the abdominal areas problematic.⁸¹ More recently, Nock et al. have investigated a series of compounds, one based on a GRP receptor antagonist as well as four other GRP receptor agonists. Demobesin-1 is based on the potent antagonist D⁶Phe⁶,Leu-NHET¹³,des-Met¹⁴-BN(6-14),⁸² to which they attached an open chain tetraamine (N₄) chelator for labeling with $^{99\text{m}}\text{Tc}$ (see Figure 28.1). Although this compound showed minimal internalization in prostate cancer cells, it demonstrated very high and persistent uptake in PC-3 human xenografts in nude mice.⁸³ This group went on to develop compounds based on GRP receptor agonists, as agonists are known to undergo receptor-mediated endocytosis which allows residualization of the radiometal within the cell. Using the tetraamine chelator, four further compounds were developed: N₄⁰-Pro¹-Tyr⁴-BN and its Nle¹⁴ substituted analog (Demobesin-3 and -4) as well as two truncated BN analogs, (N₄-Bzdig)⁰-BN(7-14) and its Nle¹⁴ substituted analog, using a benzylaminodiglycolic acid spacer between the

chelator and the receptor-binding sequence (Demobesin-5 and -6).⁸⁴ All of the compounds showed high receptor affinity (50% inhibitory concentration) (IC_{50}) < 0.06 nmol/l in competition binding assays) and rapid internalization (~75% within 30 min) in PC-3 tumor cells. In vivo, Demobesin-3 and -4 demonstrated high tumor uptake (9–11%ID/g at 1 h post-injection, 7–9%ID/g at 4 h post-injection, where ID is initial dose) with rapid clearance from non-target tissues. These compounds proved to be much less lipophilic than the truncated BN analogs, and were excreted mainly via the kidneys. Demobesin-5 and -6 showed lower tumor uptake and largely hepatobiliary clearance. Due to the higher tumor uptake and favorable excretion route, this group plan to start clinical trials on their Demobesin-4 compound.

In other clinical studies, Scopinaro et al. have reported detection of prostate cancer using Leu¹³-BN(1–14) modified on its N-terminus to directly bind ^{99m}Tc.⁸⁵ Since this compound undergoes hepatobiliary clearance, it is probable that the Demobesin compounds will be superior in clinical trials. A [^{99m}Tc]EDDA/HYNIC-Lys³-BN compound has been developed by Ferro-Flores et al.⁸⁶ Although this compound shows predominantly renal excretion, it had relatively low uptake in PC-3 tumors in vivo.

[^{99m}Tc]BN derivatives have also been prepared via the (^{99m}Tc(H₂O)₃(CO)₃)⁺ precursor (see Figure 28.1). La Bella et al. demonstrated high binding affinity for the GRP receptor, and rapid internalization into PC-3 cells of their [^{99m}Tc(CO)₃]Nβ-histidinylacetate-BN(7–14) compound; however, tumor uptake was low and no blocking was seen. Since uptake into the pancreas was high and specific, the authors speculated that this was due to weak vascularization of the tumor xenografts. This group developed another tricarbonyl technetium bombesin conjugate: [^{99m}Tc(1)]PADA-AVA-bombesin(7–14) (where PADA is picolyaminodiacetic acid and AVA is S-amino valerianic acid), which demonstrated hepatobiliary clearance in vivo and relatively low (but specific) tumor uptake.⁸⁷ Smith et al. have also used tricarbonyl-^{99m}Tc complexes such as [^{99m}Tc(X)(CO)₃]Dpr-SSS-BN(7–14)NH₂ (where X = H₂O or P(CH₂OH)₃ and Dpr is diaminopropionic acid), demonstrating specific uptake in PC-3 tumor xenografts of 3.7 ± 0.9%ID/g at 1 h post-injection (better than that of the [^{99m}Tc]N₃S conjugate in the same animal model).^{79,88} As yet, the ^{99m}Tc(1)-carbonyl bombesin conjugates have not been investigated in humans.

Receptor scintigraphy with neurotensin analogs

Native neurotensin (NT) is a 13 amino acid peptide found in the central nervous system as well as peripheral tissues, especially in the gastrointestinal tract, where it acts as a

local hormone. Two G protein-coupled NT receptors have been identified: NTR1 which is a high affinity, low capacity receptor and NTR2, a low affinity, high capacity receptor. A further non-G protein-coupled receptor has also been identified (NTR3).²⁸ Reubi and co-workers have shown that NTR1 is expressed in Ewing's sarcoma (65%), meningioma (52%), astrocytoma (43%), medulloblastoma (38%), medullary thyroid carcinoma (29%), small-cell lung carcinoma (25%), and exocrine pancreatic tumors (75%).^{89,90} The native NT C-terminal hexapeptide, Arg⁸-Arg⁹-Pro¹⁰-Tyr¹¹-Ile¹²-Leu¹³, is the minimum sequence required for receptor binding, but as with most native peptide sequences, has a short half-life in human plasma (1.5 minutes in this case).⁹¹ However, stabilized analogs of NT(8–13) have been developed for labeling with ¹³¹I, ¹²³I, ^{99m}Tc, and ¹¹¹In (as well as ¹⁸F, ¹⁷⁷Lu, and ⁹⁰Y).^{91–96} One group of workers has concentrated on labeling with the ^{99m}Tc(1)-tricarbonyl precursor,^{93,97,98} leading to a clinical study of [^{99m}Tc(CO)₃](NβHis)Ac-Lys(ψCH₂-NH)-Arg-Pro-Tyr-Tle-Leu [^{99m}Tc]NT-XI (Tle is tertiary leucine) in ductal pancreatic adenocarcinoma, which expresses NTR1 receptors (whereas there are none in normal pancreas). Tumor was visualized in one out of four patients, the tumor tissue of which was subsequently shown to be NT receptor positive. There was also rather high non-specific kidney and liver uptake.⁹⁹ This group has gone on to develop further compounds to try to increase the target to non-target tissue ratio and improve the clearance profile.⁹⁵ Another group has focused on labeling with ¹¹¹In using DTPA and DOTA conjugates of stabilized NT analogs. Their stabilized peptide (Gly(Pip)-Pro-Gly(PipAm)-Arg-Pro-Tyr-tBuGly-Leu-OH) incorporates amino acid mimics in the enzymatic cleavage positions of the native peptide and has high NTR1 binding affinity (Gly(Pip) is 4-piperidinyl-S-glycine, Gly(PipAm) is 4-piperidinyl-(N-amidino)-S-glycine). This compound, when conjugated to DTPA and labeled with ¹¹¹In, showed good stability and specific tumor NTR1 uptake in HT29 human adenocarcinoma tumor bearing mice.^{94,100} Clinical studies of this agent have yet to be carried out.

Other peptides

Although there are a number of groups working on radiolabeling other peptides which have receptors in various tumor types, these tend to be limited to animal experimentation thus far. An exception worth mentioning is vasoactive intestinal peptide (VIP), of which two radiolabeled analogs, [¹²³I]VIP and [^{99m}Tc]VIP, have been studied in humans.^{101–105} However, despite considerable effort from workers in the field, VIP suffers from a lack of stabilized analogs, limiting the development of good radioligands for the VPAC type receptors which are present in a number of tumor types.^{28,106}

The future of PET radiopharmaceuticals in the current routine

The purpose of this section is to give a brief overview of current PET tracers that have been clinically evaluated for oncology. Also, some PET radiopharmaceuticals with very promising preclinical data will be reviewed, including aspects of new labeling chemistry. Naturally, the selection of papers will be very much of subjective choice within the given space. An analysis of the PET oncology literature of the past 10 years reveals the dominance of 2- ^{18}F fluoro-2-deoxy-D-glucose (^{18}F FDG) compared to other clinical PET tracers (Figures 28.5 and 28.6). However, the relative roles of alternative markers are also becoming apparent. Whereas the average number of ^{11}C methionine (^{11}C MET) publications remains high, the increase of 3'- ^{18}F fluoro-3'-deoxythymidine (^{18}F FLT) articles is comparable with that of ^{18}F FDG.

Glucose transport

FDG-PET

The clinically most relevant PET tracer, ^{18}F FDG, has a long history. More than 70 years ago, Warburg discovered that malignant tumors show an increased glycolytic rate.¹⁰⁷ After PET became an established imaging modality, ^{18}F FDG as a surrogate tracer for D-glucose was prepared for the first time in 1977 by Ido et al. using electrophilic fluorination of 3,4,6-tri-O-acetyl-D-glucal.¹⁰⁸ However, the radiosynthesis had some disadvantages such as poor labeling yield and a carrier-added tracer as a product. Also, ^{18}F fluorine gas was not widely available. The breakthrough in the radiosynthesis of ^{18}F FDG came eventually in 1986 with the publication of a nucleophilic labeling method based on ^{18}F fluoride and the use of the phase transfer catalyst Kryptofix®.¹⁰⁹ This protocol provided no-carrier-added ^{18}F FDG with high yields. The biological basis of FDG-PET is the uptake of the tracer by the glucose transporter, followed by metabolic trapping after

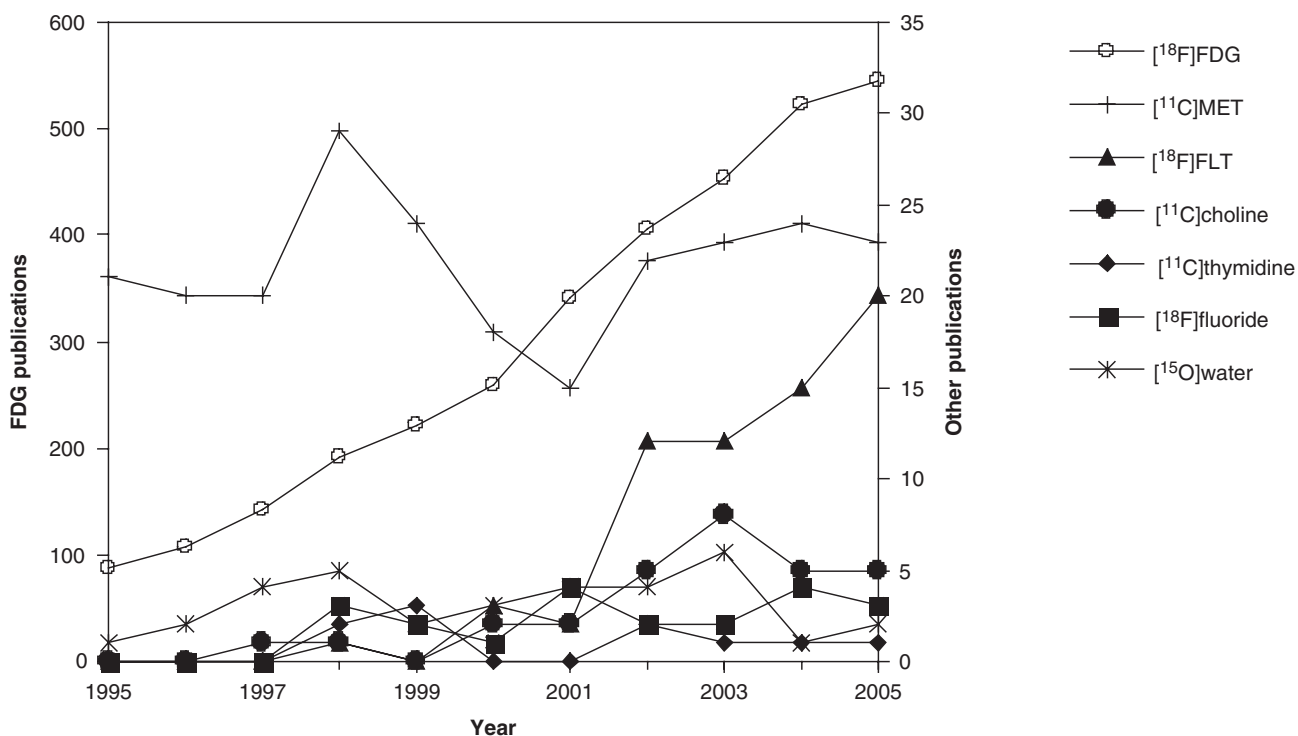


Figure 28.5

Publication statistics of routine positron emission tomography (PET) oncology tracers from 1995 to 2005 (SciFinder). FDG, fluoro-2-deoxy-D-glucose; MET, methionine; FLT, fluoro-3'-deoxy thymidine.

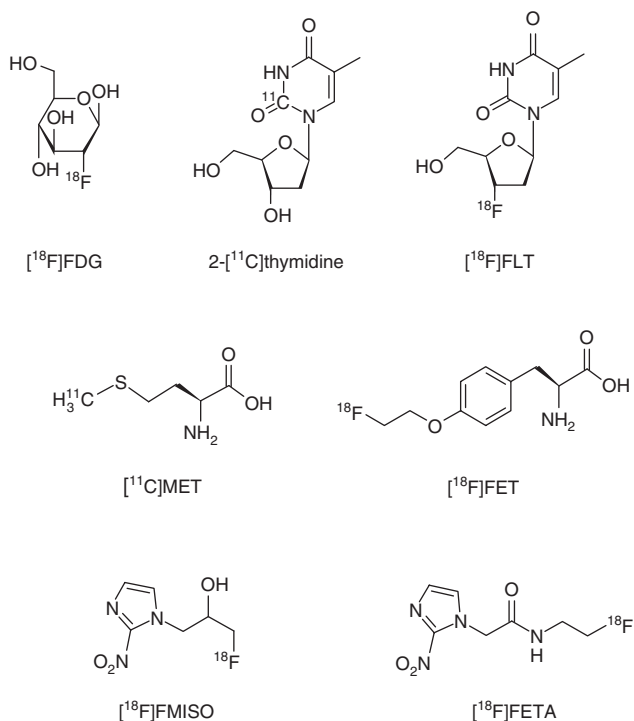


Figure 28.6

Chemical structures of $[^{18}\text{F}]$ FDG, 2- $[^{11}\text{C}]$ thymidine, $[^{18}\text{F}]$ FLT, $[^{11}\text{C}]$ MET, $[^{18}\text{F}]$ FET (fluoroethyl-L-tyrosine.), $[^{18}\text{F}]$ FMISO (fluoro-2-hydroxy propyl-2-nitroimidazole), and $[^{18}\text{F}]$ FETA (fluoroetanidazole).

phosphorylation to $[^{18}\text{F}]$ FDG-6-phosphate by hexokinase. This trapping mechanism enables subsequent PET imaging of cells with predominantly upregulated glucose metabolism. This factor, along with the radiochemistry improvements and the wide range of clinical applications of $[^{18}\text{F}]$ FDG, contributed to the acceptance of the PET method in general. For instance, diagnostic whole-body scanning and diagnosis and preoperative staging of lung cancer have now become widely recognized applications of PET in oncology.¹¹⁰

However, $[^{18}\text{F}]$ FDG as a marker for glucose metabolism is not specific for tumors. Interpreting the images requires experience and skill to identify causes of variable physiological uptake, which can occur through inflammation, wound healing, muscle contraction, and anatomic or physiological variants.^{111,112} This applies, for example, to the low uptake in hepatocellular carcinoma,¹¹³ prostate carcinoma,¹¹⁴ carcinoid,¹¹⁵ differentiated teratomas,¹¹⁶ and mucinous tumors.¹¹⁷ Also, the contribution of tumor proliferation and hypoxia to the $[^{18}\text{F}]$ FDG uptake in individual tumors remains difficult to evaluate.²² Considering these issues, the design of clinical protocols needs careful planning and standardization. There has been a European initiative to produce guidelines for the use of $[^{18}\text{F}]$ FDG for

response assessment in oncology.¹¹⁸ The role of $[^{18}\text{F}]$ FDG for monitoring tumor response to the therapy of a number of cancers has been reviewed recently.¹¹⁹

Given the high importance of $[^{18}\text{F}]$ FDG, various groups are currently investigating further improvements to the automated radiosynthesis. In a proof-of-principle study, it was shown that $[^{18}\text{F}]$ FDG can also be produced on a micro-fabricated device.¹²⁰ This concept allows simplified automation, improved control of reaction parameters, batch fabrication of disposable components, and, most important, very short reaction times. The prototype microchip produced acetyl-protected $[^{18}\text{F}]$ FDG in radiochemical yields of 20–49% in less than 20 seconds.¹²⁰ Using a similar set-up, other researchers reported radiochemical yields of 50% in only 4 seconds.¹²¹ A highly sophisticated microfluidic device was reported by Lee et al. (Figure 28.7).¹²² Here, the chip incorporated the complete radiosynthesis of $[^{18}\text{F}]$ FDG, including initial water removal, fluoridation, and deprotection. This device produced $[^{18}\text{F}]$ FDG in 38%

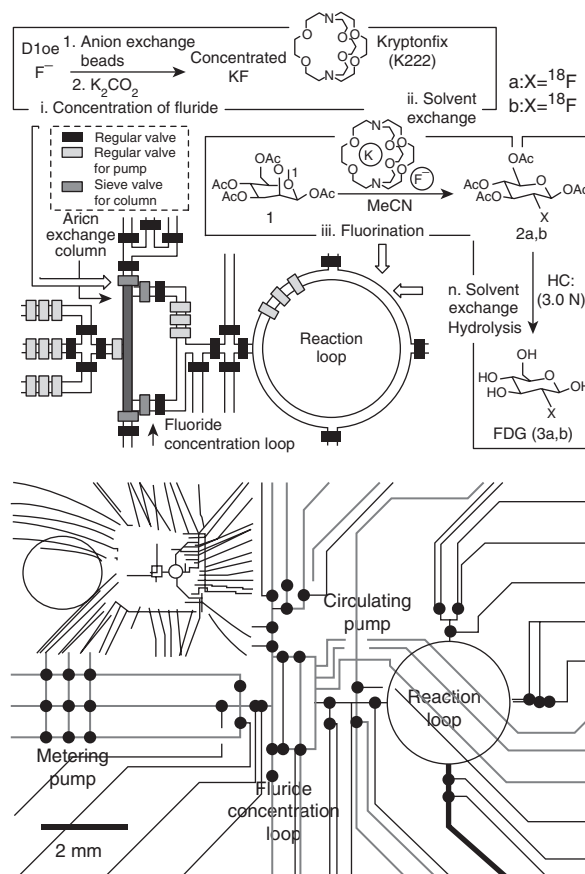


Figure 28.7

Microfluidic device for integral $[^{18}\text{F}]$ FDG synthesis that includes $[^{18}\text{F}]$ fluoride concentration, ^{18}F -fluoridation, and deprotection steps. (From reference 122 reprinted with permission from the American Society for the Advancement of Science (AAAS).)

radiochemical yield and 97.6% radiochemical purity. The isolated radioactivity (190 μCi) was sufficient for a microPET scan of a tumor bearing mouse. Microfabricated devices still have shortcomings such as not delivering sufficient amounts of radioactive tracer for human scanning and poor chip stability to organic solvents. However, the chips are being improved, and ample opportunities for future PET radiochemistry applications can be expected.

Proliferation markers

Radiolabeled nucleosides

^{18}F FDG-PET scanning of the brain for malignant lesions is usually complicated due to the high physiological background signal. In addition, ^{18}F FDG does not measure specifically the rate of DNA synthesis, a more characteristic assessment criteria for developing tumor tissue. A specific proliferation marker would therefore have enormous potential for PET oncology to monitor treatment response. The carbon-11 (half-life 20 min) labeled nucleoside 2- ^{11}C thymidine (Figure 28.6) has been used as a PET tracer to directly measure tumor cell proliferation. The tracer is considered to be a substrate of thymidine kinase (TK1), and is taken up by the salvage pathway (Figure 28.8).¹²³ Vander Borgh et al. carried out initial clinical studies to image brain tumors using 2- ^{11}C thymidine.¹²⁴ Compared with surrounding tissue, an 80% increased uptake of

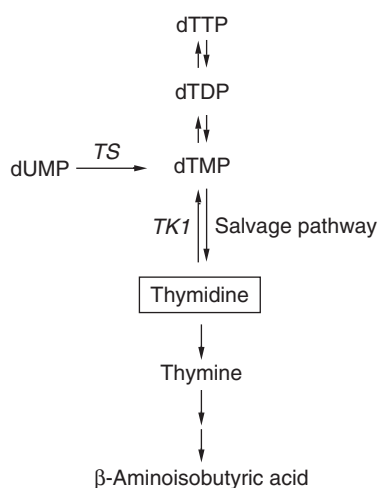


Figure 28.8

Thymidine metabolism and salvage pathway. dUMP, deoxyuridine monophosphate; dTMP, deoxythymidine monophosphate; dTDP, deoxythymidine diphosphate; dTTP, deoxythymidine triphosphate; TS, thymidylate synthase; TK, thymidine kinase.

2- ^{11}C thymidine was found. The investigators also noted a better uptake of that tracer in recurrent tumors compared with ^{18}F FDG. Later, 2- ^{11}C thymidine-PET was applied to measure small-cell lung tumor response to chemotherapy shortly after the initiation of treatment using cisplatin and etoposide. It was found that responding tumors had a lower uptake of 2- ^{11}C thymidine, whereas no change in glucose metabolic activity was seen.¹²⁵

Despite these reports, the short half-life of carbon-11, the non-trivial radiosynthesis, and the complex metabolism can all be seen as disadvantages of 2- ^{11}C thymidine, preventing its general adaption as proliferation marker.

Some of these issues have been overcome with the introduction of ^{18}F FLT (Figure 28.6).¹²⁶ This tracer benefits from the longer half-life of fluorine-18 (110 min) and a straightforward radiosynthesis.^{127–129} The production of ^{18}F FLT is now supported commercially by precursor supply and automated synthesizer modules. However, the process still has some potential for improvements in the final purification step.¹³⁰

As for 2- ^{11}C thymidine, ^{18}F FLT is taken up via the salvage pathway. The fluorine substituent of ^{18}F FLT not only prevents the glycolytic degradation of the compound but also its incorporation into DNA. In a biodistribution study, ^{18}F FLT showed virtually no uptake in the brain but some physiological uptake in the liver, bone marrow, calices, and urinary bladder.¹³⁰ Thus, similarly to 2- ^{11}C thymidine, ^{18}F FLT has a great potential for imaging tumors of the brain where ^{18}F FDG gives a high background signal. Other promising indications are diagnosis and staging of breast cancer, neck tumors, and lymphoma.¹³¹ So far, clinical studies using ^{18}F FLT have been carried out to validate the tracer in comparison with ^{18}F FDG, to differentiate between benign and malignant lesions, or to investigate correlation with proliferation. It has been also reported that ^{18}F FLT uptake can be increased shortly after chemotherapy, which contradicts the concept of the salvage pathway.¹³⁰

Amino acid transporter markers

Radiolabeled amino acids can be used to measure changes in protein metabolism that are caused by the growth of neoplasms. This alternative approach to the study of glucose metabolic rate or cell proliferation has been pursued in PET oncology for many years. Various tracers have been suggested. Two of the most promising compounds that have been discovered are ^{11}C methionine (^{11}C MET, Figure 28.6),^{132,133} and O-(2- ^{18}F fluoroethyl)-L-tyrosine (^{18}F -FET, Figure 28.6).^{134,135} The tracers appear to be more tumor specific as the protein metabolism of inflammatory cells seems to be unaltered.²²

In a recent clinical study it was shown that only ^{18}F FET-PET as opposed to magnetic resonance imaging

(MRI) was able to visualize a recurrent glioma after brain surgery. This result indicated that further operative intervention was not practical.^{136,137}

Hypoxia markers

A characteristic feature of solid tumors is their tendency to become hypoxic. However, any radiation therapy relies on the generation of reactive oxygen radical species. Thus, hypoxic tumors typically show radiation resistance. This phenomenon is also known for chemotherapy agents such as mitomycin C or porfiromycin.²² In addition, the cell response to hypoxia can be a complex gene expression pattern. This includes, for instance, the expression of growth factor genes for adaptive cell response, leading to increased tumor cell vascularization.²² There is currently great interest in the nuclear medicine community to be able to characterize individual tumors in order to improve planning of the radiation therapy regimen. Therefore, various prospective hypoxia markers have been evaluated.

One class of hypoxia markers for PET oncology is based on the 2-nitroimidazole function. A well known PET tracer for hypoxia, 1H-1-(3-[¹⁸F]fluoro-2-hydroxypropyl)-2-nitroimidazole ([¹⁸F]FMISO, Figure 28.6), was proposed by Grierson et al.¹³⁸ The radiosynthesis of [¹⁸F]FMISO has since been further improved and automated.^{139,140} A first clinical study proved the prognostic impact of [¹⁸F]FMISO-PET for imaging of hypoxia in non-small cell lung cancer and head-and-neck cancer before radiotherapy.¹⁴¹ A recently published derivative of [¹⁸F]FMISO is [¹⁸F]fluoroetanidazole ([¹⁸F]FETA, Figure 28.6).¹⁴² Early reports suggest similar in vivo properties as for [¹⁸F]FMISO. However, in a preclinical study, [¹⁸F]FETA proved to be more stable, with a lower liver accumulation and a lower amount of circulating and urinary metabolites.¹⁴³

Bioreductive metal complexes

Pyruvaldehyde-bis (N⁴-methylsemicarbone) (PTSM) readily forms complexes with copper, and has been used in conjunction with the generator-produced, positron emitting

radionuclide copper-62. Cu-PTSM is non-selectively trapped in cells because its redox potential is higher than that of the ubiquitous NADH (reduced nicotinamide adenine dinucleotide) and can therefore be used as a perfusion marker. Diacetyl-bis (N⁴-methylsemicarbone) (ATSM), on the other hand, has a lower redox potential and is trapped only in hypoxic tissues,¹⁴⁴ most likely because of selective reduction of the copper to a reactive intermediate. Cu-ATSM shows higher tumor uptake and more rapid clearance from normal tissues than does FMISO.

Peptide receptor markers

Radiolabeled peptides for targeting receptor expressing tumors are another area of intense research in PET oncology. As described above in the 'SPECT radiopharmaceuticals' section, peptides are regarded as a worthwhile labeling substrate – mostly because they can be easily tailored for specific purpose with nanomolar receptor affinities, they can be designed to be small and stabilized against metabolic degradation, and their biological half-life matches the physical half-life of typical PET nuclides. In this context, fluorine-18 can be seen as an almost ideal positron emitter for peptide labeling. However, the direct introduction of fluorine-18 into peptide precursors is still elusive. Therefore, various approaches based on pre-labeled prosthetic groups have been devised. These labeling agents have been reviewed earlier.^{145–148}

A widely adapted concept relies on the preparation of active esters for conjugation with primary peptide amino groups. Here, *N*-succinimidyl-*p*-[¹⁸F]fluorobenzoate ([¹⁸F]SFB, Figure 28.9) was introduced by Vaidyanathan and Zalutsky¹⁴⁹ in 1992. Later, the radiosynthesis of [¹⁸F]SFB was improved by others.^{148,150} The preparation was also automated, but still requires three radioactive steps, which are time consuming and lower radiochemical yields.^{151,152} In addition, the bulky phenyl moiety can cause unwanted alterations of molecular properties of smaller peptides. So far, [¹⁸F]SFB conjugation has not yet been used for human studies.

A smaller active ester for introducing ¹⁸F into peptides is 2-[¹⁸F]fluoropropionic acid 4-nitrophenylester ([¹⁸F]FPNP,

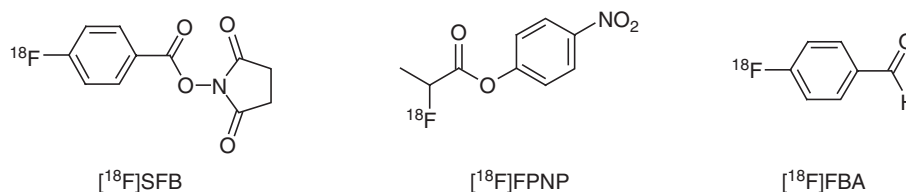


Figure 28.9

Chemical structures of [¹⁸F]SFB (succinimidyl fluorobenzoate), [¹⁸F]FPNP (fluoropropionic acid 4-nitrophenylester), and [¹⁸F]FBA (fluorobenzaldehyde).

Figure 28.9).^{153–155} Although the necessary synthetic effort for preparing [¹⁸F]FPNP is the same as for [¹⁸F]SFB, the labeling synthon can now be obtained in sufficient amounts to label peptides for clinical studies. Beer et al. recently published a study based on peptide labeling using [¹⁸F]FPNP.¹⁵⁶ The authors reported on the biodistribution and pharmacokinetics of [¹⁸F]galacto-RGD in 19 cancer patients with metastases of malignant melanoma, sarcoma, and osseous metastases (Figures 28.10 and 28.11). The [¹⁸F]galacto-RGD tracer allowed the first ever assessment of the $\alpha_v\beta_3$ receptor status in humans as a measure of the degree of angiogenesis.^{157,158} It was found that the tracer uptake varied widely for different tumor types. PET imaging of angiogenesis for monitoring treatment with new

antiangiogenic drugs is a promising field and more studies can be expected.¹⁵⁹

Recently, an interesting new method for chemoselective peptide labeling with fluorine-18 was published by Poethko et al.¹⁶⁰ Here, the prosthetic group p-[¹⁸F]fluorobenzaldehyde ([¹⁸F]FBA, Figure 28.9)¹⁶¹ is prepared in one high yielding labeling step and subsequently conjugated to a modified peptide bearing an aminoxy function. This radiochemistry does not require amino protecting groups, and efficiently results in a very stable oxime bond. Schottelius et al. used [¹⁸F]FBA to prepare the octreotide analog Cel-S-Dpr([¹⁸F]FBOA)TOCA (Figure 28.10) for imaging of the somatostatin receptor.¹⁶² The radiolabeled peptide could be obtained in high yields (65–85%) and

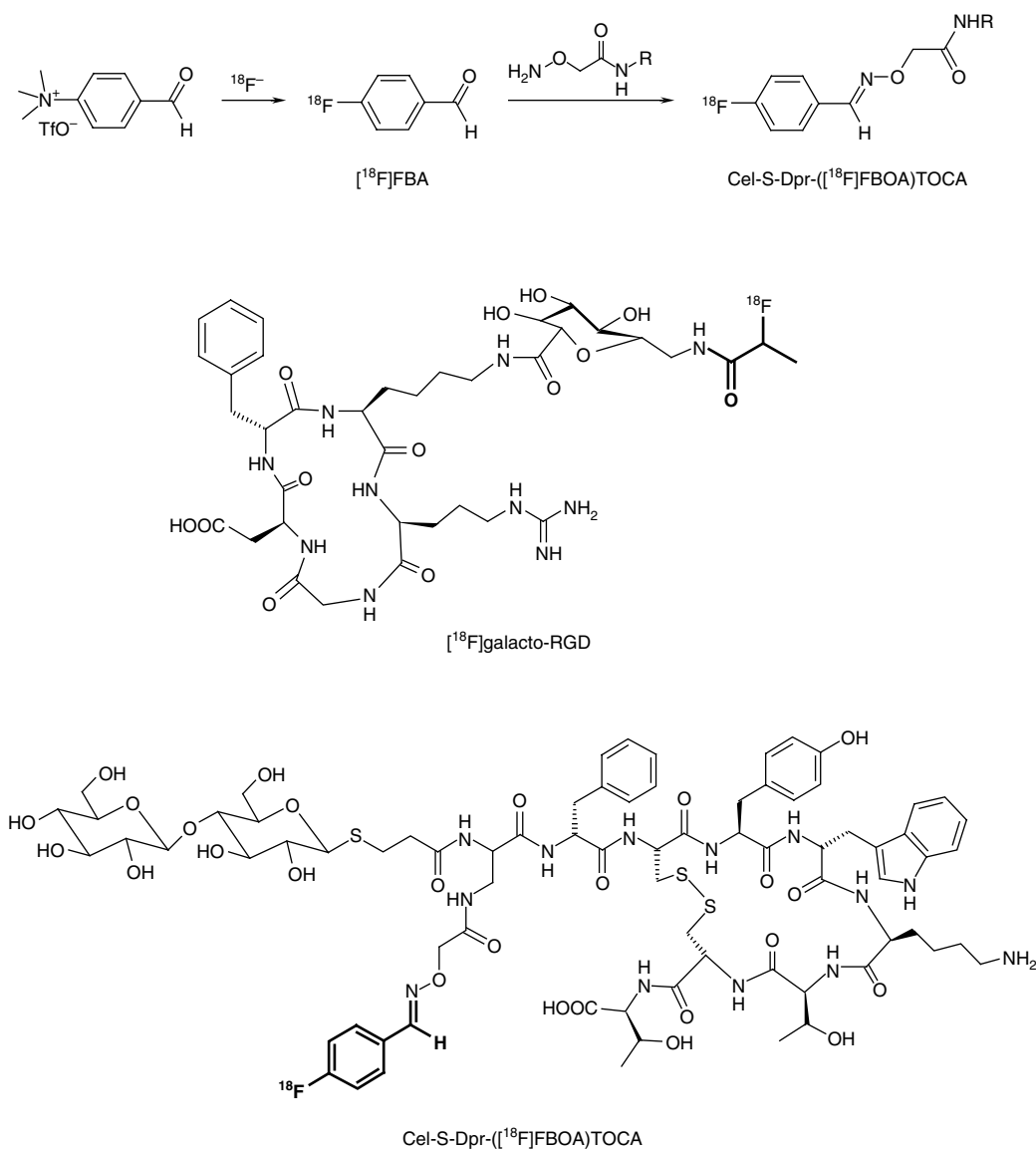


Figure 28.10

Radiosynthesis of Cel-S-Dpr([¹⁸F]FBOA)TOCA, and chemical structures of [¹⁸F]galacto-RGD (Arg-Gly-Asp) and Cel-S-Dpr([¹⁸F]FBOA)TOCA.

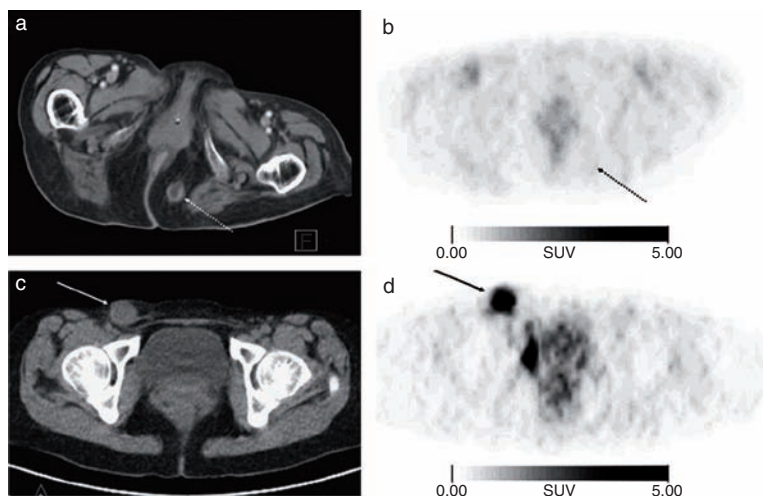


Figure 28.11

$[^{18}\text{F}]$ galacto-RGD scans of two patients with metastases from malignant melanoma showing different tracer uptake. (a) Computed tomography (CT) of 89-year-old female patient with metastasis in subcutaneous fat in gluteal area on left side (arrow), (b) no uptake with $[^{18}\text{F}]$ galacto-RGD; (c) CT of 36-year-old female patient with lymph node metastasis in right groin (arrow); (d) The $[^{18}\text{F}]$ galacto-RGD-PET scan shows intense tracer uptake 89 minutes after injection (arrow, standardized uptake value (SUV) = 6.8). (Reprinted by permission of the Society of Nuclear Medicine from reference 156.)

with fast radiochemistry (50 minutes vs. 3 hours for the $[^{18}\text{F}]$ FPNP chemistry of the same peptide). The tumor accumulation in pancreatic tumor-bearing mice was excellent (15.1 ± 2.5 % of injected dose/g after 1 h) with a low uptake in non-target organs.

Other PET oncology markers

Various fluorinated estrogen analogs have been suggested as diagnostic tools for breast cancer. However, 30–40% of these tumors are not estrogen receptor positive (ER+), and up to 50% of the ER+ tumors will not respond to endocrine therapy.²² Most data in this field have been obtained with 16α - $[^{18}\text{F}]$ fluoroestradiol- 17β -($[^{18}\text{F}]$ FES). Dehdashti et al. were able to show that tamoxifen-responding ER+ patients had reduced $[^{18}\text{F}]$ FES uptake.¹⁶³ The data also revealed local $[^{18}\text{F}]$ FDG accumulation, which was caused by ‘metabolic flare’.

Choline as a marker for membrane lipid metabolism has been radiolabeled with carbon-11 by Hara et al.¹⁶⁴ This tracer and the recently published $[^{18}\text{F}]$ choline¹⁶⁵ are now preferred markers for prostate cancer, with encouraging results.¹⁶⁶

The readily available sodium $[^{18}\text{F}]$ fluoride is a well-established marker for osseous metabolism. The tracer gave good results for skeletal metastases of breast cancer.¹⁶⁷ Due to the higher sensitivity of the PET modality, bone scanning with sodium $[^{18}\text{F}]$ fluoride is superior to existing SPECT diagnostics.

Conclusions

A broad range of alternative and specific markers are now available which are complementary to the limitations of $[^{18}\text{F}]$ FDG-PET. Some of the current anticancer agents can

be cytostatic rather than cytotoxic. Therefore, for optimal diagnosis and treatment decisions, morphological imaging modalities have to be coupled with functional imaging. This need is already reflected by the fact that PET–CT is now a standard instrumentation, and there is no stand-alone PET scanner available on the market. Also, sophisticated PET oncology markers for molecular imaging will have great impact on successful Intensity Modulated Radiation Therapy towards a personalized medicine.

Acknowledgment

Comments from Edward Robins and Erik Årstad on the manuscript of this section are gratefully acknowledged.

References

1. Nunn AD. The cost of developing imaging agents for routine clinical use. *Invest Radiol* 2006; 41: 206–12.
2. Hakumaki JM, Liimatainen T. Molecular imaging of apoptosis in cancer. *Eur J Radiol* 2005; 56: 143–53.
3. Boersma HH, Kietselaer BL, Stolk LM et al. Past, present, and future of annexin A5: from protein discovery to clinical applications. *J Nucl Med* 2005; 46: 2035–50.
4. Kasina S, Rao TN, Srinivasan A et al. Development and biologic evaluation of a kit for preformed chelate technetium-99m radiolabeling of an antibody Fab fragment using a diamide dimercaptide chelating agent. *J Nucl Med* 1991; 32: 1445–51.
5. Boersma HH, Liem IH, Kemerink GJ et al. Comparison between human pharmacokinetics and imaging properties of two conjugation methods for 99mTc -annexin A5. *Br J Radiol* 2003; 76: 553–60.
6. Verbeke K, Kieffer D, Vanderheyden JL et al. Optimization of the preparation of 99mTc -labeled Hynic-derivatized Annexin V for human use. *Nucl Med Biol* 2003; 30: 771–8.

7. Haberkorn U, Kinscherf R, Krammer PH, Mier W, Eisenhut M. Investigation of a potential scintigraphic marker of apoptosis: radioiodinated Z-Val-Ala-DL-Asp(O-methyl)-fluoromethyl ketone. *Nucl Med Biol* 2001; 28: 793–8.
8. Bauer C, Bauder-Wuest U, Mier W, Haberkorn U, Eisenhut M. ¹³¹I-labeled peptides as caspase substrates for apoptosis imaging. *J Nucl Med* 2005; 46: 1066–74.
9. Haubner RH, Wester HJ, Weber WA, Schwaiger M. Radiotracer-based strategies to image angiogenesis. *Q J Nucl Med* 2003; 47: 189–99.
10. Giersing BK, Rae MT, CarballidoBrea M, Williamson RA, Blower PJ. Synthesis and characterization of ¹¹¹In-DTPA-N-TIMP-2: a radiopharmaceutical for imaging matrix metalloproteinase expression. *Bioconjug Chem* 2001; 12: 964–71.
11. Koivunen E, Arap W, Valtanen H et al. Tumor targeting with a selective gelatinase inhibitor. *Nat Biotechnol* 1999; 17: 768–74.
12. Zheng QH, Fei X, DeGrado TR et al. Synthesis, biodistribution and micro-PET imaging of a potential cancer biomarker carbon-11 labeled MMP inhibitor (2R)-2-[[4-(6-fluorohex-1-ynyl)phenyl]sulfonylamino]-3-methylbutyric acid [¹¹C]methyl ester. *Nucl Med Biol* 2003; 30: 753–60.
13. Aumailley M, Gurrath M, Muller G et al. Arg-Gly-Asp constrained within cyclic pentapeptides. Strong and selective inhibitors of cell adhesion to vitronectin and laminin fragment P1. *FEBS Lett* 1991; 291: 50–4.
14. Haubner R, Wester HJ, Reuning U et al. Radiolabeled alpha(v)beta3 integrin antagonists: a new class of tracers for tumor targeting. *J Nucl Med* 1999; 40: 1061–71.
15. Haubner R, Wester HJ, Weber WA et al. Noninvasive imaging of alpha(v)beta3 integrin expression using ¹⁸F-labeled RGD-containing glycopeptide and positron emission tomography. *Cancer Res* 2001; 61: 1781–5.
16. Janssen M, Oyen W, Massuger L et al. Comparison of a monomeric and dimeric radiolabeled RGD-peptide for tumor imaging. *Cancer Biother Radiopharm* 2002; 17: 641–6.
17. Wester HJ, Kessler H. Molecular targeting with peptides or peptide-polymer conjugates: just a question of size? *J Nucl Med* 2005; 46: 1940–50.
18. Line BR, Mitra A, Nan A, Ghandehari H. Targeting tumor angiogenesis: comparison of peptide and polymer-peptide conjugates. *J Nucl Med* 2005; 46: 1552–60.
19. Kaspar M, Zardi L, Neri D. Fibronectin as target for tumor therapy. *Int J Cancer* 2006; 118: 1331–9.
20. Demartis S, Tarli L, Borsi L, Zardi L, Neri D. Selective targeting of tumor neovasculature by a radiohalogenated human antibody fragment specific for the ED-B domain of fibronectin. *Eur J Nucl Med* 2001; 28: 534–9.
21. Santimaria M, Moscatelli G, Viale GL et al. Immunoscintigraphic detection of the ED-B domain of fibronectin, a marker of angiogenesis, in patients with cancer. *Clin Cancer Res* 2003; 9: 571–9.
22. Couturier O, Luxen A, Chatal A et al. Fluorinated tracers for imaging cancer with positron emission tomography. *Eur J Nucl Med* 2004; 31: 1182–206.
23. Ballinger JR, Imaging hypoxia in tumors. *Semin Nucl Med* 2001; 31: 321–9.
24. Mannan RH, Somayaji VV, Lee, J et al. Radioiodinated 1-(5-iodo-5-deoxy-beta-D-arabinofuranosyl)-2-nitroimidazole (iodoazomycin arabinoside: IAZA): a novel marker of tissue hypoxia. *J Nucl Med* 1991; 32: 1764–70.
25. Linder KE, Chan YW, Cyr JE et al. TcO(PnA.O-1-(2-nitroimidazole)) [BMS-181321], a new technetium-containing nitroimidazole complex for imaging hypoxia: synthesis, characterization, and xanthine oxidase-catalyzed reduction. *J Med Chem* 1994; 37: 9–17.
26. Melo T, Duncan J, Ballinger JR, Rauth AM. BRU59-21, a second-generation ^{99m}Tc-labeled 2-nitroimidazole for imaging hypoxia in tumors. *J Nucl Med* 2000; 41: 169–76.
27. Zhang X, Melo T, Ballinger JR, Rauth AM. Studies of ^{99m}Tc-BnAO (HL-91): a non-nitroaromatic compound for hypoxic cell detection. *Int J Radiat Oncol Biol Phys* 1998; 42: 737–40.
28. Reubi JC. Peptide receptors as molecular targets for cancer diagnosis and therapy. *Endocr Rev* 2003; 24: 389–427.
29. Lamberts SW, Koper JW, Reubi JC. Potential role of somatostatin analogs in the treatment of cancer. *Eur J Clin Invest* 1987; 17: 281–7.
30. Pollak MN, Schally AV. Mechanisms of antineoplastic action of somatostatin analogs. *Proc Soc Exp Biol Med* 1998; 217: 143–52.
31. Krenning EP, Kwekkeboom DJ, Bakker WH et al. Somatostatin receptor scintigraphy with [¹¹¹In-DTPA-D-Phe1]- and [¹²³I-Tyr3]-octreotide: the Rotterdam experience with more than 1000 patients. *Eur J Nucl Med* 1993; 20: 716–31.
32. Warner RR, O'Dorisio TM. Radiolabeled peptides in diagnosis and tumor imaging: clinical overview. *Semin Nucl Med* 2002; 32: 79–83.
33. Blum J, Handmaker H, Lister-James J, Rinne N. A multi-center trial with a somatostatin analog Tc-99m depreotide in the evaluation of solitary pulmonary nodules. *Chest* 2000; 117: 1232–8.
34. Reubi JC, Schar JC, Waser B et al. Affinity profiles for human somatostatin receptor subtypes SST1-SST5 of somatostatin radiotracers selected for scintigraphic and radiotherapeutic use. *Eur J Nucl Med* 2000; 27: 273–82.
35. Wild D, Schmitt JS, Ginj M et al. DOTA-NOC, a high-affinity ligand of somatostatin receptor subtypes 2, 3 and 5 for labelling with various radiometals. *Eur J Nucl Med Mol Imaging* 2003; 30: 1338–47.
36. Ginj M, Chen J, Walter MA et al. Preclinical evaluation of new and highly potent analogs of octreotide for predictive imaging and targeted radiotherapy. *Clin Cancer Res* 2005; 11: 1136–45.
37. Wild D, Macke HR, Waser B et al. ⁶⁸Ga-DOTANOC: a first compound for PET imaging with high affinity for somatostatin receptor subtypes 2 and 5. *Eur J Nucl Med Mol Imaging* 2005; 32: 724.
38. Decristoforo C, Mather SJ, Cholewinski W et al. ^{99m}Tc-EDDA/HYNIC-TOC: a new ^{99m}Tc-labeled radiopharmaceutical for imaging somatostatin receptor-positive tumors; first clinical results and intra-patient comparison with ¹¹¹In-labeled octreotide derivatives. *Eur J Nucl Med* 2000; 27: 1318–25.
39. Bangard M, Behr M, Gohlke S et al. Detection of somatostatin receptor-positive tumors using the new Tc-99m-tricine-HYNIC-D-Phe(1)-Tyr(3)-octreotide: first results in patients and comparison with In-111-DTPA-D-Phe(1)-octreotide. *Eur J Nucl Med* 2000; 27: 628–37.

40. Decristoforo C, Melendez-Alafort L, Sosabowski JK, Mather SJ. ^{99m}Tc -HYNIC-[Tyr3]-octreotide for imaging somatostatin-receptor-positive tumors: preclinical evaluation and comparison with ^{111}In -octreotide. *J Nucl Med* 2000; 41: 1114–19.
41. Decristoforo C, Cholewinski W, Donnemiller E et al. Detection of somatostatin receptor-positive tumors using the new ^{99m}Tc -tricine-HYNIC-D-Phe1-Tyr3-octreotide: first results in patients and comparison with ^{111}In -DTPA-D-Phe1-octreotide. *Eur J Nucl Med* 2000; 27: 1580.
42. Parisella M, D'Alessandria C, van de Bossche B et al. ^{99m}Tc -EDDA/HYNIC-TOC in the management of medullary thyroid carcinoma. *Cancer Biother Radiopharm* 2004; 19: 211–17.
43. Plachcinska A, Mikolajczak R, Maecke HR et al. Clinical usefulness of ^{99m}Tc -EDDA/HYNIC-TOC scintigraphy in oncological diagnostics: a preliminary communication. *Eur J Nucl Med Mol Imaging* 2003; 30: 1402–6.
44. Gabriel M, Froehlich F, Decristoforo C et al. ^{99m}Tc -EDDA/HYNIC-TOC and (18) F-FDG in thyroid cancer patients with negative (131) I whole-body scans. *Eur J Nucl Med Mol Imaging* 2004; 31: 330–41.
45. Plachcinska A, Mikolajczak R, Maecke H et al. Clinical usefulness of ^{99m}Tc -EDDA/HYNIC-TOC scintigraphy in oncological diagnostics: a pilot study. *Cancer Biother Radiopharm* 2004; 19: 261–70.
46. Plachcinska A, Mikolajczak R, Maecke HR et al. ^{99m}Tc -EDDA/HYNIC-TOC scintigraphy in the differential diagnosis of solitary pulmonary nodules. *Eur J Nucl Med Mol Imaging* 2004; 31: 1005–10.
47. Storch D, Behe M, Walter MA et al. Evaluation of [^{99m}Tc /EDDA/HYNIC]octreotide derivatives compared with [^{111}In -DOTA0,Tyr3,Thr8]octreotide and [^{111}In -DTPA0]octreotide: does tumor or pancreas uptake correlate with the rate of internalization? *J Nucl Med* 2005; 46: 1561–9.
48. Nikolopoulou A, Maina T, Sotiriou P, Cordopatis P, Nock BA. Tetraamine-modified octreotide and octreotate: labeling with ^{99m}Tc and preclinical comparison in AR4-2J cells and AR4-2J tumor-bearing mice. *J Pept Sci* 2006; 12: 124–31.
49. Kopecky M, Trejtnar F, Laznicek M et al. ^{99m}Tc demotate 1: biodistribution and elimination characteristics in rats. *Nucl Med Commun* 2005; 26: 549–54.
50. Maina T, Nock B, Nikolopoulou A et al. [^{99m}Tc]Demotate, a new ^{99m}Tc -based [Tyr3]octreotate analogue for the detection of somatostatin receptor-positive tumors: synthesis and preclinical results. *Eur J Nucl Med Mol Imaging* 2002; 29: 742–53.
51. Gabriel M, Decristoforo C, Maina T et al. ^{99m}Tc -N4-[Tyr3]octreotate versus ^{99m}Tc -EDDA/HYNIC-[Tyr3] octreotide: an inpatient comparison of two novel Technetium-99m labeled tracers for somatostatin receptor scintigraphy. *Cancer Biother Radiopharm* 2004; 19: 73–9.
52. Decristoforo C, Maina T, Nock B et al. ^{99m}Tc -Demotate 1: first data in tumor patients—results of a pilot/phase I study. *Eur J Nucl Med Mol Imaging* 2003; 30: 1211–19.
53. Spradau TW, Edwards WB, Anderson CJ, Welch MJ, Katzenellenbogen JA. Synthesis and biological evaluation of Tc- 99m -cyclopentadienyltricarbonyltechnetium-labeled octreotide. *Nucl Med Biol* 1999; 26: 1–7.
54. Schibli R, Schubiger PA. Current use and future potential of organometallic radiopharmaceuticals. *Eur J Nucl Med Mol Imaging* 2002; 29: 1529–42.
55. Reubi JC, Schaer JC, Waser B. Cholecystokinin (CCK)-A and CCK-B gastrin receptors in human tumors. *Cancer Res* 1997; 57: 1377–86.
56. Reubi JC, Waser B. Unexpected high incidence of cholecystokinin-B/gastrin receptors in human medullary thyroid carcinomas. *Int J Cancer* 1996; 67: 644–7.
57. Schmitz F, Otte JM, Stechele HU et al. CCK-B/gastrin receptors in human colorectal cancer. *Eur J Clin Invest* 2001; 31: 812–20.
58. Behr TM, Jenner N, Behe M et al. Radiolabeled peptides for targeting cholecystokinin-B/gastrin receptor-expressing tumors. *J Nucl Med* 1999; 40: 1029–44.
59. Behe M, Becker W, Gotthardt M, Angerstein C, Behr TM. Improved kinetic stability of DTPA-dGlu as compared with conventional monofunctional DTPA in chelating indium and yttrium: preclinical and initial clinical evaluation of radiometal labeled minigastrin derivatives. *Eur J Nucl Med Mol Imaging* 2003; 30: 1140–6.
60. Behe M, Behr TM. Cholecystokinin-B (CCK-B)/gastrin receptor targeting peptides for staging and therapy of medullary thyroid cancer and other CCK-B receptor expressing malignancies. *Biopolymers* 2002; 66: 399–418.
61. Behr TM, Behe MP. Cholecystokinin-B/gastrin receptor-targeting peptides for staging and therapy of medullary thyroid cancer and other cholecystokinin-B receptor-expressing malignancies. *Semin Nucl Med* 2002; 32: 97–109.
62. Aloj L, Caraco C, Panico M et al. In vitro and in vivo evaluation of ^{111}In -DTPAGlu-G-CCK8 for cholecystokinin-B receptor imaging. *J Nucl Med* 2004; 45: 485–94.
63. Reubi JC, Waser B, Schaer JC et al. Unsulfated DTPA- and DOTA-CCK analogs as specific high-affinity ligands for CCK-B receptor-expressing human and rat tissues in vitro and in vivo. *Eur J Nucl Med* 1998; 25: 481–90.
64. de Jong M, Bakker WH, Bernard BF et al. Preclinical and initial clinical evaluation of In-111-labeled nonsulfated CCK8 analog: a peptide for CCK-B receptor-targeted scintigraphy and radionuclide therapy. *J Nucl Med* 1999; 40: 2081–7.
65. Kwekkeboom DJ, Bakker WH, Kooij PP et al. Cholecystokinin receptor imaging using an octapeptide DTPA-CCK analogue in patients with medullary thyroid carcinoma. *Eur J Nucl Med* 2000; 27: 1312–17.
66. Aloj L, Panico M, Caraco C et al. In vitro and in vivo characterization of Indium-111 and Technetium-99m labeled CCK-8 derivatives for CCK-B receptor imaging. *Cancer Biother Radiopharm* 2004; 19: 93–8.
67. Laverman P, Behe M, Oyen WJ et al. Two technetium-99m-labeled cholecystokinin-8 (CCK8) peptides for scintigraphic imaging of CCK receptors. *Bioconjug Chem* 2004; 15: 561–8.
68. Nock BA, Maina T, Behe M et al. CCK-2/gastrin receptor-targeted tumor imaging with (99m) Tc-labeled minigastrin analogs. *J Nucl Med* 2005; 46: 1727–36.
69. von Guggenberg E, Behe M, Behr TM et al. ^{99m}Tc -labeling and in vitro and in vivo evaluation of HYNIC- and (Nalpa-His)acetic acid-modified [D-Glu1]-minigastrin. *Bioconjug Chem* 2004; 15: 864–71.
70. Reubi JC, Wenger S, Schmuckli-Maurer J, Schaer JC, Gugger M. Bombesin receptor subtypes in human cancers: detection

- with the universal radioligand (125)I-[D-TYR(6), beta-ALA(11), PHE(13), NLE(14)] bombesin(6-14). *Clin Cancer Res* 2002; 8: 1139–46.
71. Reubi JC, Korner M, Waser B, Mazzucchelli L, Guillou L. High expression of peptide receptors as a novel target in gastrointestinal stromal tumors. *Eur J Nucl Med Mol Imaging* 2004; 31: 803–10.
 72. Decristoforo C, Mather SJ. The influence of chelator on the pharmacokinetics of 99mTc-labeled peptides. *Q J Nucl Med* 2002; 46: 195–205.
 73. Baidoo KE, Lin KS, Zhan Y et al. Design, synthesis, and initial evaluation of high-affinity technetium bombesin analogs. *Bioconjug Chem* 1998; 9: 218–25.
 74. Lin KS, Luu A, Baidoo KE et al. A new high affinity technetium-99m-bombesin analogue with low abdominal accumulation. *Bioconjug Chem* 2005; 16: 43–50.
 75. Lin KS, Luu A, Baidoo KE et al. A new high affinity technetium analogue of bombesin containing DTPA as a pharmacokinetic modifier. *Bioconjug Chem* 2004; 15: 1416–23.
 76. Gali H, Hoffman TJ, Sieckman GL et al. Synthesis, characterization, and labeling with 99mTc/188Re of peptide conjugates containing a dithia-bisphosphine chelating agent. *Bioconjug Chem* 2001; 12: 354–63.
 77. Karra SR, Schibli R, Gali H et al. 99mTc-labeling and in vivo studies of a bombesin analogue with a novel water-soluble dithiadiphosphine-based bifunctional chelating agent. *Bioconjug Chem* 1999; 10: 254–60.
 78. Smith CJ, Gali H, Sieckman GL et al. Radiochemical investigations of (99m)Tc-N(3)S-X-BBN[7-14]NH(2): an in vitro/in vivo structure-activity relationship study where X = 0-, 3-, 5-, 8-, and 11-carbon tethering moieties. *Bioconjug Chem* 2003; 14: 93–102.
 79. Smith CJ, Volkert WA, Hoffman TJ. Gastrin releasing peptide (GRP) receptor targeted radiopharmaceuticals: a concise update. *Nucl Med Biol* 2003; 30: 861–8.
 80. Van de Wiele C, Dumont F, Vanden Broecke R et al. Technetium-99m RP527, a GRP analogue for visualisation of GRP receptor-expressing malignancies: a feasibility study. *Eur J Nucl Med* 2000; 27: 1694–9.
 81. Van de Wiele C, Dumont F, Dierckx RA et al. Biodistribution and dosimetry of (99m)Tc-RP527, a gastrin-releasing peptide (GRP) agonist for the visualization of GRP receptor-expressing malignancies. *J Nucl Med* 2001; 42: 1722–7.
 82. Wang LH, Coy DH, Taylor JE et al. des-Met carboxyl-terminally modified analogs of bombesin function as potent bombesin receptor antagonists, partial agonists, or agonists. *J Biol Chem* 1990; 265: 15695–703.
 83. Nock B, Nikolopoulou A, Chiotellis E et al. [99mTc] Demobesin 1, a novel potent bombesin analogue for GRP receptor-targeted tumor imaging. *Eur J Nucl Med Mol Imaging* 2003; 30: 247–58.
 84. Nock BA, Nikolopoulou A, Galanis A et al. Potent bombesin-like peptides for GRP-receptor targeting of tumors with 99mTc: a preclinical study. *J Med Chem* 2005; 48: 100–10.
 85. Scopinaro F, De Vincentis G, Varvarigou AD et al. 99mTc-bombesin detects prostate cancer and invasion of pelvic lymph nodes. *Eur J Nucl Med Mol Imaging* 2003; 30: 1378–82.
 86. Ferro-Flores G, de Murphy CA, Rodr Guez-Corte SJ, Pedraza-Lo Pez M, Ram Rez-Iglesias MA. Preparation and evaluation of 99mTc-EDDA/HYNIC-[Lys3]-bombesin for imaging gastrin-releasing peptide receptor-positive tumors. *Nucl Med Commun* 2006; 27: 371–6.
 87. La Bella R, Garcia-Garayoa E, Langer M et al. In vitro and in vivo evaluation of a 99mTc(I)-labeled bombesin analogue for imaging of gastrin releasing peptide receptor-positive tumors. *Nucl Med Biol* 2002; 29: 553–60.
 88. Smith CJ, Sieckman GL, Owen NK et al. Radiochemical investigations of gastrin-releasing peptide receptor-specific [(99m)Tc(X)(CO)3-Dpr-Ser-Ser-Ser-Gln-Trp-Ala-Val-Gly-His-Leu-Met-(NH2)] in PC-3, tumor-bearing, rodent models: syntheses, radiolabeling, and in vitro/in vivo studies where Dpr = 2,3-diaminopropionic acid and X = H₂O or P(CH₂OH)₃. *Cancer Res* 2003; 63: 4082–8.
 89. Reubi JC, Waser B, Friess H, Buchler M, Laissue J. Neurotensin receptors: a new marker for human ductal pancreatic adenocarcinoma. *Gut* 1998; 42: 546–50.
 90. Reubi JC, Waser B, Schaer JC, Laissue JA. Neurotensin receptors in human neoplasms: high incidence in Ewing's sarcomas. *Int J Cancer* 1999; 82: 213–18.
 91. Chavatte K, Terriere D, Jeannin L et al. Labelling and evaluation of new stabilised neurotensin (8-13) analogues for single photon emission tomography (SPET). *J Lab Comp Radiopharm* 1999; 42: 423–35.
 92. Terriere D, Chavatte K, Ceusters M, Tourwe D, Mertens J. Radiosynthesis of new radio neurotensin (8-13) analogues. *J Lab Comp Radiopharm* 1998; 41: 19–27.
 93. Garcia-Garayoa E, Blauenstein P, Bruehlmeier M et al. Preclinical evaluation of a new, stabilized neurotensin(8–13) pseudopeptide radiolabeled with (99m)tc. *J Nucl Med* 2002; 43: 374–83.
 94. Achilefu S, Srinivasan A, Schmidt MA et al. Novel bioactive and stable neurotensin peptide analogs capable of delivering radiopharmaceuticals and molecular beacons to tumors. *J Med Chem* 2003; 46: 3403–11.
 95. Maes V, Garcia-Garayoa E, Blauenstein P, Tourwe D. Novel 99mTc-labeled neurotensin analogs with optimized biodistribution properties. *J Med Chem* 2006; 49: 1833–6.
 96. Bergmann R, Scheunemann M, Heichert C et al. Biodistribution and catabolism of (18)F-labeled neurotensin(8-13) analogs. *Nucl Med Biol* 2002; 29: 61–72.
 97. Schubiger PA, Allemann Tannahill L, Egli A et al. Catabolism of neurotensins – implications for the design of radiolabeling strategies of peptides. *Q J Nucl Med* 1999; 43: 155–8.
 98. Bruehlmeier M, Garayoa EG, Blanc A et al. Stabilization of neurotensin analogs: effect on peptide catabolism, biodistribution and tumor binding. *Nucl Med Biol* 2002; 29: 321–7.
 99. Buchegger F, Bonvin F, Kosinski M et al. Radiolabeled neurotensin analog, 99mTc-NT-XI, evaluated in ductal pancreatic adenocarcinoma patients. *J Nucl Med* 2003; 44: 1649–54.
 100. de Visser M, Janssen PJ, Srinivasan A et al. Stabilised 111In-labeled DTPA- and DOTA-conjugated neurotensin analogs for imaging and therapy of exocrine pancreatic cancer. *Eur J Nucl Med Mol Imaging* 2003; 30: 1134–9.
 101. Thakur ML, Marcus CS, Saeed S et al. Tc-99m-labeled vasoactive intestinal peptide analog for rapid localization of tumors in humans. *J Nucl Med* 2000; 41: 107–10.

102. Hennesius C, Bader M, Meinhold H et al. Vasoactive intestinal peptide receptor scintigraphy in patients with pancreatic adenocarcinomas or neuroendocrine tumors. *Eur J Nucl Med* 2000; 27: 1684–93.
103. Raderer M, Kurtaran A, Yang Q et al. Iodine-123-vasoactive intestinal peptide receptor scanning in patients with pancreatic cancer. *J Nucl Med* 1998; 39: 1570–5.
104. Raderer M, Kurtaran A, Vorbeck F et al. Iodine-123 vasoactive intestinal peptide (VIP) receptor scintigraphy in patients with colorectal cancer. *J Nucl Med* 1998; 39: 146.
105. Virgolini I, Raderer M, Kurtaran A et al. I-123 Vasoactive-intestinal-peptide (VIP) receptor scanning – update of imaging results in patients with adenocarcinomas and endocrine tumors of the gastrointestinal-tract. *Nucl Med Biol* 1996; 23: 685–92.
106. Reubi JC. In vitro evaluation of VIP/PACAP receptors in healthy and diseased human tissues. Clinical implications. *Ann N Y Acad Sci* 2000; 921: 1–25.
107. Warburg O. The metabolism of tumors. 1931: 129–69.
108. Ido T, Wan CN, Fowler JS, Wolf AP. Fluorination with F₂. A convenient synthesis of 2-deoxy-2-fluoro-D-glucose. *J Org Chem* 1977; 42: 2341–2.
109. Hamacher K, Coenen HH, Stoecklin G. Efficient stereospecific synthesis of NCA 2-[¹⁸F]fluoro-2-deoxy-2-fluoro-D-glucose using aminopolyether supported nucleophilic substitution. *J Nucl Med* 1986; 27: 235–8.
110. Anderson H, Price P. What does positron emission tomography offer oncology? *Eur J Cancer* 2000; 36: 2028–35.
111. Stahl A, Wieder H, Piert M et al. Positron emission tomography as a tool for translational research in oncology. *Mol Imaging Biol* 2004; 6: 214–24.
112. Pacak K, Eisenhofer G, Goldstein DS. Functional imaging of endocrine tumors: role of positron emission tomography. *Endocr Rev* 2004; 25: 568–80.
113. Torizuka T, Tamaki N, Inokuma T et al. In vivo assessment of glucose metabolism in hepatocellular carcinoma with FDG-PET. *J Nucl Med* 1995; 36: 1811–17.
114. Hofer C, Laubenbacher C, Block T et al. Fluorine-18-fluorodeoxyglucose positron emission tomography is useless for the detection of local recurrence after radical prostatectomy. *Eur Urol* 1999; 36: 31–5.
115. Adams S, Baum R, Rink T et al. Limited value of fluorine-18 fluorodeoxyglucose positron emission tomography for the imaging of neuroendocrine tumors. *Eur J Nucl Med* 1998; 25: 79–83.
116. Bender H, Schomburg A, Albers P, Ruhlmann J, Biersack HJ. Possible role of FDG-PET in the evaluation of urologic malignancies. *Anticancer Res* 1997; 17: 1655–60.
117. Stahl A, Ott K, Weber W et al. FDG PET imaging of locally advanced gastric carcinomas: Correlation with endoscopic and histopathological findings. *Eur J Nucl Med Mol Imaging* 2003; 30: 288–95.
118. Young H, Baum R, Cremerius U et al. Measurement of clinical and subclinical tumor response using [¹⁸F]-fluorodeoxyglucose and positron emission tomography: review and 1999 EORTC recommendations. *Eur J Cancer* 1999; 35: 1773–82.
119. Giannopoulou C. The role of SPET and PET in monitoring tumor response. *Eur J Nucl Med Mol Imaging* 2003; 30: 1173–200.
120. Jeffery NT, Luthra SK, Manz A et al. Radiochemistry of microfabricated devices: proof of principle. *J Nucl Med* 2004; 45: 51P.
121. Gillies JM, Prenant C, Chimon GN et al. Microfluidic technology for PET radiochemistry. *Appl Rad Isot* 2006; 64: 333–6.
122. Lee C-C, Sui G, Elizarov A et al. Multistep synthesis of a radiolabeled imaging probe using integrated microfluidics. *Science* 2005; 310: 1793–6.
123. Wells P, West C, Jones T, Harris A, Price P. Measuring tumor pharmacodynamic response using PET proliferation probes: The case for 2-[¹¹C]-thymidine. *Biochim Biophys Acta* 2004; 1705: 91–102.
124. Vander Borgh T, Pauwels S, Lambontte L et al. Brain tumor imaging with PET and 2-[carbon-11]thymidine. *J Nucl Med* 1994; 35: 974–82.
125. Shields AF, Mankoff DA, Link JM et al. Carbon-11-thymidine and FDG to measure therapy response. *J Nucl Med* 1998; 39: 1757–62.
126. Shields AF, Grierson JR, Dohmen BM et al. Imaging proliferation in vivo with [F-18]FLT and positron emission tomography. *Nat Med* 1998; 4: 1334–6.
127. Teng B, Wang S, Fu Z et al. Semiautomatic synthesis of 3'-deoxy-3'-[¹⁸F]fluorothymidine using three precursors. *Appl Rad Isot* 2005; 64: 187–93.
128. Cleij MC, Steel CJ, Brady F et al. An improved synthesis of 3'-deoxy-3'-[¹⁸F]fluorothymidine ([¹⁸F]FLT) and the fate of the precursor, 2,3'-anhydro-5'-O-(4,4'-dimethoxytrityl)-thymidine. *J Lab Comp Radiopharm* 2001; 44: S871–3.
129. Martin SJ, Eisenbarth JA, Wagner-Utermann U et al. A new precursor for the radiosynthesis of [¹⁸F]FLT. *Nucl Med Biol* 2002; 29: 263–73.
130. Been LB, Suurmeijer AJH, Cobben DCP et al. [¹⁸F]FLT-PET in oncology: current status and opportunities. *Eur J Nucl Med Mol Imaging* 2004; 31: 1659–72.
131. Mier W, Haberkorn U, Eisenhut M. [¹⁸F]FLT; portrait of a proliferation marker. *Eur J Nucl Med* 2002; 29: 165–9.
132. Vaalburg W, Coenen HH, Crouzel C et al. Amino acids for the measurement of protein synthesis in vivo by PET. *Nucl Med Biol* 1992; 19: 227–37.
133. Kim S, Chung JK, Im SJ et al. ¹¹C-Methionine PET as a prognostic marker in patients with glioma: comparison with ¹⁸F-FDG PET. *Eur J Nucl Med Mol Imaging* 2005; 32: 1367–72.
134. Wester H-J, Herz M, Weber W et al. Synthesis and radiopharmacology of O-(2-[¹⁸F]fluoroethyl)-L-tyrosine for tumor imaging. *J Nucl Med* 1999; 40: 205–12.
135. Heiss P, Mayer S, Herz M et al. Investigation of transport mechanism and uptake kinetics of O-(2-[¹⁸F]fluoroethyl)-L-tyrosine in vitro and in vivo. *J Nucl Med* 1999; 40: 1367–73.
136. Pauleit D, Floeth F, Hamacher K et al. O-(2-[F-18]fluoroethyl)-L-tyrosine PET combined with MRI improves the diagnostic assessment of cerebral gliomas. *Brain* 2005; 128: 678–87.
137. Machulla HJ. PET-Diagnostika in der Onkologie. *Pharm Zeit* 2005; 34: 490–497.
138. Grierson JR, Link JM, Mathis CA. A radiosynthesis of fluorine-18 fluoromisonidazole. *J Nucl Med* 1989; 30: 343–50.
139. Tang G, Wang M, Tang X, Gan M, Luo G. Fully automated one-pot synthesis of [¹⁸F]fluoromisonidazole. *Nucl Med Biol* 2005; 32: 553–8.

140. Kämäräinen E-L, Kyllönen T, Nihtilä O, Björk H, Solin O. Preparation of fluorine-18-labeled fluoromisonidazole using two different synthesis methods. *J Lab Comp Radiopharm* 2004; 47: 37–45.
141. Eschmann SM, Paulsen F, Reimold M et al. Prognostic impact of hypoxia-imaging with ¹⁸F-Misonidazole-PET in non-small-cell lung cancer and head-and-neck cancer prior to radiotherapy. *J Nucl Med* 2005; 46: 253–60.
142. Tewson TJ. Synthesis of [¹⁸F]fluoroetanidazole: a potential new tracer for imaging hypoxia. *Nucl. Med Biol* 1997; 24: 755–60.
143. Rasey JS, Hofstrand PD, Chin LK, Tewson TJ. Characterization of [¹⁸F]fluoroetanidazole, a new radiopharmaceutical for detecting tumor hypoxia. *J Nucl Med* 1999; 40: 1072–9.
144. Fujibayashi Y, Taniuchi H, Yonekura Y et al. Copper-62-ATSM: a new hypoxia imaging agent with high membrane permeability and low redox potential. *J Nucl Med* 1997; 38: 1155–60.
145. Wilbur DS. Radiohalogenation of proteins: an overview of radionuclides, labeling methods, and reagents for conjugate labeling. *Bioconjugate Chem* 1992; 3: 433–70.
146. Okarvi SM. Recent progress in fluorine-18 labeled peptide pharmaceuticals. *Eur J Nucl Med* 2001; 28: 929–38.
147. Lundqvist H, Tolmachev V. Targeting peptides and positron emission tomography. *Biopolymers* 2002; 66: 381–92.
148. Wester H-J, Hamacher K, Stoecklin G. A comparative study of N.C.A. fluorine-18 labeling of proteins via acylation and photochemical conjugation. *Nucl Med Biol* 1996; 23: 365–72.
149. Vaidyanathan G, Zalutsky MR. Labeling proteins with fluorine-18 using N-succinimidyl 4-[¹⁸F]fluorobenzoate. *Nucl Med Biol* 1992; 19: 275–81.
150. Wüst F, Hultsch C, Bergmann R, Johannsen B, Henle T. Radiolabelling of isopeptide N-ε-(γ-glutamyl)-L-lysine by conjugation with N-succinimidyl-4-[¹⁸F]fluorobenzoate. *Appl Rad Isot* 2003; 59: 43–8.
151. Mäding P, Füchtner F, Wüst F. Module-assisted synthesis of the bifunctional labelling agent N-succinimidyl 4-[¹⁸F]fluorobenzoate ([¹⁸F]SFB). *Appl Rad Isot* 2005; 63: 329–32.
152. Zijlstra S, Burchert W. Synthesis and evaluation of a ¹⁸F-labeled recombinant annexin-V derivative, for identification and quantification of apoptotic cells with PET. *Appl Rad Isot* 2003; 58: 201–7.
153. Guhlke S, Wester H-J, Bruns C, Stoecklin G. (2-[¹⁸F]Fluoropropionyl-(D)phe¹)-octreotide, a potential radiopharmaceutical for quantitative somatostatin receptor imaging with PET: Synthesis, radiolabeling, in vitro validation and biodistribution in mice. *Nucl Med Biol* 1994; 21: 819–25.
154. Guhlke S, Coenen HH, Stoecklin G. Fluoroacylation agents based on small N.C.A. [¹⁸F]fluorocarboxylic acids. *Appl Radiat Isot* 1994; 45: 715–27.
155. Wester HJ, Guhlke S, Stoecklin G. Regioselective [¹⁸F]fluoropropionylation of peptides and proteins in aqueous solution. *J Lab Comp Radiopharm* 1994; 35: 297–9.
156. Beer AJ, Haubner R, Goebel M et al. Biodistribution and pharmacokinetics of the α_vβ₃-selective tracer ¹⁸F-Galacto-RGD in cancer patients. *J Nucl Med* 2005; 46: 1333–41.
157. Eliceiri BP, Cheresch DA. The role of α_v integrins during angiogenesis: Insights into potential mechanisms of action and clinical development. *J Clin Invest* 1999; 103: 1227–30.
158. Haubner R, Wester H-J, Weber WA et al. Noninvasive imaging of α_vβ₃ integrin expression using ¹⁸F-labeled RGD-containing glycopeptide and positron emission tomography. *Cancer Res* 2001; 61: 1781–5.
159. Van de Wiele C, Oltenfreiter R, de Winter O et al. Tumor angiogenesis pathways: related clinical issues and implications for nuclear medicine imaging. *Eur J Nucl Med* 2002; 29: 699–709.
160. Poethko T, Schottelius M, Thumshirn G et al. Two-step methodology for high-yield routine radiohalogenation of peptides: ¹⁸F-labeled RGD and octreotide analogs. *J Nucl Med* 2004; 45: 892–902.
161. Haka SM, Kilbourn MR, Watkins GL, Toorongian SA. Aryltrimethylammonium trifluoromethanesulfonates as precursors to aryl [¹⁸F]fluorides: improved synthesis of [¹⁸F]GBR-13119. *J Lab Comp Radiopharm* 1989; 27: 823–33.
162. Schottelius M, Poethko T, Herz M et al. First ¹⁸F-labeled tracer suitable for routine clinical imaging of sst receptor-expressing tumors using positron emission tomography. *Clin Cancer Res* 2004; 10: 3593–606.
163. Dehdashti F, Flanagan FL, Mortimer JE et al. Positron emission tomographic assessment of ‘metabolic flare’ to predict response of metastatic breast cancer to antiestrogen therapy. *Eur J Nucl Med* 1999; 26: 51–6.
164. Hara T, Kosaka N, Kondo T, Kishi H, Kobori O. Imaging of brain tumor, lung cancer, esophagus cancer, colon cancer, prostate cancer and bladder cancer with [¹¹C]choline. *J Nucl Med* 1997; 38 (Suppl): 1058.
165. Hara T. ¹⁸F-Fluorocholine: a new oncologic PET tracer. *J Nucl Med* 2002; 42: 1815–17.
166. Price DT, Coleman RE, Hiao RP et al. Comparison of [¹⁸F]fluorocholine and [¹⁸F]fluorodeoxyglucose for positron emission tomography of androgen dependent and androgen independent prostate cancer. *J Urol* 2002; 168: 273–80.
167. Petren-Mallmin M, Andreasson I, Ljunggren O et al. Skeletal metastases from breast cancer: uptake of ¹⁸F-fluoride measured with positron emission tomography in correlation with CT. *Skeletal Radiol* 1998; 27: 72–6.

Radiopharmaceuticals for therapy

Margaret S Cooper and John Buscombe

Background

The use of therapeutic radiopharmaceuticals to target cancer is possibly as close as medicine has come to achieving the dream of the 'magic bullet', first proposed by Paul Ehrlich. A therapeutic radiopharmaceutical consists of two parts, a vector and a radioisotope. The vector takes the radioisotope to the tumor cells, where the radioactivity kills the tumor cells leaving normal cells unharmed. The choice of vector and isotope is critical for achieving an effective radiopharmaceutical.

Vectors

In an ideal world, the vector would be completely specific for the target, binding only to the cancer cells and not to any normal tissue. It would be able to reach its target tissue, the cancer cells, easily, and it would not cause unwanted side-effects such as allergic reactions or toxicity of any kind.

One of the main problems in finding an ideal vector for targeting cancer cells is that the cancer cells are so similar to normal cells. However, the process that induces malignancy results in changes on the surface of the tumor cell such that it can be recognized as being different from a normal cell. These changes on the surface of the tumor cells give rise to tumor specific markers, or antigens, that can be used to target the vector specifically to the cancer cell. Most of these differences that arise are not due to the appearance of entirely novel cell surface markers but to altered expression of a normal cellular constituent; for example, a protein may be glycosylated aberrantly during its passage through to the surface of the tumor cell, or a marker which exists on normal cells may be overexpressed on the tumor cell. So, in fact, it is more helpful to think of these markers as tumor associated antigens rather than tumor specific antigens.

Vectors can be identified that bind specifically to these tumor associated antigens; for example, it is possible to raise antibodies against these antigens. Although many

antibodies in clinical use such as Bexxar® and Zevalin® are based on conventional mouse monoclonal antibodies, there may be some advantages offered by engineered antibodies in terms of factors such as reduced binding to leukocyte Fc receptors or reduction of binding to Brambell receptors in the liver.¹ Alternatively, it may be possible to identify peptides that bind to the tumor associated antigens using techniques such as phage display technology.

Tumor associated antigens have been exploited in radioimmunotherapy for various tumors; for example, the TAG72 antigen, the AC170 antigen, the L6 antigen, high molecular weight adenocarcinoma-associated membrane and cytoplasmic antigen, the E4 antigen, and prostate specific membrane antigen (PSMA) have all been targets for radioimmunotherapy in prostate cancer.²

Radioisotopes

As well as a good vector, the choice of radioisotope is crucial for tumor cell kill (Table 29.1). The β emitting isotopes ^{131}I and ^{90}Y have commonly been used, and these isotopes are employed for the two commercially available radioimmunotherapeutics, Bexxar and Zevalin. The high energy and 2.7-day half-life of ^{90}Y have made it increasingly attractive for radioimmunotherapy. However, several studies have used α -particle emitting radionuclides, and there is some evidence that the short path length offers the potential for more specific tumor cell killing with less damage to surrounding normal tissues than with β -emitters.³ ^{90}Y and ^{111}In have commonly been used for radionuclide therapy with peptides, although there is also increasing interest in using ^{177}Lu .⁴ It is unclear which isotope is ideal, and indeed, the choice may be dependent on the nature of the cancer and possibly on the vector itself. However, practical issues such as availability, radiation safety, and of course cost need to be taken into account. The main challenge may actually be in targeting solid tumors, which are relatively radioresistant. The use of higher injected activities of radioisotopes and targeting smaller tumors as well as novel approaches to

Table 29.1 Radioisotopes used or proposed for therapeutic applications

<i>Radionuclide</i>	<i>Particle</i>	<i>Half-life</i>	<i>Maximum particle energy (MeV)</i>	<i>Maximum range in tissue</i>
Yttrium-90 (⁹⁰ Y)	β	2.7 days	2.28	12.0 mm
Iodine-131 (¹³¹ I)	β	8.0 days	0.61	2.4 mm
Lutetium-177 (¹⁷⁷ Lu)	β	6.7 days	0.50	1.8 mm
Rhenium-188 (¹⁸⁸ Re)	β	17.0 hours	2.11	10.8 mm
Rhenium-186 (¹⁸⁶ Re)	β	3.8 days	1.08	5.0 mm
Indium-111 (¹¹¹ In)	Internal conversion electrons	2.8 days	0.25	0.6 mm
Samarium-153 (¹⁵³ Sm)	β	2.0 days	0.81	3.0 mm
Bismuth-212 (²¹² Bi)	α	1.0 hour	8.8	87.0 μm
Astatine-211 (²¹¹ At)	α	7.2 hours	6.8	65.0 μm

therapy such as pre-targeting and intracavity injection may go some way to meeting this challenge.⁵

Manufacturing therapeutic antibodies

It is essential that radioactive antibodies are manufactured to a high quality in aseptic conditions for clinical studies. The considerations required to achieve these standards can make the manufacture difficult at the practical level, especially in routine hospital radiopharmacies, since many of the materials and reagents used are generally manufactured for laboratory and not clinical use. Recent European legislation has enshrined these requirements into a set of directives and rules which are then transposed into national law of member states, but are generally known as 'good manufacturing production' or GMP. The requirements are not only the need to ensure that all components of a product are themselves made to a similar standard of sterility and purity, but also to ensure that each item is traceable to source.

Antibodies have been radiolabeled with iodine for several decades,^{6,7} although improvements have been made in the methodology. However, radioiodination has largely been surpassed by metal ion chelation, using most commonly ⁹⁰Y and ¹¹¹In. Direct radiolabeling using these radiometals is not possible; instead an immunoconjugate needs to be prepared that can then be radiolabeled. There are several benefits to using these radiometals over radioiodination, especially in pharmaceutical terms. The main advantage is that, once the conjugation is complete, the radiolabeling methodology is fairly straightforward. In addition, there is

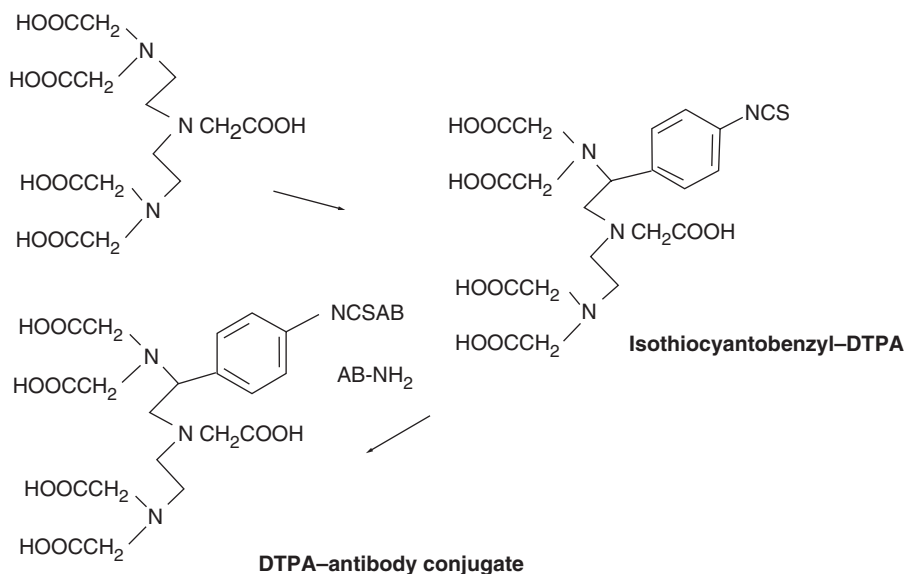
greater consistency between one radiolabeling episode and the next, and less dependency on operator technique. High radiolabeling efficiency is usually achieved, making a purification step unnecessary in most cases. There are also advantages in that it is possible to achieve high-quality standards during manufacture, since the main part of the process can be carried out in advance ensuring sterility, ability to bind to the target, purity, and robust radiolabeling. It can also be argued that the radiolabeling is safer for the operator using a pure β emitter such as ⁹⁰Y, compared with using ¹³¹I which also has high energy γ emissions.

Conjugation of antibodies with bifunctional ligands

Unlike radioiodination, antibodies cannot be directly labeled with metal ions. Instead, it is necessary to make a chemical modification to the antibody by attaching a bifunctional ligand. The ligand is bifunctional in that it (1) attaches itself to the antibody, usually via the amino side chain of lysine residues within the antibody, and (2) it chelates the radiometal. The method of radiolabeling can be described as a three-step process:

- conjugation – a chemical reaction between the antibody and the ligand
- purification – removal of excess ligand from the newly formed immunoconjugate
- radiolabeling.

Diethylenetriaminepentaacetic acid (DTPA) was the first such ligand to be used in these conjugation reactions, the

**Figure 29.1**

Method of producing a backbone substituted DTPA (diethylenetriaminepentaacetic acid) for better chelating of radiometals.

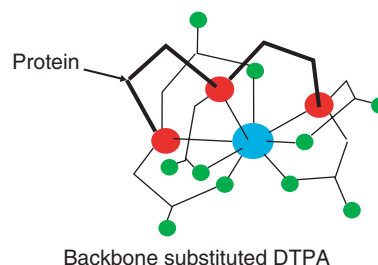
attachment to the antibody being via a peptide bond formed between the amino side chain of a lysine residue and one of the carboxylic acid groups of the DTPA.⁸ However, the radioactive complexes formed following radiolabeling were not very strong, since only four carboxylic acid groups remained available for chelation with the metal ion. Instead, backbone substituted DTPA derivatives have been used, and conjugation is achieved via a thiourea bond between the isothiocyanatobenzyl DTPA derivative and the amino side chain of the lysine residue⁹ (Figure 29.1). Further substitutions on the backbone of the DTPA derivative confer greater stability to the radiolabeled antibody and can influence biodistribution.¹⁰ The theory is that the increased rigidity of the chelate ring system might provide enhanced radioisotope complex stability.¹¹ Novel ligands such as 2-(4-isothiocyanatobenzyl)-1,4,7,10-tetraaza-1,4,7,10-tetra-(2-carbamoylmethyl)-cyclododecane (4-NCS-Bz-TCMC) and 2-(4-isothiocyanatobenzyl)-1,4,7,10,13,16-hexaazacyclododecane-1,4,7,10,13,16-hexaacetic acid (HEHA-NCS) for chelation of lead isotopes (²⁰³Pb and ²¹²Pb) and actinium (²²⁵Ac) respectively have also been synthesized,^{12,13} and there are reports of other ligands in the literature where backbone substitutions confer greater in vitro and in vivo stability and can be used for radiolabeling both α and β emitters.¹⁴ However, the theory behind conjugation to the antibody remains the same.

Greater stability can be achieved by using 1,4,7,10-tetraazacyclododecane-N,N',N'',N'''-tetraacetic acid (DOTA) rather than DTPA derivatives (Figures 29.2 and 29.3), but not without the practical problem that heating is required for achieving radiolabeling, and this limits the usefulness of DOTA as a bifunctional ligand for antibodies. However, it is

an extremely useful ligand for radiolabeling peptides where heating to 100°C is usually not a problem.

The initial conjugation step is pH sensitive; optimal conjugation occurs at ~pH 8.5 (for example in HEPES buffer (4-(2-hydroxyethyl)-1-piperazineethanesulfonic acid)). The conditions for the conjugation reaction can be varied to achieve varying ligand/antibody ratios. The exact conditions will be dependent on the ligand and antibody; however, satisfactory conjugation can usually be achieved following overnight incubation of the antibody with the ligand at 2–8°C.

It is critical that throughout the conjugation and purification steps the level of metal ions present is kept to a minimum. This can be achieved by preparing buffers using high-purity reagents with low metal ion content and low metal leaching consumables, such as sterile polypropylene containers, and avoiding the use of metal, for example metal needles and spatulas. If metal ions are present, they

**Figure 29.2**

Three-dimensional model of metal binding of backbone substituted DTPA.

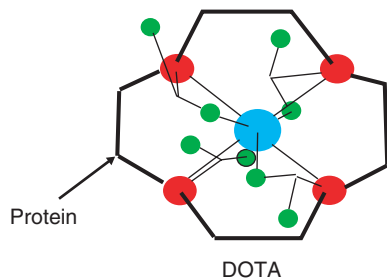


Figure 29.3

Three-dimensional model of metal labeling of DOTA (tetraazacyclododecanetetraacetic acid).

can poison the ligand in that they will be chelated by the ligand in the same way as the radiometal and prevent the ligand being available for radiolabeling.

Following conjugation, excess ligand must be removed from the newly formed immunconjugate. This purification step achieves two goals, that of removing the excess ligand but also allowing a buffer transfer step, leaving the immunconjugate in a more suitable buffer for storage and/or radiolabeling.

Purification can be carried out by a number of methods, but the preferred methods are ultracentrifugation or tangential flow filtration (TFF). Both methods work on the same principle: a membrane filter allows the passage of small molecules such as the buffer components and the excess ligand but does not allow passage of the antibody. In this way, the excess material is removed from the immunconjugate and fresh buffer can be introduced into the system. Ultracentrifugation is very useful for small scale developmental work, but TFF is more suitable for large scale production and has the advantage of being quicker and having smaller in-process losses of antibody material.

Quality control checks should be carried out on the purified immunconjugate. The necessary tests include: full test labeling with the radiometal to be used; testing for sterility and pyrogenicity; protein concentration; purity, usually assessed by high performance liquid chromatography (HPLC) sodium dodecylsulfate or (SDS) gel; immunoreactivity; ligand to antibody ratio; and stability assays.¹⁵

The immunconjugate can be packed in quantities suitable for single patient use and stored. Depending on the exact radiolabeling method chosen and the buffer used for storage, the radiolabeling method is usually quite simple, requiring the addition of the radiometal to the immunconjugate possibly following buffering to achieve an optimal pH for radiolabeling to occur. Ascorbic acid¹⁶ or human serum albumin¹⁷ can be added to prevent radiolysis.

Radiolabeling efficiencies in excess of 99% are usually achieved, but, if necessary, a chelating agent such as DTPA or ethylenediaminetetraacetic acid (EDTA) can be added to

the radiolabeled antibody to chelate free radiometal which will be excreted via the kidneys.

⁹⁰Y-labeled antibodies show much promise in the clinical setting. Zevalin ([⁹⁰Y]ibritumomab tiuxetan) is now a commercially available therapeutic radiopharmaceutical for the treatment of relapsed or refractory low-grade follicular or transformed B-cell non-Hodgkin's lymphoma.¹⁸

However, there are other applications of ⁹⁰Y antibodies under investigation. It is likely that the most effective approach may be to use a combination of radioimmunotherapy and conventional chemotherapy in treating solid tumors.¹⁹ Richman et al. have investigated using [⁹⁰Y]MUC1 (mucin-1) monoclonal antibody, m170, combined with low dose paclitaxel for treating metastatic prostate and breast cancer. A similar strategy was used for treatment of non-small-cell lung cancer using an antibody targeting the tumor associated glycoprotein-72 (TAG72).²⁰ In addition, Kelly et al.²¹ have studied combination therapy using an anti-Lewis Y monoclonal antibody (hu3S193) combined with paclitaxel in a breast cancer model. Biodistribution studies demonstrated excellent tumor targeting and limited normal tissue uptake. This antibody has also been used in combination with the epidermal growth factor receptor inhibitor, AG1478, in a human cancer xenograph model.²²

Another approach to treating prostate cancer has been to target mindin/RG-1 protein expression on prostate cancers. Studies using a fully human antibody, 19G9, showed significant antitumor effects with single administration of the radiolabeled antibody in animal studies.²³ The identification of new targets such as these will be crucial for effective therapy in the future.

The manner in which the treatment is given may also be important for effective therapy and reduction of unwanted side-effects. It is proposed that fractionation of therapy could reduce myelotoxicity compared with single dose administration.²⁴ In a study by Vallabhajosula et al. using an anti-PSMA monoclonal antibody to treat prostate cancer, it was found that patients receiving their treatment as three separate doses suffered reduced myelotoxicity compared with patients receiving a single treatment dose.

A novel approach to radioimmunotherapy has been to use ²¹²Pb as an in vivo generator of ²¹³Bi. This strategy has been adopted in a pre-targeted approach using NR-LU-10-antibody-streptavidin conjugate and ²¹²Pb/²¹²Bi chelate of DOTA-biotin.²⁵ This approach is of interest since the short half-life of ²¹³Bi (46 min) limits its usefulness in conventional radioimmunotherapy.

The use of ¹⁸⁸Re and ¹⁸⁶Re should also be mentioned. The potential usefulness of these isotopes stems from their chemical similarity to the commonly used γ emitting isotope ^{99m}Tc, making them a tantalizing choice for an effective diagnostic/therapeutic strategy. In addition, ¹⁸⁸Re can be eluted from an on-site installable ¹⁸⁸W/¹⁸⁸Re generator, which has a useful shelf-life of several months.

However, labeling with rhenium has proved somewhat more problematic than labeling with technetium, with the complexes being more difficult to radiolabel and often possessing unsatisfactory stability.^{26,27} Improvements in radiolabeling techniques have enabled the preparation of [¹⁸⁸Re]anti-CD20 antibody²⁸ for non-Hodgkin's lymphoma, and the potential to radiolabel other antibodies in this way exists and may lead to the development of some interesting ¹⁸⁸Re-labeled antibodies.

Antibody fragments

The strategy of radiolabeling antibodies with metal ions or with iodine can be applied to antibody fragments as well as to whole antibodies. Due to their smaller molecular size, antibody fragments have shown rapid tumor targeting and blood clearance, a more uniform tumor distribution, and a lower potential to elicit a human immune response. However, there is also increased risk of renal toxicity as the antibody fragments are cleared rapidly from the blood through the kidney. Strategies using a variety of isotopes have recently been employed, including ¹³¹I, ⁹⁰Y, ¹¹¹In, ⁶⁴Cu, and ¹⁷⁷Lu,²⁹ for targeting neuroblastomas, renal cell carcinomas, ovarian carcinomas, endometrial carcinomas, gastric carcinomas, gliomas, and hepatocellular carcinomas.^{30–32} Improved tumor targeting can be achieved by increasing avidity using diabodies and minibodies. Such strategies have been employed using anti-carcinoembryonic antigen (CEA) fragments.³³

Pre-targeting strategies

Pre-targeting is an alternative to directly radiolabeled antibodies. The theory behind pre-targeting is that a bifunctional antibody conjugate is first injected. One functionality binds to the tumor while the other functionality acts as a 'hook' to catch a subsequently administered radiolabeled complex. Several different approaches exist, but most commonly this hook is provided by streptavidin, which is bound to the antibody. In an (optional) second stage a macromolecule clearing agent is administered to remove circulating conjugate from the bloodstream. Finally a radioactive molecule which binds to the 'hook' is injected (in the case of the streptavidin conjugated antibody this would be biotin), and this binds to the antibody conjugate pre-targeted to the tumor. There are several advantages to this method, in particular the potential of lower radiation dose to normal tissue and more specific localization of radioactivity at the tumor site, resulting in higher tumor cell kill. This is achieved because the time taken for antibodies to localize at the tumor site (usually

several hours) means that when they are directly radiolabeled there is the potential for radiation damage to occur to normal tumor cells; however, in the pre-targeting approach, the antibody has time to localize at the target before the smaller, radioactive moiety is introduced, which is capable of quickly reaching its target causing less radiation damage to surrounding tissues. Studies in a variety of hematologic and solid tumor models have shown advantages of pre-targeting compared with directly radiolabeled immunoglobulin G (IgG) for therapy, and there are several clinical studies under way that are also showing promising results.^{34,35} This approach can also be applied using antibody fragments.³⁶

Several pre-targeting strategies have been proposed, but only those using the biotin–avidin recognition system and those using bispecific antitumor × antihapten antibodies have been tested in the clinic for both immunoscintigraphy and radioimmunotherapy.^{37,38} Because pre-targeting is a multistep process, it initially met with some resistance, but simpler procedures have been introduced meaning that it is likely that the next generation of targeting agents will employ pre-targeting approaches to optimize radionuclide delivery for a wide range of applications.³⁹

Radiopeptide therapy

Octreotide derivatives

The field of radiopeptide therapy has been dominated by the use of radiolabeled somatostatin analogs. The use of octreotide and its derivatives has been covered in depth in Chapter 21. Initially, therapeutic studies used high-dose [¹¹¹In]octreotide, taking advantage of the internal conversion electrons from ¹¹¹In.⁴⁰ However, more recently, DOTA-DPhe¹-Tyr³-octreotide (DOTA-TOC)⁴¹ has been radiolabeled with ⁹⁰Y for effective treatment of neuroendocrine tumors. Other derivatives, such as DOTA-Tyr³-Thr⁸-octreotate (DOTA-TATE), in theory offer advantages due to increased specificity for the somatostatin receptor subtype 2 (hSST2),⁴² but in clinical practice little if any benefit over DOTA-TOC is seen.⁴³ [¹⁷⁷Lu]DOTA-TOC or [¹⁷⁷Lu]DOTA-TATE may offer some advantages over the ⁹⁰Y-labeled derivatives since ¹⁷⁷Lu has a lower β particle energy and shorter range, and may be more effective in treating small lesions.⁴⁴

Beyond octreotide derivatives

The future of radiopeptide therapy is not limited to somatostatin, and many potential targets exist which could be explored (Tables 29.2 and 29.3). These receptor targets

Table 29.2 Targets for radiopeptide therapy

<i>Target</i>	<i>Tumor</i>	<i>Radiopeptide therapy examples</i>
Somatostatin receptors	Endocrine tumors, neuroendocrine tumors, other tumors: small-cell lung cancer (SCLC), medullary thyroid cancer, breast cancer, renal cancer, thyroid cancer, lymphoma, brain tumor: medulloblastoma and glioma	Octreotide, DOTA-TOC, DOTA-TATE
Gastrin releasing peptide receptors	Prostate cancer, breast cancer, lung cancer, SCLC, colonic cancer, glioblastoma	Bombesin and analogs, [¹⁷⁷ Lu]AMBA
Substance-P (SP) receptors	Medullary thyroid cancer, SCLC, breast tumors, gliomas	[⁹⁰ Y]DOTA-substance P
Integrin ($\alpha_v\beta_3$) receptors	Glioma, ovarian tumors, breast cancer, prostate cancer	[⁹⁰ Y]RGD peptides
α -Melanocyte stimulating hormone (α -MSH) receptors	Melanoma	DOTA- α -MSH

DOTA, tetraazacyclododecanetetraacetic acid; TOC, Tyr³-octreotide; TATE, Tyr³-octreotate; AMBA, aminomethylbenzoic acid; RGD, Arg-Gly-Asp.

are overexpressed in many primary human cancers compared with adjacent normal tissue, and this gives a targeting advantage for molecules that bind to the receptors. Many of the peptides under investigation are naturally occurring, but one of the advantages of using peptides is that they can be designed synthetically as novel molecules, with the potential of giving increased binding affinity compared with their naturally occurring counterparts. Other advantages of using peptides compared with antibodies or antibody fragments are excellent permeability, lack of antigenicity, minimal side-effects, ease of radiolabeling, and rapid clearance from the body.

Many of the targets have been investigated for their potential in diagnostic imaging. Theoretically these receptors are also targets for radiopeptide therapy, but in fact there are far fewer reports in the literature relating to radiopeptide therapy compared with radiopeptide imaging. One of the reasons may be the inability to achieve high enough tumor to background ratios. This is not such a

problem with the diagnostic applications as long as uptake in other organs does not interfere with interpretation of the scan. However, for therapy, it is vital to obtain good uptake solely in the tumor and not in other organs, where radiation damage is likely to become a dose-limiting factor.

RGD peptides

Angiogenesis is an important factor for the development of cancers. The $\alpha_v\beta_3$ receptor is present on developing but not developed vasculature. This means that it is highly expressed on activated endothelial cells, and tumor cells but not on dormant endothelial cells or normal cells, and so presents an attractive target for tumor therapy. The peptide Arg-Gly-Asp (known as the RGD peptide) binds to $\alpha_v\beta_3$ receptors but is not rigid enough to be an effective vector for targeting radionuclides. However, several groups

Table 29.3 Potential future targets for radiopeptide therapy

<i>Target</i>	<i>Tumor</i>
Cholecystokinin B/gastrin (CCK-2) receptors	Medullary thyroid cancer, gastrointestinal stromal tumors (GIST), SCLC, insulinomas
Vasoactive intestinal peptide (VIP) receptors	Adenocarcinomas, SCLC, neuroendocrine tumors, lymphoma
Neurotensin (NT1) receptors	Exocrine pancreatic cancer, meningioma, Ewing's sarcoma
Neuropeptide Y (NPY) receptors	Breast cancer (NPY-1), sex cord stromal ovarian tumor and adrenal tumor (NPY-1 and NPY-2)
Glucagon-like peptide 1 receptors (GLP-1)	Insulinoma, medullary thyroid cancer, gastrinoma
Corticotropin-releasing factor (CRF) receptors	Pituitary adenoma, paraganglioma

have used this peptide as a starting point for designing agents which can bind specifically to the receptor, for example by using cyclic RGD peptide, doubly cyclized CDCRGDCFC (RGD4C) peptide, or peptide derivatized to other molecules such as copolymers.^{45,46} These agents can then be radiolabeled with radioisotopes such as ⁹⁰Y, ¹¹¹In, or ²¹⁰Po following conjugation to a suitable bifunctional ligand such as DOTA or cyclohexyl (CHX)-A-DTPA. These peptides have been studied in animal models with promising results, and may prove valuable in the treatment of solid tumors.⁴⁷

Bombesin and its analogs

Gastrin releasing peptide (GRP) receptor is expressed on a variety of tumors including breast and prostate cancer. Bombesin (BN), a 14 amino acid peptide, has a high affinity for the GRP receptor and hence is of interest for radiolabeled peptide therapy. BN and its analogs have been radiolabeled with ⁹⁰Y, ¹¹¹In, and ¹⁷⁷Lu as potential agents for treating prostate, breast, and lung cancers. Specific and high uptake of the peptides has been shown, and there are encouraging results in terms of response to treatment in animal models.^{48–50}

Other targets

Several other receptor targets exist which could be utilized for radiolabeled peptide therapy. α -Melanocyte stimulating hormone (α -MSH, α -melanotropin) has been conjugated to DOTA with the potential for radiolabeling with a variety of radiometals. Such agents would be useful for targeting melanomas.⁵¹ Similarly, conjugation of substance-P with

DOTA offers the possibility of treating medullary thyroid cancer, small-cell lung cancer (SCLC), breast tumors, and gliomas, and radiolabeled analogs of neurotensin, vasoactive intestinal peptide (VIP), bombesin (BN), and gastrin/cholecystokinin (CCK) are all being studied and evaluated for potential clinical application.⁵² However, much of this work is in its early stages, and it remains to be seen which of these radiopeptides will be able to make an impact in the treatment and management of patients with solid tumors.

Changing the target: genetic modification

Whilst most work in the development of therapeutic nuclear medicine has been directed towards the development of better molecules which have more precise and higher affinity for the target an alternative solution would be to change the target. It is known that the antigen used for tumor targeting is encoded by a specific gene, for example the gene encoding BRAC1 means a woman has a higher chance of developing breast cancer, but its expression also means that effective treatment is possible from Herceptin®.⁵³

It is one step from identifying a gene which is responsible for a particular antigen, and the ability to use this to provide specific therapy.

A classic example is the sodium iodide symporter (NIS) gene whose expression is normal in thyroid and some breast tissue. When the NIS gene is expressed, it will allow the target cell to accumulate radioactive iodine. The trick, however, is to find a vector which will carry the gene into the target cell (Figure 29.2). Normally the vector used is a virus, and adenovirus has been used as a successful vector for the NIS gene in an animal model⁵⁴ (Figure 29.4). The advantage is that once a cell is transfected it will allow

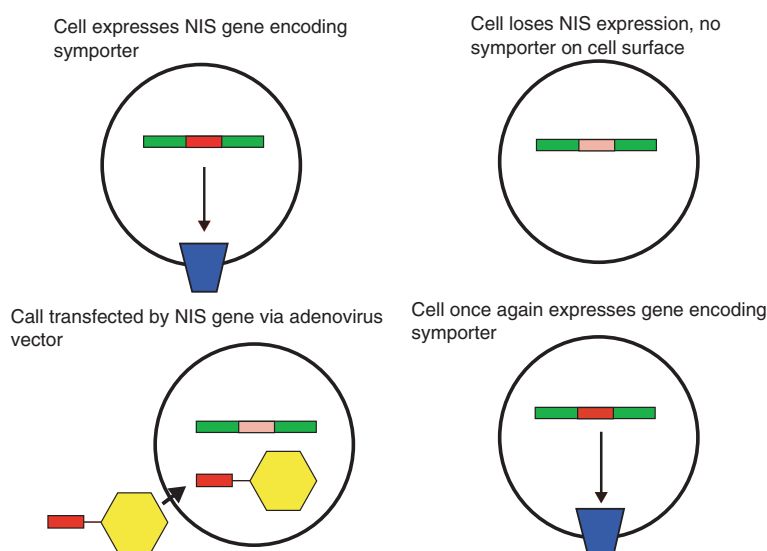


Figure 29.4

Schematic showing the transfection of cells with the sodium iodide symporter (NIS) gene using an adenovirus vector.

uptake of a cheap radiopharmaceutical such as ^{131}I , though there is evidence that such uptake may be limited for about 6 weeks, which seems to be the mean time for a transfected cell to express the genes carried to it by the viral vector. There is also another theoretical problem in that, unlike thyroid cells, there is no mechanism for the organification and hence retention of the ^{131}I within the transfected cell, though pretreatment with lithium salts may help to increase residency within the cell type.

Other genes may also be targets, including the genes encoding the amine uptake of [^{131}I]MIBG (metaiodobenzylguanidine) and the gene for the somatostatin-type 2 receptor; all have the advantage that imaging can be used to determine whether transfection is high enough to allow therapy before a therapeutic dose is given. The best hope may be to 're-infect' those thyroid cancers which have become ^{131}I -resistant.

An alternative is to use a physical vector, and this has been shown to allow transfection of hepatocellular cells with [^{131}I]lipiodol, into which is dissolved an EGF (epidermal growth factor) promoter gene which will allow the tumor cells to be attacked by antivascular therapies. In this case, the ^{131}I is used as a marker of targeting.⁵⁵

Whilst this area of work remains highly speculative and limited to animal studies, there is some suggestion that it could lead to extension of the use of radionuclide therapies in a range of cancers; this may be of particular importance in view of the generally non-toxic nature of these treatments compared to other chemotherapy-based approaches.

Conclusions

There is much work being undertaken to improve the range of therapeutic radiopharmaceuticals available. This includes a variety of radioisotopes and chelators. The carrier molecules for therapy include whole antibodies, fragments of antibodies, peptides, and potentially the cell itself, by gene therapy. As always, however, commercial pressure will determine which of these agents is most successful.

References

- Hale G, Berrie E, Bird P. Design and manufacture of monoclonal antibodies for radioimmunotherapy. *Q J Nucl Med Mol Imaging* 2004; 48: 258–66.
- Smith-Jones PM. Radioimmunotherapy of prostate cancer. *Q J Nucl Med Mol Imaging* 2004; 48: 297–304.
- Mulford DA, Scheinberg DA, Jurcic JG. The promise of targeted alpha-particle therapy. *J Nucl Med* 2005; 46: 199S–204S. Zalutsky MR, Pozzi OR. Radioimmunotherapy with alpha-particle emitting radionuclides. *Q J Nucl Med Mol Imaging* 2004; 48: 289–96.
- Teunissen JJ, Kwekkeboom DJ, de Jong M et al. Endocrine tumors of the gastrointestinal tract. Peptide receptor radionuclide therapy. *Best Pract Res Clin Gastroenterol* 2005; 19: 595–616.
- Rogers BE, Roberson PL, Shen S et al. Intraperitoneal radioimmunotherapy with a humanized anti-TAG-72 (CC49) antibody with a deleted CH2 region. *Cancer Biother Radiopharm* 2005; 20: 502–13.
- Hunter WM, Greenwood FC. Preparation of Iodine-131 labelled human growth hormone of high specific activity. *Nature* 1962; 194: 495.
- Fraker PJ, Speck JC. Protein and cell membrane iodinations with a sparingly soluble chloroamide, 1,3,4,6-tetrachloro-3a,6a-diphenylglycoluril. *Biochem Biophys Res Commun* 1978; 80: 849–57.
- Hnatowitch DJ, Childs RL, Lantaigne D, Najafi A. DTPA-coupled antibodies radiolabelled with metallic radionuclides: an improved method. *J Immunol Meth* 1983; 65: 147–57.
- Esteban JM, Schlom J, Gansow OA et al. New method for the chelation of indium-111 to monoclonal antibodies; biodistribution and imaging of athymic mice bearing human colon carcinoma xenografts. *J Nucl Med* 1987; 28: 861–70.
- Quadri SM, Vriesendorp HM. Effects of linker chemistry on the pharmacokinetics of radioimmunoconjugates. *Q J Nucl Med* 1998; 42: 250–61.
- Chong HS, Milenic DE, Garmestani K et al. In vitro and in vivo evaluation of novel ligands for radioimmunotherapy. *Nucl Med Biol* 2006; 33: 459–67.
- Chappell LL, Dadachova E, Milenic DE et al. Synthesis, characterization, and evaluation of a novel bifunctional chelating agent for the lead isotopes ^{203}Pb and ^{212}Pb . *Nucl Med Biol* 2000; 27: 93–100.
- Chappell LL, Deal KA, Dadachova E, Brechbiel MW. Synthesis, conjugation and radiolabeling of a novel bifunctional chelating agent for (^{225}Ac) radioimmunotherapy applications. *Bioconjug Chem* 2000; 11: 510–19.
- Chong HS, Milenic DE, Garmestani K et al. In vitro and in vivo evaluation of novel ligands for radioimmunotherapy. *Nucl Med Biol* 2006; 33: 459–67.
- Mather SJ. Radiolabeling of monoclonal antibodies. In: Shepherd P, Dean C, eds. *Monoclonal Antibodies*. Oxford: Oxford University Press; 2000: 207–36.
- Chakrabarti MC, Le N, Paik CH, De Graff WG, Carrasquillo JA. Prevention of radiolysis of monoclonal antibody during labeling. *J Nucl Med* 1996; 37: 1384–8.
- Zimmer AM, Kazikiewicz JM, Webber DI et al. Stability of radioiodinated monoclonal antibodies: in vitro storage and plasma analysis. *Int J Rad Appl Instrum B* 1989; 16: 691–6.
- Crawford LM Jr. From the Food and Drug Administration. *JAMA* 2002; 287: 1640.
- Richman CM, Denardo SJ, O'Donnell RT et al. High-dose radioimmunotherapy combined with fixed, low-dose paclitaxel in metastatic prostate and breast cancer by using a MUC-1 monoclonal antibody, m170, linked to indium-111/yttrium-90 via a cathepsin cleavable linker with cyclosporine to prevent human anti-mouse antibody. *Clin Cancer Res* 2005; 11: 5920–7.
- Forero A, Meredith RF, Khazaeli MB et al. Phase I study of 90Y-CC49 monoclonal antibody therapy in patients with

- advanced non-small cell lung cancer: effect of chelating agents and paclitaxel co-administration. *Cancer Biother Radiopharm* 2005; 20: 467–78.
21. Kelly MP, Lee FT, Smyth FE, Brechbiel MW, Scott AM. Enhanced efficacy of ⁹⁰Y-radiolabeled anti-Lewis Y humanized monoclonal antibody hu3S193 and paclitaxel combined-modality radioimmunotherapy in a breast cancer model. *J Nucl Med* 2006; 47: 716–25.
 22. Lee FT, Mountain AJ, Kelly MP et al. Enhanced efficacy of radioimmunotherapy with ⁹⁰Y-CHX-A'-DTPA-hu3S193 inhibition of epidermal growth factor receptor (EGFR) signalling with EGFR tyrosine kinase inhibitor AG1478. *Clin Cancer Res* 2005; 11: 7080s–6s.
 23. Parry R, Schneider D, Hudson D et al. Identification of a novel prostate tumor target, mindin/RG-1, for antibody-based radiotherapy of prostate cancer. *Cancer Res* 2005; 65: 8397–405.
 24. Vallabhajosula S, Goldsmith SJ, Kostakoglu L et al. Radioimmunotherapy of prostate cancer using ⁹⁰Y- and ¹⁷⁷Lu-labeled J591 monoclonal antibodies: effect of multiple treatments on myelotoxicity. *Clin Cancer Res* 2005; 11: 7195s–200s.
 25. Su FM, Beaumier P, Axworthy D, Atcher R, Fritzbeg A. Pretargeted radioimmunotherapy in tumored mice using an in vivo ²¹²Pb/²¹³Bi generator. *Nucl Med Biol* 2005; 32: 741–7.
 26. Griffiths GL, Goldenberg DM, Diril H, Hansen HJ. Technetium-99m, rhenium-186 and rhenium-188 direct-labelling antibodies. *Cancer* 1994; 73: 761–8.
 27. Juweid M, Sharkey RM, Swayne LC, et al. Pharmacokinetics, dosimetry and toxicity of rhenium-188-labelled anti-carcinoembryonic antigen monoclonal antibody, MN-14, in gastrointestinal cancer. *J Nucl Med* 1998; 39: 39–42.
 28. Ferro-Flores G, Torres-Garcia E, Garcia-Pedroza L et al. An efficient, reproducible and fast preparation of ¹⁸⁸Re-anti-CD20 for the treatment of non-Hodgkin's lymphoma. *Nucl Med Commun* 2005; 26: 793–9.
 29. Grunberg J, Novak-Hofer I, Honer M et al. In vivo evaluation of ¹⁷⁷Lu- and ^{67/64}Cu-labeled recombinant fragments of antibody chCE7 for radioimmunotherapy and PET imaging of L1-CAM-positive tumors. *Clin Cancer Res* 2005; 11: 5112–20.
 30. Chen ZN, Mi L, Xu J et al. Targeting radioimmunotherapy of hepatocellular carcinoma with iodine (¹³¹I) metuximab injection: clinical phase I/II trials. *Int J Radiat Oncol Biol Phys* 2006; 65: 435–44.
 31. Kim JC, Hong HK, Roh SA et al. Efficient targeting of gastric cancer cells using radiolabeled anti-carcinoembryonic antigen-specific T84.66 fragments in experimental radioimmunoguided surgery. *Anticancer Res* 2004; 24: 663–70.
 32. Boskovitz A, Akabani GH, Pegram CN, Bigner DD, Zalutsky MR. Human/murine chimeric 81C6 F(ab')(2) fragment: preclinical evaluation of a potential construct for the targeted radiotherapy of malignant glioma. *Nucl Med Biol* 2004; 31: 345–55.
 33. Yazaki PJ, Wu AM, Tsai SW et al. Tumor targeting of radiometal labeled anti-CEA recombinant T84.66 diabody and t84.66 minibody: comparison to radioiodinated fragments. *Bioconj Chem* 2001; 12: 220–8.
 34. Paganelli G, Bartolomei M, Grana C et al. Radioimmunotherapy of brain tumor. *Neurol Res* 2006; 28: 518–22.
 35. Boerman OC, van Schaijk FG, Oyen WJ, Corstens FH. Pretargeted radioimmunotherapy of cancer: progress step by step. *J Nucl Med* 2003; 44: 400–11.
 36. Forster GJ, Santos EB, Smith-Jones PM, Zanzonico P, Larson SM. Pretargeted radioimmunotherapy with a single-chain antibody/streptavidin construct and radiolabeled DOTA-biotin: strategies for reduction of the renal dose. *J Nucl Med* 2006; 47: 140–9.
 37. Gruaz-Guyon A, Raguin O, Barbet J. Recent advances in pretargeted radioimmunotherapy. *Curr Med Chem* 2005; 12: 319–38.
 38. Gautherot E, Rouvier E, Daniel L et al. Pretargeted radioimmunotherapy of human colorectal xenografts with bispecific antibody and ¹³¹I-labeled bivalent hapten. *J Nucl Med* 2000; 4: 480–7.
 39. Sharkey RM, Karacay H, Cardillo TM et al. Improving the delivery of radionuclides for imaging and therapy of cancer using pretargeting methods. *Clin Cancer Res* 2005; 11: 7109s–21s.
 40. Valkema R, De Jong M, Bakker WH et al. Phase I study of peptide receptor radionuclide therapy with [In-DTPA] octreotide: the Rotterdam experience. *Semin Nucl Med* 2002; 2: 110–22.
 41. Bodei L, Cremonesi M, Grana C et al. Receptor radionuclide therapy with ⁹⁰Y-[DOTA] (0)-Tyr(3)-octreotide (⁹⁰Y-DOTA-TOC) in neuroendocrine tumors. *Eur J Nucl Med Mol Imaging* 2004; 7: 1038–46.
 42. Reubi J, Schaer J, Waser B et al. Affinity profiles for human somatostatin receptor subtypes SST1-SST5 of somatostatin radiotracers selected for scintigraphic and radiotherapeutic use. *Eur J Nucl Med* 2000; 27: 273–82.
 43. Forrer F, Uusijarvi H, Waldherr C et al. A comparison of ¹¹¹In-DOTATOC and ¹¹¹In-DOTATATE: biodistribution and dosimetry in the same patients with metastatic neuroendocrine tumors. *Eur J Nucl Med Mol Imaging* 2004; 31: 1257–62.
 44. Kwekkeboom D, Mueller-Brand J, Paganelli G et al. Overview of results of peptide receptor radionuclide therapy with 3 radiolabelled somatostatin analogues. *J Nucl Med* 2005; 46: 625–65.
 45. Mitra A, Nan A, Papadimitriou JC, Ghandehari H, Line BR. Polymer-peptide conjugates for angiogenesis targeted tumor radiotherapy. *Nucl Med Biol* 2006; 33: 43–52.
 46. Chen X, Hou Y, Tohme M et al. Pegylated Arg-Gly-Asp peptide: ⁶⁴Cu labeling and PET imaging of brain tumor alphavbeta3-integrin expression. *J Nucl Med* 2004; 45: 1776–83.
 47. Janssen M, Frielink C, Dijkgraaf I et al. Improved tumor targeting of radiolabeled RGD peptides using rapid dose fractionation. *Cancer Biother Radiopharm* 2004; 19: 399–404.
 48. Zhang H, Chen J, Waldherr C et al. Synthesis and evaluation of bombesin derivatives on the basis of pan-bombesin peptides labeled with indium-111, lutetium-177, and yttrium-90 for targeting bombesin receptor-expressing tumors. *Cancer Res* 2004; 64: 6707–15.
 49. Breeman WA, de Jong M, Erion JL et al. Preclinical comparison of (¹¹¹In)-labeled DTPA- or DOTA-bombesin analogs for receptor-targeted scintigraphy and radionuclide therapy. *J Nucl Med* 2002; 43: 1650–6.
 50. Lantry LE, Cappelletti E, Maddalena ME et al. ¹⁷⁷Lu-AMBA: synthesis and characterization of a selective ¹⁷⁷Lu-labeled

- GRP-R agonist for systemic radiotherapy of prostate cancer. *J Nucl Med* 2006; 47: 1144–52.
51. Eberle AN, Froidevaux S. Radiolabeled alpha-melanocyte-stimulating hormone analogs for receptor-mediated targeting of melanoma: from tritium to indium *J Mol Recognit* 2003; 16: 248–54.
 52. Heppeler A, Froidevaux S, Eberle AN, Maecke HR. Receptor targeting for tumor localisation and therapy with radiopeptides. *Curr Med Chem* 2000; 7: 971–94.
 53. Skaso E, Pasko Z, Niwinska A et al. The presence of hereditary BRCA1 gene mutation in women with familial breast and ovarian cancer and the frequency of occurrence of these tumors in their relatives. *Eur J Gynaecol Oncol* 2004; 25: 470–4.
 54. Boland A, Ricard M, Opolon P et al. Adenovirus mediated transfer of the thyroid sodium/iodide symporter gene into tumors for targeted radiotherapy *Cancer Res* 2000; 60: 3484–92.
 55. Kawashita Y, Ohtsuru A, Miki F et al. Eradication of hepatocellular carcinoma xenografts by radiolabelled, lipiodol-inducible gene therapy. *Gene Ther* 2005; 12: 1633–9.

New concepts in dosimetry and radiation protection

Michael Lassmann, Manuel Bardies, Carlo Chiesa, Wolfgang Eschner, Glenn Flux, Myriam Monsieurs, Sauli Savolainen, and Sven-Erik Strand

Background

Nuclear medicine contributes significantly to the health, healthcare, and quality of life of European citizens, particularly in major clinical areas such as cancer and cardiovascular disease. Every year in Europe, over 10 million patients benefit from a nuclear medicine procedure, 90% of which are diagnostic (planar, positron emission tomography (PET), single photon emission computed tomography (SPECT)) and 10% therapeutic. These radionuclide therapies (or targeted radiotherapy, TRT) will increase in importance and number in the coming years, in particular with the introduction of new molecules and radiopharmaceuticals, including radioimmunotherapy, through rapid developments in molecular biology and medicine. TRT (e.g. radioimmunotherapy) with new radiopharmaceuticals coupled to β - or α -emitting isotopes is a promising form of radiotherapy for the treatment of different forms of cancer.

According to a survey carried out by the European Association of Nuclear Medicine (EANM) radionuclide therapy committee¹ in 1999, there were 82 892 patients treated with radionuclides in 18 European countries, i.e. 191 treatments per million inhabitants. The most frequent therapy indication was and is 'benign thyroid disease' with ¹³¹I (69.1%). Another 26.6% of the indications were for malignant diseases. These numbers underline the necessity to carry out accurate dosimetry:

1. To comply with the EU council directive 97/43/ EURATOM (June 1997)² in which it is stated that 'For all medical exposure of individuals for radiotherapeutic purposes ... exposures of target volumes shall be individually planned; taking into account that doses of non-target volumes and tissues shall be as low as

reasonably achievable and consistent with the intended radiotherapeutic purpose of the exposure'. Individualized treatment planning has become routine practice for patients undergoing external beam radiotherapy, and this directive is now becoming incorporated into national legislation, such as the Ionising Radiation (Medical Exposure) Regulations (IRMER) regulations in the UK.³

2. To fulfill the clinical need for reliable individual patient dosimetry estimates to improve the efficacy of targeted radiotherapy.

A number of centers worldwide have conducted theoretical as well as (pre)clinical experimental studies for TRT. Significant progress in the development of selective radionuclide carriers and optimal radioisotopes has been achieved in several centers. Evaluation of the efficacy of TRT by unsealed sources of radiation⁴ depends on calculating the absorbed dose delivered to the patient's organ and tissues.⁵ Oncology is the most common context in which these therapeutic methods are implemented, in which case the absorbed doses delivered are determined in both tumor targets and the normal tissues that are to be preserved.⁶ As the administered activities are very high, deterministic radiation effects are to be expected.

Individual patient dosimetry is currently the only possible way to:

- establish an individual minimum effective absorbed dose and maximum tolerated absorbed dose to tissue
- predict tumor response and normal organ toxicity on the basis of pretherapy dosimetry
- increase the knowledge of clinical radionuclide radiobiology by correlation calculations and observed effects post-therapy

- relate and compare the results to the radiation dosimetry routinely performed for external beam radiotherapy
- Increase radiation safety to both patients and staff.

Absorbed dose calculations are based on modeled biodistribution data and on quantitative imaging procedures. The biodistribution of radioactive tracers should be assessed separately for each individual patient, as it depends on a number of patient-specific parameters, such as gender, and size of the subject as well as the extent and nature of the disease. However, to date, technicalities and knowledge have had to be augmented and stimulated in order to achieve a more satisfactory correlation between absorbed dose estimates and treatment response or correlation with organ toxicity. Due to this, almost all TRT treatments today are based on empirical fixed administered activities, activities modified by clinical and/or pathological findings. This approach certainly leads to suboptimal under- or overdosing, as it is not individually tailored. (For the sake of safety, empirical-based treatments are in general far below the toxicity threshold.)

Currently, the errors of internal dosimetry calculations for diagnostic or therapeutic studies are in the order of magnitude of 30–100% or even higher, so that the situation is comparable to the situation of external beam therapy 30 or more years ago. Lower accuracy in quantitative imaging in combination with more demanding patient study and analysis time for internal dosimetry in TRT is maybe the reason for this delay with respect to external beam therapy. Nevertheless, improvements in quantification accuracy and specifically designed hardware and, above all, software can be conceived. Obviously resources are needed. It is a fact that, at present, technological means and human and time resources for internal dosimetry are small compared to external beam therapy. The influence of the individual patient's radiation sensitivity and the knowledge of radiation-induced biological effects are not taken into account when patient absorbed doses are calculated.

Dosimetry, however, is very demanding, particularly in TRT. Today administered activities in the order of GBq cause deterministic effects in, for example, bone marrow and are close to 50% lethal dose (LD_{50}) without any good, accurate internal dosimetry.

Internal Dosimetry in Nuclear Medicine today can be divided into two main approaches, one is the dosimetry for the diagnostic application of radionuclides, and the second approach is the patient-specific dosimetry for TRT. Both approaches can be based on the so-called 'MIRD formalism'. As stated below for dosimetry in diagnostics, the possibility of having any correlation with biological effect is then limited. The second approach demands the development of dose planning systems for individual patient dosimetry. It is driven by the use of high activities in radionuclide therapy, where the goal is methodology able to estimate any relationship between absorbed dose and biological effect.

Definition of 'absorbed dose'

In many publications the term dose is used to describe the administered activity as well as the 'absorbed dose'. It is, however, mandatory to distinguish between these two terms. The appropriate term for the quantity of interest in dosimetry, however, is absorbed dose (D), expressed in units of gray (Gy).

The absorbed dose is defined as the energy (E) absorbed in a particular mass of tissue, divided by the tissue mass (m):

$$D = \frac{E}{m} \quad (1)$$

In radionuclide therapy E represents the number of radionuclide disintegrations in a particular volume multiplied by the energy emitted per disintegration of the radionuclide and multiplied by the fraction of emitted energy that is absorbed by a particular (target) mass.

The concept of absorbed dose is only applicable on a macroscopic scale as it is generally done in nuclear medicine dosimetry. In macrodosimetry, one considers mean parameters (mean doses). It should be noted that the mean absorbed dose can be calculated for a large (i.e. organ) volume or at the microscopic level, as long as the criteria applicable to macrodosimetry are met.^{7,8} The energy deposition, however, is a stochastic process and shows inherent statistical fluctuations. If particle flux – and energy deposition – is large enough then the mean absorbed dose is relevant, as the standard deviation due to stochastic fluctuations is small.

In microdosimetry, the whole process of energy deposition is followed, and the results are given as a probability distribution of energy deposition events. Microdosimetry has to be applied in a situation when the statistical fluctuations of the energy deposition events become apparent. A typical example for the applicability of microdosimetry in nuclear medicine is treatment with α emitters such as ^{212}Bi or ^{223}Ra . As a detailed description of microdosimetry and the related concepts is beyond the scope of this book, the reader is referred to the International Commission on Radiation Units (ICRU) 'Report 36'.⁷

Conventional dosimetry formalism

Methods for calculating the absorbed dose from the administration of a radiopharmaceutical were first standardized in the 1960s by the Medical Internal Radiation Dosimetry (MIRD) committee (see, for example, reference 9) with the initial aim of estimating average doses to critical organs resulting from diagnostic procedures. Essentially this

methodology allows the calculation of absorbed dose using the *simplified* version of the basic equation:

$$\bar{D}(r_k \leftarrow r_h) = \bar{A}_h S(r_k \leftarrow r_h) \quad (2)$$

$\bar{D}(r_k \leftarrow r_h)$: the mean absorbed dose to a target region r_k from the cumulated activity in source region r_h .

\bar{A}_h : the cumulated activity (i.e. the integral of the activity–time curve from zero to infinity) in a given source region r_h .

$S(r_k \leftarrow r_h)$: the radionuclide specific S factor for target region r_k and source region r_h per unit cumulated activity in source region r_h .

\bar{A} denotes the total number of radioactive decays occurring within an organ in which a radiopharmaceutical accumulates (the ‘source organ’). The MIRD S factor accounts for the energy released from each radioactive decay and the relative geometry of the source organ and the organ for which the absorbed dose is to be calculated. Thus, the cumulated activity is dependent on biological parameters whilst the S factor deals with the physical components of the absorbed dose.

There is no assumption made concerning the source or target, other than that the radioactive distribution is homogeneous in the source h . The source and target can be of any size or composition. Theoretically, if the activity in the source has a heterogeneous distribution, it is possible to subdivide the source into smaller volumes in which the activity can be considered to be homogeneous.

As the cumulated activity constitutes the sum of all radioactive emissions during the time considered, the energy deposition rate with time is not taken into account, although the absorbed dose rate (Gy s^{-1}) is known to impact on the biological consequences of the irradiation.¹⁰ The relevance of this is indicated by the fact that the aim of most dosimetric studies is to relate a physical parameter (i.e. energy absorbed per unit mass) to the observed biological effect: the relation between these two parameters may not be simple, and scientifically sound dosimetric protocols are simply a prerequisite for subsequent radiobiological studies.

MIRD S factors have been published as look-up tables for any given pair of relative organs for a comprehensive range of clinically relevant radionuclides.¹¹ For a full exposition of the MIRD schema, the reader is referred to the various pamphlets and books published by the MIRD committee. Further methodologies for dosimetry have been developed,^{12,13} although the basic principles behind each are essentially identical.

Whilst MIRD methodology, as traditionally employed, provides a relatively simple means to perform internal dosimetry, adaptations and alternative methods are required to deal with *therapeutic* applications of radiopharmaceuticals.

Whilst the basic principles of dosimetry hold for all dosimetric calculations, the application of these methods, and in particular in the determination of the required input parameters, is not straightforward. The method of administration may be intravenous, intra-arterial, or by direct

infusion, as well as oral. Different methods of administration, for example, will require different approaches to dosimetry calculations. For example, in the case of an intratumoral administration of a radiopharmaceutical, the absorbed dose gradient can be dramatic, and a mean absorbed dose over the whole tumor can be meaningless. For intracavitary administration, the absorbed dose to the cavity wall has been calculated using an absorbed fraction of 0.5 rather than 1, since only half of the energy is assumed to be deposited in the wall.

Furthermore, an increasing range of radionuclides are being employed for TRT, including α and pure β emitters as well as low energy electron emitters such as Auger electron emitters, and the mechanism and localization of uptake can vary for different therapy procedures. To be clinically useful, dosimetric calculations must be performed for both target organs (which may include focal and primary lesions) and for organs-at-risk, which frequently include the red marrow as well as organs such as the kidneys, liver, and heart. In particular, the accuracy with which dosimetry may be carried out is adversely affected by heterogeneity of radiopharmaceutical uptake on both a macroscopic and a microscopic scale and by non-standard organ geometries.¹⁴ In a recent publication of the ICRU, different aspects on the heterogeneity of activity uptake in tissues and tumors have been addressed.¹⁵

One example of a recent clinical application of dosimetry is the application of [⁹⁰Y] ibritumomab tiuxetan (the first radiopharmaceutical for radioimmunotherapy which is licensed in Europe and the USA) to the radioimmunotherapy of non-Hodgkin’s lymphoma (NHL) by Wiseman et al.¹⁶ In this study, pre-therapeutic image-based dosimetry for an administration of 15 MBq/kg [⁹⁰Y] ibritumomab tiuxetan (Zevalin®) radioimmunotherapy for NHL was performed. Patients were given a tracer administered dose of 185 MBq [¹¹¹In] ibritumomab tiuxetan on day 0, evaluated with dosimetry, and then a therapeutic administered activity of 7.4–15 MBq/kg [⁹⁰Y] ibritumomab tiuxetan on day 7. The residence times for ⁹⁰Y in blood and major organs were estimated from ¹¹¹In.¹⁷ One of the findings was that the median absorbed dose for ⁹⁰Y was 0.97 Gy (sacral image-derived method) to red marrow, and that the hematological toxicity did not correlate with estimates of red marrow absorbed dose.¹⁷

The lack of standardized dosimetric practice is due in part to the relatively low numbers of patients treated at any one center and also due to the lack of medical physicists involved in dosimetry. However, the increasing number of multicenter trials involving TRT will enable more data to be collated and processed according to similar protocols.^{18–27}

Patient-specific absorbed dose calculations for tumors and for normal organs present two main challenges. The first, and arguably the most significant, barrier to routine accurate dosimetry is that of image quantification, by which the counts recorded in an image may be converted to

absolute values of activity or activity concentration. The second issue that arises is that of the absorbed dose calculation itself, and particularly the need to deal with problems caused by a non-uniform uptake of activity and by non-standard organ geometries. A comprehensive overview of methods and instrumentation for dosimetry is compiled by the MIRD committee and published in pamphlet form.²⁸ The ICRU Report 67¹⁵ summarizes the current status of internal dosimetry, including small-scale and macrodosimetry as well as radiobiological considerations. For assessment of the biokinetics (the 'time-activity curve') for pre-therapeutic or therapeutic dose calculations several methods can be used according to their respective capabilities.

The ICRP has published several summaries of absorbed doses in nuclear medicine, all based on the MIRD concept and mean absorbed doses.^{29,30} These data can be considered as useful in the diagnostic setting, but not applicable in any therapeutic applications or for predicting biologic effects.

Scintillation camera imaging in nuclear medicine dosimetry

Photons are emitted in the patient and undergo a certain number of interactions until they are (or are not) finally detected. Photon transport depends on the interaction probabilities in tissue, which vary within the body, arising in attenuation and scatter of the photons. A minor portion of the photons emerging from the patient body pass through a collimator, whose role is to make sure that only orthogonal projections of the source will impinge on the crystal. The photons then interact in the crystal, creating scintillation light that is detected by a position sensitive array of light sensitive detectors (i.e. PMTs, photomultiplier tubes). By using appropriate electronics for conversion of the light to an electrical signal, the position and the energy of the impinging photon, which falls within a pre-determined energy window, are registered as a count on the image. The counts are then used to quantify the activity distribution in the patient by using, for example, region of interest (ROI) techniques. All these processes have to be considered for activity quantification calculations (Figure 30.1). The main corrections needed for absolute quantification are attenuation, scatter, collimator efficiency, detector sensitivity, septal penetration, and eventually high count rate corrections. Only a minor part of the emitted photons will be detected (about 10^{-6}).

At a low pulse rate, the number of counts collected during a preset time interval is limited, which makes the statistical uncertainty high and produces noisy images. However, the time resolution of the camera has to be considered at high activities (such as those encountered for therapeutic applications) and thus for high fluence rates of photons that impinge on the scintillation crystal.

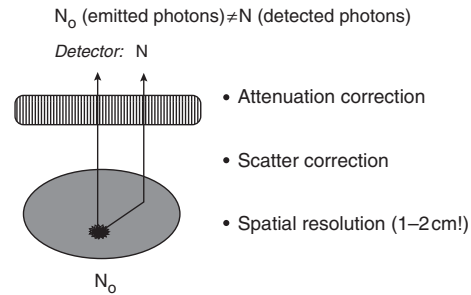


Figure 30.1

General problem in nuclear medicine: the number of emitted photons is not equal to the number of detected photons.

When using radionuclides emitting high energy photons, large septal penetration can occur, and therefore images can no longer be considered as orthogonal projections of an activity distribution. An accurate method of revealing such effects is to use Monte Carlo methods for simulating the total process of photon transport and interactions. For example, for ^{131}I , the scatter component is complex, due to the higher principal energy (364 keV), and the contribution of non-negligible higher energy photons (637 and 723 keV). Interactions that need to be modeled occur in the patient, the collimator, and the camera head, and include septal penetration.³¹

Planar image-based dosimetry

To date, the majority of dosimetric calculations, where they have been carried out, have employed planar images. Mostly the conjugate-view method has been used for quantification. Imaging is possible with γ emitting radionuclides that are used for therapy (e.g. ^{131}I , ^{153}Sm , ^{186}Re , and ^{188}Re), whilst in cases where pure β -emitters have been administered, dose estimates have been made using a surrogate radioisotope such as ^{111}In for ^{90}Y .³² Planar imaging is less resource intensive than SPECT- or PET-based imaging, and has a spatial resolution around 10 mm, although contrast is decreased and it is necessary to distinguish tumor or organ uptake from uptake in underlying or overlying organs. Also, for the A/P method the matching of the two projections and the transmission image is crucial for accurate quantification. Planar imaging has been used widely in many recent clinical studies.³³⁻⁴⁴

The contribution from overlapping tissue activity has been calculated for some organs.⁴⁵ As an example for $^{99\text{m}}\text{Tc}$: in the images, the kidney activity was overestimated by up to a factor of 34 for some time points, due to activity and scatter from overlapping organs partly caused by excretion of activity through the intestines. The residence times calculated for ^{131}I were for some organs more than ten times higher than the true residence time, resulting in 6-7 times

higher calculated absorbed dose to those organs than was the actual mean absorbed dose.⁴⁶

SPECT image-based dosimetry

The disadvantage of planar imaging is the lack of three-dimensional (3D) information. This can be partially solved by the addition of three-dimensional anatomical images from computed tomography (CT) or magnetic resonance imaging (MRI),^{33,47–52} although this will not yield the true 3D distribution of radioactivity. As the conjugate view method cannot correct appropriately for overlapping tissues (see above), quantitative SPECT imaging leads to a more accurate determination of the actual tissue activity concentration. It is particularly advantageous for measuring organ activities in body structures with overlying structures.²⁸ Examples of the application of this technique to preclinical and clinical studies can be found in the literature.^{53–80} As well as the increased resources required to obtain a time-sequential series of SPECT scans following the administration of a therapy or pre-therapy tracer, post-acquisition image processing is also more involved. The most notable of these is image reconstruction, for which a number of algorithms have been developed. However, the ability of SPECT imaging to identify the distribution of uptake within the target organ offers the potential in many cases for improved dosimetric accuracy. A flow chart describing the methodology of the quantification procedure and evaluation is shown in Figure 30.2.⁷⁴

Quantitative SPECT imaging

Emission tomography methods significantly reduce the macroscopic superposition of activity in the reconstructed data and permit determination of the activity volume on a macroscopic scale. Tomographic image reconstruction can be performed by analytical methods, using filtered back-projection, although many contemporary reconstruction methods now work on an iterative basis where the aim is to generate a set of estimated projections from a first guess of the activity distribution. The estimated projections are compared to the measured projections and updated based on the differences. The comparison, updating, and stopping criteria can be performed based on various approaches, e.g. the maximum-likelihood or ordered-subsets expectation maximization algorithms. An advantage of the iterative methods is that compensation for physical limitations can be modeled in the reconstruction process.⁸¹ It is also possible to account for scatter during the iterative reconstruction process.⁸² A detailed review of reconstruction algorithms in SPECT is found in an article by Bruyant⁸³ and the textbook by Wernick and Aarsvold.⁸⁴

In SPECT imaging, the attenuation of homogeneous regions can be estimated using a body contour and a single value of the effective attenuation coefficient. For non-homogeneous regions, a patient-specific attenuation map is required. This can be obtained from scintillation-camera transmission scanning,⁸⁵ or CT,^{86,87} or by using segmented scatter-emission images.^{88,89} Attenuation corrections can be performed on the projection images, on the reconstructed images, or as part of an iterative reconstruction method.

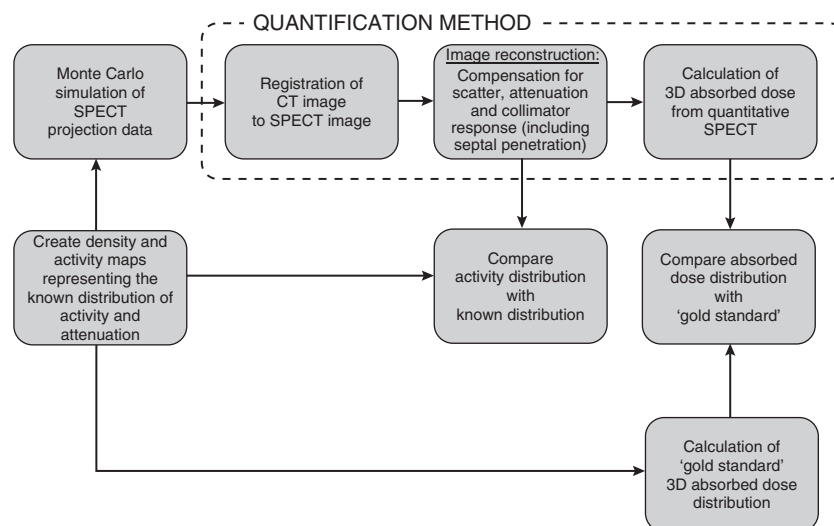


Figure 30.2

Flow chart describing methodology of quantification procedure and evaluation. Known activity map and gold standard absorbed dose distribution are compared with corresponding maps obtained from quantitative single photon emission computed tomography (SPECT) calculation scheme. (Redrawn from reference 74.)

A full review of attenuation correction for emission tomography is given by Zaidi and Hasegawa⁹⁰ and is also addressed in the above textbook.⁸⁴

The problem of image quantification for therapy radionuclides, particularly for ¹³¹I, is exacerbated by the fact that most cameras are optimized for diagnostic imaging with ^{99m}Tc.

PET-based dosimetry

PET is currently the most accurate method for the determination of activity concentrations in tissue. PET is based on electronic collimation, and thereby offers a wide acceptance angle for detecting emitted annihilation photons. Consequently, the sensitivity of PET per disintegration with comparable axial fields of view is two orders of magnitude greater than that of SPECT cameras. Quantification techniques are well established with PET. For dosimetry, PET offers improved spatial resolution over SPECT. The measured line integrals must be corrected for a number of background and physical effects before reconstruction, such as subtraction of random coincidences, detector normalization, dead time, attenuation, and scatter corrections.

In PET, correction for attenuation depends on the total distance traveled by both annihilation photons, and is independent of the emission point along the ray defined by these photons. The most accurate attenuation correction techniques are based on measured transmission data acquired before (pre-injection), during (simultaneous), or after (post-injection) the emission scan. Alternative methods to compensate for photon attenuation in reconstructed images use assumed distribution and boundary of attenuation coefficients, segmented transmission images, or consistency condition criteria.⁹¹

PET imaging can be considered for treatment planning but ideally requires the use of a radioisotope from the same element as that used for treatment (for example ¹²⁴I for ¹³¹I or ⁸⁶Y for ⁹⁰Y). ¹²⁴I was applied to dosimetric assessments as early as 1986,⁹² particularly for the dosimetry of radioiodine therapy of benign thyroid diseases.^{93,94} In 1991 the use of ¹²⁴I was proposed for quantifying in vivo tumor concentration and biodistribution for radioimmunotherapy.^{95–97} An additional application was the approach to treatment planning of [¹³¹I]MIBG (metaiodobenzylguanidine) targeted radiotherapy.⁹⁸ Due to the complex decay process of ¹²⁴I, the quantification procedure cannot be performed in the same way as for ¹⁸F. Pentlow et al.⁹⁹ measured resolution, linearity, and the ability to quantify the activity contents of imaged spheres of different sizes and activities in different background activities. It was shown that the quantification process for ¹²⁴I could reproduce the activities administered. Compared to conventional PET nuclides, resolution and quantification were only slightly degraded.^{100,101} In addition, the sphere detectability was

also only slightly worse if imaging time was increased to compensate for the lower positron abundance.

PET with ¹²⁴I was also successfully applied to the measurement of thyroid volume.^{101,102} Today's state of the art of PET ¹²⁴I-based thyroid dosimetry is described in a recent paper by Sgouros et al.,¹⁰³ in which it is shown that, when using the PET results as input to a fully 3D dose planning program, spatial distributions of absorbed dose, isodose contours, dose–volume histograms, and mean absorbed dose estimates can be obtained.

Another application of PET quantification to dosimetry is the use of ⁸⁶Y for the therapy planning of somatostatin receptor positive tumors.^{104–111} The complex decay process of ⁸⁶Y, however, makes the use of extensive corrections for quantification necessary, which are not easily implemented into standard PET or PET–CT scanners. Helisch et al.¹⁰⁹ For example, showed that the image quality and quantification process is superior when using ⁸⁶YDOTA-Phe¹-Tyr³-octreotide (where DOTA is tetraazacyclododecanetetraacetic acid) compared to [¹¹¹In]pentetreotide. They conclude that, compared to ⁸⁶Y, dosimetry with ¹¹¹In overestimated doses to the kidneys and spleen, whereas the absorbed dose to the tumor-free liver was underestimated. However, both dosimetric approaches detected the two patients with an exceptionally high radiation burden to the kidneys that carried a potential risk of renal failure following radionuclide therapy.¹¹⁰

When applying appropriate corrections to the PET images a dose dependence of the radiation nephrotoxicity after [⁹⁰Y]DOTA-TOC (where TOC is Tyr³-octreotide) therapy was shown.¹¹¹ Individual renal volume, dose rate, and fractionation play important roles in accurate dosimetry estimation that enables the prediction of risk of renal function impairment.¹¹¹

Other radioisotopes such as ⁶⁶Ga,¹¹² or ¹³⁴Ce/¹³⁴La, a radionuclide generator producing an Auger electron- and positron-emitting radionuclide,¹¹³ may also play an important role in PET-based dosimetry for targeted radiotherapy.

Problems that have to be overcome include but are not limited to the following:

1. Many of the surrogate isotopes used have such a short half-life that the time–activity curve does not reflect the complete biokinetics of the radionuclide used for therapy (such as ⁸⁶Y/⁹⁰Y).
2. Special quantification procedures have to be performed, as the standard quantification procedures fail due to additional γ emissions of the isotopes used which are detected in the coincidence window (such as ⁸⁶Y) of the PET systems.
3. The availability of the PET radiopharmaceutical is often restricted to very few centers which have access to a cyclotron for nuclide production.
4. The software of newer PET–CT systems does not easily allow the application of non-standard ([¹⁸F]-based) corrections.

Monte Carlo methods in nuclear medicine dosimetry

Dosimetric estimates require both quantitative imaging and dose calculation. These can be referred to as the two terms of equation (1) above. Dose calculation can be carried out by multiplying the cumulated activity (which requires quantitative imaging and pharmacokinetics assessment) by the relevant S factor (the dose conversion factor, which is relevant for a given geometry and isotope).

Monte Carlo techniques can be used in both fields. Historically, Monte Carlo simulations were first used for S factor calculations, but now the trend seems to be to use these techniques more and more in the field of quantitative nuclear medicine imaging.

S factor calculations

S factor calculations seem to be the obvious field for the use of Monte Carlo methods in nuclear medicine. Analytical description of radiation transport is only feasible in a restricted number of cases – basically for very simple geometries and uniform propagation media. The pioneer work of Berger¹¹⁴ was first used for Monte Carlo determination of dose point kernels (DPKs) that were previously determined by numerical solving of the radiation transport equations.^{115,116} A further step was reached with the modeling of dose deposition in heterogeneous phantoms,¹¹⁷ which eventually led to the publication of the MIRD S factor tables for an adult reference man.¹¹⁸ Cristy and Eckerman¹¹⁹ published S factors for six anthropomorphic phantoms representing the newborn, and 1-, 5-, 10- and 15-year-old child (at the time considered as equivalent to the reference women – a statement that would not be accepted today) and the reference adult male. These were later integrated in the MIRDOSE software (version 2). At the time, due to calculation time constraint, a large degree of uncertainty had to be accepted. Since then, the availability of ever increasing computing power has allowed the generation of more sophisticated mathematical phantoms, including ethnic phantoms, or male or female phantoms of varying size and weight.^{120–122}

Patient specific dose calculation through Monte Carlo simulation was difficult to achieve – at least when the whole patient body was considered. The example given by Xu¹²³ emphasizes this point: the reference man, when segmented with a (quite good) sampling of $0.30 \times 0.3 \times 1$ mm leads to a 4-Gbyte data set, which exceeds the limits of most 32-byte workstations. It is also generally felt that dealing with digital phantoms (i.e. the closest data set to a 'real' patient image) dramatically increases the calculation time required for performing Monte Carlo simulations.¹²⁴ However,

some examples have recently been published that seem to indicate that patient specific dose calculation using Monte Carlo techniques is feasible, and may become more widespread in the near future.^{124–129}

Imaging

Sufficient image quantification is only possible if all effects that degrade the quantitative content of the image have been corrected for. Monte Carlo simulations are an appealing tool that can help to model interactions occurring in the patient and in the detector system. This is helpful to develop and test correction techniques, and to help define detector geometries better suited to quantitative imaging. As a consequence, there are a growing number of articles^{130,131} and textbooks^{132,133} being published in the field of nuclear medicine that involve Monte Carlo techniques, particularly with respect to quantitative imaging.

There are basically two kinds of Monte Carlo codes that can be used in nuclear imaging: generic Monte Carlo codes and specific Monte Carlo codes.

Generic Monte Carlo codes come from the world of high energy physics. They were mostly created in major nuclear research centers, and were developed to deal with radiation propagation in matter. Codes such as ETRAN and its derivatives,¹¹⁴ EGS,¹³⁴ MCNP,¹³⁵ or Geant¹³⁶ belong to that category. They have been widely used by the scientific community and possess an established user database. They are usually part of an extensive research program, i.e. involving several permanent people committed to the development, debugging, and maintenance of the code. This explains why these codes can generally be considered as standards against which other codes can be benchmarked. One major drawback is that they usually have not been designed to deal with nuclear imaging explicitly. This often makes it very difficult to use them within that area. For example, it is important to make sure that 'low energies' such as those encountered in nuclear imaging are dealt with correctly.

Specific Monte Carlo codes, on the other hand, have been especially designed for nuclear imaging. They can be differentiated by the way that detection modeling is dealt with. In SPECT for example, some codes model interactions that occur in the collimator, and others just consider photons that impact on the detection head with the right solid angle (optical selection). The main possible drawback of 'homemade' Monte Carlo codes is the lack of support with time: being mostly the product of a single laboratory, the continuity of a given code is often not granted. Also, the way physics interactions are dealt with is in general less reviewed – or at least reviewed by a smaller user community – than for generic Monte Carlo codes.

A collaborative effort has been carried out recently by a group of laboratories involved in the field in order to create a

Monte Carlo code dedicated to nuclear imaging but based on a generic Monte Carlo code. That code, Gate,¹³⁷ is based on Geant4. The user can create the experiment through the use of a macro-language via a dedicated scripting mechanism that extends the native command interpreter of Geant4 and allows performing and controlling the Monte Carlo simulation in an intuitive manner (<http://www.lphe.epfl.ch/~PET/research/gate/>). As an example, in Figure 30.3 a Monte Carlo simulation of the influence of septal penetration and scatter of ¹³¹I photons on a high energy collimator of a γ camera is shown (Figure 30.3a: resulting image; Figure 30.3b: scatter only; Figure 30.3c: septal penetration; Figure 30.3d: geometric photons). The numbers in the upper right corner denote the percentage of photons. In the case of ¹³¹I only 47% of detected photons counted by a γ camera are geometric photons. The rest come from either septal penetration or scatter.

One major limit of Monte Carlo methods is linked to the statistics required to accurately simulate a given experimental setting: the number of simulated particles has to be very high, and therefore implies heavy computing power.

In SPECT, photons that reach the detector head first impact the collimator. Since only one out of 10 000 photons – or fewer – that hit the detector head actually cross the collimator and are detected, this highlights how inefficient this process is from a computing perspective.

In order to decrease computing time, analytical modeling of physical effects can sometimes be carried out, such as

optical selection of photons that impinge the collimator, but this may not be always feasible. For example, when modeling γ cameras for high energy radionuclides such as ¹³¹I, one has to consider explicit interaction modeling in the collimator, since septal penetration cannot be neglected in that case.

Variance reduction techniques can be implemented, but are not available in every code proposed to the scientific community. The validation of those techniques is itself a field of research, so one has to be very cautious when dealing with variance reduction.

Monte Carlo modeling of radiation interactions in matter fall in the ‘embarrassingly parallel problem’ category: photons that interact with the detector are independent, and therefore it is equivalent to simulate 10^9 photons on a single machine or 10^8 photons on ten different machines, thus paving the way for cluster computing.¹³⁸ Apart from the trivial caveat related to random seed generation, one has to be aware of some specific aspects of image detection; for example, dead-time modeling, or pile-up effect implementation, requires serious attention to the simulation set-up in a parallel environment.

Another drastic limitation is the difficulty in validating the results given by a simulation. Experimental validation has to be carried out in a simple, i.e. feasible, practice setting, which may not allow as thorough a validation as would be required.

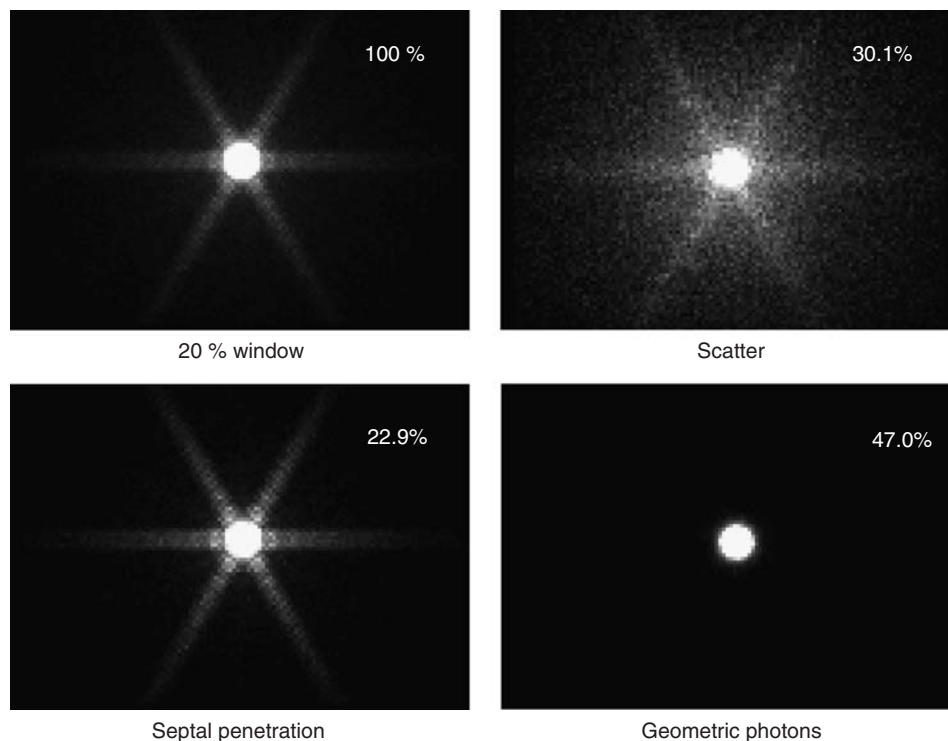


Figure 30.3

Monte Carlo simulation of the influence of septal penetration and scatter of ¹³¹I photons on a high energy collimator of a γ camera ((a) resulting image; (b) scatter only; (c) septal penetration; (d) geometric photons).

Computer codes and tools for dosimetry

Several software packages have been developed to implement the S value methodology (see equation (2) above). Basically there are two groups of computer codes.

The *first* group use planar conjugate view quantitative imaging and/or SPECT imaging for determining patient-specific organ cumulated activities or residence times. Typical codes that have been published are NUCLIDOSE¹³⁹ (Figure 30.4) or ULMDOS.¹⁴⁰

The results can be inserted into a group of computer codes which use the cumulated activities or residence time as input. As an output the doses are calculated according to the MIRD formalism. One of the first and the most widely used codes is MIRDOSE3.¹⁴¹ This code incorporates S factors for 223 radionuclides and ten different anthropomorphic models, including standard male, female, and pediatric geometries. With the exception of the 'nodule module', a part of the program which calculates the self-dose to spheres of varying diameters, patient specific parameters such as organ weight and/or organ size could not be corrected for directly. This software is no longer distributed. It has been replaced by Organ Level Internal Dose Assessment (OLINDA; Vanderbilt University).¹⁴² OLINDA received US Food and Drug Administration (FDA) exemption (premarket notification, 510K). It includes S values specific to ten phantoms and

five organ models for more than 800 radionuclides, including α particle emitters, which were not previously included in S value tabulations. The program also includes a pharmacokinetic module that may be used to determine organ cumulated activities. A typical output is shown in Figure 30.5.

MABDOSE (University of Colorado), another package that also implements fixed geometry, allows the user to place spherically shaped tumors within the simplified anatomic model originally described by the MIRD committee. To do this, an on-the-fly Monte Carlo simulation was incorporated into the code.^{143,144} This method could accommodate tumor dosimetry within the idealized geometry defined by the MIRD committee.

The consequence of using these programs is that in general it is not possible to include or recalculate patient-specific S factors. How much this fact contributes to the uncertainty in the dose assessment is highly dependent upon the disease and the radiopharmaceutical used. In some cases the patient specificity does not influence the result greatly, whereas in other cases a complete over- or underestimation of the dose is possible.

In volumes of interest (VOIs) that are large relative to the spatial resolution of the imaging system for a given radionuclide, it is often possible to discern a heterogeneous uptake of a radiopharmaceutical throughout a tumor or organ. In this case it can be misleading to quote a mean absorbed dose, with the problem exacerbated by the difficulty

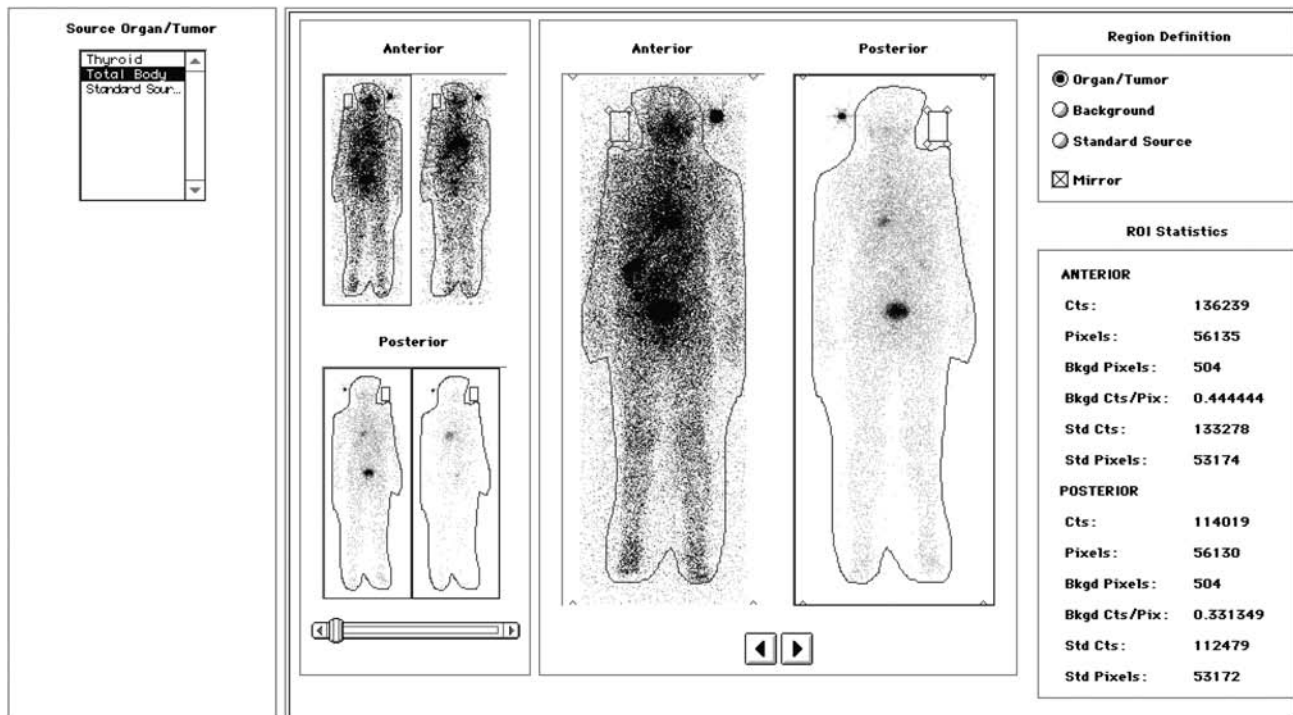


Figure 30.4

Example of the use of a computer code for the quantification of whole body scans (conjugate views) using NUCLIDOSE in a patient with differentiated thyroid cancer.

Portion of Sample Output from OLINDA/EXM 1.0

Organ	Dose to target organs*				No. disintegrations in source organs†
	α	β	Photon	Total	
Adrenals	0.00E+00	4.38E-02	8.05E-02	1.24E-01	
Brain	0.00E+00	4.38E-02	2.94E-02	7.32E-02	
Breasts	0.00E+00	4.38E-02	2.84E-02	7.22E-02	
Gallbladder wall	0.00E+00	4.38E-02	6.14E-02	1.05E-01	
Lower large intestine wall	0.00E+00	4.38E-02	6.02E-02	1.04E-01	
Small intestine	0.00E+00	4.38E-02	6.09E-02	1.05E-01	
Stomach wall	0.00E+00	4.38E-02	6.70E-02	1.11E-01	
Upper large intestine wall	0.00E+00	4.38E-02	5.78E-02	1.02E-01	
Heart wall	0.00E+00	4.38E-02	5.07E-02	9.46E-02	
Kidneys	0.00E+00	1.30E+00	2.40E-01	1.54E+00	3.50E+00
Liver	0.00E+00	2.61E-02	4.70E-02	7.32E-02	4.50E-01
Lungs	0.00E+00	1.33E-01	4.94E-02	1.83E-01	1.20E+00
Muscle	0.00E+00	4.38E-02	4.25E-02	8.64E-02	
Ovaries	0.00E+00	4.38E-02	6.19E-02	1.06E-01	
Pancreas	0.00E+00	4.38E-02	9.28E-02	1.37E-01	
Red marrow	0.00E+00	1.08E-01	5.27E-02	1.60E-01	1.50E+00
Osteogenic cells	0.00E+00	1.52E-01	5.52E-02	2.07E-01	
Skin	0.00E+00	4.38E-02	2.54E-02	6.92E-02	
Spleen	0.00E+00	1.33E+00	2.73E-01	1.61E+00	2.20E+00
Testes	0.00E+00	4.38E-02	4.04E-02	8.42E-02	
Thymus	0.00E+00	4.38E-02	4.07E-02	8.45E-02	
Thyroid	0.00E+00	4.38E-02	3.81E-02	8.19E-02	
Urinary bladder contents					1.98E+00
Urinary bladder wall	0.00E+00	5.64E-01	1.51E-01	7.15E-01	
Uterus	0.00E+00	4.38E-02	7.45E-02	1.18E-01	
Total body	0.00E+00	5.75E-02	4.41E-02	1.02E-01	
Remainder					2.91E+01

*mSv/MBq; nuclide, ^{131}I (8.02E00 day); adult male.

†MBq-h/MBq ($\mu\text{Ci-h}/\mu\text{Ci}$).

Figure 30.5

Example of the output of OLINDA (Organ Level Internal Dose Assessment) used for preliminary dose assessment in a patient with differentiated thyroid cancer. (From reference 142)

of delineating an outline within which the absorbed dose is to be calculated. One possible solution is to quote a maximum absorbed dose, although overall response is likely to be dependent on the extent of the volume that receives a low absorbed dose. A more comprehensive approach is to calculate the absorbed dose distribution throughout the tumor and generate dose-volume histograms.¹⁴⁵ This can be achieved by registering sequential tomographic data so that each voxel within the VOI occupies the same coordinate throughout the series of scans. The mean absorbed dose in each voxel can then be calculated independently for each coordinate. For this technique voxel S values are required. The MIRD pamphlet 17¹⁴⁶ gives S values for a range of radionuclides for voxels with edge 0.1 mm, 3 mm and 6 mm. Image registration is becoming a more routinely used tool in medicine, due largely to an increasing interest in the incorporation of functional and MR data with CT for external beam radiotherapy planning, and by the advent of dual modality scanners.

Therefore, the *second* group completely relies upon 3D imaging and voxel-based dosimetry. Many researchers have pursued and contributed to 3D imaging-based patient-specific dosimetry.^{61,136-155} A typical output of such a code is shown in Figure 30.6 applied to [^{131}I]MIBG treatment.

In principle, the codes take the distribution of a radiopharmaceutical for a given patient (from SPECT or PET) and combine it with anatomic information (from CT or MRI) to yield absorbed dose estimates that are specific to a particular patient's biodistribution and anatomy.¹⁵⁶ In addition, some of the codes introduce the concept of dose-volume histograms for internally administered radionuclides. Dose calculations can be done applying either Monte Carlo or point kernel based calculations. More recently, the computer code 3D-ID has been used in thyroid cancer patients with ^{124}I -PET data and CT.⁹⁹ The DOSIMG software developed by the Lund group has been used with mathematical anthropomorphic phantoms to examine the impact of different quantitative SPECT

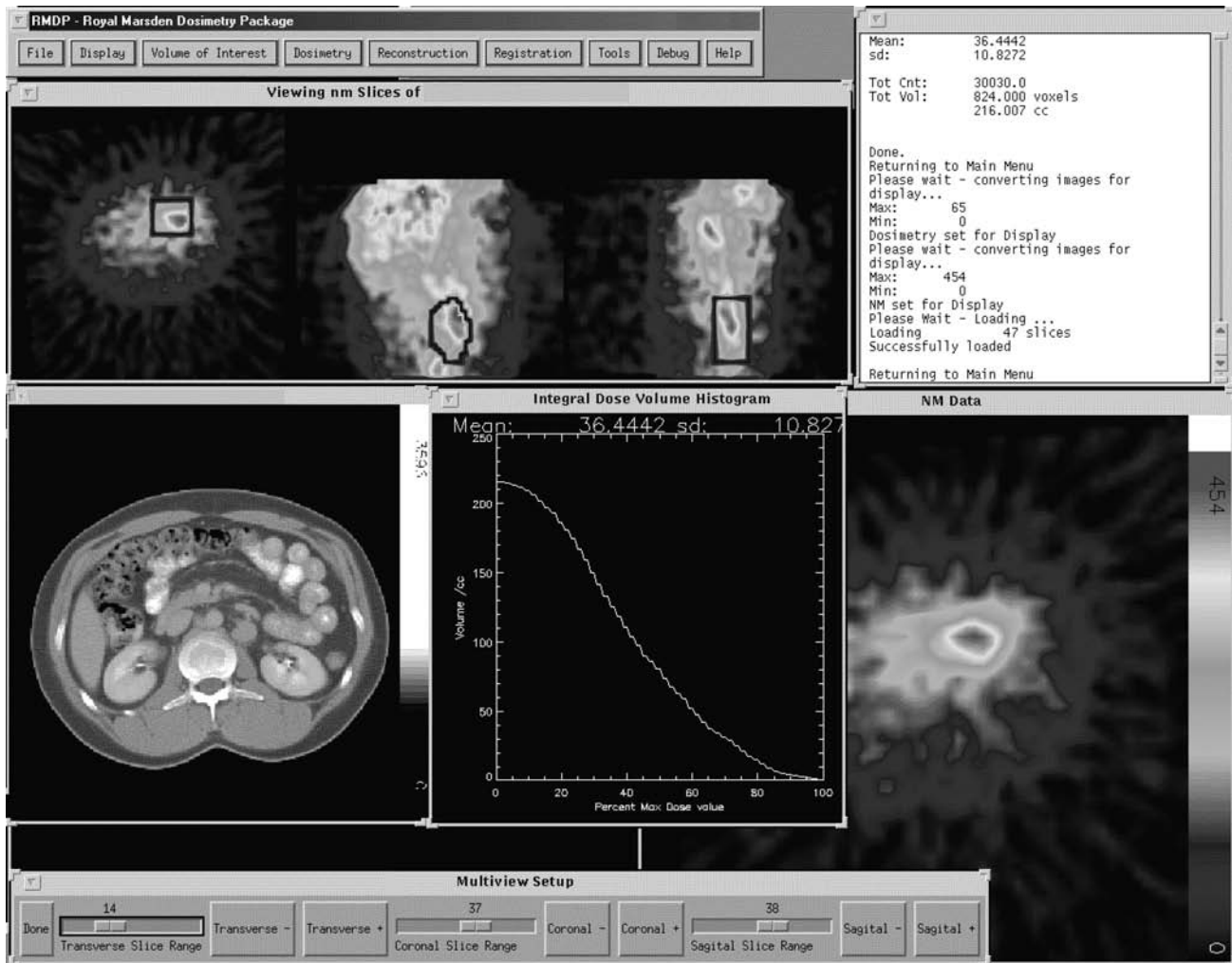


Figure 30.6

Montage of dosimetry package output for an abdominal node, imaged using $[^{131}\text{I}]\text{MIBG}$ (metaiodobenzylguanidine). (a) (left–right) Transverse, coronal, sagittal SPECT slices including volume of interest (VOI), and dialog window. (b) (left–right) Transverse abdominal computed tomography (CT), integral dose–volume histogram (DVH), and transverse SPECT slices.

algorithms on Monte Carlo derived absorbed dose calculations. Mathematical phantom derived CT and SPECT images were generated, and dose calculations derived from these were compared with ‘true’ dose results derived from the actual mathematical phantom data.¹⁵³ The SPECT quantitation methodologies derived from this work were subsequently applied to $^{111}\text{In}/^{90}\text{Y}$ dosimetry.¹⁵³

An example of the application of SPECT to three-dimensional dose calculations is shown in Figure 30.7 in which a transaxial slice of a dose distribution resulting from $[^{131}\text{I}]\text{MIBG}$ therapy of neuroblastoma can be seen. In Figure 30.7a a SPECT slice acquired post-therapy, in Figure 30.7b the corresponding absorbed dose distribution, in Figure 30.7c the rendered view of absorbed dose distribution, and in Figure 30.7d the isodose contours from targeted therapy superimposed onto the registered CT slice are shown.⁶¹

Dosimetry on tissue and cellular levels and heterogeneity in activity and absorbed dose distributions

Small-scale dosimetry

All nuclear medicine procedures are based on physiological processes, where the administered radiopharmaceutical is distributed in the tissues governed by its chemical properties. Most radiopharmaceuticals are taken up or accumulated in certain cells in the tissues, which in fact is the basis for nuclear medicine and functional imaging.

Considering that most radiopharmaceuticals inherently, due to their behavior, will distribute heterogeneously in

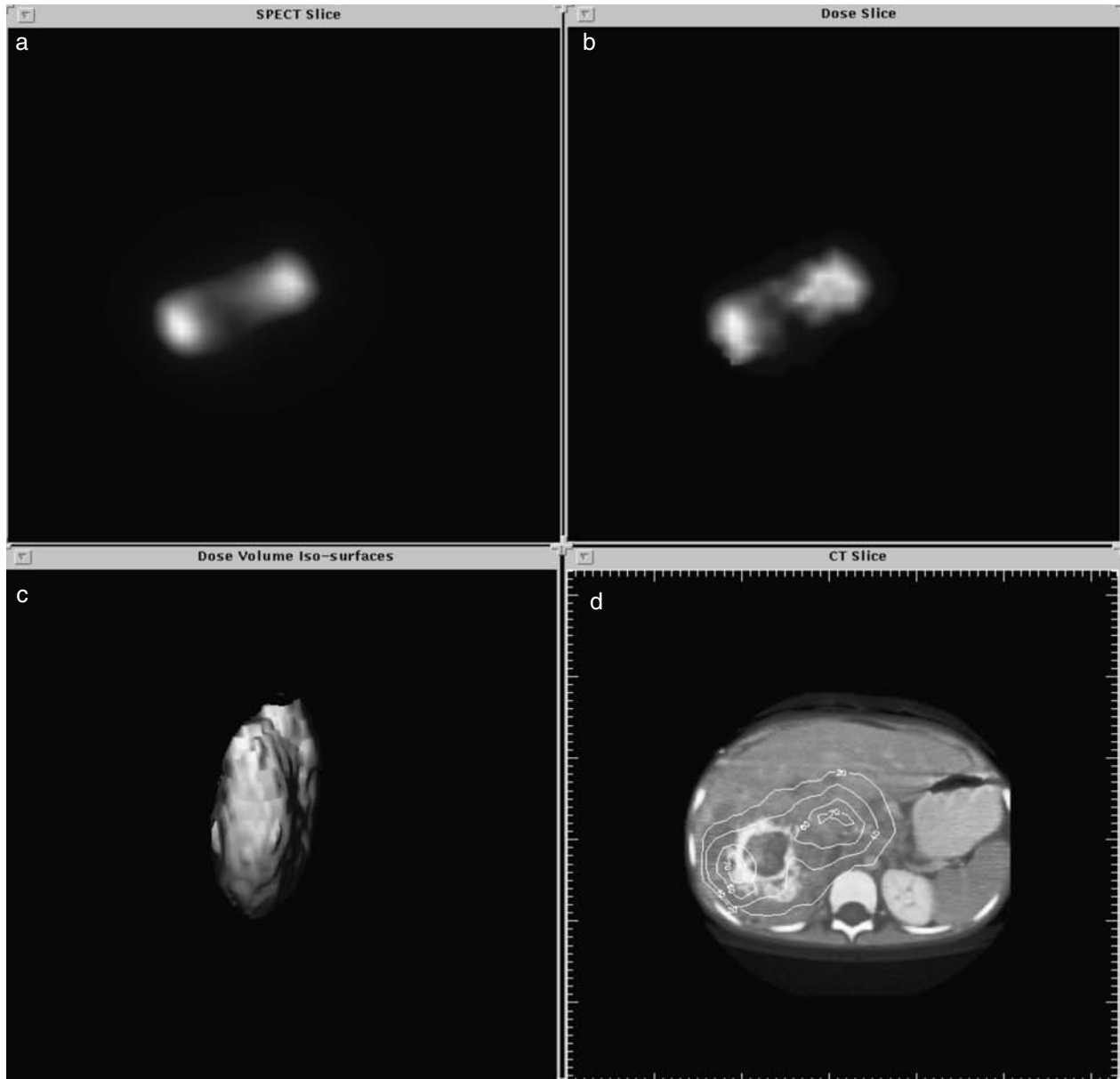


Figure 30.7

Transaxial slice of a dose distribution resulting from $[^{131}\text{I}]$ MIBG therapy of neuroblastoma. (a) SPECT slice acquired post-therapy; (b) corresponding absorbed dose distribution; (c) rendered view of absorbed dose distribution; (d) isodose contours from targeted therapy superimposed onto registered CT slice.

most organs and tissues, internal dosimetry must address this fact, in order to obtain the realistic activity and absorbed dose distribution. Not only the geometry for radiation emission in the tissue must rely on realistic distributions; also the activity must be quantified in vivo with high precision and the pharmacokinetics must be followed for a sufficient time period.

Figure 30.8 indicates that with different imaging techniques, different levels of resolution will determine how accurately absorbed dose distributions can be elucidated.

For example, with in vivo imaging with a scintillation camera, SPECT, or PET, the resolution is very low, in that only mean absorbed dose calculations can be obtained. Although a heterogeneous activity distribution mostly is present it will not be revealed with such imaging. Complementary imaging techniques are needed based on tissue sampling, such as biopsies in patients or experimental animal data. Then more realistic activity distributions can be obtained.

The dosimetry can be divided into three categories, macro-, small-scale, and micro-dosimetry, with no clear

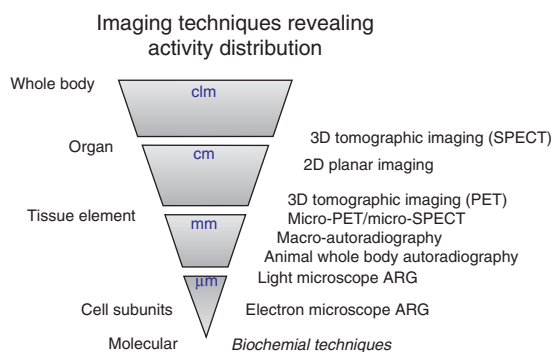


Figure 30.8

Different levels of resolution determine how accurate absorbed dose distributions will be. ARG, autoradiography. (Redrawn from reference 15.)

distinction between the first two which can be dealt with by the basic MIRD formalism with absorbed fractions and related S values.

Different models for more realistic organ/tissue dosimetry have been developed, and one example is a new model for crypt cell dosimetry in the intestines.¹⁵⁷ Another factor in radionuclide therapy that can affect the mean absorbed dose to a tumor is its shrinkage during therapy. It was shown¹⁵⁸ for one tumor that the absorbed dose calculation differed by 75% due to this.

On the tissue level, the heterogeneous distribution of radioactivity will in most cases result in great deviation of the tissue dose distribution from the mean absorbed dose. Absorbed dose heterogeneity will be obtained if there is no radiation equilibrium or charged particle equilibrium in the volume.

Heterogeneous uptake causing great deviations from mean absorbed dose is illustrated in the paper by Gardin et al.¹⁵⁹ where the absorbed dose to Kupfer cells was 15 000 times higher than the mean absorbed dose to the liver for [^{99m}Tc]sulfur colloids. Also, Makrigiorgos et al.¹⁶⁰ showed for individual lung cells an absorbed dose variation of a factor of 30 000 for ^{99m}Tc-labeled microspheres.

The cellular distribution of radioactivity is of great importance, especially when dealing with short-ranged particles, which will have great impact especially for α emitters and Auger emitters.

In a study by Linden et al.¹⁶¹ it was shown that the uptake of [^{99m}Tc]Fab' anti-CD22 in lymphoma cells varied, and depended on the CD22 expression, where the mean absorbed dose to the cells could vary between 10^{-7} and 10^{-1} Gy. When the activity was evenly distributed within the cytoplasm or on the cell surface the absorbed dose to the cell nucleus was either 16×10^{-3} or 9×10^{-3} Gy. Thus, the absorbed dose within cells can vary considerably, especially for low energy Auger electron emitters. Interestingly, it was found in that study that only five atoms per cell for ^{99m}Tc will be targeted, whereas in a therapeutic setting

with ⁹⁰Y the number of atoms per cell will increase to 480. This is considerably less than suggested by Humm¹⁶² for eradicating tumor cells.

Microdosimetry for internal emitters has to be considered when the energy deposition density is highly variable and the statistical fluctuations in energy deposition increase when smaller volumes are considered. In a study by Humm et al.¹⁶³ it was stated that when the relative deviation of the specific energy from the mean absorbed dose was larger than 20% then stochastic effects should be taken into account.

One example of the importance of the heterogeneity of activity distribution is the use of α particles for therapy. Elqvist et al.¹⁶⁴ studied the absorbed dose distribution at different distances from the center of different sized tumor cell clusters for ²¹¹At-labeled monoclonal antibody MX35 in experimental ovarian cancer. They showed that for cell clusters of 25 μ m radius with 400 kBq intraperitoneal injection, then an absorbed dose of 126 Gy was obtained with homogeneous activity distribution. However, if the activity was only on the cluster surface, then the absorbed dose declined to 29 Gy. For tumors with radii larger than 62 μ m (range of α particles), then the absorbed dose outside the range became zero, with a large decreasing gradient.

Radiobiological aspects

Up to now the role of the rate of dose delivery has been completely neglected in TRT. The key concepts have been known for a decade,¹⁶⁵ and are currently in use in external radiotherapy (XRT) dosimetry, but they were never applied in the clinical practice of TRT dosimetry. This could be one of the reasons why the situation of dosimetry in targeted radiation therapy is comparable to the situation of dosimetry in external beam therapy 30 or more years ago. In XRT it is well known that the same dose given with different fractionation schema gives a different biological response. TRT could be seen as a sequence of tiniest dose fractions, so frequent that a continuous delivery takes place. A latent question is the absence of toxicity to healthy organs in spite of the XRT dose limit being surpassed by the sum of the absorbed dose in therapeutic cycles (see for instance [¹³¹I]MIBG or [¹¹¹In]DTPA-octreotide (where DTPA is diethylenetriaminepentaacetic acid) cycles without liver damage, or [¹⁷⁷Lu]DOTA-TATE (where TATE is Tyr³-octreotate) and [¹¹¹In]DTPA-octreotide with unexpectedly low kidney toxicity). On the other hand [⁹⁰Y]DOTA-TOC more often gave renal problems in spite of the fact that the evaluated kidney doses of these three peptides were almost the same.¹⁶⁶ In the case of [¹⁶⁶Ho]DOTMP applying conventional clinical dosimetry for bone metastasis treatment, calculated kidney doses were less than 10 gray,¹⁶⁷ but the pharmaceutical gave rise to radiation-induced nephritis¹⁶⁸ and it was suspended from use.

Another recent dosimetry failure hopefully opened the gate to use of the biological effective dose (BED) in TRT. Pauwels et al. conducted an individualized dosimetric study in 18 patients to be treated with [⁹⁰Y]DOTA-TOC.¹¹¹ Dosimetry was based on PET imaging of the DOTA-TOC molecule labeled by ⁸⁶Y, a positron emitter (14.7 hours half-life).

The treatment planning was to give a kidney dose of 27 Gy to each patient. Note that the XRT threshold for kidney toxicity (5% in 5 years) TD_{5/5} is 23 Gy, and TD_{50/5} is 28 Gy.¹⁶⁹ Patients were administered in some cases with a single batch, and in other cases with more (up to five) injections, with a 30–45 day interval. Eventual late renal toxicity was monitored through percentage creatinine loss per year in a follow-up period of minimum 18–maximum 65 months.

The observed effects on the kidney following a supposed identical absorbed dose were astonishing: the radio-induced creatinine loss per year varied from 0 to 60%. Absolutely no correlation between absorbed dose and effect was found.

Having seen the failure of this high-technology, pretreatment dosimetry, the authors improved the dosimetric accuracy retrospectively by measuring individual kidney volume. They manually implemented individual mass correction after the use of MIRDOSE3 based dosimetry. For only one calculation, which for a pure β emitter consists of multiplying the self-irradiation S by the ratio between standard mass and actual mass, ROIs on any single kidney CT slice were drawn. The correlation between absorbed dose and effect rose slightly to $r = 0.54$, but was considered insufficient by the authors.

A further and radical improvement was undertaken looking at the basis of the biological effect of radiation. The dose rate effect and the number of activity administrations were included quantitatively in the dosimetric evaluation using the biological effective dose (BED, not to be confused with effective dose, see next paragraph). The dose–effect curve $F = (1 - \exp(-\alpha D))^b$ fitted experimental data with $r = 0.93$, $p < 0.0001$. The five out of 18 patients with creatinine loss per year greater than 20% were well separated in the creatinine loss vs. BED plot. A BED threshold for kidney toxicity could be set at BED = 45 Gy. According to this study, which unfortunately is still unique, the effect correlates not with the absorbed dose D, but with the BED (which in any case is based upon D). Prudence is necessary, because three of the five patients suffered from hypertension, a risk factor for impaired kidney function. Also, the damage parameterization is not universally accepted. Nevertheless, the role of dose rate in TRT must be investigated quantitatively. Absorbed dose, though the base of any dosimetric evaluation, is not sufficient for description of the biological effects. The key point is the competition between the rate of sublethal cellular damage and the cellular repair rate. But ‘nihil novum sub soli’, since the linear quadratic (LQ) model has been known since 1982,¹⁷⁰ and is currently employed in XRT when a sequence of treatment needs modification.

Radiobiological linear quadratic model and TRT

The LQ model was developed in order to explain the cellular survival curves as a function of absorbed dose, for different dose rates. For the sake of simplicity, we consider only one type of radiation, i.e. we discard relative biological efficacy (RBE) problems. LQ in TRT was introduced by Dale in 1996, but it was applied only recently in order to quantitatively account for the [⁹⁰Y]DOTA-TOC kidney dose–effect relationship.^{171,172}

Two kinds of damage to DNA are taken into account (Figure 30.9). A type damage, in which a single interaction breaks both DNA strands, and B type damage, in which the two strands are broken by two independent ionizations, separated by a time interval. The amount of A type damage depends on the number of incident ionizing events, i.e. is proportional to the absorbed dose D through the radiosensitivity α . The B type damage is proportional to the probability of two independent interactions happening in the same place. This probability is proportional to the product of two independent probabilities; hence, the quadratic term D^2 is necessary. Moreover, in B type damage, being two interactions separated by a time interval, enzymatic repair can occur if the time interval is long enough. So, the competition between dose rate and repair rate becomes the crucial point.

Biological effects in an in vitro irradiated cellular population are described by the survival fraction S as a function of the absorbed dose D. The LQ model starting point is:

$$S = \exp(-\alpha D - \beta D^2) \quad (3)$$

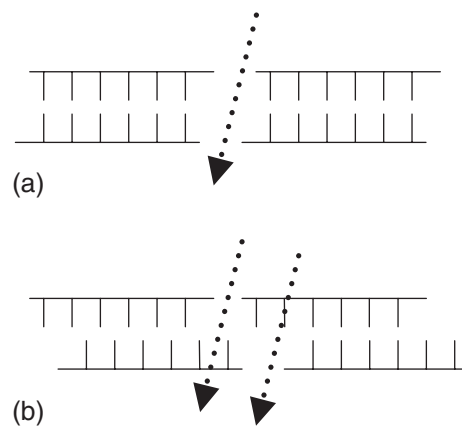


Figure 30.9

(a) A type damage (lethal): one single interaction breaks both DNA strands. Linear dependence on the absorbed dose D.
 (b) B type damage (sublethal): two independent ionizations break one DNA strand each. Dependence upon D^2 : as the two events are separated by a time interval, enzymes can repair the first damage before the second occurs, if enough time is given. This effect depends on competition between the cellular repair time and the dose rate.

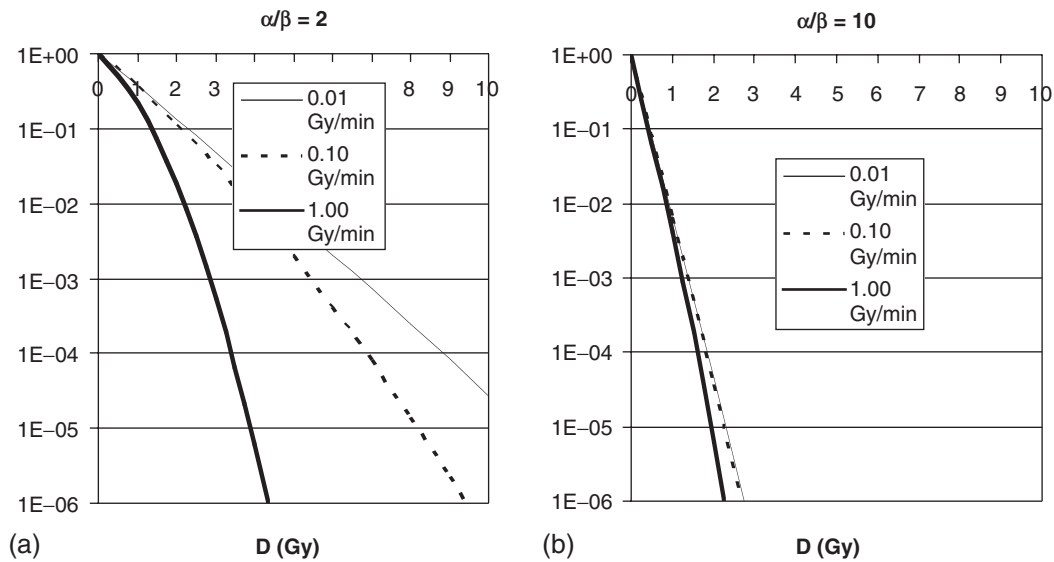


Figure 30.10

Hypothetical cellular survival curves vs. absorbed dose for low α/β ((a) slow cellular replication tissues), and high α/β ((b) tumors and slow cellular replication tissues). The sparing effect is evident in (a) since the same absorbed dose with a low dose rate gives much less damage.

Where α is radiosensitivity to A type damage, β to B type damage.

From XRT, it is known that low α/β values are characteristic of tissues with slow replication (indirect oxygen effect negligible): this includes healthy organs, except red marrow, with α/β around 2–5 Gy. High α/β values, about 5–25 Gy, are typical of fast-replicating tissues (tumors) (substantial indirect oxygen effect). Hypothetical examples of S curves for $\alpha/\beta=2$ Gy and $\alpha/\beta=10$ Gy are given in Figure 30.10.

As it is easy to understand from Figure 30.10(a), low α/β tissues allow a ‘sparing effect’ by dose rate reduction. This fact had been investigated at the beginning of XRT in order to optimize the present irradiation scheme, and to fix the dose fraction per day (usually 2 Gy). TRT is nowadays at that point. Optimization should be based on the biological effective dose (BED, not to be confused with effective dose (ED)):

$$BED = -\ln(S)/\alpha \quad (4)$$

The presence of α as the denominator makes the comparison between BEDs of tissues with different radiosensitivities meaningless. BED is useful for comparison of different irradiation conditions on the same tissue.

BED (measured in Gy) is conveniently factorized as the product of absorbed dose D and the relative efficacy (RE):

$$BED = D \times RE \quad (5)$$

Equation (5) shows the predominant importance of the absorbed dose, modulated by RE.

In the case of XRT treatment with daily fraction d, we have:

$$RE = 1 + d/(\alpha/\beta) \quad (6)$$

In the case of nuclear medicine TRT to an organ with mono-exponential clearance with effective decay constant λ , initial dose rate R_0 , and cellular repair rate constant μ , we have:

$$RE = 1 + R_0/[(\mu + \lambda)(\alpha/\beta)] \quad (7)$$

So, the relative efficacy, i.e. the biological response for a fixed absorbed dose, depends upon the following key parameters (in case of monoexponential clearance):

- R_0 , initial dose rate
- $\mu = \ln(2)/t_{1/2}^{rep}$, repair half-time of cellular sublethal damage
- $\lambda = \ln(2)/t_{1/2}^{eff}$, effective half-life
- α/β , radiosensitivity ratio for A type over B type damage.

Pauwels¹¹¹ applied a derivation of the above formula (5) which includes the sum over more than one administration:

$$BED = \sum_i D_i + \beta/\alpha \cdot t_{1/2}^{rep}/(t_{1/2}^{rep} + t_{1/2}^{eff}) \cdot \sum_i D_i^2 \quad (8)$$

All problems seem to be solved. Unfortunately, among the above listed parameters, only R_0 and $t_{1/2}^{eff}$ can be measured

Table 30.1 Radiosensitivity ratio (α/β) and repair half-time of cellular sublethal damage ($t_{1/2}^{\text{rep}} = \ln(2)/\mu$) for mouse kidney according to different authors

α/β (Gy)	1.6–3.2	1.8	2.3	0–3.5	5.0
$t = \ln(2)/\mu$ (h)	1.3	2.1			

in patients. The radiobiological parameters α/β and $t_{1/2}^{\text{rep}}$ are known with large uncertainties, or even unknown. They allow ad hoc choices and easy manipulation to obtain a good fit. Table 30.1, for instance, shows radiobiological values in mice obtained by different authors.

For kidneys, Pauwels et al.¹¹¹ adopt $\alpha/\beta = 2.6$ Gy and $t_{1/2}^{\text{rep}} = 2.8$ h.

As an example of quantitative LQ model application, consider that XRT dose rates are around 1–10 Gy/min, with 2 Gy/day fractions, while [⁹⁰Y]DOTA-TOC gives an initial kidney dose rate of 0.003 Gy/min, which continuously and exponentially decays with $t_{1/2}^{\text{eff}}$ of about 30 h. In XRT there is a consensus for kidney $\alpha/\beta = 3.0$ Gy. Using this value,¹⁷² the XRT tolerable dose of 23 Gy can be translated to a limit BED of 38 Gy, while in nuclear medicine TRT with [⁹⁰Y]DOTA-TOC, a dose limit of 27 Gy corresponds to BED = 30 Gy in the case of three equal administrations, or to BED = 37 Gy in the case of a single administration.

Dose rate to tumors and tumor cell replication rate

The low dose rate in TRT monotonically decays following the effective half-time. Dosimetric calculations consider the whole dose given below the integral of the time–activity curve until infinite time to be effective. But if the dose rate is too low, competition of cellular repopulation may occur.¹⁷¹ The BED must be corrected subtracting the repopulation factor RF:

$$\text{BED} = D \times \text{RE} - \text{RF} \quad (9)$$

A proposed but also much debated expression for RF includes the average doubling tumor time t_{av} , the irradiation duration T, and tumor radiosensitivity α :

$$\text{RF} = \ln(2)T/(\alpha t_{\text{av}}) \quad (10)$$

From equation (10) the critical dose rate for repopulation is:

$$R_{\text{crit}} = \ln(2)/(t_{\text{av}}\alpha) \quad (11)$$

Absorbed dose imparted with a dose rate below this limit is ineffective. The situation worsens for low radiosensitivity and fast-replicating tumors. This effect, although theoretically well understood, is again difficult to take into consideration in practice as we are ignorant about the radiobiological parameters.

Radiation protection for β -emitters

There had long been an understanding that using very high activities (> 10 GBq) of ¹³¹I in a therapeutic regimen tends to create concerns in terms of radiation protection for personnel, as well as the public. This is particularly true in all cases where a significant amount of the administered activity is retained in the patient's body, while it is of lesser importance in therapy of thyroid carcinoma, where $> 90\%$ of the activity is excreted within the very first hours.

The radiation protection issues with ¹³¹I are quite well understood, and can rather easily be quantified because of the γ radiation component of ¹³¹I which makes detection and measurement of the amount and distribution of activity a fairly simple task.

The latter is not the case with nuclides that have no γ emission at all or only minute γ components. The most prominent of such nuclides is ⁹⁰Y, which is used for quite a number of TRTs, the most prominent being the therapy with ⁹⁰Y labeled Zevalin®. Of all the β -decaying nuclides currently in use in nuclear oncology, ⁹⁰Y also has the highest maximum β energy (E_{β} endpoint = 2280 keV). This section thus focuses on radiation safety considerations with respect to ⁹⁰Y.

Radiation protection for workers

External exposure

⁹⁰Y is a pure β emitter with maximum β energy of 2.28 MeV. Its average path length in soft tissue is approximately 5 mm. Significant exposure to the skin of personnel is to be expected unless proper shielding is used. The highest absorbed doses occur for workers in the radiochemistry laboratory during radiolabeling and the physician, nurse, or technician when handling the syringe during administration. Table 30.2 lists skin absorbed doses from a number of source configurations.¹⁷³ Direct contact with 1000 MBq ⁹⁰Y in a syringe without shielding for only 1 minute, e.g. stabilizing it during administration, would result in a dose of approximately 725 mSv to the fingertips and could thus exceed the regulatory limit of 500 mSv per any square cm of skin.

Table 30.2 External exposure from ^{90}Y in different configurations

Configuration	Dose rate (mSv h^{-1})
Point source 1 MBq in air at 30 cm distance	1.08×10^{-1}
10-ml glass vial with 1 MBq at 100 cm distance	7.11×10^{-5}
Contact with 1 MBq in 5-ml plastic syringe	43.5
Contamination with 1-kBq droplet	1.35

During the whole process of radiopharmaceutical preparation and administration, ^{90}Y must be handled in shields or, where this is impossible, at least with tweezers to increase the distance between source and skin.

Lead or tungsten shields for syringes or vials are inappropriate in this case, because the high atomic number of these elements results in generating high amounts of bremsstrahlung, which would counteract the reduction in β radiation. Instead, shields made of low-Z (low atomic number) material such as glass, acrylic, or aluminum should be used, possibly combined with an outer layer of high-Z material.¹⁷⁴ Such shields were shown to reduce the dose rate by three orders of magnitude, e.g. from 3.66 Gy/h to 1–2 mGy/h during preparation of 1.55 GBq [^{90}Y]ibritumomab tiuxetan or from 12.87 Gy/h to 2–3 mGy/h while handling a 10-ml syringe with 1147 MBq of the same substance.¹⁷⁵

As is the case in all procedures that involve manual handling of β -only emitters, hands and clothing should be monitored frequently for external contamination.

Once the ^{90}Y has been administered to the patient, the only source of external exposure to workers is the bremsstrahlung generated within the patient. As man primarily consists of low-Z elements, the resulting dose rate is very small. Wiseman et al. measured deep dose equivalent rates $H_p(10)$ ('personal deep dose equivalent': dose equivalent at 10 mm depth below the point of the body where the personal dosimeter is worn) from bremsstrahlung at 1 m distance from the patient immediately after administration of 15 MBq/kg [^{90}Y]Zevalin[®] to an average 2.95 μSv per hour (range 2.4–3.9 $\mu\text{Sv/h}$).¹⁷⁶ Similar values had been predicted from computations.¹⁷⁷

Taking decay into account, no person can receive a dose of more than 1 mSv even if he or she remains at 1 m distance from a patient at all times.

Internal exposure

Internal exposure could result from inhalation of airborne radioactivity or (accidental) ingestion.

Contrary to iodine which, due to its vapor pressure, causes measurable concentrations in the air even when handled in liquid form, none of the other β emitters is known to yield any significant airborne activity concentrations. Yet, performing the radiochemical procedures under a fume hood with filtering at the exhaust would be considered 'good medical practice', and at the same time reduce the probability of accidental incorporation, e.g. from breakage of a container. The dose coefficients for intake of ^{90}Y are 2.7×10^{-9} Sv/Bq from ingestion and 1.6×10^{-9} Sv/Bq from inhalation.¹⁷³ The accidental ingestion of 1 MBq ^{90}Y would thus result in an effective dose of 2.7 mSv.

Radiation protection for helping persons and the public

External exposure

As mentioned above, external exposure from a patient is very low. In most countries, the administration of [^{90}Y]ibritumomab tiuxetan (Zevalin[®]) is therefore performed on an outpatient basis. In order to minimize the exposure of persons otherwise not involved, all patients are supplied with instructions for adequate behavior after therapy (see below).

Absorbed dose measurements for those family members having the closest contact to a patient yielded an average value $H_p(10)$ of 35 μSv (range 14–79 μSv), measured over 1 week beginning immediately after administration.¹⁷⁸ The exposure of relatives is thus within the range of background radiation.

Internal exposure

Internal exposure of persons in the vicinity of the patient could most likely result from spilled urine. In a worst case scenario, a helping person is assumed to incorporate 0.1% of all activity excreted by the patient. Total excretion via urine was measured to be $7.3 \pm 3.2\%$ of the administered activity for [^{90}Y]ibritumomab tiuxetan.¹⁷⁹ Assuming the maximum administered activity of 1200 MBq and an excretion of 10%, the helping person would ingest at most 0.12 MBq ^{90}Y , resulting in an effective dose of 0.2 mSv. Any realistic exposure is certainly one order of magnitude lower if the situation is understood by the persons involved and precautionary measures are taken.

Radioecological considerations

In order to clear the way for regulatory exemption of [^{90}Y]Zevalin[®] treatment from the requirement of inpatient

treatment in Germany, a radioecological model calculation was performed to ascertain that there could be no significant exposure to the public from excretions of the patients. Even under most conservative assumptions, the activity concentration in surface water would not exceed 0.5% of the regulatory limit.¹⁷⁹ Keeping the requirement of a minimum stay of 48 hours in a nuclear therapy ward would have reduced that concentration by no more than one-half.

Instructions to patients

From the abovementioned aspects it becomes clear that instructions to patients after a [⁹⁰Y]ibritumomab tiuxetan administration can be moderate compared to those for patients after radioiodine therapy.¹⁸⁰ It seems that the simple set of rules laid out in Table 30.3 is agreed upon internationally.¹⁸¹

Conclusion

β Emitters in nuclear oncology require certain radiation protection measures, but these are easy to implement. During preparation and administration of the radiopharmaceutical, the general rules for handling β emitters apply: no direct contact, use of plastic shields and/or tools to manipulate vials and syringes. Once in the patient, the radionuclide constitutes hardly any radiation risk: exposure to helping persons and the general public is generally within the range of background radiation exposure.

Table 30.3 Instructions for patients after [⁹⁰Y]ibritumomab tiuxetan therapy

<i>Time after treatment</i>	<i>Instructions</i>
3 days	Avoid contact with patient's body fluids (clean up spilled urine, dispose of body fluid-contaminated material by flushing it through toilet) Wash hands frequently and thoroughly, especially after using the toilet
1 week	Use condoms during sexual intercourse
1 year	Avoid pregnancy, breastfeeding should be discontinued completely

Conclusions and future aspects

Nuclear medicine dosimetry is still controversial because of its faint correlation with biological effects. This has been mostly emphasized in radionuclide therapy, where several efforts have been made to find this correlation, with limited success.

The MIRD scheme divides the dosimetric process into two parts: cumulated activity determination and dosimetric calculations. It is therefore common practice to consider these two components independently. However, this is not entirely the case.

Organ-based dosimetry relies on quantitative imaging; organ definition and functional or anatomical segmentation are based on patient images. Anatomical segmentation is most often based on CT with a resolution that is superior to that of functional (nuclear medicine) imaging. However, it is acknowledged that absorbed dose gradients are likely to be observed at small distances from the emission point: the majority of β emitters deliver their energy in the sub-millimeter to millimeter range. Any heterogeneous activity distribution at that level will not be visualized by conventional nuclear medicine imaging alone. Without additional means to assess radiopharmaceutical uptake at the millimeter level (or less), one is left with the assumption that activity is distributed homogeneously in the smallest quantifiable image volume element.

Any progress made in quantitative imaging impacts directly on the dosimetric calculation: voxel-based activity determination enables voxel-based absorbed dose calculations. It can be argued that the absorbed dose calculations themselves present less uncertainty than the activity determination, so that the limiting step in obtaining accurate dosimetry estimates is that of image quantification. It is hoped that fast and reliable Monte Carlo-based absorbed dose calculations will become available for nuclear medicine departments. With this methodology it is possible to account for heterogeneity of the activity distribution.

Whilst crude dosimetric estimates based on or extrapolated from anthropomorphic phantoms may be considered sufficiently accurate for radiation protection purposes, there is an increasingly strong requirement in the targeted therapy community for accurate tumor dosimetry. At present the single largest factor in need of improvement and further development is that of image quantification. It is hoped that as these issues are addressed, standardized procedures can be formulated that may be introduced into routine clinical practice.

In summary, for an accurate dosimetry estimate and to get closer to the goal of having a dosimetry that can predict the biological effect, a combination of macro–small-scale–microdosimetry needs to be explored and further developed.

References

1. Chatal JF, Hoefnagel CA. Radionuclide therapy. *Lancet* 1999; 354: 931–5.
2. Nuis A. Health protection of individuals against the dangers of ionising radiation in relation to medical exposure. Council directive 97/43/EURATOM. 30-6-1997.
3. Department of Health. The Ionising Radiation (Medical Exposure) Regulations 2000. SI 2000 No. 1059.
4. DeNardo SJ. Tumor-targeted radionuclide therapy: trial design driven by patient dosimetry. *J Nucl Med* 2000; 41: 104–6.
5. Hoefnagel CA, Clarke SE, Fischer M et al. Radionuclide therapy practice and facilities in Europe. EANM Radionuclide Therapy Committee. *Eur J Nucl Med* 1999; 26: 277–82.
6. Howell RW, Wessels BW, Loevinger R et al. The MIRD perspective 1999. Medical Internal Radiation Dose Committee. *J Nucl Med* 1999; 40: 3S–10S.
7. Microdosimetry. International Commission on Radiation Units and Measurements: Washington, DC: 1983.
8. Bardiés M, Pihet P. Dosimetry and microdosimetry of targeted radiotherapy. *Curr Pharm Des* 2000; 6: 1469–502.
9. Loevinger RB. MIRD primer for absorbed dose calculations. New York: Society of Nuclear Medicine, 1988.
10. Dale R, Carabe-Fernandez A. The radiobiology of conventional radiotherapy and its application to radionuclide therapy. *Cancer Biother Radiopharm* 2005; 20: 47–51.
11. Snyder WS, Ford MR, Warner GG, Watson SB. S, absorbed dose per unit cumulated activity for selected radionuclides and organs (Part 1). Reston, VA: Society of Nuclear Medicine 1975.
12. Marinelli L, Quimby E, Hine G. Dosage determination with radioactive isotopes. II Practical considerations in therapy and protection. *Am J Roentgenol Radium Ther* 1948; 59: 260–80.
13. International Commission on Radiological Protection. Radiation dose from radiopharmaceuticals. ICRP Publication 53. New York; Pergamon Press, 1988.
14. Langmuir VK, Fowler JF, Knox SJ et al. Radiobiology of radiolabeled antibody therapy as applied to tumor dosimetry. *Med Phys* 1993; 20: 601–10.
15. Dose Specifications in Nuclear Medicine. ICRU Report 67. Bethesda, MD: ICRU, 2002.
16. Wiseman GA, Leigh B, Erwin WD et al. Radiation dosimetry results for Zevalin radioimmunotherapy of rituximab-refractory non-Hodgkin lymphoma. *Cancer* 2002; 94: 1349–57.
17. Wiseman GA, White CA, Stabin M et al. Phase I/II Y-90-Zevalin (yttrium-90 ibritumomab tiuxetan, IDEC- Y2B8) radioimmunotherapy dosimetry results in relapsed or refractory non-Hodgkin's lymphoma. *Eur J Nucl Med* 2000; 27: 766–77.
18. Vose JM, Wahl RL, Saleh M et al. Multicenter phase II study of iodine-131 tositumomab for chemotherapy-relapsed/refractory low-grade and transformed lowgrade B-cell non-Hodgkin's lymphomas. *J Clin Oncol* 2000; 18: 1316–23.
19. Kostakoglu L, Goldsmith SJ, Buchegger F et al. Preliminary results of a multicenter dosimetry, efficacy and safety study with iodine-131 tositumomab in treatment of non-Hodgkin's lymphoma (NHL). *Eur J Nucl Med* 2001; 28: OS73.
20. Wiseman GA, White CA, Sparks RB et al. Biodistribution and dosimetry results from a phase III prospectively randomized controlled trial of Zevalin (TM) radioimmunotherapy for low-grade, follicular, or transformed B-cell non-Hodgkin's lymphoma. *Crit Rev Oncol Hematol* 2001; 39: 181–94.
21. Rajendran JG, Eary JF, Bensinger W et al. High-dose Ho-166-DOTMP in myeloablative treatment of multiple myeloma: pharmacokinetics, biodistribution, and absorbed dose estimation. *J Nucl Med* 2002; 43: 1383–90.
22. Virgolini I, Britton K, Buscombe J et al. In-111- and Y-90-DOTA-lanreotide: results and implications of the MAURITIUS trial. *Semin Nucl Med* 2002; 32: 148–55.
23. Flower MA, Fielding SL. Radiation dosimetry for I-131-MIBG therapy of neuroblastoma. *Phys Med Biol* 1996; 41: 1933–40.
24. Luster M, Sherman SI, Skarulis MC et al. Comparison of radioiodine biokinetics following the administration of recombinant human thyroid stimulating hormone and after thyroid hormone withdrawal in thyroid carcinoma. *Eur J Nucl Med Mol Imaging* 2003; 30: 1371–7.
25. Koral KF, Dewaraja Y, Li J et al. Update on hybrid conjugate-view SPECT tumor dosimetry and response in 131I-tositumomab therapy of previously untreated lymphoma patients. *J Nucl Med* 2003; 44: 457–64.
26. Kendler D, Donnemiller E, Oberladstatter M et al. An individual dosimetric approach to 153Sm-EDTMP therapy for pain palliation in bone metastases in correlation with clinical results. *Nucl Med Commun* 2004; 25: 367–73.
27. Meredith R, Shen S, Macey D et al. Comparison of biodistribution, dosimetry, and outcome from clinical trials of radionuclide-CC49 antibody therapy. *Cancer Biother Radiopharm* 2003; 18: 393–404.
28. Siegel JA, Thomas SR, Stubbs JB et al. MIRD pamphlet no. 16: Techniques for quantitative radiopharmaceutical biodistribution data acquisition and analysis for use in human radiation dose estimates. *J Nucl Med* 1999; 40: 37S–61S.
29. Radiation dose to patients from radiopharmaceuticals. ICRP Publication 80. *Ann ICRP* 1998; 28: 3; Oxford: Pergamon Press.
30. Radiation dose to patients from radiopharmaceuticals. ICRP Publication 53. *Ann ICRP* 1987; 18: 1–4; Oxford: Pergamon Press.
31. Autret D, Bitar A, Ferrer L, Lisbona A, Bardiés M. Monte Carlo modeling of gamma cameras for I-131 imaging in targeted radiotherapy. *Cancer Biother Radiopharm* 2005; 20: 77–84.
32. DeNardo SJ, Kramer EL, O'Donnell RT et al. Radioimmunotherapy for breast cancer using indium-111/yttrium-90 BrE-3: results of a phase I clinical trial. *J Nucl Med* 1997; 38: 1180–5.
33. Sjogreen K, Ljungberg M, Strand SE. An activity quantification method based on registration of CT and whole-body scintillation camera images, with application to I-131. *J Nucl Med* 2002; 43: 972–82.
34. Koral KF, Zasadny KR, Swailm FM et al. Importance of intra-therapy single-photon emission tomographic imaging in calculating tumor dosimetry for a lymphoma patient. *Eur J Nucl Med* 1991; 18: 432–5.
35. Erdi AK, Wessels BW, Dejager R et al. Tumor-activity confirmation and isodose curve display for patients receiving

- iodine-131-labeled 16.88-human monoclonal-antibody. *Cancer* 1994; 73: 932–44.
36. Koral KF, Zasadny KR, Kessler ML et al. CT-SPECT fusion plus conjugate views for determining dosimetry in iodine-131-monoclonal antibody therapy of lymphoma patients. *J Nucl Med* 1994; 35: 1714–20.
 37. Korppi-Tommola ET, Kairemo KJA, Jekunen AP, Niskanen EO, Savolainen SE. Double-tracer dosimetry of organs in assessment of bone marrow involvement by two monoclonal antibodies. *Acta Oncol* 1996; 35: 357–65.
 38. DeNardo SJ, DeNardo GL, Kukis DL et al. Cu-67-2IT-BAT-Lym-1 pharmacokinetics, radiation dosimetry, toxicity and tumor regression in patients with lymphoma. *J Nucl Med* 1999; 40: 302–10.
 39. Koral KF, Li J, Dewaraja Y et al. I-131 anti-B1 therapy/tracer uptake ratio using a new procedure for fusion of tracer images to computed tomography images. *Clin Cancer Research* 1999; 5: 3004S–9S.
 40. Lundqvist H, Lubberink M, Tolmachev V et al. Positron emission tomography and radioimmunotargeting – general aspects. *Acta Oncol* 1999; 38: 335–41.
 41. Koral KF, Dewaraja Y, Li J et al. Initial results for hybrid SPECT-conjugate-view tumor dosimetry in I-131-anti-B-1 antibody therapy of previously untreated patients with lymphoma. *J Nucl Med* 2000; 41: 1579–86.
 42. Koral KF, Dewaraja Y, Clarke LA et al. Tumor-absorbed-dose estimates versus response in tositumomab therapy of previously untreated patients with follicular non-Hodgkin's lymphoma: preliminary report. *Cancer Biothe Radiopharm* 2000; 15: 347–55.
 43. Koral KF, Francis IR, Kroll S et al. Volume reduction versus radiation dose for tumors in previously untreated lymphoma patients who received iodine-131 tositumomab therapy – conjugate views compared with a hybrid method. *Cancer* 2002; 94: 1258–63.
 44. Orlova A, Hoglund J, Lubberink M et al. Comparative biodistribution of the radiohalogenated (Br, I and At) antibody A33. Implications for in vivo dosimetry. *Cancer Biother Radiopharm* 2002; 17: 385–96.
 45. Jonsson L, Ljungberg M, Strand SE. Evaluation of accuracy in activity calculations for the conjugate view method from Monte Carlo simulated scintillation camera images using experimental data in an anthropomorphic phantom. *J Nucl Med* 2005; 46: 1679–86.
 46. Jönsson L, Ljungberg, M, Strand S-E. 2007; personal communication.
 47. Siegel JA, Wu RK, Maurer AH: The buildup factor – effect of scatter on absolute volume determination. *J Nucl Med* 1985; 26: 390–4.
 48. Guy MJ, Castellano-Smith IA, Flower MA et al. DETECT – dual energy transmission estimation CT – for improved attenuation correction in SPECT and PET. *IEEE Trans Nucl Sci* 1998; 45: 1261–7.
 49. Kolbert KS, Sgouros G, Scott AM et al. Implementation and evaluation of patient-specific three-dimensional internal dosimetry. *J Nucl Med* 1997; 38: 301–8.
 50. Laitinen JO, Kairemo KJA, Jekunen AP, Korppi-Tommola T, Tenhunen M. The effect of three dimensional activity distribution on the dose planning of radioimmunotherapy for patients with advanced intraperitoneal pseudomyxoma. *Cancer* 1997; 80: 2545–52.
 51. Sgouros G, Squeri S, Ballangrud AM et al. Patient-specific, 3-dimensional dosimetry in non-Hodgkin's lymphoma patients treated with I-131-anti-B1 antibody: assessment of tumor dose-response. *J Nucl Med* 2003; 44: 260–8.
 52. Papavasileiou P, Flux GD, Flower MA, Guy MJ. Automated CT marker segmentation for image registration in radionuclide therapy. *Phys Med Biol* 2001; 46: N269–79.
 53. Strand SE, Jonsson BA, Ljungberg M, Tennvall J. Radioimmunotherapy dosimetry – a review. *Acta Oncol* 1993; 32: 807–17.
 54. Holmes T, Mackie TR. A filtered backprojection dose calculation method for inverse treatment planning. *Med Phys* 1994; 21: 303–13.
 55. Larson SM, Divgi CR, Scott A et al. Current status of radioimmunotherapy. *Nucl Med Biol* 1994; 21: 785–92.
 56. Strand SE, Ljungberg M, Tennvall J, Norrgren K, Garkavij M. Radio-immunotherapy dosimetry with special emphasis on SPECT quantification and extracorporeal immunoadsorption. *Med Biol Eng Comput* 1994; 32: 551–61.
 57. Turner JH, Claringbold PG, Klemp PFB et al. Ho-166-microsphere liver radiotherapy – a preclinical SPECT dosimetry study in the pig. *Nucl Med Commun* 1994; 15: 545–53.
 58. Giap HB, Macey DJ, Bayouth JE, Boyer AL. Validation of a dose-point kernel convolution technique for internal dosimetry. *Phys Med Biol* 1995; 40: 365–81.
 59. Giap HB, Macey DJ, Podoloff DA. Development of a SPECT-based 3-dimensional treatment planning system for radioimmunotherapy. *J Nucl Med* 1995; 36: 1885–94.
 60. Siegel JA, Zeiger LS, Order SE, Wallner PE. Quantitative bremsstrahlung single-photon emission computed tomographic imaging – use for volume, activity, and absorbed dose calculations. *Int J Radiat Onco Biol Phys* 1995; 31: 953–8.
 61. Furhang EE, Chui CS, Sgouros G. A Monte Carlo approach to patient-specific dosimetry. *Med Physics* 1996; 23: 1523–9.
 62. Tristram M, Alaamer AS, Fleming JS, Lewington VJ, Zivanovic MA. Iodine-131-metaiodobenzylguanidine dosimetry in cancer therapy: risk versus benefit. *J Nucl Med* 1996; 37: 1058–63.
 63. Behr TM, Sharkey RM, Juweid ME et al. Variables influencing tumor dosimetry in radioimmunotherapy of CEA-expressing cancers with anti-CEA and antimucin monoclonal antibodies. *J Nucl Med* 1997; 38: 409–18.
 64. Behr TM, Sharkey RM, Juweid ME et al. Phase I/II clinical radioimmunotherapy with an iodine-131-labeled anti-carcinoembryonic antigen murine monoclonal antibody IgG. *J Nucl Med* 1997; 38: 858–70.
 65. Flux GD, Webb S, Ott RJ, Chittenden SJ, Thomas R. Three-dimensional dosimetry for intralesional radionuclide therapy using mathematical modeling and multimodality imaging. *J Nucl Med* 1997; 38: 1059–66.
 66. Furhang EE, Chui CS, Kolbert KS, Larson SM, Sgouros G. Implementation of a Monte Carlo dosimetry method for patient-specific internal emitter therapy. *Med Phys* 1997; 24: 1163–2.
 67. Koral KF, Lin SH, Fessler JA, Kaminski MS, Wahl RL. Preliminary results from intensity-based CT-SPECT fusion

- in I-131 anti-B1 monoclonal-antibody therapy of lymphoma. *Cancer* 1997; 80: 2538–44.
68. Leichner PK, Akabani G, Colcher D et al. Patient-specific dosimetry of indium-111-and yttrium-90-labeled monoclonal antibody CC49. *J Nucl Med* 1997; 38: 512–16.
 69. Tempero M, Leichner P, Baranowska-Kortylewicz J et al. High-dose therapy with (90)yttrium-labeled monoclonal antibody CC49: a phase I trial. *Clin Cancer Res* 2000; 6: 3095–102.
 70. Colnot DR, Quak JJ, Roos JC et al. Phase I therapy study of Re-186-labeled chimeric monoclonal antibody U36 in patients with squamous cell carcinoma of the head and neck. *J Nucl Med* 2000; 41: 1999–2010.
 71. Van Laere K, Koole M, Kauppinen T et al. Nonuniform transmission in brain SPECT using Tl-201, Gd-153, and Tc-99m static line sources: anthropomorphic dosimetry studies and influence on brain quantification. *J Nucl Med* 2000; 41: 2051–62.
 72. Gonzalez DE, Jaszczak RJ, Bowsher JE, Akabani G, Greer KL. High-resolution absolute SPECT quantitation for I-131 distributions used in the treatment of lymphoma: a phantom study. *IEEE Trans Nucl Sci* 2001; 48: 707–14.
 73. Thierens HM, Monsieurs MA, Brans B et al. Dosimetry from organ to cellular dimensions. *Comput Med Imaging Graph* 2001; 25: 187–93.
 74. Ljungberg M, Sjogreen K, Liu XW et al. A 3-dimensional absorbed dose calculation method based on quantitative SPECT for radionuclide therapy: evaluation for I-131 using Monte Carlo simulation. *J Nucl Med* 2002; 43: 1101–9.
 75. Dewaraja YK, Wilderman SJ, Ljungberg M et al. Accurate dosimetry in 131I radionuclide therapy using patient-specific, 3-dimensional methods for SPECT reconstruction and absorbed dose calculation. *J Nucl Med* 2005; 46: 840–9.
 76. Boucek JA, Turner JH. Validation of prospective whole-body bone marrow dosimetry by SPECT/CT multimodality imaging in (131)I-anti-CD20 rituximab radioimmunotherapy of non-Hodgkin's lymphoma. *Eur J Nucl Med Mol Imaging* 2005; 32: 458–69.
 77. De Jong M, Valkema R, Van Gameren A et al. Inhomogeneous localization of radioactivity in the human kidney after injection of [(111)In-DTPA]octreotide. *J Nucl Med* 2004; 45: 1168–71.
 78. King M, Farncombe T. An overview of attenuation and scatter correction of planar and SPECT data for dosimetry studies. *Cancer Biother Radiopharm* 2003; 18: 181–90.
 79. Ljungberg M, Frey E, Sjogreen K et al. 3D absorbed dose calculations based on SPECT: evaluation for 111-In/90-Y therapy using Monte Carlo simulations. *Cancer Biother Radiopharm* 2003; 18: 99–107.
 80. Guy MJ, Flux GD, Papavasileiou P, Flower MA, Ott RJ. RMDP: a dedicated package for 131I SPECT quantification, registration and patient-specific dosimetry. *Cancer Biother Radiopharm* 2003; 18: 61–9.
 81. Sjogreen K, Ljungberg M, Strand SE. Parameters influencing volume and activity quantitation in SPECT. *Acta Oncol* 1996; 35: 323–30.
 82. Beekman FJ, Kamphuis C, Frey EC. Scatter compensation methods in 3D iterative SPECT reconstruction: a simulation study. *Phys Med Biol* 1997; 42: 1619–32.
 83. Bruyant PP. Analytic and iterative reconstruction algorithms in SPECT. *J Nucl Med* 2002; 43: 1343–58.
 84. Wernick M, Aarsvold J. *Emission Tomography: The Fundamentals of PET and SPECT*. New York: Academic Press, 2004.
 85. Bailey DL. Transmission scanning in emission tomography. *Eur J Nucl Med* 1998; 25: 774–87.
 86. Ljungberg M, Strand SE. Attenuation and scatter correction in SPECT for sources in a nonhomogeneous object: a Monte Carlo study. *J Nucl Med* 1991; 32: 1278–84.
 87. Damen EM, Muller SH, Boersma LJ, de Boer RW, Lebesque JV. Quantifying local lung perfusion and ventilation using correlated SPECT and CT data. *J Nucl Med* 1994; 35: 784–92.
 88. King MA, Tsui BM, Pan TS, Glick SJ, Soares EJ. Attenuation compensation for cardiac single-photon emission computed tomographic imaging: Part 2. Attenuation compensation algorithms. *J Nucl Cardiol* 1996; 3: 55–64.
 89. Licho R, Glick SJ, Xia W et al. Attenuation compensation in 99mTc SPECT brain imaging: a comparison of the use of attenuation maps derived from transmission versus emission data in normal scans. *J Nucl Med* 1999; 40: 456–63.
 90. Zaidi H, Hasegawa B. Determination of the attenuation map in emission tomography. *J Nucl Med* 2003; 44: 291–315.
 91. Zaidi H, Montandon ML, Slosman DO. Magnetic resonance imaging-guided attenuation and scatter corrections in three-dimensional brain positron emission tomography. *Med Phys* 2003; 30: 937–48.
 92. Akbari RB, Ott RJ, Trott NG, Sharma HL, Smith AG. Radionuclide purity and radiation dosimetry of 124I used in positron tomography of the thyroid. *Phys Med Biol* 1986; 31: 789–91.
 93. Ott RJ, Batty V, Webb BS et al. Measurement of radiation dose to the thyroid using positron emission tomography. *Br J Radiol* 1987; 60: 245–51.
 94. Flower MA, Irvine AT, Ott RJ et al. Thyroid imaging using positron emission tomography—a comparison with ultrasound imaging and conventional scintigraphy in thyrotoxicosis. *Br J Radiol* 1990; 63: 325–30.
 95. Westera G, Reist HW, Buchegger F et al. Radioimmuno positron emission tomography with monoclonal antibodies: a new approach to quantifying in vivo tumour concentration and biodistribution for radioimmunotherapy. *Nucl Med Commun* 1991; 12: 429–37.
 96. Pentlow KS, Graham MC, Lambrecht RM, Cheung NK, Larson SM. Quantitative imaging of I-124 using positron emission tomography with applications to radioimmunodiagnosis and radioimmunotherapy. *Med Phys* 1991; 18: 357–66.
 97. Larson SM, Pentlow KS, Volkow ND et al. PET scanning of iodine-124-3F9 as an approach to tumor dosimetry during treatment planning for radioimmunotherapy in a child with neuroblastoma. *J Nucl Med* 1992; 33: 2020–3.
 98. Ott RJ, Tait D, Flower MA, Babich JW, Lambrecht RM. Treatment planning for 131I-MIBG radiotherapy of neural crest tumours using 124I-MIBG positron emission tomography. *Br J Radiol* 1992; 65: 787–91.
 99. Pentlow KS, Graham MC, Lambrecht RM et al. Quantitative imaging of iodine-124 with PET. *J Nucl Med* 1996; 37: 1557–62.

100. Lubberink M, Lundqvist H, Westlin JE et al. Positron emission tomography and radioimmunotargeting—aspects of quantification and dosimetry. *Acta Oncol* 1999; 38: 343–9.
101. Crawford DC, Flower MA, Pratt BE et al. Thyroid volume measurement in thyrotoxic patients: comparison between ultrasonography and iodine-124 positron emission tomography. *Eur J Nucl Med* 1997; 24: 1470–8.
102. Eschmann SM, Reischl G, Bilger K et al. Evaluation of dosimetry of radioiodine therapy in benign and malignant thyroid disorders by means of iodine-124 and PET. *Eur J Nucl Med Mol Imaging* 2002; 29: 760–7.
103. Sgouros G, Kolbert KS, Sheikh A et al. Patient-specific dosimetry for ¹³¹I thyroid cancer therapy using ¹²⁴I PET and 3-dimensional-internal dosimetry (3D-ID) software. *J Nucl Med* 2004; 45: 1366–72.
104. Rosch F, Herzog H, Stolz B et al. Uptake kinetics of the somatostatin receptor ligand [Y-86]DOTA-DPhe(1)-Tyr(3)-octreotide ([Y-86]SMT487) using positron emission tomography in non-human primates and calculation of radiation doses of the Y-90-labelled analogue. *Eur J Nucl Med* 1999; 26: 358–66.
105. Forster GJ, Engelbach MJ, Brockmann JJ et al. Preliminary data on biodistribution and dosimetry for therapy planning of somatostatin receptor positive tumours: comparison of (86)Y-DOTATOC and (111)In-DTPA-octreotide. *Eur J Nucl Med* 2001; 28: 1743–50.
106. Jamar F, Barone R, Mathieu I et al. ⁸⁶Y-DOTA(0)-D-Phe1-Tyr3-octreotide (SMT487)—a phase 1 clinical study: pharmacokinetics, biodistribution and renal protective effect of different regimens of amino acid co-infusion. *Eur J Nucl Med Mol Imaging* 2003; 30: 510–18.
107. Palm S, Enmon RM Jr, Matei C et al. Pharmacokinetics and biodistribution of (86)Y-Trastuzumab for (90)Y dosimetry in an ovarian carcinoma model: correlative microPET and MRI. *J Nucl Med* 2003; 44: 1148–55.
108. Buchholz HG, Herzog H, Forster GJ et al. PET imaging with yttrium-86: comparison of phantom measurements acquired with different PET scanners before and after applying background subtraction. *Eur J Nucl Med Mol Imaging* 2003; 30: 716–20.
109. Helisch A, Forster GJ, Reber H et al. Pre-therapeutic dosimetry and biodistribution of ⁸⁶Y-DOTA-Phe1-Tyr3-octreotide versus ¹¹¹In-pentetreotide in patients with advanced neuroendocrine tumours. *Eur J Nucl Med Mol Imaging* 2004; 31: 1386–92.
110. Barone R, Borson-Chazot F, Valkema R et al. Patient-specific dosimetry in predicting renal toxicity with (90)Y-DOTATOC: relevance of kidney volume and dose rate in finding a dose-effect relationship. *J Nucl Med* 2005; 46: 99S–106S.
111. Pauwels S, Barone R, Walrand S et al. Practical dosimetry of peptide receptor radionuclide therapy with (90)Y-labeled somatostatin analogs. *J Nucl Med* 2005; 46: 92S–8S.
112. Lubberink M, Lundqvist H, Tolmachev V. Production, PET performance and dosimetric considerations of Ce-134/La-134, an Auger electron and positron-emitting generator for radionuclide therapy. *Phys Med Biol* 2002; 47: 615–29.
113. Ugur O, Kothari PJ, Finn RD et al. Ga-66 labeled somatostatin analogue DOTA-DPhe1-Tyr3-octreotide as a potential agent for positron emission tomography imaging and receptor mediated internal radiotherapy of somatostatin receptor positive tumors. *Nucl Med Biol* 2002; 29: 147–57.
114. Berger MJ. Monte Carlo calculation of the penetration and diffusion of fast charged particles. In: Alder B, Fernbach S, Rotenberg M, eds. *Methods in Computational Physics Vol. 1* Academic Press: New York: 1963.
115. Berger MJ. *Improved point kernels for electrons and beta-ray dosimetry*. Gaithersburg, MD: National Bureau of Standards, 1973.
116. Berger MJ. MIRD Pamphlet No. 7: Distribution of absorbed doses around point sources of electrons and beta particles in water and other media *J Nucl Med* 1971; 12: 5–23.
117. Snyder WS, Ford MR, Warner GG, Fisher HL. MIRD Pamphlet No. 5: Estimates of absorbed fractions for monoenergetic photon sources uniformly distributed in various organs of a heterogeneous phantom. *J Nucl Med* 1969; 10: (Suppl 3): 5–52.
118. Snyder WS, Ford MR, Warner GG, Watson SB. MIRD Pamphlet No. 11: ‘S’, absorbed dose per unit cumulated activity for selected radionuclides and organs. New York: The Society of Nuclear Medicine, 1975.
119. Cristy M, Eckerman KF. Specific absorbed fractions of energy at various ages from internal photon sources. I Methods, II One year old, III Five year old, IV Ten year old, V Fifteen year old male and adult female, VI New-born and VII Adult male. Oak Ridge, TN: Oak Ridge National Laboratory, 1987.
120. Saito K, Wittmann A, Koga S et al. Construction of a computed tomographic phantom for a Japanese male adult and dose calculation system. *Radiat Environ Biophys* 2001; 40: 69–75.
121. Clairand I, Bouchet LG, Ricard M et al. Improvement of internal dose calculations using mathematical models of different adult heights. *Phys Med Biol* 2000; 45: 2771–85.
122. Xu XG, Chao TC, Bozkurt A. VIP-man: an image-based whole-body adult male model constructed from color photographs of the visible human project for multi-particle Monte Carlo calculations. *Health Phys* 2000; 78(5): 476–86.
123. Xu XG. Specific absorbed fractions from image-based VIP-man body model and EGS4-VLSI Monte Carlo code: internal electron emitters. *Phys Med Biol* 2001; 46: 901–27.
124. Caon M. Voxel-based computational models of real human anatomy: a review. *Radiat Environ Biophys* 2004; 42: 229–35.
125. Peter J, Tornai MP, Jaszczak RJ. Analytical versus voxelized phantom representation for Monte Carlo simulation in radiological imaging. *IEEE Trans Med Imaging* 2000; 5: 556–64.
126. Xu G. Stylized versus tomographic: an experience on anatomical modelling at RPI. Presented at Monte Carlo 2005 Topical Meeting, Chattanooga, Tennessee, April 17–21, American Nuclear Society, LaGrange Park, IL, 2005.
127. Yoriyaz H, Stabin MG, dos Santos A. Monte Carlo MCNP-4B-based absorbed dose distribution estimates for patient-specific dosimetry. *J Nucl Med* 2001; 42(4): 662–9.
128. Descalle MA, Hartmann Siantar CL, Dauffy L, et al. Application of MINERVA Monte Carlo simulations to targeted radionuclide therapy. *Cancer Biother Radiopharm* 2003; 18: 71–9.
129. Chiavassa S, Aubineau-Lanièce I, Bitar A et al. Validation of a personalised dosimetric evaluation tool (Oedipe) for

- targeted radiotherapy based on the Monte Carlo MCNPX code. *Phys Med Biol* 2006; 51: 601–616.
130. Zaidi H. Relevance of accurate Monte Carlo Modeling in nuclear medical imaging. *Med Phys* 1999; 26: 574–608.
 131. Buvat I, Castiglioni I. Monte Carlo simulations in SPET and PET. *Nucl Med* 2002; 46: 48–61.
 132. Ljungberg M, Strand SE, King MA. Monte Carlo Calculation in Nuclear Medicine: Applications in Diagnostic Imaging. Bristol: IOP Publishing, 1998.
 133. Haidi H, Sgouros G. Therapeutic Applications of Monte-Carlo Calculations in Nuclear Medicine. Bristol: IOP Publishing, 2003.
 134. Nelson WR, Hirayama H, Rogers DWO. The EGS4 code system. Stanford Linear Accelerator Center report SLAC-265, 1985.
 135. Briesmeister JF, ed MCNP – A General Monte Carlo N-Particle Transport Code. Los Alamos National Laboratory report LA-12625-M, November, 1993.
 136. Agostinelli S, Allison J, Amakoe K, et al. Geant4 – a simulation toolkit. *Nucl Instrum Meth Phys Res* 2003; A 506: 250–303.
 137. Jan S, Santin G, Strul D et al. GATE: a simulation toolkit for PET and SPECT. *Phys Med Biol* 2004; 49: 4543–61.
 138. Dewaraja Y K, Ljungberg M, Bose A, Majumdar A, Koral K. A parallel Monte Carlo code for planar and SPECT imaging: implementation, verification and applications in I-131 SPECT. *Comput Meth Prog Biomed* 2002; 67: 115–24.
 139. Erwin WD, Groch MW, Macey DJ et al. A radioimmunoimaging and MIRD dosimetry treatment planning program for radioimmunotherapy. *Nucl Med Biol* 1996; 23: 525–32.
 140. Glatting G, Landmann M, Kull T et al. Internal radionuclide therapy: the ULMDOS software for treatment planning. *Med Phys* 2005; 32: 2399–405.
 141. Stabin MG. MIRDOSE: personal computer software for internal dose assessment in nuclear medicine. *J Nucl Med* 1996; 37: 538–46.
 142. Stabin MG, Sparks RB, Crowe E. OLINDA/EXM: the second-generation personal computer software for internal dose assessment in nuclear medicine. *J Nucl Med* 2005; 46: 1023–7.
 143. Johnson TK, McClure D, McCourt S. MABDOSE. I: Characterization of a general purpose dose estimation code. *Med Phys* 1999; 26: 1389–95.
 144. Johnson TK, McClure D, McCourt S. MABDOSE. II: Validation of a general purpose dose estimation code. *Med Phys* 1999; 26: 1396–403.
 145. Sgouros G, Barest G, Thekkumthala J et al. Treatment planning for internal radionuclide therapy – 3-dimensional dosimetry for non-uniformly distributed radionuclides. *J Nucl Med* 1990; 31: 1884–91.
 146. Bolch WE, Bouchet LG, Robertson JS et al. MIRD pamphlet No. 17: The dosimetry of nonuniform activity distributions – radionuclide S values at the voxel level. *J Nucl Med* 1999; 40: 11S–36S.
 147. Chiavassa S, Bardies M, Guiraud-Vitoux F et al. OEDIPE: a personalized dosimetric tool associating voxel-based models with MCNPX. *Cancer Biother Radiopharm* 2005; 20: 325–32.
 148. Lehmann J, Hartmann Siantar C, Wessel DE et al. Monte Carlo treatment planning for molecular targeted radiotherapy within the MINERVA system. *Phys Med Biol* 2005; 50: 947–58.
 149. Dewaraja YK, Wilderman SJ, Ljungberg M et al. Accurate dosimetry in ¹³¹I radionuclide therapy using patient-specific, 3-dimensional methods for SPECT reconstruction and absorbed dose calculation. *J Nucl Med* 2005; 46: 840–9.
 150. Lehman J, Hartmann Siantar C, Wessel DE et al. Monte Carlo treatment planning for molecular targeted radiotherapy within the MINERVA system. *Phys Med Biol* 2005; 50: 947–58.
 151. Petoussi-Hens N, Zankl M, Nosske D. Estimation of patient dose from radio-pharmaceuticals using voxel models. *Cancer Biother Radiopharm* 2005; 20: 103–9.
 152. Wolf I, Zankl M, Scheidhauer K et al. Determination of individual S-values for ¹³¹I using segmented CT data and the EGS4 Monte Carlo code. *Cancer Biother Radiopharm* 2005; 20: 98–102.
 153. Sjogreen K, Ljungberg M, Wingardh K, Minarik D, Strand SE. The LundADose method for planar image activity quantification and absorbed-dose assessment in radionuclide therapy. *Cancer Biother Radiopharm* 2005; 20: 92–7.
 154. Larsson E, Jonsson BA, Jonsson L, Ljungberg M, Strand SE. Dosimetry calculations on a tissue level by using the MCNP4c2 Monte Carlo code. *Cancer Biother Radiopharm* 2005; 20: 85–91.
 155. Sgouros G. Dosimetry of internal emitters. *J Nucl Med* 2005; 46 (Suppl 1):18S–27S.
 156. Hasegawa B, Tang HR, Da Silva AJ et al. Dual-modality imaging. *Nucl Instrum Meth Phys Res A* 2001; 471: 140–4.
 157. Jonsson L, Liu X, Jonsson BA, Ljungberg M, Strand SE. A dosimetry model for the small intestine incorporating intestinal wall activity and cross-doses. *Nucl Med* 2002; 43: 1657–64.
 158. Hindorf C, Linden O, Stenberg L, Tennvall J, Strand SE. Change in tumor-absorbed dose due to decrease in mass during fractionated radioimmunotherapy in lymphoma patients. *Clin Cancer Res* 2003; 9: 4003S–6S.
 159. Gardin I, Linhard NC, Petiet A, Bok BD. Dosimetry at the cellular level of Kupffer cells after technetium-99m-sulphur colloid injections. *J Nucl Med* 1992; 33: 380–4.
 160. Makrigrigios GM, Adelstein, SJ, Kassis AI. Cellular radiation dosimetry and its implications for estimating of radiation risks. *JAMA* 1990; 264: 592–5.
 161. Linden O, Hindorf C, Tennvall J et al. Single tumor cell uptake and dosimetry of technetium-99m Fab' or minute anti-CD22 in low-grade B-cell lymphoma *Cancer* 2002; 94: 1270–4.
 162. Humm JL. A microdosimetric model of Astatine-211 labeled antibodies for radioimmunotherapy. *Int J Radiat Oncol Biol Phys* 1987; 13: 1767–73.
 163. Humm JL, Roeske JC, Fisher DR, Chen GTY. Microdosimetric concepts in radioimmunotherapy. *Med Phys* 1993; 20: 535–41.
 164. Elgqvist J Andersson H, Bäck T et al. Therapeutic efficacy and tumor dose estimations in radioimmunotherapy of intraperitoneally growing OVCAR-3 cells in nude mice with ²¹¹At-labeled monoclonal antibody MX35. *J Nucl Med* 2005; 46: 1907–15.
 165. Dale RG Dose-rate effects in targeted radiotherapy. *Phys Med Biol* 1996; 41: 1871–84.
 166. Kwekkeboom DJ, Mueller-Brand J, Paganelli G et al. An overview of the peptide receptor radionuclide therapy with

- 3 different radiolabeled somatostatin analogues. *J Nucl Med* 2005; 46: 62S–6S.
167. Breitz H, Wendt R, Stabin M, Bouchet L, Wessels B. Dosimetry of high dose skeletal targeted radiotherapy (STR) with ^{166}Ho -DOTMP. *Cancer Biother Radiopharm* 2003; 18: 225–30.
168. Breitz H. Clinical aspects of radiation nephropathy. *Cancer Biother Radiopharm* 2004; 19: 359–62.
169. Emami B, Lyman J, Brown A et al. Tolerance of normal tissue to therapeutic irradiation. *Int J Radiat Oncol Biol Phys* 1991; 21: 109–22.
170. Barendsen GW. Dose fractionation, dose rate and iso-effect relationships for normal tissue responses. *Int J Radiat Oncol Biol Phys* 1982; 8: 1981–97.
171. Dale R. Use of the linear-quadratic radiobiological model for quantifying kidney response in targeted radiotherapy. *Cancer Biother Radiopharm* 2004; 19: 363–70.
172. Konijnenberg MW. Is the renal dosimetry for ^{90}Y -DOTA0, Tyr3]octreotide accurate enough to predict thresholds for individual patients? *Cancer Biother Radiopharm* 2003; 18: 619–25.
173. Delacroix D, Guerre JP, Leblanc P, Hickman C. Radionuclide and radiation protection data handbook 2nd edition (2002). *Radiat Prot Dosimetry* 2002; 98: 9–168.
174. Rödel R, Ebert A, Reichmann K et al. [Effectiveness of syringe shieldings using radionuclides in radiation synovectomy]. *Nuklearmedizin* 2003; 42: 50–3.
175. Zimmer A, Carey A, Spies S. Effectiveness of specific vial shields in reducing radiation exposure from ^{90}Y Zevalin. *J Nucl Med* 2002; 43: 45P.
176. Wiseman G, Leigh B, Witzig T, Gansen D, White C. Radiation exposure is very low to the family members of patients treated with yttrium-90 Zevalin anti-CD20 monoclonal antibody therapy for lymphoma. *Eur J Nucl Med* 2001; 28: 1198.
177. Zanzonico PB, Binkert BL, Goldsmith SJ. Bremsstrahlung radiation exposure from pure beta-ray emitters. *J Nucl Med* 1999; 40: 1024–8.
178. Wiseman G, Leigh B, Erwin W. Urinary clearance of ^{90}Y activity following Zevalin radioimmunotherapy of B-cell non-Hodgkin's lymphoma. *J Nucl Med* 2001; 42: 268P.
179. Schomacker K, Dietlein M, Schnell R et al. [Radioimmunotherapy with yttrium-90 ibritumomab tiuxetan. Clinical considerations, radiopharmacy, radiation protection, perspectives]. *Nuklearmedizin* 2005; 44: 166–77.
180. Radiation protection following iodine-131 therapy (exposures due to out-patients or discharged in-patients). Brussels: European Commission, 1998.
181. Zhu X. Radiation safety considerations with yttrium 90 ibritumomab tiuxetan (Zevalin). *Semin Nucl Med* 2004; 34: 20–3.

Advances in nuclear medicine imaging in oncology

Carlo Chiesa, Roberta Matheoud, Marco Brambilla, and Gian Luca Poli

Background

The main task of imaging in oncology is the detection of the smallest lesion in the whole body of a patient. Hence lesion detectability is our goal. In the simplest imaging theory, where the influence of the observer is neglected, a lesion is detectable if the signal to noise ratio (some authors refer to this ratio more rigorously as the contrast to noise ratio, see reference¹) exceeds the value of 4–5. Thus we have two parameters.

The *signal* has to be interpreted as the contrast of the lesion with respect to the surrounding background:

$$\frac{N_t - N_b}{N_b}$$

where N_t and N_b are the average count per pixel in the tumor and in the background respectively. Contrast depends upon the intrinsic contrast (uptake) of the lesion, upon the imaging methodology (tomographic techniques were developed to offer better contrast with respect to the planar view), upon the background level (where scatter plays a major role in whatever nuclear medicine imaging, while random coincidences are an additional contribution only in positron emission tomography (PET)), and upon the spatial resolution, which is strongly dependent on the reconstruction method and parameters.

The *noise* is the image pixel fluctuation (relative standard deviation σ) which masks the signal. Nature forces the noise to obey Poisson's law, according to which $\sigma/\sqrt{N_b} = 1/\sqrt{N_b}$. This means that, in order to improve the signal/noise by a factor of two for fixed contrast and acquisition conditions, the acquisition must be prolonged four times. Since acquisition time reduction, or patient throughput increase, is a general goal, only two chances are left: injecting higher activities or improving the system sensitivity. These two options, in PET, are not independent, because the noise

equivalent count rate (NECR) implies that an excessive injected activity deteriorates the count rate capabilities (besides giving higher radiation dose to the patient).

NECR improvement has been the leading force in recent PET scanner development. However, this focuses only on the second parameter (noise). Moreover, the NECR is related only to raw data collection, while in tomography the noise is also strongly dependent on data handling methods and reconstruction parameters.

Recent years have seen technological improvements in imaging equipment, moderate and continuous in γ cameras, and explosive in PET scanners. The number of newly developed PET models is difficult to account for. The new era of three-dimensional (3D) PET posed difficult challenges to the manufacturers. Industrial research aimed to fully exploit the 3D power, trying to solve two major problems: limited count rate capability with bismuth germanate (BGO) crystals, and scatter fraction. March 2006 was the dawn of a new era of PET scanners based on the time-of-flight (TOF) PET technique. The old dream is the reality of today. TOF further reduces the noise.

New scanner models have been, up to now, compared according to individual physical parameters which cannot be easily related to lesion detectability. The issue of 'the best scanner' or 'the best lesion detectability' is still open.

Single detection

Planar γ cameras

The γ camera is a device that produces digital images representing the radioactivity distribution within the body of a patient. It basically consists of a detector mounted on a gantry for easy positioning close to the patient, and an electronic processing console. Modern γ cameras are connected to a computer for image processing and display.^{2,3}

The *detector* is a scintillation crystal, usually thallium-activated sodium iodide NaI(Tl), which converts the absorbed energy of the γ -ray into light flashes. The light is converted into electronic signals by photomultiplier tubes (PMTs) optically coupled to the crystal. The large area detector is viewed by an array of usually up to 59 PMTs, or 95 PMTs in the most refined models (GE Infinia™ VC with 1-in thick crystal, 94 PMTs in the Sopha™ DST-XL). Signals from PMTs are amplified and finally processed by the position-energy circuit that furnishes the (x,y) position of interaction of the γ -ray and its energy. The interaction location of the γ -ray on the crystal is determined by using the relative levels of the PMT signals (Anger logic) and can be determined with an error of approximately 3–4 mm. This important characteristic is called *intrinsic spatial resolution* (typical values are reported in Table 31.1). In modern γ cameras, the NaI(Tl) crystal is usually of rectangular shape, with dimensions of about $40 \times 60 \text{ cm}^2$ in the case of whole body studies and $25 \times 40 \text{ cm}^2$ for cerebral studies.

Another main characteristic of the detector is its *intrinsic efficiency*, which means its capability of detecting γ -rays. It depends on the γ -ray energy (E_γ) and strongly decreases when medium and high energy isotopes are used, due to the $1/E_\gamma^3$ dependence of the photoelectric effect probability. Efficiency can be improved by increasing the standard 3/8-in detector thickness. For this reason, larger detector thicknesses of 4/8 in, 5/8 in, or 6/8 in were also adopted for commercially available γ cameras. Unfortunately this brings a loss of intrinsic spatial resolution, since in a thicker crystal the spark of light photons will spread over a larger extent before reaching the PMTs. The crystal thickness is usually 3/8 in when the 140-keV γ emission of $^{99\text{m}}\text{Tc}$ has to be

detected; this value in fact represents a good compromise between efficiency (about 90% at 140 keV) and good spatial resolution.

A recent technological improvement is represented by the 1-in thick Starbright™ grooved crystal, which offers a sensitive increase of intrinsic efficiency for medium and high energies containing the loss of spatial resolution (see Table 31.1). This kind of detector, which is mounted on the GE Infinia VC and Siemens e.cam™, is pixelated on the rear (Figure 31.1). This limits the spread of the light photons. Intrinsic efficiency for 364-keV γ -rays of ^{131}I photons with a 1-in Starbright™ detector is about twice with respect to a 3/8-in thick crystal. The only disadvantage of the 1-in thick crystal is its high cost.

Examples of spatial resolution measurements obtained at Istituto Nazionale Tumori with this type of crystal are shown in Table 31.2. Physicians at this center are not able to distinguish the technetium bone studies acquired with a 3/8-in crystal from those obtained with a 1-in thick Starbright™ detector (Figure 31.2).

In the case of cerebral imaging, where the isotopes employed are usually $^{99\text{m}}\text{Tc}$ ($E_\gamma = 140.5 \text{ keV}$) and ^{123}I ($E_\gamma = 159 \text{ keV}$), the optimal choice is the typical thickness of 3/8 in and dedicated small field γ cameras.

Intrinsic efficiency and spatial resolution combine their influence on system performance through the type and structure of the collimator. This has essentially the function of identifying the direction of flight of the γ -rays. In fact two points are needed to define a straight line in space, while single emitters provide only the point of interaction on the crystal, and this is not enough to produce an image. Therefore, the collimator has the aim of projecting the radionuclide distribution within the organ being imaged on the crystal surface. Due to the absorption in the collimator, only a small fraction (of the order of 10^{-4}) of the emitted photons actually reaches the detector surface. This huge loss

Table 31.1 Examples of intrinsic spatial resolution (full width half maximum (FWHM) in central field of view (CFOV)) with $^{99\text{m}}\text{Tc}$

Producer	Model	Crystal thickness (in)	FWHM (producer specification) (mm)
Siemens	e.cam	3/8	≤ 3.8
Siemens	e.cam	5/8	≤ 4.5
Siemens	e.cam	1	≤ 5.5
GE	Infinia	3/8	≤ 3.8
GE	Infinia VC	1	≤ 4.5
Philips	EPIC-AZ detectors	3/8	3.3
Philips	EPIC-AZ detectors	5/8	3.9
Mediso	Spirit DH-V	3/8	3.6

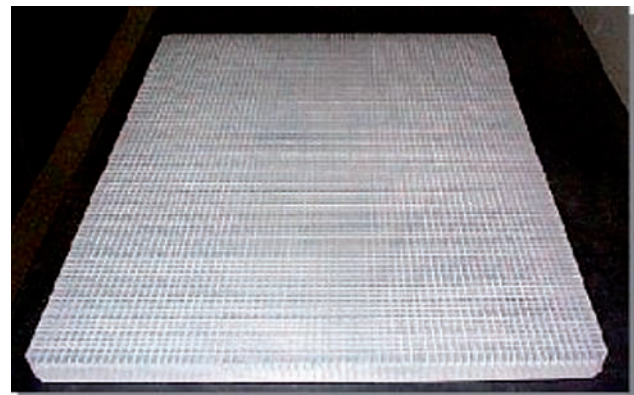


Figure 31.1

The rear of a 1-in thick Starbright™ NaI detector. (Courtesy of General Electric Medical Systems.)

Table 31.2 Dependence on crystal thickness of the system spatial resolution without scatter at 10 cm with LEHR collimator (CFOV)

Producer	Model	Crystal thickness (in)	FWHM (producer specification) (mm)	Authors' (mm)
Siemens	e.cam	3/8	7.4	7.1
Siemens	e.cam	5/8	7.8	7.8
Siemens	e.cam	1	8.5	NA
GE	Infinia	3/8	7.4	NA
GE	Infinia VC	1	8.1	8.0
Philips	Forte with EPIC-AZ detectors	3/8	7.4	NA
Philips	Forte with EPIC-AZ detectors	5/8	7.7	NA

of photons is the main drawback of single detection compared to coincidence detection, where no collimator is necessary. The most widely used type of collimator is the *parallel hole collimator*. It consists of small holes perpendicular to the crystal separated by thin lead septa. A γ -ray perpendicular to the detector can pass through the holes, while an oblique γ -ray is stopped by the lead septa. The quality of the final image will strongly depend on the collimator specifications.

The collimator lead septa are usually of hexagonal shape with a 'bees' nest' configuration. Recently, efforts were made to reduce the annoying visibility of the collimator hexagonal structure in images obtained with high energy isotopes such as ^{131}I (Figure 31.3). A first simple shrewdness

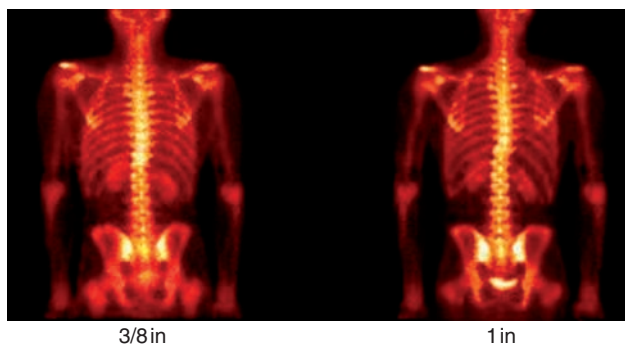


Figure 31.2 Comparison of technetium bone scan acquired with 3/8-in and 1-in Starbright™ crystal thicknesses. (Courtesy of General Electric Medical Systems.)

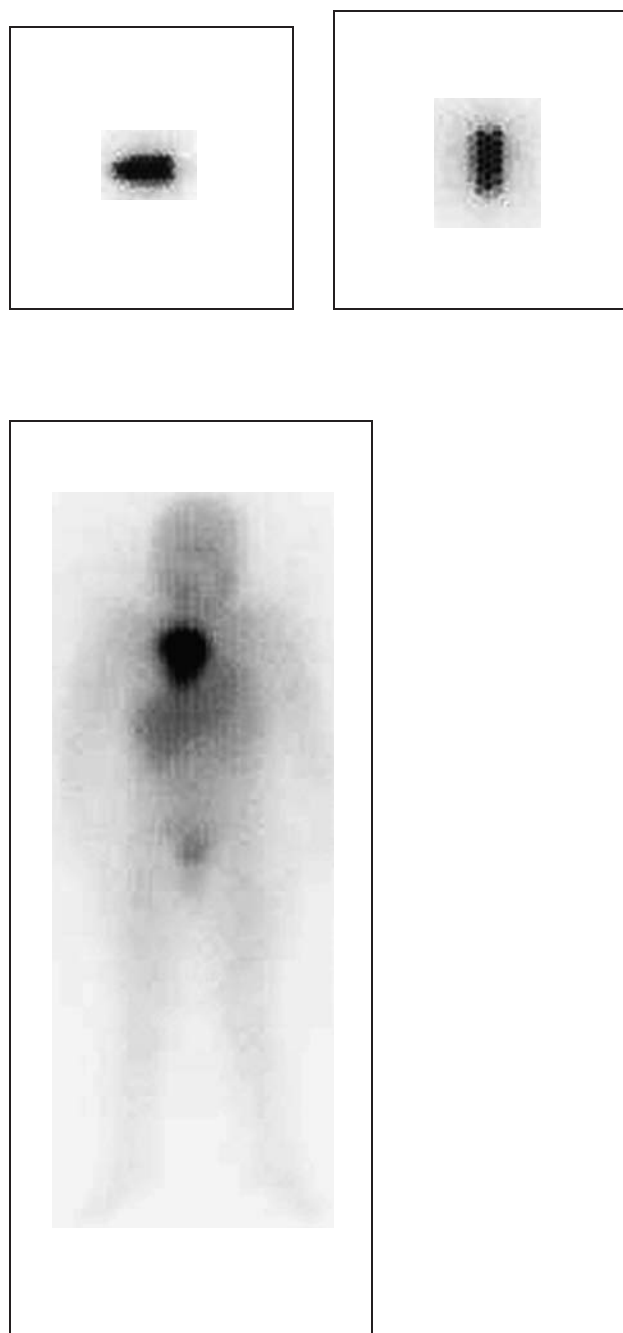


Figure 31.3 The same 20-ml ^{131}I vial lain at contact of high-energy collimator of Sopha DHD (top left) and Toshiba 7200 (top right). The vial axis in both cases is parallel to the hole rows. The better image quality on Sopha is evident. Note also in the bottom image the vertical rows of holes on Toshiba 7200, which causes marked stripes in whole-body studies (^{131}I]MIBG (metaiodobenzylguanidine scan 96 h post-therapeutic injection).

that the manufacturer can adopt to reduce these effects at least in whole-body studies is to avoid lines of holes parallel to the longitudinal direction.

The theory developed by Formiconi et al.⁴ establishes that by placing the high energy collimator at an appropriate distance from the crystal, disappearance of the 'bees' nest' effect will be obtained. Such optimal distance depends upon the collimator specification, and for ¹³¹I should be about 15 mm. The unavoidable loss of resolution should be negligible. To date, no γ camera exploits such an expedient.

The system sensitivity of a γ camera is defined as the count rate (number of events per second) for a specified

amount of activity. This parameter influences the acquisition time or the statistics of the acquired image. The system sensitivity depends on detector efficiency (i.e. on crystal thickness, γ -ray energy, and on the width of energy window) and on the collimator sensitivity, which is determined by its geometric parameters.

Table 31.3 compares the sensitivities for some commercial γ cameras according to the data furnished by the manufacturers and according to the results of acceptance tests by the authors, performed with an International Electrotechnical Commission (IEC) phantom (flat polymethylmethacrylate (PMMA) disc 15 cm in diameter, 1 cm thickness).

Table 31.3 System sensitivity comparison of modern γ cameras

<i>Producer</i>	<i>Model</i>	<i>Crystal thickness (in)</i>	<i>Collimator</i>	<i>Energy window width (%)</i>	<i>Isotope</i>	<i>Point source (producer specification) (cpm/μCi)</i>	<i>Authors' IEC phantom measurement (cpm/μCi)</i>
Siemens	e.cam HD4	3/8	LEHR	15	^{99m} Tc	202	219
Siemens	e.cam HD4	3/8	LEHR	20	^{99m} Tc	NA	232
Siemens	e.cam HD4	5/8	LEHR	15	^{99m} Tc	225	219
Siemens	e.cam HD4	5/8	LEHR	20	^{99m} Tc	—	233
Siemens	e.cam HD4	5/8	LEUHR	15	^{99m} Tc	NA	94
Siemens	e.cam HD4	5/8	LEUHR	20	^{99m} Tc	NA	100
Siemens	e.cam HD4	5/8	HE	15	¹³¹ I	NA	224
Siemens	HD4	1	LEHR	15	^{99m} Tc	230	224
GE	Infinia	3/8	LEHR	20	^{99m} Tc	160	NA
GE	Infinia	3/8	HEGP	20	¹³¹ I	114	NA
GE	Infinia VC	1	LEHR	20	^{99m} Tc	171	182
GE	Infinia VC	1	HEGP	20	¹³¹ I	190	213
GE	Millennium MG	3/8	LEHR	15	^{99m} Tc	135	NA
GE	Millennium MG	3/8	LEHR	20	^{99m} Tc	NA	178
GE	Millennium MG	3/8	HEGP	20	¹³¹ I	180	161
Philips	EPIC-AZ detectors	3/8	LEGP	20	^{99m} Tc	265	NA
Philips	EPIC-AZ detectors	3/8	LEHR	20	^{99m} Tc	146	NA
Philips	EPIC-AZ detectors	5/8	LEGP	20	^{99m} Tc	285	NA
Mediso	Spirit DH-V	3/8	LEHR	NA	^{99m} Tc	160	NA

LEHR, low energy high resolution; LEUHR, low energy ultrahigh resolution; HE, high energy; HEGP, high energy general purpose; LEGP, low energy general purpose; NA, not available.

The system spatial resolution of a γ camera is defined as the least distance between two point sources that allows to distinguish them. It is another fundamental characteristic for image quality. In fact, the partial volume effect consists of a loss of contrast for lesions smaller than about twice the spatial resolution. A quantitative evaluation of the spatial resolution is given by the width of the peak at half maximum (FWHM) obtained, projecting along an axis the counts of a point or a linear source imaged at different distances from the collimator surface.

Spatial resolution depends on the intrinsic characteristics of the detector system (intrinsic resolution), on the geometric resolution of the collimator, and on the distance of the source from the collimator. When a point source is placed in front of the γ camera at a close distance to the collimator, the γ -rays will pass only through a small number of holes and the point source will be imaged with high resolution. In contrast, when the same point source is placed at a distance from the collimator, the γ -rays from the source will pass through many more holes, 'illuminating' a larger area of the detector with a consequent loss of spatial resolution. Hence, it is very important that the collimator remains as close as possible to the patient surface. For this purpose the GE and Siemens γ cameras are equipped with infrared-based automatic systems that maintain the heads at the closest distance from the surface of the patient during whole-body or single photon emission computed tomography (SPECT) studies.

The collimator spatial resolution depends on its geometric characteristics which, on the other hand, are strictly correlated to the energy of the used isotope. It increases with decreasing hole diameter and increasing hole length. Unfortunately this leads inevitably to a reduction of system sensitivity. In fact, an approximate relationship between efficiency and collimator spatial resolution is $\epsilon \approx (\text{FWHM})^2$. Collimator spatial resolution can be improved only at the expense of efficiency; hence, once the isotope is fixed, the choice of collimator has to be made according to a compromise between good spatial resolution and high efficiency. From this point of view, oncology requires the use of collimators with good resolution, with the purpose of detecting lesions as small as possible.

Various types of collimators are commercially available; these are classified according to the radiation energy of the used isotopes and their spatial and efficiency characteristics. The principal characteristics of the collimators in more common use are summarized in Table 31.4.

In the field of neurological imaging, considering the usually used isotopes and the small dimensions of the organ of study, the most suitable collimators are the low energy high resolution (LEHR) (or low energy ultrahigh resolution, LEUHR) and the fan beam collimators described later on.

The most probable interaction mechanism for nuclear medicine photons emerging from a lesion is *Compton scatter* with surrounding tissues. γ -Rays which undergo

Compton scatter within the patient lose part of their energy and change their flight direction. If these kinds of events are scattered perpendicularly to the crystal, they can be detected, giving wrong information about the position where the photon was originally emitted. These events have to be eliminated because they cause a loss of resolution and contrast, since they do not give any useful information to the image. Scatter events can be reduced by accepting only the photons with an energy within a prefixed energy window centered on the primary energy. Discrimination between valid and scatter events is more selective, decreasing energy window. On the other hand, the loss of sensitivity represents a limit to reduction of the energy window, because of the finite energy resolution. In other words, the energy window is inevitably of finite dimensions (15–20% of the peak energy); this causes an image contrast loss due to the fact that, if the γ -ray scatter angle is small, the energy loss is also small, and the scattered photon will probably be accepted as a valid event.

The typical *energy resolution* in modern γ cameras is about 10% at 140 keV (Table 31.5) and the typical energy window is 20%, wide enough to include the majority of the non-scattered events in the window. In some cases a 15% energy window or an asymmetric window shifted towards the high-energy range can be taken, in order to reduce scatter more efficiently. The better is the detector's energy resolution, the smaller is the energy window that can be taken and the better is the scatter rejection.

Another functional aspect of a γ camera is its *count rate* performance, which refers to the ability of the system to keep strict proportionality between the activity and recorded counts. Nevertheless, count rate performance is not a problem with γ cameras for typical *diagnostic* activities. In contrast, a large count underestimation affects early post-therapy scintigraphy. This fact poses severe quantification problems in dosimetric studies during the therapeutic phase.⁵

SPECT

The main problem of planar imaging with the γ camera is that images are a bidimensional representation of distributions of three-dimensional (3D) sources. Therefore, the image of a given anatomical structure is somewhat hidden by under- and overlying structures, resulting in low image contrast.

With SPECT, the 3D radioactivity distribution within transverse slices is reconstructed from 2D projection images acquired at different angles around the patient. The reconstructed image will have a better contrast resolution, defined as the smallest detectable size for a fixed lesion to background ratio, especially for deeply located lesions.⁶

Table 31.4 Comparison of collimator specifications

Collimator	Hole diameter (mm)	Hole length (mm)	Septal thickness (mm)	Crystal thickness (in)	System resolution at 10 cm (mm)	Sensitivity at 10 cm (cpm/ μ Ci)	Isotope
LEHR, Siemens	2.54	24.05	0.36	3/8	15.6	1020	^{99m}Tc
LEAP, Siemens	1.45	24.1	0.20	3/8	9.4	330	^{99m}Tc
LEHR, Siemens	1.11	24.05	0.16	3/8	7.4	202	^{99m}Tc
LEUHR, Siemens	1.16	35.8	0.13	3/8	6.0	100	^{99m}Tc
LEFB, Siemens	1.53	35	0.16	3/8	7.3	280	^{99m}Tc
MELP, Siemens	2.94	40.64	1.14	3/8	12.5	310	^{67}Ga
HE, Siemens	3.4	50.8	2	3/8	14.5	135	^{131}I
LEGP, Philips	1.40	24.7	0.18	3/8	8.8	265	^{99m}Tc
LEHR, Philips	1.40	32.8	0.152	3/8	7.4	146	^{99m}Tc
VXGP, Philips	1.78	42.0	0.152	3/8	7.8	159	^{99m}Tc
VXHR, Philips	2.03	54.0	0.152	3/8	7.4	132	^{99m}Tc
VXUR, Philips	1.78	54.0	0.152	3/8	6.7	106	^{99m}Tc
MEGP, Philips	2.95	48.0	1.143	3/8	11.3	212	^{67}Ga
HEGP, Philips	3.81	60.0	1.727	3/8	12.5	106	^{131}I
HEHR, Philips	3.06	60.0	1.95	3/8	10.4	53	^{131}I
LEGP, GE Infinia	1.9	35	0.2	3/8	9.0	270	^{99m}Tc
LEHR, GE Infinia	1.5	35	0.2	3/8	7.4	160	^{99m}Tc
MEGP, GE Infinia	3.0	58	1.05	3/8	9.4	144	^{67}Ga
MEGP, GE Infinia	3.0	58	1.05	1	11.5	144	^{67}Ga
HEGP, GE Infinia	4.0	66	1.8	3/8	10.7	97	^{131}I
HEGP, GE Infinia	4.0	66	1.8	1	15.7	97	^{131}I
Fan beam, GE Infinia	1.5	40	0.2	3/8	7.0	NA	
Fan beam, GE Infinia	1.5	40	0.2	1	7.4	NA	

LEHS, low energy high sensitivity; LEAP, low energy all purpose; LEFB, low energy fan beam; MELP, medium energy low penetration; VXGP, vertex general purpose; VXHR, vertex high resolution; VXUR, vertex ultrahigh resolution; MEGP, medium energy general purpose; HEHR, high energy high resolution.

In order to perform SPECT, γ cameras able to rotate around the patient are needed. Different types of γ cameras can perform tomographic studies, and the main difference is the *number of heads* that can vary from one to three. As the number of heads increases, system *sensitivity* increases, and therefore, presuming that all other parameters such as acquisition time are fixed, the statistical noise of the image decreases. Currently the two-headed γ camera is the most common type, because it can attain a good performance level and is very versatile.

The ability to visualize small lesions with SPECT is strongly influenced by the *tomographic spatial resolution* of the γ camera, which is measured by calculating the FWHM of a point source imaged in SPECT geometry at different SPECT radii. Since spatial resolution worsens with the distance of the source from the collimator, an important criterion for optimizing the spatial resolution in SPECT is to have the γ camera rotating as close as possible to the patient. For this purpose different strategies have been developed, including rotation of the γ camera around the

Table 31.5 Intrinsic energy resolution

<i>Producer</i>	<i>Model</i>	<i>Crystal thickness (in)</i>	<i>Producer specification (%)</i>	<i>Authors' measured value (%)</i>
Siemens	e.cam	3/8	≤9.9	9.6
Siemens	e.cam	5/8	≤9.9	9.6
Siemens	e.cam	1	≤10.4	NA
GE	Infinia	3/8	≤9.8	NA
GE	Infinia VC	1	≤9.8	9.1
Philips	EPIC-AZ detectors	3/8	≤9.5	NA
Philips	EPIC-AZ detectors	5/8	≤9.7	NA
Mediso	Spirit DH-V	3/8	9.7	NA

patient with non-circular orbits. In the case of cerebral SPECT, the 'as close as possible' condition can be reached, avoiding the shoulders of the patient in the detector sight; in fact, the obstacle represented by the shoulders would involve an excessive moving apart of the detectors in correspondence to some angular projections, with consequent worsening of the resolution. In this case a decentralized zoom can be used; this kind of zoom allows magnification of views of the patient's head starting from the detector's edge, thus leaving the patient's shoulders external to the detector field of view.

Spatial resolution in SPECT is tightly correlated with the planar spatial resolution; the tomographic spatial resolution measured according to National Electrical Manufacturers Association (NEMA) specifications, in terms of FWHM, can be assumed to be approximately 20–30% higher than the planar spatial resolution. Obviously, the clinical resolution in SPECT will strongly depend also on the reconstruction algorithm. For cerebral studies, tomographic spatial resolutions vary typically between 8 and 12 mm, according to the type of collimator in use; moreover, the spatial resolution in the cortex is slightly better in comparison to that in the center of the skull.

When the organ under study is small compared to the crystal dimensions, such as for example in cerebral SPECT studies, and parallel hole collimators are used, only a partial use of the detector area is possible, with a consequent limit on the efficiency. It is possible to take better advantage of the detector surface by using special collimators for tomography, the so-called *fan beam collimators*. These convergent collimators have tilted holes focused along a line parallel to the γ camera axis of rotation. This determines a magnifying effect, with a consequent increase of detection efficiency.

Also, for this type of collimator, there is an improvement of spatial resolution with decreasing distance, but at the same time this determines a loss of efficiency because of

the smaller image magnification effect. This means that for fan beam collimators there is a fixed distance (typically 13–15 cm) that guarantees the best compromise between efficiency and spatial resolution. With appropriate holes and septa size, fan beam collimators guarantee, for the same efficiency, superior performance in terms of spatial resolution in comparison to parallel hole collimators.

The magnification effect of the fan beam collimators also implies a dependence of the image dimension on the distance from the collimator, with a consequent image distortion; however, this distortion is corrected by the fan beam dedicated reconstruction software.

In tomographic imaging, both SPECT and PET, an additional crucial influence on the final images is furnished by the reconstruction algorithm and by the filtering parameters (some notes on a new reconstruction algorithm are presented below in 'software improvement').

One of the main problems in SPECT is *attenuation*: γ -rays emitted inside the patient can undergo photoelectric absorption or Compton scatter, resulting in a loss of detected counts. The degree of attenuation depends on the energy of the γ -ray, on the type of material it passes through, and on the distance it travels through the attenuating material. Attenuation brings an underestimation of emission activity coming from deep organs within the body, and hence the necessity to perform a correction for attenuation. In cerebral SPECT images, for instance, attenuation gives an underestimation of the activity concentration in the inner areas of the skull.

One of the first approaches to attenuation correction, which is still widely used, is Chang's method.⁷ This method assumes a uniform attenuation coefficient in the different tissues within the SPECT image. The intensity of each pixel in the reconstructed image is changed according to the attenuation probability which is correlated to the depth of the pixel from the surface. The optimal attenuation coefficient

has to be experimentally determined on a single γ camera, because Compton scatter partially compensates the attenuation effect. Chang's method provides a reasonable estimation of attenuation in areas of uniform density. This is the reason why it gives particularly good results in the case of cerebral SPECT studies, since the constancy of the attenuation coefficient hypothesis is practically correct.

Unfortunately, with a few exceptions, the attenuation coefficient varies dramatically within the body; the degree of attenuation non-uniformity is more severe in regions such as the thorax, where the photons may encounter structures with very different attenuation coefficients. In this case, Chang's method shows its limits.

A more recent method consists of correcting for attenuation on the basis of a transmission image obtained with external sources.⁸ In this method a map of densities within the body (μ map) is obtained, and then can be utilized in an iterative reconstruction algorithm to correct for the effects of non-uniform attenuation. This method requires additional radioactive sources (usually ^{153}Gd , ^{133}Ba , or ^{57}Co) positioned in such a way that their photons pass through the patient before reaching the opposing detector. Different configurations of the external sources have been used for simultaneous transmission and emission measurements. As an example, three-headed SPECT systems allow the use of one of the heads in conjunction with a rod or point source to obtain attenuation maps of the patient from transmission data.

Another example is the Siemens e.cam profile attenuation correction system that utilizes dual arrays of ^{153}Gd transmission sources to simultaneously illuminate both detectors. A multiple line array utilizes a series of individual stationary line sources that, when appropriately spaced and positioned at an adequate distance from the detector, appear as a sheet source.

More recently, the computed tomography (CT)-based attenuation correction method has been implemented in SPECT-CT systems, discussed later, which improves the image quality of SPECT studies. The method is practically identical to what is done with PET-CT systems: the CT numbers are used, after scaling for different photon energies, to calculate the μ map for attenuation correction.

SPECT-CT

A general limit of nuclear medicine images is the scarce morphological information. The location of radioactive accumulation is sometimes difficult to find without additional anatomical information. Commercially available registration software allows the co-registration of nuclear medicine images with images from other modalities such as magnetic resonance imaging (MRI) or CT; these kinds of imaging modalities furnish excellent anatomical details

thanks to their high spatial resolution, and can be correlated to the accumulation of radioactivity in SPECT images. Software image fusion is often successful for the brain, which can substantially be considered as a rigid body whose form is determined by the skull, but does not work as well for the rest of the body. The problem is mainly the non-identical positioning of the patient during scans with different imaging modalities.

The employment of SPECT-CT hybrid systems is a more direct (and more accurate) method of integrating the physiological and functional data furnished by SPECT images with the anatomical data furnished by CT images. With these kinds of scanners, in which SPECT and CT are combined in a single system, emission and transmission images are acquired during the same session with the patient in the same position, eliminating any imaging co-registration problem.

As previously discussed, another advantage of a SPECT-CT system is that one can use the transmission images of the CT to correct SPECT images for attenuation.

The first system able to perform simultaneous CT and SPECT brain studies was reported in 1992. Currently, SPECT-CT systems are becoming more and more common in nuclear medicine departments; examples are Infinia VC and HawkeyeTM by GE, PrecedenceTM by Philips, and SymbiaTM by Siemens. The main difference between these commercial systems is that the CT mounted by Siemens and Philips is a spiral CT, which works independently of the SPECT, allowing fast rotation and acquisition. On the other hand, in the GE system, the CT image is produced using an X-ray tube which rotates together with the γ camera's heads. In this case the CT acquisition time is much higher and can reach 20 minutes for a thorax. Moreover, the slice thickness with the GE system is much larger; obviously these differences are reflected by the cost of the various systems. The Hawkeye price is about one-half that of a γ camera, while the Symbia CT costs more than a γ camera.

Dedicated brain-SPECT systems

There are three- and four-head γ camera systems commercially available that constitute the most sophisticated instruments for cerebral SPECT, reaching spatial resolutions as low as 6 mm. As an example, the NuclineTM X-Ring-4R digital γ camera produced by Mediso is a four-head γ camera with internal dimensions of about 25 cm, and can reach tomographic resolutions of 5.6 mm with LEUHR.

With the purpose of increasing the efficiency, ring dedicated systems were developed for cerebral SPECT, such as, for example, Sprint II,⁹ CeraSPECT,¹⁰ and FAST-SPECT.¹¹ These systems have mainly been used for research, and they are not found in a typical nuclear medicine department.

Future developments

In the future, new types of detectors may be employed in nuclear medicine. For example, semiconductor detectors such as those including cadmium zinc telluride (CdZnTe) show a better energy resolution with respect to NaI(Tl), and do not need PMTs. On the other hand, their detection efficiency is lower than that of NaI(Tl). At the moment their most promising application is in mobile systems.

One of the main limitations of mechanically collimated γ cameras is that sensitivity is dramatically reduced by the collimator, and can be improved only at the expense of spatial resolution. An alternative to mechanical lead collimation for single-photon imaging is represented by 'electronically collimated' or '*Compton cameras*',¹²⁻¹⁴ which have the potential for dramatic improvement in sensitivity without sacrificing spatial resolution. These systems need two separate detectors to estimate the direction from which the γ -ray originated. Figure 31.4 shows the functioning principle of the system. A γ -ray from the patient undergoes Compton scatter within the first detector; subsequently the scattered photon proceeds toward the second detector. Both detectors determine the interaction position and the deposited energy. The sum of the deposited energies gives the energy of the incident photon. From the energy deposited in the first detector and the relative position of interaction within the two separated detectors a cone of possible flight directions of the γ -ray can be determined. In order to have good spatial resolution, the position in the first detector must be determined with good precision and one of the two detectors must have very good energy resolution. In fact, only in this case can the energy of the scattered photon be determined with good precision and the

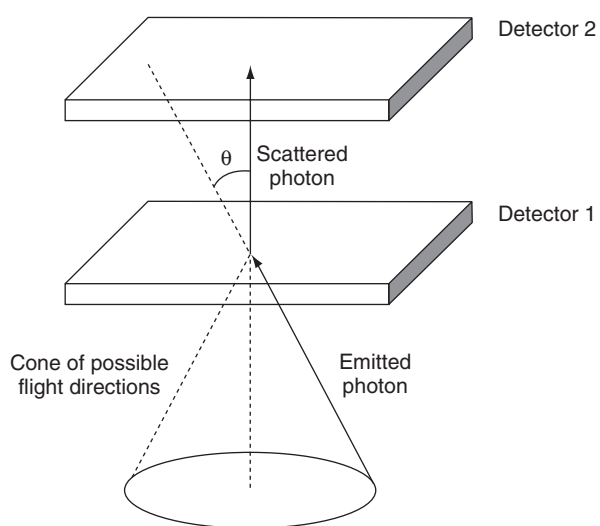


Figure 31.4
Schematic drawing showing the functioning principle of electronic collimation.

surface of the cone in 3D space be accurately determined. With many of these cones, the source distribution within the patient can be reconstructed.

These kinds of systems present an increase in sensitivity with respect to traditional γ cameras, by a factor of 100. The necessary good resolution can be obtained using semiconductor detectors and liquid nitrogen cooling.

Compton camera prototypes show promising performance, especially with isotopes of higher energies with the dominating Compton scatter. The C-SPRINT Compton camera¹⁵ uses pixelated, low-noise, position-sensitive silicon as the first detector, and a sodium iodide scintillation detector ring as the second detector. The system consists of a single $4.5 \times 1.5 \times 0.03$ -cm³ silicon pad detector module with ~ 2 keV energy resolution centered at the front face of a 50-cm diameter, 12-cm long sodium iodide detector annulus.

Coincidence detection

Introduction: the aims of PET scanner evolution

The fascinating possibility of fully exploiting the counting capability of a dedicated PET scanner by the 3D mode is the force which drives actual research in PET technology. As a matter of fact, the recent evolution of dedicated PET scanners has moved mainly towards solutions to the two non-trivial problems raised by the 3D PET modality:¹⁶

- the rather limited BGO system count rate performance in 3D
- the large scatter fraction in whole-body 3D (no matter the type of crystal) with respect to the 2D modality.

Shortly after the introduction of 3D PET with BGO, the main idea was to improve its count rate performance, probably with the aim of shortening the acquisition time rather than improving the image quality. Systems were developed in this direction, leaving behind BGO, 'prince' of 2D imaging: Siemens PET AccelTM and PET-CT BiographTM with lutetium oxyorthosilicate (LSO); Philips PET AllegroTM and PET-CT GeminiTM with gadolinium oxyorthosilicate (GSO). The price in terms of injected activity necessary to fully exploit first-generation fast-crystal scanners was rather high. Probably for this reason, GE changed the PET crystal structure from Discovery LS to Discovery ST, but kept BGO. Changes in electronics were adopted, and significant improvements were made (Siemens: from Biograph to Biograph equipped with Pico 3D, Philips: from Gemini to Gemini GXL, GE: from Discovery ST to Discovery STE, the only scanner keeping 2D and 3D modalities with BGO).

This industrial competition towards the best count rate performance seems to focus on the fundamental goal of imaging in oncology (90% of PET studies), which is lesion detectability. This is only partially true, since better statistics in principle means easier lesion localization through higher signal to noise ratio (SNR). But many other factors contribute to the visibility of a small region: spatial resolution and scatter fraction are the most important figures of merit. For these reasons, another improvement line was towards better spatial resolution (see, for example, the structural changes from Discovery ST to STE). Moreover, other elements which play a crucial role in the tomographic imaging process must be mentioned: data handling, corrections, and reconstruction algorithms. These elements can be grouped under the generic term 'software'. Regarding the intrinsic statistical noise of PET data, it has been said¹⁷ that 'reconstruction can cause image noise to be as much as an order of magnitude higher'.

In the wake of image quality improvement from the aspect of SNR, the next revolution has been under way since March 2006: Philips officially presented the first commercial time-of-flight (TOF) PET-CT scanner (Gemini TF). TOF-PET means the ability to detect the infinitesimal difference in detection time between two annihilation photons.

However, the following fundamental oncological question still remains open.

Which scanner gives the best lesion detectability?

This question is accompanied by several others. What is the price in terms of injected activity in clinical routine? What is the inferior limit to the acquisition time? It must be clearly stated that the monoparametric approach used to date is far from giving the answer; i.e. the count rate capability (NECR) used to compare different scanners is only one factor among many others.

We should point out that answers to these questions are not available, being the front line of current research. In the following, we hope to summarize elements for better understanding of the multiparametric jungle in which answers have to be sought.¹⁸ A useful mental framework could be the following:

Hardware	crystal material scanner structure electronics
Software	data handling correction and reconstruction algorithm

An even more exciting technology under development is research in small-animal PET, but this is beyond the aims of this chapter.

Basis of coincidence detection

Classical and new positron emitters

Beyond the usual four cyclotron-produced clinical positron emitters (¹¹C, ¹³N, ¹⁵O, ¹⁸F), further isotopes could be more extensively considered.¹⁸ As a matter of fact, copper (⁶²Zn/⁶²Cu), gallium (⁶⁸Ge/⁶⁸Ga), rubidium (⁸²Sr/⁸²Rb), and lanthanum (¹³⁴Ce/¹³⁴La) have been clinically used, and are characterized by the noticeable advantage of being distributable as generators, similarly to technetium. However, the mind of the nuclear physician could easily sweep the possible clinical applications of ¹²⁴I (half-life 4.18 days), both as a free iodine isotope (thyroid pathologies) and in bound form (metaiodobenzylguanidine (MIBG)), monoclonal antibodies (mAb). Similar important applications could be immediately thought of with ⁸⁶Y (half-life 14.7 hours) bound to somatostatin receptor targeting peptides or anti-CD20 mAb. The application of these isotopes is not problem-free, since quantification is difficult because there are other simultaneous γ emissions besides the coincidence photons. Specific corrections must be implemented for commercial scanners (see Chapter 30 by M. Lassmann for more detail) and careful calibrations must be performed.

Nevertheless, it is a fact that such kinds of isotopes, though available, are of extremely restricted distribution and use. An important role regarding these topics could be played by cyclotron- and PET scanner-producing companies. Regarding new positron emitters, to date no specific target and related process system has been proposed commercially. Not even correction and calibration for the abovementioned isotopes are implemented on commercial scanners. Rather, the company responsibility mechanism prevents the final user implementing such corrections themselves, both by legal argument and in practice by delivering inaccessible software.

This forced 'black box acceptance' of any imaging system is certainly a negative modern trend, absent in the pioneering phase of PET (1970s–1990s).

Coincidence detection

Coincidence detection requires two almost collinear ($180^\circ \pm 0.25^\circ$) 511-keV annihilation photons to 'simultaneously' interact in two detectors coupled to a coincidence unit (Figure 31.5). Such an 'electronic black box' has two input gates, and accepts two incoming signals. As soon as the first gate is triggered (start signal), the second gate stays alert for a fixed time interval τ , the resolving coincidence time. An output logical signal of 'good event' is produced if a second pulse enters the second gate within the time interval τ . Since annihilation photons are indistinguishable, and we cannot say which one arrives first without detecting it, a fundamental physics symmetry law imposes the correct

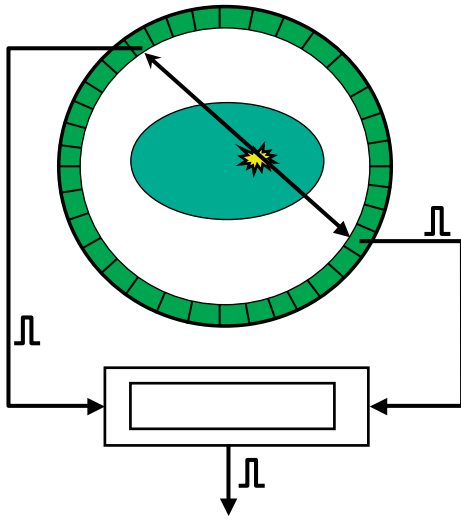


Figure 31.5

Coincidence detection. An event is detected (OK) by the coincidence unit if the two pulses arrive at the two gates within $\pm\tau$. τ is named coincidence resolution time.

statement ‘an event is detected if the two pulses arrive within $\pm\tau$.¹⁹

Figure 31.6 represents the components of the response of a coincidence detection system. Singles are uncoupled counts in only one detector; trues are really correlated photons coming from the same positron annihilation; randoms are couples of uncorrelated photons coming from different annihilations; scatters are pairs in which photons were deflected and degraded in energy (Compton effect) within the extended source or within the detector.

Scanner structure

Scanner structure is based on tens of thousands of single scintillating crystals. In order to reduce the number of necessary photomultipliers (PMTs) in the block design (Figure 31.7), an array of $n \times n$ crystals are subtended by a few PMTs (typically four). The interaction position is given

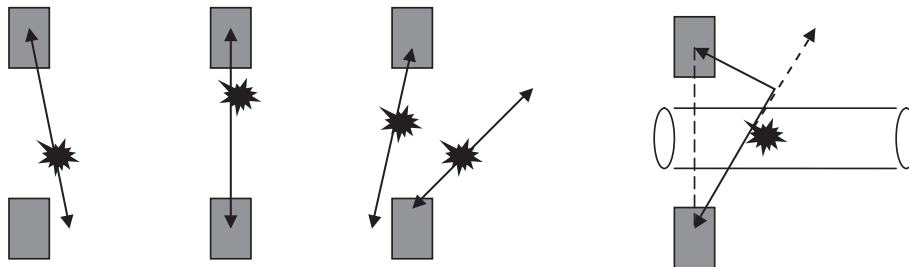


Figure 31.6

Components of response of a coincidence detection system.

in discrete single crystal steps, weighting the relative amplitude of the four-PMT output. Many blocks surround the patient in a cylindrical geometry. In 2D each detector ring can accept coincidences from itself or from adjacent rings. The sensitivity of the system is limited by the small solid angle seen by a point source at the center of the axial field of view (AFOV). In this case, inter-ring lead or tungsten septa mechanically collimate scatter photons, reducing the scatter fraction to about 10%. In 3D mode, septa are removed (in GE scanners) or absent (Siemens and Philips 3D-only scanners). The scanner count rate increases ten times with respect to the 2D mode, but scatter photons enter the detector rings also from outside the AFOV, giving typically 30–40% scatter fraction.

An alternative to block design is the large crystal design. The ADAC C-PETTM is an example of this structure. The potential advantage of this kind of structure with respect to the block design is the improved energy resolution, i.e. potentially lower scatter fraction. In fact, in the block design, the crystals are in different positions with respect to the sensitive part of the PMT, the photocathode, and for this reason equal light sparks give different PMT output signals from different crystal positions, deteriorating the system energy resolution.

On the other side, the large crystal structure is subtended by an Anger type location system. This implies that many PMTs are involved, in principle, after each interaction, causing count rate limitations. Specific electronics had to be developed in order to isolate the centroid of the light spark, and to process simultaneous events, provided that they are spatially separated. This is also the basic limitation of coincidence γ cameras. In the block structure, each PMT works independently from the others, and the system count rate can be higher.

The most recent variation of the large crystal design is the Philips PIXELARTM technology, used in Allegro and Gemini scanners, in which the inner part of the cylinder is constituted by small single crystals, as in the block design. The crystals are subtended by a large light guide (flat panel), which faces on its opposite side the Anger logic PMT array. In this intermediate configuration, the best of both designs should be pursued.

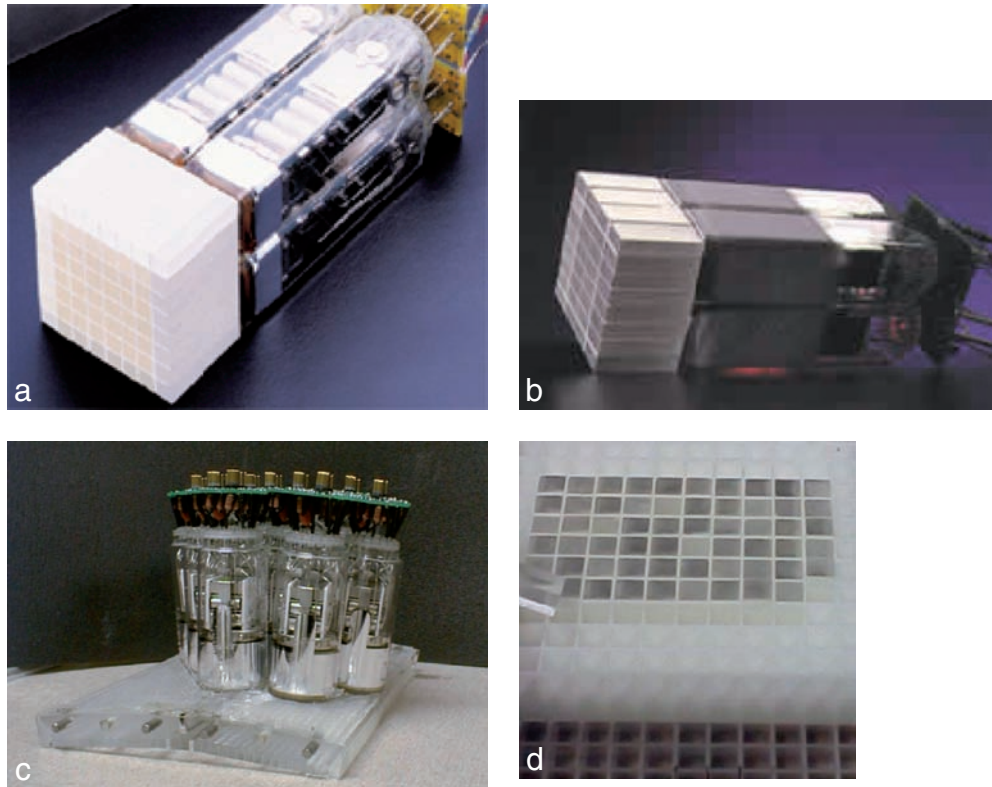


Figure 31.7

Scanner design: (a, b) block design; (c, d) flat panel design. (a) Siemens Biograph; (b) GE Discovery ST; (c, d) Philips Gemini.

Both in block and in flat panel design, the elementary detection unit is a couple of crystals in coincidence. The volume between them is defined as the line of response (LOR). The possibility of electronically identifying the traveling direction of photons eliminates the collimator (which is necessary in single detection with γ cameras). This raises the system sensitivity by two or three orders of magnitude. If we consider a fixed transaxial section and a fixed projection angle, we have a sequence of parallel LORs whose counts give a count profile, which is stored in a row of a matrix. Changing the projection angle we have another vector which is stored as the second row of the matrix. The complete matrix is called a sinogram. This is the raw data set for each slice. The name derives from the fact that a point source coordinate as seen as a function of the projection angle varies as the sine function.

Random coincidences and timing electronics

Now we consider the elementary timing circuit shown in Figure 31.8. We replaced the coincidence unit, which gives only a yes/no answer, with a time amplitude converter, whose output is a signal of amplitude proportional to the

time interval between the photon arrival instant. Given the infinitesimal time scale under study, it is also necessary to properly balance the traveling time of the electric pulses in the two strands of the electronic chain. In fact, if the difference in traveling was too long, i.e. larger than 2τ , no valid

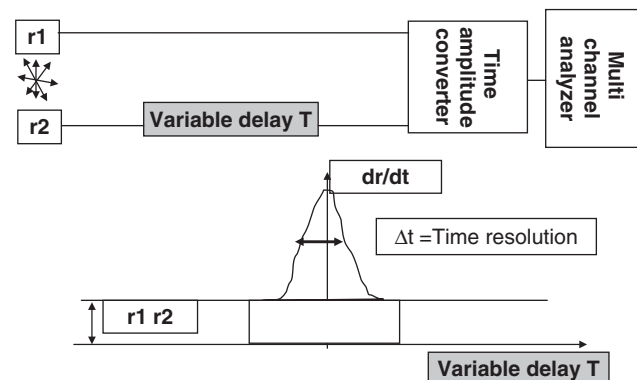


Figure 31.8

Elementary timing circuit and spectral time distribution plot in case of coincidence emitter. Varying the delay T , true coincidences (below the Gaussian peak) are lost. For any other arbitrary delay, a constant rate is observed: it is the random distribution.

coincidence output would result. The interesting point is that, even with totally unbalanced strands, a constant number of counts is detected on average. Since there is no correlation between such couples of photons, they are named random coincidences. It is also easy to quantify their rate. r_1 (cps) is the singles rate in detector 1. Each pulse in strand 1 opens gate 2 for 2τ . So, in each second, gate 2 remains opened for a fraction of time equal to $2\tau r_1$. In this fraction, the rate of random pulses coming from gate 2 is:

$$R = 2\tau r_1 r_2 \quad (1)$$

The random rate R (equation (1)) is the area of the acceptance rectangle, if the delay is too large. Note that R is an average value, and that the statistical nature of nuclear decay adds fluctuation (noise) to it.

Equation (1) has three important consequences:

1. Since the singles rates r_1 and r_2 are proportional to the activity of the source, in a fixed 2D or 3D modality, R increases with the square of the injected activity, while the true rate T has a linear dependence on the activity (ideally).
2. If we pass from 2D to 3D, since septa are removed, R jumps by one order of magnitude, and random events become a problem.
3. Equation (1) gives the first method of measuring R for each LOR, on the basis of the singles rates, named 'single based' estimation of random coincidences. With this random correction method the average of R can be subtracted on-line from T ; in this case, for the law of propagation of errors, the resulting error on T is raised. Since all kinds of coincidence rates are much smaller than the singles rates, the statistical Poisson noise of R according to equation (1) is small. This method of random correction is 'noiseless', but is reliable only if singles rates are measured at an appropriate point in the data processing stream.¹

A second method for random correction is based on Figure 31.8. Split the dual coincidence circuit in two dual strands and use one strand properly balanced, while the second strand has a totally unbalanced delay. We collect total coincidence events in the first strand and only random events in the second strand; trues are calculated as the difference of the two. This method is 'noisy', because random noise enters the two collected sinograms and propagates to the result of the subtraction.

No matter the correction method, *the optimal choice would be to reduce the random rate*. We can obtain this reduction either mechanically by inserting septa in 2D mode, or again using equation (1) in 3D mode. In fact, the narrower is the coincidence window, the lower is the unwanted random background rate. So the idea is to reduce τ , but we have two limits. As shown in Figure 31.8, the peak in

the time spectrum has a certain width, whose FWHM is defined as:

$$\Delta t = \text{time resolution of the coincidence circuit}$$

No real detector has an infinitely narrow peak, i.e. infinite time resolution ($\Delta t = 0$). This extremely important feature depends mainly upon the crystal scintillation timing properties, but also on the electronic chain, as will be described below. So 2τ cannot be reduced to less than about $2\Delta t$, otherwise true coincidences will be lost. In other words, the timing resolution of the system imposes an inferior limit to the coincidence resolving time.

Since technology advances quickly, we could conceive, in the not too distant future, improvements in timing resolution, so that this first limit might become meaningless. Unfortunately a second physical constant will stop our dream: the finite speed of light (3×10^{10} cm/s) implies that the γ rays need 3.3 nanoseconds to cross a 1-m diameter PET detector ring. We cannot close the second gate before the second γ has arrived. Hence, in any case, it must be:

$$\tau > 3.3 \text{ ns (speed of light limit)} \quad (2)$$

Scatter

The second unwanted event in the crystal is that of scattered photons. The problem is more familiar than the random event, and is well known on collimated γ cameras. What is new in 3D PET is the amount of scatter caused by the absence of any collimation. Figure 31.9 shows an example obtained by a NaI scanner, the source being a 20-cm diameter, 70-cm length cylindrical phantom (NaI should have the best energy resolution, i.e. the best scatter rejection).²⁰

Scatter contribution can be reduced mechanically by using septa in 2D mode, or in 3D mode by raising the lower

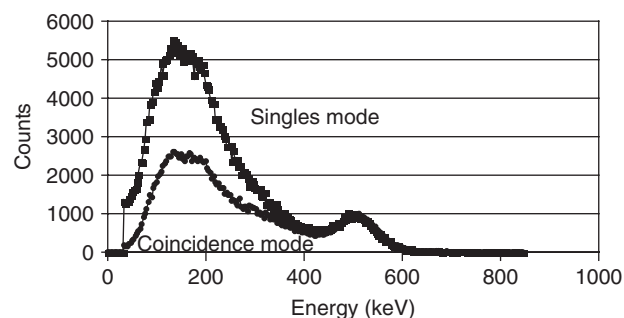


Figure 31.9

The scatter problem in three-dimensional positron emission tomography (3D PET). Energy spectra obtained by ADAC C-PET NaI scanner from a 20-cm diameter, 70-cm long cylindrical phantom. (Reproduced with permission of Edizioni Minerva Medica from reference 20.)

threshold of the discrimination energy window. The sensitivity loss unavoidably related to narrowing the energy window is less evident the narrower is the photo peak, i.e. the better is the system energy resolution. Here again, average scatter can be somewhat estimated by suitable correction algorithms, but the scatter-related noise will always enter the system, increasing the image noise. While randoms can be quantitatively measured, at least in terms of their average value, scatter cannot be exactly quantified. Scatter depends critically upon the volume of the extended source, so it increases during the same PET study in moving the AFOV from the head of the patient to the thorax and the abdomen. In 3D mode, scatter depends also on the activity outside the AFOV.

General PET scanner performance parameters

Spatial resolution

In oncology, spatial resolution is one of the most important parameters in lesion detectability, but it is not the only one. The partial volume effect reduces the contrast of spheres of constant lesion to background activity as their diameter diminishes below twice or three times the spatial resolution (see the IEC recovery coefficient test²¹ and the NEMA 2001 image quality test).²²

In full ring PET scanners, maximum spatial resolution depends upon:

1. Positron range in tissue (minor dependence). This effect depends only upon the used isotope.
2. Non-perfect colinearity of annihilation photons. This is associated with scanner structure, since blurring is greater if the ring diameter is larger: $\text{FWHM} \cong 0.0022 \times D$ (cm). For this reason, dedicated brain scanners were produced in the past.
3. Crystal dimension, w . Ideally, the related FWHM is $w/2$. The resolution could be improved by a reduction of w , limited at present mainly by PMT dimensions. For this reason, a number of alternative solutions are under study.¹⁶ Position sensitive PMT (PSPMT) is one line of research. Such a device is already implemented in small-animal PET scanners (microPET by Concorde Microsystems). Another completely new trend aims to replace PMT with pixelated semiconductor solid state photodetectors.
4. Parallax error (Figure 31.10). This bias worsens for smaller ring diameter. As a matter of fact, this effect forces the actual human scanner to have a detector ring much larger than the patient port, with a consequent loss of spatial resolution (see point 2) and necessity of a

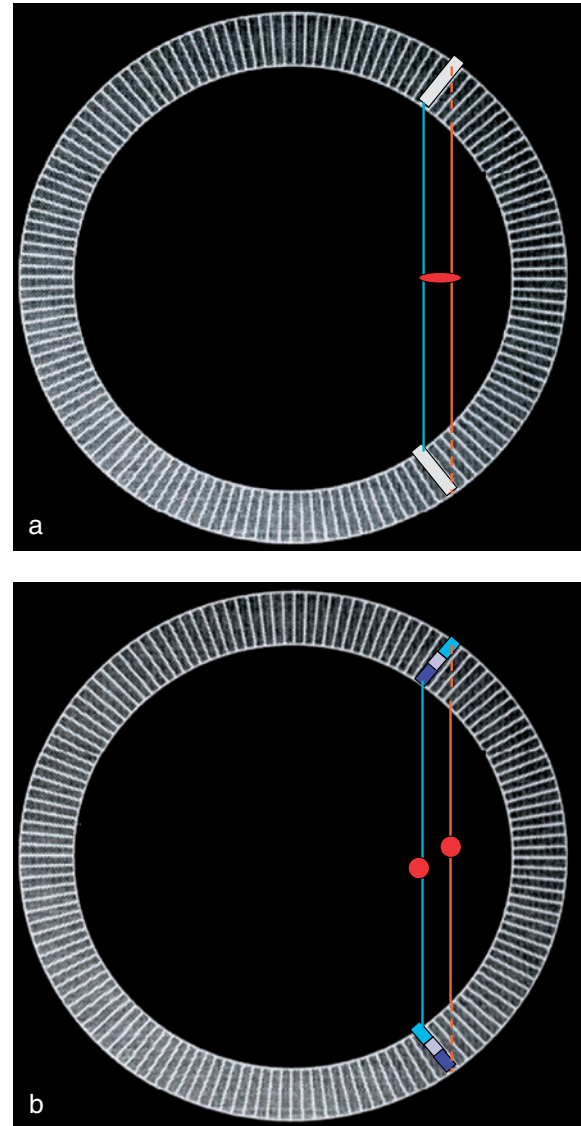


Figure 31.10

The parallax error. (a) The orange correct line of response (LOR) is mispositioned. The point source is distorted radially. (b) The depth-of-interaction (DOI) measurement by phoswich detector reduces parallax error and improves radial resolution.

larger amount of scintillation crystal (which is the most expensive scanner component). The solution to this problem falls under the term ‘depth-of-interaction’ (DOI) measurement. Many prototypes have been realized in different laboratories, mostly following the philosophy of a stacked detector in the radial direction (phoswich). The stack can be obtained by layers of different crystals, or by different doping levels of the same scintillator. Other prototypes measure the DOI by means of two photodetectors: one PMT on the back of the crystals (as usual) and one photodiode at the entrance to the crystals. The difference between front

and back light amount is correlated to the DOI. To date, no human scanner allows DOI measurement.

One must keep in mind that, in clinical studies, spatial resolution is worsened with respect to the NEMA measured value. The presence of the scatter medium and the reconstruction filters is responsible for this reduction.

Sensitivity

Sensitivity is in general the ratio between the true count rate and the activity in a fixed source. NEMA NU 2-2001 protocol defines a precise way to determine the scanner sensitivity without scatter. Sensitivity depends on the crystal material, on its packing fraction, on the AFOV, and, of course, on the acquisition modality (2D vs. 3D). The goal of sensitivity gain in PET guided the efforts from the very beginning. NaI, which is very suitable with 140-keV ^{99m}Tc photons, was abandoned (apart from very few exceptions equipped with thicker crystals) for BGO, the most efficient crystal at 511 keV.

Now let us carry out a 'gedanken experiment'. This paradox uncouples one important parameter in generic image quality (the statistics of accumulated counts) from sensitivity. Any imaging system undergoes Poisson statistics, according to which the relative image noise is proportional to $1/\sqrt{N}$, where N is a generic number of counts. Now, following this paradox, extremely low sensitivity could be overcome by extremely long acquisition times. So, sensitivity is not a problem, if one has enough time.

Coming back to the real world, where shortening the acquisition time is imperative, in 3D mode the alternative solution, i.e. to increase the injected activity, is not trivial. While in 2D clinical PET an increase of injected activity gives a proportional increase in the scanner count rate, this is dramatically false in 3D mode. One reason for this is the scatter increase due to the absence of septa. Another is the huge jump in random rate, following the square dependence on the singles rate (activity). For this reason, in 3D PET, other, more sophisticated parameters should be considered for scanner comparison.

The simpler one is the *peak trues* (see Figure 31.18), which is a generalization of linearity curves of usual singles detection systems. Trues after random and scatter subtraction cannot be proportional to an arbitrarily high injected activity, because of the dead time count loss (known also as saturation), but even working at the true peak rate is not the optimal condition. Corrected trues can be useless if accompanied by excessive noise. This is the deep meaning of the NEC parameter.

Noise equivalent count rate

One of the most important concepts in imaging theory is the signal to noise ratio (SNR).²³ In a uniformity image it

can be thought of as the ratio between the average value of the pixel count divided by their standard deviation. The noise equivalent count (NEC) is a general parameter related to the SNR by the relationship:

$$\text{SNR} = \text{cons} \times \sqrt{\text{NEC}} \quad (3)$$

Equation (3) is quite similar to Poisson's law, which states that the average counts of a detector in a fixed time divided by their standard deviation is proportional to \sqrt{N} . Pay attention to the fact that we are speaking of total collected counts.

The formula for NEC was introduced in PET by Strother et al.²⁴ in the strict assumption of a uniform cylinder. In the original Strother paper, T is the total collected true counts. Many other authors report a formula for the noise equivalent count rate (NECR) similar to the following (from Brasse et al.¹):

$$\text{NECR} = \frac{T^2}{T + S + f_{\text{FOV}}(1+k)R} \quad (4)$$

where T , R , S are the rates for trues, scatter, random, and $k=0$ for noiseless random correction method, $k=1$ for noisy delayed random correction method, and f_{FOV} is the fraction of field of view occupied by the object.

It is of great importance to keep in mind the difference between noise equivalent count NEC (which is directly related to the SNR) and noise equivalent count rate (NECR), which can be linked to the former by multiplication by the scan duration. Unfortunately, in PET literature, there is a misleading convention of indicating both parameters by 'NEC'.

Examples of experimental NECR curves as a function of phantom activity are shown in the 'performance comparison' section below. It is meaningless to use activities higher than that corresponding on the abscissa of the NECR peak. The maximum useful true count rate is the ordinate of the NECR peak.

According to Daube-Witherspoon et al.,¹⁷ 'It should be noted that the NEC is a fairly global parameter and does not describe local noise in the image'. This means that other forms of signal to noise ratio could be considered when predicting lesion detectability. In other words, *NECR is no more than an effective count rate*. It gives the trues rate, corresponding to a situation of identical noise if scatter and random were absent. While it is easy to calculate the NECR for cylindrical phantoms, it is less trivial to relate NECR to the injected activity in patients. Theoretical optimization of activity to be injected in patients was performed on the basis of the NECR.²⁵ Comparison of image quality on the basis of the NECR is meaningful only for a fixed scanner, fixed acquisition time, and reconstruction algorithm. More complicated is drawing a conclusion after having compared

NECRs on different scanners. The NECR is not the unique parameter for the final choice of best scanner performance. It affects only the denominator of the contrast to noise ratio. Prolonging the acquisition time always improves the image quality in terms of SNR through the NEC. On the other hand, for example, exceptional count rate capability without spatial resolution would result in poor lesion detectability (low contrast).

This should be said in another way. *The competition between scanner designers focused recently first on improving the scanner count rate performance (i.e. improving patient throughput), mainly to overcome the problems posed by the 3D mode. There is no experimental evidence that these improved count rate performances, obtained passing from 2D to 3D and further passing from 3D BGO to 3D fast crystals, correspond to the expected improvement in lesion detectability, defined as contrast to noise ratio.*

Scatter fraction

Quality control protocols precisely define the method of scatter fraction determination. Numerical values will be reported in the section below regarding scanner comparison. Bear in mind that the tabulated values are valid for 20-cm diameter phantom studies. The actual clinical scatter fraction on the thorax or abdomen is surely higher.

We remark that *the reduction of the high 3D scatter fraction is the second aim of 3D scanner manufacturers after the improvement of NECR.* As values show, only a minor improvement in this field was attained. The obese patient still remains a problem in 3D. One trend of the present research is devoted to optimizing acquisition protocols for such patients.

Lesion detectability

After having been impressed by the rate of production of new models with new crystals, researchers are now addressing the real focal problem in oncology: lesion detectability. Apparently, the current tool for testing it is the NEMA NU 2-2001 ‘image quality test’. This name is rather misleading, since the image quality (IQ) test is a complicated but conventional measure of lesion to background *contrast* in an abdomen phantom: hot spheres are surrounded by activity with a 4:1 or 8:1 concentration ratio. An evaluation of the noise of the background is included. The total activity must be 60 MBq. The presence of activity outside the AFOV is prescribed.

This test is not a signal to noise ratio or, to define it more rigorously, a contrast to noise measurement. It takes into account only the denominator of the contrast to noise ratio. For this reason, IQ evaluation is independent of count rate. So the NEMA IQ test shows some limitation, since various

centers have started to vary the injected activity to be closer to the clinical average situation, but also in order to see the dependence of NEMA ‘image quality’ upon the NECR. However, scatter fraction surely plays a more direct and simpler role. From this point of view, a comparison with the ‘old’ 2D BGO mode is mandatory. Other figures of merit for scanner comparison have been introduced.¹ No data have been published yet.

Another huge topic under research is the influence of data handling and correction and the reconstruction algorithm. ‘Reconstruction can cause image noise to be as much as an order of magnitude higher.’¹⁷ NECR characterizes the acquisition condition without taking into account reconstruction parameters. We believe that a demonstrated answer should be found in order to assure proper patient diagnosis.

Technology past and future

New inorganic scintillation crystals for 3D mode

Intrinsic efficiency

The recent most impressive technological development concerns scintillator crystals. The probability t of photoelectric interaction, i.e. of detecting primary undeflected photons coming from a lesion, depends roughly upon:

$$t \div \rho Z_{\text{eff}}^4 / E_{\gamma}^3 \quad (5)$$

where ρ is the material density (g/cm^3), Z_{eff} is the effective detector atomic number, and E_{γ} is the incident γ energy. For Compton scatter we have:

$$\sigma \div \rho Z_{\text{eff}} / E_{\gamma} \quad (6)$$

For photon energies below pair production ($E_{\gamma} < 1022 \text{ keV}$), the linear attenuation coefficient is:

$$\mu = t + \sigma \quad (7)$$

The attenuation of N_0 impinging photons by a crystal in a single detection is given by:

$$N_{\text{stopped}}(x) = N_0 [1 - \exp(-\mu x)] \quad (8)$$

where x is the crystal radial dimension.

The need for high intrinsic efficiency ϵ_s (ratio of interacting to impinging photons) for single detection:

$$\epsilon_s(x) = N_{\text{stopped}}(x) / N_0 = [1 - \exp(-\mu x)] \quad (9)$$

derives from their high energy. This obliges us to consider inorganic scintillators for their high μ . μ is characteristic of the material, and $\epsilon_s(x)$ additionally, improves with higher detector radial dimension. Note that μ and $\epsilon_s(x)$ include both photoelectric (PE) and Compton interaction in the detector. However, some of the Compton interacting photons are rejected, and equation (9) is the upper limit of real efficiency. The physical parameters of inorganic scintillators are reported in Table 31.6.

The need for high efficiency in detection coincidence is further stressed by the total interaction probability, which is the product of single interactions:

$$\epsilon_{\text{COINCIDENCE}} = \epsilon_s \times \epsilon_s \quad (10)$$

This reduces quadratically the coincidence intrinsic efficiency, i.e. the system sensitivity. This explains why NaI coincidence γ cameras have one-twentieth sensitivity with respect to a BGO scanner. For the same reason, BGO is the best crystal in terms of coincidence intrinsic efficiency (see the μ column in Table 31.6), but the other crystals have values that are not much lower, except NaI. What is special in BGO is its highest 40% PE probability. Unfortunately, photoelectric interaction cannot be sharply distinguished from Compton interaction in the crystal, because of the low BGO energy resolution.

Energy resolution

Energy resolution impacts on the scatter fraction of the scanner.

Scintillation converts one γ photon into thousands of light photons through the decay of excited molecular electron-hole pairs to their ground state. In general emission and absorption visible spectra overlap. Hence, scintillation would be self-absorbed. For this reason, an activating doping element is added (ppm). The activator is usually thallium (Tl) or cerium (Ce) indicated at right of the chemical formula for the scintillator, e.g. NaI(Tl). The excited electrons fall to excited levels of the intermediate doping element and their subsequent fall to the ground state originates a new, visible emission spectrum, which is not absorbed. It is clear that if the doping is not uniform between crystals or within a single crystal, the system or single crystal energy resolution will be degraded. BGO emission and absorption light spectra do not overlap (self-activated scintillator), so it does not need any activator.

Intrinsic crystal energy resolution depends on the number of information carriers N according to the Poisson statistic $1/\sqrt{N}$. It is measured in laboratory conditions with one single crystal at the center of a PMT. This depends on the incident energy, because N , the number of visible photons produced in the crystal, is proportional to the γ -ray energy. So the light yield (column $N_{\text{photon}}/\text{MeV}$ in Table 31.6) plays an indirect role in scatter rejection.

Finally, the transparency to light within the crystal depends on its shape. Crystals used in scanner design are necessarily 20–30 mm thick in radial dimension and 3–5 mm wide in the other dimensions. This deteriorates energy resolution with respect to cubic crystals. The intrinsic crystal energy resolutions in Table 31.6 were measured with 662-keV ^{137}Cs photons on single crystals.

Additional factors influence the system energy resolution. The first of these is the number of information carriers, which initially is the number of light photons. At the entrance to the PMT they are converted into electrons. Here we have the nuclear medicine bottleneck to energy resolution: the photocathode. The number of carriers drops by a factor of five, its quantum efficiency being only 20–30% maximum. Another problem could be the matching between the scintillator emission light spectrum and photocathode absorption spectrum (peaked at visible wavelength around 390–410 nm). The BGO emission spectrum is partly above 500 nm.

Reflection of light at the photocathode is low if the refractive index of the crystal is close to the value for glass of 1.5. BGO is the worst case.

We have already mentioned that, in the block design, the system energy resolution is suboptimal because crystals are in different positions with respect to the photocathode. Flat panel technology seems to overcome the problem only partially (see Table 31.6).

The final component contributing to energy spread is the electronic PMT noise which is, luckily, small. Table 31.6 summarizes energy resolution according to different authors.

Research in photodetectors

The second scanner component after the crystal is the photodetector. Many laboratories are working in this field with the intent of improving both energy and spatial resolution.¹⁶ In this direction we find the position sensitive PMT (PSPMT), but even more promising is the study of the possibility of replacing the PMT with a semiconductor photodetector, i.e. photodiodes (PDs). Good features of the PMT are high gain (10^5), stability, low electronic noise, good linearity, and good scintillator-photocathode spectral matching. Weak points are lower limits in dimension (limit to spatial resolution) and, above all, the low photocathode quantum efficiency (low energy resolution, poor scatter rejection). For these reasons PDs are attractive: they have high quantum efficiency (70%), and possible high spatial resolution in the pixelated shape. Features to be improved are the low gain (1 in simple PD), high noise, and poor spectral match (absorption in the infrared region at 1000 nm).

Photodiodes are grouped into PIN (positive, intrinsic, negative) diodes, avalanche photodiodes (APDs), and

Table 31.6 Physical properties of inorganic scintillators used in human positron emission tomography (PET) scanners or old 'time of flight' prototype scanners

Scintillator	Composition	Density (g/cm ³)	Z _{eff}	1/μ(mm)	Photoelectric probability (%)	N _{photon} /MeV (× 10 ³)	Light yield relative to NaI (%)	λ _{max} (nm)	τ _{scint} (ns)	Crystal time resolution (ps)	Refraction index	Crystal energy resolution ²⁰ 662-keV ¹³⁷ Cs photons (%)	Crystal energy resolution ¹⁶ 511-keV photons (%)	System energy resolution ²⁶ (%)
NaI	NaI:Tl	3.7	51	29.1	17	41	100	410	230		1.85	6.6	8.0	
BGO	Bi ₄ Ge ₃ O ₁₂	7.1	75	10.4	40	9	15	480	300	6000	2.15	10.2	18.0	13
LSO	Lu ₂ SiO ₅ :Ce	7.4	66	11.4	32	30	75	420	40	300	1.82	10.0	7.3 (662)	11
LYSO	(10% Y)	7.1	66	12.0			90		40	450				10
GSO	Gd ₂ SiO ₅ :Ce	6.7	59	14.1	25	8	20	430	60		1.85	8.5	9.0	
BaF ₂	BaF ₂	4.9	53				12	310	0.8		1.49			
CsF	CsF	4.6	53				5	390	4		1.48			
LaBr ₃		5.3	47	21.0			150		35	400				3
LuAP	LuAlO ₃ :Ce	8.3	65	10.5	30	12		365	18	160*	1.94			
										1160 [†]				

*With 1300-keV ⁶⁰Co photons; [†]with 511-keV annihilation photons.Z_{eff}, effective detector atomic number; μ, linear attenuation coefficient; N_{photon}, number of photons; λ_{max}, wavelength of the maximum intensity; τ_{scint}, scintillation time constant.

silicon drift detectors. PIN diodes have 70% quantum efficiency, but unit gain and high noise. They are candidates for small-animal PET. APDs operate at much higher reverse bias than PINs, so their gain is 1000. The noise is again high, and the major impairment is the strong dependence upon temperature: 2.5% of gain variation per °C. Silicon drift detectors show lower quantum efficiency, but low noise, and above all they can be produced as large surfaces. These are candidates for human PET scanners. Prototypes of scintillators with PDs are many (a dozen references in reference 16), and they are usually coupled to LSO. Examples of energy resolution with a CsI(Tl) scintillator using ^{137}Cs (662 keV) are: 6.6% (APD), 7.1% (PMT), and 7.9% (PD). Pixel dimensions range from $1 \times 1 \text{ mm}^2$ to $3 \times 3 \text{ mm}^2$ (good spatial resolution). Time resolution is low with LSO: 2800–4000 picoseconds, but new technologies promise 2000 picoseconds.

Nowadays, PDs outperform PMTs in some features, but not globally. The hope behind PDs is that PMTs were extensively studied for decades and all their possibilities were reached, while the research into semiconductor devices is among the more active. Besides that, photodiode cost is definitely lower.

Detector time response

After the primary γ interaction in a crystal, which can be considered instantaneous, the scintillation light production follows an exponential law in time:

$$\text{scintillation light} = \text{const} \exp(-t/\tau_{\text{scint}}) \quad (11)$$

This is true if late ‘afterglow’ phenomena consequent to crystal or doping imperfection are absent. Any spectrometry detector can be modeled as a simple circuit with a resistor and a capacitor in series. The charge of the capacitor follows the charge collection, and in our case it is characterized by the constant of time τ_{scint} . The tail of the pulse depends upon the circuit time constant RC. This second value is arbitrary, but in order to collect the whole charge must be $RC \gg \tau_{\text{scint}}$, otherwise the capacitor will start to discharge before being completely charged. Moreover, the best energy resolution is attained by collecting the whole charge, i.e. using $RC \gg \tau_{\text{scint}}$. In simpler, other words, the pulse following an interaction is a bi-exponential curve, whose leading edge rises with τ_{scint} and tail decays with RC. Then the scintillation process through τ_{scint} seems to dictate the inferior limit to the system dead time.

Actually, this is not always true, because in some lucky cases it is possible to obtain the timing information by sampling the leading edge before it reaches its top. Unfortunately, this is only possible if the light yield is high.

For instance, in NaI ADAC C-PET, the leading edge is sampled (or ‘clipped’) at 140 nanoseconds with τ_{scint} (NaI) = 230 ns and RC = 240 ns.²⁰ This is not possible with BGO (τ_{scint} = 300 ns, RC = 770 ns). For this reason, BGO shows poor count rate capability in 3D. Its dead time is too long, and it cannot be bypassed due to its low emission of light. This is the reason why faster scintillation crystals were developed: LSO first of all (τ_{scint} = 40 ns) and then GSO (τ_{scint} = 60 ns). LYSO is a light modification of LSO (with yttrium).

A last element must be analyzed, and it is the following. How can be the system timing resolution Δt be less than the coincidence resolution time $\tau = 12$ nanoseconds (BGO) if the signal lasts for 300 + 770 nanoseconds?

The point is that the time resolution is related to the scintillation time constant by the following absolutely fundamental equation (see in reference 16 from reference 27):

$$\Delta t = \tau_{\text{SCINT}}/\text{number scintillation photons} \quad (12)$$

Equation (12) is rarely fulfilled by common crystals. In fact a high light yield (many scintillation photons) usually requires a long scintillation time to be produced. There is only one exception: the LSO crystal. This is the fundamental characteristic which makes LSO unique nowadays. Thanks to its exceptional time resolution, a new generation of commercial PET scanners was born in March 2006: the time-of-flight (TOF) PET scanners.

Summary remarks about scintillators

BGO features are excellent for 2D imaging, showing the highest intrinsic efficiency, but its light yield and consequently its energy resolution are low. The worst BGO parameter is its very low time resolution. Other detectors have been introduced (LSO, GSO, LYSO) with better time resolution, but only LSO and LYSO have been maintained in further technological development. LSO is second in efficiency only to BGO; it gives a high light yield (good energy resolution), and it has a fast scintillation time. Both properties result in excellent time resolution. LSO is the only crystal capable of measuring the time of flight of photons across the ring. Minor drawbacks with LSO are an observed non-linear response with γ energy, differences in energy and time resolution from different batches (probably related to non-identical concentrations of doping Ce), and the presence in the natural lutetium of 2.6% of the radioactive isotope ^{176}Lu (4×10^{10} years half-life), which gives 10 kcps of background count rate in a clinical scanner (not a negligible rate in small-animal PET where low count rates are the rule).

Time-of-flight PET

Time-of-flight PET theory²⁸

In 1966, Anger realized that in coincidence detection, the possibility of determining the exact position of annihilation could be at the basis of a new reconstruction algorithm. It is almost obvious that if we could measure exactly each annihilation position along the propagation line (LOR), no reconstruction would be necessary in order to obtain an image. Such a possibility is now open thanks to the extremely quick response of the new crystals. Note that we are speaking of measuring the difference in arrival times at opposite sides of the detector ring of two photons traveling at the speed of light, $c=300\,000\text{ km/s}$. Unfortunately, present technologies cannot *exactly* determine such an infinitesimal difference, but only approximately. We are facing again a resolution problem, but in terms of time.

Consider now Figure 31.11. A system with an extremely high time resolution (narrow peak), with exactly equal electronic traveling time in the two strands of the chain, with the source exactly at half the distance (point A) between the two crystals, would record coincidences in a very sharp peak in time, positioned at abscissa zero. The peak enlargement (time resolution=FWHM) gives the system uncertainty of measuring the arrival times.

If now the source is moved to the point B, closer to detector D1 by a distance Δx , photons will be detected earlier in detector D1 with an anticipated arrival time of $\Delta t_1 = -\Delta x/c$, while in D2 they will arrive $\Delta t_2 = +\Delta x/c$. The time difference between the two signals is then:

$$\Delta_{\text{arrival time}} = \Delta t_2 - \Delta t_1 = 2\Delta x/c \quad (13)$$

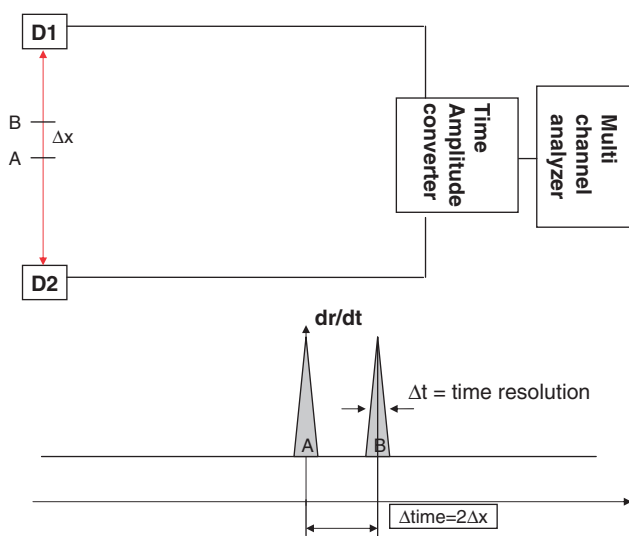


Figure 31.11

Time-of-flight (TOF) coincidence detection with high time resolution.

Table 31.7 Time resolution and annihilation position uncertainty

Time resolution, Δt (ps)	Position uncertainty Δx (cm)	
50	0.75	Reconstruction not necessary Present spatial resolution reached
300	4.5	
500	7.5	
650	9.75	Gemini TF

The factor 2 derives from the fact that one photon gains time and the other loses time by the same amount, $\Delta x/c$.

Now equation (13) is fundamental to understanding TOF. If, instead of an extremely high time resolution Δt , we had a large time uncertainty Δt similar to Figure 31.8, we would not be able to distinguish whether the source is in position A or B, the two peaks being completely overlapped. If Δt becomes smaller but finite, we can reduce the position uncertainty, though without being able to exactly fix a point. Time resolution Δt and the consequent position uncertainty (both as FWHM) are related by equation (13). Table 31.7 reports some examples of values. With 50 picoseconds (50×10^{-12} seconds) time resolution, the reconstruction would be unnecessary, since the position uncertainty would be equal to the present spatial resolution.

TOF improves the signal to noise ratio

Since actual technology cannot reach $\Delta t=50$ ps, what can be the advantage of a time resolution of some hundreds of picoseconds? We have to consider Figure 31.12 and the principle of back projection.

In conventional back projection, the whole activity contained within the volume between a couple of detectors contributes to back projected counts and noise. In TOF reconstruction only a part of that volume contributes to counts, and, most important, to image noise. This is the part confined to the position uncertainty Δx . So, for a uniform cylinder of diameter D , the signal to noise ratio will be approximated by:²⁹

$$\text{SNR}_{\text{TOF}} = \sqrt{\frac{D}{\Delta x}} \text{SNR}_{\text{CONVENTIONAL}} = \sqrt{\frac{2D}{c\Delta t}} \text{SNR}_{\text{CONVENTIONAL}} \quad (14)$$

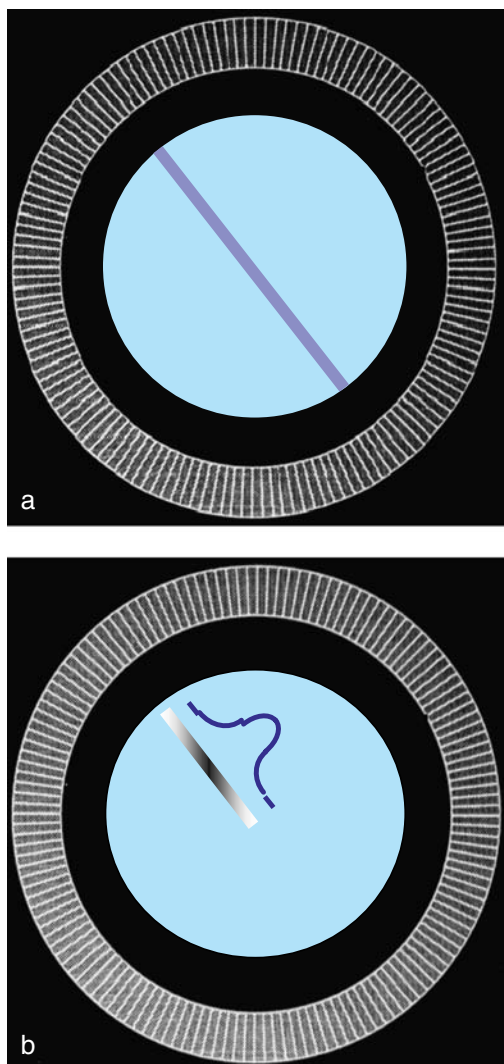


Figure 31.12

Noise reduction by TOF reconstruction. (a) In standard back projection all the voxels along a LOR contribute to the noise. (b) In TOF back projection, only the voxels within the position uncertainty Δx contribute to the noise.

This simple formula indicates that the gain over noise is greater if the time resolution is better (smaller Δt) or, for a fixed Δt (i.e. for a fixed scanner), if the patient is larger. Note that the noise reduction applies also to random and scatter coincidences. In other words, a better time resolution and TOF reconstruction algorithm should increase the NECR peak, and this could be decisive in solving the problem of obese patients in 3D. Figure 31.13 demonstrates the effect.

Old and new technological TOF implementations

A number of PET cameras incorporating TOF were built in the early 1980s and the predicted gains were observed. However, the scintillators used (BaF_2 and CsF) were poor in intrinsic efficiency, having low density and low effective atomic number (see Table 31.6). Their system sensitivity was too low. The TOF PET was abandoned. The recent revolution came from a new crystal, LSO, which in addition to suitable intrinsic efficiency, energy resolution, and fast scintillation time, is characterized by a time resolution of 300 ps under ideal conditions. Other changes in the use of PET required TOF improvement: whole-body oncological studies rather than the brain or heart studies of the 1980s, and 3D mode with a multi-ring system rather than the 2D mode of old scanners with few rings. Other technological advances now allow TOF PET: an improvement in timing performance of PMTs and miniaturization of integrated circuits.

The first experimental confirmation of the TOF noise reduction theory came in 2005.²⁹ Conti et al. implemented TOF reconstruction in the CPS Hi-Rez PET scanner both with 2D filtered back projection and with 3D iterative reconstruction. They adapted and optimized a scanner not conceived for TOF in the most important features (time alignment and scatter correction). A time resolution of 1200 ps was attained. The coincidence window was set at 4.5 ns. Coincidence data were acquired in list mode (interesting results have been obtained regarding the possibility of avoiding list mode data storage.³⁰) Noise was measured as the standard deviation of counts in a cold region in a phantom divided by the mean value in the same region. In a simulated phantom of 40 cm in diameter, an undoubted NECR gain larger than 2 was determined. In a real phantom of 50 cm diameter, 20 cm length, an inner cylinder of 10 cm in diameter with 85% activity concentration with respect to the surroundings became visible only after TOF reconstruction.

The Gemini TF by Philips is the first commercially available scanner designed for time-of-flight PET. The GSO crystal, poor in light yield and consequently with low time resolution (equation (12)), was abandoned for the more suitable LYSO, with 450 ps time resolution. The PMT cathode became a curve instead of being traditionally flat, in order to keep the PMT time resolution of ≈ 100 ps uniform over the photocathode area. New electronics have been developed in order to preserve time resolution with only an additional 100 ps uncertainty. A system time resolution of 650–750 picoseconds is reported.

A second, important innovation is the new stability in electronics, with the current small drift after 70 hours to be compared with the stability of minutes in the 1980s. The time calibration today takes 10 minutes against hours in the 1980s. These are real advances! The amount of collected

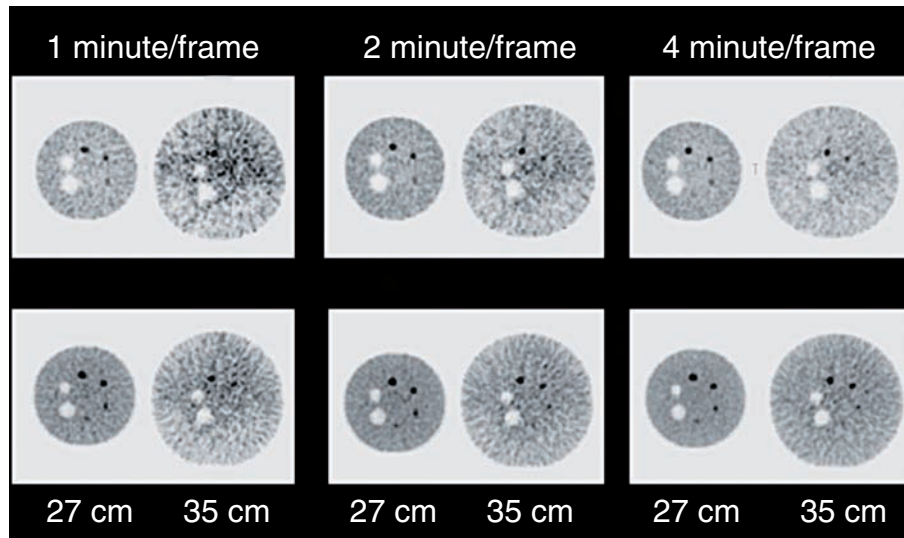


Figure 31.13

Effect of time-of-flight noise reduction on phantom images in a system with 460 picoseconds time resolution. The improvement in image quality is evident in terms of signal to noise ratio passing from not TOF (upper row) to TOF reconstruction (lower row). (Courtesy of Philips Medical Systems.)

data could not be processed in the absence of the tremendous improvement in processor performance. Unique in this feature, Gemini TF employs all the LOR from the detector pairs. Data must be collected in list mode. A RAMLA (row action maximum likelihood approach, see below) iterative algorithm is used for reconstruction by a multiple parallel processor architecture.

The results obtained in phantom studies and the design of a fully dedicated time of flight PET scanner hopefully will dissipate one of the two problems of 3D PET. Obese patient imaging will be sensitively improved by the gain in signal to noise ratio obtained by TOF. Research is going further, looking towards newer crystals for TOF: lanthanum bromide³¹ (see Table 31.6).

Extinct evolution lines

Time passes, causing a natural selection of the systems. The tomograph C-PET with curved NaI crystal 1 in thick is no longer produced by Philips. This should be a clear and interesting sign for those who sustained NaI technology in PET.

Coincidence γ cameras still survive among users thanks to their extremely low prices, but the disappearance of a NaI tomograph with much better performance with respect to coincidence γ cameras should be a strong indication. We remark that coincidence γ cameras are not provided even with random, scatter, or dead time corrections.

Software improvements

We must always keep in mind that tomographic imaging is a sequence of actions starting with acquisition, passing through on-line corrections, and followed by off-line corrections during the reconstruction process. It is clear that image quality depends critically also on this third step, i.e. upon the method of creation of the image starting from the raw data. This remark is necessary because the final lesion detectability could be destroyed by bad reconstruction methods, even starting from the best raw data acquired with a scanner with the highest performances. In this respect, Brasse et al. introduced several figures of merit in order to evaluate image quality.¹ The first, the NEC, applies only to sinograms, i.e. raw data, and does not take into account the reconstruction process. We say again that NEC is only one parameter among many figures which contribute to the imaging process.

Rebinning or fully 3D algorithm

The huge increase of the number of LORs passing from 2D to 3D PET posed data reconstruction problems, which were solved with the shortcut of rearranging 3D data in 2D form, and followed by the use of standard 2D reconstruction algorithms. The simplest method is 'single slice rebinning' (SSRB), in which an event with LOR oblique with respect to the axial direction is assigned to the transaxial

plane corresponding to midway along the LOR segment. This distorts the real activity distribution in the longitudinal direction. Improved but not perfect rebinning methods are multislice rebinning (MSRB) and Fourier rebinning (FORE). Of course, any rebinning method degrades the potential information of the whole set of 3D data.

For this reason, the most recent development in PET reconstruction methods focuses on fully 3D algorithms.

Filtered back projection supplanted by iterative reconstruction methods

Any experienced user of nuclear medicine imaging systems knows that important software improvements took place in recent decades regarding tomographic reconstruction algorithms. It is a fact that iterative methods supplanted filtered back projection (FBP). This possibility derives from a parallel technological improvement in computer performance, since the main obstacle to the use of iterative reconstruction methods is their computational time demand.

The filtered back projection algorithm was born in the CT world and transferred to SPECT, where its application is not optimal because various physical factors do not fulfill the assumptions on which FBP relies: (1) photons do not impinge strictly perpendicular to the crystals; in SPECT the collimator hole sees a cone of activity rather than a line; the resolution degrades with the distance from the crystals; (2) attenuation, (3) scatter, and (4) statistical fluctuations are present. Corrections try to partially compensate such effects. Only 2D methods are possible.

On the other hand, iterative reconstruction methods can more correctly take into account the abovementioned physical effects, which can be modeled in the algorithm, starting from a fully 3D architecture. Flash 3D™ technology is an example of fully 3D iterative (ordered subsets expectation maximization, OSEM) methods with beam modeling and attenuation correction³² implemented by Siemens on new e.soft™ γ camera workstations.

In the FBP, basic principle is to project counts from projection space to the opposite direction along their propagation path. Counts are added to all the image pixels on entire segments over the reconstruction matrix (see Figure 31.12), giving origin to the well known strike artifacts outside the patient contour. Projections of the unknown image x are the starting point of the reconstructed images.

In an iterative reconstruction algorithm, the starting point is a hypothetical image y_0 , which is mathematically projected by a projector operator A simulating the acquisition process, in order to obtain simulated projections g :

$$g = Ay_0 \quad (15)$$

The probability, or 'expectation value', $P(g|x)$ of obtaining the projections g from the real image x is calculated. This probability is then maximized by a mathematical function called maximum likelihood (ML). A new image y_1 is created, which is a better approximation of the real image x . The procedure is then iterated. The maximum likelihood expectation maximization (MLEM) algorithm was introduced in 1992. Its main drawback is the large number of iterations required for convergence, which is the reduction of the difference between the estimated and the real projection data below a fixed threshold. MLEM is time consuming. The greater is the number of iterations, the better is the approximation of the reconstructed image y_n to the target real image x , and the higher is the spatial resolution, and noise. The noise problem is reduced by the so-called 'overiteration + post-filtering' philosophy. The Gaussian smoothing post-filters pose the usual trade-off between noise limitation and loss of resolution.

A reduction of computational time is furnished by a variation of the above method by grouping projections uniformly distributed around the source volume in 'subsets', and with MLEM applied to these subgroups. The resulting OSEM algorithm, introduced in 1994, converges more rapidly and is less time consuming. The number of subsets is suggested to be as large as possible (minimum eight for 64 or 128 projections), but not to exceed one-quarter of the number of views. OSEM is now the most widely used iterative reconstruction method both in SPECT and in PET.

RAMLA (row action maximization likelihood algorithm) works at each step on one row of the system matrix (i.e. it considers one single projection at each step). RAMLA is not an extraordinary innovation, apart from a particular application which considers as a fundamental mathematical entity special functions instead of the commonly used pixels or voxels. The idea is to describe the volume of the patient by a number of 3D partially overlapping functions, radially symmetric, bell shaped, called 'blobs'. These mathematically constitute a 'base' in the object space, i.e. any activity distribution can be described as a linear combination of these functions, in perfect analogy with the possibility in FBP of describing an image as a superimposition of many sine functions in Fourier space. The spatial frequency interval covered by the blobs gives the degree of noise and resolution included in the reconstructed images. RAMLA can be either 2D (rebinning and bidimensional blobs) or 2.5D (rebinning and 3D blobs), or completely 3D (no rebinning, 3D blobs). Philips adopted a fully 3D (without data rebinning) RAMLA algorithm on CT-PET, Allegro, and Gemini PET scanners. They sustain³³ that the use of proper blobs allows a reduction in the image noise without losing resolution, which is the typical problem following the common 3D Gaussian post-filtering (smoothing).

Performance comparison of commercially available scanners

Since the introduction of positron emission tomography (PET) several decades ago, there has been a constant improvement in technology and in physical performance of PET scanners. In particular, in the last 2 years a sudden acceleration of this process took place. The introduction of integrated PET–CT systems, which provide a combination of metabolic and anatomic imaging, further increased this process. On the one hand, CT data provide an attenuation map for the quantification of PET emission data that can be collected rapidly from the patient, reducing the overall duration of the examination, typically from about 45 minutes on a stand-alone 2D PET scanner to about 20 minutes on an integrated 3D system.^{34,35} On the other hand, CT data provide a high-quality anatomical image co-registered with the PET functional image that is fundamental for a correct localization and interpretation of radiotracer concentrations.

Integrated PET–CT scanners became commercially available in 2001.³⁶ Although these systems are more expensive than traditional PET scanners, evidence of their superiority imposed this technology on the market, and nowadays PET–CT examinations are performed in the staging of cancer patients.

This section examines the performance of state-of-the-art PET–CT scanners published in the literature or reported in manufacturers' pamphlets, and compares these performances to those of the corresponding former generation of PET scanners (Discovery ST (GE),^{37,38} Allegro (Philips),³⁹ Biograph (Siemens)).⁴⁰

PET systems

The main requirements in PET oncology are high-contrast detailed imaging to detect subcentimetric lesions accumulating [¹⁸F]fluoro-2-deoxy-D-glucose (FDG). The principal parameters of a PET scanner that account for them are sensitivity, spatial resolution, scatter fraction, noise equivalent count rate, and NEMA NU 2-2001 image quality, which up until now was erroneously considered the most important objective parameter correlated to lesion detectability. To this extent, the characteristics of state-of-the-art PET–CT scanners for principal manufacturers are examined in the following paragraphs, evidencing the improvements in these parameters with respect to the former generation of PET scanners, showing how PET technology has improved, especially in the last 5–10 years.

The three state-of-the-art PET scanners are based on GSO, LSO, and BGO detector crystals. Two of them that use fast detectors, the Biograph Hi-Rez-pico3D (LSO)⁴¹ and Gemini GXL (GSO), choose to have only 3D geometry to

take full advantage of the main characteristics of these detectors. The Discovery STE, with extendable septa, has the possibility of a dual acquisition modality and is based on BGO crystals.

In these scanners, the total number of detector crystals is increased (> 13 000) and multiple full detector rings (24–39 rings) are disposed over 360° around the imaging volume, covering an axial field of view of 15–18 cm, creating 40–90 imaging planes of about 2 mm each.

In the following, a detailed analysis of the characteristics and performance of the latest PET tomographs commercially available is reported.

Spatial resolution

As described previously, crystal dimensions directly influence spatial resolution. In current scanners, the reduction of axial and tangential crystal dimensions (3–6 mm, compared to ~6 mm of the former generation) leads to an overall improvement in spatial resolution of about 1 mm, as can be observed from Table 31.8 and Figure 31.14.

The greatest improvement in spatial resolution is observed for the Hi-Rez-pico3D, even if this tomograph shows the highest dependence on the point of measure in the FOV (coefficient of variation, CV=10.3%). The Discovery STE for both modalities shows a better uniformity of spatial resolution values (CV=8%).

Sensitivity

3D geometry increases the sensitivity about five-fold relative to the 2D modality (8.5 kcps/MBq vs. 2.0 kcps/MBq, for Discovery STE). Among 3D tomographs, the Hi-Rez-pico3D shows the lowest sensitivity (Figure 31.15), which is mainly due to a reduced depth of the detector crystal in the radial direction (20 mm), with respect to Gemini GXL and Discovery STE (30 mm). The highest sensitivity observable for the Discovery STE/3D is mostly due to the use of BGO as detecting material, which is the most efficient crystal at 511 keV.

With respect to the former Philips scanner, the Gemini GXL shows a two-fold increase in sensitivity, mainly due to an important improvement in the electronics of signal processing.

Scatter fraction

The increase in sensitivity deriving from the 3D modality leads to an increase also in the scatter fraction (32–36%)

Table 31.8 State of the art positron emission tomography–computed tomography (PET–CT) scanners: technical parameters (manufacturers' data)

<i>Parameter</i>	<i>Discovery STE, GE</i>	<i>Gemini GXL, Philips</i>	<i>Hi-Rez-pico3D, Siemens</i>
Number of detector rings	24	29*	39
Ring diameter (mm)	886	885	830
Number of individual crystals	13 440	17 864	24 336
Crystal material	BGO	GSO	LSO
Crystal size (mm)	4.7×6.3×30	4×6×30	4×4×20
Number of crystals/ring	560	616	624
PMT number		420	144
Number of crystals/block	—	—	13×13
Acquisition mode	2D/3D	3D	3D
Interplane septa	0.8 mm tungsten, 5.4 cm long	—	—
Energy window width (keV)	375 (2D) 425 (3D)	410–590	425–650
Coincidence window (ns)	11.05 (2D) 9.75 (3D)	7.5	4.5
Transaxial FOV (mm)	70	57.6	58.5
Axial FOV (mm)	15.7	18.0 (physical)	16.2
Number of image planes	47	90	81
Slice thickness (mm)		2	2.0
Patient port diameter (cm)	70	70	70
Axial sampling interval (mm)	3.27	2	2.0

PMT, photomultiplier tube; 2D, two-dimensional; 3D, three-dimensional; FOV, field of view.

*Theoretical ring.

with respect to the 2D mode (9–18%) (Table 31.9 and Figure 31.16). The improvement in energy resolution of the fast crystals (present energy resolution of 15% for 3D Gemini GXL and Siemens Hi-Rez-pico3D, comparable to that of 2D systems) allows an increase in the lower limit of the energy window, and this feature, together with the implementation of accurate and sophisticated algorithms for scatter evaluation and subtraction, reduces the problem. In new systems, indeed, we observe a reduction in the scatter fraction of about 20% with respect to the old ones, as shown in Figure 31.16.

Noise equivalent count rate

Improvements in the parameters described above result in an improvement also in the peak of the noise equivalent

count rate (NECR), an important parameter describing PET count rate performance in relation to the activity present in the field of view. While for 2D systems the NECR increases with increasing activity in the patient (for the clinical range of activities), for the 3D scanners there is a precisely defined value of activity in the FOV which corresponds to the peak in the NECR. This peak position and value depend on the shape of the source. As in 3D mode randoms increase faster with respect to the 2D mode (see above), a limitation of unrelated coincidence events is achieved by using fast electronics with a narrow coincidence window. Figure 31.17 shows the NECR curves for the latest scanners, for which the NECR peak is between 60 and 80 kcps; the square symbols superimposed refer to previous systems.

The abovementioned technological improvements between the last two generations of scanner result in an increase of the NECR peak, which is evident especially for

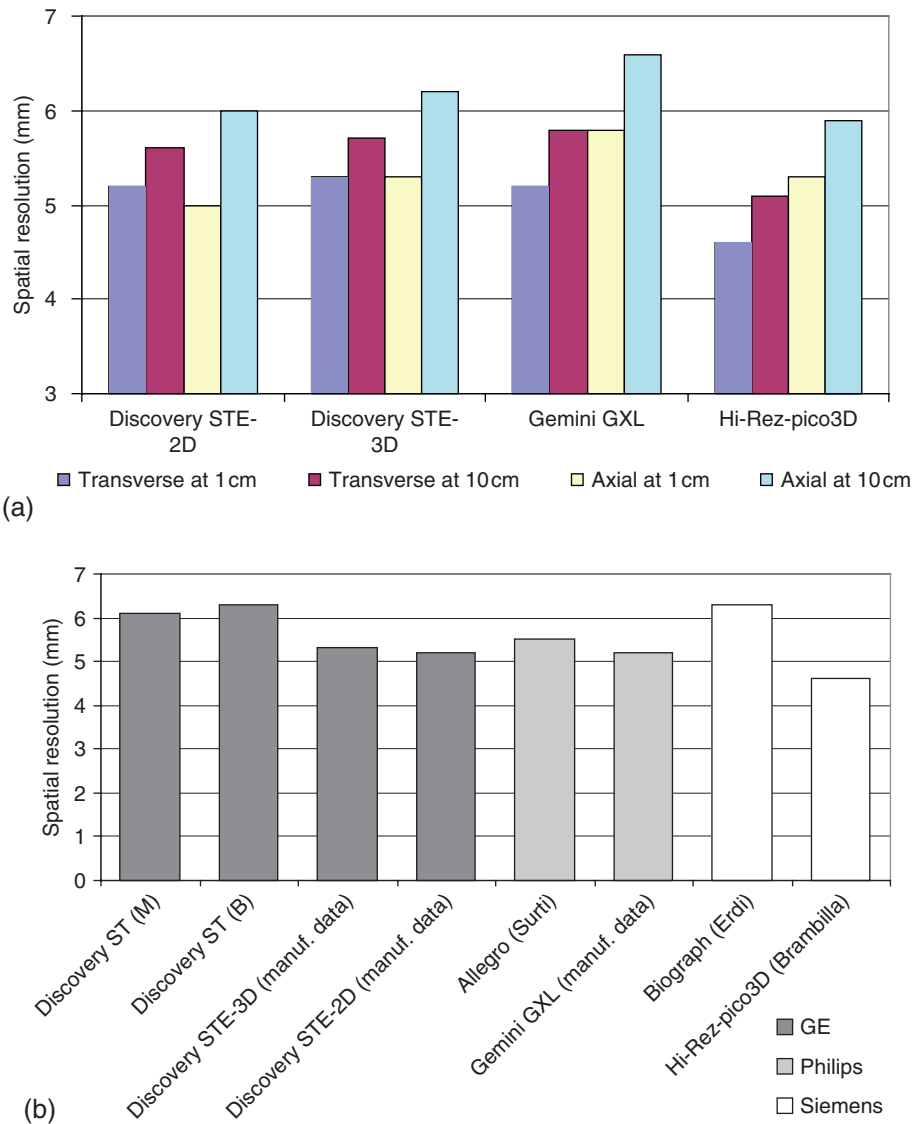


Figure 31.14

(a) Spatial resolution data for Discovery STE (2D and 3D modes), Gemini GXL (manufacturer's data) and Hi-Rez-pico3D.⁴¹

(b) Transverse spatial resolution at 1 cm: comparison between former and latest PET scanner generations.^{37–41} Discovery ST B or M refers to Bettinardi⁴⁰ or Mawllawi⁴¹ data.

Siemens and Philips systems, for which the older NECR curves were fairly low with respect to GE systems. In the Hi-Rez-pico3D, beyond the increase in NECR peak from 44 to about 60 kcps, also a horizontal shift is observable from 15 to 22 kBq/ml. This important improvement in the Siemens scanner is the result of the presence of fast electronics and a narrow coincidence window (4.5 ns) that allow the rejection of 'bad' coincidence events. The difference between GE and other systems is explained by the higher BGO sensitivity.

In the Gemini GXL the increase in NECR peak is more than twice with respect to the Allegro, and the reason

can be found in the improvements in both electronics and the energy window. The Discovery STE shows a limited increase in peak NECR (12%), because the former GE system had already reached an excellent NECR peak value.^{37,38}

Similar considerations apply to the true count rate (curves and data are reported in Figure 31.18). It must be mentioned that the concentration of the trues peak is not the optimal working condition for a scanner, because it neglects the noise influence, which on the other hand is included in the NECR.

Table 31.9 Physical performance of state of the art PET–CT scanners

	<i>Discovery STE, GE*</i>	<i>Gemini GXL, Philips*</i>	<i>Hi-Rez-pico3D, Siemens⁴¹</i>
Transverse spatial resolution at 1 cm (mm)	5.2 (2D) 5.3 (3D)	5.2	4.6
Transverse spatial resolution at 10 cm (mm)	5.6 (2D) 5.7 (3D)	5.8	5.1
Axial spatial resolution at 1 cm (mm)	5.0 (2D) 5.3 (3D)	5.8	5.3
Axial spatial resolution at 1 cm (mm)	6.0 (2D) 6.2 (3D)	6.6	5.9
System sensitivity (kcps/MBq)	2.0 (2D) 8.5 (3D) (average on-axis/10 cm off-axis)	8.0 (center) 8.3 (10 cm off-center)	4.87 (center) 4.97 (10 cm off-center)
Scatter fraction (%)	19 (2D) 36 (3D)	35	33
Energy resolution (%)		15	15
Peak noise equivalent count rate	84 kcps at 49 kBq/ml (2D) 75 kcps at 12 kBq/ml (3D)	55 kcps at 5.3 kBq/ml	58.99 kcps at 21.68 kBq/ml (k=2)
Maximum trues		235 kcps at 5.14 kBq/ml	171 kcps at 17 kBq/ml
Reconstruction algorithm	VUE point iterative reconstruction (ML-OSEM)	2D FBP, 2D OSEM, 2.5D RAMLA, 3D RAMLA	Fourier rebinning (FORE) attenuation, weighted-ordered subsets expectation
Random correction method	Direct from singles and real-time delayed window	Delayed window (160 ns)	Delayed window
Scatter correction method		Single scatter simulation (micro-Monte Carlo) inside 3D LOR algorithm; with 'energy selection'; with 'Background subtraction'	
Adjacent bed overlap (%)	Not given	50	28

*Manufacturers' data.

ML-OSEM, maximum likelihood-ordered subsets expectation maximization; FBP, filtered back projection; RAMLA, row action maximization likelihood algorithm; LOR, line of response.

CT systems

The CT scanners of combined PET–CT systems nowadays are based on a 16-slice spiral tomograph, providing bases for not only attenuation correction of emission [¹⁸F]FDG data but also high-resolution and -contrast images. The use of CT as a transmission source has several advantages over the application of conventional sources such as ⁶⁸Ge or ¹³⁷Cs, among which we must consider higher signal to noise ratio and a reduced acquisition time.

The CT image is a map of attenuation coefficients normally obtained at 120 kV_p that corresponds to a mean X-ray energy of 80 keV. These attenuation coefficients are scaled to 511 keV energy for the three typical materials of body composition, soft tissue, bone, and lung, using dedicated software.

CT examination is performed using submillimeter slice sampling and a variable pitch with fast rotation times (0.4–0.5s) that improve image quality, increasing lesion detectability.

Figure 31.15
Sensitivity in new and old tomographs.³⁷⁻⁴¹

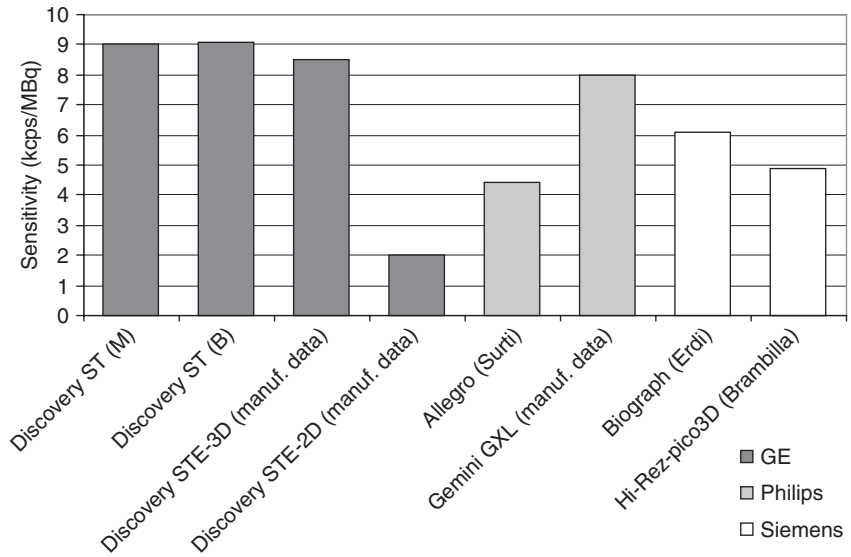


Figure 31.16
Scatter fraction in new and old tomographs.³⁷⁻⁴¹

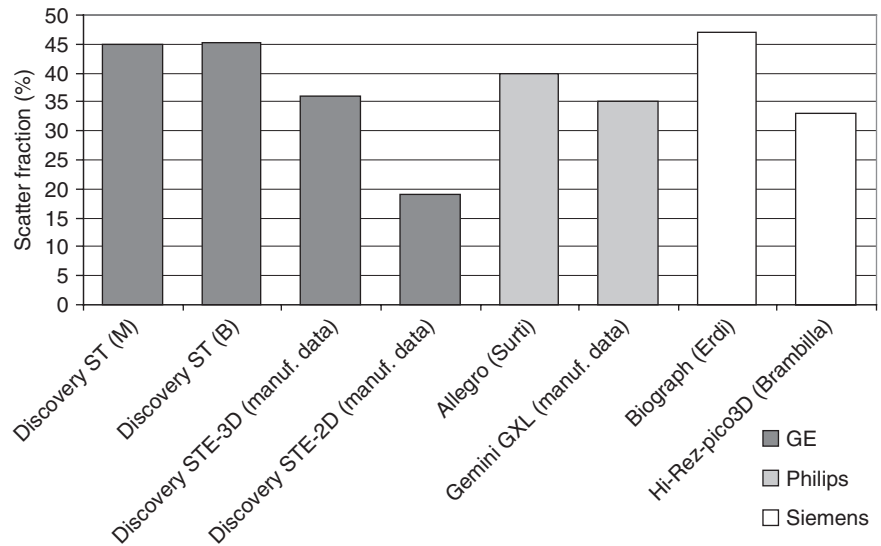
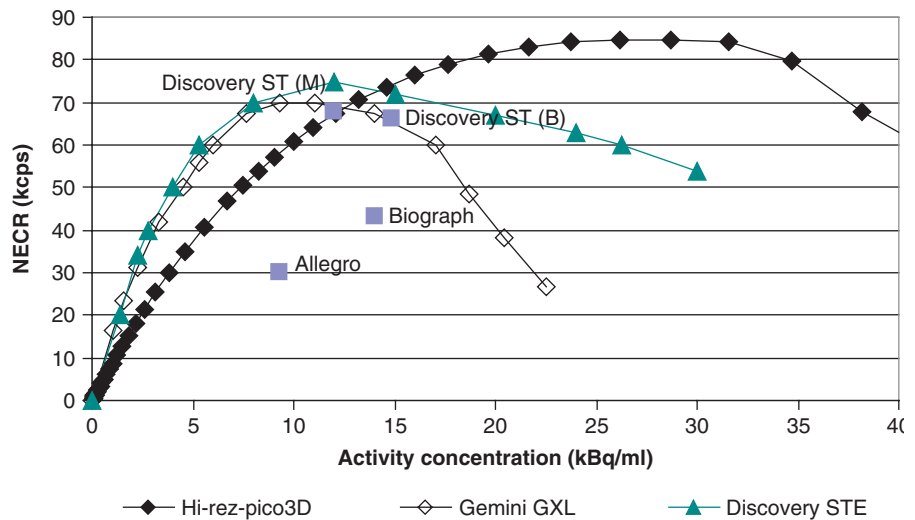
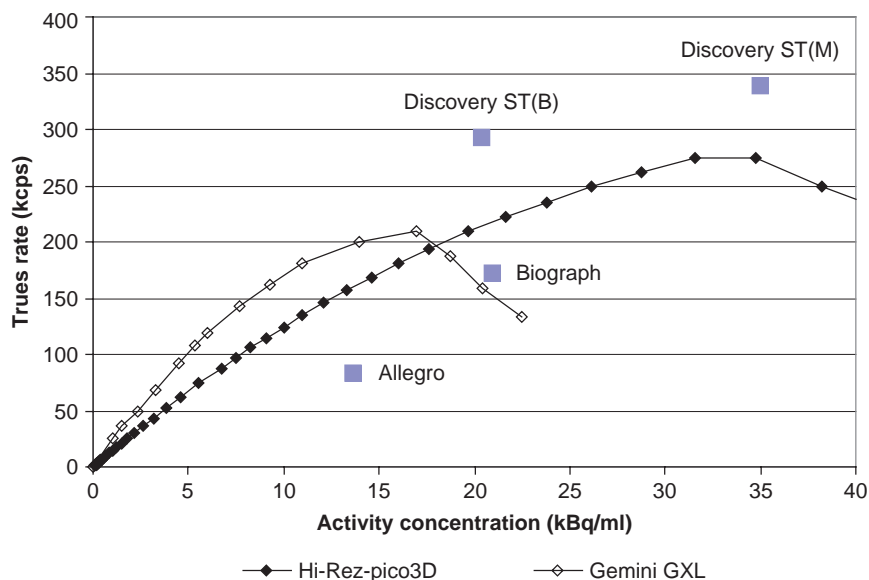


Figure 31.17
Noise equivalent count rate (NECR) curves ($k=1$) for Gemini GXL (manufacturer's data), Discovery STE (manufacturer's data), and Hi-Rez-pico3D.⁴¹ Square symbols refer to the peak NECR of previous-generation scanners.



**Figure 31.18**

True rate vs. activity concentration. Curves are reported for Gemini GXL (manufacturer's data) and Hi-Rez-pico3D⁴¹ (no data supplied by GE). Square symbols refer to the true peak of former-generation systems.

The principal parameters of the CT scanners in modern hybrid PET–CT systems are presented in Table 31.10.

Dedicated PET scanners

The state-of-the-art PET–CT scanners described above are designed to optimize their performance in the study of whole-body imaging. These scanners are used to diagnose and stage several types of tumors. In the case of the breast and the prostate, the distance between these organs and PET detectors (20–30 cm) limits the sensitivity of this technique.

This paragraph describes some dedicated scanners for breast and prostate PET imaging, which at present are not commercialized but represent only prototypes.

Breast cancer

Mammography allows the detection of very small lesions, and nowadays has become the screening modality of choice. However, this technique has a limited sensitivity in the detection of microcalcifications in dense and fibrocystic breasts, and poor specificity in differentiating between malignant and benign lesions.

Dedicated PET systems for breast imaging, positron emitting mammography (PEM) instruments, overcome this limitation, being designed especially for the imaging of this organ.⁴² Normally, PEMs consist of two planar detectors positioned parallel to each other, operating in coincidence. The detectors used can be pixellated BGO crystals⁴³

or arrays of LSO crystals⁴⁴ coupled to position sensitive photomultiplier tubes. One of these systems⁴³ is coupled to a traditional mammography unit and co-registers the [¹⁸F]FDG emission with the X-ray transmission images, allowing valuable information to be obtained about the localization and characterization of suspicious lesions.

Prostate cancer

Dedicated scanners for prostate PET imaging⁴⁵ use two curved detector banks, each composed of 40 conventional block detectors with septa extended to 5 cm to limit scatter and random counts. The banks are positioned above and under the patient, respectively, on the prostate region; they can be tilted and their relative distance can be adjusted in order to maximize sensitivity.

Concluding remarks

The evolution of imaging in oncology is characterized by fast technological steps forward, especially in the PET field. Scanner improvement has occurred mainly in count rate performance, and its impact on noise reduction. The same goals are pursued by the most recent revolution, time-of-flight PET technology.

There is no single figure of merit that summarizes PET scanner performance, since performance ultimately depends on the diagnostic task being performed.⁴⁶ Nonetheless, to provide a common set of metrics that assesses performance

Table 31.10 Technical parameters of CT tomographs (manufacturers' data)

Parameters	Somatom 16, Siemens	Lightspeed 16, GE	Brilliance, Philips
Scan mode	Helical, axial, scout	Helical, axial, scout	Helical, axial, scout
Aperture (cm)	70	70	70
Transverse scan field (cm)	50	50	25, 50
Maximum number of CT slices	16	16	16
Nominal slice width (mm)	0.6, 0.75, 1.0, 1.5, 2.0, 3.0, 4.0, 5.0, 6.0, 7.0, 8.0, 10.0	0.625, 1.25, 2.5, 3.75, 5.0, 7.5, 10	0.6, 0.75, 1.5, 3.0, 4.5, 6.0
Tube voltage (kV)	80, 100, 120, 140	80, 100, 120, 140	90, 120, 140
Tube current (mA)	28–500	10–440; 5 mA increments.	20–500; 1 mA increments
Detector material	Solid state (ultrafast Ceramic, UFC™)		Solid state GOS
Number of elements along z-axis	24	24	6, 10, 16 slices, 24 detectors along z for a total covered length of 24 cm
Total number of detectors	16 128	21 888	16 128
Total effective length of detectors array (mm)	24	24	24
Rotation times (s)/360° rotation	0.42, 0.5, 0.75, 1.0, 1.5	0.5, 0.6, 0.7, 0.8, 0.9, 1.0, 2.0, 3.0, 4.0	0.4, 0.5, 0.75, 1.0, 1.5, 2.0
Pitch factor (volume pitch)	0.5–2.0 (1–20)	0.5625, 0.9375, 1.375, 1.75	0.13–1.7 continuously
Spiral scan time (s)	100		
Helical interpolation algorithms available	AMPR (adaptive multi-plane reconstruction)		
Heat capacity (MHU)	5.3		8.0
Maximum power (kW)	60	53.2	60
Focal spot (mm)	0.5 × 0.7/7° 0.8 × 1.2/8°	0.7 × 0.6 0.9 × 0.9	Large: 1.0 × 1.0 Small: 0.5 × 1.0
GOS, gadolinium oxysulfide.			

of PET scanners, the National Electrical Manufacturers Association (NEMA) introduced in the NU 2-2001 standard,²² among other tests already present in the 1994 standard (spatial resolution, sensitivity, scatter fraction, and count rate performances), an 'image quality' test, in which contrast recovery and background variability are assessed for a standardized situation, which is supposed to simulate a clinical imaging condition.

It must be stressed that inferences regarding lesion detectability in a patient cannot be directly extrapolated from such a test, which is subject to many limitations. For instance, the counting rate characteristics of the phantom used in the NEMA standard, at a given activity concentration, are not similar to those found in patients, probably as a result of the higher concentration of activity in the

scanner field of view and lower attenuation than in patients.⁴⁰ Moreover, a single activity concentration is unlikely to represent the wide range of activity concentrations that may be found in patients as a result of the different activity administration schemes adopted in clinical practice. Still more relevant, several groups have previously shown that visualizing a lesion in a uniform background when the location is known (as is the case with the IEC phantom) is much easier than detecting a lesion of unknown location in a heterogeneous background.⁴⁷

Lesion detection can be assessed using human observers (i.e. receiver operating characteristic (ROC), localization receiver operating characteristic (LROC), alternative free-response receiver operating characteristic (AFROC) studies), numerical observers (non-prewhitening matched filters,

channelized Hotelling observers), or, more theoretically, sound figures of merit (i.e. contrast to noise ratio), and requires a large number of studies (human observers), multiple noise realization (numerical observers), or anthropomorphic phantoms in order to assess the ability to detect a lesion in a heterogeneous background, as is the case in a patient study.^{46–51}

The front lines of actual research focus on the dependence of lesion detectability on the scanner structure, reconstruction algorithm, injected activities, and scan duration.

References

1. Brasse D, Kinahan PE, Lartzien C et al. Correction methods for random coincidences in fully 3D whole body PET: impact on data and image quality. *J Nucl Med* 2005; 46: 859–67.
2. Cherry SR, Sorenson JA, Phelps ME. *Physics in Nuclear Medicine*. Saunders, 2003.
3. Webb S. *The Physics of Medical Imaging*. Bristol: Institute of Physics Publishing, 1993.
4. Formiconi AR, Gunter DL, Vanzi E. A design strategy for suppression of hole pattern artifacts in high energy collimators. *IEEE Trans Nuc Sci* 2007; 53: 1179–87.
5. Ferrer L, Delpon G, Lisbona A, Bardies M. Dosimetric impact of correcting count losses due to deadtime in clinical radioimmunotherapy trials involving iodine-131 scintigraphy. *Cancer Biother Radiopharm* 2003; 18: 117–240.
6. Devous MD. Instrumentation, radiopharmaceuticals, and technical factors. In: Van Heertum RL, Tikofsky RS, eds. *Functional Cerebral SPECT and PET Imaging*, 3rd edn. Baltimore: Lippincott Williams & Wilkins, 2000.
7. Chang LT. A method for attenuation correction in radionuclide computed tomography. *IEEE Trans Nucl Sci* 1978; 25: 638–43.
8. Bailey D. Transmission scanning in emission tomography. *Eur J Nucl Med* 1998; 25: 774–87.
9. Rogers WL, Clinthorne NH, Shao L et al. SPRINT II: a second-generation single-photon ring tomograph. *IEEE Trans Med Imaging* 1988; 7: 291–7.
10. Genna SG, Smith AP. The development of ASPECT, an annular single crystal brain camera for high efficiency SPECT. *IEEE Trans Nucl Sci* 1988; 35: 654–8.
11. Rowe RK, Aarsvold NJ, Barrett HH et al. A stationary hemispherical SPECT imager for three-dimensional brain imaging. *J Nucl Med* 1993; 34: 474–80.
12. Rohe RC, Valentine JD. An energy-subtraction Compton scatter camera design for in vivo medical imaging of radiopharmaceuticals. *IEEE Trans Nucl Sci* 1996; 43: 3256–63.
13. Meier D, Czermak A, Jalocha P et al. Silicon detector for a Compton camera in nuclear medicine imaging. Presented at IEEE Nuclear Science Symposium and Medical Imaging Conference, Lyon, France, 2000.
14. Yang Y, Gono Y, Motomura S et al. A Compton camera for multitracer imaging. *IEEE Trans Nucl Sci* 2001; 48: 656–61.
15. LeBlanc JW, Bai X, Clinthorne NH et al. ^{99m}Tc Imaging Performance of the C-SPRINT Compton Camera. Nuclear Science Symposium Conference Record, IEEE 1999; 1: 545–52.
16. Humm JL, Rosenfeld A, Del Guerra A. From PET detectors to PET scanners. *Eur J Nucl Med Mol Imaging* 2003; 30: 1574–97.
17. Daube-Witherspoon M, Zubal GI, Karp JS. Development in instrumentation for emission computer tomography. *Semin Nucl Med* 2003; 33: 28–41.
18. Zanzonico P. Positron emission tomography: a review of basic principles, scanner design and performance, and current systems. *Semin Nucl Med* 2004; 34: 87–111.
19. Knoll GF. *Radiation Detection and Measurement*. John Wiley & Sons.
20. Muehlethner G, Karp JS, Surti S. Design consideration for PET scanners. *Q J Nucl Med* 2002; 46: 16–23.
21. IEC 61675-11998 Radionuclide imaging devices – Characteristics and test conditions – Part 1: positron emission tomographs. Geneva: IEC, 1998.
22. NEMA Standard publication NU 2-2001: performance measurement of positron emission tomographs. Washington, DC: National Electrical Manufacturers Association (NEMA), 2001.
23. ICRU report 54. Medical imaging – The assessment of image quality. Bethesda MD: International Commission on Radiation Units and Measurements, 1996.
24. Strother SC, Casey ME, Hoffmann EJ. Measuring PET scanner sensitivity: relating count rate to image signal-to-noise ratios using noise equivalent counts. *IEEE Trans Nucl Sci* 1990; 37: 783–8.
25. Lartzien C, Comtat C, Trebossen R et al. Optimization of the injected dose based on noise equivalent count (NEC) rates for 2D and 3D whole body PET. *J Nucl Med* 2002; 43: 1268–78.
26. Photonic Materials web site. As reported by Maniawsky J. *TruFlight PET Technology*, Philips XNGT-0210056 Rev A, 2005.
27. Balcerzyk M, Moszinsky M, Kapusta M, Szawlowski M. Timing properties of LuAP: Ce studies with large area avalanche photodiodes. *IEEE Trans Nucl Sci* 2001; 48: 2344–7.
28. Moses W. Time of flight PET revisited. *IEEE Trans Nucl Sci* 2003; 50: 1325–30.
29. Conti M, Bendriem B, Casey M et al. First experimental results of time-of-flight reconstruction on an LSO PET scanner. *Phys Med Biol* 2005; 50: 4507–26.
30. Vandenberghe S, Daube-Whiterspoon ME, Lewitt RM, Karp JS. Fast reconstruction of 3D time-of-flight PET data by axial rebinning and transverse mashing. *Phys Med Biol* 2006; 51: 1603–21.
31. Karp et al. Characterization of a TOF PET scanner based on lanthanum bromide. MIC Conference Record, Philips Research, Briarcliff, NY, 2005.
32. Vija H, Hawman EG, Engdahl JC. Analysis of a SPECT OSEM reconstruction method with 3D beam modelling and optional attenuation correction: phantom studies. *IEEE Trans Nucl Sci* 2003; 50: 2662–6.
33. Daube-Witherspoon ME, Matej S, Karp JS, Lewitt RM. Application of the row action maximum likelihood algorithm with spherical basis functions to clinical PET imaging. *IEEE Trans Nucl Sci* 2001; 48: 24–30.
34. Beyer T. Acquisition protocol considerations for combined PET/CT imaging. *J Nucl Med* 2004; 45 (Suppl 1): 25S–35S.
35. Townsend DW. PET/CT today and tomorrow. *J Nucl Med* 2004; 45 (Suppl 1): 4S–14S.

36. Siegel BA. Oncologic PET/CT: current status and controversies. *Eur Radiol* 2005; 15 (Suppl 4): D127–32.
37. Bettinardi V, Danna M, Savi A et al. Performance evaluation of the new whole-body PET/CT scanner: Discovery ST. *Eur J Nucl Med Mol Imaging* 2004; 31: 867–81.
38. Mawlawi O, Podoloff DA, Kohlmeyer S et al. Performance characteristics of a newly developed PET/CT scanner using NEMA standards in 2D and 3D modes. *J Nucl Med* 2004; 45: 1734–42.
39. Surti S, Karp JS. Imaging characteristics of a 3-dimensional GSO whole-body PET camera. *J Nucl Med* 2004; 45: 1040–9.
40. Erdi YE, Nehmeh SA, Mulnix T, Humm J, Watson CC. PET performance measurements for an LSO-based combined PET/TC scanner using the National Electrical Manufacturers Association NU 2-2001 standard. *J Nucl Med* 2004; 45: 813–21.
41. Brambilla M, Secco C, Dominiotto M et al. Performance characteristics obtained for a new 3-dimensional lutetium oxyorthosilicate-based whole-body PET/CT scanner with the National Electrical Manufacturers Association NU 2-2001 Standard. *J Nucl Med* 2005; 46: 2083–91.
42. Freifelder R, Karp JS. Dedicated PET scanners for breast imaging. *Phys Med Biol* 1997; 42: 2463–80.
43. Bergman AM. Technique to obtain positron emission mammography images in registration with x-ray mammograms. *Med Phys* 1998; 25: 2119–29.
44. Doshi NK, Shao Y, Silverman RW, Cherry SR. Design and evaluation of an LSO PET detector for breast cancer imaging. *Med Phys* 2000; 27: 1535–43.
45. Huber J, Derenzo SE, Qi J et al. Conceptual design of a compact positron tomograph for prostate imaging. *IEEE Trans Nucl Sci* 2001; 48: 1506–11.
46. Fruruie SS, Herman GT, Narayan TK, Kinahan PE, Karp JS, Lewitt RM, and Matej S. A methodology for testing for statistically significant differences between fully 3D PET reconstruction algorithms. *Phys Med Biol* 1994; 39: 341–354.
47. Lartizien C, Kinahan PE, and Comtat C. Volumetric model and human observer comparison of tumor detection for whole-body PET. *Academic Radiol* 2004; 11: 637–648.
48. Farquhar TH, Llacer J, Sayre J, Tai Y, and Hoffman EJ. ROC and LROC analyses of the effects of lesion contrast, size and signal-to-noise ratio on detectability in PET images. *J Nucl Med* 2000; 41: 745–754.
49. Cheng PM, Kinahan PE, Comtat C, Kim JS, Lartizien C, and Lewellen TK. Effect of scan duration on lesion detectability in PET oncology imaging. In: 2004 IEEE International Symposium on Biomedical Imaging, Arlington, VA, USA April 15–18, IEEE 2004.
50. Raylman R, Kison PV, and Wahl RL. Capabilities of two- and three-dimensional FGD-PET for detecting small lesions and lymph nodes in the upper torso: a dynamic phantom study. *Eur J Nucl Med* 1999; 26: 39–45.
51. Everaert H, Vanhove C, Lahoutte T, Muylle K, Caveliers V, Bossuyt A, Franken PR. Optimal dose of 18F-FDG required for whole-body PET using an LSO PET camera. *Eur J Nucl Med Mol Imaging* 2003; 30: 1615–1619.

Nuclear medicine-guided radiotherapy

Diano Salvo, Annibale Versari, Cinzia Iotti, and Marta Paiusco

Background

Radiation therapy (RT) plays a very important role in cancer treatment. About 50% of patients with cancer, during the course of their lives, receive radiation treatment, with curative intent (with or without chemotherapy) in at least 30% of cases.

The main goal of radical radiation therapy is local control of the tumor, with preservation of the functional status and a satisfying quality of life. This means delivering a high tumoricidal dose to the target volume while minimizing the dose to the adjacent healthy tissues. In the past, the major constraints to the uncomplicated cure of cancer were the poor anatomical knowledge of the volumes to be irradiated and the possibility of delivering an effective dose to the tumor without exciting the tolerance of the surrounding tissue. However, in recent decades radiation therapy technology has witnessed an extraordinary evolution. The introduction of computed tomography (CT) imaging into treatment planning (in the late 1970s) combined with the later development of fast computers and new planning and delivery techniques has led to highly tailored dose distribution around three-dimensional (3D) targets of any shape with steep gradients falling away from them. The paradigmatic term for these advanced techniques is intensity modulated radiation therapy (IMRT). IMRT is the delivery of a non-uniform intensity of radiation to produce a non-uniform absorbed dose to satisfy, as much as possible, fixed goals. The first advantage allowed by this approach is a more precise and conformal dose distribution around concave surfaces and invaginations of the tumor volume, with a very rapid dose decrease at its periphery. This allows dose escalation without the concomitant increasing risk of radio-induced injury to normal tissue, or reduced toxicity for treatment with conventional doses. Furthermore, IMRT permits the shift from multifractionated radiotherapy to hypofractionated radiotherapy (radiosurgery). Actually, it is assumed that the high-fraction dose is more effective on the tumor while improving protection of the healthy tissue. Another attractive characteristic of IMRT is the possibility to deliver different dose levels to multiple targets simultaneously. This means delivering, with the same plan

and during the same session, lower prophylactic doses to regions at risk of subclinical disease and higher doses to the macroscopic tumor, and also to boost parts of the tumor regarded as more radioresistant. In other words, it is possible to produce a controlled non-homogeneous dose distribution inside the target (dose painting).

The expected clinical result of these new high-precision techniques is an improvement of local control rate of the tumor, and hence the survival probability of the patient, with the lowest possible risk of acute and late toxicity. The advances in radiotherapy techniques require equivalent progress in the use of imaging in treatment planning. Unless there is a comparable level of precision in definition of the disease extent and localization, any benefit expected from the new techniques can be lost. It is now recognized that cancer is not a homogeneous ensemble of cells with similar attributes, but that it contains areas responding to treatment variously, because of hypoxia, intrinsic resistance to X-ray damage, high proliferation rate, high aggressiveness, and so on. The ability of IMRT to 'sculpt' the dose around different target volumes is a spur for the identification of multiple aspects of the tumor, in order to treat them differently.

Thus, the main need of the radiation oncologist is knowledge of the distribution and extent of the disease, in order to avoid missing the tumor, with consequent reduction of local control probability, and, on the other hand, avoiding the unjustified irradiation of healthy tissue, leading to unacceptable side-effects. Furthermore, correct definition of the disease stage is mandatory for selection of the most appropriate therapeutic strategy and intent. The other very important need for the radiation oncologist is the knowledge of the tumor and tissue biological characteristics, which could affect the response to radiotherapy, and so be useful for optimized and personalized treatment strategy planning.

Modern radiation therapy

The advance of new technology has had a significant impact on the practice of radiotherapy and has improved

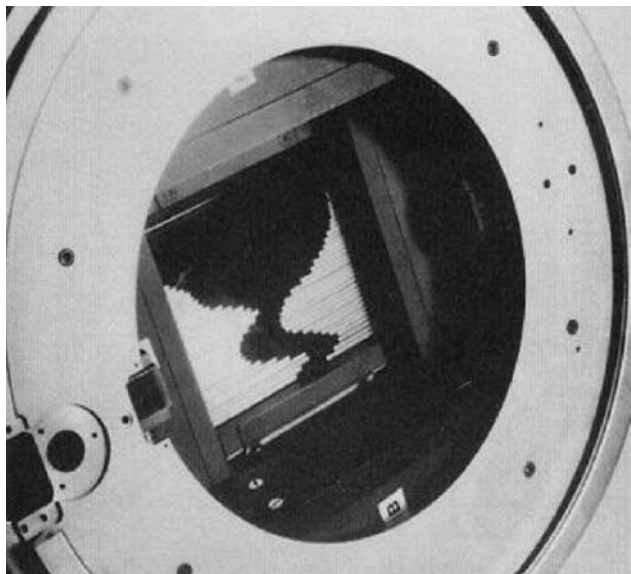


Figure 32.1
A multileaf collimator.

its therapeutic efficacy. Development of the computer controlled multileaf collimator (MLC) system has been one of the main technical advances in the past decade.^{1,2} The MLC is quite a standard feature in the medical linear accelerator (linac). It is an intensity modulator consisting of 20–60 pairs of movable leaves (Figure 32.1). The first application of the MLC is to replace conventional blocking with a more practical method, to conform the geometrical shape of the field to the planning target volume (PTV). This led in the 1990s to the concept of conformal radiotherapy, in which the high-dose volume is tailored to the PTV, trying to spare the organs at risk (OAR).³

Actually, the major advantage of the MLC is to make IMRT clinically practical.

IMRT is considered one of the most significant technological breakthroughs in cancer treatment. In IMRT, instead of a single large radiation beam passing through the body, the radiation, thanks to MLC, is broken up into thousands of tiny pencil-thin radiation beams, each with different intensity. This results in a high dosage to the tumor with high gradients on its edges, lowering the dose to the adjacent sensitive structures. The IMRT delivery approach can be static or rotational.

Static IMRT delivery

In static (cone beam) IMRT, a standard MLC is used to modulate the fluence of a fixed gantry field. There are two methods of modulating beam intensity: the ‘segmental IMRT’ and ‘dynamic IMRT’. In the first mechanism, also

called ‘step and shoot’ (S&S), the shape of the field is constant during irradiation and changes while the beam is off. Superimposing a series of segments of uniform intensity produces a non-uniform pattern of fluence. In dynamic IMRT, leaves are instructed to move during the entire irradiation time. To date, the most common mechanism used has been the sliding window modality, where the MLC leaf pair defines a gap sweeping across the target volume with various velocities to create the modulation.

Rotational IMRT delivery

The rotational modality includes a fan beam technique such as tomotherapy and the IMAT (intensity modulated arc therapy) technique, using a standard dynamic MLC.^{1,2,4,5}

Tomotherapy is a modality inspired by the tomography technique. The IMRT is delivered through a narrow slit while the gantry is rotating. The first commercially available system is known as serial tomotherapy, as it employs a slice-by-slice beam delivery where a binary beam modulator produces modulation of the beam intensity. The intensity modulating collimator consists of two banks of 20 leaves, and is mounted on the gantry of the linear accelerator. While the gantry rotates around the patient and the beam is on, the binary modulator opens and closes with an electropneumatic action. Originally, the couch had to be moved after every slice of treatment, but recently an autocrane system has been introduced to move the table automatically to the next index. The newer tomotherapy machine is called TomoTherapy Hi-Art System® (Figure 32.2a). Essentially it is a marriage of two types of technology: spiral CT scanning and intensity modulated radiation therapy. As with a CT scanner, the patient moves through the gantry while a 6-MV X-ray spirally rotates around him. The binary modulator used has 64 leaves. These are pneumatically driven in and out of the radiation, and the opening patterns, which change as a function of the gantry position, modulate the beam.

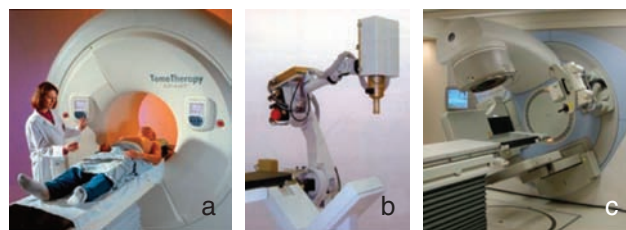


Figure 32.2
Modern devices for radiotherapy delivery: (a) TomoTherapy® Hi-Art System®; (b) Cyber Knife®; (c) linear accelerator with kV and MV conebeam computed tomography (CT).

An important feature of the TomoTherapy Hi-Art is the on-board detector system that allows the acquisition of megavoltage computed tomography (MVCT) images prior to treatment. These images may be used for patient positioning and to compare the actual delivered dose to the planned one. This, in principle, makes it possible to adapt the treatment according to the displacements.

IMAT is a technique employing a conventional accelerator (Figure 32.2c). While the gantry rotates, the dynamic MLC moves continuously, changing the shape of the field. Multiple overlapping arcs, each with a different set of field shapes, create the intensity modulation.

CyberKnife®

A robotic linear accelerator has been proposed as a treatment device delivering the IMRT plan: the CyberKnife® (Figure 32.2b).^{1,2} The system consists of a compact 6-MV linear accelerator assembled on a computer controlled robotic arm. The CyberKnife system's image guidance technology is capable of tracking the skeletal and lesion orientations throughout the treatment process. It correlates live radiographic images with preoperative CT scans to determine patient and tumor position repeatedly during the course of treatment. The imaging information is transferred from the computer's operating system to the robot so that it may compensate for any changes in patient position by repositioning the linac.

The main advantages of the CyberKnife are the huge degrees of freedom, improving conformity for irregularly shaped volumes, and the rotational X-ray (RX) image guidance system that makes adaptive radiotherapy possible.

Adaptive radiotherapy is a new standard in treatment delivery. Linac machines are now equipped with cone beam CT able to generate MV or KV images of the patient in the treatment position. Software, merging a reference CT with the daily image, calculates how much the couch needs to be moved to align the planned isocenter with the beam. This is a new integrated technology that performs as a fully automated patient positioning system for more accurate tumor targeting. The goal of cone beam CT is the possibility of identifying the exact location of the organ before radiotherapy to adapt the treatment, or dose distribution, to the patient, fraction by fraction. However, due to internal organ motion and patient positioning differences, the tumor can move both during a radiation treatment session and from one treatment session to another. Because of these changes the tumor could move out of the prescribed treatment range and might not receive the planned amount of radiation, or normal tissues may receive more radiation than they can tolerate. One way to overcome this problem is to minimize the motion. A great effort is now being directed towards the control of breathing movement.

To reach this goal, a respiratory gating system has been developed.⁶ An infrared marker is set on the abdomen of the patient while an infrared video camera, attached to the CT ceiling, is used to detect respiratory motion and to trigger the CT scan. Normally, the system is gated to only one tidal cycle phase, mainly the exhalation one. It means that a CT scan is acquired only when the respiratory motion amplitude detected by the camera is correlated to the exhalation phase. This would reasonably guarantee that the tumor would be in the same position for every scan. By carrying out a 3D-CT study synchronized to a respiratory phase we are indeed acquiring a 4D-study, the fourth dimension being time. At the treatment machines, thanks to the same infrared system, the radiation beam will be turned on only when the patient is in the same phase of the respiratory cycle and, probably, the tumor in the same position as planned on the 4D-CT scan.

Positron emission tomography imaging in radiation therapy planning

Rationale

CT is still the gold standard for radiotherapy planning (RTP) for a variety of reasons, ranging from its spatial reliability to the availability of tissue density information for dose calculation. Nevertheless, morphologic imaging is often unable to define in detail the tumor extent and its characteristics. The recent development of biologic imaging allows additional information, about both cancer and healthy tissues. The expression 'biologic' embraces metabolic, biochemical, physiologic and functional classes of images, and also molecular, genotypic, and phenotypic ones.

Nuclear medicine, with positron emission tomography (PET) and single photon emission computed tomography (SPECT), can offer significant contributions to define the volume of interest in treatment planning (Figure 32.3). In addition, this technology is easily upgradable with the use of different radiotracers. Thanks to technology progress, biological imaging can be fused and registered with CT and magnetic resonance imaging (MRI) and then incorporated into radiation treatment planning for a better definition of the target volumes.

The terminology for the target volumes in radiotherapy includes three main concepts: GTV, CTV, and PTV.⁷ The GTV (gross tumor volume) represents the macroscopic, demonstrable disease, including the primary site and all other nodal and/or distant localizations. The CTV (clinical target volume) contains the GTV plus any regions estimated to be at risk of subclinical disease (e.g. locoregional

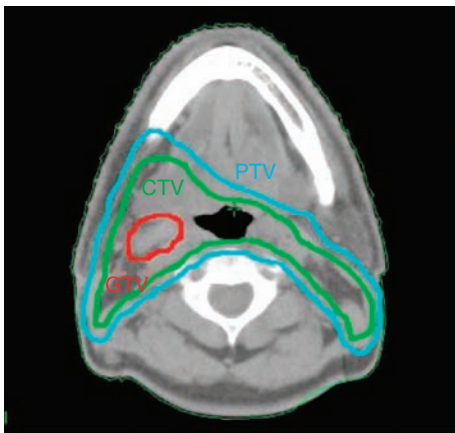


Figure 32.3

The target volumes for radiation therapy. The GTV (gross tumor volume) is shown in red, representing macroscopic visible disease. In light green is the CTV (clinical target volume), i.e. the region adjacent to gross tumor and the lymph node areas at risk of occult disease. In cyan, is the PTV (planning target volume), the three-dimensional (3D) expansion to CTV accounting for geometric uncertainties.

lymph nodal areas). The addition to the CTV of a margin accounting for geometric uncertainties (set-up errors and organ motion) generates the PTV (planning target volume). The introduction of functional imaging to treatment planning leads to the definition of a new target concept, the biological target volume (BTV).⁸ The BTV is not a substitute for CT-based volumes. Depending on the radiotracer used, the BTV expresses different functional properties of the tumor that can be variously considered in the treatment design. Bentzen defined ‘theragnostic’ imaging as the multimodality imaging employed as a guide to design the highest dose spots in the context of the tumor. In substance, the difference between this new concept and diagnostic imaging is that it provides information to determine how and not purely where radiation therapy should be delivered.⁹ Furthermore, attention can be focused on the functional aspects and importance of the healthy tissue, so as to reduce radioinduced damage. In conclusion, the use of multimodal imaging can lead to personalized radiation therapy, biologically optimized for the individual patient instead of the population of patients. The expected clinical result of such an approach is improvement of the locoregional control, and subsequently of survival, with the lowest possible risk of severe iatrogenic complications.

The first goal of the inclusion of functional imaging in treatment planning is to improve the cancer staging and to help the physician in identification of the tumor volume, using anatomical imaging as a frame for the dose calculation.

The inclusion of fluoro-2-deoxy-D-glucose (FDG)-PET in RTP, because of the improvement in cancer staging, may have significant effects.^{10,11} The impact of PET on target

delineation is related to the accuracy of the study (sensitivity and specificity) for the type of tumor to be treated. The way in which the treatment planning is affected by PET hinges on the radiation oncologist’s goal. If missing the tumor is the major concern, sensitivity is the attribute required, and the interpretation criteria should be stringent. On the other hand, if the purpose is healthy tissue protection and, thus, its exclusion from the high dose volume, specificity is the most important quality demanded.¹²

Another advantage provided by PET–CT image co-registration is a reduction of the interobserver variability in target delineation, especially among practitioners less expert in imaging.¹³

However, in addition to the benefit in definition of the PTV, the most promising use of multimodality imaging is the characterization of biochemical and physiological features of the tumor, providing a guide for the delineation of tumor subvolumes to be boosted. In this context, the benefit offered by multimodal imaging makes the ideal match with IMRT, because of its particular ability to paint the dose close to selected volumes. For example, if the uptake intensity of FDG is related to tumor burden, the IMRT plan can be designed to deliver an additional dose in this area, to maximize the local control probability.

While dose escalation in metabolically active areas is still experimental, the use of FDG-PET for more precise and accurate localization of the disease has entered into clinical use, at least for specified solid cancer types.

A further possibility offered by functional imaging is prediction of the responsiveness to radiotherapy during the early phase of treatment. Monitoring the reduction of FDG uptake or standardized uptake value (SUV) variation can allow the treatment optimization and correction of the original strategy. Another possible role of nuclear medicine in RT planning regards the definition of healthy tissue to be spared, instead of tumor volume delineation. More exactly, SPECT imaging can allow the identification of non-functional tissue and thus guide the beam set-up.

The use of multimodal imaging in radiation treatment planning implies several successive steps. First, image fusion, that is the transfer of information from one study to another. The second step is image co-registration, the correct spatial mapping of corresponding points of the images. The third step is delineation of the volume of pathologic tracer uptake. In fact, unlike the nuclear physician who makes his analysis mostly in a qualitative way, the radiation oncologist needs a quantitative evaluation.

Image fusion and co-registration

As Ling et al. write in ‘Towards multidimensional radiotherapy (MD-CRT): biological imaging and biological

conformality', '... the current technology for delivering may have exceeded our ability to localize tumors and normal tissue by conventional imaging technique'.⁸ Regarding this, there is growing evidence that the integration of PET with morphological imaging such as CT and MRI leads to a better delineation of target volume.

An accurate image co-registration process is required to incorporate PET into treatment planning. This means determining a geometrical transformation that maps an acquired image onto another acquired with the same or different modalities. Different manual or automated methods have been proposed.¹⁴ They are based on geometrical features such as point-based registration, or on voxel similarity measures.^{15,16}

The case of PET–CT or PET–MRI fusion is complicated by the lack of anatomical features and deviation from the rigid-body model, assumed in most of the commercially available registration algorithms. To reduce tissue deformation and volumetric distortion on the different images, the

position of a patient must be well reproduced using appropriate immobilization systems and a flat table such as those used for RT (Figure 32.4).

Fiducial markers, filled with CT contrast and FDG, can be necessary to guide the registration and to improve the matching accuracy (Figure 32.5). Another important consideration is the necessity to place lasers in the room. Lasers are commonly used in a CT room to set up the patient or to localize the isocenter position, as in the treatment room. The placement of lasers in the PET room will guarantee the accuracy of patient positioning.

It needs to be pointed out that the accuracy of registration must always be checked by phantom measurements, as this could be a limiting factor for using PET in tumor delineation.^{17–19}

Actually, registration accuracy appears to be variable, depending on the anatomical region investigated. For tumors of the head and neck (H&N), the deviation between the center of the tumor as defined by CT and as

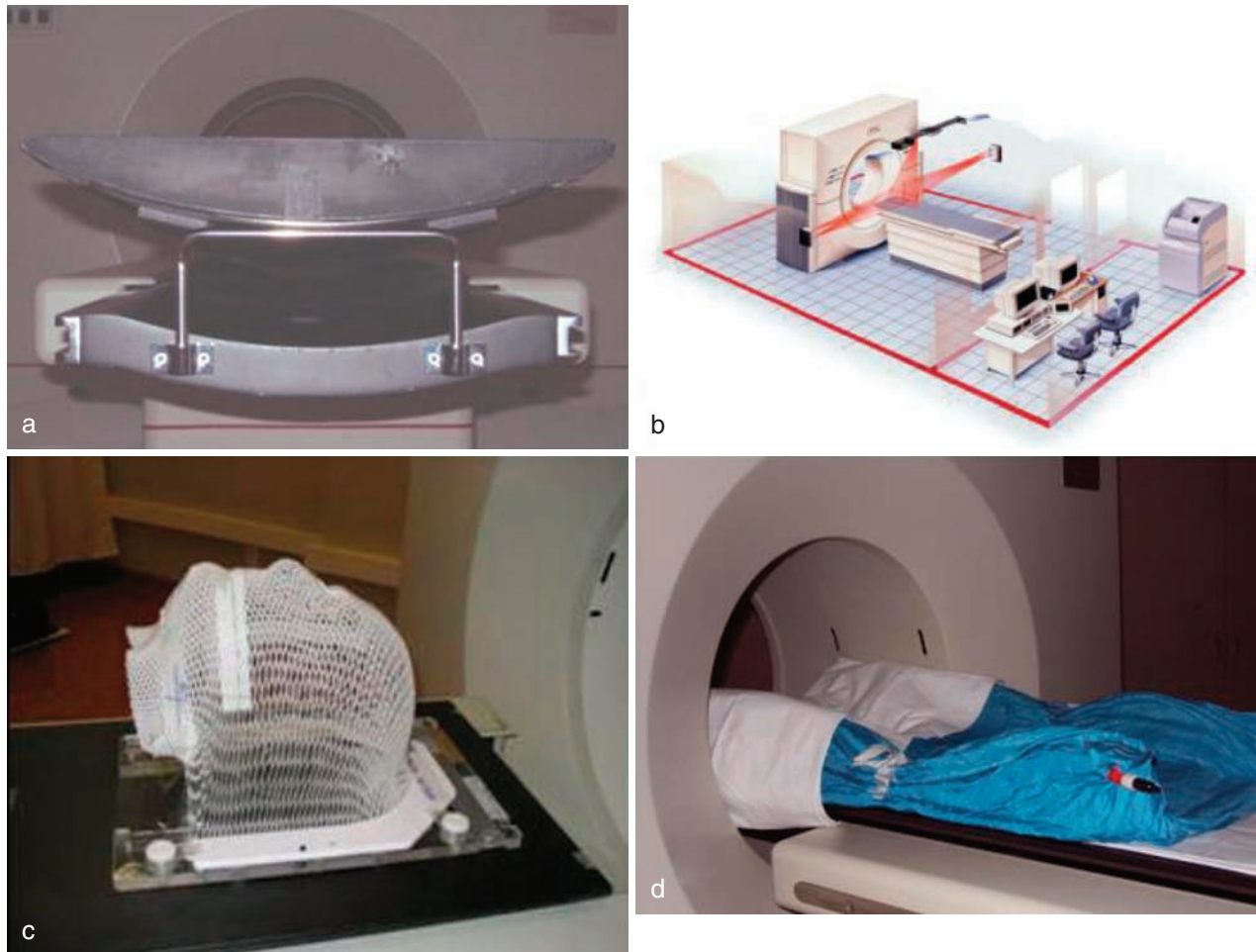


Figure 32.4

Patient position reproducibility: (a) flat bed, (b) laser positioning system, (c, d) immobilization systems.

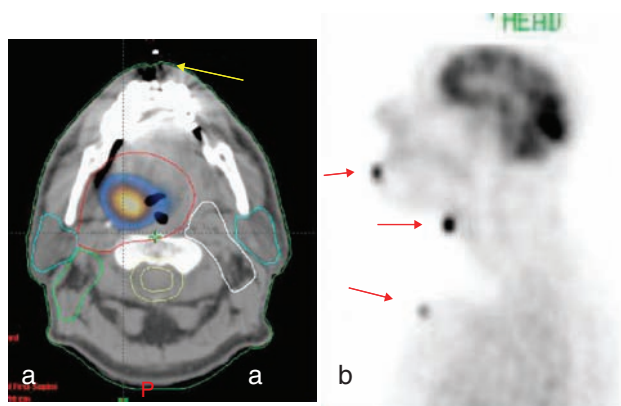


Figure 32.5

Fiducial markers in CT (a) and positron emission tomography (PET) (b) images. These markers, filled with CT contrast and fluoro-2-deoxy-D-glucose (FDG), can be used to guide registration and improve matching accuracy.

defined by PET was found to be about 0.15 cm.²⁰ Maximal deviation was found in the chest region, and ranged up to 0.64 cm in the x and y directions with a range of 0.8–0.4 cm in the z direction. This mismatch in the thorax is mainly a breathing effect, which is different in CT and PET.

Acquisition is rapid with CT, and the resulting image is a virtual snapshot of the diaphragm position that could be markedly different from the average position obtained with a 5-minute PET scan. This phenomenon could be so pronounced as to result in marked mislocalization of a lesion that would appear to be located in the wrong position. Osman et al. reported that in evaluating 250 PET–CT scans, in which free breathing was allowed, there were six cases of mislocalization of liver metastasis, which appeared to be in the lung on the CT image.²¹

Regarding this, use of the PET–CT scan seems to be the future. Equipped with a gantry as large as possible, so that special immobilization devices used during radiotherapy treatment can fit through the PET–CT, it might solve the problem of patient positioning, thanks to scans being acquired on the same machine. Nevertheless, involuntary patient motion and motion due to breathing are not solved with this new technology, and a gating capability for respiration should be provided.

Gross tumor volume delineation

Accurate delineation and localization of the GTV is especially critical when the volume has a deep impact on the treatment plan results, as in IMRT treatment, or when considering a dose escalation. The co-registration of CT and

PET may improve the definition of a given tumor because of the functional imaging, but the volume definition in a functional image is a very critical step.²² This is strictly related to the nature of PET imaging. Factors such as the size of the tumor, the background signal, and the algorithm used for image reconstruction, which define the full width half maximum (FWHM), could affect the resultant size of an image in PET. Furthermore, PET volumes displayed on the screen may look large or small depending on the display window/level settings (Figure 32.6) and this underlines the importance of robust volume segmentation tools. Different segmentation methods have been proposed, principally based on a threshold value defined by phantom study. Using CT volume as a standard, Erdi et al. define an optimal threshold in relation to the signal to background ratio (S/B).²³ A value ranging from 36% to 44% of the lesion maximum signal is indicated for volumes larger than 4 ml, where the measure is less sensitive to partial volume effects. Due to the edge blurring effect of the background, this value must be increased for volumes smaller than 4 ml (Figure 32.7).

As the SUV is a standard parameter used in diagnostic nuclear medicine, it has been suggested as a criterion to define gross tumor volume. A value of 2.5 (SUV_{2.5}), the same as used in diagnostic studies, has been proposed by Paulino and Johnstone.²⁴ Comparison between the Erdi criterion and the SUV_{2.5} shows that, compared to CT–GTV, the first criterion underestimates the volume. Black et al. found a linear correlation between the SUV threshold and the mean target SUV: the higher the mean SUV is, the greater is the threshold SUV.²⁵ The important concept reported by Black et al. is that the background activity concentration and the sphere volume have no independent effect on the SUV threshold. Again, this segmentation overestimates the extent of a target volume with respect to the Erdi method.

A different segmentation method is proposed by Nestle et al.²⁶ In this case the criterion is defined in terms of signal intensity. The intensity threshold is an increasing linear function of the mean intensity inside the lesion and of the intensity background. This criterion underestimates the volume with respect to the SUV_{2.5} method, and overestimates it with respect to Erdi.

A different relation between the threshold value and the S/B ratio has been investigated by Daisne et al.: the determined value is higher for less contrasted images. A new aspect introduced by Daisne et al. is that the value is related to the image reconstruction algorithm used.²⁷ The method proposed by these authors has been validated using surgical specimens for pharyngolaryngeal carcinoma: the FDG–PET–GTV appeared to be more accurate than CT- and MRI–GTV, even if it was still larger than the surgical one.²⁸

The results of the above described studies underline that the segmentation method is an unsolved crucial problem and further evaluation must be done.

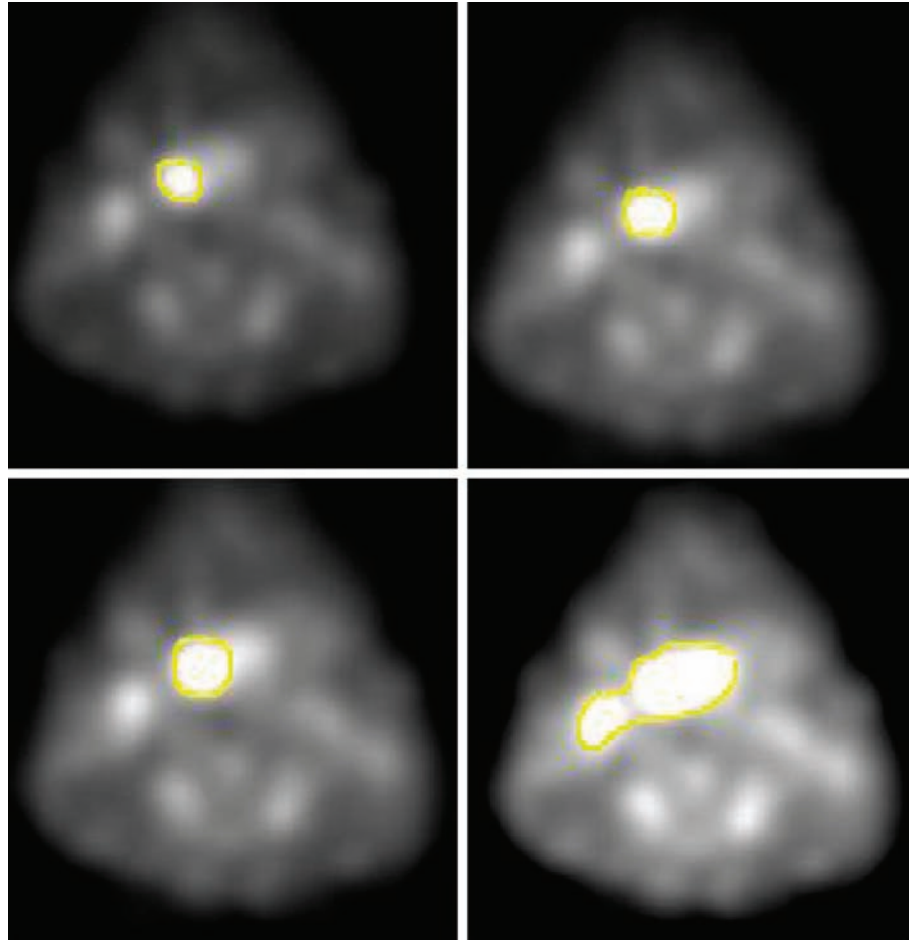


Figure 32.6

Images of the same PET scan are shown with different window level settings on the treatment planning system screen. In the upper right image a threshold value of 65% of the maximum is set, while a value of 40% is set in the lower left image. It is evident that the window level defines a different dimension of the lesion.

Clinical applications

Many authors have demonstrated that FDG-PET is a very effective imaging modality for managing oncologic patients. Gambhir et al. published a review (419 articles and abstracts) reporting a global sensitivity (18 402 patients) and specificity (14 264 patients) of 84% and 88% respectively; the management of patients ($n = 5062$) was changed by PET in 30% of cases.²⁹ Dizendorf et al. evaluated the impact of whole-body FDG-PET on the staging and managing of patients for radiation therapy in 202 consecutive cases. The radiation therapy strategy was changed in 27% of patients.³⁰ Similar results have been reported by other authors.^{31,32}

The recent development of PET imaging regarding integrated acquisition PET-CT has been an important step towards true morpho-functional imaging. Ciernik et al.

investigated the usefulness of hardware co-registered PET-CT images for target volume definition in 39 patients with various solid tumors. CT and FDG-PET were obtained in the treatment position, and co-registered images were used for treatment planning. In 56% of cases, GTV delineation changed significantly. In 16% of cases, PET-CT revealed distant metastases, changing the treatment strategy from curative to palliative.²⁰

In radiotherapy planning, PET-CT is particularly useful when the patient has poorly defined target volumes (e.g. brain tumors or lung cancer), or is candidate for dose-escalated radiotherapy (e.g. H&N cancer, lung carcinoma, prostate carcinoma), which needs accurate definition of the metabolically active tumor volume and its differentiation from surrounding healthy tissue (Figure 32.6).³³

The following sections provide a view on the clinical applications of PET (Figure 32.8), and a look also at

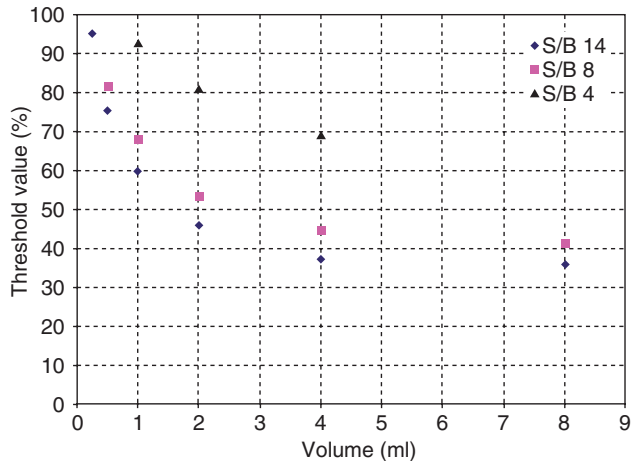


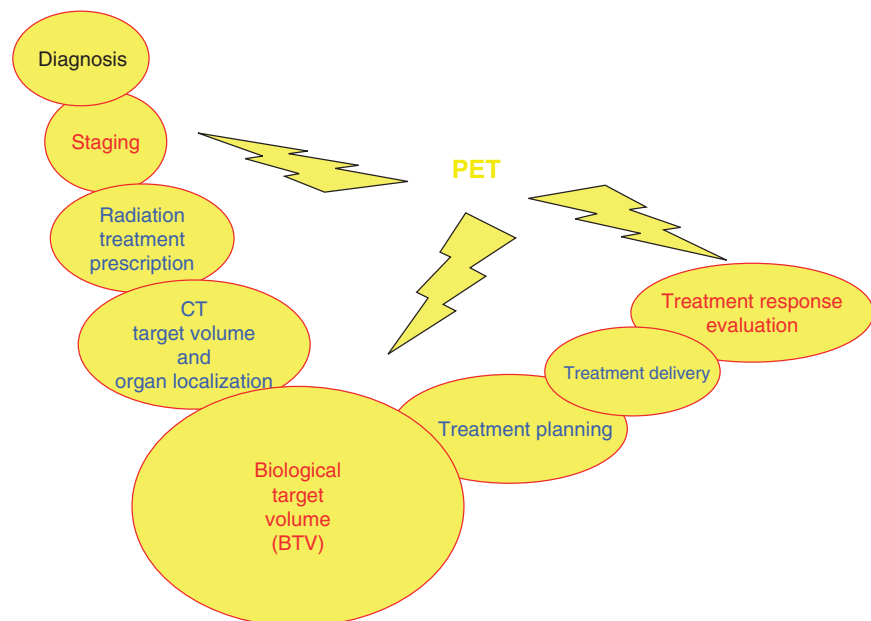
Figure 32.7

Segmentation of PET volumes. The threshold value required to visualize spheres of defined dimension is shown for different source to background ratios (S/B). A phantom including spheres of volumes 0.2, 0.5, 1.0, 2.0, 4.0, 8.0 ml was used. For lesions bigger than 4 ml and a S/B equal to 8, the graphic exhibits a plateau, to indicate that a threshold of 40% may be used for automated segmentation. For smaller lesions the threshold is a function of the tumor dimension, and a single segmentation value cannot be defined.

SPECT, in the radiation treatment planning for several tumor sites. The most common tracer employed is FDG, and the main goal of its use is definition of the GTV. More experimental applications of FDG and the use of alternative radiotracers for different purposes – such as assessment of biological tissue properties (i.e. for BTV definition) – will be discussed separately.

Figure 32.8

The sequence of radiation therapy. The figure shows the phases of patient management in radiation therapy in which FDG-PET imaging plays a major role (staging, biological target volume definition, and treatment response evaluation).



Lung cancer

Lung cancer is the most deadly form of cancer. The most effective therapy is surgery, but unfortunately only a few patients are operable. The outcome of radiation therapy is poor: the long-term survival in inoperable lung cancer receiving only RT ranges from 6% to about 30% for stage I–II, decidedly worse for the advanced stages.

Even if the main event affecting the prognosis is the appearance of distant metastases, there is a significant number of patients relapsing inside the treatment field. This demonstrates the necessity to improve the local control. The current trend to improve survival is towards dose escalation only in the radiographically evident tumor, combined with systemic therapy. In fact, the elimination of prophylactic irradiation of the mediastinal region reduces the toxicity, leaving more room for dose escalation on the GTV.

It has been proved that FDG-PET plays an important role in the management of non-small-cell lung cancer (NSCLC) patients. As a meta-analysis by Toloza et al. has shown, PET is a valuable diagnostic and staging tool. PET-FDG has a sensitivity and specificity, for mediastinal staging, of 84% and 89%, respectively, compared to 57% and 84% for CT (Figure 32.9).³⁴ A recent study of the relationship between the SUV obtained from FDG-PET and the treatment response/survival of inoperable NSCLC seems to indicate SUV_{max} as an important prognostic factor for survival and a predictive factor for treatment response.³⁵ The FDG SUV appears to be a good indicator for selecting patients for different treatment strategies.

The incorporation of PET into radiation therapy seems to improve tumor coverage and normal tissue sparing,

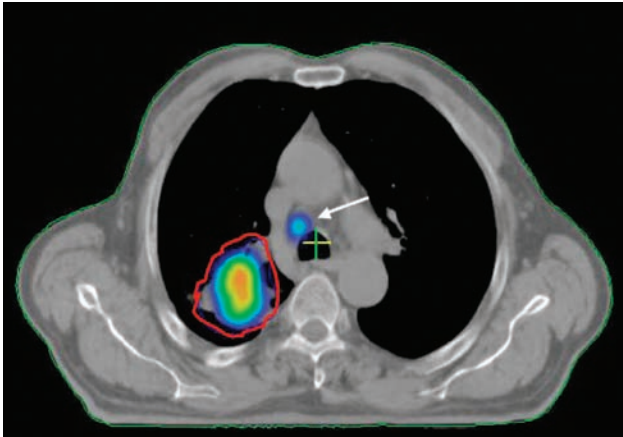


Figure 32.9

FDG-PET uptake in a case of non-small-cell lung cancer (NSCLC). The red contour represents the GTV defined on a CT basis only. Without PET imaging, the GTV would have been underestimated because of missing one mediastinal node not described as pathologic by CT (arrow).

which may lead to less toxicity and the possibility of dose escalation.^{36–38}

Actually, the integration of FDG-PET images into radiotherapy planning is an issue of recent interest. Therefore, most of the reported studies have analyzed the impact of FDG-PET on radiation therapy without the help of fusion images, but using other methods to incorporate functional information. Despite this, there is clear evidence that PET has the potential to affect both management and radiation treatment planning.³⁹ PET imaging, combined with CT, can dramatically alter the GTV definition. Because of the higher sensitivity of PET in detecting lymph node metastases compared to CT, it may lead to an increase in the size of the GTV. Nestle et al., in a retrospective study, reported that incorporating PET would have altered the radiotherapy plan in 12 of 34 patients (35%).⁴⁰ Vanuytsel et al., comparing the GTV defined by only CT and by CT integrated with PET, asserted that radiation portals were altered in 45 of 75 patients (62%).⁴¹ Messa et al. changed the CTV after the inclusion of PET–CT data, in 55% of cases.⁴² The same is reported by Munley et al.: 34% of the treatment plans would be influenced by PET images.⁴³

In more recent studies, the effect of PET on target definition via image fusion has been investigated.^{44–47} Mah et al. recruited 30 patients only referred for radiation therapy with radical intent.⁴⁴ CT and PET data sets were acquired in the treatment position. The inclusion of PET showed a significant change in disease location, size, and shape, and in identifying affected lymph nodes that were borderline on CT. The study reports that in 12 cases radiation treatment was changed. A significant finding is that seven of 30 patients were actually not suitable for radiation treatment because of the extent of the disease. In agreement with this,

McManus et al. reported that 30% of patients with locally advanced NSCLC became ineligible for radical radiotherapy treatment because of distant metastasis or extrathoracic disease.¹⁰ An interesting result, confirmed by other studies, is that the integration of PET and CT lowers observer variation, providing a more consistent definition of GTV.^{20,45} In this paper¹⁰ the ratio between the largest and the smallest GTV, as drawn on a CT image had a variability ranging from 1.06 to 7.66. The range was narrowed to between 1.09 and 2.77 when PET information was included.

A reduction of the delineation variability is proved by Steenbakkers et al.⁴⁸ In this study the three-dimensional observer variation was reduced from 1.0 cm to 0.4 cm (standard deviation, SD) using matched CT-FDG-PET. The largest reduction was seen in the atelectasis region.

Likewise, Bradley et al. found that PET changed the American Joint Committee on Cancer (AJCC) clinical stage in eight of 26 patients.⁴⁹ The radiation therapy planning was changed in over 50% of patients in comparison with CT targeting because of variation of PTV.

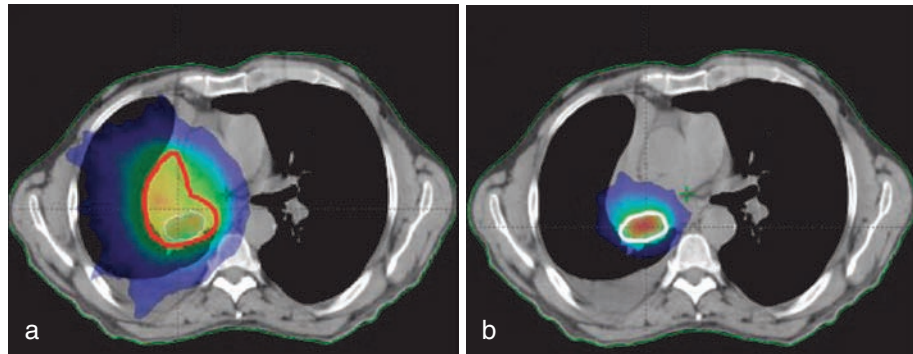
It needs to be pointed out that there is no agreement regarding the definition of ‘significant variation of tumor volume’. Bradley et al. have adopted as a criterion ‘a clear difference between contours, i.e. nodal regions contoured as tumor on PET–CT data sets and not contoured only on CT’, while other authors define criteria related to minimum percentage volume differences from GTV on PET/CT and GTV on PET.^{20,39} Strictly related to this is the rule used to identify the lesion boundary on PET images. Mah et al. set a window level equal to 50% of the maximum;⁴⁵ Bradley et al. define a threshold value of 40%,⁵⁰ while Erdi et al. consider a variable threshold related to the background signal.⁴⁵ Ashamalla et al. have also addressed this issue: a criterion equal to a SUV value of 2 ± 0.4 is defined.⁵⁰ The lack of a general consensus regarding these criteria, which are subject to debate, means that, even if the benefits of PET scans are well established, the correct integration of metabolic information in radiotherapy treatment is still an open issue.

Recently, Deniaud-Alexandre et al. studied 101 patients who underwent CT and FDG-hybrid PET for simulation treatment. A significant variation of the GTV, i.e. a difference of 25% between GTV-CT and GTV-PET–CT, was found. The GTV was decreased by CT–PET image fusion in 21 patients (23%), and increased in 24 patients (26%). Because of the PET-modified GTV, the percentage of total lung volume receiving > 20 Gy increased in 15 cases and decreased in 22. The multivariate analysis demonstrated that tumor with atelectasia was the single independent factor that resulted in a significant effect on the modification of the size of the GTV.³⁸ Due to the ability of PET to distinguish tumor from atelectasis, a review of published data suggests a reduction in the CT-derived GTV in 15% of cases (Figure 32.10).⁴⁸

Respiratory motion is an important factor that degrades PET image quality and reduces its potential.

Figure 32.10

A case of NSCLC in which the CT-based GTV overestimated the true extent of disease because of inclusion of an area of atelectasia. (a) In blue is shown the distribution of a dose potentially dangerous for the lung. (b) Reduction of the target volume, allowed by PET imaging integration, led to much better sparing of healthy lung tissue.



Respiration creates artifacts and blurring, and reduces the image quality, the ability to quantify FDG uptake, the target to background contrast, and, consequently, the capability to define the lesion size. Due to respiratory motion, usually, we see an increase in the planning target volume that limits dose escalation. Some authors have suggested that the ‘smearing’ of the lesions due to motion might indicate the exact margin to add to a GTV to avoid a mismatch of the tumor and its underdosage.^{51–54} The best solution for motion is the respiratory gating.⁵³ PET data are acquired synchronized to the respiratory cycle, in a similar way that PET is already designed in terms of cardiac gating. A patient study has shown that when gating is applied, the GTV is reduced by 28% and the SUV increased by 56.5%. This recent approach with respiratory gating in PET certainly represents a new line of development.

Patients with NSCLC often have inhomogeneous lung perfusion, and its evaluation can be useful in planning and monitoring the radiation treatment.

Christian et al. suggested using a SPECT scan to design radiotherapy treatments that limit the dose to healthy perfused lung. In six patients they optimized 3D-conformal plans using SPECT images to define the volume of perfused ‘functioning’ lung. This procedure was helpful for patients with large perfusion deficits.⁵⁵

Zhang et al. evaluated radiation-induced lung injury in 19 patients receiving thoracic 3D conformal radiotherapy for lung cancer. SPECT lung perfusion scans and X-ray or CT scans before RT, and after 40–50 Gy radiation, were performed. A decreased post-RT lung perfusion was observed in six patients, whereas a relatively increased post-RT lung perfusion was observed in 13. The authors concluded that SPECT lung perfusion scanning is a simple, convenient, and useful method for assessing pre-RT regional lung function and monitoring the changes in regional lung function after irradiation.⁵⁶

Seppenwoolde et al. studied regional differences in lung radiosensitivity by evaluating the incidence of radiation pneumonitis (RP) in relation to regional dose distribution. They registered chest CT and SPECT lung perfusion scans in 106 patients before curative radiotherapy for NSCLC. The incidence of RP correlated significantly with the mean lung dose and the mean regional dose. They found that by

weighting the local dose with the local perfusion it is possible to improve the dose–effect relationship, particularly important for caudally located lung tumors, resulting in a greater risk of radiation pneumonitis.⁵⁷

Regional lung functional impairment in patients with lung cancer was also assessed by Suga et al. using co-registered respiratory-gated ventilation/perfusion SPECT–CT images. Twenty untreated and three irradiated patients underwent gated ^{99m}Tc-labeled Technegas/macroaggregated albumin (MAA) SPECT, using a triple-headed SPECT unit and a respiratory synchronizer. The conclusion was that detailed functional–morphological correlation on co-registered gated SPECT–CT images contributes to the accurate assessment of regional functional impairment, and may be useful for surgical planning, prediction of postoperative function, and assessment of external beam radiotherapy effects in patients with lung cancer.⁵⁸

Head and neck cancer

Head and neck cancer represents an elective indication for IMRT techniques, because of the anatomic complexity of the region in which a variety of critical structures lies in close proximity to the tumor. Consequently, the ability of IMRT to spare normal tissue is particularly helpful in this area. Xerostomia is an example of radioinduced injury affecting most heavily the quality of life of the patient treated for H&N cancer. Thus, the preservation of salivary function is one of the most important goals in H&N treatment planning. Obviously, by reducing the dose to radiosensitive tissue, IMRT also gives more room for dose escalation to the macroscopic disease. Head and neck cancers are at high risk of lymph node metastases, and anatomical imaging (CT and MRI), with its dimensional and morphologic criteria, can fail in the differentiation between neoplastic and non-neoplastic lymph nodes. For this reason, it is usual to treat all neck regions deemed to be at more than 10–15% risk for subclinical disease. This approach, combined with the necessity to improve local control by dose escalation and combination with chemotherapy, makes this kind of treatment very aggressive

and toxic. Therefore, the best possible disease localization and description is one condition to improve the therapeutic ratio, i.e. the ratio between the probability of cure and the risk of induced damage. The main justification for PET imaging in H&N RT planning is its superiority for lymph node disease detection; several studies also report good performance in the detection rate of primary tumor sites (ranging from 88% to 98%).^{28,59–67} PET may also be helpful in finding the primary site in patients with lymph node metastases of unknown origin.^{68,69} Yet, in these cases, some authors have reported a significant incidence of false-positive findings, warning against making treatment decisions

unless proven by biopsy.⁷⁰ Finally, PET may show undetected distant metastases and synchronous second primary. It must be underlined that PET interpretation in the head and neck region is not easy because of physiological FDG uptake in certain areas (i.e. tonsils, base of the tongue, parotid glands, thyroid, masticatory muscles). Co-registration with CT can improve image understanding and allow correct anatomical localization of the lesions and the detection of smaller ones (Figure 32.11). The relatively rigid nature of the H&N region and the possibility of immobilizing it properly are a good basis to fully evaluate the role of PET on target volume definition.

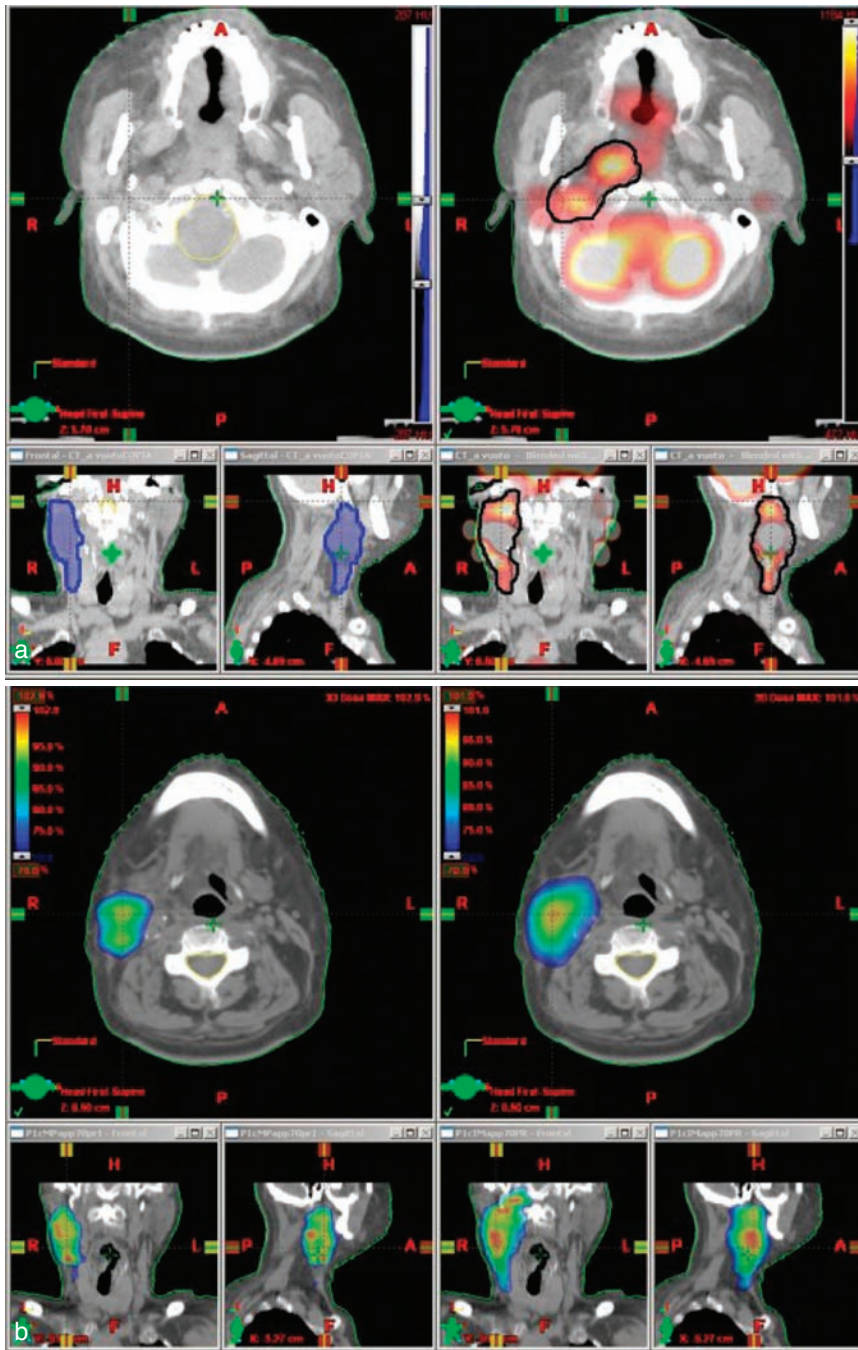
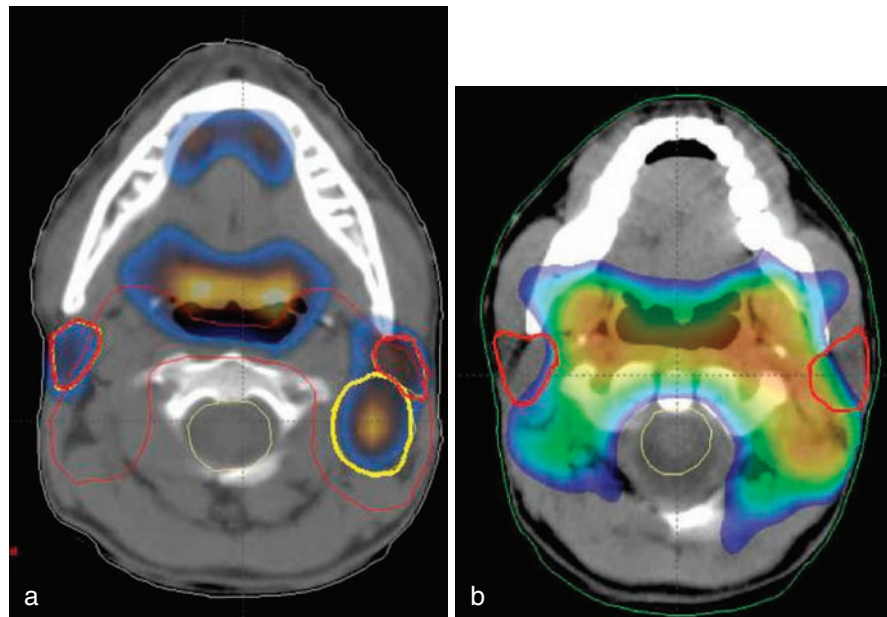


Figure 32.11

(a) The GTV variation consequent to PET–CT registration in a case of right parotid cancer with homolateral nodal disease. On the left, in blue, is shown the CT-based GTV. On the right, in black, is the PET–CT GTV. In the axial section displayed there is no target defined on CT imaging, while PET reveals a parapharyngeal nodal involvement. After PET integration, the GTV increased by about 100%. Note the absence of uptake corresponding to a necrotic area inside a massive lymph node metastasis. (b) The prescribed dose distribution corresponding to the two different GTVs.

Figure 32.12

A case of rhinopharynx cancer with nodal metastases at the 2° left level of the neck. (a) The yellow contour represents the pathologic FDG-PET uptake and the red the parotid glands. (b) Intensity modulated radiation therapy (IMRT) plan dose distribution: the proven absence of disease near the right parotid allowed its sparing without risk of missing the tumor.



On the whole, FDG-PET is helpful in target delineation, and may greatly influence the radiation treatment plan, also playing a role in normal tissue sparing (particularly parotid glands) (Figure 32.12).

There are several published studies on the influence of FDG-PET in head and neck radiotherapy. Nisioka et al. studied the PET influence on RT planning for oro- and nasopharynx cancer.⁷¹ In their experience, after the inclusion of PET information, only two of 21 patients had a beam geometry variation, but the dimension changed by about 50%. Furthermore, parotid gland sparing was planned with more confidence because of the more precise GTV localization. Ciernik et al. reported a GTV modification by $\geq 25\%$ in six of 12 patients; the volume increased in four patients, and decreased in two.²⁰

Scarfone and colleagues investigated the influence of PET on the delineation of target volume in head and neck cancer.⁷² The inclusion of PET findings led to GTV changes in five of the six patients evaluated (one patient was not evaluated because PET was negative after induction chemotherapy). In all cases the volume was enlarged by an average of 15%. Heron and colleagues investigated the effect of the use of hybrid PET-CT simulation for treatment volume definition in 21 patients with H&N cancer. In all cases PET images showed increased uptake in the known primary tumor site, while CT failed in its visualization in three cases. The primary volume defined by PET was smaller than the CT-based one in all patients (ratio CT-GTV/PET-GTV, 3.1). In contrast, the volume of abnormal lymph nodes as defined by PET was overall larger than in CT images (ratio CT nodal volume/PET nodal volume, 0.7). PET detected more pathologic nodes in nine patients. The better performance of PET imaging in

primary tumor identification can partly be explained by its lesser susceptibility to artifacts generated by metal dental work.⁷³

Geets and co-workers evaluated the influence of FDG-PET in the treatment of 18 patients with pharyngolaryngeal squamous cell carcinoma. All patients underwent pretreatment CT, MRI, and PET.⁷⁴ The GTVs that were PET based, and the related CTVs and PTVs, were smaller than those based on morphologic imaging. This reduction led to a significant decrease of the irradiated volumes and to better healthy tissue, namely parotid gland, sparing. The patients were also studied using the same procedure after a mean dose of 46 Gy. CT and MRI showed a GTV reduction, but, because of radiotherapy-induced inflammation, PET automated segmentation was not usable.

Wang et al. studied 28 patients with H&N carcinoma.⁷⁵ PET led to changes in disease staging in 16 patients (57%) and found a second primary cancer in one other patient. GTV variation was evaluated in 16 patients by comparing PET-CT-GTV to CT-GTV. The authors reported a potential overestimation of the disease extent by CT in nine patients (volume changes 11–40%) and underestimation in five patients (volume changes 14–31%).

Paulino and colleagues examined 40 patients with head and neck squamous cell carcinoma who underwent CT-simulation and PET-CT. After image co-registration, the CT-GTV and the PET-GTV were delineated. The aim of their study was to define the adequacy of PET-GTV dose coverage if radiation treatment was planned on a CT basis only. The primary tumor identified by PET was underdosed by the CT-based plan in ten (25%) patients. In seven patients it was caused by the detection of additional neoplastic areas (PET-GTV > CT-GTV), while in the other

three cases it was because of non-overlapping PET- and CT-GTVs.⁷⁶ For 36 in the same patient series, Koshy et al. reported the staging and therapy variation consequent to PET-CT image fusion. Changes in TNM score and AJCC stage were registered in 36% and 14% of the patients, respectively. In addition, PET allowed the detection of the primary site in two cases with cervical node metastases from an unknown primary. Nine patients (25%) had a modification of their treatment strategy. The pattern of changes (in some cases overlapping in the same patient) included: shift of treatment intent from curative to palliative because of metastatic disease; exclusion of radiotherapy for detection of synchronous advanced lung cancer; modification of treatment volume (larger in two patients, smaller in three); variation of treatment dose (higher in three patients, lower in one); and variation of chemotherapy management.⁷⁷

Versari et al. reported the results of PET application in 36 H&N curative IMRT. According to PET-CT findings, the stage of disease changed in 22.2% (8/36) of cases. GTV modifications led to changes in high dose volumes in 10/36 patients (27.8%). In two cases (5.6%) the radiation therapy intent shifted from a curative to a palliative purpose as a consequence of the detection of distant metastases. In the group of patients (22/36) with a follow-up longer than 6 months, no local failures have been observed in regions excluded from the high dose because of PET negativity.⁷⁸

To fully exploit the potential of IMRT, Scwhartz et al. examined 20 H&N patients and studied the potential impact of PET-CT imaging for more tailored IMRT plans, targeted to PET-CT-GTV only, with the exclusion of prophylactic irradiation of PET-negative regions. The theoretical plan created can greatly reduce the dose to normal tissue, and contextually can leave more room for intensive irradiation of the macroscopic disease. Obviously, this promising approach requires that FDG-PET-CT is fully validated. The benefit of FDG-PET on head and neck radiotherapy outcome is still unknown, and its use for target delineation should be regarded as a research tool.⁷⁹

It should be mentioned that there is no consensus about the usefulness of FDG-PET in H&N cancer staging and RT planning.⁸⁰ The reason advocated to justify this position is the small advantage of PET in the definition of primary tumor and its failure in the demonstration of microscopic nodal metastases, considerably frequent in H&N tumors.

Besides staging purposes, FDG uptake can be considered for treatment response prediction. The early monitoring of treatment can provide help in distinguishing responders from non-responders (particularly useful in organ preservation protocols) and allow the identification, before therapy, of the most aggressive tumors.⁸¹

FDG-PET imaging plays also an important role in the detection of residual/relapsing disease after radiation treatment. In this context, the limits of morphologic imaging (CT and MRI) in the characterization of abnormal tissue become evident, and the superiority of PET imaging

is acknowledged.^{82–84} Greven et al. evaluated 45 patients before radiotherapy and at 1, 4, 12, and 24 months afterwards. The study showed a high accuracy in both positive and negative findings at 4 months after radiotherapy, but not as accurate at earlier intervals (namely for negative scans).⁸⁵ However, it seems reasonable that a gap of 8 weeks is enough to prevent the majority of false results.⁸⁶ The early detection of disease recurrence is imperative, improving the salvage therapy outcome.⁸⁷ Besides, the predictive value of a negative scan is high enough to postpone biopsy specimens. The avoidance of repeated unjustified biopsies is particularly useful in the head and neck region, namely after larynx radiotherapy, because they can promote severe tissue damage and also precipitate necrosis.⁸⁸

Other cancer sites

The number of tumor sites investigated for PET-guided treatment planning is rapidly increasing. Some of these are not well detected with FDG, and can require the use of alternative radiotracers or single photon emission technology instead of PET. The results are still preliminary, but it is likely that clinical application of nuclear medicine technology in the radiotherapy sector will become gradually more important for a variety of cancer types.

Cervical cancer

Radiation therapy has a major role in cervical cancer. For early-stage cervical cancer the treatment is radical surgery and/or radiation therapy, whereas for patients with locally advanced disease the treatment of choice is combined chemoradiotherapy. The radiotherapy planning consists of brachytherapy (intracavitary implants) and external beam radiation therapy.

FDG is the main tracer used for PET studies in cervical cancer. Its role is important in the primary staging of untreated advanced disease, in post-treatment surveillance with suspicion of recurrence, and in restaging of potentially curable recurrent cervical cancer.

An application of PET imaging in radiotherapy planning is the identification of positive para-aortic lymph nodes (PALNs). In fact, the conventional treatment of this region, because of the dose limit due to the adjacent organs at risk, is ineffective, and the prognosis of patients with positive PALNs is poor. A possible solution is to escalate the dose to the positive nodes using PET-guided IMRT.

Esthappan et al. attempted to determine guidelines regarding the selection of appropriate treatment and organ-specific parameters for intensity modulated radiotherapy planning for PALNs. They developed treatment plans that deliver 59.4 Gy to the positive PALNs and 50.4 Gy to

the para-aortic region using CT–PET-guided IMRT, achieving acceptable sparing of the stomach, liver, and colon.⁸⁹

Another application of PET is to guide the brachytherapy dose distribution to assure adequate tumor coverage, as reported by some authors.^{90–92}

Esophageal cancer

Leong and co-workers examined the impact of PET–CT in the delineation of GTV in 21 patients with esophageal carcinoma, and found significant differences between the volumes generated with and without PET contribution. PET-avid disease regions were excluded from GTV-CT in 11 patients. Consequently, radiotherapy plans based only on CT imaging would have failed to cover the tumor adequately in five of these patients (31%). The main cause of discrepancy was the longitudinal extent of the disease. Furthermore, PET findings led to a staging variation in eight of 21 cases (38%) and to a change of therapeutic intent (from curative to palliative) in five.⁹³

Moureau-Zabotto et al. studied 34 patients scheduled for concomitant chemoradiotherapy. In two cases the detection of unsuspected distant metastases excluded curative radiotherapy. The inclusion of FDG-PET in target definition led to the reduction of GTV in 12 patients (35%) and to its increase in seven (21%). A GTV variation $\geq 25\%$ was observed in six patients. Consequently, the lung volume exposed to radiation damage was also affected by CT and FDG-PET image fusion. The definitive clinical impact of these variations has still to be defined.⁹⁴

Konski and colleagues described their experience with 25 patients with esophageal cancer who underwent CT, PET, and endoscopic ultrasound (EUS). The authors concluded that FDG-PET in addition to EUS is able to provide information useful for more precise and accurate target definition.⁹⁵

Vrieze and co-workers evaluated the impact of FDG-PET for the delineation of lymph nodal target volume in patients with locally advanced esophageal cancer. They studied 30 patients using CT, EUS, and FDG-PET. In 14 cases (47%) the FDG-PET features appeared to be discordant with the CT/EUS ones. In six of these patients, the PET information would have led to a change in treatment volume (enlargement in three, reduction in three). Because of the high specificity of PET for esophageal cancer the authors consider the possibility of using it in the treatment planning in the case of positive findings. In contrast, its low sensibility warns about the exclusion of PET-negative nodes appearing pathologic with CT/EUS.⁹⁶

Lymphoma

FDG-PET is very sensitive and specific for Hodgkin's and non-Hodgkin's lymphomas, and is widely used as a staging

procedure and for post-treatment evaluation. The use of PET to optimize the treatment volume is still under investigation. It is justified by the necessity to reduce the irradiation volume as much as possible, in order to lower the risk of late side-effects (namely secondary cancer and permanent pulmonary toxicity) in these long-surviving patients. In the retrospective study conducted by Lee and colleagues of 17 thoracic lymphomas, PET showed different findings from CT in all but one patient. These results could lead to substantial changes in treatment field definition. However, the additional value of PET could be more relevant if moving from the conventional anterior–posterior technique towards more conformal and innovative approaches such as IMRT of smaller 'lymph-node fields'.⁹⁷

Brain tumors

Brain tumors are frequently treated with radiosurgery or with stereotactic radiotherapy. These very precise and conformal therapies are delivered in one or a few high-dose fractions and require careful localization of the tumor.⁹⁸

Other than for PET imaging, brain tumors represent a field of interest also for SPECT applications. Grosu and colleagues examined 66 patients with resected malignant gliomas and evaluated the influence of the incorporation of [¹²³I]α-methyl-tyrosine-SPECT (IMT-SPECT) imaging in the postoperative radiotherapy treatment planning.⁹⁹ Their results showed substantial differences between the volumes of MRI abnormalities and IMT uptake. Because of the high specificity of IMT-SPECT, these findings can be used for the definition of target volume, especially for localization of the high-dose volume. In a more recent work, Grosu et al. demonstrated a similar result with the use of L-(methyl-¹¹C)-labeled methionine-PET (MET-PET), an imaging modality having a higher specificity and sensibility than MRI for the differentiation of unspecific tissue modifications and residual tumor after surgical resection of high-grade gliomas.¹⁰⁰

Prostate cancer

The low sensitivity of FDG-PET in prostate cancer has limited its use in this field. The development of new PET radiopharmaceuticals will probably allow the use of functional and biological imaging to support parallel developments in radiotherapy techniques for prostate cancer. The ultimate goal is a coordinated diagnostic and therapeutic approach to individualize and optimize the treatment plan for patients with prostate cancer.¹⁰¹

Choline-PET and acetate-PET are promising tracers in the diagnosis of prostate cancer, but their validity in local tumor demarcation, lymph node diagnosis, and detection of recurrence has to be defined in future clinical trials.^{102–104}

Future perspectives

Multitracer PET–CT

The heterogeneity of the biologic properties of the tissues makes the individual response to radiation extremely varied. Knowledge of the incidence and intensity of the events leading to tissue damage is really interesting for the radiation oncologist, in order to predict the responsiveness of both tumor and normal tissues. Prediction of the response can give information about the prognosis and efficacy of a determined gold-standard treatment, and can also allow the identification of patient subgroups for whom an altered/new therapeutic strategy could be superior.

For a long time, the radiation oncologist has tried to measure the predictors of response to radiotherapy, such as surviving fraction to 2 Gy, potential tumor doubling time, thymidine labeling index, and tumor hypoxia. Unfortunately, the methods used to measure these factors were mostly invasive and prone to sampling errors. Now, some properties influencing the radiotherapy effect may be assessed by means of non-invasive and repeatable techniques. The images that provide information about factors affecting the responsiveness to radiation therapy can be described as radiobiological.

Nuclear medicine, using PET and SPECT, allows the determination of various tissue properties potentially affecting the outcome of radiotherapy. However, it must be emphasized that the first aim is demonstration of the correlation between the imaging and biological features of the tissue. The second issue is verification of the temporal constancy of a specified functional property.

Tumor hypoxia

Tumor hypoxia is one of the main causes of radioresistance and poor prognosis. The main mechanism of radiation injury at the molecular level is mediated by the production of free radicals, and requires the presence of oxygen. If the partial oxygen pressure is low, the repair of free radical damage, and hence cell survival, increases. In the hypoxic condition, the dose required to achieve the same level of cell kill is 2–3 times higher than in well-oxygenated tissue. The radiation therapy community has invested important resources to evaluate techniques able to overcome the radioresistance caused by hypoxia. The identification of hypoxia markers is an offshoot of research into radiosensitizer drugs.

Chapman et al. described clearly which requisites the best hypoxia tracer should exhibit.¹⁰⁵ It should have a high hypoxia-specific factor (HSF), i.e. good sensitivity for the hypoxic cells relative to the aerobic ones. At the same time it should identify tumor cells with oxygen levels above the range defining the radiobiologic oxygen effect. Furthermore,

acquisition of the hypoxia-specific signal should be done at the time at which the hypoxia/background signal is maximal. The hypoxia tracers under investigation belong to three different classes.

The first group (also called ‘vanilla’ markers) contains the 2-nitroimidazole (azomycin) moiety. The family includes: misonidazole (MISO); fluoromisonidazole (FMISO); the azomycin nucleosides (IAZAF, IAZGP, IAZXP); and EF-5.¹⁰⁵ These markers, upon reduction, can covalently bind to cellular molecules. Among these markers, those labeled with ¹⁸F are very difficult to image because, soon after administration, the hypoxia signal is covered by the signal coming from non-specific markers not yet excreted.

In the second group (the ‘chocolate’ markers), the selective bond with hypoxic cells is due to the reduction of a chelated metal. The best known tracer of this group is [⁶⁰Cu]diacetyl-bis(N₄-methylthiosemicarbazone) ([⁶⁰Cu]ATSM). This agent shows a HSF lower than that of the first group, and a heterogeneous dependence on oxygen concentration. The third class of markers (the ‘chocolate swirl’ markers) bind to hypoxic cells by means of the reduction of a metal-chelating ligand coupled with an azomycin compound. These products combine the tissue distribution and uptake asset of the chocolate class with the bioreduction properties of the azomycin. The main, and still unresolved, problem with the use of hypoxia markers in radiotherapy is the demonstration that the uptake into tumor regions correlates with the individual tumor radioresistance.

For H&N patients, Chao et al. demonstrated the feasibility of a novel [⁶⁰Cu] ATSM-guided IMRT approach through co-registering hypoxia [⁶⁰Cu]ATSM-PET with the corresponding CT images.¹⁰⁶

Dehdashti et al. investigated whether pretreatment tumor hypoxia assessed by [⁶⁰Cu]ATSM-PET predicts responsiveness to subsequent therapy in cervical cancer. Fourteen patients were studied by PET with [⁶⁰Cu]ATSM before initiation of radiotherapy and chemotherapy. The study revealed that tumor uptake was inversely related to progression-free survival and overall survival. PET furnished clinically relevant information about tumor oxygenation that was predictive of tumor behavior and response to therapy.¹⁰⁷

Eschmann et al. studied 40 patients with advanced H&N cancer ($n = 26$) or NSCLC ($n = 14$) to evaluate the ability of FMISO-PET to predict tumor recurrence after radiotherapy. Dynamic (0–15 min) and static PET scans were acquired. The results indicated that the outcome after radiotherapy can be predicted on the basis of the kinetic behavior of FMISO in tumor tissue. An accumulation-type curve, high SUV, and high tumor-to-muscle and tumor-to-mediastinum ratios at 4 hours after injection are highly suggestive of an incomplete response to treatment and might be used to select patients for intensified therapy protocols.¹⁰⁸

The [^{60}Cu]ATSM images show the best contrast early after injection, but these images are confounded by blood flow. FMISO has been criticized as inadequate because of its clearance characteristics, but its uptake after 2 hours is probably the most purely reflective of regional partial oxygen pressure at the time that the radiopharmaceutical is used. FMISO images show less contrast than those of [^{60}Cu]ATSM because of its lipophilicity and slower clearance.

In conclusion, many radiopharmaceuticals have been proposed for hypoxia imaging. To date, only FMISO and [^{60}Cu]ATSM have been evaluated in patients, but other promising tracers are under investigation.

Tumor proliferation and clonogenic cell density

Several randomized controlled trials have provided evidence on the importance of overall treatment time, especially in squamous-cell carcinoma of the H&N, with evidence from other tumor sites being less strong.^{109,110} This feature has been linked to rapid tumor-cell proliferation during RT as a resistance mechanism in fractionated RT. Proliferating cells in the S-phase (also called 'growth fraction') represent a part, ranging from 3% to 15%, of the entire tumor volume. Appearance of the radiation response and tumor volume shrinkage are generally faster when the growth fraction is higher. Knowledge of the clonogenic activity within the GTV is important for treatment planning and maybe more so for evaluating treatment response.

Numerous *in vitro* and *in vivo* studies have documented that FDG uptake is an indicator of tumor grade and clonogenic activity.^{111–114} Nevertheless, only three studies have documented a relationship of FDG uptake to local response.

Rege and colleagues reported their data in 12 patients with epidermoidal cancer of the head and neck.¹¹⁵ Pretreatment metabolic activity, as expressed by FDG-PET findings, is related to local control probability. This information could be used to identify the patients who could benefit from more aggressive or somewhat altered treatment instead of a conventional one.

Brun et al. reported that a low metabolic rate of glucose in 17 patients with H&N cancer after RT (15–36 Gy) or one cycle of chemotherapy is predictive of complete remission.¹¹⁶ Allal et al. studied 63 patients with H&N cancer and suggested that tumors with high pretreatment FDG uptake require stronger approaches.¹¹⁷

Unfortunately, FDG is an indicator of consuming energy activities, as cell division is, but also, other activities of tumor and non-tumor cells require glucose consumption. Therefore, information provided by FDG uptake can be ambiguous. Consequently, different and more focused radiotracers have been investigated.

Radiolabeled nucleosides

Thymidine is the only base incorporated uniquely into DNA. ^{11}C -labeled thymidine is a tracer produced with ^{11}C in two different positions (methyl-5 or ring-2 position); both forms are rapidly metabolized after their injection and consequently their assessment requires complex time-activity models to distinguish tumor uptake from the metabolites produced. There are some clinical data demonstrating a difference of [^{11}C]thymidine uptake in various human cancers.^{118,119} This behavior could reflect different proliferation profiles, but the data are still insufficient to draw any conclusion.

Radiolabeled deoxyuridine

To overcome difficulties related to the rapid metabolism of thymidine and the short half-life of ^{11}C , radiolabeled thymidine analogs have been developed. The [^{131}I], [^{124}I] deoxyuridine, and [^{77}Br]deoxyuridine, have a half-life long enough to allow delayed imaging. Preliminary clinical investigations are inconclusive because of technical issues of measurement (low statistical count and high background activity).^{120,121}

New radiopharmaceuticals more resistant to *in vivo* metabolism are to be studied. The most interesting is an ^{18}F analog, [^{18}F]FLT (3'-deoxy-3'-fluorothymidine).

Radiolabeled amino acids

Tumor cells incorporate a large amount of amino acids. One fraction of these amino acids is addressed to protein synthesis and one fraction to other use (such as energy supply or production of secretory substances). Despite that protein synthesis requires only a small portion of the amino acids pooled in the tumor cell, generally the signal produced by radiolabeled amino acids represents the proliferation grade of the tumor. Furthermore, the registered signal is a little hampered by the inflammatory component, because of its lower protein metabolism.¹²⁴ The most investigated amino acids are [^{11}C]MET and [^{11}C]tyrosine (Tyr), because of their simple synthesis and low metabolite interference. Despite preclinical studies showing a correlation between MET uptake and proliferation activity better than FDG in H&N cancer cell lines, clinical studies have demonstrated a correlation in brain and lung tumors but not in head and neck cancer and lymphoma.^{123–126} However, the studies published failed to clearly demonstrate the predictive value of MET-PET.^{127,128}

Apoptosis

Two different kinds of cell death can occur after radiation injury: interphase death and mitosis-related death. The first type is usually expressed by an apoptotic mechanism;

the second can happen with both apoptotic and necrotic processes. Apoptosis (or programmed cell death) is the dominant mechanism of lymphoid cell radio-induced death, while seeming to be less important in carcinoma cells. Apoptosis develops early and reaches its peak 3–6 hours after irradiation. There is evidence that the peak of apoptosis varies among different tumors and is related to the radiotherapy outcome. Studies of non-Hodgkin's lymphoma and prostate, bladder, and rectal cancer correlate high pretreatment apoptosis levels with good tumor regression.^{129–131} In H&N and cervical carcinoma the utility of pretreatment assessment is dubious.^{132,133} However, reports aiming to demonstrate a correlation between spontaneous apoptosis in non-irradiated tissue and the peak of apoptosis after irradiation have shown opposing results. Thus, the measurement of apoptotic response after the first fraction of radiotherapy is the best way to define the apoptotic response of the tumor and, consequently, the expected efficacy of treatment. Annexin 5 is a protein with high affinity for membrane phosphatidylserine; it is normally located at the inner membrane surface, but becomes externalized when the cell dies. The use of radiolabeled annexin 5 and its assessment by means of SPECT has been studied for purposes other than cancer cure, but this kind of application is now under investigation.^{134,135}

Tumor growth factor receptor status

Many tumor cells overexpress on their surface the receptors for epidermal growth factor (EGFR). EGFR is involved in the signal transduction of cellular response to various growth-stimulating factors. Consequently, amplification of the receptor status correlates with increased growth rate and worsens prognosis. There are several studies aimed at finding an association between high expression of EGFR and the response to radiation.^{136–138} All but one demonstrated a poor outcome in EGFR overexpression.¹³⁹ The interest in EGFR is determined by the possibility of targeting the receptors to block the signal transduction pathway. This can be accomplished by various substances such as monoclonal antibodies (e.g. IMC-225) and tyrosine kinase inhibitors (ZD1839). The *in vivo* assessment of EGFR expression can represent a predictive marker for radiotherapy outcome. For this purpose, several radiolabeled peptides and antibodies have been produced for various cancer types.¹⁴⁰ Furthermore, the concomitant delivery of these new therapeutic factors (in particular IMC-225 and Iressa®) and radiotherapy seems to improve the tumor response; to date, the most significant preclinical and clinical data concern head and neck and colorectal cancer.^{141,142} However, the clinical impact of radiolabeled EGF imaging is still to be defined.

The future

To fully exploit the IMRT dose-painting ability, the next step should be to tailor the dose distribution on the functional image. A great effort needs to be made to improve patient management in terms of much more individualized radiotherapy. Xing et al. have coined the idea of new 4D data for radiotherapy: 3D structural plus 1D metabolic.^{143,144} As PET imaging includes functional information, it can provide more than one method to better define the treatment volume. The information on tumor biology and functional properties of sensitive structures is valuable for guiding a spatial non-uniform dose distribution. The goal is to obtain a true biologically driven dose distribution, taking full advantage of the voxel by voxel metabolic information and IMRT features. The objective is to generate a different formalism for dose optimization that, instead of working in the PTV geometrical domain, will work in a voxel domain, dealing with biological heterogeneity.

In this way, radiotherapy will be a full image-guided process in which the dose would be escalated according to the functional signal. A rationale for delivering a dose in relation to the PET activity distribution is, for example, for FDG uptake, the correlation between signal and cell proliferation rate. Many authors have demonstrated the technical feasibility of planning in accordance with a metabolic map.^{143–147} Nevertheless, another important issue arises from this new concept of integration of functional information in radiation therapy.

To achieve a biologically conformal dose instead of a geometrical dose distribution means, first of all, defining a metric of tumor metabolism that gives us the possibility to quantify the metabolic signal, allowing us to define an abnormal signal. Second, it will be necessary to understand the correlation between the abnormal signal and the radiation dose and, in the meantime, to define the normal tissue tolerance on a voxel basis, according to functional importance. There is work being done in this direction, trying to establish a suitable metric for different functional imaging modalities, and this will be an active area of research.

References

1. van Dyk J. *The Modern Technology of Radiation Oncology*. Madison: Medical Physics Publishing; 1999.
2. Webb S. *Intensity Modulated Radiation Therapy. The Physics of Conformal Radiotherapy: Advances in Technology*. Bristol: IOP Publishing, 2001.
3. Webb S. *The Physics of Conformal Radiotherapy: Advances in Technology*. Philadelphia: IOP Publishing, 1997.
4. Ezzel GA, Galvin JM, Low D et al. Guidance document on delivery, treatment planning, and clinical implementation of IMRT: report of the IMRT subcommittee of the AAPM radiation therapy committee. *Med Phys* 2003; 30: 2089–15.

5. Mackie TR, Holmes T, Swerdloff S et al. Tomotherapy: a new concept for the delivery of dynamic conformal radiotherapy. *Med Phys* 1993; 20: 1709–19.
6. Yu CX, Yan D, Du MN, Zhou S, Verhey LJ. Optimization of leaf positions when shaping radiation fields with multileaf collimators. *Phys Med Biol* 1995; 40: 305–8.
7. International Commission on Radiation Units and Measurements. Prescribing, recording and reporting photon beam therapy. Report 50. Washington DC: International Commission on Radiation Units and Measurements, 1993.
8. Ling CC, Humm J, Larson S et al. Towards multidimensional radiotherapy (MD-CRT): biological imaging and biological conformality. *Int J Radiat Oncol Biol Phys* 2000; 47: 551–60.
9. Bentzen SM. Theragnostic imaging for radiation oncology: dose-painting by numbers. *Lancet Oncol* 2005; 6: 112–17.
10. McManus MP, Hicks RJ, Ball DI et al. F-18 fluorodeoxyglucose positron emission tomography staging in radical radiotherapy candidates with nonsmall cell lung carcinoma: powerful correlation with survival and high impact on treatment. *Cancer* 2001; 92: 886–95.
11. Vanuytsel LJ, Vansteenkiste JF, Stroobants SG et al. The impact of (18)FDG-PET lymph node staging on the radiation treatment volumes in patients with non-small cell lung cancer. *Radiother Oncol* 2000; 55: 317–24.
12. Gregoire V. Is there any future in radiotherapy planning without the use of PET? Unraveling the myth . . . *Radiother Oncol* 2004; 73: 261–3.
13. Schoder H, Erdi YE, Larson SM et al. PET/CT: a new imaging technology in nuclear medicine. *Eur J Nucl Med Mol Imaging* 2003; 30: 1419–37.
14. Hill DL, Batchelor PG, Holden M, Hawkes DJ. Medical image registration. *Phys Med Biol* 2001; 46: R1–45.
15. Kanatani K. Analysis of 3-D rotation fitting. *IEEE Trans Pattern Anal Match Intell* 1994; 16: 543–9.
16. Wells WM, Viola PA, Atsumi H, Nakajima S, Kikinis R. Multi-modal volume registration by maximization of mutual information. *Med Image Anal* 1996; 1: 35–51.
17. Matic S, Dempsey JF, Bosch WR et al. Multimodality image registration quality assurance for conformal three dimensional treatment planning. *Int J Radiat Oncol Biol Phys* 2001; 51: 255–60.
18. Daisne JF, Sibomana M, Bol A et al. Evaluation of multi-modality (CT, MRI and PET) coregistration procedure on phantom and head and neck cancer patients: accuracy, reproducibility and consistency. *Radiother Oncol* 2003; 69: 237–45.
19. Senan S, De Ruysscher D. Critical review of PET-CT for radiotherapy planning in lung cancer. *Crit Rev Oncol Hematol* 2005; 56: 345–51.
20. Ciernik IF, Dizendorf E, Baumert BG et al. Radiation treatment planning with an integrated positron emission and computer tomography (PET/CT): a feasibility study. *Int J Radiat Oncol Biol Phys* 2003; 57: 853–63.
21. Osman MM, Cohade C, Nakamoto Y et al. Clinically significant inaccurate localization of lesions with PET-CT: frequency in 300 patients. *J Nucl Med* 2003; 44: 240–3.
22. Yaremko B, Riauka T, Robinson D, et al. Threshold modification for tumour imaging in non-small-cell lung cancer using positron emission tomography. *Nucl Med Commun* 2005; 26: 433–40.
23. Erdi Y, Mawlawi O, Larson SM et al. Segmentation of lung lesion volume by adaptive positron emission tomography image thresholding. *Cancer* 1997; 80 (Suppl): 2505–9.
24. Paulino AC, Johnstone PA. FDG-PET in radiotherapy treatment planning: Pandora's box? *Int J Radiat Oncol Biol Phys* 2004; 59: 4–5.
25. Black QC, Grills IS, Kestin LL et al. Defining a radiotherapy target with positron emission tomography. *Int J Radiat Oncol Biol Phys* 2004; 60: 1272–82.
26. Nestle U, Kremp S, Schuler AS et al. Comparison of different methods for delineation of F-FDG PET positive tissue for target volume definition in radiotherapy of patients with non small cell lung cancer. *J Nucl Med* 2005; 46: 1342–8.
27. Daisne JF, Sibomana M, Bol A et al. Tri-dimensional automatic segmentation of PET volumes based on measured source to background ratios: influence of reconstruction algorithms. *Radiother Oncol* 2003; 69: 247–50.
28. Daisne JF, Duprez T, Weynand B et al. Tumor volume in pharyngolaryngeal squamous cell carcinoma: comparison at CT, MR imaging, and FDG PET and validation with surgical specimen. *Radiology* 2004; 233: 93–100.
29. Gambhir SS, Czernin J, Schwimmer J et al. A tabulated summary of the FDG PET literature. *J Nucl Med* 2001; 42: 1S–93S.
30. Dizendorf EV, Baumert BG, Von Schulthess GK, Lutolf UM, Steinert HC. Impact of whole-body 18F-FDG PET on staging and managing patients for radiation therapy. *J Nucl Med* 2003; 44: 24–9.
31. Gabriele P, Malinverni G, Moroni GL et al. The impact of 18F-deoxyglucose positron emission tomography on tumor staging, treatment strategy and treatment planning for radiotherapy in a department of radiation oncology. *Tumori* 2004; 90: 579–85.
32. Grosu AL, Piert M, Weber WA et al. Positron emission tomography for radiation treatment planning. *Strahlenther Onkol* 2005; 181: 483–99.
33. Herrmann T. Radiation oncology and functional imaging. *Nuklearmedizin* 2005; 44 (Suppl 1): S38–40.
34. Toloza EM, Harpole L, McCrory DC. Non invasive staging of non small cell lung cancer: a review of the current evidence. *Chest* 2003; 123: 137S–46S.
35. Dawood M, Lang N, Jiang X, Schafers KP. Lung motion correction on respiratory gated 3-D PET/CT images *IEEE Trans Med Imaging*. 2006; 25: 476–85.
36. van Baardwijk A, Baumert BG, Bosmans G et al. The current status of FDG-PET in tumour volume definition in radiotherapy treatment planning. *Cancer Treat Rev* 2006; 32: 245–60.
37. Borst GR, Belderbos JS, Boellaard R. FDG uptake: a prognostic factor for inoperable non-small cell lung cancer. *Eur J Cancer* 2005; 41: 1533–41.
38. Deniaud-Alexandre E, Touboul E, Lerouge D et al. Impact of computed tomography (CT) and 18F-deoxyglucose-coincidence detection emission tomography (FDG-CDET) image fusion for optimisation of conformal radiotherapy in non-small-cell lung cancers. *Cancer Radiother* 2005; 9: 304–15.
39. Nestle U, Hellwig D, Schmidt S et al. 2-Deoxy-2-18Ffluoro-D-glucose positron emission tomography in target volume definition for radiotherapy of patients with non small cell lung cancer. *Mol Imaging Biol* 2002; 4: 257–63.

40. Nestle U, Walker K, Schmidt S et al. 18F-deoxyglucose positron emission tomography (FDG-PET) for the planning of radiotherapy in lung cancer: high impact in patients with atelectasis. *Int J Radiat Oncol Biol Phys* 1999; 44: 593–7.
41. Vanuytsel LJ, Vansteenkiste JF, Stroobants SG et al. The impact of 18-fluoro-2-deoxy-D-glucose positron emission tomography (FDG-PET) lymph node staging on the radiation treatment volumes in patients with non-small cell lung cancer. *Radiother Oncol* 2000; 55: 317–24.
42. Messa C, Ceresoli GL, Rizzo G et al. Feasibility of (18F) FDG-PET and coregistered CT on clinical target volume definition of advanced non-small cell lung cancer. *Q J Nucl Med Mol Imaging* 2005; 49: 259–66.
43. Munley MT, Marks LB, Scarfone C et al. Multimodality nuclear medicine imaging in three dimensional radiation treatment planning for lung cancer: challenges and prospects. *Lung Cancer* 1999; 23: 167–77.
44. Mah K, Caldwell BC, Ung YC et al. The impact of FDG-PET on target and critical organs in CT based treatment planning of patients with poorly defined non small cell lung carcinoma: a prospective study. *Int J Radiat Oncol Biol Phys* 2002; 52: 339–50.
45. Erdi YE, Rosenzweig K, Erdi AK et al. Radiotherapy treatment planning for patients with non-small cell lung cancer using positron emission tomography (PET). *Radiother Oncol* 2002; 62: 51–60.
46. Grosu AL, Piert M, Weber WA. Positron emission tomography for radiation treatment planning. *Strahlenther Onkol* 2005; 181: 483–99.
47. Brianzoni E, Rossi G, Ancidei S et al. Radiotherapy planning: PET/CT scanner performances in the definition of gross tumour volume and clinical target volume. *Eur J Nucl Med Mol Imaging* 2005; 32: 1392–9.
48. Steenbakkers RJ, Duppen JC, Fitton I et al. Reduction of observer variation using matched CT-PET for lung cancer delineation: a three-dimensional analysis. *Int J Radiat Oncol Biol Phys* 2006; 64: 435–48.
49. Bradley J, Thorstad WL, Mutic S et al. Impact of FDG-PET on radiation therapy volume delineation in non small cell lung cancer. *Int J Radiat Oncol Biol Phys* 2003; 57: 853–63.
50. Ashamalla H, Rafla S, Parikh K et al. The contribution of integrated PET/CT to the evolving definition of treatment volumes in radiation treatment planning in lung cancer. *Int J Radiat Oncol Biol Phys* 2005; 63: 1016–23.
51. Lavrenkov K, Partridge M, Cook G, Brada M. Positron emission tomography for target volume definition in the treatment of non-small cell lung cancer. *Radiother Oncol* 2005; 77: 1–4.
52. Caldwell CB, Mah K, Skinner M, Danjoux CE. Can PET provide the 3D extent of tumor motion for individualized internal target volumes? A phantom study of the limitation of CT and the promise of PET. *Int J Radiat Oncol Biol Phys* 2003; 55: 1381–93.
53. Nehmeh SA, Erdi YE, Ling CC et al. Effect of respiratory gating on reducing lung motion artefacts in PET imaging of lung cancer. *Med Phys* 2002; 29: 366–71.
54. Yaremko B, Riauka T, Robinson D et al. Thresholding in PET images of static and moving targets. *Phys Med Biol* 2005; 50: 5969–82.
55. Christian JA, Partridge M, Nioutsikou E. The incorporation of SPECT functional lung imaging into inverse radiotherapy planning for non-small cell lung cancer. *Radiother Oncol* 2005; 77: 271–7.
56. Zhang WJ, Zheng R, Zhao LJ, Wang LH, Chen SZ. Utility of SPECT lung perfusion scans in assessing early changes in pulmonary function of patients with lung cancer after radiotherapy. *Ai Zheng* 2004; 23: 1180–4.
57. Seppenwoolde Y, De Jaeger K, Boersma LJ, Belderbos JS, Lebesque JV. Regional differences in lung radiosensitivity after radiotherapy for non-small-cell lung cancer. *Int J Radiat Oncol Biol Phys* 2004; 60: 748–58.
58. Suga K, Kawakami Y, Zaki M et al. Clinical utility of co-registered respiratory-gated (99m)Tc-Technegas/MAA SPECT-CT images in the assessment of regional lung functional impairment in patients with lung cancer. *Eur J Nucl Med Mol Imaging* 2004; 31: 1280–90.
59. Launbenbacher C, Saumweber D, Wagner-Manslau C et al. Comparison of fluorine-18-fluorodeoxyglucose PET, MRI and endoscopy for staging head and neck squamous-cell carcinomas. *J Nucl Med* 1995; 36: 1747–57.
60. Schechter NR, Gillenwater AM, Byers RM et al. Can positron emission tomography improve the quality of care for head-and-neck cancer patients? *Int J Radiat Oncol Biol Phys* 2001; 51: 4–9.
61. Rege S, Maas, Chaiken L et al. Use of positron emission tomography with fluorodeoxyglucose in patients with extracranial head and neck cancers. *Cancer* 1994; 73: 3047–58.
62. Adams S, Baum RP, Stuckensen T et al. Prospective comparison of 18F-FDG PET with conventional imaging modalities (CT, MRI, US) in lymph node staging of head and neck cancer. *Eur J Nucl Med* 1998; 25: 1255–60.
63. Fischbein NJ, Os AA, Caputo GR et al. Clinical utility of positron emission tomography with 18F-fluorodeoxyglucose in detecting residual/recurrent squamous cell carcinoma of the head and neck. *Am J Neuroradiol* 1998; 19: 1189–96.
64. Li P, Zhuang H, Mozley PD et al. Evaluation of recurrent squamous cell carcinoma of the head and neck with FDG positron emission tomography. *Clin Nucl Med* 2001; 26: 131–5.
65. Greven KM, Williams DW III, Keyes JW Jr et al. Positron emission tomography of patients with head and neck carcinoma before and after high dose irradiation. *Cancer* 1994; 74: 1355–9.
66. Hannah A, Scott AM, Tochon-Danguy H. Evaluation of 18F-fluorodeoxyglucose positron emission tomography and computed tomography with histopathologic correlation in the initial staging of head and neck cancer. *Ann Surg* 2002; 236: 208–17.
67. Paulus P, Sambon A, Vivegnis D et al. 18FDG-PET for the assessment of primary head and neck tumors: clinical, computed tomography, and histopathological correlation in 38 patients. *Laryngoscope* 1998; 108: 1578–83.
68. Johansen J, Eigtved A, Buchwald C. Implication of 18F-fluoro-2-deoxy-D-glucose positron emission tomography on management of carcinoma of unknown primary in the head and neck: a Danish cohort study. *Laryngoscope* 2002; 112: 2009–14.
69. Fogarty GB, Peters LJ, Stewart J. The usefulness of fluorine 18-labelled deoxyglucose positron emission tomography in

- the investigation of patients with cervical lymph-adenopathy from an unknown primary tumor. *Head Neck* 2003; 25: 138–45.
70. Greven KM, Keyes JW, Williams DW. Occult primary tumors of head and neck. Lack of benefit from positron emission tomography imaging with 2-(F18)fluoro-2-deoxy-D-glucose. *Cancer* 1999; 86: 114–18.
71. Nishioka T, Shiga T, Shirato H et al. Image fusion between 18FDG-PET and MRI/CT for radiotherapy planning of oropharyngeal and nasopharyngeal carcinomas. *Int J Radiat Oncol Biol Phys* 2002; 53: 1051–7.
72. Scarfone C, Lavelly WC, Cmelak AJ et al. Prospective feasibility trial of radiotherapy target definition for head and neck cancer using 3-dimensional PET and CT imaging. *J Nucl Med* 2004; 45: 543–52.
73. Heron DE, Andrade RS, Flickinger J et al. Hybrid PET-CT simulation for radiation treatment planning in head-and-neck cancers: a brief technical report. *Int J Radiat Oncol Biol Phys* 2004; 60: 1419–24.
74. Geets X, Daisne JF, Tomsej M et al. Impact of the type of imaging modality on target volumes delineation and dose distribution in pharyngo-laryngeal squamous cell carcinoma: comparison between pre- and per-treatment studies. *Radiother Oncol* 2006; 78: 291–7.
75. Wang D, Schultz CJ, Jursinic PA et al. Initial experience of FDG-PET/CT guided IMRT of head and neck carcinoma. *Int J Radiat Oncol Biol Phys* 2006; 65: 143–51.
76. Paulino AC, Koshy M, Howell R et al. Comparison of CT- and FDG-PET-defined gross tumor volume in intensity-modulated radiotherapy for head-and-neck cancer. *Int J Radiat Oncol Biol Phys* 2005; 61: 1385–92.
77. Koshy M, Paulino AC, Howell R et al. F-18 FDG PET-CT fusion in radiotherapy treatment planning for head and neck cancer. *Head Neck* 2005; 27: 494–502.
78. Versari A, Iotti C, Iori M et al. Role of FDG-PET in head and neck IMRT planning. *J Nucl Med* 2006; 47: 109–10 (abstr).
79. Schwartz DL, Ford E, Rajendran J et al. FDG-PET/CT imaging for preradiotherapy staging of head and neck squamous cell carcinoma. *Int J Radiat Oncol Biol Phys* 2005; 61: 129–36.
80. Rohren EM, Turkington TG, Coleman RE et al. Clinical applications of PET in oncology. *Radiology* 2004; 231: 305–32.
81. Lowe VJ, Dunphy FR, Varvares M et al. Evaluation of chemotherapy response in patients with advanced head and neck cancer using 18F-fluorodeoxyglucose positron emission tomography. *Head Neck* 1997; 19: 666–74.
82. Terhaard CH, Bongers V, Van Rijk PP et al. F-18-fluoro-deoxy-glucose positron emission tomography scanning in detection of local recurrence after radiotherapy for laryngeal/pharyngeal cancer. *Head Neck* 2001; 23: 933–41.
83. Kao CH, Shiau YC, Shen YY et al. Detection of recurrent or persistent nasopharyngeal carcinomas with technetium-99m methoxyisobutylisonitrile single photon emission computed tomography and computed tomography: comparison with 18-fluoro-2-deoxyglucose positron emission tomography. *Cancer* 2002; 94: 1981–6.
84. Wong RJ, Lin DT, Schoder H. Diagnostic and prognostic value of (18F)-fluorodeoxyglucose positron emission tomography for recurrent head and neck squamous cell carcinoma. *J Clin Oncol* 2002; 20: 4199–208.
85. Greven KM, Williams DW III, McGuirt WF Sr et al. Serial positron emission tomography scans following radiation therapy of patients with head and neck cancer. *Head Neck* 2001; 23: 942–6.
86. Schöder H, Yeung HWD. Positron emission imaging of head and neck cancer, including thyroid carcinoma. *Seminars Nucl Med* 2004; 34: 180–97.
87. Myers E, Leffall L. *Head and Neck Oncology: Diagnosis, Treatment, and Rehabilitation*. Boston: Little Brown, 1991.
88. McGuirt W, Greven K, Keyes J et al. Positron emission tomography in the evaluation of laryngeal carcinoma. *Ann Otol Rhinol Laryngol* 1995; 104: 274–8.
89. Esthappan J, Mutic S, Malyapa RS et al. Treatment planning guidelines regarding the use of CT/PET-guided IMRT for cervical carcinoma with positive paraaortic lymph nodes. *Int J Radiat Oncol Biol Phys* 2004; 58: 1289–97.
90. Mutic S, Grigsby PW, Low DA et al. PET-guided three-dimensional treatment planning of intracavitary gynecologic implants. *Int J Radiat Oncol Biol Phys* 2002; 52: 1104–10.
91. Lin LL, Mutic S, Malyapa RS et al. Sequential FDG-PET brachytherapy treatment planning in carcinoma of the cervix. *Int J Radiat Oncol Biol Phys* 2005; 63: 1494–501.
92. Malyapa RS, Mutic S, Low DA. Physiologic FDG-PET three-dimensional brachytherapy treatment planning for cervical cancer. *Int J Radiat Oncol Biol Phys* 2002; 54: 1140–6.
93. Leong T, Everitt C, Yuen K et al. A prospective study to evaluate the impact of FDG-PET on CT-based radiotherapy treatment planning for esophageal cancer. *Radiother Oncol* 2006; 78: 254–61.
94. Moureau-Zabotto L, Touboul E, Lerouge D et al. Impact of CT and 18F-deoxyglucose positron emission tomography image fusion for conformal radiotherapy in esophageal carcinoma. *Int J Radiat Oncol Biol Phys* 2005; 63: 340–5.
95. Konski A, Doss M, Milestone B et al. The integration of 18-fluoro-deoxy-glucose positron emission tomography and endoscopic ultrasound in the treatment-planning process for esophageal carcinoma. *Int J Radiat Oncol Biol Phys* 2005; 61: 1123–8.
96. Vrieze O, Haustermans K, De Wever W et al. Is there a role for FDG-PET in radiotherapy planning in esophageal carcinoma? *Radiother Oncol* 2004; 73: 269–75.
97. Lee YK, Cook G, Flower MA et al. Addition of 18-FDG-PET scans to radiotherapy planning of thoracic lymphoma. *Radiother Oncol* 2004; 73: 277–83.
98. Levivier M, Wikler D Jr, Massager N et al. The integration of metabolic imaging in stereotactic procedures including radiosurgery: a review. *J Neurosurg* 2002; 97: 542–50.
99. Grosu AL, Feldmann HJ, Dick S et al. Implications of IMT-SPECT for postoperative radiotherapy planning in patients with gliomas. *Int J Radiat Oncol Biol Phys* 2002; 54: 842–54.
100. Grosu AL, Weber WA, Riedel E et al. L-(methyl-11C) methionine positron emission tomography for target delineation in resected high-grade gliomas before radiotherapy. *Int J Radiat Oncol Biol Phys* 2005; 63: 64–74.
101. Carey BM. Imaging for prostate cancer. *Clin Oncol (R Coll Radiol)* 2005; 17: 553–9.
102. Oyama N, Miller TR, Dehdashti F et al. 11C-acetate PET imaging of prostate cancer: detection of recurrent disease at PSA relapse. *J Nucl Med* 2003; 44: 549–55.

103. Sandblom G, Sorensen J, Lundin N, Haggman M, Malmstrom PU. Positron emission tomography with C11-acetate for tumor detection and localization in patients with prostate-specific antigen relapse after radical prostatectomy. *Urology* 2006; 67: 996–1000.
104. Picchio M, Messa C, Landoni C et al. Value of [11C]choline-positron emission tomography for re-staging prostate cancer: a comparison with [18F]fluorodeoxyglucose-positron emission tomography. *J Urol* 2003; 169: 1337–40.
105. Chapman JD, Bradley JD, Eary JF et al. Molecular (functional) imaging for radiotherapy applications: an RTOG symposium. *Int J Radiat Oncol Biol Phys* 2003; 55: 294–301.
106. Chao KS, Bosch WR, Mutic S et al. A novel approach to overcome hypoxic tumor resistance: Cu-ATSM-guided intensity-modulated radiation therapy. *Int J Radiat Oncol Biol Phys* 2001; 49: 1171–82.
107. Dehdashti F, Grigsby PW, Mintun MA et al. Assessing tumor hypoxia in cervical cancer by positron emission tomography with ⁶⁰Cu-ATSM: relationship to therapeutic response – a preliminary report. *Int J Radiat Oncol Biol Phys* 2003; 55: 1233–8.
108. Eschmann SM, Paulsen F, Reimold M et al. Prognostic impact of hypoxia imaging with 18F-misonidazole PET in non-small cell lung cancer and head and neck cancer before radiotherapy. *J Nucl Med* 2005; 46: 253–60.
109. Bernier J, Bentzen SM. Altered fractionation and combined radiochemotherapy approaches: pioneering new opportunities in head and neck oncology. *Eur J Cancer* 2003; 30: 560–71.
110. Bentzen SM. Repopulation in radiation oncology: perspective of clinical research. *Int J Radiat Oncol Biol Phys* 2003; 79: 581–5.
111. Smith TAD. FDG uptake, tumour characteristics and response to therapy: a review. *Nucl Med Commun* 1998; 19: 97–105.
112. Vesselle H, Schmidt RA, Pugsley JM et al. Lung cancer proliferation correlates with F-18 fluorodeoxyglucose uptake by positron emission tomography. *Clin Cancer Res* 2000; 6: 3837–44.
113. Smith TA, Titley J. Deoxyglucose uptake by head and neck squamous carcinoma: influence of change in proliferative fraction. *Int J Radiat Oncol Biol Phys* 2000; 47: 219–23.
114. Avril N, Menzel M, Dose J et al. Glucose metabolism of breast cancer assessed by F-18-FDG PET: histologic and immunohistochemical tissue analysis. *J Nucl Med* 2001; 42: 9–16.
115. Rege S, Safa AA, Chaiken L et al. Positron emission tomography: an independent indicator of radiocurability in head and neck carcinomas. *Am J Clin Oncol* 2000; 23: 164–9.
116. Brun E, Ohlsson T, Erlandsson K et al. Early prediction of treatment outcome in head and neck cancer with 2-(18)FDG PET. *Acta Oncol* 1997; 36: 741–7.
117. Allal AS, Dulguerov P, Allaoua M et al. Standardized uptake value of 2-(F-18) fluoro-2-deoxy-D-glucose in predicting outcome in head and neck carcinomas treated by radiotherapy with or without chemotherapy. *J Clin Oncol* 2002; 20: 1398–404.
118. Mankoff DA, Dehdashti F, Shields AF. Characterizing tumors using metabolic imaging: PET imaging of cellular proliferation and steroid receptors. *Neoplasia* 2000; 2: 71–88.
119. Krohn KA. Evaluation of alternative approaches for imaging cellular growth. *Q J Nucl Med* 2001; 45: 174–8.
120. Blasberg RG, Roeleke U, Weinreich R et al. Imaging brain tumor proliferative activity with (124I) iododeoxyuridine. *Cancer Res* 2000; 60: 624–35.
121. Tjuvajev JG, Macapinlac HA, Daghighian F et al. Imaging of brain tumor proliferative activity with iodine-131-iododeoxyuridine. *J Nucl Med* 1994; 35: 1407–17.
122. Kubota R, Kubota K, Yamada S et al. Methionine uptake by tumor tissue: a microautoradiographic comparison with FDG. *J Nucl Med* 1995; 36: 484–92.
123. Lindholm P, Leskinen S, Lapela M. Carbon-11-methionine uptake in squamous cell head and neck cancer. *J Nucl Med* 1998; 39: 1393–7.
124. Derlon JM, Petit-Taboue MC, Chapon F et al. The in vivo metabolic pattern of low grade brain gliomas: a positron emission tomography study using 18F-fluorodeoxyglucose and 11C-methylmethionine. *Neurosurgery* 1997; 40: 276–87.
125. Lindholm P, Leskinen-Kallio S, Lapela M. Carbon-11-methionine uptake in squamous cell head and neck cancer. *J Nucl Med* 1998; 39: 1393–7.
126. Miyazawa H, Arai T, Lio M et al. PET imaging of non-small-cell lung carcinoma with carbon-11-methionine: relationship between radioactivity uptake and flow-cytometric parameters. *J Nucl Med* 1993; 34: 1886–91.
127. Nuutinen J, Jyrkkio S, Lehtikainen P et al. Evaluation of early response to radiotherapy in head and neck cancer measured with (11C) methionine-positron emission tomography. *Radiother Oncol* 1999; 52: 225–32.
128. Kubota K, Yamada S, Ishiwata K et al. Evaluation of treatment response of lung cancer with positron emission tomography and L-(methyl-11C)methionine: a preliminary study. *Eur J Nucl Med* 1993; 20: 495–501.
129. Scott N, Hale A, Deakin M et al. A histopathological assessment of the response of rectal adenocarcinoma to combination chemo-radiotherapy: relationship to apoptotic activity, p53 and bcl-2 expression. *Eur J Surg Oncol* 1998; 24: 169–73.
130. Rodel C, Grabenbauer GG, Papadopoulos T et al. Apoptosis as a cellular predictor for histopathologic response to neoadjuvant radiochemotherapy in patients with rectal cancer. *Int J Radiat Oncol Biol Phys* 2002; 52: 294–303.
131. Rodel C, Grabenbauer GG, Rodel F et al. Apoptosis, p53, bcl-2, and Ki67 in invasive bladder carcinoma: possible predictors for response to radiochemotherapy and successful bladder preservation. *Int J Radiat Oncol Biol Phys* 2000; 46: 1213–21.
132. Bartelink H, Begg A, Martin JC, et al. Towards prediction and modulation of treatment response. *Radiother Oncol* 1999; 50: 1–11.
133. Corvò R, Antognoni P, Sanguinet G. Biological predictors of response to radiotherapy in head and neck cancer: recent advances and emerging perspectives. *Tumori* 2001; 87: 355–63.
134. Collingridge DR, Glaser M, Osman S et al. In vitro selectivity, in vivo biodistribution and tumor uptake of annexin V radiolabelled with a positron emitting radioisotope. *Br J Cancer* 2003; 89: 1327–33.
135. Van de Wiele C, Lahorte C, Vermeersch H et al. Quantitative tumor apoptosis imaging using technetium-99m-HYNIC

- annexin V single photon emission computed tomography. *J Clin Oncol* 2003; 21: 3483–7.
136. Magné N, Pivot X, Bensadoun RJ et al. The relationship of epidermal growth factor receptor levels to the prognosis of unresectable pharyngeal cancer patients treated by chemoradiotherapy. *Eur J Cancer* 2001; 37: 2169–77.
 137. Grandis JR, Melhem MF, Gooding WE et al. Levels of TGF- α and EGFR protein in head and neck squamous cell carcinoma and patient survival. *J Natl Cancer Inst* 1998; 90: 824–32.
 138. Maurizi M, Amadori G, Ferrandina G et al. Prognostic significance of epidermal growth factor receptor in laryngeal squamous cell carcinoma. *Br J Cancer* 1996; 74: 1253–7.
 139. Smith BD, Smith GL, Carter D et al. Molecular marker expression in oral and oropharyngeal squamous cell carcinoma. *Arch Otolaryngol Head Neck Surg* 2001; 127: 780–5.
 140. Mendesohn J, Baird A, Fan Z et al. Growth factors and their receptors in epithelial malignancies. In: Mendesohn J, Howley PM, Israel MA et al., eds. *The Molecular Basis of Cancer*. Philadelphia: WB Saunders; 2001: 137–53.
 141. Robert F, Ezekiel MP, Spencer SA et al. Phase I study of anti-epidermal growth factor receptor antibody cetuximab in combination with radiation therapy in patients with advanced head and neck cancer. *J Clin Oncol* 2001; 19: 3234–43.
 142. Williams KJ, Telfer BA, Stratford IJ et al. ZD1839 (Iressa), a specific oral epidermal growth factor receptor – tyrosine kinase inhibitor, potentiates radiotherapy in a human colorectal cancer xenograft model. *Br J Cancer* 2002; 86: 1157–61.
 143. Xing L, Cotrutz C, Hunjan S et al. Inverse planning for functional image guided intensity modulated radiation therapy. *Phys Med Biol* 2002; 47: 3567–78.
 144. Xing L, Hunjan S, Lian J et al. Toward biologically conformal radiotherapy: functional and molecular image guided intensity modulated radiation therapy. In: *Proceedings of the XIV International Conference on Use of Computers in Radiation Therapy*, Seoul, Korea, 2004: 36–9.
 145. Albe M, Paulsen F, Eschmann SM, Machulla HJ. On biologically conformal boost dose optimisation. *Phys Med Biol* 2003; 48: N31–5.
 146. Yang Y, Xing L. Towards biologically conformal radiation therapy (BCRT): selective IMRT dose escalation under the guidance of spatial biology distribution. *Med Phys* 2005; 32: 1473–84.
 147. Das SK, Miften MM, Zhou S et al. Feasibility of optimizing the dose distribution in lung tumors using fluorine-18-fluorodeoxyglucose positron emission tomography and single photon emission computed tomography guided dose prescriptions. *Med Phys* 2004; 31: 1452–61.

Index

N.B. Page numbers in *italic* denote material in Figures or Tables.

- [¹¹C]acetate 119, 121, 512
- acute myeloid leukemia
 - signaling pathways 12
 - treatment-related 310–11
- ADAC C-PET 477
- adenocarcinomas, esophageal 89
- adenomas
 - benign 69–70
 - of pituitary gland 25, 43
 - radionuclide imaging 35
- adrenal glands 177
- adrenal hyperplasia 183
 - bilateral 179
- adrenal metastases 72
- adrenal tumors 177–88
 - adrenocortical scintigraphy 181–7
 - adrenocortical tumors 177–8
 - diagnostic modalities 181–7
 - imaging 183
 - CT 178, 179, 182, 182, 185, 186
 - dexamethasone suppression 183
 - FDG-PET 177, 181, 183, 185–7
 - HED-PET 184–5, 187
 - HED-PET-CT 182, 186
 - L-DOPA-PET 185, 187
 - MIBG scintigraphy 180, 181, 183–4, 185, 187
 - drug interactions 184
 - MRI 178
 - NP-59 181–3
 - drug interactions 182
 - interpretation 182–3
 - patient preparation 181
 - pitfalls 182
 - technique 181–2
 - PET 182, 183, 184–5, 186, 187
 - PET-CT 182, 186
 - scintigraphy 179
 - adrenocortical 181–3
 - sympathetic nervous system tumor 183–7
 - SPECT 178, 179, 180, 181–4, 185
 - SPECT-CT 178, 179, 182, 184, 185
 - medullary tumors 178–9
 - metastatic disease 177, 179, 180, 181
- adrenocortical carcinoma 177
- adrenocorticotrophic hormone (ACTH) 177, 181, 182–3
- affinity enhancement system (AES) 294, 295
- Akt 2, 6, 9
- alcohol injection 353
- aldosteronism, primary 177
- aldosteronomas 183
- Allegro 475, 477, 489, 490, 492, 492, 494–5
- α -fetoprotein 352
- alveolar rhabdomyosarcomas 240, 242
- American Joint Committee on Cancer (AJCC)
 - staging system
 - esophageal cancer 89, 90
 - malignant melanoma 253, 254
- American Thoracic Society (ATS) lung cancer tests 61, 62
- amino acid transporter markers 424–5
- amino acids, radiolabeled 37–9, 514
- [¹¹C]aminoisobutyric acid (AIB) 244
- anaplastic astrocytomas 24, 41, 42
- anaplastic oligodendrogliomas 24, 42
- androgen receptor 19
- aneuploidy 1
- Ang 9, 10
- Anger camera (γ -camera) *see* γ -camera (Anger camera)
- angiogenesis 9–10
 - inhibitors 10
 - molecular basis 10
 - molecular targets in imaging 19
 - new radiopharmaceuticals 414–15
 - regulation 9
 - signaling molecules 10
- angiogenic factors
 - pro-/anti-angiogenic 9
 - in tumorigenesis 8
- angiosarcomas 231, 240
- annexin 5 20
- anti-carcinoembryonic antigen (CEA) 294–5, 295, 296
- anti-CD20 Ab 304
- antiapoptotic genes 6
- antibodies 383
 - 776.1 386, 387
 - AC6C3-2B12 392
 - AE1 391–2
 - anti-CEA antibodies 359, 360, 361–2, 363
 - B43.13 386, 387
 - B72.3 386, 390, 393
 - bispecific 294, 361–2
 - CC49 386, 390, 393, 393
 - chimeric (humanized) 303
 - clinical applications, parameters for 384
 - conjunction with bifunctional ligands 434–7
 - evolution of radioimmunotherapy 303
 - fragments 437
 - HMF61 386, 387–8, 393
 - hu3S193 386, 391
 - IgM antibody 392
 - MN-14 386, 388
 - MOv18 386, 388–9
 - MX35 386, 390–1
 - therapeutic, manufacturing 434–7
 - and tumor physiology 384
 - see also* monoclonal antibodies
- antibody-dependent cellular cytotoxicity (ADCC) 390
- antibody-directed enzyme pro-drug therapy (ADEPT) system 361
- antigens
 - CEA 386, 388
 - gp38 (aFR) 386, 388
 - gp95 386, 390
 - HER2/neu 391–2
 - Lewis Y 386, 391
 - MUC1 386, 387, 393
 - MUC16/CA125 386, 387
 - TAG72 386, 389–90, 393, 394
- antigens (*Continued*)
 - tumor-associated, in therapy 433
 - tumor-expressed 383
- antigrowth signals 3
- APAF1 2
- Apomate 413–14
- apoptosis
 - extrinsic (death receptor-mediated) pathway 5
 - intrinsic pathway 5–6
 - molecular targets in imaging 20
 - new radiopharmaceuticals 413
 - protection from 6
 - regulatory proteins 2
 - vs* necrosis 5
- apparent diffusion coefficient (ADC) 30, 31
- astatine-211 302
- astrocytomas 24, 367
 - classification 41
 - genetic changes 26
 - imaging 34
 - magnetic resonance image 28
- ATM 2
- autologous stem cell transplantation (ASCT) 306, 308
- autophagy 6, 7
- avidin–biotin model 374
- axillary node dissection (AND) 143, 144
- axillary node involvement 150
- B-cell lymphomas 25, 300
 - signaling pathways 12
- Bak 2
- basal-cell carcinoma signaling pathways 12
- Bax 2
- Bcl-2 2, 6
- Bcl-XL 6
- BCNU 372
- BECN1 7
- benign cortical irregularity of distal femur (BCIDF) 230
- Bexxar *see* tositumomab (Bexxar)
- biochemistry of apoptosis 5
- Biograph 475, 478, 490, 492, 494–5
 - Sensation 406
- biopsies
 - fine needle aspiration (FNAB)
 - CUP imaging 267
 - thyroid cancer imaging 161, 162–3
 - ultrasound-guided 161–3, 162, 165
 - glioma imaging 27
 - PET-CT-guided 27
 - primary brain tumors 27
 - sentinel lymph node (SLNB)
 - breast cancer imaging 143–4, 149, 155
 - malignant melanoma imaging 254–5
- bioreductive metal complexes 416, 425
- BMI1 pathway 12
- BMS181,321 416, 416
- bombesin/bombesin analogs 118, 120, 320, 417
 - peptide receptor scintigraphy 420–1
 - radiopeptide therapy 438–9

- bombesin receptors 316
- bone cysts
aneurysmal (ABC) 228, 229, 230
simple 228, 229
unicarmel 229
- bone islands 227, 230
- bone marrow toxicity 332
- bone metastases 151, 156, 341–50
background 341–2
from breast cancer 150, 150, 152, 152
chemotherapy 346–7
implications 341
from lung cancer 70
from neuroendocrine tumors 328
procedures 344–8
antitumor therapy 345–6
new treatment strategies 346–7
pain therapy 344–5, 348
from prostate cancer 115, 116–17, 124, 124, 125, 348
radiation dose calculation 343
radionuclide therapy 344–6
with bone marrow support 349
with chemotherapy 346–7
repeated dose 347, 349
therapeutic approaches 342–3
from thyroid cancer 169, 285
tumor formation 342–3
of unknown primary 267
- bone scintigraphy
breast cancer 156
cancer of unknown primary (CUP) 267
prostate cancer metastases 116–17
vs [¹⁸F]fluoride-PET-CT 125, 125
- bone tumors
chemotherapy 233
classification
benign tumors 228
malignant tumors 231
common sites 227, 228, 231
diagnosis 223
etiology/pathogenesis 227
grading 223
medullary thyroid cancer 296
metastatic disease 233, 236
radiopharmaceuticals 224–6
recent advances/future trends 243–4
staging 223, 223
- bortezomib 19
- brachialplexopathy 153
- brain metastases from lung cancer 72
- brain tumors 367–81
blood–tumor barrier/blood–brain barrier 372
classification 367–8, 369, 370
WHO system 368, 369
grading 368
location 368
patient age 368
precursor cells 368
primary 23–50
background 23
calcification patterns 29–30
classification 23–6, 41
diagnosis 26–7, 39, 40
epidemiology 23, 24
grading 32
hemorrhage 29
imaging 27–39
CT 23, 27–30
diffusion-weighted MRI 30, 30
future outlook 39–41
MRI 23, 27–31, 30, 30
MRS 23, 31–2
PET 23, 33, 35–9
radionuclide imaging 33–9
SPECT 23, 33–5
tumorigenesis 26
radiotherapy 512
- brain tumors (*Continued*)
recurrence 376
screening artifact 367
secondary 211–12
tenascin expression 374–5, 375
therapy
brachytherapy 371–2
chemotherapy 372–3
adjuvant 373
with radiotherapy 373
future directions 379
PAGRIT
with chemotherapy 378
locoregional 376–7, 378
systemic 376
radioimmunotherapy 373–9
avidin–biotin model 374
clinical applications 374–6
dosimetry evaluation 378–9
isotope characteristics 374
pre-targeting 374
three-step strategy 375, 377, 379
radiosurgery 371, 372
radiotherapy 370–2
with chemotherapy 373
surgery 370, 377
pre-radioimmunotherapy 377
- breast cancer 143–60
axillary node dissection 143, 144
dedicated scanners 495
diagnostic work-up, current 144
follow-up 144
imaging
bone scintigraphy 156
CT 153
FDG-PET 147, 147–8, 148, 149, 152, 155–6
problems 153
recurrent disease 151
therapy response 153, 154
FDG-PET-CT 147, 151, 151, 152
fluoroestradiol 154
[¹⁸F]fluorothymidine 154
lymphoscintigraphy 155
mammography 145, 148, 148
MET-PET 154
MIBI 146
MRI 148, 148
normoprogesterone 154
PET 143, 147–55, 148, 149
diagnosis, primary 147–8
PET-CT 143, 147, 148
recurrent disease 151–3
scintimammography 155
sentinel lymph node biopsy 155
[^{99m}Tc]sestamibi 145–6, 145, 155
SPECT 146–7
[^{99m}Tc]tetrofosmin 145, 146, 155
tyrosine 154
ultrasound 148
metastatic disease 150, 151, 152, 152, 156
FDG-PET 154
radioimmunotherapy 436
recurrent disease 151–3, 151
screening 148
sentinel lymph node biopsy 143–4, 149
signaling pathways 12
staging 144
FDG-PET 149–50
lymph node evaluation 148–9
metastases, detection of 149–50
therapy response 154
breast metastases of unknown primary 268
Breslow microstaging method 253
brown adipose tissue 172, 260, 260
BRU59-21 416, 416
butylene amine oxime (BnAO) 416
CA125 measurement 133, 138
- calcification patterns
lung cancer 65
primary brain tumors 29–30
calcitonin 293, 294
- cancer
epigenetic changes 3–5
genetic changes 1, 3–5
cancer of unknown primary (CUP) 265–72
classification 265
diagnosis 265–6
imaging
[¹¹¹In]DTPA-octreotide 268
[^{99m}Tc] EDDA/HYNIC-octreotate 269
[^{99m}Tc] EDDA/HYNIC-TATE 267
[^{99m}Tc] EDDA/HYNIC-TOC 267
FDG-PET 266, 269–70
FDG-PET-CT 268, 269–70
fine needle aspiration biopsy 267
⁶⁷Ga scintigraphy 267
L-DOPA-PET 268, 270–1
L-DOPA-PET-CT 270–1
[^{99m}Tc]MDP 267
modalities 265
[¹¹¹In]pentetreotide 268–9
[^{99m}Tc]pertechnetate 267
PET 266, 266
PET-CT 266, 266
PET-DOTA 266
PET-DOTA-NOC 271
PET-DOTA-TOC 271
[^{99m}Tc]sestamibi 268
somatostatin analogs 271
somatostatin receptor imaging 268
SPECT 266, 266
radiopharmaceuticals 266
tumor markers 265–6, 266
- cancer stem cells 11–13
signaling pathways 12
therapeutic implications 12
transplantation 12
- capromab pendetide 116
- carcinoembryonic antigen (CEA)
colorectal cancer imaging 105
colorectal cancer therapy 359, 360–1
in radioimmunotherapy 388, 392
- carcinogenesis
somatic mutation theory 3
tissue organization field theory 4–5
- carcinoid syndrome 189, 195
- carcinoid tumors 189, 197
DOTA-TOC therapy 324, 328
peptide receptor expression 417
- caspases
activation 5–6
in apoptosis 5–6
caspase-8 2
radiolabeled substrates 414
- catecholamine analogs 177, 192
- CCK-2 receptor expressing tumors 419–20
- CD20 301
- CD22 304
- CD95/Fas 2
- cell death 5–7
in cancer 7
non-apoptotic 6
programmed *see* apoptosis
- cell membrane synthesis tracers 39
- cell survival pathways 6
- cellular survival curves 457
- Central Brain Tumor Registry of US (CBTRUS) 23
- central nervous system lymphomas 25, 211–12
- cerebellar astrocytomas 24, 29
- cervical cancer 511–12
- cetuximab 19
- Chang's method 473–4
- chemokines 7–8, 9
- chemoradiotherapy
colorectal cancer 106

- chemoradiotherapy (*Continued*)
 esophageal cancer 94
 lung cancer 78
 prostate cancer metastases 111
 therapy monitoring 78, 106
- chemotherapy
 bone metastases 346–7
 brain tumors 372–3
 breast cancer 154
 colorectal cancer 362
 differentiated thyroid cancer 285–6
 hepatocellular carcinoma 353
 and hypoxia 415
 lung cancer
 combined with radiotherapy 65
 palliative 64
 predicting response to therapy 78
 lymphomas 213, 214, 215, 306, 307
 follicular lymphoma 309
 with radioimmunotherapy 309
 osteosarcomas 233
 ovarian cancer 137–8
 in ovarian cancer 390
 with PAGRIT 378–9
- Child–Pugh index 352
 children, brain tumors in 23, 25–6, 367
 [¹⁸⁶Ho]chitosan 356
 CHK2 2
 [²⁰¹Tl]chloride 67
 [⁸⁹Sr]chloride 343, 343, 344
 ‘chocolate’ markers 513
 cholangiocarcinoma 352
 cholecystokinin analogs 320, 417, 419, 420
 amino acid sequences 419
 cholecystokinin receptors 438
 cholesterol analogs 177
 [¹¹C]choline/derivatives 39, 96, 117–19, 122
 [¹⁸F]choline (FCH)/derivatives 117–19, 122–4
 distribution of FCH 123
 FCH-PET-CT 123–4
 structural formulae 118
 vs [¹⁸F]fluoride-PET-CT 124
 [¹¹C]choline-PET 244, 422, 512
 chondroblastomas 228, 229, 230
 chondromas 228
 chondromyoid fibromas 228
 chondrosarcomas 229, 231, 236–7
 chordomas 231
 choroid plexus carcinoma 26, 42
 choroid plexus papilloma 26
 chromatin modification 3, 5, 6
 chromogranin A 190
 cisplatin 346, 355
 [⁶⁷Ga]citrate 67
 coincidence detection 475–88
 basis 476
 CT systems 493–5
 detection 476–7, 477
 PET systems 475–80, 490–3
 dedicated 495
 positron emitter comparison 476
 random coincidences/timing electronics 478–9, 478
 random correction 479
 scanner choice 476
 scanner design 478, 478
 scanner structure 477–8
 scanners, commercially available 490–5
 scatter 479–80, 479
- collimators 469, 471, 472, 474, 474
 fan beam collimators 473
 multileaf collimators (MLC) 500
- colorectal cancer 99–108, 359–65
 clinical management 104–5, 104
 cost-effectiveness of imaging 105
 detection/diagnosis 99
 epidemiology 99
 etiology 359
- colorectal cancer (*Continued*)
 familial factors 359
 imaging
 anti-CEA antibody image 363
 CT 99, 100–1, 102, 103, 360, 363–4
 FDG-PET 101–2, 103, 363–4
 FDG-PET-CT 100, 101
 methods/limitations 99, 105–6
 MRI 99
 PET 99–100, 102–3
 recurrent disease 101–3
 staging 100–1
 PET-CT 100, 100, 101, 103–4
 ultrasound 99, 101
 liver metastases 363–4
 signaling pathways 12
 staging 359, 360
 therapy 359–62, 364
 anti-CEA antibodies 359, 360
 with chemotherapy 362
 with hyperthermia 362
 ¹³¹I-labeled 360–1, 361
 with radiotherapy 362
 ⁹⁰Y-labeled 361
 β-emitting isotopes 361
 bispecific antibodies 361–2
 monitoring 106
 radiolabeled antibodies 360
 surgery 359
- complement-dependent cytotoxicity (CDC) 390
 completion thyroidectomy 278
 computed tomography (CT) *see* CT (computed tomography)
 copper-semicarbazone complexes 416
 corticotropin-releasing factor (CRF) receptors 438
 CT (computed tomography)
 adrenal tumor imaging 178, 179, 182, 182, 185, 186
 bone tumor imaging 224, 225, 237
 breast cancer imaging 153
 colorectal cancer imaging 99, 100–1, 104, 105, 360, 363–4
 esophageal cancer imaging 90, 92
 staging 93
 vs PET or PET-CT 93
 head/neck cancer imaging 51
 radiotherapy planning 510
 hepatocellular carcinoma 351, 352, 356, 357
 instrumentation, new 407
 lung cancer imaging 70
 detection of recurrence 76–7
 diagnosis 65–6, 68
 radiotherapy planning 77, 78
 staging 72, 73, 75, 76
 comparison with FDG-PET 74, 74
 distant metastases 69–70
 lymph node evaluation 73
 lymphoma imaging 203, 204, 208, 209, 210, 211
 limitations 204
 vs FDG-PET 209, 213, 214
 malignant melanoma imaging 254, 257, 257, 258, 259
 megavoltage computed tomography (MVCT) 501
 neuroendocrine tumor imaging 190
 ovarian cancer imaging 133, 134, 135, 137
 recurrent disease 138, 140
 pleural disease 79
 primary brain tumors 23, 27–30, 39, 40
 traditional findings 42–3
 prostate cancer imaging 113, 115–16
 radiotherapy planning 501
 soft tissue tumor imaging 225, 241, 242
 thyroid cancer imaging 172, 172
 vs [¹⁸F]galacto-RGD 427
 see also PET-CT; SPECT-CT
- CUP *see* cancer of unknown primary (CUP)
 Cushing’s syndrome 177, 178
 CyberKnife 500, 501
- cystic tumors 29
 cytokines 7–8
- death induced signaling complex (DISC) 5
 death receptor-mediated (extrinsic) apoptosis pathway 5
 dedicated imaging devices *see* imaging devices, dedicated
 Demobesin compounds 420, 421
 Demogastrin-2 420
 deoxyuridine, radiolabeled 514
 depreotide-based ligands 319–20
 depreotide (NeoTect) 318, 418
 lung cancer imaging 66, 67
 depreotide-SPECT 196
 desmoplastic fibromas 228
 dexamethasone suppression 183
 differentiated thyroid cancer (DTC) 161, 167, 275–91
 characteristics 275
 guidelines 275
 follow-up 283
 hormone therapy 282–3
 radioiodine 279–80
 surgery 276–7, 278, 279
 metastatic disease 278, 285
 prognosis 276
 recurrent disease 284–5, 285, 286
 staging
 fine needle aspiration cytology 276, 279
 preoperative 276
 ultrasound 276
 therapy 275–86
 central lymph node dissection 278–9
 CT 282
 cytotoxic therapy 285–6
 external beam radiotherapy 283
 metastatic disease 285
 FDG-PET 282, 284, 285, 286
 FDG-PET-CT 284
 fine needle aspiration cytology 275, 278
 follow-up 275, 283–5
 guidelines 283
 metastatic disease 285
 recurrent disease 284–5
 remission 285
 hormone therapy 282–3
 lobectomy 277
 multimodal 275, 275
 radioiodine 279–82, 285, 286
 ablative 279–80
 adverse effects 282
 guidelines 279–80
 metastatic disease 285
 patient preparation 280
 recent advances 275
 SPECT-CT 275, 281–2, 282, 284
 surgery 276–9, 276, 286
 complications 279
 follicular (FTC) 277–8
 guidelines 276–7, 278, 279
 metastatic disease 285
 papillary (PTC) 277
 thyroidectomy 278
 thyroidectomy 276, 278
 ultrasound-guided 275
 vitamin A derivatives 285
- differentiation 1, 3
 diffuse astrocytomas 41, 42
 diffusion tensor imaging (DTI) 31, 31
 digital rectal examination (DRE) 109
 dihydroxyphenylalanine-PET *see* L-DOPA-PET
 Discovery ST 475, 478, 490, 492, 494–5
 Discovery STE 475, 490, 491, 492, 492, 493, 494–5
 [^{99m}Tc]DMSA scintigraphy
 bone tumor imaging 226, 237
 soft tissue tumor imaging 225, 226
 DNA damage 456

- DNA methylation 3–4
Doppler ultrasound 133, 134
dosimetry 443–58
 absorbed dose 454
 calculation 444, 445
 patient-specific 445–6
 definition of 444
 distribution 455
 distribution/activity heterogeneity 453–8
 clinical applications 445
 computer codes/tools 450, 451–3, 451
 conventional formalism 444–6
 dose rate to tumors 458
 heterogenous uptake 455
 individual patient 443–4
 microdosimetry 444
 Monte Carlo methods 446, 449–50, 450, 452
 imaging 449–50
 limitations 450
 S factor calculations 445, 449
 variance reduction techniques 450
 need for 458
 point kernel based calculations 452
 radiobiological aspects 455–6
 radiobiological linear quadratic model 456–8
 scintillation camera imaging 446–8
 PET-based dosimetry 448
 planar image-based dosimetry 446–7
 SPECT image-based dosimetry 447
 SPECT imaging, quantitative 447–8
 quantification procedure 447
 small-scale 453–5
 SPECT 450, 453
 on tissue/cellular levels 453–8
 tumor cell replication rate 458
DOSIMG software 452
DOTA
 linker in anti-CEA antibody therapy 361
 manufacture 435
 metal labeling 436
 PET-based dosimetry 448
 in radioimmunotherapy 386, 387, 388, 389
 structure 414
DOTA-biotin 436
DOTA-BOC-ATE 318, 318
DOTA-LAN 317, 318, 319, 321, 328, 328, 329
 dose/administration 330
 neuroendocrine tumor therapy 328
 quality of life parameters 331, 332
 time to progression 331
 toxicity 332
DOTA-LAN-PET 322, 329
DOTA-NOC 317, 318, 318, 419
 neuroendocrine tumor imaging 198
 neuroendocrine tumor therapy 328
 vs OctreoScan 328
DOTA-NOC-ATE 318, 318, 419
DOTA-TATE 317, 318, 326, 330
 neuroendocrine tumor therapy 323–4, 327, 327
 quality of life parameters 332
 radiolabeling 437
 time to progression 331
 toxicity 332
DOTA-TOC 317, 317, 318, 321, 328, 329, 418, 419
 cancer of unknown primary (CUP) imaging 271
 dose/administration 330
 follow-up 324, 326
 neuroendocrine tumor imaging 199
 neuroendocrine tumor therapy 322–3, 328
 pharmacokinetics 330
 quality of life parameters 332
 radiolabeling 437
 time to progression 331
 toxicity 332
 treatment results 323
 treatment scheme 324
DOTA-TOC/DOTA-TATE 327
DOTA-TOC-PET scans 322, 323, 326, 328
DOTA-TOC scintigraphy 322
DOTA-TOC-SPECT 322
‘doughnut’ sign 229
doxorubicin 346, 347
drug resistance 2
DTPA 418
 backbone-substituted 435
 DTPA-antibody conjugate 435
 linker in anti-CEA antibody therapy 361
 manufacture 434–5
 in radioimmunotherapy 390
 structure 414
DTPA-OC 332
DTPA-octreotide (DTPA-OC) (OctreoScan)
 CUP imaging 268
 neuroendocrine tumor imaging 191, 192, 192,
 193, 198, 268, 269, 416
 neuroendocrine tumor therapy 317, 317, 318,
 321, 322
 see also OctreoScan
Dukes staging method 359, 360
e-selectin 19
Early Lung Cancer Action Program (ELCAP)
 study 65, 68
[^{99m}Tc] EDDA/HYNIC-octreotate 269
[^{99m}Tc] EDDA/HYNIC-TATE 267
[^{99m}Tc] EDDA/HYNIC-TOC 196, 197, 267, 318
[¹⁵³Sm] EDTMP 342, 343, 343
 in antitumor therapy 346
 with bone marrow support 349
 in pain therapy 344, 345
embryonal rhabdomyosarcomas 240
enchondromas 229
endocrine pancreatic tumors 189
endoscopic ultrasound (EUS)
 esophageal cancer imaging 89–90, 512
 staging 93
 neuroendocrine tumor imaging 190–1
ependymomas 25, 42
epidermal growth factor receptor (EGFR) 8, 8, 515
epigenetic changes
 in cancer 3–5
 combined with genetic changes 4
epirubicin and [¹³¹I]lipiodol 355
[⁹⁰Y] epratuzumab 304
erlotinib 18
esophageal cancer 89–97
 advanced disease 96
 diagnostic modalities 89–93
 computed tomography 90
 endoscopic ultrasound 89–90
 PET
 FDG-PET 90–1
 FDG-PET-CT 91
 other radiopharmaceuticals 96
 positivity criteria 91, 93
 epidemiology 89
 and esophagitis 95
 follow-up 96
 metastases 89, 93–4, 94
 lymph node evaluation 90, 95
 neoadjuvant therapy, response to 94–6, 95
 radiotherapy 512
 relapse 93–4, 94
 staging 89–90, 90, 93
 therapy 89
 esophagitis 95
 estramustine 347
 estrogen receptor (ER) 19
Ewing’s sarcomas 229, 231, 235, 236
 extraskeletal 240, 243
 see also primitive neuroectodermal tumor
 (PNET)
 ‘onion peel’ appearance 235
 extracellular matrix proteins 415
 extrinsic (death receptor-mediated) apoptosis
 pathway 5
farnesylation 9
Fas see CD95/Fas
[¹⁸F]FBA 426
 structure 425
Cel-S-Dpr([¹⁸F]FBOA)TOCA 426, 426
FCH-PET-CT 123–4, 123, 124, 125
 vs [¹⁸F]fluoride-PET-CT 124
FDG 18, 35–7, 38, 90, 99
 biodistribution 208–9
 brain tumor imaging 36
 head/neck imaging 53
 lymphoid tissue hyperplasia 54
 retro-mandibular nodes 54
 lung cancer imaging 67
 radiotherapy planning 77
 structure 423
 synthesis, microfluidic device for 423
 vs radiolabeled amino acids 37
FDG-PET
 adrenal tumor imaging 177, 181, 183, 185–7
 bone tumor imaging 224, 226, 235, 237, 238–9,
 238
 recent advances 243–4
 brain tumor imaging 18, 19, 35, 36–7
 indications 44
 multimodal 40
 traditional findings 42–3
 breast cancer imaging 147, 147–8, 148, 149,
 152, 155–6
 metastatic disease 154
 problems 153
 recurrent disease 151
 therapy response 153, 154
 breast cancer staging 149–50
 colorectal cancer imaging 101–2, 103, 104–5,
 363–4
 limitations 105–6
 liver metastases 52, 104
 therapy monitoring 106
 cost-effectiveness of imaging 105
 CUP imaging 266, 269–70
 esophageal cancer imaging 90, 93
 follow-up 96
 lymph node evaluation 95
 sensitivity/specificity 93
 staging 93
 therapy response 94, 95
 head/neck cancer imaging 511
 sensitivity/specificity 55, 57
 HNSCC post-therapy evaluation 52, 53, 56–8, 57
 pretreatment baseline 57
 lung cancer imaging 67, 68–9, 79, 506–8
 cost-effectiveness 79
 detection of recurrence 75
 diagnosis 66, 68–9, 70
 false-positive findings 71
 patient preparation 67
 predicting/monitoring response to therapy
 78, 79
 radiotherapy planning 78
 sensitivity/specificity 68–9, 72
 staging
 comparison with CT 74, 74
 distant metastases 71–3
 lymph node evaluation 73–4
 small-cell lung cancer 79–80
 techniques 67
 lymphoma imaging 203, 208–16
 extranodal lymphoma 211–12
 in HD vs NHL 214
 limitations/pitfalls 215
 protocol 208–9
 recurrent disease 215
 residual/recurrent disease 214
 staging 209, 211
 therapy response 212–13, 212, 213, 214–15
 vs CT 209, 213, 214
 vs Ga-SPECT 209, 215–16

- FDG-PET (*Continued*)
 malignant melanoma imaging 254, 255–6, 257–8
 false-negative 259
 pitfalls 260–1
 recurrent disease 258, 259
 risk stratification 260
 therapy response 259
 and tumor stage 256
 neuroendocrine tumor imaging 192, 196, 198, 323
 new radiopharmaceuticals 0–4
 ovarian cancer imaging 134, 135–6, 137
 recurrent disease 138–9, 140
 pleural disease 79
 prostate cancer imaging 117
 publication statistics 422
 radiotherapy planning 505, 505
 cervical cancer 511
 esophageal cancer 512
 radiotherapy target delineation 502
 soft tissue tumor imaging 226, 242, 242
 biopsy guidance 240–1, 241
 diagnosis/staging 240, 241, 243, 243
 limitations 241
 metastatic disease 241
 recurrent disease 241
 therapy response 241–2, 241
 thyroid cancer imaging 161, 164–5, 169–71, 170
- FDG-PET-CT
 breast cancer imaging 147, 151, 151, 152
 CUP imaging 268, 269–70
 esophageal cancer imaging 91
 lung cancer imaging 66, 68, 69, 70
 detection of recurrence 76
 staging 72, 73, 75, 76
 lymphoma imaging 209, 210, 215
 malignant melanoma imaging 257, 257, 258, 259, 259
 ovarian cancer imaging 136–7
 prostate cancer recurrence 121, 122
 thyroid cancer imaging 164, 165, 165, 168, 172
- FES 427
 FET-PET 424–5
 FHDT-PET 19
 FIAU 40
 fibrosarcomas 231, 240
 fibrous dysplasia, monostotic 229, 230, 230
 fibrous histiocytomas
 benign 228
 malignant 231, 240
 fiducial markers in co-registration 503–4, 504
 fine needle aspiration biopsy (FNAB)
 CUP imaging 267
 thyroid cancer imaging 161, 162–3
 US-guided thyroid cancer imaging 161–3, 162, 165
 fine needle aspiration cytology (FNAC) 275
 5-FU 362
 flare effect 346
 FLT 19
 malignant melanoma imaging 261
 structure 423
 FLT-PET 424
 brain tumor imaging 39
 breast cancer imaging 154
 lymphoma imaging 216
 publication statistics 422, 422
 fluid attenuated inversion recovery (FLAIR) 28
 fluorescence resonance energy transfer (FRET) 17
 [¹⁸F]fluoride 124–5
 [¹⁸F]fluoride-PET 422
 bone tumor imaging 226
 soft tissue tumor imaging 226
 [¹⁸F]fluoride-PET-CT
 vs bone scintigraphy 125, 125
 vs FCH-PET-CT 124
 [¹⁸F]fluoro-2-deoxy-D-glucose (FDG) *see* FDG
 [¹⁸F] fluoro-5-dihydrotestosterone PET (FDHT-PET) *see* FHDT-PET
- 16β-[¹⁸F]fluoro-5α-dihydrotestosterone (FDHT)
 119–20
 structural formula 118
 [¹⁸F]fluoro-L-thymidine *see* FLT
 [¹⁸F]fluoroacetate 119
 [¹⁸F]fluorocholesterol 39
 fluoroestradiol 154
 [¹⁸F]fluoroethylcholine (FECH) 118, 119, 122
 [¹⁸F]fluoromisonidazole (FMISO)
 brain tumor imaging 38–9
 hypoxia imaging 513–14
 [¹⁸F]fluorothymidine 154
 3'-deoxy-3'-fluorothymidine (FLT) 19, 39
 FNAB *see* fine needle aspiration biopsy
 follicular lymphoma 309
 follicular thyroid cancer (FTC) 172
 metastatic disease 278
 prognosis 276
 surgery 277
 therapy 276–7
 Fourier rebinning (FORE) 489
 [¹⁸F]FPNP 425–6, 427
 structure 425
 FTC *see* thyroid cancer, follicular
 functional brain mapping 39
 functional genomics 17
 functional magnetic resonance imaging (fMRI)
 31, 31
- ⁶⁷Ga (gallium-67) scintigraphy 205
 bone tumor imaging 225, 226, 230, 237
 soft tissue tumor imaging 225, 226, 239, 242
⁶⁷Ga scintigraphy 267
 Ga-SPECT lymphoma imaging 203
 extranodal lymphoma 206–7, 206
 imaging protocol 205–6
 residual/recurrent disease 207
 staging/restaging 206, 207
 therapy response/prognosis 207
 vs FDG-PET 209, 215–16
 [¹⁸F]galacto-RGD 426, 426
 scans 427
 [¹⁸F]galacto-RGD-PET 427
 γ-camera (Anger camera) 146
 advances made 467–71
 collimator 469, 472
 electronic 474, 474
 spatial resolution 471
 Compton camera 474
 count rate performance 471
 detector 468, 468
 thickness 469
 energy resolution 471
 intrinsic efficiency 468
 sensitivity 470, 470
 spatial resolution 468, 468, 469
 system 471
 γ probes in lymph node evaluation 74
 gastrin analogs 320, 419
 gastrin receptors 438
 gastrin-releasing peptide (GRP) 320
 gastrin-releasing peptide (GRP) receptors 438, 439
 gastrinomas 417
 gastrointestinal stromal tumors 242–3, 242
 gemcitabine 347
 Gemini scanners 477
 Gemini GXL 490, 491, 491, 492, 493, 494–5
 Gemini TF 487, 488
 PET-CT Gemini 475, 477, 478
 gene defects in tumorigenesis 7
 genetic changes
 in cancer 1, 3–5
 combined with epigenetic changes 4
 primary brain tumors 26
 genetic modification 439–40, 439
 genomics 17
 German Pneumology Society lung cancer tests
 61, 62
- 'ghost tumors' 25
 giant cell tumors (osteoclastomas) 228, 229
 Gleason grading system 109–10
 Gliadel wafers 372
 glioblastoma multiforme (GBM) 367
 brachytherapy 371
 glioblastomas 23, 24
 classification 41, 368
 epidemiology 367
 genetic changes 26
 imaging 31, 32, 34
 neuroimaging findings 42
 signaling pathways 12
 gliomas 23–4
 biopsy 27
 classification 41
 genetic changes 26
 high vs low grade 376–7
 imaging 32, 33, 34, 36–7, 38
 high vs low grade 38
 magnetic resonance imaging 28
 neuroimaging findings 42
 therapy 370, 376–7
 glucagon-like peptide (GLP) 190, 191, 192
 glucagon-like peptide (GLP) receptors 438
 glucose transporters 18, 36
 gross tumor volume (GTV) 501, 502
 delineation 504
 ground-glass appearance 65
 growth factor receptors
 in primary brain tumors 26
 upregulation/overexpression in tumors 1
 growth factors
 from cancer cells 1
 in primary brain tumors 26
 growth signaling
 in cancer development 1
 ligand-independent signaling 1
- [¹³¹I]haptan 295, 297
 HD *see* Hodgkin's disease (HD)
 head/neck cancer imaging
 radiotherapy 508–11
 recurrent disease 511
 head/neck squamous cell carcinomas (HNSCCs)
 51–60
 FDG-PET 56–8
 PET 52–5
 post-therapy evaluation 51, 56–8
 staging 51, 54–5
 tongue squamous cell carcinomas 51
 HED-PET 184–5, 187
 HED-PET-CT 182, 186
 hedgehog (HH) pathway 7
 [¹⁸⁶Re]HEDP 342, 343, 343
 in antitumor therapy 346
 in pain therapy 344, 348
 repeated dose 347, 349
 scintigraphy 348
 hemangioendothelial sarcomas 231
 hepatocellular carcinoma (HCC) 351–8
 causative agents 351
 diagnosis, confirmation of 352
 epidemiology 351
 fibrolamellar variant 352
 grading 352, 352
 imaging
 CT 351, 352, 356, 357
 MRI 351, 352
 measurement 352
 metastases 352
 natural history 352
 staging 351–2, 352
 therapy 353–7
 chemotherapy 353
 radionuclide therapy 353–7
 catheter placement 353, 354
 surgery 356

- HER/erbB receptors/ligands 8
- hexokinase 17, 18
- Hi Rez PET scanner 487
- Hi-Rez-pico3D 490, 491, 491, 492, 493, 494–5
- histone modification 4
- HL91 416, 416
- HNSCCs *see* head/neck squamous cell carcinomas (HNSCCs)
- Hodgkin's disease (HD) 203, 206, 237
- radiotherapy planning 512
- therapy 299
- hormone therapy 111, 119
- 5-HTP-PET 192, 198
- human anti-chimeric antibodies (HACA) 303
- human anti-murine antibodies (HAMA) 302, 303, 305
- H₂ receptor cell (oxyphilic) carcinoma 277
- [¹¹C]hydroxyephedrine (HED-PET) *see* HED-PET
- [^{99m}Tc]HYNIC core 414, 414
- [^{99m}Tc]HYNIC-octreotide 317, 322
- [^{99m}Tc]HYNIC-TOC 324
- hyperandrogenism 177
- hypercortisolism 182
- hypertension 178, 180
- hypoxia 10–11, 415–16
- markers 425
- measurement 415
- radiopharmaceuticals 416
- radioresistance 513
- in radioresistance/chemoresistance 20
- tracers 513
- hypoxia-inducible factors (HIFs) 10–11, 11, 20
- ¹³¹I-labeled anti-AFP 353
- ¹³¹I-labeled anti-CEA antibodies 360–1, 361
- ¹³¹I-SPECT 282
- ¹²³I 163, 164, 166
- thyroid stunning 281
- ¹³¹I 166–8, 170, 279, 281
- for DTC therapy 279–82
- for lymphomas 301–2
- for ovarian cancer 386
- patient preparation for scintigraphy 281
- IAPs 2
- IAZA 416, 416
- [⁹⁰Y]ibritumomab tiuxetan (Zevalin) 300, 305–6, 433, 436
- adverse effects 306, 310
- characteristics 306
- and chemotherapy 309
- dosimetry 445
- dosing schedule 308–9
- indications 307–8
- instructions for patients 460
- patient preparation 308
- preparation 310
- safety data 310
- therapeutic regimen 307
- [^{99m}Tc]IL-2 261
- imaging devices, dedicated 403–5
- interoperative probes 405
- nuclear mammographic imaging 403–5
- prostate imaging, positron emission 405
- imatinib 18
- immunoglobulins
- IgG 384
- IgM 392
- [¹²³I] IMP (N-isopropyl-p-[¹²³I]iodoamphetamine) 261
- IMP-SPECT 261
- IMT-SPECT 512
- inflammatory cells 7–8
- instrumentation 397–412
- combined molecular–morphological imaging 406–10
- see also* PET-CT; PET-MRI; SPECT-CT
- dedicated imaging devices 403–5
- past/future 482–5
- insulinomas 417
- integrins 9, 19, 415
- receptors 438
- intensity-modulated radiation therapy (IMRT) 499
- 4D data 515
- ATSM-guided 513–14
- CyberKnife 500, 501
- dose-painting ability 515
- dynamic 500
- future perspectives 515
- head/neck cancer imaging 508–11, 510
- multileaf collimators (MLC) 500
- PET-CT image co-registration 502
- rotational delivery 500–1
- segmental (step and shoot) 500
- static (cone beam) delivery 500
- [^{99m}Tc]interleukin-2 261
- interleukin-8 (IL-8) 8
- International Agency for Research on Cancer (IARC) 23
- International Staging System (ISS) 61, 63
- interoperative probes 405
- N-isopropyl-p-[¹²³I]iodoamphetamine ([¹²³I] IMP) 261
- Kaposi's sarcoma 239–40
- ketoconazole 346
- Krytoxif 422
- L-DOPA-PET
- adrenal tumor imaging 185, 187
- CUP imaging 268, 270–1
- neuroendocrine tumor imaging 192, 198
- L-DOPA-PET-CT 270–1
- L3,4-dihydroxy-2-phenylalanine-PET *see* L-DOPA-PET (L3,4-dihydroxy-2-phenylalanine)
- Langerhans cell histiocytosis 229
- lanreotide 418
- lanreotide-based ligands 319
- laparoscopic lymphadenectomy 113
- leiomyosarcomas 240
- lesion detectability 467, 482
- letrozole 19
- leucovorin 362
- leukemias 3
- [¹³¹I]lipiodol 354–6, 354
- and chemotherapy 355
- extended use 355–6
- first results 355
- [¹⁸⁸Re]lipiodol 356
- liposarcomas 240
- liver metastases
- breast cancer 150
- from colorectal cancer 51, 363–4
- liver tumors 351–8
- causative agents 351
- diagnosis, confirmation of 352
- epidemiology 351
- fibrolamellar variant 352
- grading 352, 352
- imaging
- CT 351, 352, 356, 357
- MRI 351, 352
- measurement 352
- metastases 352
- natural history 352
- staging 351–2, 352
- therapy 353–7
- chemotherapy 353
- radionuclide therapy 353–7
- catheter placement 353, 354
- surgery 356
- low-grade cerebellar astrocytomas 24
- lung cancer 61–87
- adrenal metastases 181
- classification 61
- cost-effectiveness of imaging 79
- detection of recurrence 75
- lung cancer (*Continued*)
- diagnostic accuracy 68
- diagnostic modalities 65–6, 67, 68–9
- conventional imaging 65–6
- nuclear imaging 66, 67, 68–9
- false-positive findings 71
- diagnostic strategies 62
- imaging
- [²⁰¹Tl]chloride 67
- [⁶⁷Ga]citrate 67
- CT 70
- detection of recurrence 76–7
- diagnosis 65–6, 68
- radiotherapy planning 77, 78
- staging 69–70, 72, 73, 73, 74, 74, 75, 76
- depreotide 66, 67
- FDG 67, 77
- FDG-PET 67, 68–9, 79
- cost-effectiveness 79
- detection of recurrence 75
- diagnosis 66, 68–9, 70
- false-positive findings 71
- patient preparation 67
- predicting/monitoring response to therapy 78, 79
- radiotherapy planning 78
- sensitivity/specificity 68–9, 72
- staging 71–4, 74, 79–80
- techniques 67
- FDG-PET-CT 66, 68, 69, 70
- detection of recurrence 76
- staging 72, 73, 75, 76
- MIBI 67, 78
- PET 68
- comparison with PET 74
- cost-effectiveness 79
- predicting/monitoring response to therapy 78
- radiotherapy planning 77–8
- staging small-cell lung cancer 79
- PET-CT 68, 68, 70
- comparison with PET 74
- detection of recurrence 75, 76–7
- predicting/monitoring response to therapy 78–9
- radiotherapy planning 77
- staging 72, 73, 75, 76, 80
- somatostatin receptor imaging 67
- [^{99m}Tc]tetrofosmin 67
- radiotherapy 506–8
- radiotherapy planning 77–8
- solitary pulmonary nodules 65
- staging 72, 73, 75, 76, 79–80
- distant metastases 69–73
- conventional imaging 69–70
- nuclear imaging 71–3
- lymph node evaluation 73–4, 74
- comparison of modalities 74, 74
- conventional imaging 73
- nuclear imaging 73–4
- restaging 76–7
- systems 61–2
- therapy indications 62
- therapy response 78–9
- treatment options 62, 64–5
- lung nodules *see* solitary pulmonary nodules (SPNs)
- lymph node evaluation 55
- procedures by level 63
- sampling methods 62
- lymph node involvement 169
- lymph nodes, thoracic 63
- lymphadenectomy, laparoscopic 113
- lymphangiography 112
- lymphoblastic leukemia 12
- lymphocytic lymphoma 206
- lymphomas 203–22, 299–314
- of bone, primary 231, 237, 238

- lymphomas (*Continued*)
 chemotherapy 213, 214, 215
 follow-up 204
 imaging
 anatomical modalities 204–5
 functional modalities 203, 205–8
 metabolic modalities 208–16
 metastatic disease 204, 206–7, 206, 211–12
 lymph node involvement 205
 primary brain tumors 25, 43
 magnetic resonance imaging 30
 prognostic evaluation, early 214–15
 radioimmunotherapy 208, 214, 299–300
 adverse effects 310–11
 choice of target antigen 300–1, 301
 dosing schedule 308–9
 indications 307–8
 integration into NHL chemotherapy 309
 patient preparation 308
 precautions 309–10
 radionuclide selection 301–2, 302
 safety data 310
 radiotherapy 512
 residual/recurrent disease 204, 205, 207, 214
 early detection 215
 restaging 207
 staging 206, 209, 211
 therapy response 204, 205, 207, 212, 212, 213,
 214–15
 tumor biology 209
 see also Hodgkin's disease (HD); non-Hodgkin's
 lymphoma (NHL)
- lymphosarcoma of bone 231
- lymphoscintigraphy
 breast cancer 143
 breast cancer imaging 155
 malignant melanoma imaging 254, 255, 255
 prostate cancer 115
- MABDOSE 451
^[99mTc]macro-aggregated albumin (MAA) 353
- magnetic resonance imaging (MRI) see MRI
 (magnetic resonance imaging)
- magnetic resonance mammography (MRM) 148
- magnetic resonance spectroscopy (MRS) see MRS
 (magnetic resonance spectroscopy)
- malignant melanoma 253–64
 etiology/pathogenesis 253
 future directions 261
 imaging 260–1
 brown fat as pitfall 260, 260
 CT 254, 257, 257, 258, 259
 FDG-PET 254, 255–6, 257–8
 false-negative 259
 pitfalls 260–1
 recurrent disease 258, 259
 risk stratification 260
 therapy response 259
 and tumor stage 256
 FDG-PET-CT 257, 257, 258, 259, 259
 lymphoscintigraphy 254, 255, 255
 MRI 254, 257, 258
 PET-CT 256, 257
 pitfalls 260–1
 sentinel lymph nodes 255
 sentinel lymph node biopsy 254–5
 interferon reaction mimicking 260, 261
 metastatic disease 256–8, 257, 258
 in-transit metastases 256
 lymph node evaluation 253–6
 outcome prediction 260
 recurrent disease 258–9
 risk stratification 260
 staging 253
 AJCC system 254
 distant metastases 256–8
 nodal 253–6
 therapy response 259–60
- MALT (mucosa-associated lymphoid tissue)
 lymphoma 206, 211
- mammary gland carcinoma 4
- mammographic imaging devices 403–5
 positron emission mammography 405
 single photon emission mammography 404–5
- mammography
 breast cancer imaging 145, 148, 148
 dedicated scanners 495
- markers 17
 cancer of unknown primary 265–6, 266
 neuroendocrine tumors 190
- matrix metalloproteinases (MMPs) 415
- MAURITIUS (Multicenter Analysis of Universal
 Receptor Imaging and Treatment Initiative:
 eUropean Study) 319, 328, 330, 331
- Max 3
- MDM2 2
- ^[99mTc]MDP 267
- ^[99mTc]MDP bone scan 70
- ^[99mTc]MDP scans
 bone tumor imaging 224, 225, 226, 227,
 229–30, 229, 234
 soft tissue tumor imaging 226, 242
- mediastinoscopy 62
- Medical Internal Radiation Dosimetry (MIRD)
 committee 444–5, 446, 451, 452
- medullary thyroid cancer (MTC) 190, 293–8
 bone metastases 296
 epidemiology 293
 imaging 293
 CT 293
 DOPA-PET 293
 FDG-PET 293
 MRI 293
 peptide receptor expression 417
 prognosis 293, 294
 therapy
 MIBG 294
 radioimmunotherapy, pre-targeted 294–7, 295
 affinity enhancement system 294, 295
 hematological toxicity risk 296
 pre-targeting strategies 294
 procedure 296–7
 survival 297
 survival, effect on 296
 surgery 293–4
 therapy response 296, 297
- medulloblastomas 25, 43
 signaling pathways 12
- megavoltage computed tomography
 (MVCT) 501
- α-melanocyte stimulating hormone (α-MSH)
 receptors 438, 439
- meningiomas 25, 43, 417
- MET-PET 37–8, 424
 in brain tumor imaging
 multimodal 40
 radiotherapy planning 512
 traditional findings 42–3
 breast cancer imaging 154
 colorectal cancer imaging 106
 lymphoma imaging 216
 publication statistics 422, 422
 vs FDG-PET 38
 vs MRI 37
- ^[123I]meta-isomer of iodobenzylguanidine (MIBG)
 scintigraphies see MIBG scintigraphy
- metal complexes, bioreductive 416, 425
- metastases
 adrenal 72
 brain 72
 breast 268
 FDG-PET detection 55
 in HNSCCs 55
 liver 51, 150, 363–4
 pulmonary 62
 spleen 150
- metastases (*Continued*)
 see also bone metastases; cancer of unknown
 primary (CUP)
 metastatic brain tumors 24
^[11C]methionine-PET (MET-PET) see MET-PET
^[99mTc]methoxyisobutylisonitrile (MIBI) see MIBI
 methylation 3–4
^[99mTc] methylene diphosphonate bone
 scintigraphy see MDP bone scintigraphy
 L-[3-¹⁸F]methyltyrosine (FMT) 38, 244
 bone tumor imaging 244
 MGMT promoter methylation 373
^[131I]MIBG 439–40
 PET-based dosimetry 448
 MIBG scintigraphy 18
 adrenal tumor imaging 180, 181, 183–4, 185, 187
 drug interactions 184
 with ^[90Y]DOTA-TOC 328–9
 neuroendocrine tumor imaging 189, 191, 192,
 196–9, 197
 biodistribution 197
 vs somatostatin analogs 197–8
^[131I]MIBG therapy 453, 454
 MIBI (^[99mTc]methoxyisobutylisonitrile)
 bone tumor imaging 226, 235, 235, 237
 brain tumor imaging 34–5
 breast cancer imaging 146
 lung cancer imaging 67
 predicting response to therapy 78
 lymphoma imaging 208
 soft tissue tumor imaging 226
 mindin/RG-1 protein 436
 minigastrin analogs 417, 419, 420
 amino acid sequences 419
 MIRDOSE software 448, 451, 456
 misonidazole 362
 misonidazole derivatives 20
 mitotic catastrophe 7
 MLH1 4, 5
 molecular markers 17
 molecular targets see targets, molecular
- monoclonal antibodies (mAb)
^[177Lu]CC49 393, 394
¹³¹I-labeled anti-HLA-DR mAb (Lym-1) 304
 radioimmunotherapy 383
 evolution of 302–3
 non-myeloablative 304–6
 structure 385
- monoclonal antibody therapy
 brain tumors 373–4, 375, 377
 efficacy 383
 lymphoma imaging 208
 medullary thyroid cancer 294
 non-Hodgkin's lymphoma 299
 ovarian cancer 383
 and radiotherapy 515
 in SPECT 35, 208
 see also radioimmunotherapy
- morphology, cellular 5
- MRI (magnetic resonance imaging) 70
 adrenal tumor imaging 178
 apparent diffusion coefficient (ADC) 30, 31
 bone tumor imaging 223–4, 225, 232, 234,
 236, 237
 STIR 235, 236
 breast cancer imaging 148, 148
 colorectal cancer imaging 99
 diffusion-weighted 30, 30, 31
 functional (fMRI) 31, 31
 head/neck cancer imaging 51
 hepatocellular carcinoma 351, 352
 lung cancer staging 70, 73
 lymphoma imaging 205, 209, 211
 malignant melanoma imaging 254, 257, 258
 neuroendocrine tumor imaging 190
 ovarian cancer imaging 133, 134, 137
 recurrent disease 138, 140
 perfusion-weighted 31

- MRI (magnetic resonance imaging) (*Continued*)
 primary brain tumors 23, 27–31, 39, 40
 astrocytoma 28
 cerebellar pilocytic astrocytomas 29
 gliomas 28
 traditional findings 42–3
 prostate cancer imaging 113, 115–16
 radiotherapy planning 510
 soft tissue tumor imaging 225, 241, 242
 diagnosis/staging 243
- MRS *see* magnetic resonance spectroscopy (MRS)
- MRS (magnetic resonance spectroscopy)
 multivoxel 32, 33
 primary brain tumors 23, 31–2, 39
 grading 32
 prostate cancer imaging 113
 sensitivity *vs* specificity 32
 short echo time (TE) sequences 32
 single-voxel 32, 33
- Multicenter Study Differentiated Thyroid Carcinoma (MSDS) trial 277, 279
- multiple neuroendocrine neoplasia (MEN) 190
- multislice rebinning (MSRB) 489
- multitracer imaging 125, 513–15
- Myc 2, 3
- myelodysplastic syndromes (MDS) 310–11
- myeloma (plasmacytoma) 237
- N_4 Tc chelating system 414
- nasopharyngeal SCC 56
- neck cancers *see* head/neck squamous cell carcinomas (HNSCCs)
- necrosis 6
 molecular targets in imaging 20
 and SPECT imaging 34
vs apoptosis 5
- NeoTect (NeoSpect) (P829) 319
- nerve sheath tumors, malignant peripheral 243, 243
- neuroblastomas
 adrenal 179, 181, 185, 185, 186, 187
 metastatic 231
- neuroendocrine tumors 315–39
 classification 189, 190, 315
 derivation 189
 diagnosis 190
 diagnostic work-up 191
 family of tumors 315–16
 follow-up 326
 gastroenteropancreatic 189–202
 classification 189, 190
 imaging 197
- imaging
 catecholamine analogs 192
 CT 190
 depreotide-SPECT 196
 DTPA-octreotide 191, 192, 192
 [^{99m}Tc]EDDA/HYNIC-TOC 196, 197
 FDG-PET 192, 196, 198
 GLP 190, 192
 5-HTP-PET 192, 198
 L-DOPA-PET 192, 198
 MIBG 189, 191, 192, 196–9, 197
 biodistribution 197
vs somatostatin analogs 197–8
 MRI 190
 octreotide 191, 192–5
 pentetreotide 192, 193, 194, 194, 195
 radioguided surgery 195
 PET 191, 198–9
 PET-CT 191, 198
 PET-DOTA-NOC 198
 PET-DOTA-TOC 199
 planar scintigraphy 192, 193
 radiopharmaceuticals 191, 192
 somatostatin analogs 191, 192, 192, 195–6, 197–8
 somatostatin receptors 191, 193–4
 SPECT 191, 193, 195
- neuroendocrine tumors (*Continued*)
 SPECT-CT 195, 197
 [^{99m}Tc]TP3654 196
 ultrasound 190–1
 VIP 190, 192
- markers 190
- metastatic disease 197, 268
- molecular targets in 18
- peptide receptor expression 316
- radiopeptides 316–21
 bombesin 320
 cholecystokinin analogs 320
 depreotide-based ligands 319–20
 gastrin analogs 320
 gastrin-releasing peptide (GRP) 320
 lanreotide-based ligands 319
 neurotensin analogs 320
 octreotide-based ligands 316–19
 substance P 320–1
 VIP-based analogs 320
- receptor-mediated imaging 316–21
 impact of 321
- secretions 315
- therapeutic approaches 321–9
 chemoembolization 315
 diagnostic/dosimetric evaluation 330
 discontinuation 330
 management, optimal 315–16
 procedures 329–33
 radiopeptides 328
 dose/administration 330–1
 patient selection 329–30
 somatostatin analogs 315
 surgery 315
- therapy response
 biochemical parameters 331
 long-term effects 332–3
 quality of life parameters 331–2
 radiopeptide side-effects 332
 regression/progression 331
 tumor burden 331
- of unknown primary 266, 269
see also neuroblastomas; pheochromocytomas;
 sympathoadrenal tumors
- neuroepithelioma, peripheral 243
- neurofibromas 243
- neurofibromatosis 243, 243
- neuron-specific enolase (NSE) 190
- neuropeptide Y receptors 438
- neurotensin analogs 320, 417
 peptide receptor scintigraphy 421
- neurotensin receptors 438
- NFKB 2, 6
- NHL *see* non-Hodgkin's lymphoma (NHL)
- NIS *see* sodium iodide symporter (NIS)
- nitroimidazoles 416
- NOC 418
- NOC-ATE 418
- nociceptors 341–2
- noise equivalent count rate 467, 481–2
- non-Hodgkin's lymphoma (NHL) 25, 204, 237, 299–300
 classification 203, 204, 300
 epidemiology 299
 grading 299
 radioimmunotherapy 294, 436
 radiotherapy planning 512
- therapy
 antibody-targeted 299–300
 integration of radioimmunotherapy 309
 response monitoring 212
- non-ossifying fibromas 228, 229
- non-small-cell lung cancer (NSCLC) 61
 cost-effectiveness of imaging 79
 CT overestimation 508
 FDG-PET
 in management 506
 studies 71–3
- non-small-cell lung cancer (NSCLC) (*Continued*)
 uptake 507
 PET-CT 508
 pleural disease assessment 79
 predicting/monitoring response to therapy 78–9
 radioimmunotherapy 436
 radiotherapy planning 78, 508
 staging 72, 73, 75, 76
 restaging 76–7
 therapy by stage 63, 64
 [^{131}I]6 β -iodomethyl-19-norcholesterol (NP-59) *see* NP-59
- normoprogesterone 154
- Notch pathway 12
- NP-59 181–3
 drug interactions 182
 interpretation 182–3
 patient preparation 181
 pitfalls 182
 technique 181–2
- nuclear factor KB (NFKB) 6
- nuclear medicine-guided radiotherapy *see under* radiotherapy
- nucleosides, radiolabeled 424, 514
- NUCLIDOSE 451, 451
- ^{15}O labeled water 244
- OctreoScan *see* DTPA-octreotide (DTPA-OC)
- octreotide 418–19, 418
 brain tumor imaging 18, 35
 neuroendocrine tumor imaging 191, 192–5
 octreotide-based ligands 316–19
 radiopeptide therapy 437
- Okuda grading system 352
- Okuda staging system 352
- oligoastrocytomas 24
- oligodendrogliomas 24, 370
 neuroimaging findings 42
- OLINDA (Organ Level Internal Dose Assessment) 451
 sample output 452
- oncogenes
 in cancer development 1
 in tumorigenesis/apoptosis/drug resistance 2
- 'onion peel' appearance 235
- orchiectomy 111
- osteoblastomas 228
- osteochondromas 228, 229, 230
- osteoclastomas (giant cell tumors) 228, 229–30, 229
- osteogenic sarcomas (osteosarcomas) 229, 231, 231, 235
 diagnosis 233
 [^{99m}Tc]MDP scans 234
 metastatic disease 233
 [^{99m}Tc]MIBI scan 235, 235
 MRI scans 232, 234
 radiographs 232, 234
 staging systems 233
 therapy response 233
- osteoid osteomas 228, 229
 radionuclide scintigraphy 227
- osteosarcomas *see* osteogenic sarcomas (osteosarcomas)
- ovarian cancer 133–42, 383–96
 CA125 measurement 133, 138
 diagnosis, importance of 133
 diagnostic modalities 133–4, 137, 139–40
 recurrent disease 138
 follow-up 134
 functional imaging 134–7
 recurrent disease 138–9
- imaging
 CT 133, 134, 135, 137
 Doppler ultrasound 133, 134
 FDG-PET 134, 135–6, 137
 FDG-PET-CT 136–7
 MRI 133, 134, 137
 PET 134, 135–6, 135, 136, 137

- ovarian cancer (*Continued*)
 PET-CT 136–7, 137
 ultrasound 133, 134, 137
 malignancy determination 133, 134, 137, 137
 management 133
 chemotherapy 137–8
 second-look laparoscopy 138
 pelvic examination 133
 peritoneal involvement determination 134–5,
 135, 136
 prognosis 133
 radioimmunotherapy 385
 clinical studies 392–4, 393
 glycoproteins 383, 386, 388–91
 isotopes used 385, 386
 mucins 383, 386–8, 386
 radiolabeling technique 385–6
 saccharide antigens 386, 391
 targets 386–92, 386
 three-step strategy 392
 recurrent disease 137–40
 imaging
 CT 138, 140
 FDG-PET 138–9, 140
 MRI 138, 140
 PET 139–40, 140
 PET-CT 139–40, 140
 staging 133, 134, 135, 137
 overstaging/understaging 134
 restaging 134
 ultrasound 133
 oxygen-15 38
 oxygen deprivation *see* hypoxia
 oxyphilic (H₁thle cell) carcinoma 277
- P13K 2
 P13K–Akt signaling pathway 6, 7
 p16 4
 p53 2, 6
 P829 (NeoTect) (NeoSpect) 319
 [^{99m}Tc(1)] PADA-AVA-bombesin(7-14) 421
 Paget's sarcomas 235
 PAGRIT 374, 378
 with chemotherapy 378
 locoregional 376–7, 378
 systemic 376
 pain
 bone metastases 341–2
 breakthrough 341
 pancreatic peptide (PP) 190
 papillary thyroid cancer (PTC) 161, 166
 prognosis 276
 recurrent disease 285, 286
 surgery 277
 therapy 276
 para-aortic lymph nodes (PALN) 511–12
 paragangliomas 417
 parecoxib 362
 Patient Care Evaluation Study of thyroid cancer
 (PCES) 279
 PDGF *see* platelet derived growth factor (PDGF)
 pelvic lymph node dissection (PLND) 112–13
 pentetreotide 268–9
 neuroendocrine tumor imaging 192, 193, 194,
 194, 195
 radioguided surgery 195
 peptide receptor proteins 417
 peptide receptor scintigraphy
 bombesin analogs 420–1
 CCK-2 receptor expressing tumors 419–20
 neurotensin analogs 421
 VIP-based analogs 421
 peptide receptor therapy *see* radiopeptide
 therapy
 perineal prostatectomy 111
 [^{99m}Tc]pertechnetate 267
 [^{99m}Tc]pertechnetate
 thyroid cancer imaging 162, 163–4
- PET (positron emission tomography) 18, 51, 52
 adrenal tumor imaging 182, 183, 184–5, 186, 187
 brain tumor imaging 44
 breast cancer imaging 148, 149
 colorectal cancer imaging 99–100, 101, 102–3,
 102, 104, 105
 combined methods 39, 40
 CT-based attenuation correction 408–9
 contrast agents, effect of 409
 energy scaling of attenuation map 408
 motion artifacts 409
 resolution scaling 409
 CUP imaging 266, 266
 detection of residual/recurrent disease 56, 101
 esophageal cancer imaging 90–1, 92
 advanced disease 96
 metastases 92
 positivity criteria 91, 93
 staging 93
 therapy response 95
 vs PET-CT or CT 93
 head/neck cancer imaging 51, 52–4, 56
 sensitivity/specificity 55
 staging 54–5
 instrumentation *see* PET scanners
 lung cancer imaging 68
 comparison with PET 74
 cost-effectiveness 79
 predicting/monitoring response to therapy 78
 radiotherapy planning 77–8
 staging small-cell lung cancer 79
 lymphoma imaging 208, 209, 210, 211
 neuroendocrine tumor imaging 191, 198–9
 ovarian cancer imaging 134, 135–6, 135, 136, 137
 recurrent disease 139–40, 140
 primary brain tumors 23, 33, 35–9
 traditional findings 42–3
 proliferation markers 424–5
 prostate cancer imaging 117–25
 [¹¹C]acetate 119, 121
 bombesin derivatives 120
 [¹¹C]choline/derivatives 117–19, 122
 [¹⁸F]choline/derivatives 117–19, 122–4
 FDG 120–1
 [¹⁸F]fluoride 124–5
 16β-[¹⁸F]fluoro-5α-dihydrotestosterone
 119–20
 [¹⁸F]fluoroacetate 119
 future perspectives 120
 multitracer imaging 125
 with radiolabeled amino acids 37
 radiopharmaceuticals, new 413
 radiotherapy planning
 head/neck cancer 509, 510
 image fusion/co-registration 502–4
 lymphomas 512
 rationale 501–2
 sensitivity/specificity 102
 thyroid cancer imaging 172
 tracers 421
 structures 423
see also specific PET-tracers
 whole body, for metastases 55, 58, 58, 71
see also FDG-PET; FDHT-PET; FLT-PET; HED-
 PET; MET-PET; PET scanners; PET-CT
- PET scanners 397–9
 'afterglow' phenomena 485
 detector technology
 avalanche photodiodes 399
 inorganic scintillators 397–8
 photomultiplier tubes 399
 detector time response 485
 developments 401–3
 2D vs 3D 402
 depth of interaction 402
 time of flight 402–3, 482–5
 extinct evolution lines 487–8
 Fourier rebinning (FORE) 489
- PET scanners (*Continued*)
 inorganic scintillators 397–8, 482, 484, 485
 energy resolution 483
 intrinsic efficiency 482–3
 maximum likelihood expectation maximization
 (MLEM) 489
 multislice rebinning (MSRB) 489
 ordered subsets expectation maximization
 (OSEM) 489
 photodetector research 483, 485
 photodiodes 482–3
 RAMLA 489
 scanner evolution 475–80
 scanner performance parameters 480–2
 depth of interaction 402, 480–1
 image quality (IQ) 482
 lesion detectability 482
 noise equivalent count rate 481–2, 490–1, 494
 parallax error 480, 480
 peak trues 481, 494
 scatter fraction 482, 490–1, 494
 sensitivity 481, 490, 494
 signal:noise ratio 481, 482
 spatial resolution 480–1, 490, 492
 scintillators *see* PET scanners, inorganic
 scintillators
 single slice rebinning (SSRB) 488–9
 software improvements 488–9
 filtered back projection 489
 fully 3D algorithm 488–9
 iterative reconstruction methods 489
 rebinning 488–9
 time of flight 402–3, 486–8
 annihilation position uncertainty 486
 coincidence detection 486
 noise reduction 487, 488
 signal:noise ratio improvement 486–7
 technological implementations 487–8
 theory 486
 time resolution 486
- PET Accel 475
 PET-CT
 adrenal tumor imaging 182, 186
 bone tumor imaging 224, 237, 238, 239, 243
 breast cancer imaging 147, 148
 recurrent disease 151–3
 co-registration of images 406
 colorectal cancer imaging 100, 100, 101, 103–4
 inline vs software fusion 103–4
 limitations 106
 cost-effectiveness of imaging 105
 CUP imaging 266, 266
 esophageal cancer imaging 91, 92
 metastases 94
 vs PET or CT 93
 example image 408
 head/neck cancer imaging 52–3
 movement artifacts 53, 54
 post-therapy evaluation 57
 for radiotherapy target volume 57
 stripe artifact 55
 hypopharyngeal SCC 55
 instrumentation, new 406, 408, 409
 lung cancer imaging 68, 68, 70
 comparison with PET 74
 detection of recurrence 75, 76–7
 predicting/monitoring response to therapy
 78–9
 radiotherapy planning 77
 staging 72, 73, 75, 76
 small-cell lung cancer 80
 lung cancer staging
 distant metastases 70
 lymph node evaluation 74
 small-cell lung cancer 80
 lymphoma imaging 203, 208, 210, 211, 215
 malignant melanoma imaging 256, 257
 multitracer imaging 513–15

- PET-CT (*Continued*)
 apoptosis 514–15
 clonogenic cell density 514
 tumor growth factor receptor status 515
 tumor hypoxia 513–14
 tumor proliferation 514
 neuroendocrine tumor imaging 191, 198
 ovarian cancer imaging 136–7, 137
 recurrent disease 139–40, 140
 prostate cancer imaging 120
 radiotherapy image co-registration 502
 radiotherapy planning 503, 505
 esophageal cancer 512
 head/neck cancer 509, 510, 511
 imaging 512
 lung cancer 507, 508
 scanner 171
 soft tissue tumor imaging 242–3
 biopsy guidance 240–1
 metastatic disease 241
 recurrent disease 241
 therapy response 241–2
 thyroid cancer imaging 161, 171–3, 172
 volume segmentation 503, 505
 whole body, for metastases 58, 58
- PET-CT scanners
 state of the art scanners 494
 physical performance 493, 494–5
 spatial resolution 492
 technical parameters 491
 time of flight 476
- PET-DOTA 266
- PET-DOTA-NOC
 cancer of unknown primary (CUP) imaging 271
 CUP imaging 271
 neuroendocrine tumor imaging 198
- PET-DOTA-TOC
 cancer of unknown primary (CUP) imaging 271
 CUP imaging 271
 neuroendocrine tumor imaging 199
- PET-MRI 409–10, 503
- PGF *see* placenta growth factor (PGF)
- pheochromocytomas 178–9, 180, 187
 metastatic disease 182, 197
 peptide receptor expression 417
- pilocytic astrocytomas 24
 classification 41
 magnetic resonance imaging 29
 neuroimaging findings 42
- pilomatricomas 12
- pituitary adenomas 25, 43, 417
- PIXELAR 477
- placenta growth factor (PGF) 8
- planar scintigraphy
 neuroendocrine tumor imaging 192, 193
 soft tissue tumor imaging 226
- plasmacytoma (myeloma) 237
- platelet derived growth factor (PDGF) 9, 10
 from cancer cells 1
- pleomorphic rhabdomyosarcomas 240
- pleural disease 79
- positron emission mammography 405
- positron emission prostate imaging 405
- positron emission tomography (PET) *see* PET (positron emission tomography)
- positron emitting mammography (PEM)
 instruments 495
- pRb *see* retinoblastoma protein (pRb)
- pre-targeted antibody-guided
 radioimmunotherapy (PAGRIT) 374
 with chemotherapy 378
 locoregional 376–7, 378
 systemic 376, 378
- pre-targeting strategies 437
- primary bone lymphoma 231, 237, 238
- primary brain tumors
 differential diagnosis 26
- primary brain tumors (*Continued*)
 histopathology 26
 imaging 244
 symptoms 27
- primitive neuroectodermal tumor (PNET) 240, 243, 367
- procarbazine 373
- proliferation
 control of 5
 molecular targets in imaging 19
- ProstaSci 116
- prostate cancer 109–31
 bone metastases 344–5
 characteristics 109
 cost-effectiveness of imaging 116
 dedicated scanners 495
 imaging 113, 115–17
 bone metastases/scintigraphy 115, 116–17, 124, 124
 CT 113, 115–16
 FDG-PET-CT 121, 122
 lymphoscintigraphy 115
 MRI 113, 115–16
 MRS 113
 PET 120
 [¹¹C]acetate 119, 121
 bombesin derivatives 120
 [¹¹C]choline 117–19, 122
 [¹⁸F]choline 122–4
 FDG 117, 120–1
 [¹⁸F]fluoride 124–5
 16β-[¹⁸F]fluoro-5α-dihydrotestosterone 119–20
 [¹⁸F]fluoroacetate 119
 future perspectives 120
 multitracer imaging 125
- PET-CT 120
- radioimmunoscintigraphy 116
- SPECT 117
- transrectal ultrasound (TRUS) 113
- metastases 111, 112, 116–17
 lymph node detection 113, 115, 115
- prognostic factors 109–11
 grading 109–10, 110
 prostate specific antigen 110–11
 staging 109, 110
- radioimmunotherapy 436
- radiotherapy 512
- recurrence 109, 121, 122
- risk stratification 111
- sentinel lymph nodes 112–13, 114, 115
- staging
 M staging 115–16
 N staging 113, 115
 T staging 113
- therapy 111–12
 follow-up 111–12
 hormone therapy 111, 119
 surgery 111, 113
- prostate imaging, positron emission 405
- prostate specific antigen (PSA) 109, 110–11
 in follow-up therapy 111–12, 116
 PSA doubling time 112
- prostate specific membrane antigen (PSMA) 116
- prostatectomies 111
- protease inhibitors 4
- protein degradation 6–7
- protein kinase B (PKB) 9
- proteomics 17
- PSA *see* prostate specific antigen (PSA)
- PTC *see* papillary thyroid cancer (PTC)
- PTEN 2, 7, 9, 26
- PTEN pathway 12
- radiation protection 458–60
 for β-emitters 458
 external exposure 458–9, 459
 for helpers/public 459
- radiation protection (*Continued*)
 instructions for patients 460, 460
 internal exposure 459
 radioecological considerations 459–60
 for workers 458–9
- radiation therapy *see* radiotherapy
- radical prostatectomies 111
- radiofrequency ablation 353
- radiography, plain
 bone tumor imaging 224, 232, 234, 235, 236
 soft tissue tumor imaging 224
- radioimmunodetection 302
- radioimmunoimaging 302
- radioimmunoscintigraphy 295, 297
 prostate cancer imaging 116
- radioimmunotherapy 208, 214
 antibodies
 776.1 386, 387
 AC6C3-2B12 392
 AE1 391–2
 B43.13 386, 387
 B72.3 386, 390, 393
 CC49 386, 390, 393, 393
 HMF61 386, 387–8, 393
 hu3S193 386, 391
 IgM antibody 392
 MN-14 386, 388
 MOv18 386, 388–9
 MX35 386, 390–1
- antigens
 CEA 386, 388
 gp38 (aFr) 386, 388
 gp95 386, 390
 HER2/neu 391–2
 Lewis Y 386, 391
 MUC1 386, 387, 393
 MUC16/CA125 386, 387
 TAG72 386, 389–90, 393, 394
- brain tumors 373–9
 avidin–biotin model 374
 clinical applications 374–6
 dosimetry evaluation 378–9, 379
 pre-targeting 374
 clinical progress of, for NHL 304–7
 evolution 302–4
 glycoproteins 386, 388–91
 isotopes used 385, 386
 mucins 386–8, 386
 myeloablative 306–7
 non-myeloablative 304–6
 ovarian cancer 385
 radiolabeling technique 385–6
 targets 386–92, 386
- pre-targeted 294–7
 hematological toxicity risk 296
 pre-targeting strategies 294, 437
 procedure 296–7
 survival, effect on 296
- principles 300
- saccharide antigens 386, 391
- three-step strategy 375, 377, 379, 392
 vs external beam radiotherapy 300
- radioiodine therapy 166–8, 167, 170
 differentiated thyroid cancer 279–82
 ablative radioiodine therapy 279–80, 283–4
 guidelines 279–80
 controversy 281
 papillary thyroid cancer 280
 patient preparation 280
 side-effects 280
- radioisotopes 433–4
 therapeutic applications 434
- radiolabeled amino acids 37–9
- radionuclide imaging *see* PET (positron emission tomography); SPECT (single photon emission computed tomography)
- radionuclide scintigraphy
 bone tumor imaging 223–4, 224

- radionuclide scintigraphy (*Continued*)
 benign tumors 227, 229–31
 malignant tumors 231, 233–7
 brain tumor imaging 33–9
 soft tissue tumor imaging 223–4, 224, 239–40
- radionuclide therapy
 bone metastases 341, 342, 342
 dosimetry 443–58
 hepatocellular carcinoma 353–7
- radionuclides 321–2
 physical properties 321, 343
- radiopeptide therapy
 bombesin analogs 438–9
 octreotide derivatives 437
 RGD peptides 438–9
 targets 438
 future 438
- radiopharmaceuticals
 in bone/soft tissue imaging 224–6, 343
 cancer of unknown primary 266
 chelating systems 414
 new developments
 antibodies
 fragments 437
 manufacturing 434–7
 for diagnosis 413–32
 genetic modification 439–40
 hypoxia markers 425
 peptide receptor markers 425–7
 PET 413, 421–7
 pre-targeting strategies 437
 problems/opportunities 413
 proliferation markers 424–5
 radioisotopes 433–4, 434
 radiopeptide therapy
 bombesin analogs 438–9
 octreotide derivatives 437
 RGD peptides 438–9
 receptor-binding peptide-based 416–21
 SPECT 413–21
 for therapy 433–42
 vectors 433
 organ doses/whole-body dose 343, 343
 in PET 52
- radiosensitivity ratio 458
- radiosensitizers 346, 362
- radiotherapy 502–4
 4D data 515
 biological target volume (BTV) 502
 brain tumors 370–2, 512
 cervical cancer 511–12
 clinical applications 505–12
 clinical target volume (CTV) 501–2, 502
 esophageal cancer 512
 future perspectives 513–15
 gross tumor volume (GTV) 501, 502
 delineation 504, 505, 509
 head/neck cancer 508–11
 lung cancer 64–5, 506–8
 planning 77–8
 lymphomas 512
 modern 499–500
 multidimensional (MD-CRT) 502
 fiducial markers 503–4, 504
 immobilization systems 503
 patient positioning 503
 registration accuracy 503–4
 multitracer PET-CT 513–15
 nuclear medicine-guided 499–520
 phases of patient management 505
 planning 77–8
 with PET imaging 501–4
 image fusion/co-registration 502–4
 rationale 501–2
 prostate cancer 111, 512
 tomotherapy 500
 see also intensity-modulated radiation therapy (IMRT)
- Raf 8–9
 Ras 2, 8
 Ras–Raf–MAPK pathway 1
 ras signal transduction pathway 8
 Rb 2
 see also retinoblastoma protein (pRb)
- regional cerebral blood volume (rCBV) images 30–1
- regulatory proteins 2
- renal toxicity 332
- replicative senescence 6
- reticulum cell sarcoma of bone 231
- retinoblastoma protein (pRb) 3
- retro-mandibular node imaging 54
- retropubic prostatectomy 111
- reverse transcriptase-polymerase chain reaction (RT-PCR) 266
- RGD peptides 438–9
- rhabdomyosarcomas 240, 242
- rhinopharynx cancer 510
- rituximab 299–300, 303
- SCCs see squamous cell carcinomas (SCCs)
- schwannoma, malignant 240
- scintigraphy 192
 adrenal tumor imaging 179
 adrenocortical 181–3
 sympathetic nervous system tumor 183–7
 planar, problems of 163
 whole body 161, 166–9, 167, 168, 169, 170
- scintimammography 144, 145, 146–7, 268
 breast cancer imaging 155
- sentinel lymph node biopsy (SLNB)
 breast cancer 149
 breast cancer imaging 143–4, 155
 malignant melanoma imaging 254–5
- sentinel lymph nodes (SLN)
 in breast cancer 143–4
 laparoscopic lymphadenectomy 113
 malignant melanoma imaging 255
 in prostate cancer 112–13, 114, 115
- [^{99m}Tc]sestamibi
 bone tumor imaging 225
 breast cancer imaging 146, 155
 CUP imaging 268
 soft tissue tumor imaging 225
 thyroid cancer imaging 161, 164–5, 164, 168, 169, 170
- [^{99m}Tc]sestamibi SPECT 34, 44
- [¹⁸F]SFB 425
 structure 425
- Shh pathway 12
- signaling pathways 12
- signal:noise ratio 467, 476, 486–7
- silencing of genes 3
 epigenetic 4
- single detection 467–75
 choice of scanner 476
 future developments 475
- single photon emission computed tomography see SPECT (single photon emission computed tomography)
- single photon emission mammography 404–5
- single slice rebinning (SSRB) 488–9
- SIRSpheres 362, 364, 364
- small-cell lung cancer (SCLC) 61
 classification 79
 peptide receptor expression 417
 staging 79–80
 therapy by stage 64
- 'smart' probes 17
- sodium iodide symporter (NIS) 18
- soft tissue tumors 239–44
 classification 240
 diagnosis 223
 etiology/pathogenesis 239
 grading 223, 239
 metastatic disease 242
- soft tissue tumors (*Continued*)
 radiopharmaceuticals 224–6
 recent advances/future trends 243–4
 staging 223, 223
- solitary pulmonary nodules (SPNs) 61, 65
 CT imaging 70
 FDG-PET-CT imaging 68, 69, 70
 FDG-PET imaging 70
 PET-CT imaging 70
- somatic mutation theory of carcinogenesis 3
- somatostatin 418
- somatostatin analogs 316, 418–19
 CUP imaging 271
 for diagnosis 322
 neuroendocrine tumors
 imaging 191, 192, 192, 195–6, 197–8
 after metastasis 315
 radiolabeled 418
 for therapy 322
 uptake 329
- somatostatin receptors
 binding of peptides 317
 expression 316
 neuroendocrine tumor imaging 191, 193–4
 in radiopeptide therapy 438
- somatostatin receptor imaging
 CUP imaging 268
 lung cancer
 diagnosis 66
 imaging 67
 primary brain tumors 18, 35
- SPECT (single photon emission computed tomography) 18, 454
 adrenal tumor imaging 178, 179, 180, 181–4, 185
 bombesin analogs 420
 bone tumor imaging 226
 brain tumor imaging
 indications 44
 radiotherapy planning 512
 breast cancer imaging 146
 correlated with other modalities 406
 CT-based attenuation correction 407, 408–9
 contrast agents, effect of 409
 motion artifacts 409
 resolution scaling 409
 CUP imaging 266, 266
 imaging agents 416
 instrumentation see SPECT scanners
 lung cancer radiotherapy planning 508
 lymphoma imaging 205–8
 and monoclonal antibodies 35
 neuroendocrine tumor imaging 191, 193, 195
 primary brain tumors 23, 33–5, 39
 prostate cancer imaging 117
 radiopharmaceuticals, new 413–21
 radiotherapy image co-registration 502
 sensitivity vs specificity 34
 soft tissue tumor imaging 226
 thyroid cancer imaging 161, 166–9
 tracers 33, 34–5
 see also Ga-SPECT; SPECT-CT; SPECT scanners; TI-SPECT
- SPECT scanners
 advances made 471–4
 attenuation 473
 Chang's method 473–4
 dedicated brain-SPECT systems 474–5
 developments 399–401
 attenuation correction 400
 Compton camera 400–1
 scatter correction 400
 fan beam collimators 473
 intrinsic efficiency 473
 sensitivity, system 472
 spatial resolution 472, 473
- SPECT-CT
 adrenal tumor imaging 178, 179, 182, 184, 185
 advantages 407

- SPECT-CT (*Continued*)
 bone tumor imaging 224, 243
 co-registration of images 406
 example image 407
 instrumentation, new 406, 406, 407–8, 409
 lung cancer
 radiotherapy planning 508
 staging of distant metastases 70
 neuroendocrine tumor imaging 195, 197
 VG Millennium system 406
- SPECT-CT scanners 474
- spleen metastases 150
- squamous cell carcinomas (SCCs)
 esophageal 89
 head/neck (HNSCCs)
 FDG-PET 56–8
 PET 52–5
 post-therapy evaluation 56–8
 staging 54–5
 hypopharynx 55
- staging
 bone tumors 223, 223, 233
 breast cancer 144, 148–50
 colorectal cancer 100–1, 359, 360
 esophageal cancer 89–90, 90, 93
 head/neck cancers 51, 54–5
 node evaluation 55
 hepatocellular carcinoma 351–2, 352
 lung cancer 72, 75, 79–80
 distant metastases
 conventional imaging 69–70
 nuclear imaging 71–3
 lymph node evaluation 74
 conventional imaging 73
 nuclear imaging 73–4
 restaging 76–7
 small-cell lung cancer 79–80
 systems 61–2
- lymphomas 206, 209, 211
 restaging 207
- malignant melanoma 253
 distant metastases 256–8
 nodal 253–6
- ovarian cancer 133, 134, 135, 137
 preoperative 276
- prostate cancer 109, 110, 113, 115–17
 soft tissue tumors 223, 223, 240, 241, 243, 243
- Starbright detector 468, 468
- stem cell paradigm 11
- stem cells 11–13
 signaling pathways 12
- strontium-89 342
- substance P 320–1
 receptors 438
- suppressor genes 3, 6
 suppressor proteins 2
- supratentorial ependymomas 25–6
- Survival, Epidemiology and End Results (SEER)
 project 299, 367
- sympathoadrenal tumors 181–3, 190
 associated diseases 178
 scintigraphy 183–7
- synovial sarcoma 240
- systems biology 17
- T-cell lymphomas 300
- targeted radiotherapy (TRT) *see* radionuclide therapy
- targets, molecular 17–20
 imaging
 clinically established 18
 preclinical 18–20
 therapeutic 18–19
- Taxol 394
- temozolomide 371, 373, 378
- tenascin 374–5, 375
 immunohistochemistry 375
- teratocarcinomas 4
- [⁶⁴Cu]TETA-octreotide 317
- [^{99m}Tc]tetrofosmin 35
 bone tumor imaging 226
 breast cancer imaging 146, 155
 lung cancer imaging 67
 soft tissue tumor imaging 226
 thyroid cancer imaging 161, 164–5, 165, 168, 169, 170
- thallium (²⁰¹Tl) scintigraphy *see* ²⁰¹Tl scintigraphy
- thallium (²⁰¹Tl) SPECT *see* Tl-SPECT
- thoracic lymph node stations 63
- thymidine *see* FLT
 metabolism/salvage pathway 424
- thymidine-PET 422
- thyroglobulin 161, 165–6, 167–8, 170, 170
 human (hTg)
 and cytotoxic therapy 286
 and DTC hormone therapy 282
 and DTC surgery 275
 and external beam radiotherapy 283–4
 and radioiodine therapy 280, 281, 282
 and recurrent disease 285, 286
 rTSH-stimulated thyroglobulin 161, 167–8, 172
- thyroid cancer 161–75, 275
 diagnostic modalities
 follow-up 161, 164–73
 preoperative 161–4
 hyperfunctioning nodules 163
 hypofunctioning nodules 163, 165
 imaging 168
 brown fat as pitfall 172
 radioiodine 161, 163, 164
 whole body scintigraphy 167, 169, 170
 metastatic disease 161, 165, 168, 172
 papillary vs follicular 161
 recurrent disease 161, 165
 treatment 161, 165
 thyroglobulin 161, 165–6
see also differentiated thyroid cancer (DTC); follicular thyroid cancer (FTC); medullary thyroid cancer (MTC); papillary thyroid cancer (PTC)
- thyroid stimulating hormone (TSH) 161, 165–6
 rTSH-stimulated thyroglobulin 161, 167–8, 172
 stimulation 285, 286
 suppression 283, 285
- thyroid stunning 167, 281
- thyroidectomy 276
 completion 278
- thyroiditis, radiation 282
- L-thyroxine 282, 283
- tissue inhibitors of metalloproteinases (TIMPs)
 415
- tissue organization field theory of carcinogenesis
 4–5
- ²⁰¹Tl scintigraphy
 bone tumor imaging 225, 226, 233, 235
 soft tissue tumor imaging 225, 226, 242
 thyroid cancer imaging 168
- ²⁰¹Tl-SPECT 33, 34, 233
 brain tumor imaging 44
 lymphoma imaging 208
- TNM staging system
 bone/soft tissue tumors 223, 233
 colorectal cancer 101
 esophageal cancer 89, 90
 lung cancer 61–2
 malignant melanoma 253
 prostate cancer 109, 110, 113, 115–16
- tomotherapy 500
- TomTherapy Hi-Art System 500–1
- tongue cancers 51, 56
- TOR pathway 6
- [¹³¹I]tositumomab (Bexxar) 300, 433
 adverse effects 304, 310
 characteristics 306
- [¹³¹I]tositumomab (Bexxar) (*Continued*)
 and chemotherapy 309
 dosing schedule 309
 efficacy 304–5
 indications 307–8
 non-myeloablative radioimmunotherapy 304–5
 patient preparation 308
 preparation 310
 therapeutic regimen 305
- TP53 26
- TP3654 196
- TRAIL-R 2
- transforming growth factor β (TGF β) 1, 9
- transrectal ultrasound (TRUS) 113
- trastuzumab 18
- tricarbonyl precursor 414
- tumor blood vessels 9–10
- tumor growth 7–9
- tumor necrosis factor (TNF) 5
- tumor suppressor genes 6
 repression 3
- tumorigenesis
 gene defects in 7
 primary brain tumors 26
 regulatory proteins 2
- Tyr-octreotate (TATE) 418, 418
- Tyr-octreotide (TOC) 316, 317, 418, 418
- tyrosine 154
- tyrosine kinases 19
- tyrosine kinase inhibitors 515
- ubiquitin-mediated proteolysis 6
- ULMDOS 451
- ultrasound (US)
 bone tumor imaging 224
 breast cancer imaging 148
 colorectal cancer imaging 99, 101
 endoscopic *see* endoscopic ultrasound (EUS)
 lymphoma imaging 205, 211
 neuroendocrine tumor imaging 190–1
 ovarian cancer imaging 133, 134, 137
 soft tissue tumor imaging 224
 thyroid cancer imaging 161–2, 165, 166
 transrectal (TRUS) 113
 US-FNAB thyroid cancer imaging 161–3, 162, 165
- 'vanilla' markers 513
- Vapreotide 418
- vascular endothelial growth factor receptor (VEGFR) 9, 10, 19
- vascular endothelial growth factor (VEGF) 8, 9, 10, 19
- vasoactive intestinal peptide (VIP) 190, 191
 neuroendocrine tumor imaging 190, 192
 VIP-based analogs 320, 421
 VIP receptors 316
- vectors 433, 439–40
- video-assisted thoracic surgery (VATS) 62
- vinblastine 347
- VIP-based analogs 320
- Warburg effect 52
- white matter tractography 31, 31
- whole body scanning *see under specific modality*
- Wnt pathway 4, 7, 12
- X-ray computed tomography *see* computed tomography (CT)
- ⁹⁰Y 301, 302
- ⁹⁰Y-labeled anti-CEA antibodies 361
- ⁹⁰Y-labeled humanized anti-CD22 IgG 304
- ⁹⁰Y-labeled microspheres 356–7, 362, 364, 364
- yttrium-90 342
- Zevalin *see* ibritumomab tiuxetan (Zevalin)

Advances in Nuclear Oncology

Diagnosis and Therapy

Edited by

Emilio Bombardieri

Director, Department of Diagnostic Imaging and Therapy, Nuclear Medicine Division, IRCCS Foundation, National Cancer Institute, Milan, Italy

John Buscombe

Consultant, Department of Nuclear Medicine, Royal Free Hospital, London, UK

Giovanni Lucignani

Director, Unit of Nuclear Medicine, Hospital San Paolo, Institute of Radiological Sciences, University of Milan, Milan, Italy

Otmar Schober

Director, Department of Nuclear Medicine, University of Münster, Münster, Germany

The diagnostic and therapeutic achievements in radiopharmaceuticals and nuclear medicine instrumentation – PET, SPECT, MR, CT and their hybrids PET-CT and SPECT-CT – are the result of the interdisciplinary research efforts of cell-biologists, chemists, pharmacologists, physicists, computer-scientists, engineers, nuclear medicine physicians, and oncologists. The clinical implications of these achievements have made nuclear medicine indispensable in the management of cancer. This superbly illustrated text on modern nuclear medicine applications in the diagnosis and treatment of cancer describes the state of the art and the current position of nuclear medicine in the light of these recent developments. It is intended as a valuable update also for non-nuclear medicine specialists working in oncology. Nuclear medicine as part of molecular imaging and therapy has changed radically in the last decade. The growing importance and clinical impact of these changes in the near future has impelled the internationally renowned editors and contributors to put them on record in *Advances in Nuclear Oncology*.

Section Contents:

I. Biology of Cancer

II. Diagnostic Applications

III. Therapeutic Applications

IV. Methods and Technology

Advances in Nuclear Oncology is required reading for all those working with and treating cancer patients. This excellent text

- Combines nuclear oncologic medicine (including the most up-to-date radiopharmaceuticals) with the latest in computed tomography (CT) technology and so will be at the forefront of nuclear medicine diagnostic texts
- Divided into four sections for ease of use
- 321 color and 579 black and white scans, photographs, and line drawings
- Extensively referenced
- The editors contributors are respected leaders in the field of nuclear oncologic medicine



informa
healthcare

www.informahealthcare.com